Appendix A (Updated). 3-Dimensional Hydrodynamic and Water Quality Model of Falls Lake, North Carolina

EFDC Model Setup, Calibration, and Validation
Task 3c

Prepared for:

The Upper Neuse River Basin Association
P.O. Box 270
Butner, NC 27509

Prepared for:

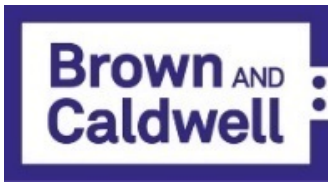

Brown and Caldwell
5430 Wade Park Blvd. Suite 200
Raleigh, NC 27607

May 30, 2023

DYNAMIC SOLUTIONS, LLC
6421 DEANE HILL DRIVE
KNOXVILLE, TENNESSEE 37919

Table of Contents

List of Figures

List of Tables

List of Acronyms and Abbreviations

AE	Average Error
CAAE	North Carolina State University Center for Applied Aquatic Ecology
CASTNET	Clean Air Status and Trends Network
CE	Coefficient of Efficiency
Chl-a	Chlorophyll-a
COD	Chemical Oxygen Demand
CSOD	Carbonaceous Sediment Oxygen Demand
DO	Dissolved Oxygen
DOC	Dissolved Organic Carbon
DOM	Dissolved Organic Matter
DON	Dissolved Organic Nitrogen
DOP	Dissolved Organic Phosphorus
DSI	Dynamic Solutions International, LLC
DWR	North Carolina Division of Water Resources
EFDC	Environmental Fluid Dynamics Code
EPA	Environmental Protection Agency
LOESS	Locally Estimated Scatterplot Smoothing
LPOC	Labile Particulate Organic Carbon
LPON	Labile Particulate Organic Nitrogen
LPOP	Labile Particulate Organic Phosphorus
MRSW	Modeling and Regulatory Support Workgroup
NADP	National Atmospheric Deposition Program
NAVD88	North American Vertical Datum of 1988
NC	North Carolina
NCDC	National Climatic Data Center
NEXRAD	Next Generation Weather Radar
NHD	National Hydrography Dataset
NOAA	National Oceanic and Atmospheric Administration
NSC	Normalized Sensitivity Coefficient
NSOD	Nitrogenous Sediment Oxygen Demand
pBias	Percent Bias
PFC	Path Forward Committee
PDF	Probability Density Function
POC	Particulate Organic Carbon
POM	Particulate Organic Matter
PON	Particulate Organic Nitrogen
POP	Particulate Organic Phosphorus
QAPP	Quality Assurance Project Plan

RE	Relative Error
RMSE	Root Mean Square Error
RPOC	Refractory Particulate Organic Carbon
RPON	Refractory Particulate Organic Nitrogen
RPOP	Refractory Particulate Organic Phosphorus
RSR	RMSE– Standard Deviation Ratio
SA	Available Silica
SOD	Sediment Oxygen Demand
SU	Particulate-Biogenic Silica
TAM	Total Active Metal
TKN	Total Kjeldahl Nitrogen
TN	Total Nitrogen
TOC	Total Organic Carbon
TON	Total Organic Nitrogen
TOP	Total Organic Phosphorus
TP	Total Phosphorus
TSS	Total Suspended Sediment
UNC	University of North Carolina at Chapel Hill
UNRBA	Upper Neuse River Basin Association
USGS	United States Geological Survey
WARMF	Watershed Analysis Risk Management Framework
WQ	Water Quality

1. Introduction and Background

The Neuse River was impounded near the City of Raleigh in central North Carolina to form the Falls of the Neuse Reservoir (Falls Lake) located at the downstream end of the Upper Neuse River Basin (Hydrologic Unit Code: 03020201) (Figure 1-1). Falls Lake is a Piedmont reservoir with a contributing drainage area of 770 square miles that includes several smaller impoundments. Falls Dam (-78.5825 N Longitude, 35.941667 W Latitude) is located in the Upper Neuse River immediately upstream of the village of Falls in Wake County, NC. The dam is located approximately 198 miles upstream from New Bern, NC; 47 miles upstream from Smithfield, NC; and about 10 miles north of Raleigh, NC. The main body of Falls Lake is in Wake and Durham counties with some of the embayments extending into Granville County. The physical characteristics of Falls Lake are a unique combination of geological and morphological aspects of the original river and its adjacent riparian area. It is a reservoir and not a natural lake.

Construction of Falls Lake dam by the U.S. Army Corps of Engineers was completed in 1981. Designated uses of Falls Lake are drinking water supply, recreation, fishing, aquatic life, and wildlife. Falls Dam is an earthen structure having a top elevation of 291.5 feet above mean seal level (msl), and an overall length of 1,915 feet with a height above the streambed of 92.5 feet. Falls Lake extends 28 miles up the Neuse River to just upstream of the confluence of the Eno and Flat Rivers. At the top of the conservation pool at an elevation of 251.5 feet, msl, the shoreline length is about 175 miles, and the lake covers an area of 12,410 acres (U.S. Army Corps of Engineers Wilmington District and the State of North Carolina, 2013).

The waters of the Upper Neuse River Basin have many challenges meeting the demands of society and achieving compliance with the environmental standards currently in place for the watershed. Falls Lake is the primary source of drinking water for the City of Raleigh and its 550,000 customers and is located immediately downstream of several urban areas, including the City of Durham. Falls Lake is a shallow Piedmont lake characterized by its inherent difficulty meeting water quality standards for Chl-a because of its geology, morphology, and its topographic location downstream of pre-existing and established land uses.

Falls Lake Nutrient Management Strategy. The Nutrient Management Strategy that was passed in 2011 by the State requires very large reductions in nutrient loading to the lake. The lake modeling and analyses used to support the technical basis for the rules were developed by the North Carolina Department of Environment and Natural Resources, Division of Water Quality on a compressed schedule with limited data. Based on this previous lake modeling effort and reflected in the Falls Lake Rules, there is considerable uncertainty about the technical basis of the required loading targets for nutrient reduction in the watershed. For this reason, the rules allow for a “reexamination” of the required nutrient load reductions.

In 2013, the Upper Neuse River Basin Association (UNRBA) developed a plan for conducting the reexamination that included a minimum of four years of water quality monitoring in the watershed and the lake that began in 2014. A primary purpose for collecting data in the lake was to support development of revised and new watershed-lake models as part of the

reexamination of the Falls Lake Nutrient Management Strategy. Additional types of data and information were also needed to support development of the models.

In 2018, the UNRBA submitted and DWR approved the Modeling and Regulatory Support Quality Assurance Project Plan (QAPP) to guide development of the models and support the reexamination of the Falls Lake Nutrient Management Strategy (Brown and Caldwell, Systech Water Resources Inc., Dynamic Solutions LLC, February 2018).

Selection of Watershed-Lake Model Framework. The UNRBA selected a watershed-lake model framework that included the WARMF model for watershed hydrology and nutrient loading; the WARMF lake model for a simplified model of water quality; the EFDC model for hydrodynamics, sediment transport (optional), and water quality; and a statistical model for the lake. As the predictions of nutrient enrichment and algal growth in the lake would be used to evaluate revisions of the nutrient management strategy, the UNRBA decided to develop multiple models to assess the lake's nutrient response. An approach based on assessment of multiple models reduces the reliance on a single model and provides corroboration for the ensemble of model results (Brown and Caldwell, Systech Water Resources Inc., Dynamic Solutions LLC., September 2018).

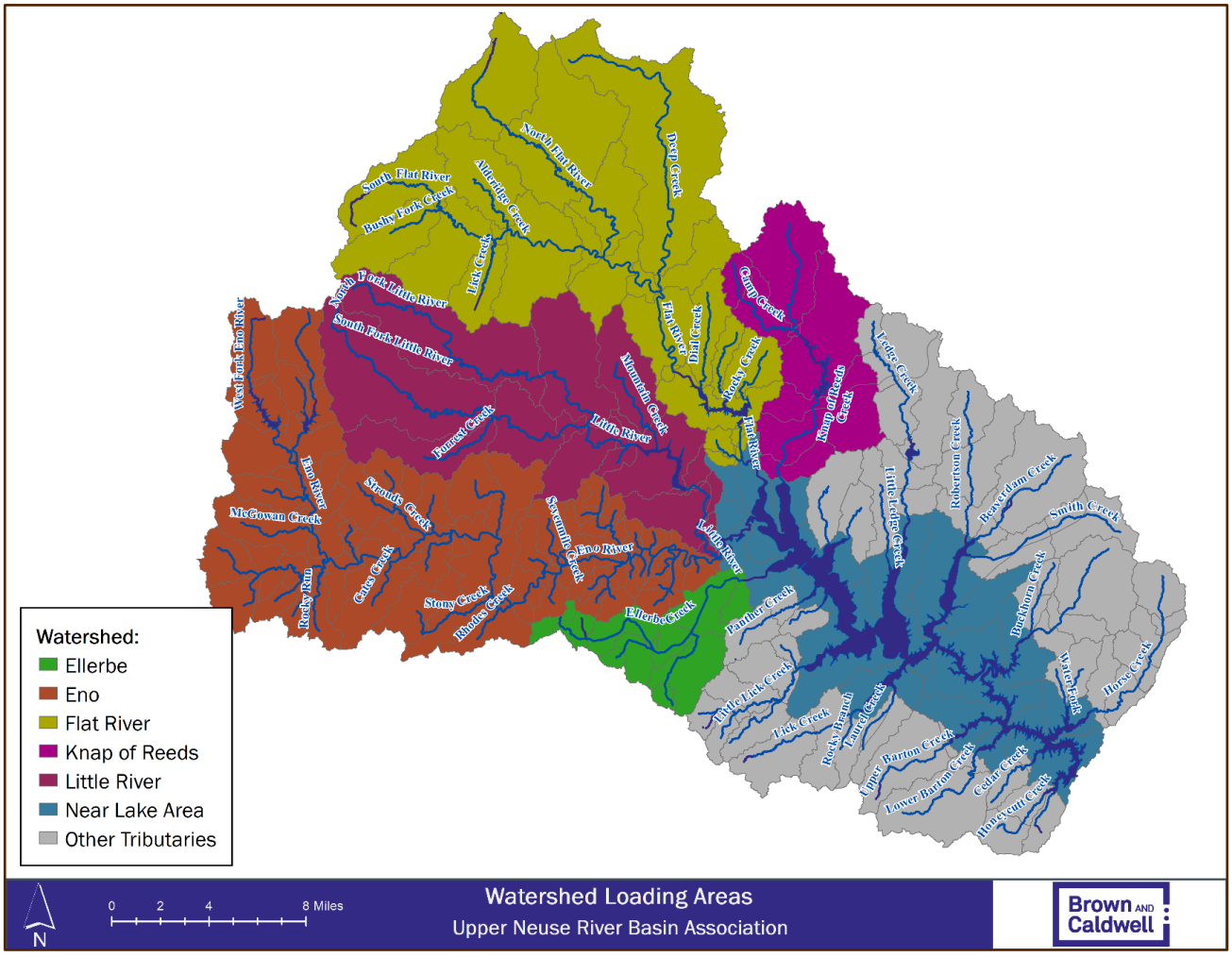

Figure 1-1 Location of Upper Neuse River Basin and Falls Lake: Hydrologic Unit Code 03020201

Dynamic Solutions LLC is responsible for (1) development of the EFDC hydrodynamic, sediment transport and water quality model for Falls Lake, and (2) evaluation of the impact of watershed load reductions of nitrogen and phosphorus as provided by the WARMF watershed model on lake water quality constituents including Chl-a. The data sources and data availability for the development of the WARMF watershed model and the EFDC lake model are documented in the UNRBA Modeling QAPP (Brown and Caldwell, Systech Water Resources Inc., Dynamic Solutions LLC, February 2018). This QAPP describes Dynamic Solution's activity performed under Phase 3 of the project for model setup, model calibration and validation, and assessment of model performance for the EFDC hydrodynamic model of Falls Lake.

Many organizations including the UNRBA, NC Collaboratory, US Geologic Survey (USGS), NC Division of Water Resources (DWR), NC Wildlife Resources Commission (WRC), NC State University Center for Applied Aquatic Ecology (CAAE), Cities of Durham and Raleigh, US Army Corps of Engineers (USACE), US Forest Service (USFS), and US Environmental Protection Agency (EPA) have conducted studies on Falls Lake or its tributaries that informed development of the three UNRBA lake models. The UNRBA has invested over $10 million in the monitoring and modeling studies of Falls Lake and its watershed. Section 4 of the main lake modeling report summarizes the extensive data sets used to develop these models.

During development of the WARMF Lake and EFDC models for Falls Lake, the modeling team, modeling staff from the DWR, the third-party reviewers funded by the NC Collaboratory, and other interested subject matter experts met to review the lake model calibrations. Discussions focused on chlorophyll-a concentrations, algal group data collected by the DWR, and sediment release studies conducted on Falls Lake. In response to this input, the UNRBA provided additional funds to test the model, improve calibration in reference to these studies, and document these efforts. Documentation of these efforts is included in Appendix D to the main lake modeling report and this appendix.

2. Development of EFDC model

2.1 Overview of the EFDC Model

EFDC is a general-purpose surface water modeling package for simulating three-dimensional (3-D) circulation, mass transport, sediment transport and biogeochemical processes in surface waters including rivers, lakes, estuaries, reservoirs, nearshore and continental shelf-scale coastal systems. The EFDC model was originally developed at the Virginia Institute of Marine Science for estuarine and coastal applications (Hamrick, 1992; 1996). EFDC has subsequently been widely used to simulate and evaluate regulatory approaches for reservoirs and lakes. Over the past decade, the US EPA has continued to support its development, and EFDC is now part of a family of public domain surface water models recommended by EPA to support water quality investigations including TMDL studies (EPA, 2020). In addition to state-of-the-art hydrodynamics with salinity, water temperature and dye tracer simulation capabilities, EFDC can also simulate cohesive and non-cohesive sediment transport, the transport and fate of toxic contaminants in the water and sediment bed, and water quality interactions that include DO, nutrients, organic carbon, algae and bacteria and a state-of-the-art sediment diagenesis model (Di Toro, 2001) that is internally coupled with the water quality model (Park et al., 2000; Hamrick, 2007). Special enhancements to the hydrodynamic code, such as vegetation resistance, drying and wetting, hydraulic structure representation, wave current boundary layer interaction, and wave-induced currents, allow refined modeling of tidal systems, wetland and marsh systems, controlled-flow systems, and near-shore wave-induced currents and sediment transport. The EFDC code has been extensively tested, documented and used in more than 100 surface water modeling studies (Ji, 2008). The EFDC model is currently used by university, government, engineering and environmental consulting organizations worldwide.

DSI has developed a version of the EFDC code that streamlines the modeling process and provides links to DSLLC's pre- and post-processing software tool EFDC_Explorer (Craig, 2018). The DSI version of the EFDC code is open source and DSI coordinates with EPA to provide ongoing updates and enhancements to DSI's version of EFDC as well as the version of the EFDC code provided by EPA.

2.2 Model Simulation Period

As part of the plan for conducting the reexamination of the Falls Lake Nutrient Management Strategy, the UNRBA began the watershed and lake monitoring data collection program in August 2014. This program continued until October 2018 to capture four years of monitoring through the end of the 2018 growing season. The current Falls Lake EFDC model described in this report was developed to support this 4–year data collection program with model calibration covering the 2-year period from January 1, 2015, through December 31, 2016, and model validation covering the 2-year period from January 1, 2017, through December 31, 2018.

2.3 Grid Development

As shown in Figure 2-1, a curvilinear orthogonal grid was developed for Falls Lake with 862 horizontal grid cells using UTM northing and easting coordinates for UTM Zone 17. Water column depth is split into ten (10) vertical Sigma Zed layers with equal thickness to represent vertical resolution of the lake model. The accuracy and scope of the modeling effort relative to grid and sediment depth development was greatly aided by the availability of the extensive bathymetric and sediment depth studies of the lake. This detail is typically not available. The following data were used to support development of the model grid and bathymetry interpolation.

- Shoreline and road shape files including numerous bridges and causeways in the Falls Lake watershed downloaded from the NHD; and
- Bathymetry data (Falls_Lake_2017_ASCII_HF_DTM_10_ft_Grid.txt) obtained from Brown and Caldwell.

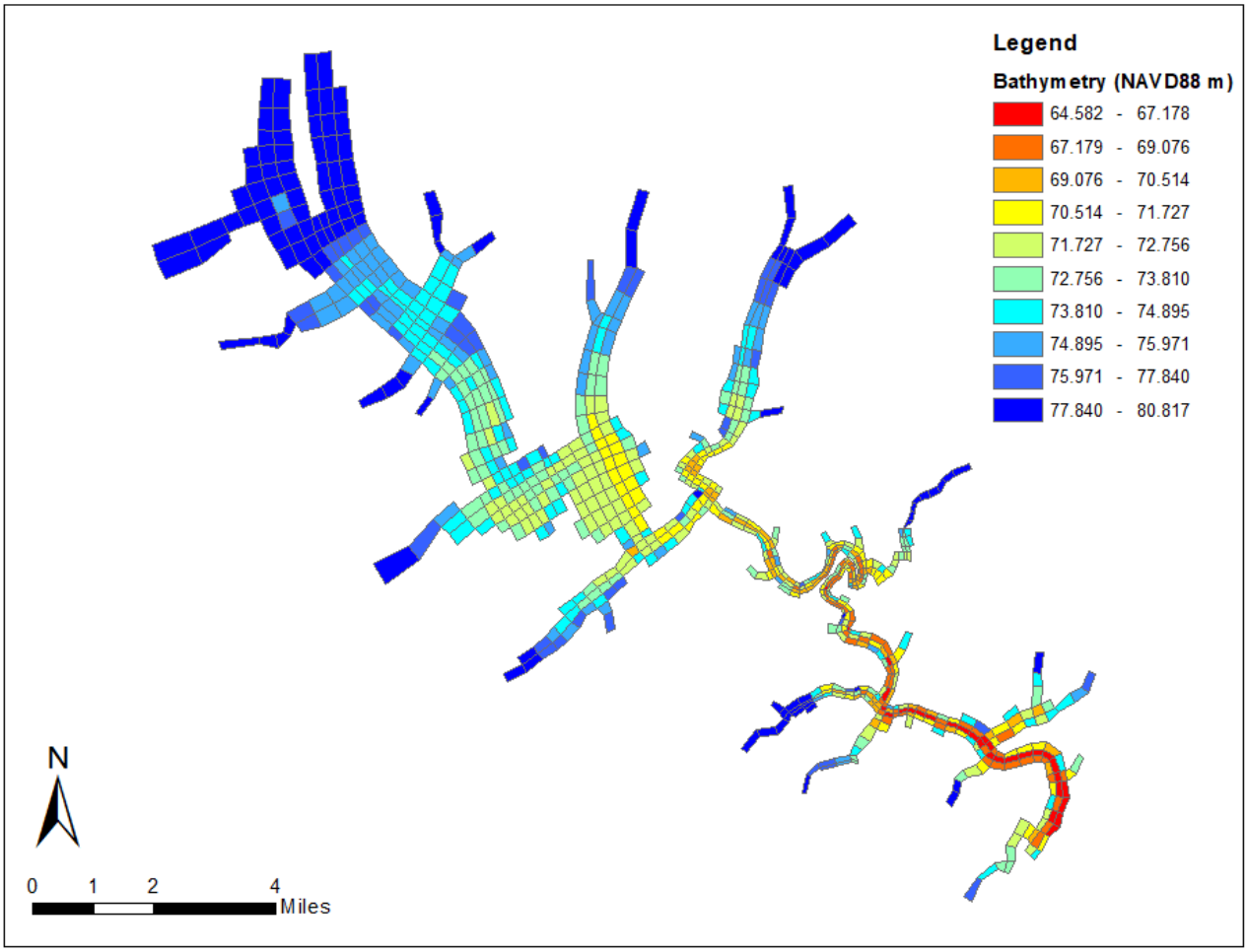

Figure 2-1 EFDC Model Grid for Falls Lake

Shoreline data (as meters, based on the UTM Zone 17N horizontal projection) was imported into the grid generator to determine the boundary of the lake. The model grid was designed such that the final model grid follows the shoreline and represents causeway flow restrictions with a spatial resolution of 862 horizontal cells. Cell sizes vary from 43 m to 686 m in the lateral direction and from 47 m to 830 m in the longitudinal direction. Spatial resolution of the model grid was chosen based on two primary considerations:

- The model grid reasonably captures bathymetric variation, meandering of the riverine segment of the lake, and shoreline; and
- Computing time for a one-year hydrodynamic, water temperature, sediment and water quality simulation are less than 12 hours to allow multiple-year simulations to be completed within a reasonable timeframe for assessment of model results.

It should be noted, however, that the spatial resolution of the grid was not fine enough to capture the old river channel along the center path of Falls Lake due to the narrowness of the old river channel compared to the width of the model grid cells.

Bathymetry data, as meters and at NAVD88, was obtained from Brown and Caldwell and used to assign bottom elevations for each grid cell. Bathymetric data points were averaged to assign a representative bottom elevation to cells with data while the Inverse Distance Weighting method was used to interpolate bathymetric observations for cells without bottom elevation data. Details related to development of the Falls Lake EFDC model grid, comparison to the DWR EFDC model grid, and locations of UNRBA sediment coring locations is provided in the main report.

2.4 Meteorological Data

Meteorological variables required by the EFDC hydrodynamic model include wind speed, wind direction, atmospheric pressure, air temperature, relative humidity, rainfall, evaporation, solar radiation, and cloud cover. Locations of the meteorological stations used for setup of the EFDC hydrodynamic model are shown in Figure 2-2 and identification information for the stations is given in Table 2-1.

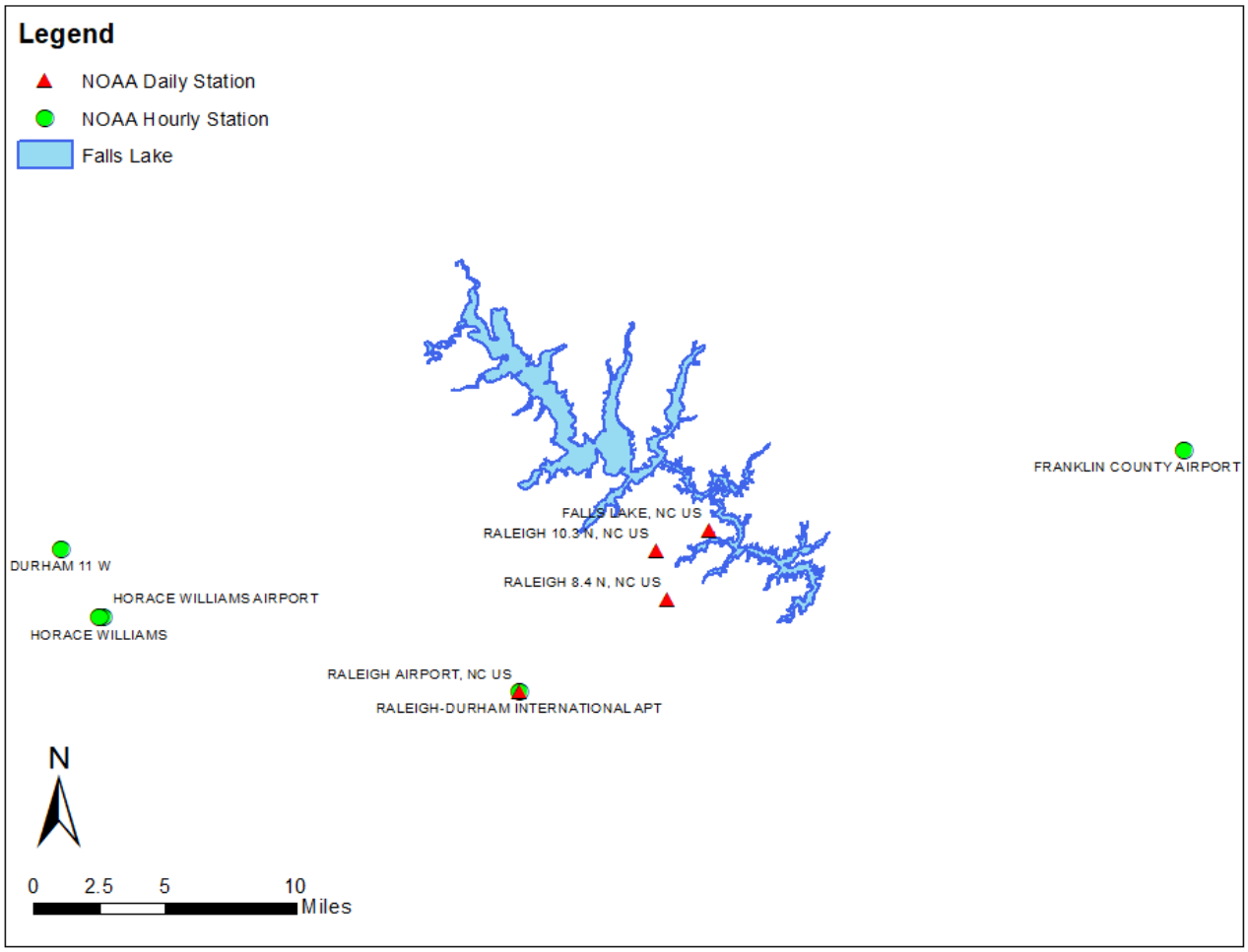

Figure 2-2 Location of the NOAA NCDC Meteorological Stations

Observed hourly evaporation was not available; therefore, hourly evaporation was internally calculated by the EFDC model. Hourly observations of wind speed, wind direction, atmospheric pressure, air temperature, relative humidity, and cloud cover were obtained from the NOAA NCDC stations shown in Figure 2-2 and listed in Table 2-1. Solar radiation data were obtained from the National Solar Radiation Database for a location defined by latitude (36.01 N) and longitude coordinates (-78.70 W) (NREL, 2020).

NEXRAD rainfall data provided by the NC State Climate Office (Brown & Caldwell and Systech Water Resources, 2023) were used to better represent spatial variation of the rainfall over the lake. A total of six (6) NEXRAD cells/time series were used to cover the whole lake. The locations of the stations are listed in Table 2-2 and shown in Figure 2-3. The time interval of the NEXRAD rainfall data was six (6) hours, and the data were disaggregated into hourly based on the hourly rainfall pattern available at the NOAA NCDC station USC00312993. The time frame for collection of meteorological data covered the years from 2014 to 2018 (initialization, calibration, and validation).

Table 2-1 Meteorological Stations Used in the EFDC Model

Station Name	Station ID	Latitude (degree)	Longitude (degree)
Falls Lake, NC US	USC00312993	35.981	-78.653
Raleigh Airport, NC US	USW00013722	35.892	-78.782
Raleigh 8.4 N, NC US	US1NCWK0061	35.943	-78.681
Raleigh 10.3 N, NC US	US1NCWK0001	35.970	-78.689
Raleigh-Durham International Apt	WBAN 13722	35.892	-78.782
Horace Williams Airport	WBAN 93785	35.933	-79.064
Horace Williams	WBAN 99999	35.933	-79.067
Durham 11 W	WBAN 3758	35.971	-79.093
Franklin County Airport	WBAN 3731	36.023	-78.330
Falls Lake, NC US	USC00312993	35.981	-78.653
Falls Lake, NC US	USC00312993	35.981	-78.653

Table 2-2 NEXRAD Station Locations

Station Name	Pixel ID	Latitude (degree)	Longitude (degree)
X370Y089_NE	71	36.0938	-78.7812
X370Y089_SE	69	36.0313	-78.7812
X371Y089_SW	52	36.0313	-78.7188
X371Y089_SE	53	36.0313	-78.6562
X371Y088_NE	59	35.9688	-78.6562
X372Y088_NW	46	35.9688	-78.5938

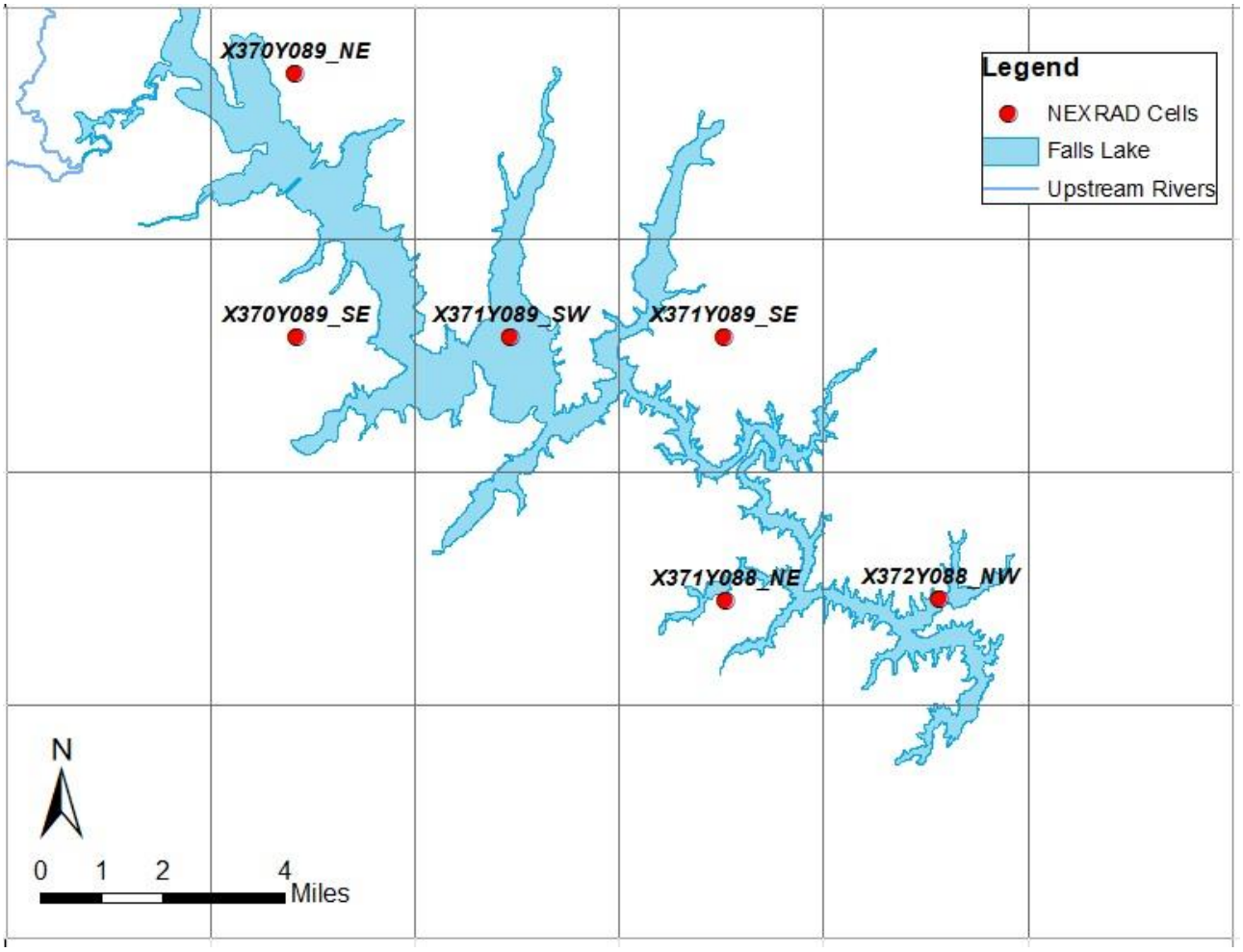

Figure 2-3 Location of the NEXRAD Stations

2.5 Boundary Conditions

Boundary conditions for EFDC must be specified for flow boundary conditions to define external inflows of water and mass loading into the EFDC model domain. Flow boundary datasets required for input to the EFDC hydrodynamic model include time series of flow and water temperature.

The Falls Lake EFDC model was developed with sixty-nine (69) tributary or overland flow inflows obtained from the WARMF watershed model, one (1) dam discharge outflow, and one (1) withdrawal outflow. Table 2-3 lists the seventy-one (71) flow boundary indexes with the number of EFDC cells assigned for the boundary and the boundary group ID corresponding to the boundary location.

External flow boundary conditions from the WARMF watershed model were assigned to EFDC grid cells based on physical location and the specific boundary condition represented in the lake model (Figure 2-4). Simulated streamflow, overland runoff, water temperature, TSS, organic carbon, nutrients, DO and algae biomass records provided by the WARMF model were used to assign flow boundaries for twenty-six (26) tributaries and forty-three (43) overland

runoff catchments for input to the lake model. WARMF model results are provided for input to the EFDC model at 6-hour time intervals (Brown & Caldwell and Systech Water Resources, 2023).

Dam discharge outflow at Falls Dam was obtained from the station USGS 0208706575 (National Water Information System, 2020). Based on the conduit info in the Falls Lake Master Plan (U.S. Army Corps of Engineers Wilmington District and the State of North Carolina, 2013), the discharge outflow was distributed over layers 4, 5, and 6 of the grid where USGS 0208706575 is located. Withdrawal outflow data were obtained from the City of Raleigh Public Utility Department (personal communication to Alix Matos, Brown & Caldwell, 4/23/2019). The withdrawal gate is near the dam. Based on the gate structure information, the withdrawal outflow was assigned to the top layer of the cell where the gate structure is located. The time series of dam discharge outflow and withdrawal outflow are shown in Figure 2-5 and Figure 2-6, respectively. The annual averages of dam discharge outflow and withdrawal outflow are shown at Figure 2-7.

Table 2-3 Falls Lake EFDC Model Flow Boundaries and Data Source

BC	Boundary Group ID	Name	Data Source	Cells
1	C0016	Lick Creek	WARMF catchment	1
2	C0030	Unknown	WARMF catchment	1
3	C0035	Sage Creek	WARMF catchment	1
4	C0037	Unknown	WARMF catchment	1
5	C0038	Unknown	WARMF catchment	1
6	C0039	Unknown	WARMF catchment	1
7	C0060	Unknown	WARMF catchment	1
8	C0084	Unknown	WARMF catchment	1
9	C0092	Beaverdam	WARMF catchment	1
10	C0094	Unknown	WARMF catchment	1
11	C0100	Unknown	WARMF catchment	1
12	C0101	Unknown	WARMF catchment	1
13	C0103	Unknown	WARMF catchment	1
14	C0108	Unknown	WARMF catchment	1
15	C0109	Jenny s Branch	WARMF catchment	1

BC	Boundary Group ID	Name	Data Source	Cells
16	C0116	Unknown	WARMF catchment	1
17	C0118	Unknown	WARMF catchment	1
18	C0119	Unknown	WARMF catchment	1
19	C0135	Unknown	WARMF catchment	1
20	C0139	Little Beaverdam Creek	WARMF catchment	1
21	C0141	Unknown	WARMF catchment	1
22	C0142	Unknown	WARMF catchment	1
23	C0143	Unknown	WARMF catchment	1
24	C0179	Pierce Creek	WARMF catchment	1
25	C0180	Unknown	WARMF catchment	1
26	C0181	Rocky Branch	WARMF catchment	1
27	C0185	Unknown	WARMF catchment	1
28	C0187	Unknown	WARMF catchment	1
29	C0190	Unknown	WARMF catchment	1
30	C0196	Unknown	WARMF catchment	1
31	C0197	Unknown	WARMF catchment	1
32	C0199	Unknown	WARMF catchment	1
33	C0213	Unknown	WARMF catchment	1
34	C0217	Unknown	WARMF catchment	1
35	C0221	Unknown	WARMF catchment	1
36	C0222	Unknown	WARMF catchment	1
37	C0229	Camp Adventure Lake	WARMF catchment	1
38	C0234	Unknown	WARMF catchment	1
39	C0235	Unknown	WARMF catchment	1
40	C0236	Unknown	WARMF catchment	1
41	C0237	Unknown	WARMF catchment	1

BC	Boundary Group ID	Name	Data Source	Cells
42	C0239	Unknown	WARMF catchment	1
43	C0257	Unknown	WARMF catchment	1
44	Dam Discharge Outflow	Falls Dam	USGS	1
45	Withdrawal Outflow	Falls Lake Raw Water Intake Structure (35.950 N, -78.582 W)	City of Raleigh Public Utility Department	1
46	R0001	Eno River	WARMF river	1
47	R0117	Flat River	WARMF river	1
48	R0139	Knap of Reeds Creek	WARMF river	1
49	R0145	Unknown	WARMF river	1
50	R0146	Unknown	WARMF river	1
51	R0147	Little Ledge Creek	WARMF river	1
52	R0148	Ledge Creek	WARMF river	1
53	R0154	Robertson Creek	WARMF river	1
54	R0157	Beaverdam Creek	WARMF river	1
55	R0159	Smith Creek	WARMF river	1
56	R0161	Buckhorn Creek	WARMF river	1
57	R0163	New Light Creek	WARMF river	1
58	R0166	Water Fork	WARMF river	1
59	R0167	Lowery Creek	WARMF river	1
60	R0168	Horse Creek	WARMF river	1
61	R0174	Unknown	WARMF river	1
62	R0175	Honeycutt Creek	WARMF river	1
63	R0180	Cedar Creek	WARMF river	1
64	R0182	Lower Barton Creek	WARMF river	1
65	R0184	Upper Barton Creek	WARMF river	1
66	R0186	Laurel Creek	WARMF river	1

BC	Boundary Group ID	Name	Data Source	Cells
67	R0187	Lick Creek	WARMF river	1
68	R0192	Chuncky Pipe Creek	WARMF river	1
69	R0200	Unknown	WARMF river	1
70	R0201	Panther Creek	WARMF river	1
71	R0203	Ellerbe Creek	WARMF river	1

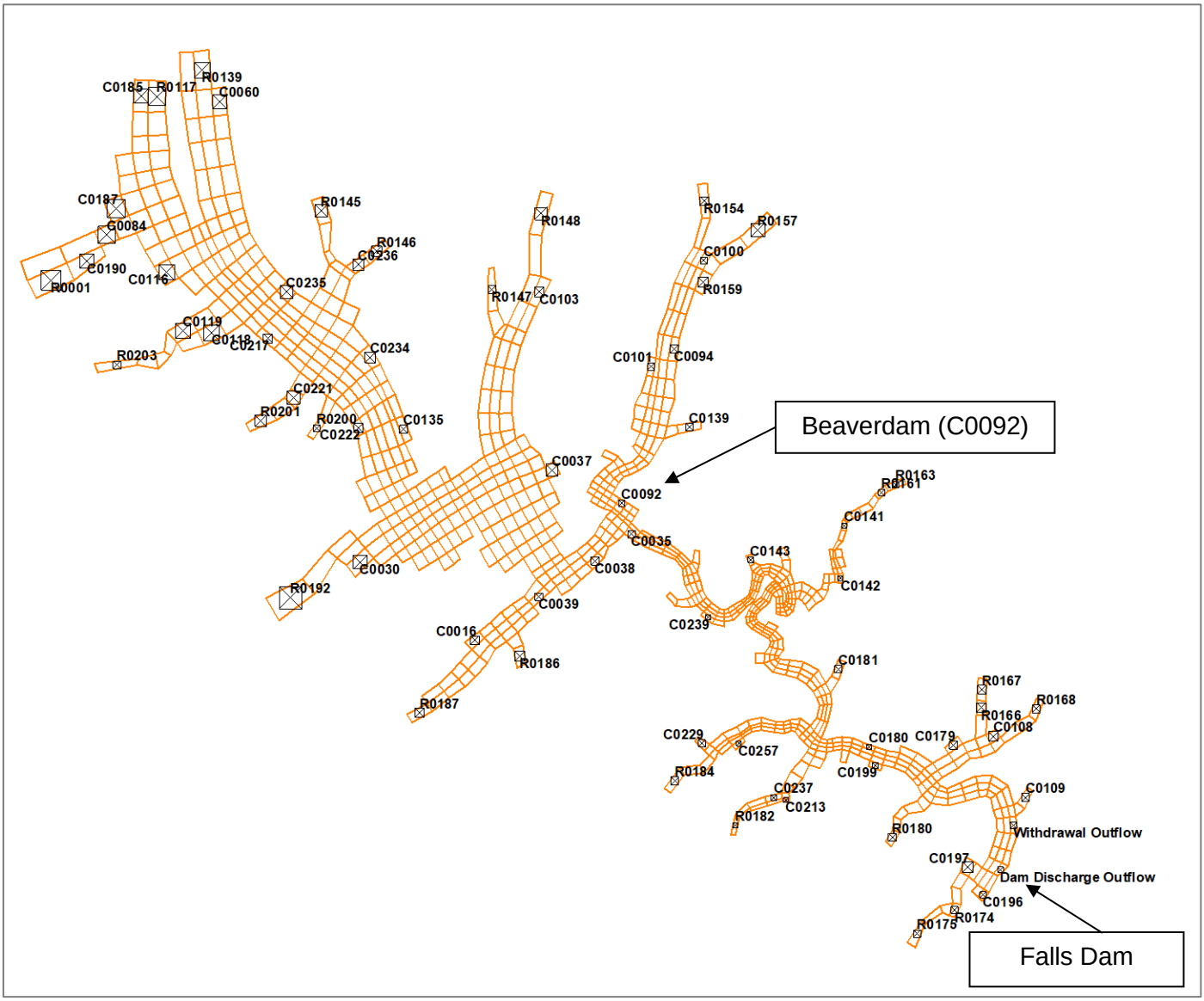

Figure 2-4 Boundary Conditions for the Falls Lake EFDC Model

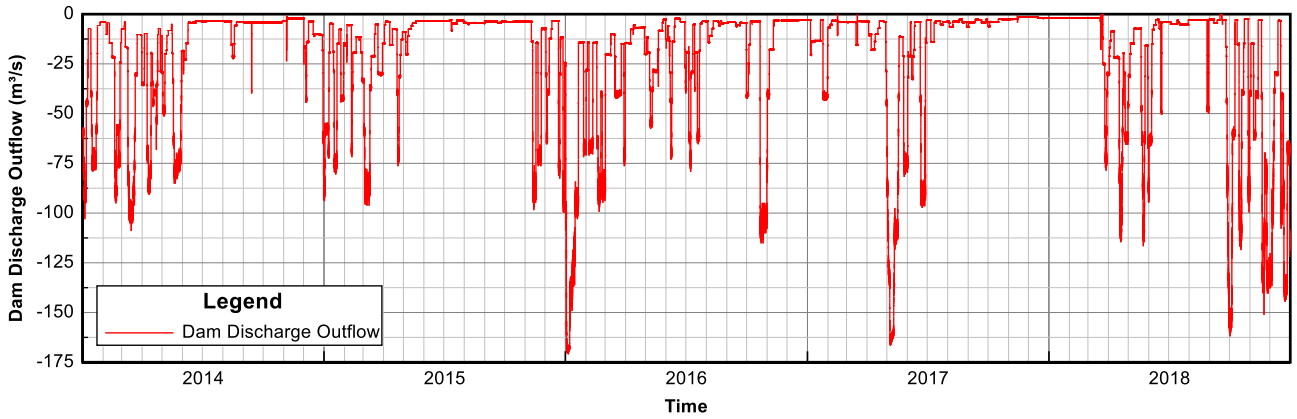

Figure 2-5 Dam Discharge Outflow at Falls Dam from USGS 0208706575

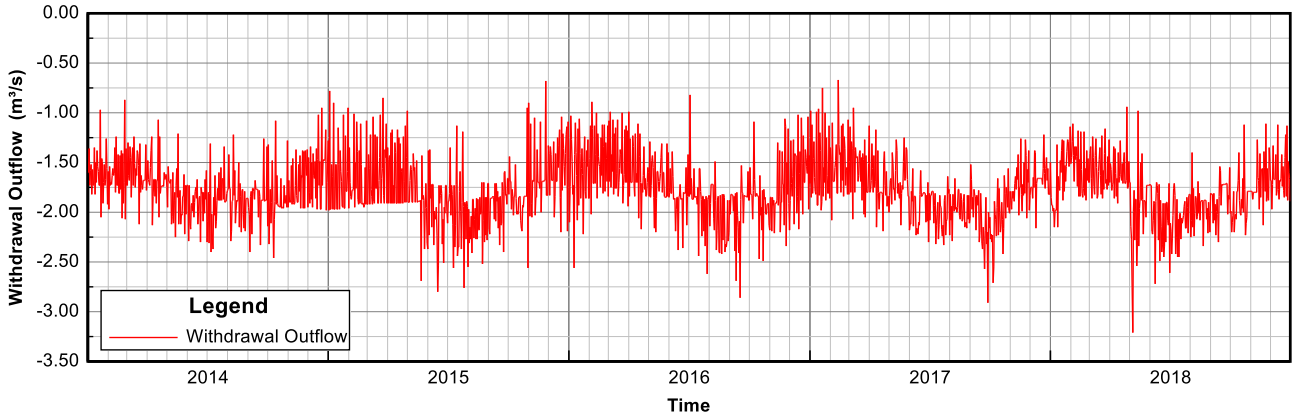

Figure 2-6 Withdrawal Outflow from City of Raleigh Public Utility Department

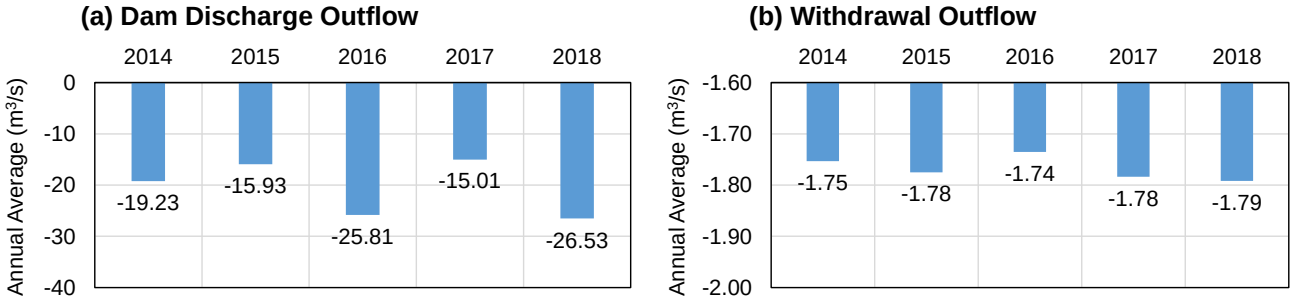

Figure 2-7 Annual Average Outflow; (a) Dam Discharge and (b) Water Intake Withdrawal

2.6 WARMF-EFDC Linkage

For the Falls Lake EFDC model, streamflow and pollutant loading from the watershed were obtained from the WARMF model. This linkage is critical both to model development and use of the developed model in the evaluation of management alternatives. Watershed changes impacting nutrient loading and the effect they have on lake water quality is the primary focus of the overall modeling effort. This linkage was not available for the DWR modeling used to

develop the current strategy. The watershed model was developed by Systech Water Resources to represent tributary flow, overland runoff, and subsurface processes within the drainage area to Falls Lake. WARMF divides a river basin into three (3) modeling units: land catchments, river/tributary segments, and stacked reservoir layers. These modeling units are linked by delineation to route runoff and pollutants from the land surface into a receiving waterbody (WARMF, 2001). The WARMF catchments and river/tributary segments used as flow boundary conditions for the EFDC model are listed in Table 2-3. Hydrologic, sediment and water quality variables of the WARMF model developed for the Falls Lake project are listed in Table 2-4.

Table 2-4 WARMF Variables and Units for the Falls Lake Project

WARMF Variable	Abbreviation	Fortran Code	Units
Flow	Flow	MFLO	m^3/s
Temperature	$\mathrm{Temp.}$	MTEMP	°C
SEDIMENT TRANSPORT			
Clay	Clay	MSED1	mg/L
Silt	Silt	MSED2	mg/L
WATER QUALITY			
Blue-green Algae	$\mathrm{Alg.\,1}\vert_{\mathrm{WARMF}}$	MALG1	µg Chl-a/L
Diatoms	$\mathrm{Alg.\,2}\vert_{\mathrm{WARMF}}$	MALG2	µg Chl-a/L
Green/Other Algae	$\mathrm{Alg.\,3}\vert_{\mathrm{WARMF}}$	MALG3	µg Chl-a/L
Detritus	$\mathrm{Det.}\vert_{\mathrm{WARMF}}$	MDET	mg C/L
Dissolved Organic Carbon	$\mathrm{DOC}\vert_{\mathrm{WARMF}}$	MOACD	mg C/L
Total Organic Carbon	$\mathrm{TOC}\vert_{\mathrm{WARMF}}$	MTOC	mg C/L
Phosphate	PO_4	MPO4	mg P/L
Total Phosphorus	$\mathrm{TP}\vert_{\mathrm{WARMF}}$	MTPO4	mg P/L
Total Kjeldahl Nitrogen	TKN	MTKN	mg N/L
Ammonia	NH_4	MNH4	mg N/L
Nitrite + Nitrate	NO_3	MNO3	mg N/L
Total Nitrogen	$\mathrm{TN}\vert_{\mathrm{WARMF}}$	MTNH4	mg NL
Dissolved Oxygen	DO	MDO	mg O2/L

The WARMF-EFDC linkage of flow, water temperature, DOC, TOC for catchments, phosphate, ammonia, nitrite + nitrate and DO is straightforward. WARMF-EFDC linkage of algae and some organic matter variables, however, requires stoichiometric transformations.. For example, EFDC needs particulate organic phosphorus, nitrogen, and carbon amounts that separate the content contained in tributary algae and algae detritus (dead algae). The algae and algal detritus are part of the particulate organic matter input to the EFDC model that is processed differently than the dissolved constituents. The WARMF model output includes three groups of living algae (diatoms, blue greens, and other) as well as algal detritus. Total loads from the watershed model can be subcategorized depending on the constituent (all as mass per volume):

- Total phosphorus output can be broken down into dissolved inorganic, dissolved organic, suspended sediment adsorbed inorganic, algae (three groups), and algal detritus.
- Total nitrogen output can be broken down into ammonia, nitrite plus nitrate, dissolved organic, sediment adsorbed inorganic, algae (three groups), and algal detritus.
- Total organic carbon output can be broken down into as dissolved, suspended sediment adsorbed, algae (three groups), and algal detritus.

The first step is to convert the WARMF output for each algal group (reported as chlorophyll-a concentrations) into estimates of particulate organic nitrogen, phosphorus, and carbon. The estimates of particulate organic nitrogen, phosphorus, and carbon are based on the WARMF model stoichiometry for milliequivalents (meq) of carbon, ammonia (NH_4), and phosphate (PO_4) in the three groups of algae.

Blue green (WARMF Algae Type 1):

$$Particulate\ Organic\ Carbon\left(\frac{mg\ C}{L}\right) = Chl_a\left(\frac{\mu g}{L}\right) * \frac{1\ meq\ C}{(20\ \mu g\ Chl_a)} * \frac{1\ mg\ C}{1\ meq\ C}$$

$$Particulate\ Organic\ Nitrogen\left(\frac{mg\ N}{L}\right) = Chl_a\left(\frac{\mu g}{L}\right) * \frac{1\ meq\ C}{(20\ \mu g\ Chl_a)} * \frac{0.0121\ meq\ NH_4 - N}{1\ meq\ C} * \frac{14.01\ mg\ NH_4 - N}{1\ meq\ NH_4 - N}$$

$$Particulate\ Organic\ Phosphorus\left(\frac{mg\ P}{L}\right) = Chl_a\left(\frac{\mu g}{L}\right) * \frac{1\ meq\ C}{(20\ \mu g\ Chl_a)} * \frac{0.00051\ meq\ PO_4 - P}{1\ meq\ C} * \frac{30.97\ mg\ PO_4 - P}{1\ meq\ PO_4 - P}$$

Diatoms (WARMF Algae Type 2):

$$Particulate\ Organic\ Carbon\left(\frac{mg\ C}{L}\right) = Chl_a\left(\frac{\mu g}{L}\right) * \frac{1\ meq\ C}{(18\ \mu g\ Chl_a)} * \frac{1\ mg\ C}{1\ meq\ C}$$

$$Particulate\ Organic\ Nitrogen\left(\frac{mg\ N}{L}\right) = Chl_a\left(\frac{\mu g}{L}\right) * \frac{1\ meq\ C}{(18\ \mu g\ Chl_a)} * \frac{0.0106\ meq\ NH_4 - N}{1\ meq\ C} * \frac{14.01\ mg\ NH_4 - N}{1\ meq\ NH_4 - N}$$

$$Particulate\ Organic\ Phosphorus\left(\frac{mg\ P}{L}\right) = Chl_a\left(\frac{\mu g}{L}\right) * \frac{1\ meq\ C}{(18\ \mu g\ Chl_a)} * \frac{0.00108\ meq\ PO_4 - P}{1\ meq\ C} * \frac{30.97\ mg\ PO_4 - P}{1\ meq\ PO_4 - P}$$

Green/Other Algae (WARMF Algae Type 3):

$$Particulate\ Organic\ Carbon\ \left(\frac{mg\ C}{L}\right) = Chl_a\left(\frac{\mu g}{L}\right) * \frac{1\ meq\ C}{(18\ \mu g\ Chl_a)} * \frac{1\ mg\ C}{1\ meq\ C}$$

$$Particulate\ Organic\ Nitrogen\ \left(\frac{mg\ N}{L}\right) = Chl_a\left(\frac{\mu g}{L}\right) * \frac{1\ meq\ C}{(18\ \mu g\ Chl_a)} * \frac{0.00518\ meq\ NH_4 - N}{1\ meq\ C} * \frac{14.01\ mg\ NH_4 - N}{1\ meq\ NH_4 - N}$$

$$Particulate\ Organic\ Phosphorus\left(\frac{mg\ P}{L}\right) = Chl_a\left(\frac{\mu g}{L}\right) * \frac{1\ meq\ C}{(18\ \mu g\ Chl_a)} * \frac{0.00024\ meq\ PO_4 - P}{1\ meq\ C} * \frac{30.97\ mg\ PO_4 - P}{1\ meq\ PO_4 - P}$$

The second step is to calculate the components contained in algal detritus:

Algal Detritus (WARMF Detritus):

$$Particulate\ Organic\ Carbon\ \left(\frac{mg\ C}{L}\right) = det\left(\frac{mg}{L}\right) * \frac{1\ meq\ C}{(1\ mg\ det)} * \frac{1\ mg\ C}{1\ meq\ C}$$

$$Particulate\ Organic\ Nitrogen\left(\frac{mg\ N}{L}\right) = det\left(\frac{mg}{L}\right) * \frac{1\ meq\ C}{(1\ mg\ det)} * \frac{0.006025\ meq\ NH_4 - N}{1\ meq\ C} * \frac{14.01\ mg\ NH_4 - N}{1\ meq\ NH_4 - N}$$

$$Particulate\ Organic\ Phosphorus\left(\frac{mg\ P}{L}\right) = det\left(\frac{mg}{L}\right) * \frac{1\ meq\ C}{(1\ mg\ det)} * \frac{0.0003\ meq\ PO_4 - P}{1\ meq\ C} * \frac{30.97\ mg\ PO_4 - P}{1\ meq\ PO_4 - P}$$

Algae and detritus were converted to nutrient and organic carbon fractions using the WARMF stoichiometry shown in Table 2-5. The functional relationships used to link the WARMF results for input to the EFDC model are documented in Table 2-6.

Table 2-5 WARMF Stoichiometry Used to Convert the Algae and Detritus Results into Nutrient and Organic Carbon Fractions (Applied to Rivers/Tributaries Only)

Particulate Matters for Rivers	Unit	Abbreviation	Conversion
Particulate Org Carbon per Blue-green Algae	mg C/L	$\mathrm{POC}\vert_{\mathrm{Alg.1}}$	$\frac{\mathrm{Alg.\ 1}\vert_{\mathrm{WARMF}}}{20}$
Particulate Org Carbon per Diatoms	mg C/L	$\mathrm{POC}\vert_{\mathrm{Alg.2}}$	$\frac{\mathrm{Alg.\ 2}\vert_{\mathrm{WARMF}}}{18}$
Particulate Org Carbon per Green/Other	mg C/L	$\mathrm{POC}\vert_{\mathrm{Alg.3}}$	$\frac{\mathrm{Alg.\ 3}\vert_{\mathrm{WARMF}}}{18}$
Particulate Org Carbon per Detritus	mg C/L	$\mathrm{POC}\vert_{\mathrm{Det.}}$	$\mathrm{Det.}\vert_{\mathrm{WARMF}}$
Particulate Org Phosphorus per Blue-green Algae	mg P/L	$\mathrm{POP}\vert_{\mathrm{Alg.1}}$	$\frac{\mathrm{Alg.\ 1}\vert_{\mathrm{WARMF}}}{20} \times 0.00051 \times 30.97$
Particulate Org Phosphorus per Diatoms	mg P/L	$\mathrm{POP}\vert_{\mathrm{Alg.2}}$	$\frac{\mathrm{Alg.\ 2}\vert_{\mathrm{WARMF}}}{18} \times 0.00108 \times 30.97$
Particulate Org Phosphorus per Green/Other	mg P/L	$\mathrm{POP}\vert_{\mathrm{Alg.3}}$	$\frac{\mathrm{Alg.\ 3}\vert_{\mathrm{WARMF}}}{18} \times 0.00024 \times 30.97$
Particulate Org Phosphorus per Detritus	mg P/L	$\mathrm{POP}\vert_{\mathrm{Det.}}$	$\mathrm{Det.}\vert_{\mathrm{WARMF}} \times 0.0003 \times 30.97$
Particulate Org Nitrogen per Blue-green Algae	mg N/L	$\mathrm{PON}\vert_{\mathrm{Alg.1}}$	$\frac{\mathrm{Alg.\ 1}\vert_{\mathrm{WARMF}}}{20} \times 0.0121 \times 14$
Particulate Org Nitrogen per Diatoms	mg N/L	$\mathrm{PON}\vert_{\mathrm{Alg.2}}$	$\frac{\mathrm{Alg.\ 2}\vert_{\mathrm{WARMF}}}{18} \times 0.0106 \times 14$
Particulate Org Nitrogen per Green/Other	mg N/L	$\mathrm{PON}\vert_{\mathrm{Alg.3}}$	$\frac{\mathrm{Alg.\ 3}\vert_{\mathrm{WARMF}}}{18} \times 0.00518 \times 14$
Particulate Org Nitrogen per Detritus	mg N/L	$\mathrm{PON}\vert_{\mathrm{Det.}}$	$\mathrm{Det.}\vert_{\mathrm{WARMF}} \times 0.006025 \times 14$
Total Org Carbon	mg C/L	TOC	$\mathrm{DOC}\vert_{\mathrm{WARMF}} + (\mathrm{POC}\vert_{\mathrm{Alg.1}} + \mathrm{POC}\vert_{\mathrm{Alg.2}} + \mathrm{POC}\vert_{\mathrm{Alg.3}} + \mathrm{POC}\vert_{\mathrm{Det.}})$
Total Phosphorus Excluding Living Part and Detritus	mg P/L	TP	$\mathrm{TP}\vert_{\mathrm{WARMF}} - (\mathrm{POP}\vert_{\mathrm{Alg.1}} + \mathrm{POP}\vert_{\mathrm{Alg.2}} + \mathrm{POP}\vert_{\mathrm{Alg.3}} + \mathrm{POP}\vert_{\mathrm{Det.}})$
Total Nitrogen Excluding Living Part and Detritus	mg N/L	TN	$\mathrm{TN}\vert_{\mathrm{WARMF}} - (\mathrm{PON}\vert_{\mathrm{Alg.1}} + \mathrm{PON}\vert_{\mathrm{Alg.2}} + \mathrm{PON}\vert_{\mathrm{Alg.3}} + \mathrm{PON}\vert_{\mathrm{Det.}})$

Table 2-6 WARMF-EFDC Linkage

EFDC HYDRODYNAMICS & SEDIMENT TRANSPORT	Units	WARMF-EFDC Linkage
Flow	m³/s	Flow
Water Temperature	°C	$\mathrm{Temp.}$
Inorganic Cohesive Solids	mg/L	$\mathrm{Clay + Silt}$
EFDC WATER QUALITY		
Cyanobacteria (Blue-green Algae)	mg C/L	$\mathrm{Alg.\,1}\vert_{\mathrm{WARMF}} \times \mathrm{C/Chl-a}\vert_{\mathrm{Alg.1}}$
Diatoms Algae	mg C/L	$\mathrm{Alg.\,2}\vert_{\mathrm{WARMF}} \times \mathrm{C/Chl-a}\vert_{\mathrm{Alg.2}}$
Green/Other Algae	mg C/L	$\mathrm{Alg.\,3}\vert_{\mathrm{WARMF}} \times \mathrm{C/Chl-a}\vert_{\mathrm{Alg.3}}$
Total Org Carbon (TOC); Catchments	mg C/L	TOC
Total Org Carbon (TOC); Rivers	mg C/L	$\mathrm{DOC}\vert_{\mathrm{WARMF}} + (\mathrm{POC}\vert_{\mathrm{Alg.1}} + \mathrm{POC}\vert_{\mathrm{Alg.2}} + \mathrm{POC}\vert_{\mathrm{Alg.3}} + \mathrm{POC}\vert_{\mathrm{Det.}})$
Total Org Phosphorus (TOP)	mg P/L	$\mathrm{TP}\vert_{\mathrm{WARMF}} - \mathrm{PO_4}$
Total Org Nitrogen (TON)	mg N/L	$\mathrm{TN}\vert_{\mathrm{WARMF}} - (\mathrm{NH_4} + \mathrm{NO_3})$
Dissolved Org Carbon	mg C/L	$\mathrm{DOC}\vert_{\mathrm{WARMF}}$
Refractory Particulate Org Carbon	mg C/L	$(\mathrm{TOC} - \mathrm{DOC}\vert_{\mathrm{WARMF}}) \times 0.25$
Labile Particulate Org Carbon	mg C/L	$(\mathrm{TOC} - \mathrm{DOC}\vert_{\mathrm{WARMF}}) \times 0.75$
Dissolved Org Phosphorus (DOP)	mg P/L	$\mathrm{TOP} \times (1 - \mathrm{POP/TOP})$
Refractory Particulate Org Phosphorus	mg P/L	$(\mathrm{TOP} - \mathrm{DOP}) \times 0.25$
Labile Particulate Org Phosphorus	mg P/L	$(\mathrm{TOP} - \mathrm{DOP}) \times 0.75$
Total Phosphate	mg P/L	$\mathrm{PO_4}$
Dissolved Org Nitrogen (DON)	mg N/L	$\mathrm{TON} \times (1 - \mathrm{PON/TON})$
Refractory Particulate Org Nitrogen	mg N/L	$(\mathrm{TON} - \mathrm{DON}) \times 0.25$
Labile Particulate Org Nitrogen	mg N/L	$(\mathrm{TON} - \mathrm{DON}) \times 0.75$
Ammonium Nitrogen	mg N/L	$\mathrm{NH_4}$
Nitrate+Nitrite Nitrogen	mg N/L	$\mathrm{NO_3}$
Dissolved Oxygen	mg O2/L	DO

Like many mechanistic lake water quality models, the EFDC model framework was developed to simulate three algae groups: cyanobacteria, diatoms, and green/other algae. WARMF also simulates algae as the same three (3) equivalent groups. The algae simulation output units for the Falls Lake project are represented as µg/L Chl-a. As EFDC units for algae are carbon (C)-based, a C/Chl-a ratio for each algal functional group is required to convert WARMF results as Chl-a biomass to organic carbon for input to EFDC. While the ratios can be set differently for each simulated algal group, they cannot be adjusted within the algal group to reflect varying environmental conditions or dominance of different algal species within the group through time. While this is a limitation, it is standard practice for these types of models. Appendix D to the main report documents the discussions and analyses regarding the dominant groups of algae in Falls Lake and the decision to use the "green/other" group to simulate algae that are neither diatoms nor cyanobacteria.

The following approaches were considered for estimation of the C/Chl-a ratio for the simulated groups:

1- Using literature values: a wide range of C/Chl-a values can be found in the literature, each specified for certain characteristics such as latitude, depth, watershed, algal diversity etc. As those characteristics varied from lake to lake, the literature values were not used to represent Falls Lake.

2- Performing regression analysis on the phytoplankton algal assemblage data: this approach is not accurate to derive the C/Chl-a ratio since it is based on the assumption that total POC only consists of algae. POC measurements consists of both algae and non-living detritus. Regression analysis, therefore, was not used.

3- Adjusting the estimated C/Chl-a ratio: The initial estimates for the C/Chl-a ratio for each algal group were based on the phytoplankton algal species assemblage data provided by DWR summarized in the UNRBA 2019 Monitoring Report (Brown and Caldwell, 2019). Initial estimates were derived using paired Chl-a and POC data for the days when certain algal groups were dominant based on biovolume data. Paired data for the selected algal group were used to estimate the C/Chl-a ratio for those days. The average of the set of C/Chl-a ratios derived for each algal group were calculated as shown in the second column of Table 2-7. As POC measurements include both algal biomass and detritus, the initial estimates of the calculated C/Chl-a ratios were generally overestimated and needed to be adjusted as described below.

   As the C/Chl-a ratio can significantly impact simulations of algal biomass as Chl-a and other water quality parameters, the C/Chl-a ratios were adjusted to reflect the actual observed field conditions as closely as possible with the following model test runs:

   - In each model test run, only diatoms were simulated with the typical growth rate of 1.0 per day. The other two algae groups were not simulated by setting the growth rates to zero.

   - The initial estimate of the C/Chl-a ratio for diatoms was adjusted with a multiplier factor less than one in each model test run;

- For all the model test runs, the average of the difference between simulated and observed Chl-a were compared for the winter and early spring periods only as diatoms are known to be the dominant algal group during this period;
- The best agreement between observed and simulated Chl-a data was obtained when the C/Chl-a ratio for diatoms was assigned an adjusted value of 0.005 mg C/µg Chl-a. The adjusted C/Chl-a ratio was based on a multiplier of approximately two-thirds of the initial estimate of diatom C/Chl-a shown in the second column of Table 2-7; and
- The same multiplier factor was then used to adjust the C/Chl-a ratios used in the lake model for the cyanobacteria and green algae groups. This method assumes that the approximate proportion of algal biomass and detrital matter in POC measurements is similar for the three algal groups.

The adjusted values of the C/Chl-a ratios shown in the third column of Table 2-7 were then used for model calibration and validation.

Table 2-7 Calculated and Adjusted C/Chl-a Ratios for Algal Species Groups

Algal Species Group	Average Ratio Based on Data (mg C/µg Chl-a)	Adjusted Ratio by Multiplying with 2/3 (mg C/µg Chl-a)
Cyanobacteria ($\mathrm{mg\ C/ug\ Chl-a}|_{\mathrm{Alg.1}}$)	0.007	0.005
Diatom ($\mathrm{mg\ C/\ ug\ Chl-a}|_{\mathrm{Alg.2}}$)	0.008	0.005
Green/Other algae ($\mathrm{mg\ C/ug\ Chl-a}|_{\mathrm{Alg.3}}$)	0.011	0.007

WARMF simulates algae biomass and detritus as state variables only for the tributaries and impoundments since overland runoff for a catchment does not support simulation of sestonic algal populations. Therefore, the POM at the river/tributary boundary conditions is mixed with the living algal biomass and non-living detritus. POC ($\mathrm{POC}|_{\mathrm{Alg.1}}$, $\mathrm{POC}|_{\mathrm{Alg.2}}$, $\mathrm{POC}|_{\mathrm{Alg.3}}$, $\mathrm{POC}|_{\mathrm{Det.}}$), organic phosphorus ($\mathrm{POP}|_{\mathrm{Alg.1}}$, $\mathrm{POP}|_{\mathrm{Alg.2}}$, $\mathrm{POP}|_{\mathrm{Alg.3}}$, $\mathrm{POP}|_{\mathrm{Det.}}$), and organic nitrogen ($\mathrm{PON}|_{\mathrm{Alg.1}}$, $\mathrm{PON}|_{\mathrm{Alg.2}}$, $\mathrm{PON}|_{\mathrm{Alg.3}}$, $\mathrm{PON}|_{\mathrm{Det.}}$) are calculated as shown in Table 2-5. These parameters are used to derive TOC and to separate TP and TN from the living algal biomass and non-living detritus. For catchments draining directly to Falls Lake, algal biomass is zero and WARMF simulations of TOC ($\mathrm{TOC}|_{\mathrm{WARMF}}$), TN ($\mathrm{TN}|_{\mathrm{WARMF}}$) and TP ($\mathrm{TP}|_{\mathrm{WARMF}}$) are used. TOC, TP and TN are then added as shown in the WARMF-EFDC linkage in Table 2-6 to derive non-living TOC, TOP and TON for input to the EFDC model.

POP/TOP and PON/TON ratios are required to calculate the dissolved fractions of TOP and TON as DOP and DON, respectively, for each tributary. These ratios were derived from lake loading data collected by UNRBA (Brown & Caldwell, 2019). Since no distinguishable seasonal pattern was observed between winter and the remainder of the year for all the 17 major

tributaries to Falls Lake, for computational simplicity the average of POP/TOP and PON/TON ratios for each tributary was calculated, respectively.

Table 2-8 lists the average ratios estimated for each tributary. Based on the set of 17 tributary-specific ratios, the overall averages for the POP/TOP and PON/TON ratios were calculated (last row of Table 2-8) and used to derive DOP and DON input concentrations for each tributary. The same overall average ratios of POP/TOP and PON/TON were also used to calculate direct runoff loading of DOP and DON to the lake from each land catchment using the watershed model simulated concentrations of total organic matter to derive the particulate and dissolved fractions of organic matter.

Table 2-8 Total Average of the POP/TOP and PON/TON Ratios at Each Tributary

Boundary Group ID	Tributary Name	POP/TOP	PON/TON
R0001 (ENR-8.3 & LTR-1.9)	Eno River	0.402	0.246
R0117 (FLR-5.0)	Flat River	0.390	0.280
R0203 (ELC-3.1)	Ellerbe Creek	0.222	0.200
R0139 (KRC-4.5)	Knap of Reed Creek	0.278	0.239
R0192 (LLC-1.8)	Little Lick Creek	0.344	0.307
R0148 (LGE-5.1)	Ledge Creek	0.309	0.281
R0187 (LKC-2.0)	Lick Creek	0.493	0.269
R0168 (HSE-1.7)	Horse Creek	0.442	0.277
R0154 (ROB-2.8)	Robertson Creek	0.286	0.254
R0182 (LBC-2.1)	Lower Barton Creek	0.345	0.318
R0157 (BDC-2.0)	Beaverdam Creek	0.315	0.313
R0163 (NLC-2.3)	New Light Creek	0.259	0.324
R0159 (SMC-6.2)	Smith Creek	0.447	0.329
R0184 (UBC-1.4)	Upper Barton Creek	0.386	0.342
R0175 (HCC-2.9)	Honeycutt Creek	0.376	0.200
R0201 (PAC-4.0)	Panther Creek	0.433	0.299
R0146 (UNT-0.7)	Unknown	0.361	0.304
Average of all Tributaries		0.361	0.279

3. Water Quality and Sediment Flux Model

For the Falls Lake EFDC model, the water quality model is internally coupled with the hydrodynamic model, a sediment transport model and a sediment diagenesis model. The hydrodynamic model describes circulation and physical transport processes including turbulent mixing, water column stratification during the summer months, and erosion of stratification during the winter months. The sediment transport model describes the water column distribution of inorganic cohesive particles resulting from transport, deposition, and resuspension processes. The sediment diagenesis model describes the coupling of POM deposition from the water column to the sediment bed, decomposition of organic matter in the bed, and the exchange of inorganic nutrients and DO across the sediment-water interface. This exchanged across the sediment-water interface is called “flux.” The UNRBA identified the critical importance of developing an effective sediment diagenesis component. It was clearly shown by research and data that sediment flux is an extremely important factor in evaluation of the long-term changes in the overall nutrient balance in this reservoir.

3.1 Water Quality Model

State variables of the EFDC hydrodynamic model (water temperature) and sediment transport model (TSS) are internally coupled with the EFDC water quality model. State variables of the EFDC water quality model include three functional groups of algae; organic carbon, inorganic phosphorus (orthophosphate), organic phosphorus; inorganic nitrogen (ammonium and nitrite + nitrate), organic nitrogen; COD and DO. The state variables represented in the Falls Lake EFDC hydrodynamic and water quality model are listed in Table 3-1.

The formulations of the EFDC water quality model are based on the kinetic processes developed for the Chesapeake Bay model (Cerco and Cole, 1995; Cerco et al., 2002). An overview of the source and sink terms for each state variable is presented in this section. Details of the state variable equations and kinetic terms for each state variable are presented in Park et al. (2000), Hamrick (2007) and Ji (2017). Tables listing the calibrated values of selected water quality model parameters and coefficients developed for the Falls Lake EFDC model are presented in Appendix A.1.

Table 3-1 EFDC State Variables

	EFDC State Variable		EFDC UNITS	Used in Model
	Flow	FLOW	m^3/s	Yes
	Water Temperature	TEM	°C	Yes
	Salinity	SAL	ppt	No
	Cohesive Suspended Sediment	COH	mg/L	Yes
	Non-cohesive Suspended Sediment	NONCOH	mg/L	No
1	Refractory Particulate Org C	ROC	mg C/L	Yes
2	Labile Particulate Org C	LOC	mg C/L	Yes
3	Dissolved Org C	DOC	mg C/L	Yes
4	Refractory Particulate Org P	ROP	mg P/L	Yes
5	Labile Particulate Org P	LOP	mg P/L	Yes
6	Dissolved Org P	DOP	mg P/L	Yes
7	Total Phosphate (PO_4)	P4D	mg P/L	Yes
8	Refractory Particulate Org N	RON	mg N/L	Yes
9	Labile Particulate Org N	LON	mg N/L	Yes
10	Dissolved Org N	DON	mg N/L	Yes
11	Ammonium N	NHX	mg N/L	Yes
12	Nitrate+Nitrite N	NOX	mg N/L	Yes
13	Particulate-Biogenic Silica	SUU	mg Si/L	No
14	Available Silica	SAA	mg Si/L	Yes
15	Chemical Oxygen Demand	COD	mg/L	Yes
16	Dissolved Oxygen	DOX	mg O2/L	Yes
17	Total Active Metal	TAM	mg/L	No
18	Fecal Coliform Bacteria	FCB	MPN/100 mL	No
19	Carbon Dioxide	CO2	mg/L	No
20	Blue Green Algae	ALG1	mg C/L	Yes
21	Diatoms Algae	ALG2	mg C/L	Yes
22	Green/Other Algae	ALG3	mg C/L	Yes

TSS

TSS in the EFDC model can be differentiated by size classes of cohesive and non-cohesive solids. For the Falls Lake model, TSS is represented as a single size class of cohesive particles. Cohesive suspended sediment is included in the model to account for the inorganic solids' component of light attenuation in the water column. Since cohesive particles derived from silts and clays are characterized by a small particle diameter (< 62 microns) and a low settling velocity, cohesive particles can remain suspended in the water column for long periods of time and contribute to light attenuation that can influence algae production. Non-cohesive particles, consisting of fine to coarse size sands, by contrast, are characterized by much larger particles (> 62 microns) with rapid settling velocities that quickly remove any resuspended non-cohesive particles from the water column.

The key processes that control the distribution of cohesive particles are transport in the water column, flocculation and settling, deposition to the sediment bed, consolidation within the bed, and resuspension or erosion of the sediment bed. In the EFDC model for Falls Lake, cohesive settling is defined by a constant settling velocity that is determined by model calibration. Deposition and erosion are controlled by the assignment of critical stresses for deposition and erosion and the bottom layer velocity and shear stress computed by the hydrodynamic model. The critical stress for erosion is typically defined with a factor of 1.2 times the critical deposition stress (Ji, 2008). Initial critical stresses for deposition and erosion of cohesive particles are taken from parameter values defined by Ji (2017) for a sediment transport model of Lake Okeechobee and then adjusted during model calibration. To account for the influence of the wind waves on the resuspension occurring in shallow water, the wind wave module was activated at the upper part of the lake (above I-85). Parameter values for deposition and erosion assigned for the calibration of cohesive solids are summarized in Table 3-2.

Table 3-2 EFDC Model Parameter Values for Cohesive Sediment

Parameter	Unit	Definition	Value
$1/\rho$	m^3/g	Sediment Specific Volume	3.77E-07
SG	---	Sediment Specific Gravity	2.65
V_S	m/s	Constant Sediment Settling Velocity	6.00E-06
τ_{cd}	m^2/s^2	Critical Stress for Deposition	1.00E-05
τ_{ce}	m^2/s^2	Critical Stress for Erosion	5.00E-05
J_r	$g/m^2/s$	Reference Surface Erosion Rate	0.0001

The units of $(m/s)^2$ shown in Table 3-2 for critical shear stress for deposition and erosion are not typical units found in the sediment transport literature. The units assigned for the EFDC model are derived by normalizing the units typically measured for shear stress (e.g., $dynes/cm^2$) by a water density of 1000 kg/m^3. A critical shear stress for erosion of 0.10 $dynes/cm^2$ is thus assigned for input to EFDC with a value of 1.0E-05 $(m/s)^2$ by multiplying the shear stress of 0.10 $dynes/cm^2$ by a factor of 1.0E-04 since 1 dyne is defined as 1 $g\text{-}cm/sec^2$.

Algae

Phytoplankton in the EFDC model can be represented by three or more different functional groups of algae. Typically, cyanobacteria, diatoms and green algal groups have been simulated in numerous water quality studies around the world in the last several decades as the key parameter values of the three groups are relatively well documented. For the Falls Lake EFDC water quality model, cyanobacteria, diatom, and green/other algae were linked directly from WARMF simulations of the three (3) equivalent groups of algae. As described in Appendix D to the main report, all other algal species recorded in Falls Lake (e.g., *Prymnesiophyceae*), other than cyanobacteria and diatoms, were grouped and simulated as green/other algae in this study.

Kinetic processes represented for the algal groups include photosynthetic production, basal metabolism (respiration and excretion), settling and predation. Photosynthetic production is described by a growth rate that is functionally dependent on a maximum growth rate, water temperature, the availability of sunlight at the surface, light extinction in the water column, the optimum light level for growth, and half-saturation dependent nutrient limitation by either nitrogen or phosphorus for all three groups and silica only for diatoms. Growth and basal metabolism are temperature dependent processes while settling and predation losses are assigned as constant parameter values.

For the Falls Lake water quality model, four (4) zones of the model domain as shown in Figure 3-1 were used to represent spatial variation in water column and algae kinetics. Zone 1 includes the portion of the lake above I-85, Zone 2 includes the portion of the lake between I-85 and Hwy 50, Zone 3 includes the portion of the lake below Hwy 50, and Zone 4 includes the embayment arms of the lake. Kinetic coefficients determined for calibration of the algae model are presented in Appendix A.1.

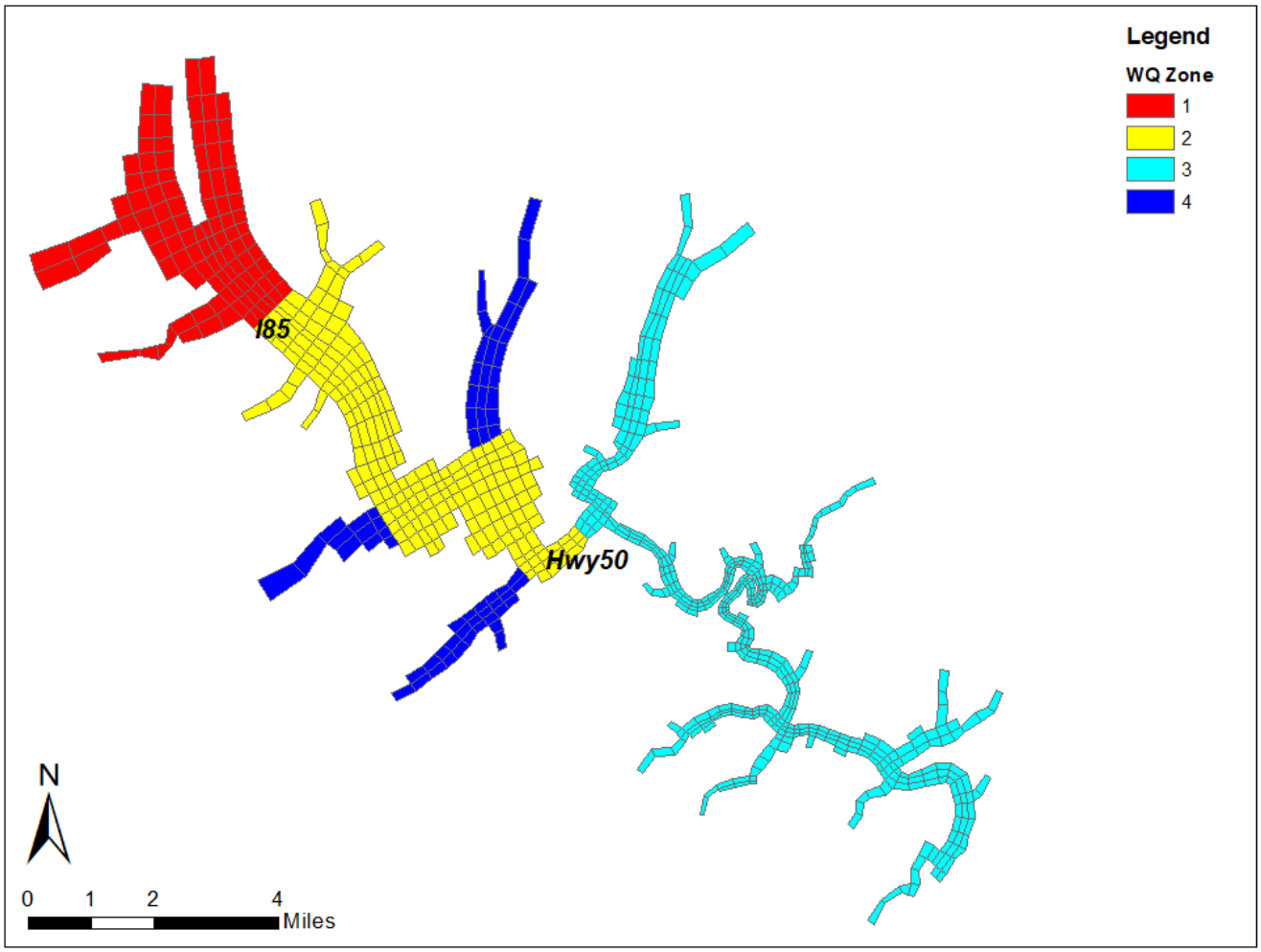

Figure 3-1 Spatial Water Column and Algae Kinetic Zones Defined for Falls Lake; Zone 1: above I-85, Zone 2: between I-85 and Hwy 50, Zone 3: below Hwy 50, Zone 4: embayment arms of the lake

Organic Carbon

TOC is represented in the model with three state variables as DOC, RPOC and LPOC. The time scale for decomposition of POM is used to differentiate refractory and labile POM with labile matter decomposing rapidly (weeks to months) while decay of refractory POM takes much longer (years). Although DOC is not termed “labile”, DOC is considered to react with a rapid time scale for decomposition (weeks to months).

Kinetic processes represented in the model for POC include algal predation, dissolution of RPOC and LPOC to DOC, and settling. Kinetic processes for DOC include sources from algal excretion and predation and dissolution of POC and losses from decomposition and denitrification. With the exception of settling of POC, the kinetic reaction processes are all temperature dependent. Minimum hydrolysis rates of DOC, RPOC and LPOC are presented in Appendix A.1.

Phosphorus

Total organic phosphorus is represented in the model with three state variables as DOP, RPOP and LPOP. As with organic carbon, the time scale for decomposition of POM is used to differentiate refractory and labile POP. Kinetic processes represented in the model for POP include algal metabolism, predation, dissolution of RPOP and LPOP to DOP, and settling. Kinetic processes for DOP include sources from algal metabolism and predation and dissolution of POP to DOP with losses of DOP from mineralization to phosphate. With the exception of settling of POP, the kinetic reaction processes are all temperature dependent.

Inorganic phosphorus is represented as single state variable for total phosphate which accounts for both the dissolved and sorbed forms of phosphate. Adsorption and desorption of phosphate is defined on the basis of equilibrium partitioning using an assigned phosphate partition coefficient for TSS. Kinetic terms for total phosphate include sources from algal metabolism and predation and mineralization from DOP. Losses for phosphate include settling of the sorbed fraction of total phosphate and uptake by phytoplankton growth. Depending on the concentration gradient between the bottom layer of the water column and sediment bed porewater phosphate, the sediment-water interface can serve as either a source or a loss term for phosphate in the water column. With the exception of the partition coefficient and the settling of sorbed phosphate, the kinetic reaction processes for phosphate are all temperature dependent.

Nitrogen

TON is represented in the model with three state variables as DON, RPON and LPON. As with organic carbon, the time scale for decomposition of POM is used to differentiate refractory and labile PON. Kinetic processes represented in the model for PON include algal metabolism, predation, dissolution of RPON and LPON to DON, and settling. Kinetic processes for DON include sources from algal metabolism and predation, dissolution of PON to DON and losses of DON from mineralization of PON to ammonium. With the exception of settling of PON, the kinetic reaction processes are all temperature dependent.

Inorganic nitrogen (ammonia, nitrite and nitrate) is represented by two state variables as (1) ammonia and (2) nitrite+nitrate. Kinetic terms for ammonia include sources from algal metabolism and predation and mineralization from DON. Losses for ammonia include bacterially mediated transformation to nitrite and nitrate by nitrification and uptake by phytoplankton growth. Depending on the concentration gradient between the bottom layer of the water column and sediment bed porewater ammonia, the sediment-water interface can serve as either a source or a loss term for ammonia in the water column. The kinetic reaction processes for ammonia are all temperature dependent. Since the time scale for conversion of nitrite to nitrate is very rapid, nitrite and nitrate are combined as a single state variable representing the sum of these two forms of nitrogen (nitrite+nitrate). Kinetic terms for nitrite/nitrate include sources from nitrification from ammonia to nitrite and nitrate. Losses include uptake by phytoplankton growth and denitrification to nitrogen gas. Depending on the concentration gradient between the bottom layer of the water column and sediment bed porewater nitrite/nitrate, the sediment-water interface can serve as either a source or a loss term for nitrite/nitrate in the water column. The kinetic reaction processes for nitrite/nitrate are all temperature dependent.

COD

In the EFDC water quality model, COD represents the concentration of reduced substances that can be oxidized through inorganic processes. The principal source of COD in freshwater is methane released from oxidation of organic carbon in the sediment bed across the sediment-water interface. Since sediment bed decomposition is accounted for in the coupled sediment diagenesis model, the only source of COD to the water column is the flux of methane across the sediment-water interface. Sources from the open water boundaries and upstream flow boundaries are set to zero for COD. The loss term in the water column is defined by a temperature dependent first order oxidation rate.

DO

DO is a key state variable in the water quality model since several kinetic processes interact with, and can be controlled by, DO. Kinetic processes represented in the oxygen model include sources from atmospheric reaeration in the surface layer and algal photosynthetic production. Kinetic loss terms include algal respiration, nitrification, decomposition of DOC, oxidation of COD, and in the bottom layer of the water column, consumption of DO from SOD. SOD is internally simulated with the sediment flux model by coupling POC deposition from the water column and decomposition of organic matter in the sediment bed. The kinetic reaction processes for DO are all temperature dependent.

Kinetic Coefficients

Most of the water quality parameters and coefficients needed by the EFDC water quality model were initialized with default values as indicated in the user's manual (Park, et.al., 1995; Hamrick, 2007). These default values are, in general, the same as the parameter values determined for the Chesapeake Bay model (Cerco and Cole, 1995). Models developed for Lake Washington (Arhonditsis and Brett, 2005) and Chesapeake Bay tributaries (Cerco et al., 2002) also provided kinetic coefficients needed for the EFDC water quality model. Kinetic coefficients and model parameters were adjusted, as needed, within ranges reported in the literature, during model calibration to obtain the most reasonable agreement between observed and simulated water quality concentrations such as TSS, algal biomass, organic carbon, DO and nutrients. A large body of literature is available from numerous advanced modeling studies developed over the past decade to provide information on reported ranges of parameter values that can be assigned for site-specific modeling projects (see Ji, 2008; Park et al, 1995; Hamrick, 2007; Dynamic Solutions, 2012).

Sensitivity analyses were conducted during model development under consultation with third-party model reviewers funded by the NC Collaboratory and DWR modelers to inform model calibration with respect to model coefficients and parameters. Kinetic coefficients and model parameters assigned for the water quality model as either global or spatially dependent zone parameters for the Falls Lake EFDC model are listed in Appendix A.1.

Atmospheric Deposition

Atmospheric deposition is represented in the EFDC model with separate source terms for dry deposition and wet deposition. Dry deposition is defined by a constant mass flux rate (as g/m^2-day) for a constituent that settles as dust or is deposited on a dry surface during a period of no precipitation. Wet deposition is defined by a constant concentration (as mg/L) of a constituent in rainfall and the time series of precipitation assigned for input to the hydrodynamic model. For the Falls Lake model, wet and dry deposition data for TN, ammonia and nitrate (Table 3-3) were obtained from the EPA CASTNET station RTP101 (Research Triangle Park, Lat.: 35.91; Long.: -78.879997) and station DUK008 (Duke Forest, Lat.: 35.974499; Long.: -79.098999) shown in Figure 3-2. The average of annual data from 2014-2018 was calculated for both stations, and then the total average value of the two was assigned to the model. Wet and dry TON were calculated by subtracting ammonia and nitrate from TN. Average concentration of DON was assumed to be 0.16 μg/m^3, based on the observations for the Duke Forest Research Facility near Chapel Hill, NC (Lin et al, 2010). The fraction of DON/TON was assumed to be the same for both wet and dry, and PON was calculated by subtracting DON from TON. A 50%-50% labile-refractory split was assumed for the wet and dry atmospheric deposition of POM.

Phosphorus is not typically measured in wet or dry deposition chemistry data. The City of Durham monitoring study analyzed but did not detect phosphorus in wet deposition; analysis of dry deposition was beyond the scope of the study (AMEC 2012). As data were not available from the CASTNET and NADP sites for phosphate, dry deposition for phosphate was estimated using annual average N/P ratios for atmospheric deposition of N and P reported for 6 monitoring sites in Iowa (Anderson and Downing, 2006). Wet organic carbon was adopted from Lin et al (2010). It was assumed that organic carbon measured from aerosol is all in the dissolved form.

Table 3-3 Dry and Wet Atmospheric Deposition for Nutrients

Parameter	Dry (g/m^2-day)	Wet (mg/L)	Data Source
DOC	Not Available	2.94E-06	Lin et al (2010), Table 1
TPO4	4.61E-06	0.0007828	Anderson & Downing (2006), Table VII
RPON	4.869E-05	4.22E-06	CASTNET & Lin et al (2010)
LPON	4.869E-05	4.22E-06	CASTNET & Lin et al (2010)
DON	1.85E-06	1.6E-07	Lin et al (2010), Table 1
NH4	3.83E-05	0.26	CASTNET (RTP101, DUK008; 2014-2018)
NO3	4.86E-05	0.101	CASTNET (RTP, DUK; 2014-2018)

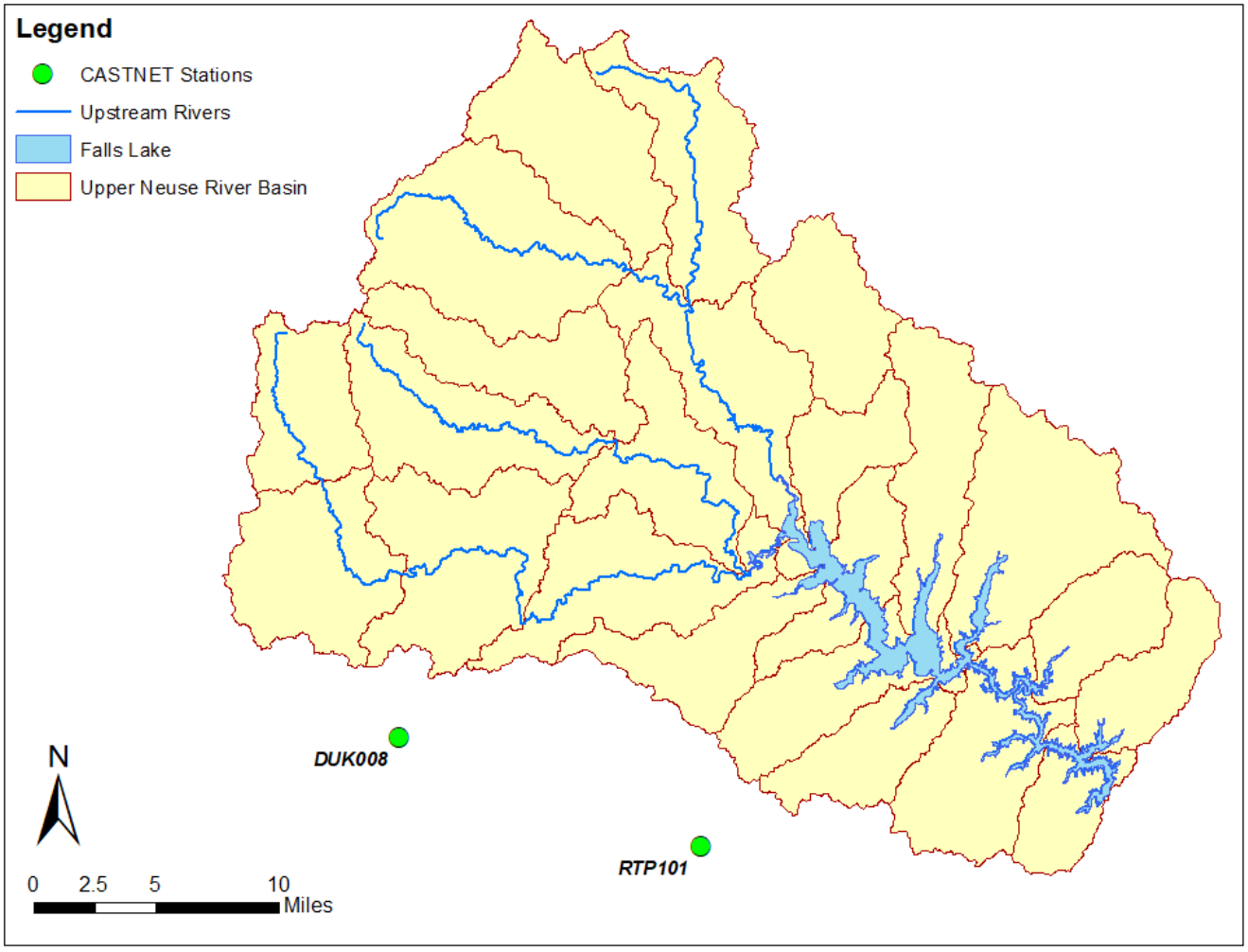

Figure 3-2 Locations of the EPA CASTNET Stations

3.2 Sediment Flux Model

The EFDC water quality model provides three options for defining the sediment-water interface fluxes for nutrients and DO. The options are: (1) externally forced spatially and temporally constant fluxes; (2) externally forced spatially and temporally variable fluxes; and (3) internally coupled fluxes simulated with the sediment diagenesis model. The water quality state variables that are controlled by diffusive exchange across the sediment-water interface include phosphate, ammonia, nitrate, silica, COD and DO. The first two options require that the sediment fluxes be assigned as spatial/temporal forcing functions based on either observed site-specific data from field surveys or best estimates based on the literature and sediment bed characteristics. These options, although acceptable for model calibration against historical data sets, do not provide the cause-effect predictive capability that is needed to evaluate future water quality conditions that might result from implementation of pollutant load reductions from watershed runoff. The third option, activation of the sediment diagenesis model developed by Di Toro (2001), does provide the cause-effect predictive capability to evaluate how water quality conditions might change with implementation of alternative load reduction or management scenarios. For the Falls Lake EFDC model, the third option was selected to

implement the sediment diagenesis model so that load allocation scenarios could be evaluated to determine an appropriate load allocation for Falls Lake.

Living and non-living POC deposition, simulated in the EFDC water quality model, is internally coupled with the EFDC sediment diagenesis model. The sediment diagenesis model, based on the sediment flux model of Di Toro (2001), describes the decomposition of POM in the sediment bed, the consumption of DO at the sediment-water interface (SOD) and the diffusive exchange of dissolved constituents (ammonia, nitrate, phosphate, silica, COD) across the sediment-water interface. State variables of the EFDC sediment flux model are sediment bed temperature, sediment bed POC, PON, and POP, porewater concentrations of phosphate, ammonia, nitrate, silica and sulfide/methane. The sediment diagenesis model computes sediment-water fluxes of COD, SOD, phosphate, ammonium, nitrate, and silica. The state variables modeled for the Falls Lake sediment flux model are listed in Table 3-4.

An overview of source and sink terms is presented with a description of each state variable group in this section. The details of the state variable equations, kinetic terms and numerical solution methods for the sediment diagenesis model are presented in Di Toro (2001), Park et al. (2000) and Ji (2017).

Table 3-4 EFDC Sediment Diagenesis Model State Variables

No.	Name	Bed Layer	Units	Activated
1	POC-G1	Layer-2	g/m^3	Yes
2	POC-G2	Layer-2	g/m^3	Yes
3	POC-G3	Layer-2	g/m^3	Yes
4	PON-G1	Layer-2	g/m^3	Yes
5	PON-G2	Layer-2	g/m^3	Yes
6	PON-G3	Layer-2	g/m^3	Yes
7	POP-G1	Layer-2	g/m^3	Yes
8	POP-G2	Layer-2	g/m^3	Yes
9	POP-G3	Layer-2	g/m^3	Yes
10	Part-Biogenic Silica	Layer-2	g/m^3	No
11	Sulfide/Methane	Layer-1	g/m^3	Yes
12	Sulfide/Methane	Layer-2	g/m^3	Yes
13	Ammonia-N	Layer-1	g/m^3	Yes
14	Ammonia-N	Layer-2	g/m^3	Yes
15	Nitrate-N	Layer-1	g/m^3	Yes
16	Nitrate-N	Layer-2	g/m^3	Yes
17	Phosphate-P	Layer-1	g/m^3	Yes
18	Phosphate-P	Layer-2	g/m^3	Yes
19	Available Silica	Layer-1	g/m^3	Yes
20	Available Silica	Layer-2	g/m^3	Yes
21	Ammonia-N-Flux		g/m^2-day	Yes
22	Nitrate-N-Flux		g/m^2-day	Yes
23	Phosphate-P-Flux		g/m^2-day	Yes
24	Silica Flux		g/m^2-day	Yes
25	SOD		g/m^2-day	Yes
26	COD Flux		g/m^2-day	Yes
27	Bed Temperature		Deg-C	Yes

Particulate Organic Matter (POM)

The sediment diagenesis model incorporates three key processes: (1) depositional flux of POM from the water column to the sediment bed; (2) diagenesis or decomposition of POM in the sediment bed; and (3) the resulting fluxes of DO, COD, sulfide/methane and nutrients across the sediment-water interface. POM is represented as carbon (POC), nitrogen (PON), and phosphorus (POP) stoichiometric equivalents based on carbon-to-dry weight and Redfield ratios for C/N, and C/P. In the water quality model, POM deposition describes the settling flux from the water column to the bed of non-living refractory and labile detrital matter and living algal biomass. In the sediment flux model, POM is split into three classes of reactivity. The labile fraction (POM-G1) is defined by the fastest reaction rate with a half-life on the order of 20 days. The refractory fraction (POM-G2) is defined by a slower reaction rate with a half-life of about one year. The inert fraction (POM-G3) is non-reactive with negligible decay before ultimate burial into the deep inactive layer of the sediment bed.

The sediment flux model represents the sediment bed as a two-layer system. The first layer is a very thin aerobic layer. The second layer is a thicker anaerobic active layer. The thickness of the aerobic layer, which is on the order of only a millimeter, is internally computed in the sediment flux model as a function of bottom layer DO concentration, the SOD rate and the diffusivity coefficient for DO. The thickness of the anaerobic active layer is assigned as a parameter for model setup. The depth of the anaerobic active layer, defined by the depth to which benthic organisms mix particles within a homogeneous bed layer, can range from ~5 to 15 cm (Ji, 2008). An active anaerobic layer thickness of ~10 cm has been determined from both theoretical considerations and field observations in estuaries (Di Toro, 2001). Any particle mass transported out of the active layer is not recycled back into the active layer since these particles are lost to deep burial out of the sediment bed.

The thickness of the active anaerobic layer controls the volume of the anaerobic layer, the amount of mass stored in the anaerobic layer and the long-term response of the sediment bed to changes in organic matter deposition from the water column. A relatively thin active layer will respond quickly to changes in watershed loading and water column deposition of particulate matter. Conversely, a thick active layer will respond slowly to changes in watershed loading and deposition of particulate materials from the water column to the bed. The rate, at which solutes stored in the anaerobic active layer are transported between the thin aerobic and thick anaerobic active layer, and potentially the overlying water column, is controlled by the mixing coefficients assigned as model parameters for particulate and dissolved substances. Anaerobic active layer thickness and diffusive mixing rates are considered to be adjustable parameters for model calibration to determine the most appropriate parameter values for each spatial zone. It should be noted that for the Falls Lake sediment flux model, three (3) zones were used. Zone 1 and zone 3 are the same as water quality zones, and zone 2 is the area of zone 2 and zone 4 of the water quality model combined (See Figure 3-1). An anaerobic layer thickness of 10 cm is assigned for each spatial zone of the sediment flux model.

Since the surface aerobic sediment layer is very thin, the depositional flux from the overlying water column is assigned to the lower anaerobic active sediment layer where decomposition then occurs. The source terms for the three “G” classes of POM are the depositional fluxes of organic matter from the overlying water column to the sediment bed. The loss terms for POM

are the temperature dependent decay (i.e., diagenesis) of POM and removal by burial from the aerobic (upper) to active anaerobic (lower) layers and from the anaerobic (lower) layer to deep burial out of the sediment bed model domain.

Dissolved Constituents

The decay or mineralization of POM results in the diagenetic production of dissolved constituents. The concentration gradients of ammonia, nitrate, phosphate, and sulfide/methane within the two porewater layers and between the surficial porewater layer and the bottom layer of the water column control the sediment fluxes computed in the model. Mineralization of POP produces phosphate which is then subject to adsorption/desorption by linear partitioning with solids in the sediment bed. Diffusive exchange is controlled by the concentration gradient of dissolved constituents, the diffusion velocity, and the bed layer thickness. Other processes that govern the mass balance of dissolved materials in the sediment bed include burial, particle mixing and removal by kinetic reactions.

Ammonia and Nitrate

Ammonia is produced in Layer 2 by temperature dependent decomposition of the reactive G1 and G2 classes of PON. Ammonia is nitrified to nitrate with a temperature and oxygen dependent process. The only source term for nitrate is nitrification in the surficial layer. Nitrate is removed from both layers by temperature dependent denitrification with the carbon required for this process supplied by organic carbon diagenesis. Nitrogen is lost from the sediment bed by the denitrification flux out of the sediments as nitrogen gas (N_2). The sediment-water fluxes of ammonia and nitrate to the overlying water column are then computed from the concentration gradients, the porewater diffusion coefficient and the thickness of the surficial bed layer.

Phosphate

Phosphate is produced by temperature dependent decomposition of the reactive G1 and G2 classes of POP in the lower layer 2 of the sediment bed. Since linear partitioning with solids is defined for phosphate, a fraction of total phosphate is computed as particulate phosphate and a fraction remains in the dissolved form. The partition coefficient for phosphate for the surficial layer 1 is functionally dependent on (a) the oxygen concentration in the overlying bottom layer of the water column based on the assignment of 2 mg/L as a critical concentration for oxygen that triggers the oxygen dependent process, (b) the magnitude of the partition coefficient assigned for the lower layer 2, and (c) an enhancement factor multiplier. There are no removal terms for phosphate in either of the two layers. The sediment-water flux of dissolved phosphate to the overlying water column is then computed from the concentration gradient, the porewater diffusion coefficient and the thickness of the surficial bed layer.

Methane/Sulfide

Sulfide is produced by temperature dependent decomposition of the reactive G1 and G2 classes of POC in the lower layer of the sediment bed. Sulfide is lost from the system by the organic carbon consumed by denitrification. Linear partitioning with solids is also defined for

sulfide to account for the formation of iron sulfide. The sediment flux model accounts for three pathways for loss of sulfide from the sediment bed: (1) temperature dependent oxidation of sulfide; (2) aqueous flux of sulfide to the overlying water column; and (3) burial out of the model domain. If the overlying water column oxygen concentration is low, then the sulfide that is not completely oxidized in the upper sediment layer can diffuse into the bottom layer of the water column. The aqueous flux of sulfide from the sediments is the source term for the flux of COD from the sediment bed to the water column.

When sulfate is depleted, methane can be produced by carbon diagenesis and oxidation of methane then consumes oxygen. In saltwater systems, such as estuaries and coastal waters, sulfate is abundant and methane production and oxidation are not represented in the sediment flux model. In freshwater systems, such as Falls Lake, sulfate is typically characterized by very low concentrations. In freshwater systems methane production and oxidation are represented in the sediment diagenesis model instead of sulfide production and oxidation.

Sediment Oxygen Demand (SOD)

The sulfide/methane oxidation reactions in the surficial layer result in an oxygen flux to the sediment bed from the overlying water column. SOD includes the carbonaceous oxygen demand (CSOD) from sulfide/methane oxidation and the nitrogenous oxygen demand (NSOD) from nitrification. The total SOD is computed as the sum of the carbonaceous and nitrogenous components of the oxygen flux.

Sediment Diagenesis Model Parameters and Kinetic Coefficients

The sediment diagenesis model requires the assignment of a large number of model parameters and kinetic coefficients. Based on the results of sediment flux models developed for estuaries, coastal systems and lakes, Di Toro (2001) has summarized parameter values used for diagenesis, sediment properties, mixing and kinetic coefficients for several different projects. The comparison of data assigned for several different projects shows the robustness of the sediment flux model since many of the parameter values and kinetic coefficients were essentially unchanged for model applications, unless there was a site-specific reason that supported the use of a different value. The exception to this generality, however, is the extreme variation in optimal nitrification velocity, which was adjusted to a value which is 1 order of magnitude smaller than the typical range given in Di Toro (2001). The reason for this adjustment is to increase NH_4 flux and decrease NO_3 flux such that they are in close agreement with the data collected by the UNRBA (Alperin, 2018). Other parameters, such as partition coefficient for PO_4 in anaerobic condition, diffusion coefficient in porewater, PO_4 sorption enhancement factor, and the factor to enhance the magnitude of SOD were also adjusted within the range of typical values.

Kinetic coefficients and parameters of the sediment flux model were initially assigned based on the compilation of parameter values reported in Di Toro (2001). Selected coefficients, were adjusted, as needed, to achieve calibration of the water quality and sediment flux model. Sensitivity analyses were conducted during model development under consultation with third-party model reviewers funded by the NC Collaboratory and DWR modelers to inform model calibration with respect to model coefficients and parameters. Kinetic coefficients and model

parameters assigned to the sediment diagenesis model as either global or spatial zone dependent parameters for the Falls Lake model are listed in Appendix A.1.

Initial Conditions for Sediment Diagenesis Model

The sediment flux model requires specification of initial conditions for POM content (as C, N, and P) and porewater concentrations of inorganic nutrients (as NH_4, NO_3, and PO_4). Setting the initial conditions for the sediment bed is an important step in the lake modeling process as it establishes the starting point from which the sediment diagenesis model performs its calculations and moves toward a dynamic equilibrium.

A UNRBA special study led by Dr. Marc Alperin (University of North Carolina-Chapel Hill) was conducted during June and July 2015 to evaluate sediment bed conditions in Falls Lake (Alperin, 2018). The study looked at sediment cores collected from fifteen (15) locations along the lake, as shown in Figure 3-3, and provides information on the characteristics of the lake sediments. The initial sediment bed organic material concentrations at each cell for the sediment diagenesis module was calculated by linear interpolation using the average sediment thickness at each cell and organic material concentration data collected at fifteen (15) locations by UNRBA (sediment thickness was used for each cell, and the core sample was used for each zone where the cell is located). The steps taken are described below:

1- The sediment bed thickness data from UNRBA sediment mapping study (UNRBA, 2019), was converted from raster to points. Then, using the point shapefile, the average sediment thickness at each grid cell was calculated;

2- It was assumed that only the top 4 inches (about 10 centimeters) of the sediment bed actively contributes to sediment nutrient flux and any sediment below the top 4 inches is effectively inactive with respect to benthic fluxes represented in the sediment flux model. Therefore, for any cells with more than 4 inches of sediment thickness including the cells where the core samples were collected, the sediment thickness of the cells was re-set to 4 inches for the purpose of interpolation;

3- It was further assumed that grid cells in the vicinity of each sampling location have the same organic matter concentrations as the sample core if the sediment thickness of the cells is equal to that of the grid cell where the core sample was collected. The area in the vicinity of each sampling location is shown in different colors in Figure 3-4 with each having the same name or number in the legend.

4- To assign the labile group (G1) of the sediment bed organic material concentration at each cell, the following linear interpolation was applied:

$$\mathrm{GPOM1}\Big|_{\text{for each color}}^{\text{for each grid cell}}{}^{(g/m^3)} = \frac{\text{Core Sample Concentration}^{(g/m^3)} \times \text{Cell Bed Thickness}^{(in)}}{4^{(in)}}$$

(Initially, it is assumed that the organic matter concentration at the cells of each zone is equal to the core sample of that zone. Then, the organic material concentration is normalized based on the ratio of the cell's thickness to the total active layer thickness

(i.e., 4 inch), to factor into both sediment thickness at each cell, and the core sample organic material concentrations from Dr. Alperin's work.)

5- The refractory group (G2) and inert group (G3) of the sediment bed organic material concentrations at each cell were calculated as the G1 group concentration multiplied by factors of 10 and 100, respectively. The factors were based on an approximation of the sediment bed as G3 (90%); G2 (9%); and G1 (1%) (Di Toro, 2001)

Figure 3-5 shows how sediment thickness which includes the inactive layer is distributed throughout the model grid based on sediment depth data collected in Falls Lake. As can be seen, the thickest sediment bed conditions are in the lower reaches of the lake. The sediment flux model initial conditions was used to simulate a spin-up (initialization) period to assign sediment bed conditions considered to be representative of external loading from the watershed model. During the model calibration process, the spin-up period was extended from 1 year (1/1/2014 to 12/31/2014) to 6 years (from 1/1/2014 to 12/31/2018). Initial conditions derived from the 6 year spin-up run of the sediment flux model were then used to run the model, beginning on 1/1/2014, to provide a better representation of sediment conditions for nutrient flux especially for PO_4flux. A spin-up period of 11 years was also tested, and while it improved PO_4flux it worsened NH_4 flux. Of the three spin-up periods tested, 6 years had the best fit to measured PO_4 and NH_4 fluxes. While the UNRBA collected a significant amount of sediment quality data in Falls Lake, many lake model grids still do not have sediment quality data and need to be populated with linear interpolation as discussed early. Model spin-up is needed to smooth out initial conditions of the sediment bed while retaining the general characteristics of the lake sediments. Nutrient flux rates take decades to change in response to changes in watershed loading inputs (Alperin 2018), so a spin-up period of six years is not expected to introduce significant uncertainty in the modeling.

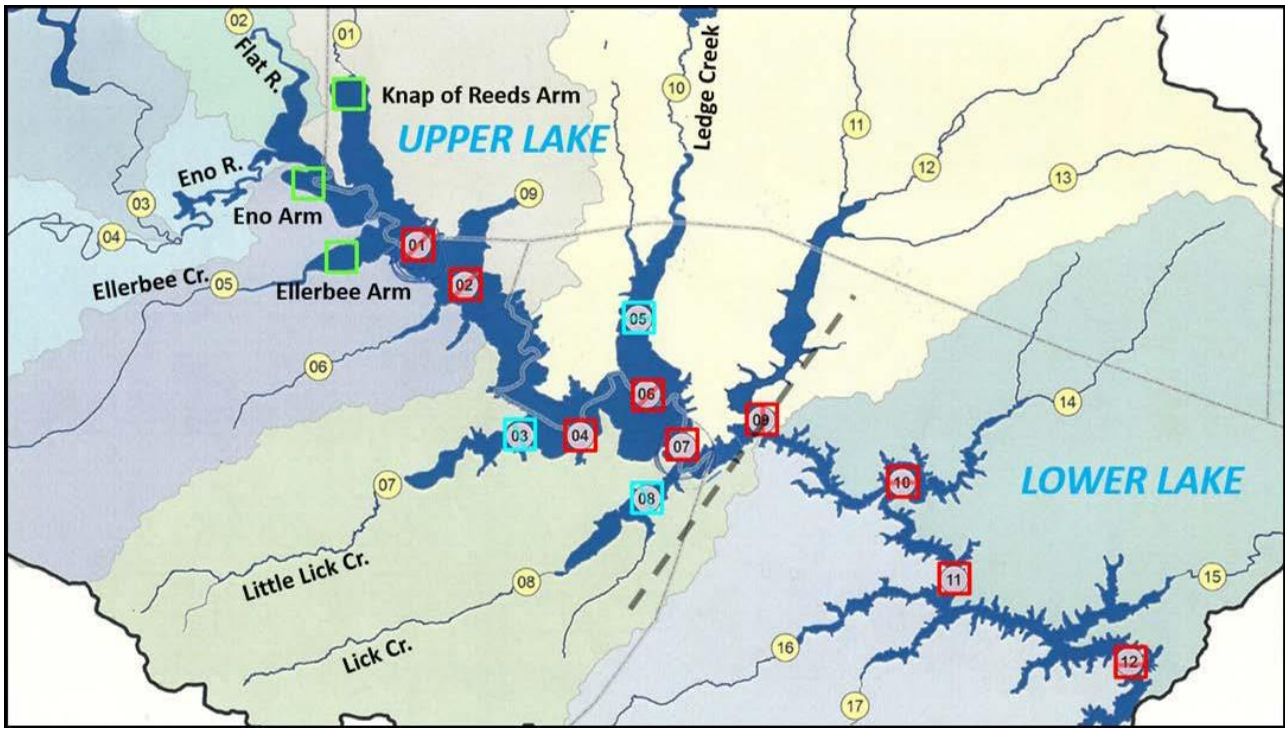

Figure 3-3 Locations of Sediment Core Sampling in Falls Lake in June 2015 (Alperin, 2018)

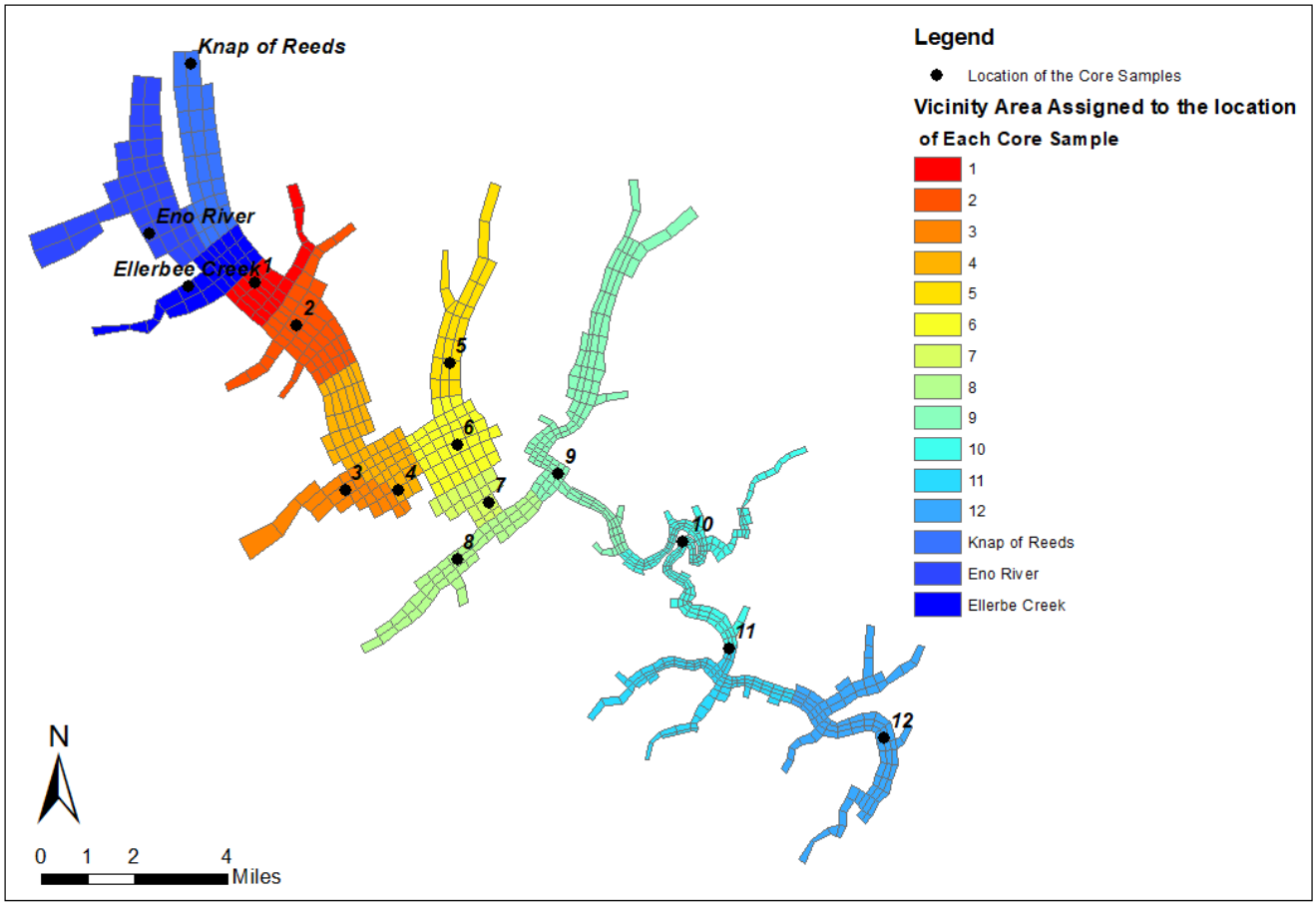

Figure 3-4 Location of the Core Samples and the Vicinity Area Assigned to the Location of each Core Sample

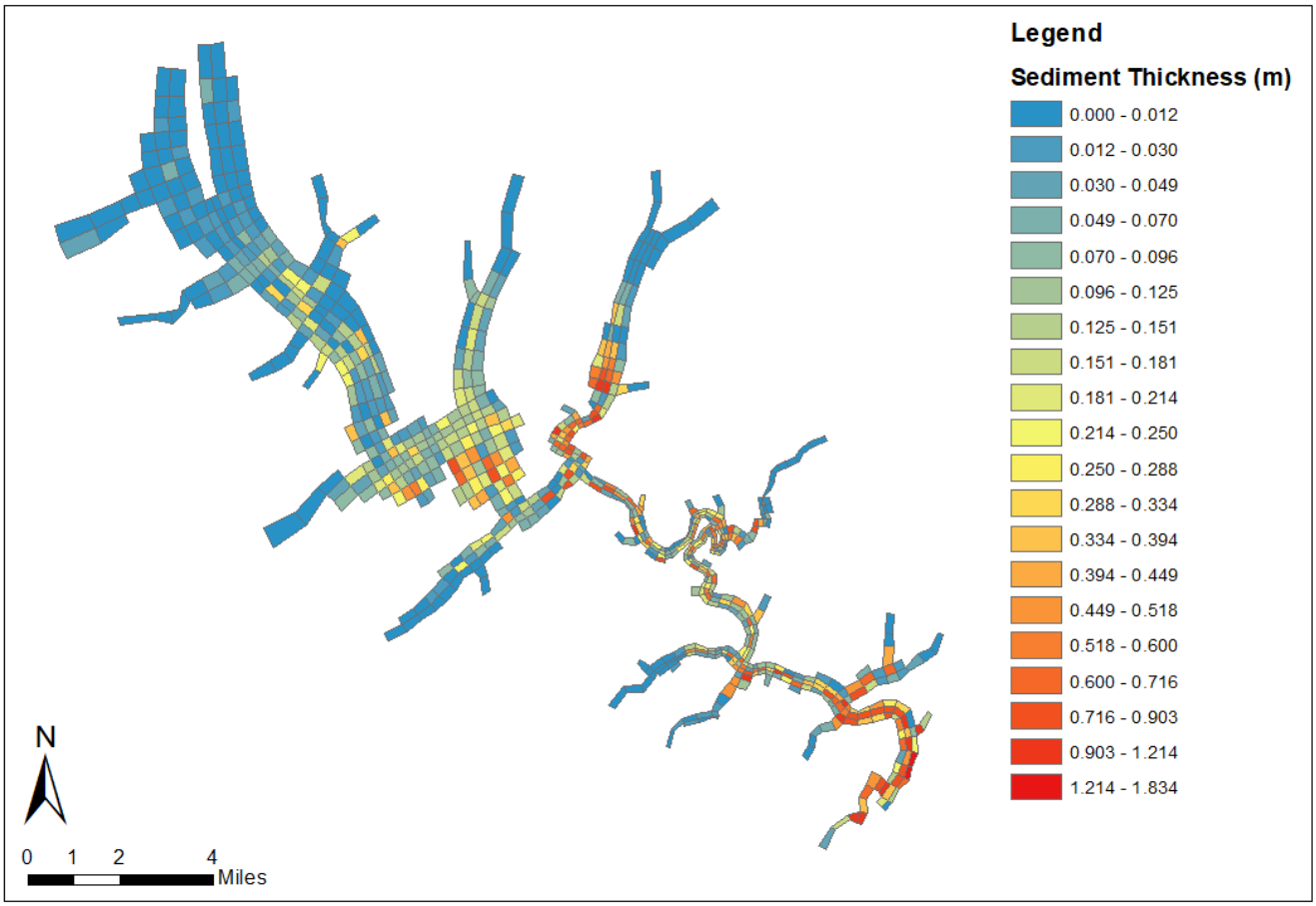

Figure 3-5 Sediment Bed Thickness Map Based on Data Collected in Falls Lake

4. Calibration and Validation Stations

The UNRBA Modeling QAPP describes the calibration and validation processes and assessment of model performance for the EFDC hydrodynamic and water quality models. While calibration was not assessed with respect to sediment fluxes, the numerous studies conducted in Falls Lake by DWR, EPA, and UNRBA were used to inform model development and improve simulations of ammonia and phosphate fluxes with respect to measurements.

4.1 Stage Calibration and Validation Stations

Observed stage data for the Falls Lake model are available at two (2) stations: (1) USGS 02087183 at Falls Dam, and (2) USGS 0208706575 at Beaverdam as shown in Figure 4-1. The former is operated in cooperation with the USACE, and the latter is operated in cooperation with the City of Raleigh, North Carolina. Stage stations are located in the forebay of the Falls Dam and forebay of the Beaver Lake Impoundment dam (Beaverdam), respectively.

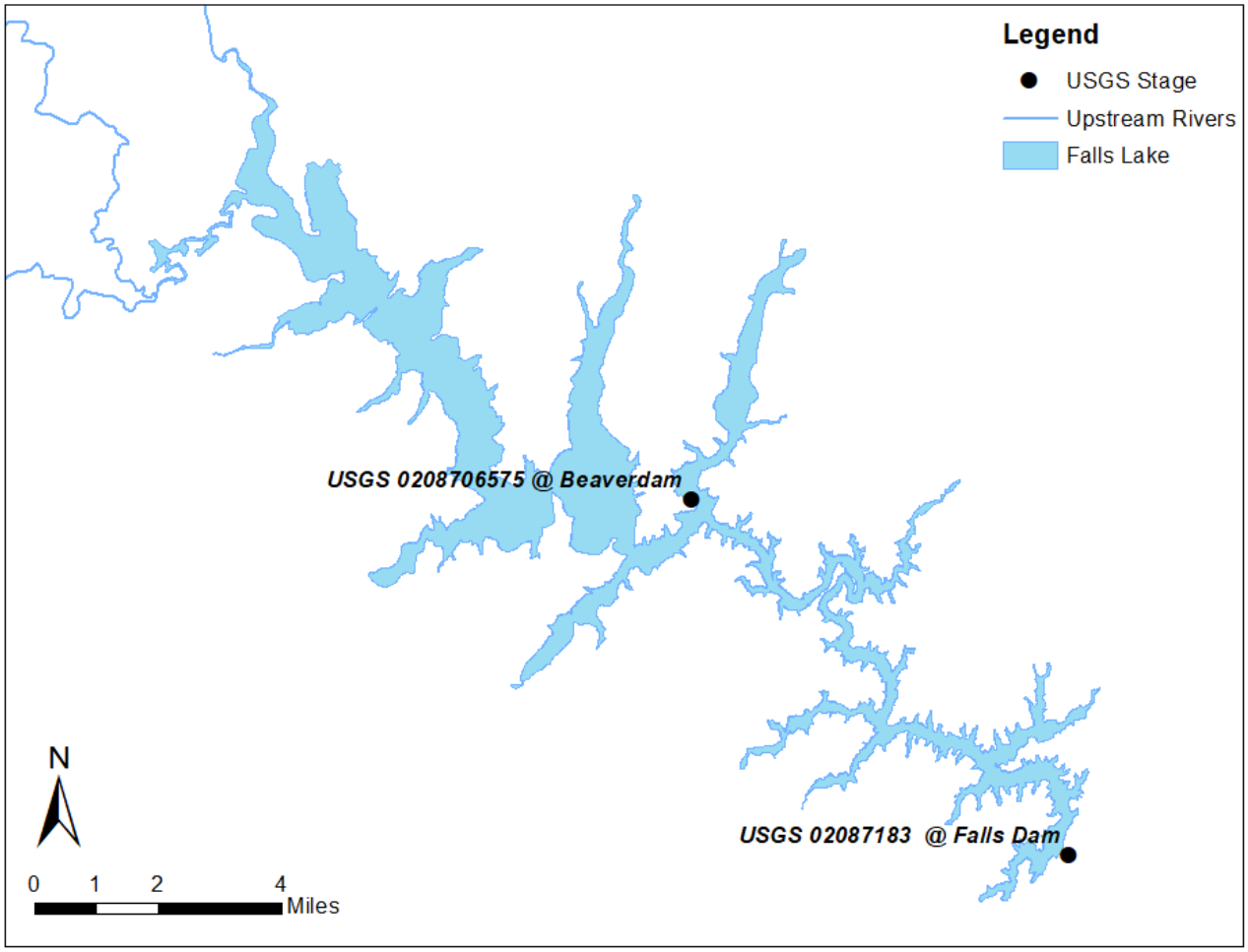

Figure 4-1 Locations of the Stage Calibration/Validation Stations in Falls Lake

4.2 Water Quality Calibration and Validation Stations

The Falls Lake EFDC model was calibrated and validated at twelve (12) DWR stations as described in the UNRBA Model QAPP. Data collected by other organizations was used to inform model development.

Station identification information for water quality calibration and validation stations is listed in Table 4-1 and station locations are shown in Figure 4-2. Water quality data were collected monthly at the lake's photic zone, corresponding to 2 x Secchi depth. Temperature and DO data were collected monthly at multiple depths. The availability of DO and temperature data at multiple depths in the water column allows for EFDC model-data comparison and assessment of model performance as surface and bottom layer time series as well as model-data "snapshots" of vertical temperature and DO profiles for days when data were collected.

Table 4-1 Location of Water Quality Calibration and Validation Stations for Falls Lake

Station Code	Location Description	Latitude (degree)	Longitude (degree)
LC01	In the Ledge Creek arm	36.04991	-78.7191
LI01	In the Lick Creek arm	36.0007	-78.7166
LLC01	Downstream of Little Lick Creek	36.01792	-78.7515
NEU013	Upstream of I-85	36.07024	-78.7795
NEU013B	Downstream of I-85	36.05928	-78.7666
NEU0171B	Between Little Lick and Ledge Creeks	36.01799	-78.7349
NEU018C	Downstream of Ledge Creek	36.02932	-78.7167
NEU018E	Upstream of Lick Creek	36.01494	-78.707
NEU019E	Downstream of Beaverdam Impoundment	36.0222	-78.6853
NEU019L	Downstream of New Light Creek	36.00507	-78.6467
NEU019P	At Hwy 98 (Durham Road)	35.97838	-78.6325
NEU020D	Upstream of dam	35.95591	-78.5844

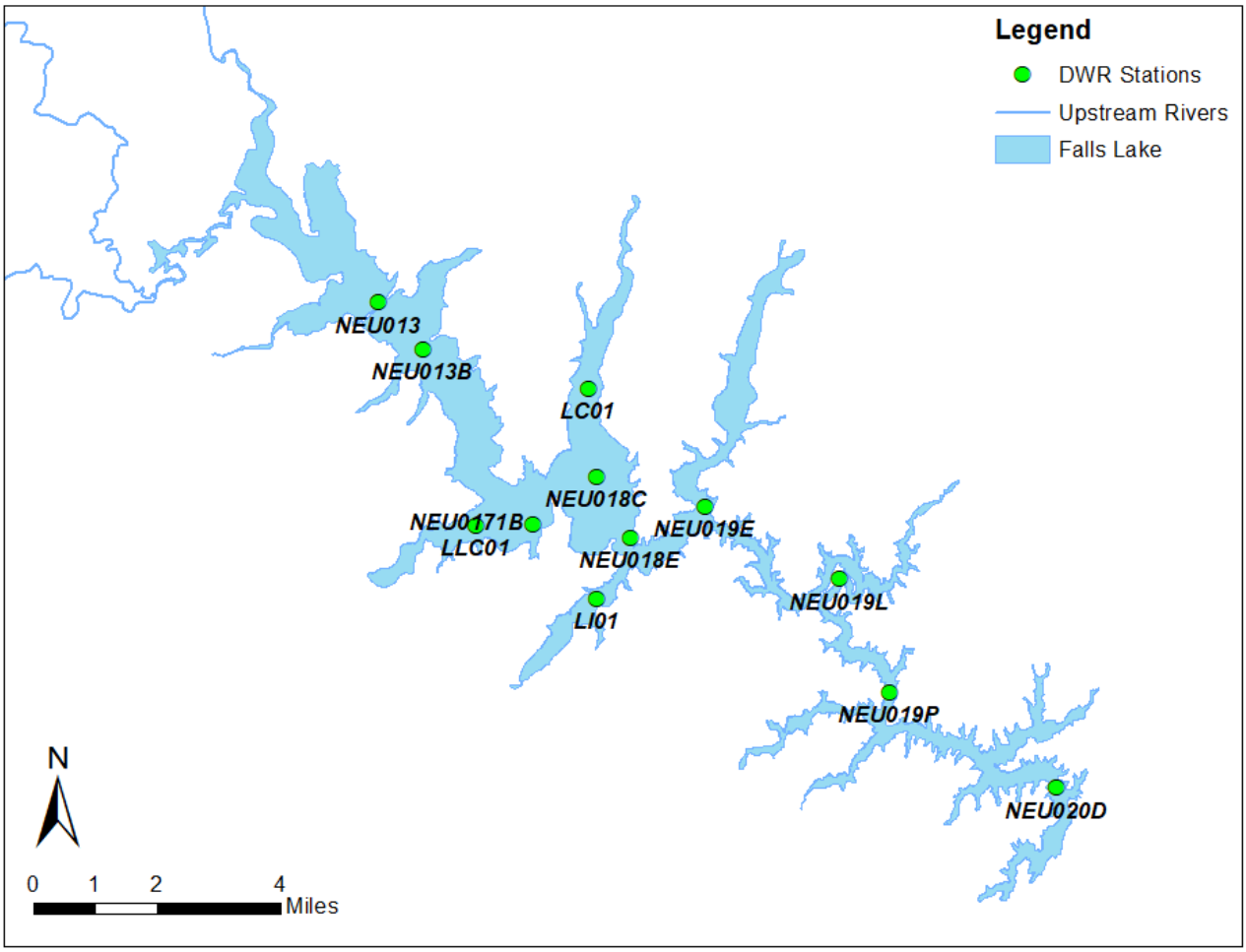

Figure 4-2 Locations of the DWR Water Quality Calibration/Validation Stations in Falls Lake

5. Model Performance Statistics

Model performance is evaluated to determine the endpoint for model calibration using a "weight of evidence" approach that has been adopted for many modeling studies. The "weight of evidence" approach includes the following steps: (a) visual inspection of plots of model results compared to observed data sets (e.g., station time series); and (b) analysis of model-data performance statistics. The "weight of evidence" approach recognizes that, as an approximation of a waterbody, perfect agreement between observed data and model results is not expected and is not specified as a performance criterion for the success of model calibration. Model performance statistics are used, not as absolute criteria for acceptance of the model, but rather, as guidelines to supplement the visual evaluation of model-data time series plots to determine the endpoint for calibration of the model. The "weight of evidence" approach used for this study thus acknowledges the approximate nature of the lake model and the inherent uncertainty in both model input data and observed data.

The model performance statistical measures selected for calibration of the hydrodynamic and water quality model are the following:

1- Coefficient of Determination (R^2): This measure estimates the combined dispersion against the single dispersion of the observed and predicted series. Its value lies between 0 and 1; A value of zero means no correlation at all whereas a value of 1 means a perfect correlation with dispersion of the prediction equal to dispersion of the observations. The expression for the R^2 is:

$$R^2 = \left(\frac{\sum_{n=1}^{N}(O_n-\overline{O})(P_n-\overline{P})}{\sqrt{\sum_{n=1}^{N}(O_n-\overline{O})^2}\sqrt{\sum_{n=1}^{N}(P_n-\overline{P})^2}} \right)^2 \qquad \text{Equation 1}$$

where $\overline{O} = \frac{1}{N}\sum_{n=1}^{N} O_n$ is the observed mean, and $\overline{P} = \frac{1}{N}\sum_{n=1}^{N} P_n$ is the predicted mean value. R^2 is used here only as a reference statistic without defined target values used for assessment of model calibration/validation.

2- Root Mean Square Error (RMSE): This measure, also known as the Standard Error of the Mean, is the average of the squared differences between observed and predicted values. This statistic has units defined by the units of each state variable of the model. The expression for the RMSE is:

$$RMSE = \sqrt{\frac{1}{N}\sum_{n=1}^{N}(P_n - O_n)^2} \qquad \text{Equation 2}$$

where N is the number of paired records of observed measurements and model results, O is the observed measurement, and P is the predicted model result.

The RMSE can be used to determine the width of the confidence interval around model predictions. The 95% confidence interval for the model is approximately equal to the model result at each point in time "+/- 2 x Standard Error". Since the RMSE represents

the same statistic as the Standard Error of the Mean, the 95% confidence interval for the model results can be determined as +/- 2 x the RMSE.

3- RMSE– Standard deviation Ratio (RSR): This measure is a normalized RMSE expressed as a percentage, and is computed as the ratio of the RMSE to the standard deviation in the observed data for each hydrodynamic and water quality constituent (Moriasi, et al., 2007). This statistic compares how well the model performs in terms of simulating the amount of variability observed in the water quality data. The expression for the RSR is:

$$RSR = \frac{RMSE}{STDEV_{Obs}} \times 100 = \frac{\sqrt{\sum_{n=1}^{N}(P_n - O_n)^2}}{\sqrt{\sum_{n=1}^{N}(O_n - \bar{O})^2}} \times 100 \qquad \text{Equation 3}$$

In evaluating the results obtained with the EFDC hydrodynamic model, a target RSR performance measure of 50% is adopted for evaluation of the comparison of model predicted results and observed measurements of water surface elevation and water temperature in the lake. For variables simulated with the EFDC water quality model, a target RSR performance measure of 50% is adopted for DO and 100% for nutrients, TOC, TN, TP, TSS, and algal biomass (as Chl-a).

4- Relative Error (RE): This measure is the ratio of the Mean Absolute Error (MAE) to the observed mean and is expressed as a percentage. The expression for the RE is:

$$RE = \frac{\frac{1}{N}\sum_{n=1}^{N}|O_n - P_n|}{\bar{O}} \times 100 \qquad \text{Equation 4}$$

RE is used here only as a reference statistic without defined target values used for assessment of model calibration/validation.

5- Average Error (AE): This measure is the average of all the differences between the predicted and observed values. The expression for the AE is:

$$AE = \frac{\sum_{n=1}^{N}(P_n - O_n)}{N} \qquad \text{Equation 5}$$

AE is used here only as a reference statistic without defined target values used for assessment of model calibration/validation.

6- Coefficient of Efficiency (CE): This measure is calculated as one minus the ratio of the error variance of the modeled time-series divided by the variance of the observed time-series. Its value lies between -∞ and 1; An efficiency less than zero (CE < 0) occurs when the observed mean is a better predictor than the model, a value of zero indicates that the model is only as good as using the mean of the observations, and a value of 1 means a perfect model with an estimation error variance equal to zero. The expression for the CE is:

$$CE = 1 - \frac{\sum_{n=1}^{N}(P_n - O_n)^2}{\sum_{n=1}^{N}(O_n - \bar{O})^2} \qquad \text{Equation 6}$$

CE is used here only as a reference statistic without defined target values used for assessment of model calibration/validation.

7- Percent Bias (pBias): The percent bias is a measure of model error relative to the observed mean. This measure is used to evaluate the systematical model results tendency towards over/under predicting the observations. A pBias of 0% would indicate that the mean of the simulated values exactly matched the mean of the observed values. The expression for pBias is:

$$\text{pBias} = \frac{\frac{1}{N}\sum_{n=1}^{N}(P_n - O_n)}{\bar{O}} \times 100 \qquad \text{Equation 7}$$

pBias is used here only as a reference statistic without defined target values used for assessment of model calibration/validation.

Observed station field data has been pre-processed to define time series for each station location for the surface layer and bottom layer (applied only to temperature and DO) of the water column. For temperature and DO, observed data is assigned to a vertical layer based on surface water elevation, station bottom elevation and the total depth of the water column estimated for the sampling date and time. Station locations are overlaid on the model grid to define a set of discrete grid cells that correspond to each monitoring site for extraction of model results. For time series of model results extracted for each grid cell (station) and surface and bottom depth layer, the match of the model simulation time with date/time of observations for comparison to the model is defined by a time tolerance parameter of +/- 1440 minutes. Model results are extracted for compilation of a set of model-data pairs if the model simulation time is within the +/- time tolerance of the observed data date/time.

For water quality parameters, DWR collects measurements as photic-zone composites. The EFDC Falls Lake model uses a Sigma-Zed grid which allows for the number of layers to vary over the model domain and maintains a uniform thickness for each layer. Each cell can use a different number of layers, though the number of layers for each cell is constant in time. The thickness of each layer varies in time to accommodate the time varying water level.

Because the layer thickness changes with the lake water level, the number of layers that represent the photic zone can vary over the simulation period. When lake levels are below normal pool (251.5 ft above mean sea level), layer thickness is approximately 0.75 meters. When lake levels are above normal pool, layer thickness is approximately 1.25 meters. An average of the values associated with layers in the photic-zone is compared to observations to assess model performance. Table 5-1 lists the layers used in the photic-zone averaging for comparison to water quality observations based on the water level in Falls Lake. The main lake report provides additional discussion about this layering approach which was approved by the UNRBA MRSW.

Table 5-1. EFDC Layers to Average for Water Quality Calibration and Comparison to Photic Zone Composites

Stations	When water level is below normal pool	When water level is above normal pool
NEU013,13B	Top layer	Top layer
LLC01; LC01; LI01; NEU017B,18C,18E,19E,19L,19P	Top 2 layers	Top layer
NEU020D	Top 3 layers	Top 2 layers

Given the lack of a general consensus across the literature for defining quantitative model performance criteria, the inherent errors in input and observed data, difficulty achieving performance criteria when observations are relatively low or show little variability, and the approximate nature of model formulations, absolute criteria for model acceptance or rejection are not appropriate for studies such as the development of the hydrodynamic and water quality model for Falls Lake. The statistical measures presented above have been used as targets or as references. They were not used as rigid rejection or acceptance criteria of model results as part of the performance evaluation of the Falls Lake Water Quality model calibration.

Model performance was reviewed iteratively as each EFDC model component was developed with the UNRBA MRSW, third-party reviewers funded by the NC Collaboratory, and modeling staff from NC DWR. Significant evaluations and modifications were made to the model to incorporate this feedback and to respond to questions. These discussions are noted throughout the main report.

6. Hydrodynamic Model Calibration and Validation

6.1 Lake Stage-Volume and Stage-Area Relationship

It is important for the EFDC model stage-volume relationship to be as close to the observed data as possible in order for the hydrodynamic model to correctly reproduce lake residence time which is critical for the simulation of Chl-a and other lake water quality constituents. Figure 6-1 shows the stage-volume comparison between the EFDC Falls Lake model and the data from WaterCube (Sloat, 2017). As can be seen, the model relationship of stage - volume demonstrates very good agreement with the observed stage - volume data. Relationship between the stage and the lake's surface area is depicted in Figure 6-2.

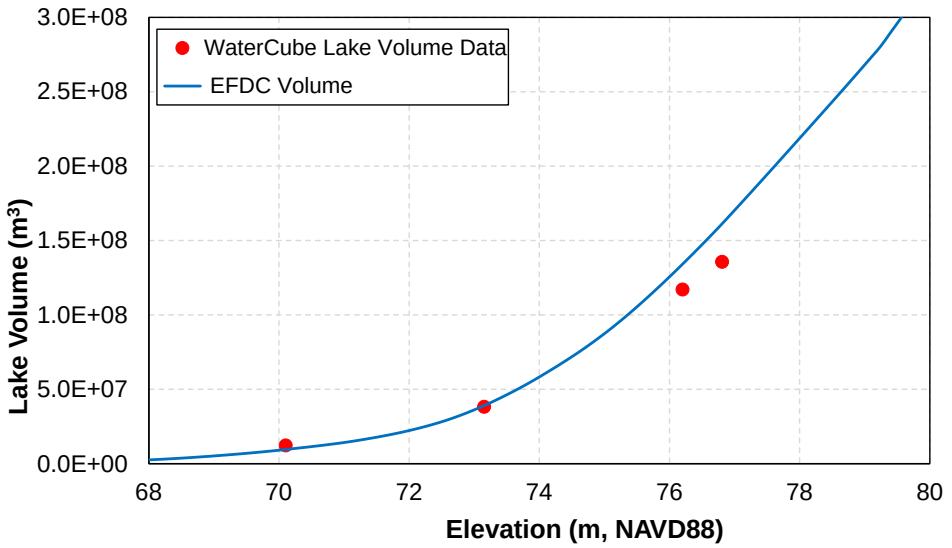

Figure 6-1 Stage-Volume Comparison Between the EFDC Model and the Data from WaterCube

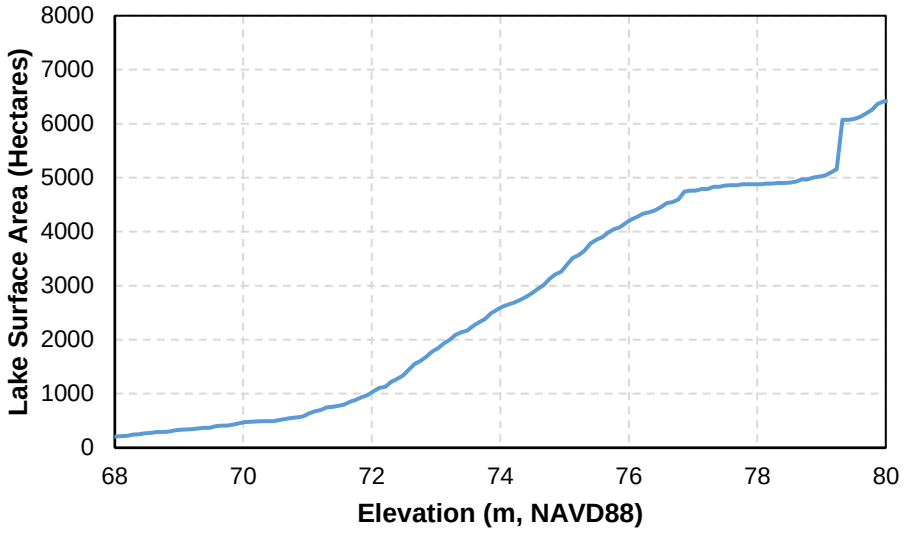

Figure 6-2 Relationship between the Stage and the Lake's Surface Area of the EFDC Model

6.2 Balance Flow Addition Procedure

Due to uncertainties in the lake inflows and outflows assigned as model inputs, the simulated lake volume (and consequently the lake surface area, and the water level) will be different than the observation. To satisfy the conservation of mass balance, the difference between the observed and simulated volumes is calculated at similar time interval and then added to the model. This procedure is called balance flow addition and is a normal part of the EFDC model development and calibration process. Potential sources of uncertainty in the lake water budget include lake-groundwater interaction, withdrawal and dam discharge measurements, lake surface evaporation, and tributary inflows. The DWR groundwater station F43X1 located in Orange County, North Carolina is relatively near the lake (See Figure 6-3). Comparison between the balance flow and the groundwater level from the station F43X1 showed no strong correlation between the two (See Figure 6-4). Furthermore, water withdrawals and dam discharges are expected to be measured with relatively high accuracy. Additionally, the uncertainty of calculating the lake surface evaporation via EFDC is too small to account for. Therefore, lake-groundwater interaction, withdrawal and dam discharge measurements, and lake surface evaporation should not be used to balance the lake's water budget. However, the uncertainty attributed to the tributary inflows is more significant. This uncertainty is mainly the result of three error sources associated with the watershed model, including the measured river/stream flows for model calibration which were derived based on the USGS stage-flow rating curves, the NEXRAD precipitation data and its temporal resolution (6 hour), and the amount of ungaged area draining to Falls Lake.

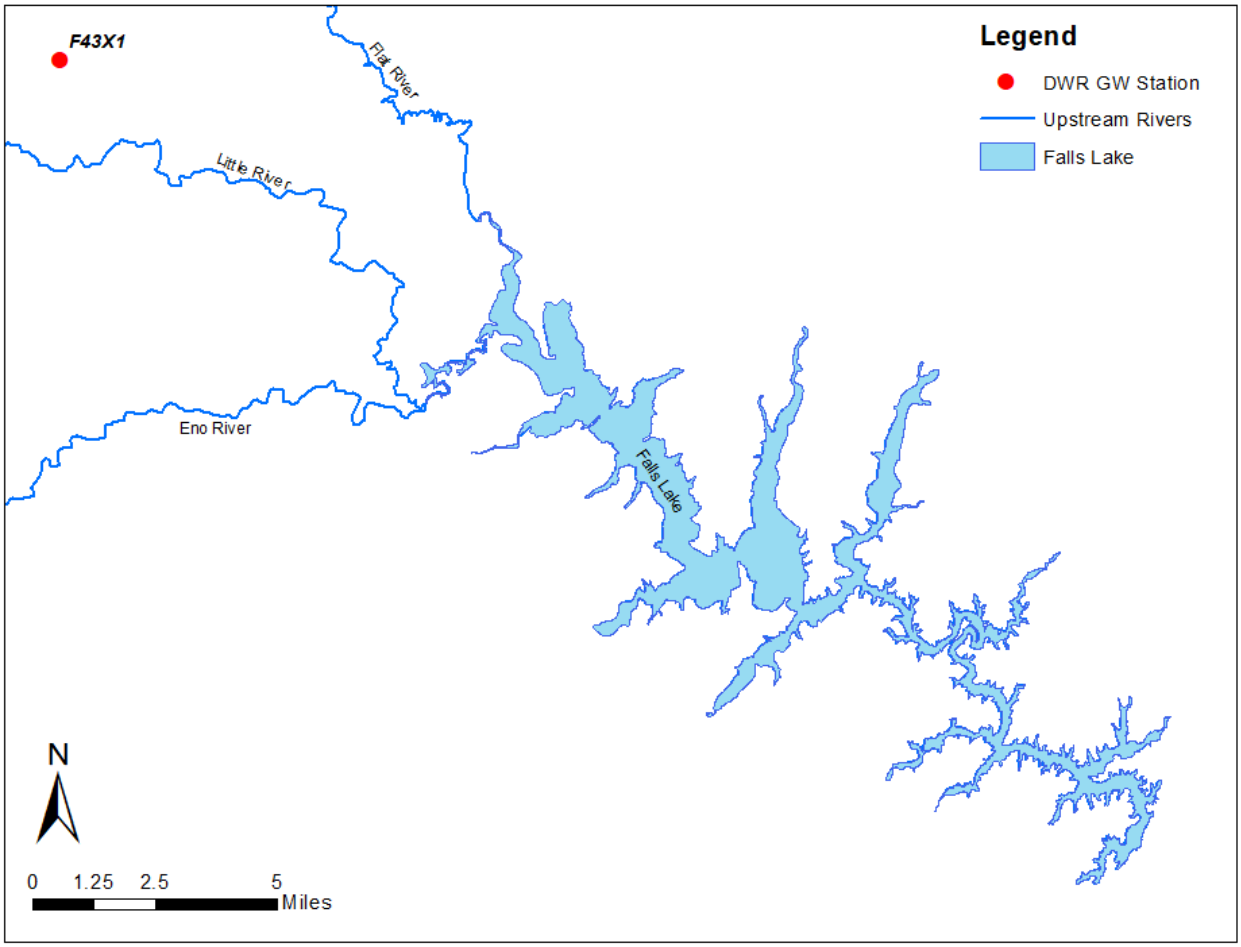

Figure 6-3 DWR Groundwater Station F43X1 Located in Orange County, North Carolina

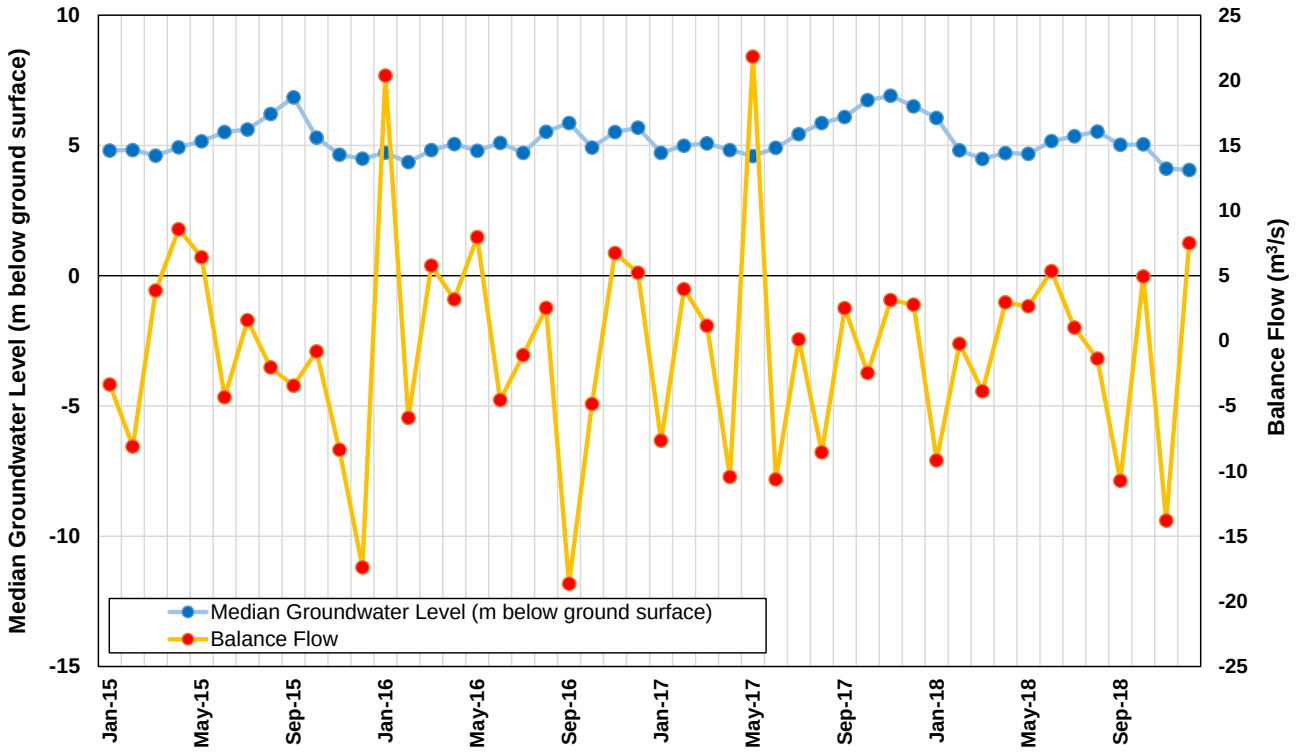

Figure 6-4 Median Monthly Groundwater Level vs. Balance Flow

To compensate for the uncertainty, the balance flow was apportioned at the tributary inputs based on ungagged drainage area. This allows to use the tributary water quality concentrations for inflows or outflows, and hence helps maintain continuity in the loads. Also, apportioning based on drainage area adds load associated with the precipitation/runoff response that contributes the most uncertainty. There is no concrete information on which tributaries/processes are generating the discrepancies. However, delineation shows that 17 major tributaries to Falls Lake, listed in Table 6-1 and shown in Figure 6-5, contribute to about 90% of the whole Falls Lake's drainage area. It should be noted that the number 17 indicates the number of the tributaries that force the model as flow boundary conditions. Of these 17 tributaries simulated as EFDC tributary model inputs, 4 of them are gaged via five (5) USGS gages located at the upstream of their confluence to the lake. They include Eno and Little Rivers (lumped in together at the boundary group ID R0001), Flat River, Knap of Reeds Creek, and Ellerbe Creek. Their gaged part of the drainage area is the area where there is the greatest confidence in the inflows. Hence the uncertainty likely comes from the small part of the drainage area downstream of those 4 tributary inputs that is ungagged. The other 13 tributaries are ungagged inflows. Located in the lower parts of the lake, they are the areas of greatest uncertainty in the water balance. Therefore, the flow additions and withdrawals were set proportional to the ungagged drainage areas of the 17 major tributaries to Falls Lake. Then, the flow additions were assigned to the model as flow boundary conditions at the cells in the lake located downstream of the cells where tributary inflows are assigned. Table 6-1 lists the total ungaged contributing area and the balance flow apportion to the 17 major tributaries.

Table 6-1 Balance Flow Apportion to the 17 Major Tributaries

Boundary Group ID	Tributary Name	Ungagged Contributing Area (sq. mi)	Balance Flow Apportion
R0001	Eno and Little Rivers	55.629	0.199
R0117	Flat River	4.910	0.018
R0139	Knap of Reed Creek	2.930	0.010
R0146	Unknown	3.394	0.012
R0148	Ledge Creek	27.815	0.099
R0154	Robertson Creek	20.133	0.072
R0157	Beaverdam Creek	13.677	0.049
R0159	Smith Creek	16.909	0.060
R0163	New Light Creek	27.209	0.097
R0168	Horse Creek	17.425	0.062
R0175	Honeycutt Creek	11.042	0.039
R0182	Lower Barton Creek	13.037	0.047
R0184	Upper Barton Creek	16.435	0.059
R0187	Lick Creek	16.204	0.058
R0192	Little Lick Creek	22.151	0.079
R0201	Panther Creek	7.856	0.028
R0203	Ellerbe Creek	2.930	0.010

On average, the balance flow represents a small fraction (about 10%) of the total watershed flow. Adding balance flows instantaneously to the model can cause numerical instabilities, particularly for shallow upstream segments. Therefore, some degree of smoothing is necessary to prevent numerical instabilities.

Smoothing was performed by applying LOESS method to the balance flow (Cleveland and Devlin, 1988). LOESS is a regression method that locally fits a second-order polynomials developed from data within a moving window defined by smoothing parameter (α or span). The span is the fraction of the overall dataset to be included in each local regression:

$$\alpha = \frac{\text{Desired window in days}}{\text{Total period of record in days}}$$ Equation 8

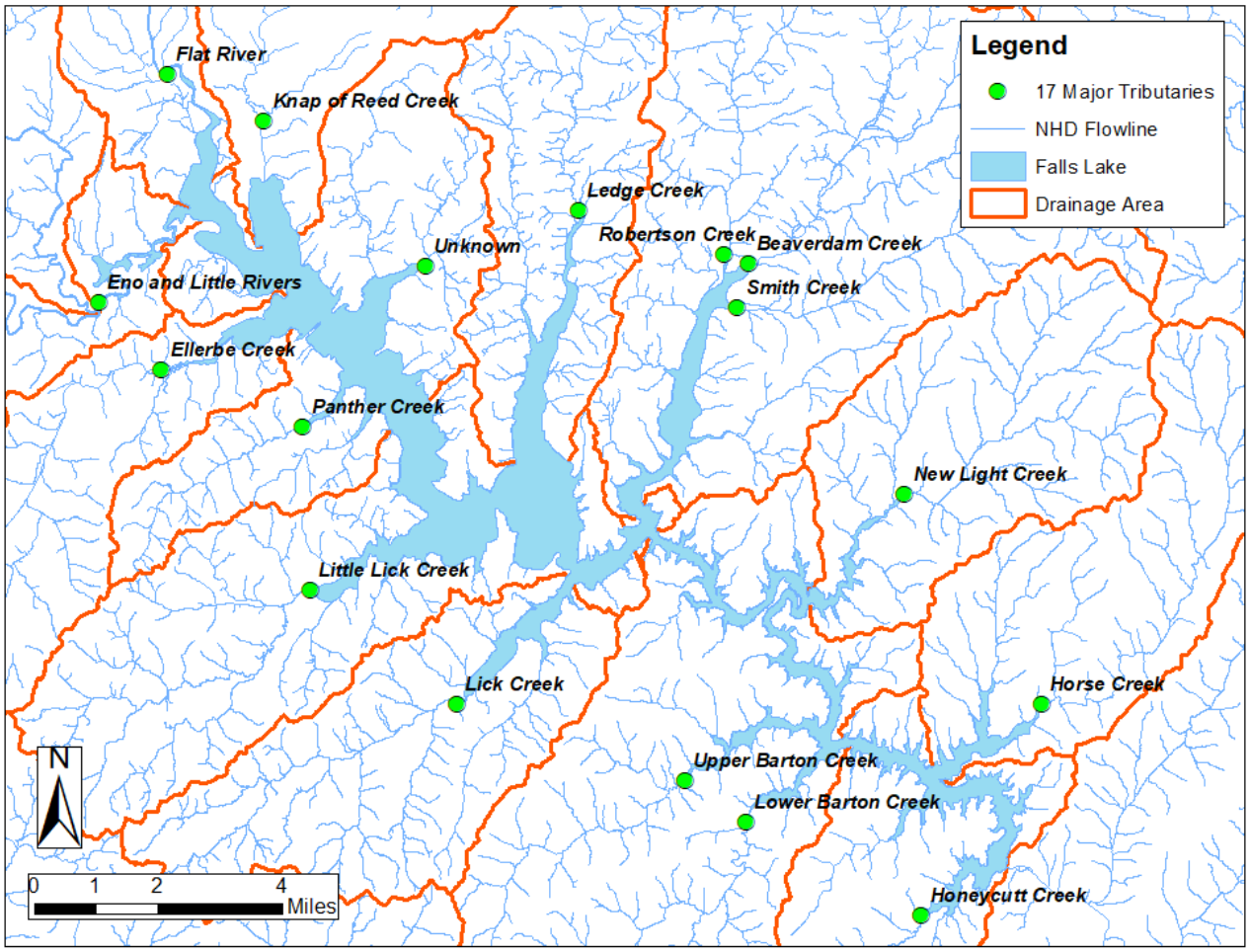

Figure 6-5 Seventeen Major Tributaries to Falls Lake

Proper determination of the span allows the model to capture seasonality, droughts, or large storms that have the largest impacts on water quality. Thus, the balance flows were closely evaluated to include meaningful scales of variation. The monthly average balance flows are depicted in Figure 6-6. It can be seen that balance flows for all four model years are mostly negative for the months of June through October and more likely to be positive in late winter and spring. This suggests that the span providing a window in the range of a month to a season may provide a good approximation for the patterns seen at Figure 6-6. As such, the span values based on 30, 60, 90, 120 and 150 days were tested. It was concluded that for a 120-day window (α=0.66) the model results after several iterations tend to approach the smallest RSR values and the calibration/validation target of the RSR value of 50%. Figure 6-7 shows the balance flow obtained after 13 iterations, smoothed with LOESS method (α=0.66).

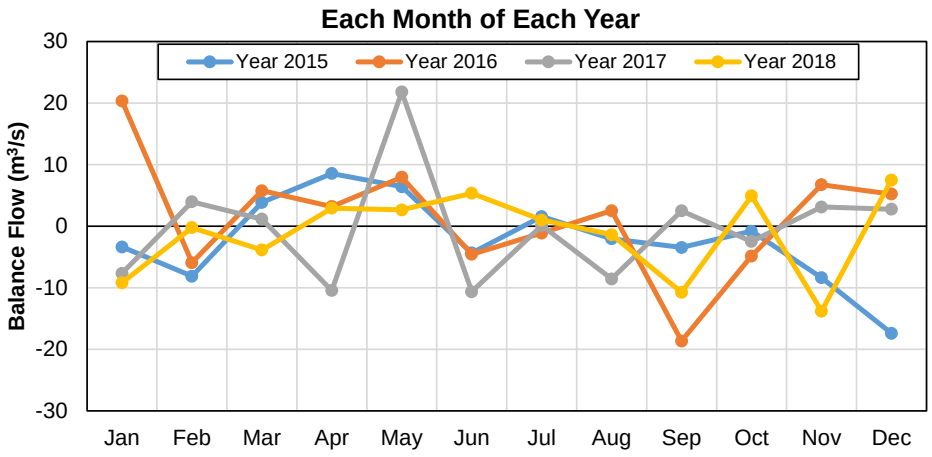

Figure 6-6 Monthly Averages of Balance Flow over 4 Years of Simulation

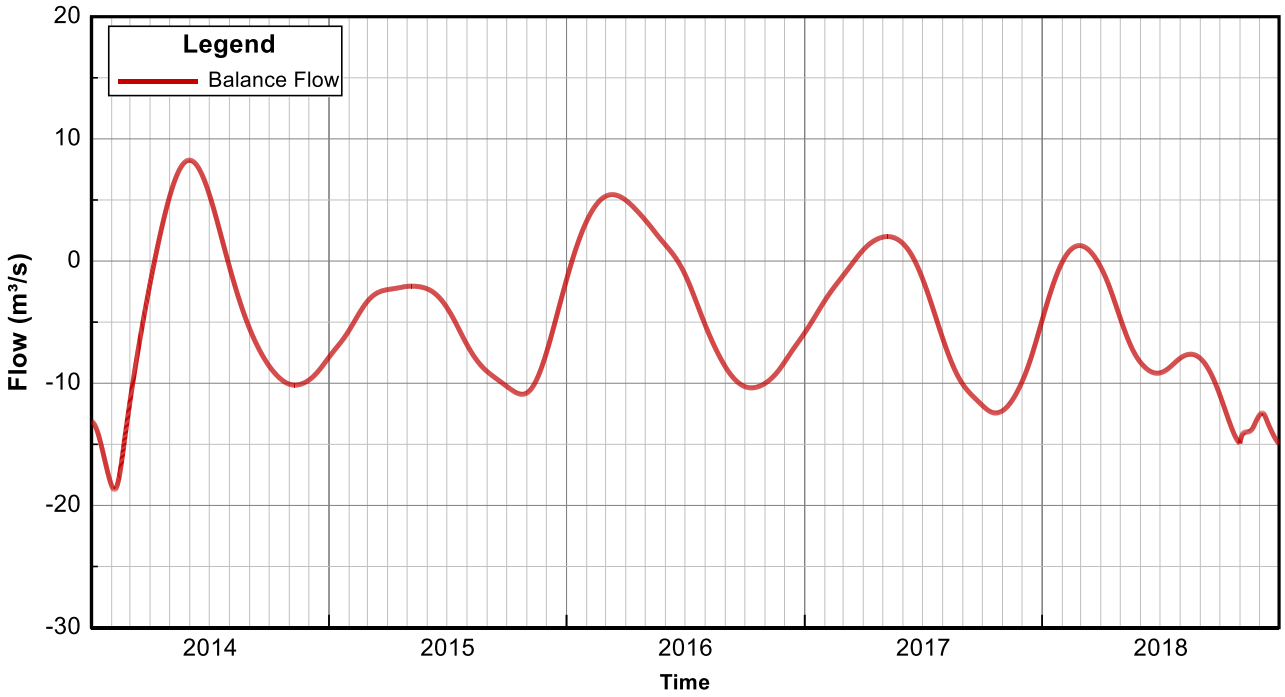

Figure 6-7 Balance Flow After 13 Iterations and Smoothed by LOESS Method

It should be noted that the recommendations regarding flow balancing proportional to 17 tributaries based on drainage area and using the LOESS smoothing technique were not part of the original methodology and performance criteria specified in the DWR-approved QAPP. During a meeting with DWR modeling staff and third-party reviewers funded by the NC Collaboratory (Nathan S. Hall and Daniel R. Obenour) on 11/30/2020, DWR contributed considerations for the development of these procedures. Based on a vote by email that closed on 1/4/2021, the MRSW voted to approve the DWR-recommended procedures used for balancing flows in the model. The third-party reviewers also agreed with these recommendations and provided some additional information on how to best determine the span.

6.3 Lake Stage Calibration

The hydrodynamic model was calibrated for the 2-year time period from January 1, 2015, to December 31, 2016. Figure 6-8 shows comparisons of the observed lake water surface elevation at USGS 02087183 (Falls Dam) and USGS 0208706575 (Beaverdam) and simulated water surface elevation extracted from grid cells at those locations. Water level data for the lake are based on the NAVD88 vertical datum in meters.

Simulated lake elevation is in good agreement with measured lake elevations for the 2-year calibration period. The simulated average stage was 76.540 m at Falls Dam, and 76.537 m at Beaverdam which is very close to the averaged observed stage of 76.541 m and 76.542 m, respectively. The calculated RMSE (see Eq. 2) was 0.279 m at Falls Dam, and 0.288 m at Beaverdam. The summary of the model performance statistics for the calibration period is given in Table 6-2.

As can be seen from Table 6-2, the stage calibration is slightly over the RSR target (see Eq. 3). The RSR target was 50% and the calculated RSR value was 50.91 % at Falls Dam, and 52.65 % at Beaverdam. There are several reasons why the calibration is above the RSR target including the following:

1- Lake's geometry: 64% of the watershed flow comes into the lake at 4 tributaries (Ellerbe Creek, Eno and Little Rivers, Flat River, and Knap of Reed Creek) that discharge at the upper part of the lake. Given that the flow is only apportioned to the small part of the drainage area downstream of these 4 tributaries, about 9% of the balance flow is given to these tributaries. The lake is about 30 miles long from the upper part (where those 4 tributaries discharge to the lake) to the forebay (USGS 02087183 at Falls Dam). Several causeways divide the lake into several segments, each having a narrow connection with the neighboring segment (I85, Cheek Rd, Hwy 50, Hwy 98, etc.). During high flow from the watershed or high dam discharge, these narrow connections create a stage difference throughout the lake from the upper part to the forebay.

2- Applying smoothing technique: During the low/high flow seasons, the direct balance flow adds/removes some amount of water to/from the model to maintain the balance in the stage. However, the positive/negative balance flow is filtered via LOESS method. As a result, rises/falls appear in the simulated stage, grow/decay over time and contribute to the overall stage difference. In other words, applying LOESS method makes less efficient use of balance flow data points that are supposed to satisfy the conservation of mass balance.

Table 6-2 Stage Calibration Statistics (NAVD88, m)

Station ID	Starting	Ending	# Pairs	Data Average (m)	Model Average (m)	R^2	RMSE (m)	RSR (%)	RE (%)	AE (m)	CE
USGS 02087183 at Falls Dam	1/1/2015	1/1/2017	2925	76.541	76.54	0.912	0.279	50.91	0.27	0.00	0.29
USGS 0208706575 at Beaverdam	1/1/2015	12/31/2016	2919	76.543	76.537	0.913	0.288	52.65	0.28	-0.01	0.27

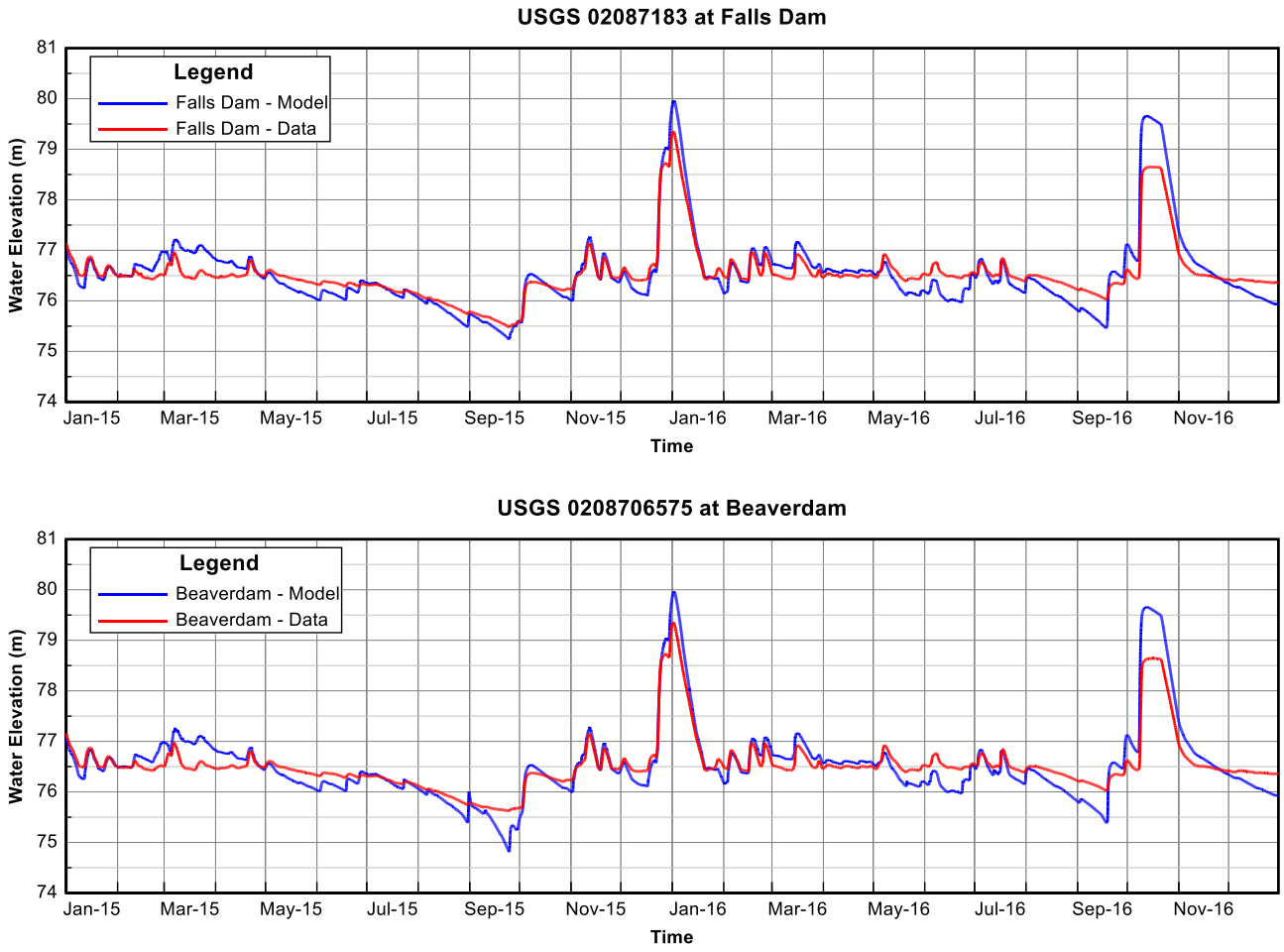

Figure 6-8 Comparison of Simulated and Observed Water Level during Jan. 2015 to Dec. 2016; Top: USGS 02087183 at Falls Dam, Bottom: USGS 0208706575 at Beaverdam

6.4 Lake Stage Validation

The Falls Lake EFDC model was validated for the 2-year time period from January 1, 2017, to December 31, 2018. The validation time series plots of surface water elevation at the two USGS stations (1) USGS 02087183 at Falls Dam and (2) USGS 0208706575 at Beaverdam are given in Figure 6-9. The summary of the model performance statistics between observed and simulated water surface elevation for the validation period is presented in Table 6-3.

Simulated water elevation at Falls Dam is in good agreement with the measured water elevation for the entire validation period. Simulated average stage was 76.486 m at Falls Dam and 76.540 m at Beaverdam which is relatively close to the averaged observed stage of 76.506 m and 76.532 m, respectively. The calculated RMSE (see Eq. 2) was 0.347 m at Falls Dam and 0.327 m at Beaverdam. The RSR (see Eq. 3) was 45.72 % at Falls Dam and 45.35 % at Beaverdam. The summary of model performance statistics for the validation period is presented in Table 6-3.

Table 6-3 Stage Validation Statistics (NAVD88, m)

Station ID	Starting	Ending	# Pairs	Data Average (m)	Model Average (m)	R^2	RMSE (m)	RSR (%)	RE (%)	AE (m)	CE
USGS 02087183 at Falls Dam	1/1/2017	12/31/2018	2917	76.506	76.486	0.914	0.347	45.72	0.38	-0.02	0.41
USGS 0208706575 at Beaverdam	1/1/2017	12/31/2018	2861	76.531	76.54	0.899	0.327	45.35	0.35	0.01	0.43

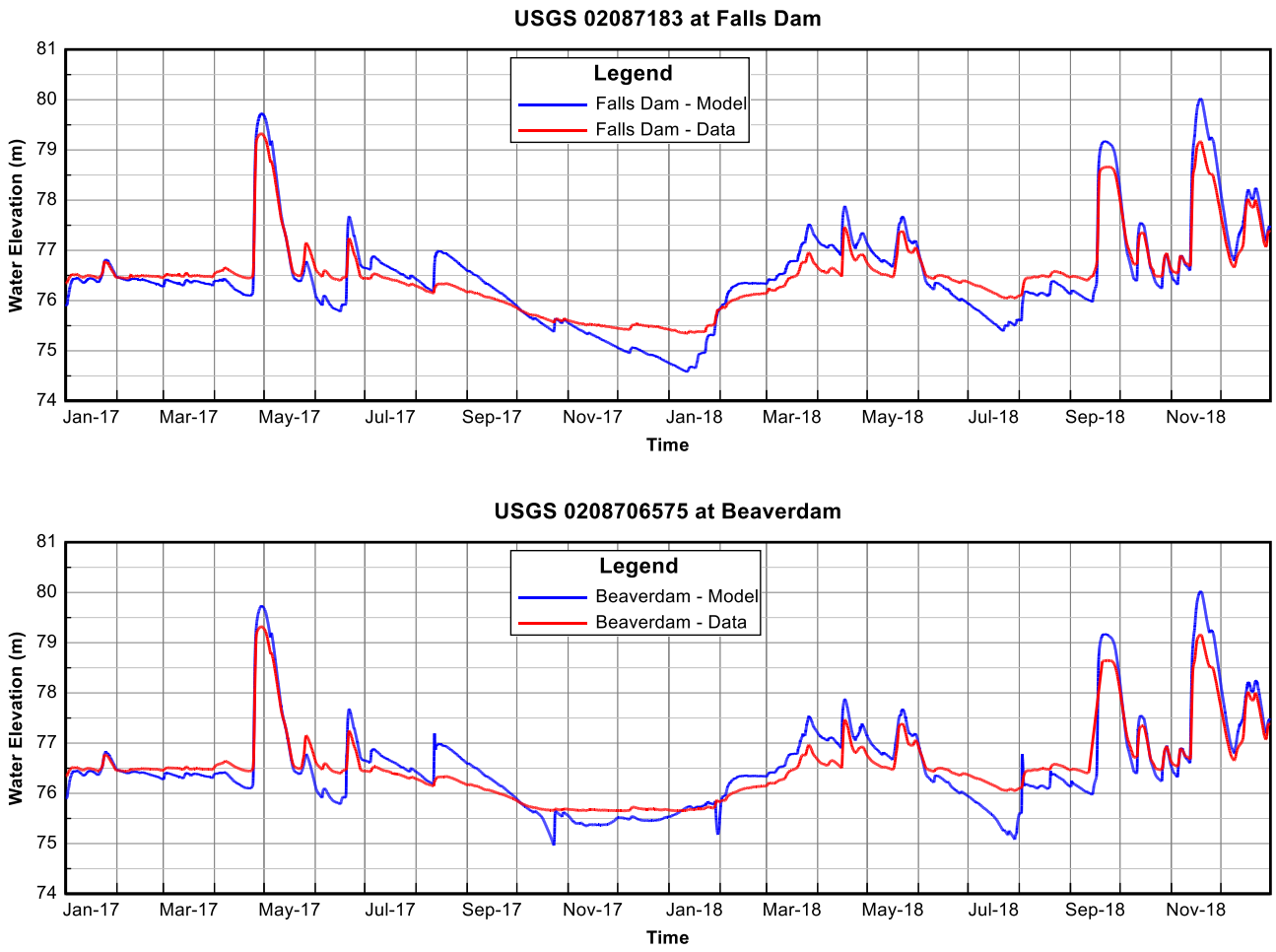

Figure 6-9 Comparison of Simulated and Observed Water Level during Jan. 2017 to Dec. 2018; Top: USGS 02087183 at Falls Dam, Bottom: USGS 0208706575 at Beaverdam

The calculated RSR values for calibration period (50.91 - 52.65 %) are slightly above the defined model performance target of 50%. For validation period (45.72 % - 45.35 %) are well within the defined model performance target. While accurate simulation of water levels is important, the major focus of this model is the prediction of water quality.

6.5 Discharge Model-Data Comparison

To evaluate the hydrodynamic model's performance for simulating discharge, a model-data comparison of discharge was performed. Discharge data was available from the constriction point sampling study conducted by UNRBA (Cardno, 2016). The study provided data collected during Jan 2016 and Oct 2016 at two locations: (1) Hwy50 (Highway 50) and (2) I85 (Interstate 85). The locations of the discharge measurements are shown in Figure 6-10. Figure 6-11 shows the model-data comparison of discharge simulated during 2016. The model results follow the trend of the data very well at Hwy50 and at I85 during Jan 2016. During Oct 2016, however, the model results underestimate the observed data at I85 which indicates an underestimate of flow generated by the watershed model simulation. Hurricane Matthew occurred in October 2016 and delivered up to ten inches of rain in some parts of the watershed.

The summary of model performance statistics between observed and simulated discharge is given in Table 6-4.

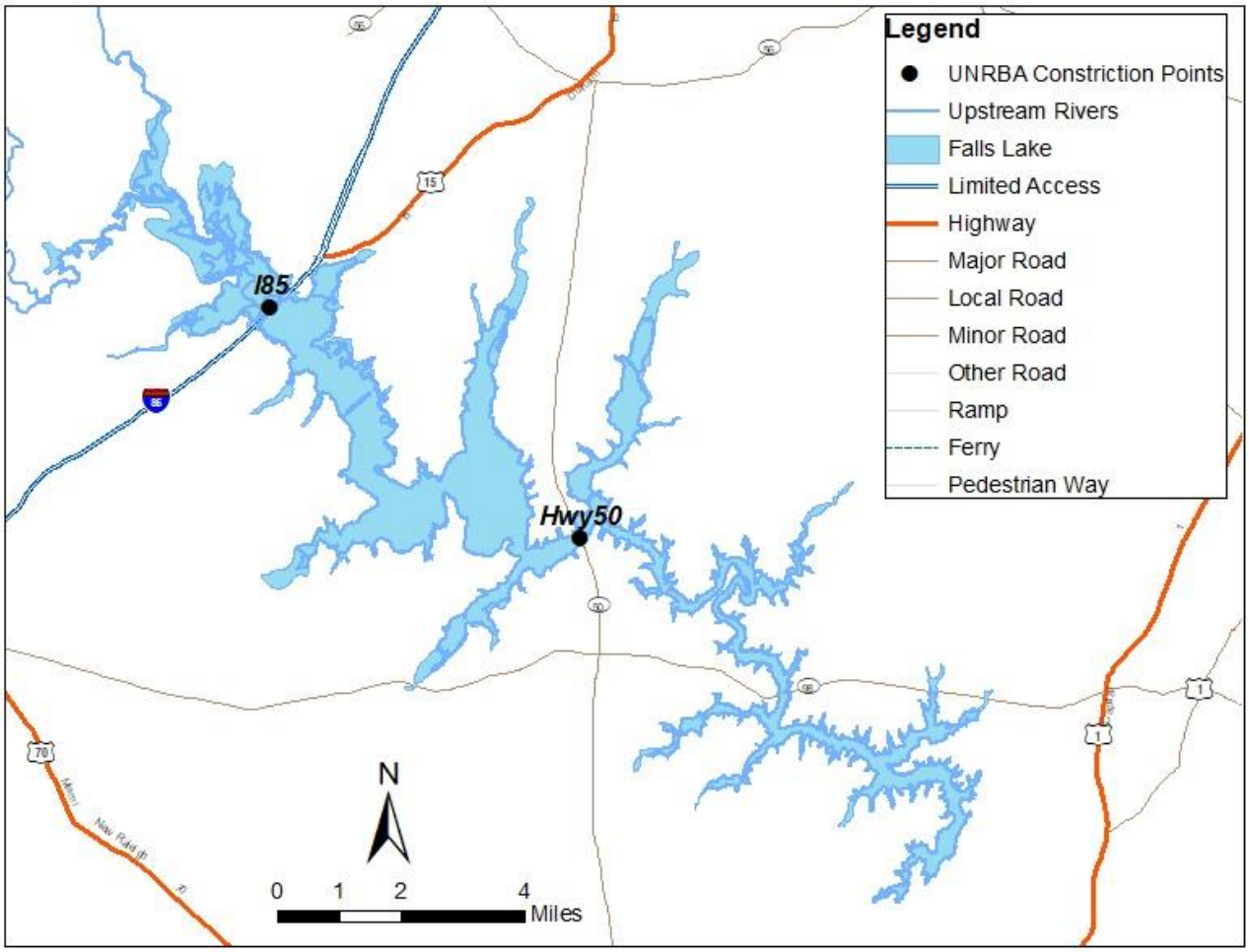

Figure 6-10 Locations of the Discharge Measurements (Adopted from the Constriction Point Sampling Study Conducted by UNRBA)

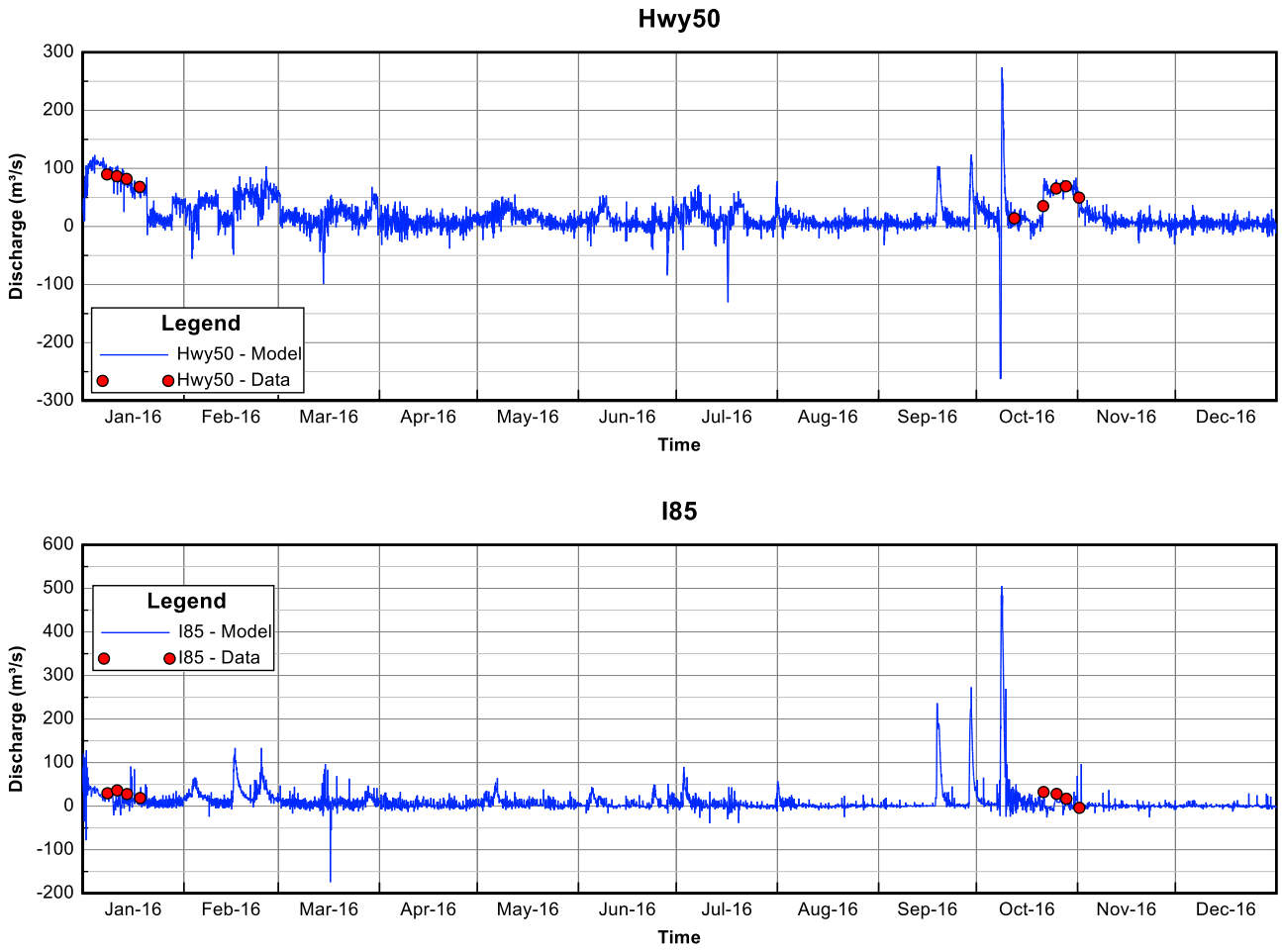

Figure 6-11 Model-Data Comparison of Discharge during Jan-2016 to Oct-2016

Table 6-4 Discharge Model-Data Comparison Statistics

Station ID	Starting	Ending	# Pairs	Data Average (m^3/s)	Model Average (m^3/s)	R^2	RMSE (m^3/s)	RE (%)	AE (m^3/s)	CE
Hwy50	1/8/2016	11/1/2016	9	62.182	61.839	0.926	9.122	12.304	-0.343	0.608
I85	1/8/2016	11/1/2016	8	23.263	10.842	0.285	16.107	62.81	-12.422	-0.546

7. Water Temperature Model Calibration and Validation

Prior to model calibration, a one-year model spin-up run was conducted to eliminate the impact of the initial conditions of water temperature on model results. Calibration of the lake model for water temperature is demonstrated with model-data comparisons as station time series and as vertical profiles for sampling date “snapshots”.

Observed data collected near the surface is compared to lake model results for the EFDC surface layer (k=10) and data collected near the bottom is compared to model results for the EFDC bottom layer. For the stations located in the shallower parts of the lake, the EFDC bottom layer is the number of sigma zed vertical layers prescribed for those stations subtracted from 10 (k=10 - # sigma zed layers). It should also be noted that at some of the stations located in the deeper parts of the lake (specially in the riverine section) there is a lack of observed data at the bottom (near the sediment bed). To this end, the EFDC bottom layer is defined as the lowest layer where there is the most observed data available. Table 7-1 lists the EFDC surface and bottom layers used for water temperature calibration and validation.

Station results are presented in this section to show model calibration and validation for the twelve (12) DWR stations in Falls Lake. The station-ID’s and location descriptions of the model calibration and validation stations are listed in Table 4-1.

Table 7-1 EFDC Surface and Bottom Layers Used for Water Temperature Model Calibration/Validation

Station Code	Location Description	Surface layer #	Bottom layer #
LC01	In the Ledge Creek arm	10	6
LI01	In the Lick Creek arm	10	5
LLC01	Downstream of Little Lick Creek	10	6
NEU013	Upstream of I-85	10	7
NEU013B	Downstream of I-85	10	7
NEU0171B	Between Little Lick and Ledge Creeks	10	7
NEU018C	Downstream of Ledge Creek	10	7
NEU018E	Upstream of Lick Creek	10	5
NEU019E	Downstream of Beaverdam Impoundment	10	5
NEU019L	Downstream of New Light Creek	10	2
NEU019P	At Hwy 98 (Durham Road)	10	1
NEU020D	Upstream of dam	10	1

7.1 Water Temperature Calibration

Systematic procedures used to calibrate the water temperature model included: (1) check the sub-watershed and grid cell linkage between WARMF and EFDC; (2) check the meteorological data to make sure the solar radiation data are in a reasonable range; and (3) adjust key parameters within reasonable ranges to best match the observed water temperature data.

Modeled water temperature results are presented for comparison to the observed data for the top and bottom layers (Table 7-1). Water temperature calibration plots for stations NEU013B and NEU019P are shown in Figure 7-1 and Figure 7-2, respectively. Station NEU013B is located in the shallow upper part of the lake where water column is typically well-mixed, whereas station NEU019P is located in the deep part of the lake where water column is typically stratified during summer time. Water temperature calibration time series for the other ten (10) stations are presented in Appendix A.2. Model performance statistics for water temperature calibration for all stations are presented in Table 7-2.

As can be seen in the model-data plots, the model results for the surface and bottom layers are in good agreement with the measured water temperature during the 2015-2016 calibration period. Modeled water temperature closely followed seasonal trends of the observed data for both the surface and bottom layers. The results for Station NEU019P demonstrate good agreement with the seasonal cycle for the onset and erosion of stratification of the water column at this station.

The calculated RMSEs ranged from 0.77 ºC at the surface layer for station NEU013B to 1.96 ºC at the bottom layer for station NEU020D as shown in Table 7-2. The calculated RSRs ranged from 9.06 % at the surface layer for station NEU013B to 44.34 % at the bottom layer for station NEU019P. Considering that the model results are well within the defined RSR model performance target of 50 % for water temperature, the model performance results for water temperature are deemed to be acceptable.

The calculated pBias ranged from -8.43 % for at the bottom layer for station NEU013 to + 5.40 % at the surface layer for station NEU020D. This indicates that there is no systematic over or under prediction during the calibration period. The temperature difference between the surface and bottom observed and modeled temperature at each station is presented as the parameter ΔT, calculated by taking the average of the water temperature observations and model results during the period of seasonal stratification from May to Oct. Good agreement between the ΔT values for observed water temperature data and model results indicates that the model results are consistent with water temperature observations collected during May through Oct. The model results suggest that the EFDC hydrodynamic model accurately represents the physical processes that control the seasonal cycles leading to the onset and erosion of water column stratification.

Table 7-2 Calibration Statistics for Water Temperature

Station ID	Starting	Ending	Layer	# Pairs	Data Average (°C)	Model Average (°C)	R^2	RMSE (°C)	RSR (%)	RE (%)	AE (°C)	CE	pBias (%)	ΔT*	
LC01	1/6/2015	12/14/2016	*Top*	23	18.66	19.16	0.99	0.93	11	3.79	0.50	0.91	2.66	*Data*	1.16
			Bottom	23	17.79	17.82	0.99	0.96	12	4.47	0.03	0.89	0.16	*Model*	2.13
LI01	1/6/2015	12/14/2016	*Top*	23	19.32	19.50	0.99	0.89	11	3.70	0.18	0.90	0.92	*Data*	2.13
			Bottom	20	16.65	16.46	0.99	0.95	13	4.77	-0.19	0.87	-1.14	*Model*	2.99
LLC01	1/6/2015	12/14/2016	*Top*	24	18.47	18.94	0.99	1.00	12	4.07	0.47	0.90	2.55	*Data*	1.27
			Bottom	24	17.66	17.56	0.99	0.87	11	4.03	-0.10	0.90	-0.57	*Model*	2.36
NEU013	1/6/2015	12/14/2016	*Top*	24	18.39	18.27	0.99	0.98	11	4.34	-0.12	0.90	-0.66	*Data*	1.66
			Bottom	12	17.29	15.84	0.98	1.87	24	8.43	-1.46	0.80	-8.43	*Model*	3.50
NEU013B	1/6/2015	11/16/2016	*Top*	23	18.93	18.94	0.99	0.77	9	2.99	0.01	0.93	0.04	*Data*	1.64
			Bottom	14	18.41	17.91	1.00	0.74	10	2.92	-0.50	0.92	-2.73	*Model*	2.49
NEU0171B	2/3/2015	12/14/2016	*Top*	23	18.96	19.26	0.99	0.91	11	3.81	0.29	0.90	1.54	*Data*	1.56
			Bottom	17	16.83	17.17	0.99	0.89	12	4.53	0.33	0.88	1.98	*Model*	1.44
NEU018C	1/6/2015	12/14/2016	*Top*	24	18.65	19.03	0.99	0.89	11	4.03	0.38	0.90	2.04	*Data*	1.17
			Bottom	19	17.85	17.76	1.00	0.90	10	3.90	-0.09	0.91	-0.52	*Model*	2.19
NEU018E	1/6/2015	12/14/2016	*Top*	24	18.81	19.02	0.99	0.87	10	3.86	0.22	0.90	1.14	*Data*	2.68
			Bottom	10	14.34	14.54	0.97	1.40	18	7.75	0.20	0.84	1.38	*Model*	2.06
NEU019E	1/6/2015	12/14/2016	*Top*	24	19.00	19.14	0.99	0.82	10	3.79	0.14	0.90	0.76	*Data*	2.77
			Bottom	20	16.05	15.59	0.98	1.38	19	6.63	-0.46	0.83	-2.85	*Model*	4.56
NEU019L	1/6/2015	12/14/2016	*Top*	23	19.86	20.44	0.99	1.03	12	4.28	0.57	0.89	2.88	*Data*	8.77
			Bottom	13	13.81	14.07	0.88	1.45	35	8.11	0.26	0.70	1.91	*Model*	9.53
NEU019P	1/6/2015	12/14/2016	*Top*	24	19.49	20.43	0.99	1.34	16	5.59	0.94	0.85	4.84	*Data*	9.06
			Bottom	14	14.71	14.57	0.82	1.76	44	8.49	-0.14	0.62	-0.92	*Model*	10.62
NEU020D	1/6/2015	12/14/2016	*Top*	24	19.51	20.56	0.99	1.35	16	5.95	1.05	0.84	5.40	*Data*	8.75
			Bottom	19	14.74	15.17	0.86	1.96	41	9.73	0.43	0.64	2.93	*Model*	9.27

*$\Delta T = T_{Top} - T_{Bottom}$ for the Stratification Period (May - Oct)

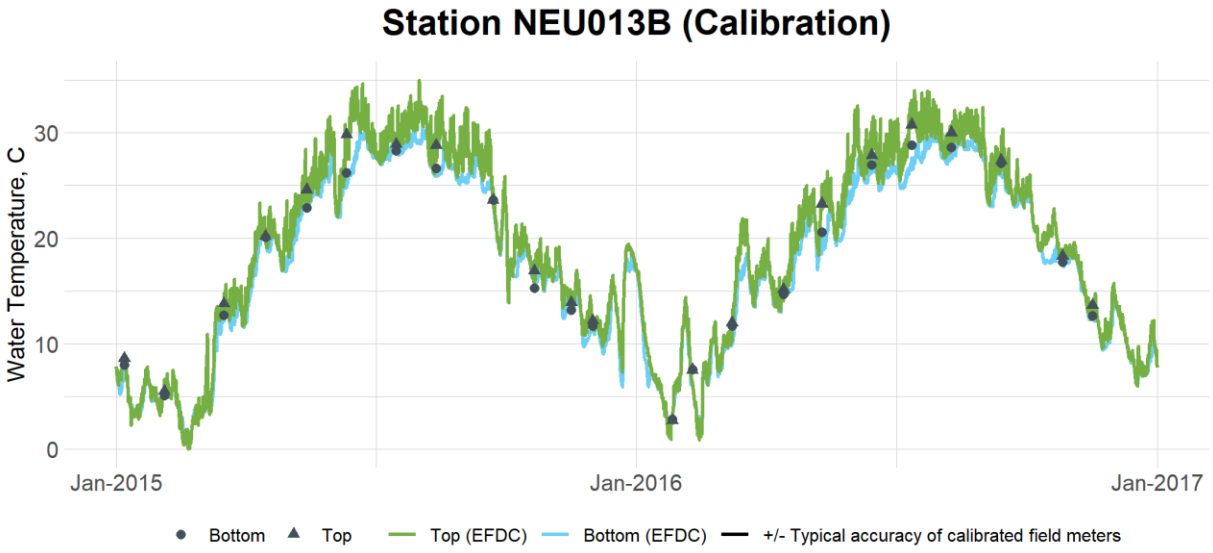

Figure 7-1 Calibration Plot of Top and Bottom Water Temperature at Station NEU013B

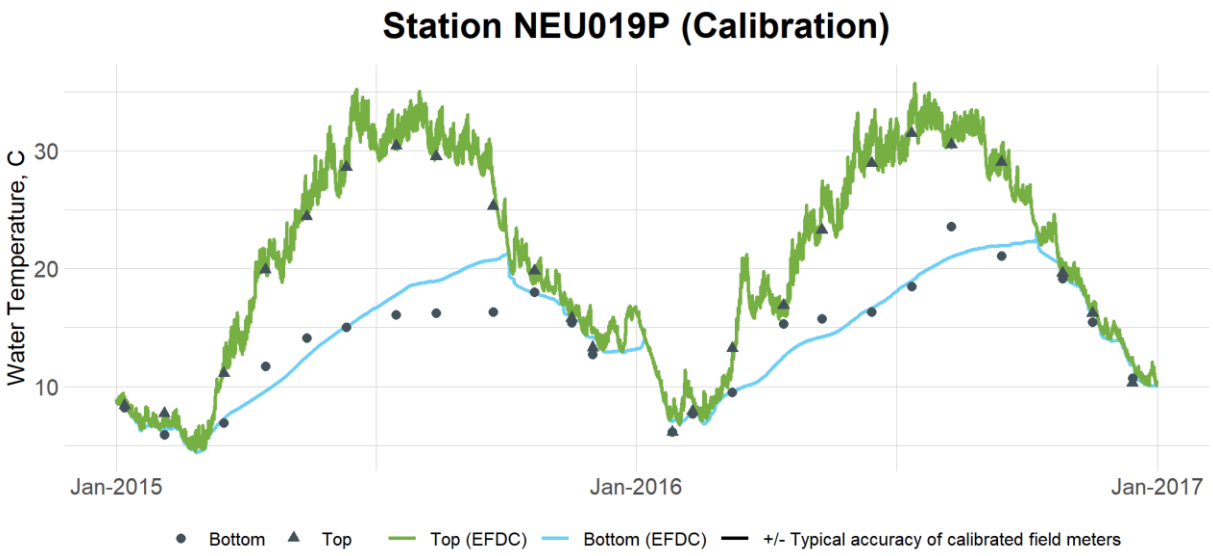

Figure 7-2 Calibration Plot of Top and Bottom Water Temperature at Station NEU019P

7.2 Water Temperature Validation

Water temperature validation time series for stations NEU013B and NEU019P are shown in Figure 7-3 and Figure 7-4, respectively, while the validation plots for water temperature for the other ten (10) stations are presented in Appendix A.2. Validation statistics for water temperature for all stations are presented in Table 7-3. As can be seen in the model-data plots,

the model results for the surface and bottom layers are in good agreement with the measured water temperature for the 2017-2018 validation period with modeled water temperature closely following the seasonal trends of the observed data.

The calculated RMSEs ranged from 0.95 ºC at the bottom layer for station NEU018C to 2.49 ºC at the bottom layer for station NEU019L as shown in Table 7-3. The calculated RSRs ranged from 12.02 % at the bottom layer for station NEU018C to 43.61 % at the bottom layer for station NEU019L. Considering that the model results are well within the defined RSR model performance target of 50% for water temperature, the results for validation of the water temperature model are deemed to be acceptable.

The calculated pBias values ranged from -9.20 % for the bottom layer for station NEU019P to +7.73 % for the surface layer for station NEU020D. This indicates that there is no systematic over or under prediction during the validation period. Comparison between the ΔT values based on the observed water temperature data and model results indicates that the model results show good agreement with the seasonal pattern of observed stratification.

Table 7-3 Validation Statistics for Water Temperature

Station ID	Starting	Ending	Layer	# Pairs	Data Average (°C)	Model Average (°C)	R^2	RMSE (°C)	RSR (%)	RE (%)	AE (°C)	CE	pBias (%)	ΔT*	
LC01	1/18/2017	10/25/2018	*Top*	21	19.32	19.22	0.97	1.63	20	6.17	-0.10	0.84	-0.51	*Data*	0.98
			Bottom	20	18.11	17.54	0.98	1.24	15	5.20	-0.56	0.87	-3.11	*Model*	1.68
LI01	1/18/2017	10/25/2018	*Top*	21	19.35	18.91	0.98	1.35	16	6.20	-0.44	0.84	-2.28	*Data*	1.81
			Bottom	15	18.22	17.35	0.99	1.32	16	6.15	-0.87	0.84	-4.79	*Model*	2.92
LLC01	1/18/2017	10/25/2018	*Top*	21	19.26	18.92	0.98	1.32	15	5.67	-0.34	0.86	-1.79	*Data*	1.52
			Bottom	19	18.19	17.59	0.99	1.10	14	4.85	-0.60	0.88	-3.27	*Model*	1.97
NEU013	1/19/2017	10/25/2018	*Top*	19	19.22	18.05	0.96	2.20	26	8.24	-1.17	0.78	-6.07	*Data*	1.33
			Bottom	14	18.77	17.25	0.97	2.05	26	9.25	-1.52	0.75	-8.11	*Model*	2.18
NEU013B	1/18/2017	10/25/2018	*Top*	20	19.71	19.17	0.97	1.73	20	6.77	-0.54	0.83	-2.72	*Data*	1.08
			Bottom	13	16.46	15.63	0.98	1.46	19	7.73	-0.83	0.81	-5.03	*Model*	1.38
NEU0171B	1/18/2017	10/25/2018	*Top*	21	19.26	19.26	0.98	1.30	15	5.38	-0.01	0.87	-0.04	*Data*	1.25
			Bottom	12	16.02	15.67	0.99	1.17	13	5.96	-0.35	0.89	-2.19	*Model*	1.81
NEU018C	1/18/2017	10/25/2018	*Top*	21	19.37	19.22	0.97	1.39	17	5.37	-0.16	0.86	-0.80	*Data*	1.24
			Bottom	16	18.80	18.64	0.99	0.95	12	3.88	-0.16	0.90	-0.85	*Model*	1.77
NEU018E	1/18/2017	10/25/2018	*Top*	20	19.36	19.45	0.98	1.17	14	4.85	0.10	0.88	0.49	*Data*	2.34
			Bottom	13	17.34	16.12	0.99	2.00	23	9.10	-1.22	0.80	-7.06	*Model*	5.00
NEU019E	1/18/2017	10/25/2018	*Top*	19	20.38	20.04	0.97	1.50	18	6.12	-0.34	0.82	-1.67	*Data*	1.89
			Bottom	15	18.83	17.79	0.98	1.70	23	7.29	-1.04	0.79	-5.54	*Model*	3.37
NEU019L	1/18/2017	10/25/2018	*Top*	18	19.59	20.13	0.97	1.64	20	6.14	0.54	0.83	2.77	*Data*	3.52
			Bottom	8	18.94	17.43	0.89	2.49	44	9.66	-1.50	0.63	-7.94	*Model*	6.23
NEU019P	2/7/2017	10/25/2018	*Top*	18	20.13	21.05	0.98	1.67	20	5.96	0.92	0.83	4.58	*Data*	3.08
			Bottom	8	16.51	14.99	0.91	2.44	39	11.37	-1.52	0.66	-9.20	*Model*	5.58
NEU020D	1/18/2017	10/25/2018	*Top*	17	19.37	20.87	0.96	2.30	28	8.34	1.50	0.77	7.73	*Data*	3.13
			Bottom	9	15.59	14.86	0.96	1.55	24	7.14	-0.73	0.82	-4.70	*Model*	5.19

*$\Delta T = T_{Top} - T_{Bottom}$ for the Stratification Period (May - Oct)

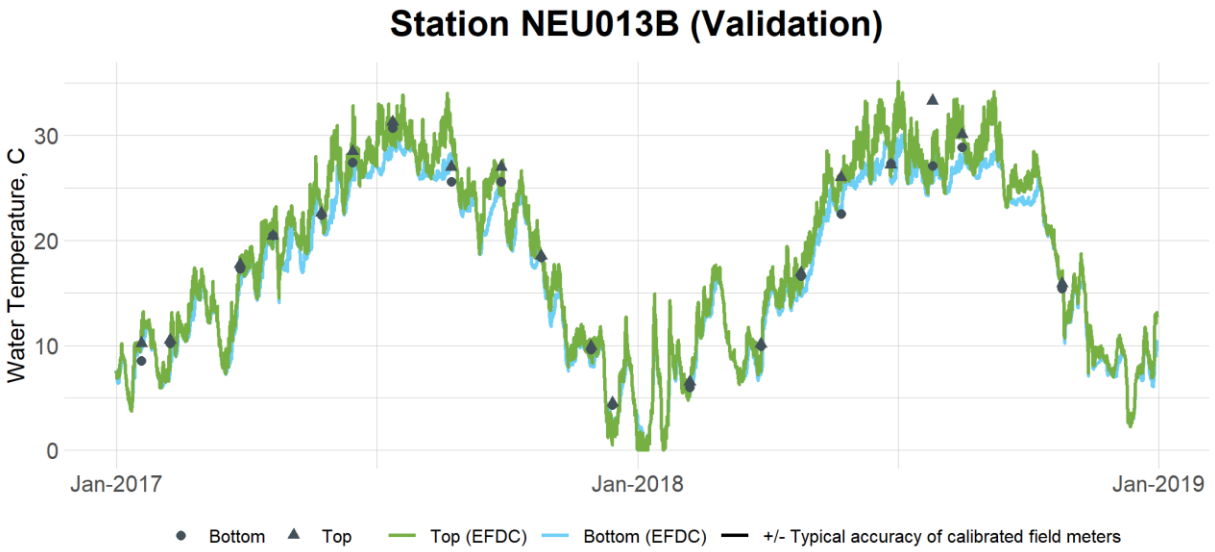

Figure 7-3 Validation Plot of Top and Bottom Water Temperature at Station NEU013B

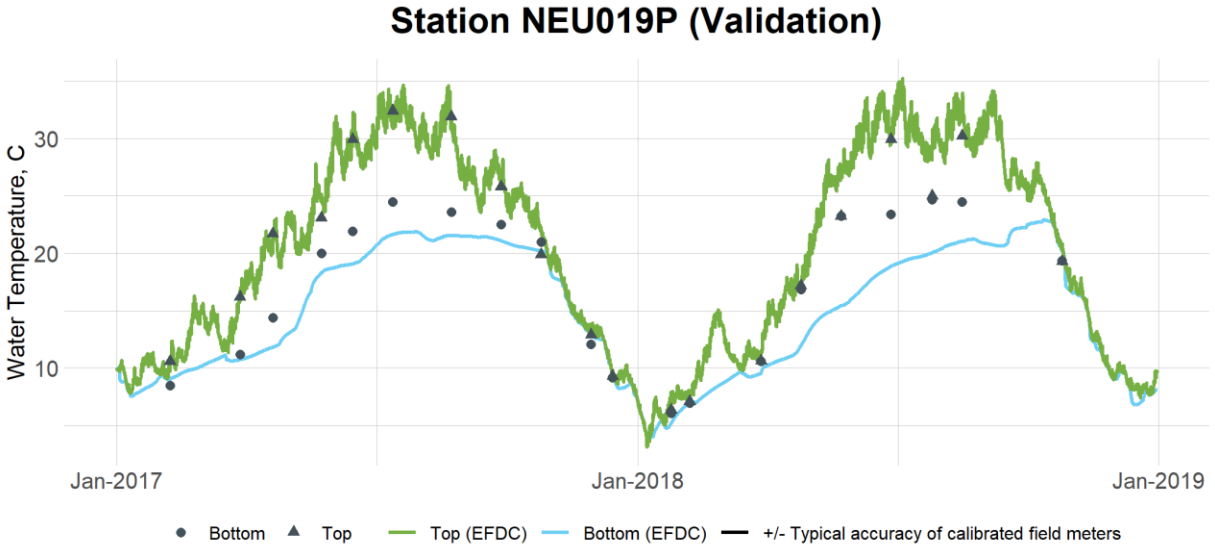

Figure 7-4 Validation Plot of Top and Bottom Water Temperature at Station NEU019P

7.3 Vertical Profiles

Comparisons of water temperature vertical profiles for stations NEU013B and NEU019P are given in Figure 7-5 and Figure 7-6, respectively. The observed water temperature data are shown with solid red dots, and the model results are depicted with the blue continuous line. Water temperature vertical profiles for the other ten (10) stations are presented in Appendix A.3. Model results are extracted as "snapshots for a time interval of the simulation that matches the observed sampling date/time records for the temperature profile. As can be seen in these model-data vertical profile plots, the modeled water temperature profile closely followed the vertical profile of the observed water temperature data in most cases.

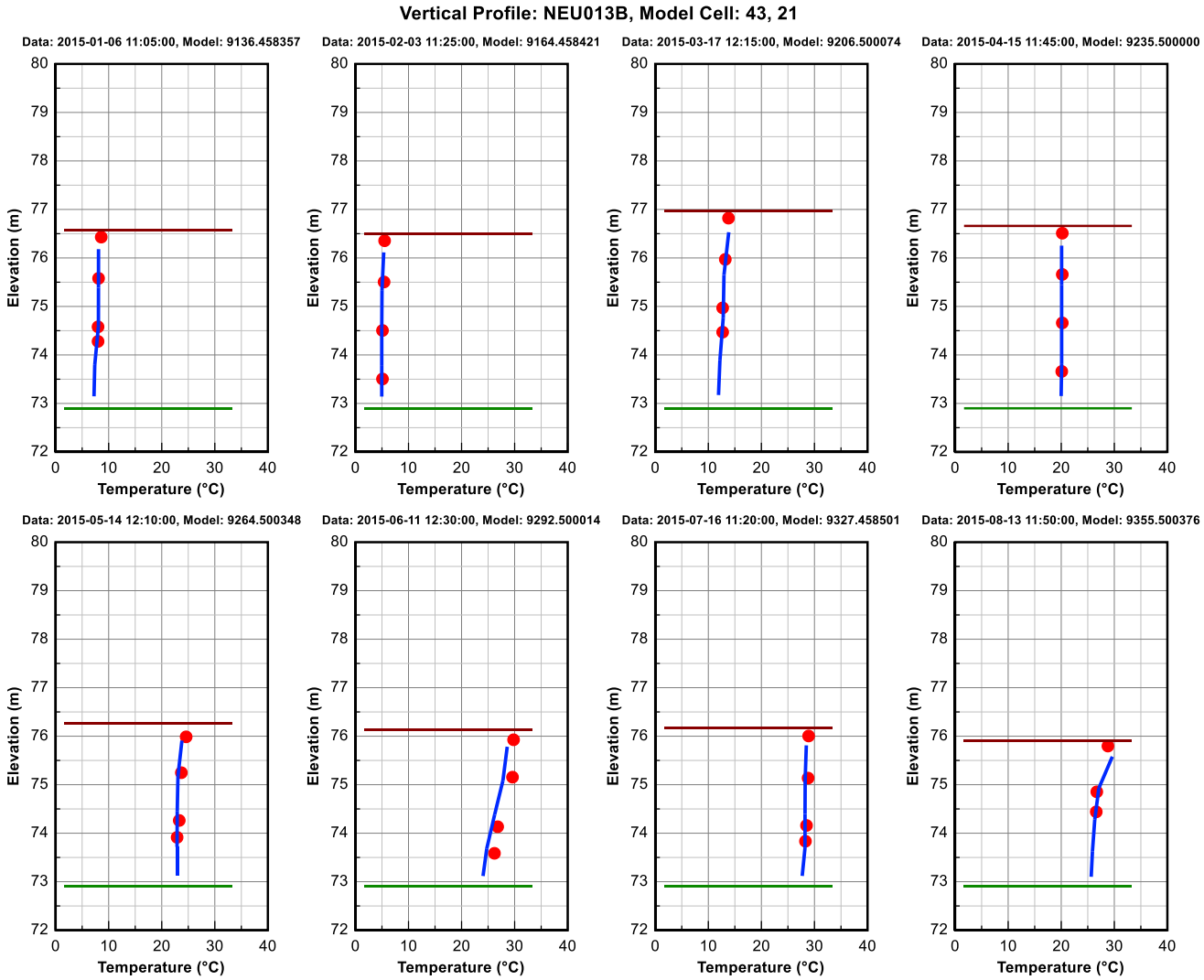

January 2015 – August 2015 (1 of 6)

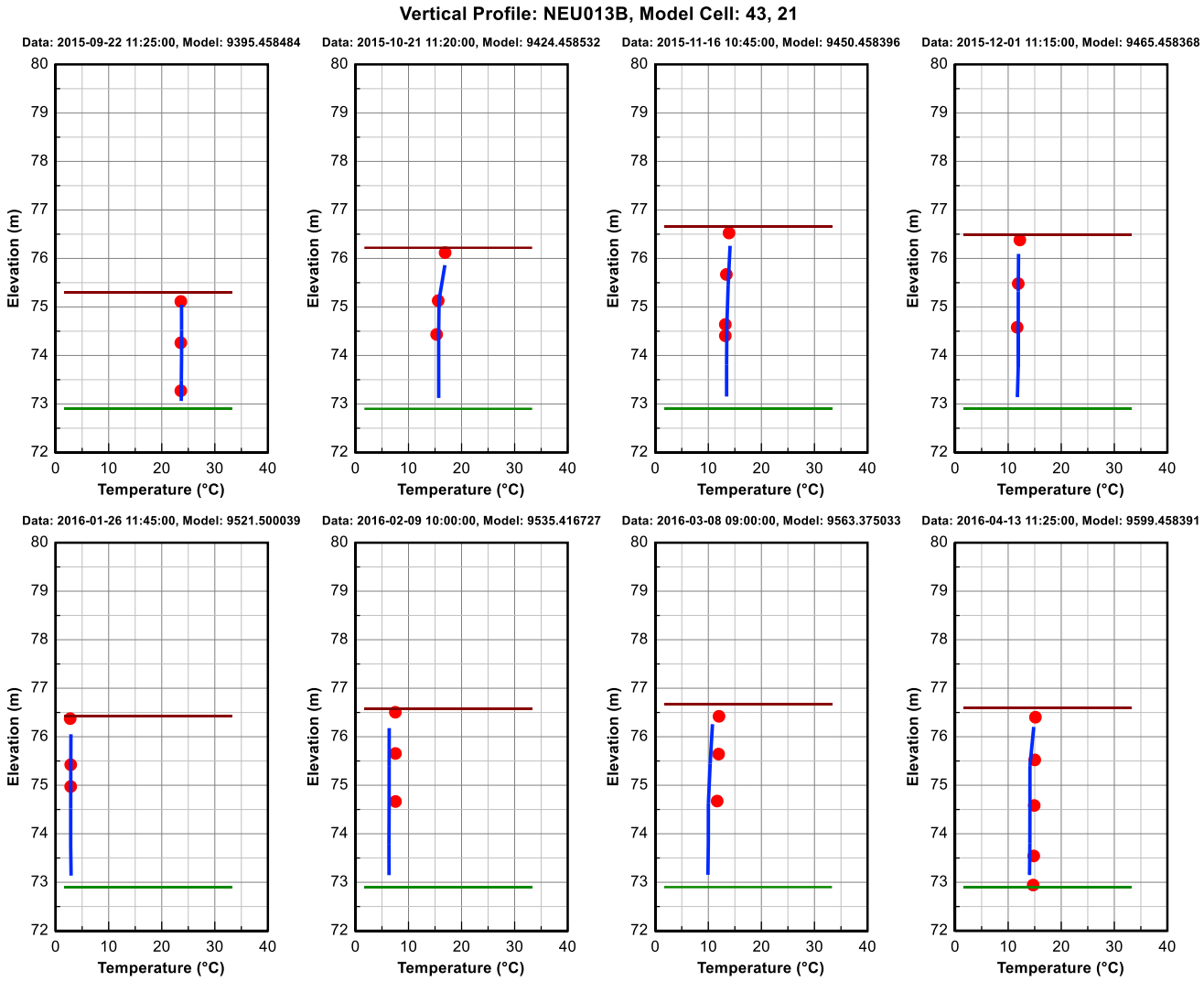

September 2015 – April 2016 (2 of 6)

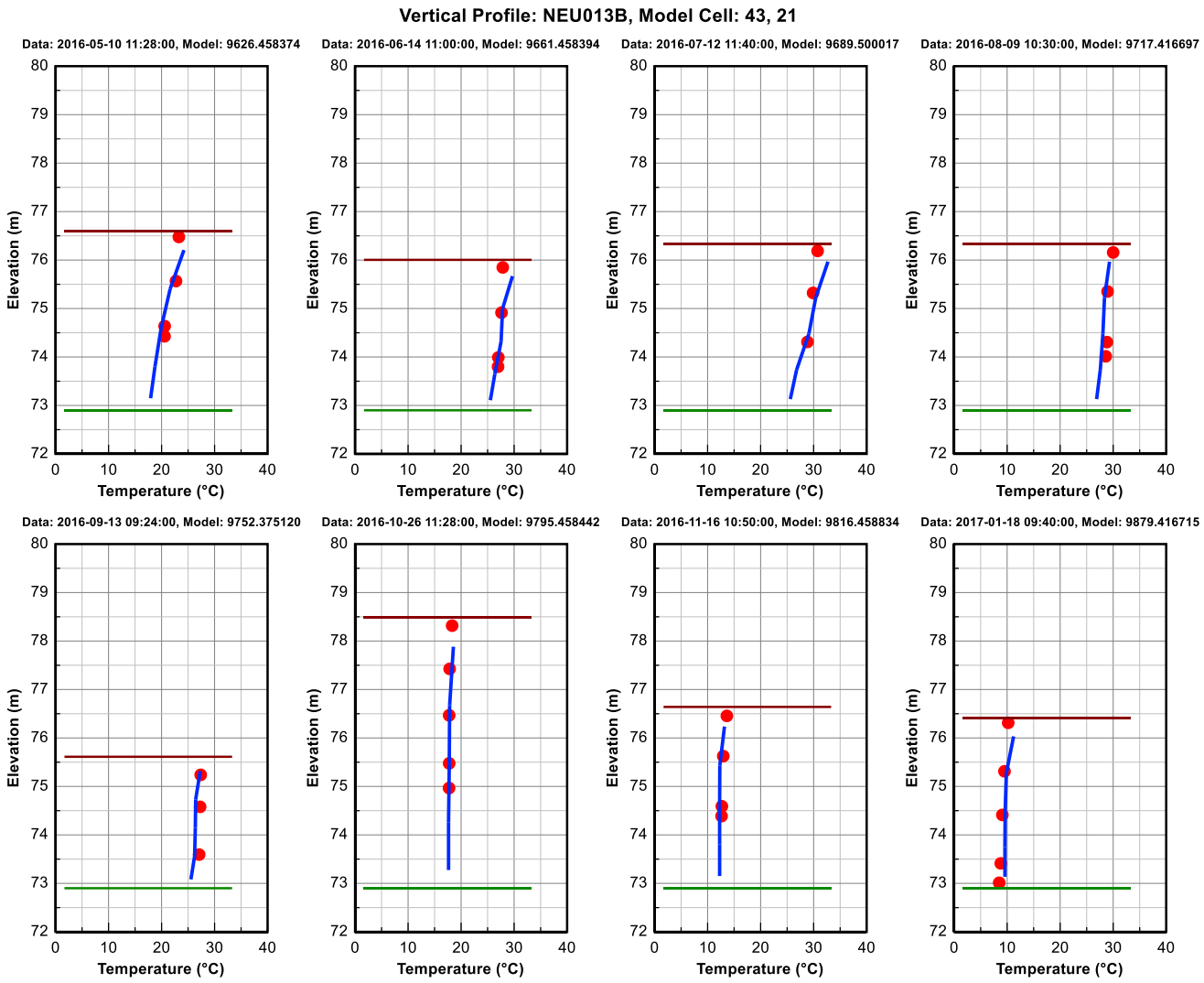

May 2016 – January 2017 (3 of 6)

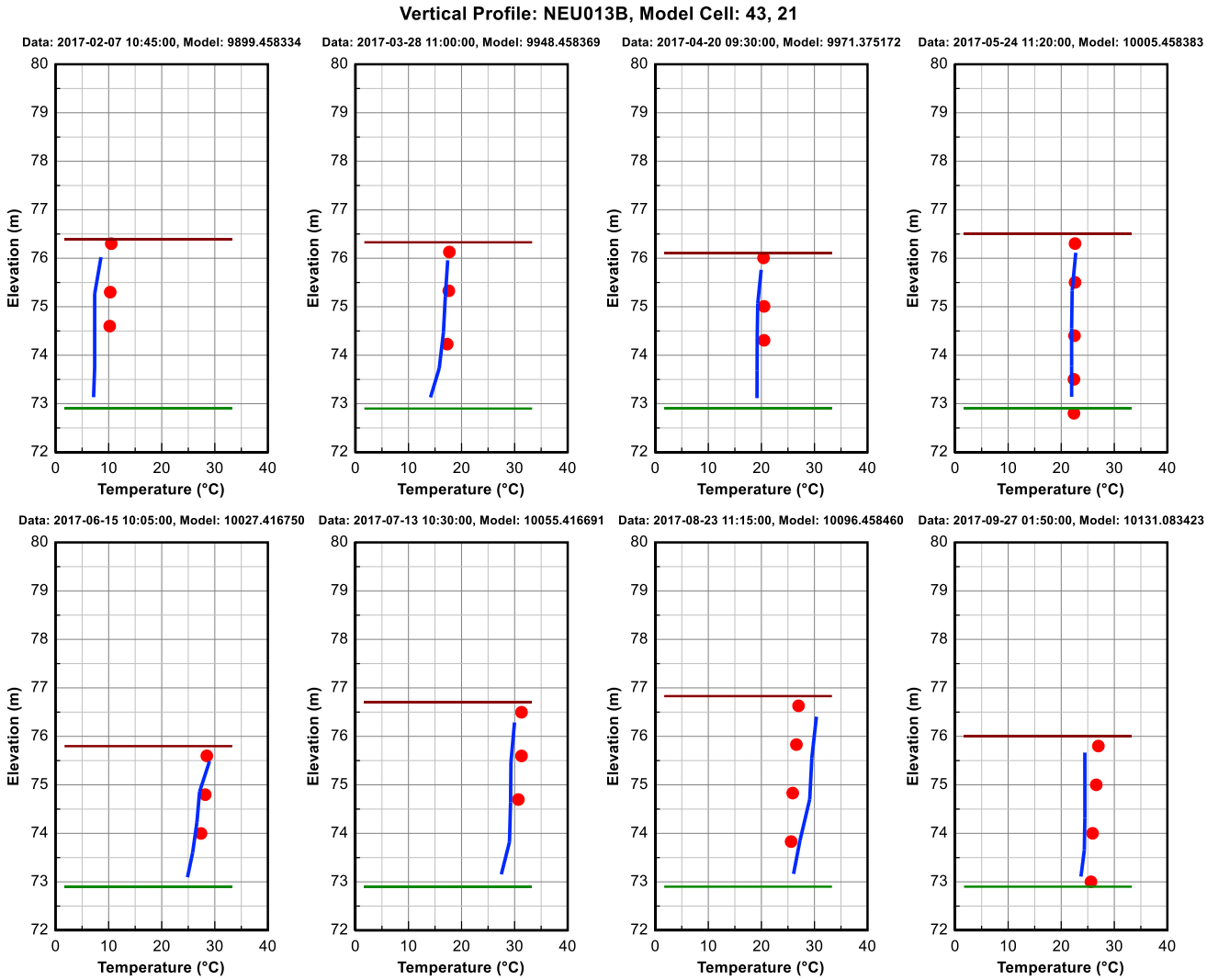

February 2017 – September 2017 (4 of 6)

Vertical Profile: NEU013B, Model Cell: 43, 21

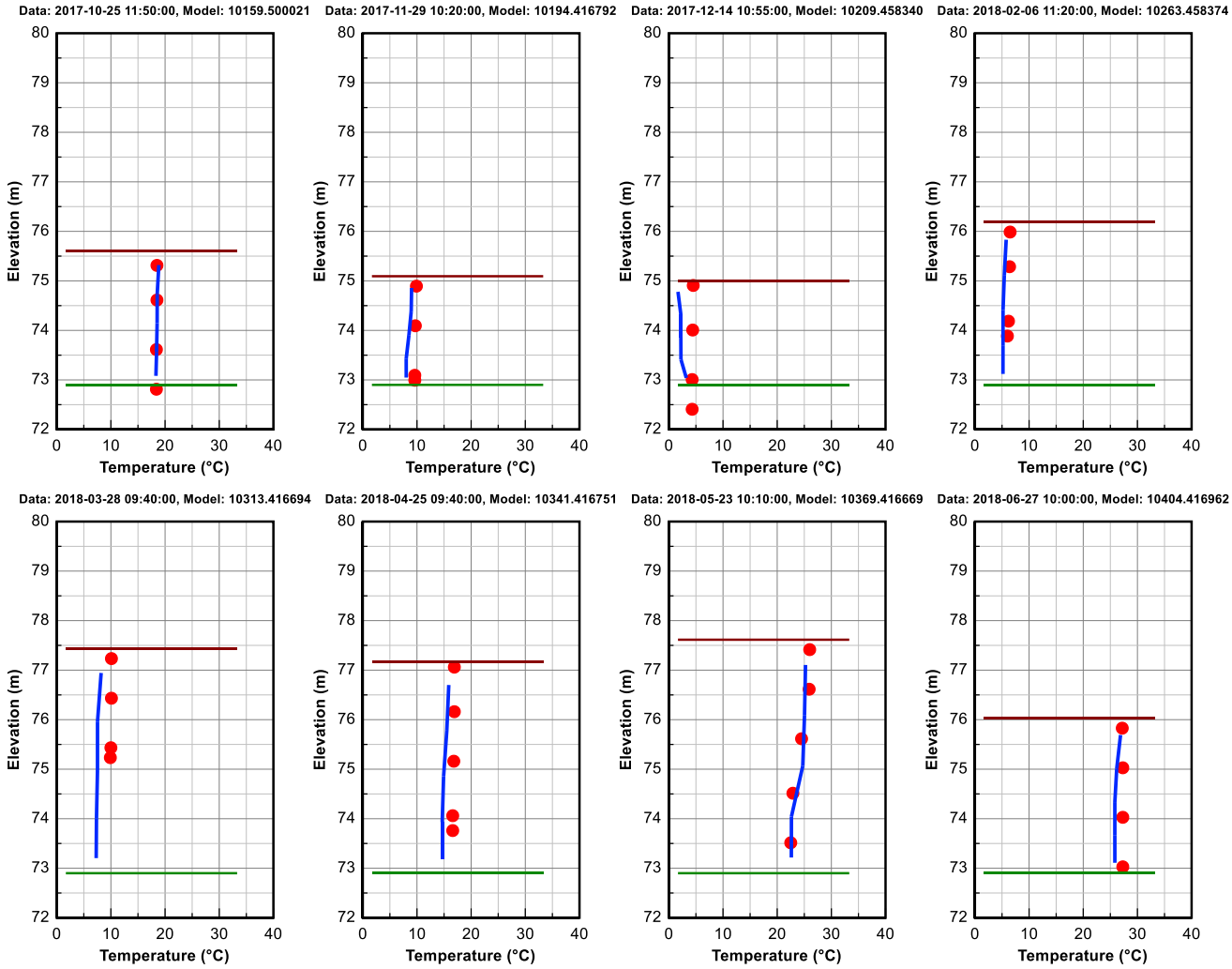

October 2017 – June 2018 (5 of 6)

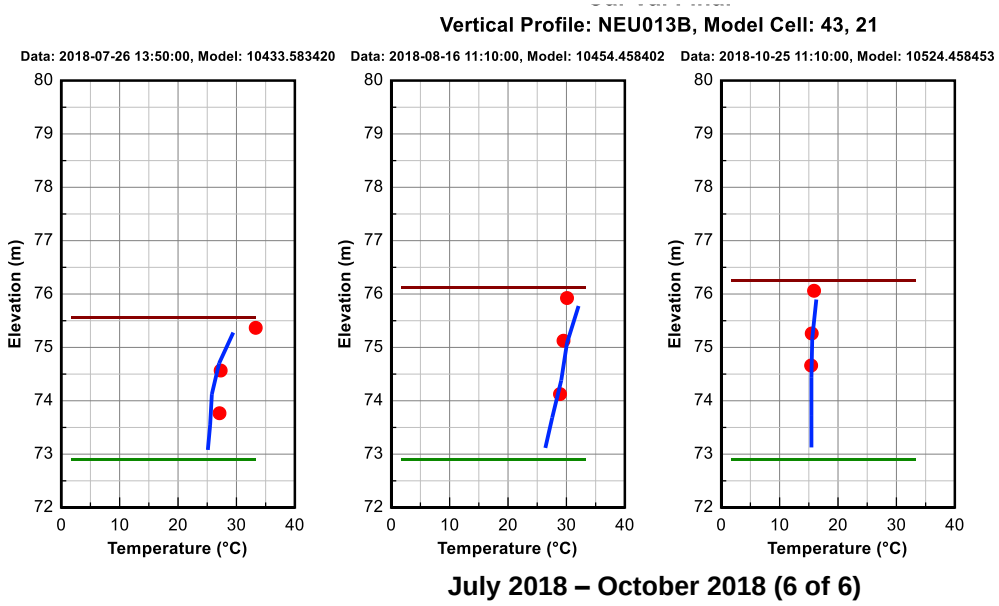

Figure 7-5 Water Temperature Vertical Profile Comparison Plot at Station NEU013B. Red dots are data, and blue continuous lines are model results.

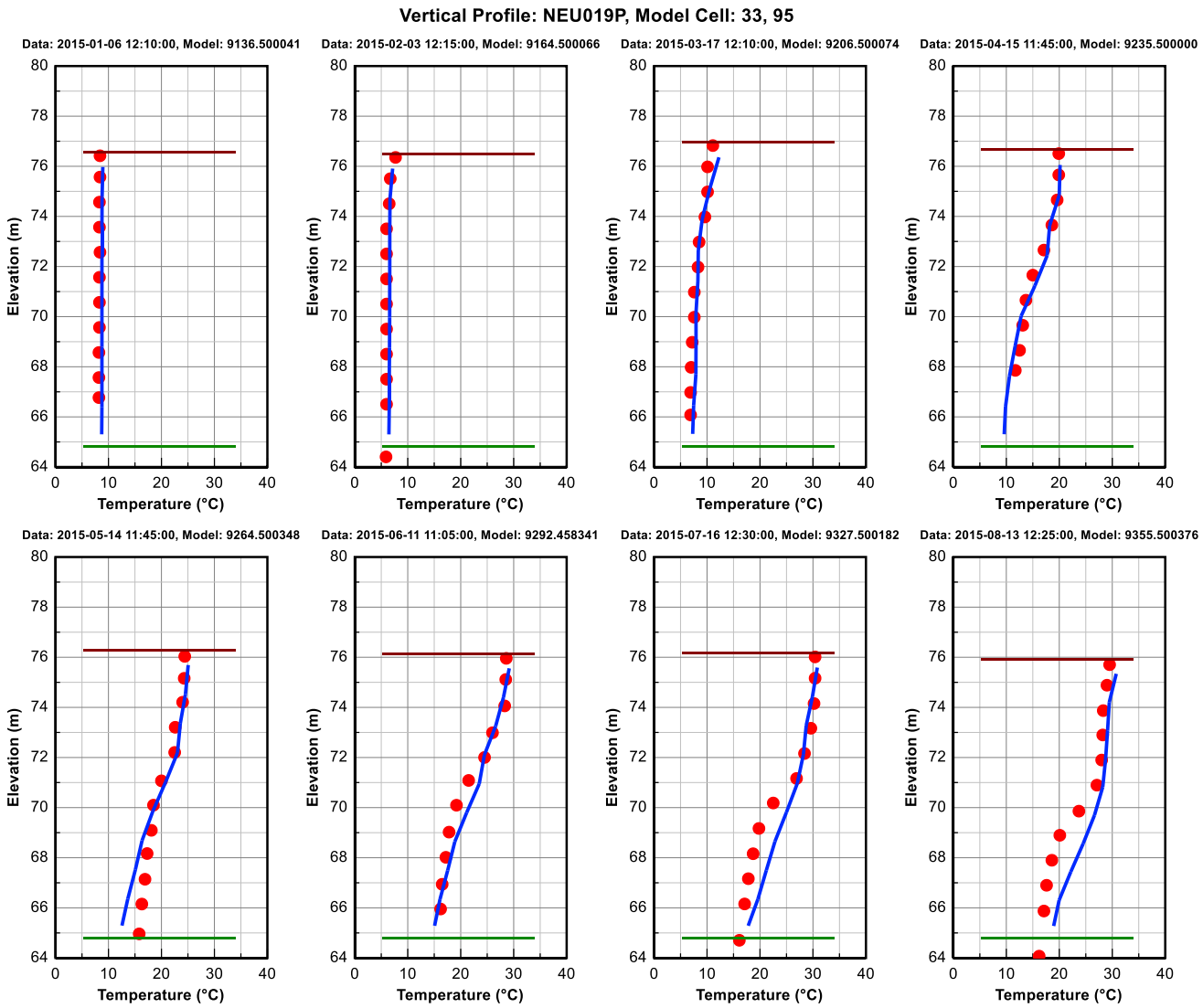

January 2015 – August 2015 (1 of 6)

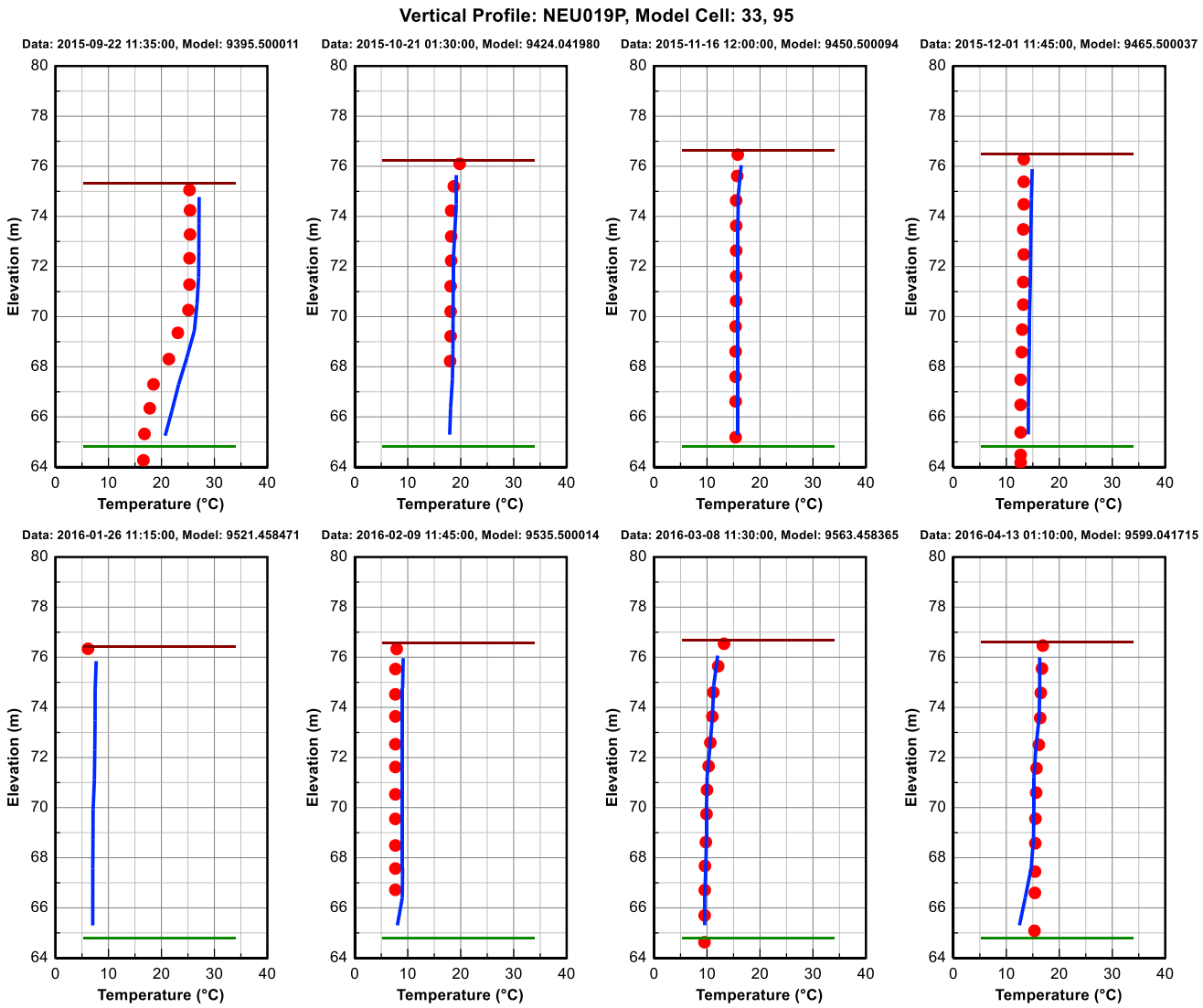

September 2015 – April 2016 (2 of 6)

Vertical Profile: NEU019P, Model Cell: 33, 95

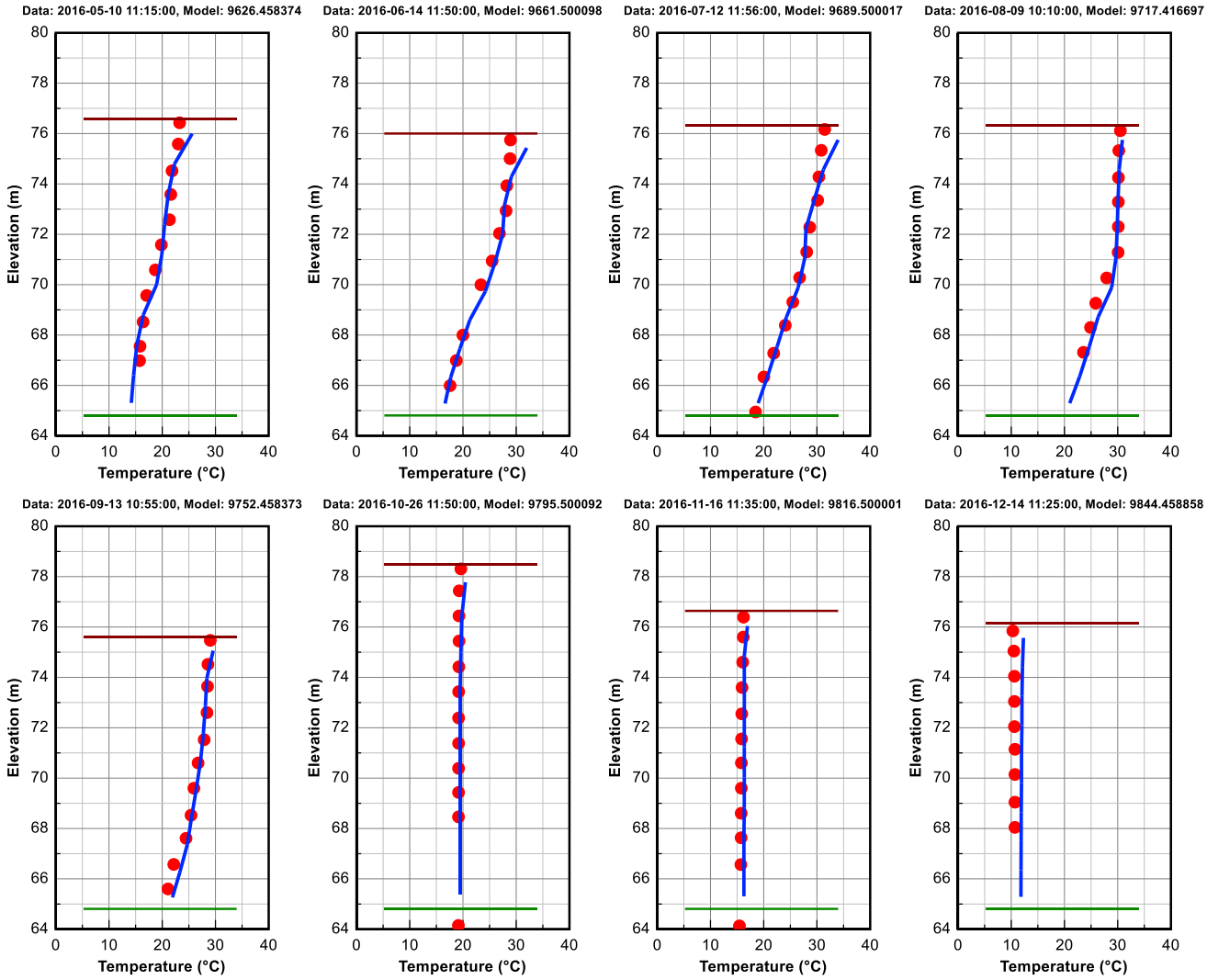

May 2016 – December 2016 (3 of 6)

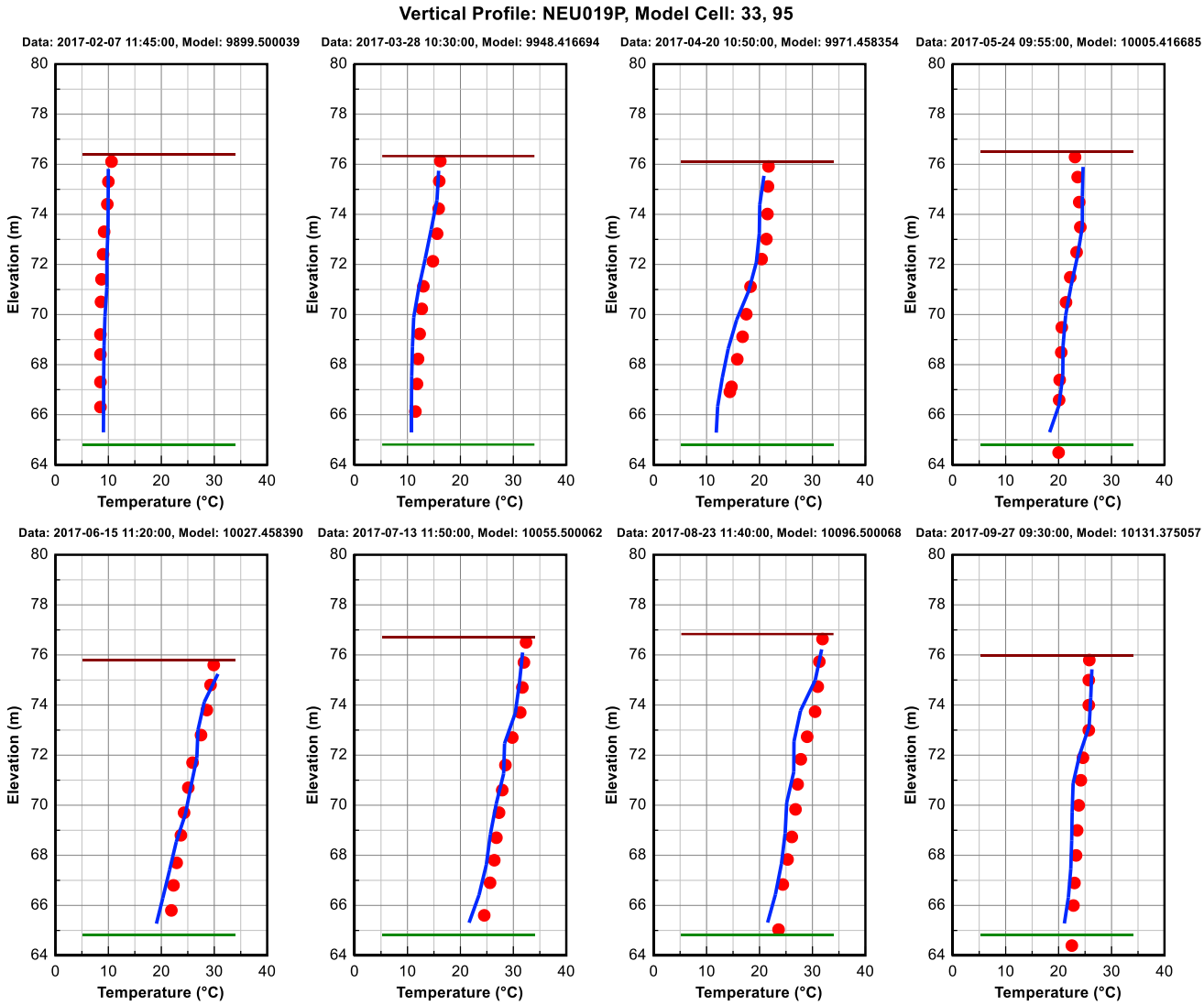

February 2017 – September 2017 (4 of 6)

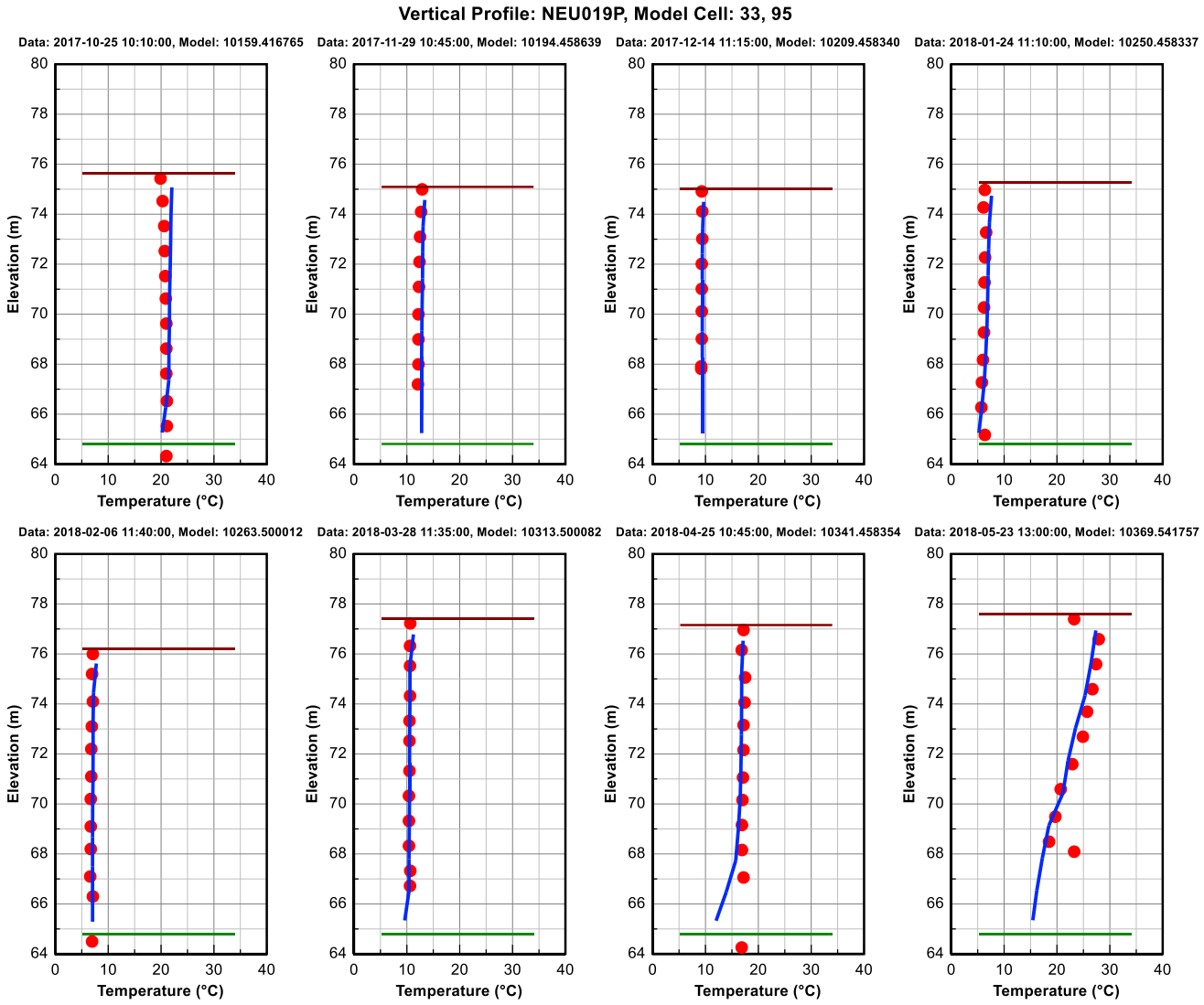

October 2017 – May 2018 (5 of 6)

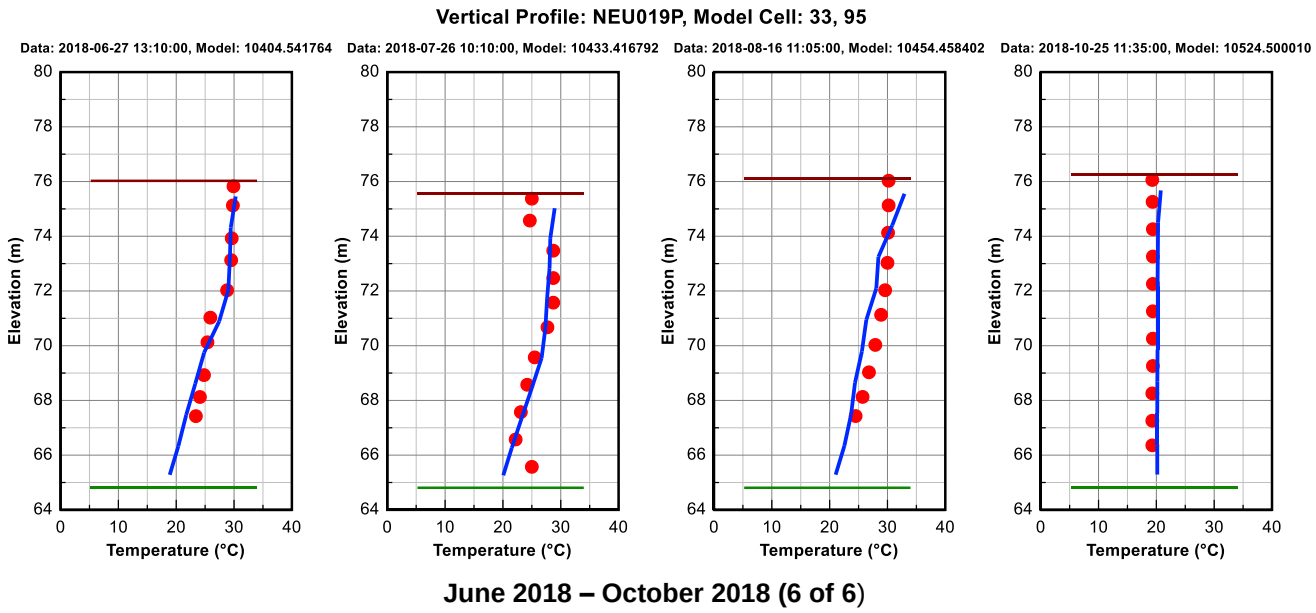

Figure 7-6 Water Temperature Vertical Profile Comparison Plot at Station NEU019P. Red dots are data, and blue continuous lines are model results.

It can be seen in Figure 7-6 for the sampling dates on 5/23/2018 and 7/26/2018 at Station NEU019P that the observed data shows that (a) the surface temperature is colder than the layers underneath and (b) the bottom temperature is warmer than the layer above. The discontinuous pattern in the water temperature data, which can be seen at some stations located in the deeper parts of the lake (e.g. NEU020D), appears to be questionable. Figure 7-7 shows the temperature vertical profile data at station NEU020D compared with that of station FLIN measured by the Center of Applied Aquatic Ecology (Data shared by Brown & Caldwell). The station locations for NEU020D and FLIN are shown in Figure 7-8. It can be seen that, as opposed to NEU020D (red full circles) the temperature profile at FLIN (black full diamonds) is continuous and water temperature decreases as depth increases.

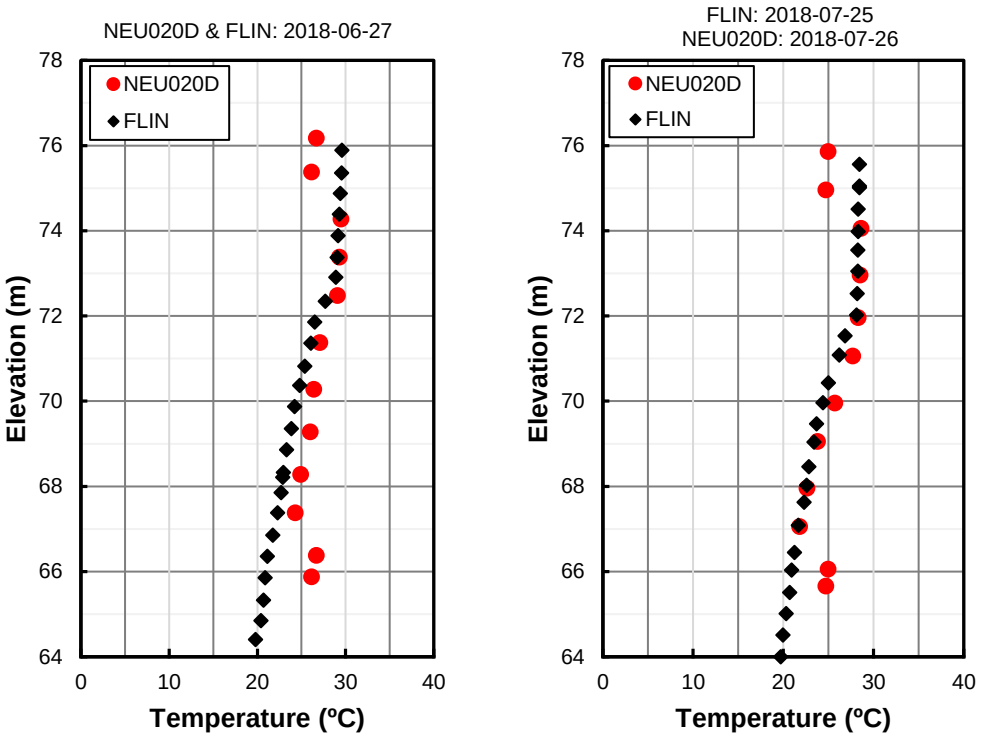

Figure 7-7 Temperature Vertical Profile Data at Station Neu020d (Red Dots) Compared with That of Station FLIN (Black Full Diamonds). Left: data at both locations were collected at 6/27/2018. Right: FLIN data was collected at 7/25/2018 and NEU020D data at 7/26/2018.

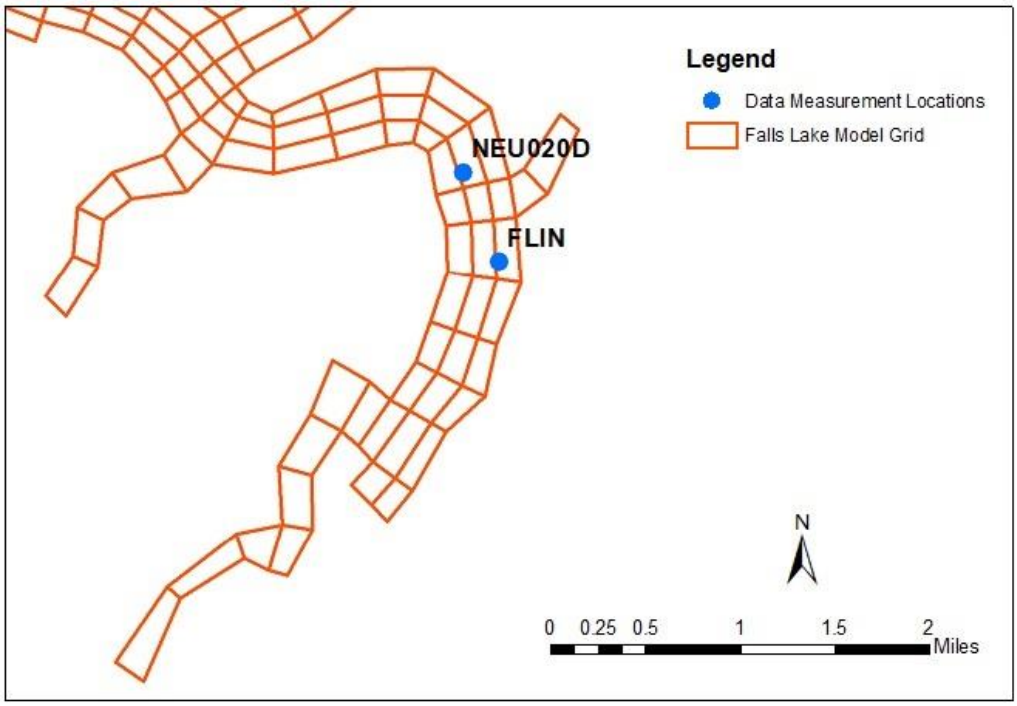

Figure 7-8 Location of UNRBA Station NEU020D and CAAE Station FLIN (Blue Full Circles) in the Model Grid.

8. Water Circulation Characteristics

The calibrated and validated hydrodynamic lake model has been used to simulate lake water quality; therefore, it is important that the hydrodynamic model is capable of simulating the circulation patterns of the lake that were observed.

8.1 Bidirectional Flow

Funded by the NC Collaboratory, Luettich et al. (2021) studied the circulation in Falls Lake by measuring the water velocity at two (2) locations, Fish Dam and Hwy 98. They identified a strong along-lake flow in response to inflows and dam operation, as well as a 5.5-hour oscillation that occurs frequently along the lake. The oscillation although relatively small (due to the minimal inflows or minimal discharge), can dominate the velocities and create a bidirectional flow when the lake stratifies in summer months. Luettich et al. (2021) observed the bidirectional flow during August 2020 at Hwy 98, mostly flowing downstream towards the dam at the surface and flowing upstream along to the bottom. The UNRBA modeling team discussed these results with Dr. Luettich and confirmed the model was simulating similar patterns. Dr. Luettich presented his work to the UNRBA Path Forward Committee (PFC) and Modeling and Regulatory Support Workgroup (MRSW) at their July 2021 meeting.

As the model simulation period ends at 12/31/2018, a direct comparison of the observed and modeled flow directions is not available. However, modeled results in February and August 2018 were chosen to compare with those observed in February and August 2019 by Luettich et al. (2021), respectively. Two drape lines were added to the grid, one at Fish Dam and the other at Hwy 98 as shown in Figure 8-1. The red lines intersect the representative cells for these 2 locations. To illustrate the bidirectional flows at those two locations, the velocity vectors throughout the water column in February and August 2018 are shown in Figure 8-2, Figure 8-3, Figure 8-4, and Figure 8-5. The vectors pointing right indicate the velocity direction towards the dam.

As can be seen in Figure 8-2 and Figure 8-3, bidirectional flow occurs quite frequently at Hwy 98. This is consistent to the observations of Luettich et al. (2021). Hwy 98 is located in the deep part of the lake where the upper layers are usually well mixed by wind action, and the lower layers are usually driven by the dominant flow along the lake from the tributaries towards the dam. However, bidirectional flow can occur when the warmer surface water flows toward the dam and cooler bottom water flows in an upstream direction. On the other hand, Fish Dam is located in the shallow part of the lake where the water column is mostly well mixed. Nevertheless, occasional bidirectional flow also occurs at this location, as depicted in Figure 8-4 and Figure 8-5. The occasional bidirectional flow at Fish Dam is mostly driven by wind.

Figure 8-1 Drape Lines at Fish Dam and Hwy 98

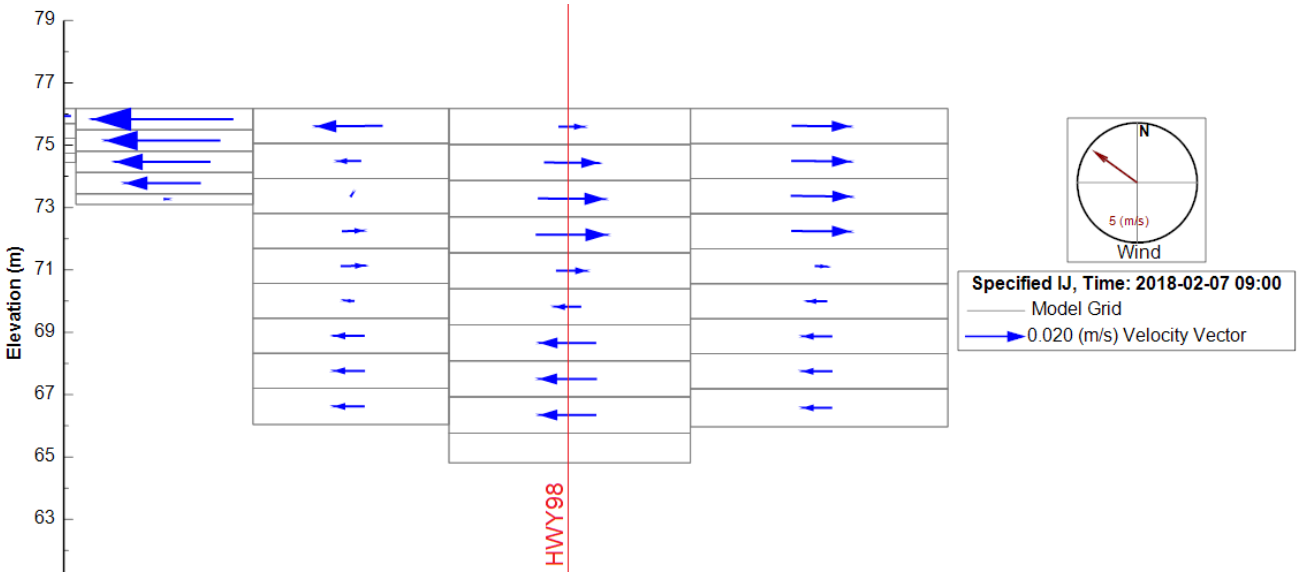

Figure 8-2 Bidirectional Flow at Hwy 98 During February 2018

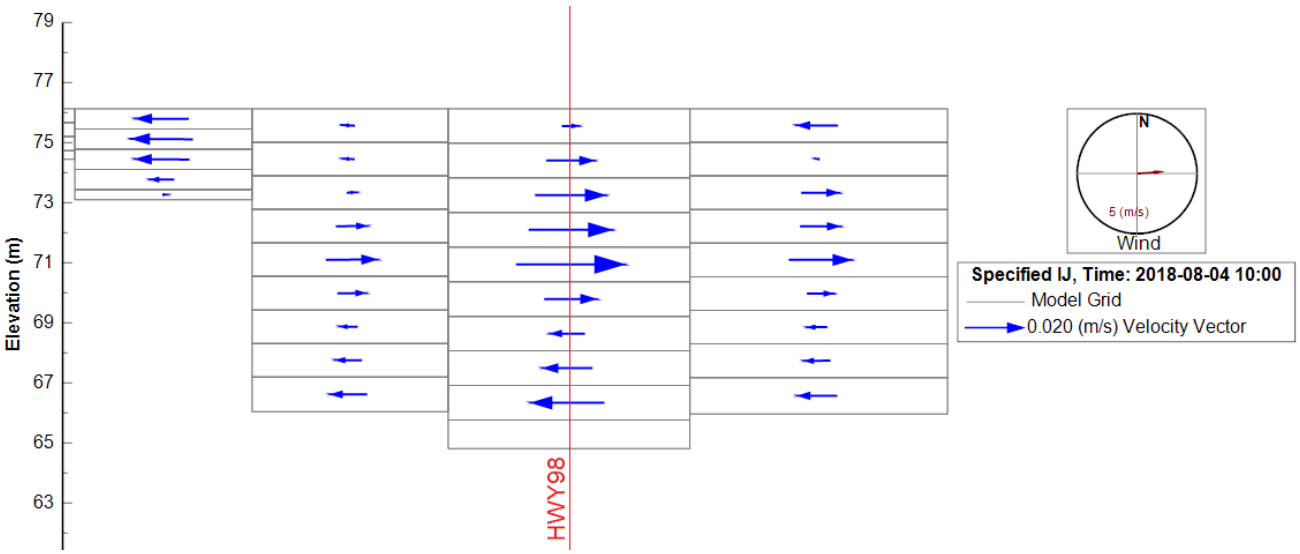

Figure 8-3 Bidirectional Flow at Hwy 98 During August 2018

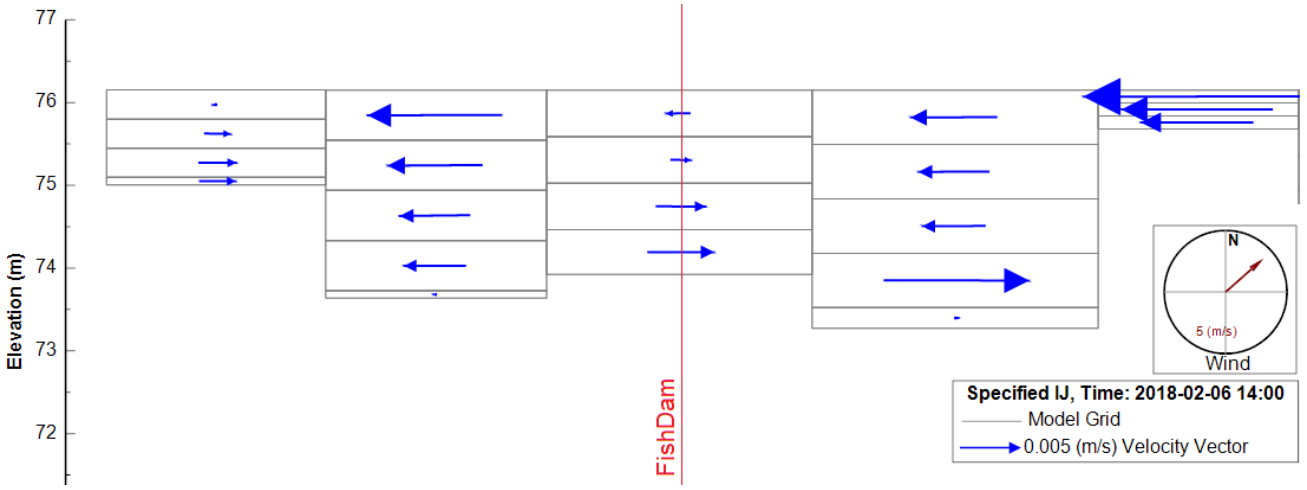

Figure 8-4 Bidirectional Flow at Fish Dam During February 2018

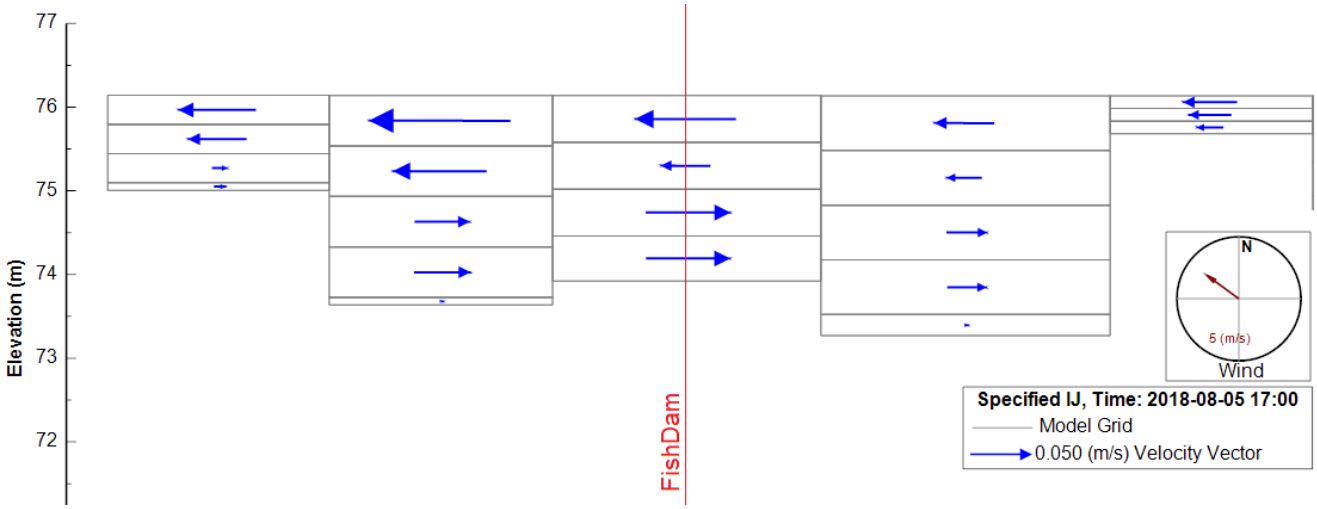

Figure 8-5 Bidirectional Flow at Fish Dam During August 2018

8.2 Residence Time Analysis

The spatial variation of physical transport processes in Falls Lake is characterized with an analysis of the residence time (or age of water) based on a dye tracer simulation. To this end, the lake was divided into 9 segments between each causeway as shown in Figure 8-6. Physical transport in Falls Lake is influenced by tributary and overland inflows throughout the lake as well as dam discharge and the water withdrawal outflow. Dam discharge which may follow a certain annual hydrologic pattern for non-regulated impoundments is not indicative of the hydrological condition of Falls Lake because it is regulated to protect downstream communities from flooding and secondarily to target normal pool (251.5 ft, msl).

As such, total annual tributary flow was examined to identify the dry and the wet years during the simulation period (2015-2018). The driest year during the simulation period represents the highest residence time. Figure 8-7 shows total annual tributary flow calculated as the sum of annual averages of the daily mean flow from the 5 major tributaries; Eno, Little, and Flat Rivers, and Knap of Reeds and Ellerbe Creeks (DWR, 2021). As can be seen for the simulation period (enclosed in the red rectangle), 2017 with the flow of 10.48 m^3/s is the driest year for the modeling period. 2017 was an average rainfall year for the area (BC and Systech Water Resources 2023).

To evaluate the residence times for the entire model domain and within the different lake segments, dye tracer simulation experiments were performed with the model. The model was run year by year, each year using the initial stage condition from the last day of its previous year, and the initial dye condition was set to 100 mg/L for the entire lake and 0 mg/L for all the inflow boundaries. Time series plots of the age of water at 2017 (the average rainfall year) for the entire lake and for each segment are presented in Figure 8-8. As shown in this plot, the age of water varies both temporally and at each segment of the lake. Table 8-1 presents summary statistics for the age of water that are computed from the time series results. As shown in the table, the 25^{th} percentile and 75^{th} percentile quartiles for the age of water range from about 7 to 35 days in segment 1 to about 62 to 127 days in segment 9, indicating a gradient in transport and mixing of the lake with the longest median residence time of 99 days computed in segment 8 (Between Beaverdam and Hwy 98) and the shortest median residence time of about 16 days computed in segment 1 (Above the railroad). The entire lake median residence time for 2017 is about 63 days.

Luettich et al. (2021) estimated a median residence time of 11 months in the lake, i.e., almost 5 times longer than what the model calculates. Their estimate was based on superimposing the water level at full pool with the 41 years discharge data and intersecting the 50^{th} percentile on the discharge curve with the full pool residence time curve, whereas the EFDC model calculates the age of water based on the instantaneous dye concentration in the cells over a shorter period (4 years) which experience average to high rainfall for the area.

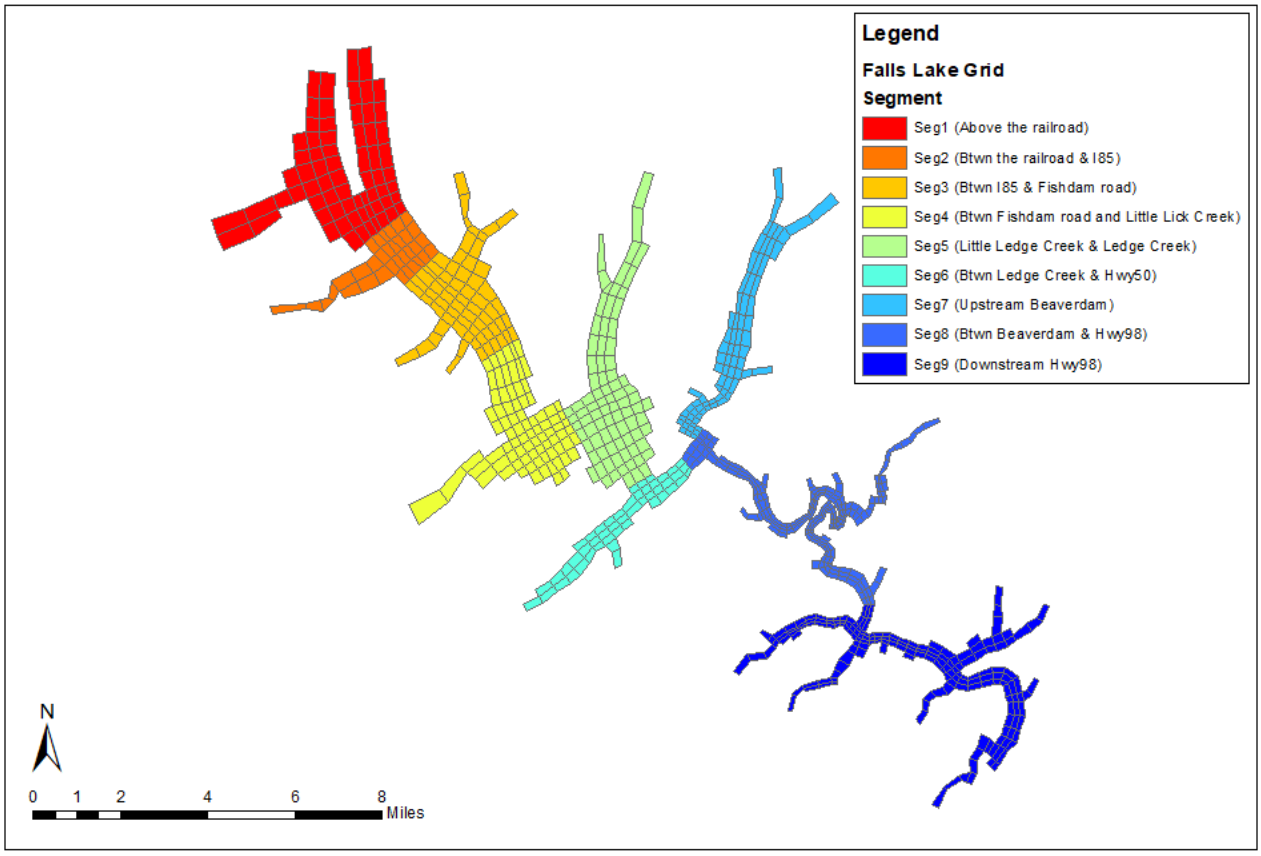

Figure 8-6 Lake Segments Between Each Causeway

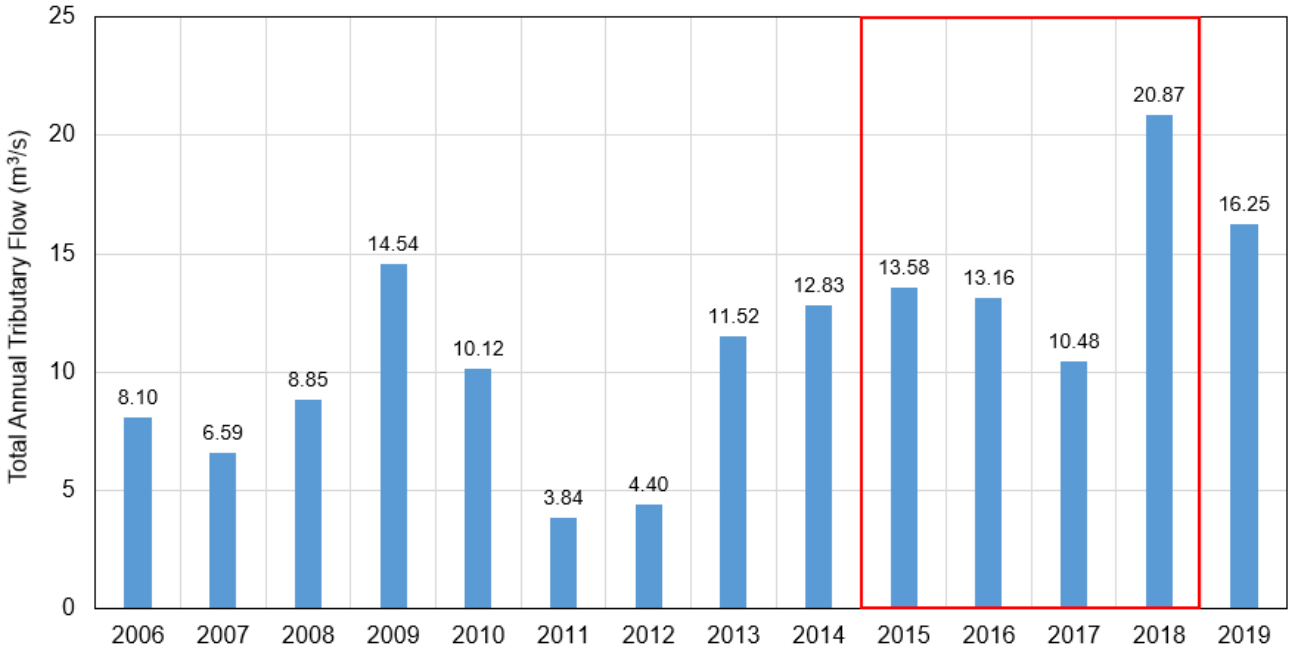

Figure 8-7 Total Annual Tributary Flow Calculated as The Sum of Annual Averages of The Daily Mean Flow from Eno, Little, and Flat Rivers, and Knap of Reeds and Ellerbe Creeks (DWR 2021 Status Report)

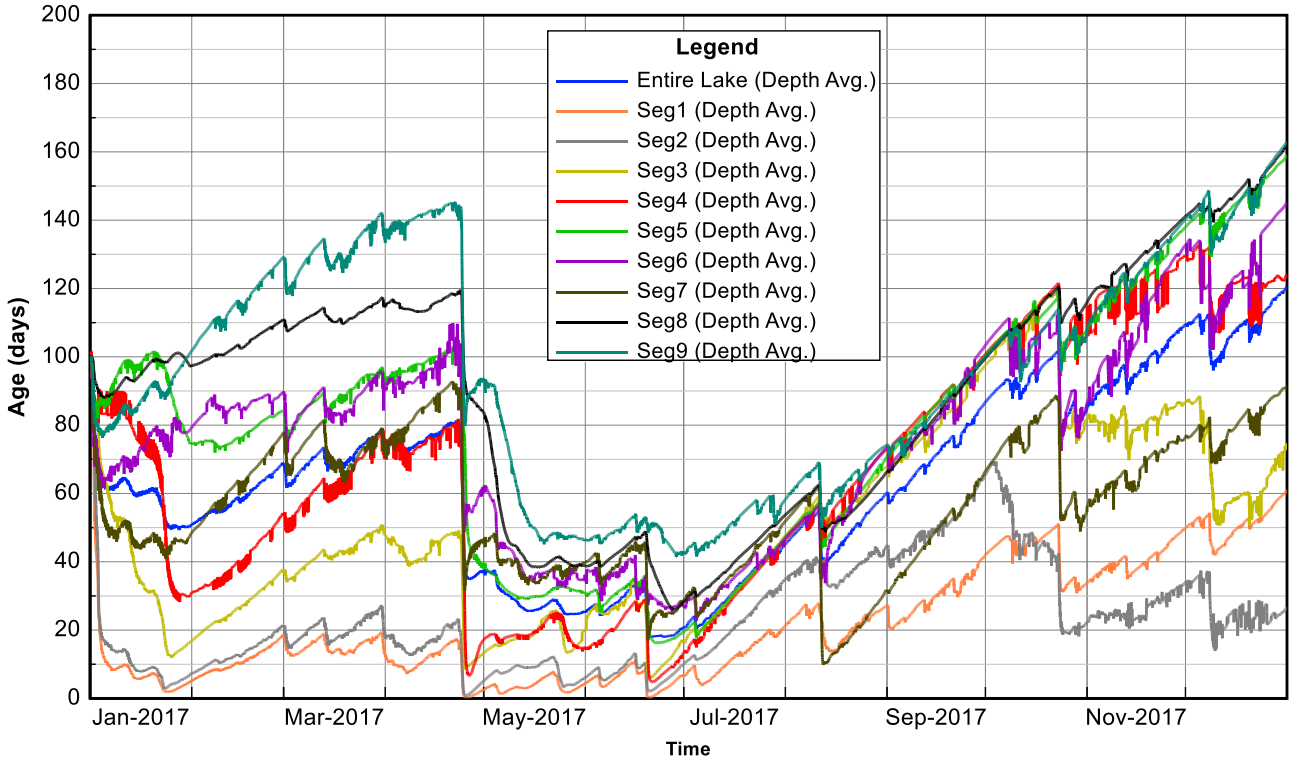

Figure 8-8 Age of Water in Falls Lake Segments during 2017 (dry year)

Table 8-1 Summary Statistics (N=8760) for Age of Water (as days) in Falls Lake Segments during 2017 (average rainfall year)

Segment #	25th Percentile	Median	75th Percentile
Segment 1	7.50	15.67	35.06
Segment 2	11.04	20.71	33.41
Segment 3	26.35	46.32	74.10
Segment 4	31.59	66.66	100.99
Segment 5	42.74	84.22	101.98
Segment 6	46.78	81.31	96.20
Segment 7	40.25	55.33	73.20
Segment 8	52.46	98.61	114.30
Segment 9	61.71	96.00	127.15
Entire Lake	39.91	62.91	82.95

9. Summary of Hydrodynamic and Temperature Model

The hydrodynamic model was calibrated using data collected during January 1, 2015, to December 31, 2016, and the model was validated to data collected during January 1, 2017, to December 31, 2018. The calibrated and validated state variables of the EFDC hydrodynamic model included stage and water temperature. Additionally, a comparison of modeled versus observed discharge during Jan 2016 and Oct 2016 showed good agreement between modeled discharge and the observed data at two constriction locations.

A balance flow time series was added to the model as an additional flow to account for the inherent uncertainty in the lake model input data. This uncertainty is mainly the result of three error sources in the watershed model including the USGS stage-flow rating curves, the 6-hr resolution of the NEXRAD precipitation data, and the ungaged areas in the watershed. To compensate for the uncertainty, the balance flow was apportioned at the tributary inputs based on ungaged drainage area. Delineation shows that seventeen (17) major tributaries to Falls Lake consist of about 90% of the whole Falls Lake's drainage area. Eno and Little Rivers (lumped in together at the boundary group ID R0001), Flat River, Knap of Reeds Creek, and Ellerbe Creek are gaged via five (5) USGS gages located at the upstream of their confluence to the lake. The gaged part of the drainage area is the area where there is the greatest confidence in the inflows to Falls Lake. Hence the uncertainty comes from the small part of the drainage area downstream of those four (4) tributaries that are ungagged. The other thirteen (13) tributaries are ungagged inflows into Falls Lake. Located in the lower parts of the lake, they are the areas of greatest uncertainty in the water balance. Therefore, the flow additions and withdrawals were set proportional to the ungagged drainage areas of the seventeen (17) major tributaries to Falls Lake. LOESS method with a 120-day window (α=0.66) was applied to smooth the balance flow.

Hydrodynamic model performance was evaluated by a combination of visual inspection and quantitative analysis of model-data performance statistics primarily based on the RMSE and the RSR. The performance target for calibration of the hydrodynamic model was adopted based on an RSR below 50%. The RSR for the lake stage during the calibration period was slightly over the 50% target with a RSR of 50.91 % for USGS 02087183 at Falls Dam and RSR of 52.65 % for USGS 0208706575 at Beaverdam. The RSR for the lake stage during the validation period was under the 50% target at both locations.

Model performance in terms of under or over predicting water temperature was evaluated using the pBias statistic. The hydrodynamic model did not show a systematic over or under prediction during the model calibration period of 2015-2016, and the model validation period from 2017-2018. The highest pBias of -9.20 %, however, is relatively small and considered to be acceptable as it less than -10 %.

The calibrated and validated hydrodynamic model was used to study the circulation patterns in Falls Lake. The model performance in simulating the bidirectional flow was verified at Hwy 98 and Fish Dam Road during Feb and Aug 2018. Also, the residence times were evaluated by performing dye tracer simulation experiments with the model for the entire model domain and within the different lake segments. The residence time analysis was performed during 2017, which is the driest year of the simulation period (an average rainfall year for the

area). The longest median residence time of 99 days was computed in segment 8 (Between Beaverdam and Hwy 98) and the shortest median residence time of about 16 days computed in segment 1 (Above the railroad). The entire lake median residence time for 2017 is about 63 days.

Overall, the performance of the Falls Lake EFDC hydrodynamic model is deemed to be acceptable. Based on the calibrated and validated hydrodynamic model, the EFDC model has approved by the MRSW and used for development of the EFDC lake water quality model. the water quality model results are presented in the next section.

10. Water Quality Model Calibration and Validation

Calibration of the water quality model is demonstrated in this report with model-data comparisons for Chl-a, TOC, DO, TN, and TP as station time series. Vertical profiles are presented for DO. For the sake of brevity, water quality calibration and validation plots are shown in the main report only for stations NEU013B and NEU020D. Station NEU013B is located in the shallow upper part of the lake where the water column is typically well-mixed and the photic zone is shallower. Station NEU020D is located in the deeper lower part of the lake where the water column is typically stratified during summer and the photic zone is deeper. Water quality calibration and validation time series plots for the other ten (10) stations are presented in Appendix A.2. In addition to the other ten (10) stations, calibration and validation results for other water quality variables are also presented in Appendix A.2 including inorganic and organic forms of nitrogen, DOC, TSS and secchi depth.

Observed data collected over the photic zone is compared to the average of lake model results simulated for the equivalent photic layers. When water levels were below the normal pool elevation, the model-layer thickness is about 0.75 m. In contrast, when the water level is above the normal pool elevation, the model layer thickness is about 1.0 to 1.5 m. The main report shows the distributions of Secchi depth at each lake monitoring station for 2014 to 2018. Secchi depth increases in the downstream direction. The model layers selected for averaging depend on the location and lake water level:

<u>Above Highway 50</u>

- At stations NEU013 and NEU013B, the photic zone is about 1 meter or less. The equivalent photic layer is the surface layer (Layer 10) at those two stations regardless of the water level in the lake.
- At the other stations above Highway 50, including the arms of embayments, the photic zone is about 1.5 meters. Depth layers were selected as follows:
  - When the water level is below normal pool elevation, the equivalent photic layer is based on the average of the top two layers (Layers 9 and 10).
  - When the water level is above normal pool elevation, the equivalent photic layer is based on the surface layer (Layer 10).

<u>Below Highway 50</u>

- At stations NEU019E, NEU019L, and NEU019P, the photic zone ranges from 1.75 m to 2.0 m. Depth layers were selected as follows:
  - When the water level is below normal pool elevation, the equivalent photic layer is the average of the top two layers (Layers 9 and 10).
  - When the water level is above normal pool elevation, the equivalent photic layer is the surface layer (Layer 10).
- At station 20D, the photic zone range is about 2.5 m. Depth layers were selected as follows:
  - When the water level is below normal pool elevation, the equivalent photic layer is the average of the top three layers (Layers 8, 9 and 10).

- When the water level is above normal pool elevation, the equivalent photic layer is the average of the top two layers (Layers 9 and 10).

Table 10-1 lists the equivalent photic layers for each station. The DO data collected near the bottom is compared to model results for the EFDC bottom layer (See Table 7-1). Station results are presented in this section to show model calibration and validation for the selected DWR stations in Falls Lake. The location of these stations is shown in Figure 4-2.

Table 10-1 Model Layers for Averaging to Equivalent Photic Layer(s)

Station ID	Water level < Normal Pool	Water level > Normal Pool
LC01	9, 10	10
LI01	9, 10	10
LLC01	9, 10	10
NEU013	10	10
NEU013B	10	10
NEU0171B	9, 10	10
NEU018C	9, 10	10
NEU018E	9, 10	10
NEU019E	9, 10	10
NEU019L	9, 10	10
NEU019P	9, 10	10
NEU020D	8, 9, 10	9, 10

As with the UNRBA Watershed Model Report, the UNRBA expressed the importance of visualizing uncertainty around laboratory measurements when comparing model output to observations. The UNRBA MRSW, DWR, and third-party model reviewers discussed methods and terminology to show the potential range of "observed" values using the relative percent difference (RPD) allowed by each laboratory when the evaluate field duplicates. Methods for dealing with observations less than the reporting limit were also discussed. For field measurements, the stated accuracy of field meters was used. The following methods were used to develop the time series comparison figures. Note this approach is different than that used in the UNRBA Watershed Modeling Report which relied primarily on UNRBA monitoring data rather than the lake model which relies on monitoring data from other organizations.

- For observations that were less than the reporting limit, the value is displayed as one-half the reporting limit. Vertical bars extend from a concentration of zero to the reporting

limit to show the potential range. This bar is labeled “Zero to the Reporting Limit”. The reporting limits change depending on the organization and parameter displayed.

- For observations that were greater than the reporting limit, vertical bars are shown on the figure and labeled in the legend as “+/- Allowable RPD of the Laboratory Duplicates”
  - CAAE observations are shown with a bar that is +/-15% of the observation point based on the CAAE monitoring QAPP
  - DWR values for chlorophyll-a, TOC, TKN, and TSS use +/-20% based on the DWR Monitoring QAPP
  - Calculated values for TN using DWR data use +-20% because the majority of the TN in Falls Lake is TKN, and the value for TKN is +/-20%
  - DWR values for ammonia, nitrate+nitrite and all phosphorus species including total use +/-10% based on the DWR Monitoring QAPP
  - City of Durham values for all parameters use +/-10% except for dissolved and total organic carbon which use +/-15% based on the City of Durham’s quality control acceptance criteria
- For field parameters
  - Temperature uses +/-0.2 C labeled “+/- Typical accuracy of calibrated field meters” as provided in the City of Durham QAPP for common field meters
  - Dissolved oxygen uses +/-0.5 mg/L labeled “+/- Allowable difference between post-sampling check readings” per the DWR QAPP (this covers the typical accuracy of field meters of +-0.1 mg/L provided in City of Durham QAPP

10.1 Chl-a

Procedures used to calibrate Chl-a included: 1) check the linkage between WARMF and EFDC to make sure that the setup of algae and other water quality boundary conditions for the EFDC model is correct; and 2) adjust the key kinetic parameters within reasonable ranges to match the observed data. These kinetic parameters include maximum growth rate, basal metabolism rate, predation rate, settling rate, optimal temperature options, P and N half-saturation constants, and nutrient fractions released during basal metabolism and predation processes. Modeled algae biomass is converted to Chl-a concentrations using the carbon to Chl-a ratios described in Section 2.6. Algae results (as Chl-a) are presented for comparison to the observed data for the equivalent photic layers as described above. In the Falls Lake model, diatoms, cyanobacteria (blue-green) and green/other algae were simulated and summed to derive simulated total algae Chl-a for comparison to Chl-a observations.

Chl-a calibration plots for stations NEU013B and NEU020D are given in Figure 10-1 and Figure 10-2, respectively. Chl-a validation plots are given in Figure 10-3 and Figure 10-4, respectively. As can be seen in these model-data plots, the model results are in good agreement with measured Chl-a concentrations. In particular, the EFDC-simulated Chl-a concentrations follow the seasonal trend of the observed Chl-a at all four stations for the calibration and validation

period reasonably well. Calibration and validation results for the other ten (10) stations are presented in Appendix A.2 as time series plots for Chl-a.

The summary statistics for model performance of Chl-a are given in Table 10-2 and Table 10-3. It can be seen that the RSR target for Chl-a is met (RSR ≤100%) during calibration period for six (6) stations. During the validation period, however, none of the stations met the RSR target. For the calibration period, the calculated RSRs ranged from 85% at station NEU020D to 151% at station NEU013B, as shown in Table 10-2. For the validation period, the calculated RSRs ranged from 121% at station LLC01 and NEU020D to 172% at station LI01, as shown in Table 10-3.

The pBias is another model performance statistic that gives good insight about model skill. For the calibration period, the pBias ranged from -9.4% at station LI01 to 16.7% at station NEU019P. Based on the approved QAPP, the pBias statistics fall within the “good” criteria for the water quality/nutrient of the watershed model calibration guidance (See Table A.7-2 of QAPP). In addition, this performance metric shows that the model is not systematically over-predicting or under-predicting Chl-a concentrations in the photic layer during the calibration period. On the other hand, for the validation period the pBias ranged from -55.8% at station NEU018E to -25.5% at station NEU013B. This shows that the model is systematically underestimating Chl-a concentrations during validation conditions. The following items are noted for consideration as an explanation of why the model is underestimating Chl-a concentrations during the validation period:

- EFDC is a mass balance-based mechanistic model and the water quality kinetic parameters such as maximum growth rate, C/Chl-a ratio, etc. are fixed for the calibration and validation periods. In reality, these kinetic parameters may change from season to season. Seasonal changes in kinetic parameters are not, however, represented in the model results.

- The average of the Chl-a concentrations during the validation period is 45% higher than the average of the Chl-a concentrations during the calibration period. However, nutrient concentrations and Secci depth were not drastically different during these periods. For mechanistic models like EFDC, nutrients and light availability are key factors in the amount of simulated algae, and the equations and kinetic parameters are fixed. If the nutrient-algae-Chl-a relationships are drastically different for the calibration and validation periods, one set of kinetic parameters cannot meet the targets for both periods.

- The biovolume data show that, in addition to diatoms and cyanobacteria (blue-greens), other algal groups also contribute to the Chl-a concentrations and biovolume levels observed in the water column, such as *Euglenophyta* and *Prymnesiophyceae* (UNRBA, 2019). Green algae are a small component of the algal biovolume observed in Falls Lake. Although the EFDC model can be setup to simulate more than three algal groups, there is very little information available to specify kinetic parameters (e.g., growth rates, half-saturation constants, optimal temperature, etc.) for the additional algal groups. Discussion of this issue with third-party reviewers and DWR modelers resulted in agreement that the Falls Lake model would be developed to account for the biomass of the additional algal groups based on the kinetic parameters assigned for the green/other

algae group. As noted above, because the kinetic parameters are fixed for each group within the model period, they cannot be changed to represent different species of algae that may dominate at different times.

- The biovolume data also shows that blooms of certain algae like *Prymnesiophyceae* sometimes correspond to high Chl-a concentrations and sometimes they do not. At other times Chl-a is relatively high and algal biovolumes for all species are relatively low. Comparisons of biovolume, Secchi depth, and Chl-a data collected in Falls Lake are provided in Appendix D of the main report.

Given all the items above, the consensus was reached that the calibration period would be the key period used to demonstrate good agreement with observed Chl-a data. Model results for Chl-a met the RSR target at the majority of lake stations and the pBias value was within the "good" criteria for the calibration period. The EFDC lake model results for Chl-a are, therefore, deemed to be acceptable.

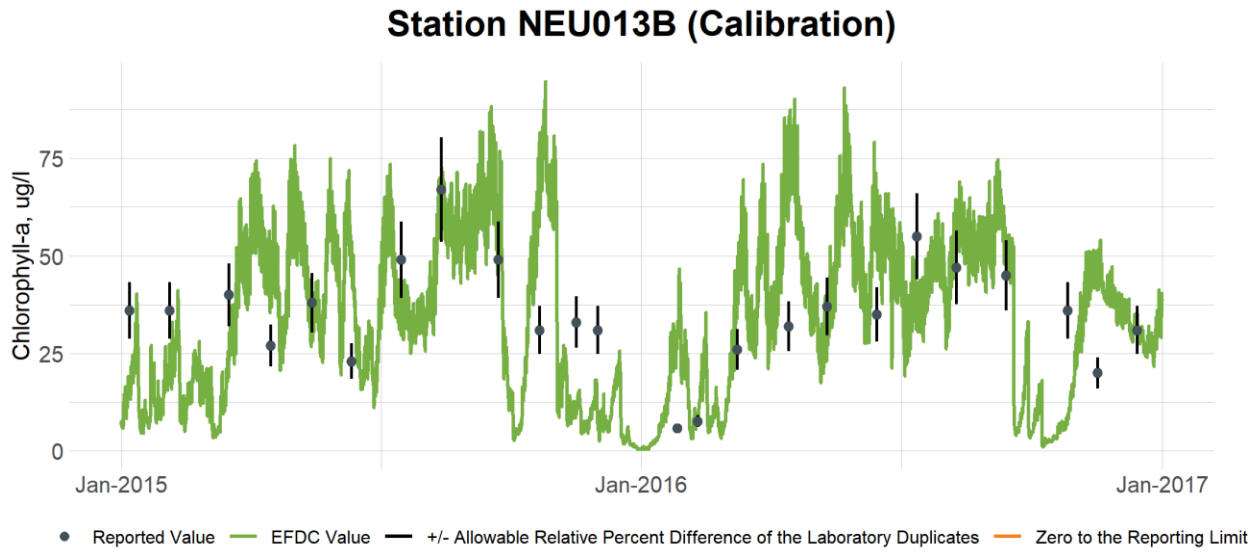

Figure 10-1 Calibration Plot of Chl-a at Station NEU013B

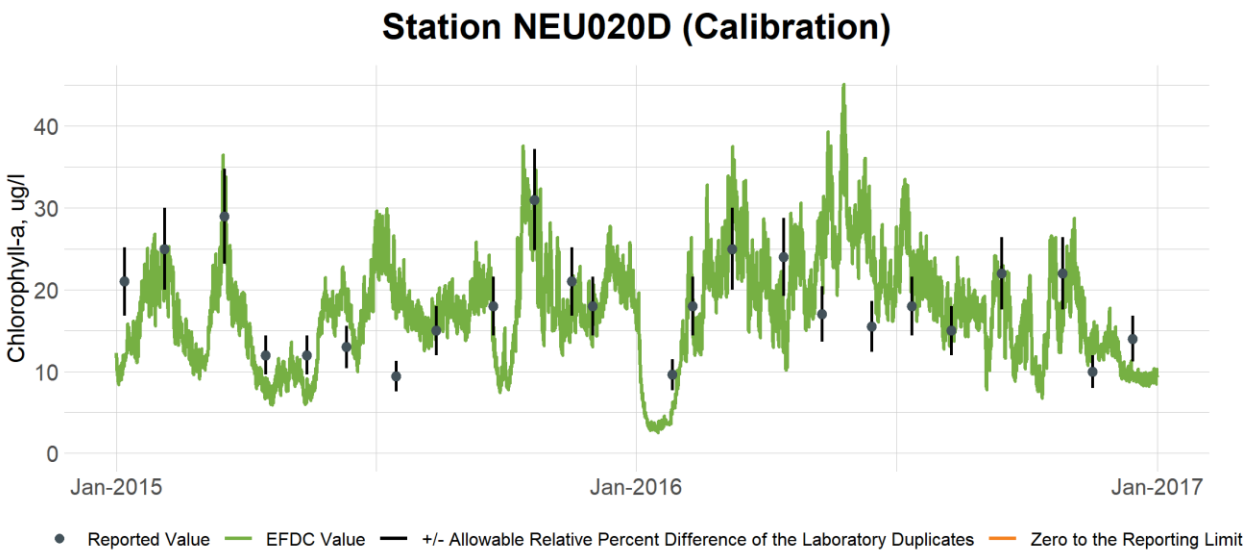

Figure 10-2 Calibration Plot of Chl-a at Station NEU020D

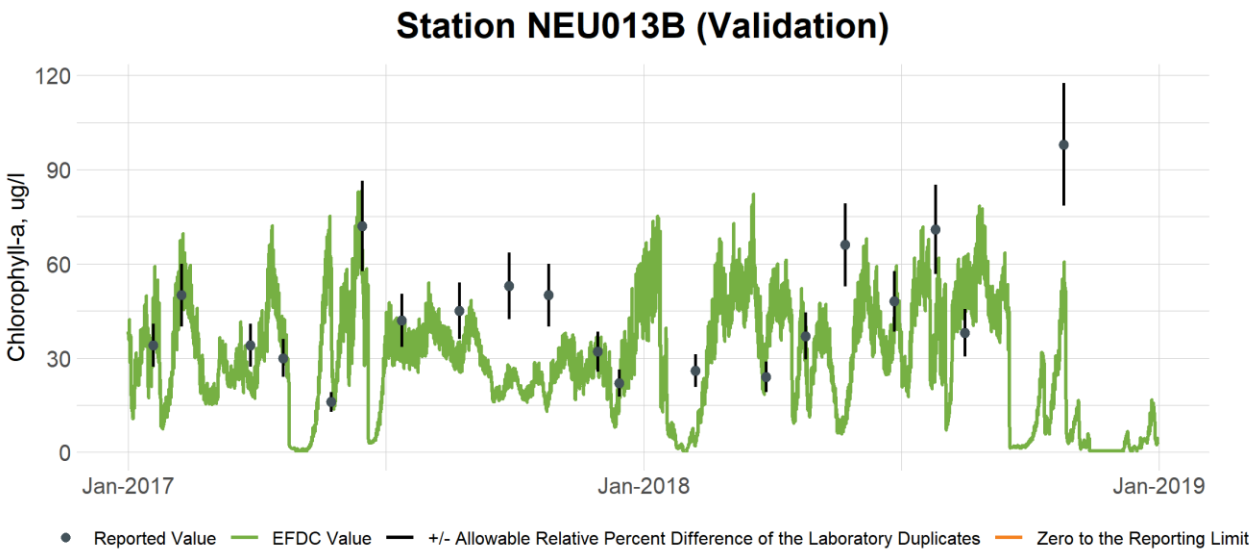

Figure 10-3 Validation Plot of Chl-a at Station NEU013B

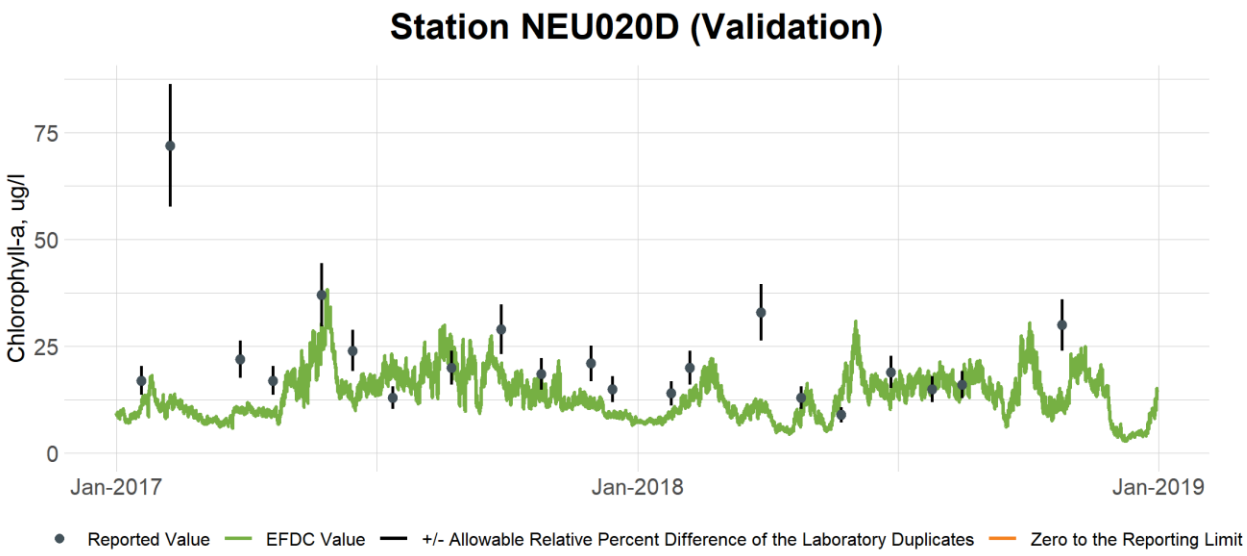

Figure 10-4 Validation Plot of Chl-a at Station NEU020D

Table 10-2 Calibration Statistics for Chl-a

Station ID	Starting	Ending	# Pairs	Data Average (µg/L)	Model Average (µg/L)	R^2	RMSE (µg/L)	RSR (%)	RE (%)	AE (µg/L)	CE	pBias (%)
LC01	1/6/2015	12/14/2016	23	24.4	27.9	0.41	8.3	122	26.3	3.5	-0.5	14.3
LI01	1/6/2015	12/14/2016	24	29.1	26.3	0.16	11.4	120	29.6	-2.7	-0.4	-9.4
LLC01	1/6/2015	12/14/2016	24	29.6	31.0	0.37	9.4	89	24.1	1.4	0.2	4.8
NEU013	---	---	---	---	---	---	---	---	---	---	---	---
NEU013B	1/6/2015	12/14/2016	24	34.9	37.4	0.09	20.2	151	48.3	2.5	-1.3	7.2
NEU0171B	1/6/2015	12/14/2016	24	30.6	29.5	0.16	11.0	100	30.8	-1.1	0.0	-3.6
NEU018C	1/6/2015	12/14/2016	24	25.1	26.6	0.21	9.3	92	29.5	1.5	0.1	5.9
NEU018E	1/6/2015	12/14/2016	24	27.8	25.5	0.00	15.0	116	39.7	-2.3	-0.3	-8.4
NEU019E	1/6/2015	12/14/2016	24	23.4	23.0	0.28	6.6	97	21.7	-0.4	0.1	-1.7
NEU019L	1/6/2015	12/14/2016	23	20.0	22.4	0.46	5.6	87	21.6	2.4	0.2	12.2
NEU019P	1/6/2015	12/14/2016	24	19.1	22.3	0.46	6.4	104	27.8	3.2	-0.1	16.7
NEU020D	1/6/2015	12/14/2016	24	18.1	17.7	0.52	5.0	85	24.3	-0.4	0.3	-2.2

Table 10-3 Validation Statistics for Chl-a

Station ID	Starting	Ending	# Pairs	Data Average (µg/L)	Model Average (µg/L)	R^2	RMSE (µg/L)	RSR (%)	RE (%)	AE (µg/L)	CE	pBias (%)
LC01	1/18/2017	10/25/2018	22	35.5	21.5	0.36	18.4	126	43.5	-14.0	-0.6	-39.5
LI01	1/18/2017	10/25/2018	21	38.9	23.9	0.04	24.5	172	49.9	-15.1	-1.9	-38.7
LLC01	1/18/2017	10/25/2018	21	40.3	24.7	0.26	22.3	121	44.9	-15.6	-0.5	-38.7
NEU013	---	---	---	---	---	---	---	---	---	---	---	---
NEU013B	1/18/2017	10/25/2018	20	44.4	33.1	0.05	25.1	128	41.1	-11.3	-0.6	-25.5
NEU0171B	1/18/2017	10/25/2018	21	41.2	25.5	0.03	24.2	146	47.7	-15.7	-1.1	-38.2
NEU018C	1/18/2017	10/25/2018	21	40.6	19.7	0.34	25.8	140	51.3	-20.8	-0.9	-51.3
NEU018E	1/18/2017	10/25/2018	21	39.8	17.6	0.18	27.4	154	55.8	-22.2	-1.4	-55.8
NEU019E	1/18/2017	10/25/2018	21	36.4	17.9	0.01	26.3	150	53.6	-18.4	-1.2	-50.7
NEU019L	1/18/2017	10/25/2018	21	34.9	16.3	0.01	26.7	147	55.0	-18.5	-1.2	-53.2
NEU019P	1/18/2017	10/25/2018	21	33.5	15.7	0.00	26.5	145	56.5	-17.8	-1.1	-53.2
NEU020D	1/18/2017	10/25/2018	21	22.6	14.2	0.01	15.8	121	45.8	-8.4	-0.5	-37.0

10.2 TOC

Procedures used to calibrate TOC included: 1) check the linkage between WARMF and EFDC to make sure that the setup of TOC and other water quality boundary conditions for the EFDC model is correct; and 2) adjust the key kinetic parameters within reasonable ranges to match the observed data.

TOC is connected with the algal production cycle; hence, algae-related kinetic parameters impact TOC model results. The settling velocity of refractory and labile organic matter also showed an impact on the distribution of TOC between the water column and the sediment bed. Since more than 90% of TOC in Falls Lake consists of DOC, kinetic parameters such as minimum heterotrophic mineralization rate and minimum hydrolysis rate of DOC also impact the TOC concentration in the water column.

TOC model results are presented for comparison to the observed data for the the equivalent photic layers. TOC calibration plots for stations NEU013B and NEU020D are given in Figure 10-5 and Figure 10-6, and the validation plots are given in Figure 10-7 and Figure 10-8, respectively. As can be seen in these model-data plots, the model results generally follow the seasonal trend of the measured data very well for both calibration and validation periods. Peak values, however, are under-predicted during the winter months of both 2015 and 2016 at both stations. Calibration and validation results for the other ten (10) stations are presented in Appendix A.2 as time series plots for TOC.

The summary statistics for model performance of TOC are given in Table 10-4 and Table 10-5. It can be seen that during the calibration period the RSR target for TOC (RSR≤100%) is met only for station LC01. During the validation periods, the RSR target for TOC is met only for station NEU0171B. For the calibration period, the calculated RSRs ranged from 99% at station LC01 to 151% at station LI01, as shown in Table 10-4. For the validation period, the calculated RSRs ranged from 86% at station NEU0171B to 197% at station LI01, as shown in Table 10-5.

For the calibration period, the pBias ranged from -20.7% at station LI01 to -9.1% at station LC01, and for the validation period the pBias ranged from -20.9% at station NEU020D to -6.2% at station NEU0171B. Based on the approved QAPP, the values of this metric falls within the “good” criteria for the water quality/nutrients of the watershed model calibration guidance (See Table A.7-2 of QAPP). However, the negative PBias values show that the lake model is systematically underestimating TOC. The reason for the underestimation is unclear. However, a few possible causes include:

- Watershed load uncertainty: Most of the observed water quality data from watershed stations are collected either before or after storm events. Some data were also collected during or immediately after storms as part of the UNRBA high-flow special studies. The watershed model was calibrated to this data which mostly represents non-storm event water quality data. Peak water quality concentrations and organic matter loading that would occur during storm events, particularly large events like hurricanes or tropical storms that cannot be safely sampled, may result in under-prediction of loads from the watershed. Four large storms (as listed by NOAA) occurred in the area between December 2015 and February 2016 (BC, 2019).

- C/Chl-a ratio: The site-specific paired data for Chl-a and POC used to derive the C/Chl-a ratio is very limited and the fraction of POC contributed only by algae sources is unknown. The sensitivity runs show that the C/Chl-a ratio has a direct impact on simulated DOC and TOC concentrations. Therefore, the C/Chl-a ratios derived for the three algal groups can be another possible cause for underestimation of TOC.

- Denitrification: During the denitrification process, NO_3 from the water column is being converted to N_2 gas and large amounts of DOC are needed for the denitrification process.

With the exception of the winter months during the calibration period of Nov 2015 through March 2016, simulated TOC generally followed the trend of the observed data fairly well during both calibration and validation years. The calculated pBias metrics for skill assessment of the model were within the good criteria established for the water quality/nutrient parameters of the watershed model calibration guidance. The model results for TOC are, therefore, deemed to be acceptable.

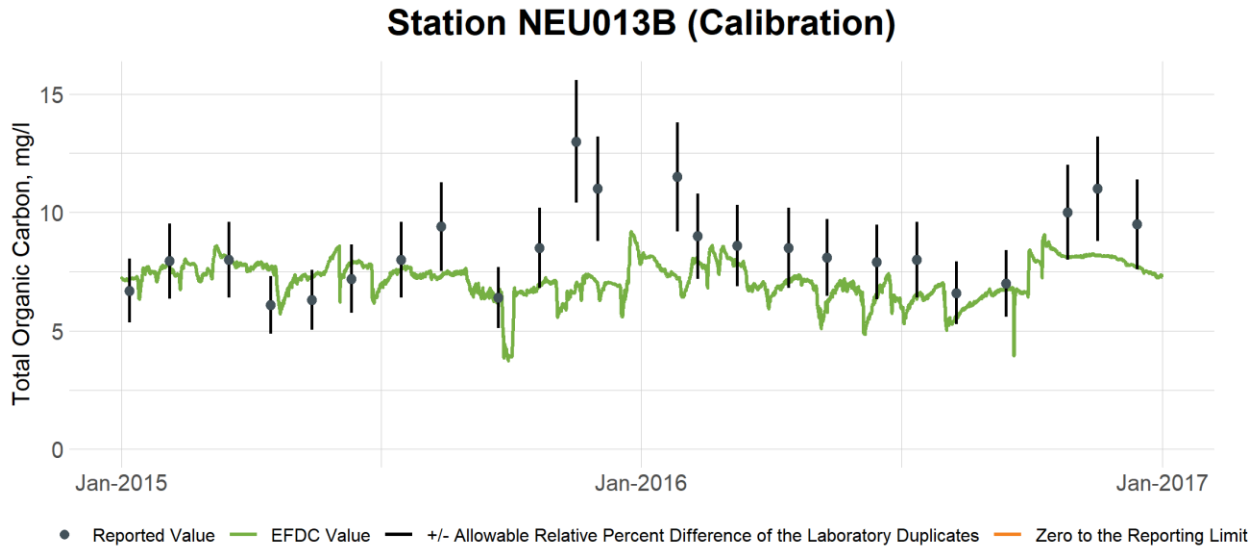

Figure 10-5 Calibration Plot of TOC at Station NEU013B

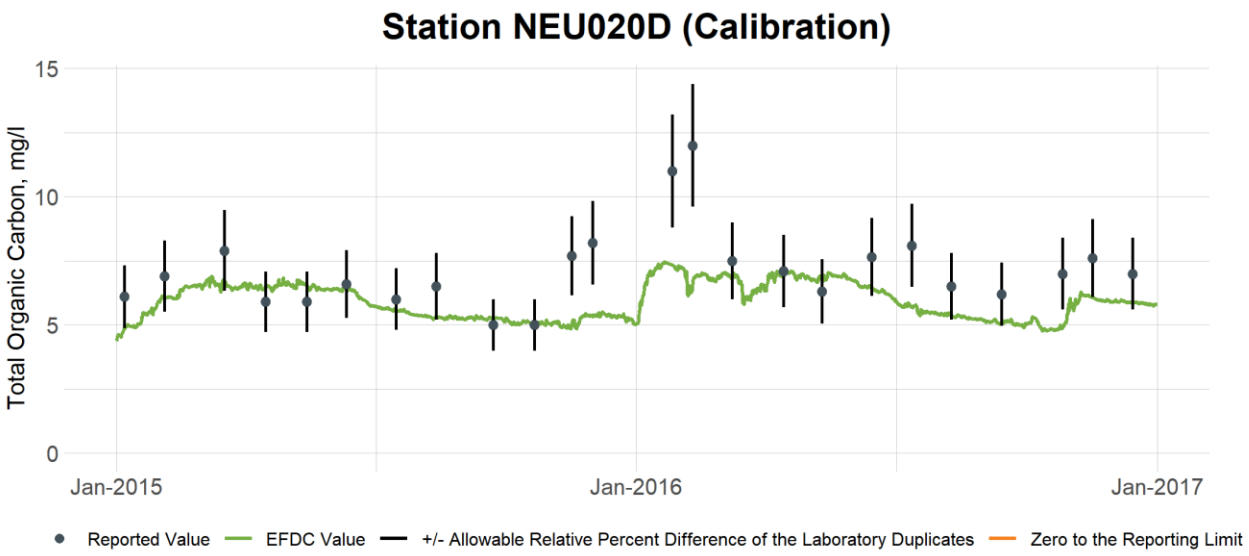

Figure 10-6 Calibration Plot of TOC at Station NEU020D

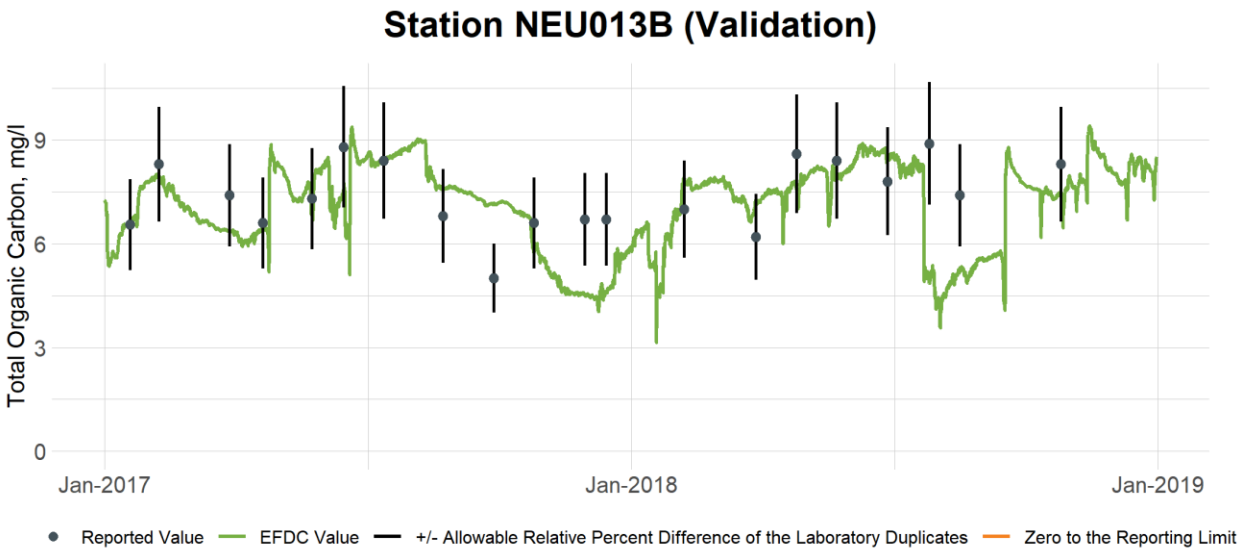

Figure 10-7 Validation Plot of TOC at Station NEU013B

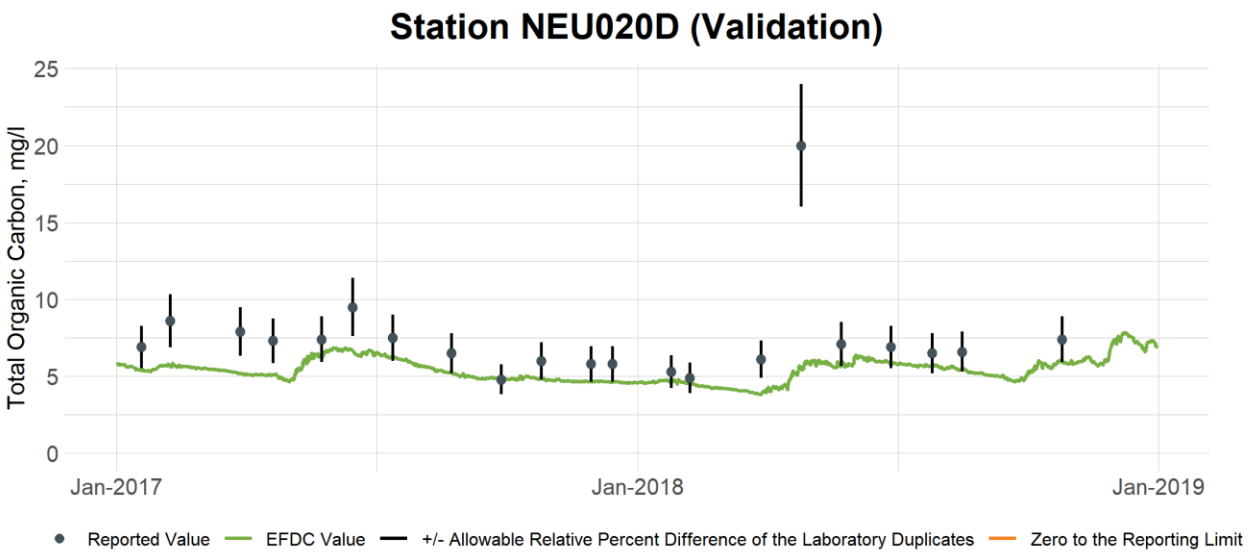

Figure 10-8 Validation Plot of TOC at Station NEU020D

Table 10-4 Calibration Statistics for TOC

Station ID	Starting	Ending	# Pairs	Data Average (mg/L)	Model Average (mg/L)	R^2	RMSE (mg/L)	RSR (%)	RE (%)	AE (mg/L)	CE	pBias (%)
LC01	1/6/2015	12/14/2016	23	8.1	7.4	0.20	1.7	99	15.7	-0.7	0.0	-9.1
LI01	1/6/2015	12/14/2016	24	8.4	6.7	0.13	2.8	151	25.0	-1.7	-1.3	-20.7
LLC01	1/6/2015	12/14/2016	24	8.2	7.3	0.00	2.1	116	18.3	-0.9	-0.3	-10.7
NEU013	1/6/2015	12/14/2016	24	8.4	6.9	0.21	2.1	126	19.6	-1.5	-0.6	-17.5
NEU013B	1/6/2015	12/14/2016	24	8.5	7.2	0.07	2.1	123	18.9	-1.3	-0.5	-15.3
NEU0171B	1/6/2015	12/14/2016	24	8.2	7.2	0.00	2.0	122	17.9	-1.0	-0.5	-11.9
NEU018C	1/6/2015	12/14/2016	24	8.0	7.1	0.01	2.0	115	18.0	-0.8	-0.3	-10.3
NEU018E	1/6/2015	12/14/2016	24	8.1	7.1	0.02	2.1	115	18.5	-1.0	-0.3	-12.1
NEU019E	1/6/2015	12/14/2016	24	8.2	7.0	0.05	2.0	122	18.9	-1.2	-0.5	-14.7
NEU019L	1/6/2015	12/14/2016	23	7.8	6.7	0.06	1.9	118	18.1	-1.1	-0.4	-13.9
NEU019P	1/6/2015	12/14/2016	24	7.7	6.5	0.22	1.8	112	17.2	-1.1	-0.2	-14.6
NEU020D	1/6/2015	12/14/2016	24	7.2	5.9	0.17	1.9	120	19.5	-1.2	-0.4	-17.1

Table 10-5 Validation Statistics for TOC

Station ID	Starting	Ending	# Pairs	Data Average (mg/L)	Model Average (mg/L)	R^2	RMSE (mg/L)	RSR (%)	RE (%)	AE (mg/L)	CE	pBias (%)
LC01	1/18/2017	10/25/2018	22	7.7	7.0	0.16	1.1	127	10.6	-0.7	-0.6	-9.0
LI01	1/18/2017	10/25/2018	21	7.6	6.4	0.04	1.5	197	16.7	-1.2	-2.9	-16.2
LLC01	1/18/2017	10/25/2018	21	7.5	7.0	0.25	1.0	104	12.5	-0.6	-0.1	-7.4
NEU013	1/19/2017	10/25/2018	20	7.6	6.6	0.05	2.2	122	20.4	-1.1	-0.5	-14.1
NEU013B	1/18/2017	10/25/2018	20	7.4	6.8	0.07	1.5	147	15.2	-0.6	-1.2	-7.6
NEU0171B	1/18/2017	10/25/2018	21	7.3	6.9	0.40	1.0	86	11.8	-0.5	0.3	-6.2
NEU018C	1/18/2017	10/25/2018	21	7.7	6.8	0.39	1.2	115	12.3	-0.9	-0.3	-11.5
NEU018E	1/18/2017	10/25/2018	21	7.4	6.7	0.41	1.1	104	12.4	-0.7	-0.1	-9.8
NEU019E	1/18/2017	10/25/2018	21	7.8	6.5	0.11	1.6	164	17.7	-1.3	-1.7	-16.3
NEU019L	1/18/2017	10/25/2018	21	7.4	6.1	0.17	1.5	171	18.2	-1.3	-1.9	-17.0
NEU019P	1/18/2017	10/25/2018	21	7.3	5.9	0.34	1.7	167	19.7	-1.4	-1.8	-19.7
NEU020D	1/18/2017	10/25/2018	21	6.7	5.3	0.54	1.6	141	21.1	-1.4	-1.0	-20.9

10.3 DO

Procedures used to calibrate DO included: 1) check the linkage between WARMF and EFDC to make sure that the setup of DO and other water quality boundary conditions for the EFDC model are correct; and 2) adjust the key kinetic parameters within reasonable ranges to obtain the best match with the observed data. These kinetic parameters include reaeration related parameters that impact surface DO, as well as SOD scaling factor that impacts bottom DO.

Time series of the modeled DO results are presented for comparison to the observed DO data at the surface layer and bottom layer of the model. DO calibration plots for stations NEU013B and NEU020D are given in Figure 10-9 and Figure 10-10, respectively. DO validation plots for stations NEU013B and NEU020D are given in Figure 10-11 and Figure 10-12, respectively. In general, the modeled DO results of both the surface and bottom layers followed the seasonal trend of the measured DO data reasonably well, as can be seen in the model-data plots. The model does very well, in particular, simulating the effect of stratification on bottom water DO at the deep water station (NEU020D) in the lower lake. Comparisons of DO vertical profiles at stations NEU013B and NEU020D are given in Figure 10-13 and Figure 10-14, respectively. As can be seen in the model-data vertical profile plots, the modeled DO profiles generally followed the vertical profile of the observed DO data fairly closely. The observed DO data are shown with solid red dots, and the model results are depicted with blue continuous line in the vertical profiles. Model-data plots for DO for the other ten (10) stations are presented as time-series in Appendix A.2 and as vertical profiles in Appendix A.3.

The summary statistics for model performance of DO are given in Table 10-6 and Table 10-7. During the calibration period, the calculated RSRs ranged from 41% at station LC01 and NEU018E to 76% at station NEU020D for the surface DO, and from 23% at station LC01 to 55% at station NEU013B for the bottom DO, as shown in Table 10-6. The surface DO RSR target (RSR≤50%) is met at five (5) stations, and the bottom DO RSR target is met at all stations except for NEU013B. During the validation period, the calculated RSRs ranged from 33% at station LC01 to 77% at station NEU020D for the surface DO, and from 33% at station NEU0171B to 60% at station NEU018C for the bottom DO, as shown in Table 10-7. The surface DO RSR target (RSR≤50%) is met at six (6) stations, mostly located in zones 2 and 4 (See Figure 3-1). The bottom DO RSR target is met at seven (7) stations.

For the calibration period, the pBias ranged from -3.2% at station NEU0171B to 4.5% at stations NEU019P and NEU020D for the surface DO, and from -3.6% at station LLC01 to 21.5% at station NEU019L for the bottom DO. Based on the approved QAPP, the pBias range for the surface layer falls within the “very good” criteria for the water quality/nutrient of the watershed model calibration guidance (See Table A.7-2 of QAPP). Within the bottom layer, the model results fall within the “good” criteria. With the exception of station LLC01, the bottom DO is overestimated, especially in zone 3 where the surface DO is also overestimated (See Figure 3-1). The overestimation of DO in this zone is seen during fall when lake overturn causes rapid mixing of DO from the surface to bottom layers.

For the validation period, the pBias ranged from -1.9% at station NEU0171B to 15.2% at station NEU020D for the surface DO, and from 0.1% at station LLC01 to 36.1% at station LI01 for the bottom DO. The pBias range for the surface layer falls within the “good” criteria for the water quality/nutrient of the watershed model calibration guidance (See Table A.7-2 of QAPP), and

the bottom layer falls within the “fair” criteria. The overestimation of bottom DO can be partially related to the underestimation of TOC during the validation period or missing the timing of the fall overturn. Questions regarding the accuracy of bottom DO measurements associated with profile data collected at some DWR stations including NEU020D is provided in Section 7.3.

In summary, the seasonal pattern of simulated DO was in good agreement with observed DO in both the surface and bottom layers and the calculated pBias metrics during calibration fall within the “very good” to “fair” criteria for the water quality/nutrient of the WARMF model calibration guidance. In particular, the effect of the onset and erosion of stratification on bottom water DO at the deep water station (NEU020D) in the lower lake was in good agreement with observations. The Falls Lake model results for DO are, therefore, deemed to be acceptable.

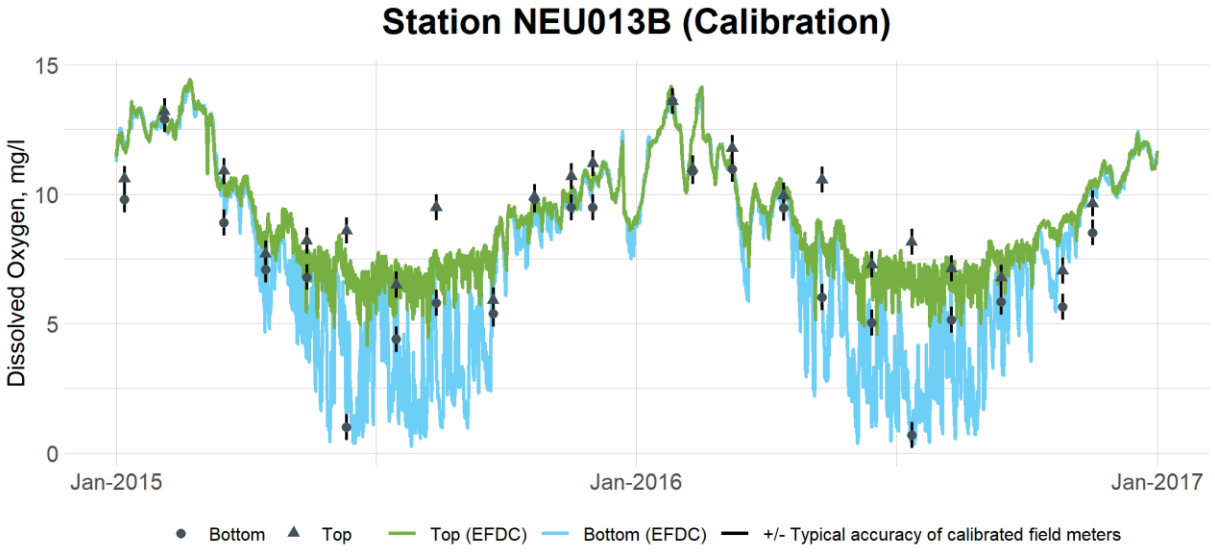

Figure 10-9 Calibration Plot of Top and Bottom DO at Station NEU013B

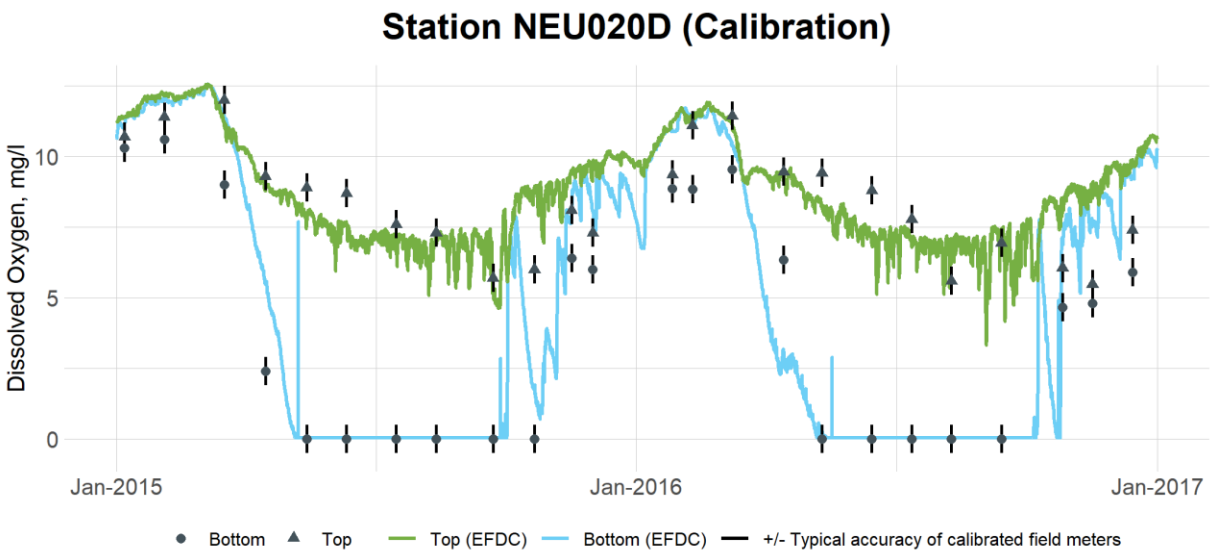

Figure 10-10 Calibration Plot of Top and Bottom DO at Station NEU020D

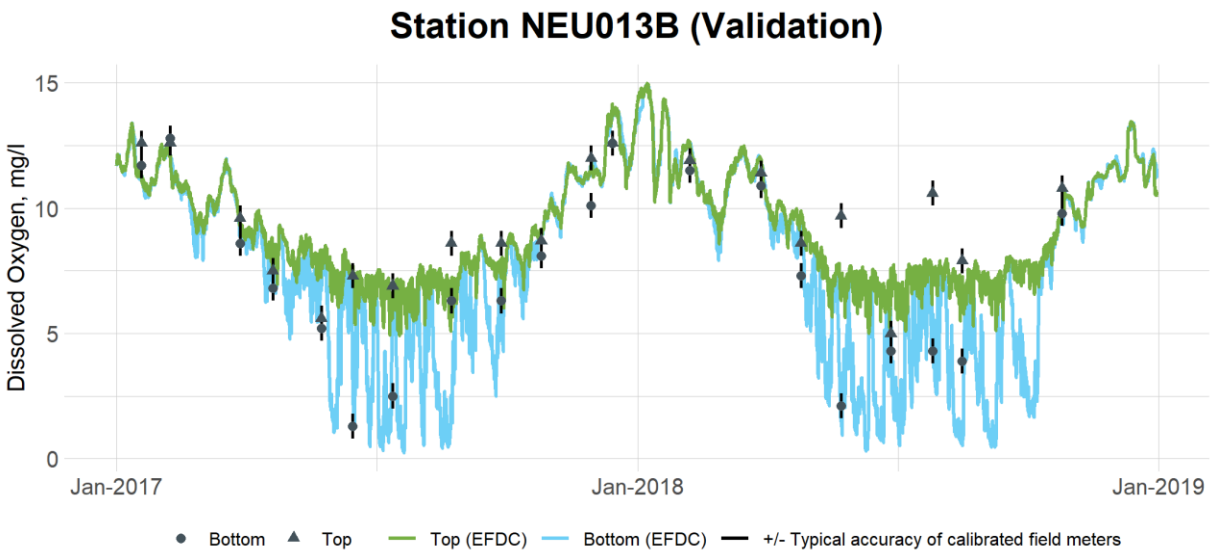

Figure 10-11 Validation Plot of Top and Bottom DO at Station NEU013B

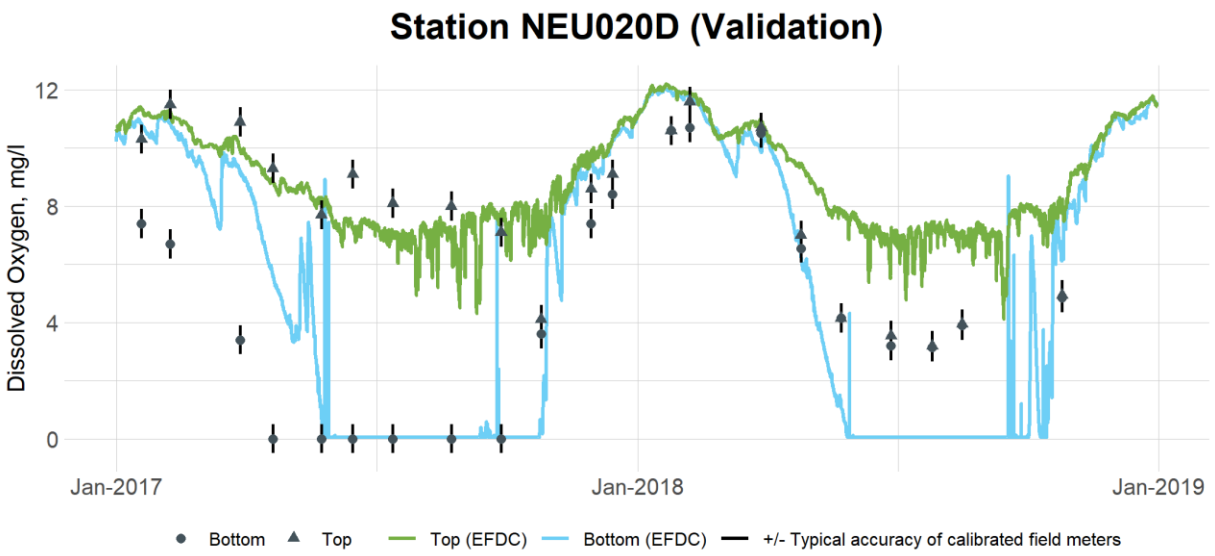

Figure 10-12 Validation Plot of Top and Bottom DO at Station NEU020D

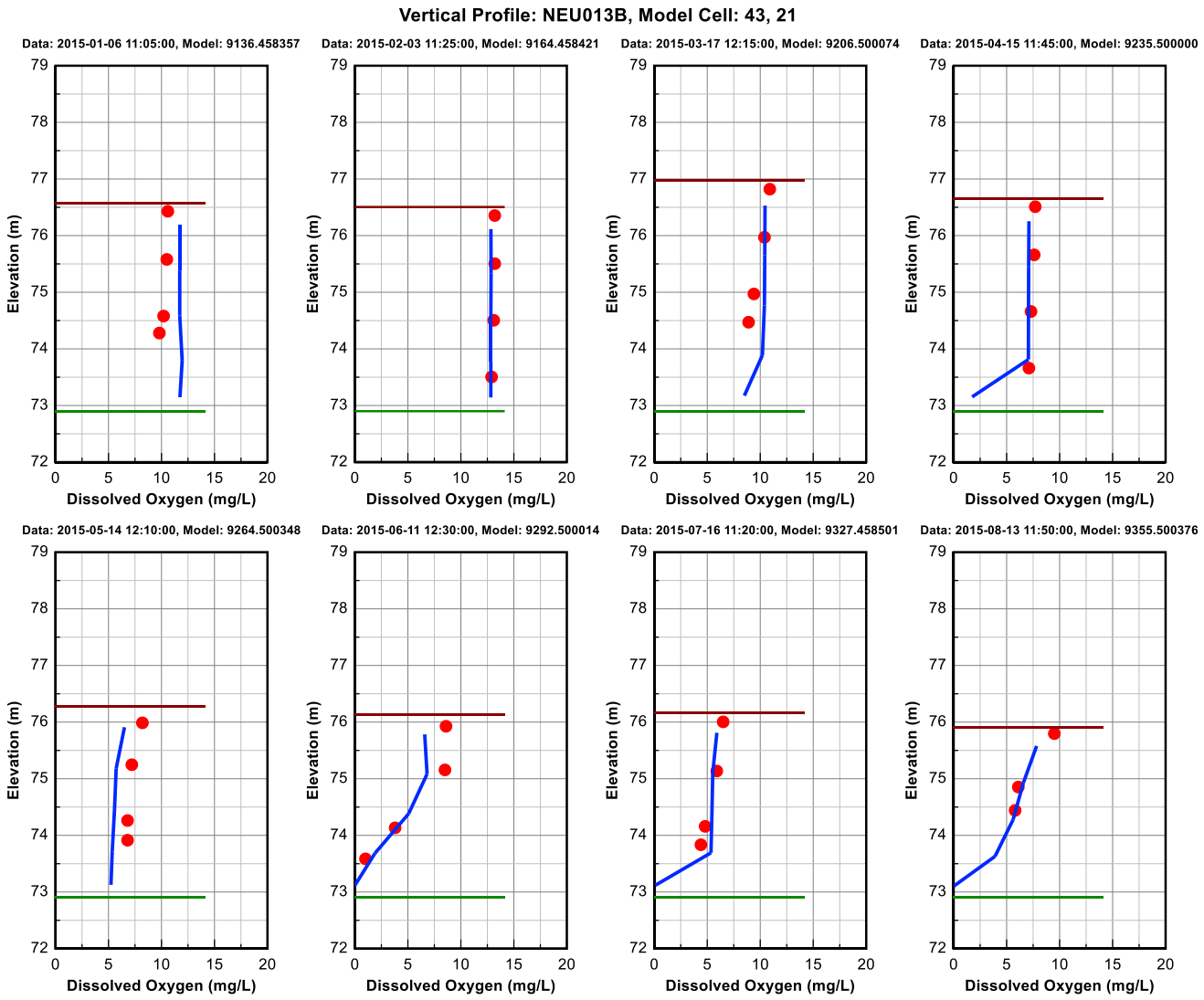

January 2015 – August 2015 (1 of 6)

Vertical Profile: NEU013B, Model Cell: 43, 21

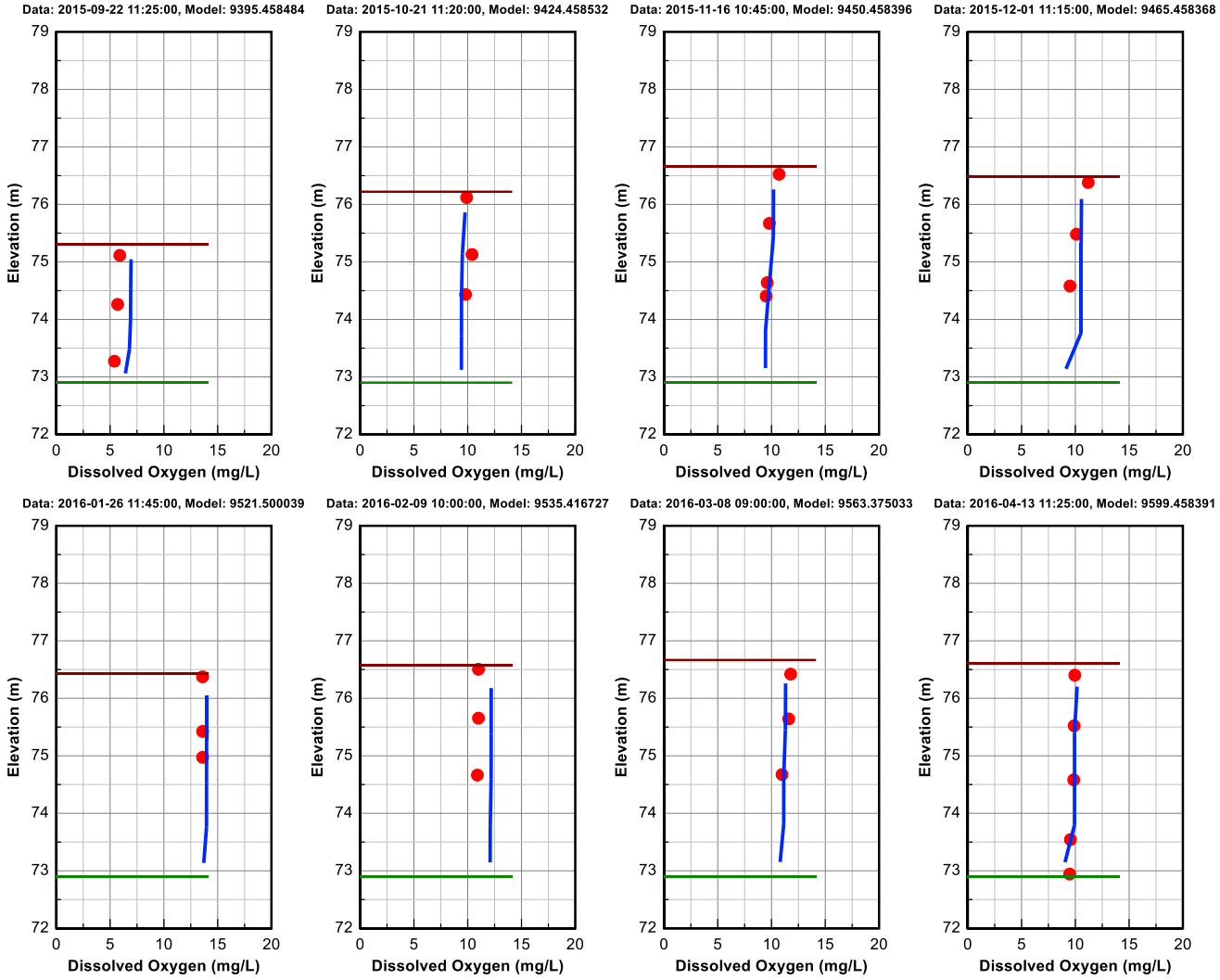

September 2015 – April 2016 (2 of 6)

Vertical Profile: NEU013B, Model Cell: 43, 21

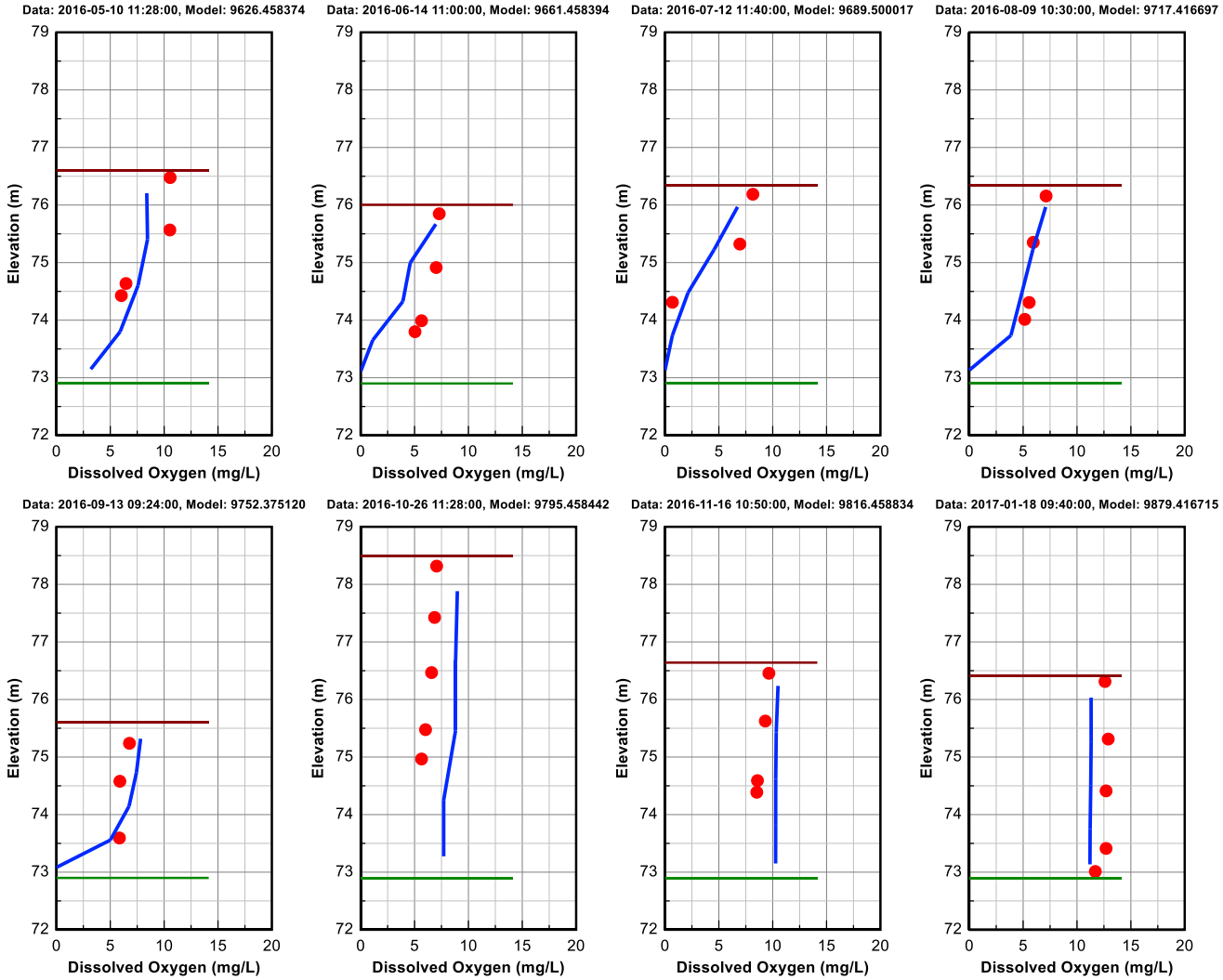

May 2016 – January 2017 (3 of 6)

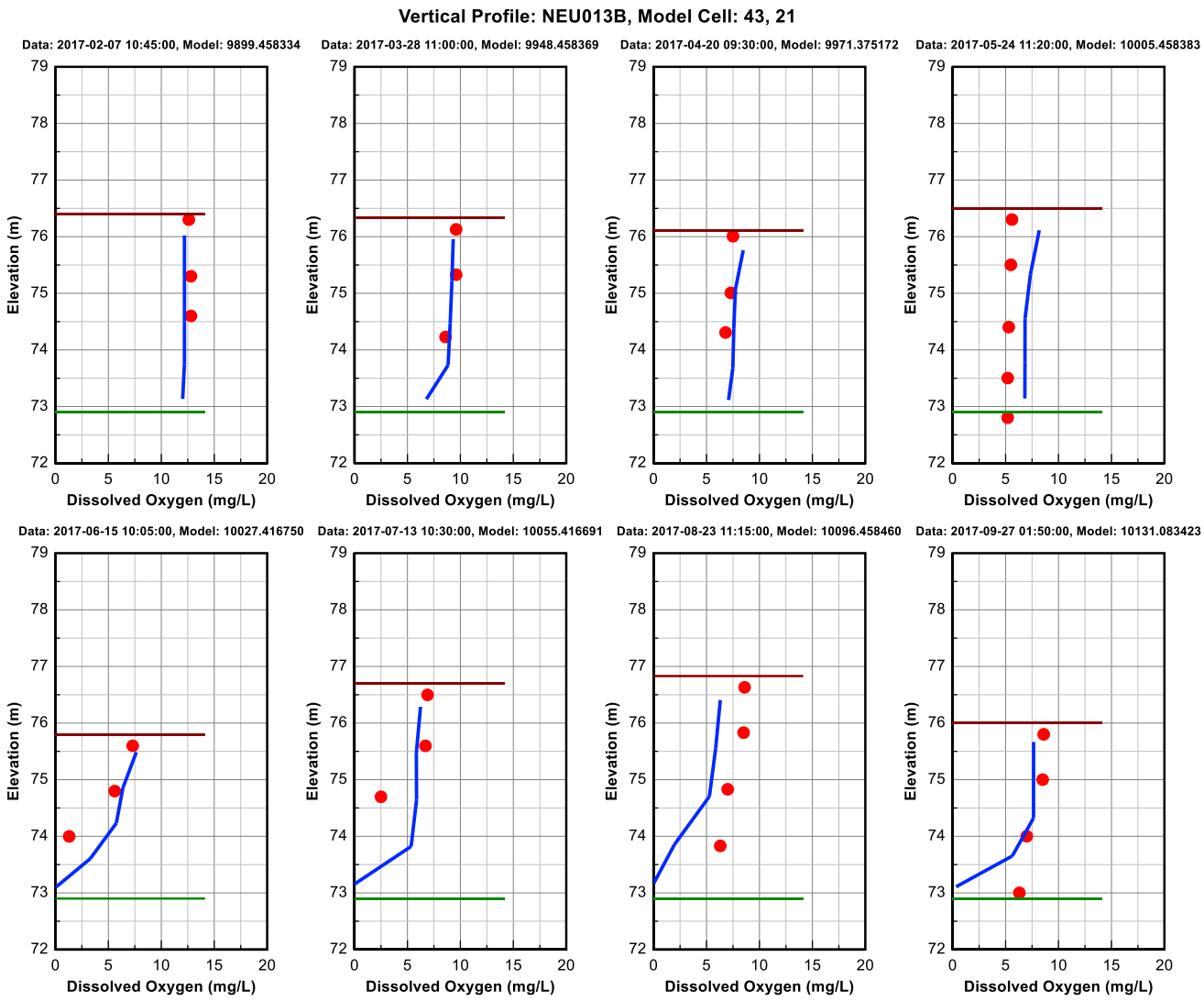

February 2017 – September 2017 (4 of 6)

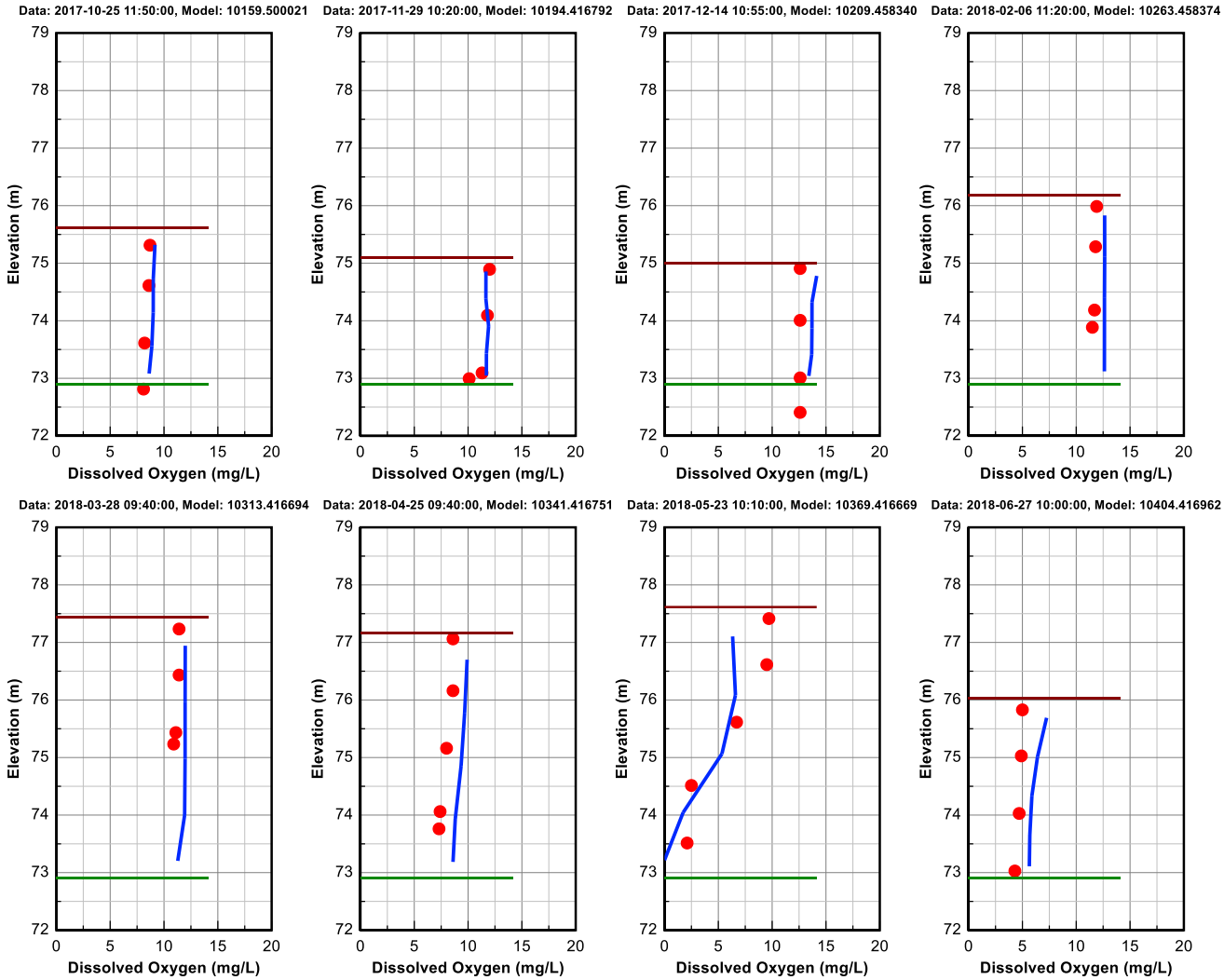

October 2017 – June 2018 (5 of 6)

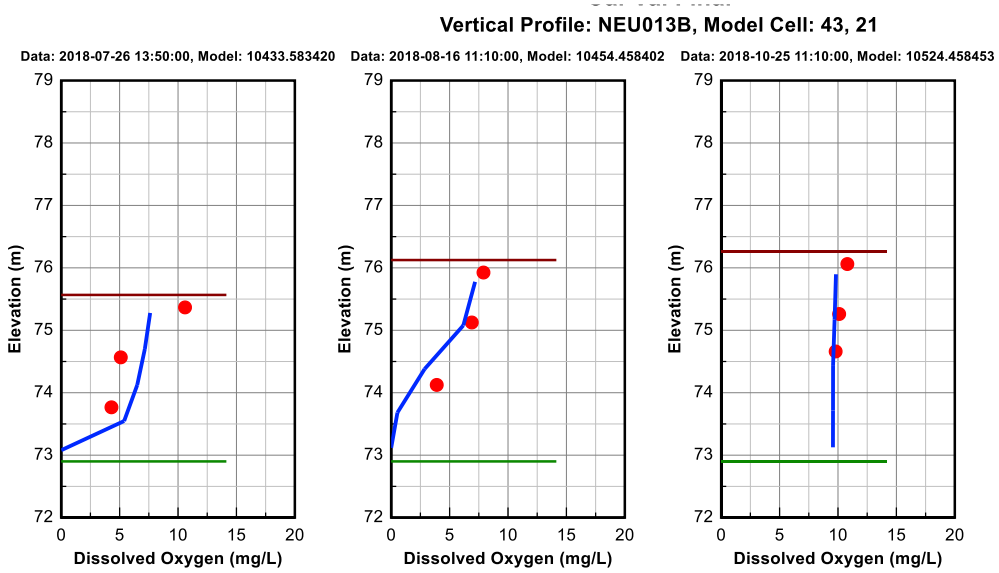

July 2018 – October 2018 (6 of 6)

Figure 10-13 DO Vertical Profile Comparison Plot at Station NEU013B. Red dots are data, and blue continuous lines are model results

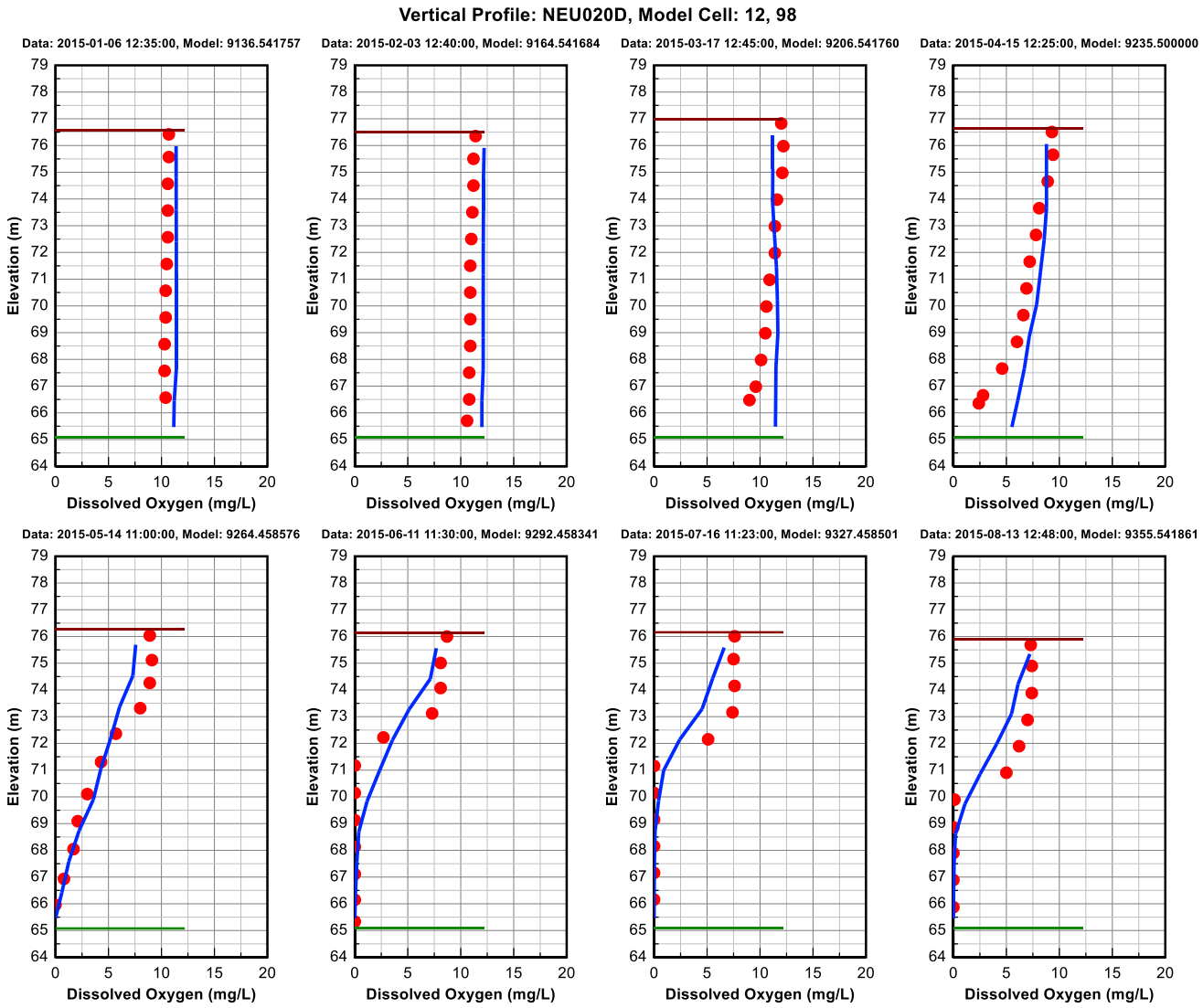

January 2015 – August 2015 (1 of 6)

Vertical Profile: NEU020D, Model Cell: 12, 98

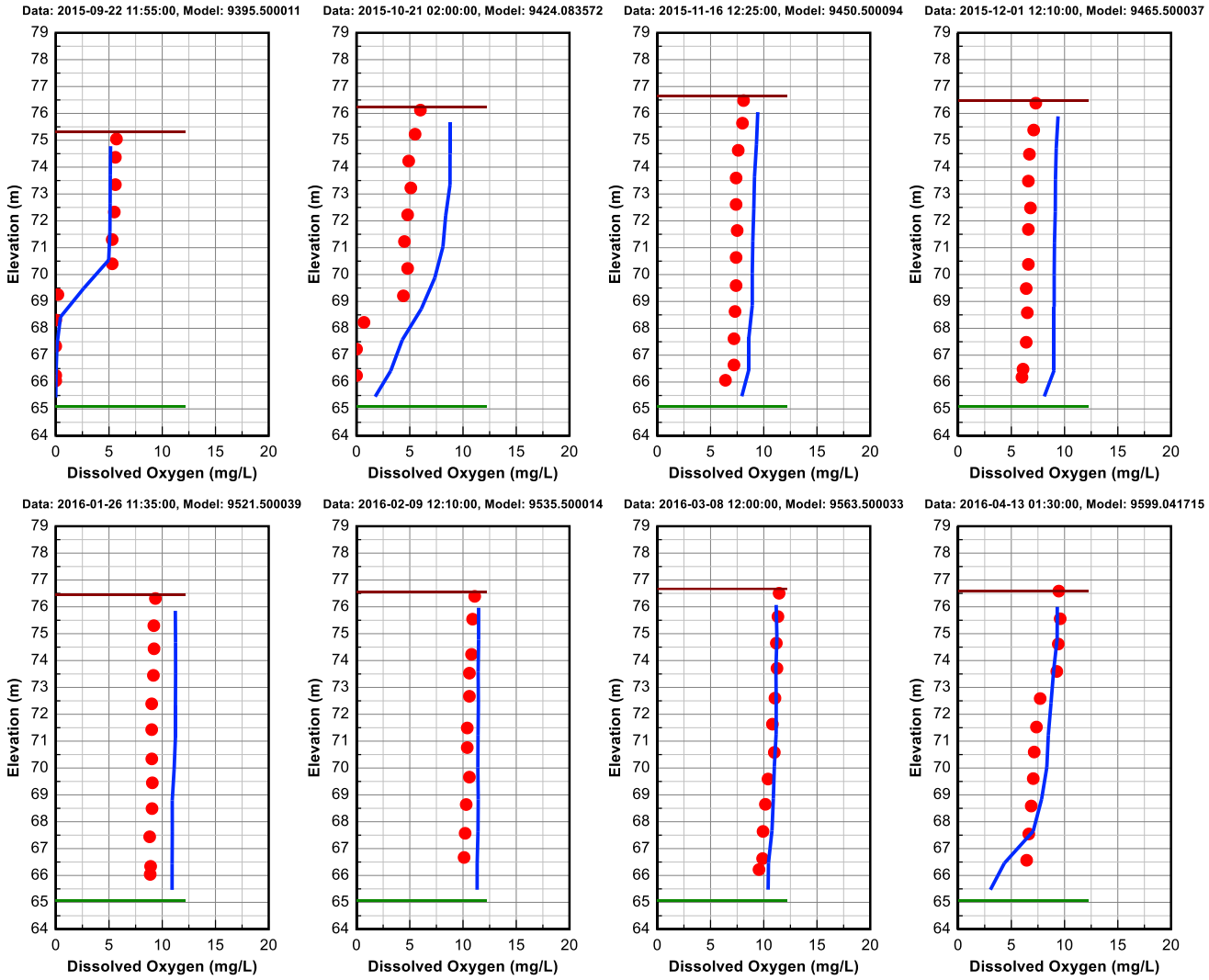

September 2015 – April 2016 (2 of 6)

Vertical Profile: NEU020D, Model Cell: 12, 98

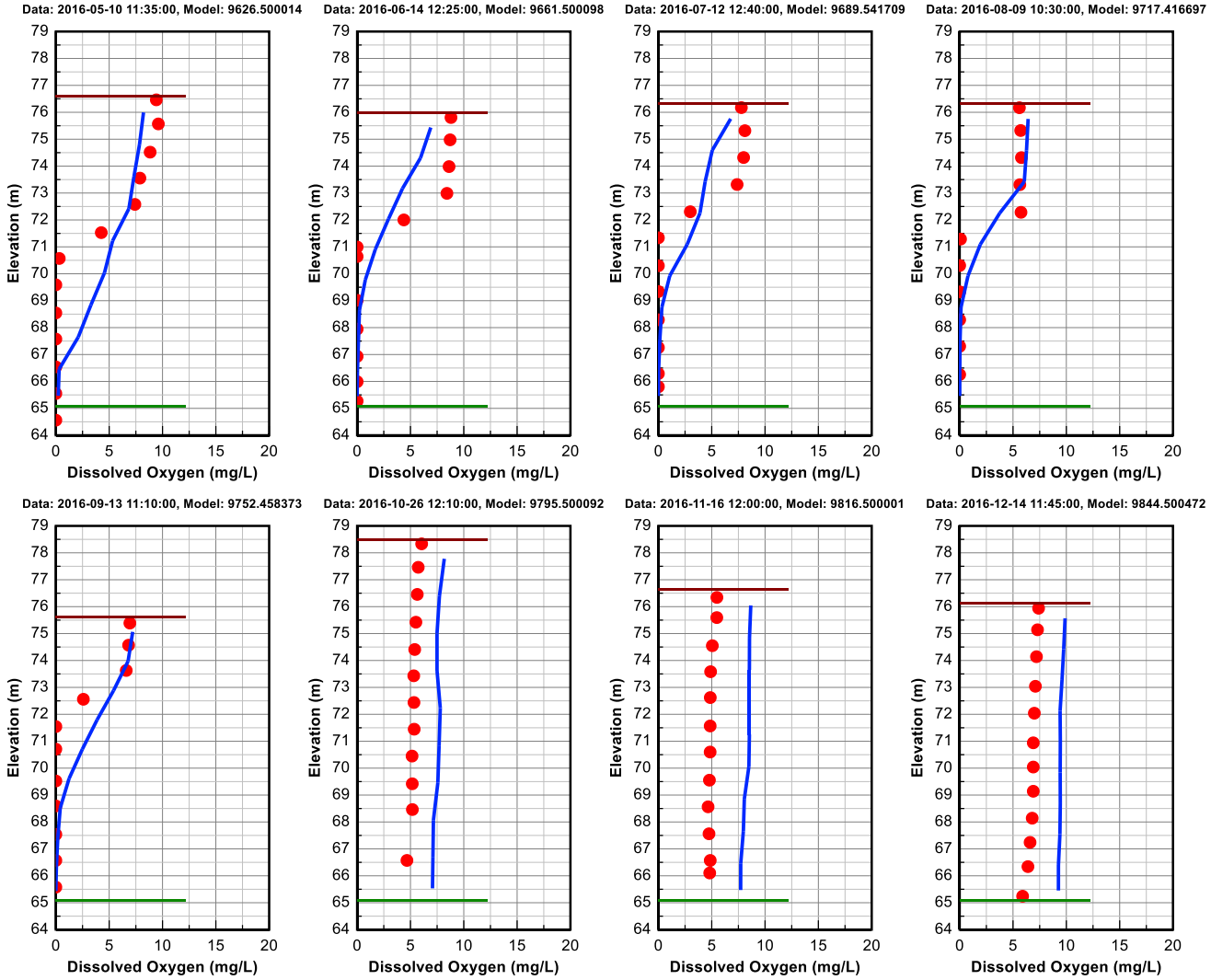

May 2016 – December 2016 (3 of 6)

Vertical Profile: NEU020D, Model Cell: 12, 98

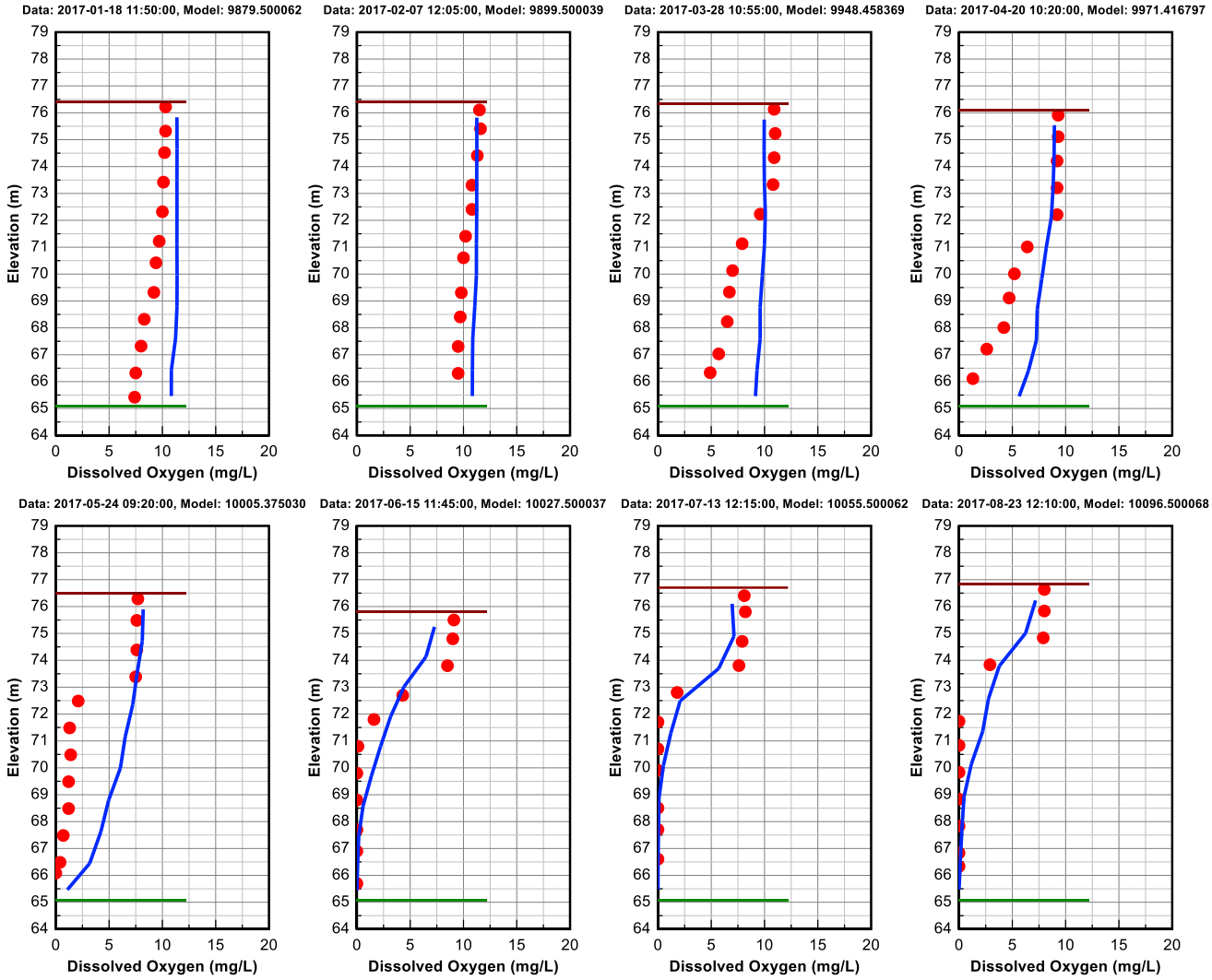

January 2017 – August 2017 (4 of 6)

Vertical Profile: NEU020D, Model Cell: 12, 98

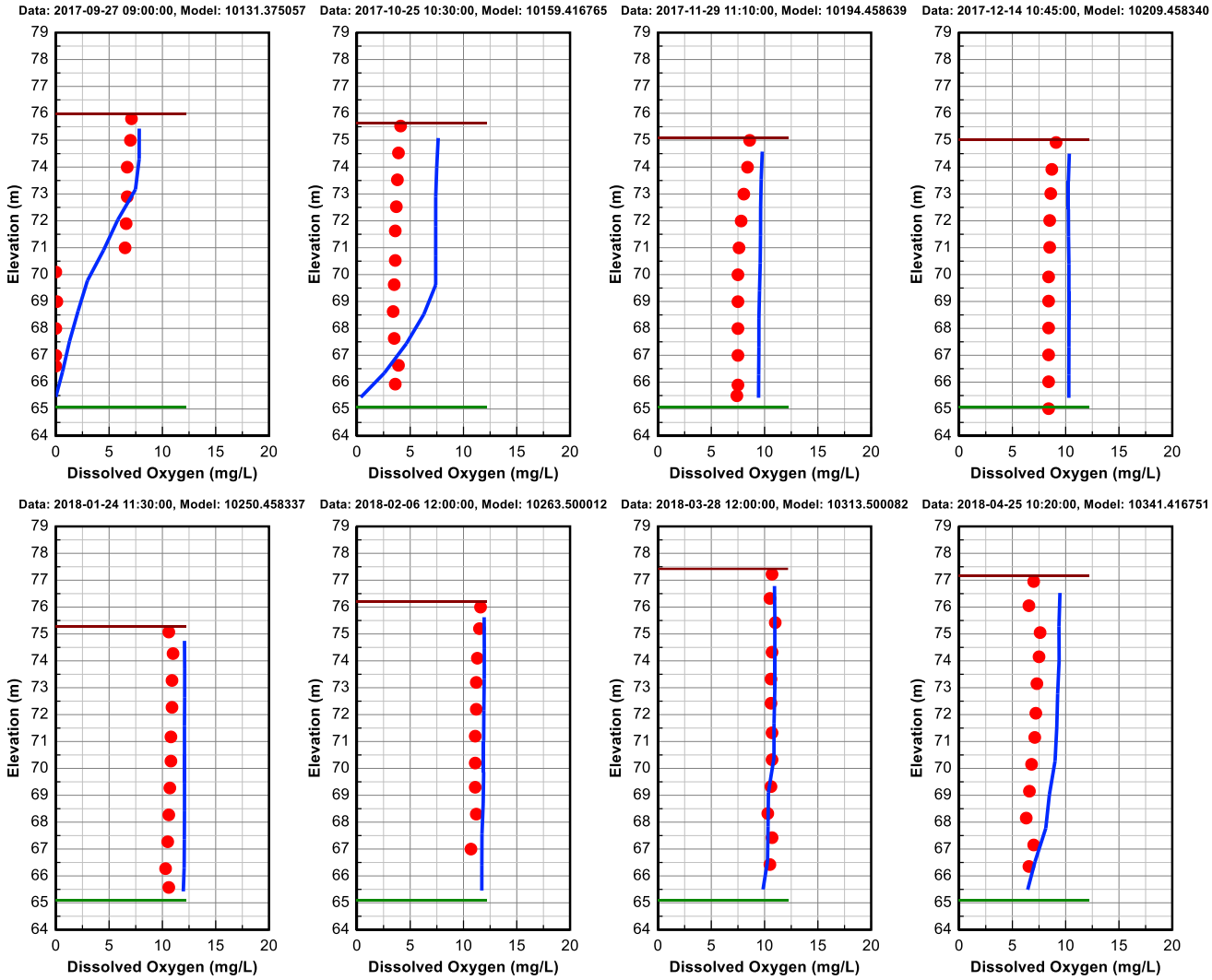

September 2017 – April 2018 (5 of 6)

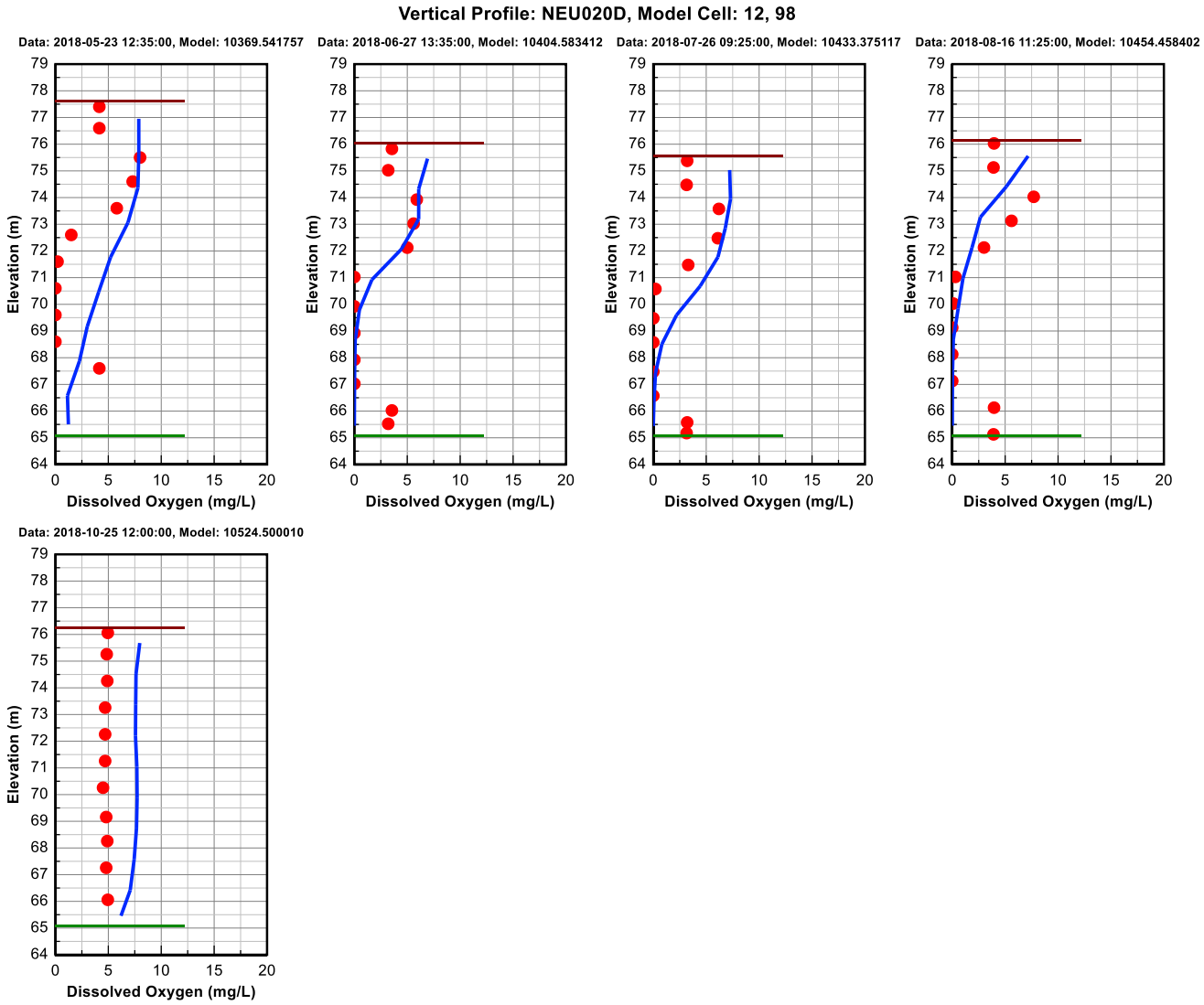

May 2018 – October 2018 (6 of 6)

Figure 10-14 DO Vertical Profile Comparison Plot at Station NEU020D. Red dots are data, and blue continuous lines are model results

Table 10-6 Calibration Statistics for DO

Station ID	Starting	Ending	Layer	# Pairs	Data Average (mg/L)	Model Average (mg/L)	R^2	RMSE (mg/L)	RSR (%)	RE (%)	AE (mg/L)	CE	pBias (%)
LC01	1/6/2015	12/14/2016	*Top*	23	8.88	9.0	0.99	0.98	41	3.76	-0.46	0.91	1.5
			Bottom	23	6.32	6.5	0.99	0.95	23	4.15	0.03	0.90	3.3
LI01	1/6/2015	12/14/2016	*Top*	23	9.06	8.8	0.99	1.03	73	4.04	-0.03	0.89	-2.5
			Bottom	20	6.19	6.9	0.99	1.85	49	4.83	0.33	0.87	11.2
LLC01	1/6/2015	12/14/2016	*Top*	24	9.43	9.2	0.99	0.86	48	5.49	-0.91	0.87	-2.1
			Bottom	24	7.03	6.8	0.99	1.54	40	5.18	0.18	0.87	-3.6
NEU013	1/6/2015	12/14/2016	*Top*	28	9.00	9.2	0.99	1.42	64	4.55	-0.06	0.90	2.3
			Bottom	12	7.62	8.2	0.98	1.15	34	7.41	1.13	0.82	8.0
NEU013B	1/6/2015	12/14/2016	*Top*	23	9.39	9.2	0.99	1.10	53	2.94	0.03	0.93	-2.3
			Bottom	14	7.16	7.3	1.00	1.58	55	3.53	0.63	0.90	2.6
NEU0171B	2/3/2015	12/14/2016	*Top*	24	9.23	9.0	0.99	0.99	50	4.14	-0.66	0.89	-3.2
			Bottom	17	7.66	8.3	0.99	1.60	45	5.11	-0.37	0.87	8.8
NEU018C	1/6/2015	12/14/2016	*Top*	23	8.95	9.1	0.99	0.80	43	4.01	-0.38	0.90	1.7
			Bottom	19	7.82	7.9	1.00	1.36	43	4.11	0.10	0.91	1.1
NEU018E	1/6/2015	12/14/2016	*Top*	24	9.41	9.2	0.99	0.78	48	3.95	-0.25	0.90	-2.8
			Bottom	10	7.87	8.1	0.98	1.98	46	7.52	-0.22	0.84	2.6
NEU019E	1/6/2015	12/14/2016	*Top*	24	8.69	8.8	0.99	1.17	58	3.99	-0.35	0.90	1.1
			Bottom	20	6.04	7.0	0.97	1.55	37	9.77	0.80	0.75	16.0
NEU019L	1/6/2015	12/14/2016	*Top*	23	8.44	8.7	0.99	1.16	62	4.62	-0.31	0.88	2.5
			Bottom	13	5.22	6.3	0.88	1.53	37	9.67	-0.70	0.64	21.5
NEU019P	1/6/2015	12/14/2016	*Top*	24	8.56	8.9	0.99	1.21	64	4.42	-0.45	0.88	4.5
			Bottom	14	4.42	4.8	0.81	1.99	47	8.86	0.65	0.60	7.8
NEU020D	1/6/2015	12/14/2016	*Top*	24	8.41	8.8	0.99	1.47	76	4.49	-0.50	0.88	4.5
			Bottom	19	4.00	4.6	0.92	1.64	41	7.4	-0.68	0.73	15.7

Table 10-7 Validation Statistics for DO

Station ID	Starting	Ending	Layer	# Pairs	Data Average (mg/L)	Model Average (mg/L)	R^2	RMSE (mg/L)	RSR (%)	RE (%)	AE (mg/L)	CE	pBias (%)
LC01	1/18/2017	10/25/2018	*Top*	22	8.86	8.9	0.99	0.87	33	3.76	-0.46	0.91	-0.4
			Bottom	20	6.81	7.4	0.99	1.62	35	4.15	0.03	0.90	8.3
LI01	1/18/2017	10/25/2018	*Top*	21	9.08	9.1	0.99	0.83	40	4.04	-0.03	0.89	-0.2
			Bottom	15	4.80	6.5	0.99	2.51	52	4.83	0.33	0.87	36.1
LLC01	1/18/2017	10/25/2018	*Top*	21	9.26	9.1	0.99	0.96	43	5.49	-0.91	0.87	-1.2
			Bottom	19	6.86	6.9	0.99	1.56	39	5.18	0.18	0.87	0.1
NEU013	1/18/2017	10/25/2018	*Top*	20	9.07	9.2	0.99	1.51	70	4.55	-0.06	0.90	1.1
			Bottom	14	7.63	8.1	0.98	1.19	34	7.41	1.13	0.82	6.7
NEU013B	1/18/2017	10/25/2018	*Top*	20	9.43	9.3	0.99	1.55	68	2.94	0.03	0.93	-1.7
			Bottom	13	8.09	8.5	1.00	1.58	52	3.53	0.63	0.90	4.5
NEU0171B	1/18/2017	10/25/2018	*Top*	21	9.45	9.3	0.99	0.85	42	4.14	-0.66	0.89	-1.9
			Bottom	12	8.86	9.1	0.99	1.17	33	5.11	-0.37	0.87	2.9
NEU018C	1/18/2017	10/25/2018	*Top*	21	9.28	9.2	0.99	0.69	35	4.01	-0.38	0.90	-0.4
			Bottom	16	6.58	7.9	1.00	2.54	60	4.11	0.10	0.91	20.2
NEU018E	1/18/2017	10/25/2018	*Top*	21	9.26	9.3	0.99	1.09	48	3.95	-0.25	0.90	-0.1
			Bottom	13	6.23	7.1	0.98	2.35	51	7.52	-0.22	0.84	14.0
NEU019E	1/18/2017	10/25/2018	*Top*	20	8.95	8.8	0.99	1.31	55	3.99	-0.35	0.90	-1.4
			Bottom	15	4.93	6.2	0.97	2.05	44	9.77	0.80	0.75	26.0
NEU019L	1/18/2017	10/25/2018	*Top*	21	8.53	8.8	0.99	1.79	63	4.62	-0.31	0.88	3.4
			Bottom	8	3.89	4.6	0.88	2.48	59	9.67	-0.70	0.64	18.9
NEU019P	1/18/2017	10/25/2018	*Top*	20	8.25	8.8	0.99	1.72	72	4.42	-0.45	0.88	6.5
			Bottom	8	4.88	5.7	0.81	1.70	39	8.86	0.65	0.60	16.3
NEU020D	1/18/2017	10/25/2018	*Top*	21	7.79	9.0	0.99	2.10	77	4.49	-0.50	0.88	15.2
			Bottom	9	5.42	5.7	0.92	1.61	39	7.4	-0.68	0.73	5.0

10.4 TN

Procedures used to calibrate the organic and inorganic forms of nitrogen included: 1) check the linkage between WARMF and EFDC to make sure that the setup of nitrogen and other water quality boundary conditions for the EFDC model is correct; and 2) adjust the key kinetic parameters within reasonable ranges to match the observed data. These kinetic parameters include minimum mineralization rate of DON, maximum nitrification rate, etc. Also, TN is connected with nitrogen release through basal metabolism and predation processes related to algal kinetics.

TN model results are presented for comparison to the observed data for the the equivalent photic layers. TN calibration plots for stations NEU013B and NEU020D are given in Figure 10-15 and Figure 10-16, and the validation plots are given in Figure 10-17 and Figure 10-18, respectively. As can be seen in these model-data plots, the model results generally follow the trend of the measured data for both calibration and validation periods. Calibration and validation results for the other ten (10) stations are presented in Appendix A.2 for ammonia, nitrate, TON and total Kjeldhal nitrogen.

The summary statistics for model performance of TN are given in Table 10-8 and Table 10-9. It can be seen that the RSR target for TN is not met (RSR≤100%) at any stations during both calibration and validation periods. For the calibration period, the calculated RSRs ranged from 111% at station NEU020D to 281% at station LI01, as shown in Table 10-8. For the validation period, the calculated RSRs ranged from 129% at station NEU019P to 332% at station LI01, as shown in Table 10-9. The highest RSR at station LI01 during calibration and validation is related to the over-estimation of NO_3.

For the calibration period, the pBias ranged from -15.5% at station NEU013 to 6.3% at station NEU019L. This shows that the model is not systematically over or under predicting TN concentration in the water column during the calibration period. On the other hand, for the validation period the pBias ranged from -20.0% at station NEU013B to 1.8% at station LI01. Except for station LLC01, the model is systematically underestimating TN during validation, which is due to the underestimation of TON.

When considered together, the RSR and pBias statistics indicate that the model is performing well on average, but not capturing the variability (or lack of variability) in the observed concentrations. Based on the approved QAPP for the water quality/nutrient of the watershed model calibration guidance (See Table A.7-2 of QAPP), the pBias values fall within the “very good” criteria for the calibration period and the “good” criteria for the validation period. The lake model results for TN, therefore, are deemed to be acceptable.

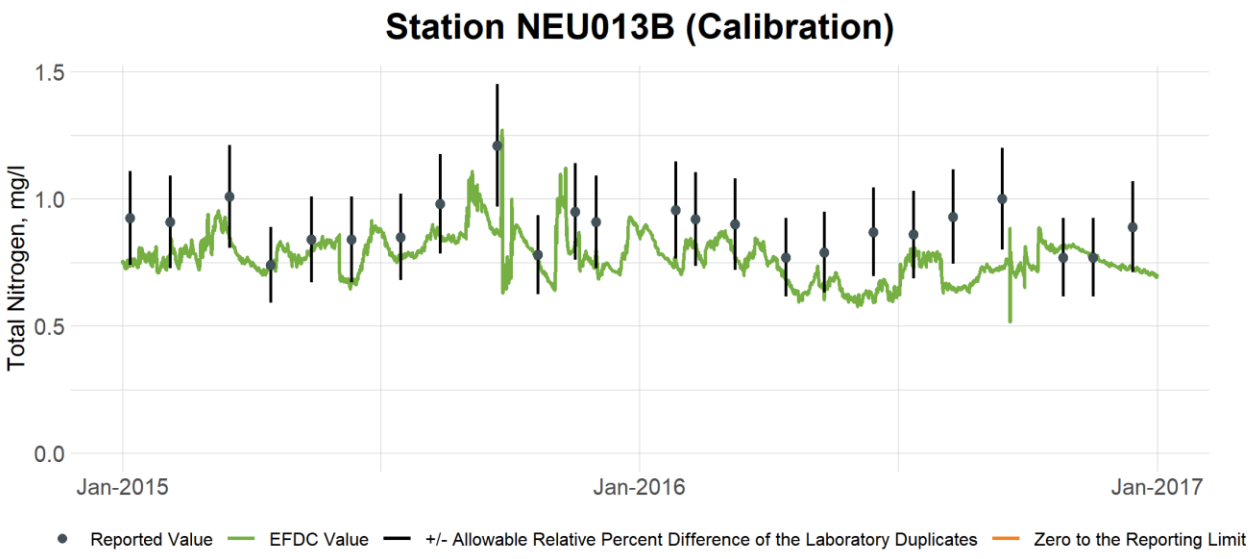

Figure 10-15 Calibration Plot of TN at Station NEU013B

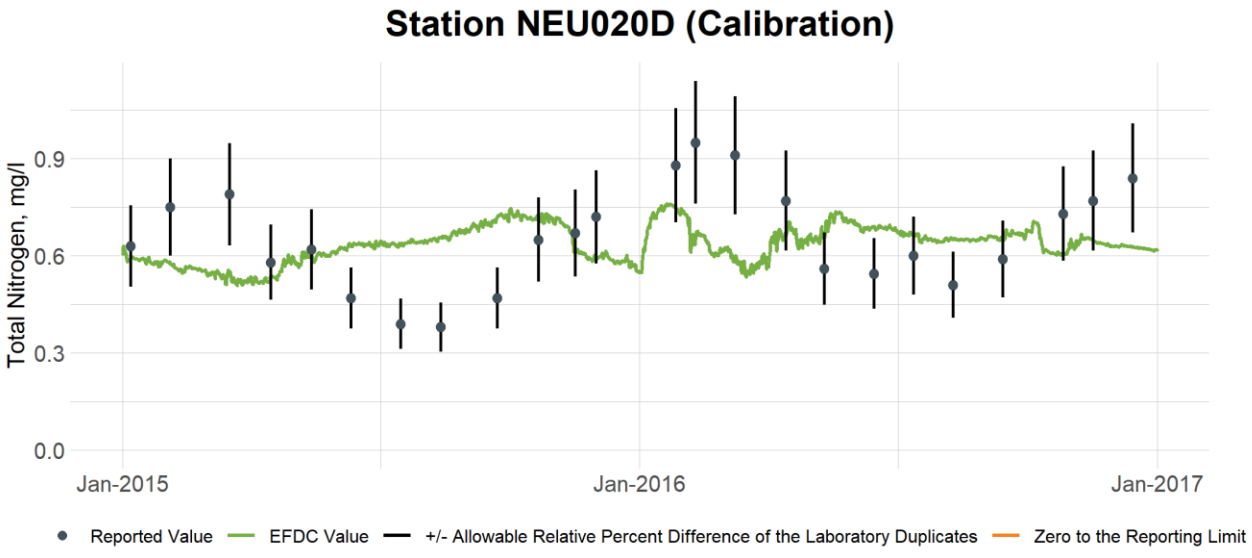

Figure 10-16 Calibration Plot of TN at Station NEU020D

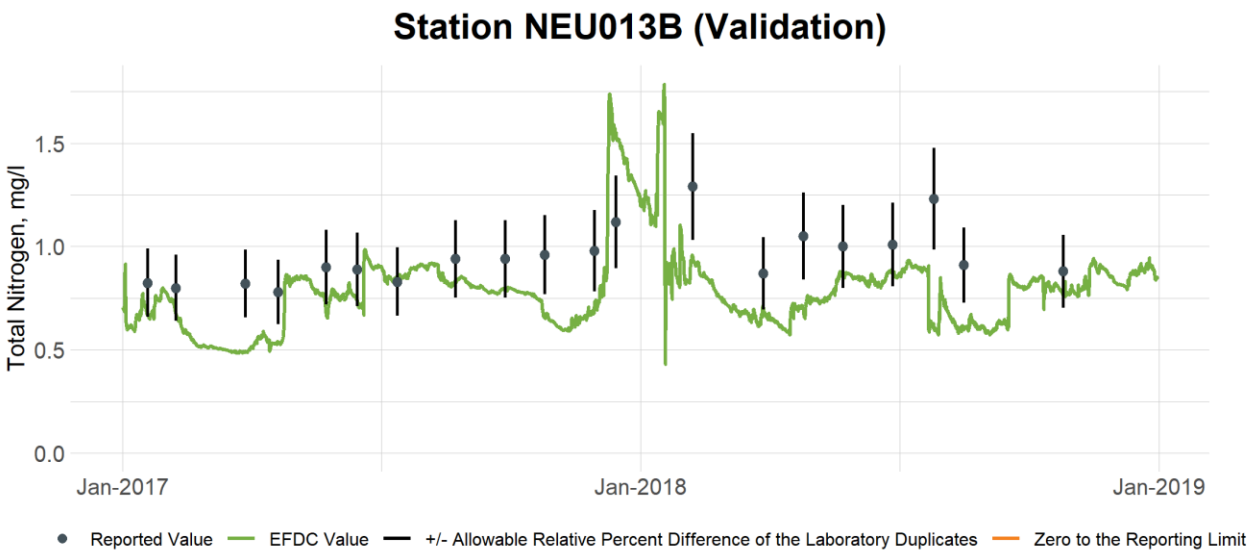

Figure 10-17 Validation Plot of TN at Station NEU013B

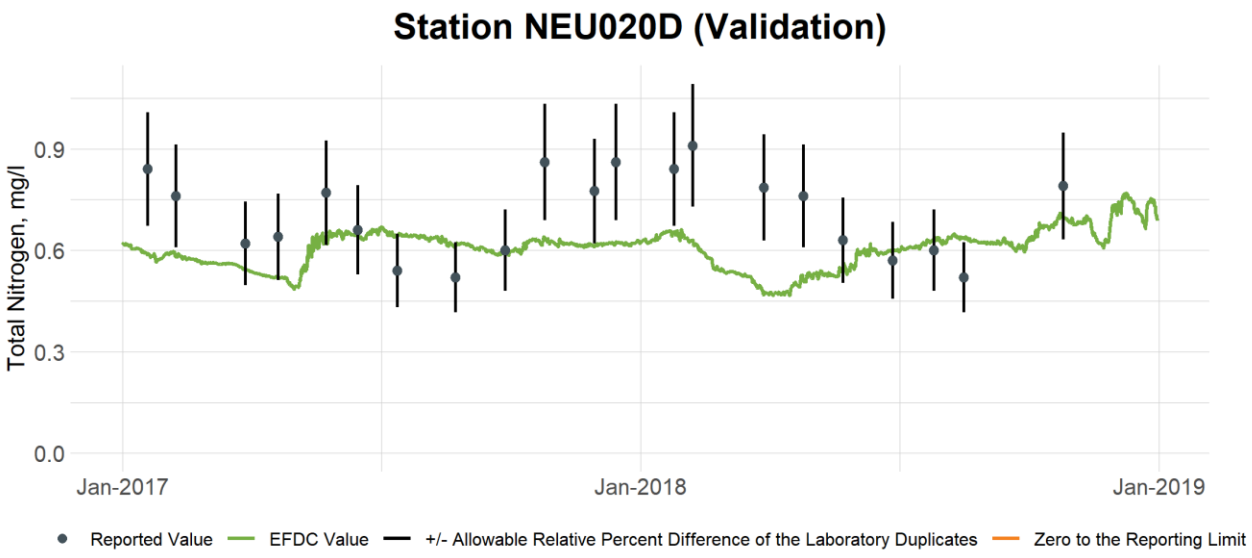

Figure 10-18 Validation Plot of TN at Station NEU020D

Table 10-8 Calibration Statistics for TN

Station ID	Starting	Ending	# Pairs	Data Average (mg/L)	Model Average (mg/L)	R^2	RMSE (mg/L)	RSR (%)	RE (%)	AE (mg/L)	CE	pBias (%)
LC01	1/6/2015	12/14/2016	22	0.750	0.749	0.001	0.107	127	12.2	-0.001	-0.60	-0.2
LI01	1/6/2015	12/14/2016	24	0.743	0.775	0.050	0.250	281	25.0	0.032	-6.94	4.3
LLC01	1/6/2015	12/14/2016	24	0.802	0.784	0.000	0.130	146	13.2	-0.019	-1.10	-2.3
NEU013	1/6/2015	12/14/2016	24	0.976	0.824	0.171	0.238	119	18.9	-0.152	-0.41	-15.5
NEU013B	1/6/2015	12/14/2016	24	0.890	0.759	0.195	0.161	160	15.4	-0.131	-1.55	-14.8
NEU0171B	1/6/2015	12/14/2016	24	0.807	0.774	0.008	0.136	133	15.0	-0.033	-0.77	-4.0
NEU018C	1/6/2015	12/14/2016	24	0.748	0.754	0.009	0.124	121	12.8	0.007	-0.45	0.9
NEU018E	1/6/2015	12/14/2016	24	0.747	0.750	0.007	0.128	119	14.3	0.003	-0.40	0.4
NEU019E	1/6/2015	12/14/2016	24	0.727	0.725	0.027	0.140	127	15.3	-0.002	-0.63	-0.3
NEU019L	1/6/2015	12/14/2016	23	0.667	0.709	0.113	0.164	134	19.9	0.042	-0.79	6.3
NEU019P	1/6/2015	12/14/2016	24	0.694	0.688	0.025	0.176	114	21.0	-0.005	-0.30	-0.8
NEU020D	1/6/2015	12/14/2016	24	0.657	0.636	0.025	0.172	111	22.5	-0.021	-0.24	-3.2

Table 10-9 Validation Statistics for TN

Station ID	Starting	Ending	# Pairs	Data Average (mg/L)	Model Average (mg/L)	R^2	RMSE (mg/L)	RSR (%)	RE (%)	AE (mg/L)	CE	pBias (%)
LC01	1/18/2017	10/25/2018	22	0.783	0.724	0.015	0.141	181	14.2	-0.059	-2.26	-7.6
LI01	1/18/2017	10/25/2018	21	0.792	0.806	0.009	0.292	332	24.8	0.015	-10.02	1.8
LLC01	1/18/2017	10/25/2018	21	0.823	0.797	0.014	0.256	278	22.3	-0.026	-6.76	-3.2
NEU013	1/19/2017	10/25/2018	20	1.015	0.822	0.047	0.313	234	26.9	-0.193	-4.42	-19.0
NEU013B	1/18/2017	10/25/2018	20	0.951	0.761	0.205	0.269	201	24.5	-0.191	-3.05	-20.0
NEU0171B	1/18/2017	10/25/2018	21	0.825	0.726	0.116	0.149	160	13.9	-0.099	-1.59	-12.0
NEU018C	1/18/2017	10/25/2018	20	0.788	0.714	0.011	0.138	172	13.6	-0.073	-1.99	-9.3
NEU018E	1/18/2017	10/25/2018	21	0.757	0.714	0.000	0.129	157	11.8	-0.043	-1.51	-5.6
NEU019E	1/18/2017	10/25/2018	21	0.736	0.707	0.020	0.146	149	15.6	-0.029	-1.20	-4.0
NEU019L	1/18/2017	10/25/2018	21	0.714	0.665	0.013	0.135	175	15.9	-0.049	-2.09	-6.8
NEU019P	1/18/2017	10/25/2018	21	0.705	0.646	0.012	0.131	129	14.4	-0.059	-0.64	-8.3
NEU020D	1/18/2017	10/25/2018	21	0.707	0.600	0.004	0.168	138	20.2	-0.107	-0.91	-15.1

10.5 TP

Procedures used to calibrate TP state variables include: 1) check the linkage between WARMF and EFDC to make sure that the setup of phosphorus and other water quality boundary conditions for the EFDC model is correct; and 2) adjust the key kinetic parameters within reasonable ranges to match the observed data. Phosphate (PO_4) is partially connected with basal metabolism and predation processes during the algae production cycle.

TP model results are presented for comparison to the observed data for the the equivalent photic layers. TP calibration plots for stations NEU013B and NEU020D are given in Figure 10-19 and Figure 10-20, and the validation plots are given in Figure 10-21 and Figure 10-22, respectively. As can be seen from Figure 10-19, during summer 2015 and spring 2016 the model is underestimating TP concentrations at station NEU013B. As described in the watershed model report (BC and Systech Water Resources, 2022), a source of nutrients is missing in the Knap of Reeds Creek watershed from late 2015 to 2016. The watershed model did not predict concentrations in this creek as high as observed, and this affects the simulated water quality at NEU013B during this period. Overall, the model results follow the trend of the measured data for both calibration and validation periods reasonably well.

The summary statistics for model performance of TP are given in Table 10-10 and Table 10-11. It can be seen that the RSR target for TP is met (RSR≤100%) only at station NEU019P during the validation period. For the calibration period, the calculated RSRs ranged from 106% at station NEU019E to 192% at station LLC01, as shown in Table 10-10. For the validation period, the calculated RSRs ranged from 100% at station NEU019P to 224% at station LLC01, as shown in Table 10-11.

For the calibration period, the pBias ranged from -28.4% at station NEU013 to 39.0% at station NEU020D. Except for stations LI01, NEU013 and NEU013B, the model is overestimating TP concentration in the water column during the calibration period, especially in zone 3 of the lower lake (See Figure 3-1). The overestimation of TP is related to the overestimation of PO_4. Similar to the calibration period, the pBias ranged from -27.2% at station NEU013 to 25.4% at station NEU020D for the model validation period which demonstrates that the model is not systematically over or under predicting TP during validation.

When considered together, the RSR and pBias statistics indicate that the model is performing well on average, but not capturing the variability (or lack of variability) in the observed concentrations. Based on the approved QAPP, the pBias values for both calibration and validation periods fall within the “fair” criteria for the water quality/nutrient of the watershed model calibration guidance (See Table A.7-2 of QAPP). The lake model results for TP are, therefore, deemed to be acceptable.

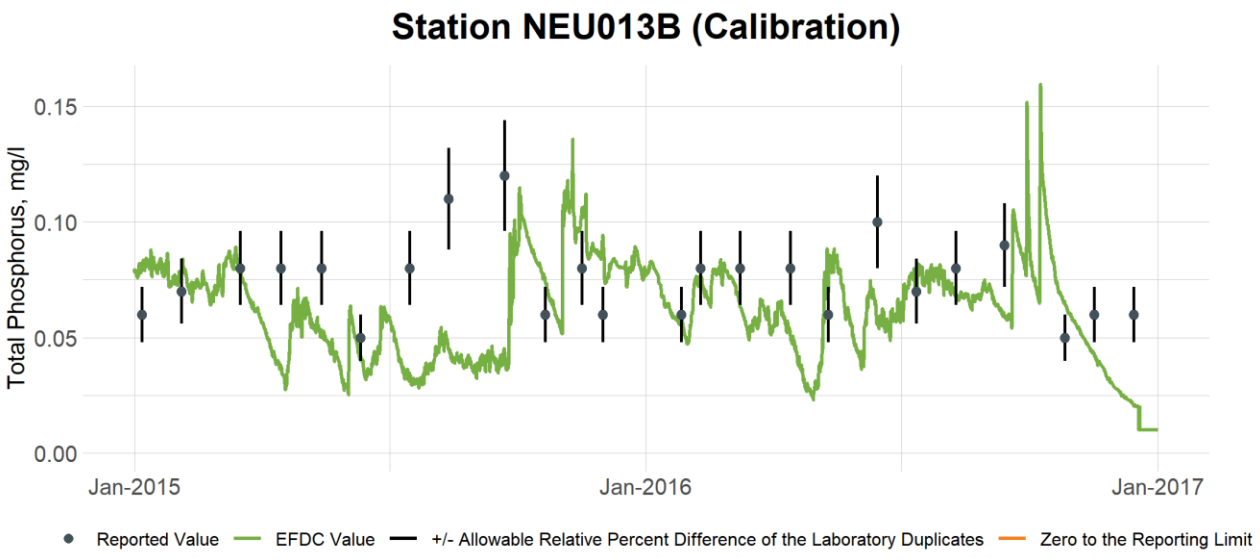

Figure 10-19 Calibration Plot of TP at Station NEU013B

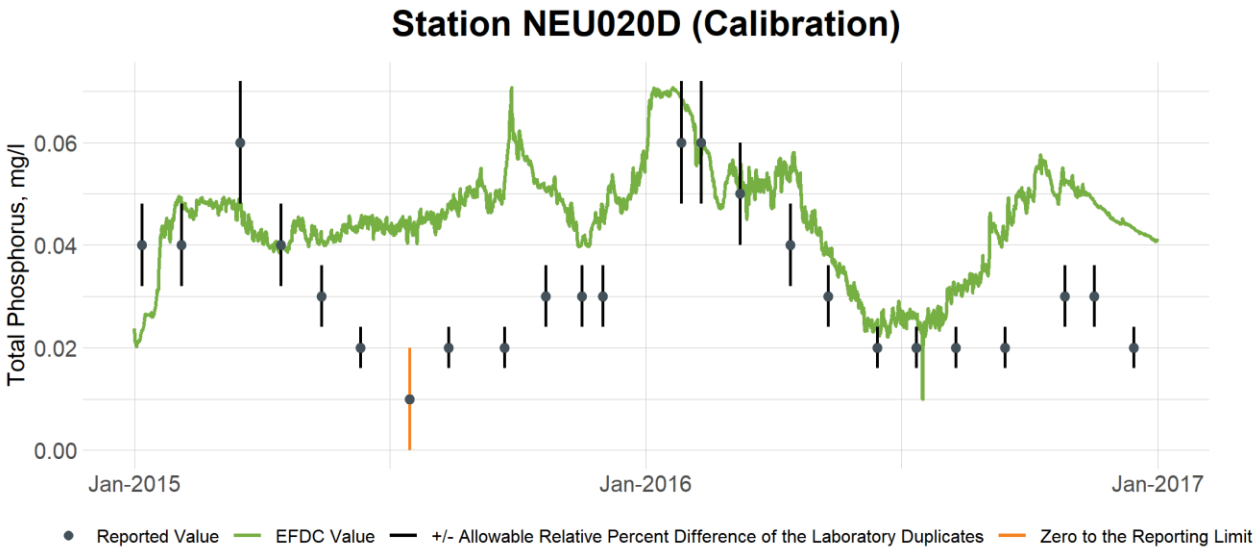

Figure 10-20 Calibration Plot of TP at Station NEU020D

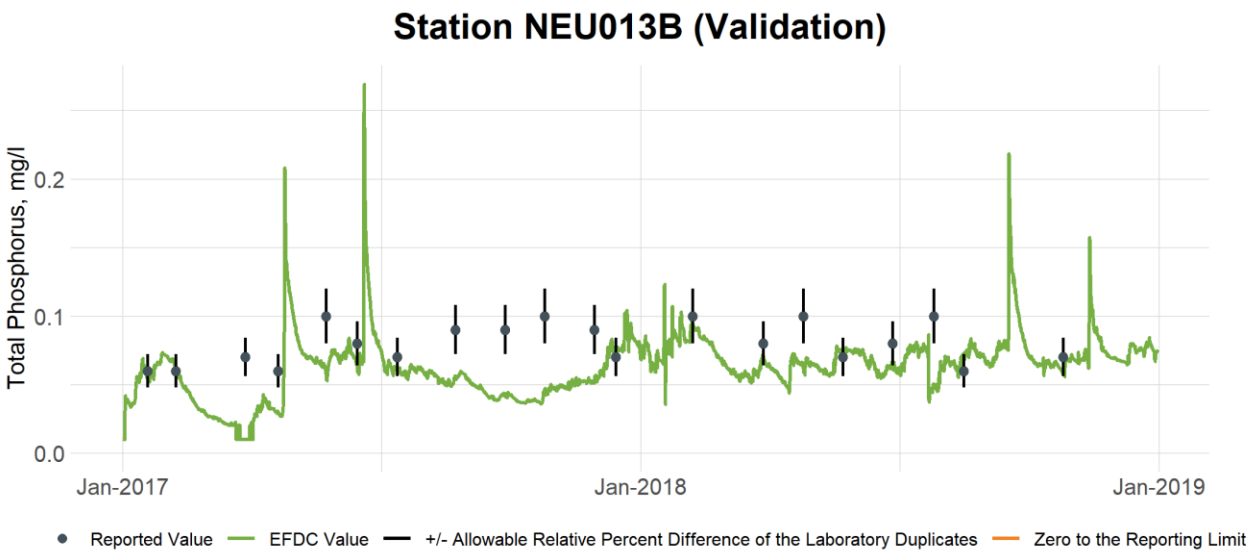

Figure 10-21 Validation Plot of TP at Station NEU013B

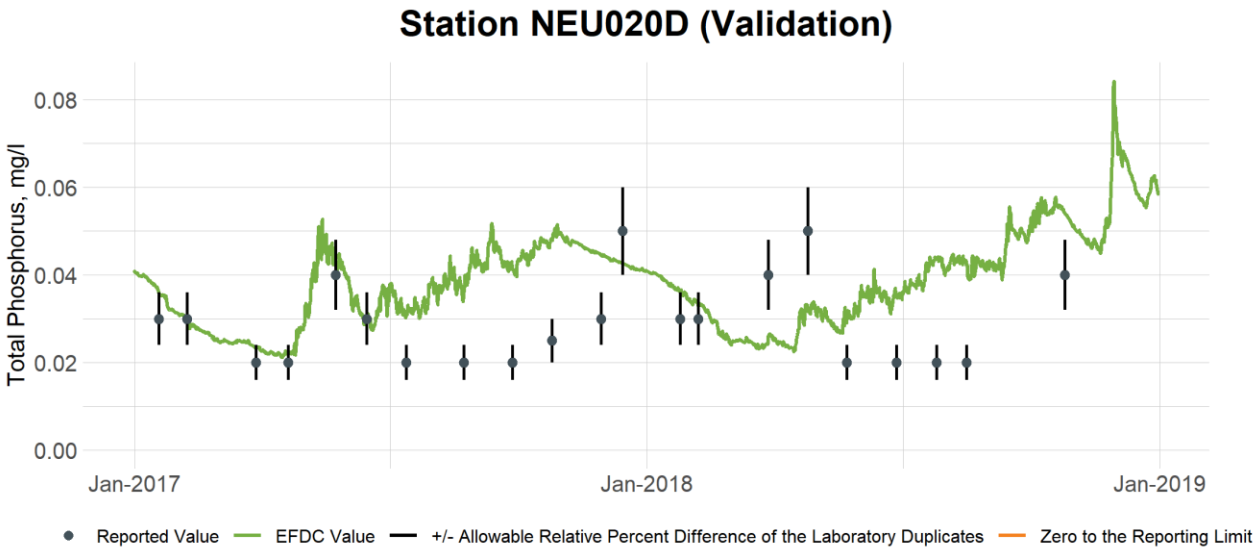

Figure 10-22 Validation Plot of TP at Station NEU020D

Table 10-10 Calibration Statistics for TP

Station ID	Starting	Ending	# Pairs	Data Average (mg/L)	Model Average (mg/L)	R^2	RMSE (mg/L)	RSR (%)	RE (%)	AE (mg/L)	CE	pBias (%)
LC01	1/6/2015	12/14/2016	22	0.047	0.053	0.351	0.015	185	25.8	0.006	-2.37	13.2
LI01	1/6/2015	12/14/2016	24	0.055	0.053	0.088	0.021	126	28.4	-0.002	-0.62	-3.3
LLC01	1/6/2015	12/14/2016	24	0.055	0.063	0.344	0.019	192	30.0	0.008	-2.57	15.2
NEU013	1/6/2015	12/14/2016	24	0.097	0.069	0.028	0.052	148	38.3	-0.027	-1.19	-28.4
NEU013B	1/6/2015	12/14/2016	24	0.075	0.061	0.031	0.031	184	32.7	-0.014	-2.26	-18.2
NEU0171B	1/6/2015	12/14/2016	24	0.055	0.058	0.202	0.017	154	24.4	0.003	-1.39	5.7
NEU018C	1/6/2015	12/14/2016	24	0.046	0.053	0.220	0.017	183	29.9	0.007	-2.74	15.5
NEU018E	1/6/2015	12/14/2016	24	0.049	0.051	0.244	0.013	133	18.6	0.002	-0.88	4.3
NEU019E	1/6/2015	12/14/2016	24	0.044	0.052	0.485	0.013	106	21.3	0.008	-0.09	19.0
NEU019L	1/6/2015	12/14/2016	23	0.036	0.049	0.406	0.015	141	35.6	0.012	-0.87	34.5
NEU019P	1/6/2015	12/14/2016	24	0.035	0.048	0.497	0.015	117	36.2	0.012	-0.46	34.5
NEU020D	1/6/2015	12/14/2016	24	0.032	0.045	0.237	0.018	127	47.5	0.013	-0.65	39.0

Table 10-11 Validation Statistics for TP

Station ID	Starting	Ending	# Pairs	Data Average (mg/L)	Model Average (mg/L)	R^2	RMSE (mg/L)	RSR (%)	RE (%)	AE (mg/L)	CE	pBias (%)
LC01	1/18/2017	10/25/2018	22	0.047	0.050	0.000	0.016	159	27.6	0.003	-1.43	7.5
LI01	1/18/2017	10/25/2018	21	0.052	0.056	0.001	0.033	219	39.9	0.004	-3.91	7.8
LLC01	1/18/2017	10/25/2018	21	0.059	0.067	0.071	0.038	224	40.7	0.008	-3.88	13.7
NEU013	1/19/2017	10/25/2018	20	0.096	0.071	0.002	0.045	161	37.6	-0.026	-1.69	-26.7
NEU013B	1/18/2017	10/25/2018	20	0.080	0.058	0.016	0.030	199	29.6	-0.022	-3.06	-27.2
NEU0171B	1/18/2017	10/25/2018	21	0.054	0.049	0.090	0.015	151	23.5	-0.005	-1.08	-9.8
NEU018C	1/18/2017	10/25/2018	20	0.044	0.044	0.152	0.011	123	21.4	0.000	-0.65	-0.2
NEU018E	1/18/2017	10/25/2018	21	0.045	0.043	0.020	0.015	145	26.3	-0.002	-1.11	-3.5
NEU019E	1/18/2017	10/25/2018	21	0.041	0.044	0.010	0.016	121	29.5	0.002	-0.58	5.9
NEU019L	1/18/2017	10/25/2018	21	0.035	0.041	0.010	0.015	145	33.0	0.005	-1.09	15.4
NEU019P	1/18/2017	10/25/2018	21	0.046	0.039	0.016	0.060	100	53.5	-0.008	0.00	-16.3
NEU020D	1/18/2017	10/25/2018	21	0.029	0.036	0.043	0.013	135	38.5	0.007	-0.91	25.4

10.6 Other Water Quality Parameters

In addition to the model-data results discussed above for Chl-a, TOC, DO, TN and TP, the lake model was also calibrated and validated for TSS, ammonia, nitrate, TKN, DOC, and TON. Time-series plots and model performance statistics for these state variables (e.g., ammonia, nitrate) and derived variables (e.g., TSS, TKN) are presented in Appendix A.2 and Appendix A.4, respectively.

The purpose of TSS calibration is to simulate a reasonable amount of suspended cohesive silt and clay in the water column such that light attenuation and the effect of available light on algae production can be properly simulated. The time series plots of TSS and Secchi depth model-data comparisons are presented in Appendix A.2 and the model performance statistics are presented in Appendix A.4. Despite the fact that TSS is generally under-predicted in terms of its mean value, the plots of Secchi depth, which ultimately determine light availability for algal growth, show good agreement between the model simulation and observed data.

In general, the model simulation results for ammonia, nitrate, and DOC were in good agreement with the observed data. Statistically, the model results for these state variables either met, or were close, to the RSR target value (RSR≤100%) during the calibration period. For TKN and TON, the pBias ranged within, or were close to, the “fair” criteria for the water quality/nutrient of the watershed model calibration guidance (See Table A.7-2 of QAPP). In addition, visual comparison of model-data results shown in the time series plots for these constituents indicate that the lake model results can be considered acceptable.

11. Discussion on Sediment Flux Model

Internal nutrient loading from sediment-water fluxes of ammonia and phosphate across the sediment-water interface of the lake sediment bed has a significant impact on water quality in the overlying water column of the lake. However, this impact is site-specific, and Falls Lake has its own unique nutrient balance characteristics. Sediment flux was identified before, during, and at completion of the model development process as one of the most important factors in making regulatory decisions. The kinetic coefficients and model parameter values assigned to the sediment flux model for Falls Lake are within reasonable range of the literature values (see Appendix A.1). To ensure that the sediment flux model performs reasonably well, the simulated sediment nutrient fluxes were compared with lake-wide estimates of nutrient loading to either observed data directly or derived/estimated values based on observed data from four (4) different data sources described below:

1- Sample sediment core data collected during the UNRBA study period (Alperin, 2019); maps for Alperin data sources are given at Figure 3-3.

2- Sediment nutrient flux measurements by USEPA in 2018 (Flexner, 2019); maps for USEPA data sources are given at Figure 11-1.

3- Sediment cores and bottom water data collected by Piehler (2019); and

4- Water column samples taken during the warm months by Hall and Paerl (2020); maps for data sources of Piehler (2019), and Hall and Paerl (2020) are given at Figure 11-2.

It should be recognized that all the observed data mentioned above were collected from sample sediment cores or benthic chambers that were much smaller than the model grid cells where the sample cores were collected.

The sediment nutrient flux measurements by USEPA at the three stations shown in Figure 11-1 indicated sediment nutrient flux increases from the upstream to downstream direction (Flexner, 2019). During the beginning of the calibration effort, the EFDC simulated sediment nutrient fluxes did not show this spatial pattern. For example, the simulated sediment PO_4 flux at station FL04 was much lower than the observed data indicated for anoxic conditions (approximately 0.03 g/m^2/day).

Following several consultations with third-party model reviewers, other engaged subject matter experts, and DWR modelers, multiple model tests were conducted to improve the performance of the sediment flux model, by increasing the simulated sediment PO_4 flux at the lower, deeper part of the lake while allowing the G1 and G2 class of organic phosphorus concentrations in the sediment bed to reach a dynamic equilibrium and stabilize throughout the lake model simulation period of 2015 to 2018.

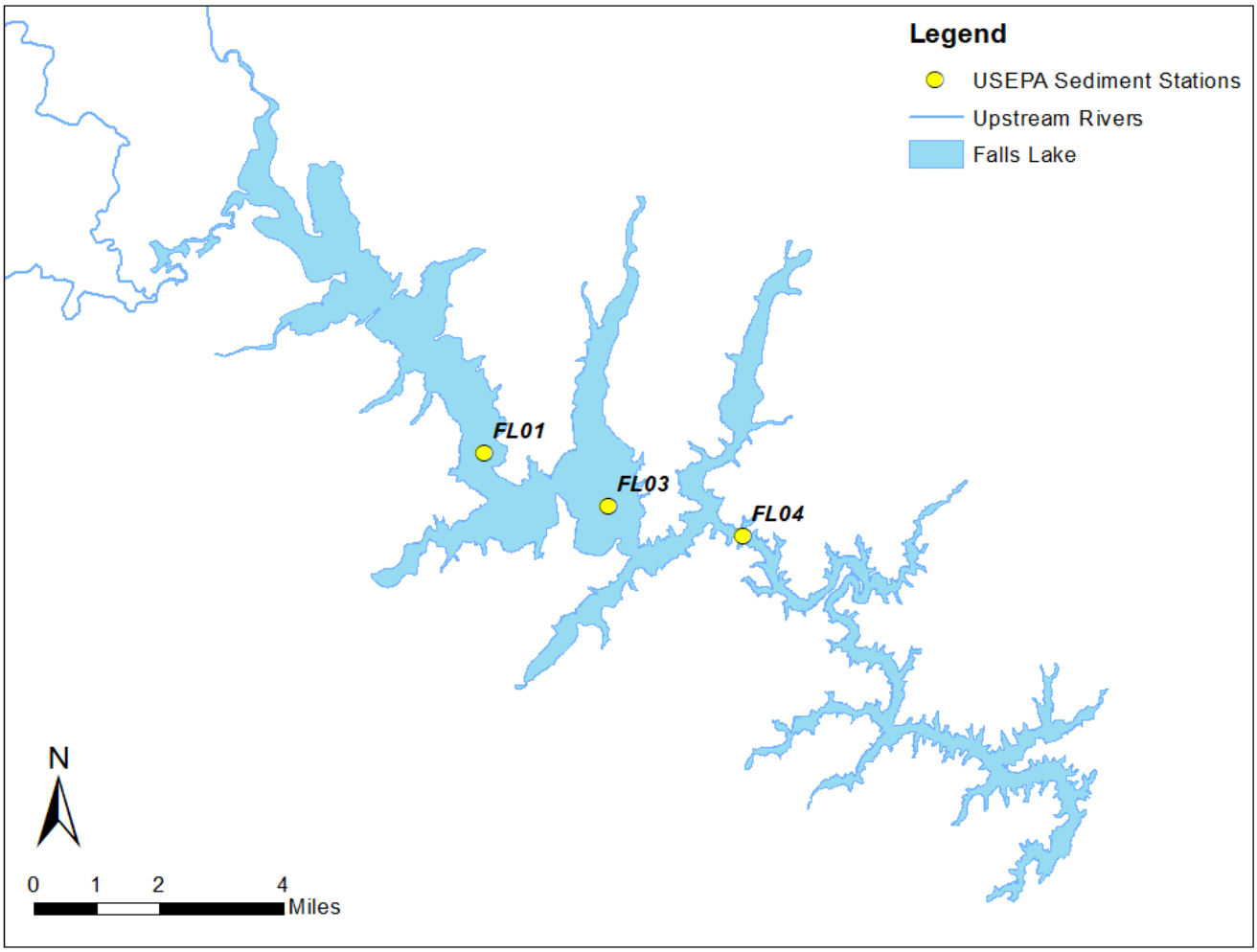

Figure 11-1 USEPA sediment data collection stations (Flexner, 2019)

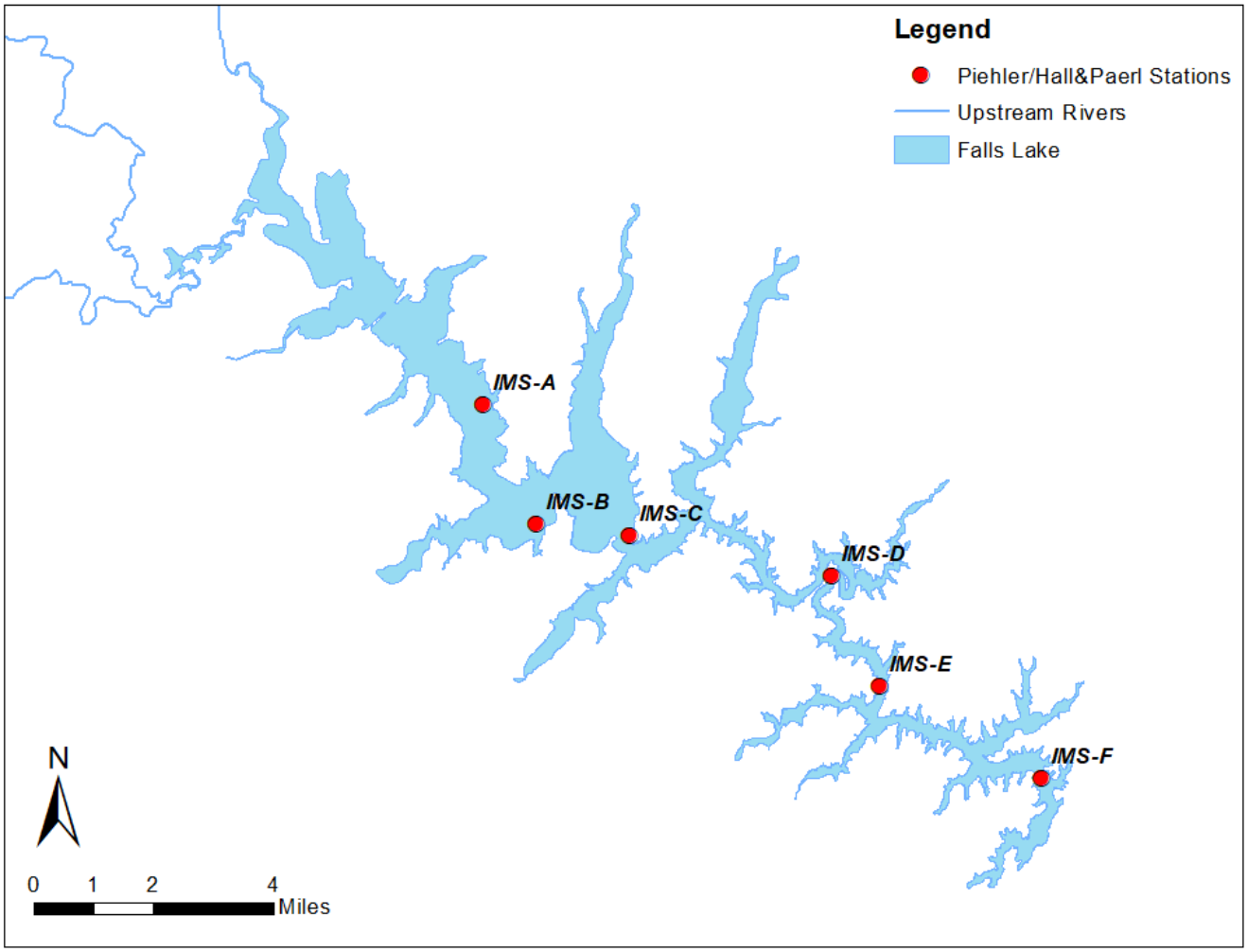

Figure 11-2 Sediment cores and bottom water data collected by Piehler (2019), and Hall and Paerl (2020)

Based on the results of the model tests, the following steps were taken to improve the sediment flux model performance relative to the studies conducted on Falls Lake:

- Decreasing the particulate organic material (POM) settling velocity to the sediment bed from the water column at the upper part of the lake to allow more POM transported downstream to settle out of the water column in the lower part of the lake;

- Recycling more algae from the water column to the sediment bed by increasing the algal growth rates, predation rates and settling velocity;

- Reducing the PO_4 sorption enhancement factor in the lower part of the lake and the forebay; and

- Changing the labile-refractory split of the POM loading from the watershed from 50%-50% to 75%-25% to allow more G1 and G2 classes into the sediment bed.

The above changes to the model did improve performance of the sediment flux model overall but did not increase the simulated PO_4 flux in the lower, deeper part of Falls Lake as high as observations. The sediment PO_4 flux could be increased to more closely agree with the observed data if the POM loading from the watershed was increased significantly. However, even an order of magnitude increase in the POM loading does not result in the 0.03 g/m^2/day PO_4 flux observed at station FL04. The sediment PO_4 flux also affects the water column concentrations of PO_4 c in lower lake. The modeling team aimed to simulate reasonable flux rates of PO_4 from the sediments and target the performance criteria described in the UNRBA Modeling QAPP for the water column concentrations.

The average annual simulated sediment nutrient loading was calculated for comparison with empirical estimates of internal loading based on the data sources described above. The average annual sediment flux nutrient loading of NH_4, PO_4, and NO_3 were calculated based on the model-simulated sediment flux time series for each model grid that was aggregated over the whole lake. Seasonal and total annual sediment flux loads of NH_4, PO_4, and NO_3 are presented in Table 11-1, Table 11-2, and Table 11-3, respectively. The EFDC model also simulates loss of nitrate to the sediment bed from the water column primarily due to the nitrate concentration gradient across the interface of the sediment bed and overlying water. This loss is provided as a negative number in Table 11-3. This loss is not the same as denitrification which is a biological process that converts nitrate to nitrogen gas. Denitrification is a loss of nitrogen from the system. While the EFDC model accounts for denitrification, it is not output in the model results.

As can be seen, the total annual lake-wide internal loading estimates obtained with the sediment flux model are comparable to the estimates derived from *in situ* sediment flux measurements. It should be noted that the empirical estimates of internal nutrient loading were obtained using core samples or benthic chambers that are very limited in the spatial distribution and areal coverage within Falls Lake. Accordingly, they provide a reasonable estimate of internal nutrient loading across the sediment-water interface in Falls Lake but not an exact lake-wide loading rate.

Table 11-1 Seasonal and Total Annual NH_4 Sediment Flux Load

Years	NH_4 Load (Nov to Apr) (lb N/yr)	NH_4 Load (May to Oct) (lb N/yr)	NH_4 Total Annual Load (lb N/yr)
2015	72,792	269,095	341,888
2016	83,690	294,175	377,865
2017	41,489	219,698	261,187
2018	31,968	240,004	271,972
Total Average	57,485	255,743	313,228
Alperin Estimate (UNRBA, 2019)			207,000
Piehler Estimate (Smiley et al, 2023)			530,000

Table 11-2 Seasonal and Total Annual PO_4 Sediment Flux Load

Years	PO_4 Load (Nov to Apr) (lb P/yr)	PO_4 Load (May to Oct) (lb P/yr)	PO_4 Total Annual Load (lb P/yr)
2015	8,505	46,164	54,668
2016	8,895	47,658	56,554
2017	6,753	40,667	47,419
2018	5,254	45,125	50,378
Total Average	7,351	44,903	52,255
Alperin Estimate (UNRBA, 2019)			14,000
Piehler Estimate (Smiley et al, 2023)			10,600

Table 11-3 Seasonal and Total Annual NO_3 Sediment Flux Load

Years	NO_3 Load (Nov to Apr) (lb N/yr)	NO_3 Load (May to Oct) (lb N/yr)	NO_3 Total Annual Load (lb N/yr)
2015	-20,548	-74,872	-95,420
2016	-32,989	-79,397	-112,386
2017	-13,911	-57,561	-71,472
2018	-14,896	-66,036	-80,933
Total Average	-20,586	-69,467	-90,053

Moreover, comparing water column nutrient concentrations with observed data is another approach that can be used to evaluate performance of the sediment flux model. Ambient nutrient levels in the water column are the result of kinetic processes in the water column and external and internal sources of nutrients including watershed loading, atmospheric loading and benthic nutrient fluxes across the sediment-water interface of the sediment bed. As described elsewhere in this section of the report, the good agreement between simulated and observed time series of nutrient concentrations in the surface and bottom layer provides an indirect indicator that the sediment flux model performs reasonably well.

12. Summary of Water Quality Model

A rigorous analysis of an extensive body of water quality and sediment data was performed to develop a conceptual model of the water quality and sediment conditions in Falls Lake. The level of data availability and efforts to assess the model development throughout the process provides an exceptional basis for confidence in this model. A detailed and continuous analysis process was used throughout model development to support the calibration and validation of 3-dimensional EFDC water quality model of Falls Lake. The EFDC water quality model of Falls Lake was calibrated using data collected during the two-year period from January 1, 2015, to December 31, 2016. The model was then validated to data collected during the two-year period from January 1, 2017, to December 31, 2018. The availability of four years of monitoring data including special studies on lake bathymetry, sediment depth and quality, and sediment nutrient flux was critical for this calibration/validation process. Calibrated and validated state variables in the EFDC water quality model included Chl-a, organic matter, nutrients, DO, and cohesive suspended sediments.

The performance of the water quality model was evaluated by a combination of visual inspection of model-data plots and quantitative analysis of model-data performance statistics that included the RSR. Third-party, subject matter expert, and DWR input was used to guide calibration decisions. All critical decisions were also reviewed and confirmed by the MRSW. As described in the DWR-approved QAPP, the performance targets adopted for calibration of the Falls Lake water quality model were based on the RSR ≤50% for DO and RSR ≤100% for nutrients, TOC, TN, TP, TSS, and algal biomass as Chl-a.

Algal Chl-a. During the calibration period, Chl-a met the RSR target at the majority of stations. An additional statistic (pBias) that measures model-data bias fell within the “good” criteria for Chl-a for the calibration period. Calibration decisions were informed by consultation with subject matter experts, third-party model reviewers, and DWR modelers and were supported by the extensive data and research available on Falls Lake. The RSR target for Chl-a for the validation period, however, was not met, and the model systematically underestimated Chl-a. The average of the Chl-a observations during the validation period was 45% higher than the average of the Chl-a observations during the calibration period, but the nutrient concentrations and Secchi depths in the lake were similar. The underestimation of Chl-a for the validation period appears to be related to (1) possible seasonal changes of the water quality kinetic parameters such as growth rate, C/Chl-a ratio, etc. are not represented in the EFDC model as these kinetic parameters are fixed over time; and (2) the lack of kinetic information, such as half saturation constants, optimal water temperature conditions, etc. for the *Euglenophyta* and *Prymnesiophyceae* groups of algae which were presented in high amounts at different times during the validation period. Although these algal groups were characterized by high biovolume measurements during the model validation period, these groups were not simulated as their own unique algal groups but were instead lumped together as part of the green/other algae group. The model provides a reasonable and effective simulation of chlorophyll-a for regulatory decision-making.

TOC. The RSR target for TOC was met only for one (1) station during both calibration and validation. In addition, the pBias metric showed that the model systematically underestimated TOC. The reason for underestimation of TOC is unclear, however, it is likely related to

(1) watershed loading uncertainty due to the lack of monitoring data collected during very large storm events, and (2) limited amount of site-specific data used to derive C/Chl-a ratios based on unknown fractions of algal and detrital POC to derive algal stoichiometry.

DO. During the calibration period, the RSR target for surface DO was met at five (5) of the twelve (12) stations. The RSR target was met for bottom DO at all stations except for NEU013B. During the validation period, the surface DO RSR target was met at six (6) of the twelve (12) stations, mostly located in zones 2 and 4, while the bottom DO RSR target was met at seven (7) stations. The pBias metric showed that bottom DO was systematically overestimated, especially in zone 3 where the surface DO was also overestimated. The overestimation of bottom DO is a possible result of lake overturn in the fall that causes rapid mixing of DO from the surface layer to the bottom layer. The systematic overestimation of bottom DO may also be related to the underestimation of TOC during validation. There is also some question of the accuracy of some of the profile measurements collected at some DWR stations when compared to data collected by other organizations at similar locations and times (Section 7.3).

TN and TP. None of the stations met the RSR target for TN during either the calibration or validation periods. However, the pBias values fell within the “very good” criteria for calibration period and within the “good” criteria for the validation period. Together, these statistics indicate that the model is performing well on average, but not capturing the variability in observed concentrations. In addition, the pBias showed that the model systematically underestimated TN during the validation period as a result of the underestimation of TON. Similar to TN, none of the stations met the RSR target for TP during both calibration and validation periods. In addition, the pBias showed that the model overestimated TP concentration in the water column during the calibration period. The overestimation of TP, especially in zone 3, is related to overestimation of PO_4.

Other Water Quality Variables. Despite the fact that TSS is generally under-predicted in terms of its mean concentration, the model-data plots of Secchi depth, which ultimately determine light availability for algal growth, show good agreement between the model results and observed data. The RSR targets for ammonia, nitrate, and DOC during the calibration period were either below, or were close to, the target of 100%. For TKN and TON, the pBias values ranged within, or were close to, the “fair” criteria. In addition to the model performance statistics, visual comparison of model-data plots for these other water quality variables showed reasonable agreement between model results and observed measurements.

Sediment Flux Model. The kinetic coefficients and model parameters values assigned to the sediment flux model were within reasonable ranges of literature values and vetted extensively throughout the review/input process. Performance of the sediment flux model was evaluated by comparing whole lake average annual internal loading of nutrients derived from the sediment flux model with empirically estimated internal loads developed from available data sources. The lake-wide average annual internal loading derived from the sediment flux model are similar in magnitude to flux rate measurements and empirical estimates of internal nutrient loading based on the available data sources.

Summary. Based on statistical skill assessment metrics, visual evaluation of model-data plots, and input from the reviewers of the modeling effort, the performance of the Falls Lake EFDC hydrodynamic and water quality model is deemed acceptable and represents a viable tool for assessing regulatory decisions for Falls Lake. The calibrated and validated water quality model was used for sensitivity analyses (Section 13) and the linked watershed (WARMF) and lake (EFDC) model framework was applied to support evaluations of the impacts of watershed load reductions of organic matter (TOC) and nutrients (TN and TP) on Chl-a and other lake water quality constituents such as DO and nutrients (Section 14).

13. Sensitivity Analysis

The purpose of the sensitivity analysis for the Falls Lake EFDC water quality model is to gain a better understanding of how perturbation of each model input parameter affects modeling results. The sensitivity analysis provides useful information regarding the physical, chemical and biological processes represented in the model and identifies the most influential parameters for improving model accuracy. This information can be insightful for future analyses, such as selecting representative data to better serve the analysis purpose. The following section summarizes the selected key kinetic coefficients, and model input parameters and sensitivity analysis results for the Falls Lake EFDC water quality model.

13.1 Sensitivity Analysis Methods

Procedure

The Falls Lake EFDC water quality model was calibrated over the 2-year period from January 1, 2015, through December 31, 2016, and validated over the 2-year period from January 1, 2017, through December 31, 2018. The calibrated and validated simulation provides the basis for comparison to the sensitivity analyses. The model was run over the whole simulation period (January 1, 2015, through December 31, 2018) to perform the sensitivity analyses. The following steps were performed to assess the sensitivity of the Falls Lake EFDC water quality model:

1- Identifying the critical model input parameters;

2- Determining the reasonable low and high perturbation levels for the model input parameter;

3- Making sure each perturbation of model input parameter value is within a reasonable range based on other modeling studies, values reported in the literature, or local research;

4- Running the EFDC model for each low and high perturbation of the model input parameter;

5- Calculating the percent difference from the calibrated model for each model input parameter value;

6- Ranking the model input parameters by Normalized Sensitivity Coefficients (NSCs) as calculated below:

$$\mathrm{NSC} = \frac{|q^{+} - q^{-}|}{|2\sigma|} \times 100 \qquad \text{Equation 9}$$

where q is the percent difference of modeled response variables from mean and is defined as:

$$q^{\pm} = \left(\frac{\sum_{n=1}^{N} Q_n(P_0 \pm \Delta P)}{\sum_{n=1}^{N} Q_n(P_0)} - 1\right) \times 100 \qquad \text{Equation 10}$$

where N is the number of model results, Q is the model response variable which in turn is a function of P the input parameter, P_0 is the base (calibrated) input value, ΔP is the change in the value of the input parameter from its base value ($|P - P_0|$), and σ is the perturbation levels of the model input parameters ($\Delta P/P_0 \times 100$).

A NSC value of 100 indicates a 1:1 sensitivity with the model producing a result in direct proportion to the input parameter change (Donigian and Love, 2007). For example, a perturbation of decrease/increase in input parameter by 50% will produce a response of increase/decrease by 50% in the model output. The higher the NSC is, the more sensitive the input parameter is.

7- Plotting time series, computing summary statistics, and preparing Box-Whisker plots for each simulation; and

8- Using NSCs to plot Tornado Diagrams to summarize response to each model input parameter value for selected response variables. The tornado diagram was created to rank the model input and parameters based on NSCs following the methodology by Donigian and Love (2007).

As described above, low and high values are determined to specify the perturbation of each model parameter selected for the sensitivity analysis. This approach is a valid statistical expression of the Point Estimate Method originally developed by Rosenblueth (1981) and subsequently modified and applied by Harr (1989), Li (1992), and Christian and Baecher (1999). In the Point Estimate Method, three values -- low, middle and high-- of the perturbed parameter are required. The three values, usually taken to be the mean and ± 1σ or ± 2σ, for each input parameter, are used to construct an estimated Probability Density Function (PDF) from model outputs by joint probability calculations. The low and high values can be based on the middle value ± some percentage, or the low and high values can be based on statistics for the model parameter (e.g., mean ± 1σ; mean ± 2σ). In applying the Point Estimate Method for the sensitivity analysis of the Falls Lake model, a simple percentage was specified as the perturbation level to the model calibration parameter values to assign low and high parameter values around the middle (calibrated) parameter values.

Response Variables and Selected Stations

The response variables for the Falls Lake EFDC water quality model selected for the sensitivity analysis include Chl-a, TOC, TN, and TP. These response variables are of particular interest to the UNRBA's reexamination of the Falls Lake Nutrient Management Strategy. Chl-a is an indicator for algal biomass, TOC has potential impact on potable water treatment and the creation of disinfection by-products in drinking water, and TN and TP represent nutrients that are linked to the growth of algae in surface waters. Considering the nature of these response variables, they were evaluated for the photic layer of the water column with the thickness corresponding to 2 x Secchi depth.

For sensitivity analysis, EFDC water quality model results were extracted from the cells where three (3) observed stations NEU013B, NEU018E, and NEU020D are located (See Figure 4-2).

These stations were selected because they represent different areas of Falls Lake: NEU013B is located in the upper part of the lake that is wide and shallow, NEU020D is located in the lower part of the lake that is deeper and narrower, and NEU018E is in the middle of the lake.

Selected Model Input Parameters and Perturbation Levels

The input parameters were selected in such a way that one could examine the change in the Chl-a and nutrient concentrations in the water column. Based on the experience gained from numerous model runs during the model calibration task, kinetic coefficients and model input parameters that significantly influenced the model results included C/Chl-a ratio, maximum algae growth rate, and algae settling velocity related to algae processes, and diffusion coefficient in pore water for the sediment nutrient flux.

Model results for Chl-a and TOC in the water column are directly related to changes in the C/Chl-a ratio, maximum algae growth rate, and algae settling velocity and indirectly related to changes in the diffusion coefficient in pore water through changes in the sediment nutrient release to the water column. Similarly, model results for TN have the same relations as Chl-a to changes in the parameters above. Based on the observed data, the majority of TN in the water column of Falls Lake is organic nitrogen. Furthermore, model results for TP are controlled considerably by algal uptake and sediment phosphate flux, especially with seasonal hypoxic conditions observed and simulated during the summer months in the deep parts of the lake. As a result, model results for TP are directly related to changes in the maximum algae growth rate, and the diffusion coefficient in pore water. Table 13-1 shows the perturbation levels chosen for the analysis of each variable.

Table 13-1 Selected Kinetic Coefficients and Input Parameters for Sensitivity Analysis

Variables	Perturbation Level		
	Low	Calibration and validation	High
C/Chl-a Ratio (mg C/µg Chl-a)	Decreased by 25%	-Specific to each simulated algal group: 0.005- 0.007	Increased by 25%
Max. Algae Growth Rate (1/day)	Decreased by 25%	Zone-Specific and Algal Group-Specific: 2.63-4.17	Increased by 25%
Algae Settling Velocity (m/day)	Decreased by 25%	Zone-Specific and Algal Group-Specific: 0.2-0.4	Increased by 25%
Diffusion Coeff. in Pore Water (m^2/day)	Decreased by 50%	Zone-Specific: 0.0024- 0.005	Increased by 50%

13.2 Sensitivity Analysis Results

Sensitivity analyses were conducted with the calibrated and validated model for the period of 2015-2018. The responsive variables, evaluated for the entire 4-year period, are Chl-a, TOC, TN, and TP. The four (4) model input parameters examined are C/Chl-a ratio, maximum algae growth rate, algae settling velocity, and diffusion coefficient in pore water.

In order to visualize and understand the sensitivity results, they are displayed in the form of time series, Box-Whisker plots, and tornado diagrams. For all four (4) response variables, these three forms of graphics are provided. Compared with time series, Box-Whisker plots provide much better visualization of the distribution of data. As an example of the Box Whisker plot shown in Figure 13-1, the blue star indicates the minimum value of the dataset; the lower end of the Whisker is the 10th percentile of the dataset; the lower end of the Box indicates the 25th percentile; the bar in the Box is the median value; the diamond shows the mean value; the upper end of the Box is the 75th percentile; the upper end of the Whisker is the 90th percentile; and the brown star is the maximum value of the dataset. Time series and Box-Whisker plots for all four (4) responsive variables are presented in Appendix A.5.

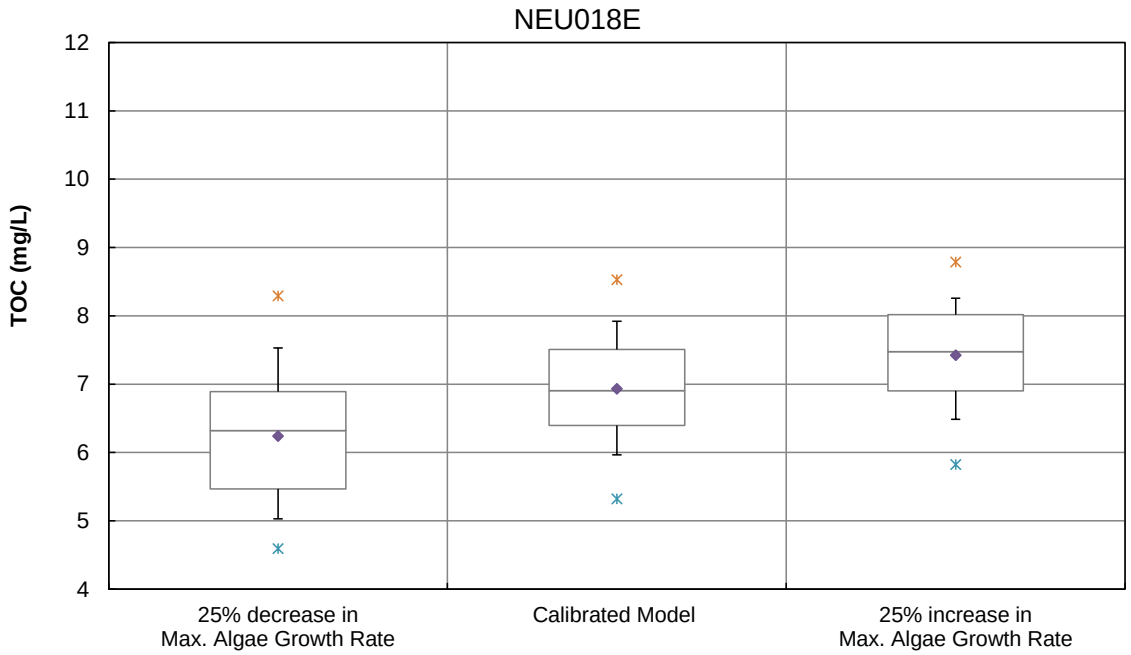

Figure 13-1 Box-Whisker Plot of TOC at NEU018E under Algal Growth Rate Perturbation

Sensitivity Analysis of Chl-a

A tornado diagram displays the range of the response variables for high and low values of each of the input parameter sets. For example, Figure 13-2 shows a tornado diagram, wherein the y-axis is the calculated NSC in percentage and the x-axis is the percent difference of modeled response variables from mean in percentage. The NSC was calculated based on the

perturbation levels for each input parameter, as shown in the tornado diagram. The model input parameters are listed in the legend on the right side of the plot based on their color.

The tornado diagrams of sensitivity analysis results of modeled Chl-a at stations NEU013B, NEU018E, and NEU020D are given in Figure 13-2, Figure 13-3, and Figure 13-4, respectively. The calculated NSCs are also given in Table 13-2. The time series plots and Box-Whisker plots of modeled Chl-a under different perturbation levels of these four (4) model input parameters at stations NEU013B, NEU018E, and NEU020D are given in Appendix A.5.

At all three stations, the positive perturbations in the maximum algal growth rate and diffusion coefficient in pore water result in the positive response in the average modeled Chl-a, or vice versa as shown in Figure 13-2, Figure 13-3, and Figure 13-4. The positive perturbation in the diffusion coefficient in pore water increases the amount of nutrient flux, which in turn stimulates the algal growth and increases the Chl-a concentration in the water column.

At all three stations, the positive perturbations in the C/Chl-a ratio and algae settling velocity lead to the negative response in the average modeled Chl-a, or vice versa. The EFDC water quality model calculates algal concentration in biomass as mg C/L. Then it uses the C/Chl-a ratio to convert the modeled algal concentrations as carbon to algal concentrations as Chl-a. As such, the positive perturbation in the C/Chl-a ratio decreases the Chl-a concentration in the water column. The positive perturbation in the algae settling velocity increases the recycling rate of algae from the water column to the sediment bed, and thus decreases the Chl-a concentration in the water column.

The maximum algal growth rate has the most impact on modeled Chl-a at all three stations. However, by moving from the upper part to the lower part of the lake the sensitivity decreases, due to the decreasing modeled nutrient (NH_4, NO_3, and TP) concentrations. The calculated NSCs at stations NEU013B, NEU018E, and NEU020D are 176.28, 105.00, and 71.08, respectively, as shown in Table 13-2. On the other hand, the diffusion coefficient in pore water has the least impact on modeled Chl-a, with the calculated NSC of 0.61 at station NEU013B, 0.33 at station NEU018E, and 0.22 at station NEU020D. At station NEU013B, in the upper part of the lake, the algae settling velocity and C/Chl-a ratio are the second and third most sensitive parameters affecting the modeled Chl-a, with the calculated NSC of 71.44 and 38.95, respectively. However, at stations NEU018E, and NEU020D this order is reversed and C/Chl-a ratio becomes the second most sensitive parameters.

Table 13-2 Calculated Normalized Sensitivity Coefficients (%) for Modeled Chl-a at Stations NEU013B, NEU018E, and NEU020D in the Photic Layer

Model Input Parameters	NEU013B	NEU018E	NEU020D
C/Chl-a Ratio	38.95	49.57	62.05
Max. Algae Growth Rate	176.28	105.00	71.08
Algae Settling Velocity	71.44	32.64	26.01
Diffusion Coeff. In Pore Water	0.61	0.33	0.22

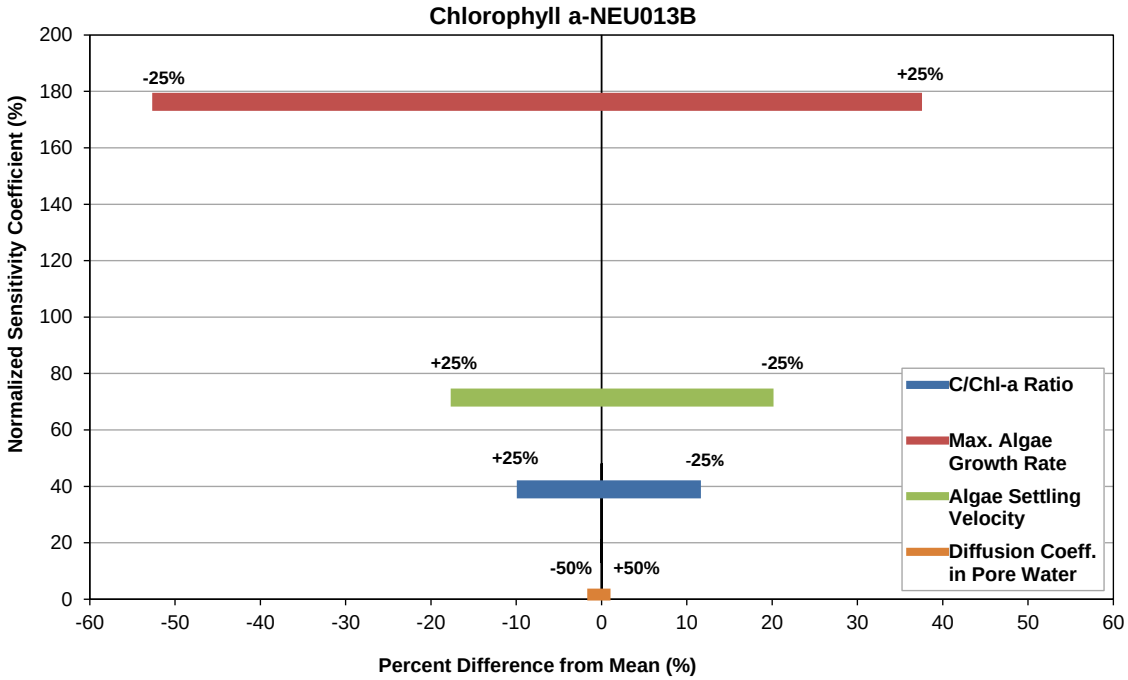

Figure 13-2 Tornado Diagram for Sensitivity Analysis of Modeled Chl-a at NEU013B

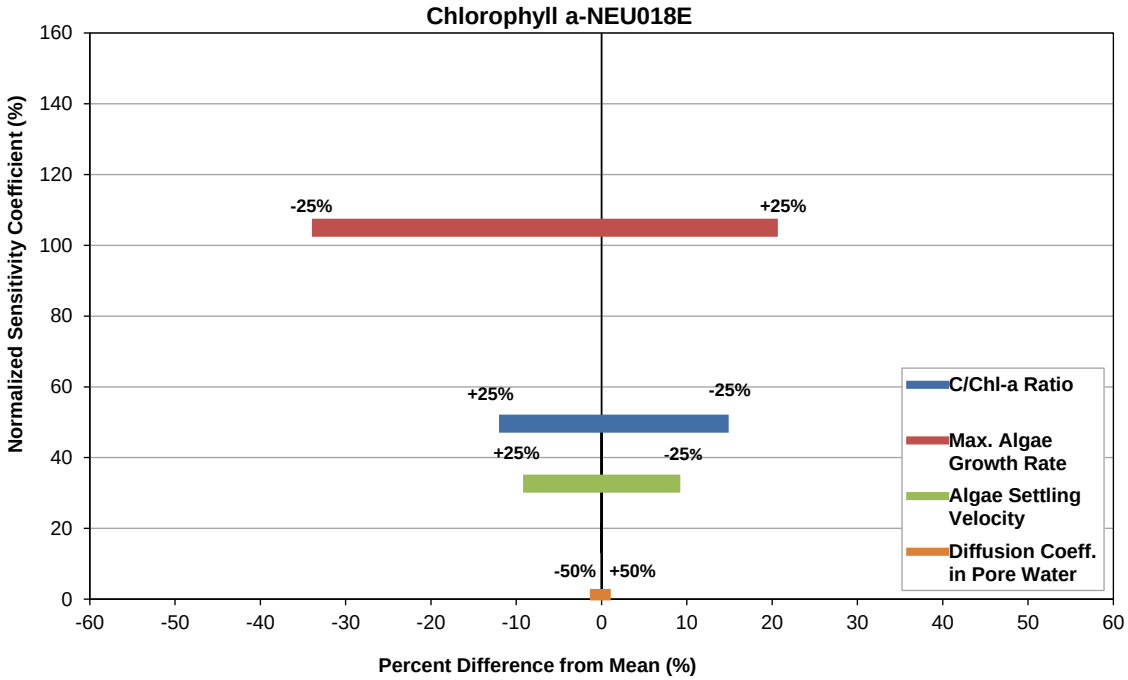

Figure 13-3 Tornado Diagram for Sensitivity Analysis of Modeled Chl-a at NEU018E

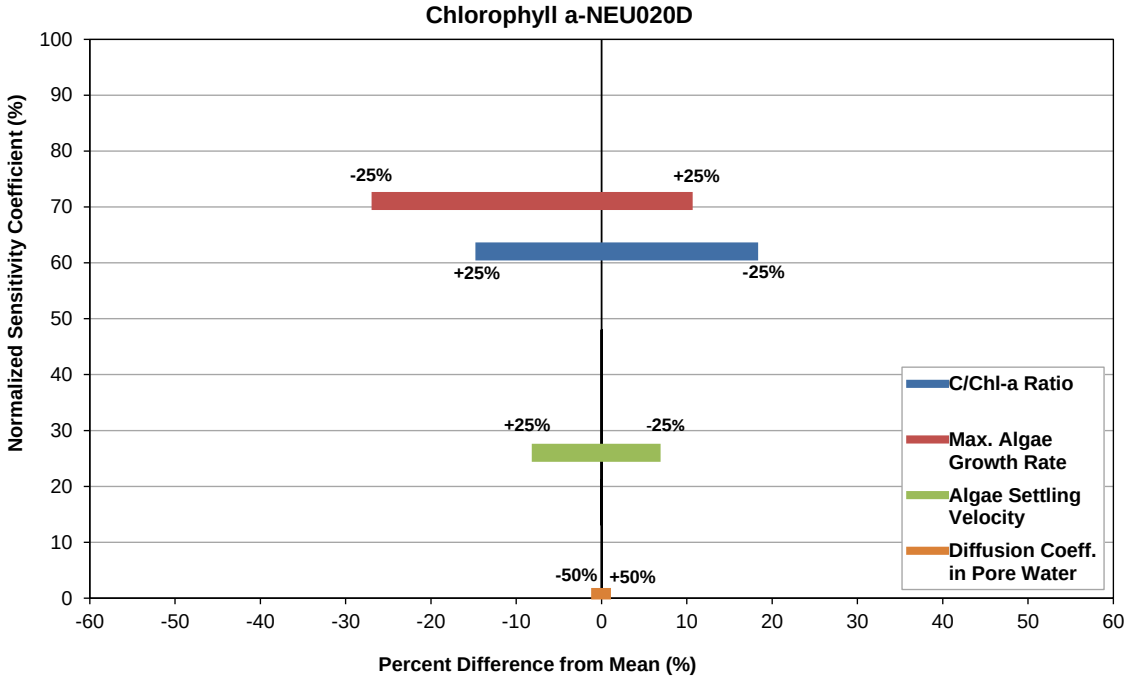

Figure 13-4 Tornado Diagram for Sensitivity Analysis of Modeled Chl-a at NEU020D

Sensitivity Analysis of TOC

The tornado diagrams of sensitivity analysis results of modeled TOC at stations NEU013B, NEU018E, and NEU020D are given in Figure 13-5, Figure 13-6, and Figure 13-7, respectively. The calculated NSCs are also given in Table 13-3. The time series plots and Box-Whisker plots of modeled TOC under different perturbation levels of these four (4) model input parameters at stations NEU013B, NEU018E, and NEU020D are given in Appendix A.5.

At all three stations, the positive perturbations in the maximum algal growth rate, C/Chl-a ratio, and diffusion coefficient in pore water result in the positive response in the average modeled TOC, or vice versa as shown in Figure 13-5, Figure 13-6, and Figure 13-7. On the other hand, the positive perturbation in the algae settling velocity leads to the negative response in the average modeled TOC, or vice versa. Based on the observed data, more than 90% of TOC in the water column of Falls Lake is DOC. The positive perturbation in the maximum algal growth rate increases the algal production and concentrations which boost algal basal metabolism and produce more DOC. However, the change in TOC due to these perturbations is much smaller than the relative effect on Chl-a because algae is a small component of TOC in Falls Lake. Note the scale of the x and y axes indicating the change in simulated TOC is scaled down from the axes displayed on the Chl-a figures (Figure 13-2, Figure 13-3, and Figure 13-4).

The maximum algal growth rate has the most impact on modeled TOC of the parameters evaluated at all three stations, with the calculated NSCs of 34.75 at station NEU013B, 34.12 at station NEU018E, and 32.08 at station NEU020D as shown in Table 13-3. By moving from the upper part to the lower part of the lake, the sensitivity of the modeled TOC to this parameter slightly decreases. On the other hand, the diffusion coefficient in pore water has the least impact on modeled TOC, with the calculated NSC of 0.19 at station NEU013B, 0.05 at station NEU018E, and 0.13 at station NEU020D. The sensitivity of the modeled TOC to the algae settling velocity and C/Chl-a ratio is in the middle of the sensitivity range. In addition, perturbations in these two (2) parameters show a similar impact on the modeled TOC at all three stations.

Table 13-3 Calculated Normalized Sensitivity Coefficients (%) for Modeled TOC at Stations NEU013B, NEU018E, and NEU020D in the Photic Layer

Model Input Parameters	NEU013B	NEU018E	NEU020D
C/Chl-a Ratio	9.94	10.98	9.82
Max. Algae Growth Rate	34.75	34.12	32.08
Algae Settling Velocity	12.72	9.12	8.13
Diffusion Coeff. In Pore Water	0.19	0.05	0.13

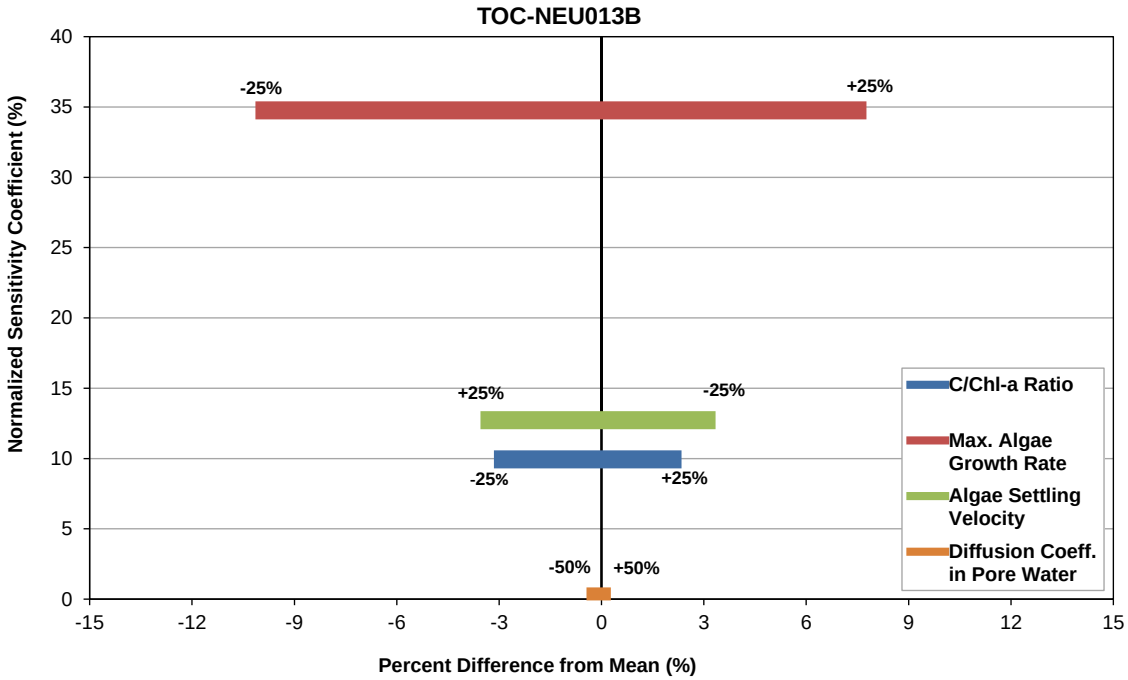

Figure 13-5 Tornado Diagram for Sensitivity Analysis of Modeled TOC at NEU013B

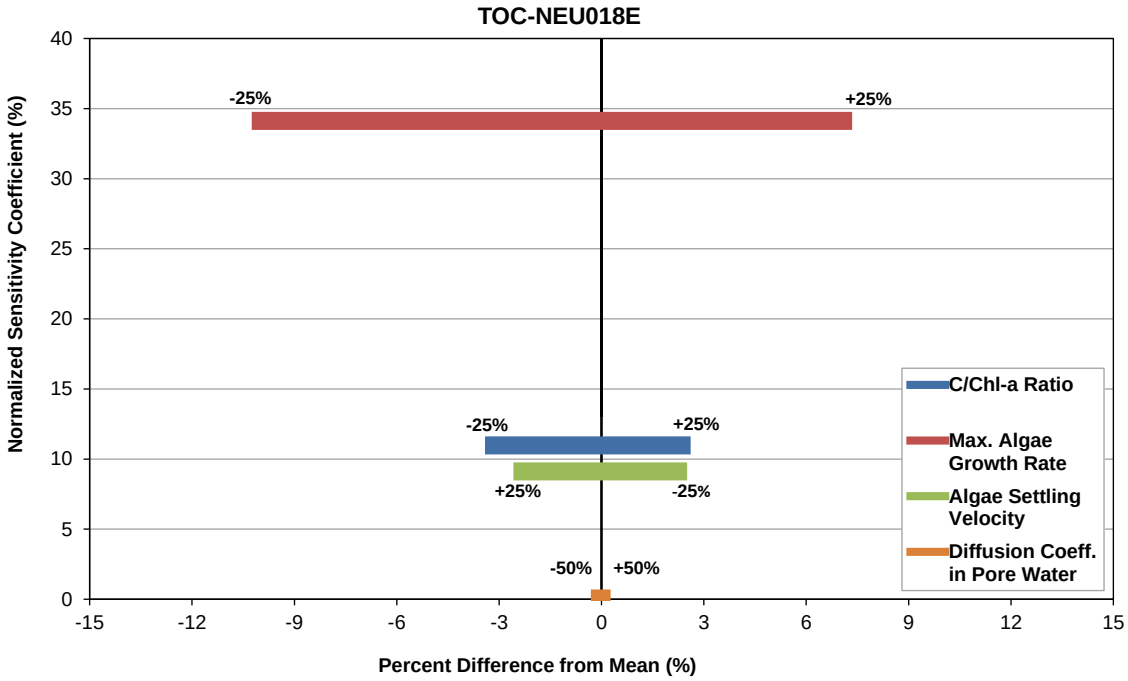

Figure 13-6 Tornado Diagram for Sensitivity Analysis of Modeled TOC at NEU018E

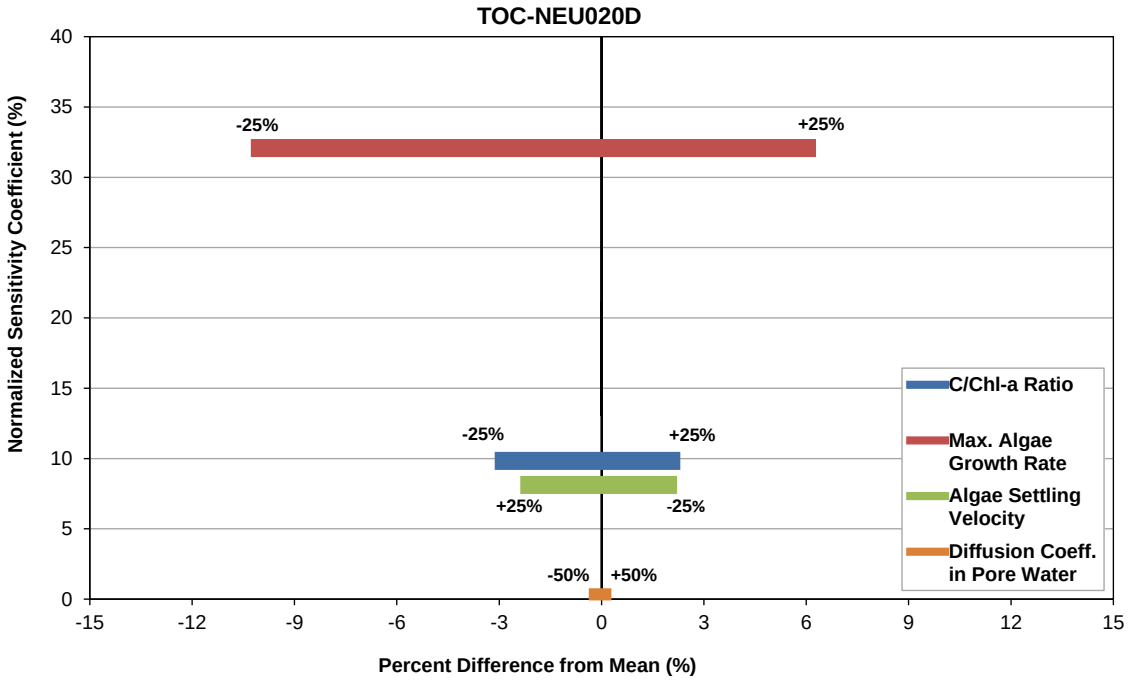

Figure 13-7 Tornado Diagram for Sensitivity Analysis of Modeled TOC at NEU020D

Sensitivity Analysis of TN

The tornado diagrams of sensitivity analysis results of modeled TN at stations NEU013B, NEU018E, and NEU020D are given in Figure 13-8, Figure 13-9, and Figure 13-10, respectively. The calculated NSCs are also given in Table 13-4. The time series plots and Box-Whisker plots of modeled TN under different perturbation levels of these four (4) model input parameters at stations NEU013B, NEU018E, and NEU020D are given in Appendix A.5.

At all three stations, the positive perturbations in the maximum algal growth rate, C/Chl-a ratio, and diffusion coefficient in pore water result in the positive response in the average modeled TN, or vice versa as shown in Figure 13-8, Figure 13-9, and Figure 13-10. On the other hand, the positive perturbation in the algae settling velocity leads to the negative response in the average modeled TN, or vice versa. Since the majority of TN in the water column of Falls Lake is organic nitrogen, part of which is contained in algae cells, the perturbation-response relation of TN is similar to that of TOC. X and Y axes on these figures are scaled smaller than preceding figure.

The maximum algal growth rate has the most impact on modeled TN at all three stations, with the calculated NSCs of 6.09 at station NEU013B, 17.45 at station NEU018E, and 18.40 at station NEU020D as shown in Table 13-4. On the other hand, the diffusion coefficient in pore water has the least impact on modeled TN, with the calculated NSC of 0.11 at station NEU013B, 0.10 at station NEU018E, and 0.23 at station NEU020D. The sensitivity of the modeled TN to the algae settling velocity and C/Chl-a ratio is in the middle of the sensitivity range. Furthermore, perturbations in these four (4) models input parameters at stations

NEU018E and NEU020D show a similar impact on modeled TN, as shown by the similar values of NSCs (Table 13-4, Figure 13-9, and Figure 13-10).

Table 13-4 Calculated Normalized Sensitivity Coefficients (%) for Modeled TN at Stations NEU013B, NEU018E, and NEU020D in the Photic Layer

Model Input Parameters	NEU013B	NEU018E	NEU020D
C/Chl-a Ratio	3.01	6.69	6.82
Max. Algae Growth Rate	6.09	17.45	18.40
Algae Settling Velocity	4.64	6.45	6.96
Diffusion Coeff. In Pore Water	0.11	0.10	0.23

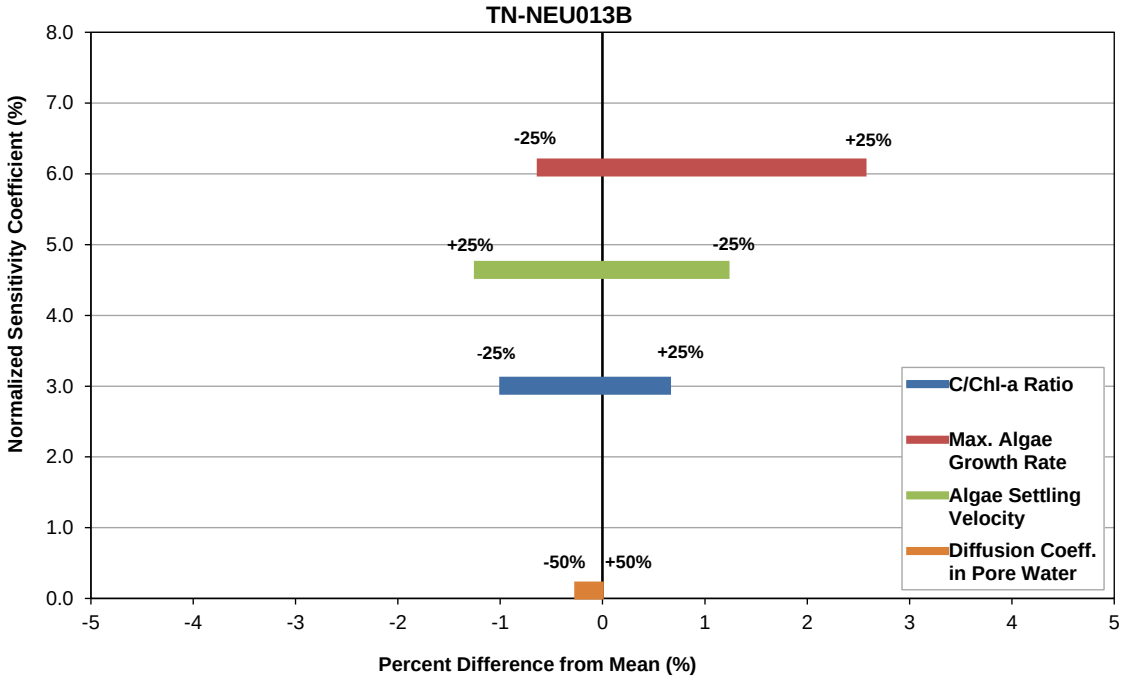

Figure 13-8 Tornado Diagram for Sensitivity Analysis of Modeled TN at NEU013B

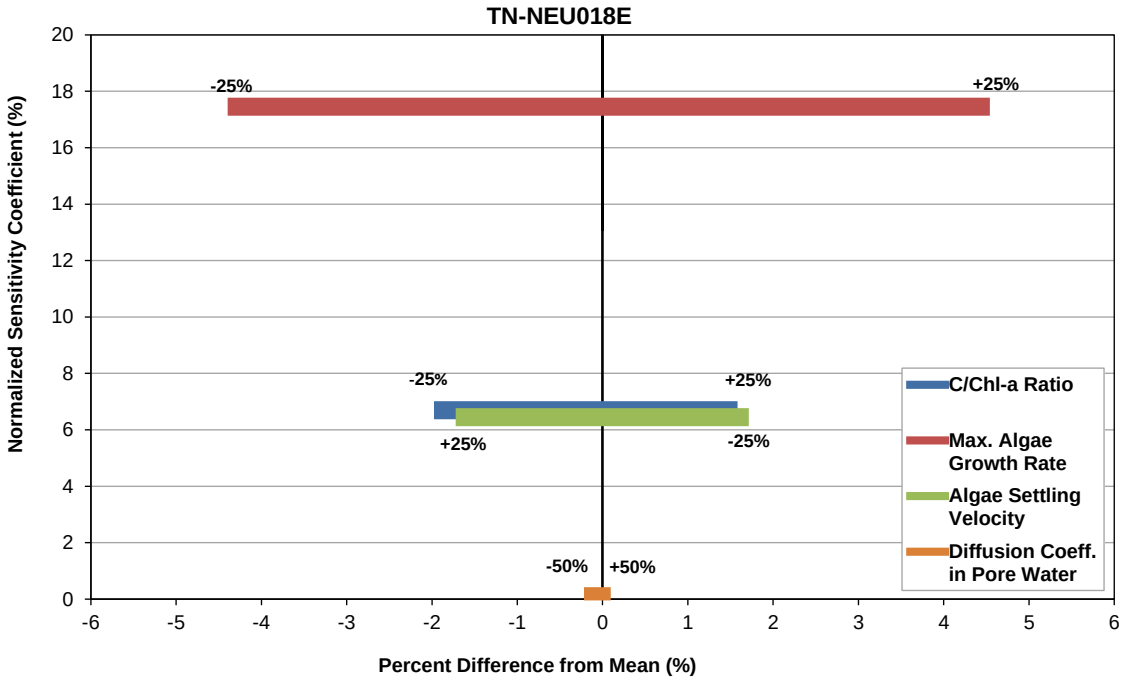

Figure 13-9 Tornado Diagram for Sensitivity Analysis of Modeled TN at NEU018E

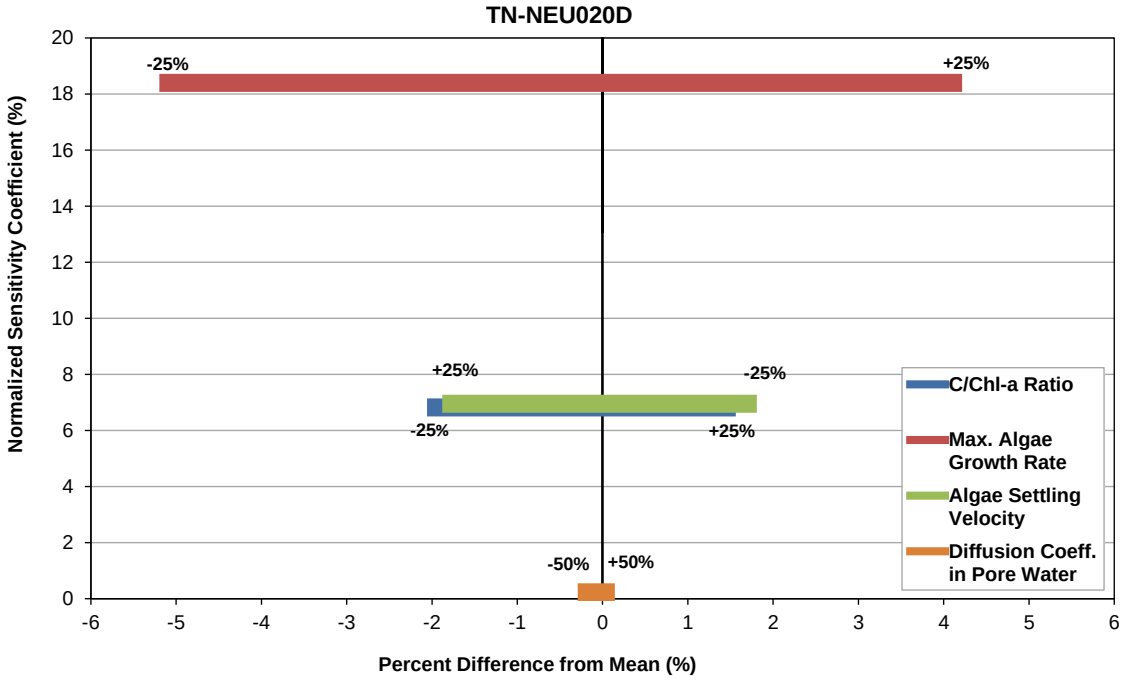

Figure 13-10 Tornado Diagram for Sensitivity Analysis of Modeled TN at NEU020D

Sensitivity Analysis of TP

The tornado diagrams of sensitivity analysis results of modeled TP at stations NEU013B, NEU018E, and NEU020D are given in Figure 13-11, Figure 13-12, and Figure 13-13, respectively. The calculated NSCs are also given in Table 13-5. The time series plots and Box-Whisker plots of modeled TP under different perturbation levels of these four (4) model input parameters at stations NEU013B, NEU018E, and NEU020D are given in Appendix A.5.

At all three stations, the positive perturbations in the maximum algal growth rate and C/Chl-a ratio result in the negative response in the average modeled TP, or vice versa as shown in Figure 13-11, Figure 13-12, and Figure 13-13. On the other hand, the positive perturbations in the algae settling velocity and diffusion coefficient in pore water lead to the positive response in the average modeled TP, or vice versa. The impact of perturbations in the maximum algal growth rate and algae settling velocity can be explained by their impact on the algal PO_4 uptake. The positive perturbation in the maximum algal growth rate increases the algal mass in the water column by increasing the algal PO_4 uptake. On the other hand, the positive perturbation in the algae settling velocity decreases the algal mass in the water column, and thus decreasing the algal PO_4 uptake.

The maximum algal growth rate has the most impact on modeled TP at all three stations, with the calculated NSCs of 48.02 at station NEU013B, 72.37 at station NEU018E, and 85.41 at station NEU020D as shown in Table 13-5. On the other hand, the algae settling velocity has the least impact on modeled TP, with the calculated NSC of 13.07 at station NEU013B, 14.47 at station NEU018E, and 13.51 at station NEU020D. It can be seen that the perturbations in the algae settling velocity have a similar impact on the modeled TP at all three stations.

At stations NEU013B and NEU018E, the diffusion coefficient in pore water and C/Chl-a ratio are the second and third sensitive parameters affecting the modeled TP. However, at station NEU020D this order is reversed, and diffusion coefficient in pore water becomes less sensitive than C/Chl-a ratio. The positive perturbation in the diffusion coefficient in pore water increases the PO_4 sediment flux during the summer months, which in turn increases PO_4 and TP in the overlaying water layer. However, at the deeper part of the lake, the mixing between the overlaying water layer and the photic layer weakens, and that leads to much smaller change in PO_4 and TP concentrations in the photic layer and less sensitivity to the changes in the diffusion coefficient at station NEU020D than at stations NEU018E and NEU013B.

Table 13-5 Calculated Normalized Sensitivity Coefficients (%) for Modeled TP at Stations NEU013B, NEU018E, and NEU020D in the Photic Layer

Model Input Parameters	NEU013B	NEU018E	NEU020D
C/Chl-a Ratio	15.07	23.83	27.84
Max. Algae Growth Rate	48.02	72.37	85.41
Algae Settling Velocity	13.07	14.47	13.51
Diffusion Coeff. In Pore Water	21.17	33.18	20.58

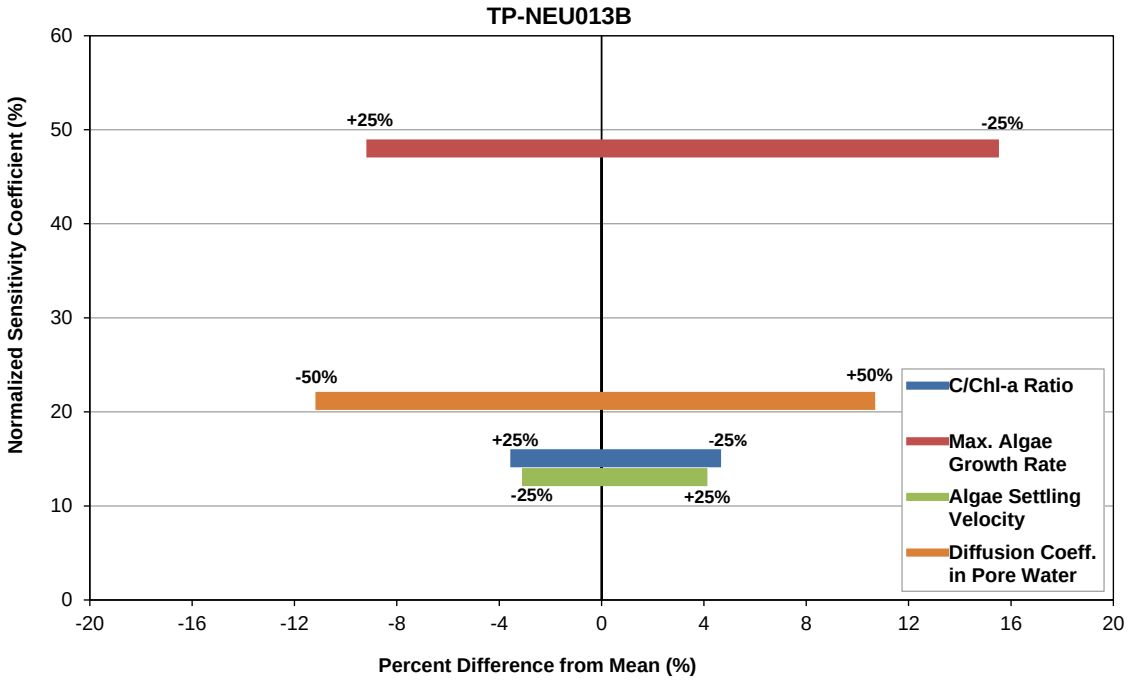

Figure 13-11 Tornado Diagram for Sensitivity Analysis of Modeled TP at NEU013B

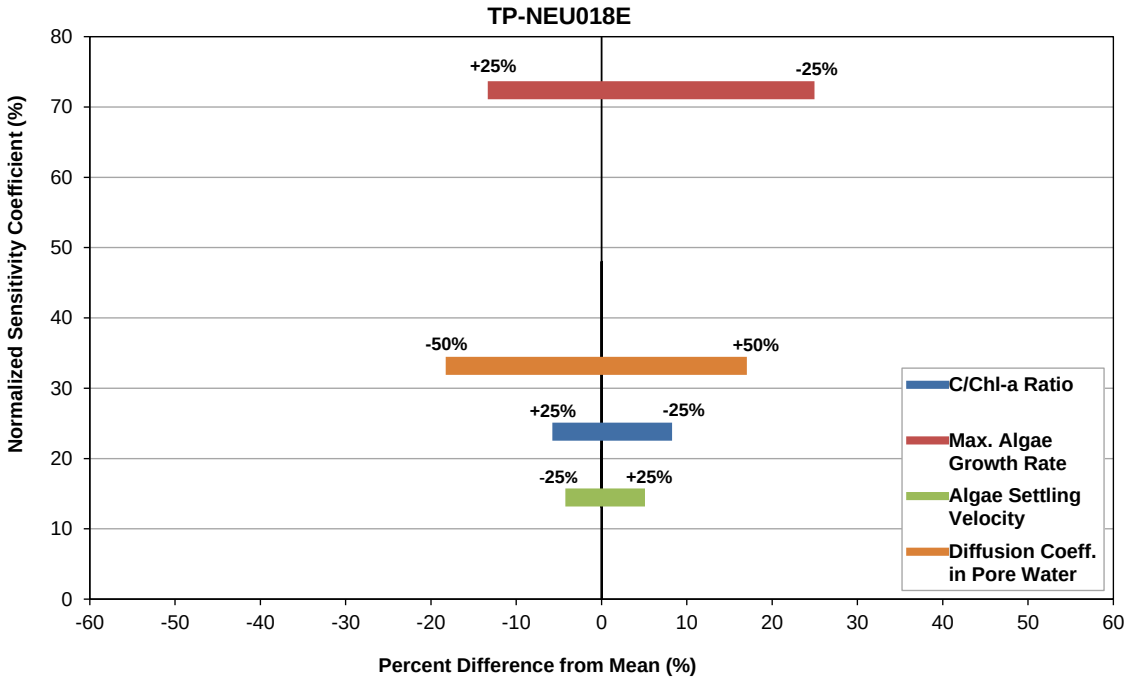

Figure 13-12 Tornado Diagram for Sensitivity Analysis of Modeled TP at NEU018E

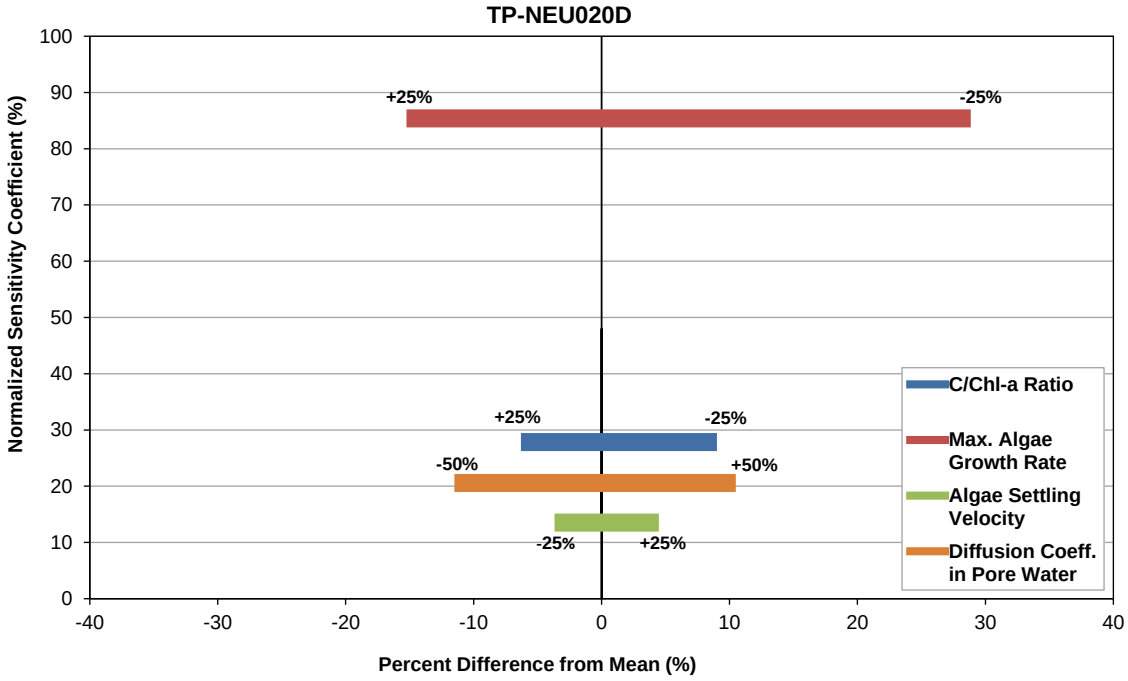

Figure 13-13 Tornado Diagram for Sensitivity Analysis of Modeled TP at NEU020D

13.3 Summary of Sensitivity Analysis

Sensitivity analyses were performed with the calibrated and validated Falls Lake EFDC water quality model. The main aim of the analyses was to evaluate the responses for Chl-a, TOC, TN and TP under the different perturbation levels of four (4) model input parameters for the period of January 1, 2015, through December 31, 2018. The four (4) model input parameters are the C/Chl-a ratio, maximum algae growth rate, algae settling velocity, and diffusion coefficient in pore water. These parameters were selected to examine the change in the algae production and the nutrient concentrations in the water column. The response variables were evaluated for the photic layer of the water column.

The time series plots, Box-Whisker plots, and tornado diagrams were presented for visual comparison of the sensitivity analysis results. The calculated NSCs were used for quantitative and graphical comparison of the sensitivity of model input parameters. Sensitivity analysis results were given at three (3) observed stations: NEU013B is located in the upper part of the lake that is wide and shallow, NEU020D is located in the lower part of the lake that is deeper and narrower, and NEU018E is in the middle of the lake.

Based on the NSCs shown in the tornado diagrams for all three stations, the maximum algal growth rate is the most sensitive parameter for all the response variables. The sensitivity response of changes to the maximum algal growth rate for Chl-a are the highest among other response variables. The sensitivity response of changes to the diffusion coefficient in pore water are less than 1% for Chl-a, TOC, and TN, making it the least sensitive parameter for these response variables. For TP, the algae settling velocity is the least sensitive parameter, with NSC less than 15%.

In the wide, shallow upper part of the lake (station NEU013B), the maximum algal growth rate and algae settling velocity have large impacts on the sensitivity results for Chl-a with NSC of 176.28% and 71.44%, respectively. Changes in these two input parameters directly affect the Chl-a concentration in the water column; the maximum algal growth rate increases algae biomass through photosynthesis, and the algae settling velocity recycles the algae from the water column to the sediment and thus reduces the Chl-a concentration in the water column. The changes in Chl-a concentration in turn impact TOC and TN to a lesser degree by affecting the portion of organic carbon and organic nitrogen coming from algae sources and TP by affecting the algal PO_4 uptake.

From the upper part (station NEU013B) to the middle of the lake (station NEU018E) and further downstream to the lower part (station NEU020D), the sensitivity of Chl-a and TOC to the maximum algal growth rate and algae settling velocity decreases. This is due to the decreasing modeled nutrient (NH_4, NO_3, and TP) concentrations from the upper part to the lower part of the lake that limits the algae growth. On the contrary, the sensitivity of Chl-a, TN, and TP to the C/Chl-a ratio increases from the upper to the lower part of the lake.

Changes in the diffusion coefficient in pore water have less impact on the sensitivity results for TP at station NEU020D in the lower part of the lake than at station NEU018E in the middle of the lake. This is due to the fact that less mixing between the bottom layer and the photic layer occurs at station NEU020D in the deeper part of the lake such that TP concentrations in the photic layer are less sensitive to the changes in the diffusion coefficient at station NUE020D

than at station NEU018E. Furthermore, changes in all four (4) model input parameters at station NEU020D and station NEU018E show similar impacts on the sensitivity results for TN.

14. Scenario Simulations

One component of the UNRBA's reexamination of the Falls Lake Nutrient Management Strategy is the development of improved modeling tools that support the evaluation of nutrient management actions and provide important input to the regulatory support component. The UNRBA formed a Scenario Screening Group to prioritize and select scenarios to evaluate with each model including real-world and boundary-type conditions. These scenarios represent an important set of information for making regulatory decisions and are summarized across models in the main lake modeling report.

The calibrated EFDC water quality model was applied to simulate the in-lake response to a series of scenarios, including long-term simulations with existing watershed loads, watershed nutrient load reduction scenarios, and a watershed nutrient load increase scenario. Analysis of the simulation results was used to understand whether or not attaining compliance with NC water quality standard for Chl-a would be feasible under a management scenario and to understand the relative stability of Chl-a in Falls Lake under potentially changing conditions.

14.1 Long-Term Simulation with the Existing Watershed Loads

One of the scenario simulations evaluates the lake water quality response by running a long-term simulation under continued existing watershed loading. Of special interest is how lake Chl-a concentration and lake sediment nutrient flux would change over time if the existing watershed loads and loading patterns of 2014-2018 were continued for 25 and 50 more years as a result of the improvements to nutrient loading that occurred in the watershed since the baseline period of the rules (2006). The long-term simulation was performed by sequentially running the model ten (10) times after the 6-yr initialization and calibration and validation period of 2014 to 2018. Table 14-1 lists the runs conducted for the long-term simulation.

For each run, watershed loads and stream flows for the period of 2014 to 2018 simulated by the WARMF model were used as input into the lake model. Water column and sediment bed conditions at the end of each run were assigned as the initial conditions for the next run. The model-simulated Chl-a concentrations and sediment bed nutrient PO_4 and NH_4 fluxes at stations NEU013B and NEU020D were evaluated after 25- and 50-year simulations.

Chl-a exceedance curves at stations NEU013B and NEU020D are shown in Figure 14-1 and Figure 14-2, respectively. Both figures show that the Chl-a exceedance curves at each station do not change after 25- and 50-year continuous simulations compared to the calibrated model (2015 and 2016). The calibration years were selected for the comparison because these years had the best model fit to observed data.

The figures indicate that with the existing watershed loads and loading patterns, the model-simulated Chl-a concentrations at these two stations would not change over the long-term. Even though significant reductions in nutrient loading have been achieved in the watershed

(BC and Systech Water Resources, 2022), the modeling period (2015 to 2018) had average to high rainfall and delivered 1.65 million pounds of TN and 183,000 pounds of TP on average. These amounts are sufficient sustain the algal population and the nutrient cycling that occurs between the lake sediments and overlying water.

Table 14-1 List of the Long-Term Simulation Runs

Run #	Period	Description
0	2014-2018	Calibrated model (run after the 6-yr initialization)
1	2019-2023	After 5 years
2	2024-2028	After 10 years
3	2029 – 2033	After 15 years
4	2034 -2038	After 20 years
5	2039 – 2043	After 25 years
6	2044 -2048	After 30 years
7	2049 – 2053	After 35 years
8	2054 -2058	After 40 years
9	2059 – 2063	After 45 years
10	2064 -2068	After 50 years

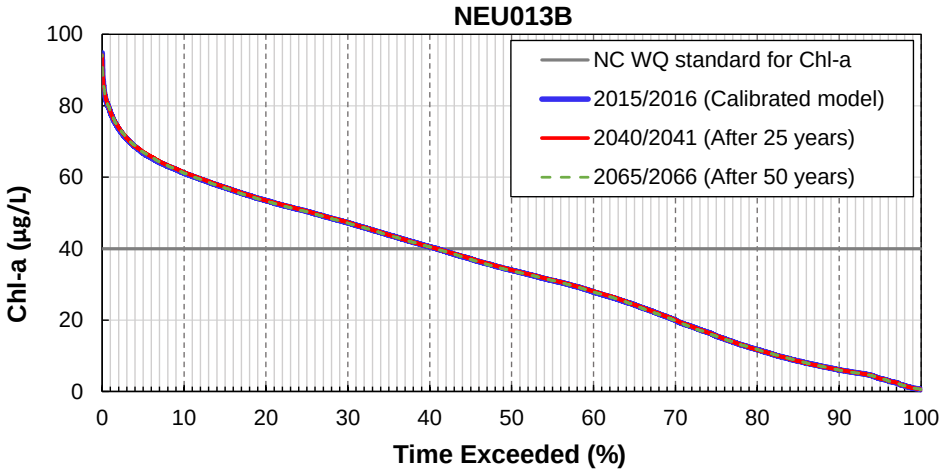

Figure 14-1 Chl-a Exceedance Curves at Station NEU013B

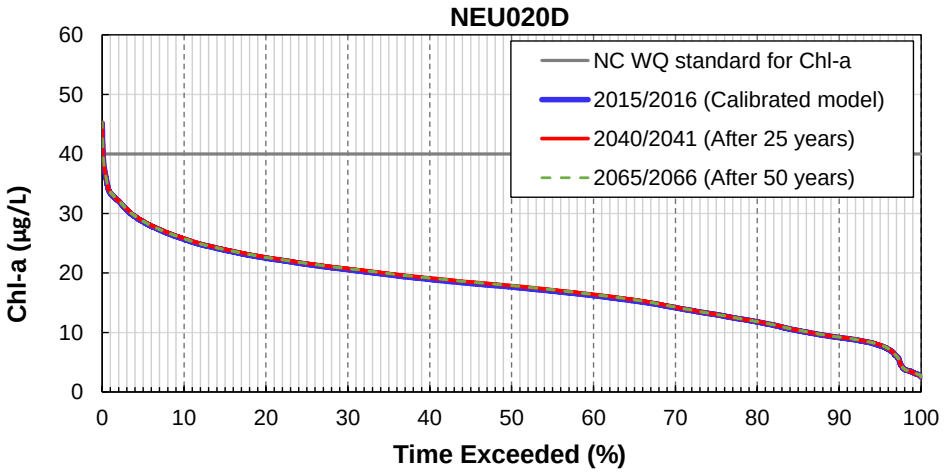

Figure 14-2 Chl-a Exceedance Curves at Station NEU020D

Figure 14-3 and Figure 14-4 display the sediment bed fluxes of PO_4 and NH_4, respectively, with station NEU013B in the top panel and station NEU020D in the bottom panel of each figure. As can be seen in Figure 14-3, after 25- or 50-year simulation (Run # 5 or Run # 10 in Table 14-1) from the calibration and validation period, the PO_4 flux slightly increases at station NEU013B in the upper part of the lake and decreases at station NEU020D in the lower part of the lake when compared to those of the calibration and validation period. This is due to the use of a smaller PO_4 sorption factor and larger diffusion coefficient for the lower part of the lake sediment compared to the upper or middle part of the lake sediment, in order to simulate a relatively large PO_4 flux from the lower and deeper part of the lake sediment. As a result, slightly higher PO_4 is released from the sediments earlier in the lower part of the lake, reducing the release rates as time progresses. Concurrently, in the upper part of the lake, less PO_4 is

released earlier, resulting in an accumulation in sediment porewater over time and slightly higher release rates for 25 or 50 years out.

As shown in Figure 14-4, there is negligible change in the sediment NH_4 fluxes between the calibrated and validated model and running the model out 25 or 50 years. This implies that a dynamic equilibrium in sediment nutrient NH_4 flux has been reached.

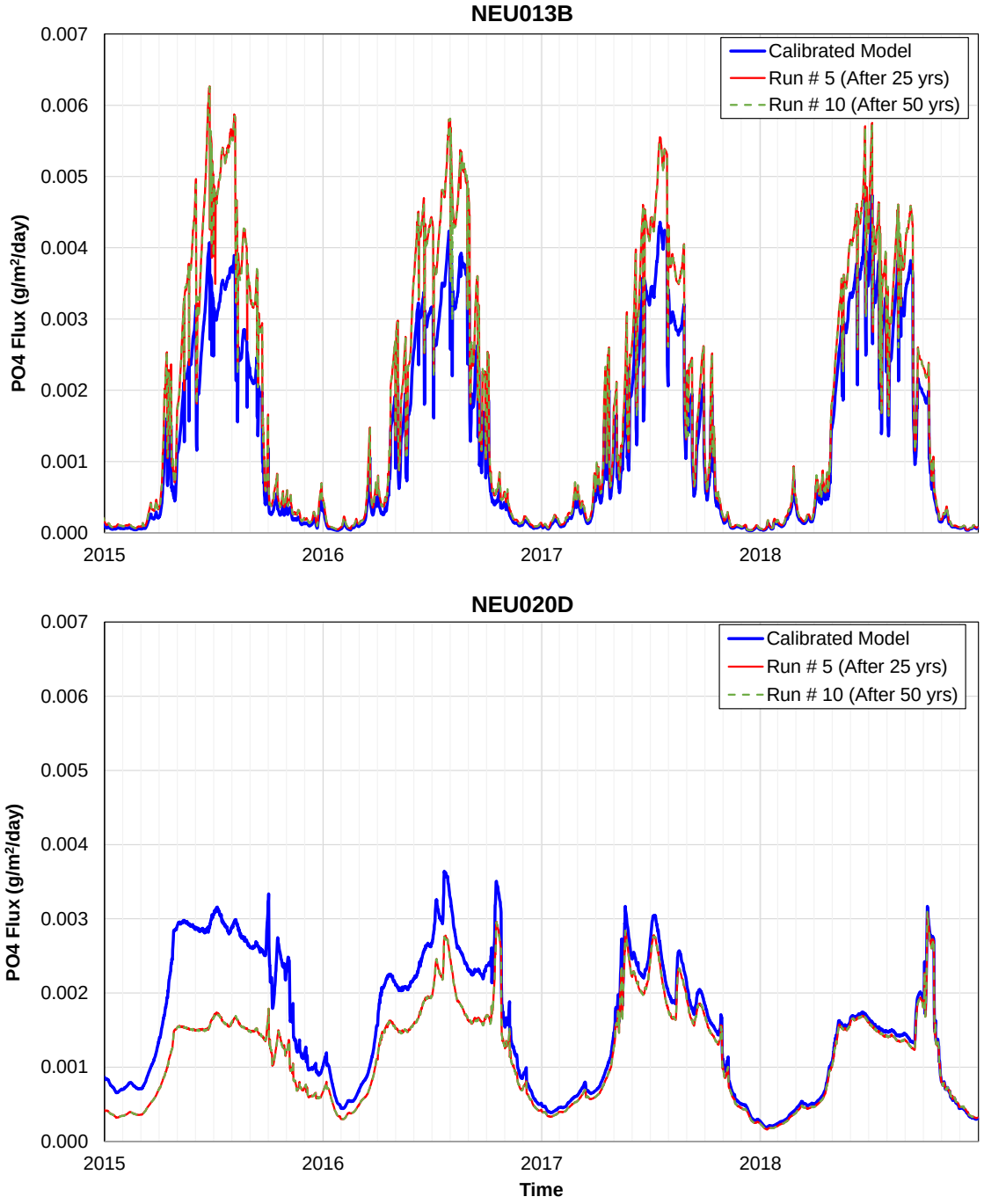

Figure 14-3 Sediment PO_4 Flux; Top: Station NEU013B in the Upper Part of the Lake, Bottom: Station NEU020D in the Lower Part of the Lake

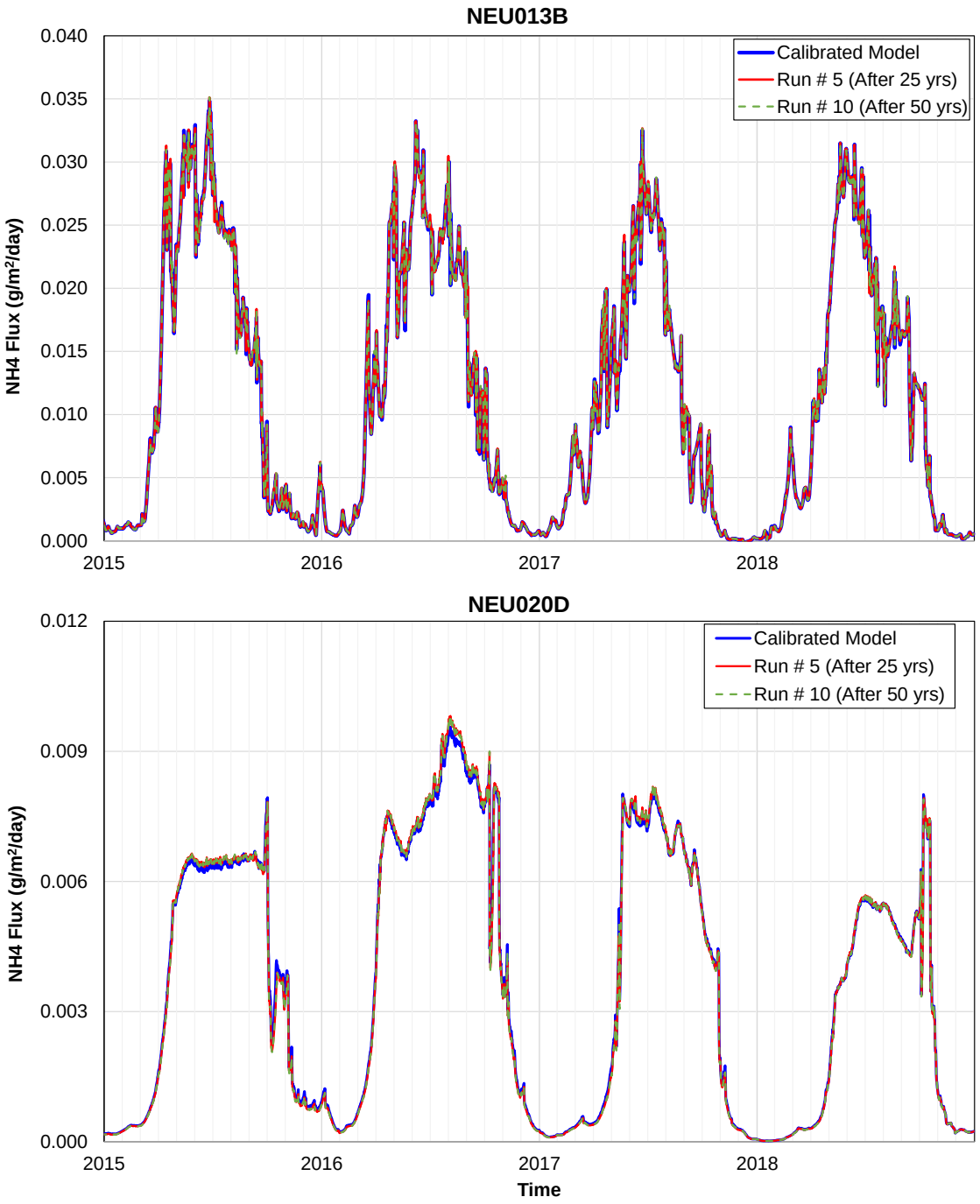

Figure 14-4 Sediment NH_4 Flux; Top: Station NEU013B in the Upper Part of the Lake, Bottom: Station NEU020D in the Lower Part of the Lake

14.2 Nutrient Load Reduction Scenario

As shown in Figure 14-1 , at station NEU013B there is about 38% percent of time that Chl-a concentrations exceed the NC water quality standard of 40 µg/L during the calibration years (2015 and 2016). The calibrated lake model (2015 to 2016) was used to evaluate several load

reduction scenarios to determine whether the Chl-a water quality targets could be achieved through watershed-based load reductions. Nutrient load reduction scenarios included 20%, 40%, and 60% reduction of TP and TN external loading simulated by the WARMF watershed model. A total of sixteen (16) simulation runs were evaluated including the calibrated model (0% reduction of TP and TN) as shown in Table 14-2. TP and TN reductions including both organic and inorganic forms were applied to all the tributary inflows obtained from the WARMF watershed model.

Table 14-2 Nutrient Load Reduction Run Matrix

TP Reduction (%)	Run #			
0	4	3	2	1
20	8	7	6	5
40	12	11	10	9
60	16	15	14	13
	60	**40**	**20**	**0**

TN Reduction (%)

The model response of Chl-a to the load reduction scenarios was examined by means of load reduction contours. Load reduction contours show the rate of exceedance of the model-prediction from the NC water quality standard for Chl-a in response to different combinations of TN and TP reductions.

The load reduction contours for station NEU013B, which was developed based on the simulated Chl-a concentration data of the 16 simulations in Table 14-2, are shown in Figure 14-5. Each contour line represents the percentage of time that Chl-a concentration would exceed the NC water quality standard of 40 µg/L for Chl-a for a series of combinations of TN and TP reductions. As shown in Figure 14-5, the Chl-a concentration at station NEU013B simulated by the calibrated model (with 0% reduction of TP and TN) indicated that approximately 40% of time the Chl-a concentration is above the NC water quality standard of 40 µg/L. To reduce the Chl-a exceedance rate to 10% or below (the blue line labeled with 10%), TN loads would have to be reduced by about 50% relative to the reductions already achieved in the watershed while no TP reduction would be needed at this level of TN reduction. The model responds more readily to TN load reduction than TP load reduction, which is consistent with the fact that nitrogen is the limiting factor for algae growth for the entire lake in

the calibrated model. At stations NEU018B and NEU020D (Figure 14-6 and Figure 14-7) and all the other DWR stations, the Chl-a exceedance rate is much lower than that simulated at station NEU013B.

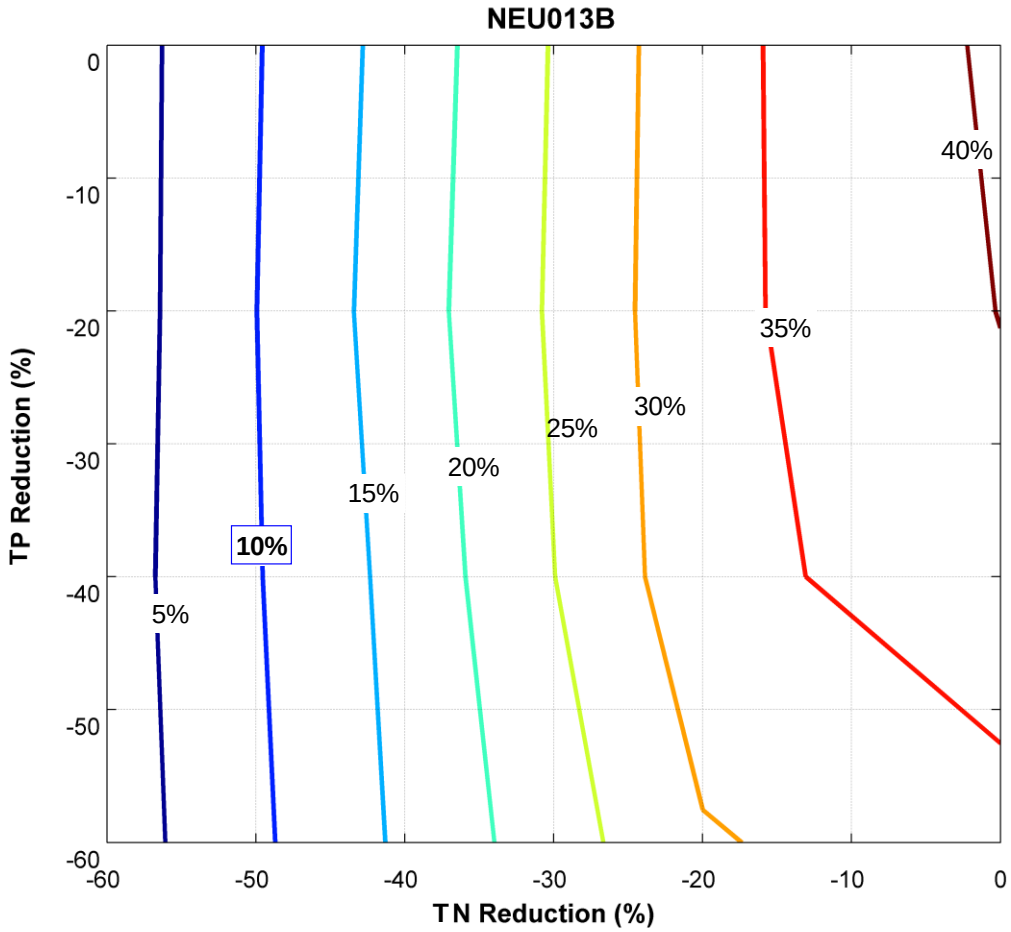

Figure 14-5 Load Reduction Contours for Station NEU013B

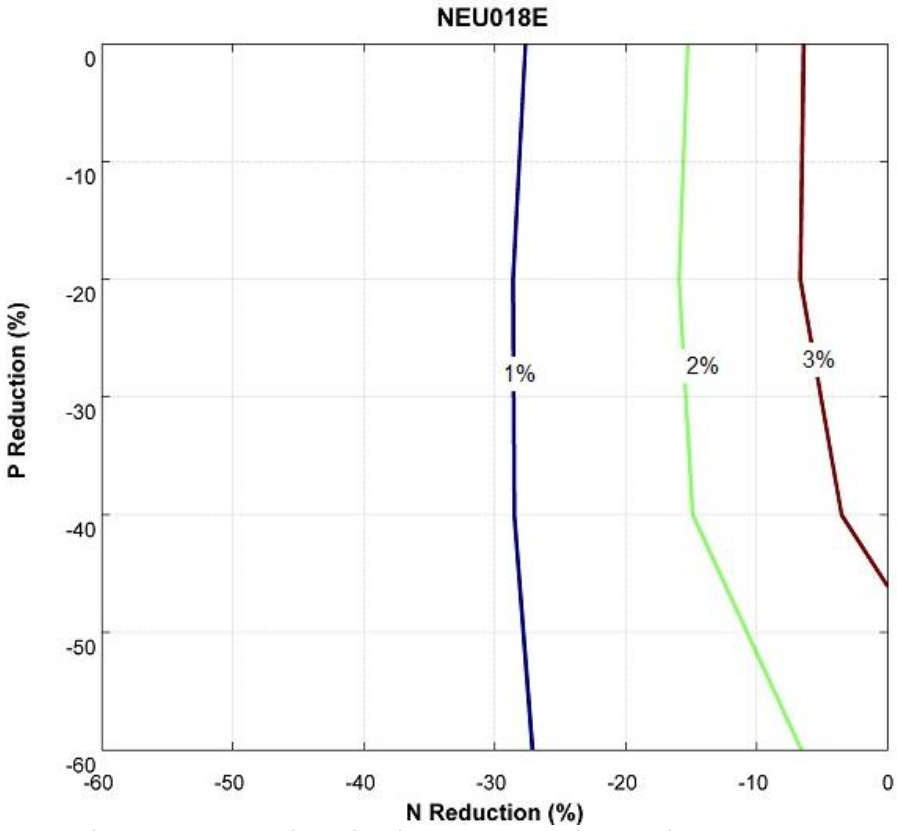

Figure 14-6 Load Reduction Contours for Station NEU018E

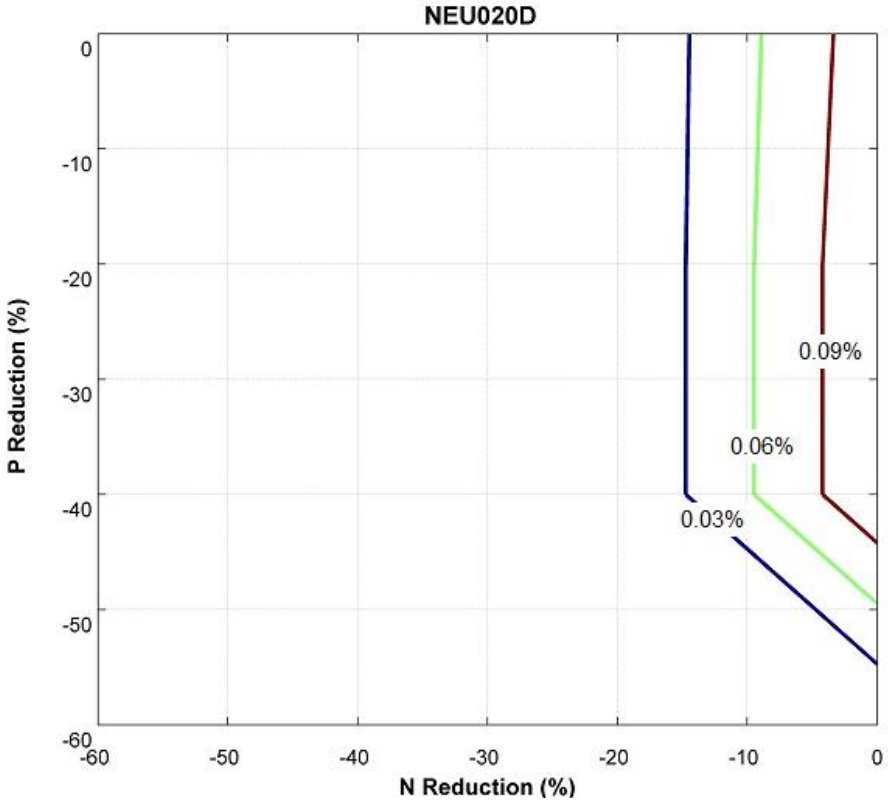

Figure 14-7 Load Reduction Contours for Station NEU020D

The results of the load reduction can also be examined by grouping multiple stations together for the upper part of the lake upstream of Hwy 50 and lower part of the lake downstream of Hwy 50. Figure 14-8 shows the Chl-a exceedance curves for equal percentage of TP and TN reductions (Runs # 1, 6, 11 and 16 in Table 14-2). The top panel of the figure compares the model-simulated exceedance curves for all the DWR stations in the upper part of the lake. To reduce the Chl-a exceedance rate to below 10% for all stations in the upper part of the lake, TP and TN loads would need to be reduced by approximately 20%. The bottom panel of Figure 14-8 shows the model-simulated exceedance curves for all the DWR stations in the lower part of the lake. As shown in the bottom panel of the figure, the Chl-a exceedance rate when the lower lake stations are evaluated together is always below 10%. The percent of time that Chl-a exceeds 40 µg/L for each combination of TP and TN load reductions shown in Figure 14-8 are listed in Table 14-3.

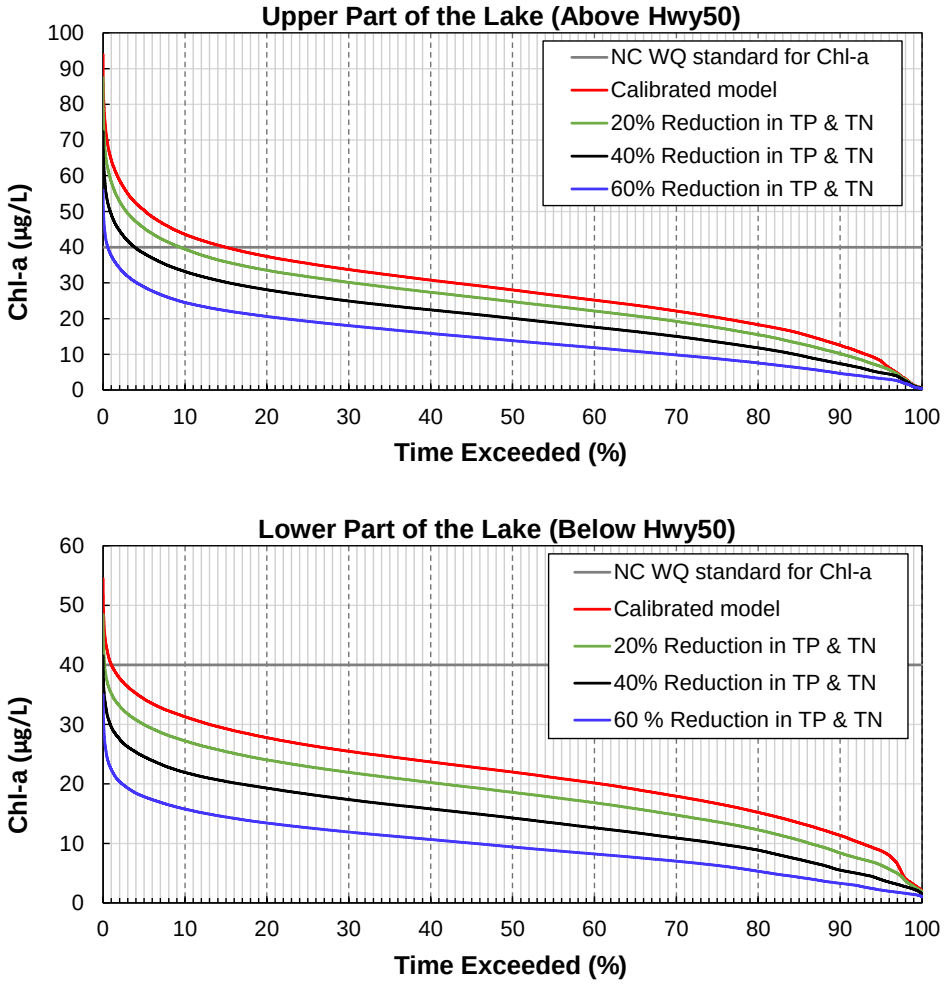

Figure 14-8 Chl-a Exceedance Curves for Equal TP and TN Reduction Scenarios; Top: All DWR Stations in the Upper Part of the Lake, Bottom: All DWR Stations in the Lower Part of the Lake

Table 14-3 Percent of Time that Chl-a Exceeds 40 µg/L for Grouped Stations

% Reduction in TP & TN	Upper Part of the Lake (Above Hwy50)	Lower Part of the Lake (Below Hwy50)
0 and 0 (Calibrated Model)	15	1
20 and 20	9	0
40 and 40	4	0
60 and 60	1	0

14.3 Nutrient Load Increase Scenario

The calibrated lake model was also used to evaluate the impact of an increase in nutrient loading from the watershed on lake water quality. One simulation was conducted with 20% TP and TN increases from external loading simulated with the WARMF watershed model. Similar to the nutrient load reduction scenario, nutrient increase was applied to all the tributary inflows simulated by the WARMF watershed model. Figure 14-9 shows the Chl-a exceedance curves for the 20% TP and TN load increase scenario. The top panel of the figure shows the model-simulated Chl-a exceedance curves of the 20% TP and TN load increase and calibrated model for station NEU013B while the bottom panel compares the model-simulated exceedance curves of the same two models for station NEU020D. At station NEU013B, the Chl-a exceedance rate increases from approximately 40% to 45% and at station NEU020D it increases from near 0% to less than 1%.

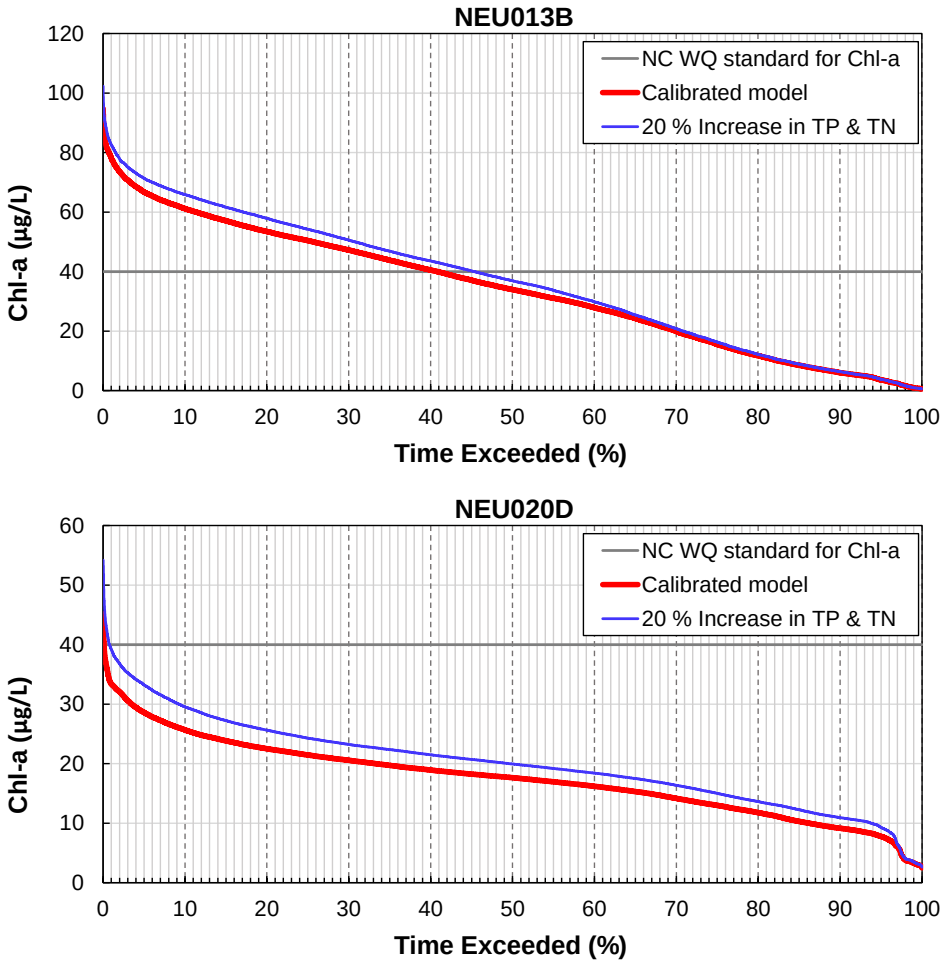

Figure 14-9 Chl-a Exceedance Curves for 20% TP and TN Load Increase Scenario; Top: Station NEU013B, Bottom: Station NEU020D

14.4 Summary of Scenario Simulations

The calibrated EFDC water quality model was applied to simulate the in-lake response to a series of scenarios including the long-term simulation with the existing watershed loads using the watershed input results from WARMF, nutrient reduction scenarios applying a percent reduction to tributary time series concentration inputs, and a nutrient increase scenario applying a percent increase to tributary time series concentration inputs. The Chl-a exceedance curves were developed at stations NEU013B in the upper part of the lake, NEU018E in the middle lake, and NEU020D in the lower and deeper part of the lake to assess the exceedance rates from the NC water quality standard of 40 µg/L.

Long-term simulation with the existing watershed load of 2014 to 2018 for 25 and 50 more years was conducted to evaluate the impact on the lake Chl-a concentrations. The results showed no difference between the Chl-a exceedance curves of the calibrated model and the long-term simulations at stations NEU013B or NEU020D. Sediment nutrient PO_4 flux slightly increased in the upper part of the lake and slightly decreased in the lower part of the lake, due to the use of a smaller PO_4 sorption factor and larger diffusion coefficient for the lower part of the lake compared to those for the upper or middle part of the lake. However, there was negligible change in the sediment NH_4 fluxes between the calibrated model and 25- or 50-year long term simulations, suggesting that a dynamic equilibrium in sediment nutrient NH_4 flux has been reached.

Nutrient load reduction scenarios were conducted to assess the impact on lake water quality. Various load reduction scenarios were conducted, including reductions of 20%, 40%, and 60% of TP and TN from external watershed loading. It was found that to reduce Chl-a exceedance rates to below 10% at station NEU013B, TN loads would need to be reduced by around 50% relative to existing loads while no TP reduction is needed. For the stations in upper part of the lake upstream of Hwy 50, TP and TN loads would need to be reduced by 20% each to achieve less than 10 percent exceedance of the Chl-a criterion of 40 µg/L whereas for the lower part of the lake, the Chl-a exceedance rate is already below 10% under the current conditions of the calibration period.

A nutrient load increase scenario was also conducted to assess the impact on lake water quality. Only one simulation was conducted for a 20% increase in TP and TN from external watershed loading. The model results showed that at station NEU013B, the Chl-a exceedance rate increased from 40% to 45%, while at station NEU020D, it increased by less than 1%.

Overall, the scenarios reflected a lake system that is significantly stabilized relative to nutrient balance, resistant to changes in watershed inputs, and extremely slow in response of algal levels and chlorophyll-a concentrations to changes in nutrient loading. This has important regulatory implications in making decisions about how to effectively manage nutrients in this system.

15. References

Alperin, M. 2018. Falls Lake Sediment Study. Report prepared for the Upper Neuse River Basin Association. UNC Department of Marine Sciences, Chapel Hill, NC. 29 pp.

AMEC. 2012. Atmospheric Deposition Study for the City of Durham, North Carolina Data Report. Prepared for the City of Durham, NC.

Anderson, K.A. and J.A. Downing. 2006. Dry and Wet Atmospheric Deposition of Nitrogen, Phosphorus and Silicon in an Agricultural Region. Water, Air, and Soil Pollution, 176:351-374.

BC and Systech Water Resources Inc. (June 2022). UNRBA Falls of the Neuse Reservoir (Lake) Watershed Modeling Report, Preliminary Draft for MRSW Review.

BC, Systech Water Resources Inc., Dynamic Solutions LLC. (February 2018). Quality Assurance Project Plan for the Upper Neuse River Basin Association; Falls Lake and Watershed Modeling. Available online at https://unrba.org/sites/default/files/reexam-files/UNRBA-Modeling-QAPP-1.0-02-28-2018-ApprovedForWebsite.pdf.

BC, Systech Water Resources Inc., Dynamic Solutions LLC. (September 2018). Data Management Plan and Description of Modeling Process and Model Files for the Upper Neuse River Basin Association; Falls Lake and Watershed Modeling. Available online at https://unrba.org/sites/default/files/reexam-files/FallsLake-ModelDataManagementPlan_September_2018-Final.pdf.

BC. (2019). Upper Neuse River Basin Association Monitoring Program Annual Report. Prepared for the UNRBA. https://unrba.org/sites/default/files/UNRBA-2019-Annual-Report-Final-Updated-Links.pdf

Cardno (May 2016). UNRBA Monitoring Program FY 2016. Raleigh, NC. https://unrba.org/sites/default/files/unrba-2016-annual-monitoring-report_final_05192016.pdf

Center of Applied Aquatic Ecology. (n.d.). Retrieved from https://caae.cals.ncsu.edu/

Cerco, C.F. and T.M. Cole. 1995. User's Guide to the CE-QUAL-ICM Three-Dimensional Eutrophication Model: Release 1.0. Prepared for U.S. Army Waterways Experiment Station, Vicksburg, MS. Technical Report 95-15.

Cerco, C.F., B.H. Johnson and H.V. Wang. 2002. Tributary refinements to the Chesapeake Bay Model. US Army Corps of Engineers, Engineer Research and Development Center, ERDC TR-02-4, Vicksburg, MS.

Christian, J.T. and G.B. Baecher (1999) Point-estimate method as numerical quadrature. Jour. GeoTech. & GeoEnviron. Eng'r, ASCE, 125(9):779-786.

Cleveland, W. S., & Devlin, S. J. (1988). Locally weighted regression: an approach to regression analysis by local fitting. Journal of the American statistical association, 83(403), 596-610.

Craig, P. (2018). User's Manual for EFDC_Explorer8.4: A Pre/Post-Processor for the Environmental Fluid Dynamics Code. Edmonds, WA: Dynamic Solutions-International, LLC.

Di Toro, D. (2001). Sediment Flux Modeling. New York, NY: Wiley Interscience.

Division of Water Resources Nonpoint Source Planning Branch (2021). 2021 Status Report: Falls Lake Nutrient Strategy. N.C. Department of Environmental Quality. Raleigh, NC.

Donigian, A.S. Jr. and J.T. Love. (2007). The Housatonic River Watershed Model: Model Application and Sensitivity/Uncertainty Analysis. 7th International IWA Symposium on System Analysis and Integrated Assessment in Water Management, May 7-9, 2007. Washington, DC.

Flexner, M., 2019. Falls Lake Nutrient Exchange & Sediment Oxygen Demand (SOD) Study Final Project Report, Version 2 (tech. rep.). Field Services Branch, Science & Ecosystem Support Division, USEPA - Region 4

Hall, N. and Paerl, H. 2020. Defining the balance between cyanobacterial N_2 fixation and denitrification in Falls of the Neuse Reservoir, NC, Annual Progress Report.

Hamrick, J. (1992). A Three-Dimensional Environmental Fluid Dynamics Computer Code: Theoretical and Computational Aspects. Gloucester Point, VA.: Special Report No. 317 in Applied Marine Science and Ocean Engineering, Virginia Institute of Marine Science. 64pp.

Hamrick, J. (1996). User's Manual for the Environmental Fluid Dynamics Computer Code. Gloucester Point, VA: Special Report No. 331 in Applied Marine Science and Ocean Engineering, Virginia Institute of Marine Science.

Hamrick, J. (2007). The Environmental Fluid Dynamics Code Theory and Computation Volume 3: Water Quality Module. Fairfax, VA: Technical report prepared by Tetra Tech, Inc.

Harr, M.E. (1989) Probabilistic estimates for multivariate analyses. Appl. Math. Modelling, 13(5):313-318.

Ji, Z.-G. (2017). Hydrodynamics and Water Quality Modeling Rivers, Lakes and Estuaries. 2nd Edition, John Wiley & Sons, Inc., Hoboken, NJ, 581 pp.

Luettich, R., Whipple, T., Seim, H., & Gilchrest, O. (2021). In situ observational study of water circulation and physical properties in Falls Lake. Talk 1 in Session 2: In-Lake Processes | Falls Lake Nutrient Management Study Research Symposium, May 19, 2021

Li, K.S. (1992) Point-estimate method for calculating statistical moments. Jour. Eng'r Mech., ASCE, 118(7):1506-1511.

Lin, M., Walker, J., Geron, C., & Khlystov, A. (2010). Organic nitrogen in $PM_{2.5}$ aerosol at a forest site in the Southeast US. Atmospheric Chemistry and Physics, 10:2145–2157.

Moriasi, D., Arnold, J., Van Liew, M., Bingner, R., Harmel, R., & Veith, T. (2007). Model Evaluation Guidelines for Systematic Quantification of Accuracy in Watershed Simulations. American Society of Agricultural and Biological Engineers, ISSN 0001-2351.

National Water Information System. Available: https://maps.waterdata.usgs.gov/mapper/index.html

NCDWR. (2008). North Carolina Drought Management Advisory Council Activities Report – 2008. North Carolina Division of Water Resources, Department of Environment and Natural Resources. Dated Oct 1, 2008 (Revised Dec. 18, 2008). https://www.ncdrought.org/files/documents/2008_annual_report.pdf

NCDWQ. (2009). Falls Lake Nutrient Response Model Final Report. Durham County: Prepared by North Carolina Department of Environment and Natural Resources, Division of Water Quality (now Division of Water Resources DWR) Planning Section, Modeling/TMDL Unit. http://portal.ncdenr.org/c/document_library/get_file?uuid=33debbba-5160-4928-9570-55496539f667&groupId=38364

NREL. (2020-08-24). NSRDB. Retrieved from National Solar Radiation Database: https://nsrdb.nrel.gov/

Park, R., Kuo, A., Shen, J., & Hamrick, J. (2000). A Three-Dimensional Hydrodynamic-Eutrophication Model (HEM-3D): Description of Water Quality and Sediment Process Submodels. Gloucester Point, Virginia: Special Report 327 in Applied Marine Science and Ocean Engineering, School of Marine Science, Virginia Institute of Marine Science, the College of William and Mary.

Piehler, M.F. 2019. Quantifying sediment nutrient processing in Falls Lake. Annual Progress Report

Smiley, A., Thompson, S., and Piehler, M. (2023). Reservoir Sediment Nutrient Flux Analysis and Model Presentation at the Falls Lake Nutrient Management Study Research Symposium, April 19, 2023. Available online: https://nutrients.web.unc.edu/2023-falls-lake-research-symposium/

Rosenblueth, E. (1981) Two-point estimates in probabilities. Appl. Math. Modelling, 5(2):329-335.

Sloat, J. (2017). Reservoir Volume and Sediment Accumulation Survey for Falls Lake. WaterCube Data Collection, Processing, & Visualization Services.

U.S. Army Corps of Engineers Wilmington District and the State of North Carolina. (2013). Falls Lake Master Plan; Neuse River Basin. Final Draft. 369 pages.

U.S. Environmental Protection Agency. (2020). Environmental Fluid Dynamics Code (EFDC). Available online at https://www.epa.gov/ceam/environment-fluid-dynamics-code-efdc-download-page

Watershed Analysis Risk Management Framework: Update One: A Decision Support System for Watershed Analysis and Total Maximum Daily Load Calculation, Allocation and Implementation, EPRI, Palo Alto, CA: 2001. 1005181.

Appendix A.1

Falls Lake EFDC Model Selected Water Quality and Sediment Diagenesis Parameters

Table of Contents

List of Tables

1. Water Column

1.1 Kinetics

Table 1-1 Light Extinction Parameters

Parameter	Unit	Definition	Value
Keb	$1/m$	Background Light Extinction Coefficient	0.045
$KeTSS$	$1/m\ per\ mg/L$	Light Extinction due to TSS	0.021
$KeCHL$	$1/m\ per\ mg/L$	Light Extinction due to Chlorophyll (use Riley's eq. if < 0):	0.062
---	---	Chlorophyll Light Extinction Exponent (ignored if using Riley's eq.):	1
$KePOC$	$1/m\ per\ mg/L$	Light Extinction due to POC (POM)	0.078
$KeDOC$	$1/m\ per\ mg/L$	Light Extinction due to DOC (DOM)	0.2

Table 1-2 Kinetics Key Parameters

Parameter	Unit	Definition	Zone 1	Zone 2	Zone 3	Zone 4
$IWQKA$	---	Reaeration Option	Constant(WQKRO)	Constant(WQKRO)	Owens & Gibbs(Modified)	Constant(WQKRO)
k_a	$1/d$	Reaeration Rate Constant	5.32	5.026	3	5.026
θ	---	Reaeration Temperature Rate Constant	1.024	1.024	1.024	1.024
R_{ea}	---	Reaeration Adjustment Factor	0.3	0.5	1.5	0.5
K_{DOC}	$1/d$	Minimum Hydrolysis Rate of DOC	0.005	0.005	0.005	0.005
K_{CD}	$1/d$	COD Decay Rate	0.1	0.1	0.1	0.1
KH_{COD}	$mg\ O_2/L$	Oxygen Half-Saturation Constant for COD Decay	1.5	1.5	1.5	1.5
WS_{RP}	m/d	Settling Velocity for RPOM	0.2	0.2	0.4	0.2
WS_{LP}	m/d	Settling Velocity for LPOM	0.2	0.2	0.4	0.2

1.2 Nutrients

Table 1-3 Nutrients Key Parameters

Parameter	Unit	Definition	Value
PHOSPHORUS			
K_{RPOP}	$1/d$	Minimum Hydrolysis Rate of RPOP	0.005
K_{LPOP}	$1/d$	Minimum Hydrolysis Rate of LPOP	0.075
K_{DOP}	$1/d$	Minimum Mineralization Rate of DOP	0.1
K_{PO4p}	g/m^3	Partition Coefficient for Sorbed/Dissolved PO_4 (to TSS or TAM):	0.04
NITROGEN			
K_{NIT}	$1/d$	Maximum Nitrification Rate	0.25
K_{RPON}	$1/d$	Minimum Hydrolysis Rate of RPON	0.005
K_{LPON}	$1/d$	Minimum Hydrolysis Rate of LPON	0.075
K_{DON}	$1/d$	Minimum Mineralization Rate of DON	0.0022
KH_{NH4}	$g\ N/m^3$	NH_4 Half-Sat Constant for Nitrification	0.025
KH_{NO3}	$g\ N/m^3$	NO_3 Half-Sat Constant for Denitrification	0.1
TR_{NIT}	^0C	Reference Temperature for Nitrification	21
$\theta_{sub,NIT}$	---	Suboptimal Temperature Coefficient for Nitrification	0.045
$\theta_{super,NIT}$	---	Superoptimal Temperature Coefficient for Nitrification	0.0045
CARBON			
K_{RPOC}	$1/d$	Minimum Hydrolysis Rate of RPOC	0.005

Parameter	Unit	Definition	Value
K_{LPOC}	$1/d$	Minimum Hydrolysis Rate of LPOC	0.075
K_{DOC}	$1/d$	Minimum Heterotrophic Mineralization Rate of DOC	0.005

1.3 Algae

General

Table 1-4 Algae General Key Parameters

Parameter	Unit	Definition	Global	Zone 1	Zone 2	Zone 3	Zone 4
Cyanobacteria							
WS_C	m/d	Settling Velocity		0.2	0.2	0.26	0.26
$CChl_C$	$mg\ C/\mu g\ Chl-a$	Carbon to Chl-a Ratio	0.005				
N/C	$g\ N/g\ C$	Nitrogen to Carbon Ratio	0.176				
Diatom							
WS_D	m/d	Settling Velocity		0.4	0.4	0.4	0.4
$CChl_D$	$mg\ C/\mu g\ Chl-a$	Carbon to Chl-a Ratio	0.005				
N/C	$g\ N/g\ C$	Nitrogen to Carbon Ratio	0.176				
Si/C	$g\ Si/g\ C$	Silica to Carbon Ratio	0.8				
Green/Other							
WS_G	m/d	Settling Velocity		0.3	0.3	0.3	0.3
$CChl_G$	$mg\ C/\mu g\ Chl-a$	Carbon to Chl-a Ratio	0.007				
N/C	$g\ N/g\ C$	Nitrogen to Carbon Ratio	0.176				

Growth

Table 1-5 Algae Growth Key Parameters

Parameter	Unit	Definition	Global	Zone 1	Zone 2	Zone 3	Zone 4
Cyanobacteria							
PM_C	$1/d$	Max Growth Rate		2.63	2.68	2.89	3.05
$D_{opt,C}$	m	Optimal Depth for Growth		1	1	1	1
$AOCR_{p,C}$	---	Photosynthesis Oxygen-to-Carbon Ratio	2.67				
KHP_C	mg/L	P Half-Saturation	0.001				
KHN_C	mg/L	N Half-Saturation	0.01				
$TM1_C$	^0C	Optimal Temp Lower Bound	24				
$TM2_C$	^0C	Optimal Temp Upper Bound	31				
$KTG1_C$	$(1/^0C)^2$	Temp Effect Coeff Below Optimal	0.0025				
$KTG2_C$	$(1/^0C)^2$	Temp Effect Coeff Above Optimal	0.002				
Diatom							
PM_D	$1/d$	Max Growth Rate		4	4.17	3.65	3.48
$D_{opt,D}$	m	Optimal Depth for Growth		1	1	1	1

Parameter	Unit	Definition	Global	Zone 1	Zone 2	Zone 3	Zone 4
$AOCR_{p,D}$	---	Photosynthesis Oxygen-to-Carbon Ratio	2.67				
KHP_D	mg/L	P Half-Saturation	0.001				
KHN_D	mg/L	N Half-Saturation	0.01				
KHS_D	mg/L	Silica Half-Saturation	0.05				
$TM1_D$	^0C	Optimal Temp Lower Bound	15				
$TM2_D$	^0C	Optimal Temp Upper Bound	18				
$KTG1_D$	$(1/^0C)^2$	Temp Effect Coeff Below Optimal	0.001				
$KTG2_D$	$(1/^0C)^2$	Temp Effect Coeff Above Optimal	0.006				
Green/Other							
PM_G	$1/d$	Max Growth Rate		4	4	4	4
$D_{opt,G}$	m	Optimal Depth for Growth		1	1	1	1
$AOCR_{p,G}$	---	Photosynthesis Oxygen-to-Carbon Ratio	2.67				
KHP_G	mg/L	P Half-Saturation	0.001				
KHN_G	mg/L	N Half-Saturation	0.01				
$TM1_G$	^0C	Optimal Temp Lower Bound	24				

Parameter	Unit	Definition	Global	Zone 1	Zone 2	Zone 3	Zone 4
$TM2_G$	^0C	Optimal Temp Upper Bound	26				
$KTG1_G$	$(1/^0C)^2$	Temp Effect Coeff Below Optimal	0.008				
$KTG2_G$	$(1/^0C)^2$	Temp Effect Coeff Above Optimal	0.008				

Metabolism

Table 1-6 Algae Metabolism Key Parameters

Parameter	Unit	Definition	Global	Zone 1	Zone 2	Zone 3	Zone 4
Cyanobacteria							
BM_C	$1/d$	Basal Metabolism Rate		0.08	0.08	0.08	0.08
$AOCR_{r,C}$	---	Respiration Oxygen-to-Carbon Ratio	2.67				
$FNR_{x,C}$	---	Fraction of N produced as RPON	0.075				
$FNL_{x,C}$	---	Fraction of N Produced as LPON	0.075				
$FND_{x,C}$	---	Fraction of N Produced as DON	0.65				
$FNI_{x,C}$	---	Fraction of N Produced as NH_4	0.2				
$FPR_{x,C}$	---	Fraction of P Produced as RPOP	0.2				

Parameter	Unit	Definition	Global	Zone 1	Zone 2	Zone 3	Zone 4
$FPL_{x,C}$	---	Fraction of P Produced as LPOP	0.2				
$FPD_{x,C}$	---	Fraction of P Produced as DOP	0.2				
$FPI_{x,C}$	---	Fraction of P Produced as PO_4	0.4				
$FCD_{x,C}$	---	Fraction of Algal DOC Excretion	1				
$KHR_{x,C}$	---	Oxygen Half-Saturation Constant for DOC Excretion	0.5				
$TR_{BM,C}$	^0C	Reference Temperature for Basal Metabolism	20				
$KT_{BM,C}$	$1/^0C$	Effect of Temperature on Metabolism	0.069				
Diatom							
BM_D	$1/d$	Basal Metabolism Rate		0.0735	0.0735	0.0735	0.0735
$AOCR_{r,D}$	---	Respiration Oxygen-to-Carbon Ratio	2.67				
$FNR_{x,D}$	---	Fraction of N Produced as RPON	0.075				
$FNL_{x,D}$	---	Fraction of N Produced as LPON	0.075				
$FND_{x,D}$	---	Fraction of N Produced as DON	0.65				
$FNI_{x,D}$	---	Fraction of N Produced as NH_4	0.2				
$FPR_{x,D}$	---	Fraction of P Produced as RPOP	0.2				

Parameter	Unit	Definition	Global	Zone 1	Zone 2	Zone 3	Zone 4
$FPL_{x,D}$	---	Fraction of P Produced as LPOP	0.2				
$FPD_{x,D}$	---	Fraction of P Produced as DOP	0.2				
$FPI_{x,D}$	---	Fraction of P Produced as PO_4	0.4				
$FSU_{x,D}$	---	Fraction of Silica Produced as SU	0.5				
$FSA_{x,D}$	---	Fraction of Silica Produced as SA	0.5				
$FCD_{x,D}$	---	Fraction of Algal DOC Excretion	1				
$KHR_{x,D}$		Oxygen Half-Saturation Constant for DOC Excretion	0.5				
$TR_{BM,G}$	^0C	Reference Temperature for Basal Metabolism	20				
$KT_{BM,G}$	$1/^0C$	Effect of Temperature on Metabolism	0.069				
Green/Other							
BM_G	$1/d$	Basal Metabolism Rate		0.0105	0.0105	0.0105	0.0105
$AOCR_{r,G}$	---	Respiration Oxygen-to-Carbon Ratio	2.67				
$FNR_{x,G}$	---	Fraction of N Produced as RPON	0.075				
$FNL_{x,G}$	---	Fraction of N Produced as LPON	0.075				
$FND_{x,G}$	---	Fraction of N Produced as DON	0.65				

Parameter	Unit	Definition	Global	Zone 1	Zone 2	Zone 3	Zone 4
$FNI_{x,G}$	---	Fraction of N Produced as NH_4	0.2				
$FPR_{x,G}$	---	Fraction of P Produced as RPOP	0.2				
$FPL_{x,G}$	---	Fraction of P Produced as LPOP	0.2				
$FPD_{x,G}$	---	Fraction of P Produced as DOP	0.2				
$FPI_{x,G}$	---	Fraction of P Produced as PO_4	0.4				
$FCD_{x,G}$	---	Fraction of Algal DOC Excretion	1				
$KHR_{x,C}$		Oxygen Half-Saturation Constant for DOC Excretion	0.5				
$TR_{BM,G}$	^0C	Reference Temperature for Basal Metabolism	20				
$KT_{BM,G}$	$1/^0C$	Effect of Temperature on Metabolism	0.069				

Predation

Table 1-7 Algae Predation Key Parameters

Parameter	Unit	Definition	Global	Zone 1	Zone 2	Zone 3	Zone 4
Cyanobacteria							
PR_C	$1/d$	Max Predation Rate		0.08	0.08	0.08	0.08
$FCRP_C$	---	Fraction of C Produced as RPOC	0.18				
$FCLP_C$	---	Fraction of C Produced as LPOC	0.12				
$FCDP_C$	---	Fraction of C Produced as DOC	0.7				
$FNRP_C$	---	Fraction of N Produced as RPON	0.33				
$FNLP_C$	---	Fraction of N Produced as LPON	0.17				
$FNDP_C$	---	Fraction of N Produced as DON	0.35				
$FNIP_C$	---	Fraction of N Produced as NH_4	0.15				
$FPRP_C$	---	Fraction of P Produced as RPOP	0.36				
$FPLP_C$	---	Fraction of P Produced as LPOP	0.39				
$FPDP_C$	---	Fraction of P Produced as DOP	0.2				
$FPIP_C$	---	Fraction of P Produced as PO_4	0.05				

Parameter	Unit	Definition	Global	Zone 1	Zone 2	Zone 3	Zone 4
Diatom							
PR_D	$1/d$	Max Predation Rate		0.3	0.288	0.288	0.3
$FCRP_D$	---	Fraction of C Produced as RPOC	0.18				
$FCLP_D$	---	Fraction of C Produced as LPOC	0.12				
$FCDP_D$	---	Fraction of C Produced as DOC	0.7				
$FNRP_D$	---	Fraction of N Produced as RPON	0.33				
$FNLP_D$	---	Fraction of N Produced as LPON	0.17				
$FNDP_D$	---	Fraction of N Produced as DON	0.35				
$FNIP_D$	---	Fraction of N Produced as NH_4	0.15				
$FPRP_D$	---	Fraction of P Produced as RPOP	0.36				
$FPLP_D$	---	Fraction of P Produced as LPOP	0.39				
$FPDP_D$	---	Fraction of P Produced as DOP	0.2				
$FPIP_D$	---	Fraction of P Produced as PO_4	0.05				
$FSUP_D$	---	Fraction of Silica Produced as SU	0.5				
$FSSP_D$	---	Fraction of Silica Produced as SA	0.5				

Parameter	Unit	Definition	Global	Zone 1	Zone 2	Zone 3	Zone 4
Green/Other							
PR_G	$1/d$	Max Predation Rate		0.258	0.258	0.258	0.258
$FCRP_G$	---	Fraction of C Produced as RPOC	0.18				
$FCLP_G$	---	Fraction of C Produced as LPOC	0.12				
$FCDP_G$	---	Fraction of C Produced as DOC	0.7				
$FNRP_G$	---	Fraction of N Produced as RPON	0.33				
$FNLP_G$	---	Fraction of N Produced as LPON	0.17				
$FNDP_G$	---	Fraction of N Produced as DON	0.35				
$FNIP_G$	---	Fraction of N Produced as NH_4	0.15				
$FPRP_G$	---	Fraction of P Produced as RPOP	0.36				
$FPLP_G$	---	Fraction of P Produced as LPOP	0.39				
$FPDP_G$	---	Fraction of P Produced as DOP	0.2				
$FPIP_G$	---	Fraction of P Produced as PO_4	0.05				

2. Sediment Diagenesis

2.1 Diagenesis rates

Table 2-1 Diagenesis Rates

Parameter	Unit	Definition	Value
$k_{POC,N,P,1}$	$1/d$	Decay Rate of POC, PON, and POP at 20^0C in Layer 2 for 1st G Class	0.035
$\theta_{POC,N,P,1}$	---	Constant for Temperature Adjustment for KPOC, N, and P for 1st G Class	1.10
$k_{POC,N,P,2}$	$1/d$	Decay rate of POC, PON, and POP at 20^0C in Layer 2 for 2nd G Class	0.0018
$\theta_{POC,N,P,2}$	---	Constant for Temperature Adjustment for KPOC, N, and P for 2nd G Class	1.15

2.2 Diagenesis kinetics and mixing

Table 2-2 Diagenesis Kinetics and Mixing

Parameter	Unit	Definition	Global	Zone 1	Zone 2	Zone 3
K_{M,D_p}	$mg\ O_2/L$	Particle Mixing Half-Saturation Constant for Oxygen	4.0			
$[O_2]_{crit,PO_4}$	mg/L	Critical Dissolved Oxygen for PO_4 Sorption	2.0			
$\pi_{PO_4,2}$	L/kg	Partition Coefficient for PO_4 in Anaerobic Condition	100			
D_d	m^2/d	Diffusion Coefficient in Porewater		0.0024	0.0024	0.0050

Parameter	Unit	Definition	Global	Zone 1	Zone 2	Zone 3
D_p	m^2/d	Particle Mixing Apparent Diffusion Coefficient		6E-05	6E-05	6E-05
κ_{NH_4}	m/d	Optimal Nitrification Velocity at 20^0C		0.02	0.02	0.02
$\kappa_{NO_3,1}$	m/d	Denitirification Velocity in 1st Layer at 20^0C		0.2	0.2	0.2
$\kappa_{NO_3,2}$	m/d	Denitirification Velocity in 2nd Layer at 20^0C		0.5	0.5	0.5
$\Delta\pi_{PO_4,1}$	---	PO_4 Sorption Enhancement Factor		60	60	1
SOD	---	Factor to Enhance Magnitude of Sediment Oxygen Demand		10	10	10

Appendix A.2

Falls Lake EFDC Model Calibration and Validation Time Series Plots

Table of Contents

List of Figures

1. Water Temperature

1.1 Water Temperature Calibration

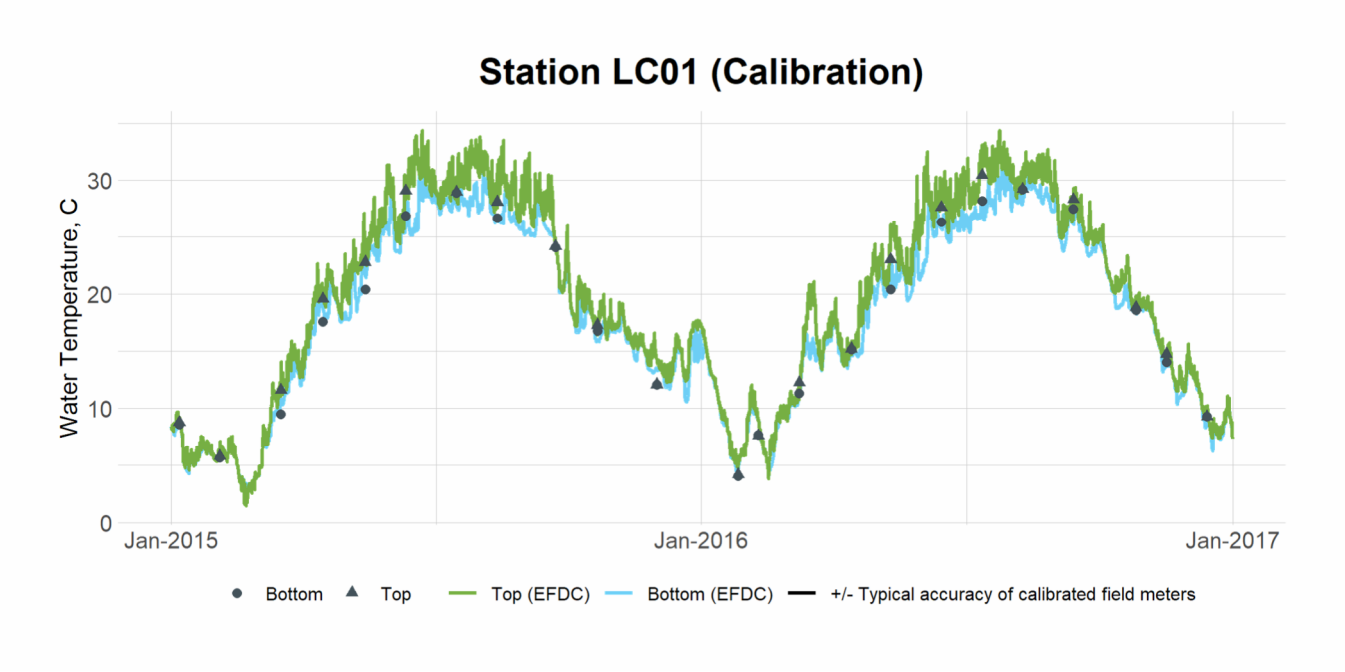

Figure 1-1 Calibration Plot of Top and Bottom Water Temperature at Station LC01

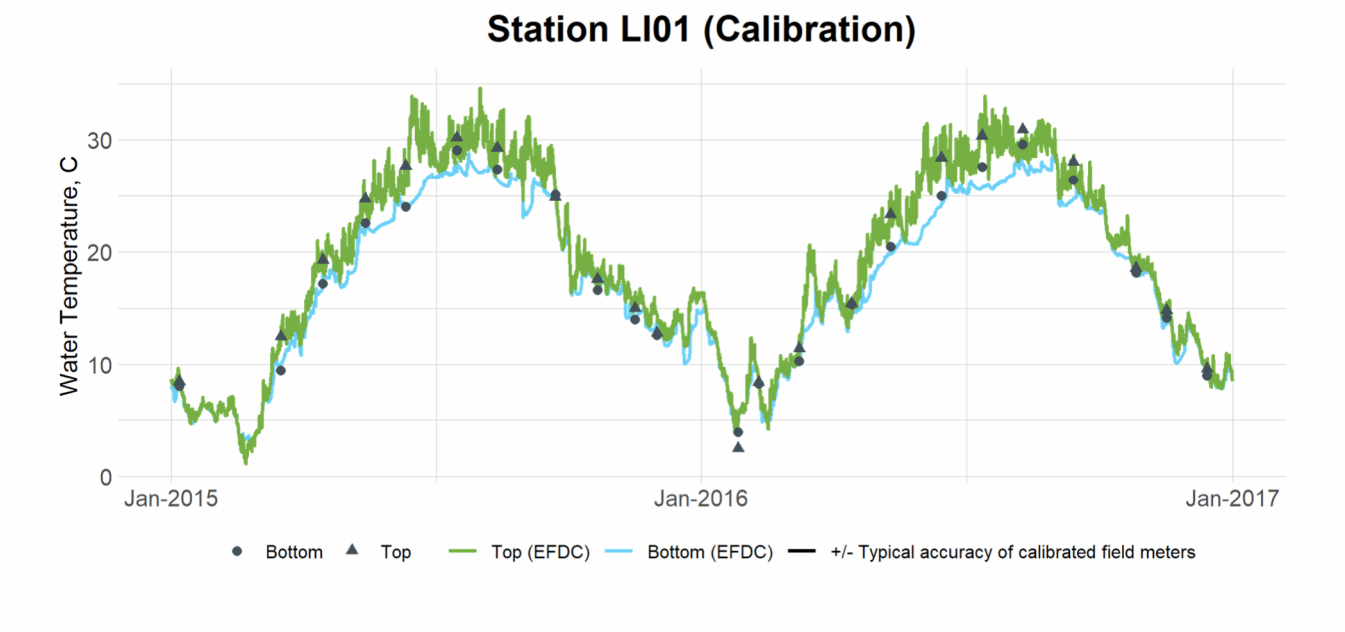

Figure 1-2 Calibration Plot of Top and Bottom Water Temperature at Station LI01

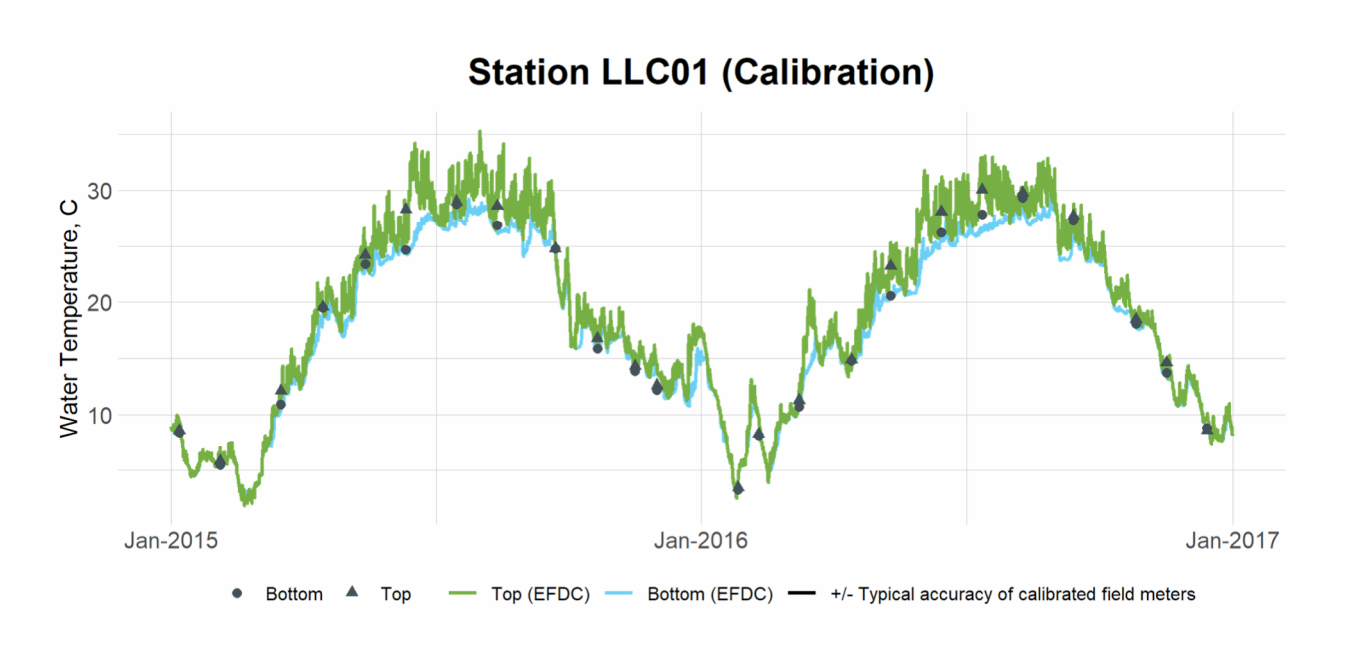

Figure 1-3 Calibration Plot of Top and Bottom Water Temperature at Station LLC01

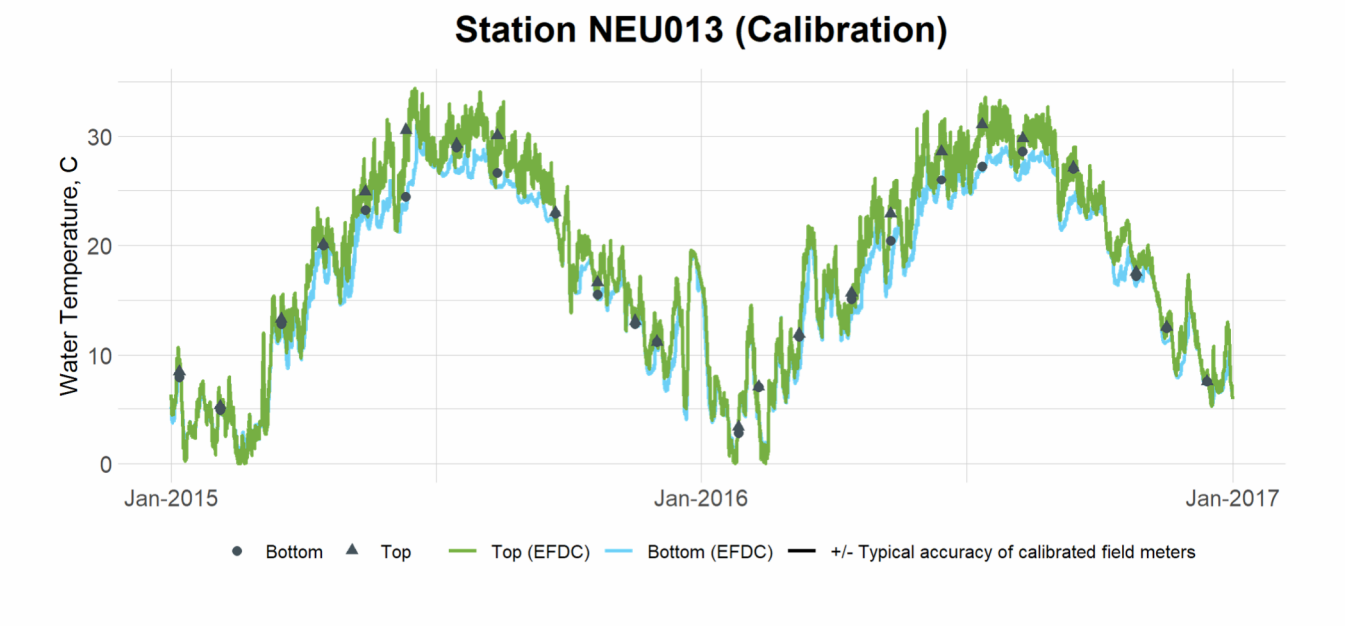

Figure 1-4 Calibration Plot of Top and Bottom Water Temperature at Station NEU013

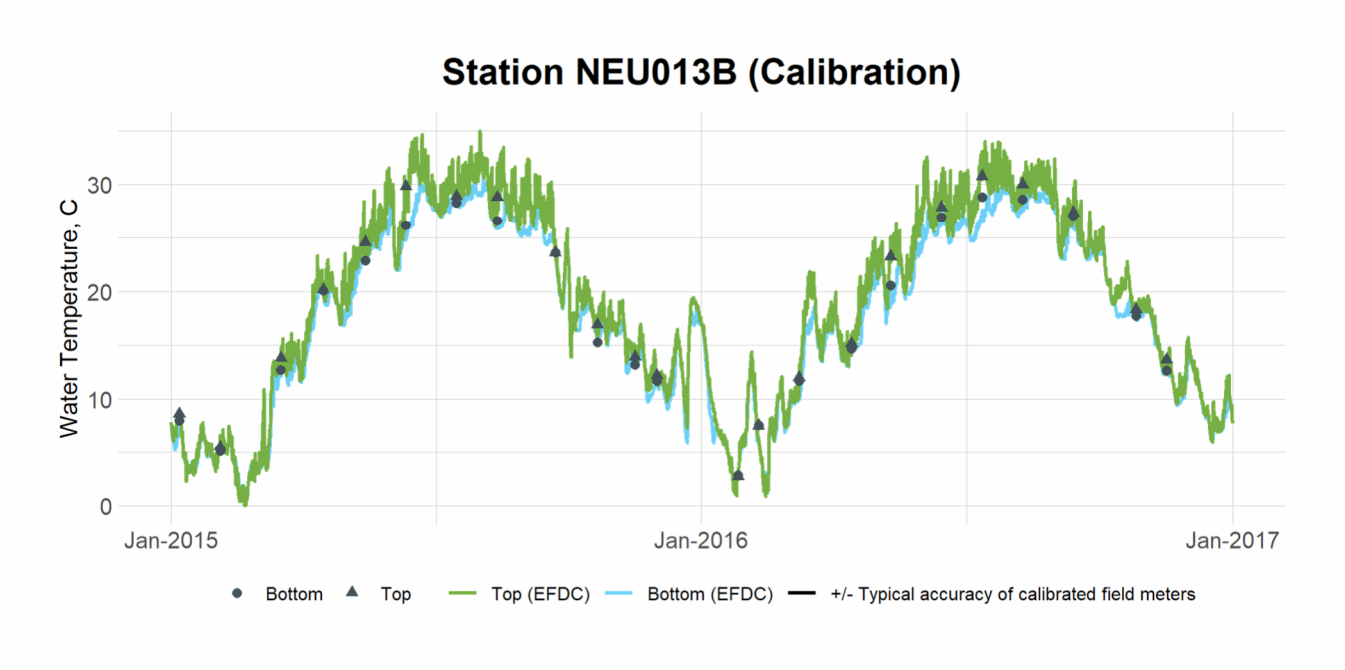

Figure 1-5 Calibration Plot of Top and Bottom Water Temperature at Station NEU013B

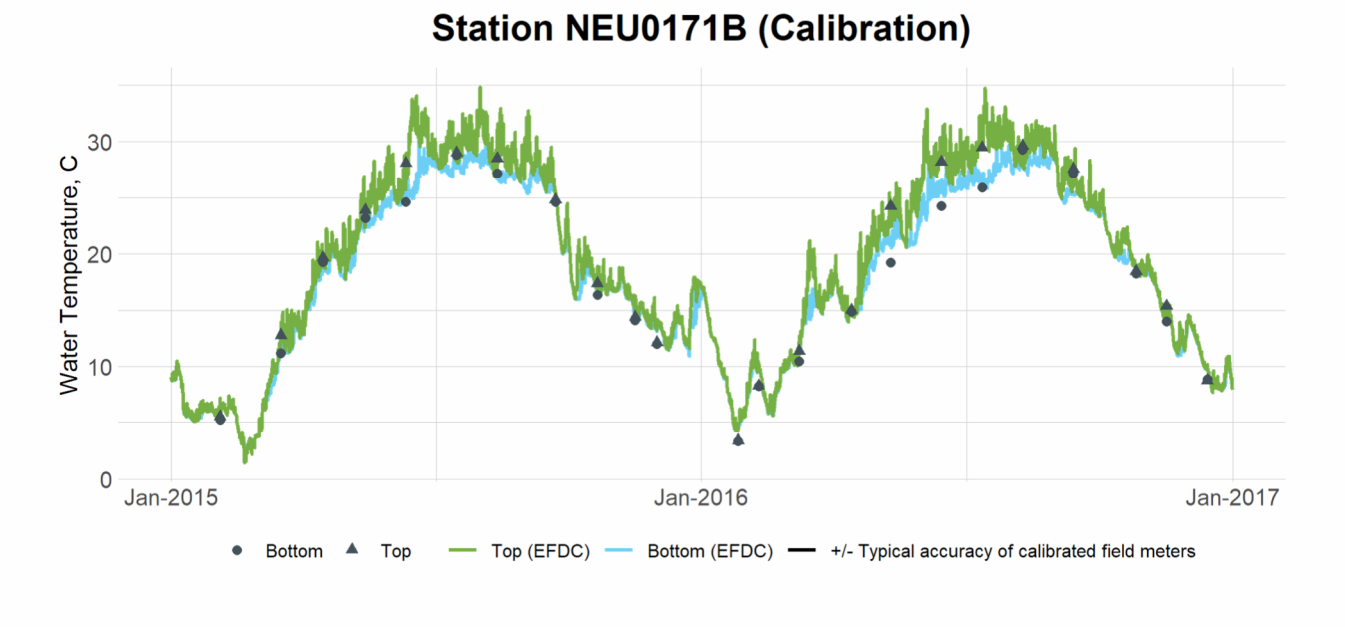

Figure 1-6 Calibration Plot of Top and Bottom Water Temperature at Station NEU0171B

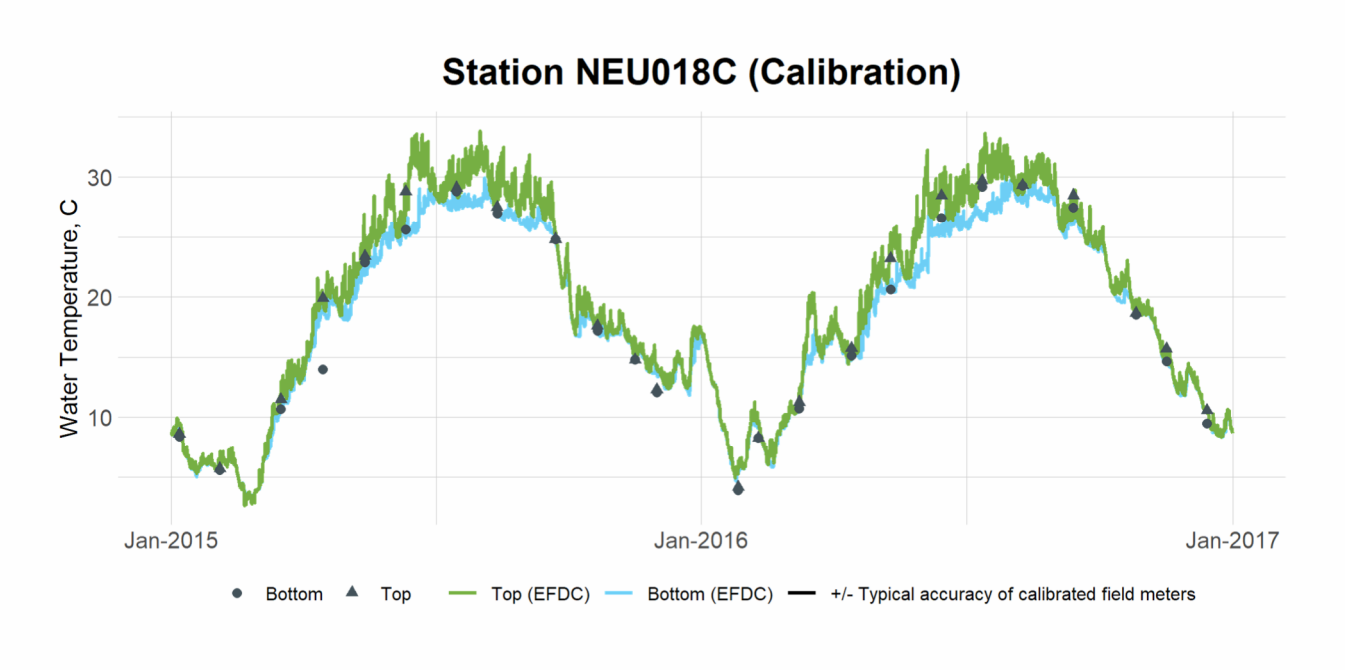

Figure 1-7 Calibration Plot of Top and Bottom Water Temperature at Station NEU018C

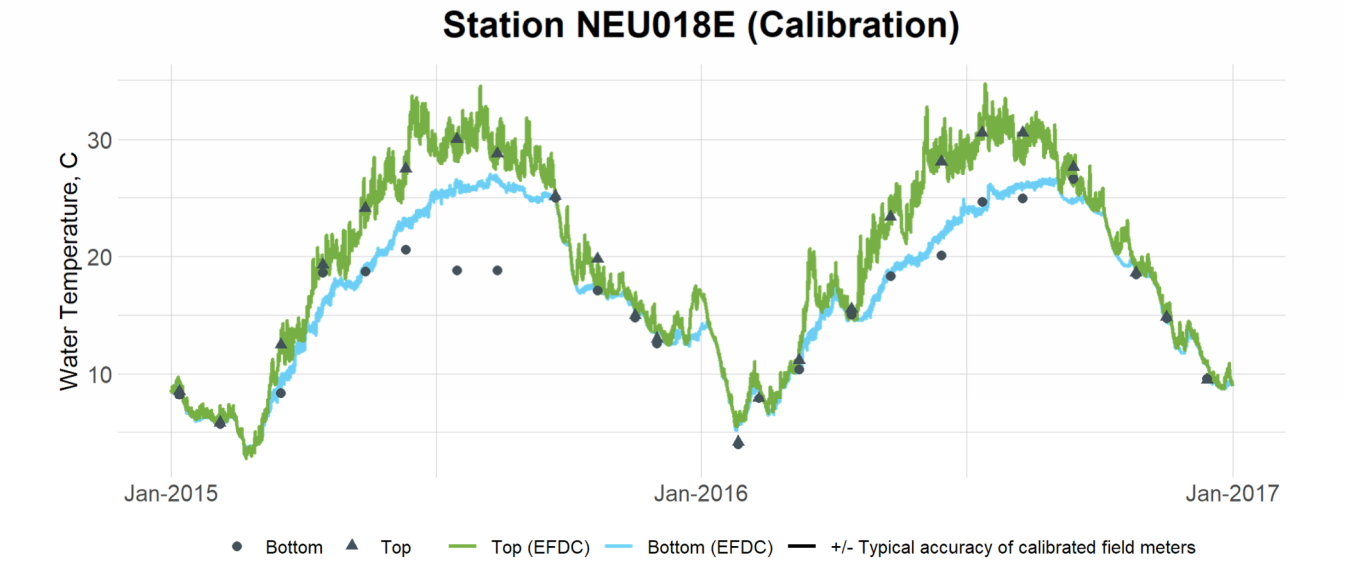

Figure 1-8 Calibration Plot of Top and Bottom Water Temperature at Station NEU018E

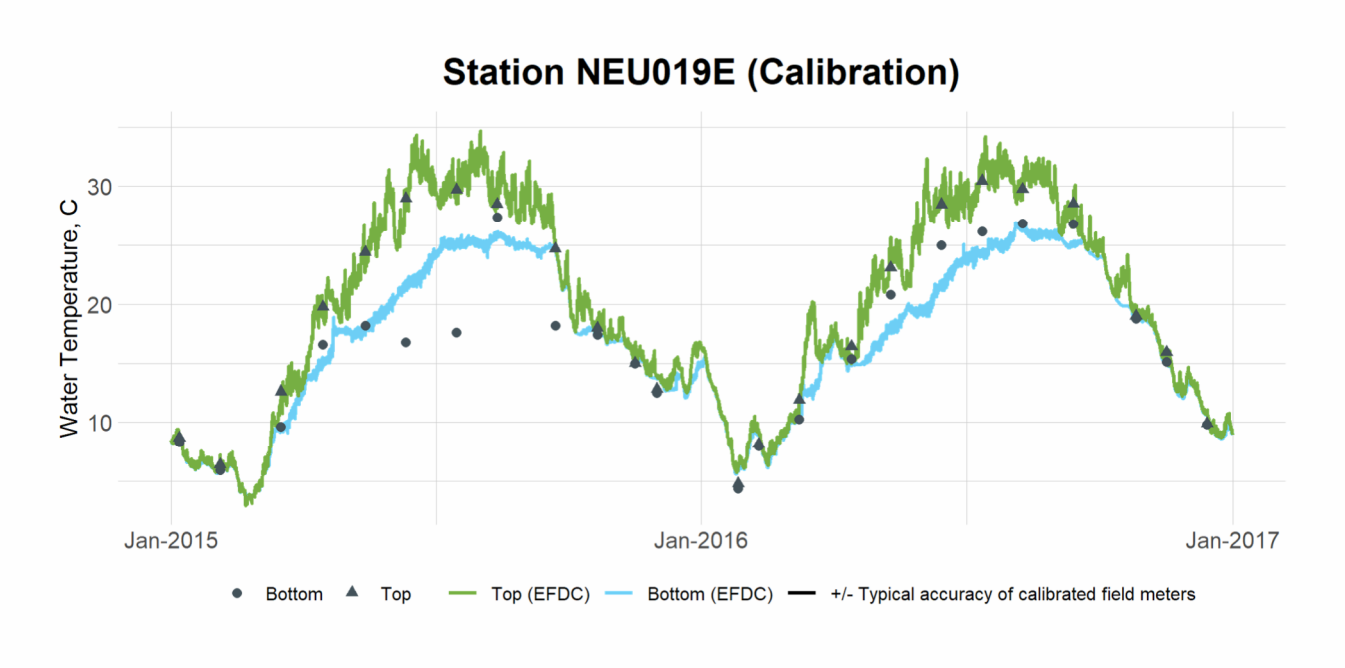

Figure 1-9 Calibration Plot of Top and Bottom Water Temperature at Station NEU019E

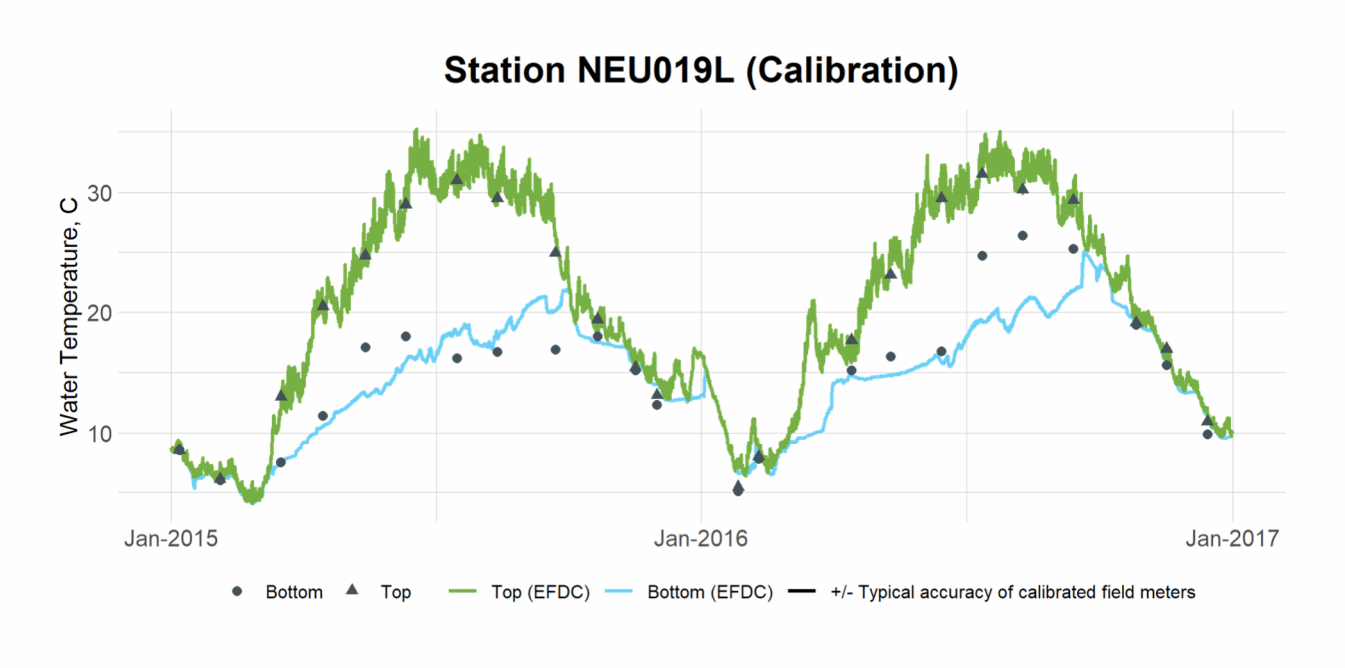

Figure 1-10 Calibration Plot of Top and Bottom Water Temperature at Station NEU019L

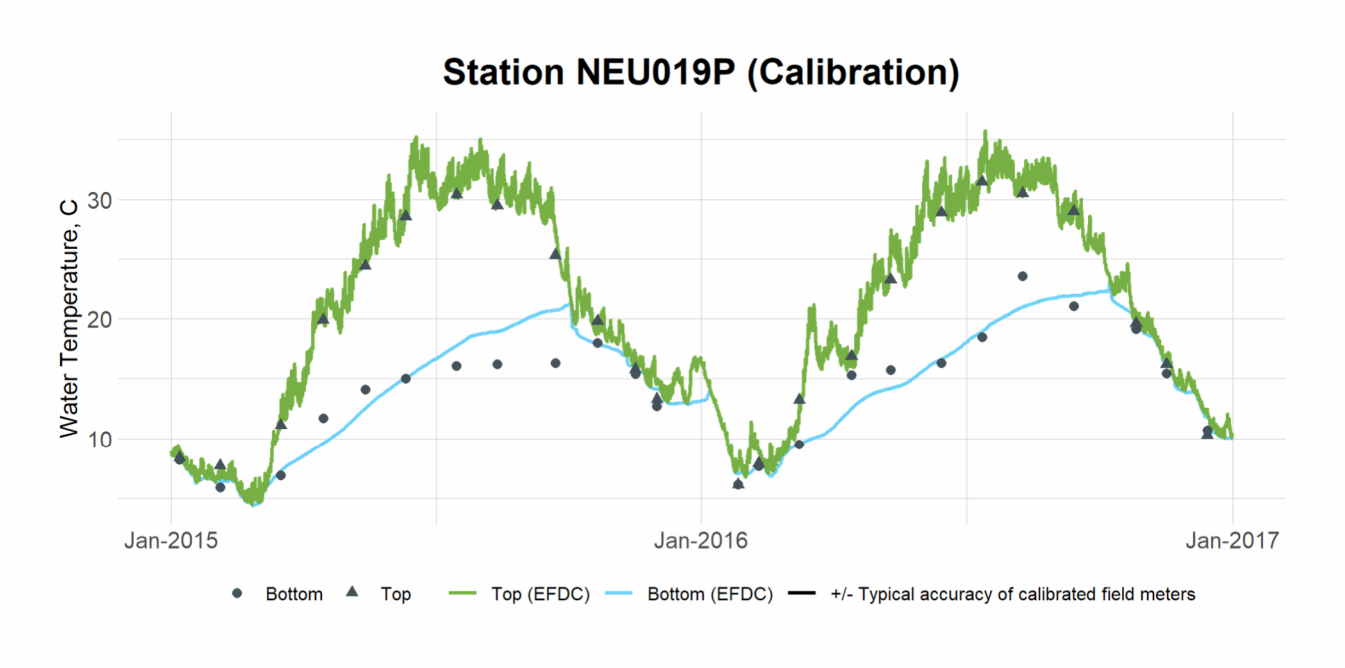

Figure 1-11 Calibration Plot of Top and Bottom Water Temperature at Station NEU019P

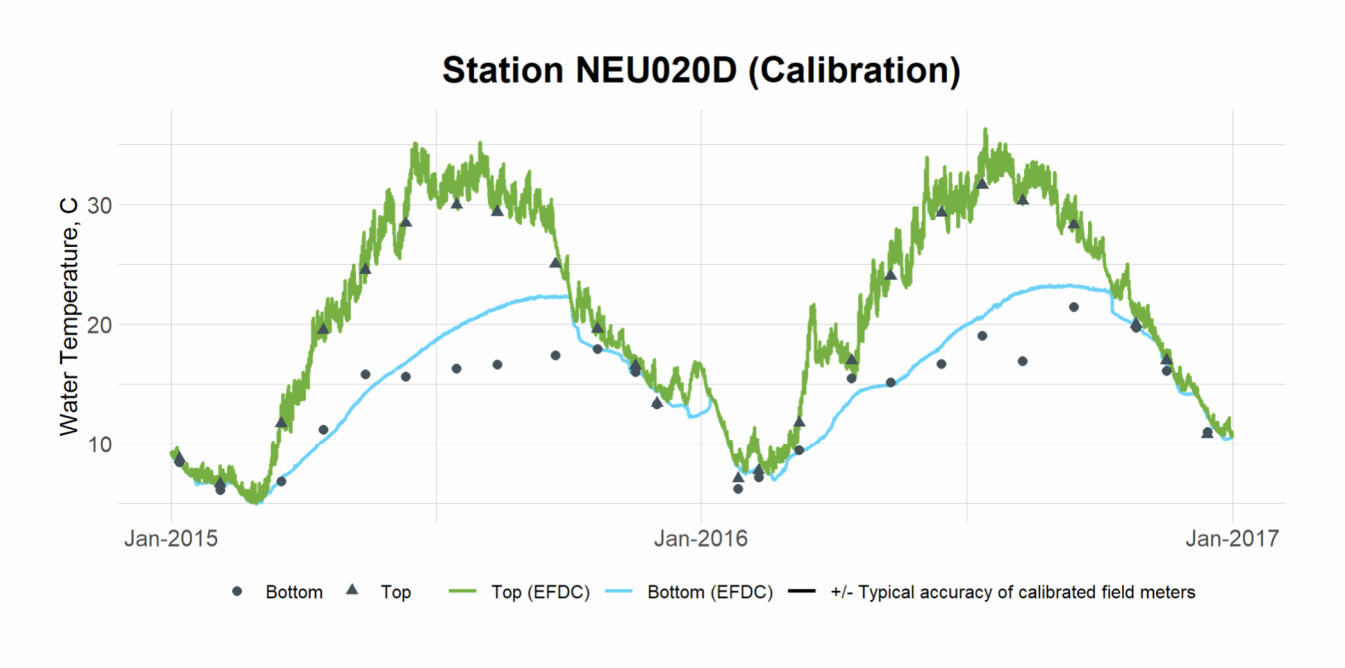

Figure 1-12 Calibration Plot of Top and Bottom Water Temperature at Station NEU020D

1.2 Water Temperature Validation

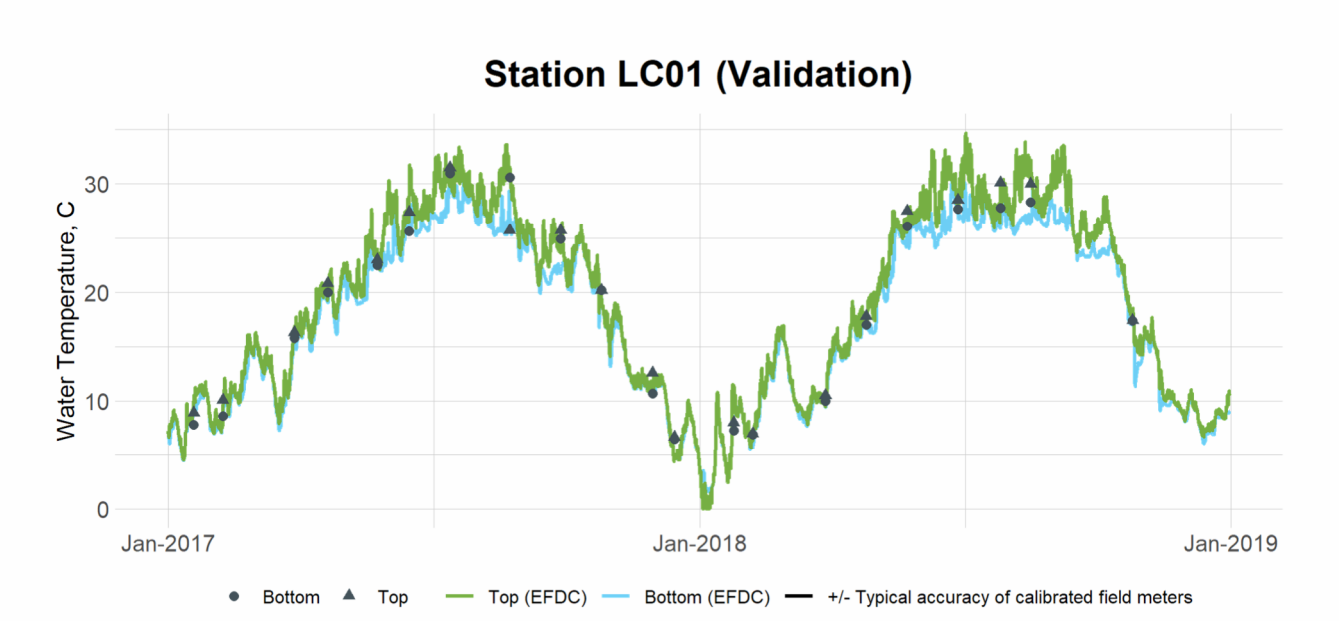

Figure 1-13 Validation Plot of Top and Bottom Water Temperature at Station LC01

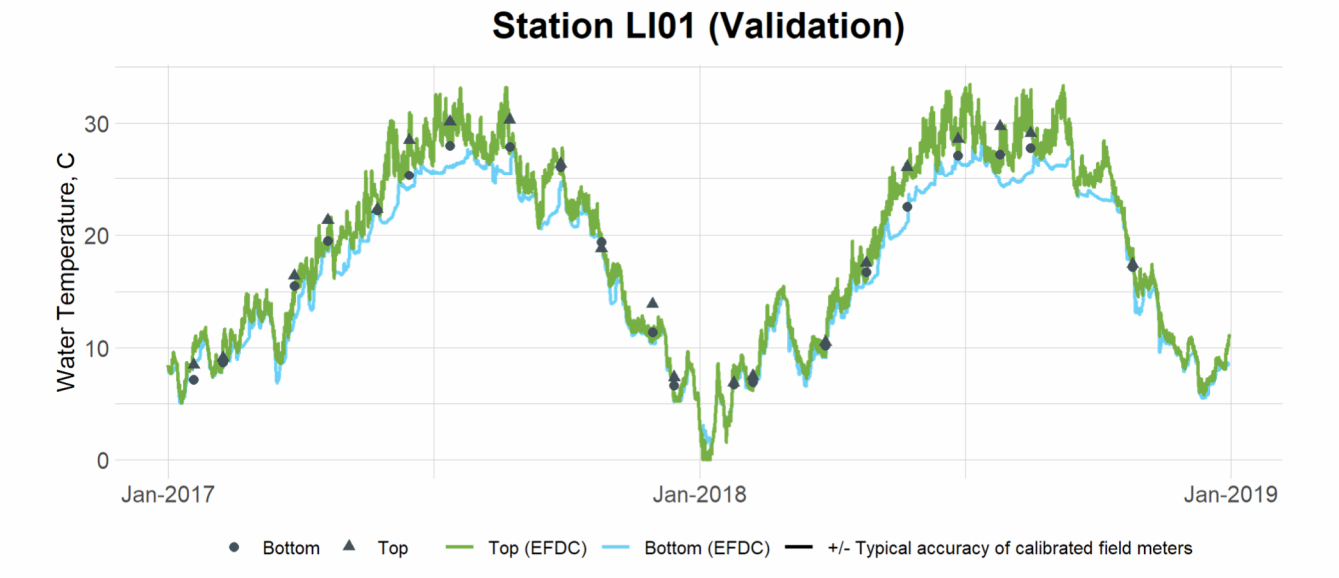

Figure 1-14 Validation Plot of Top and Bottom Water Temperature at Station LI01

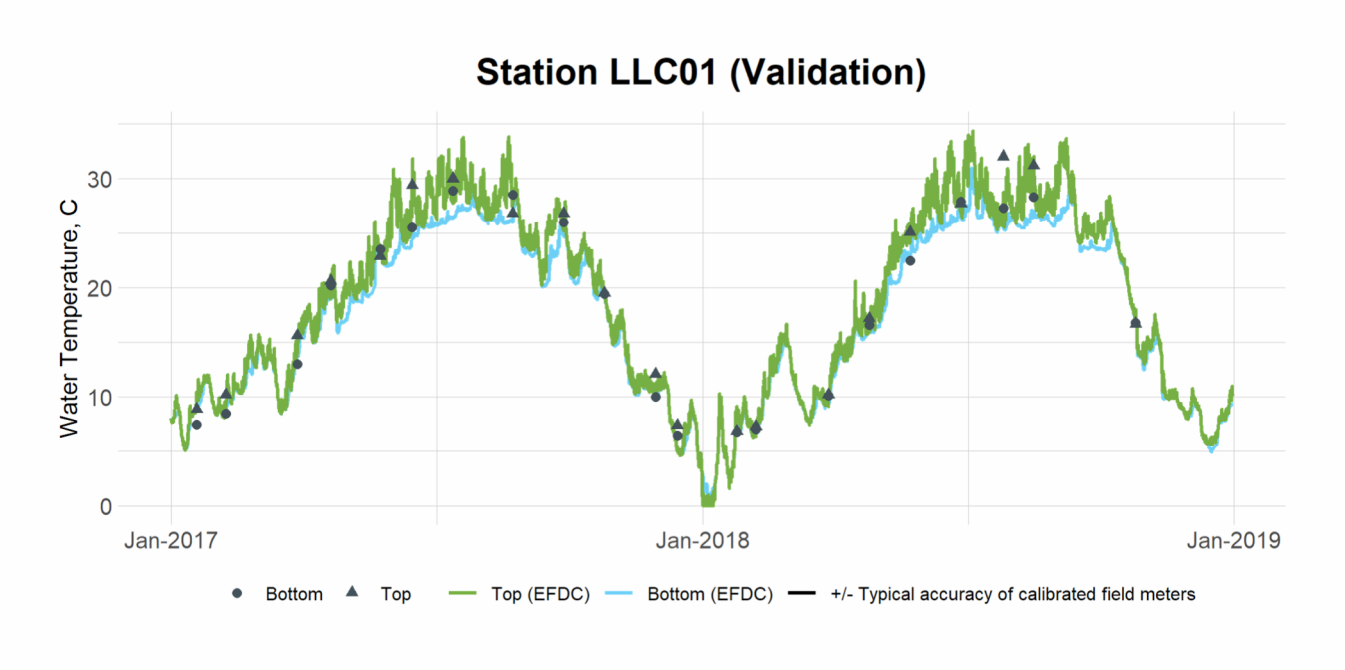

Figure 1-15 Validation Plot of Top and Bottom Water Temperature at Station LLC01

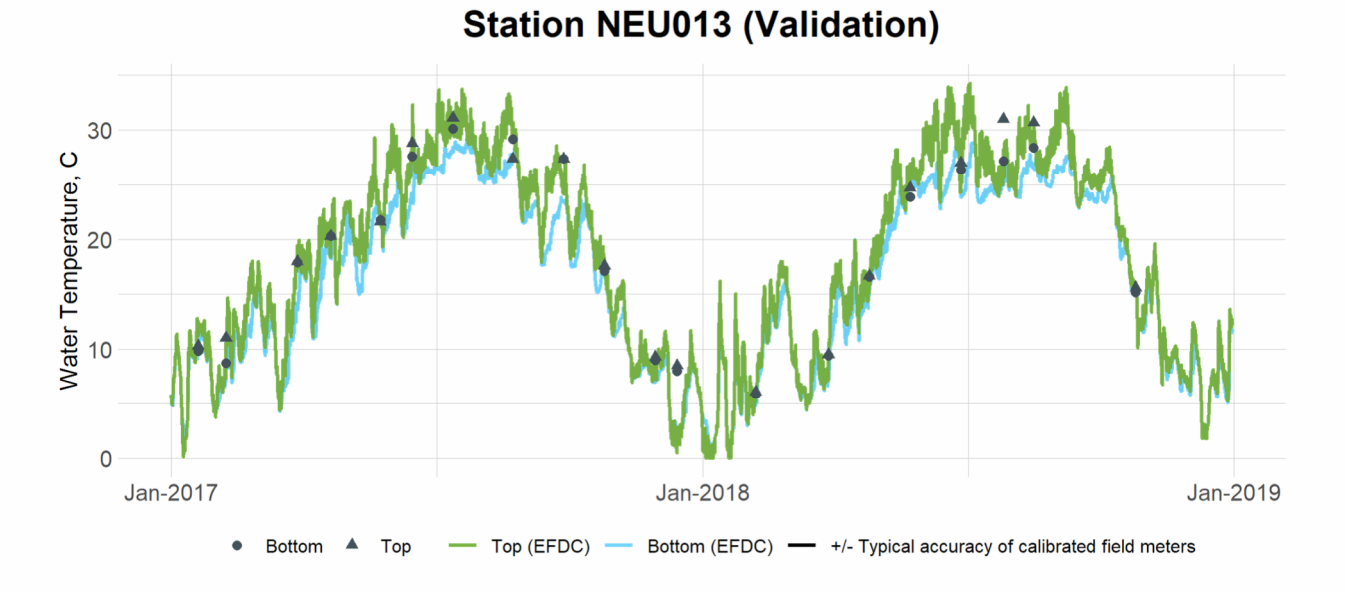

Figure 1-16 Validation Plot of Top and Bottom Water Temperature at Station NEU013

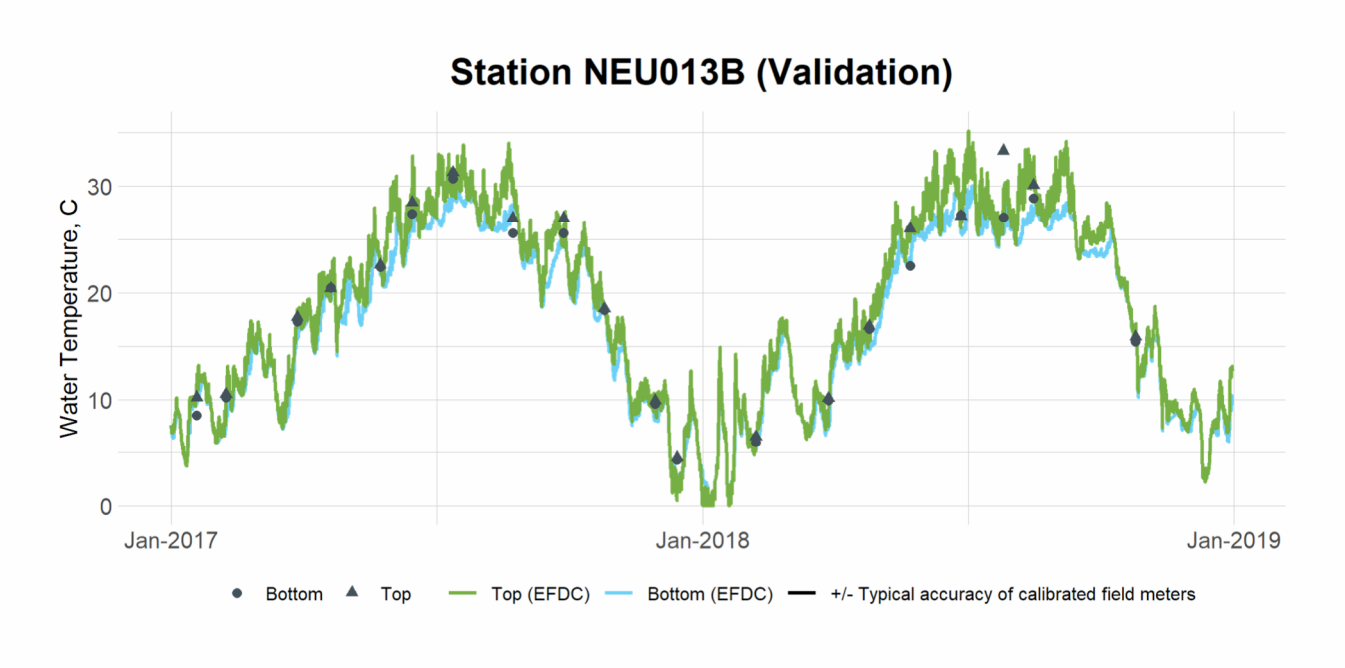

Figure 1-17 Validation Plot of Top and Bottom Water Temperature at Station NEU013B

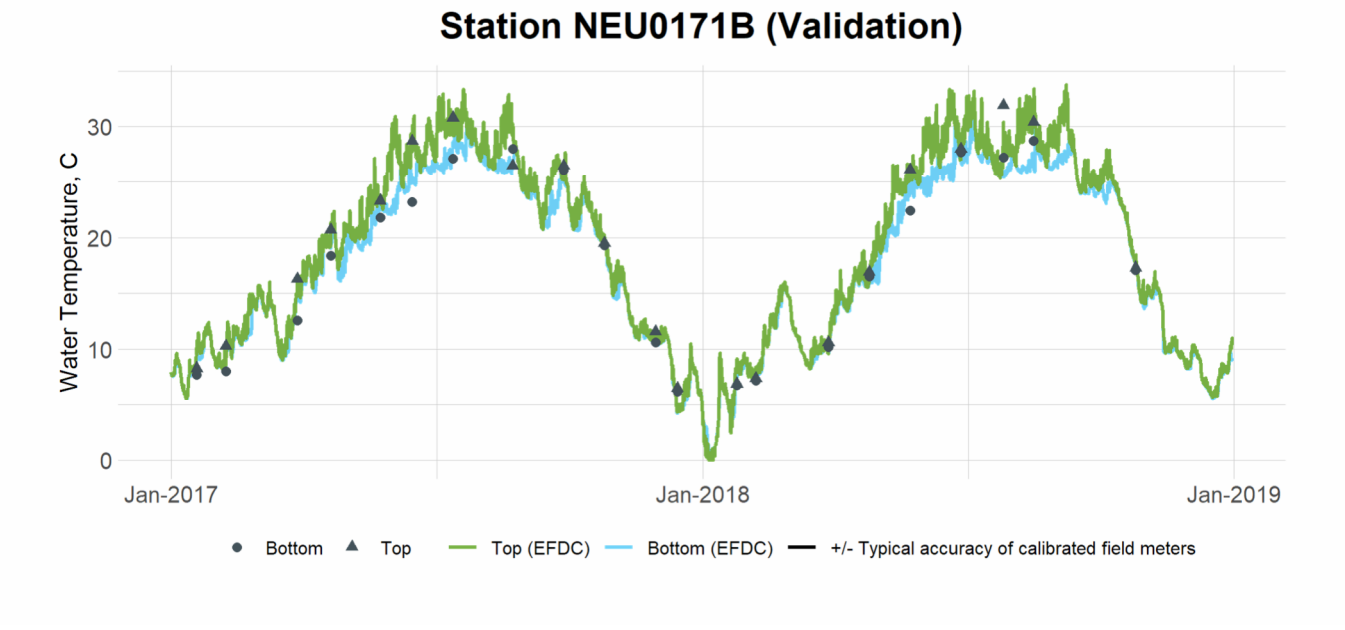

Figure 1-18 Validation Plot of Top and Bottom Water Temperature at Station NEU0171B

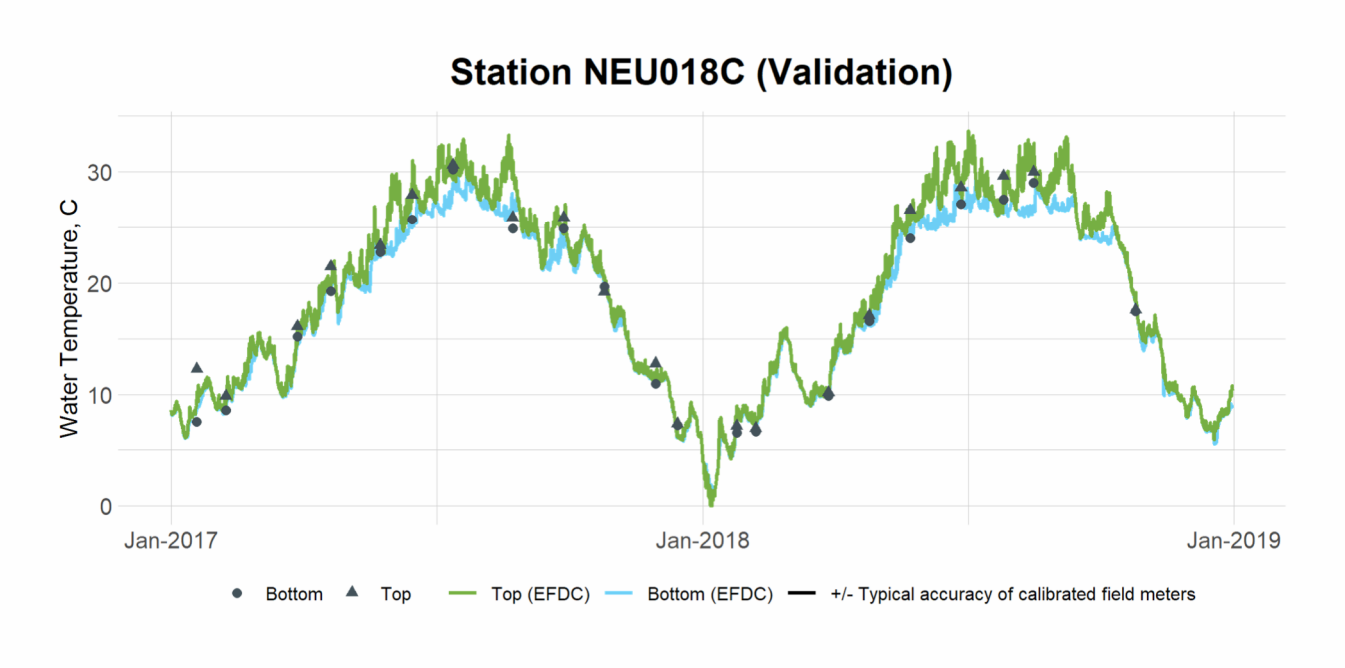

Figure 1-19 Validation Plot of Top and Bottom Water Temperature at Station NEU018C

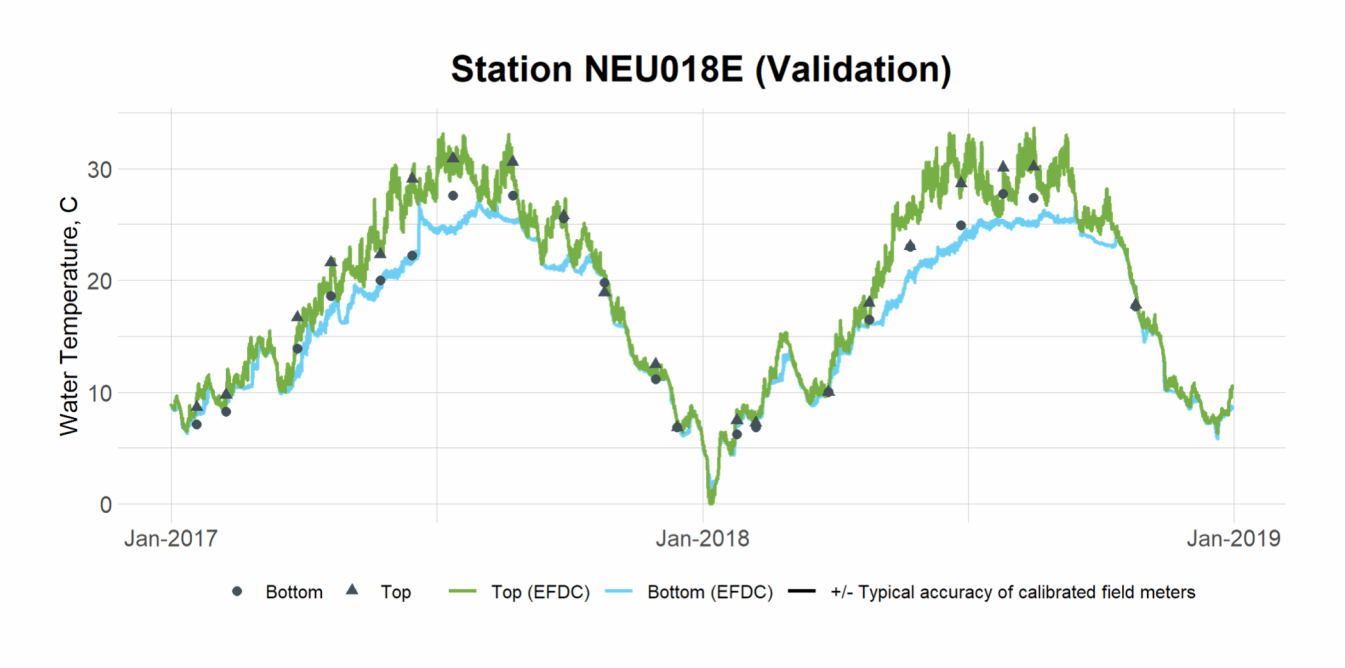

Figure 1-20 Validation Plot of Top and Bottom Water Temperature at Station NEU018E

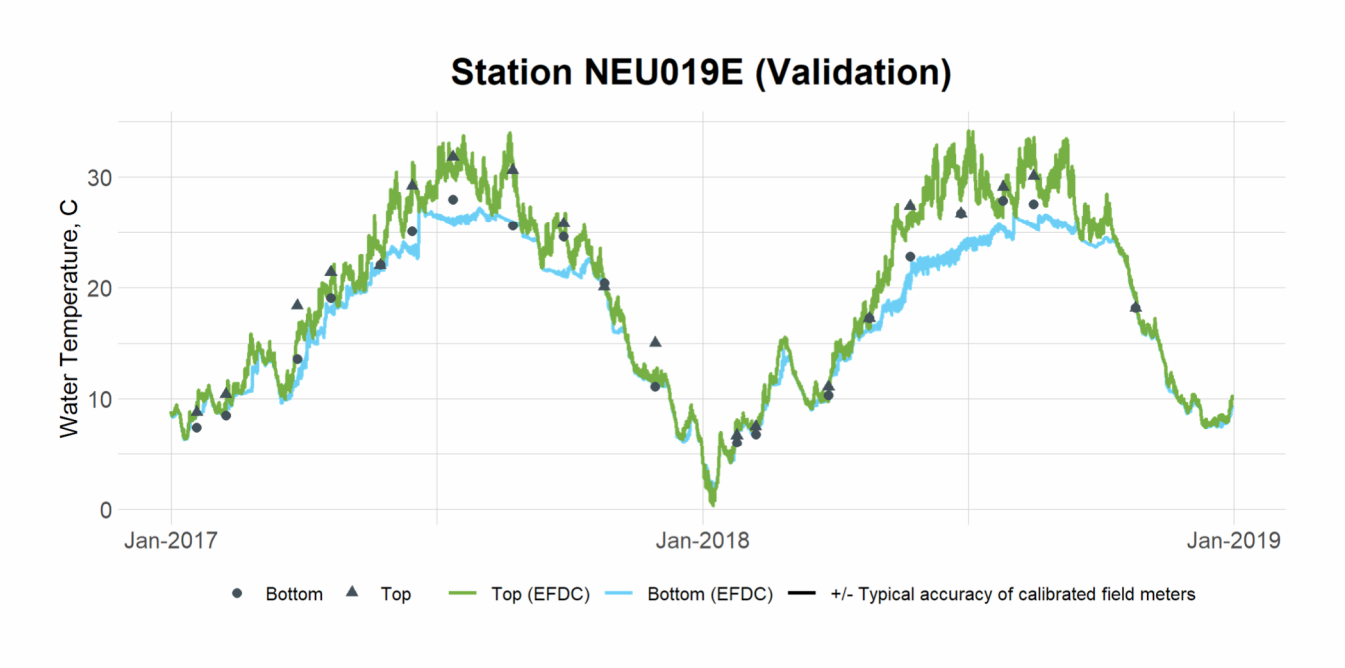

Figure 1-21 Validation Plot of Top and Bottom Water Temperature at Station NEU019E

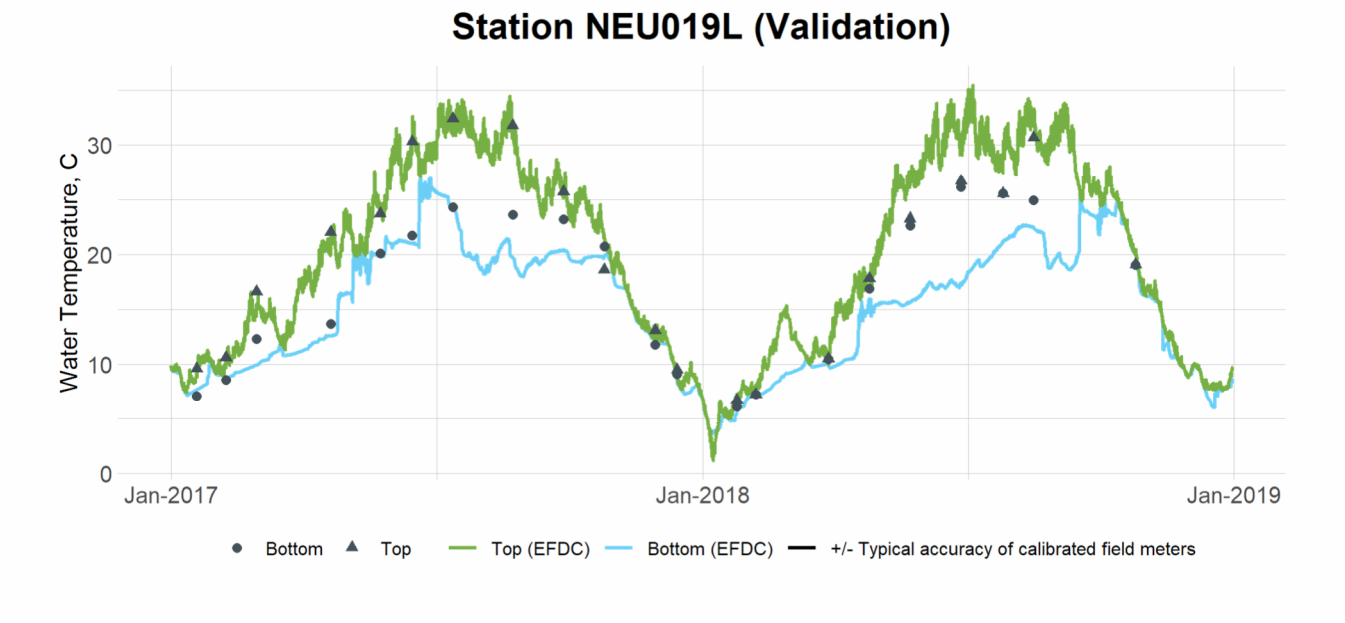

Figure 1-22 Validation Plot of Top and Bottom Water Temperature at Station NEU019L

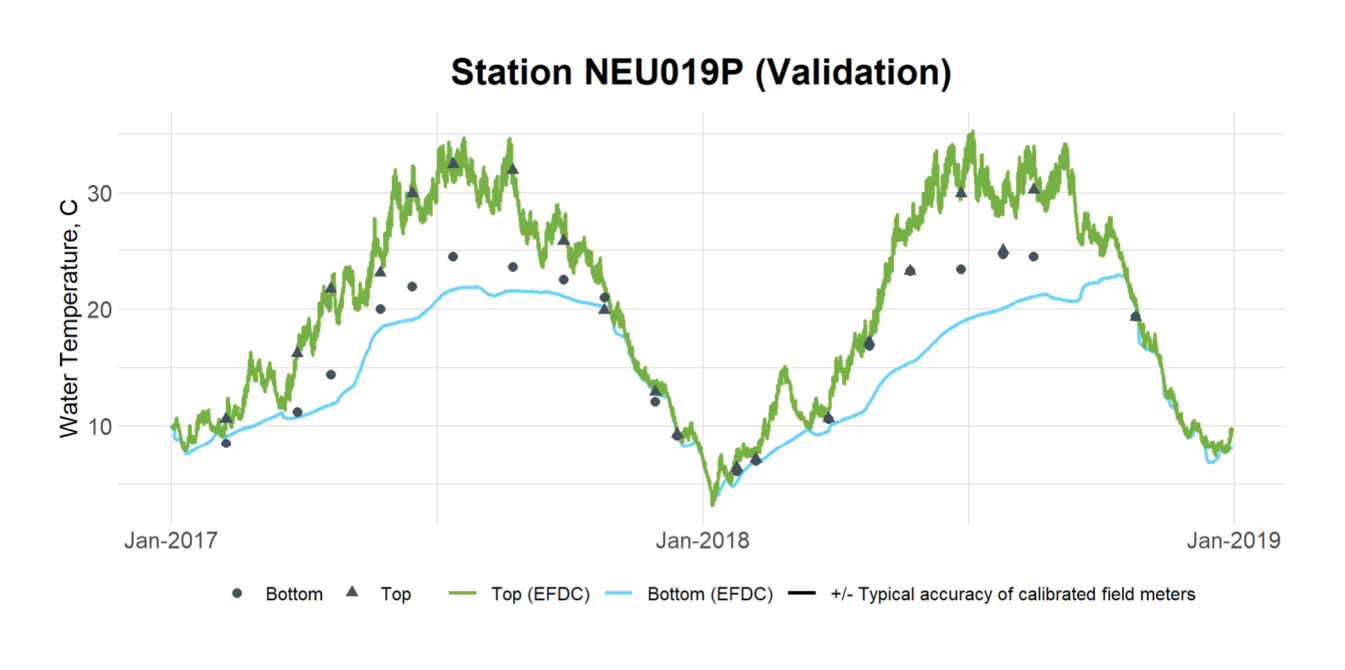

Figure 1-23 Validation Plot of Top and Bottom Water Temperature at Station NEU019P

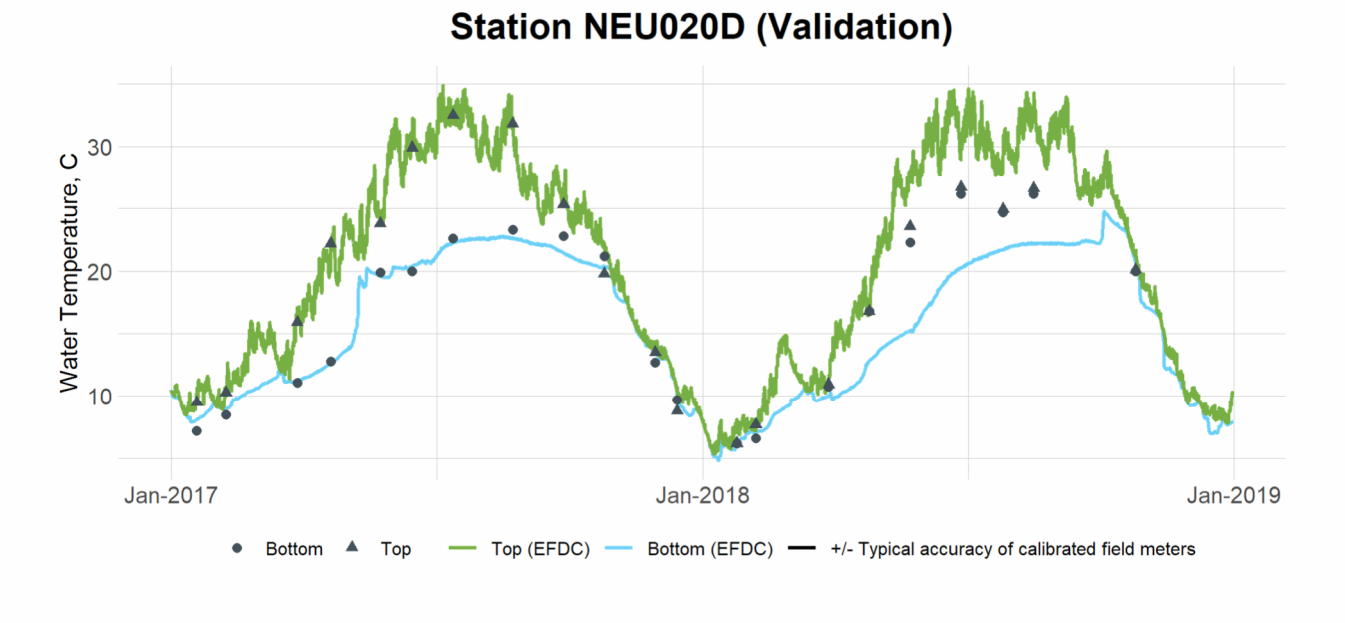

Figure 1-24 Validation Plot of Top and Bottom Water Temperature at Station NEU020D

2. Chl-a

2.1 Chl-a Calibration

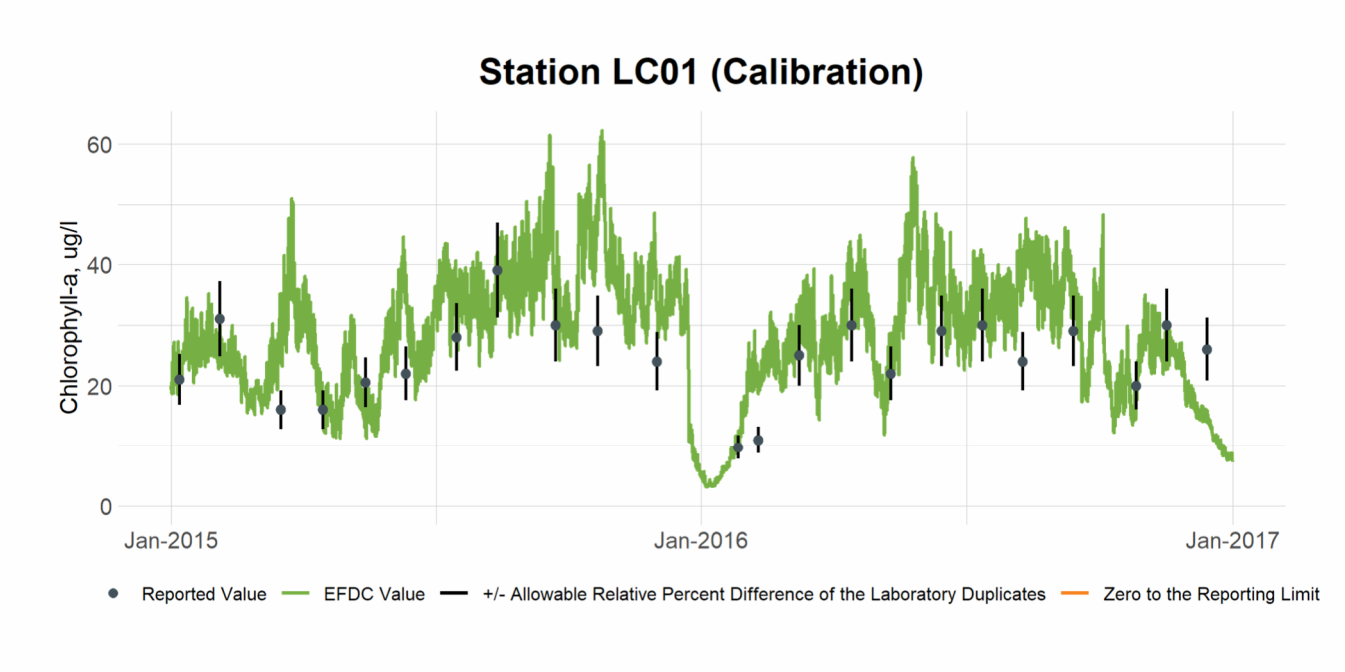

Figure 2-1 Calibration Plot of Chl-a at Station LC01

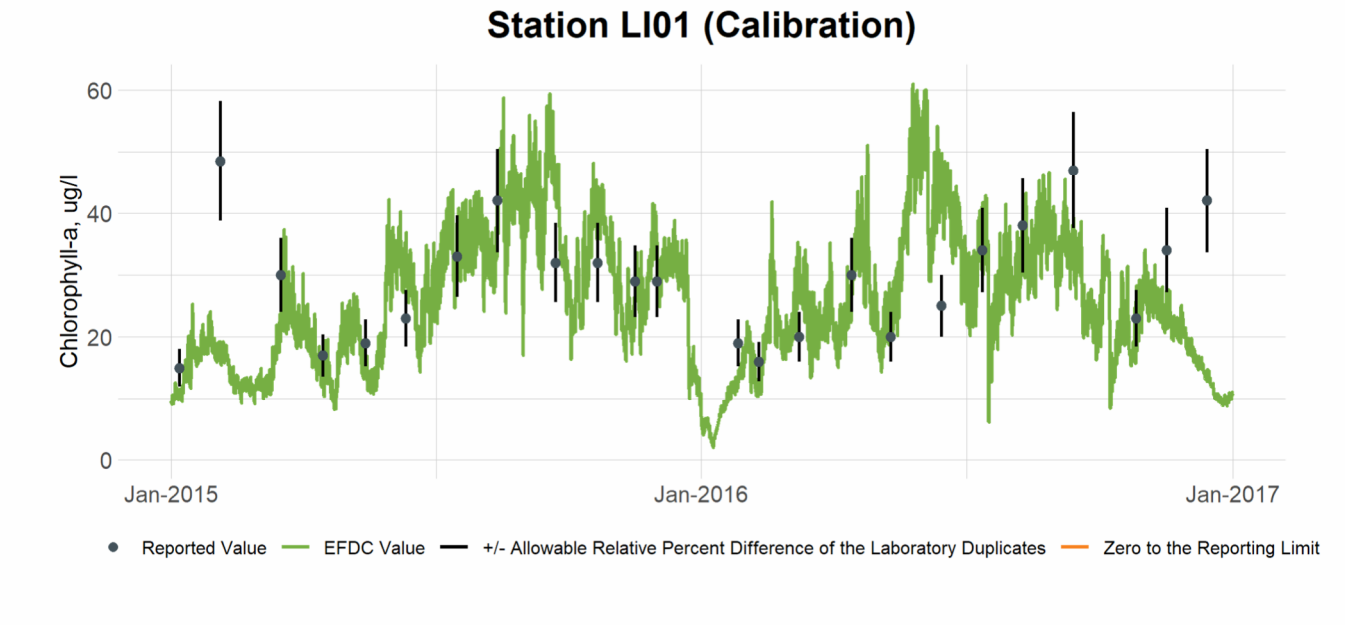

Figure 2-2 Calibration Plot of Chl-a at Station LI01

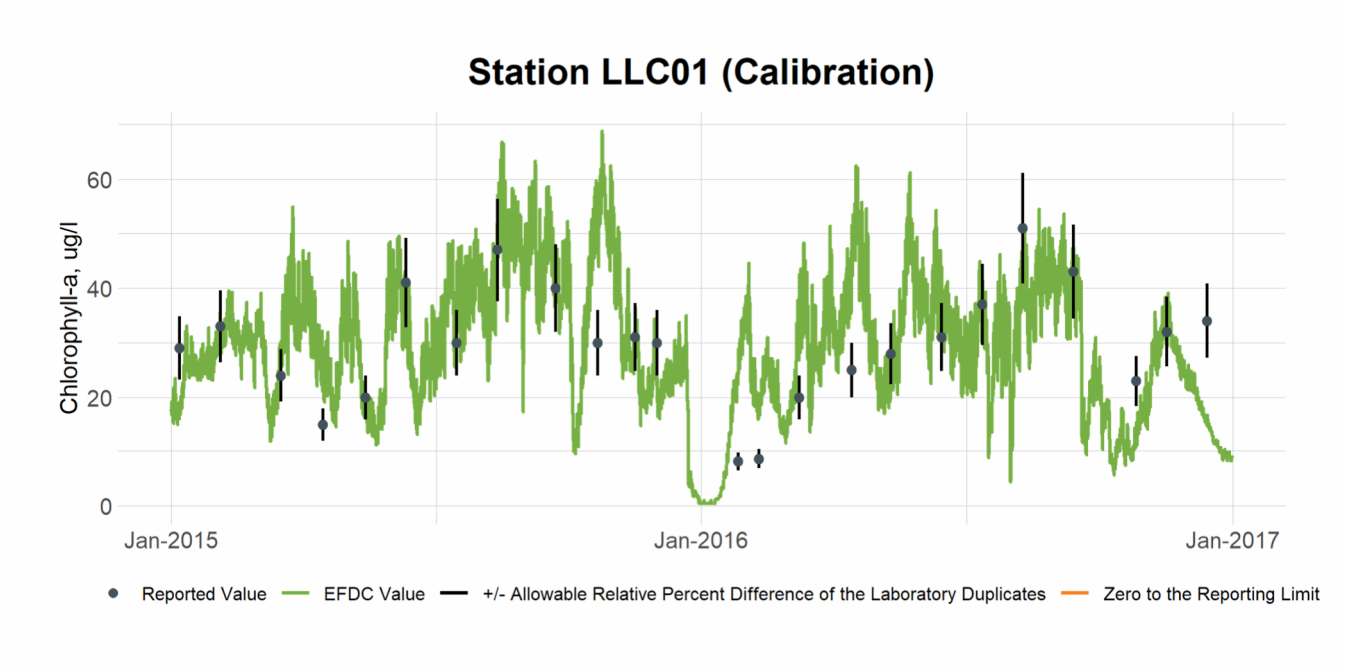

Figure 2-3 Calibration Plot of Chl-a at Station LLC01

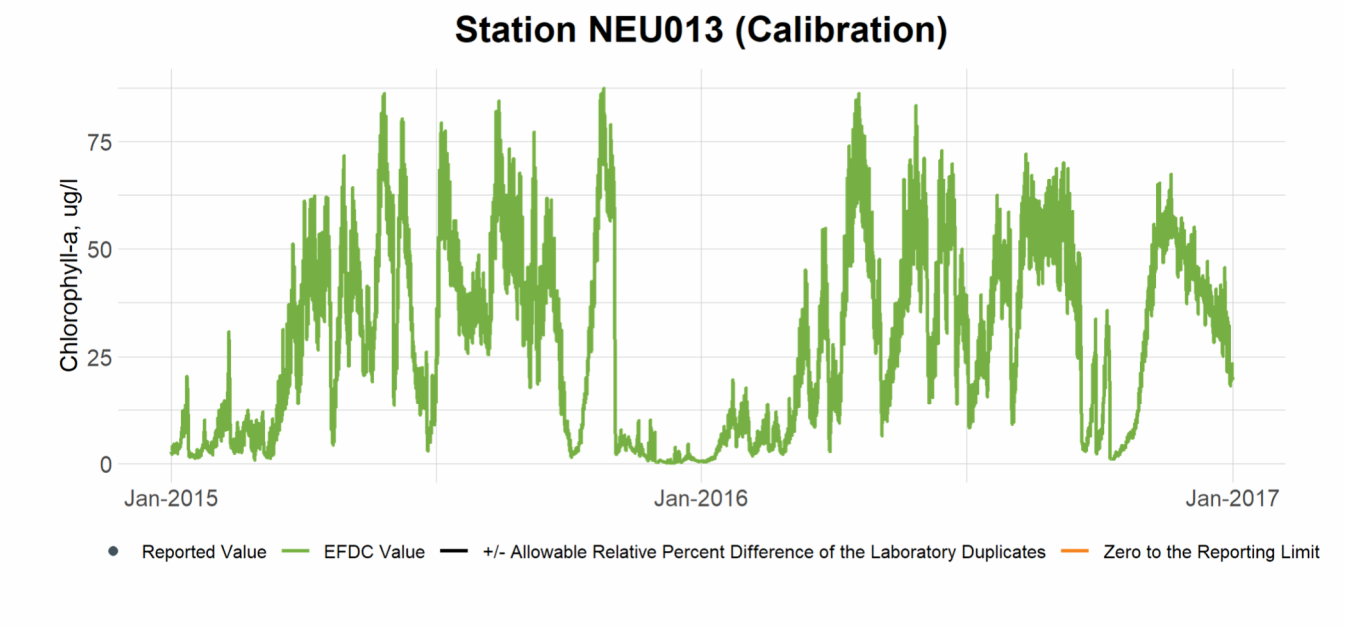

Figure 2-4 Calibration Plot of Chl-a at Station NEU013 (no observations available during this period)

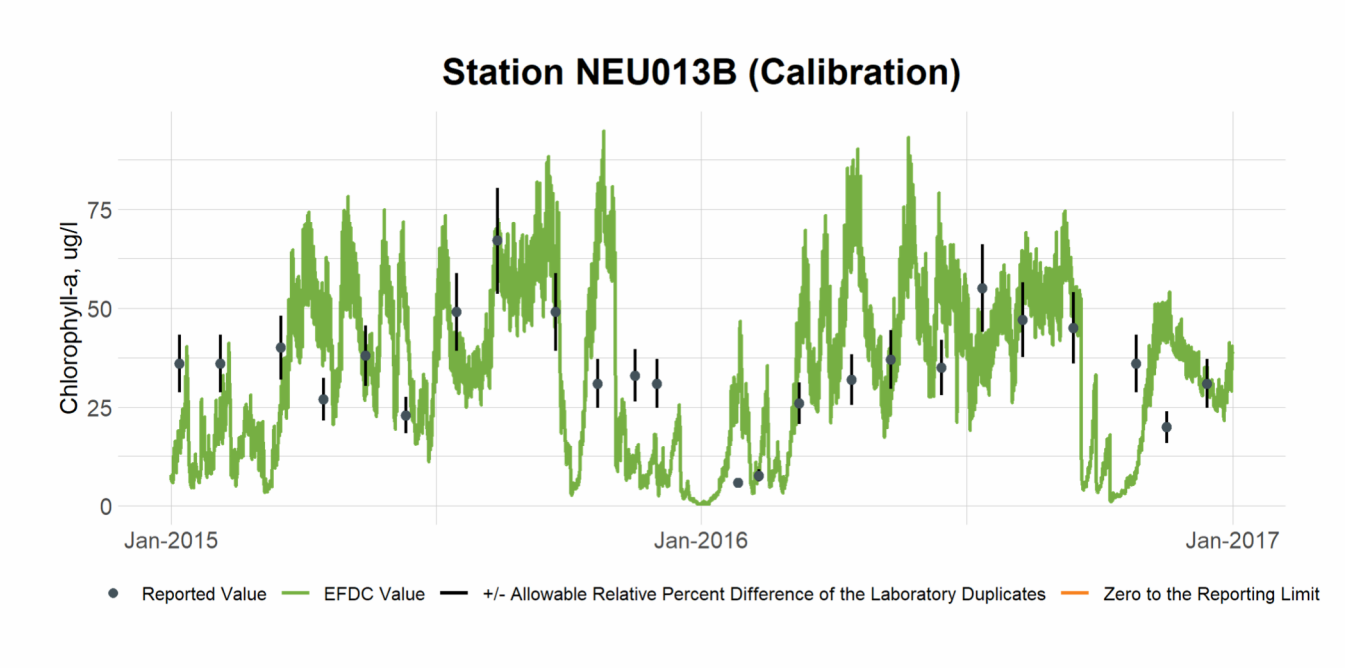

Figure 2-5 Calibration Plot of Chl-a at Station NEU013B

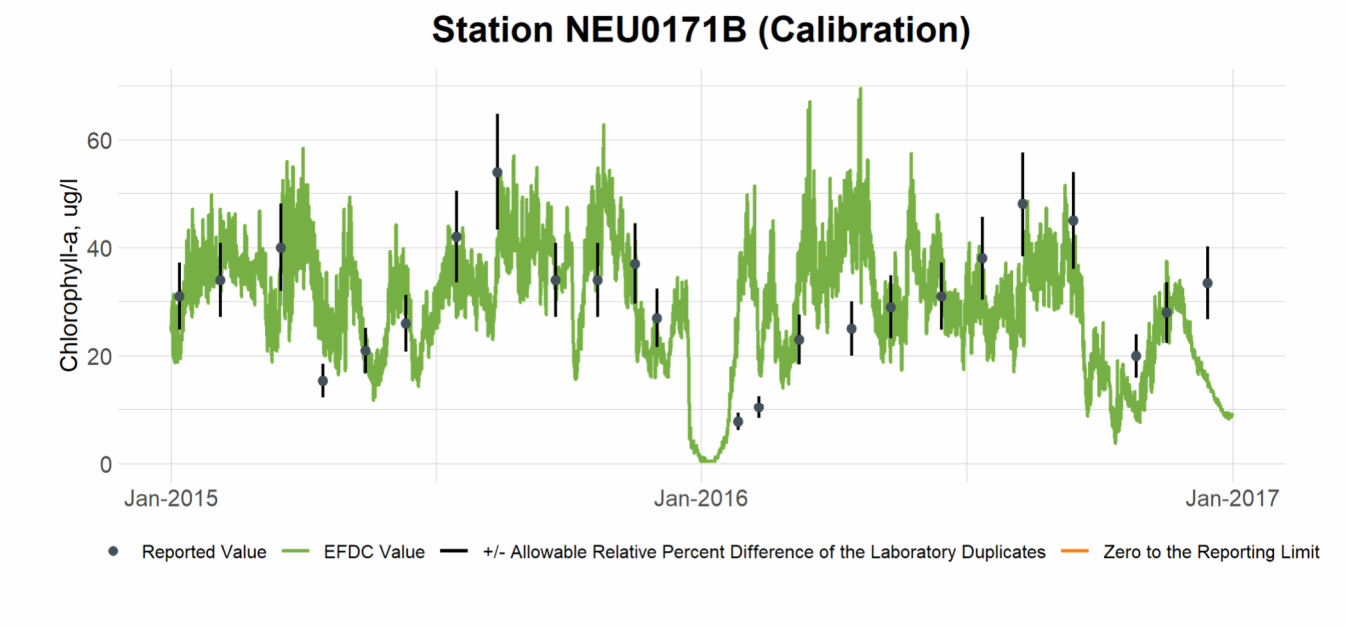

Figure 2-6 Calibration Plot of Chl-a at Station NEU0171B

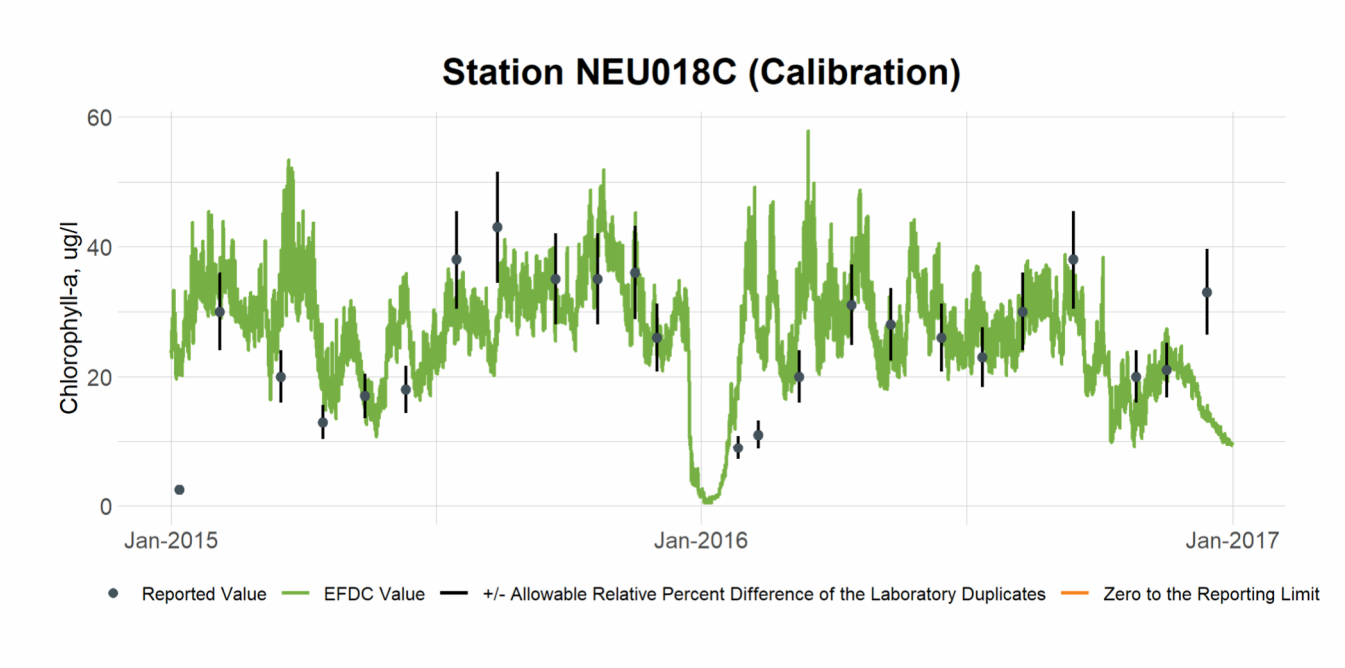

Figure 2-7 Calibration Plot of Chl-a at Station NEU018C

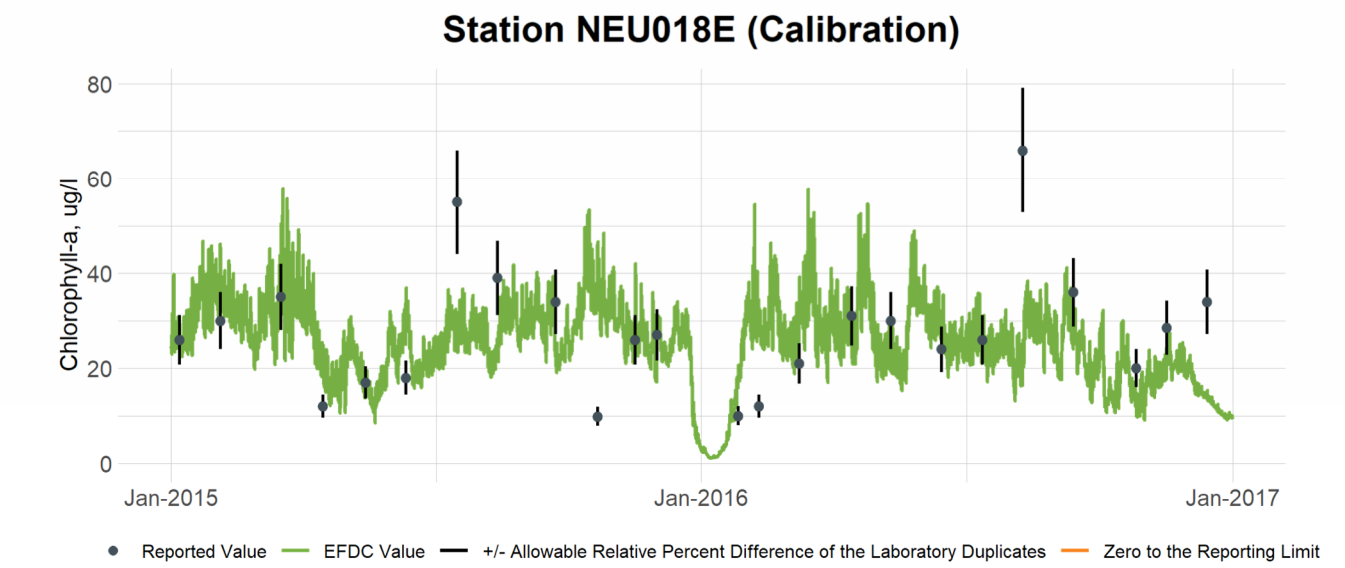

Figure 2-8 Calibration Plot of Chl-a at Station NEU018E

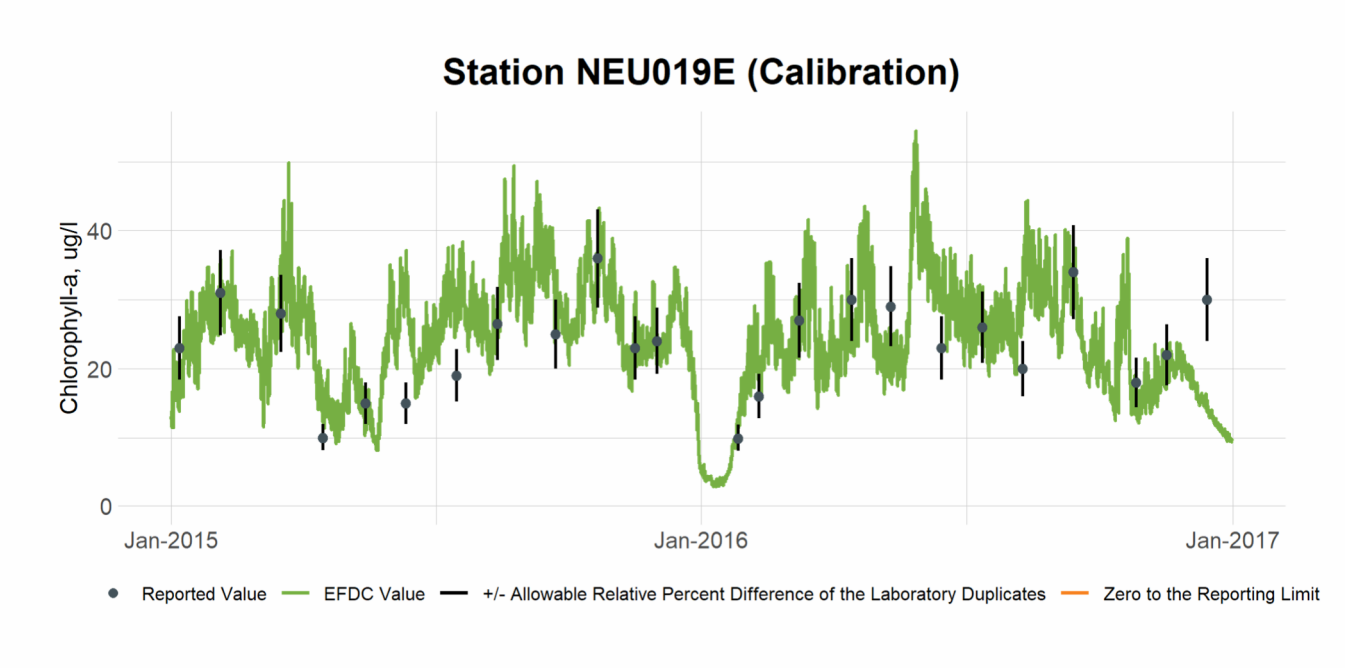

Figure 2-9 Calibration Plot of Chl-a at Station NEU019E

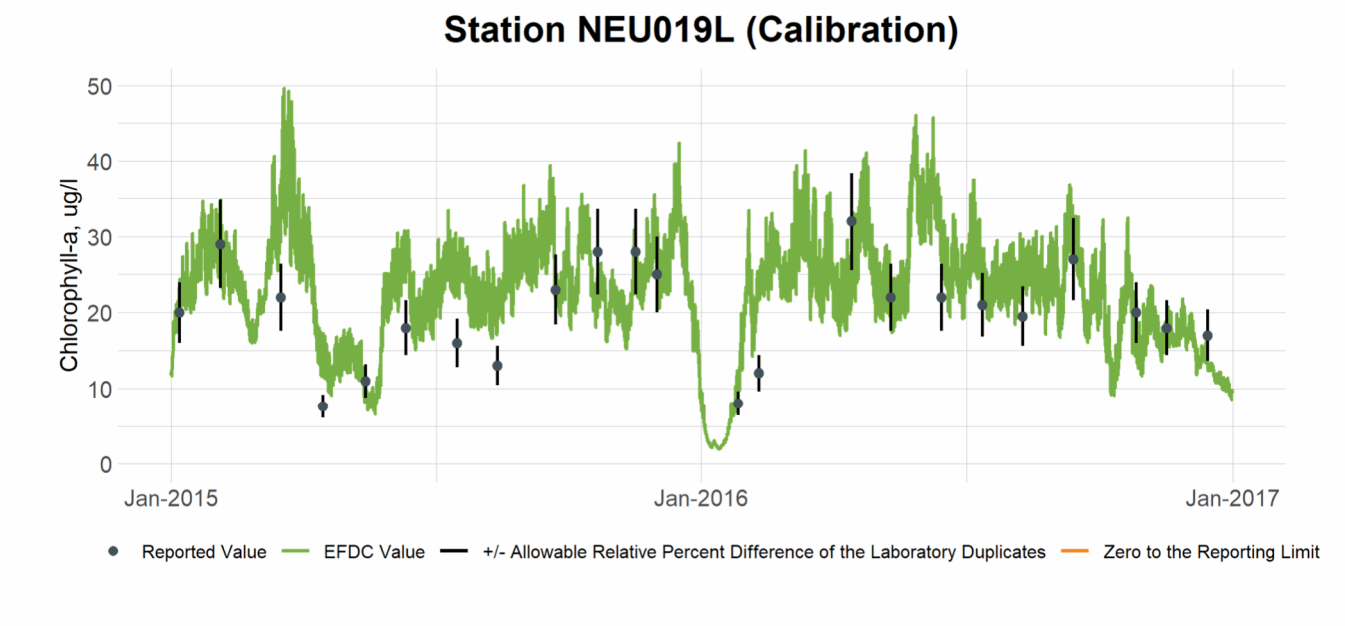

Figure 2-10 Calibration Plot of Chl-a at Station NEU019L

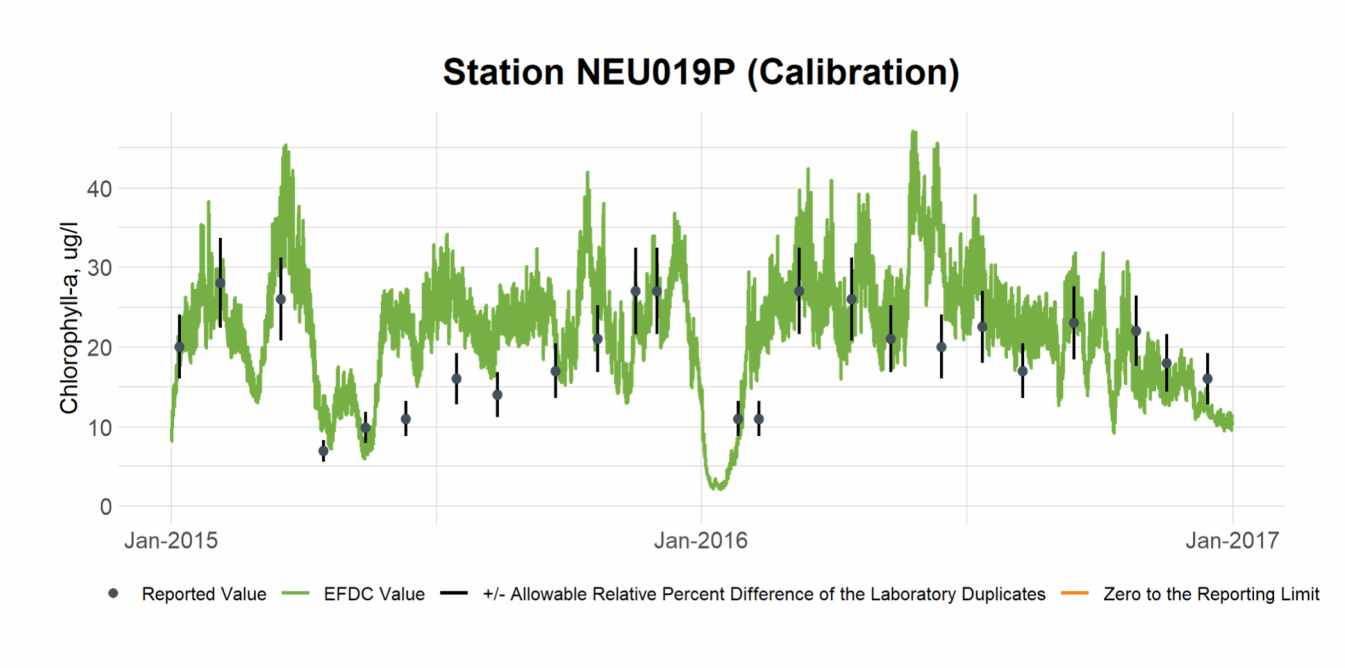

Figure 2-11 Calibration Plot of Chl-a at Station NEU019P

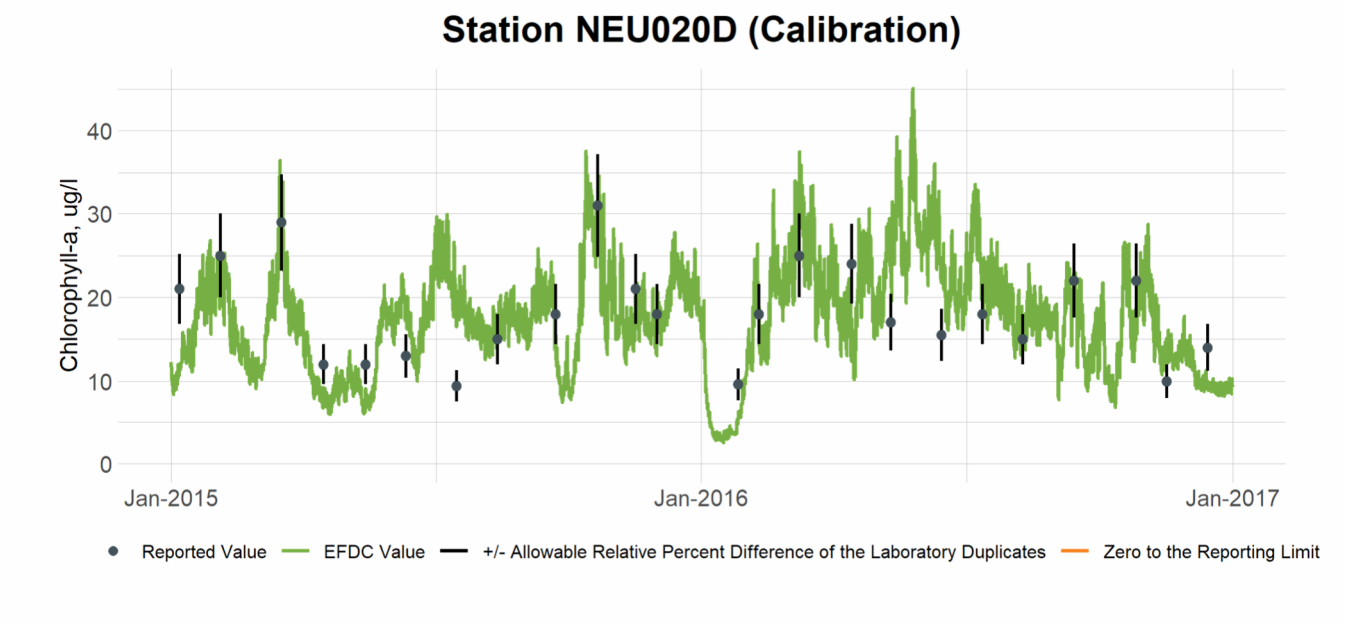

Figure 2-12 Calibration Plot of Chl-a at Station NEU020D

2.2 Chl-a Validation

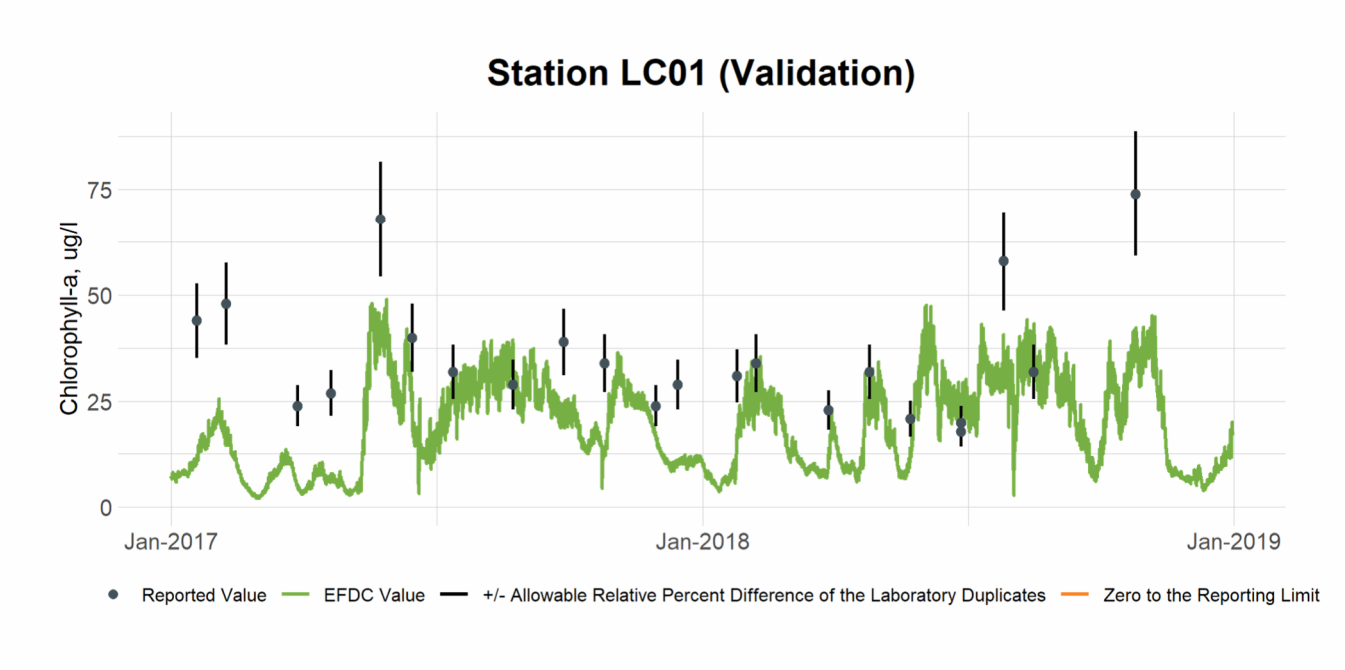

Figure 2-13 Validation Plot of Chl-a at Station LC01

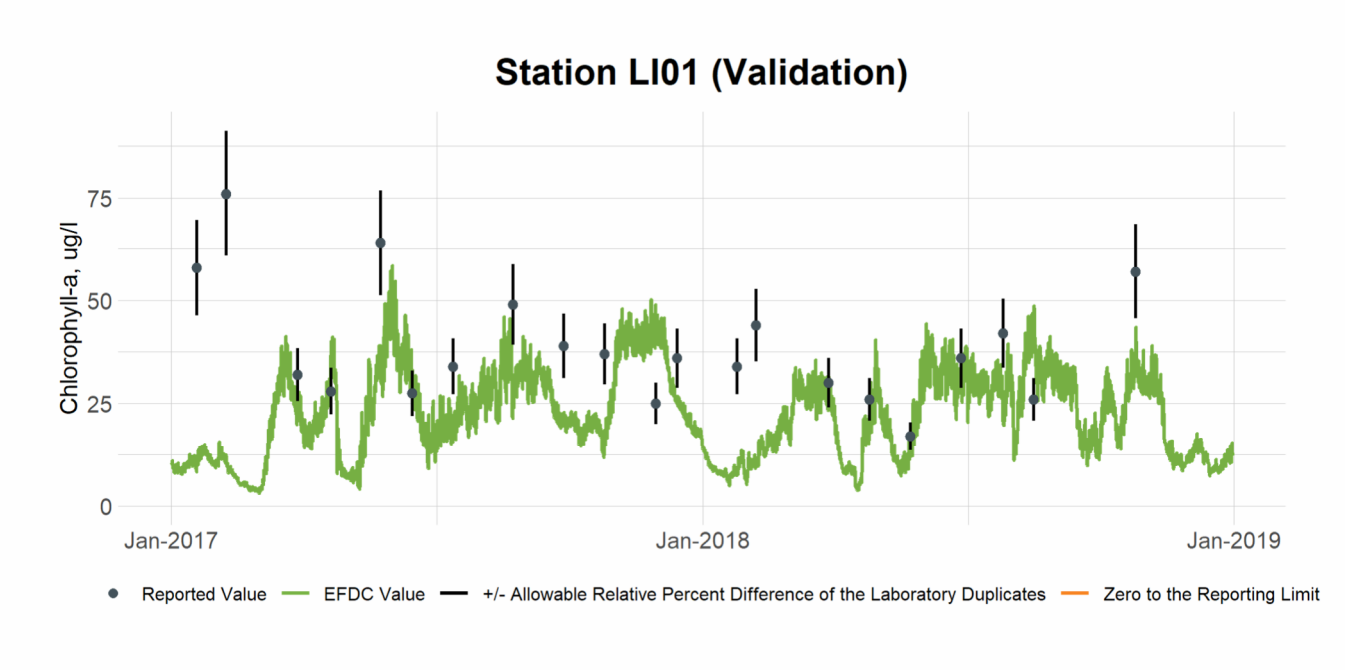

Figure 2-14 Validation Plot of Chl-a at Station LI01

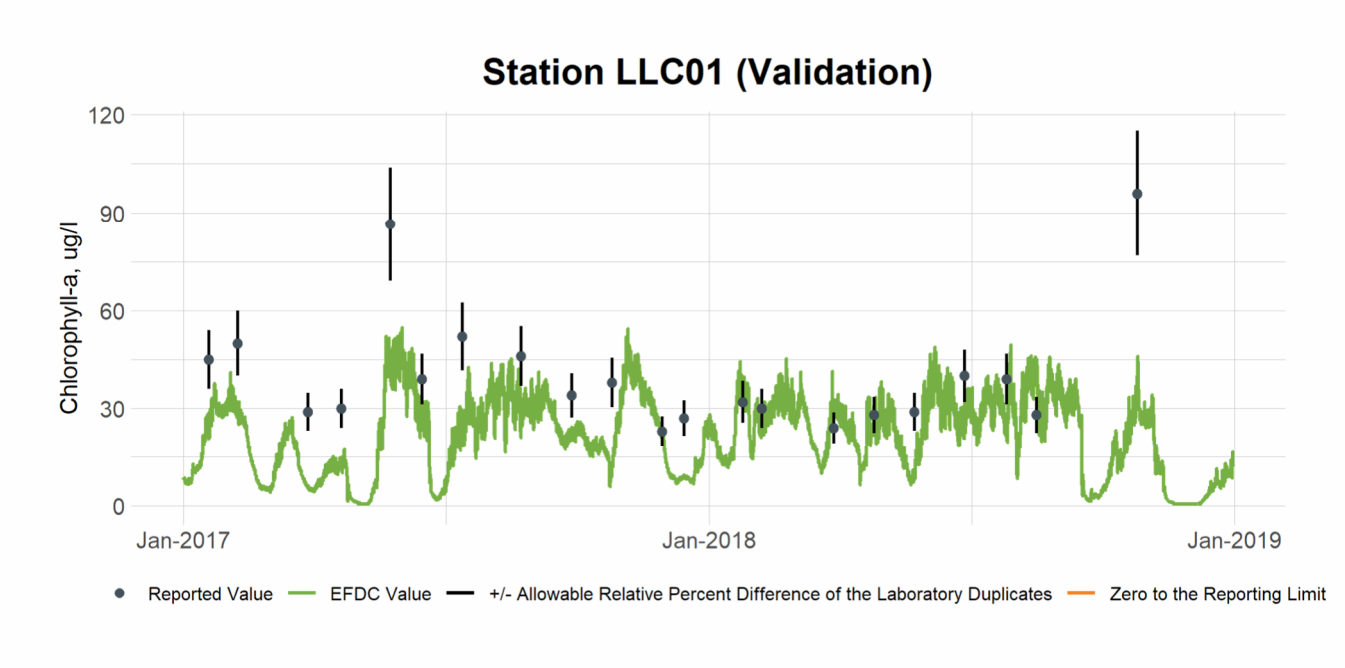

Figure 2-15 Validation Plot of Chl-a at Station LLC01

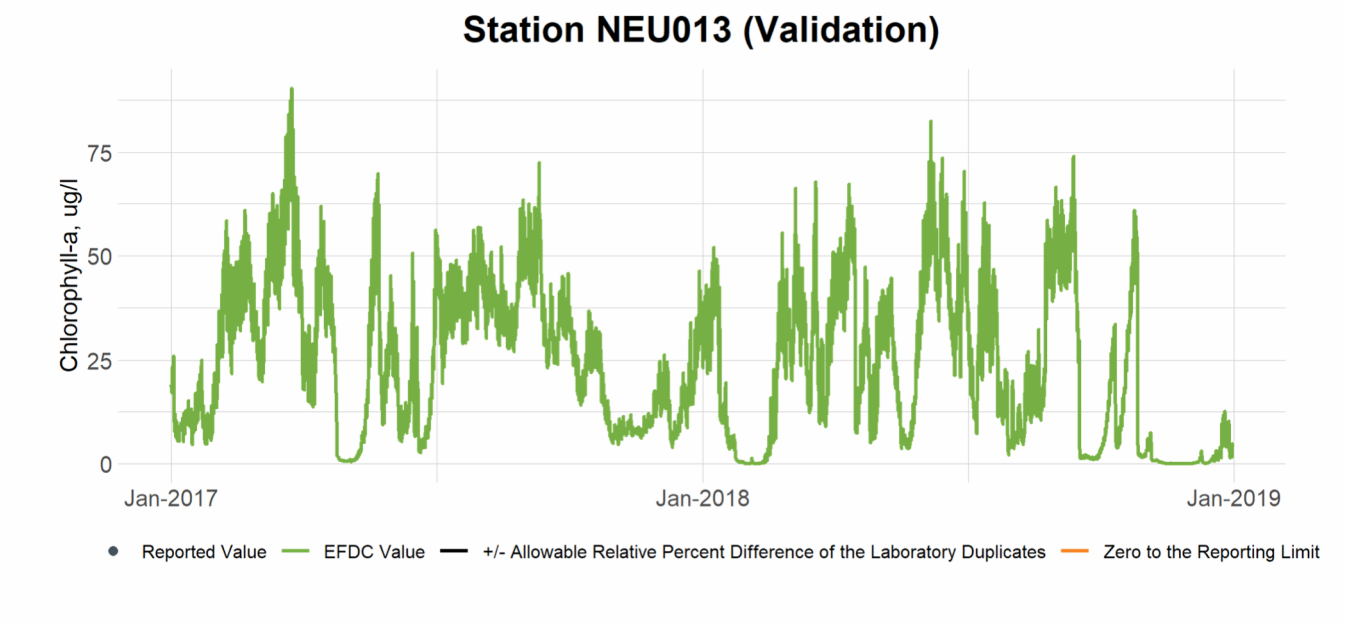

Figure 2-16 Validation Plot of Chl-a at Station NEU013 (no observations during this period)

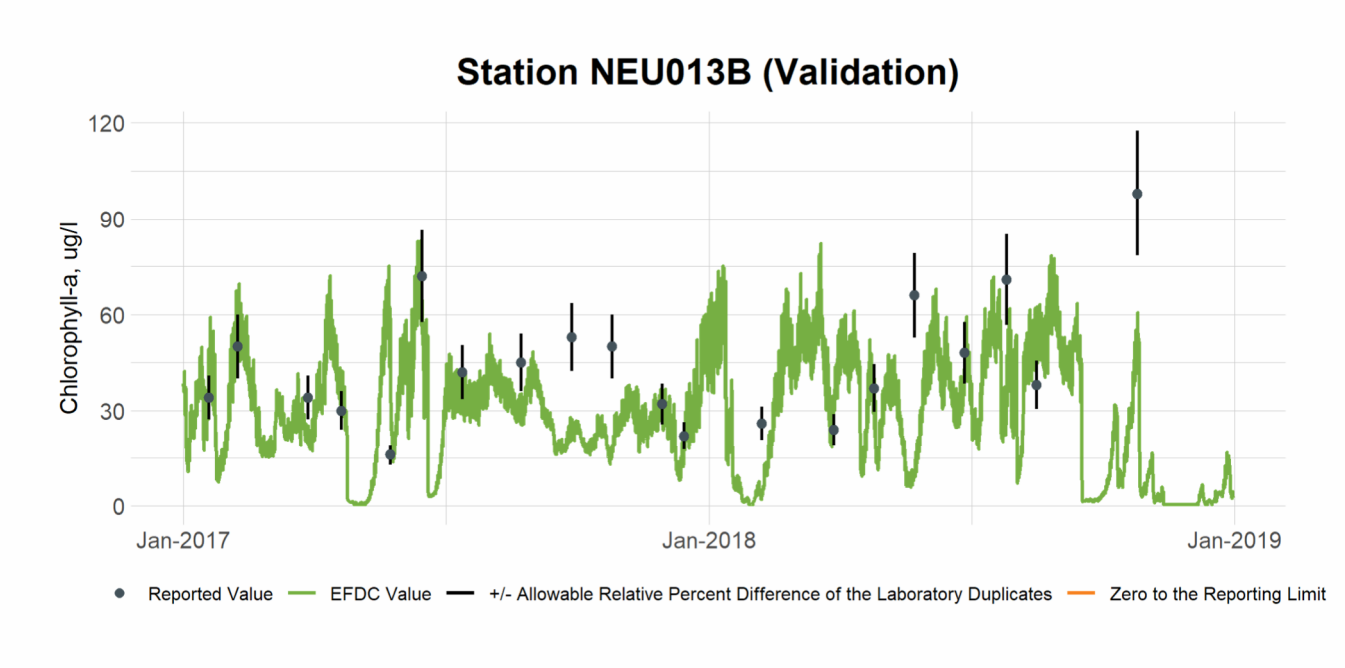

Figure 2-17 Validation Plot of Chl-a at Station NEU013B

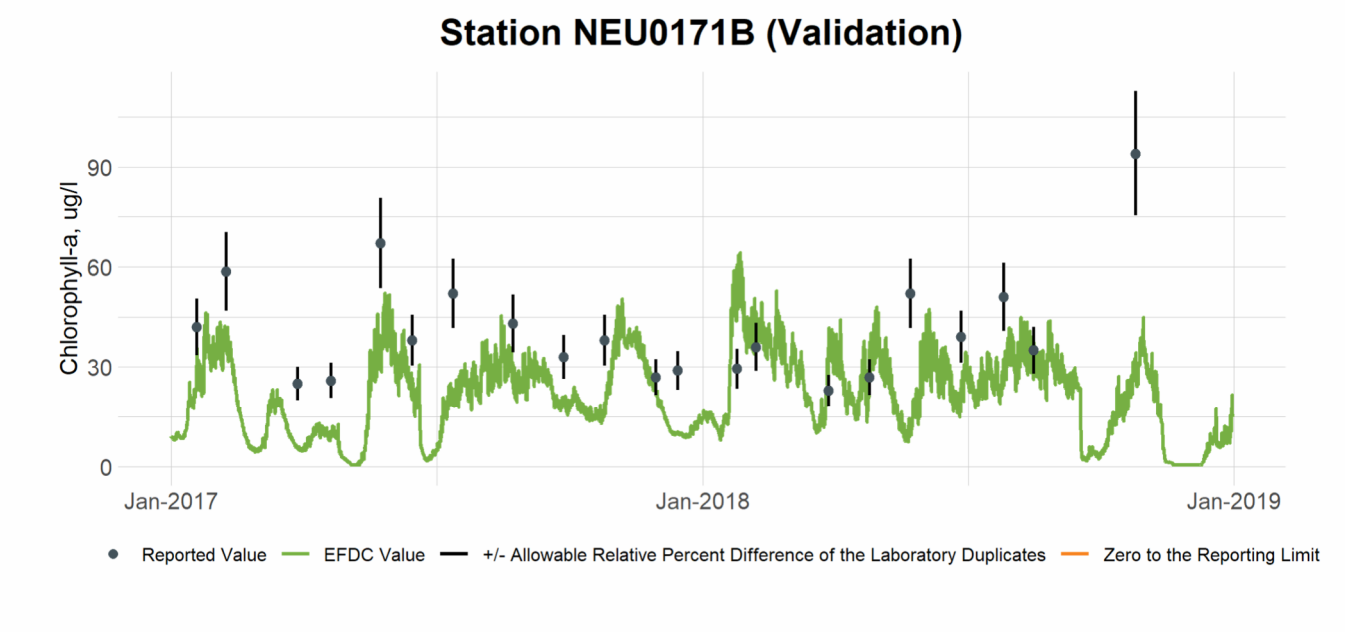

Figure 2-18 Validation Plot of Chl-a at Station NEU0171B

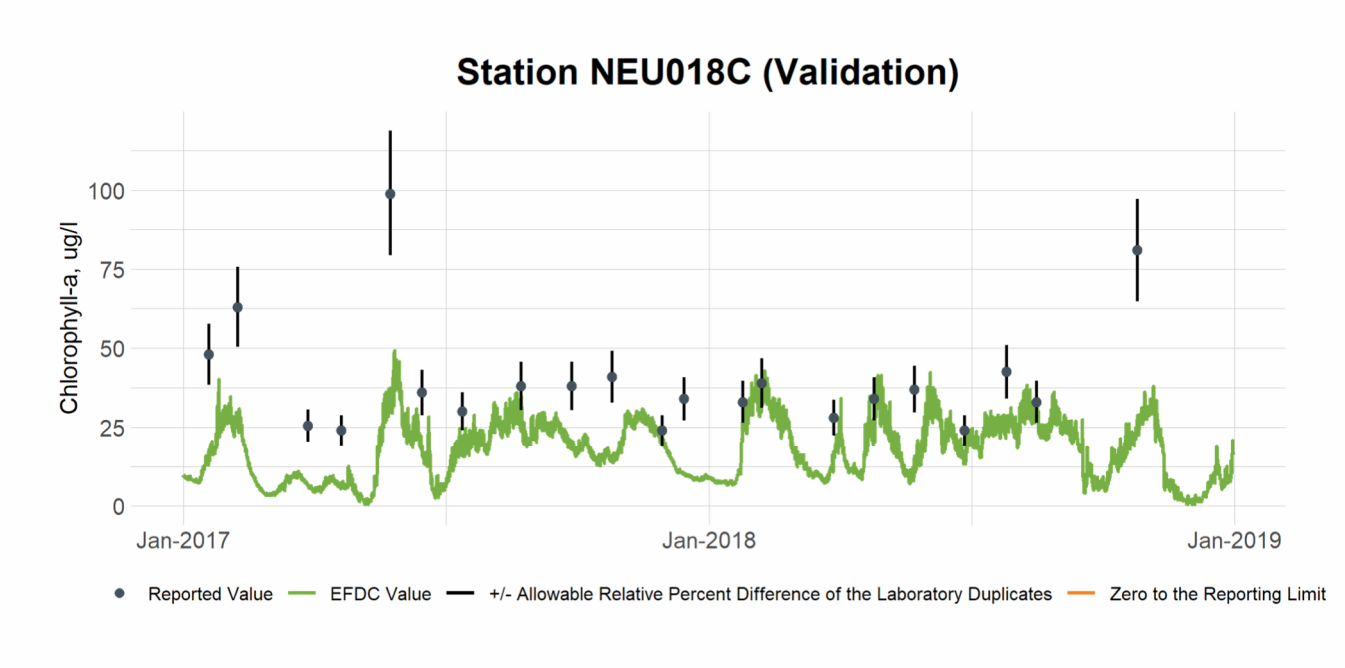

Figure 2-19 Validation Plot of Chl-a at Station NEU018C

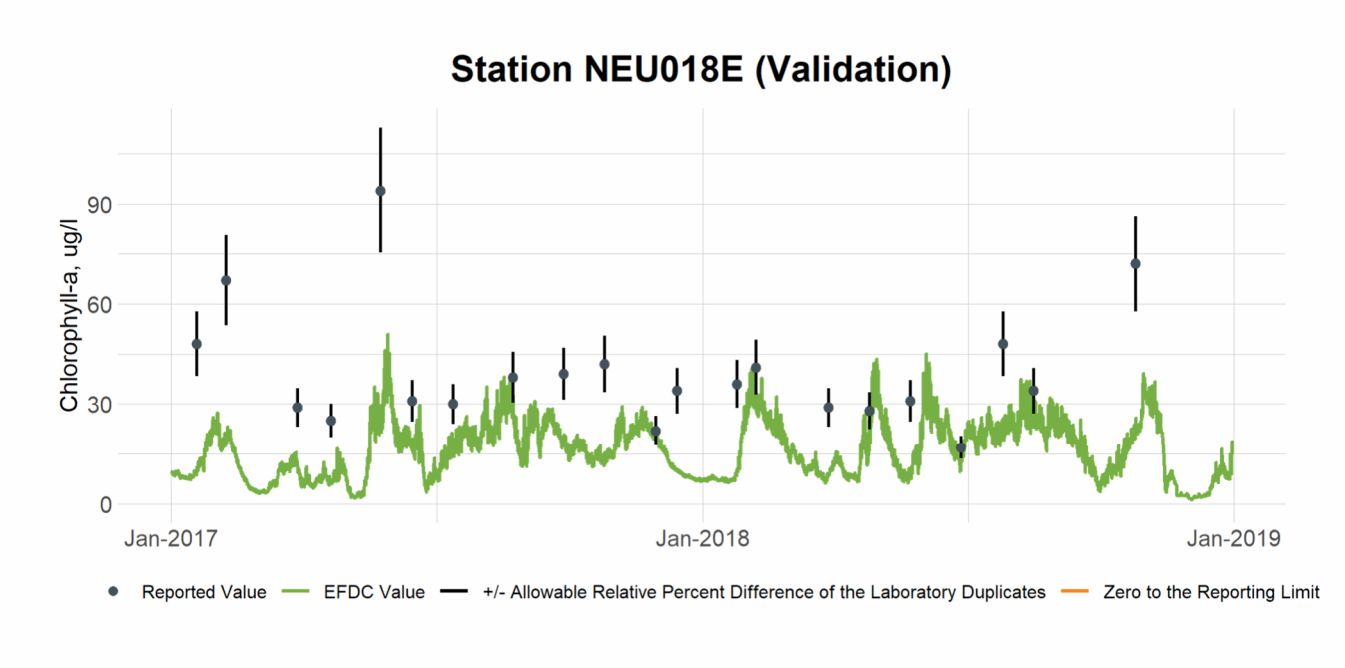

Figure 2-20 Validation Plot of Chl-a at Station NEU018E

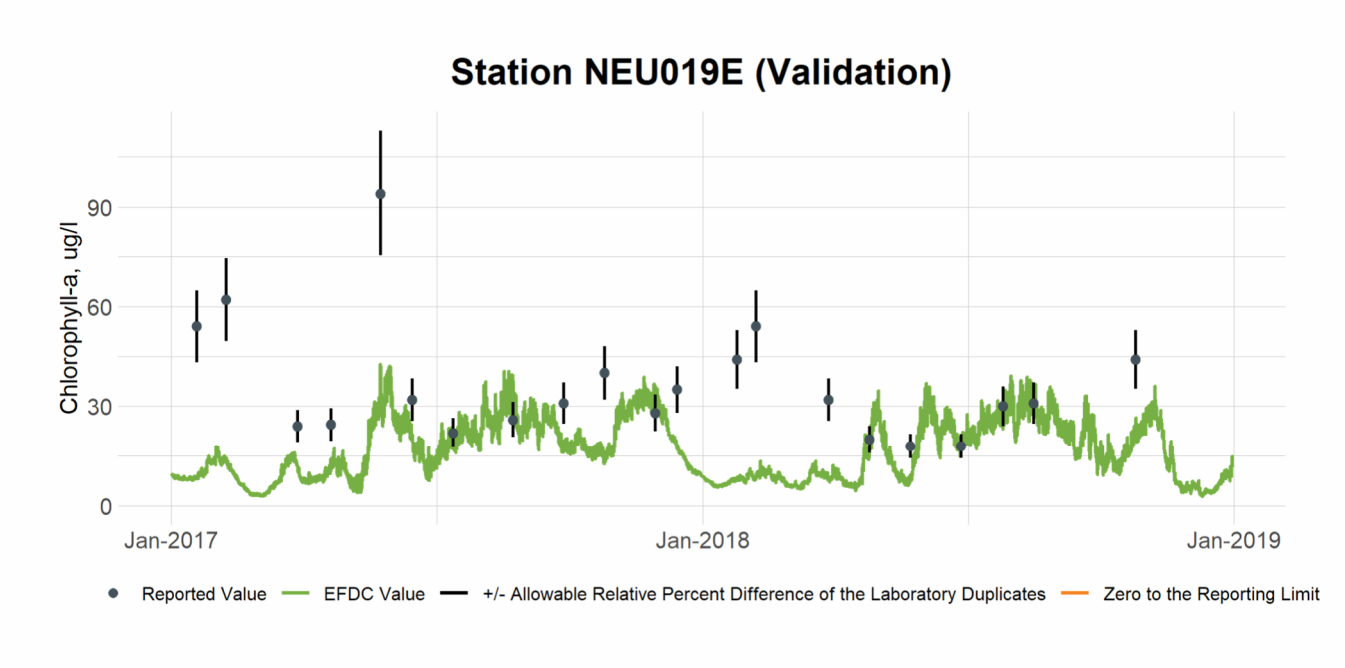

Figure 2-21 Validation Plot of Chl-a at Station NEU019E

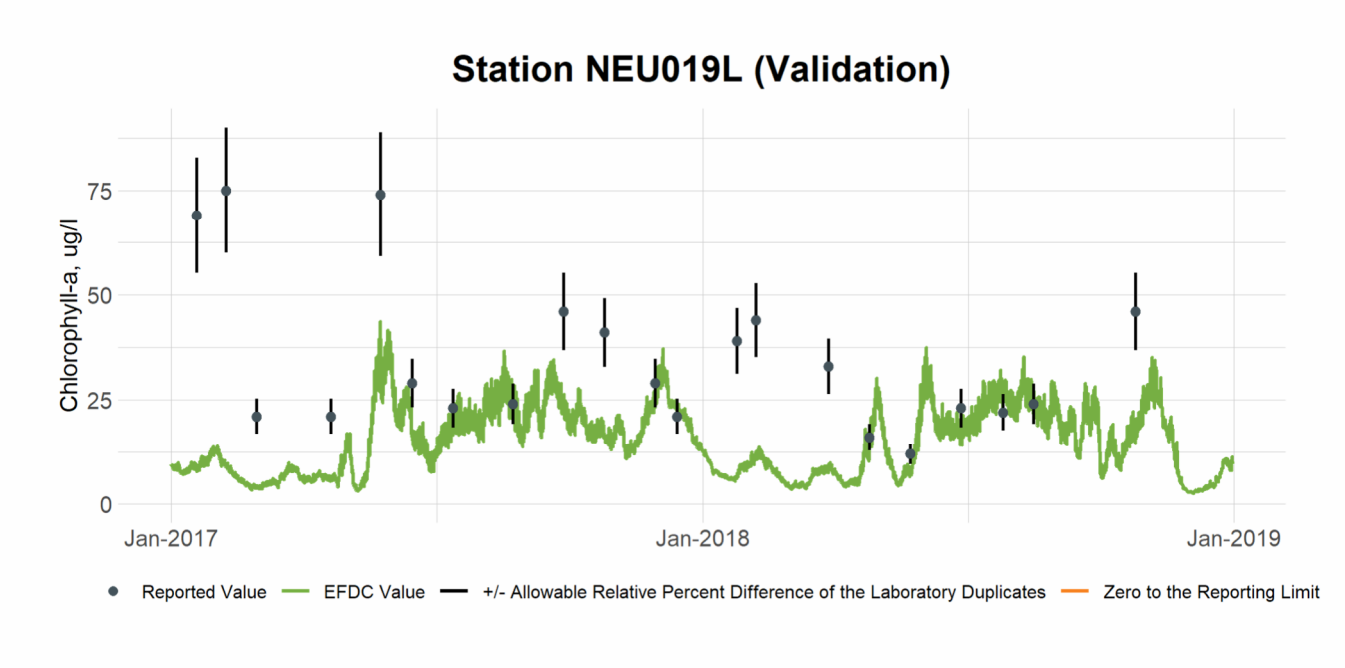

Figure 2-22 Validation Plot of Chl-a at Station NEU019L

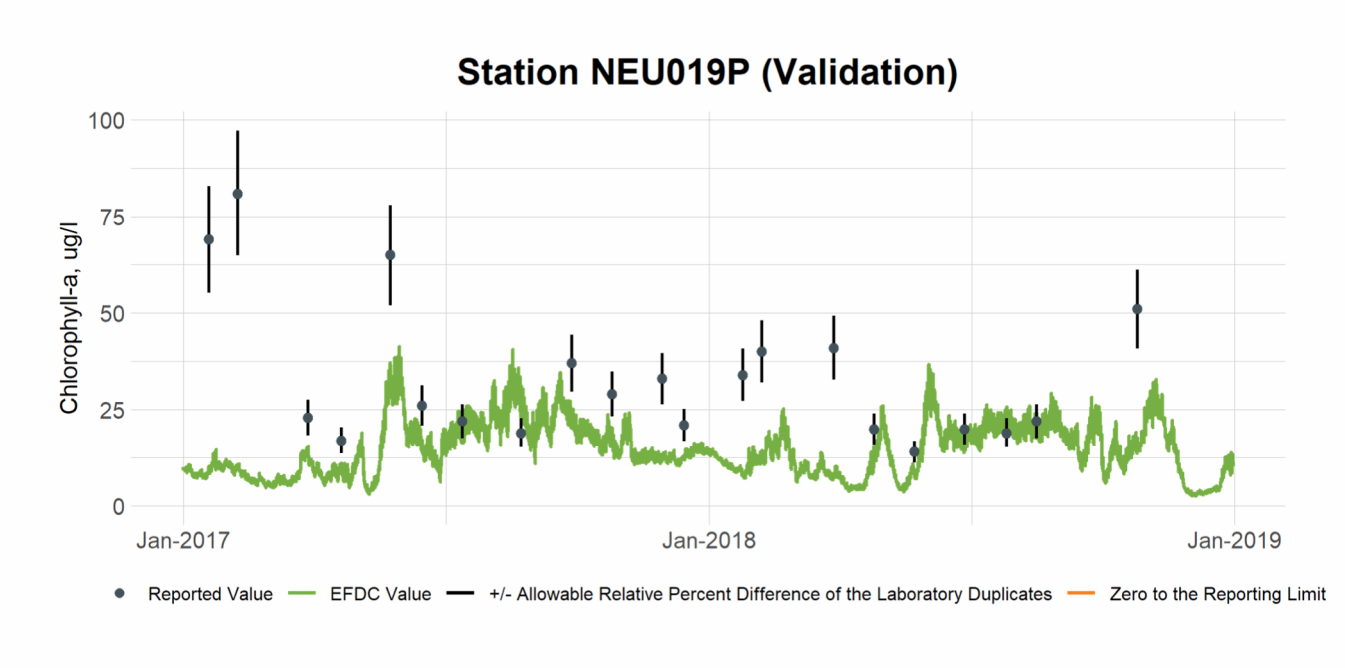

Figure 2-23 Validation Plot of Chl-a at Station NEU019P

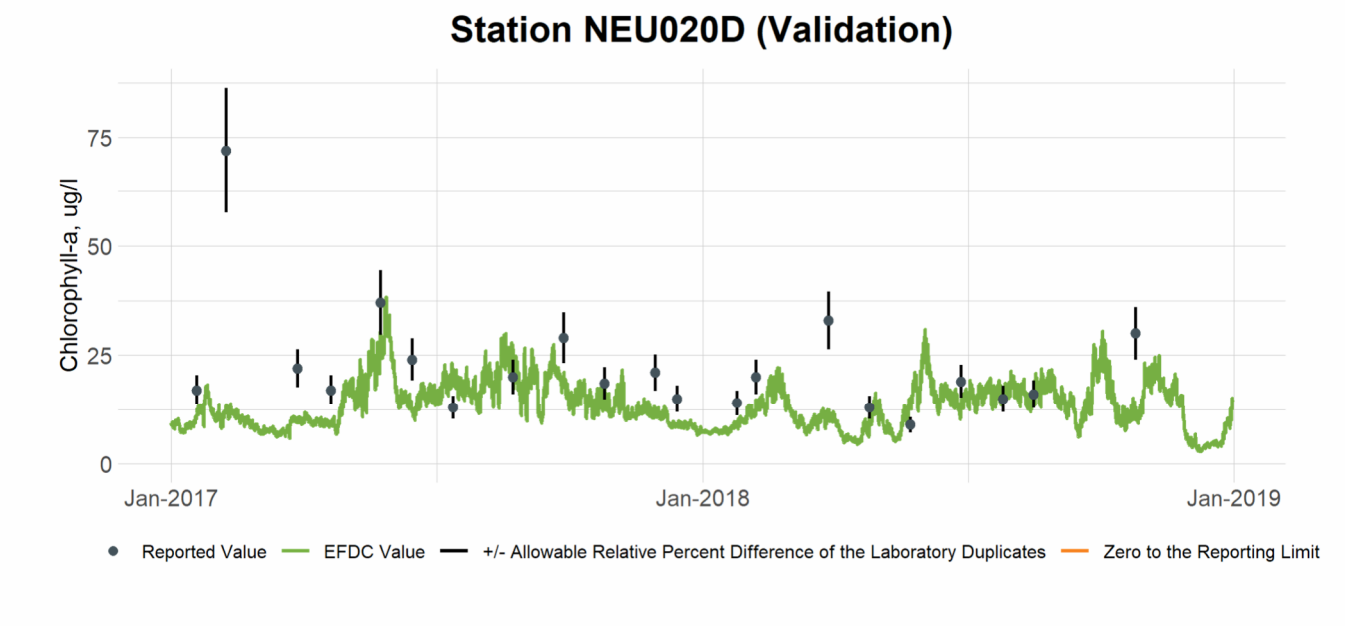

Figure 2-24 Validation Plot of Chl-a at Station NEU020D

3. TOC

3.1 TOC Calibration

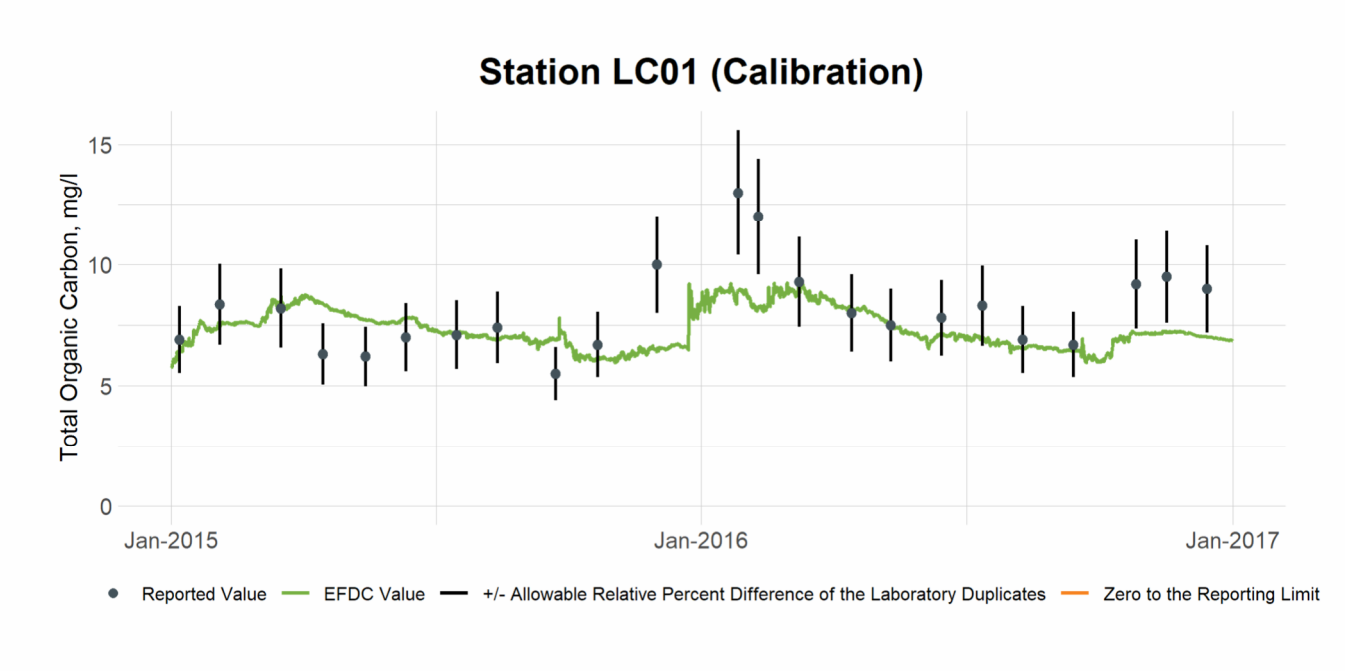

Figure 3-1 Calibration Plot of TOC at Station LC01

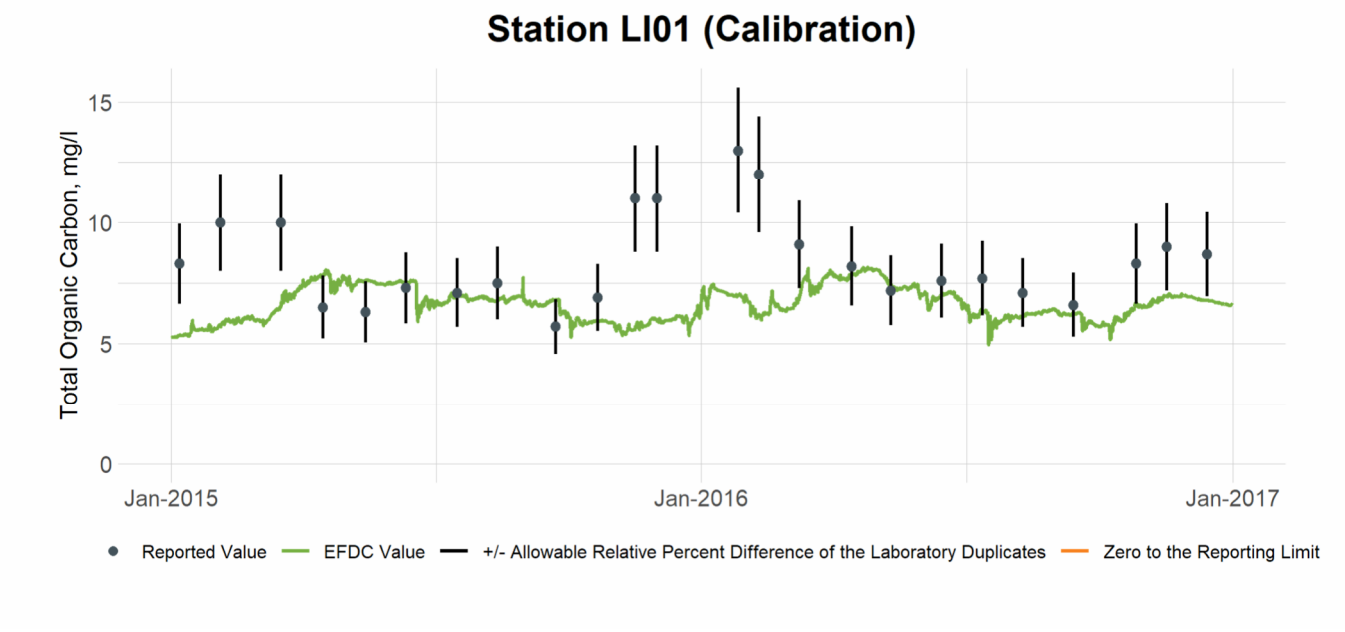

Figure 3-2 Calibration Plot of TOC at Station LI01

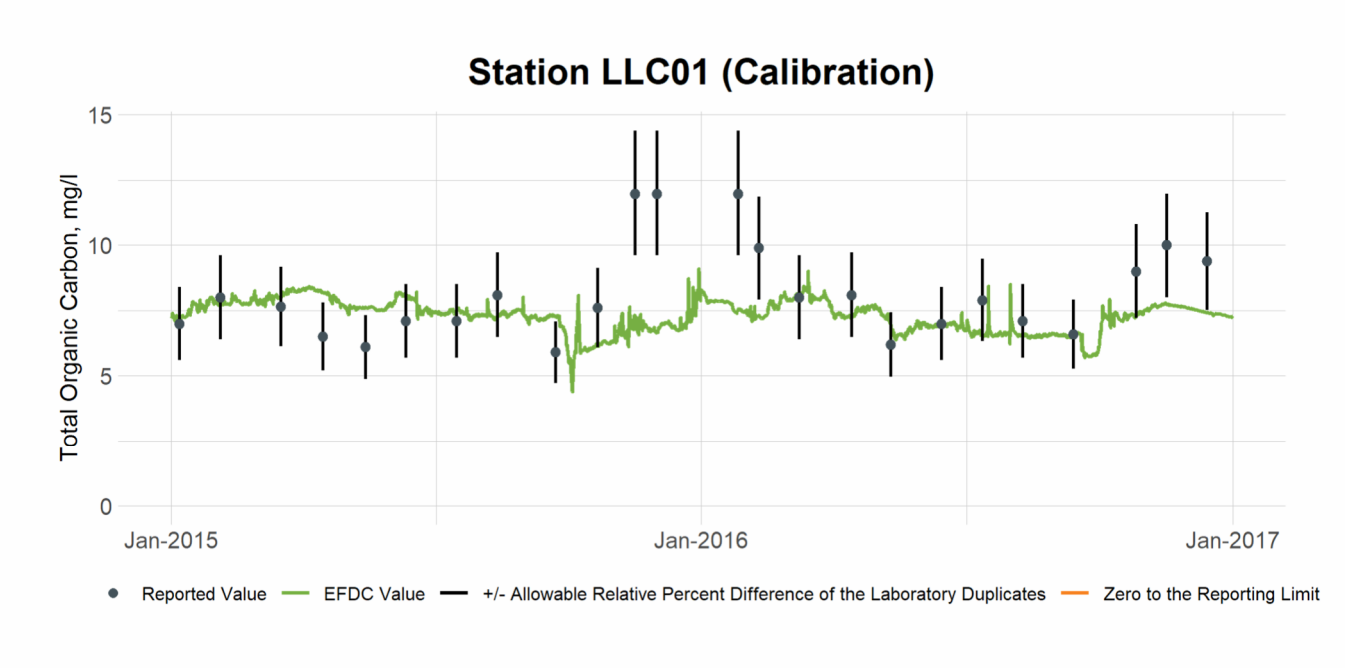

Figure 3-3 Calibration Plot of TOC at Station LLC01

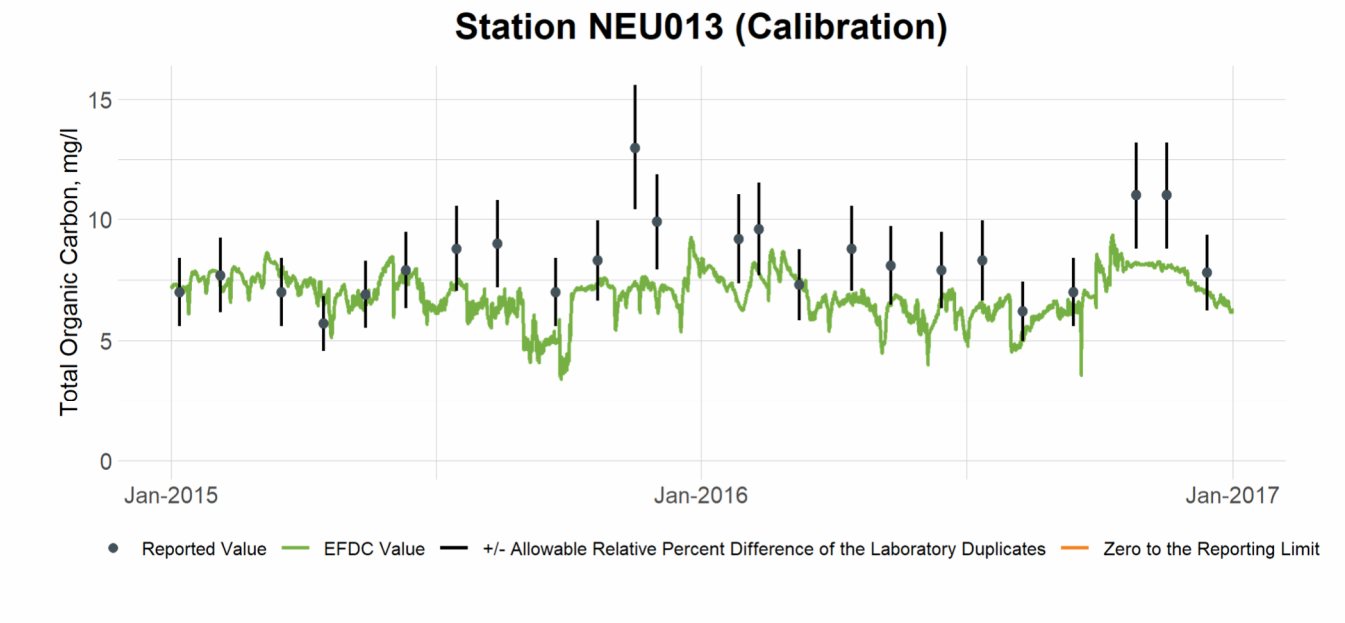

Figure 3-4 Calibration Plot of TOC at Station NEU013

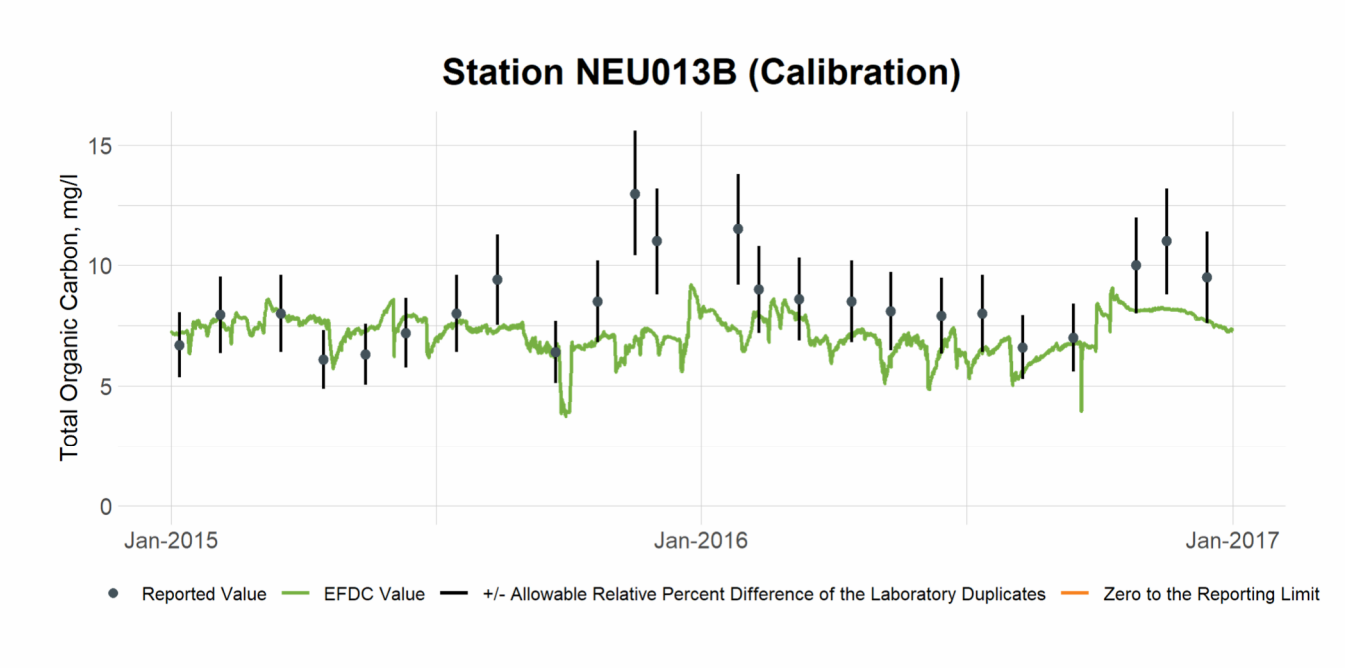

Figure 3-5 Calibration Plot of TOC at Station NEU013B

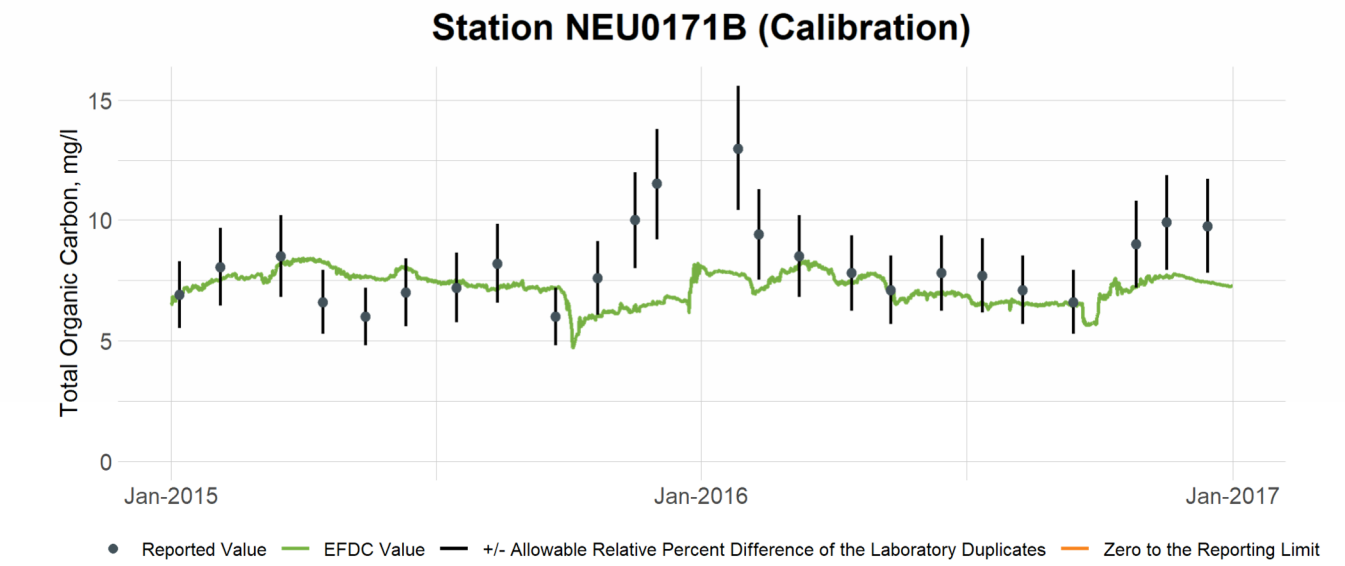

Figure 3-6 Calibration Plot of TOC at Station NEU0171B

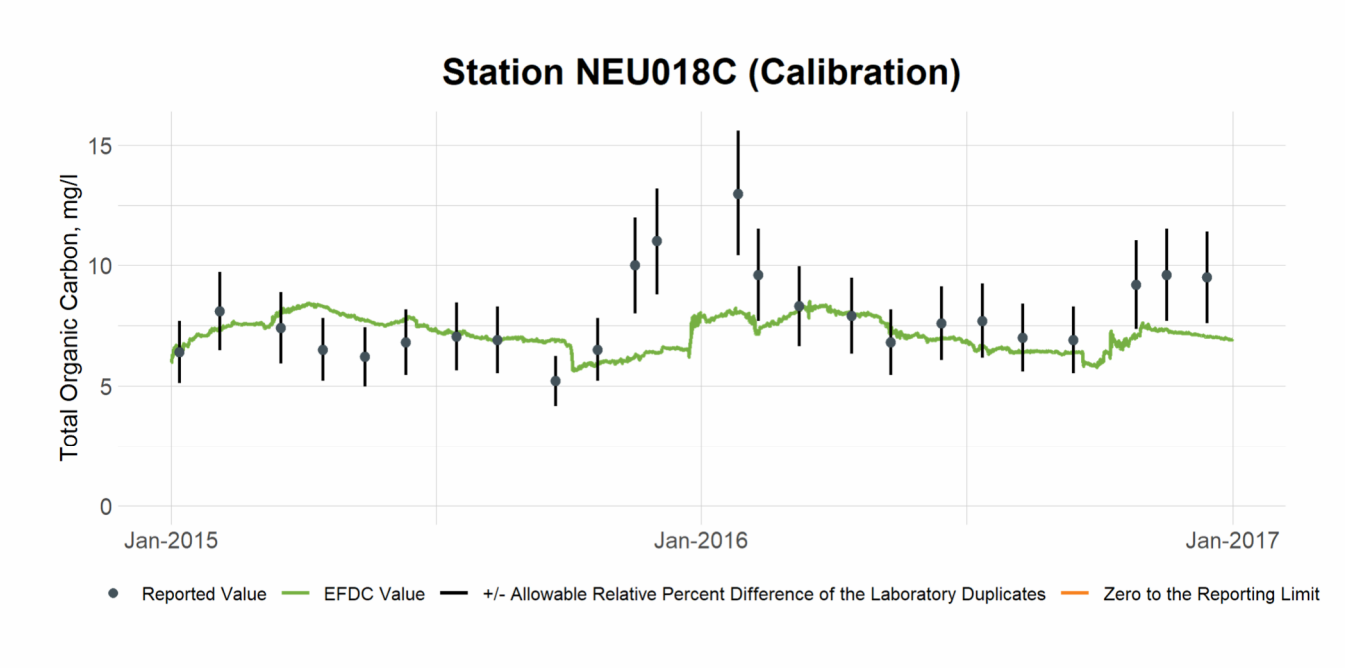

Figure 3-7 Calibration Plot of TOC at Station NEU018C

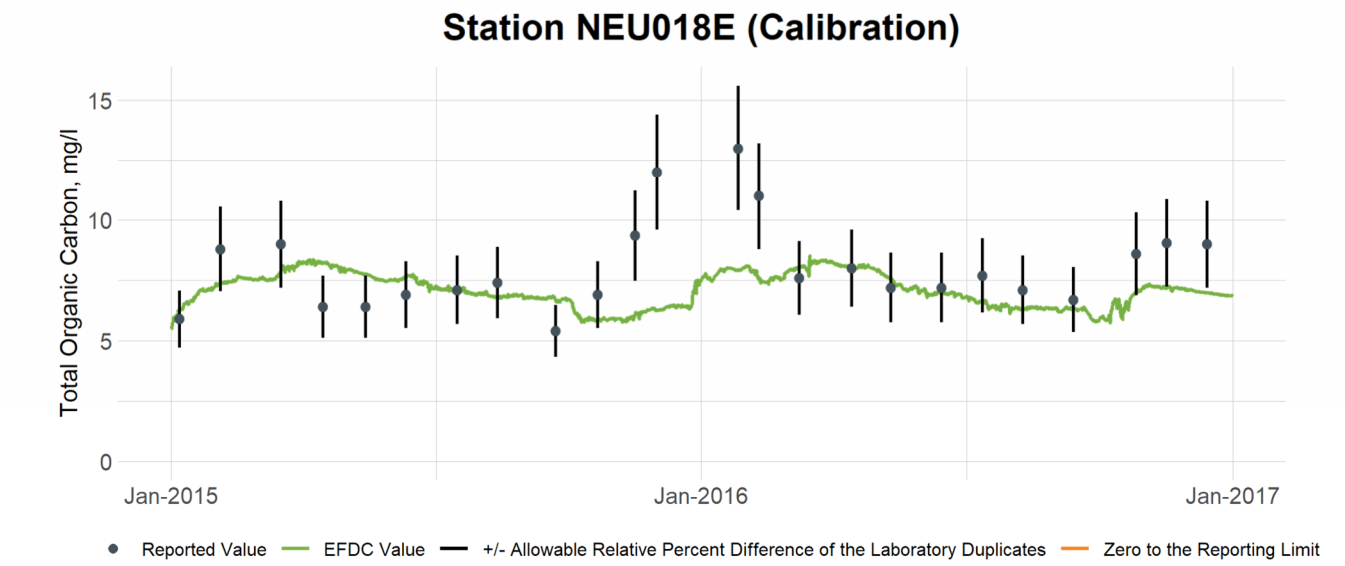

Figure 3-8 Calibration Plot of TOC at Station NEU018E

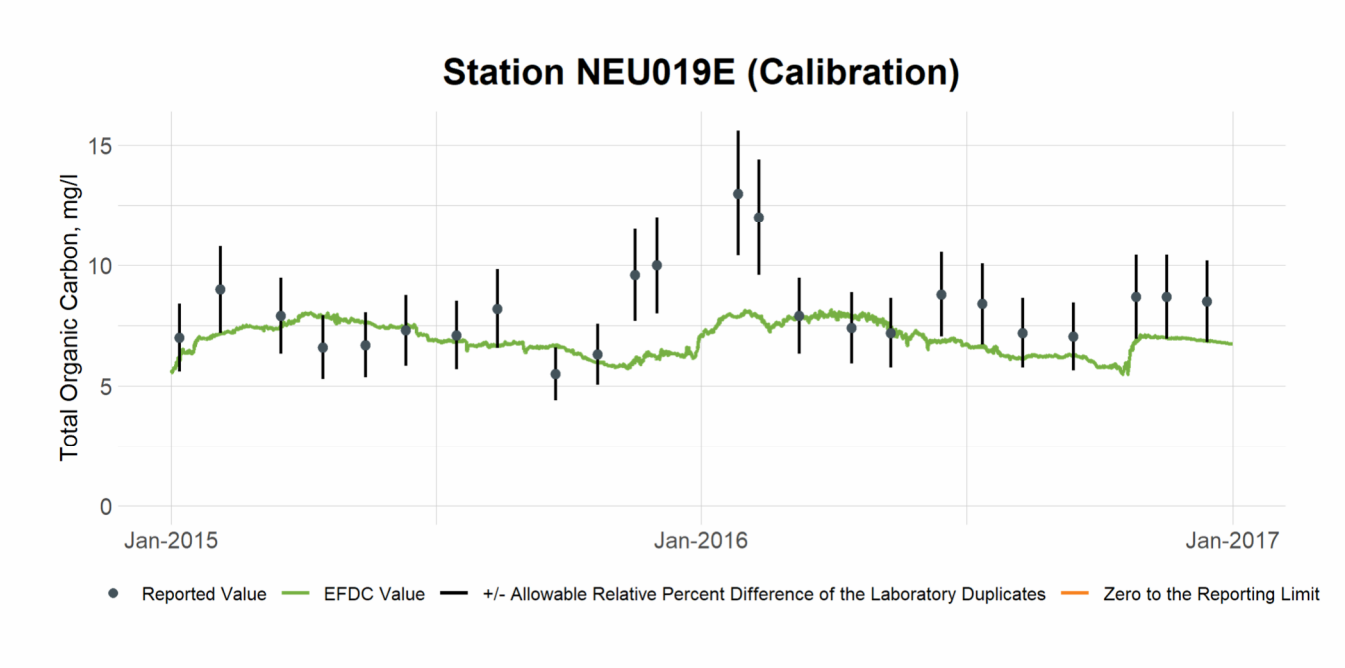

Figure 3-9 Calibration Plot of TOC at Station NEU019E

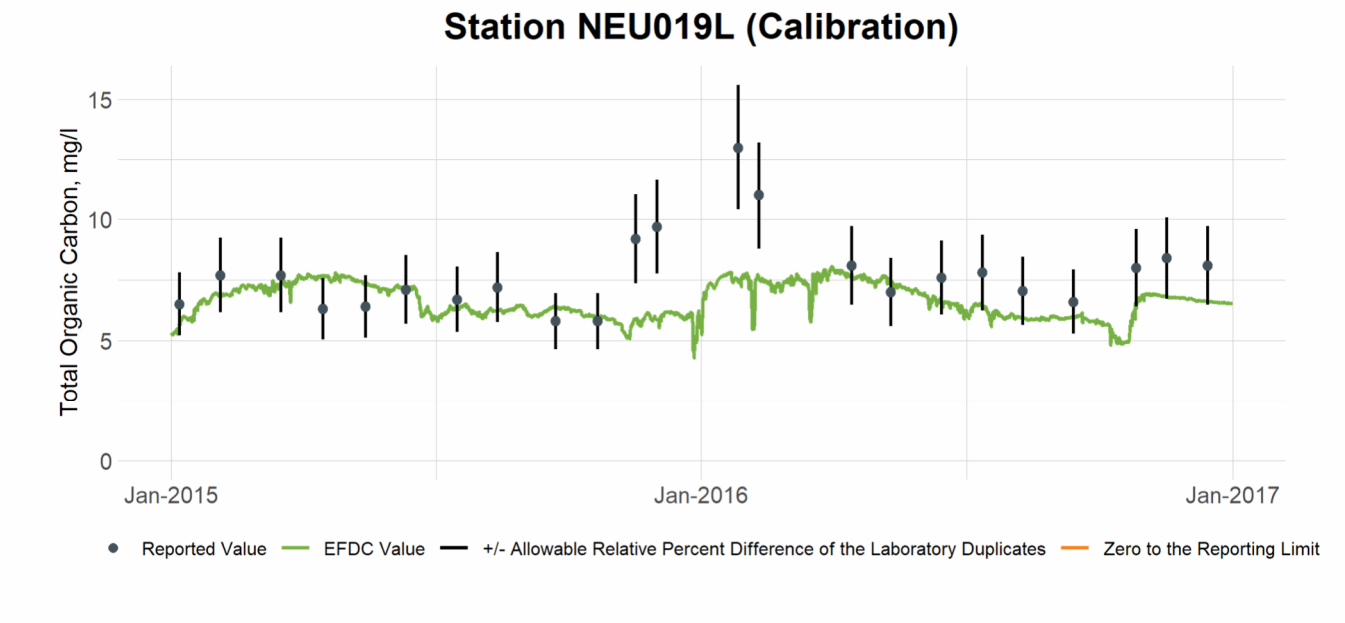

Figure 3-10 Calibration Plot of TOC at Station NEU019L

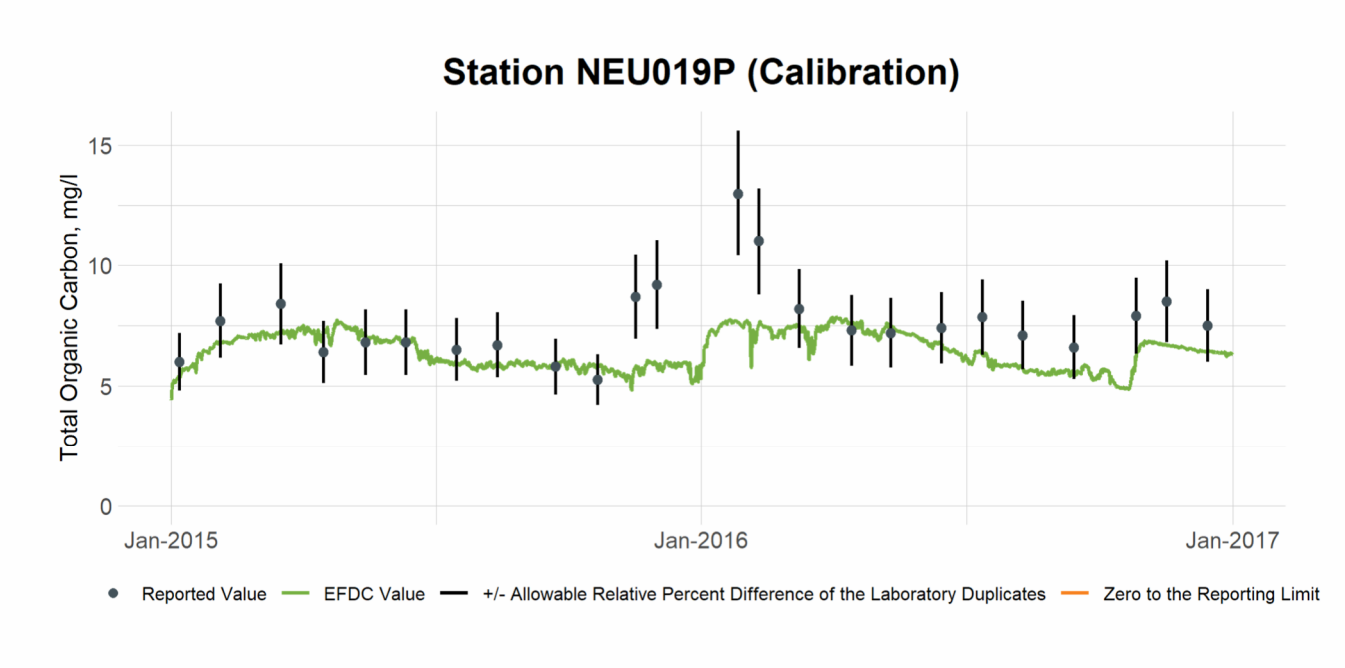

Figure 3-11 Calibration Plot of TOC at Station NEU019P

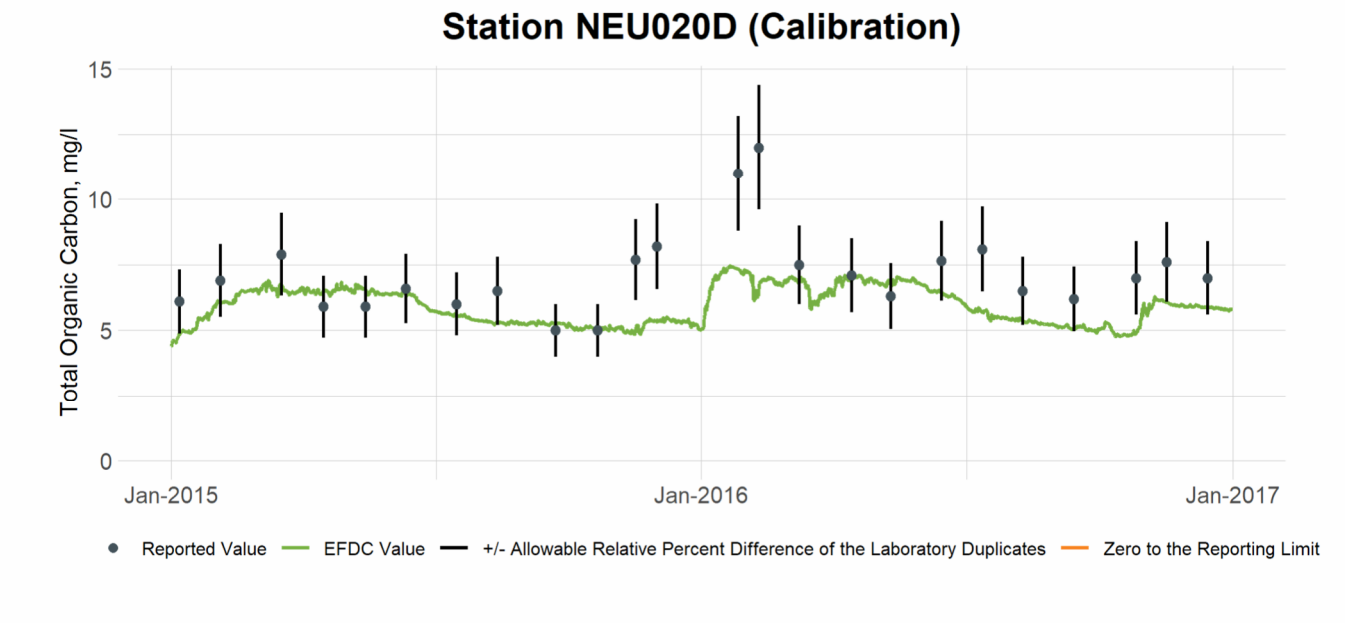

Figure 3-12 Calibration Plot of TOC at Station NEU020D

3.2 TOC Validation

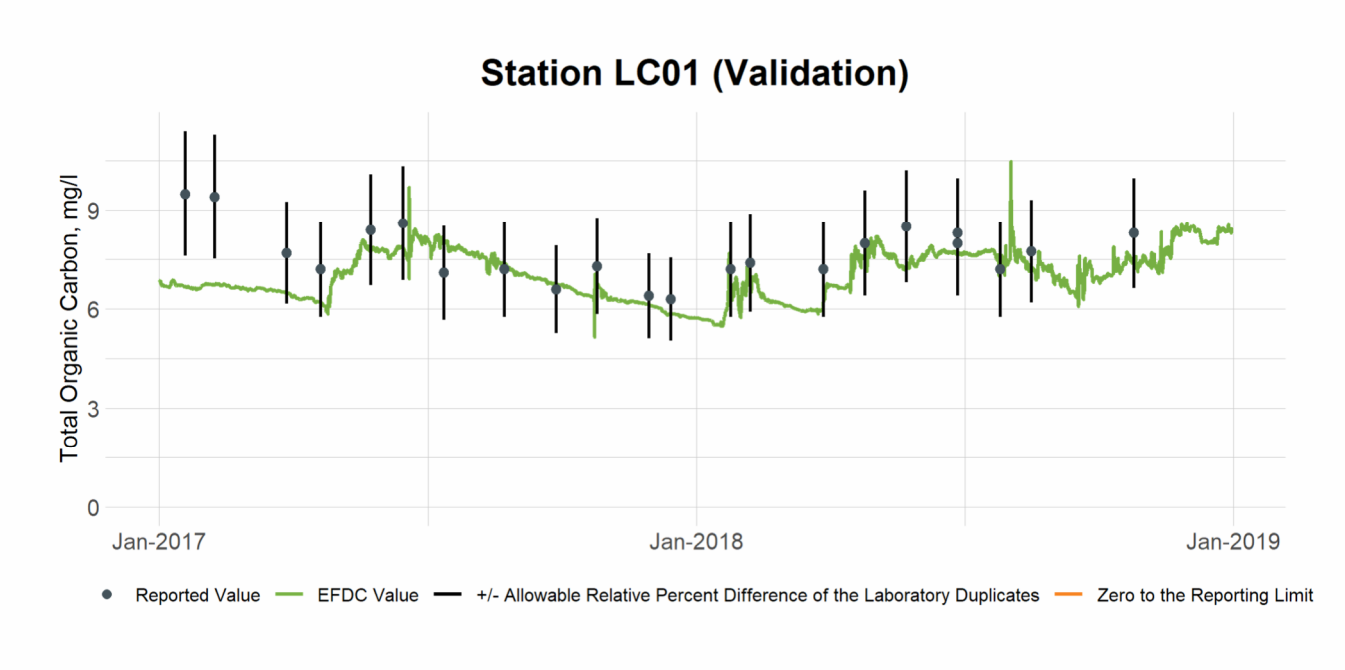

Figure 3-13 Validation Plot of TOC at Station LC01

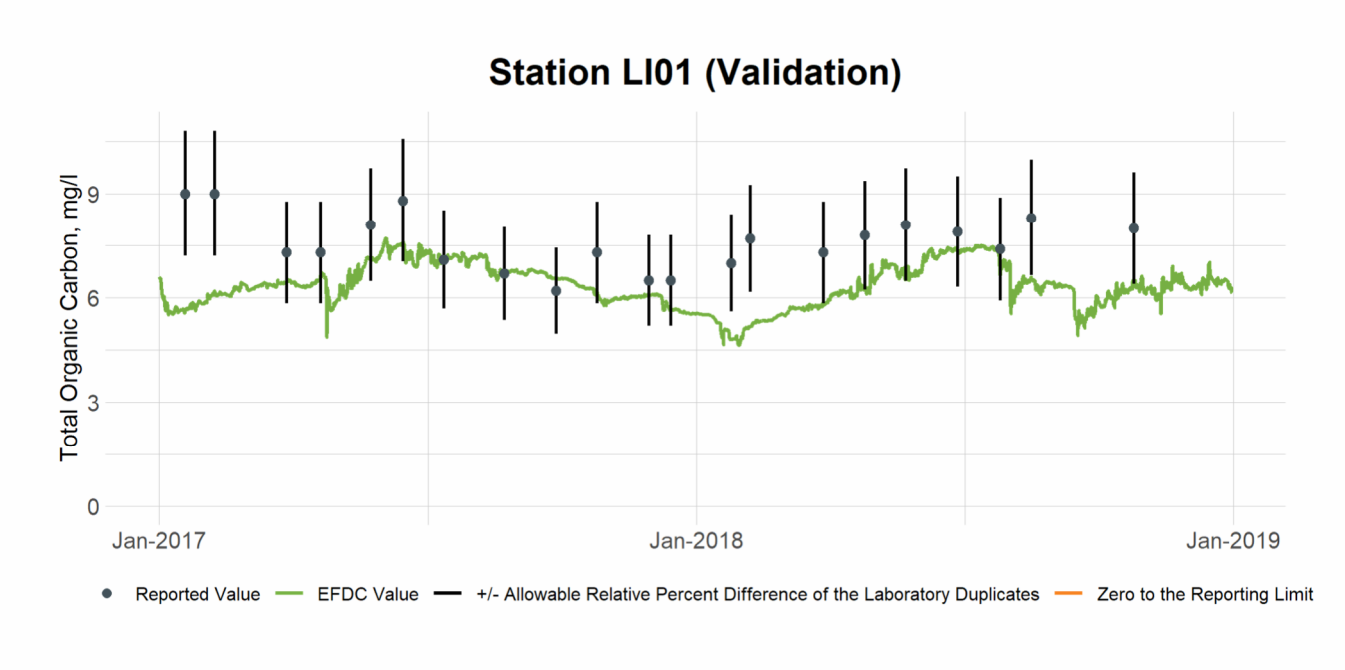

Figure 3-14 Validation Plot of TOC at Station LI01

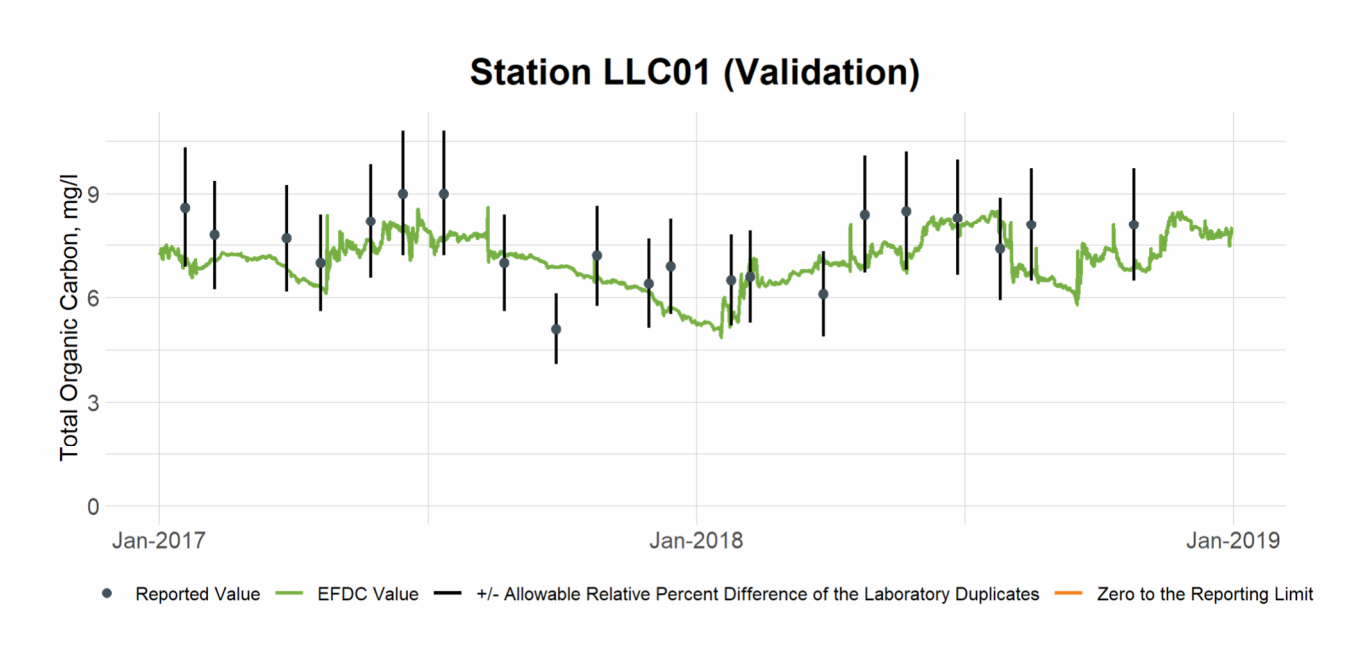

Figure 3-15 Validation Plot of TOC at Station LLC01

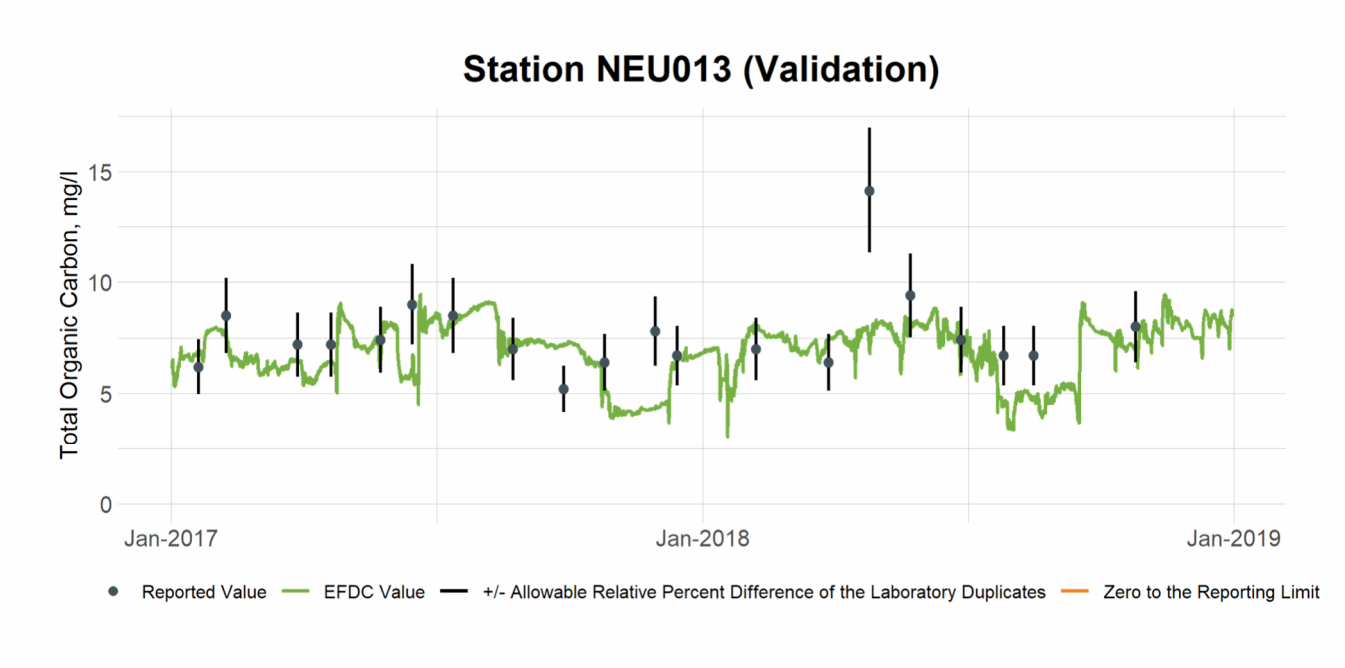

Figure 3-16 Validation Plot of TOC at Station NEU013

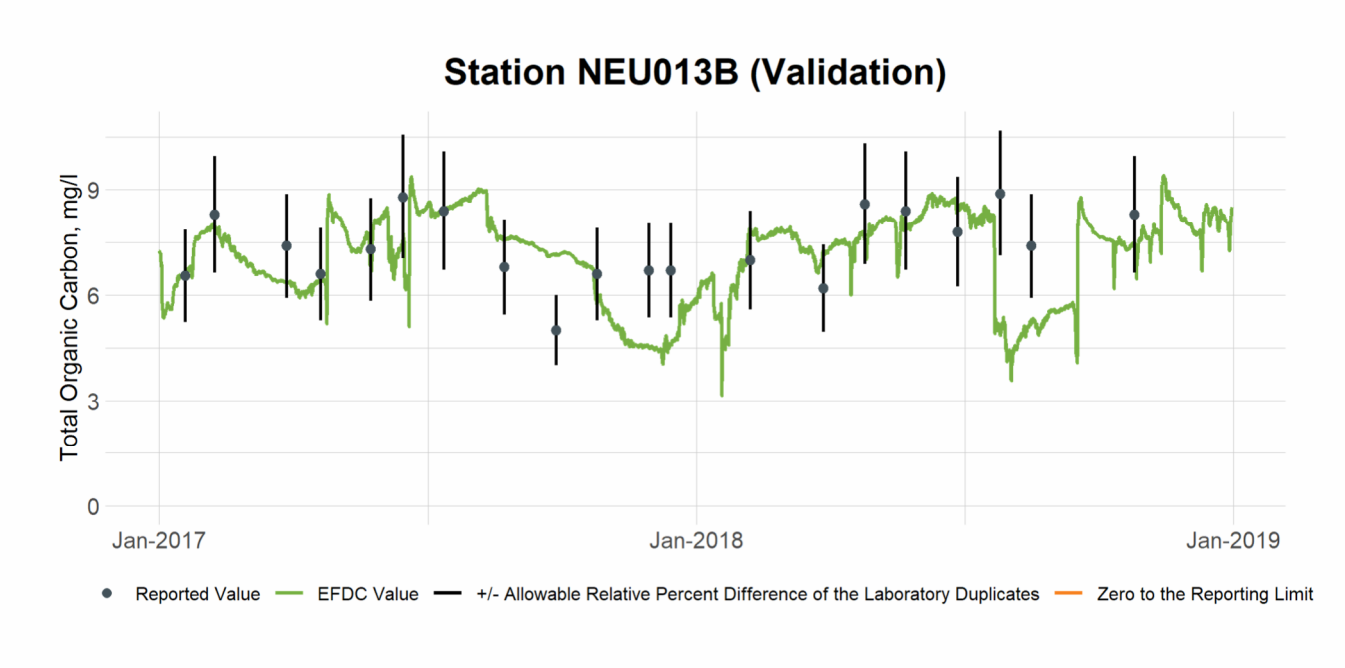

Figure 3-17 Validation Plot of TOC at Station NEU013B

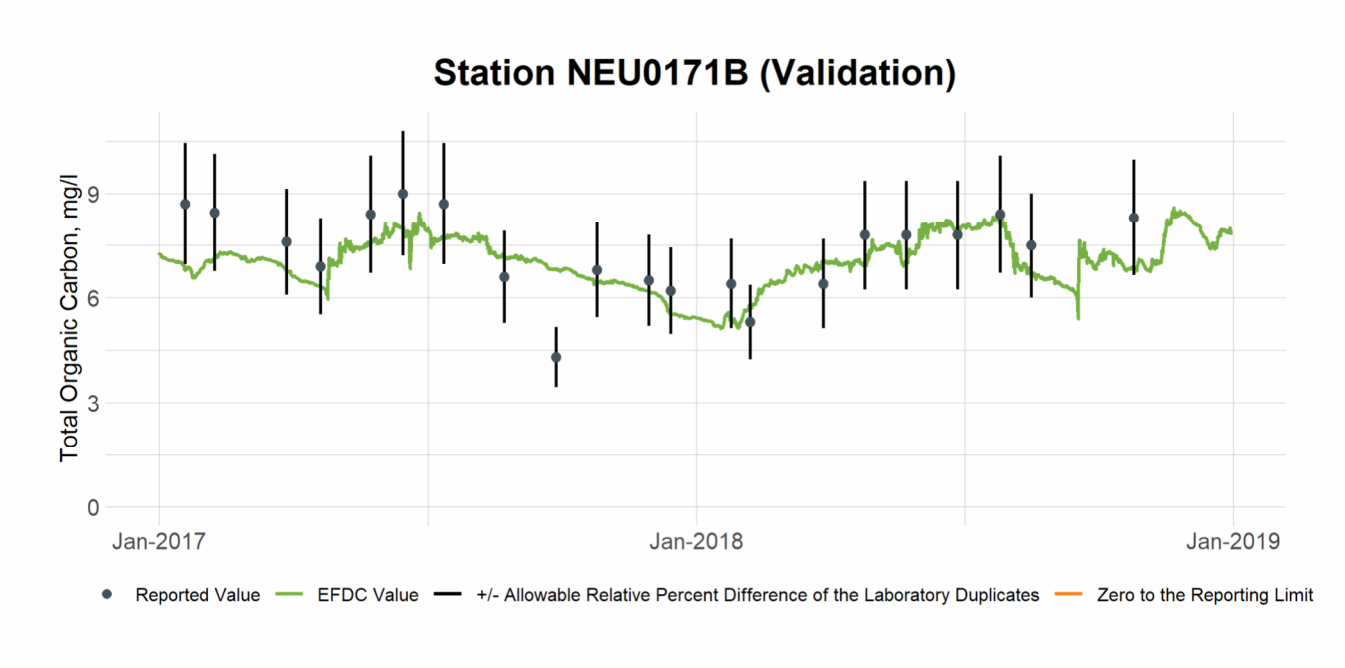

Figure 3-18 Validation Plot of TOC at Station NEU0171B

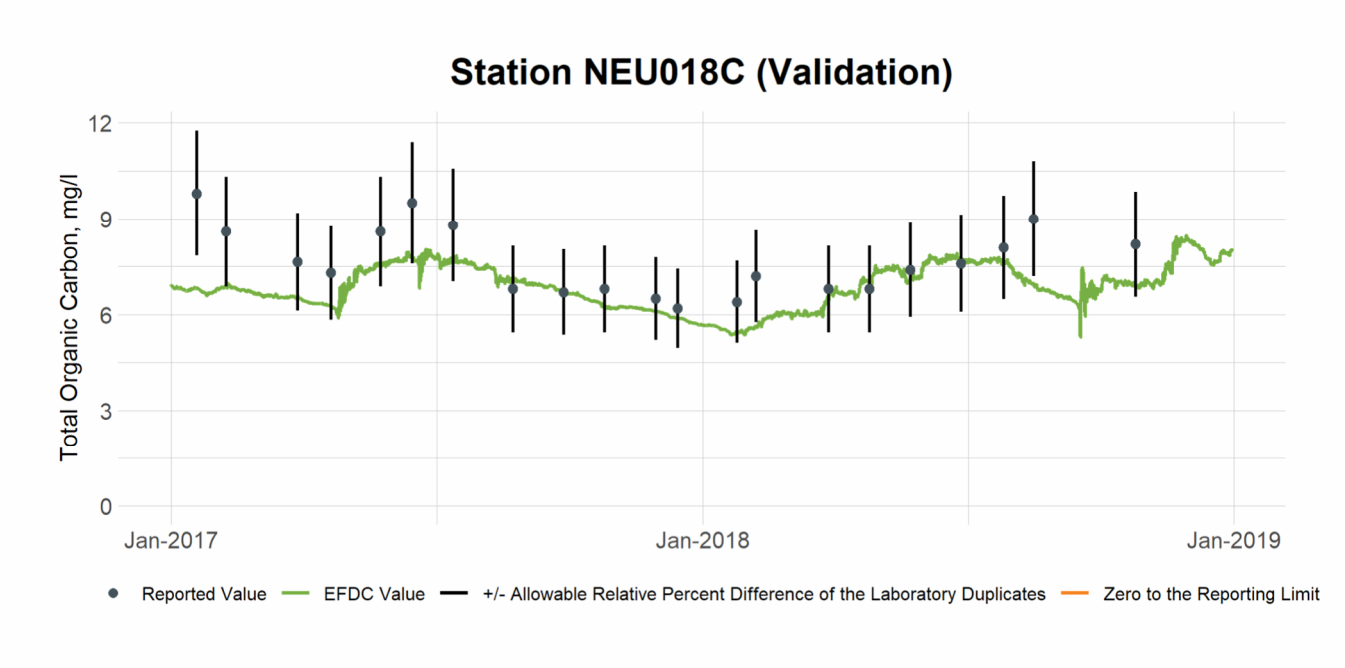

Figure 3-19 Validation Plot of TOC at Station NEU018C

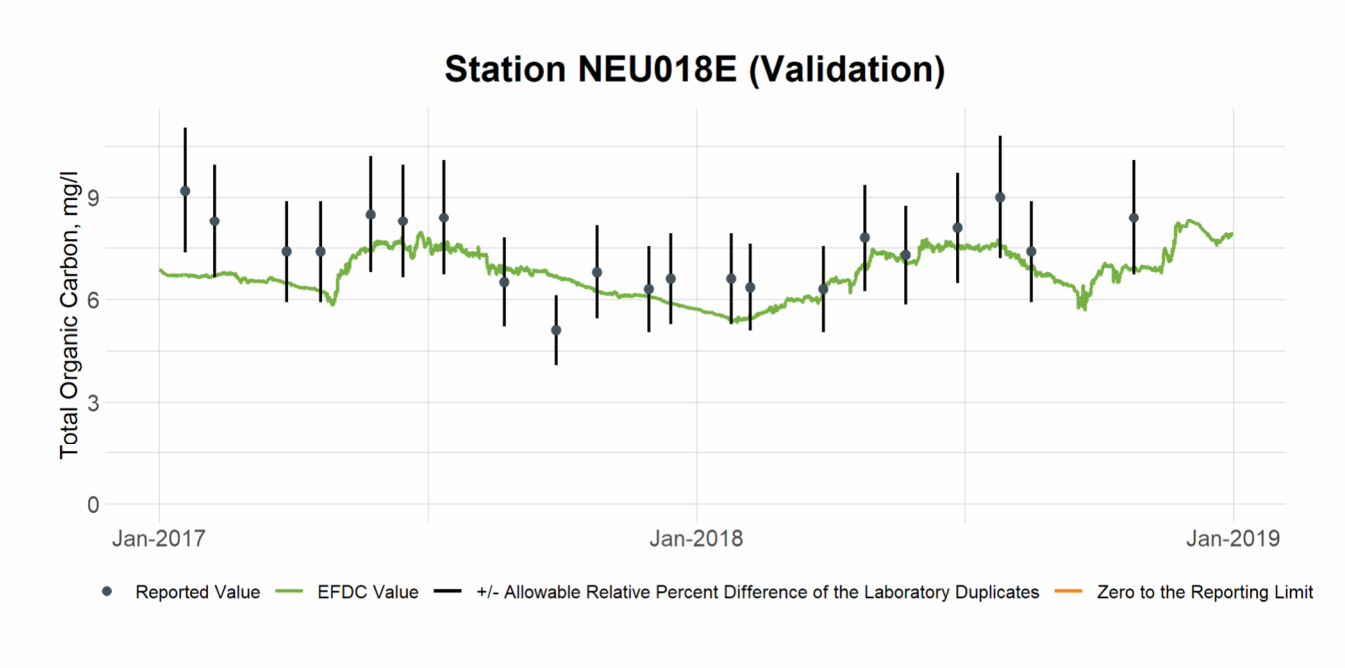

Figure 3-20 Validation Plot of TOC at Station NEU018E

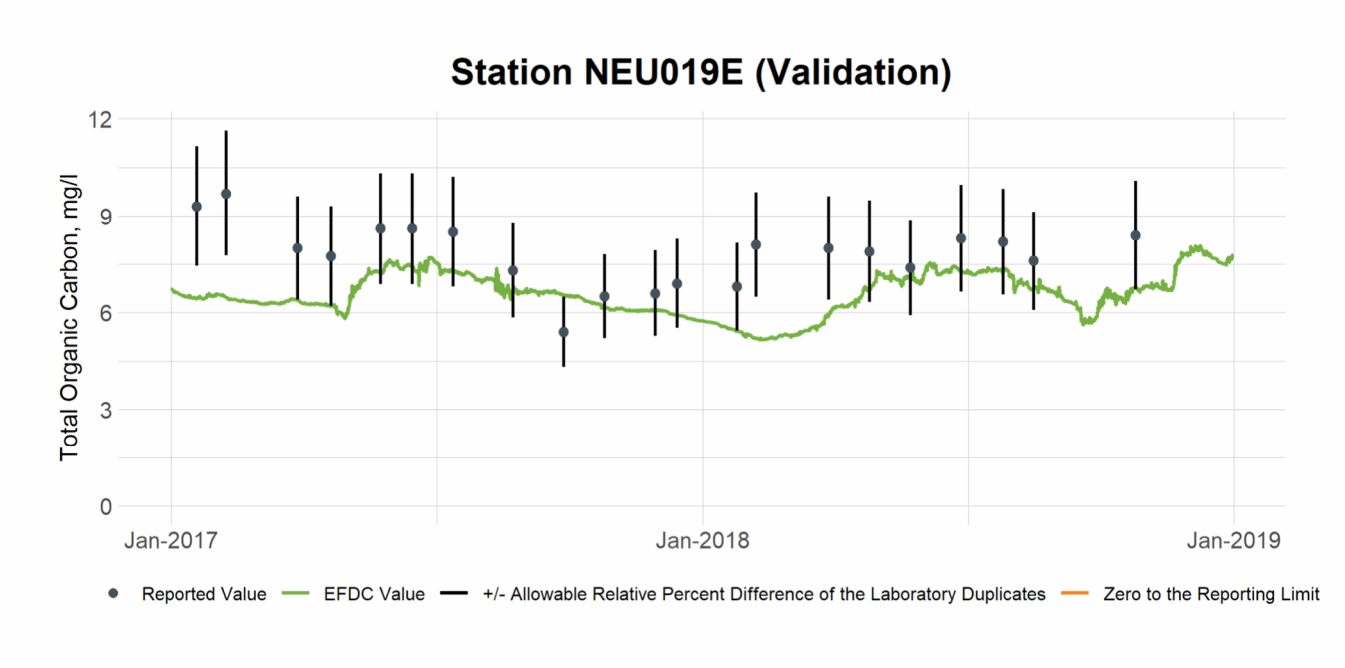

Figure 3-21 Validation Plot of TOC at Station NEU019E

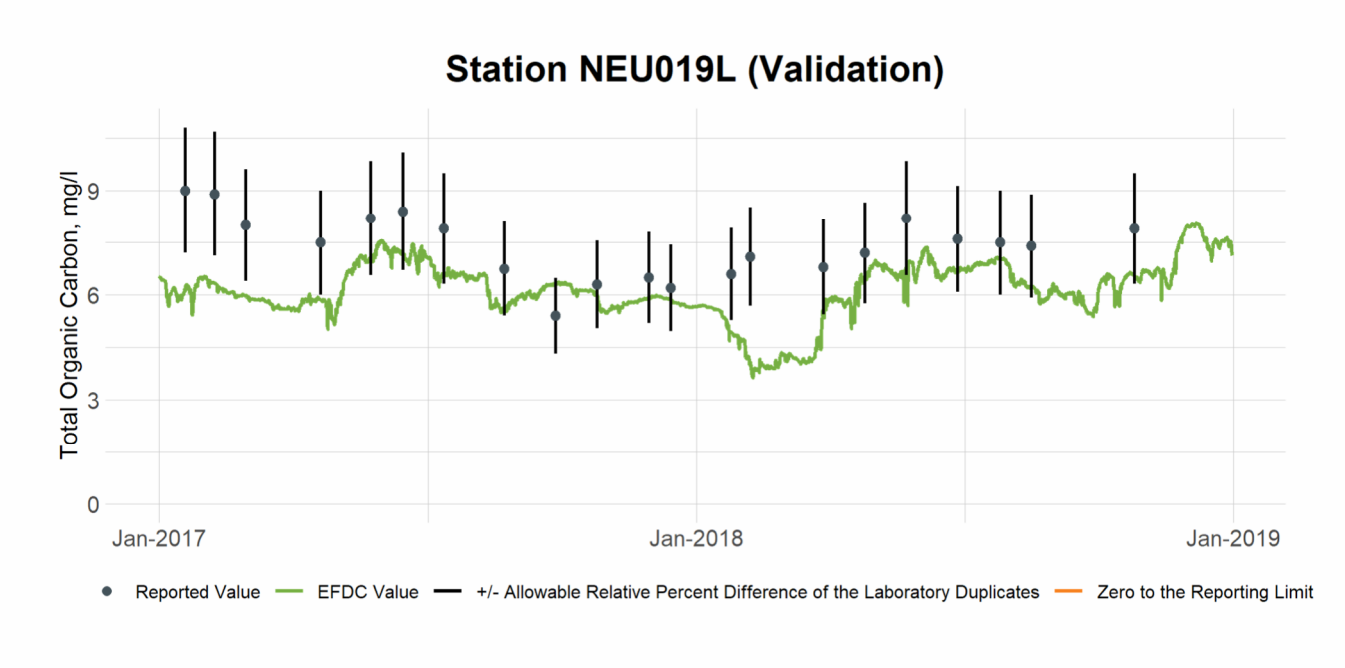

Figure 3-22 Validation Plot of TOC at Station NEU019L

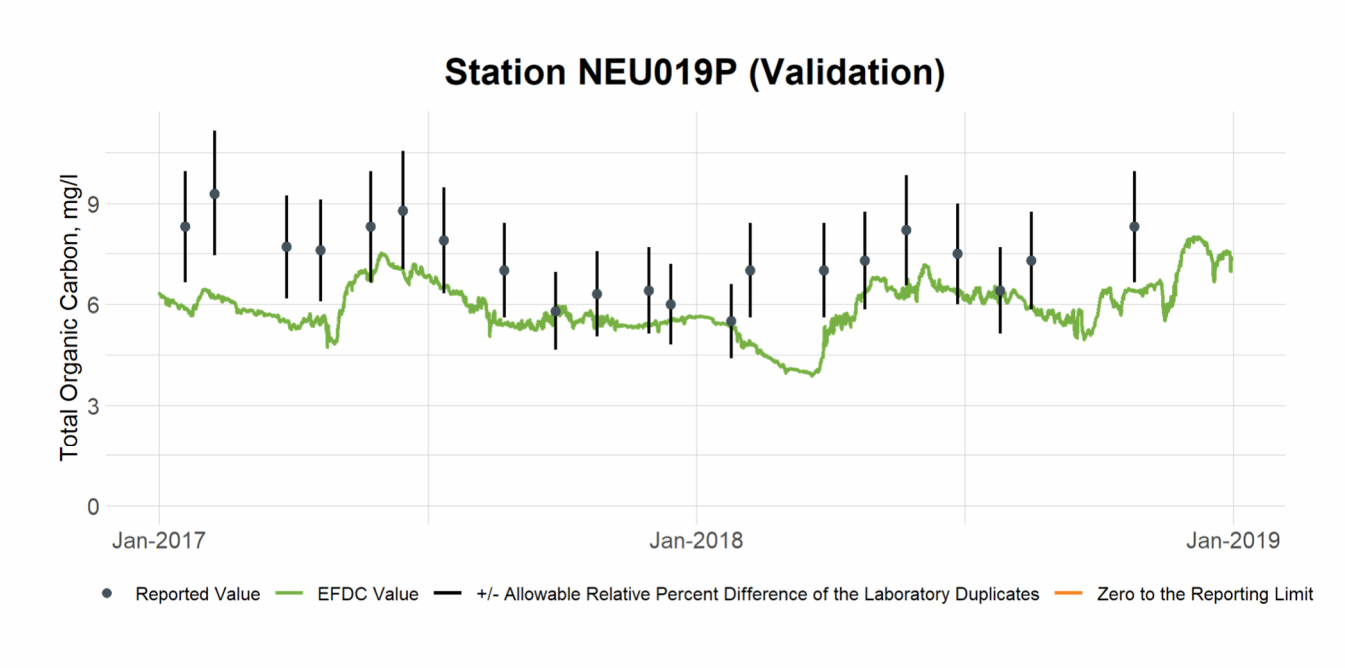

Figure 3-23 Validation Plot of TOC at Station NEU019P

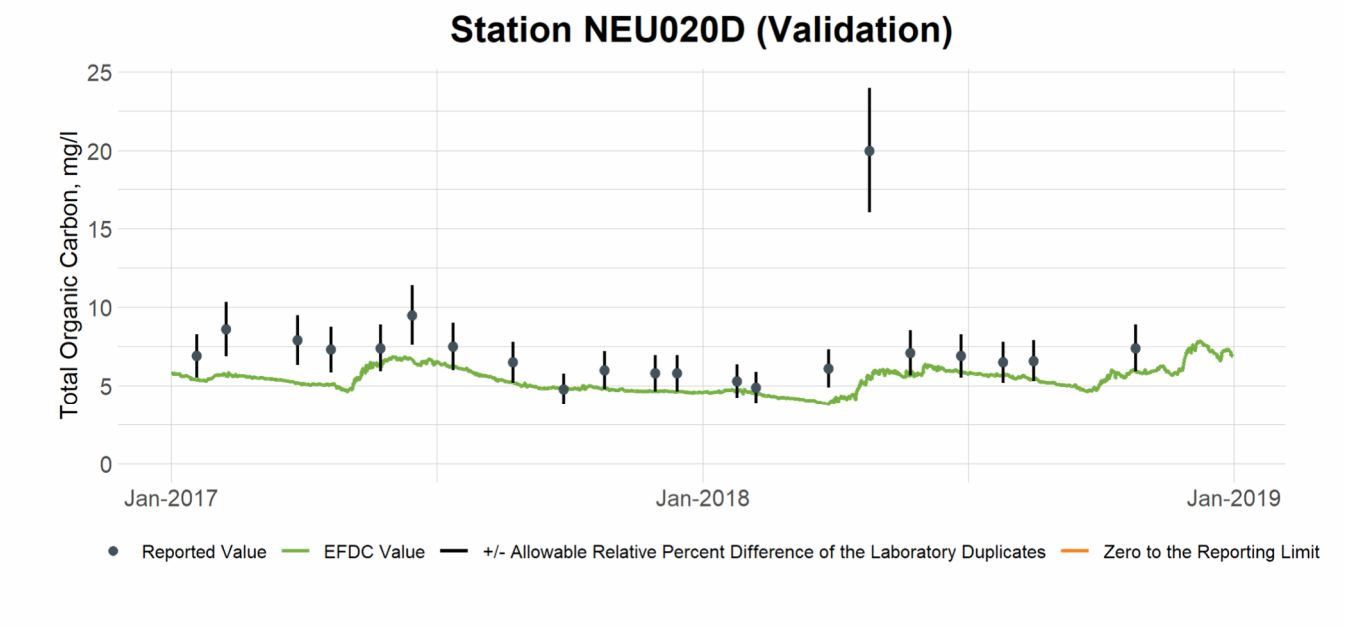

Figure 3-24 Validation Plot of TOC at Station NEU020D

4. DO

4.1 DO Calibration

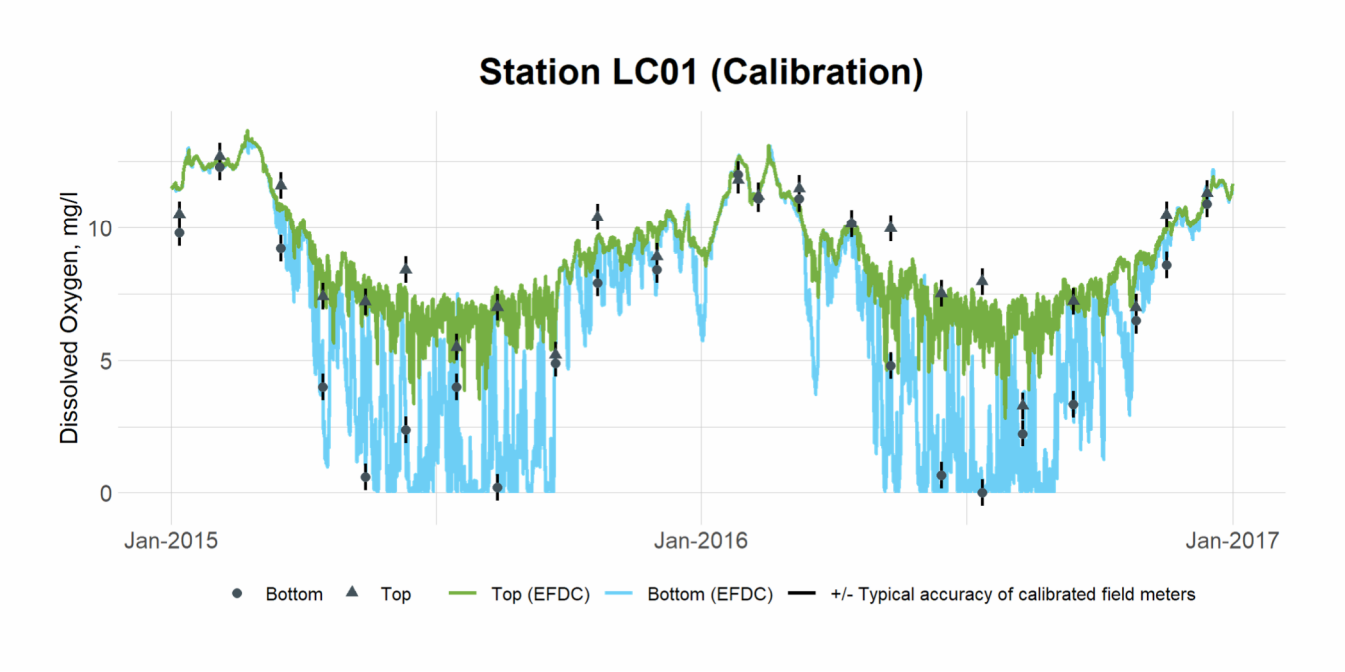

Figure 4-1 Calibration Plot of Top and Bottom DO at Station LC01

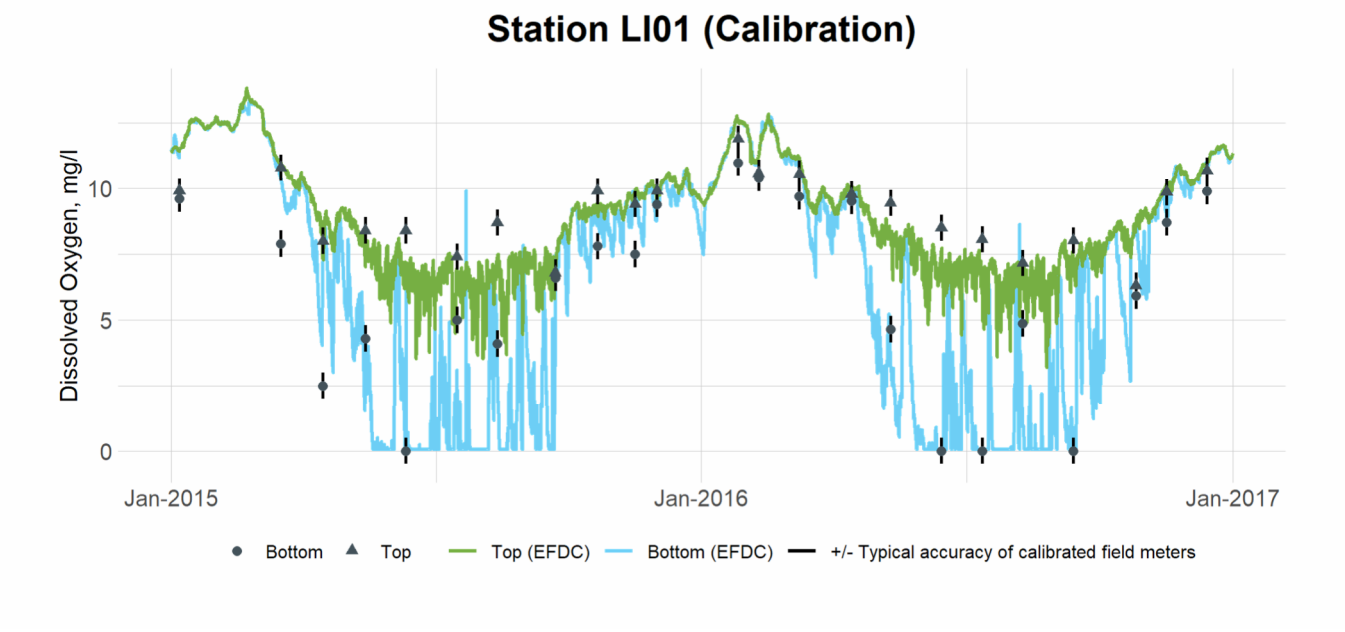

Figure 4-2 Calibration Plot of Top and Bottom DO at Station LI01

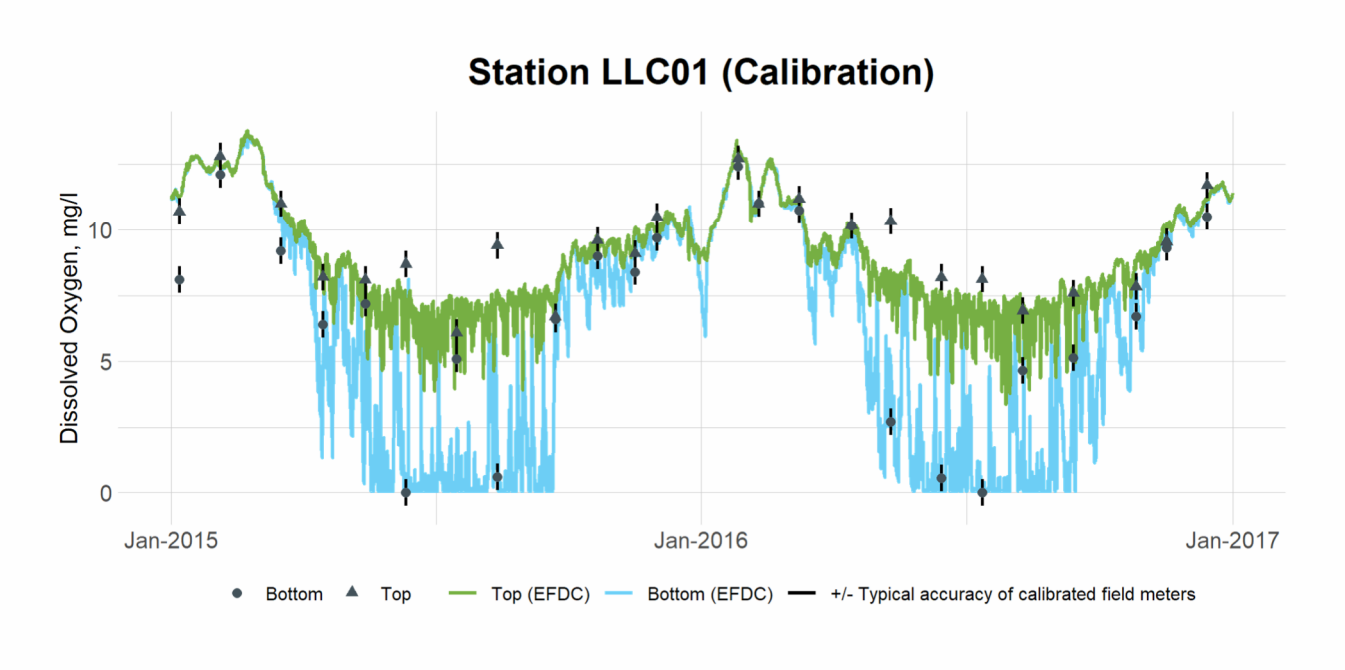

Figure 4-3 Calibration Plot of Top and Bottom DO at Station LLC01

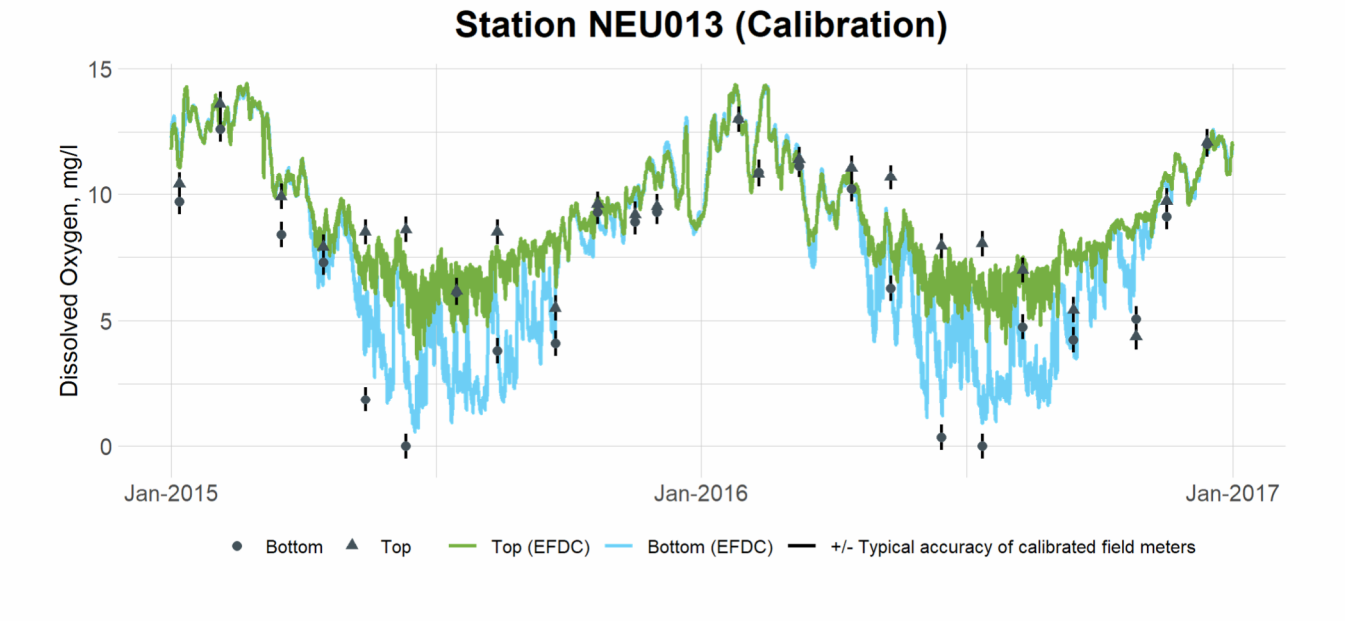

Figure 4-4 Calibration Plot of Top and Bottom DO at Station NEU013

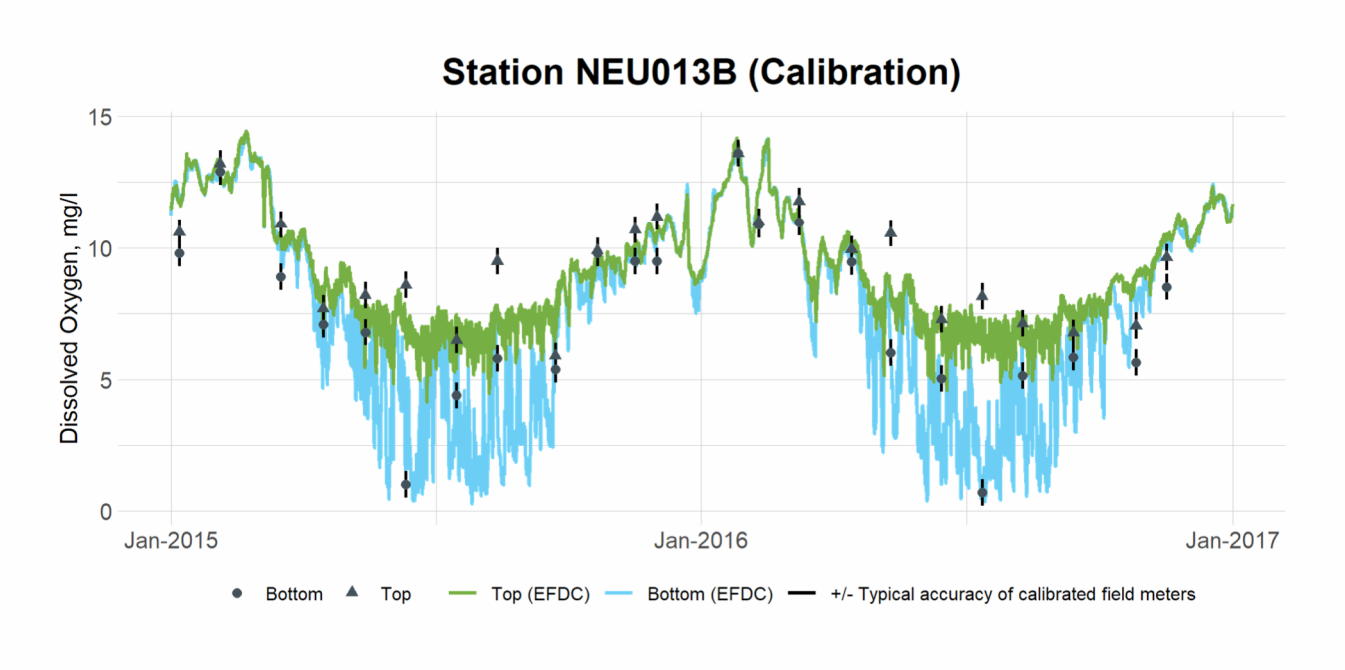

Figure 4-5 Calibration Plot of Top and Bottom DO at Station NEU013B

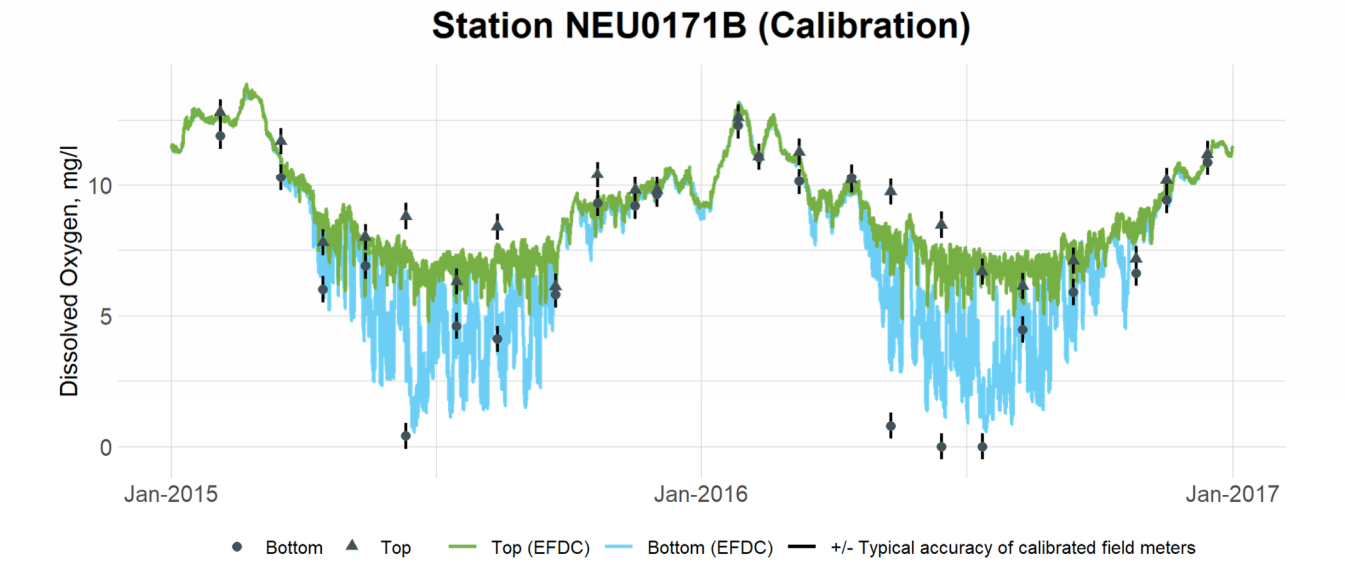

Figure 4-6 Calibration Plot of Top and Bottom DO at Station NEU0171B

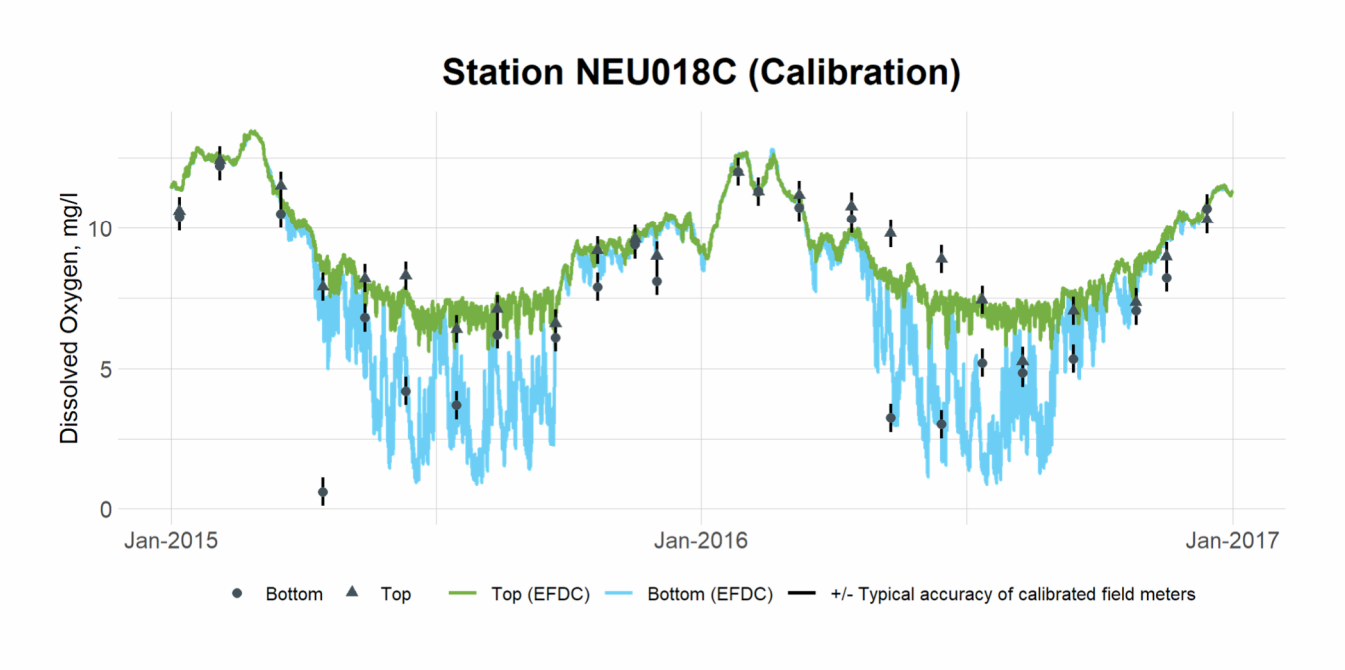

Figure 4-7 Calibration Plot of Top and Bottom DO at Station NEU018C

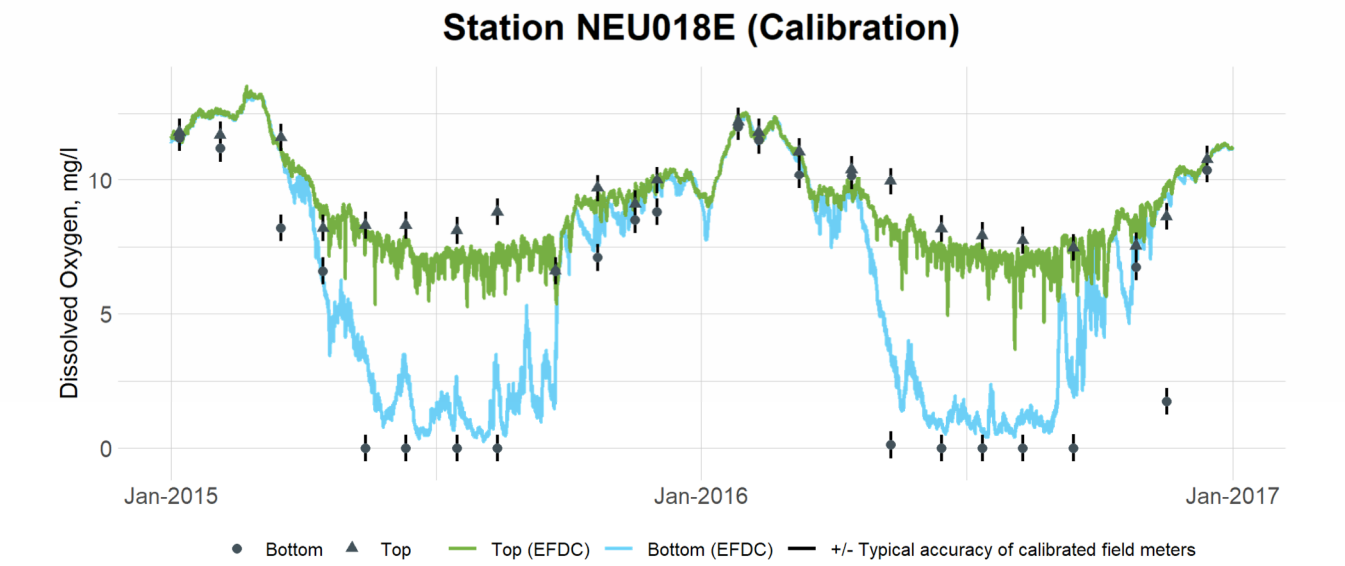

Figure 4-8 Calibration Plot of Top and Bottom DO at Station NEU018E

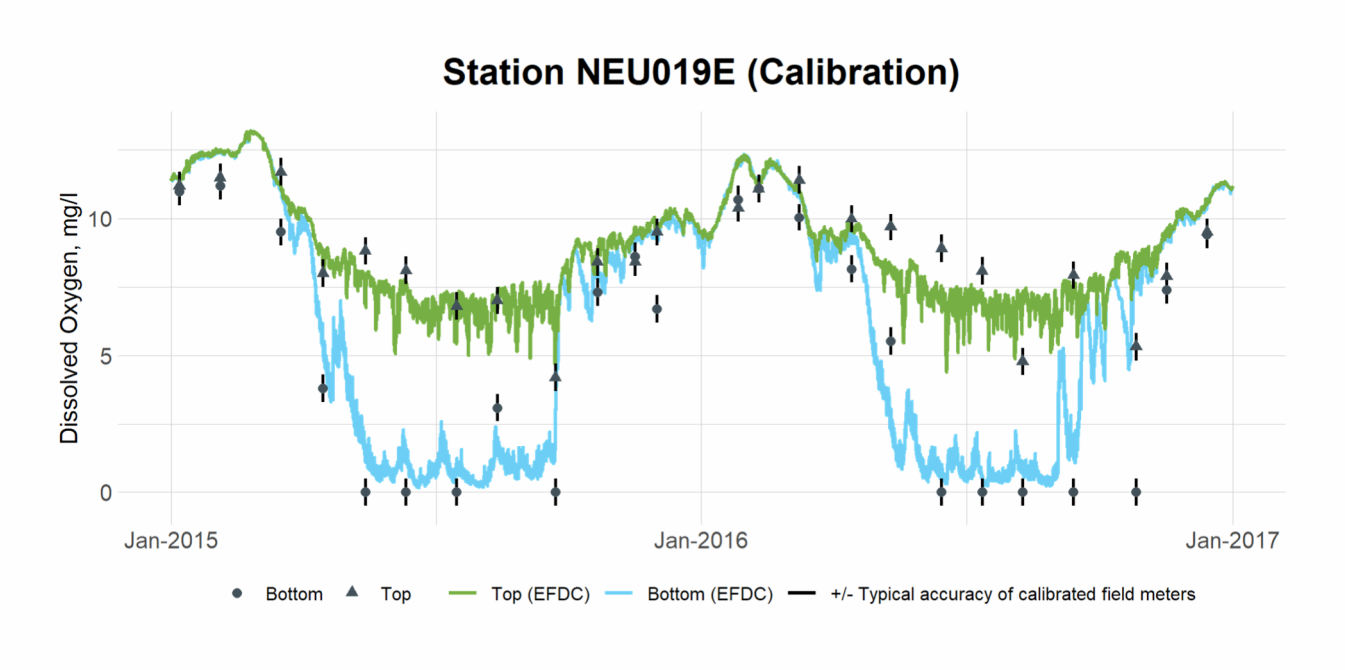

Figure 4-9 Calibration Plot of Top and Bottom DO at Station NEU019E

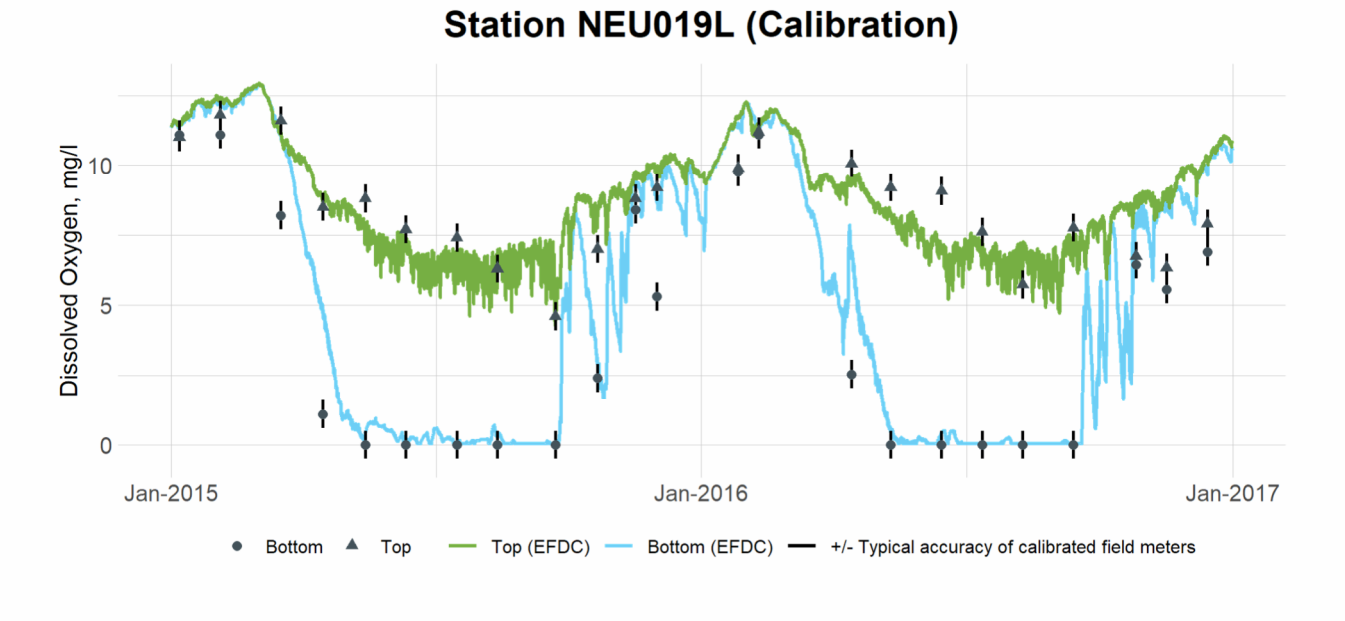

Figure 4-10 Calibration Plot of Top and Bottom DO at Station NEU019L

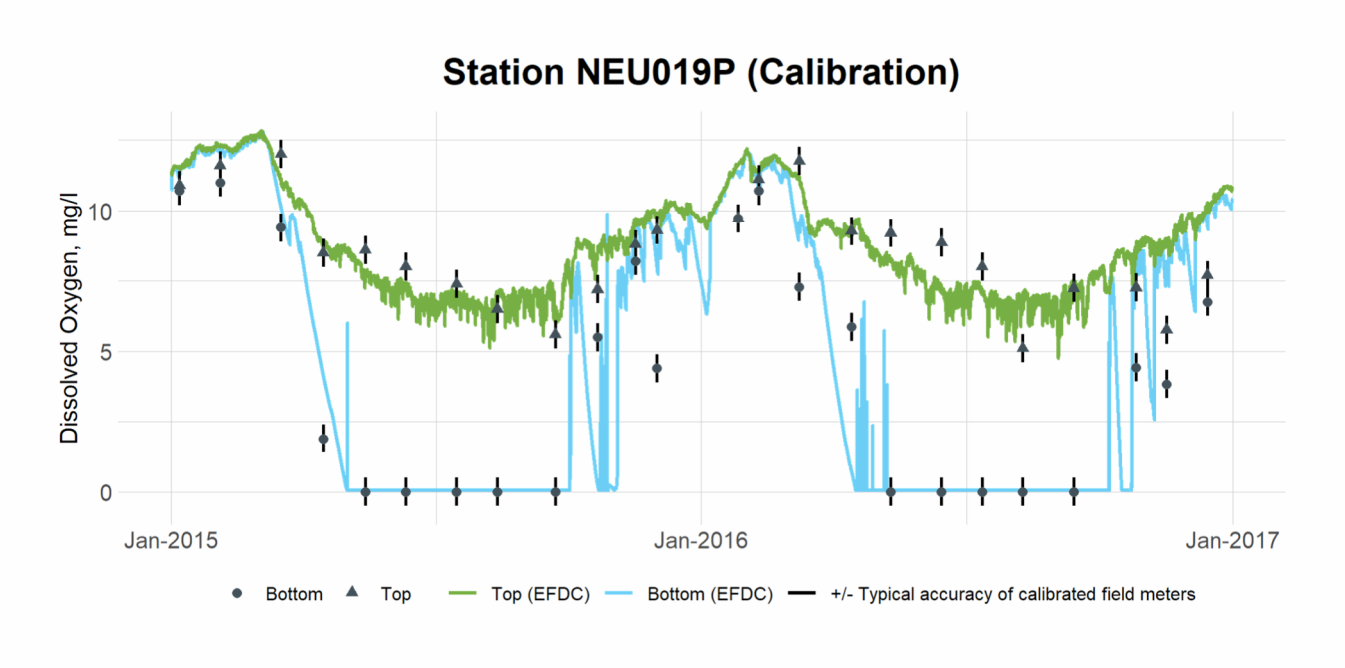

Figure 4-11 Calibration Plot of Top and Bottom DO at Station NEU019P

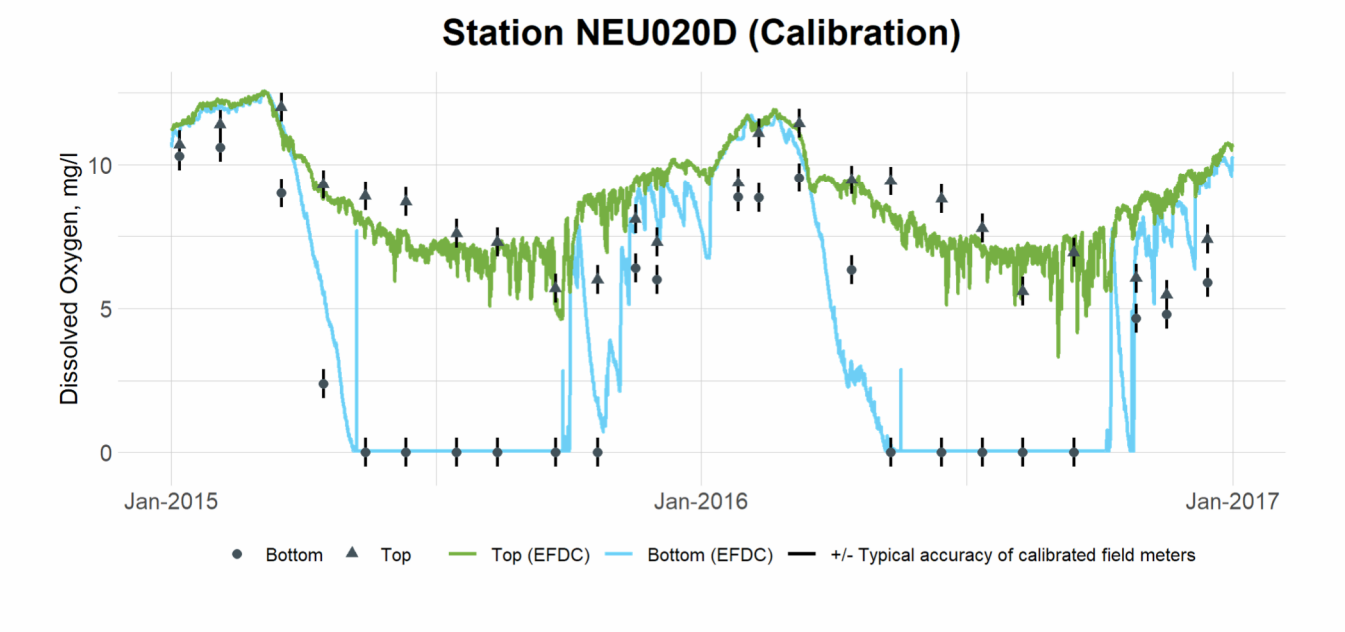

Figure 4-12 Calibration Plot of Top and Bottom DO at Station NEU020D

4.2 DO Validation

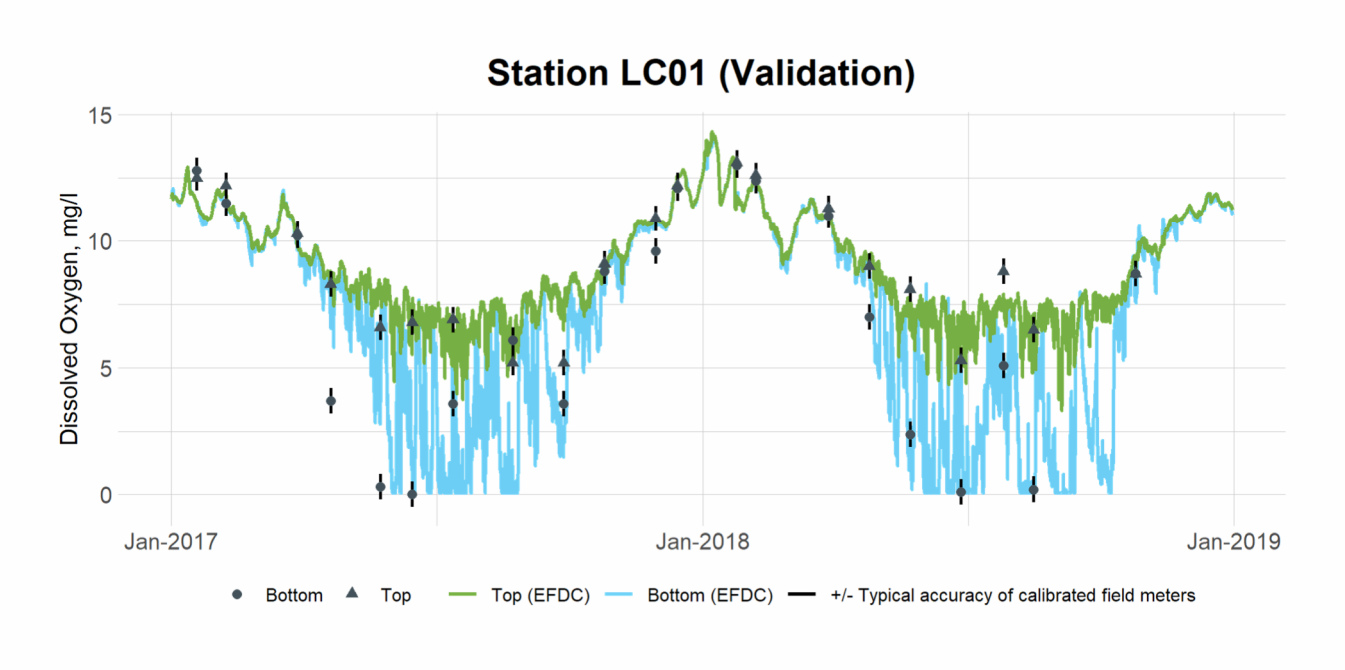

Figure 4-13 Validation Plot of Top and Bottom DO at Station LC01

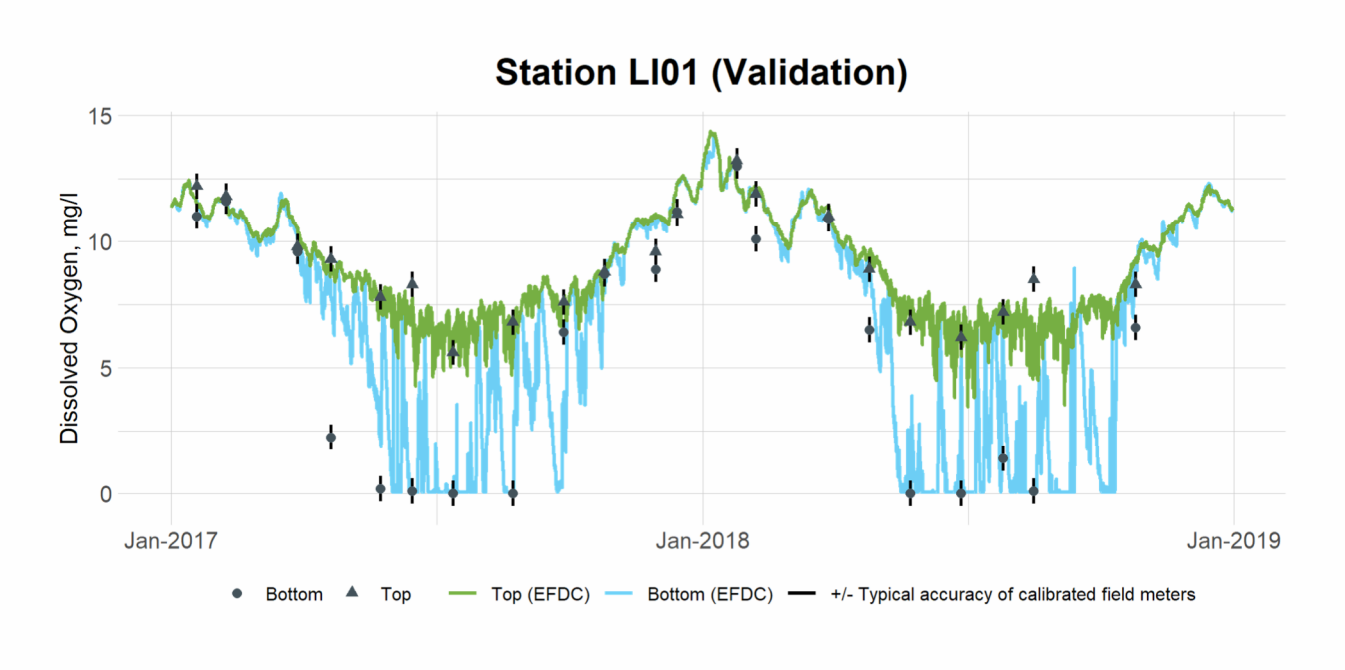

Figure 4-14 Validation Plot of Top and Bottom DO at Station LI01

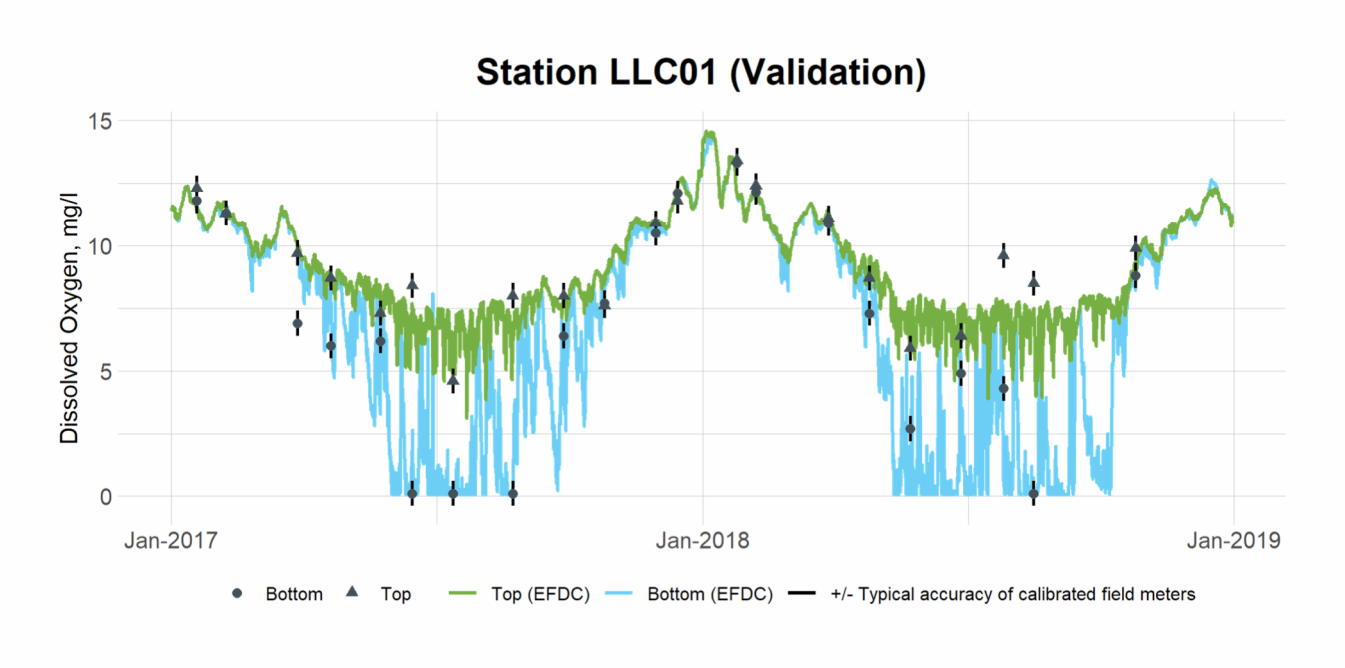

Figure 4-15 Validation Plot of Top and Bottom DO at Station LLC01

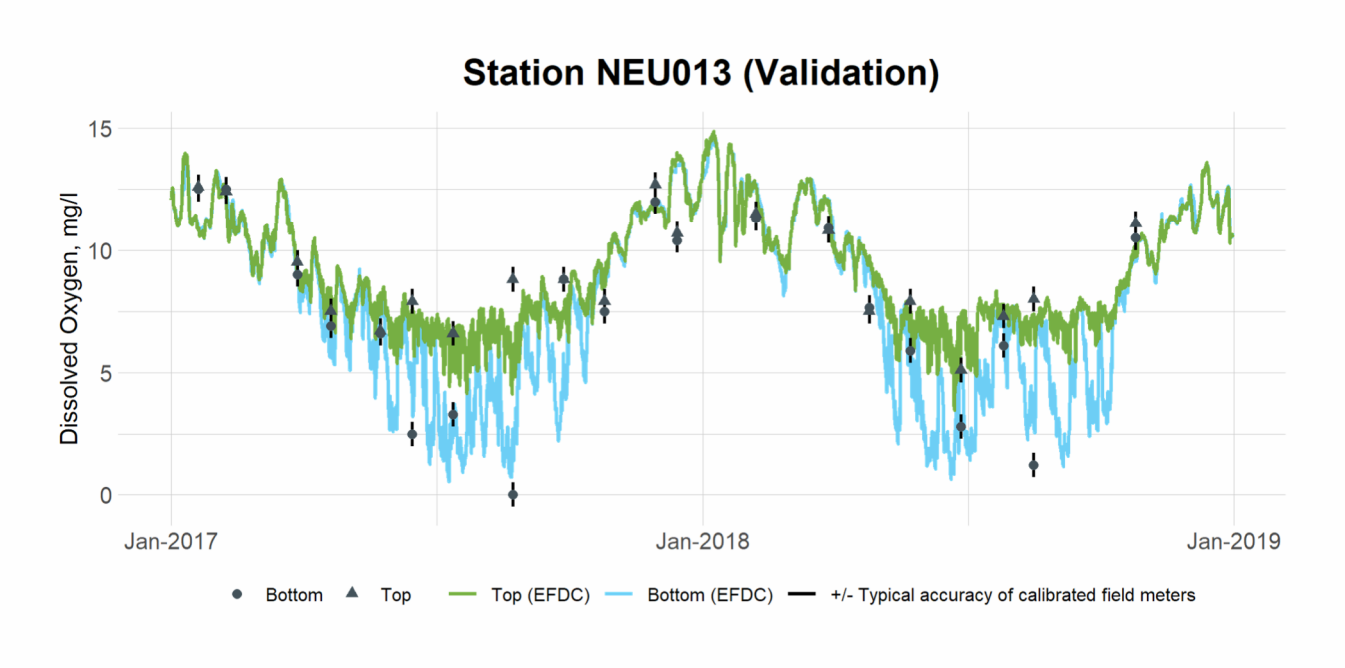

Figure 4-16 Validation Plot of Top and Bottom DO at Station NEU013

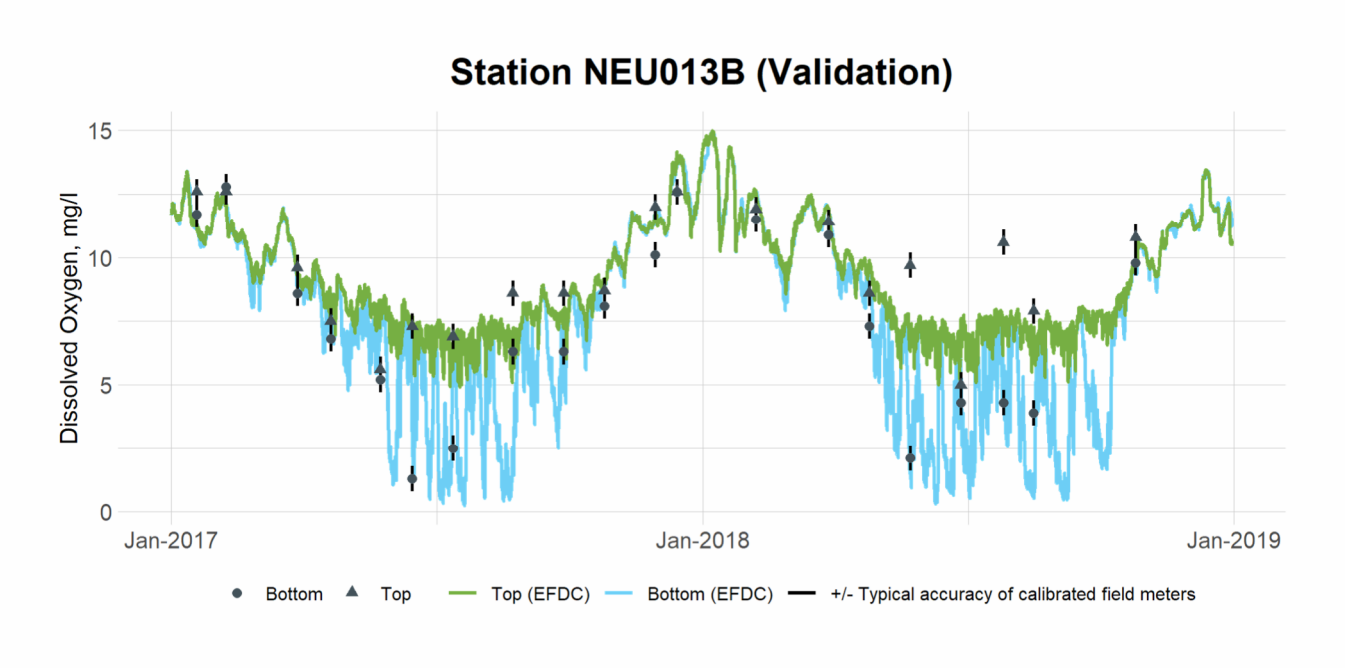

Figure 4-17 Validation Plot of Top and Bottom DO at Station NEU013B

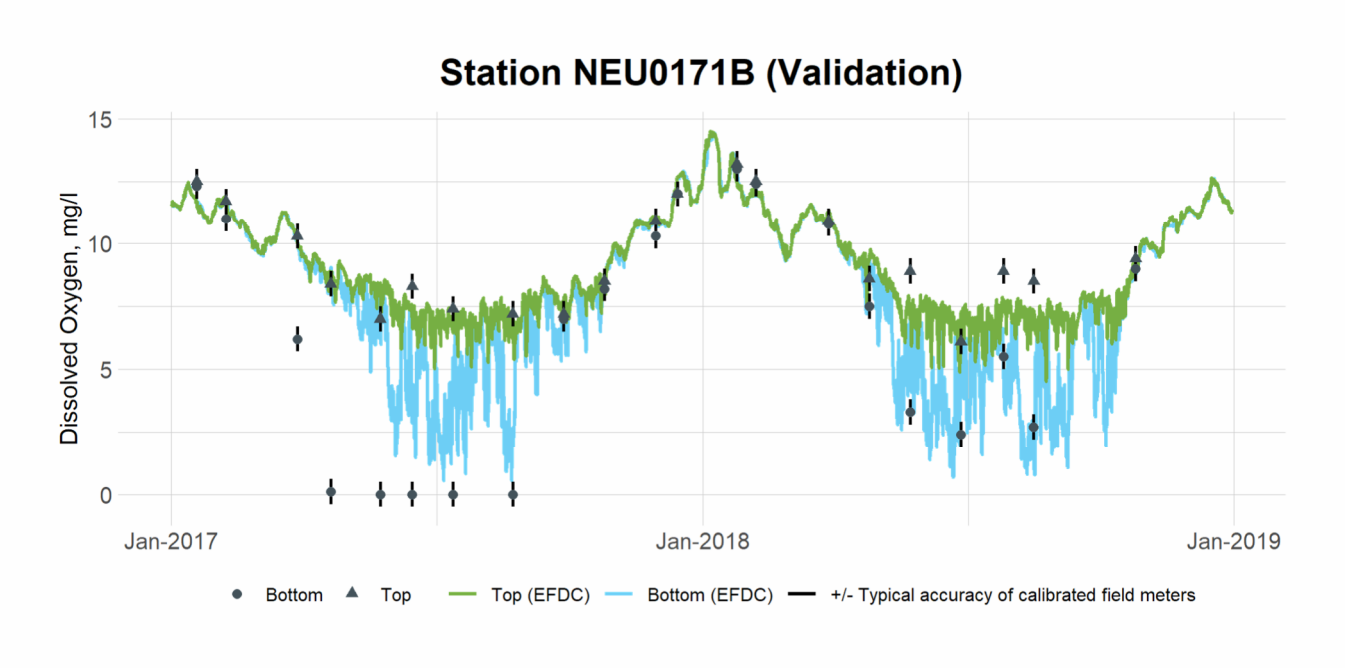

Figure 4-18 Validation Plot of Top and Bottom DO at Station NEU0171B

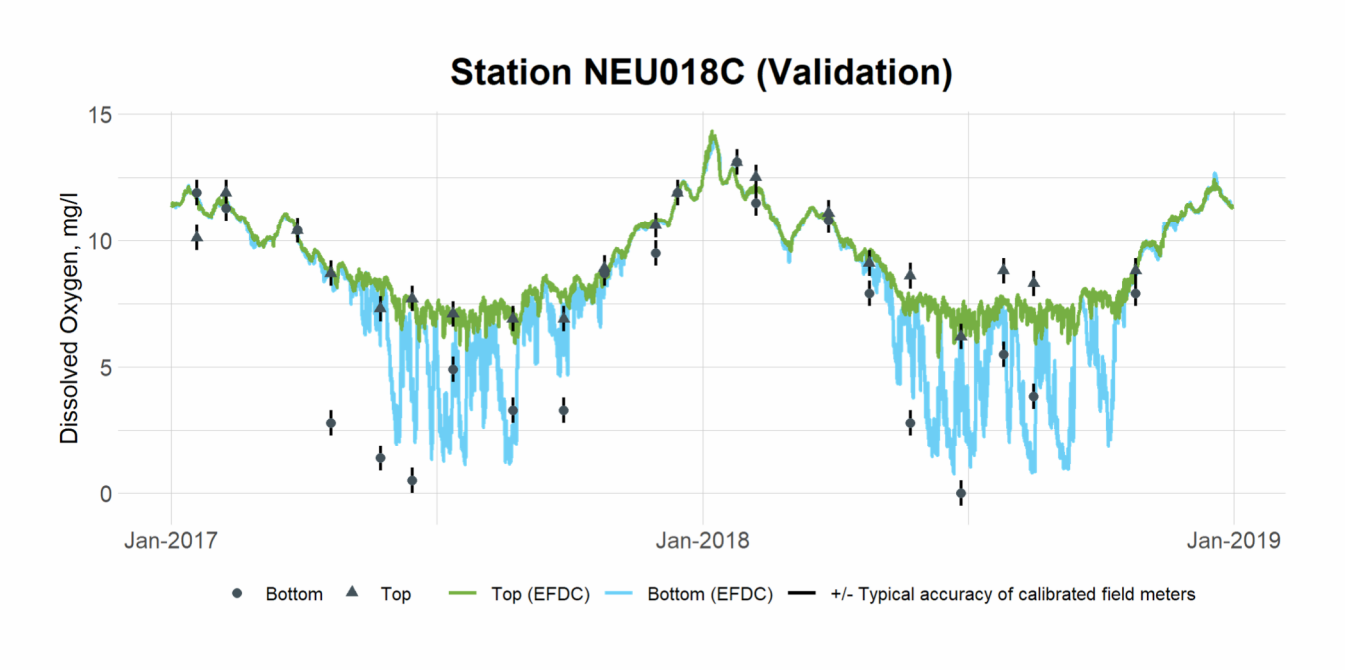

Figure 4-19 Validation Plot of Top and Bottom DO at Station NEU018C

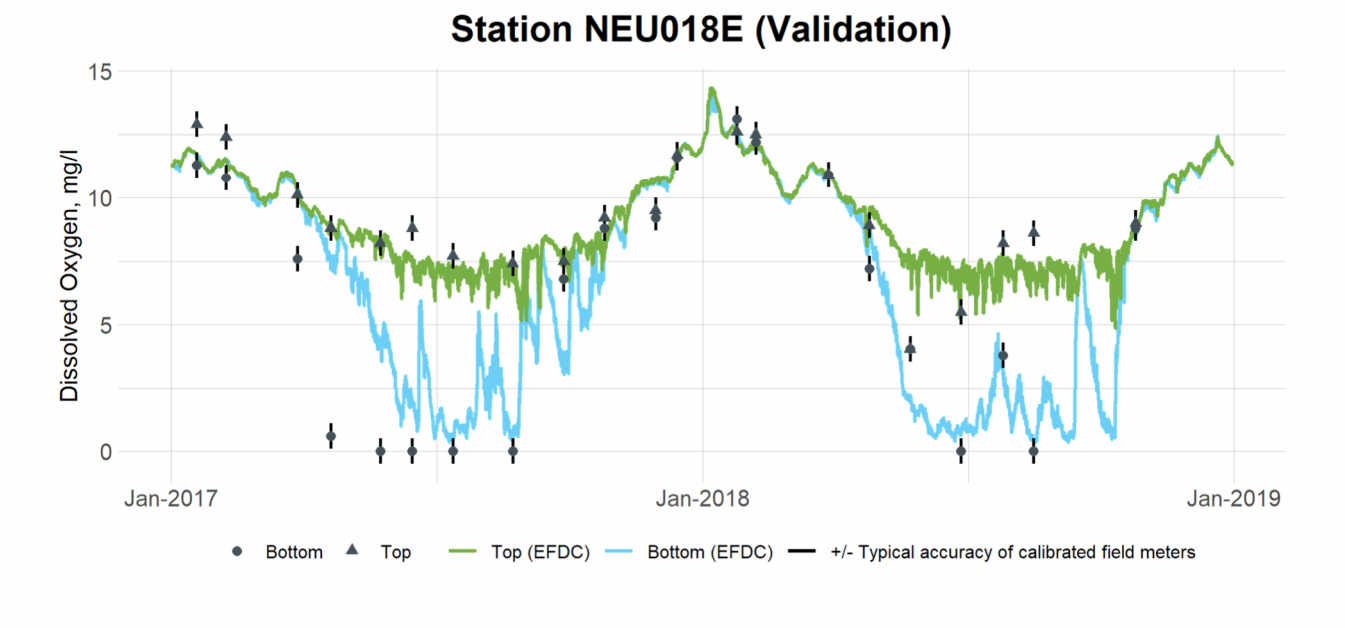

Figure 4-20 Validation Plot of Top and Bottom DO at Station NEU018E

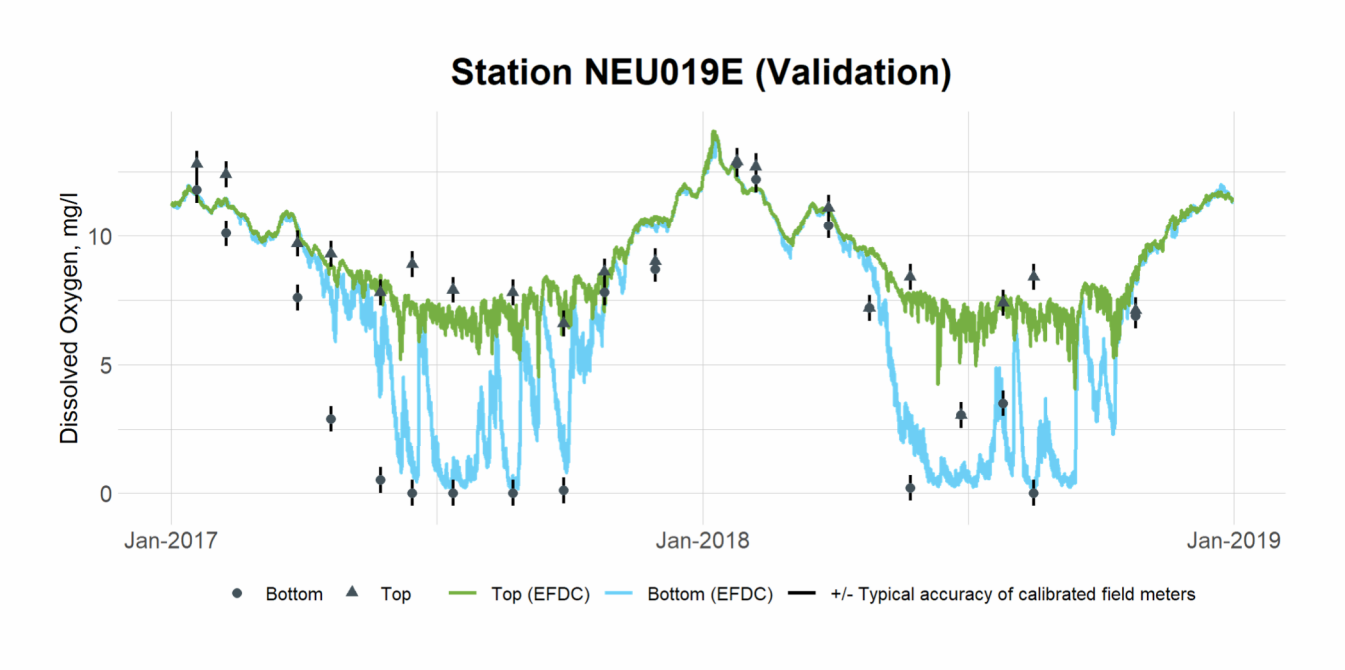

Figure 4-21 Validation Plot of Top and Bottom DO at Station NEU019E

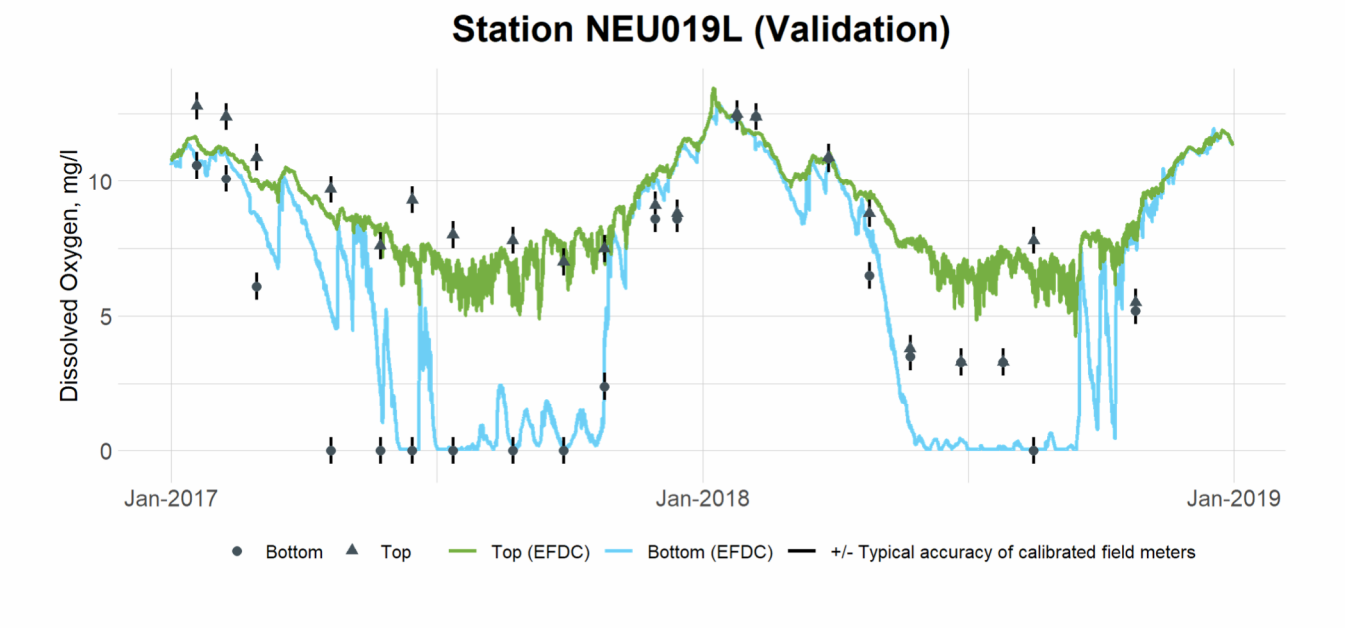

Figure 4-22 Validation Plot of Top and Bottom DO at Station NEU019L

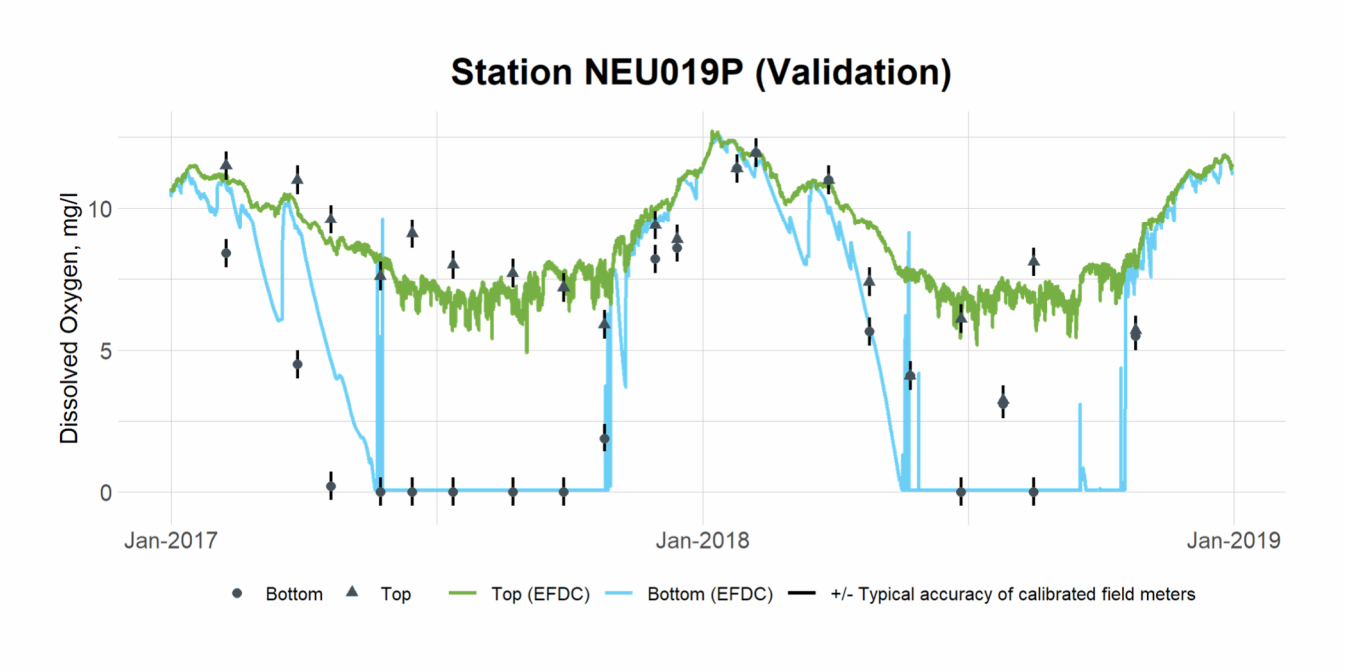

Figure 4-23 Validation Plot of Top and Bottom DO at Station NEU019P

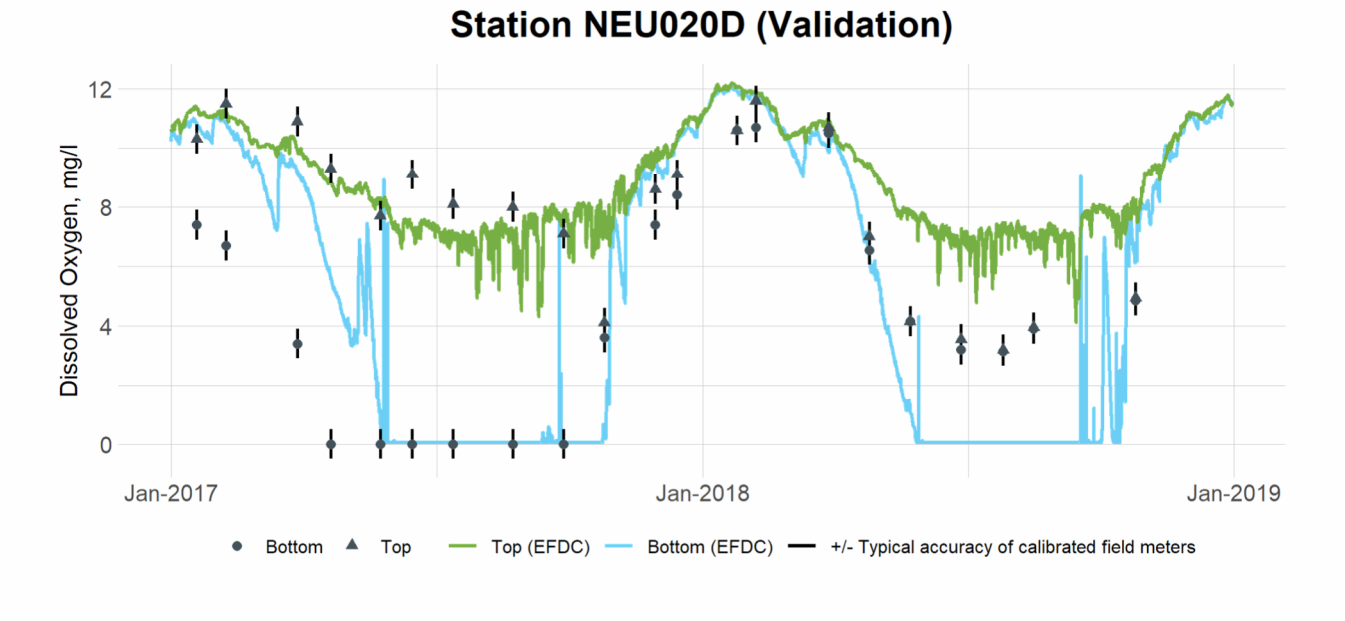

Figure 4-24 Validation Plot of Top and Bottom DO at Station NEU020D

5. TP

5.1 TP Calibration

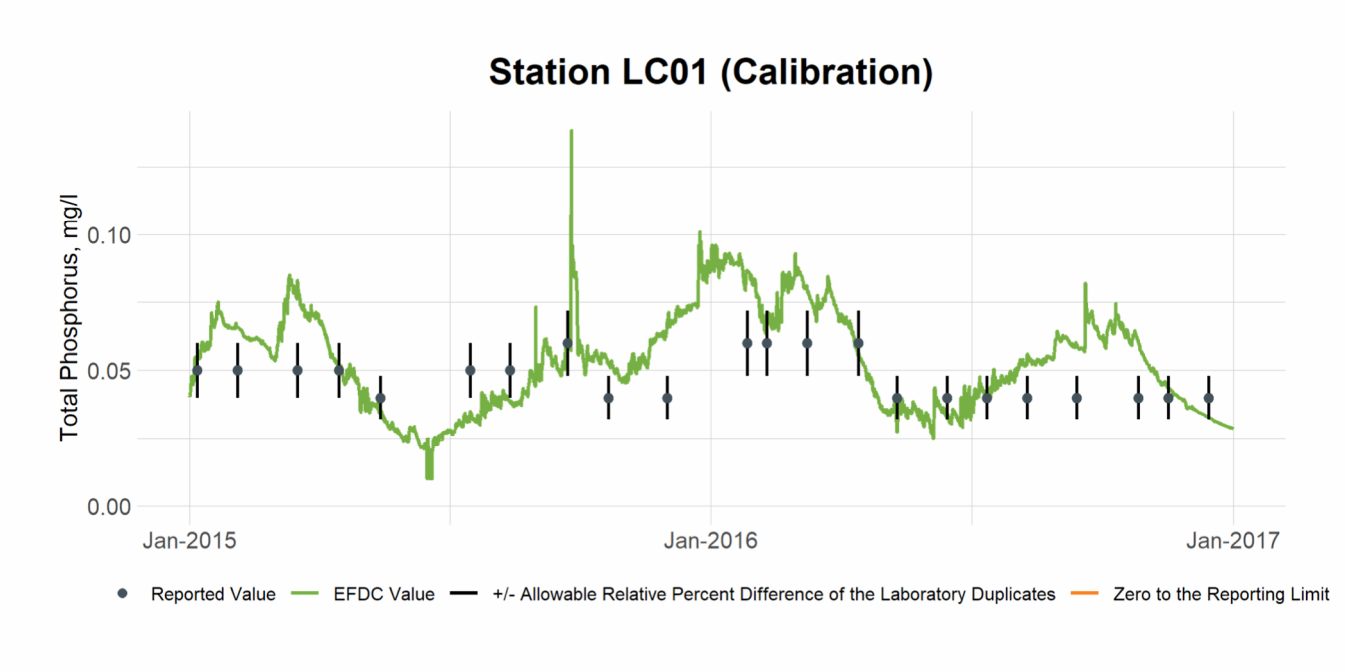

Figure 5-1 Calibration Plot of TP at Station LC01

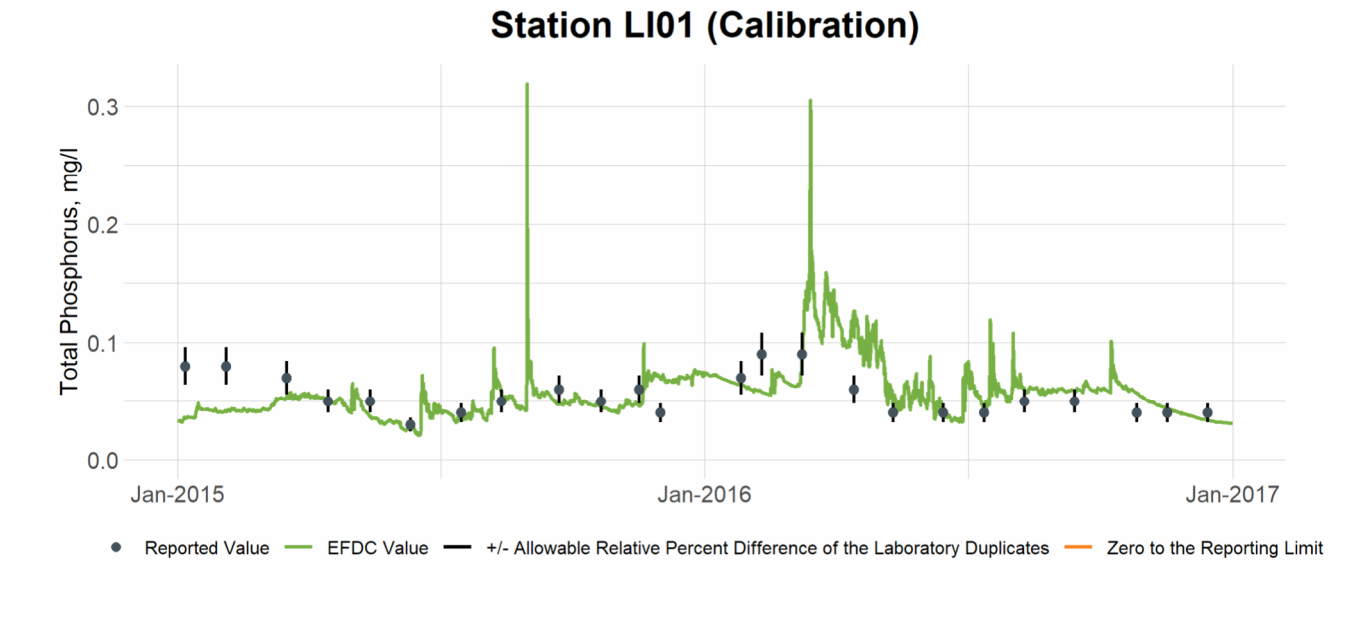

Figure 5-2 Calibration Plot of TP at Station LI01

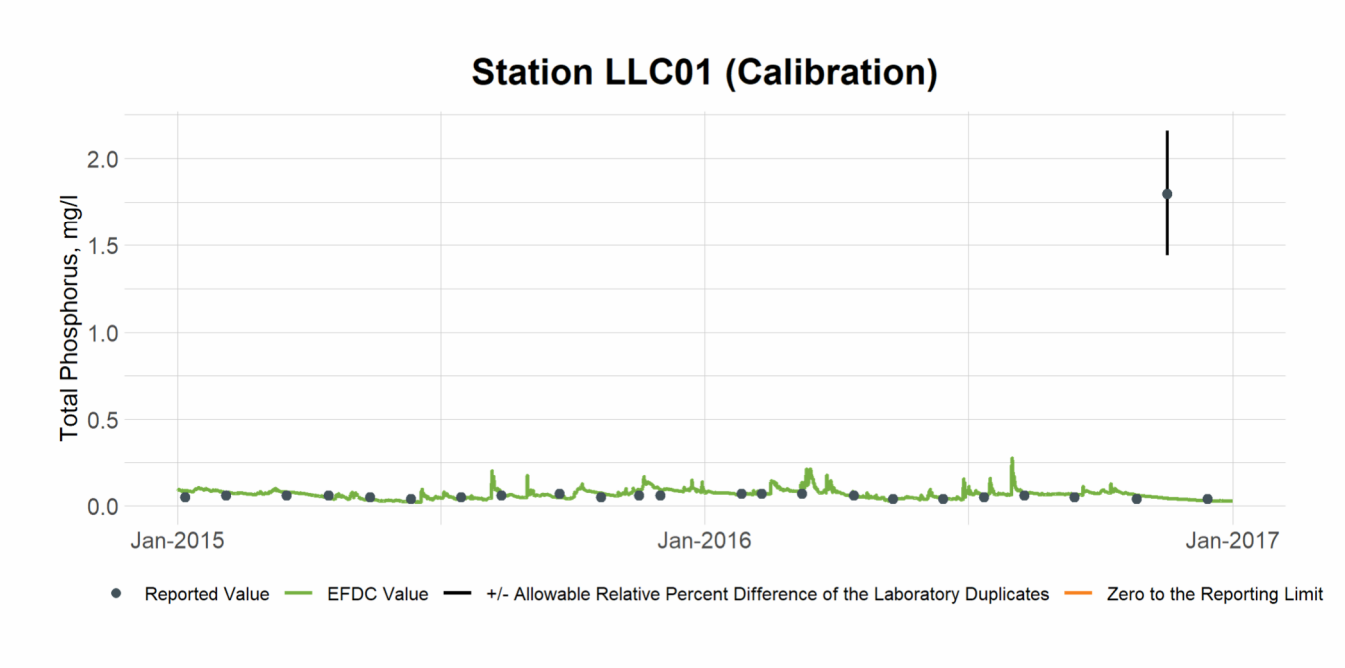

Figure 5-3 Calibration Plot of TP at Station LLC01

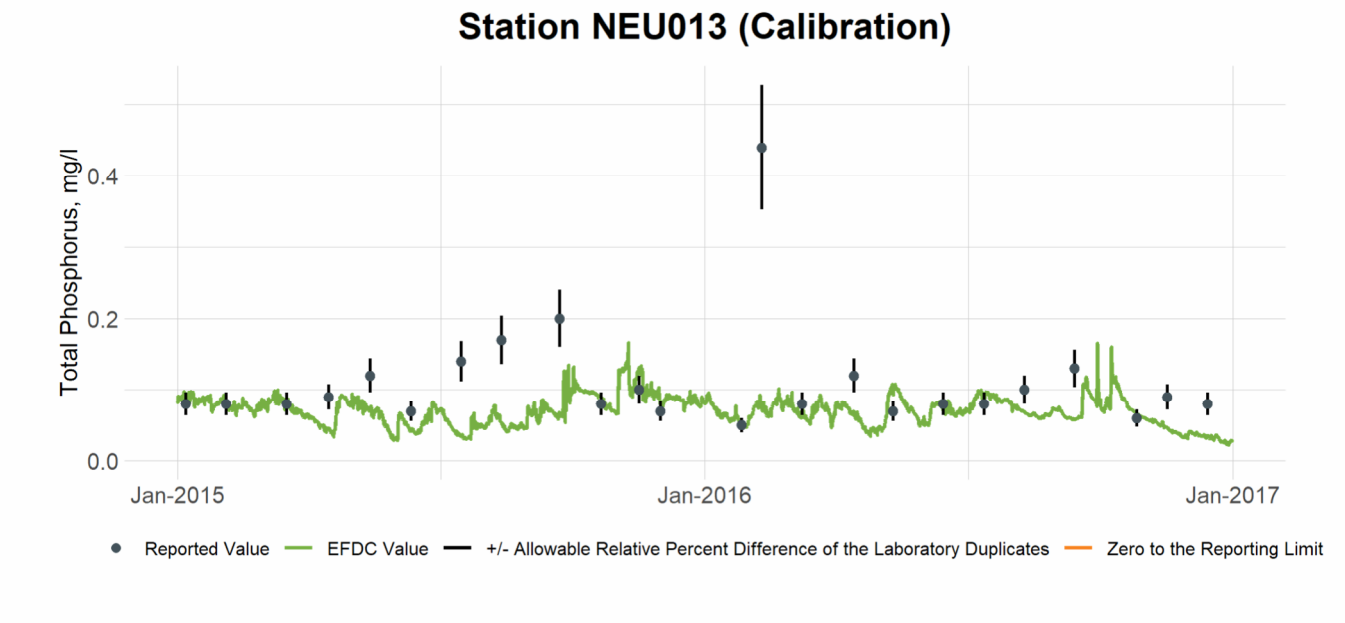

Figure 5-4 Calibration Plot of TP at Station NEU013

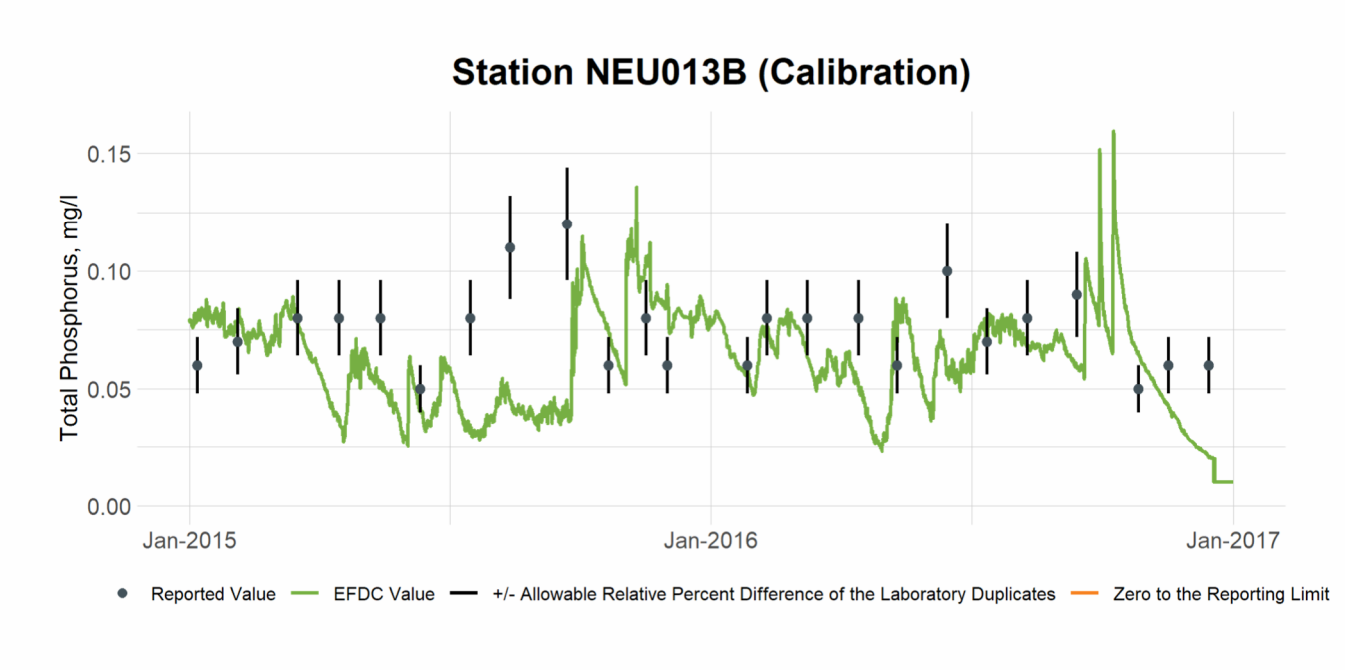

Figure 5-5 Calibration Plot of TP at Station NEU013B

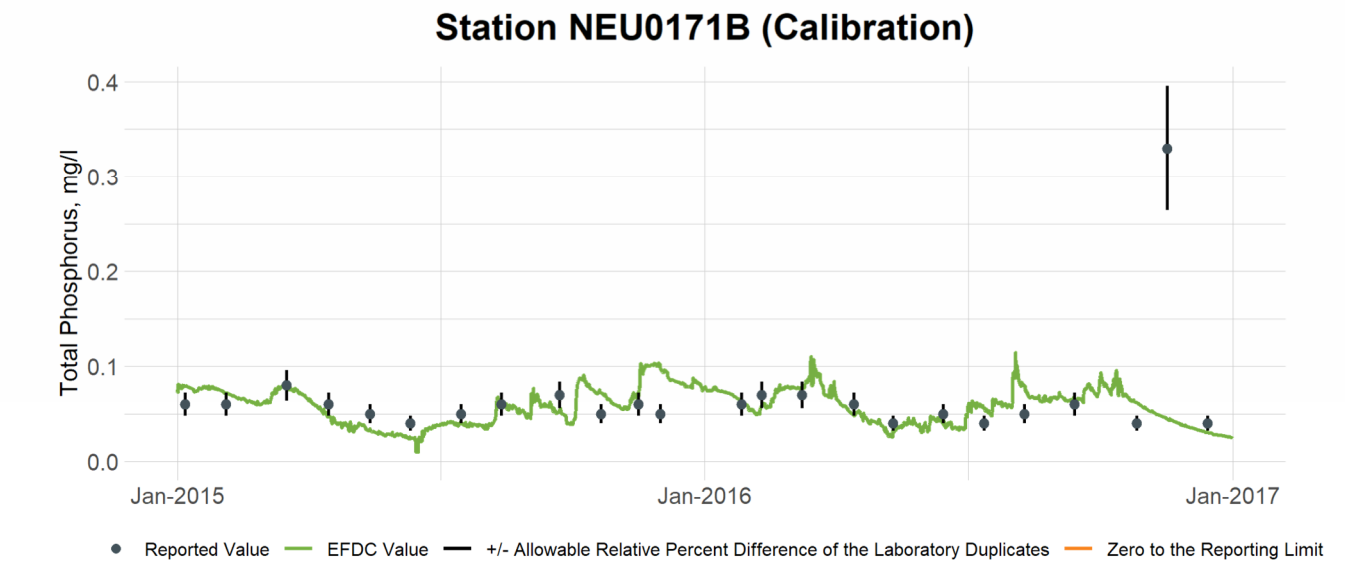

Figure 5-6 Calibration Plot of TP at Station NEU0171B

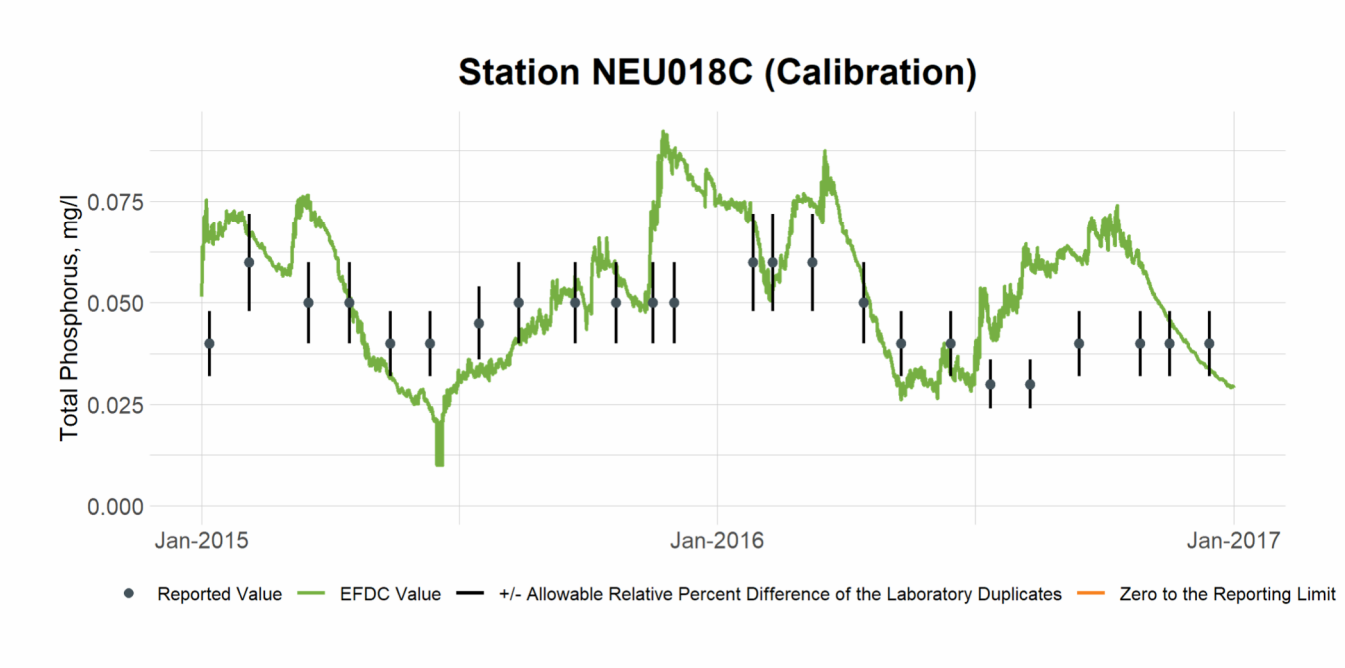

Figure 5-7 Calibration Plot of TP at Station NEU018C

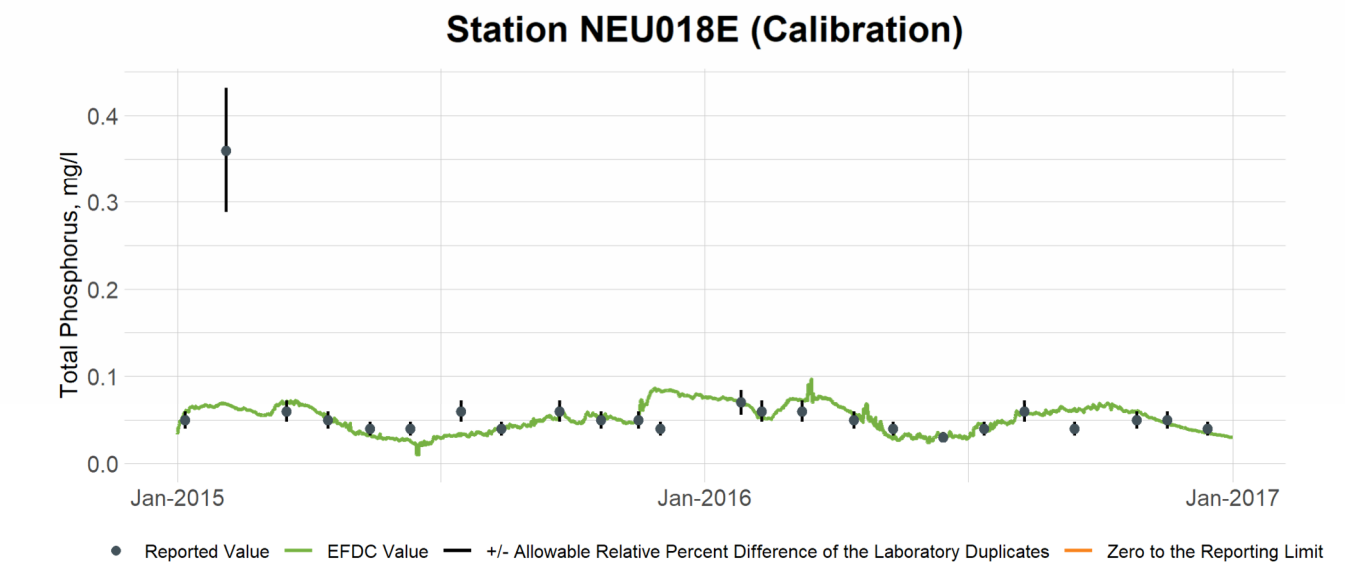

Figure 5-8 Calibration Plot of TP at Station NEU018E

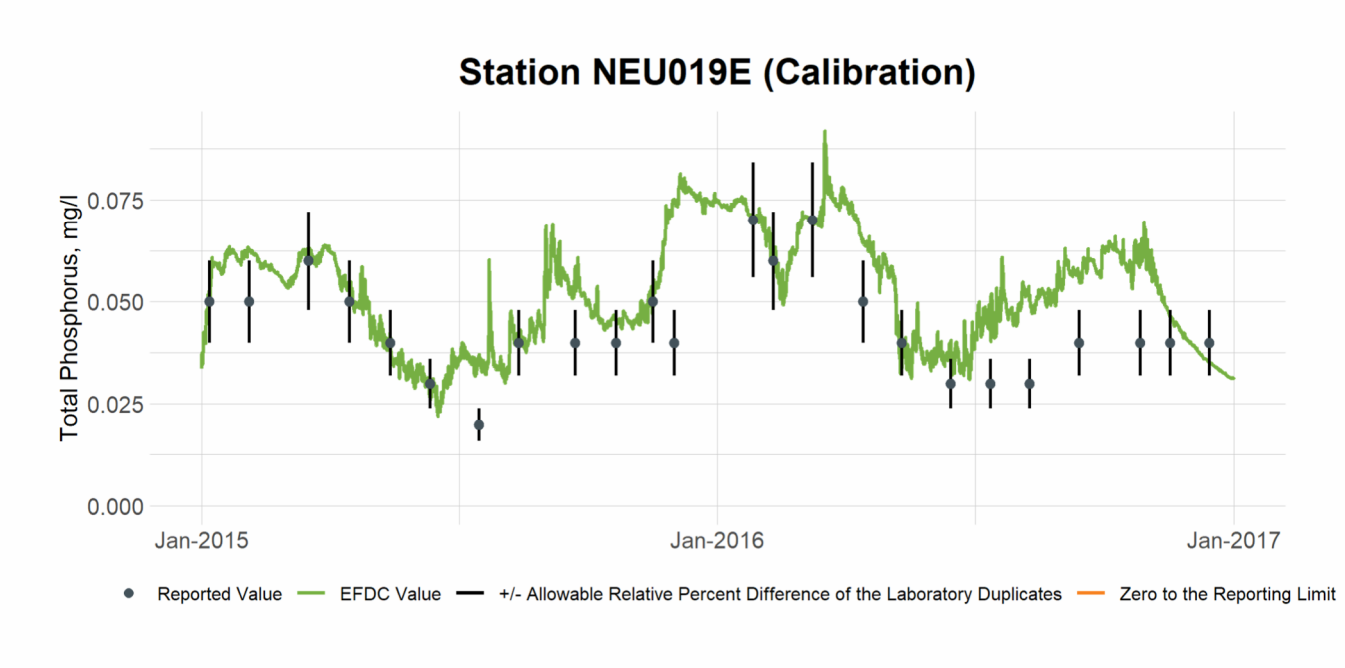

Figure 5-9 Calibration Plot of TP at Station NEU019E

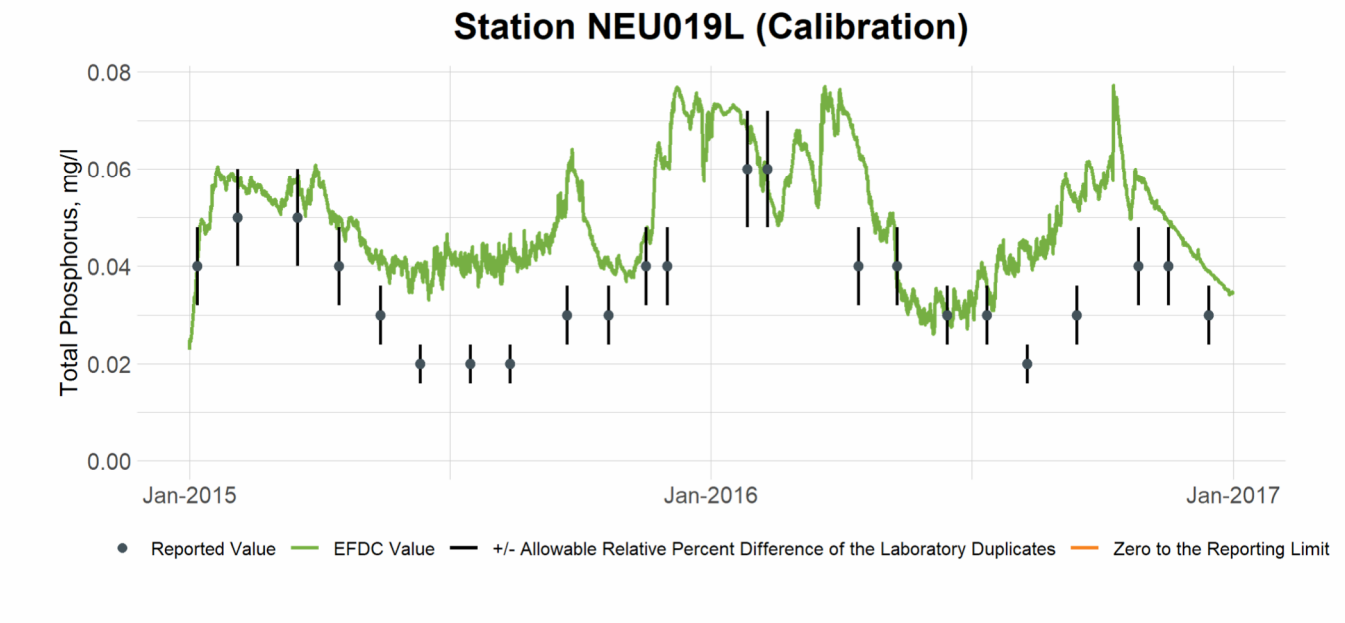

Figure 5-10 Calibration Plot of TP at Station NEU019L

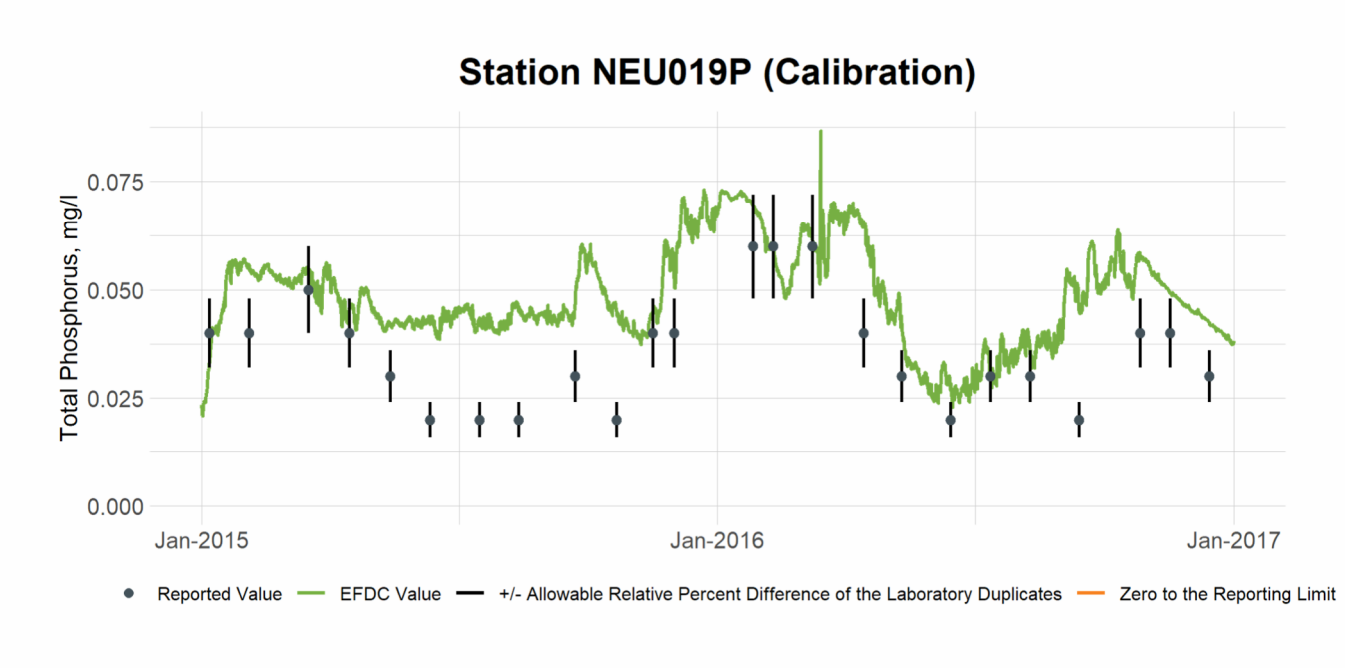

Figure 5-11 Calibration Plot of TP at Station NEU019P

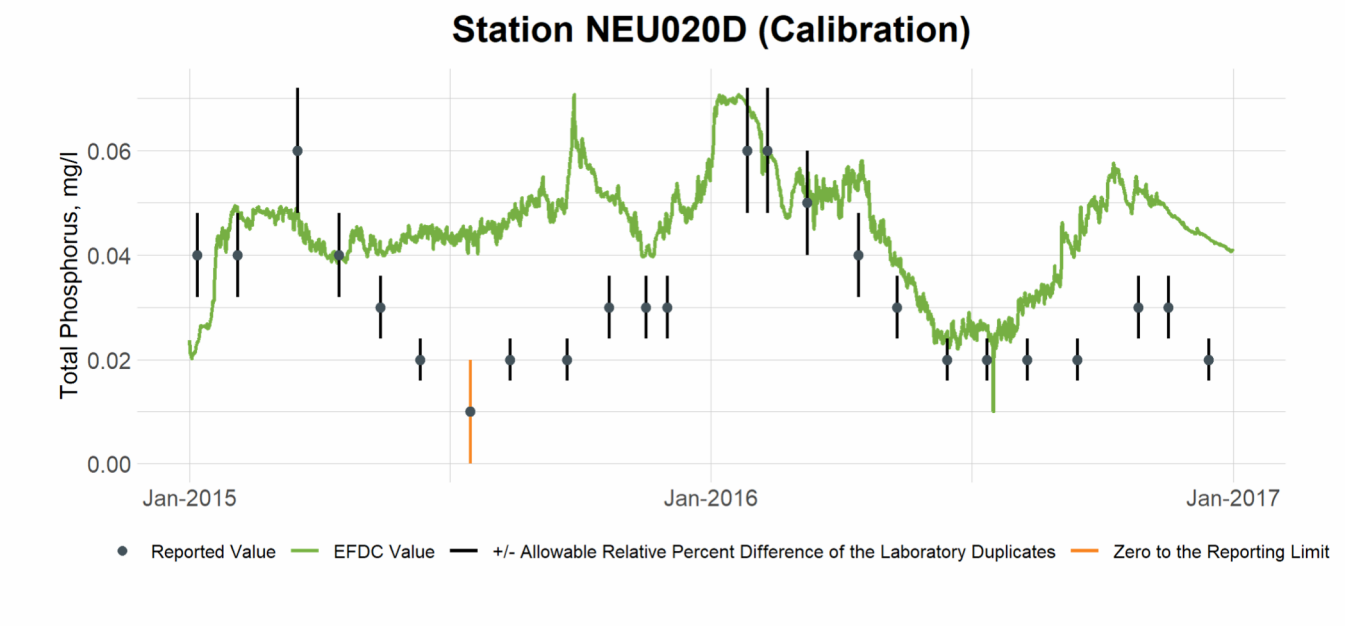

Figure 5-12 Calibration Plot of TP at Station NEU020D

5.2 TP Validation

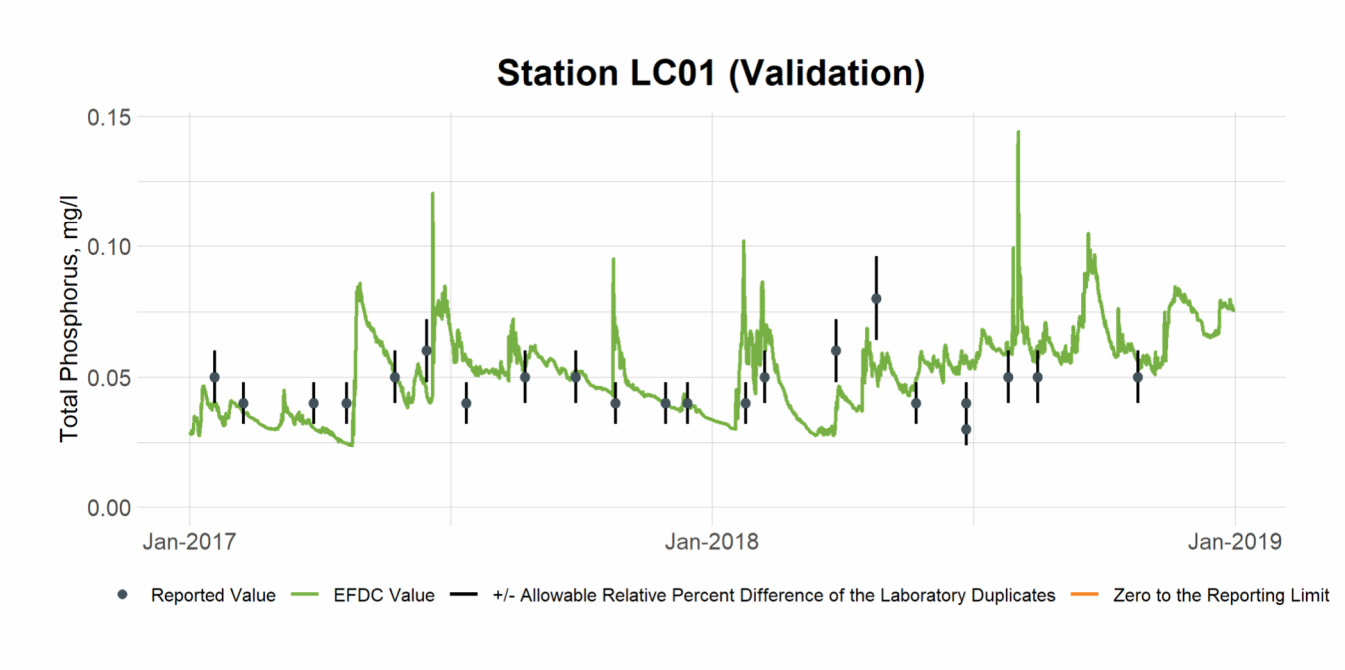

Figure 5-13 Validation Plot of TP at Station LC01

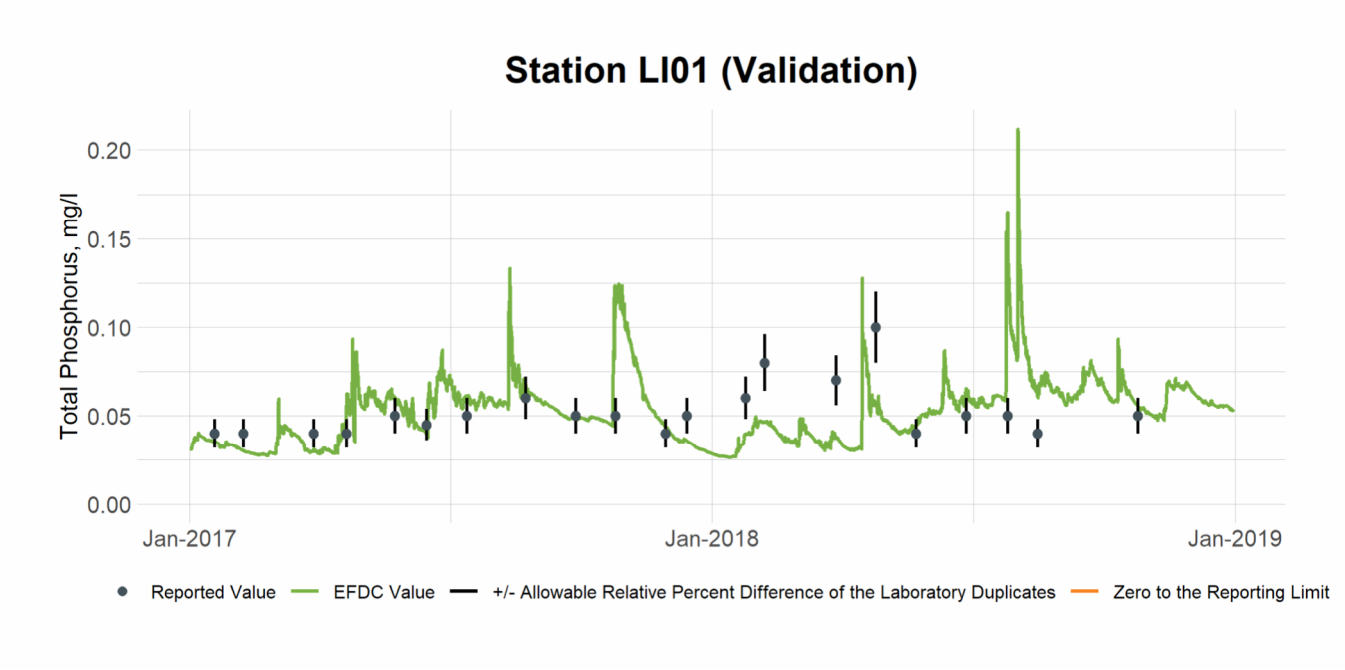

Figure 5-14 Validation Plot of TP at Station LI01

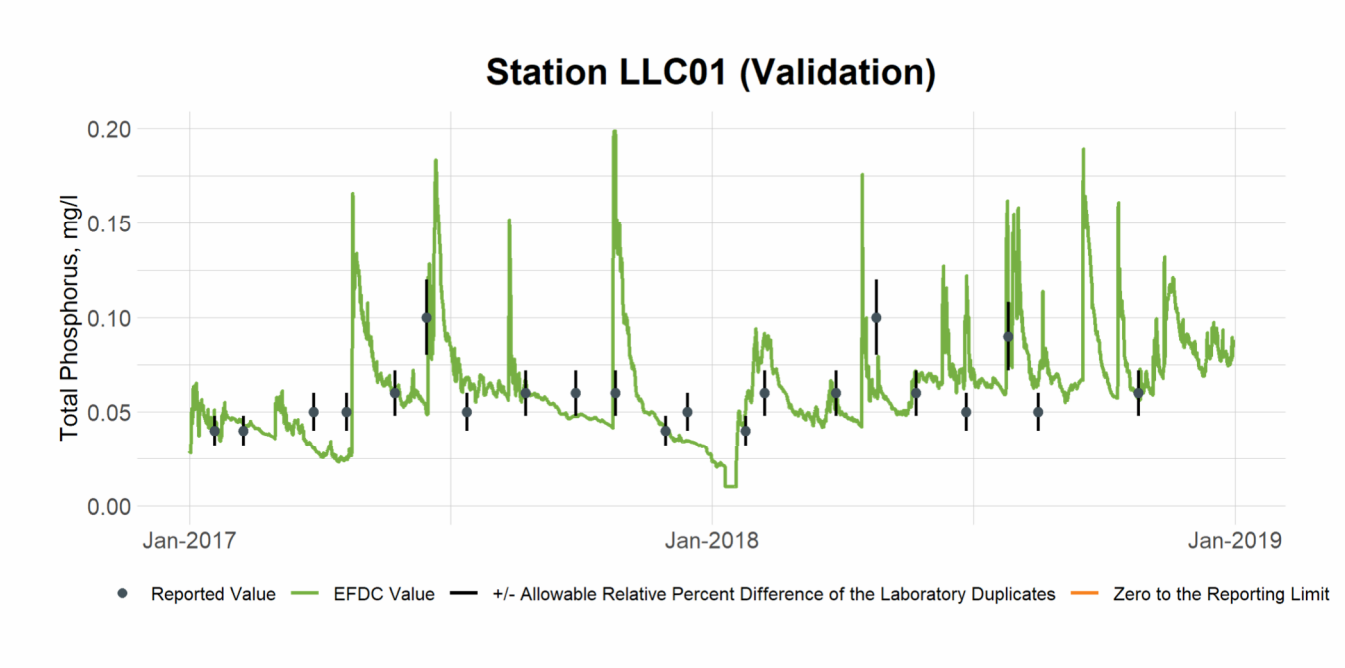

Figure 5-15 Validation Plot of TP at Station LLC01

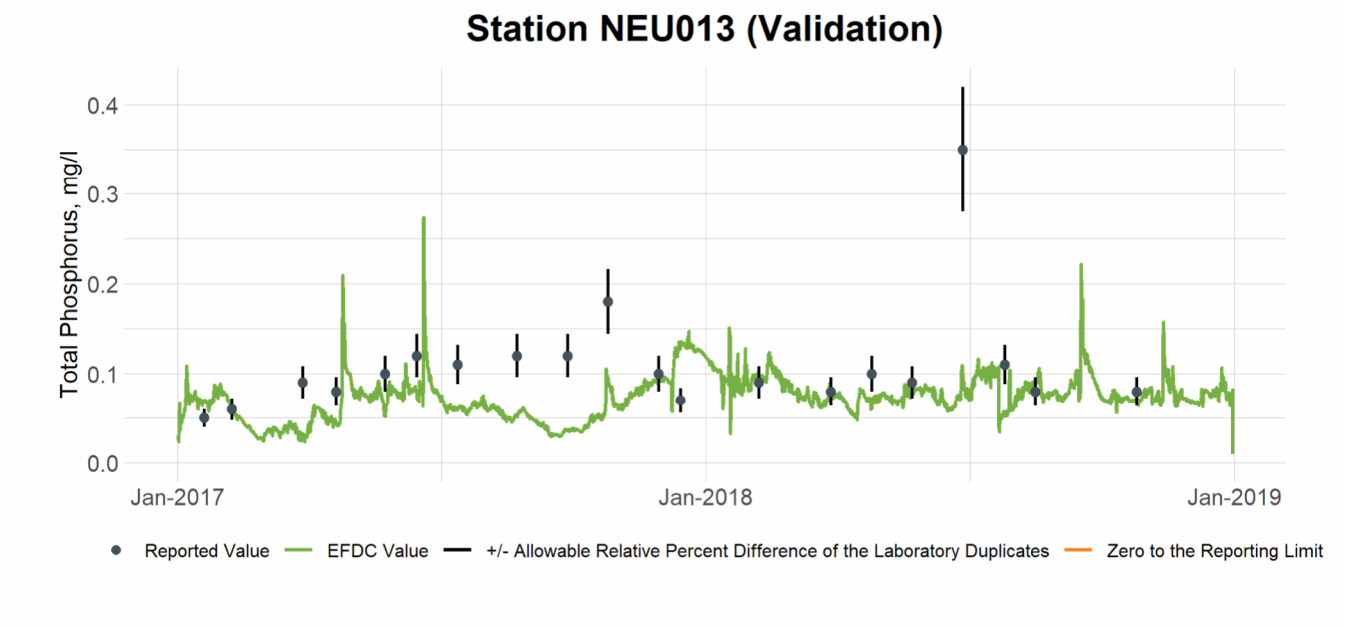

Figure 5-16 Validation Plot of TP at Station NEU013

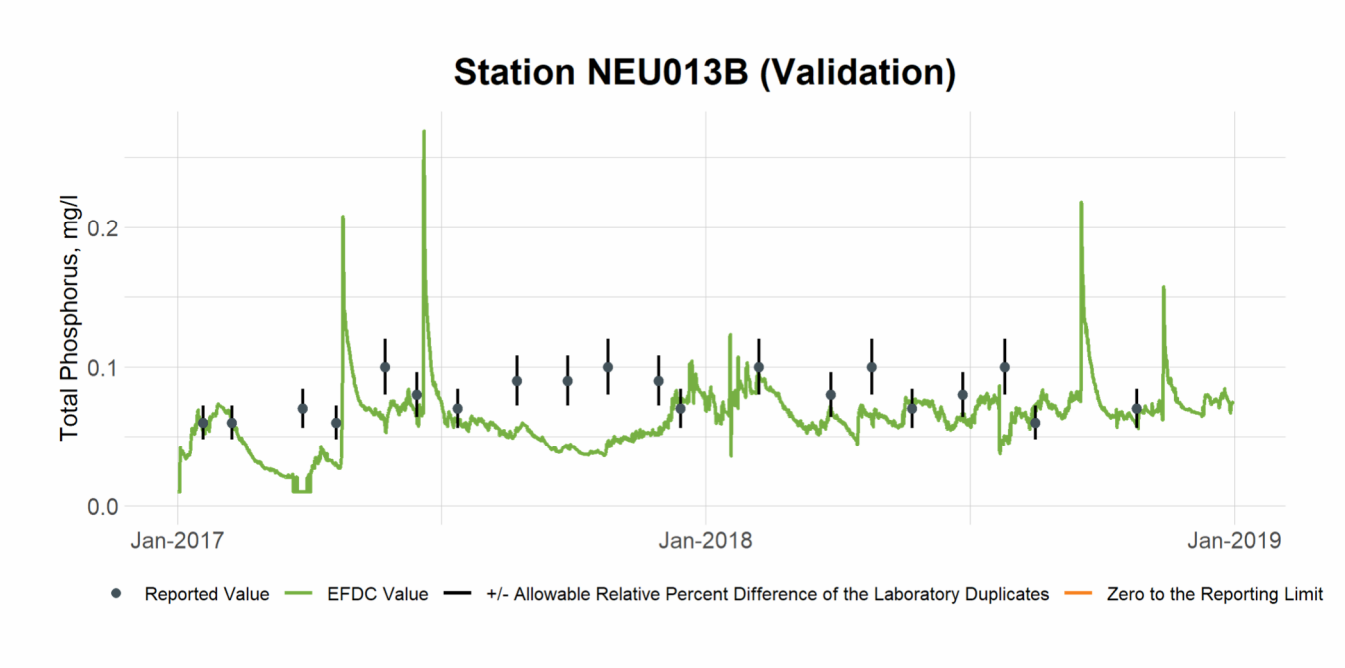

Figure 5-17 Validation Plot of TP at Station NEU013B

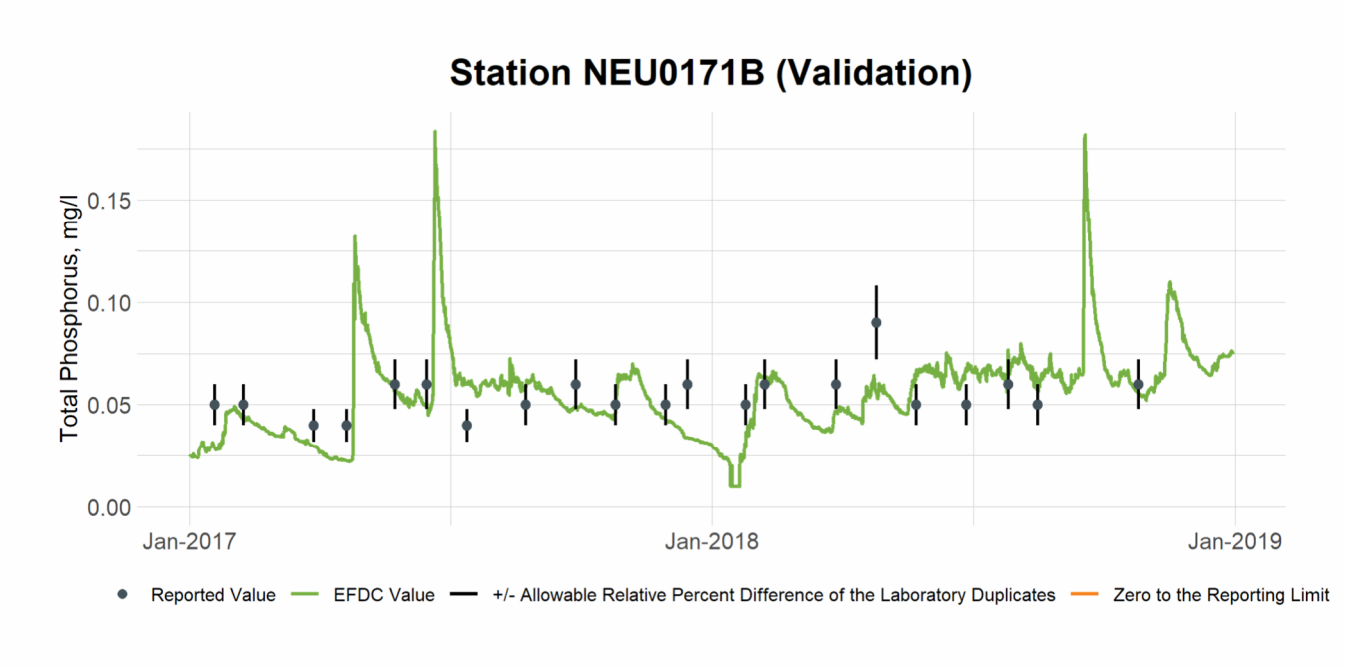

Figure 5-18 Validation Plot of TP at Station NEU0171B

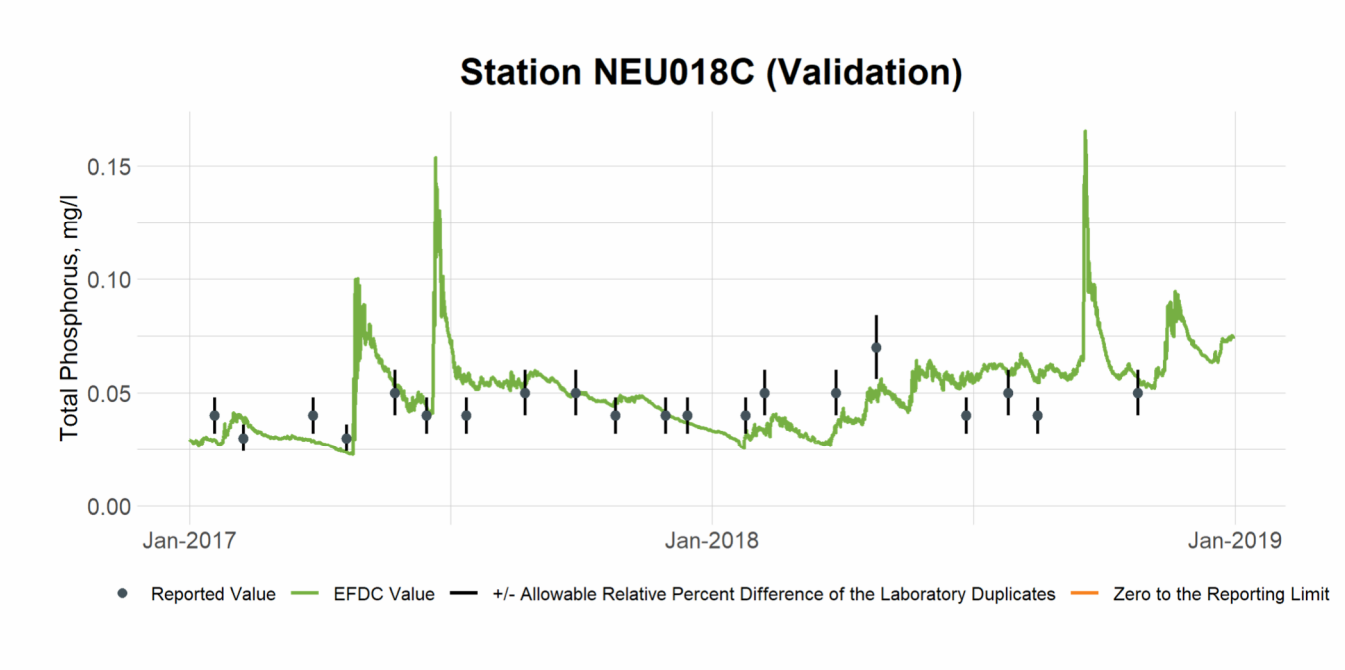

Figure 5-19 Validation Plot of TP at Station NEU018C

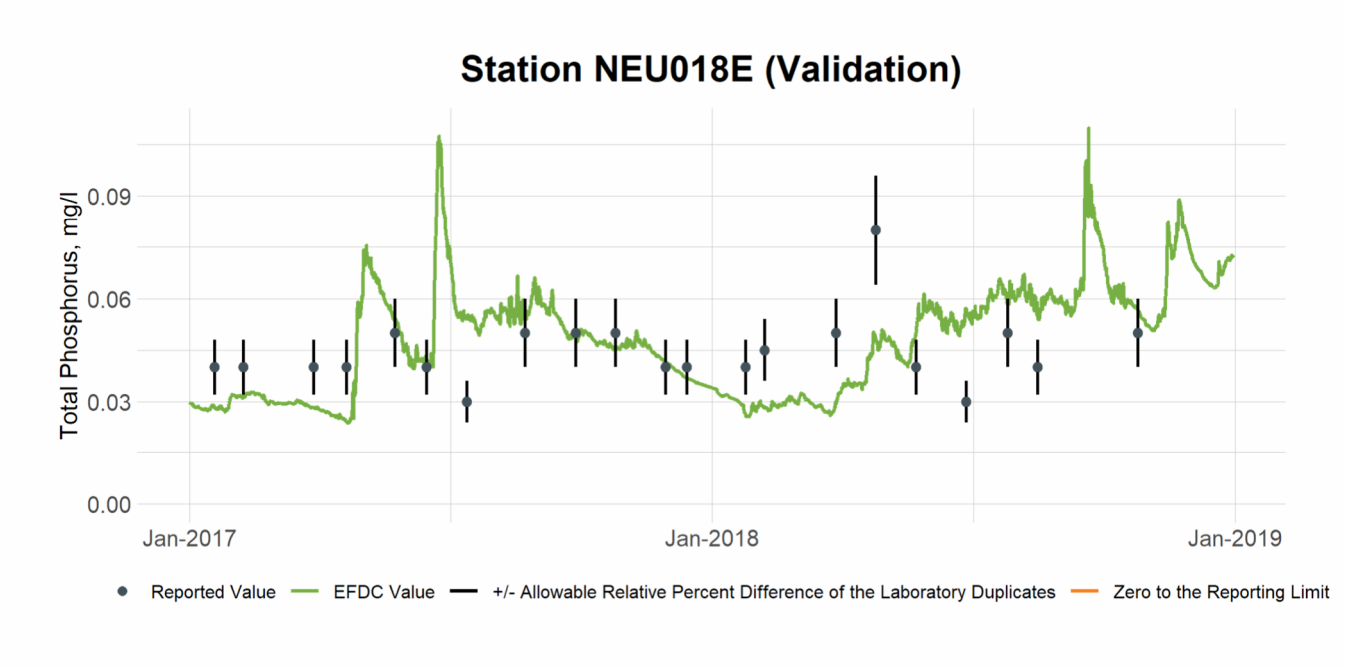

Figure 5-20 Validation Plot of TP at Station NEU018E

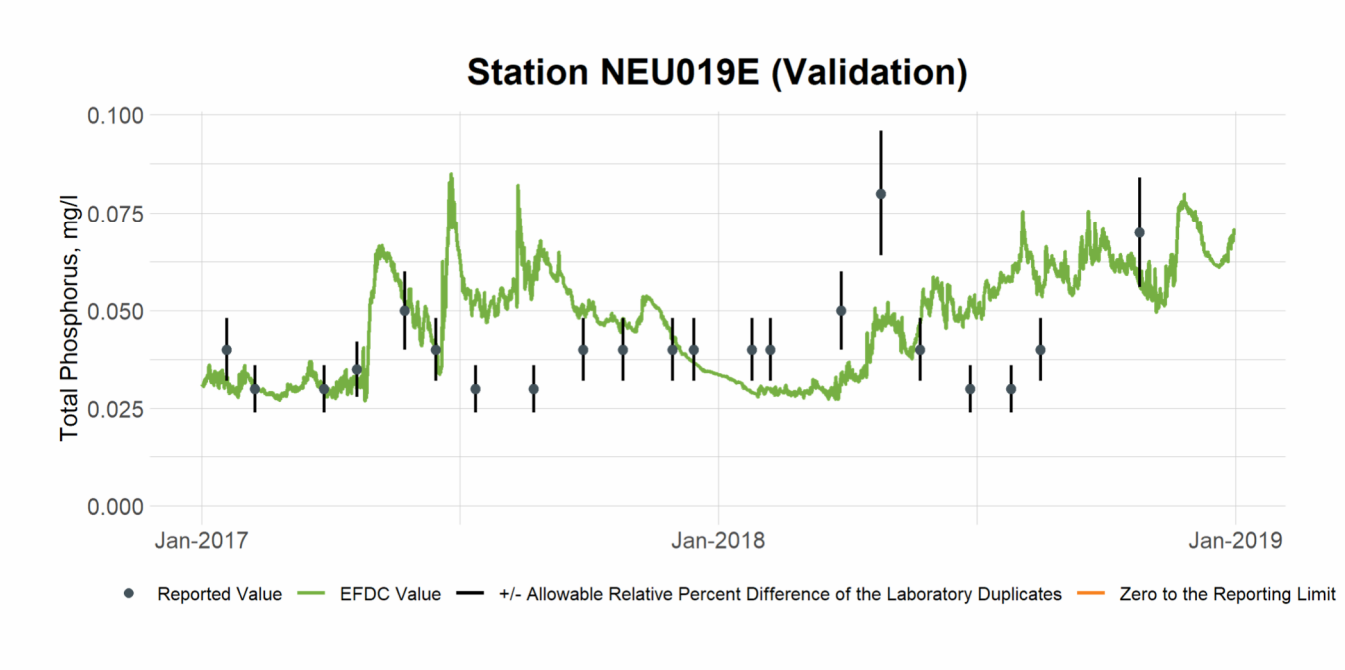

Figure 5-21 Validation Plot of TP at Station NEU019E

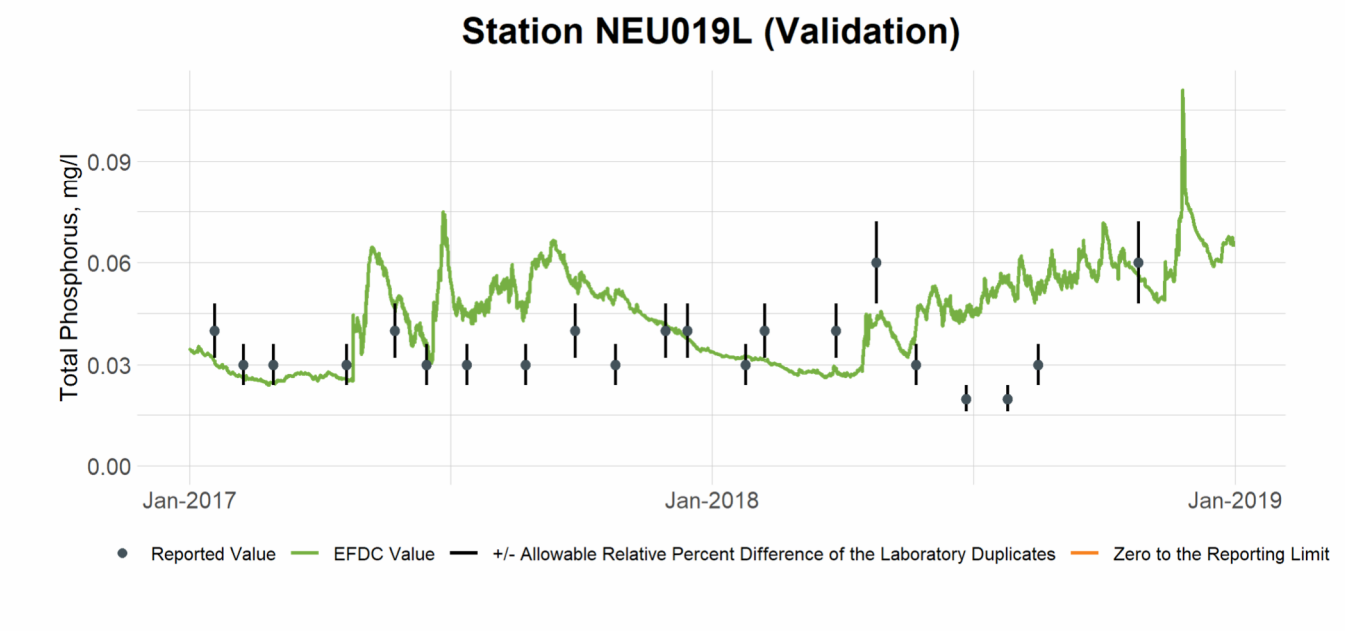

Figure 5-22 Validation Plot of TP at Station NEU019L

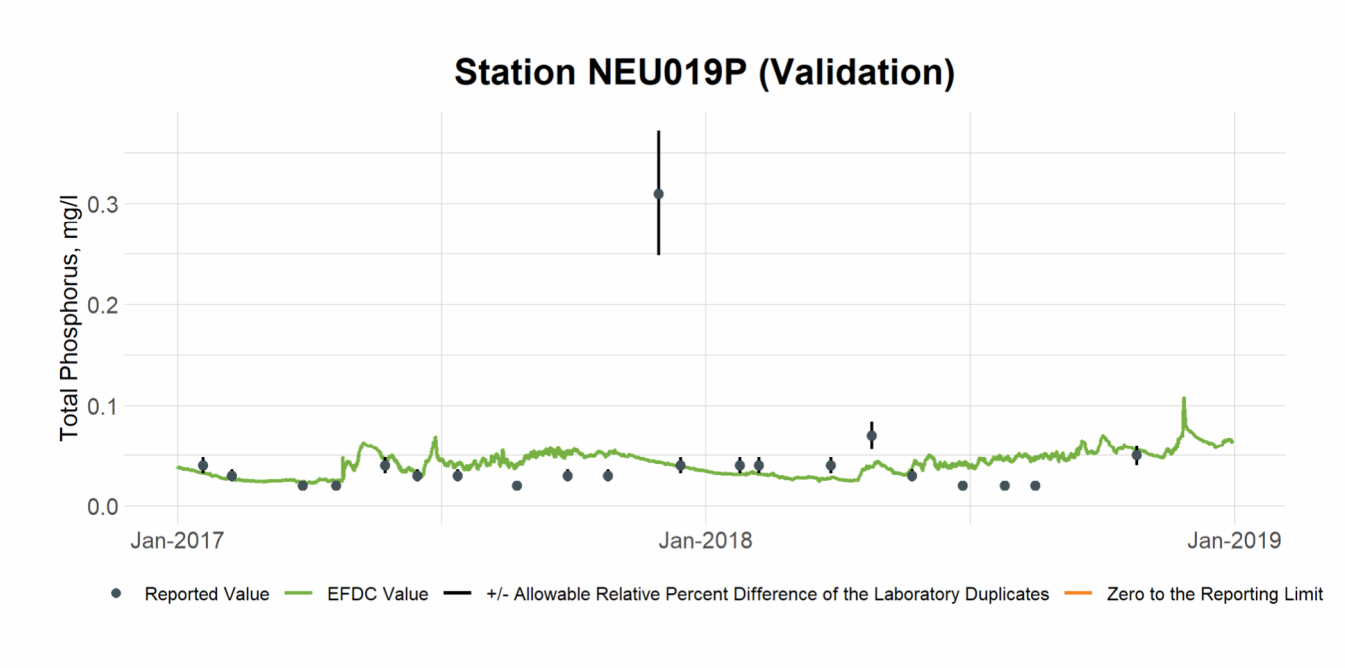

Figure 5-23 Validation Plot of TP at Station NEU019P

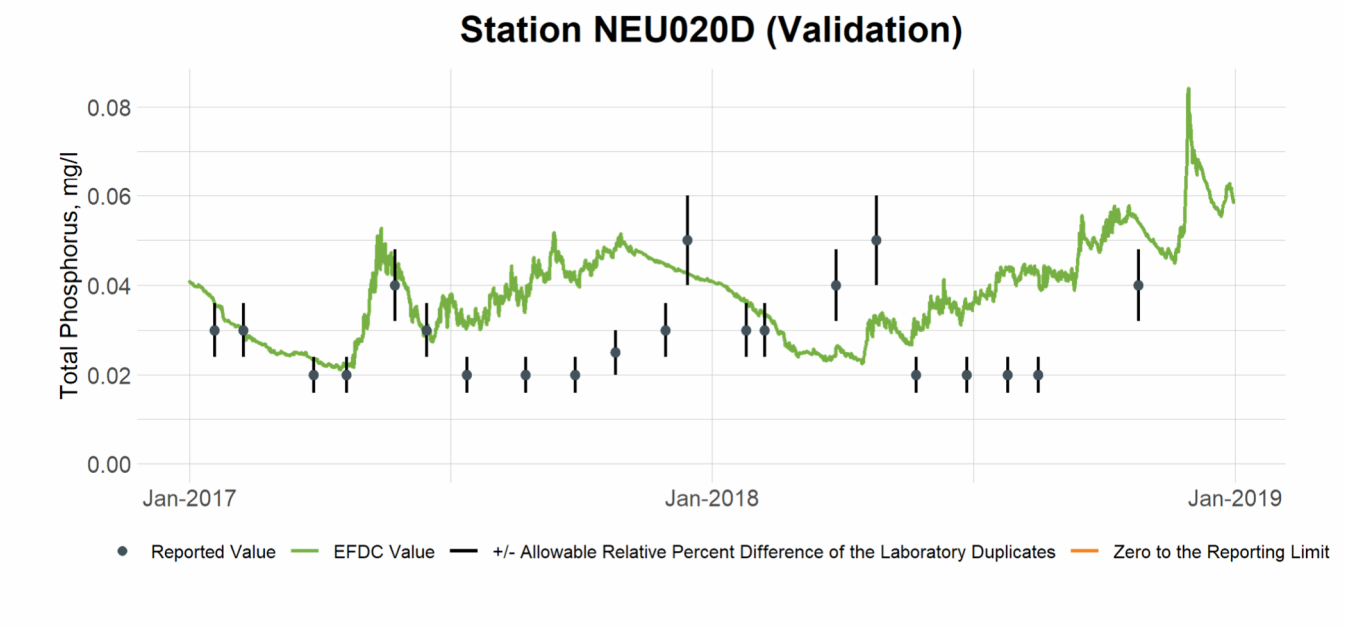

Figure 5-24 Validation Plot of TP at Station NEU020D

6. TN

6.1 TN Calibration

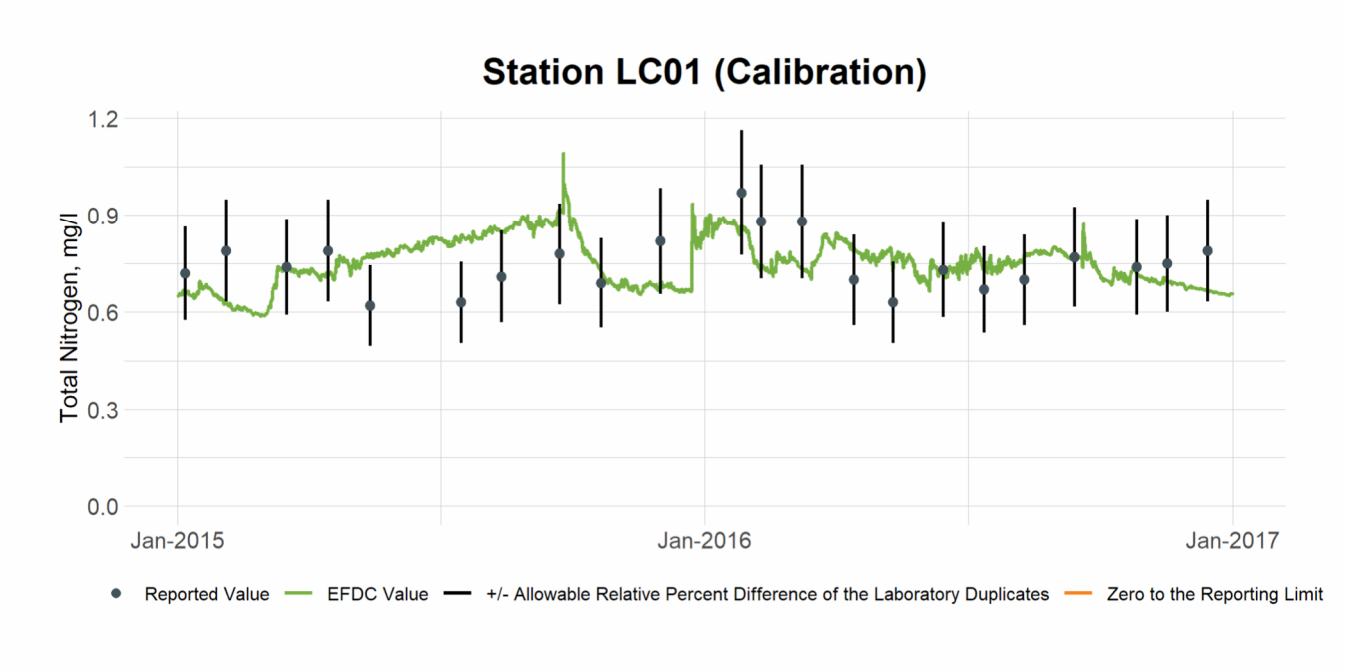

Figure 6-1 Calibration Plot of TN at Station LC01

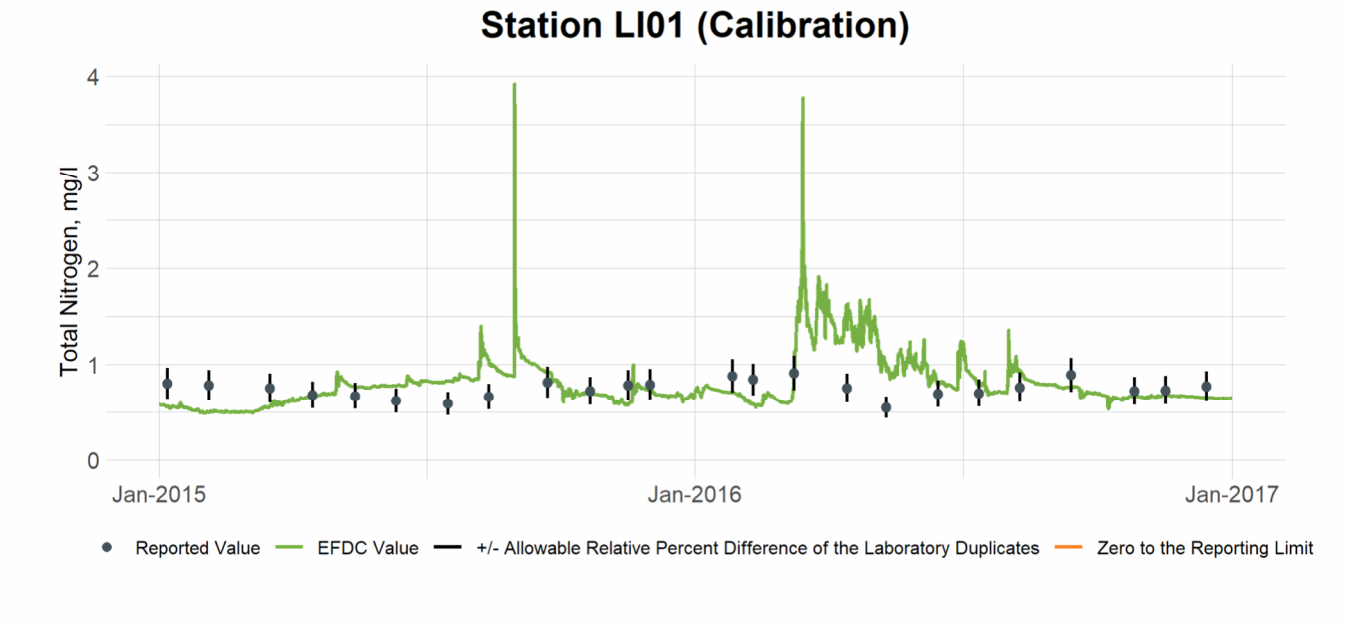

Figure 6-2 Calibration Plot of TN at Station LI01

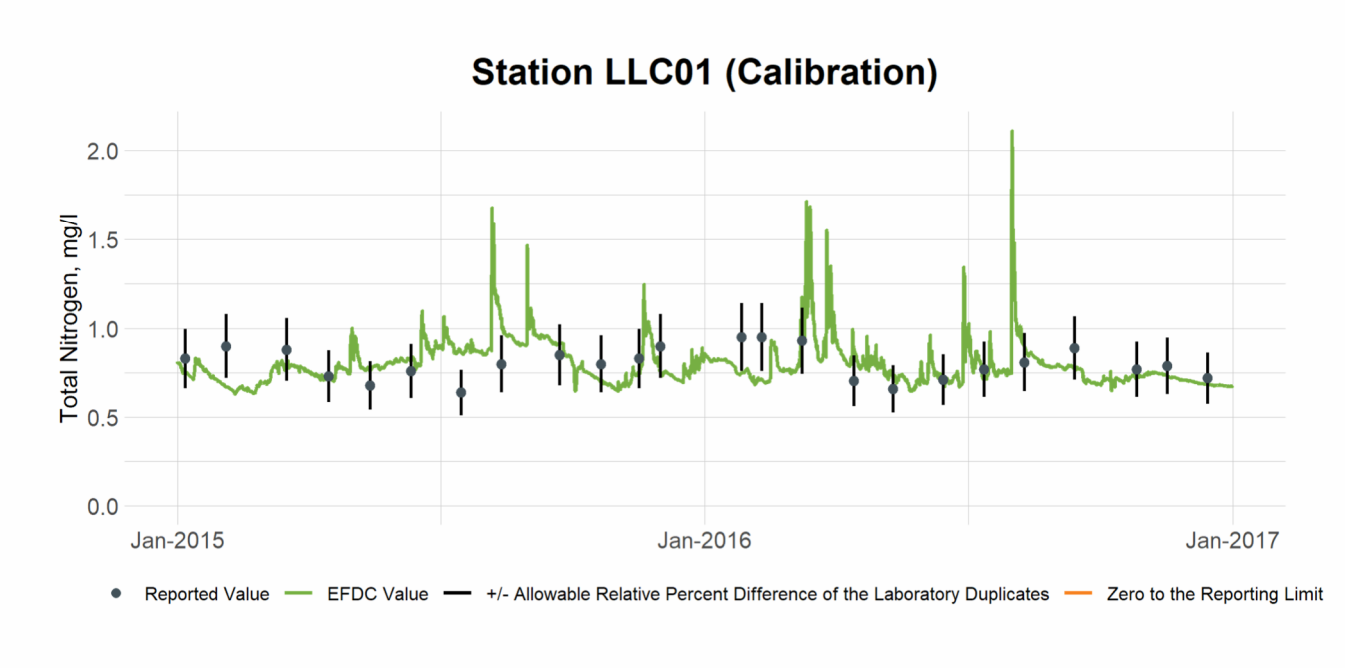

Figure 6-3 Calibration Plot of TN at Station LLC01

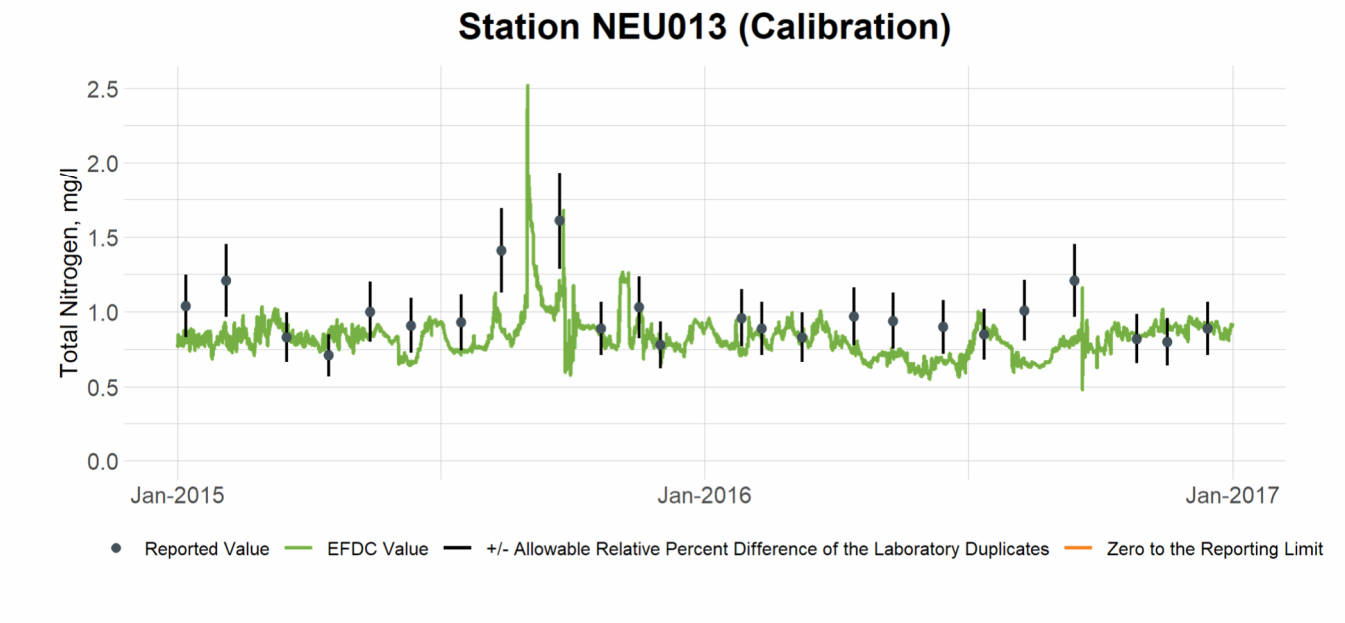

Figure 6-4 Calibration Plot of TN at Station NEU013

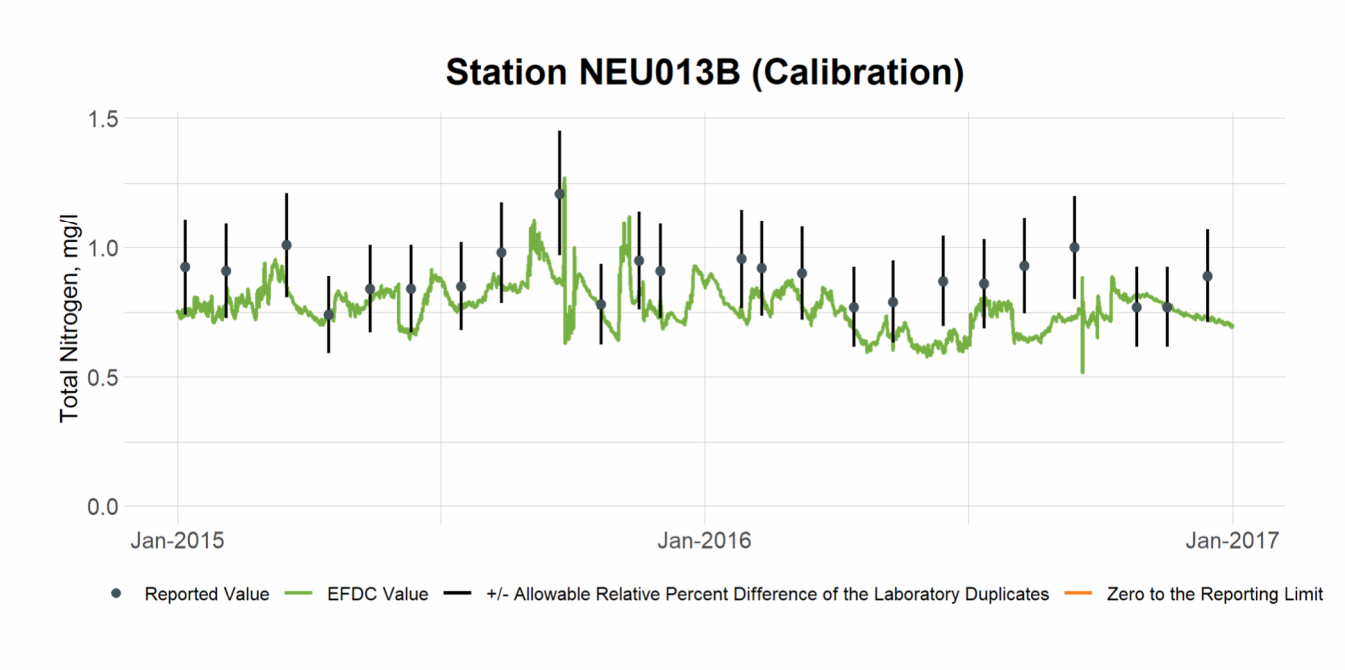

Figure 6-5 Calibration Plot of TN at Station NEU013B

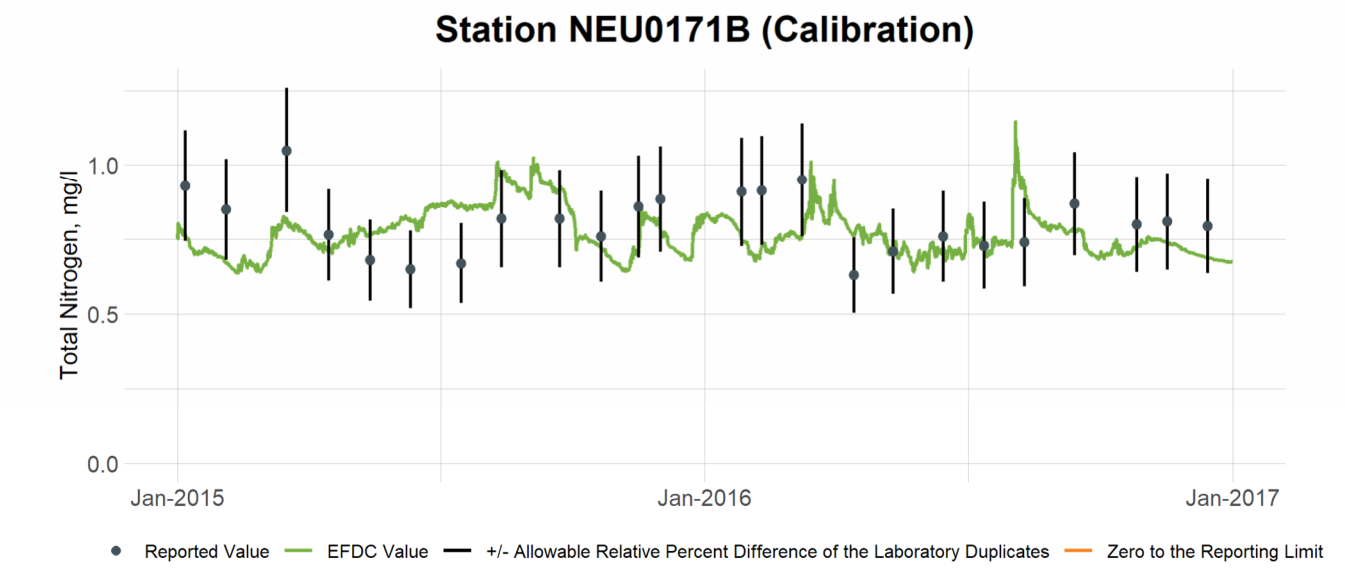

Figure 6-6 Calibration Plot of TN at Station NEU0171B

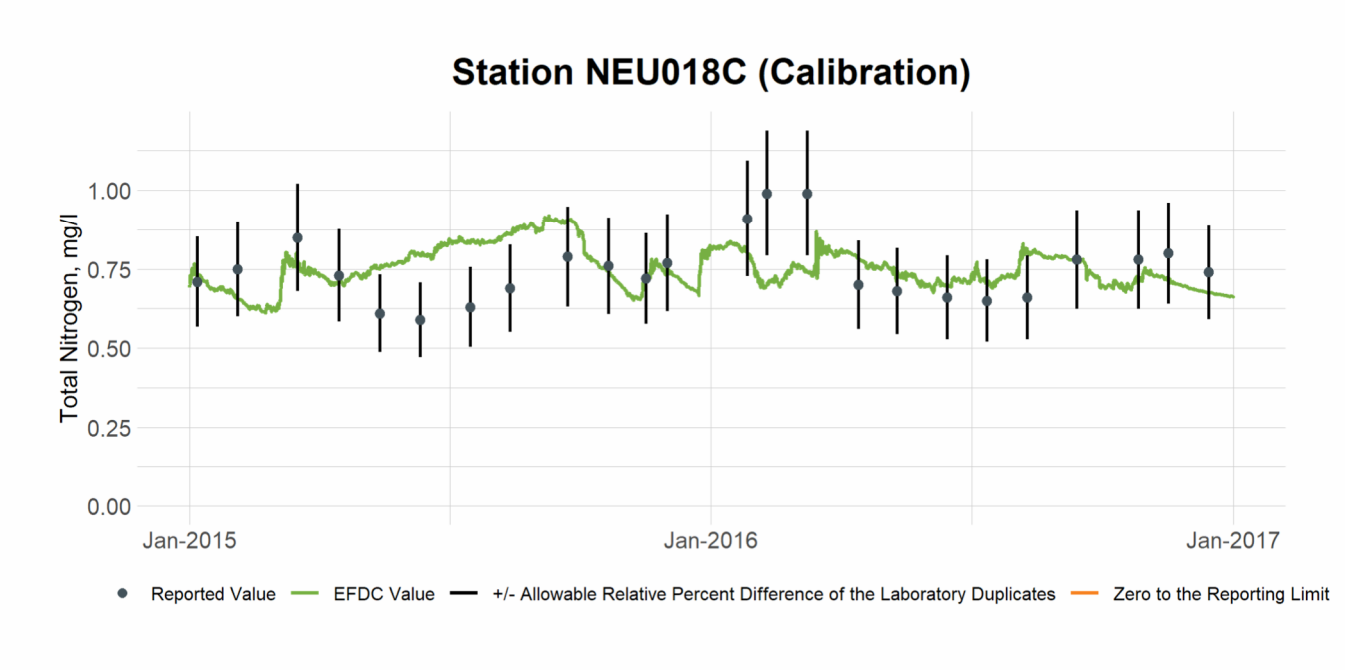

Figure 6-7 Calibration Plot of TN at Station NEU018C

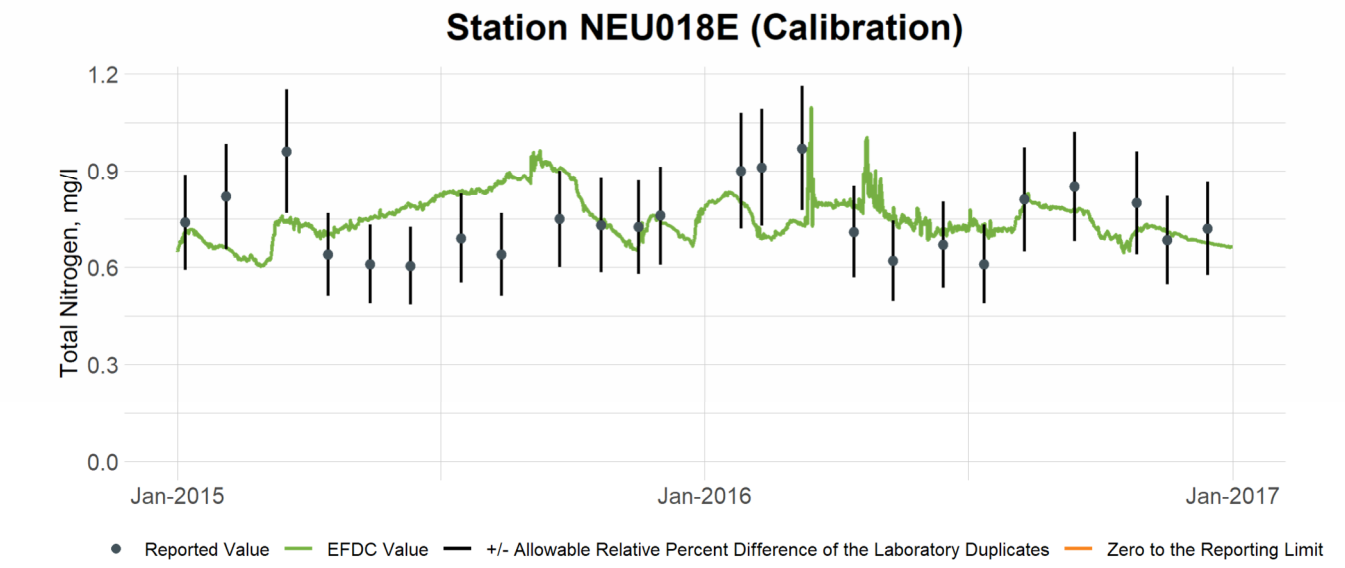

Figure 6-8 Calibration Plot of TN at Station NEU018E

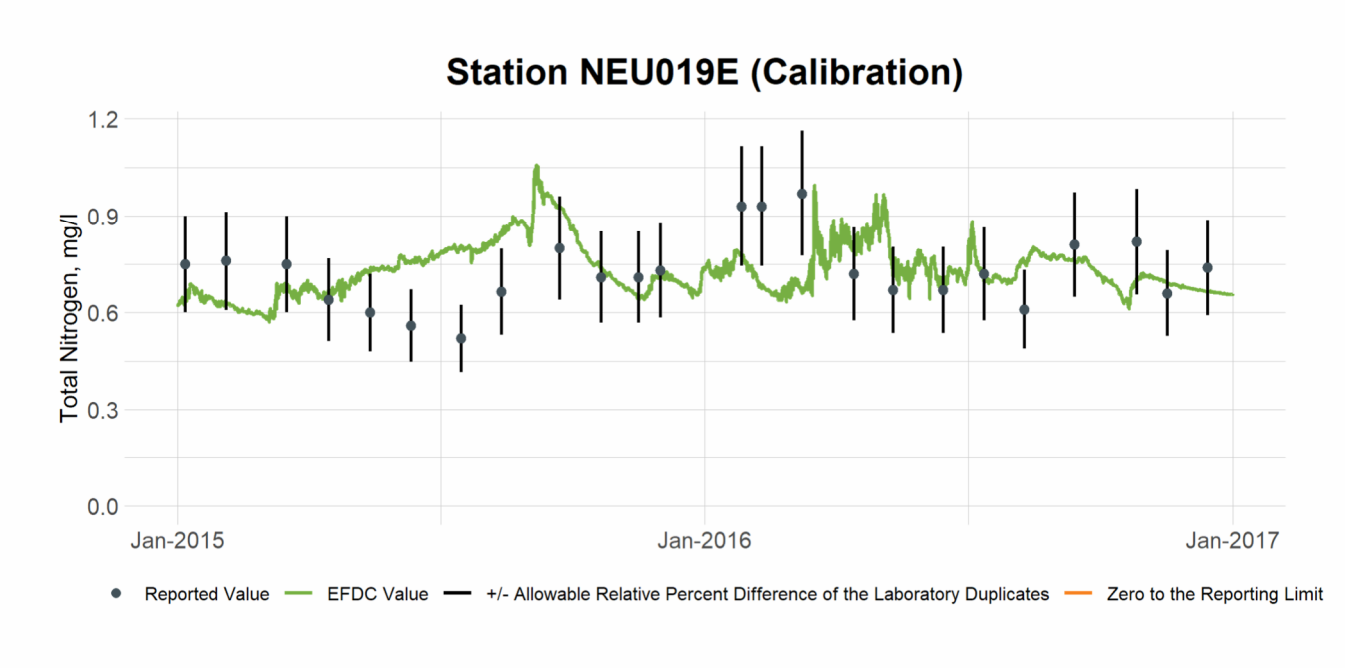

Figure 6-9 Calibration Plot of TN at Station NEU019E

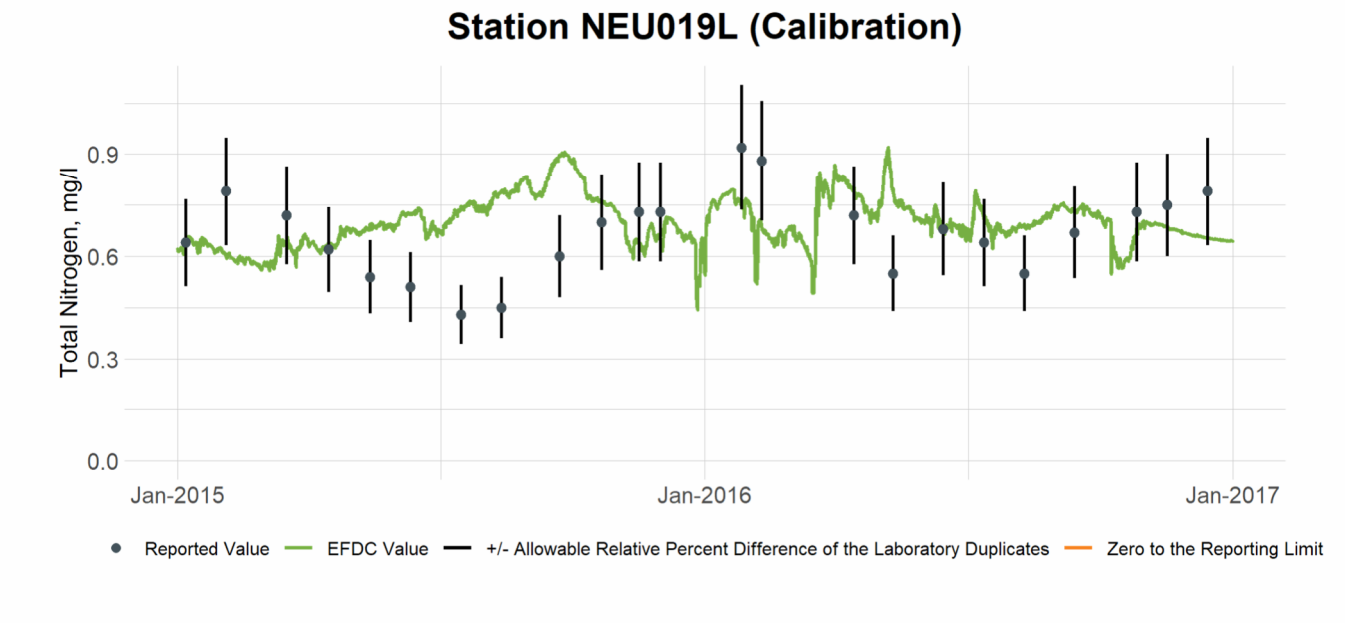

Figure 6-10 Calibration Plot of TN at Station NEU019L

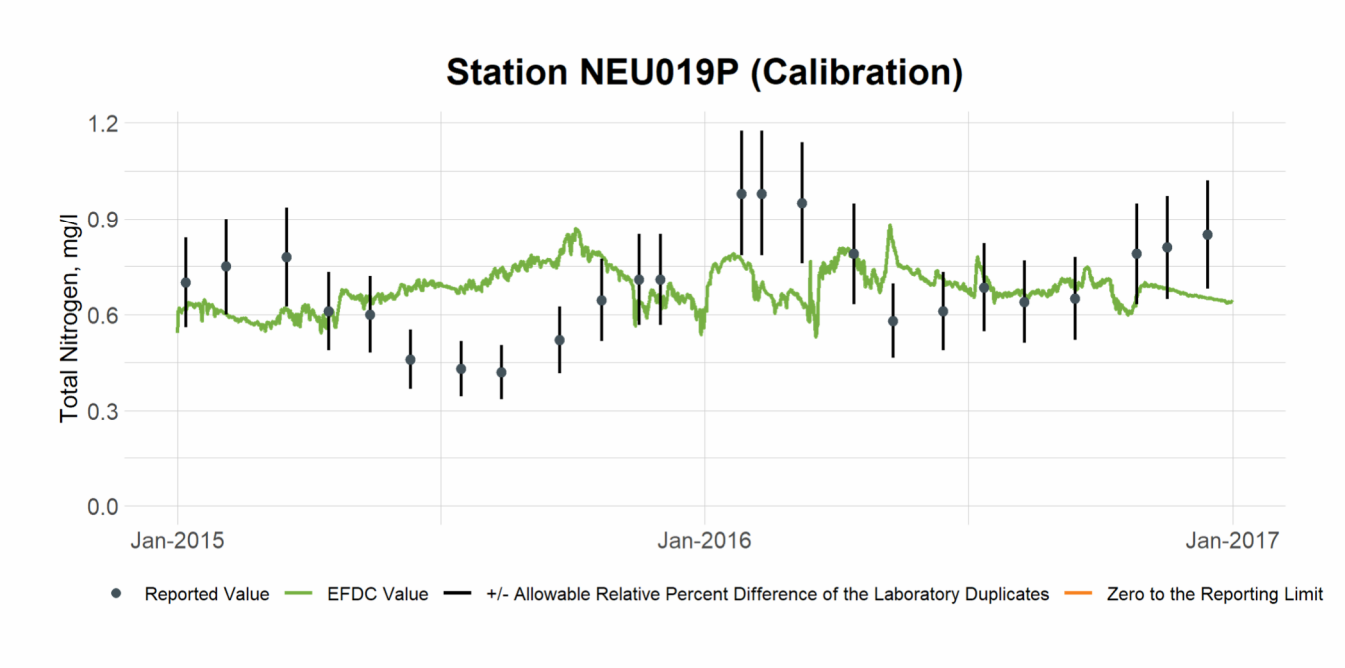

Figure 6-11 Calibration Plot of TN at Station NEU019P

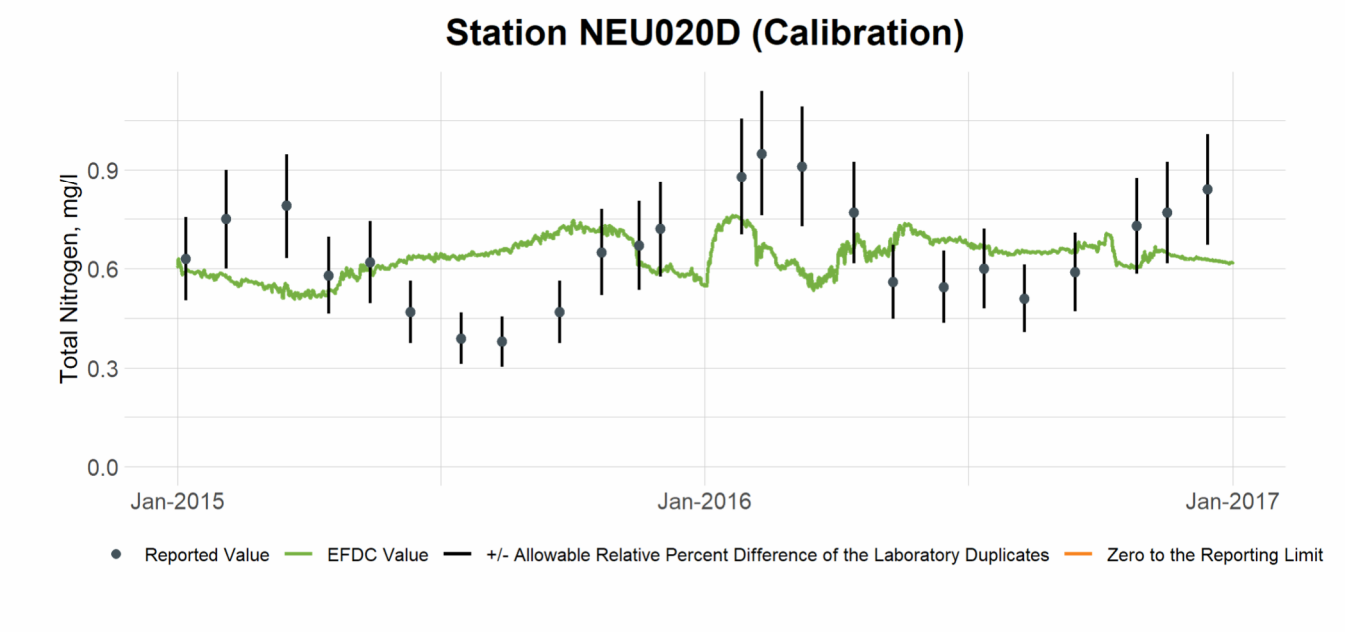

Figure 6-12 Calibration Plot of TN at Station NEU020D

6.2 TN Validation

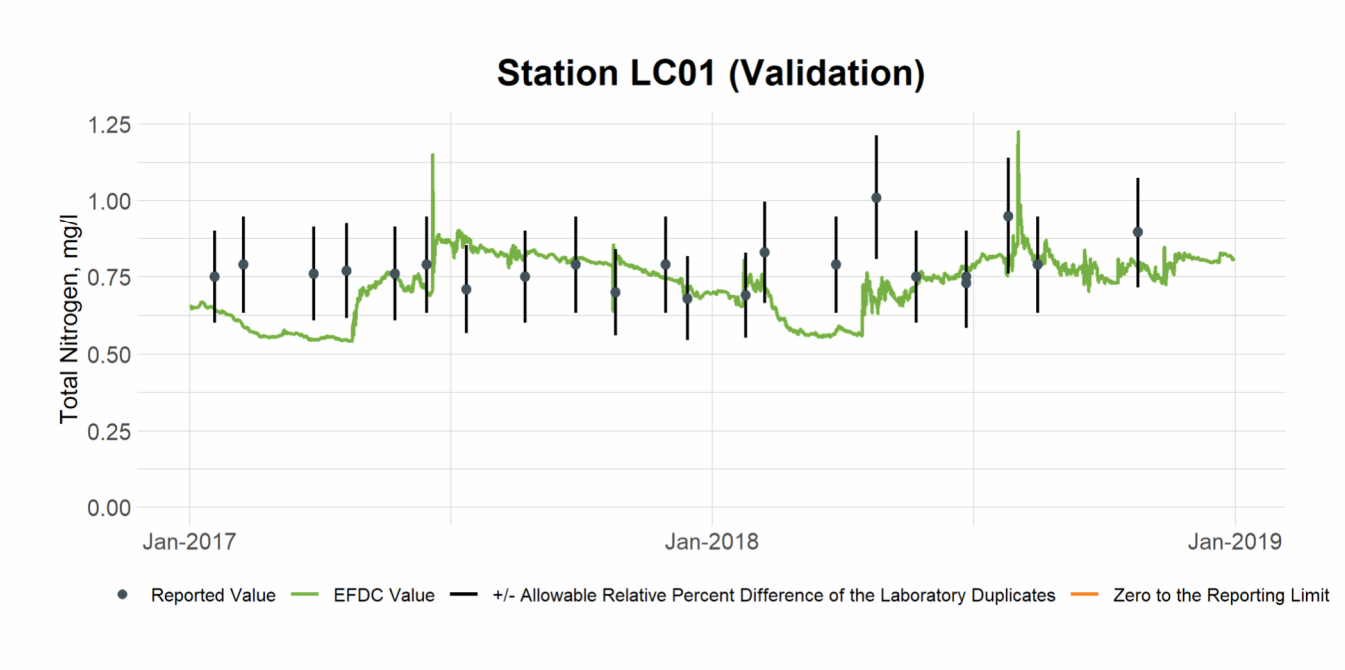

Figure 6-13 Validation Plot of TN at Station LC01

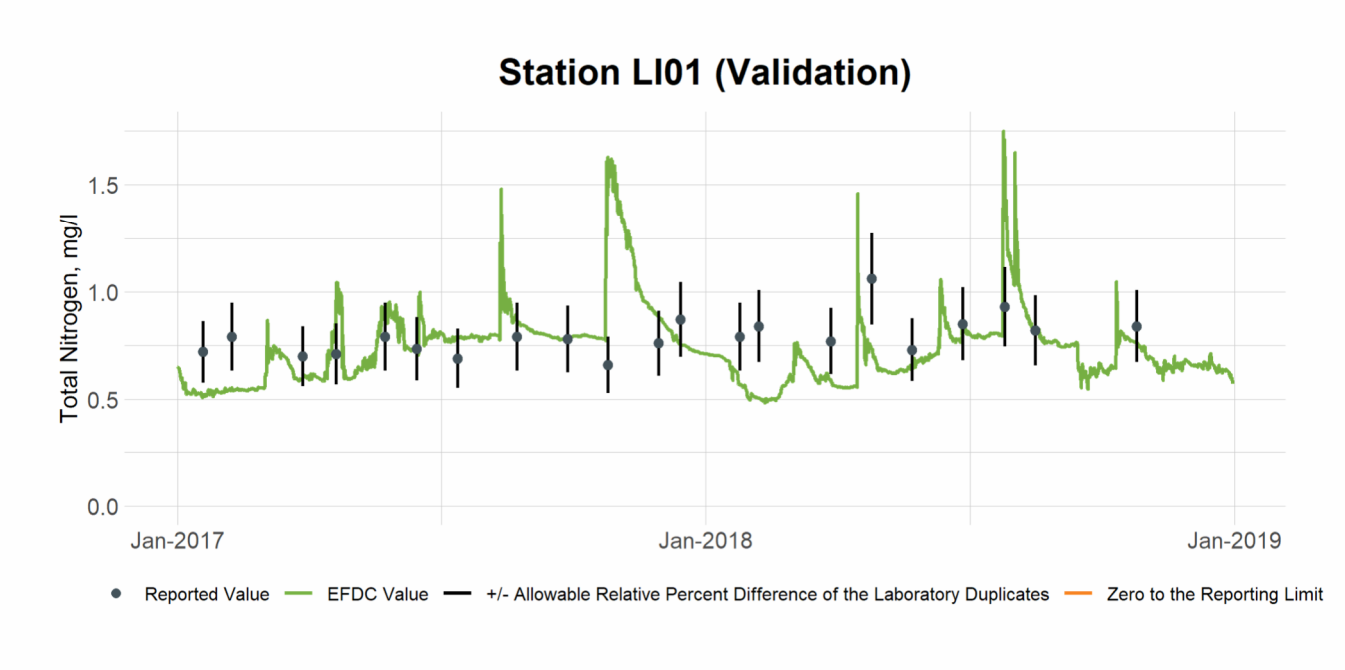

Figure 6-14 Validation Plot of TN at Station LI01

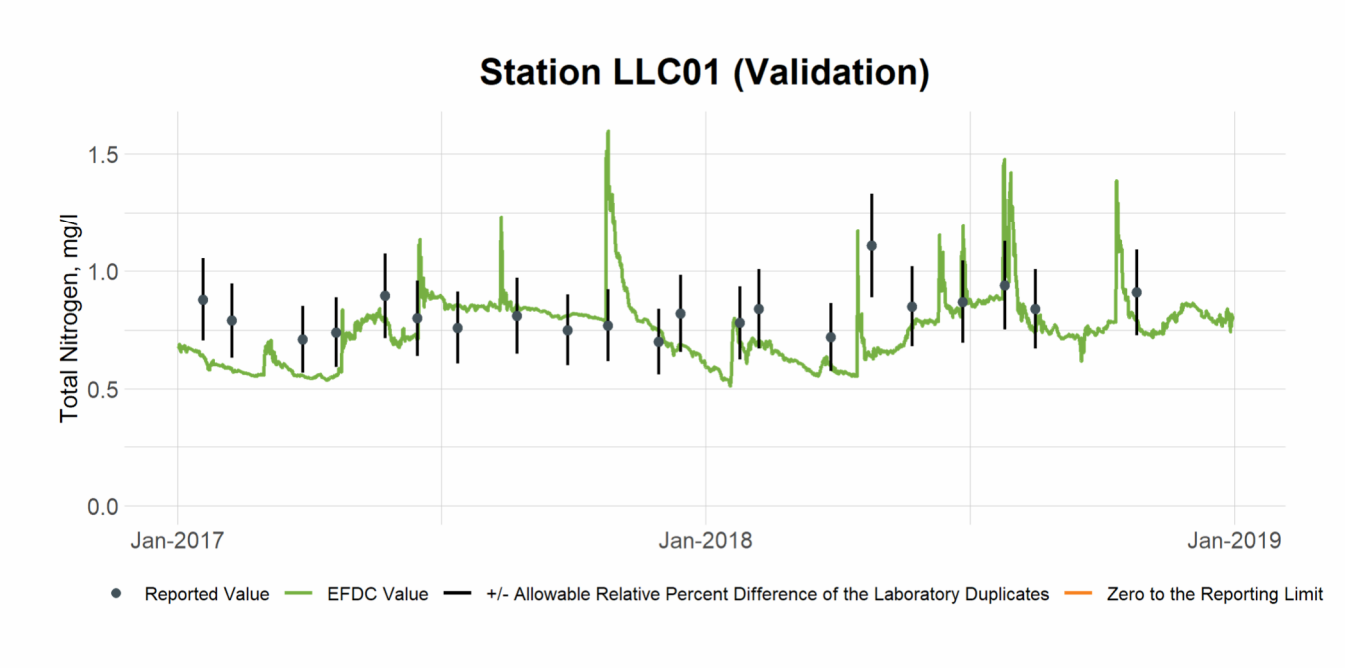

Figure 6-15 Validation Plot of TN at Station LLC01

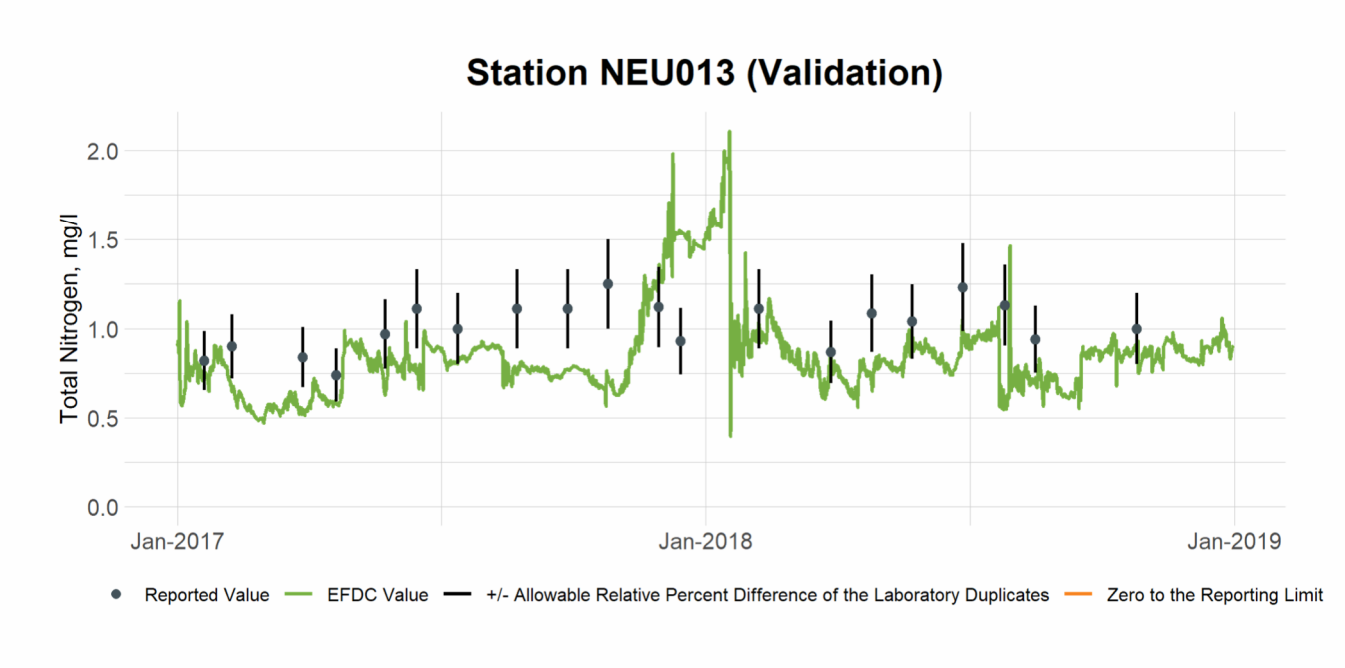

Figure 6-16 Validation Plot of TN at Station NEU013

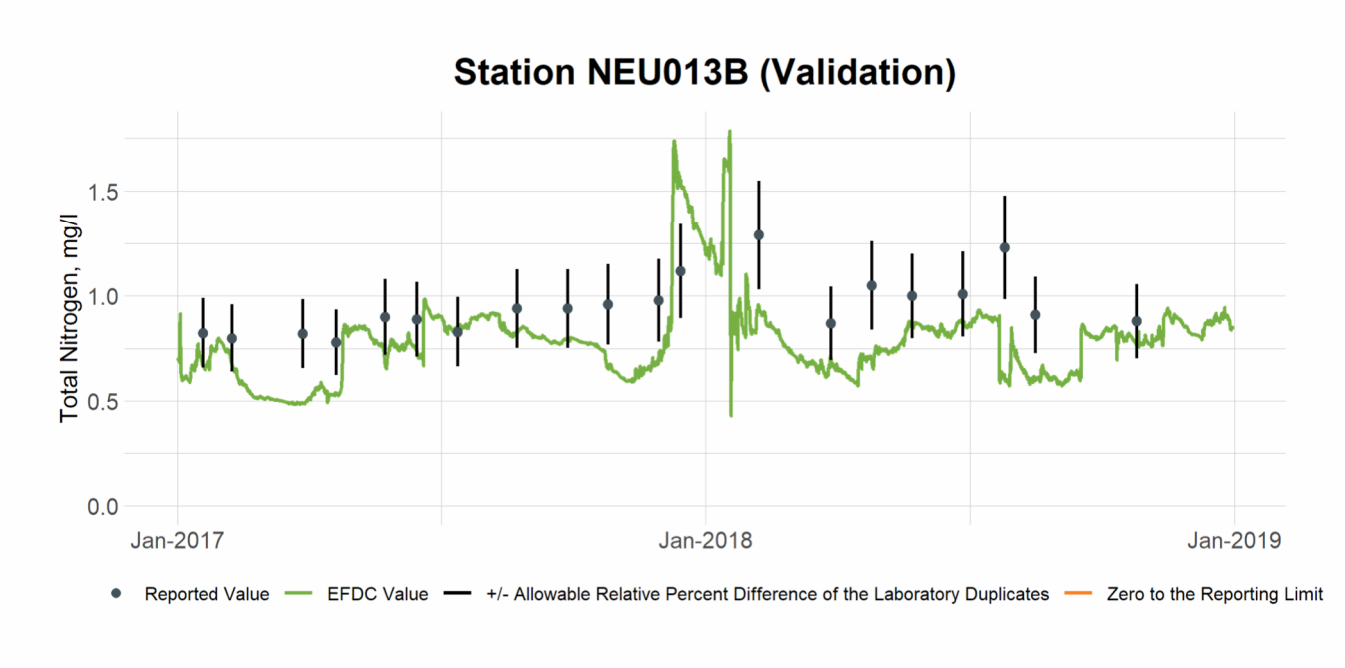

Figure 6-17 Validation Plot of TN at Station NEU013B

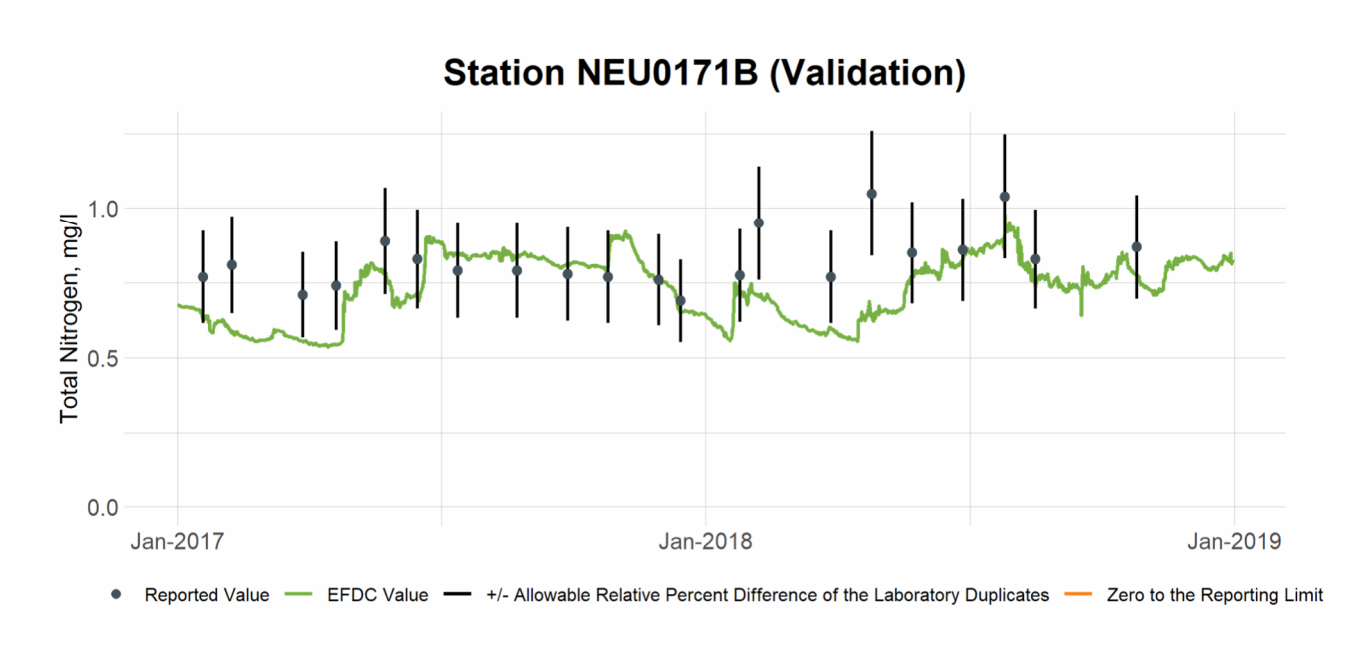

Figure 6-18 Validation Plot of TN at Station NEU0171B

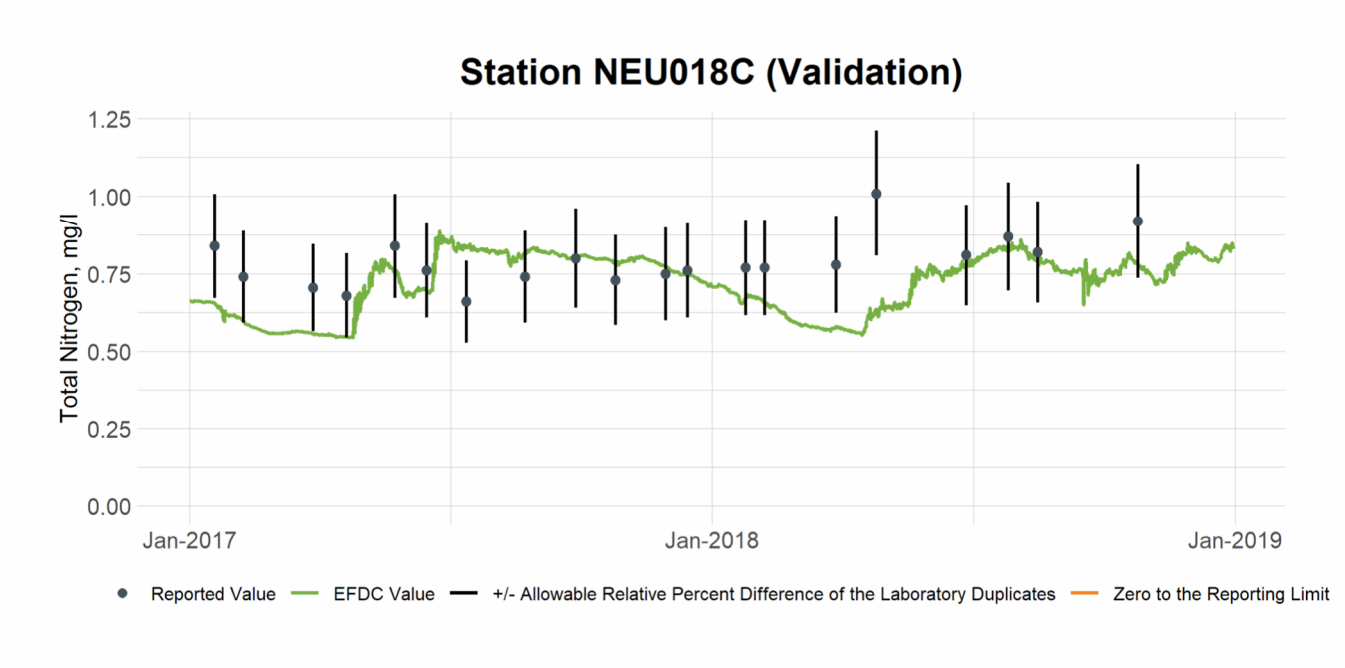

Figure 6-19 Validation Plot of TN at Station NEU018C

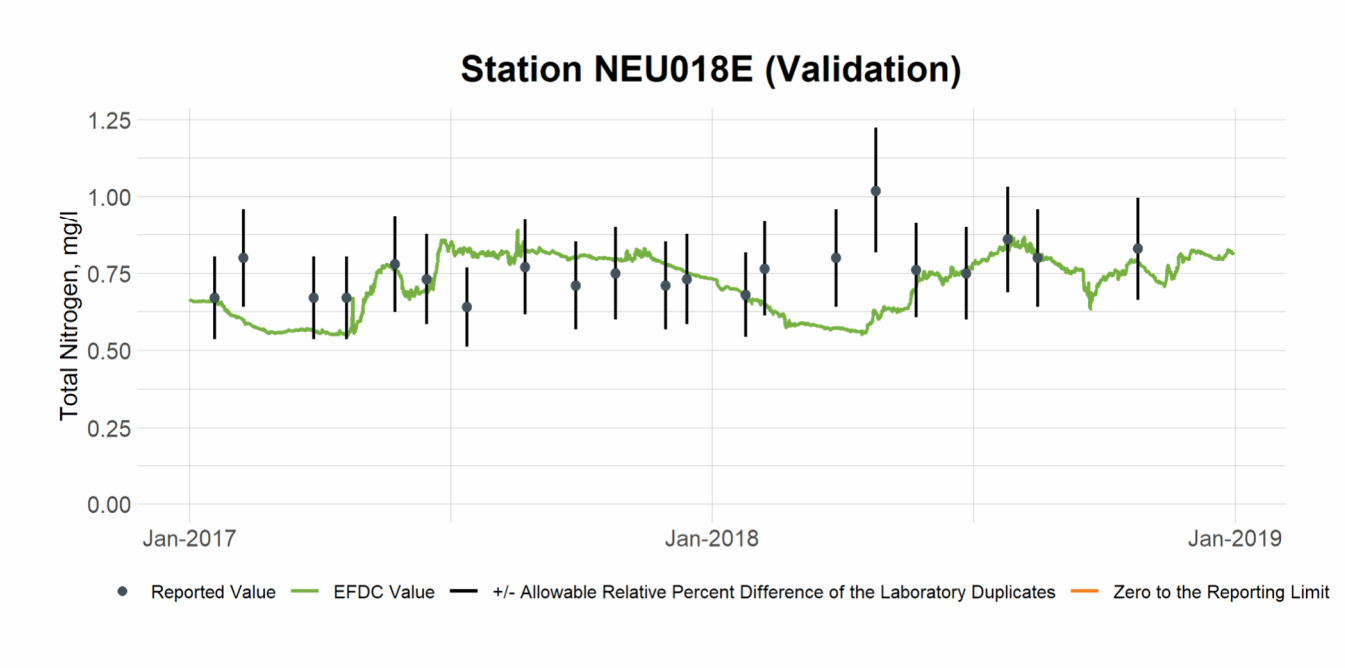

Figure 6-20 Validation Plot of TN at Station NEU018E

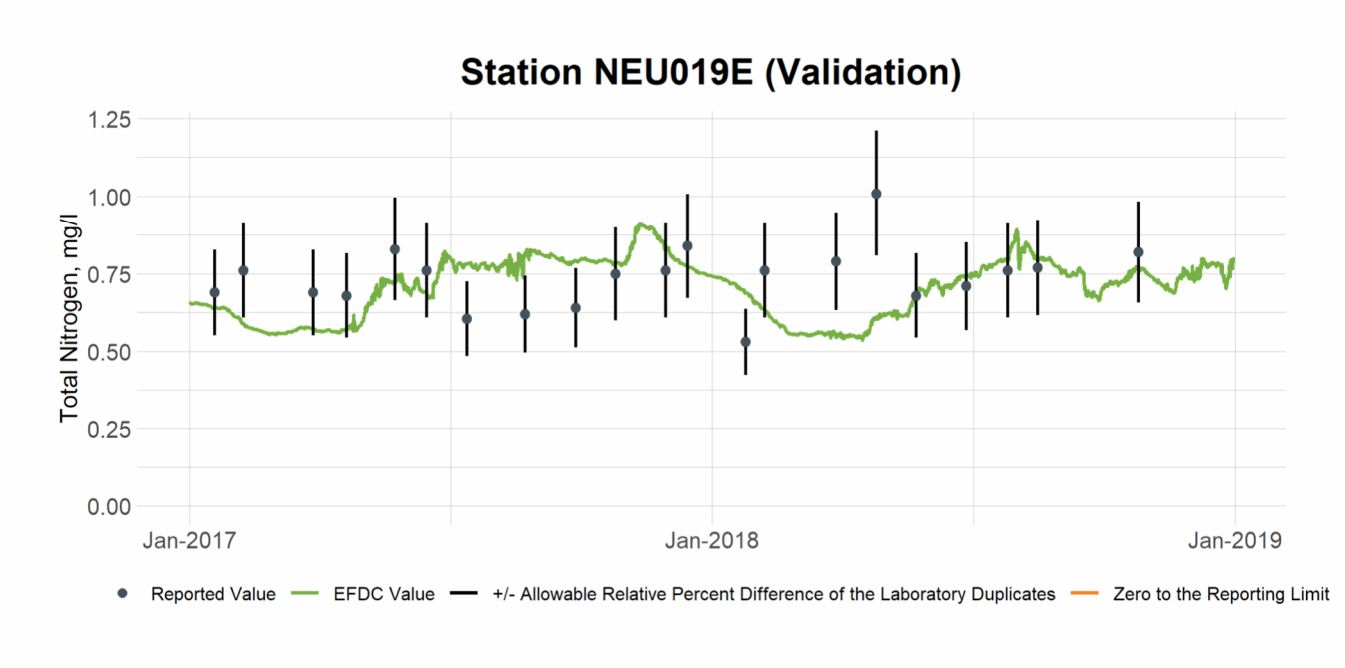

Figure 6-21 Validation Plot of TN at Station NEU019E

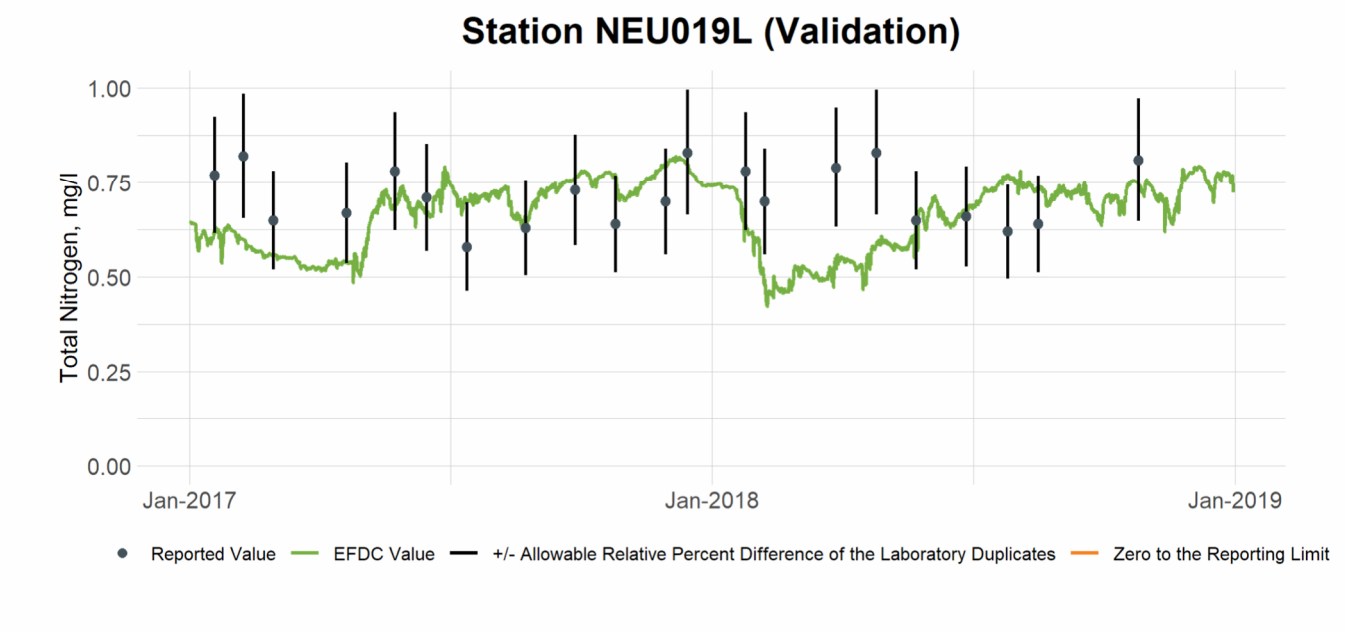

Figure 6-22 Validation Plot of TN at Station NEU019L

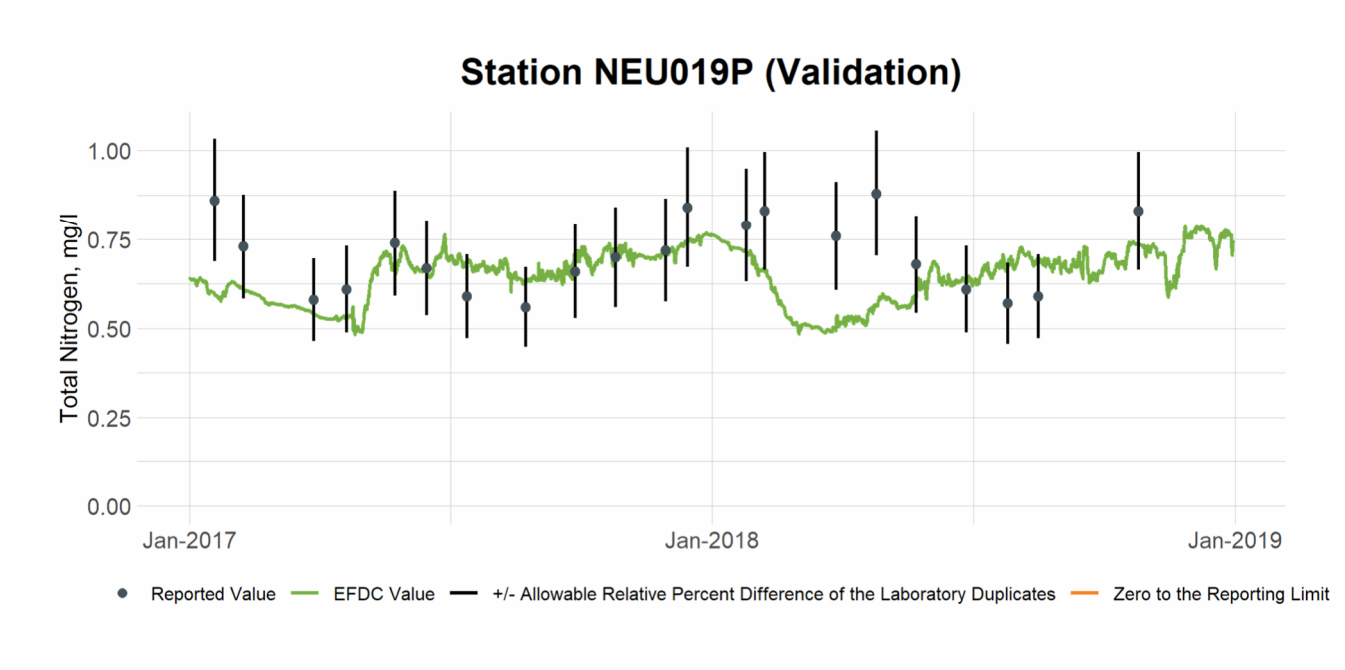

Figure 6-23 Validation Plot of TN at Station NEU019P

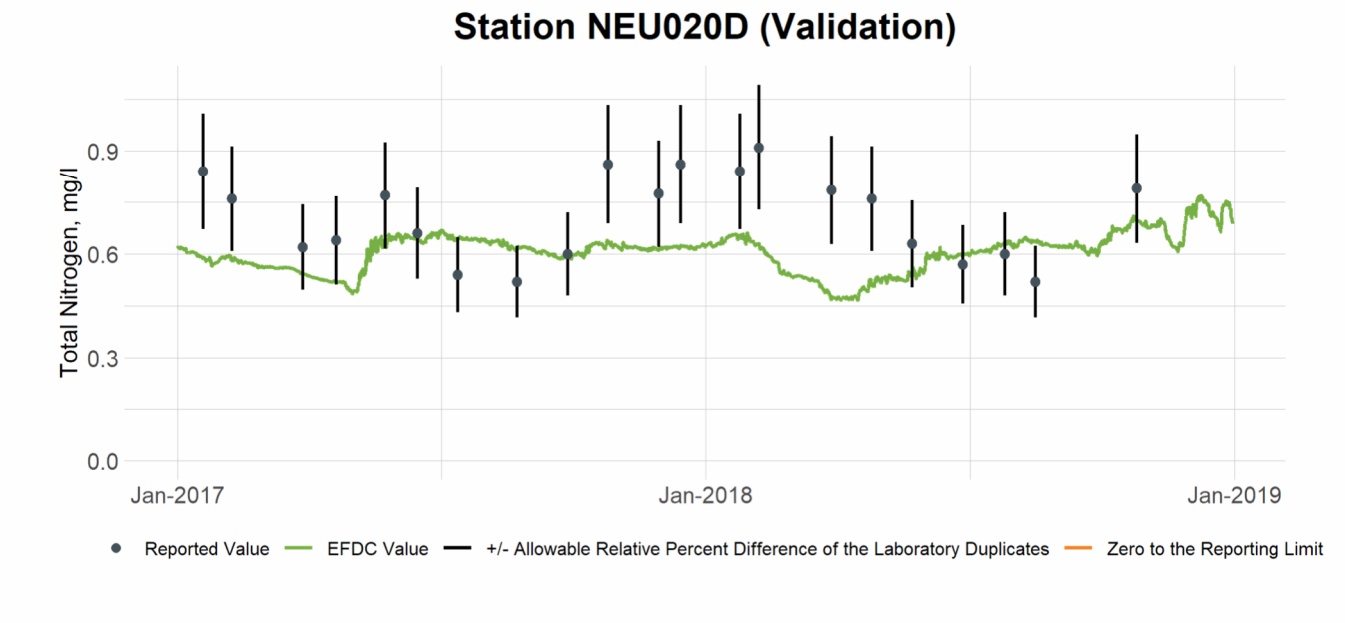

Figure 6-24 Validation Plot of TN at Station NEU020D

7. Ammonia Nitrogen (NH_4)

7.1 Ammonia Nitrogen Calibration

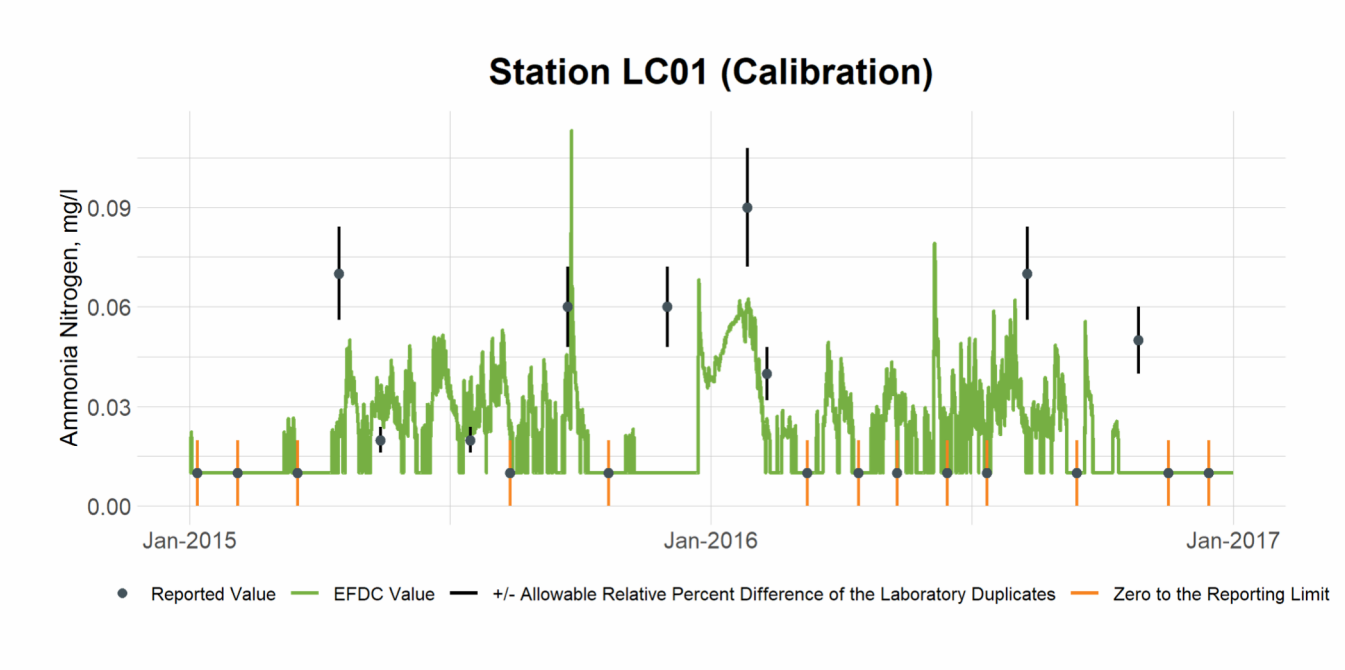

Figure 7-1 Calibration Plot of Ammonia Nitrogen at Station LC01

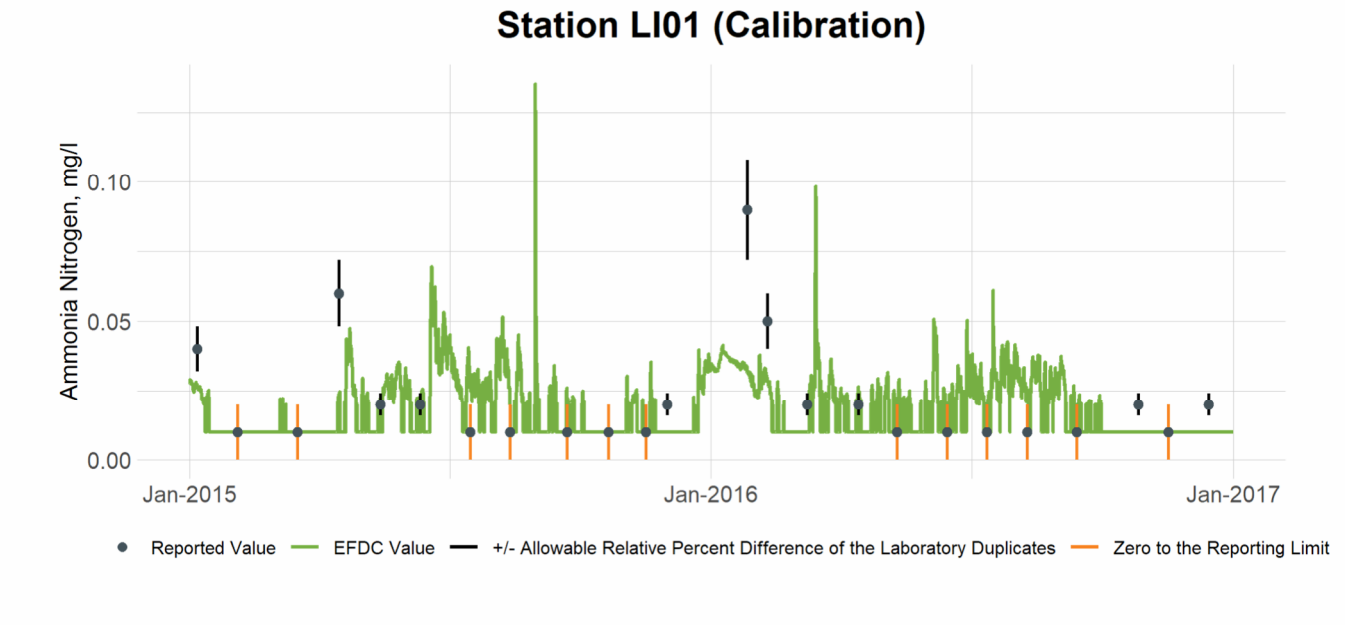

Figure 7-2 Calibration Plot of Ammonia Nitrogen at Station LI01

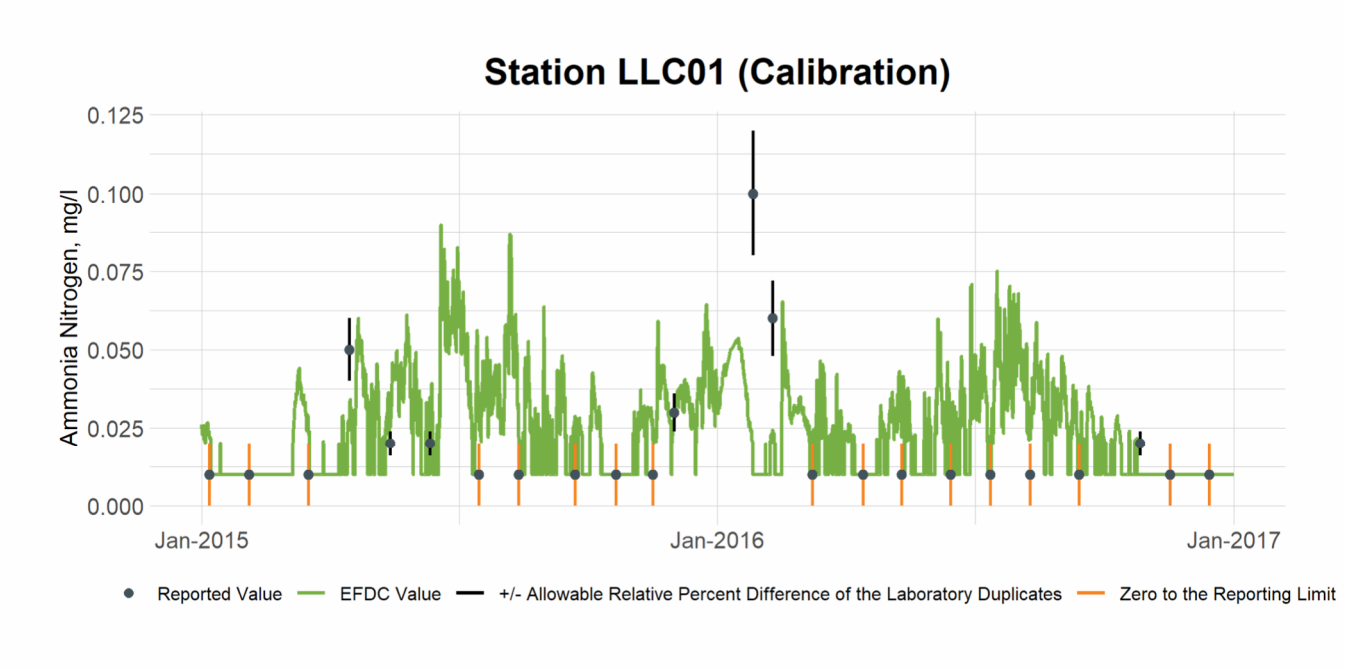

Figure 7-3 Calibration Plot of Ammonia Nitrogen at Station LLC01

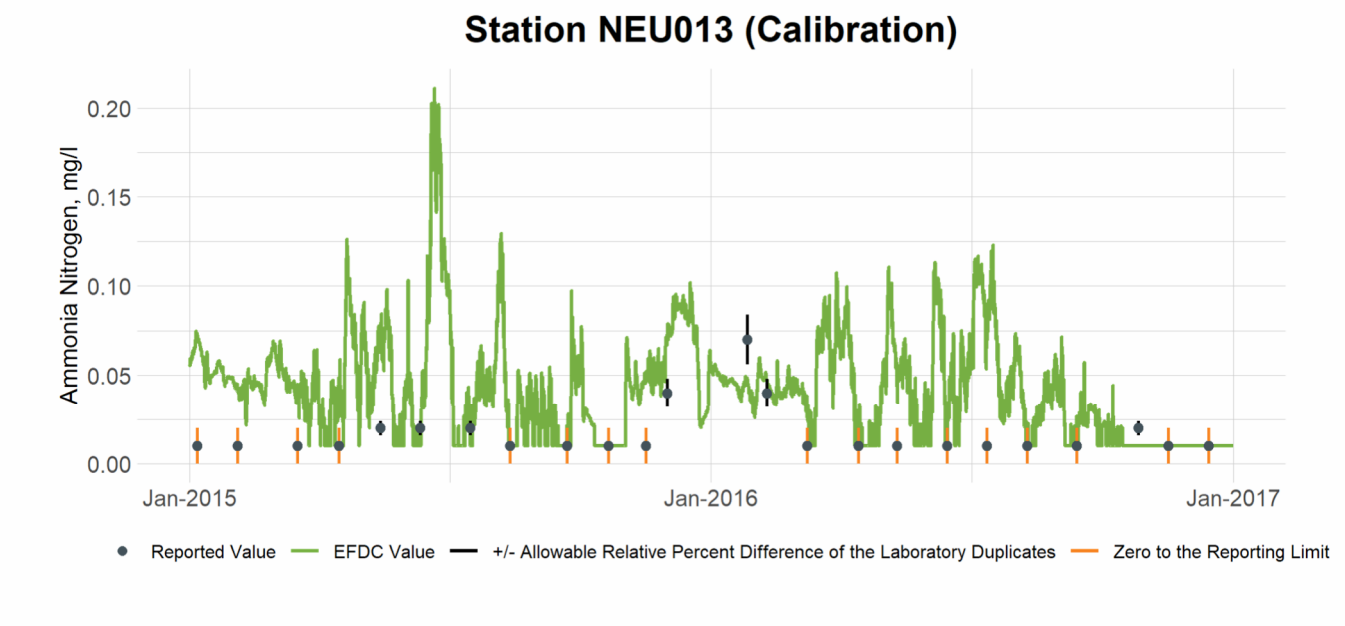

Figure 7-4 Calibration Plot of Ammonia Nitrogen at Station NEU013

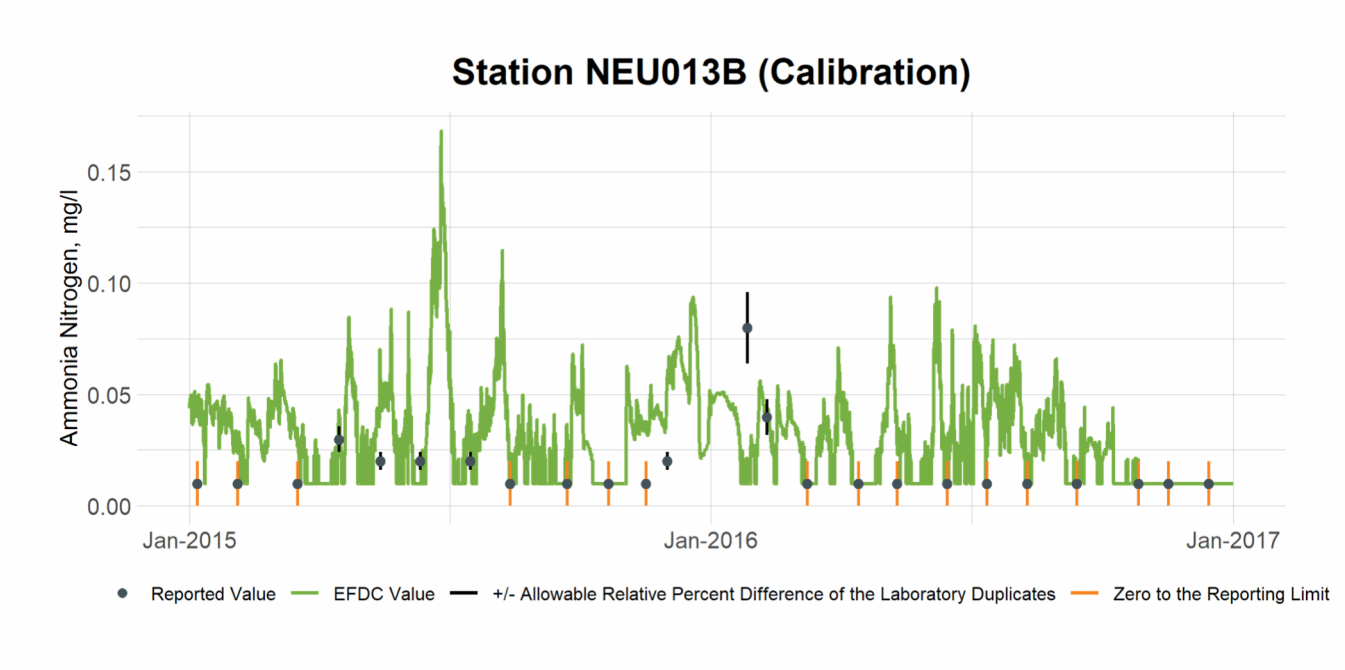

Figure 7-5 Calibration Plot of Ammonia Nitrogen at Station NEU013B

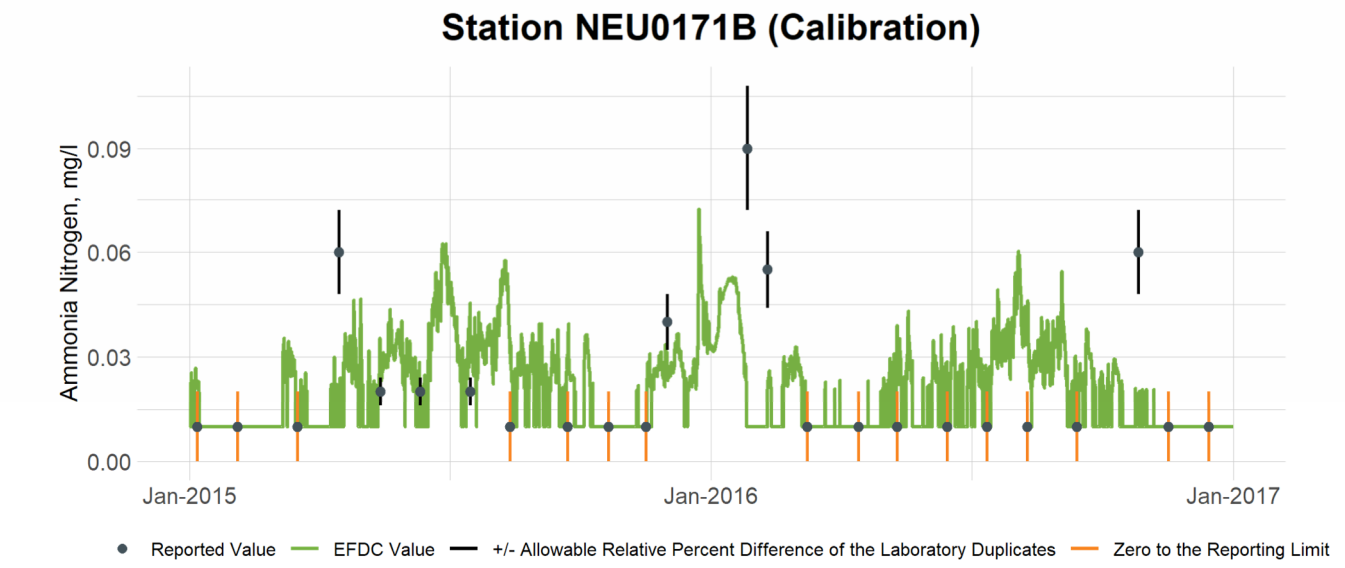

Figure 7-6 Calibration Plot of Ammonia Nitrogen at Station NEU0171B

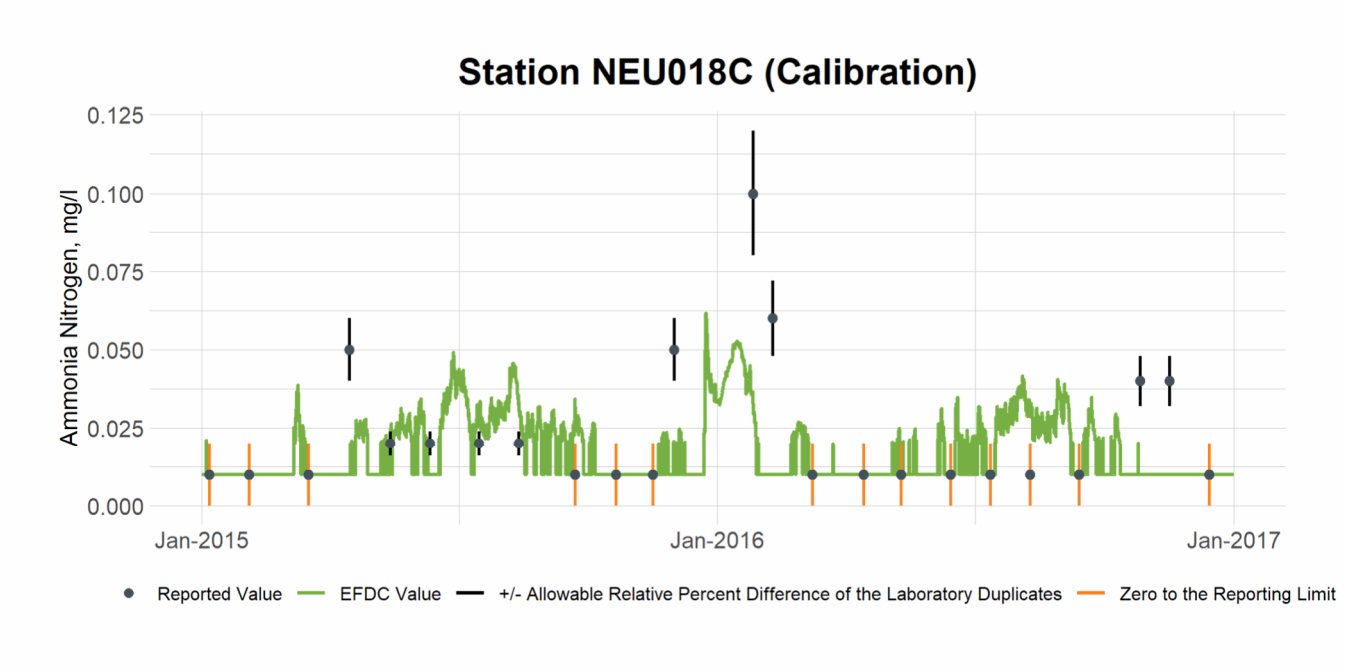

Figure 7-7 Calibration Plot of Ammonia Nitrogen at Station NEU018C

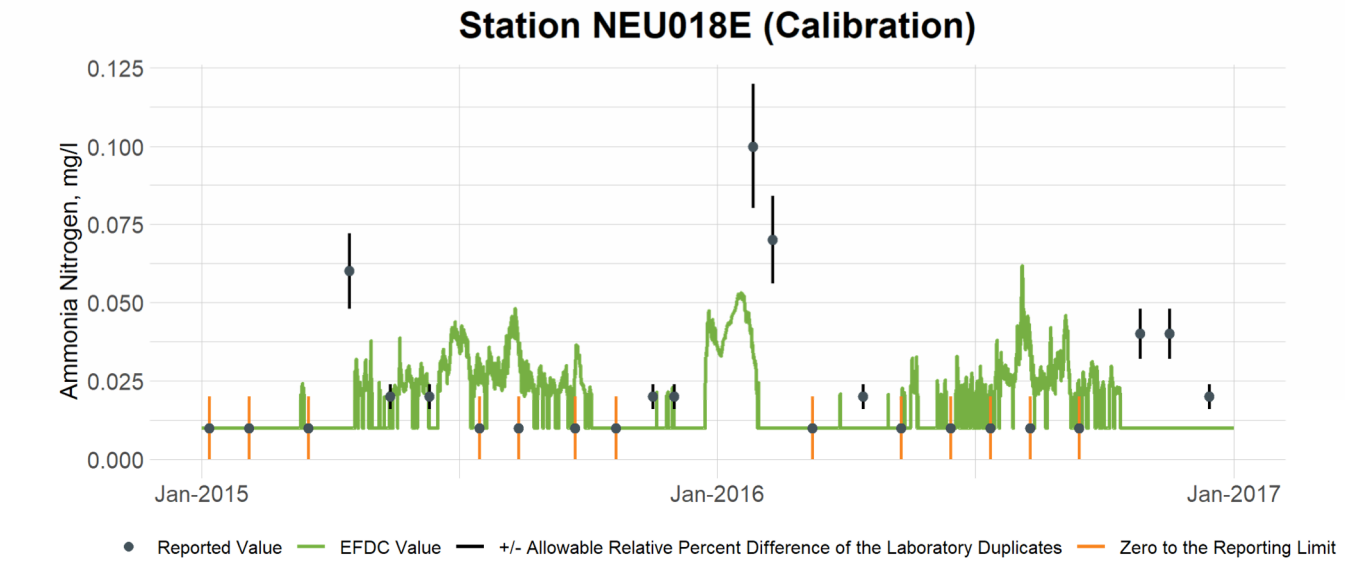

Figure 7-8 Calibration Plot of Ammonia Nitrogen at Station NEU018E

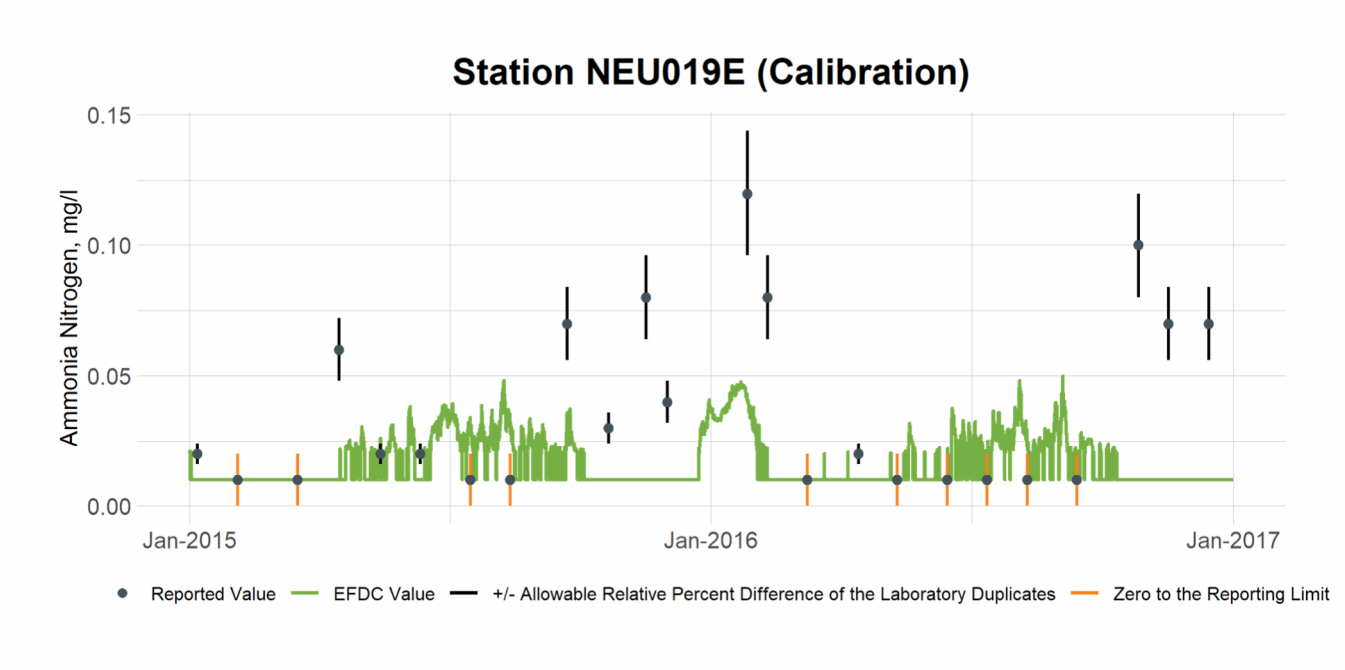

Figure 7-9 Calibration Plot of Ammonia Nitrogen at Station NEU019E

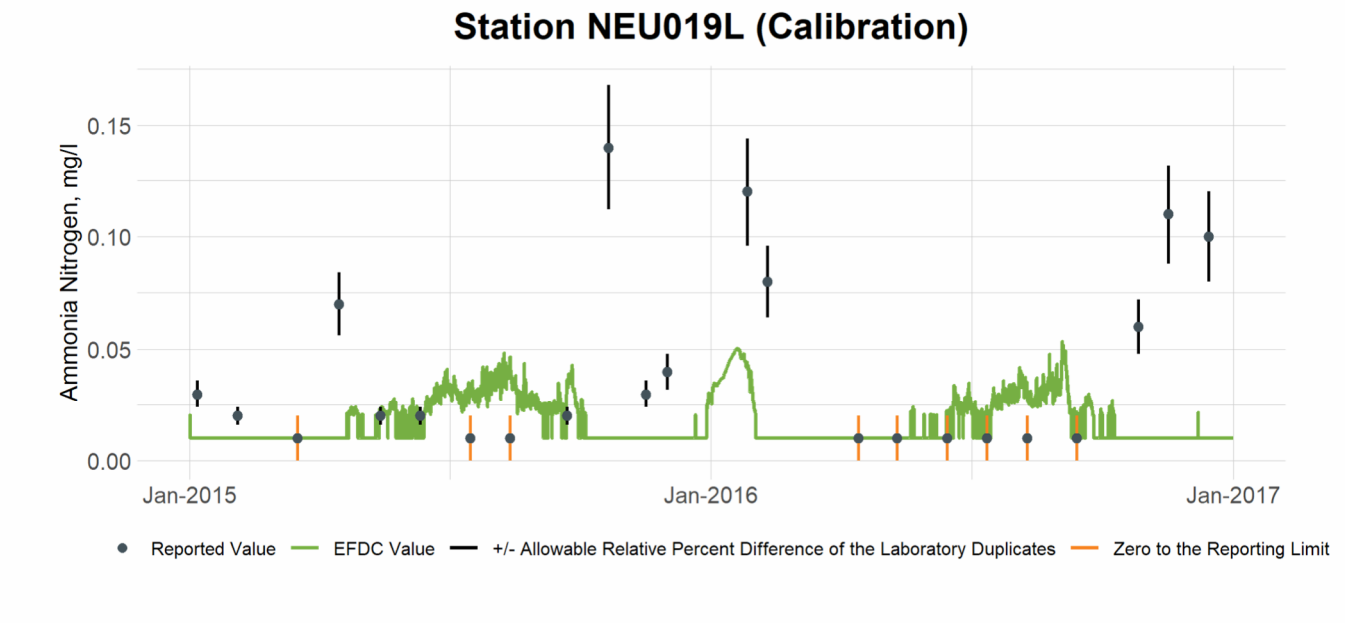

Figure 7-10 Calibration Plot of Ammonia Nitrogen at Station NEU019L

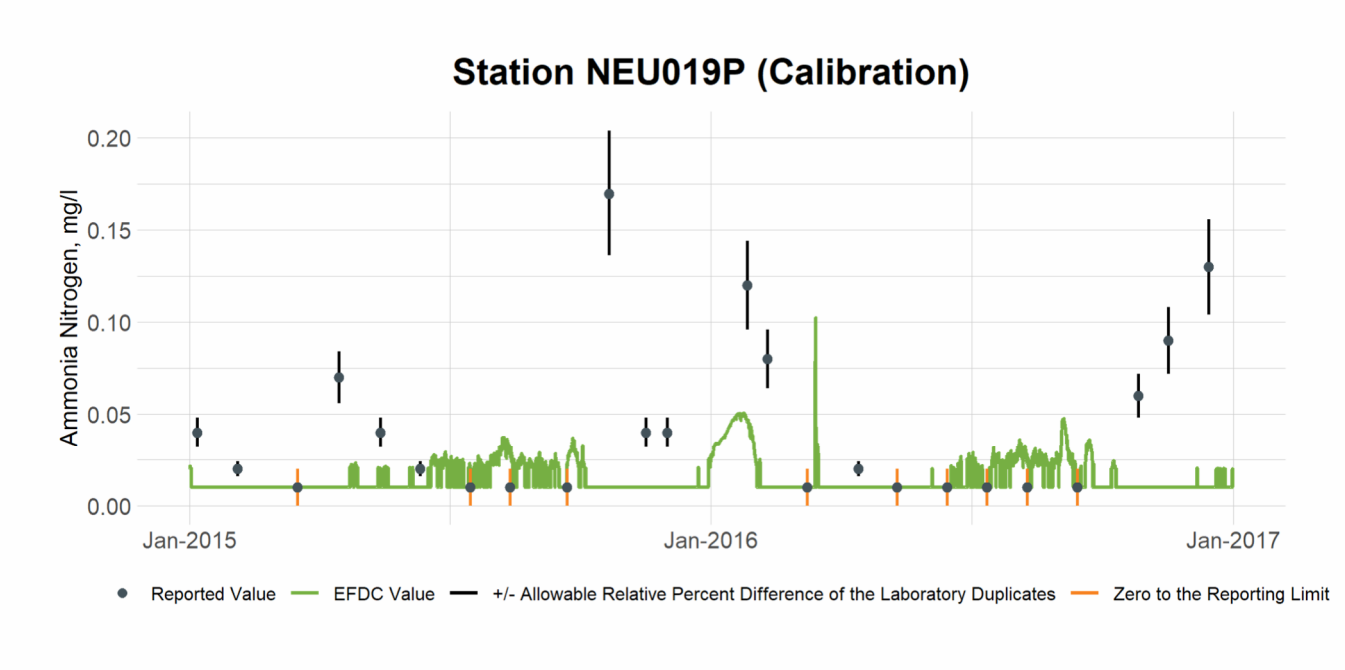

Figure 7-11 Calibration Plot of Ammonia Nitrogen at Station NEU019P

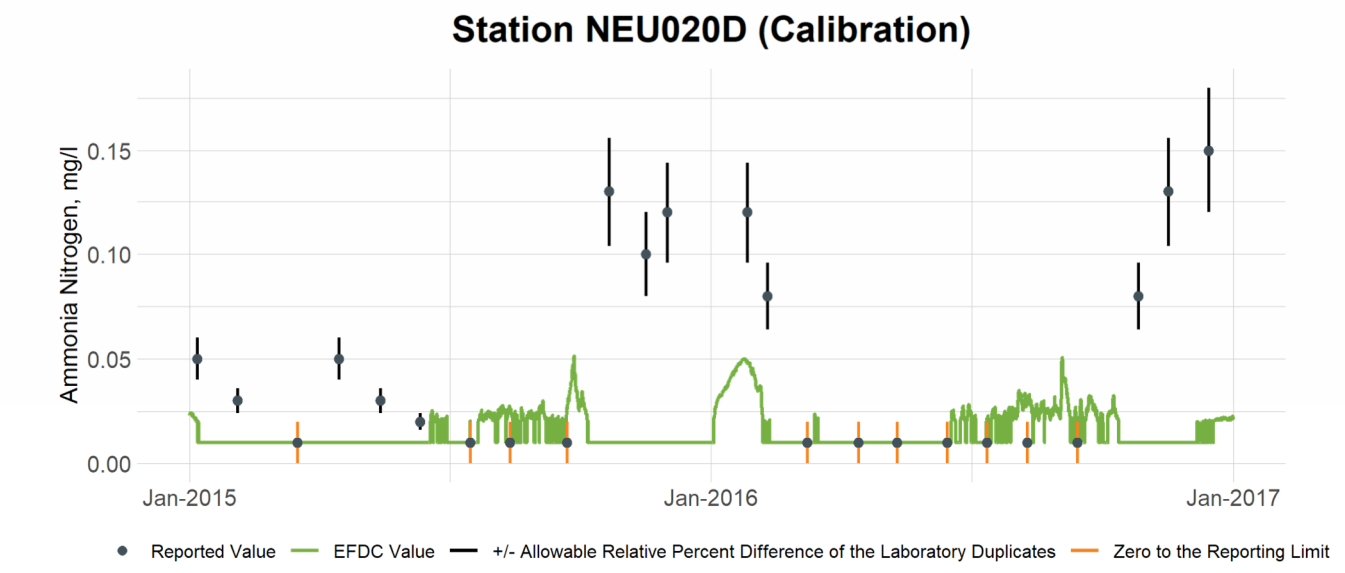

Figure 7-12 Calibration Plot of Ammonia Nitrogen at Station NEU020D

7.2 Ammonia Nitrogen Validation

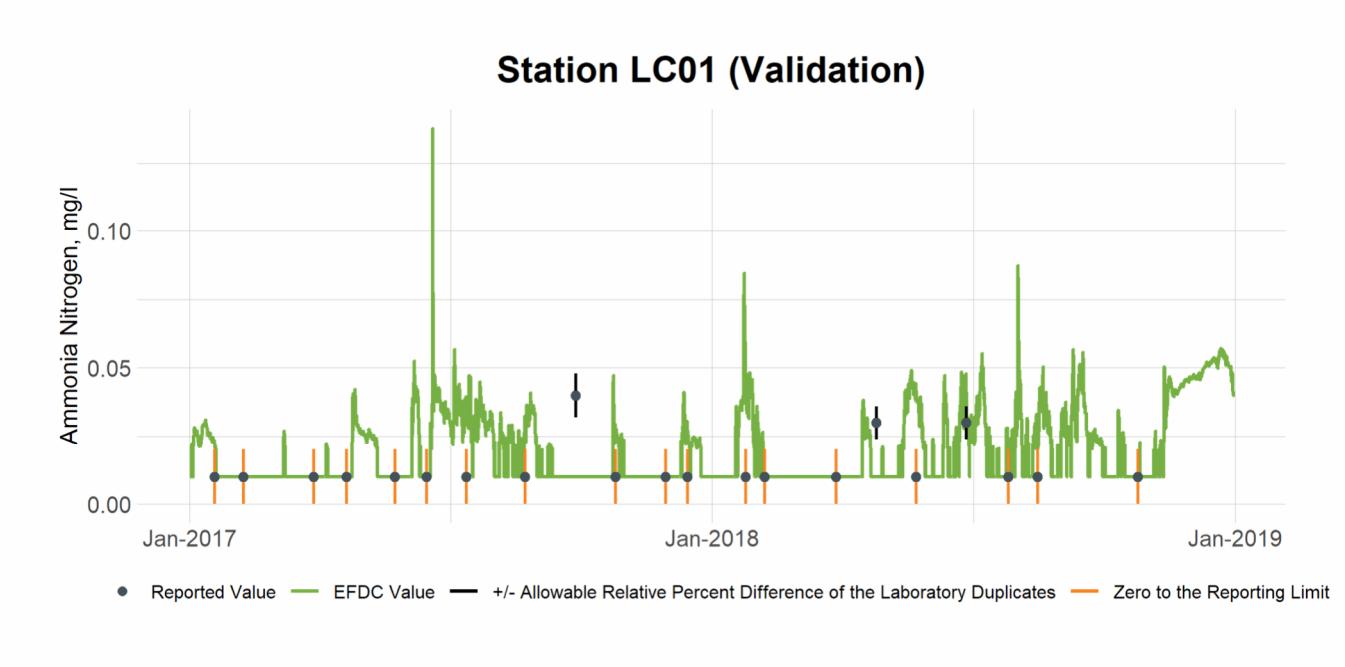

Figure 7-13 Validation Plot of Ammonia Nitrogen at Station LC01

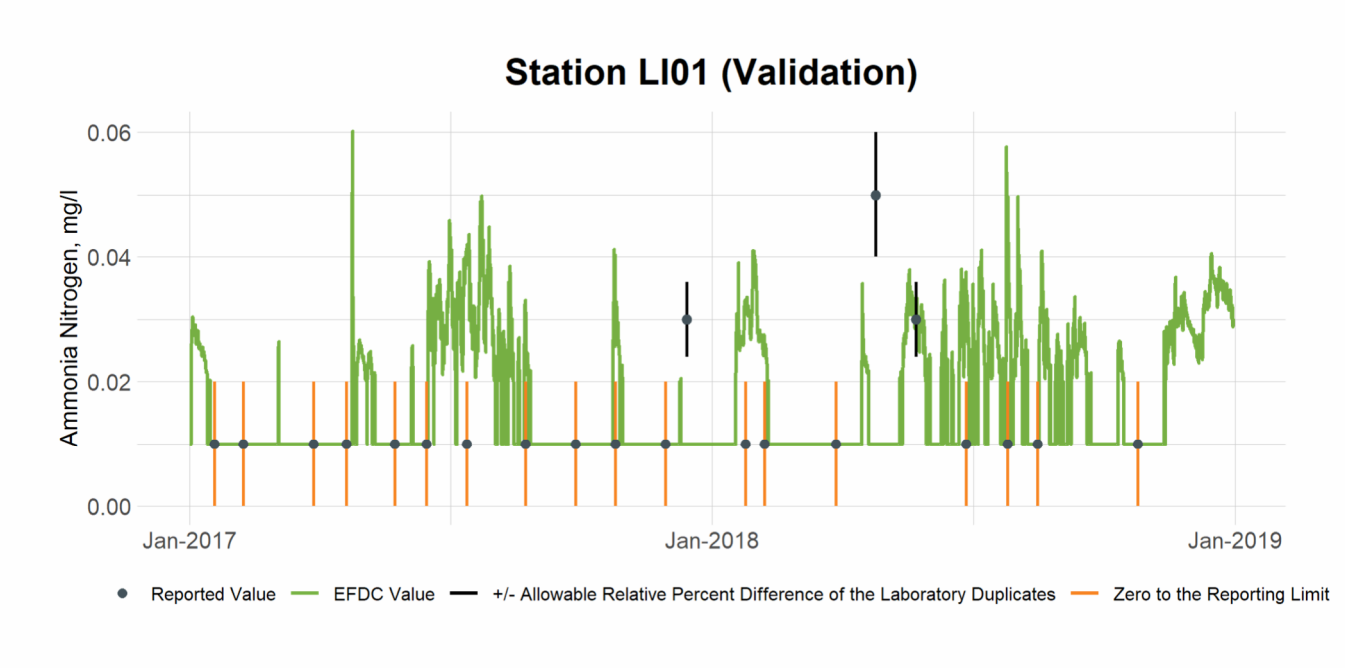

Figure 7-14 Validation Plot of Ammonia Nitrogen at Station LI01

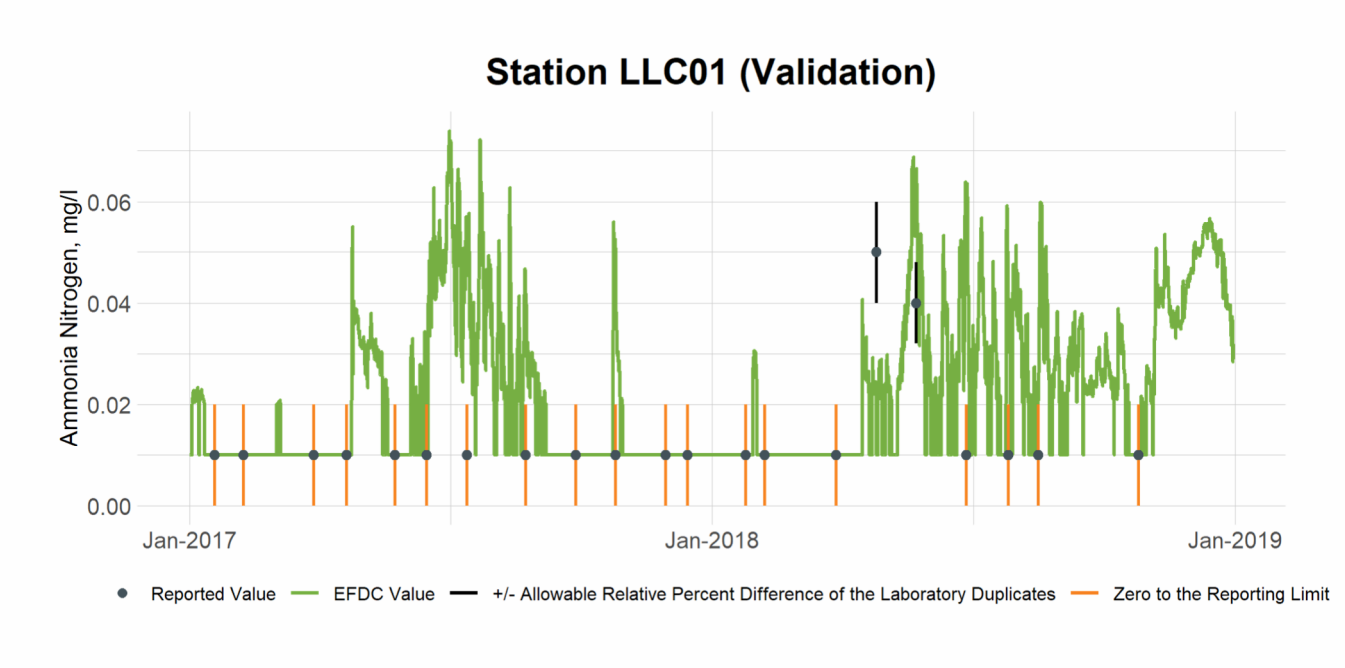

Figure 7-15 Validation Plot of Ammonia Nitrogen at Station LLC01

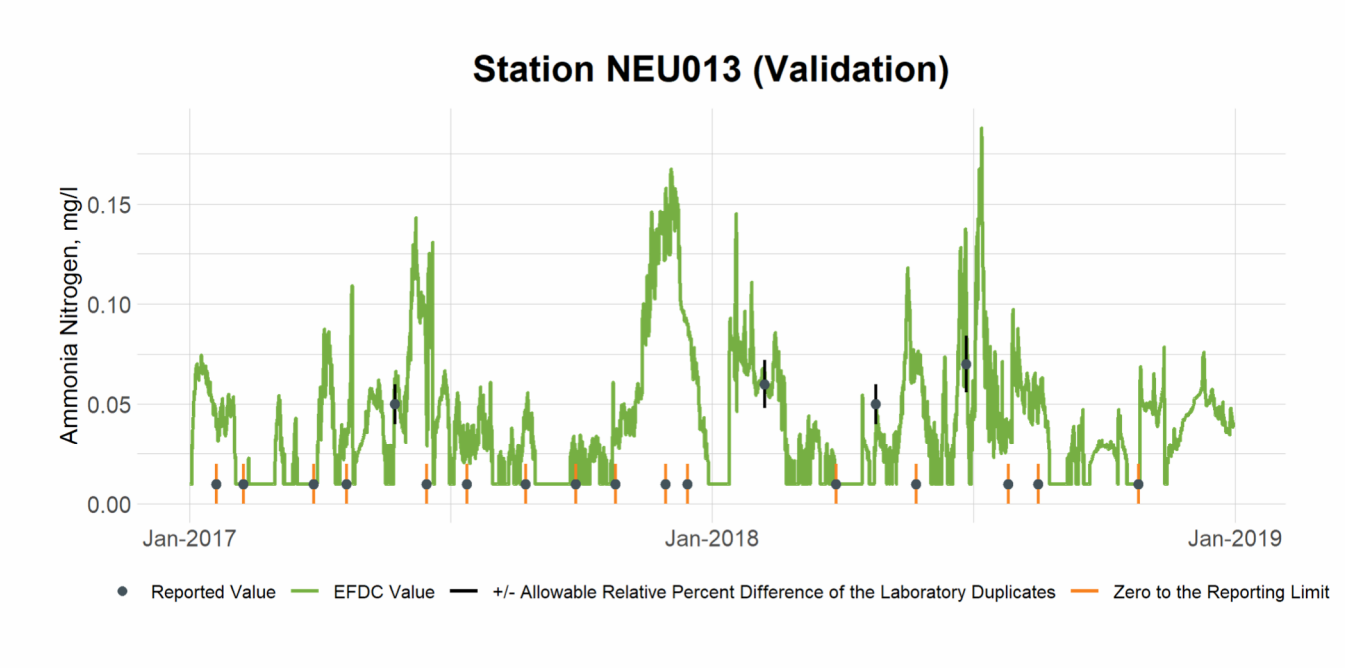

Figure 7-16 Validation Plot of Ammonia Nitrogen at Station NEU013

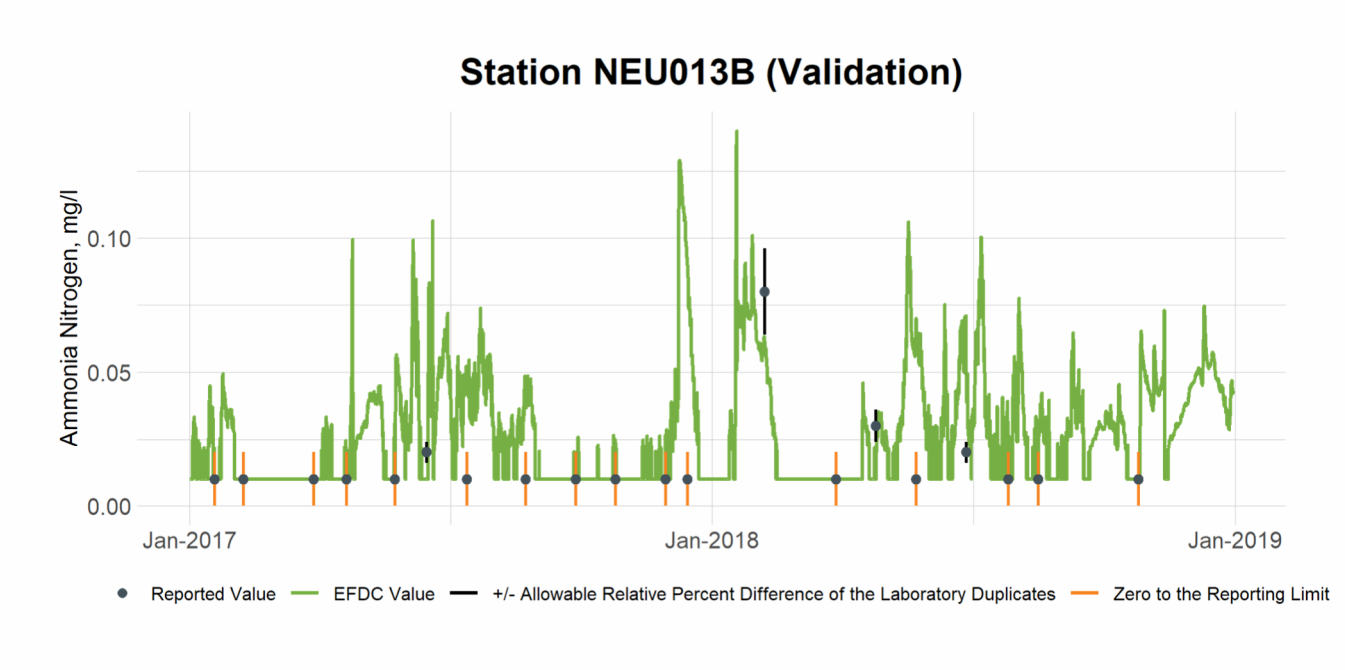

Figure 7-17 Validation Plot of Ammonia Nitrogen at Station NEU013B

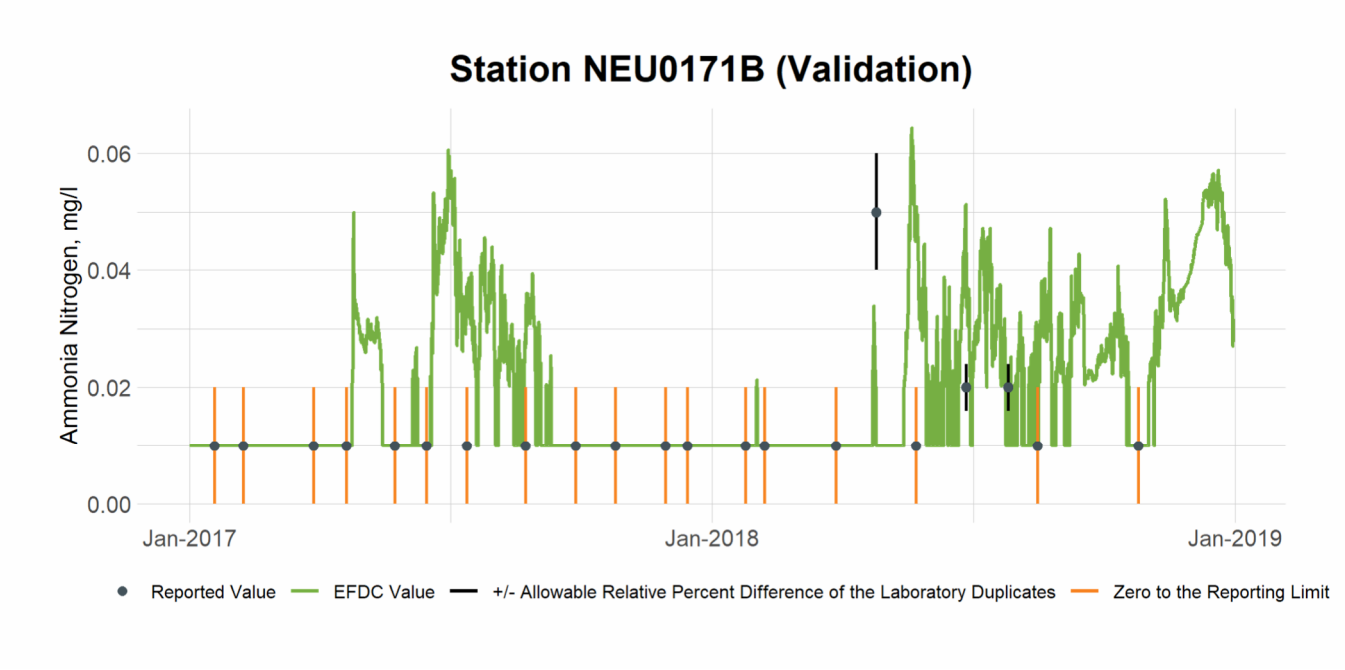

Figure 7-18 Validation Plot of Ammonia Nitrogen at Station NEU0171B

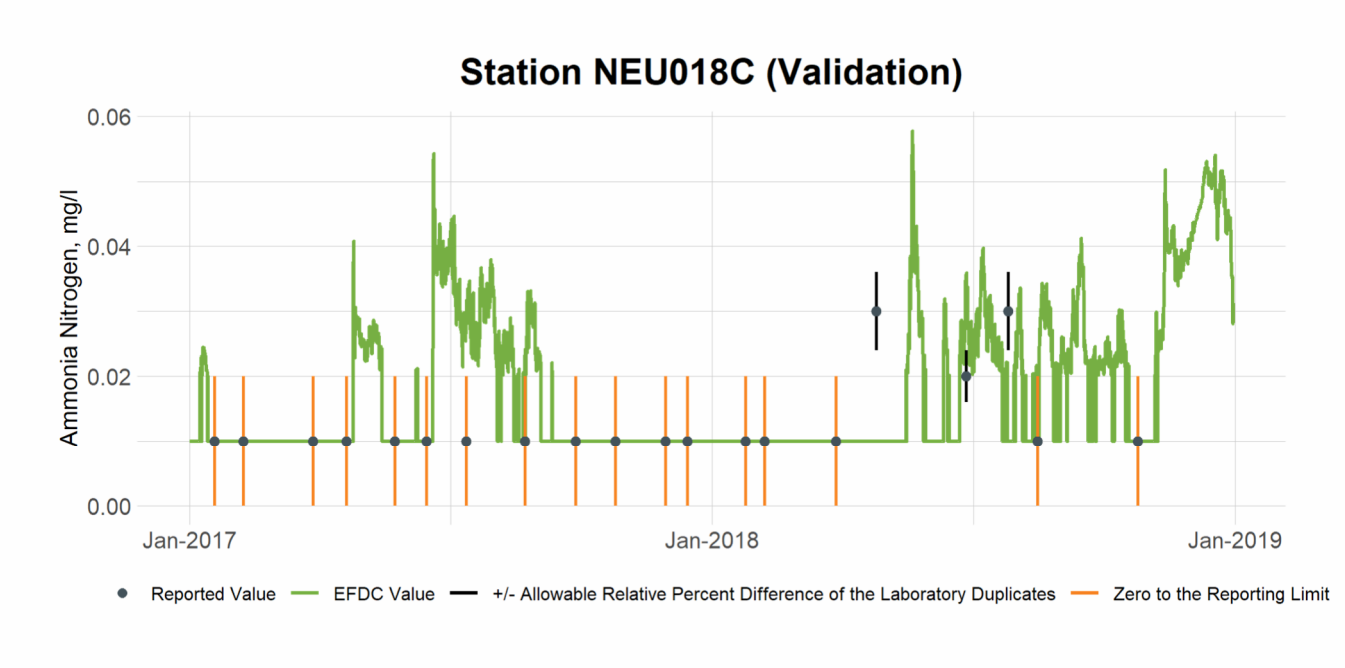

Figure 7-19 Validation Plot of Ammonia Nitrogen at Station NEU018C

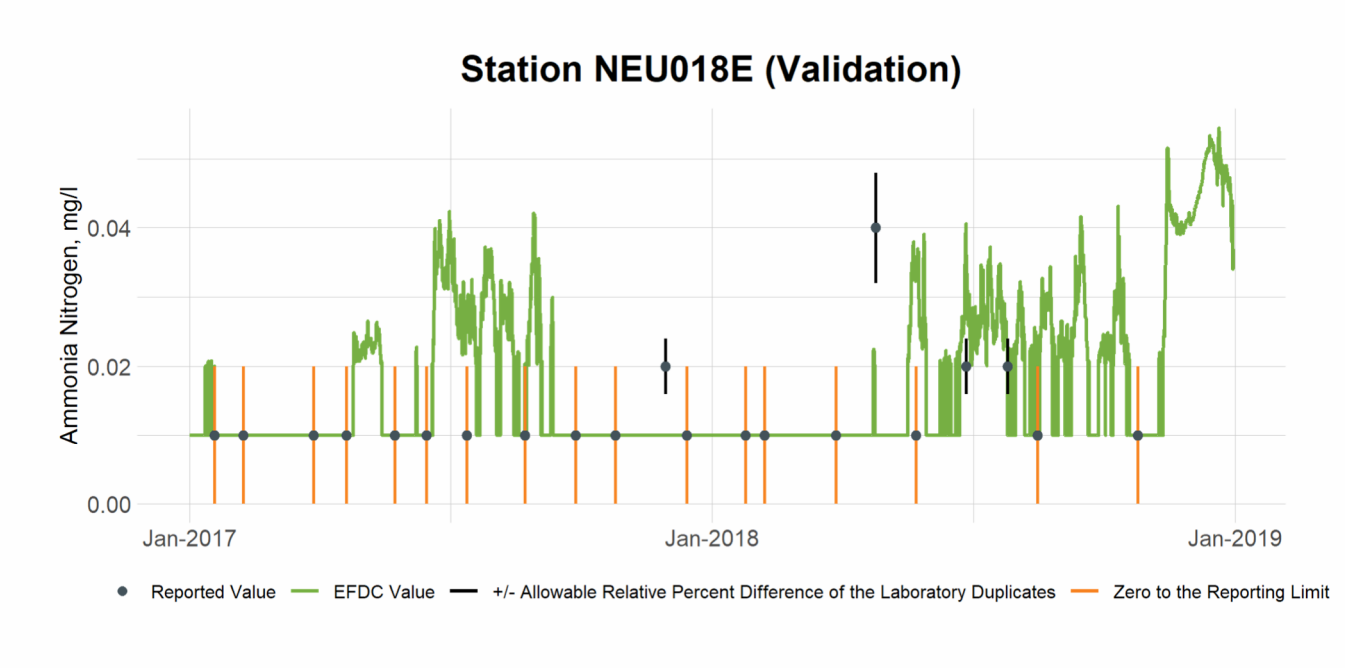

Figure 7-20 Validation Plot of Ammonia Nitrogen at Station NEU018E

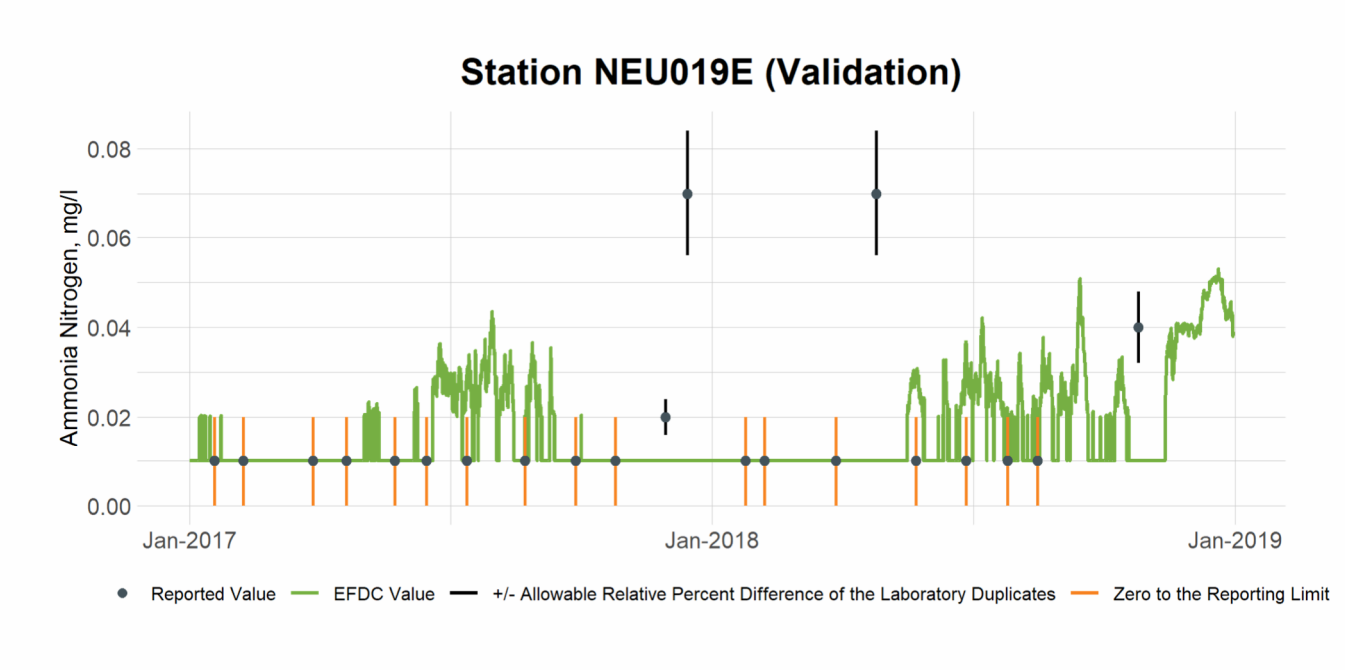

Figure 7-21 Validation Plot of Ammonia Nitrogen at Station NEU019E

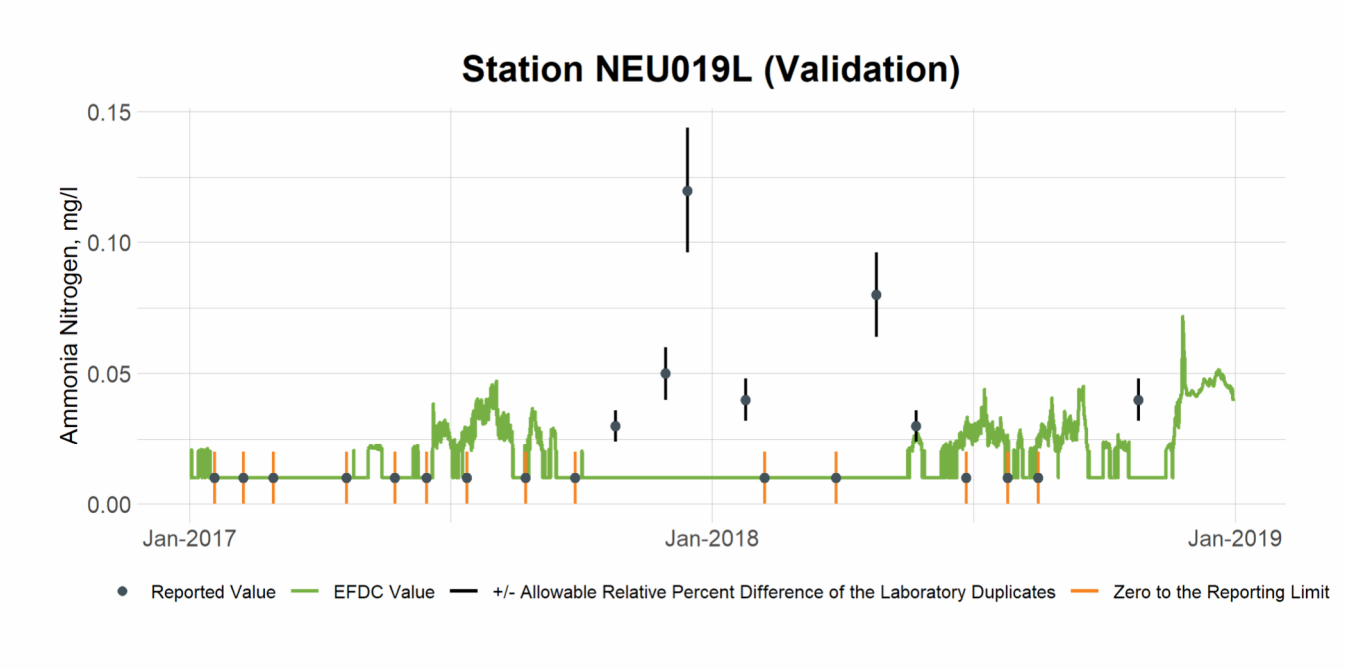

Figure 7-22 Validation Plot of Ammonia Nitrogen at Station NEU019L

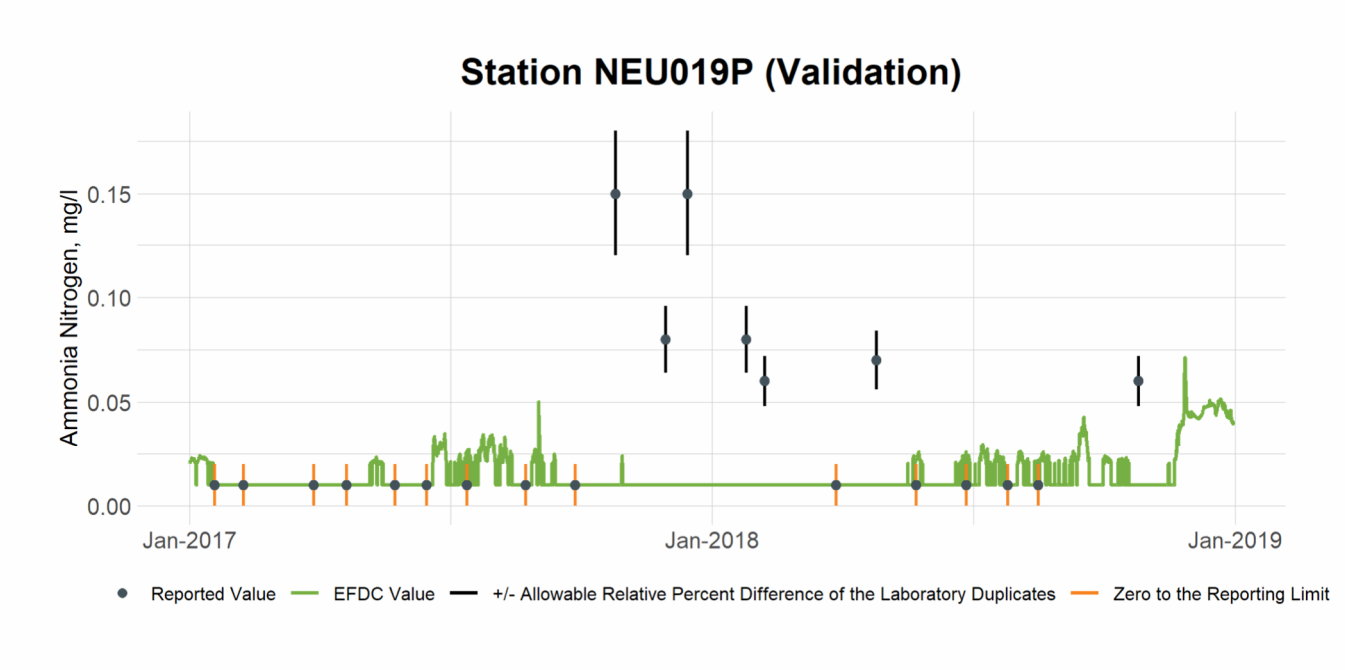

Figure 7-23 Validation Plot of Ammonia Nitrogen at Station NEU019P

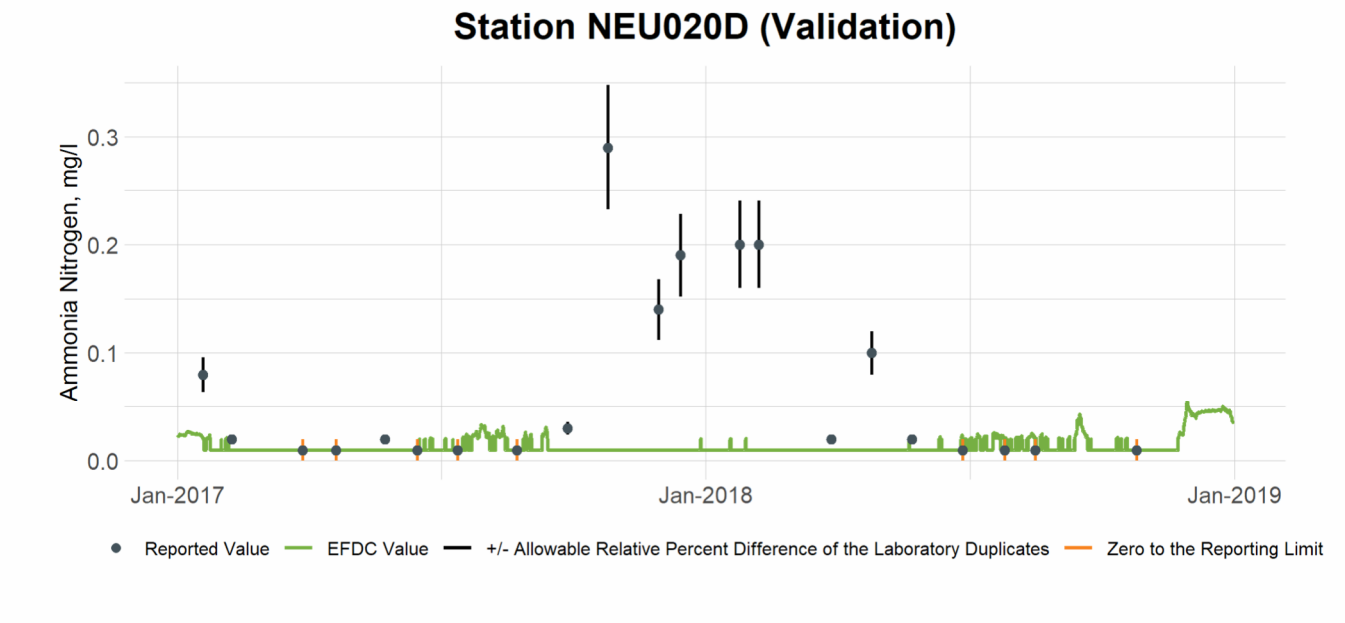

Figure 7-24 Validation Plot of Ammonia Nitrogen at Station NEU020D

8. Nitrate+Nitrite Nitrogen (NO_3)

8.1 Nitrate+Nitrite Nitrogen Calibration

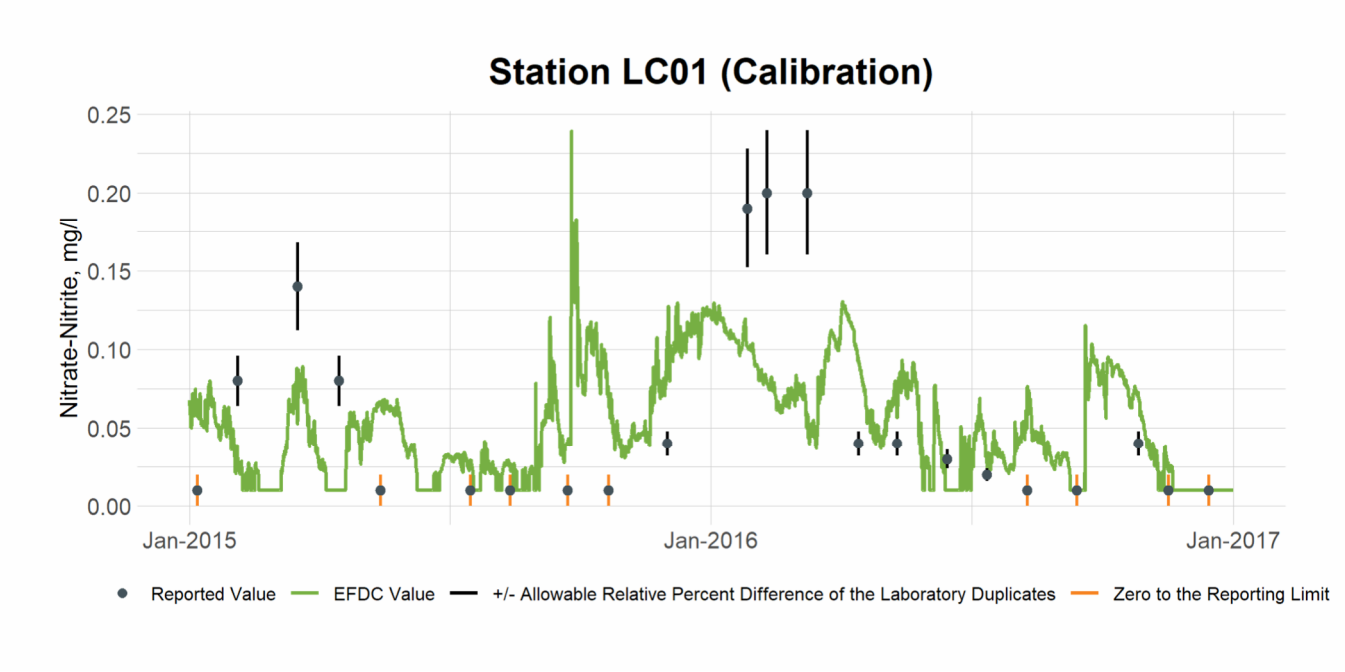

Figure 8-1 Calibration Plot of Nitrate+Nitrite Nitrogen at Station LC01

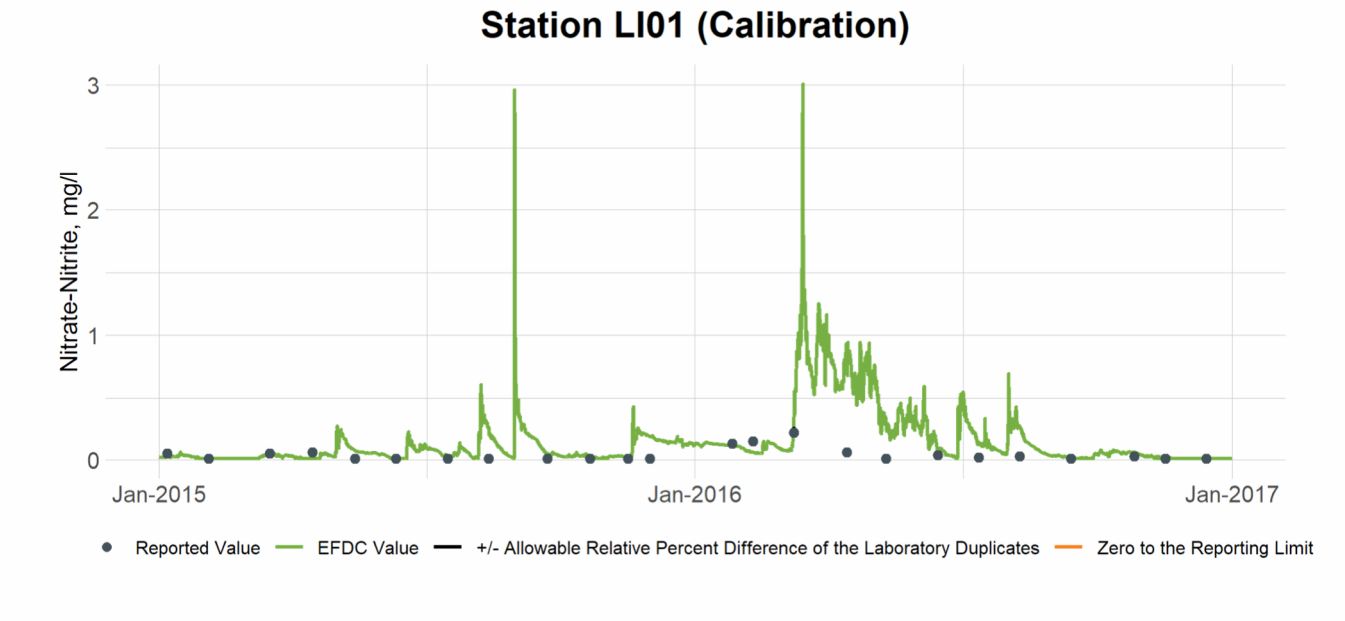

Figure 8-2 Calibration Plot of Nitrate+Nitrite Nitrogen at Station LI01

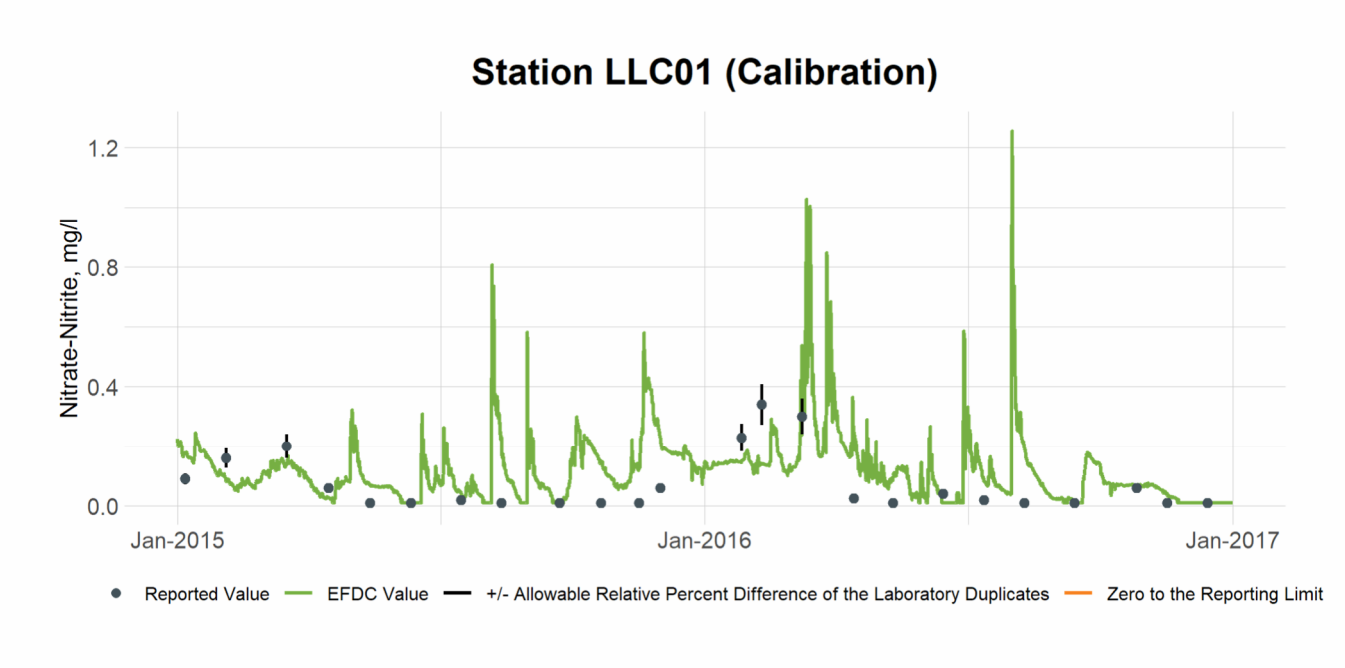

Figure 8-3 Calibration Plot of Nitrate+Nitrite Nitrogen at Station LLC01

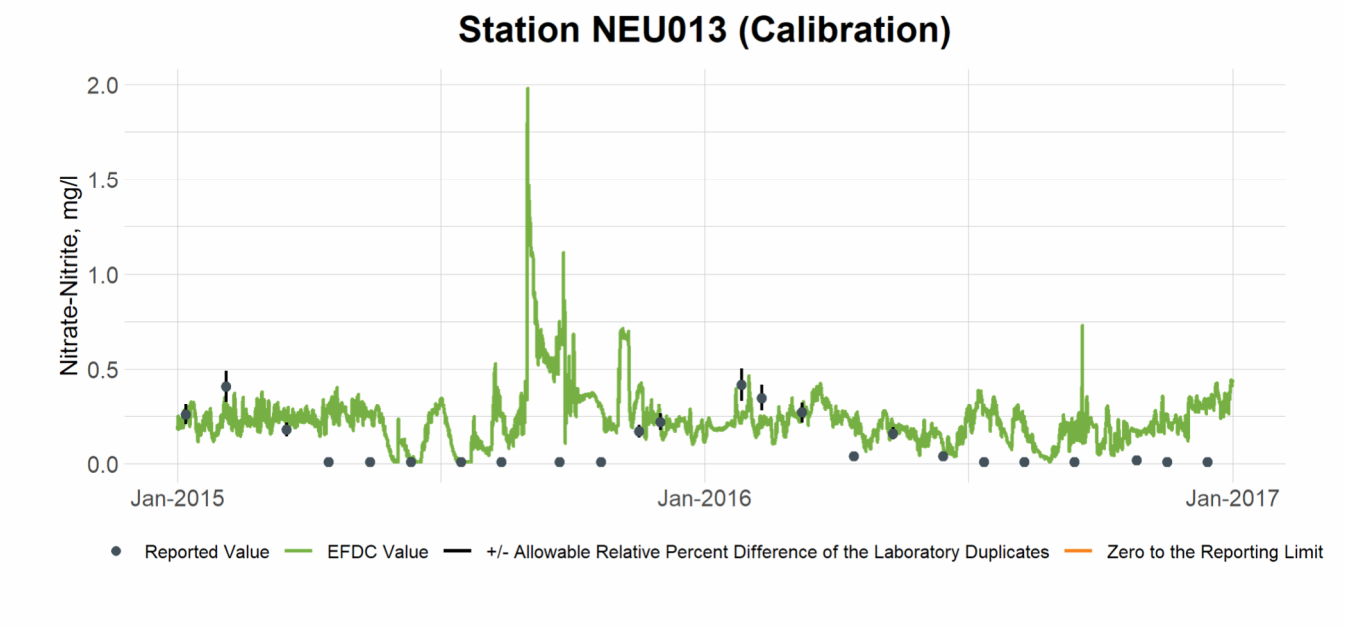

Figure 8-4 Calibration Plot of Nitrate+Nitrite Nitrogen at Station NEU013

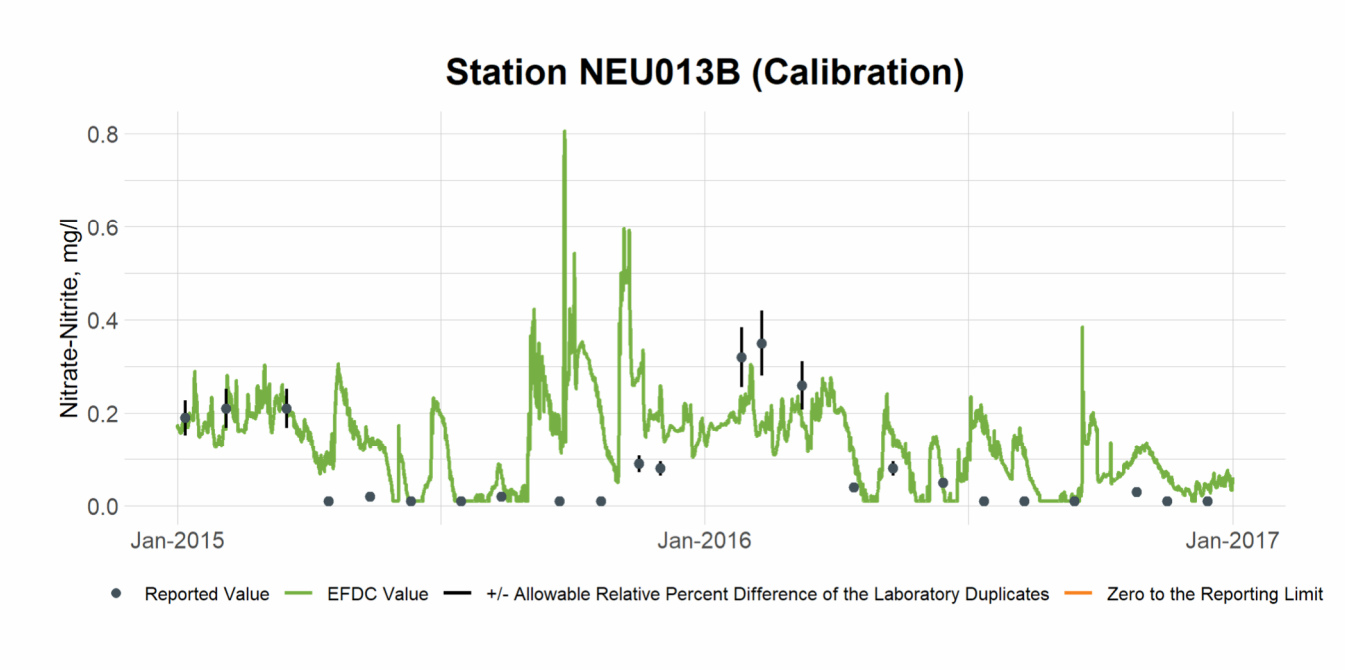

Figure 8-5 Calibration Plot of Nitrate+Nitrite Nitrogen at Station NEU013B

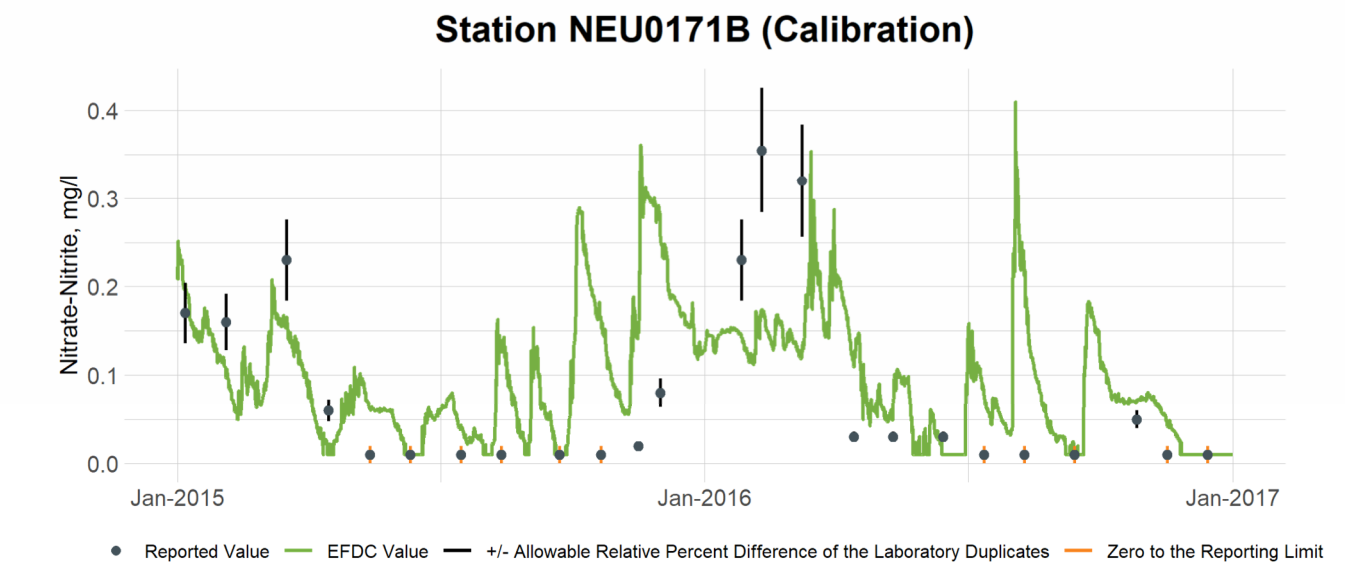

Figure 8-6 Calibration Plot of Nitrate+Nitrite Nitrogen at Station NEU0171B

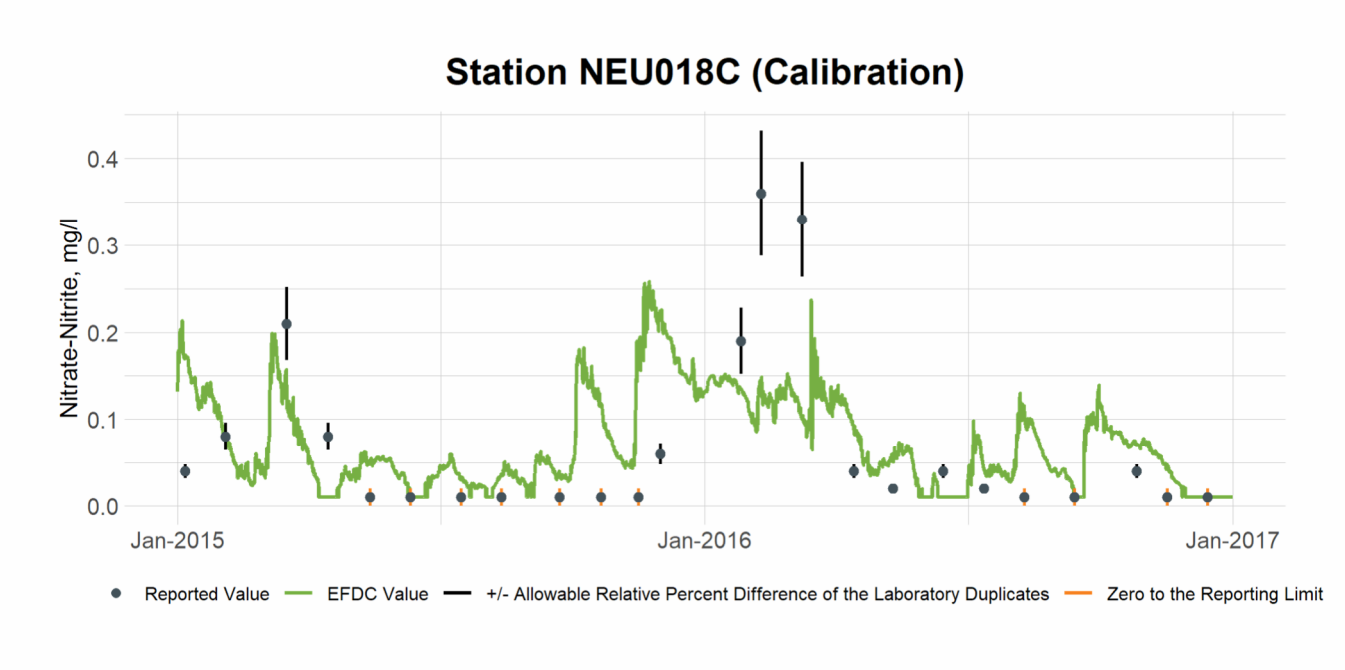

Figure 8-7 Calibration Plot of Nitrate+Nitrite Nitrogen at Station NEU018C

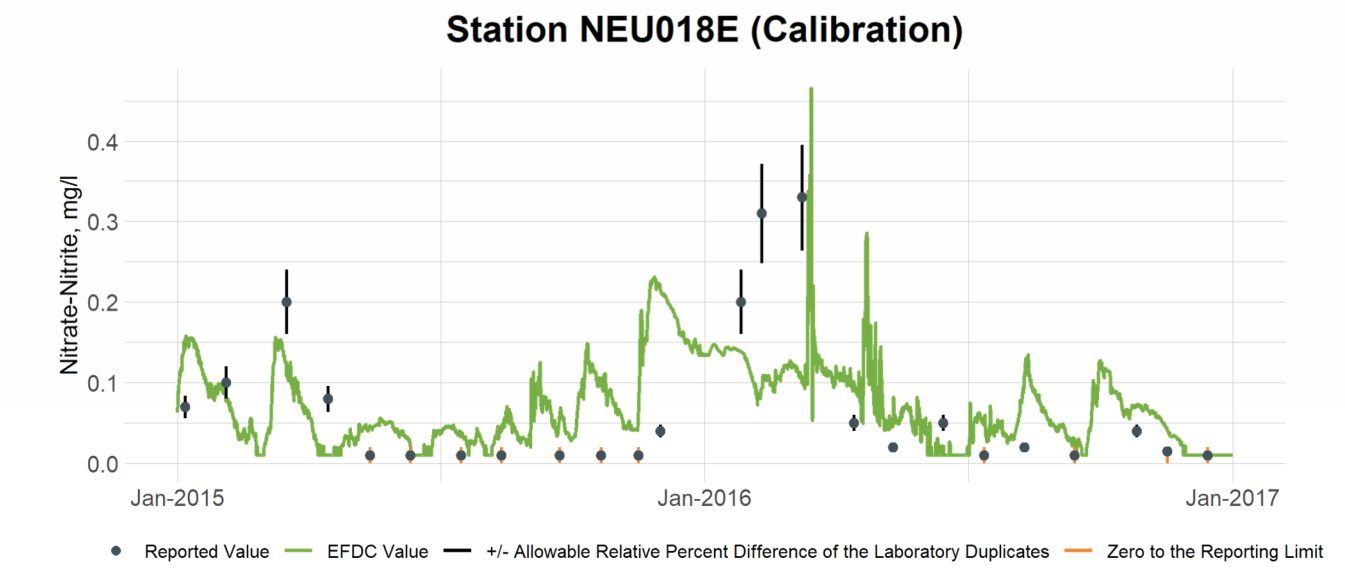

Figure 8-8 Calibration Plot of Nitrate+Nitrite Nitrogen at Station NEU018E

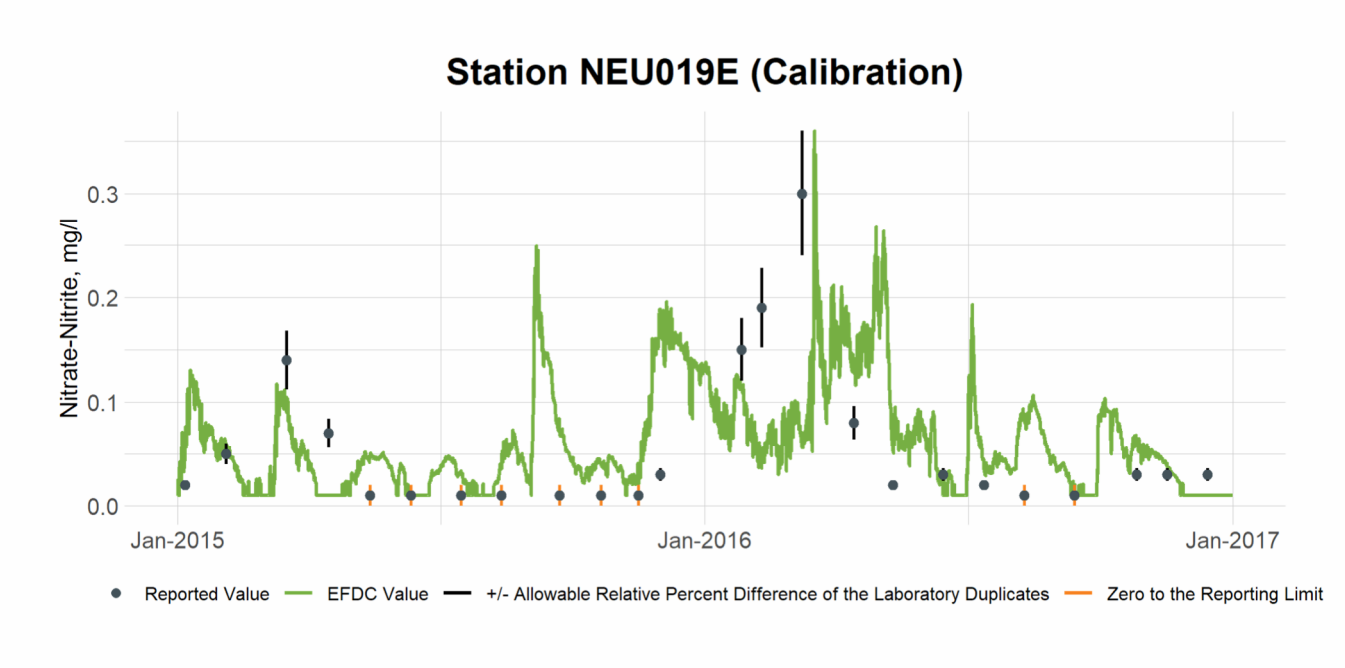

Figure 8-9 Calibration Plot of Nitrate+Nitrite Nitrogen at Station NEU019E

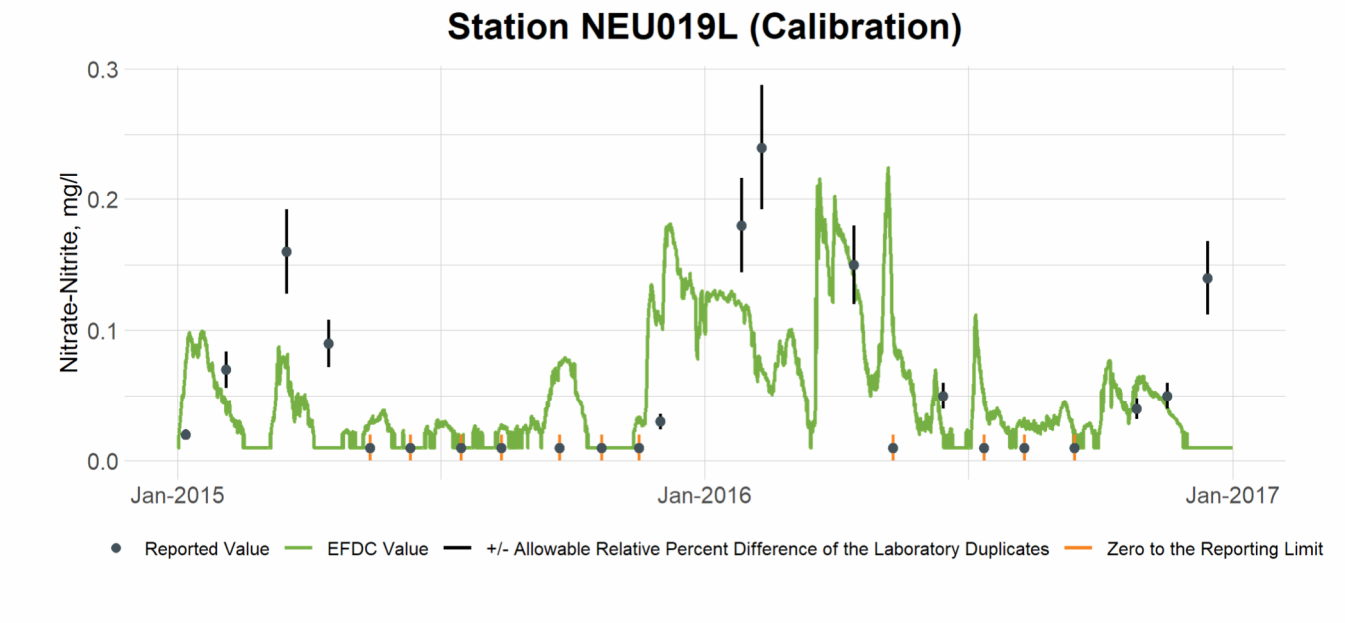

Figure 8-10 Calibration Plot of Nitrate+Nitrite Nitrogen at Station NEU019L

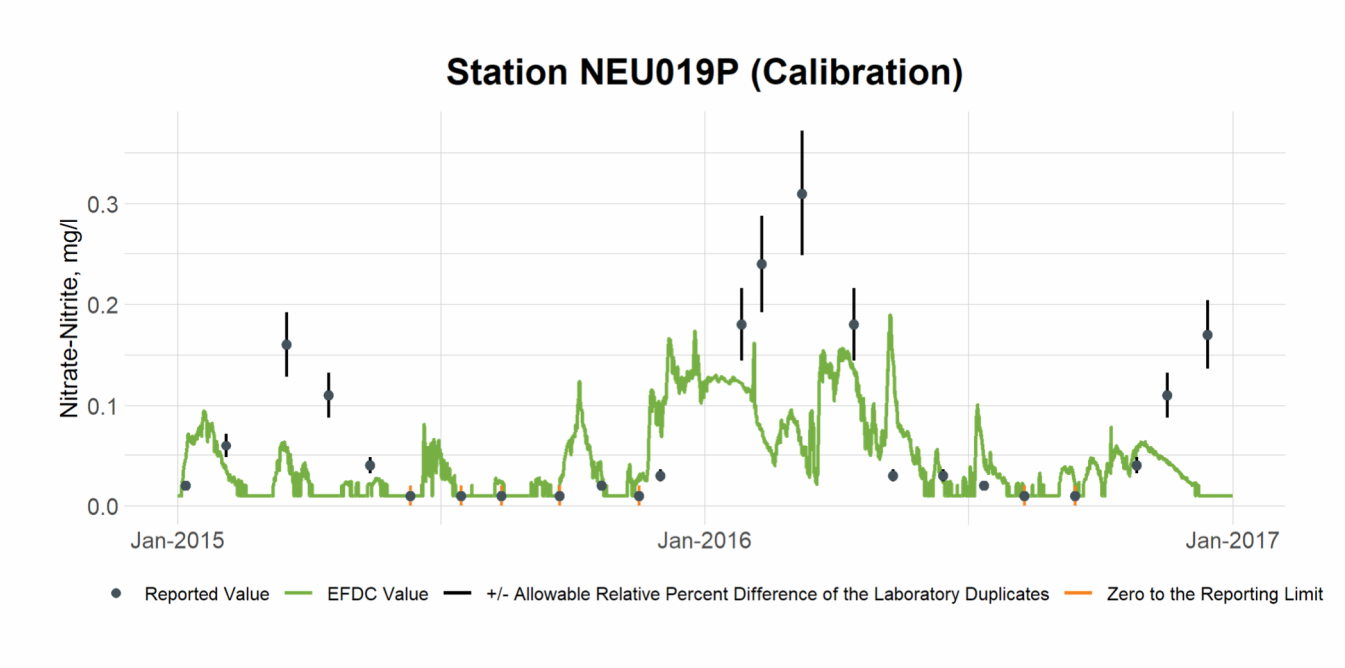

Figure 8-11 Calibration Plot of Nitrate+Nitrite Nitrogen at Station NEU019P

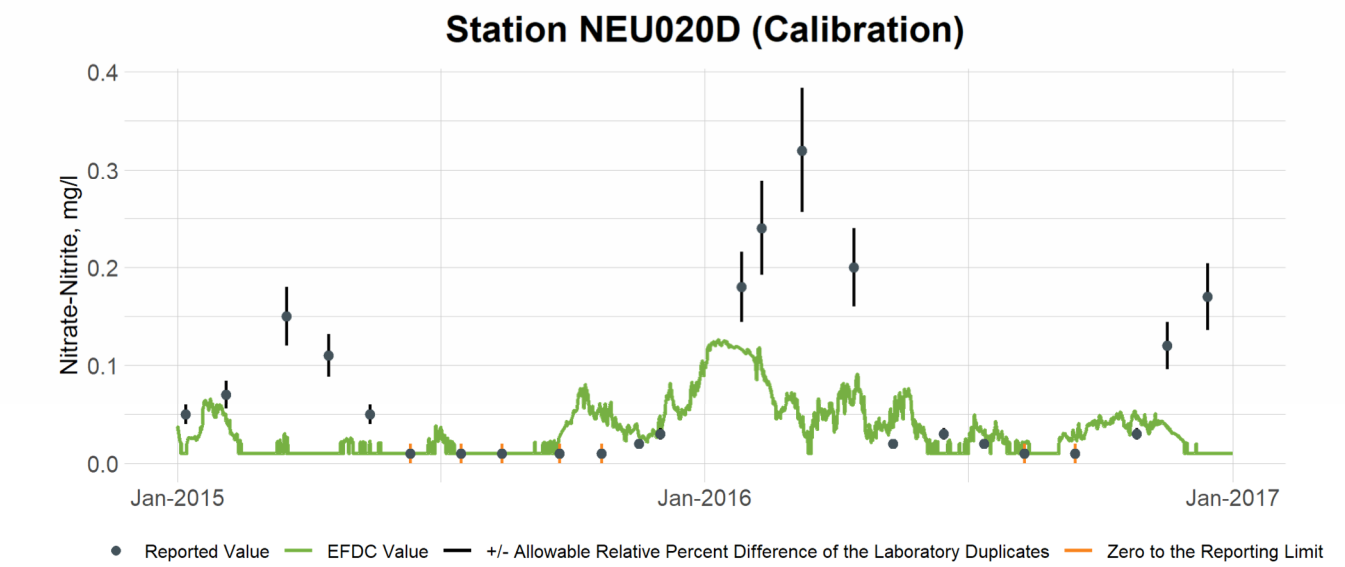

Figure 8-12 Calibration Plot of Nitrate+Nitrite Nitrogen at Station NEU020D

8.2 Nitrate+Nitrite Nitrogen Validation

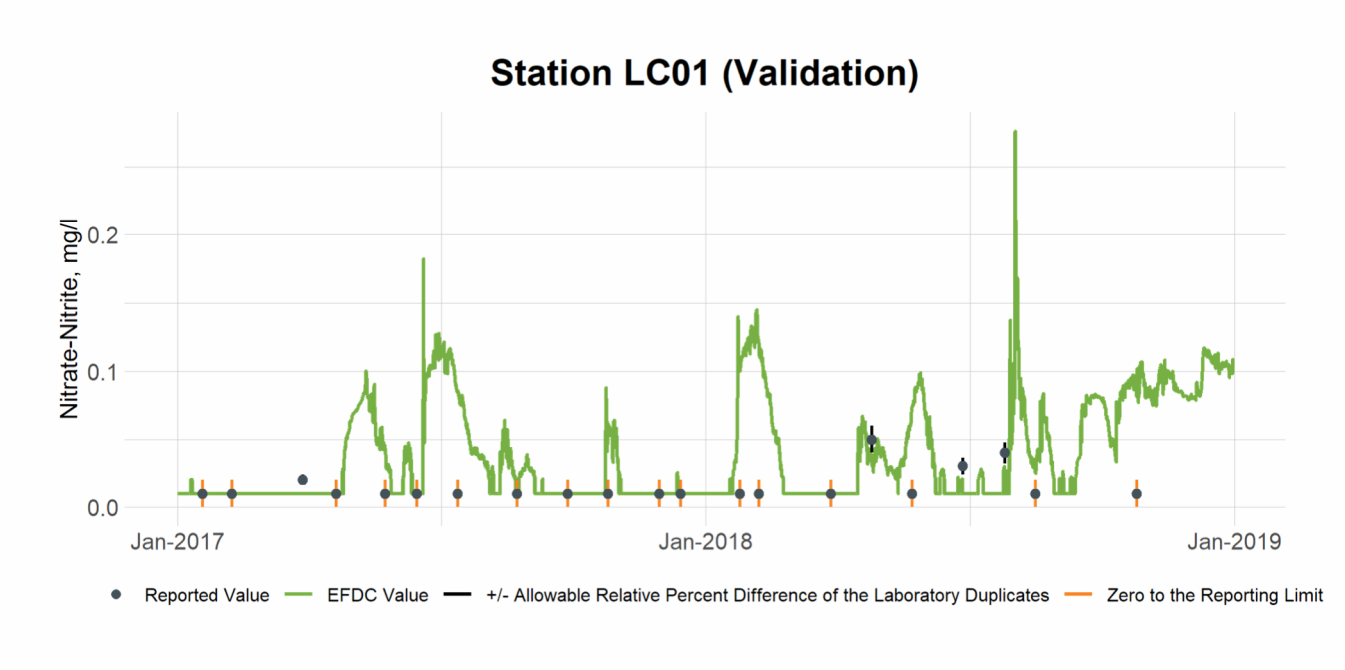

Figure 8-13 Validation Plot of Nitrate+Nitrite Nitrogen at Station LC01

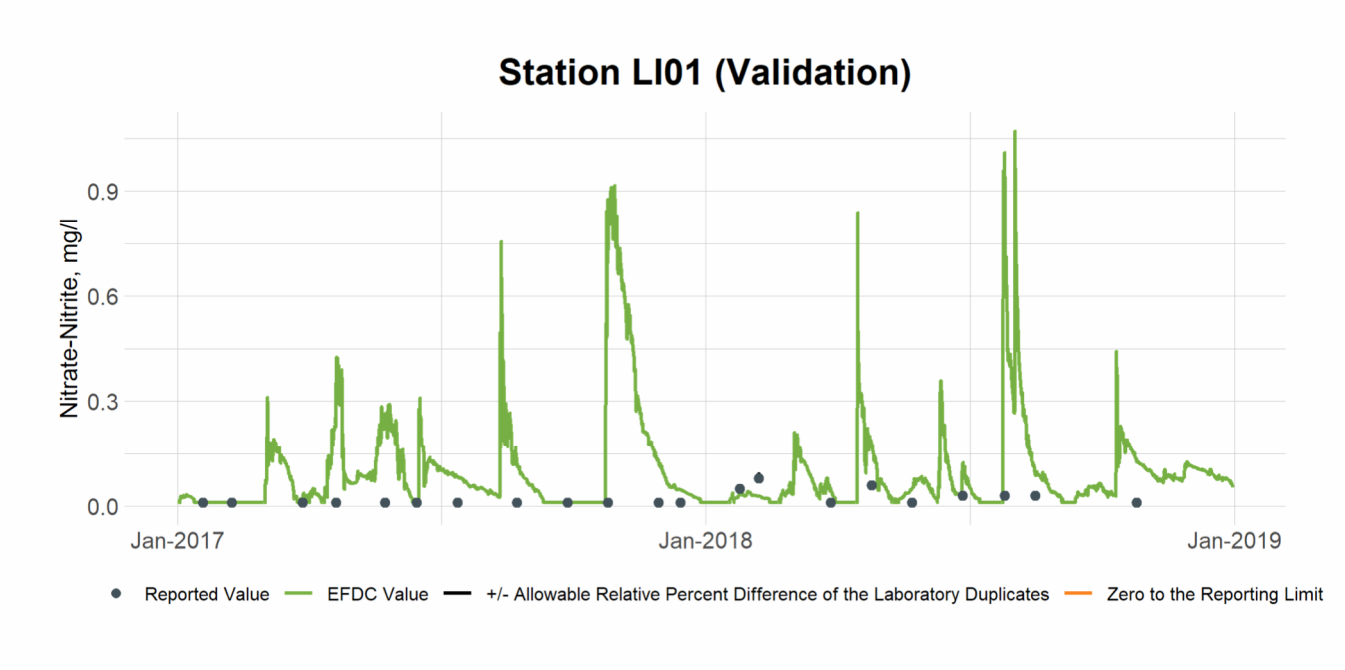

Figure 8-14 Validation Plot of Nitrate+Nitrite Nitrogen at Station LI01

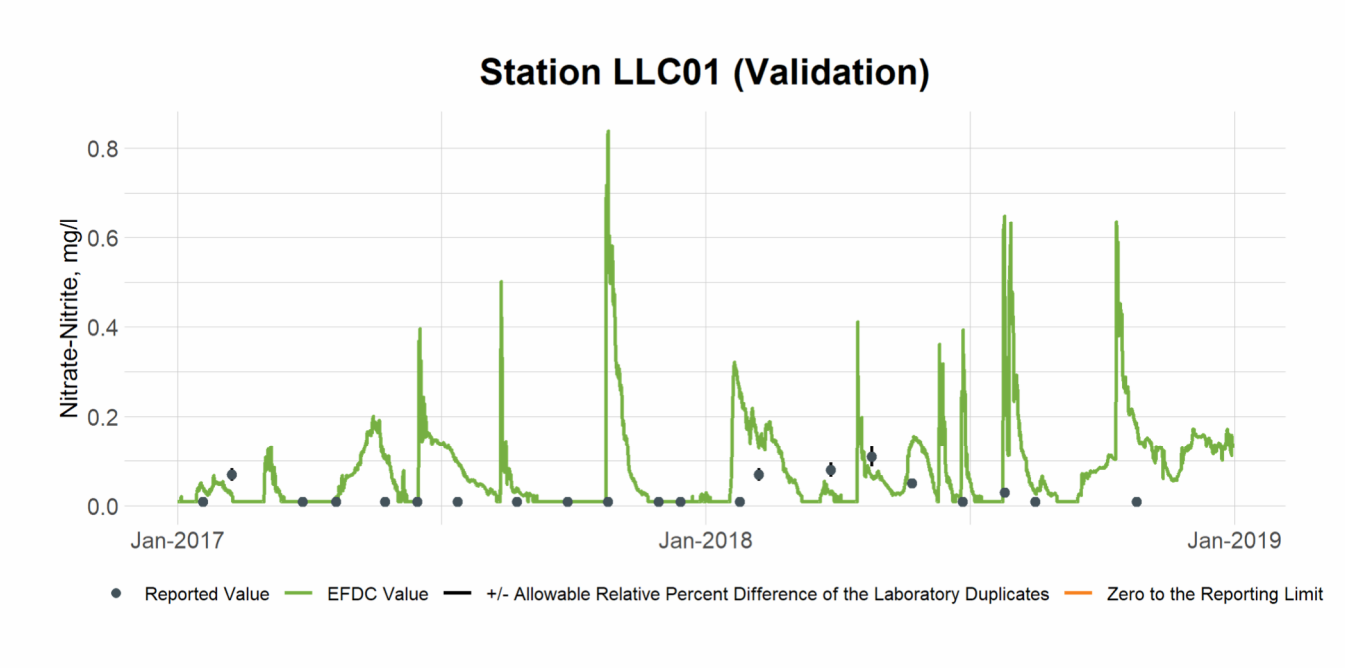

Figure 8-15 Validation Plot of Nitrate+Nitrite Nitrogen at Station LLC01

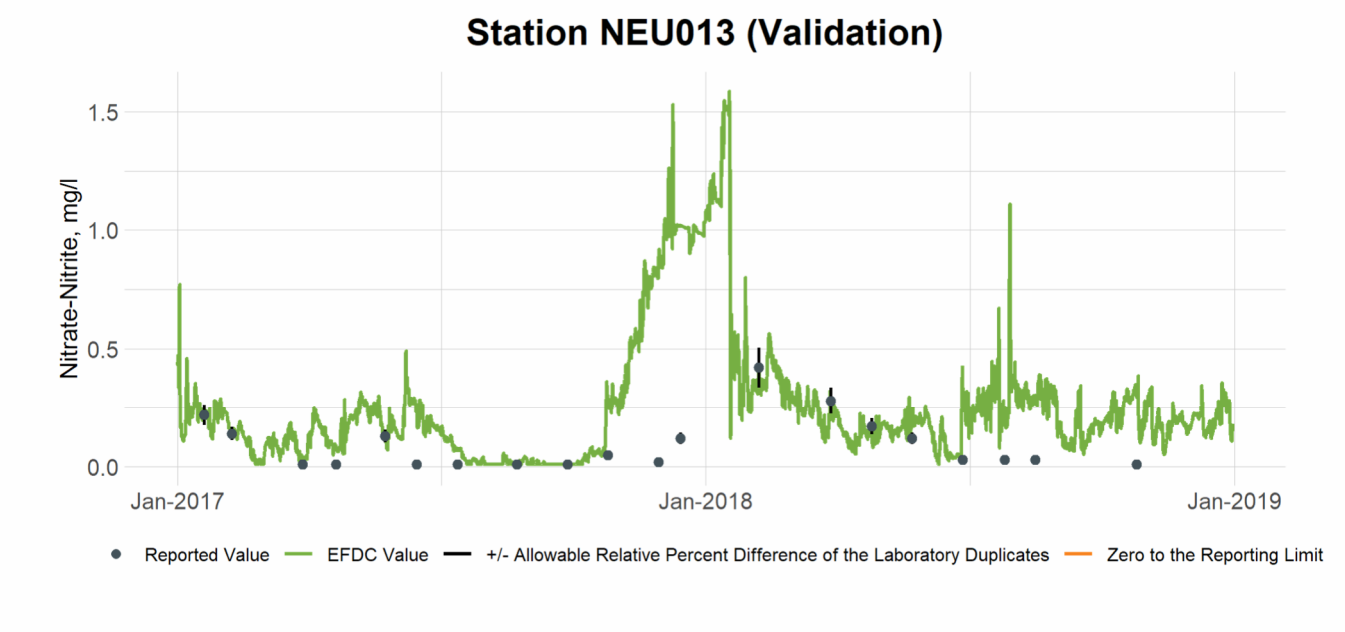

Figure 8-16 Validation Plot of Nitrate+Nitrite Nitrogen at Station NEU013

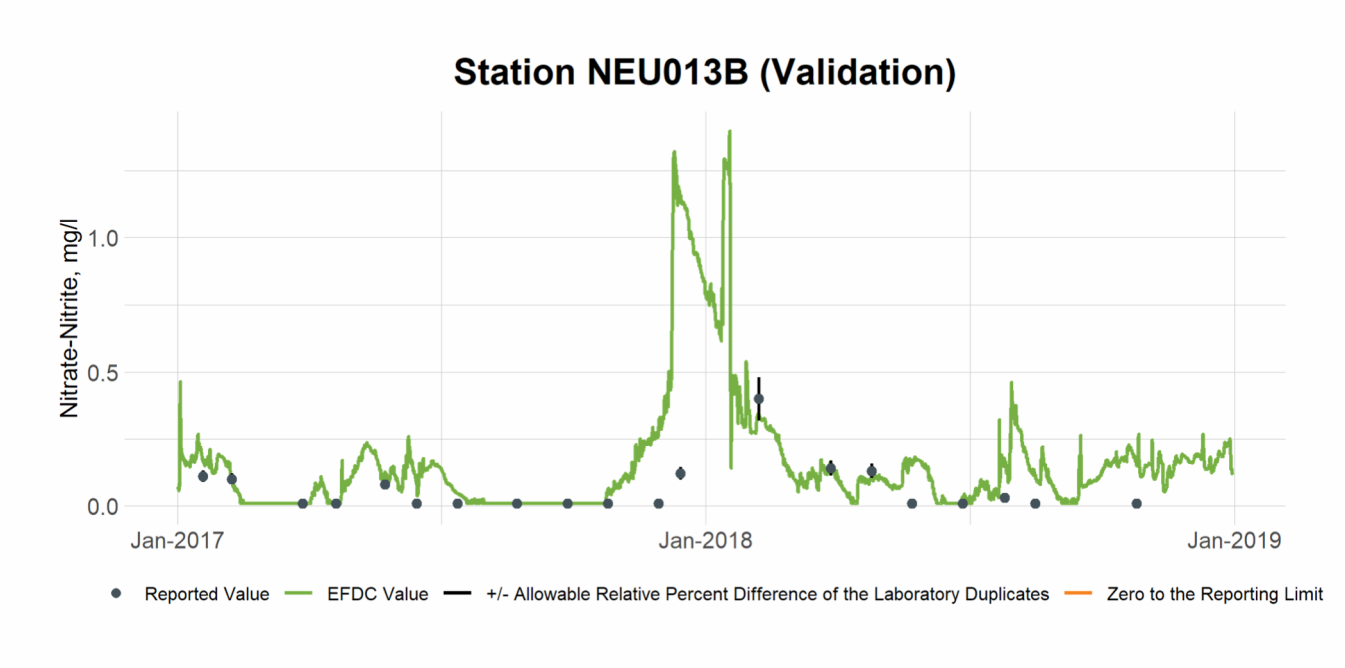

Figure 8-17 Validation Plot of Nitrate+Nitrite Nitrogen at Station NEU013B

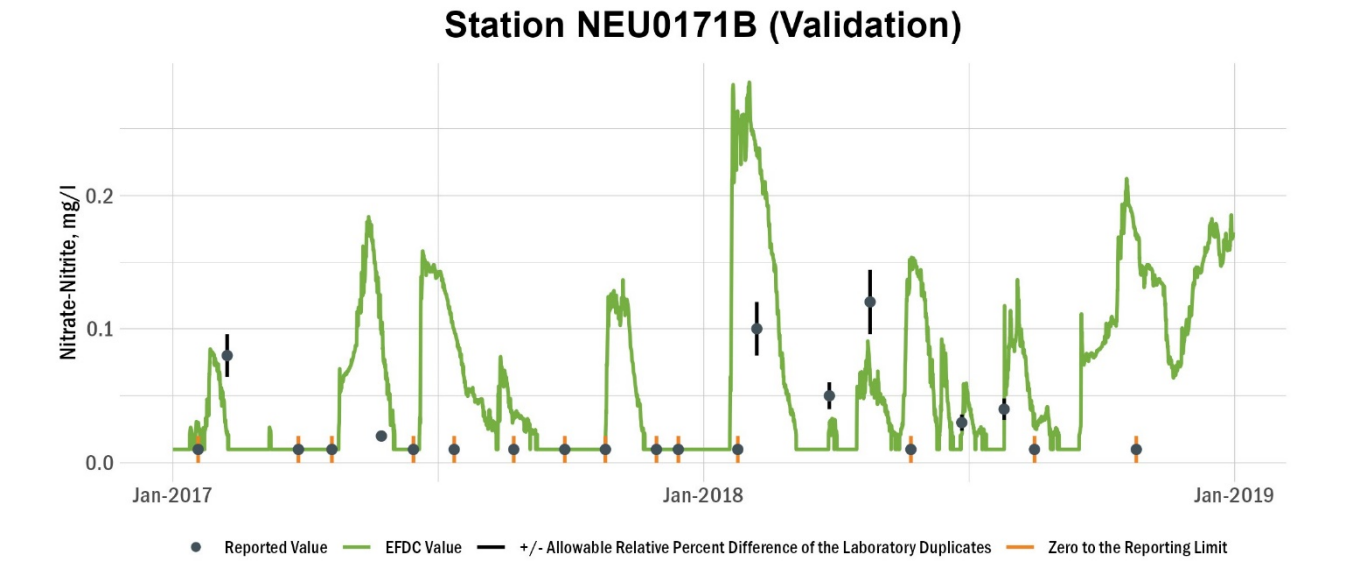

Figure 8-18 Validation Plot of Nitrate+Nitrite Nitrogen at Station NEU0171B

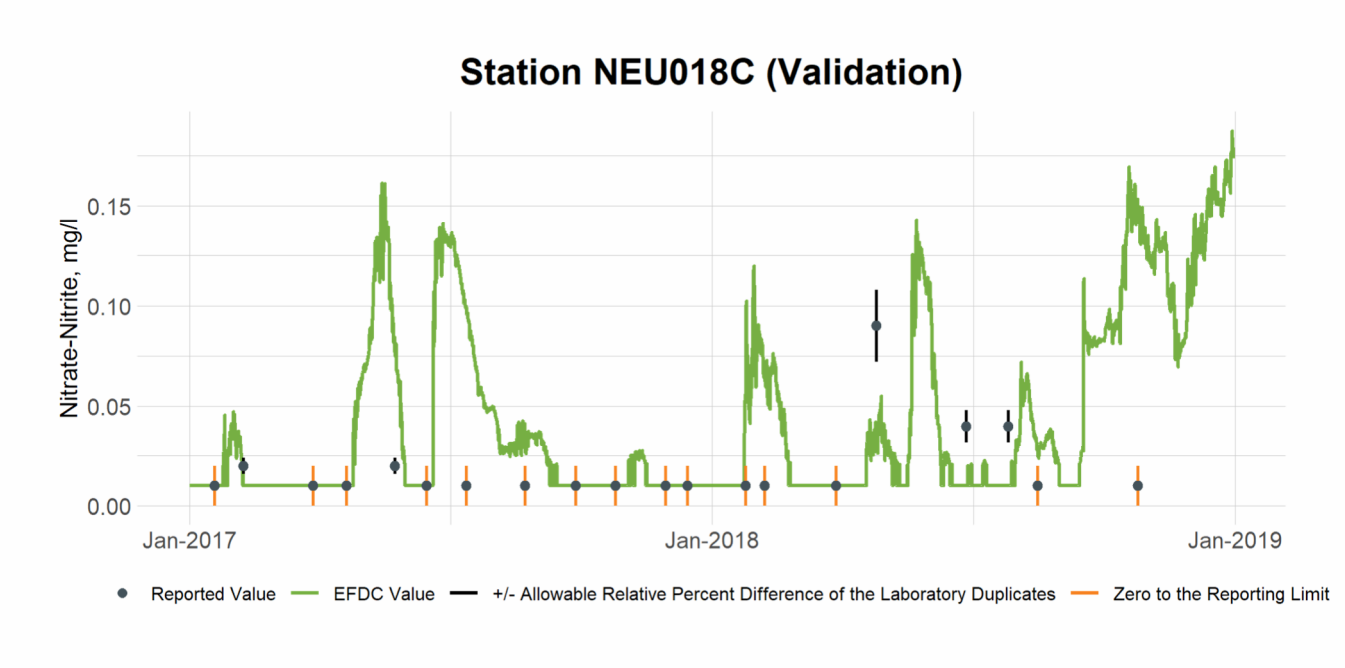

Figure 8-19 Validation Plot of Nitrate+Nitrite Nitrogen at Station NEU018C

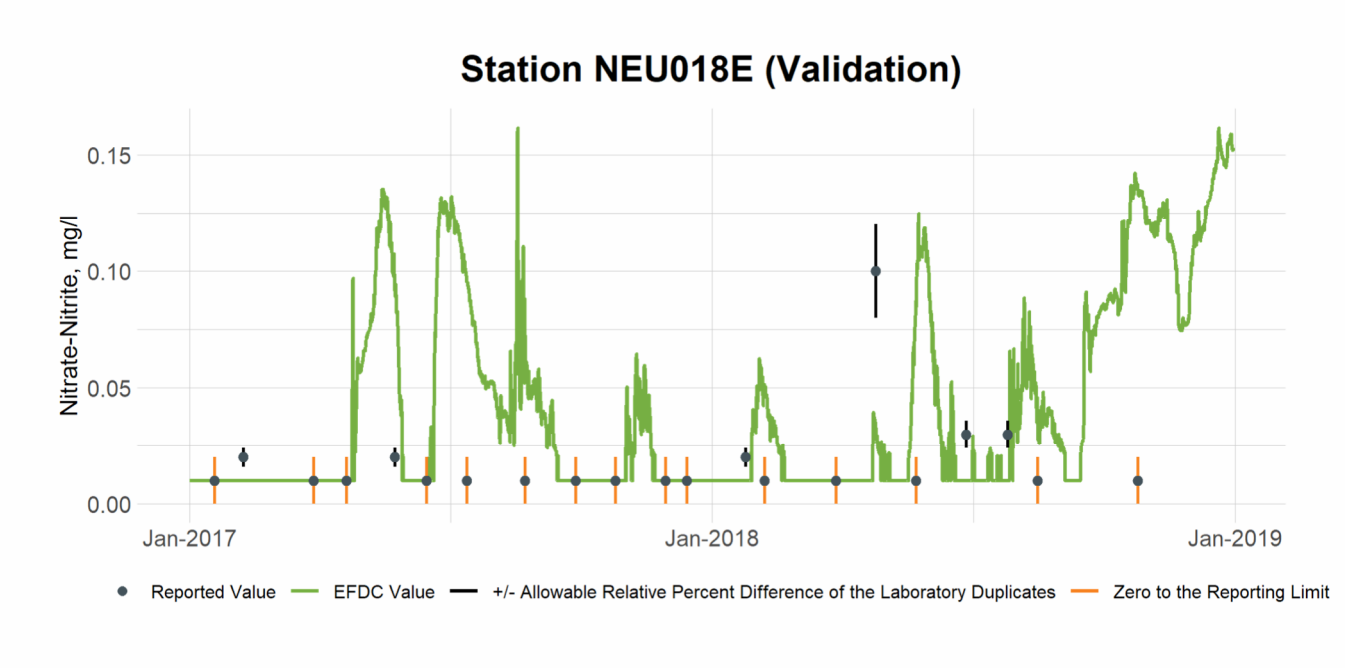

Figure 8-20 Validation Plot of Nitrate+Nitrite Nitrogen at Station NEU018E

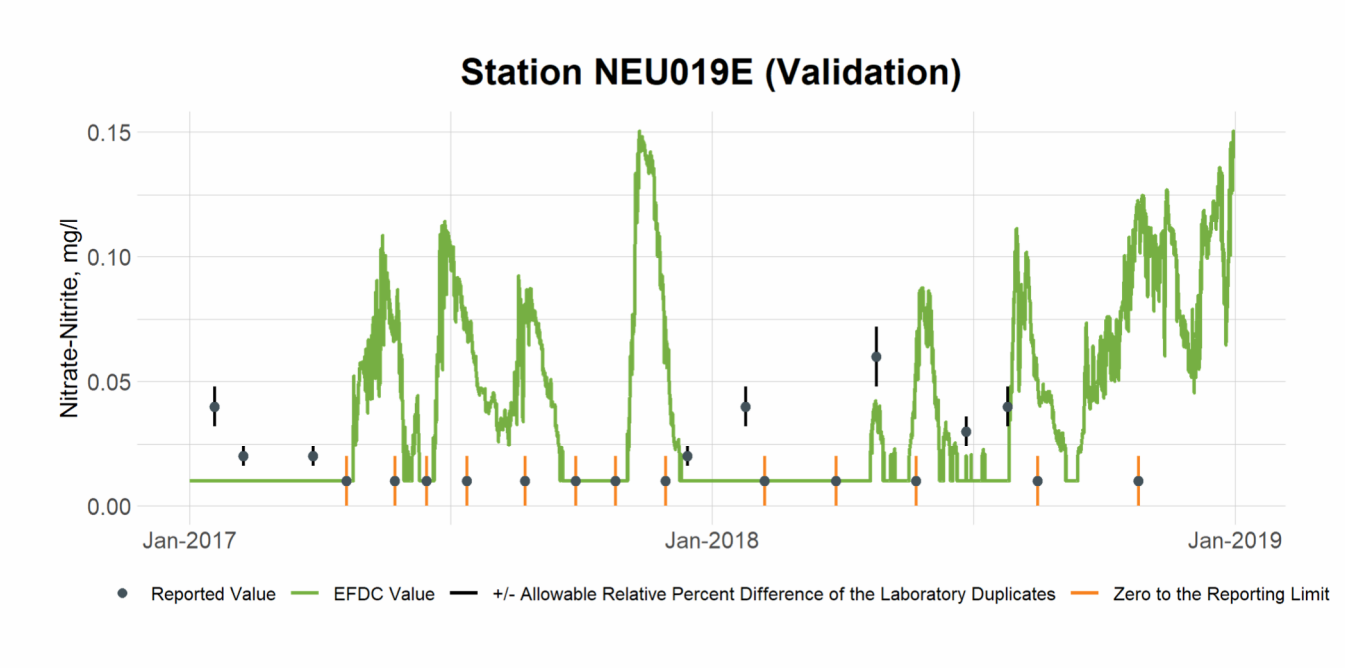

Figure 8-21 Validation Plot of Nitrate+Nitrite Nitrogen at Station NEU019E

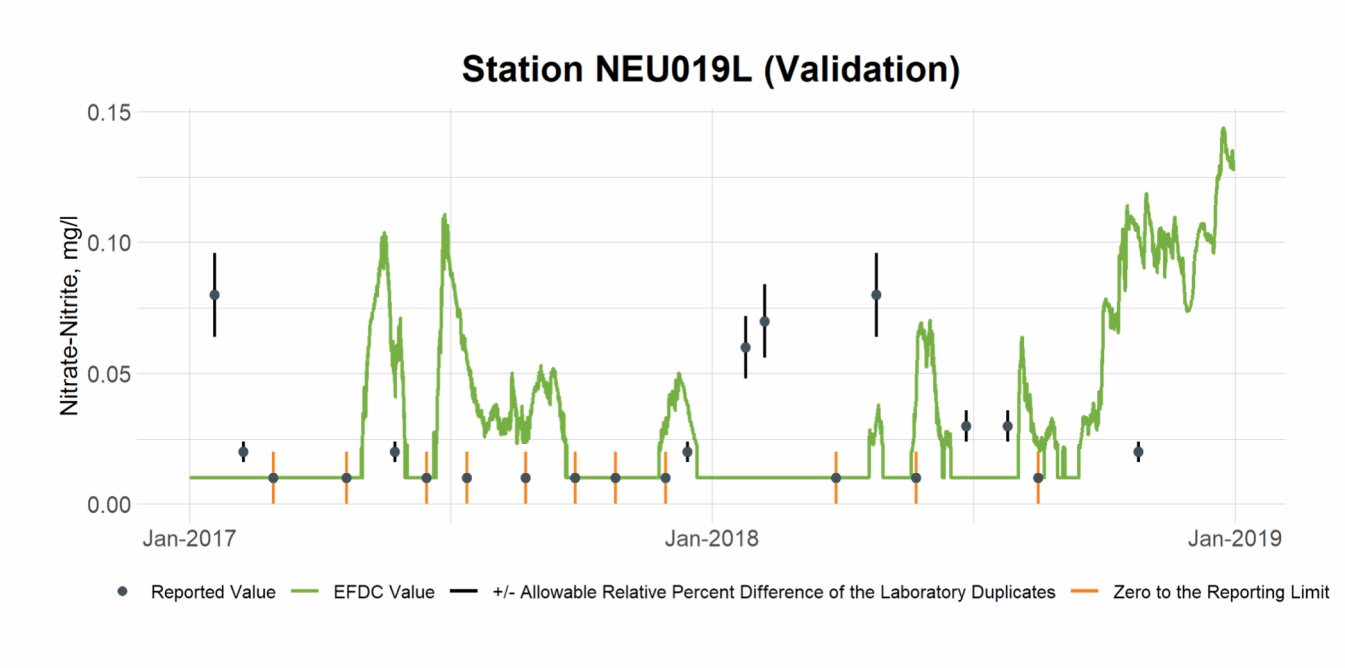

Figure 8-22 Validation Plot of Nitrate+Nitrite Nitrogen at Station NEU019L

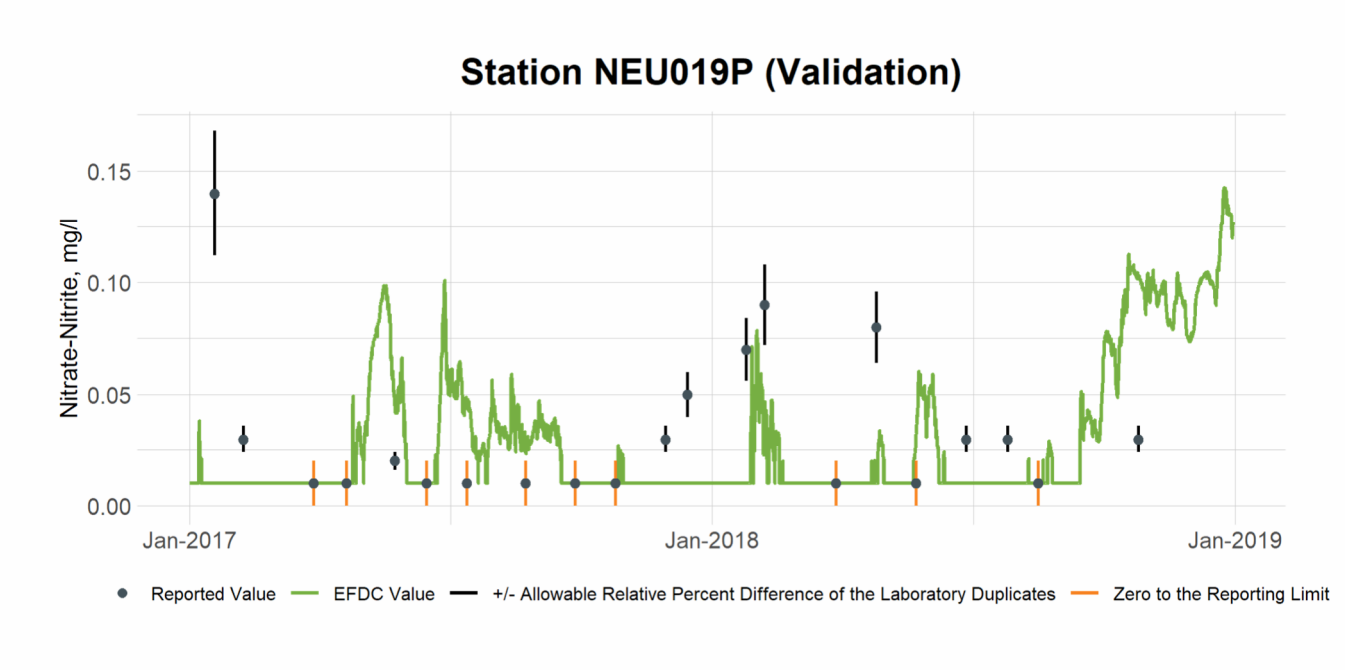

Figure 8-23 Validation Plot of Nitrate+Nitrite Nitrogen at Station NEU019P

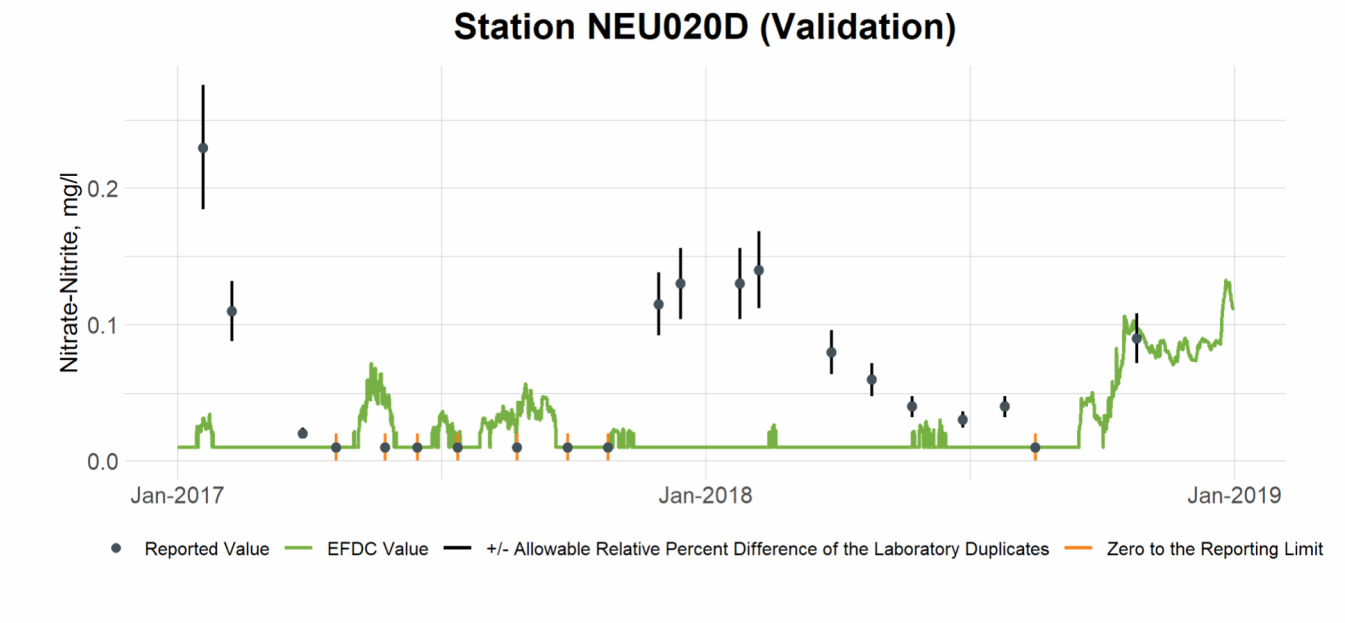

Figure 8-24 Validation Plot of Nitrate+Nitrite Nitrogen at Station NEU020D

9. DOC

9.1 DOC Calibration

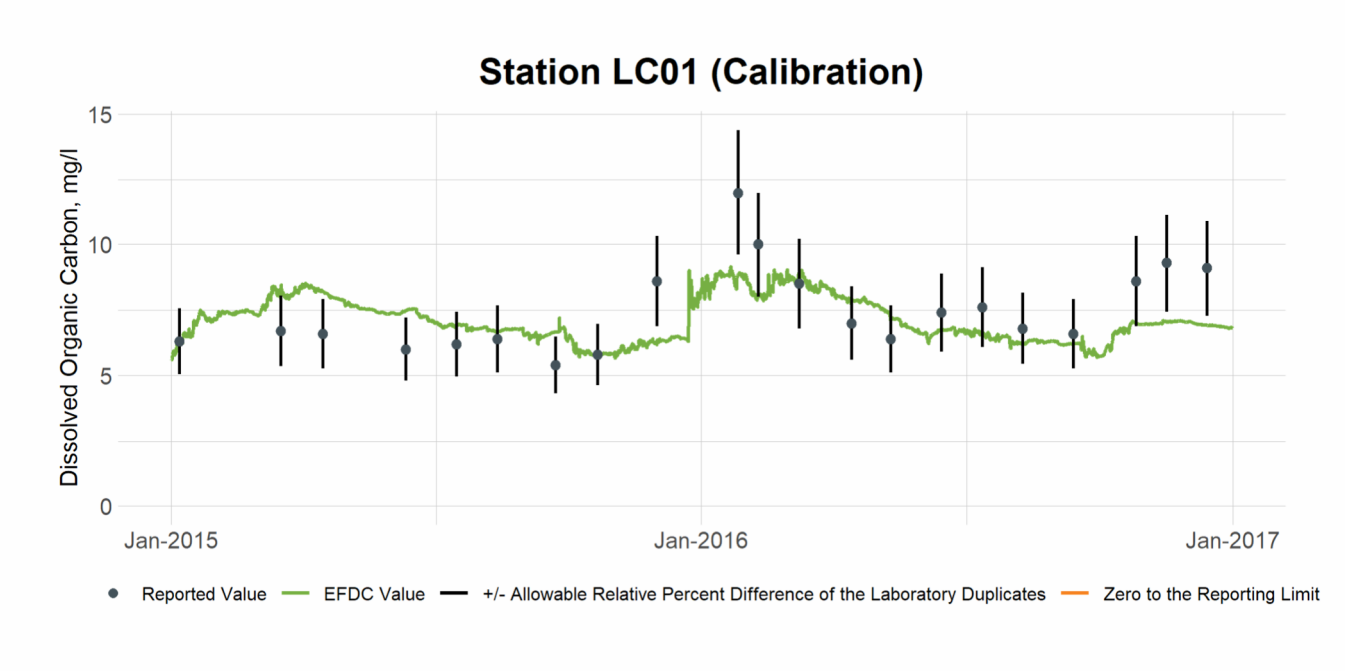

Figure 9-1 Calibration Plot of DOC at Station LC01

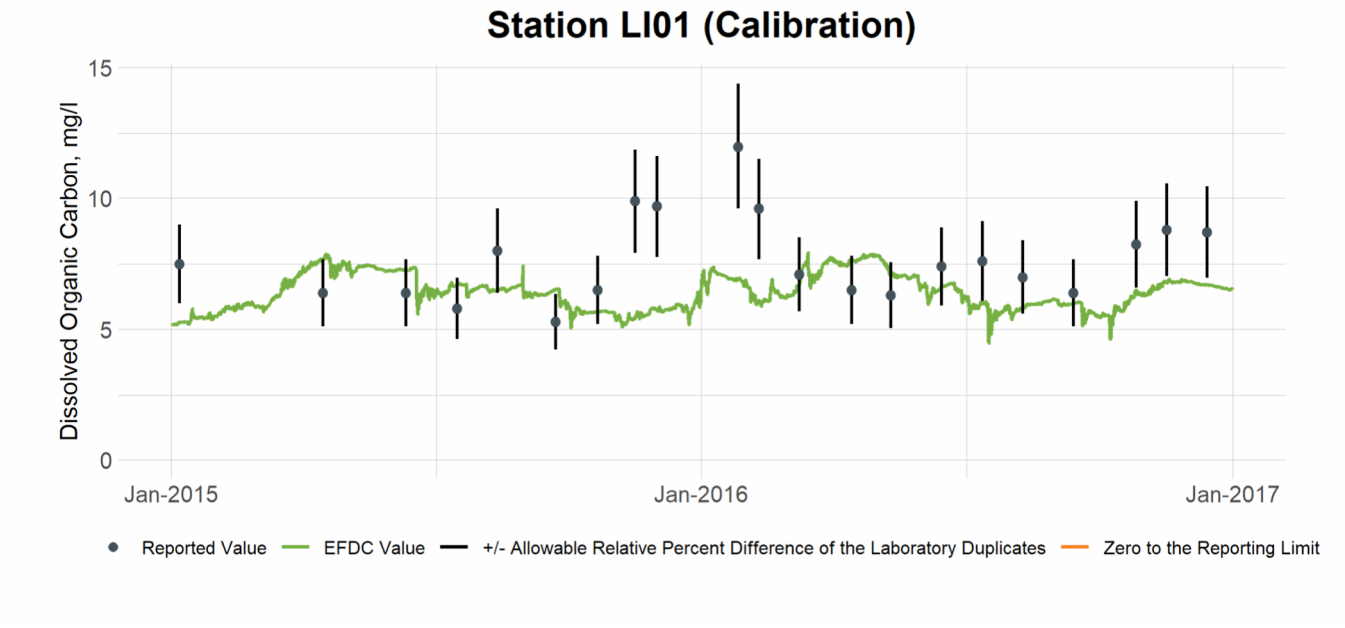

Figure 9-2 Calibration Plot of DOC at Station LI01

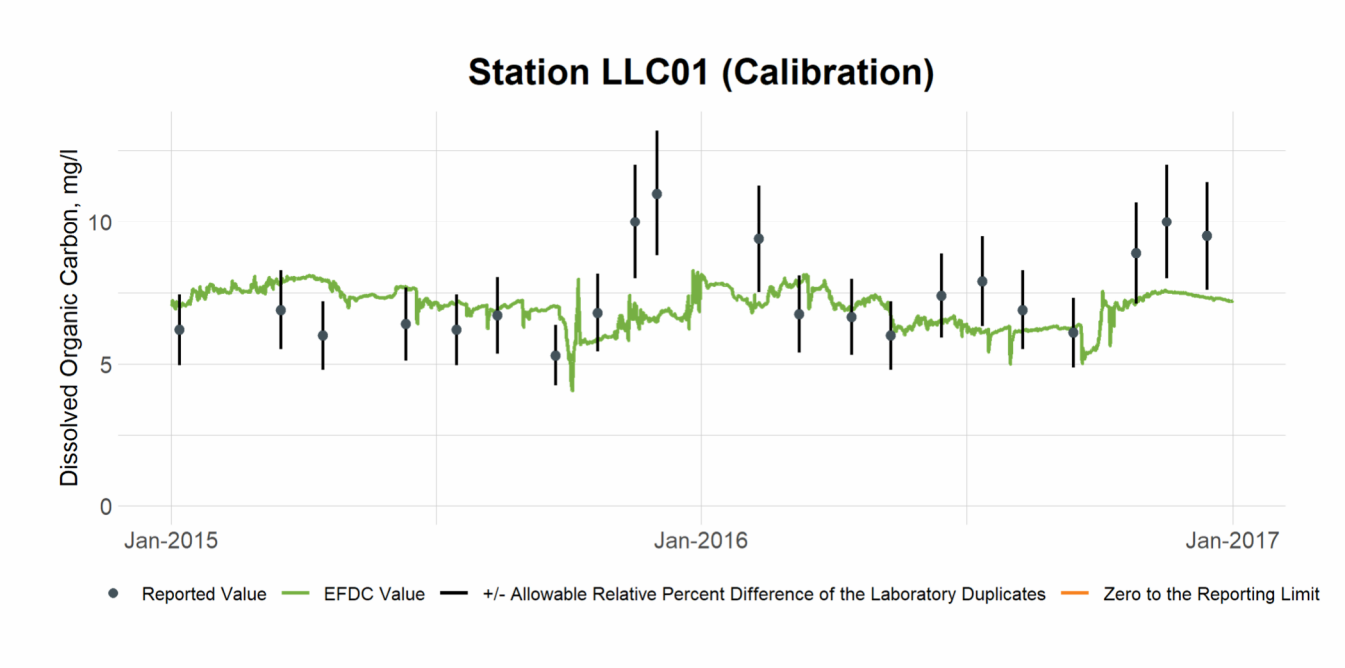

Figure 9-3 Calibration Plot of DOC at Station LLC01

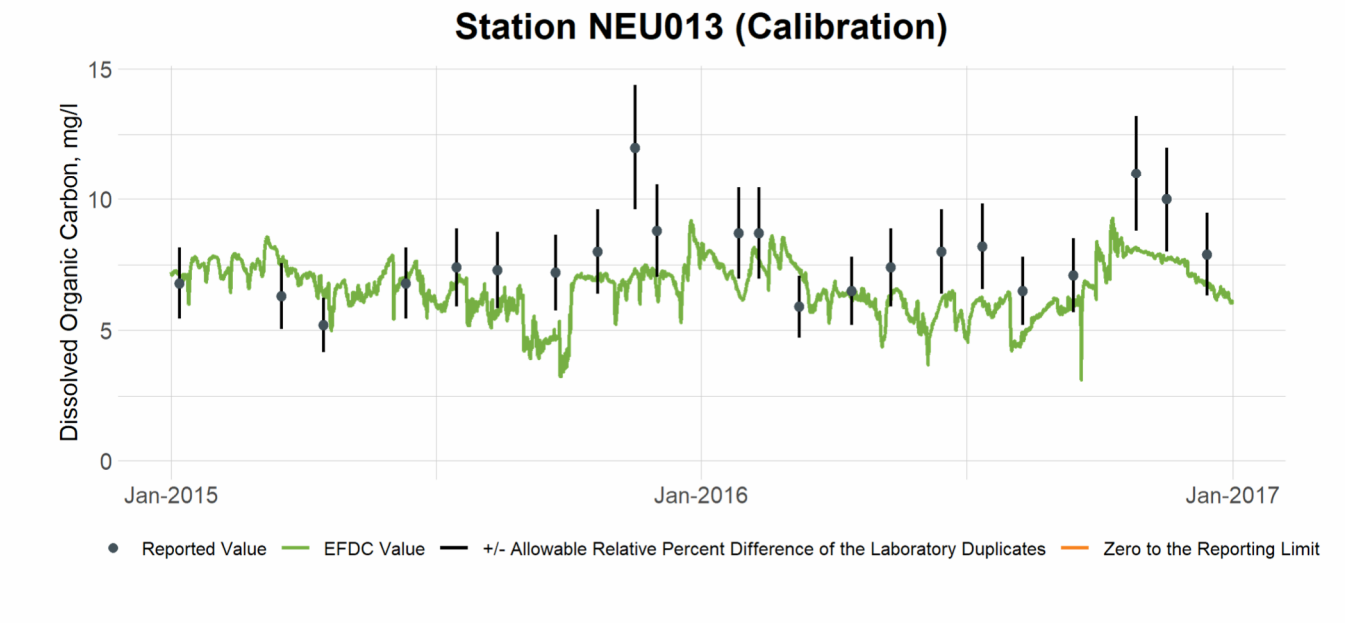

Figure 9-4 Calibration Plot of DOC at Station NEU013

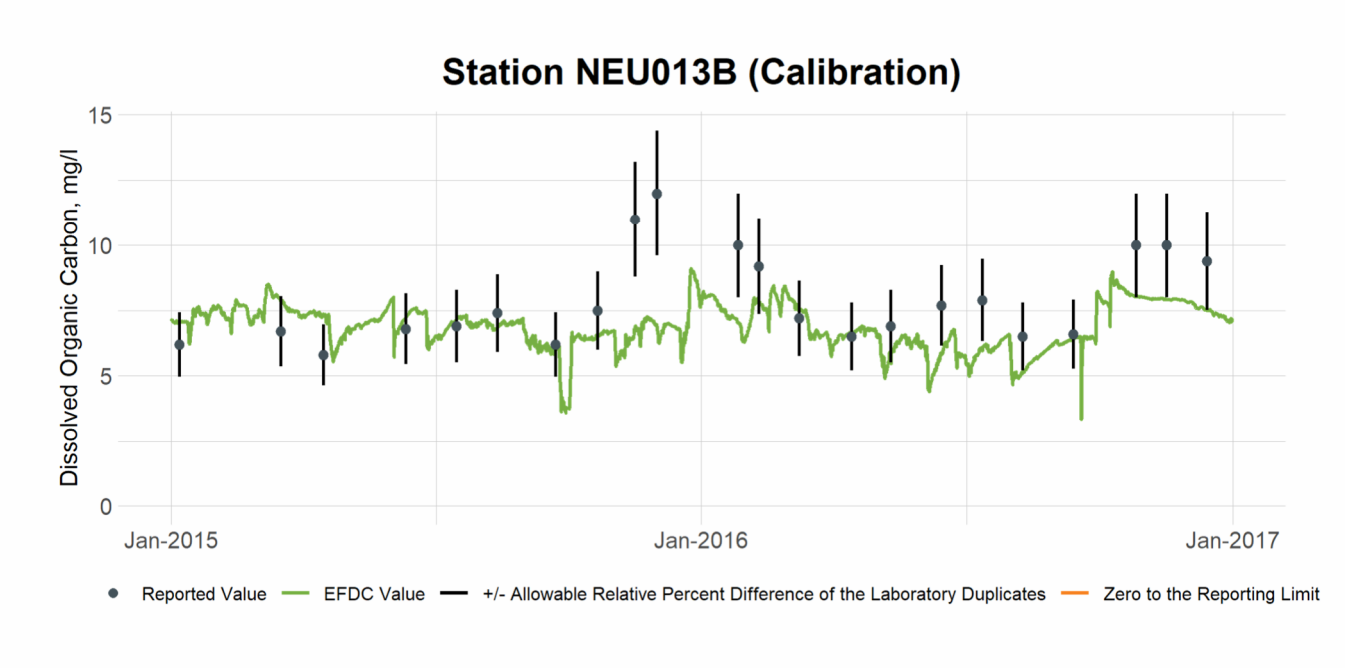

Figure 9-5 Calibration Plot of DOC at Station NEU013B

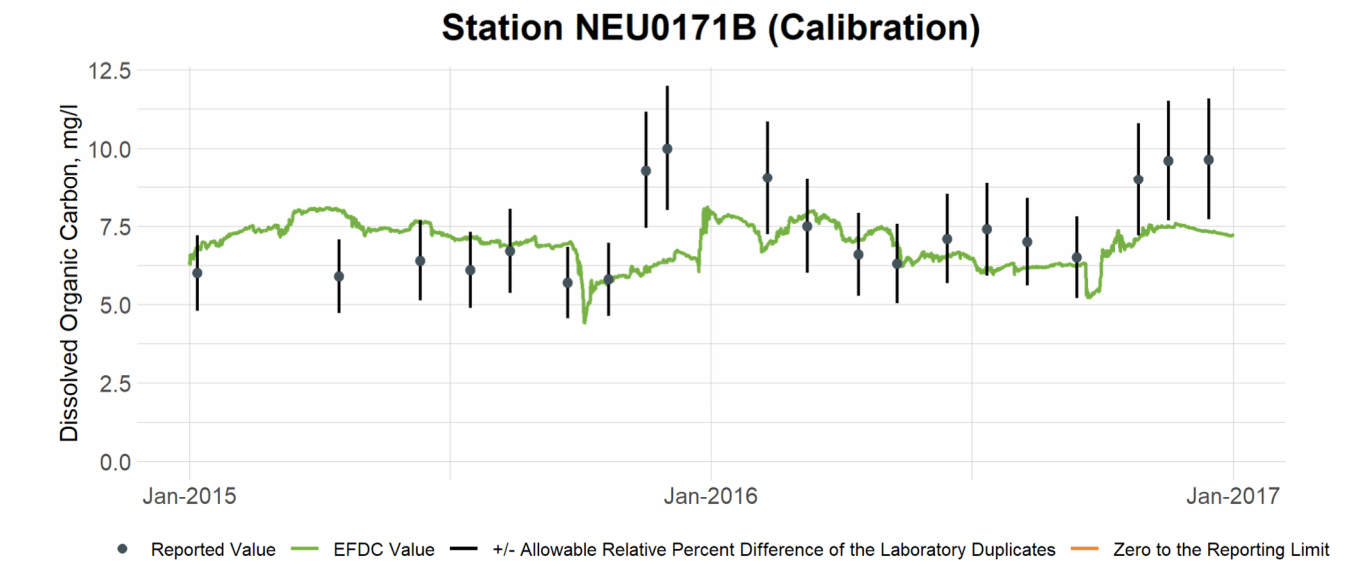

Figure 9-6 Calibration Plot of DOC at Station NEU0171B

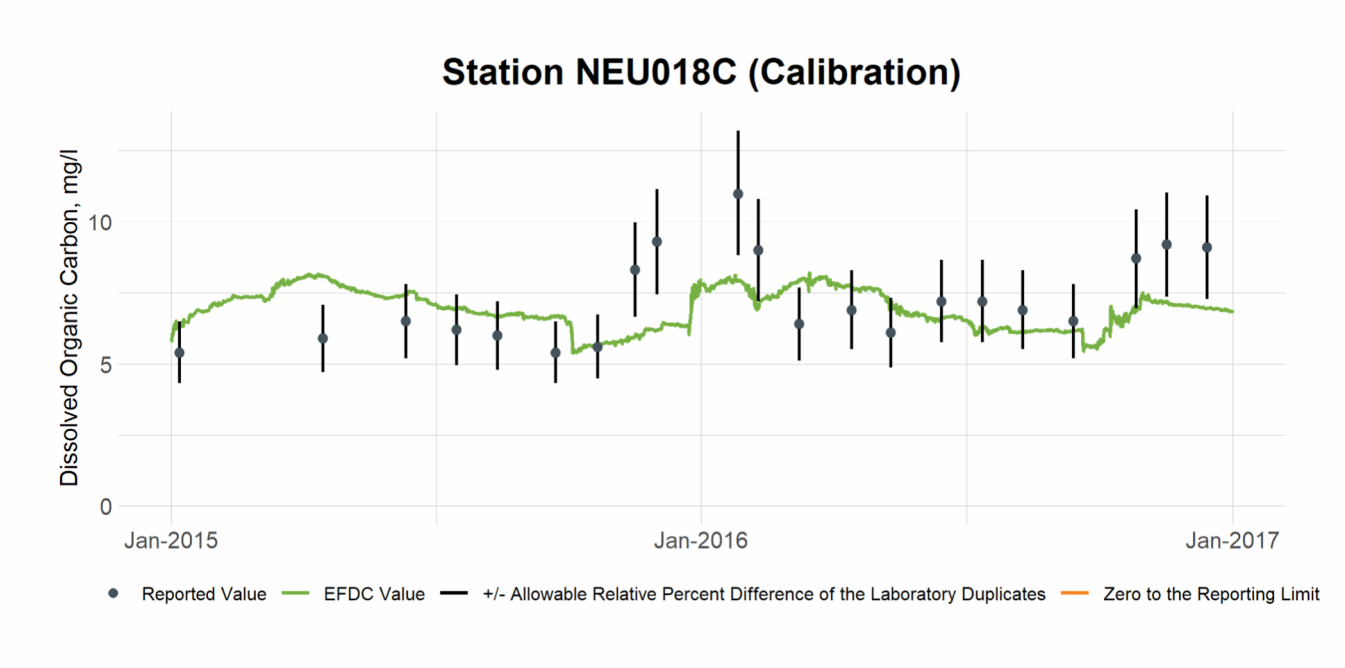

Figure 9-7 Calibration Plot of DOC at Station NEU018C

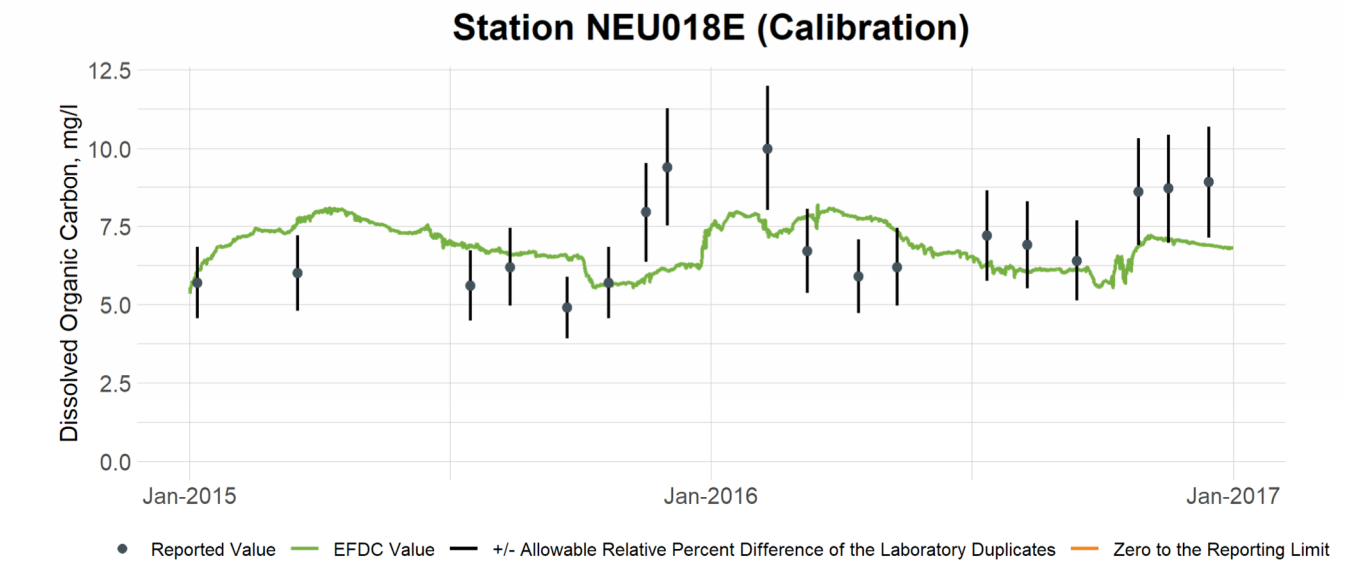

Figure 9-8 Calibration Plot of DOC at Station NEU018E

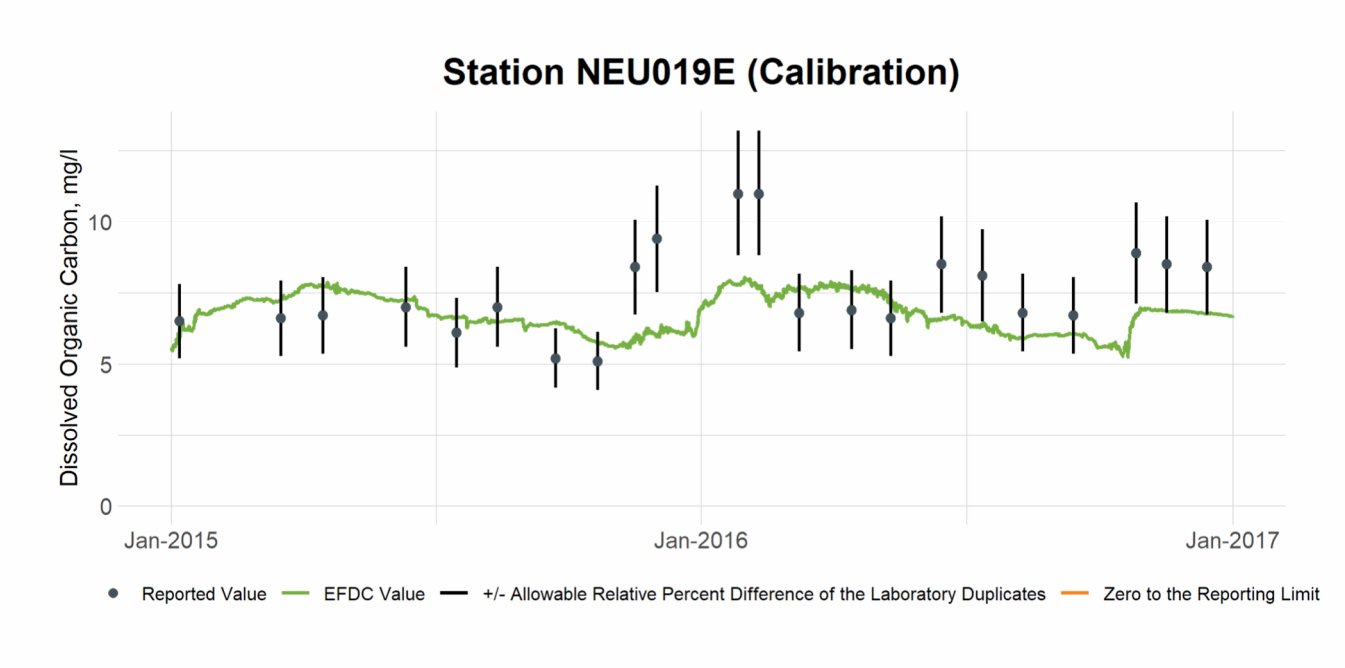

Figure 9-9 Calibration Plot of DOC at Station NEU019E

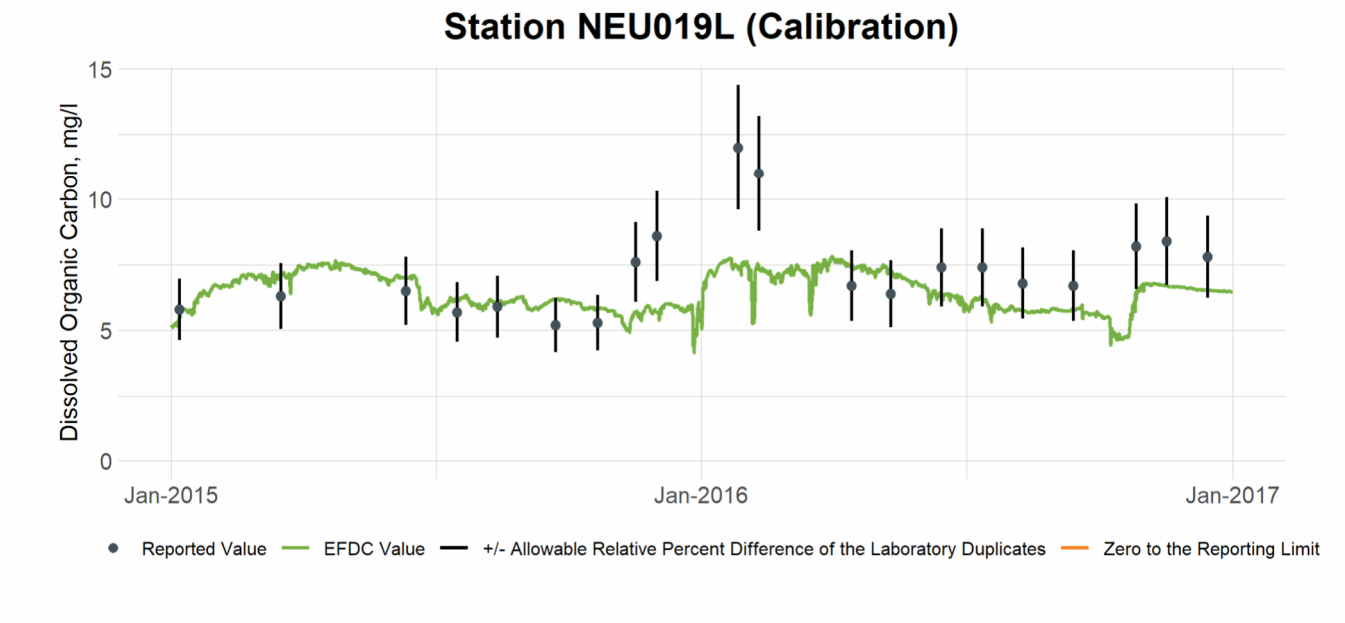

Figure 9-10 Calibration Plot of DOC at Station NEU019L

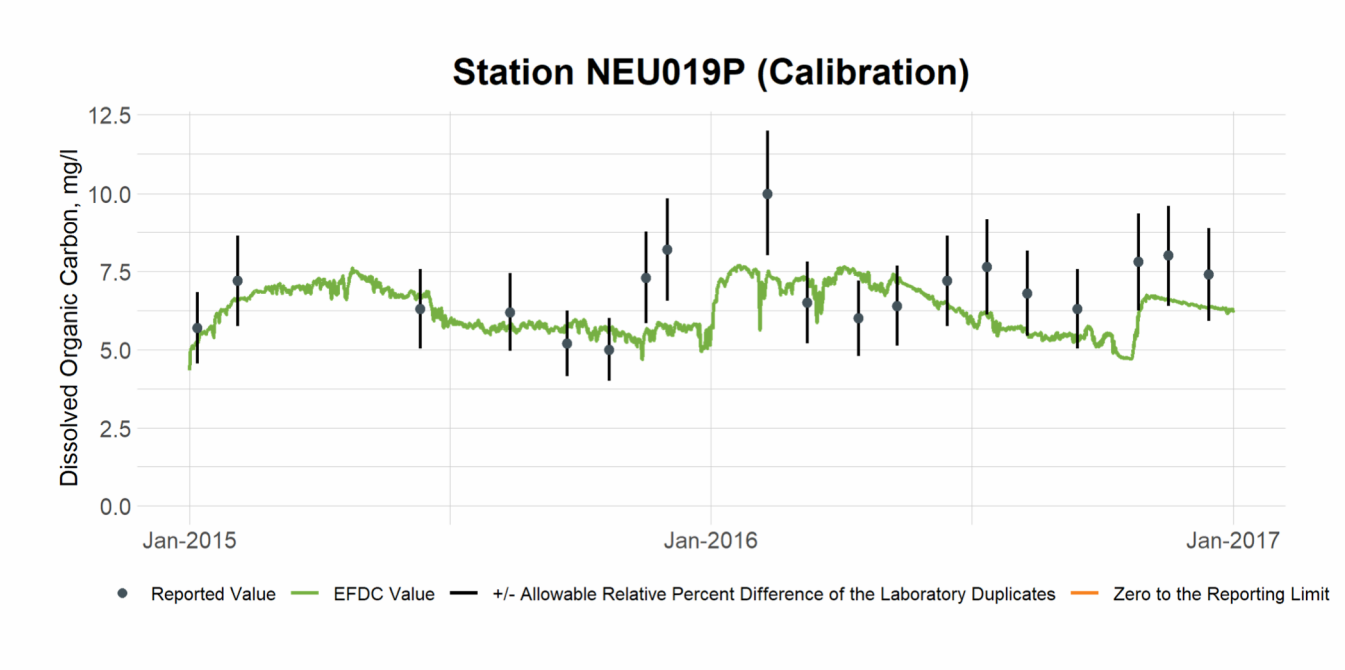

Figure 9-11 Calibration Plot of DOC at Station NEU019P

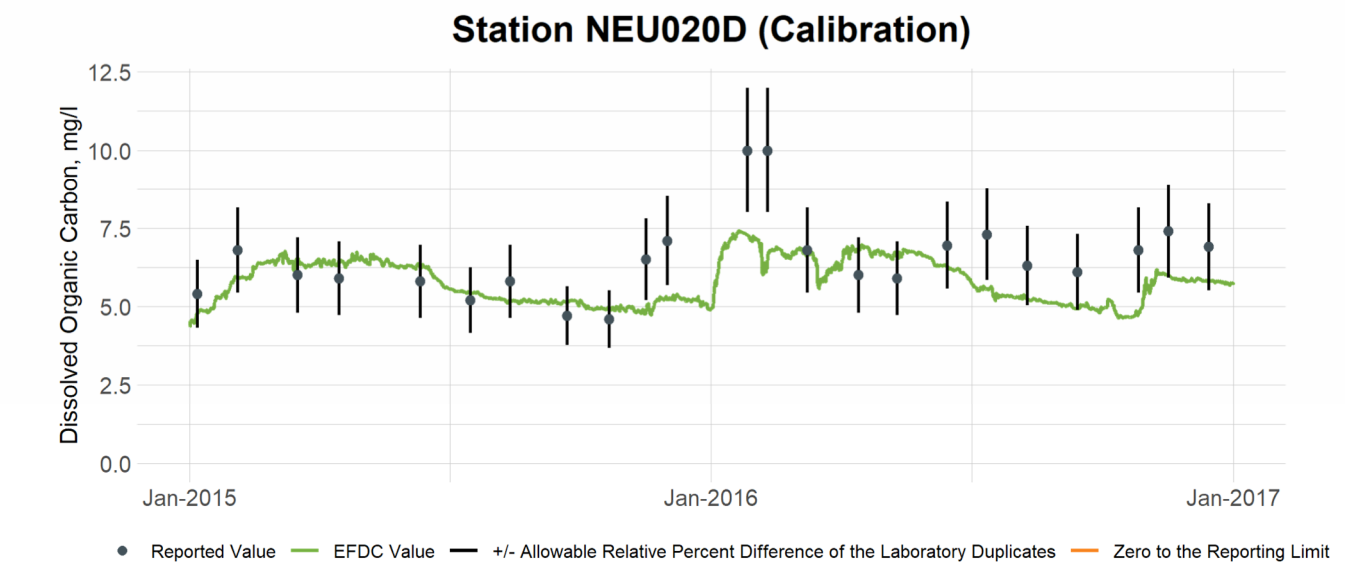

Figure 9-12 Calibration Plot of DOC at Station NEU020D

9.2 DOC Validation

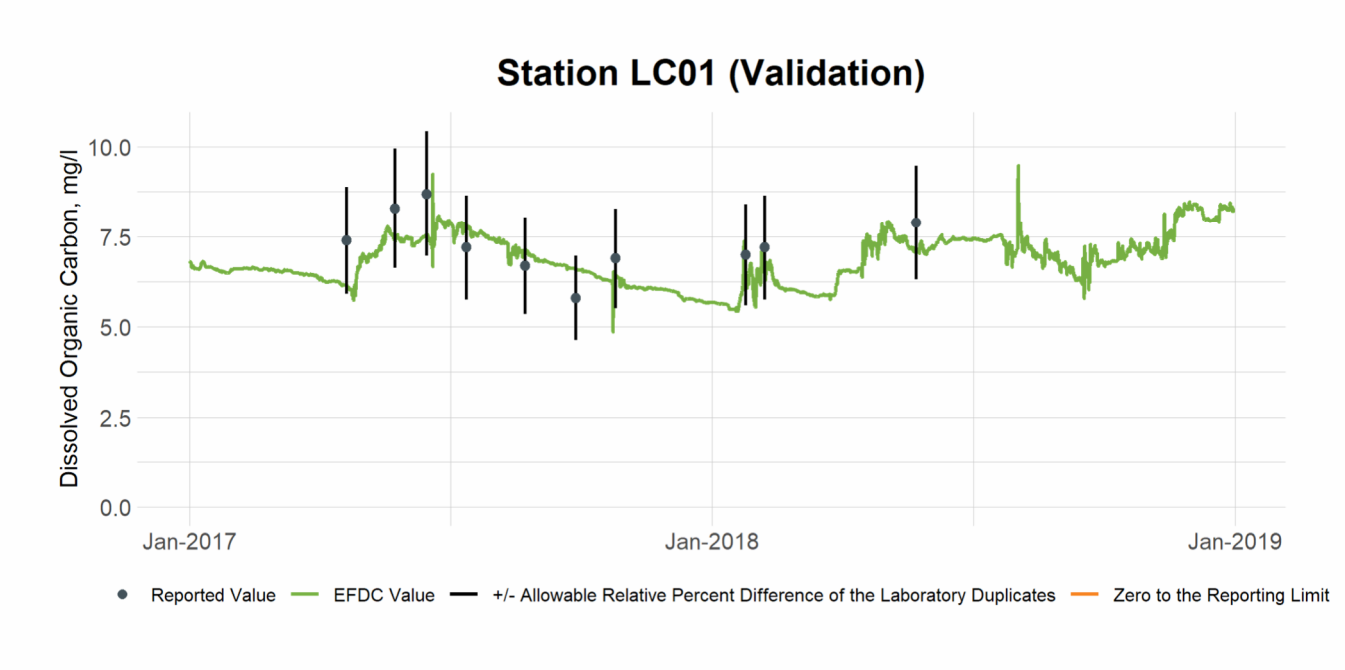

Figure 9-13 Validation Plot of DOC at Station LC01

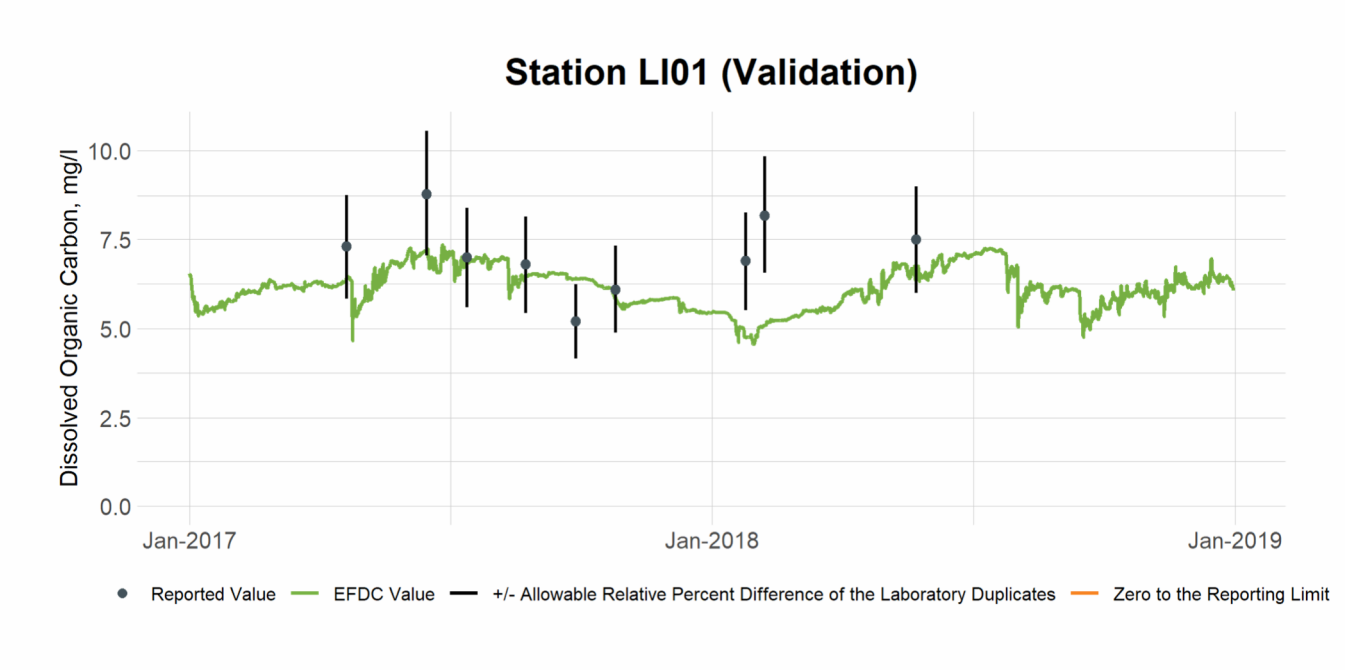

Figure 9-14 Validation Plot of DOC at Station LI01

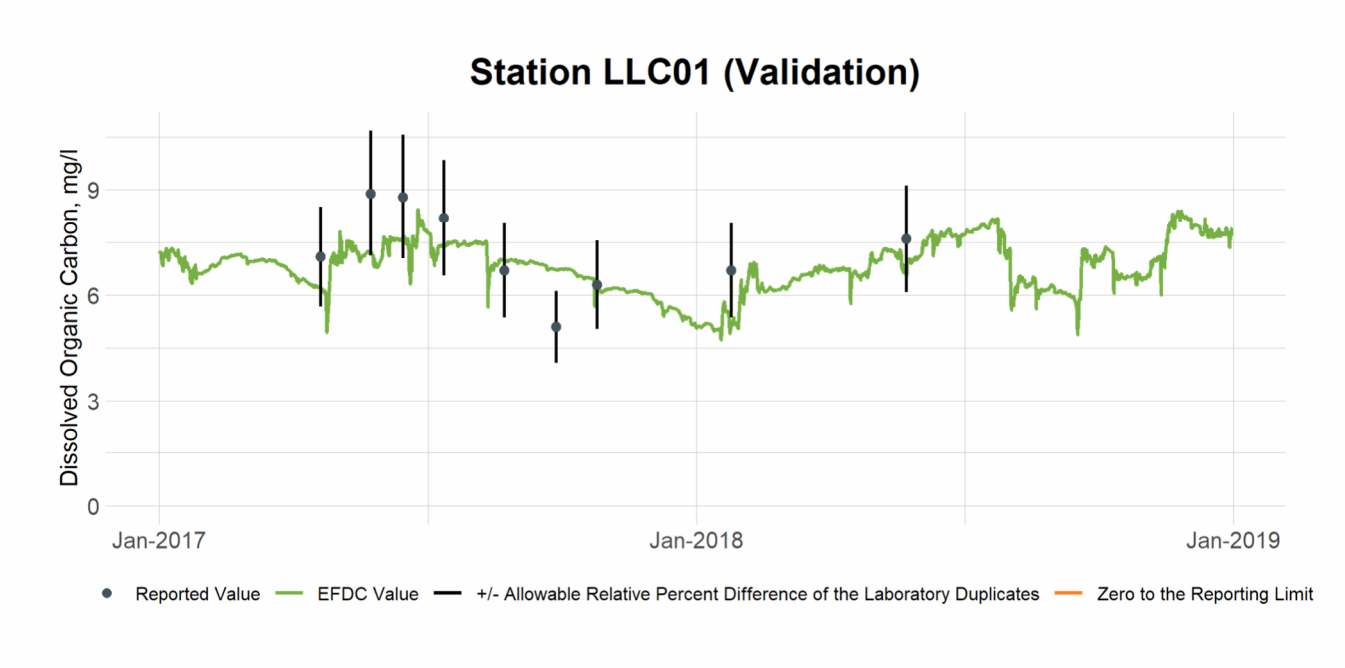

Figure 9-15 Validation Plot of DOC at Station LLC01

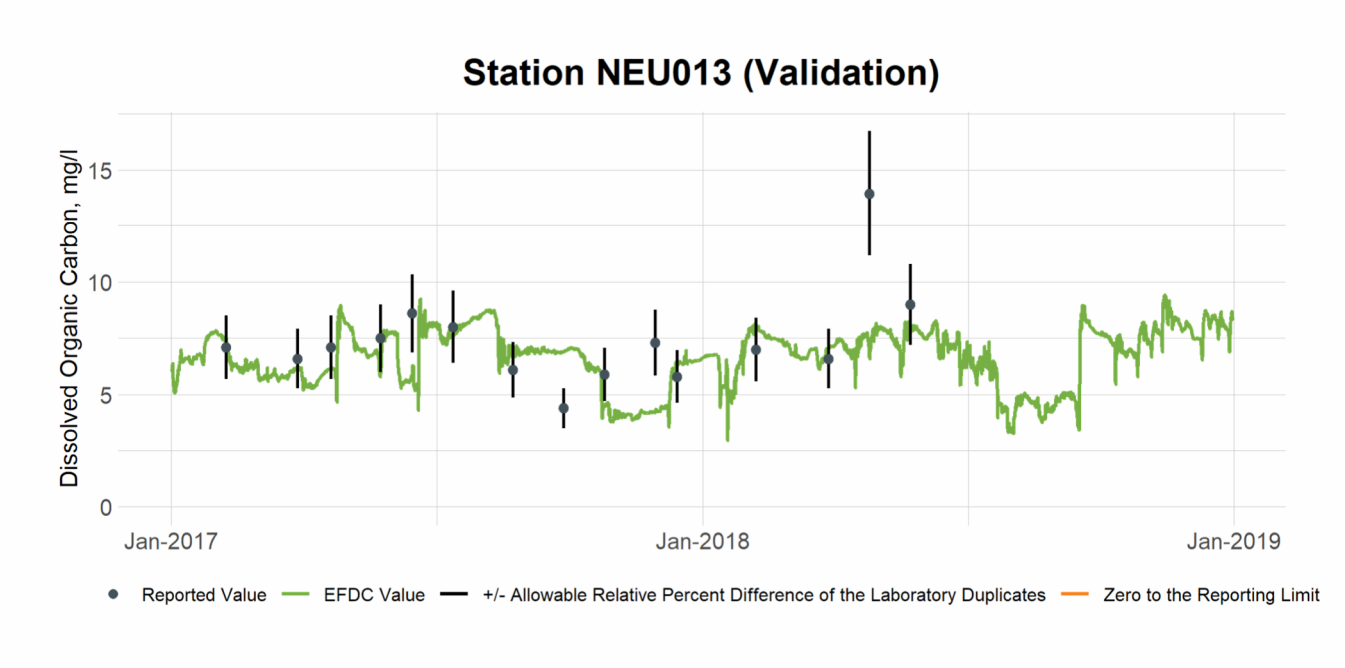

Figure 9-16 Validation Plot of DOC at Station NEU013

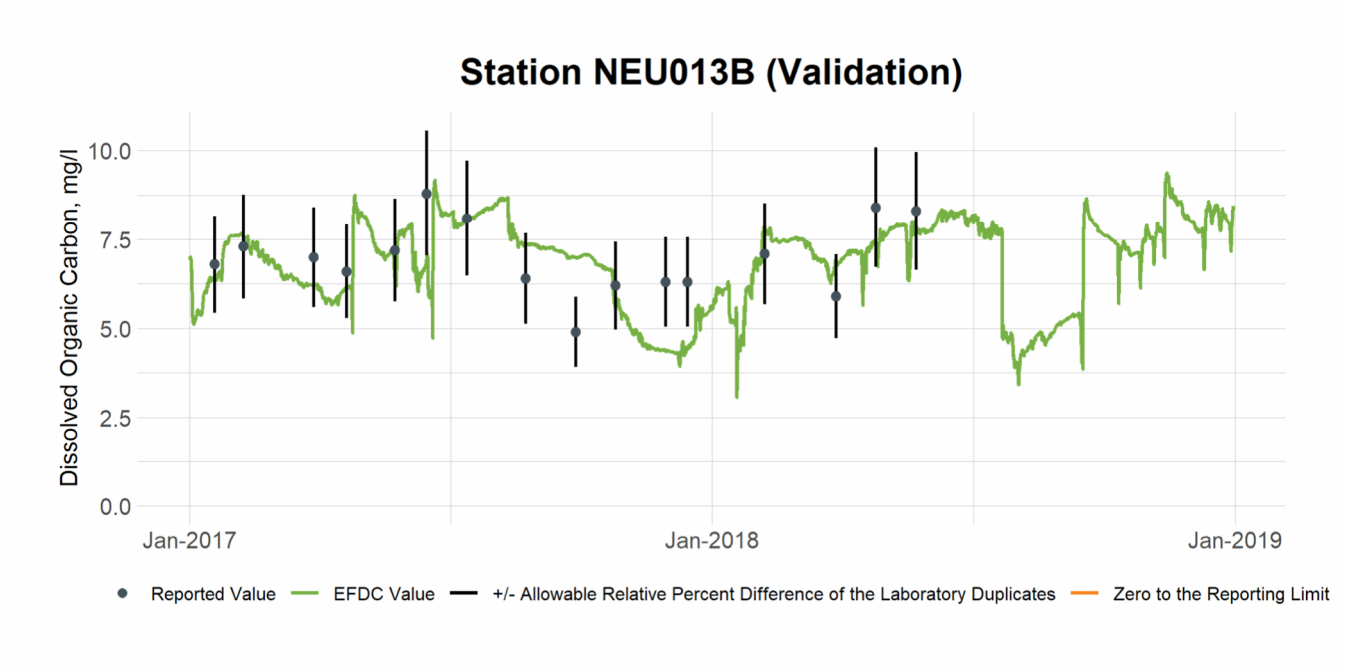

Figure 9-17 Validation Plot of DOC at Station NEU013B

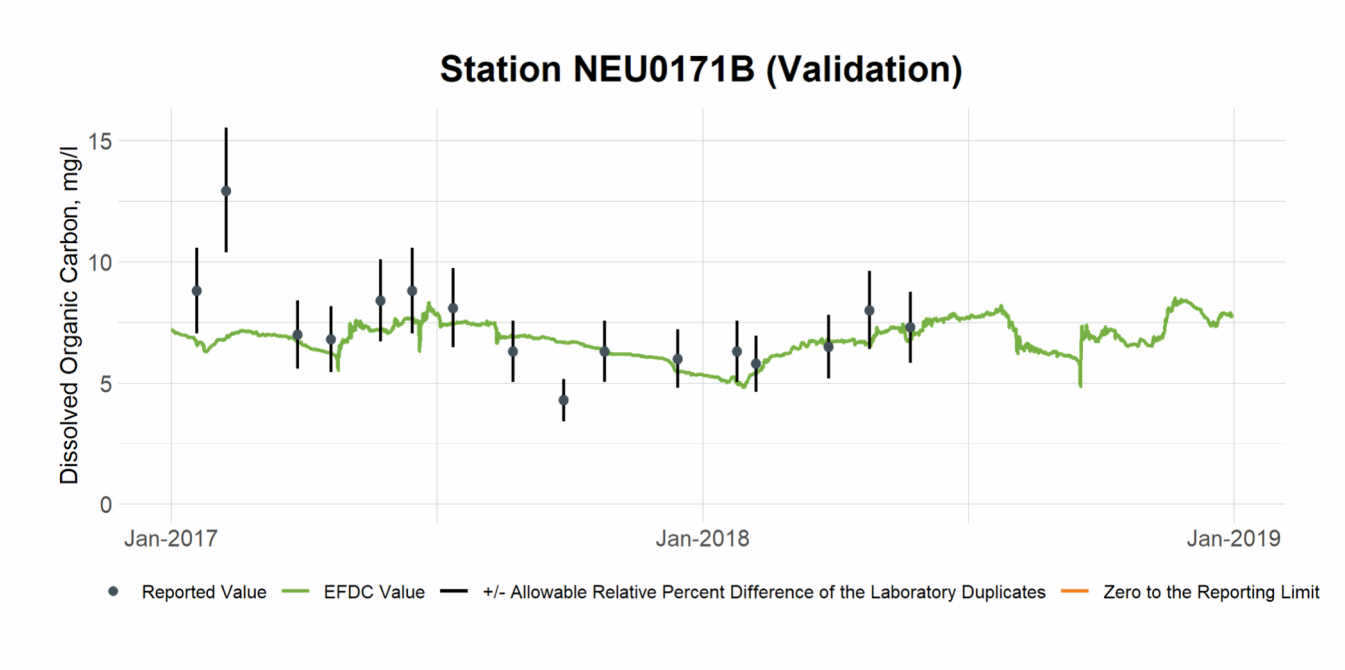

Figure 9-18 Validation Plot of DOC at Station NEU0171B

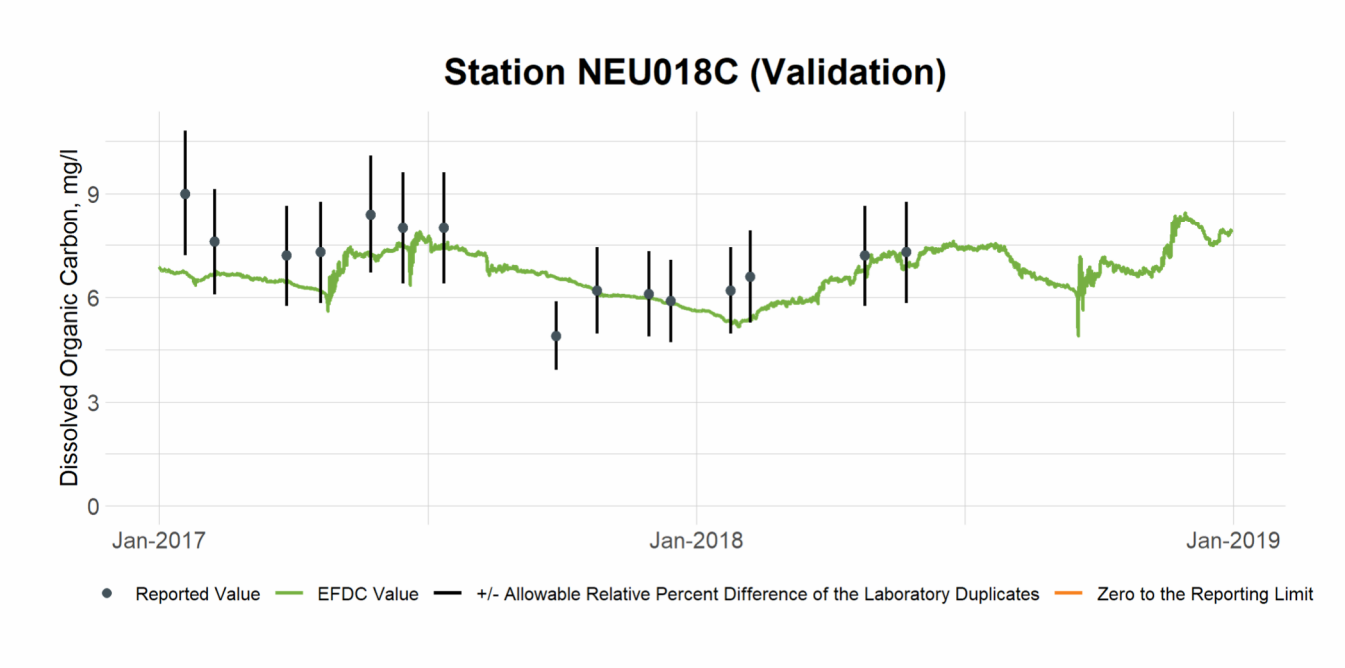

Figure 9-19 Validation Plot of DOC at Station NEU018C

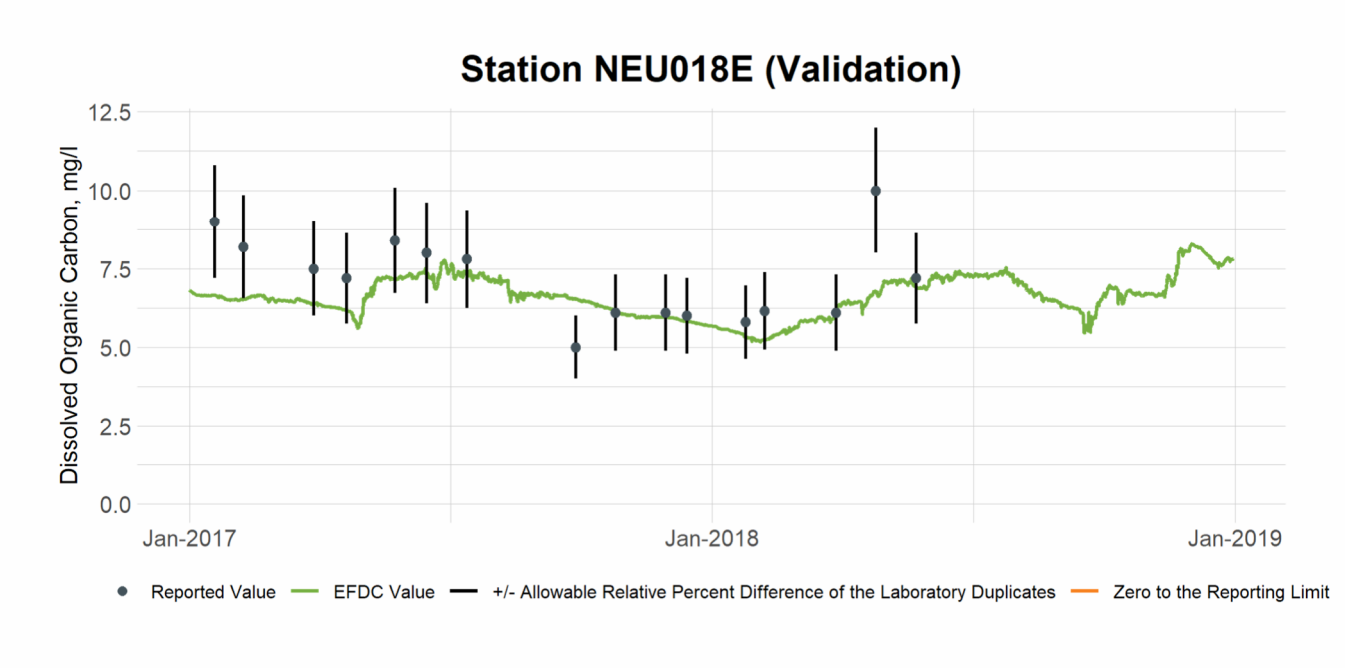

Figure 9-20 Validation Plot of DOC at Station NEU018E

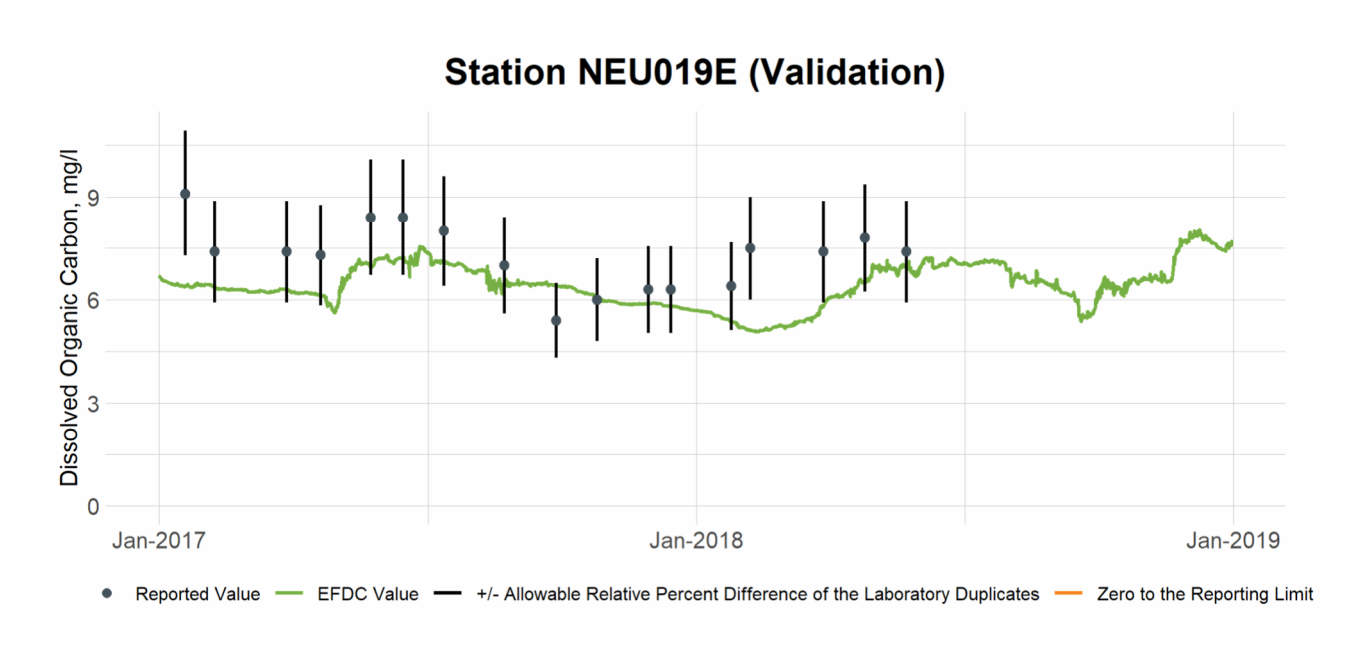

Figure 9-21 Validation Plot of DOC at Station NEU019E

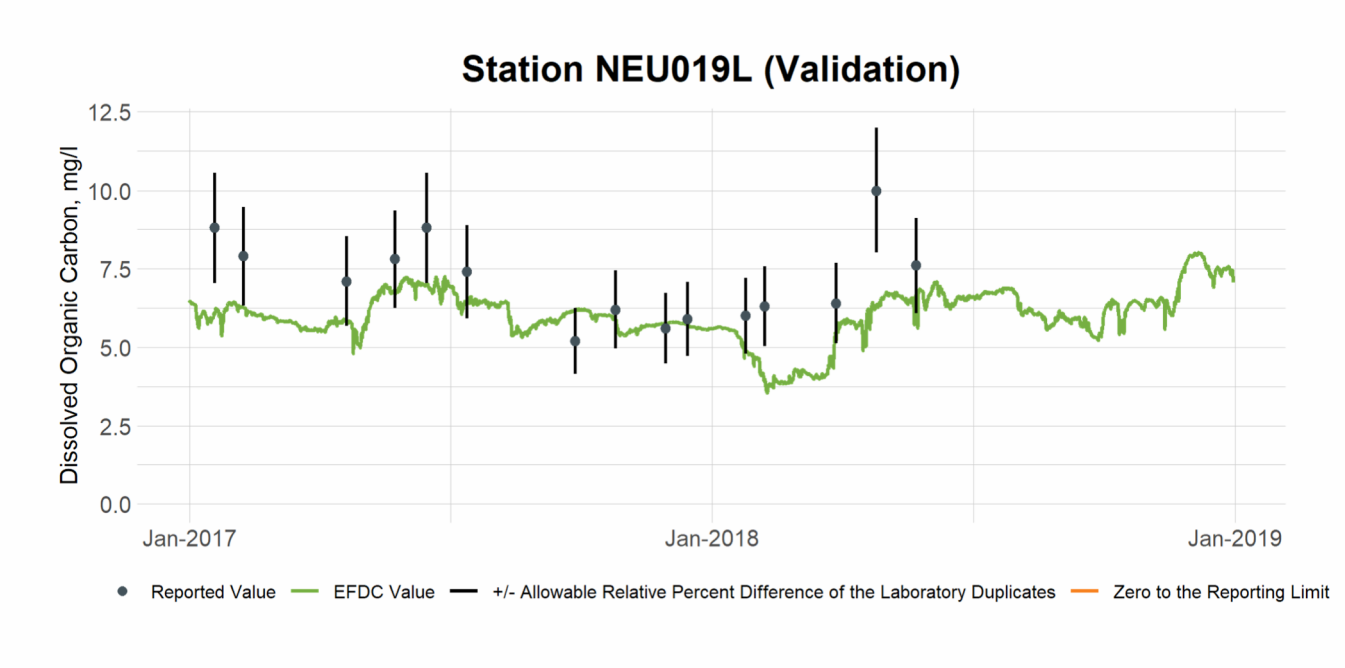

Figure 9-22 Validation Plot of DOC at Station NEU019L

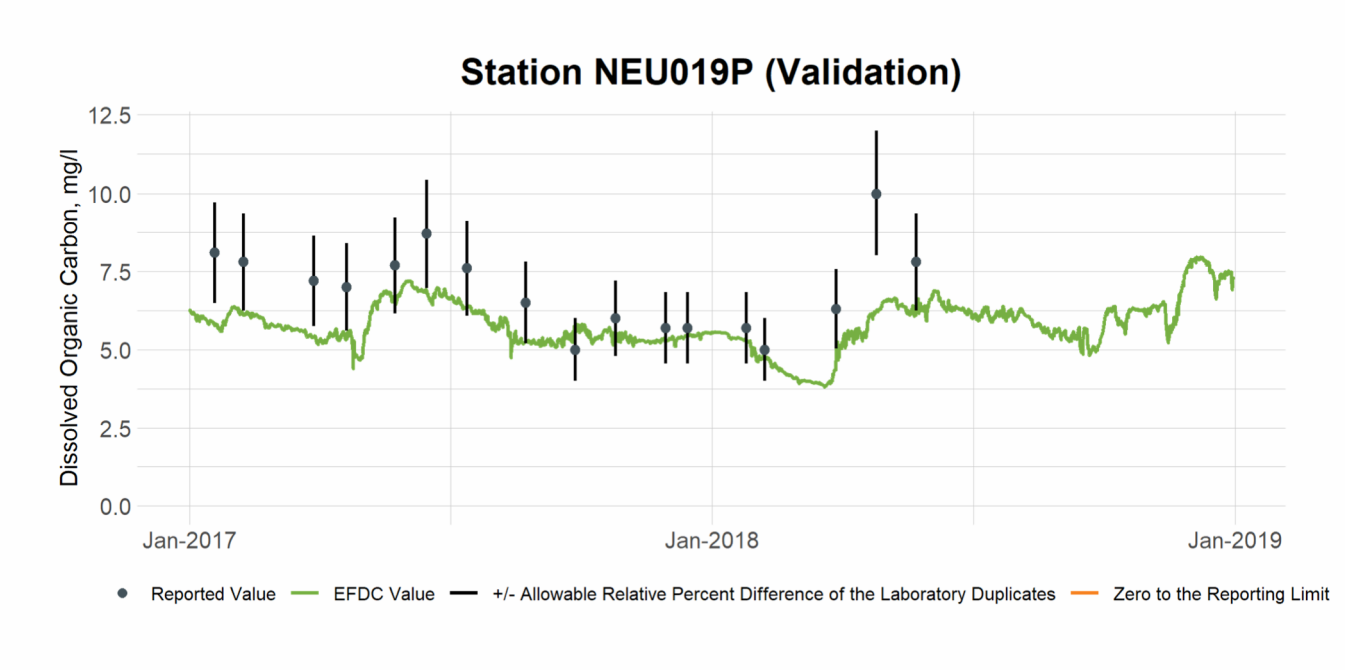

Figure 9-23 Validation Plot of DOC at Station NEU019P

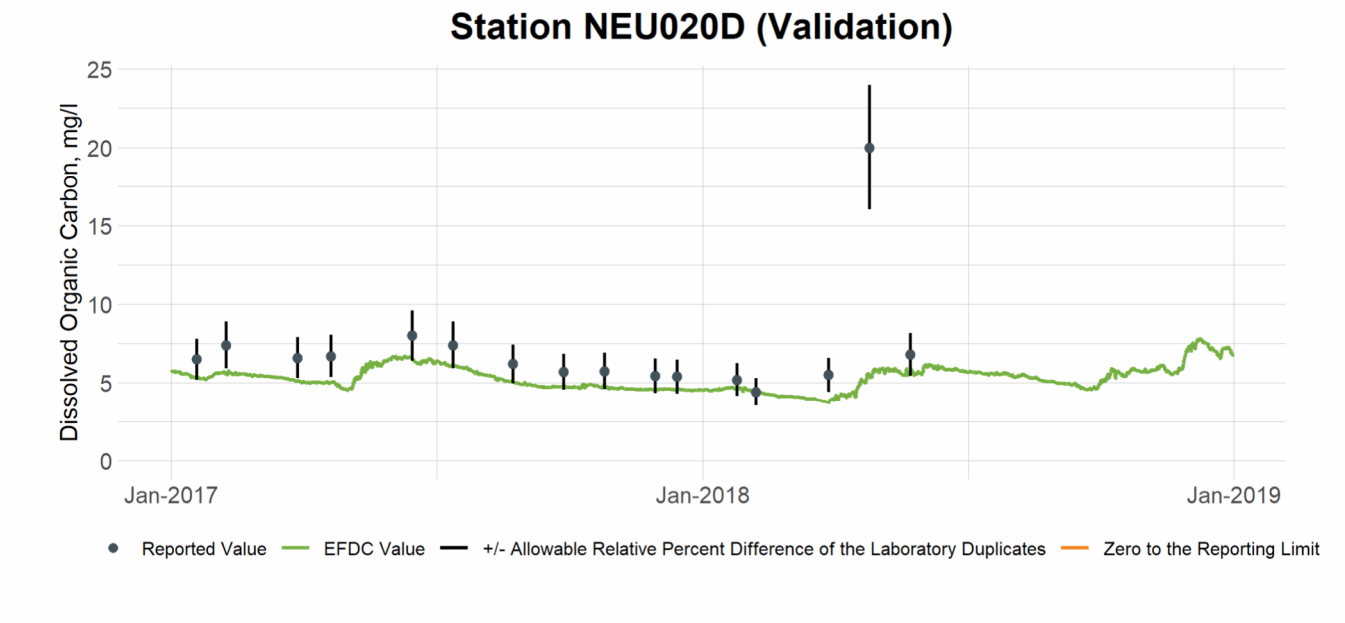

Figure 9-24 Validation Plot of DOC at Station NEU020D

10. TKN

10.1 TKN Calibration

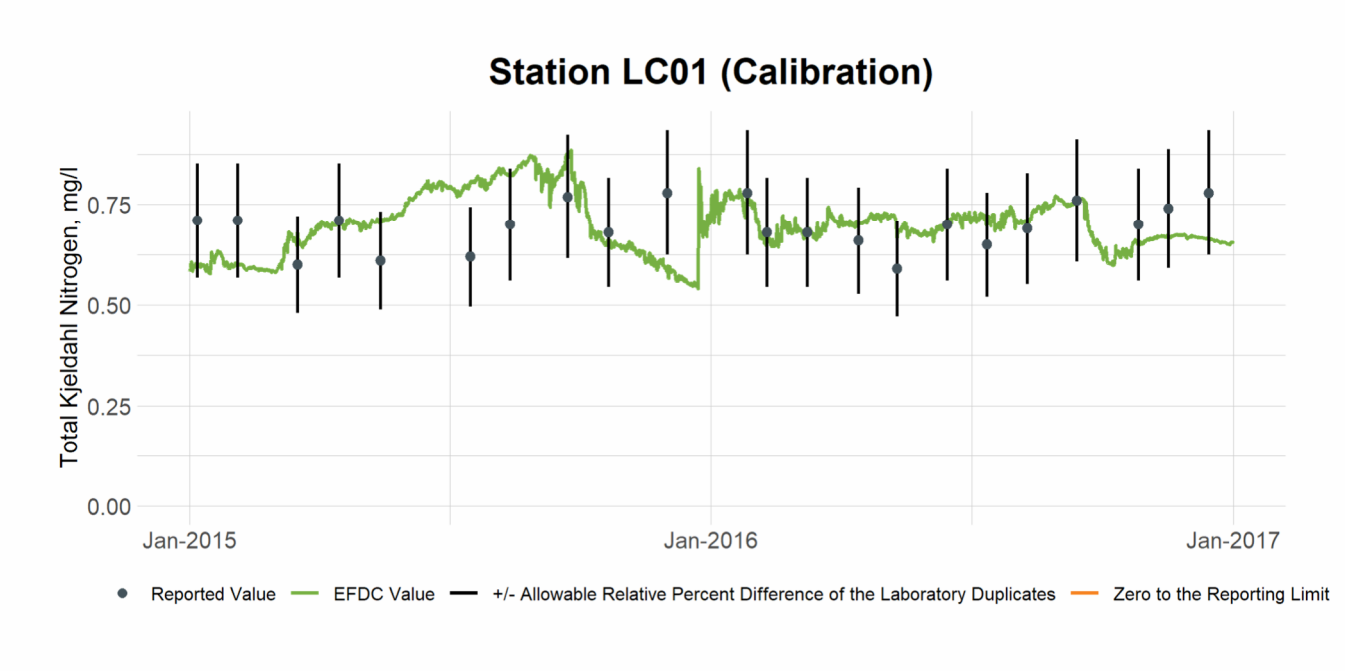

Figure 10-1 Calibration Plot of TKN at Station LC01

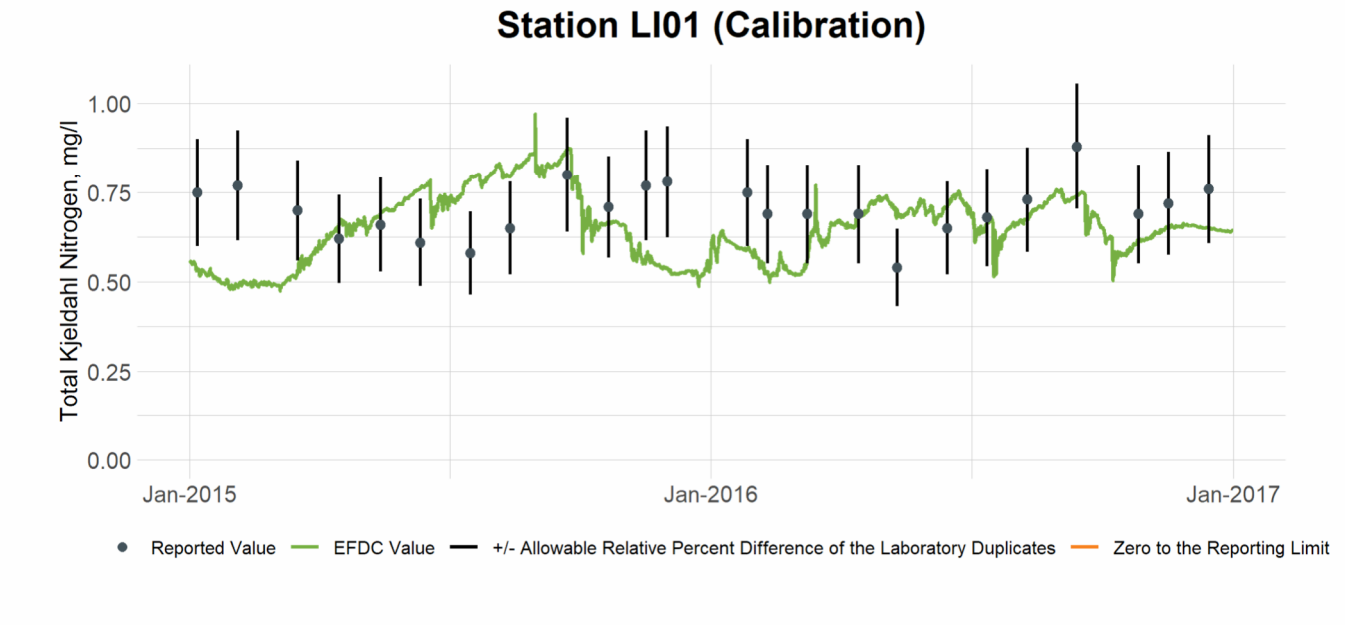

Figure 10-2 Calibration Plot of TKN at Station LI01

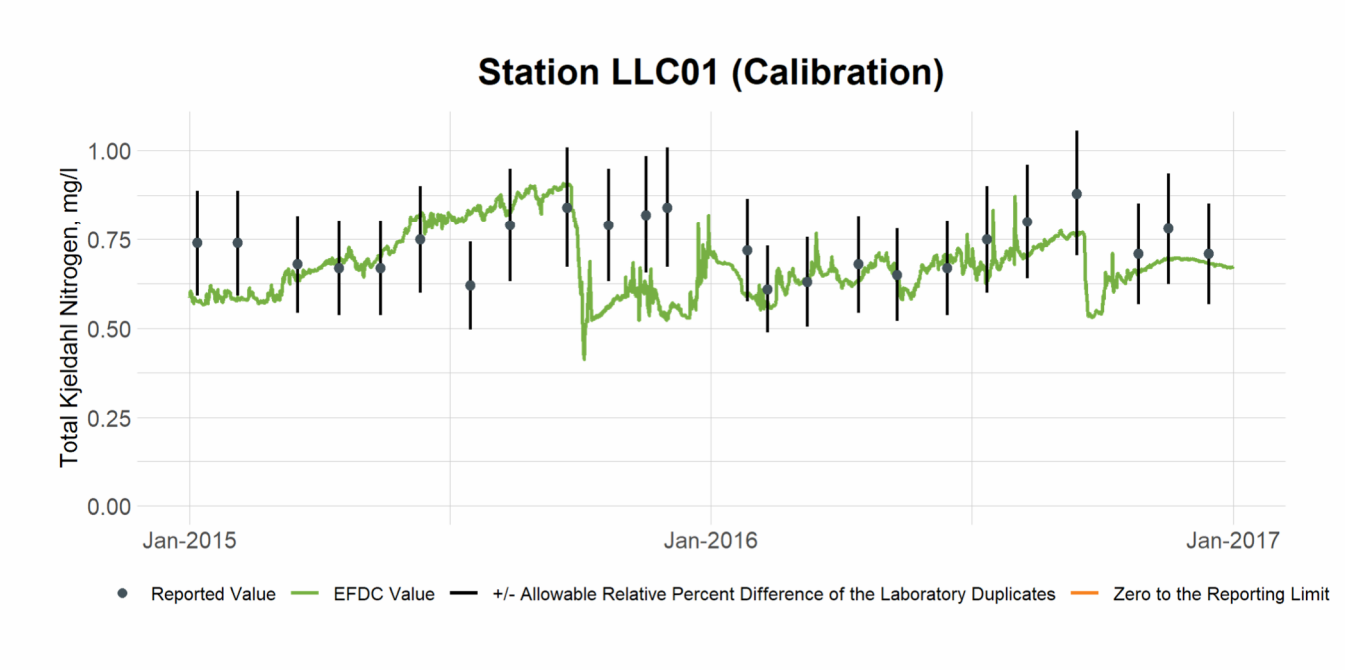

Figure 10-3 Calibration Plot of TKN at Station LLC01

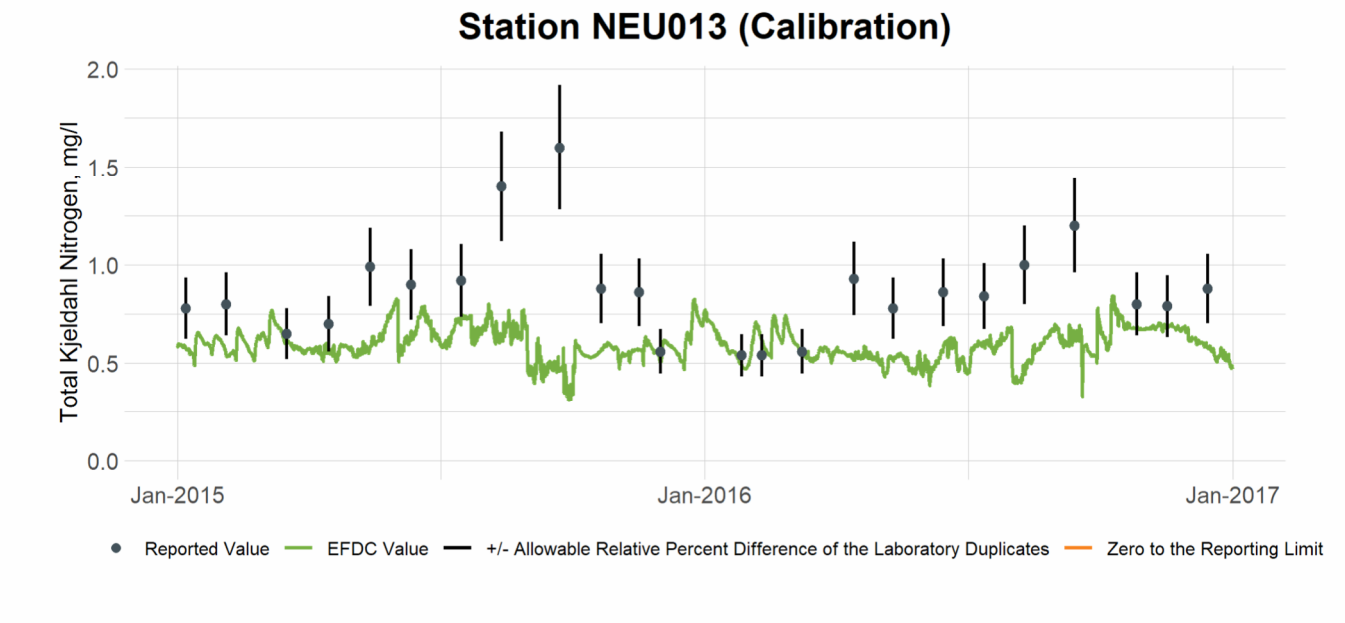

Figure 10-4 Calibration Plot of TKN at Station NEU013

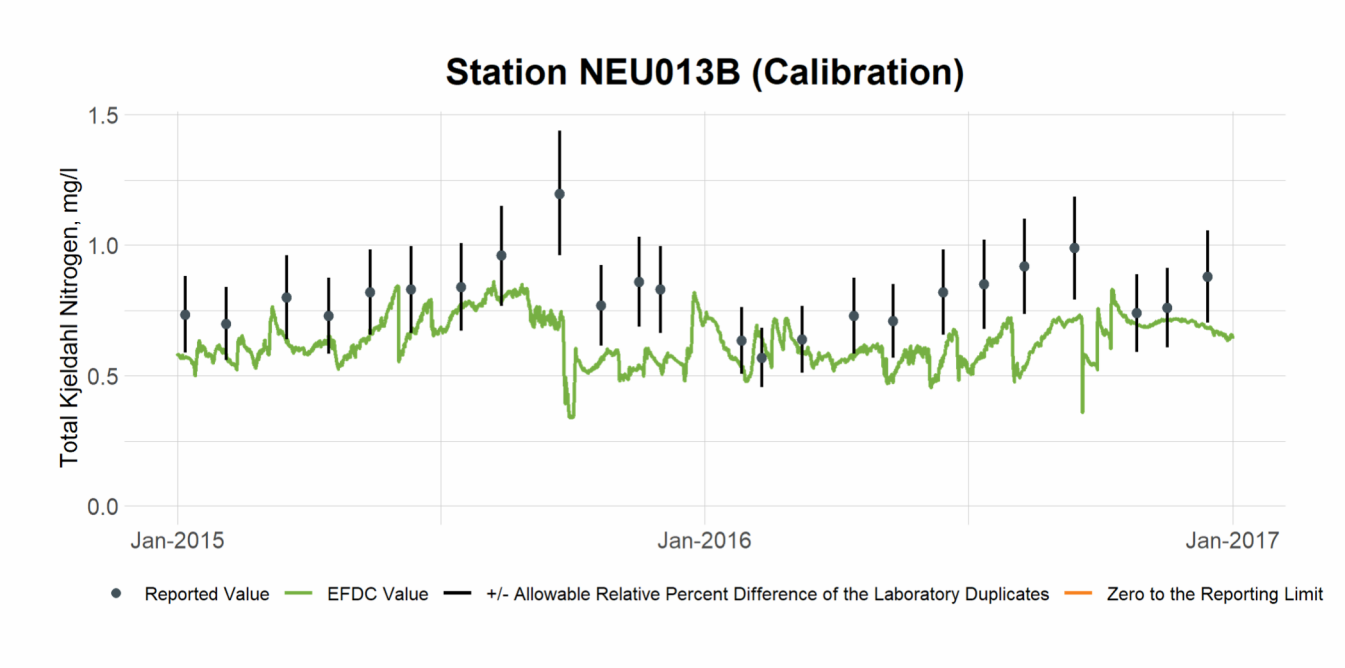

Figure 10-5 Calibration Plot of TKN at Station NEU013B

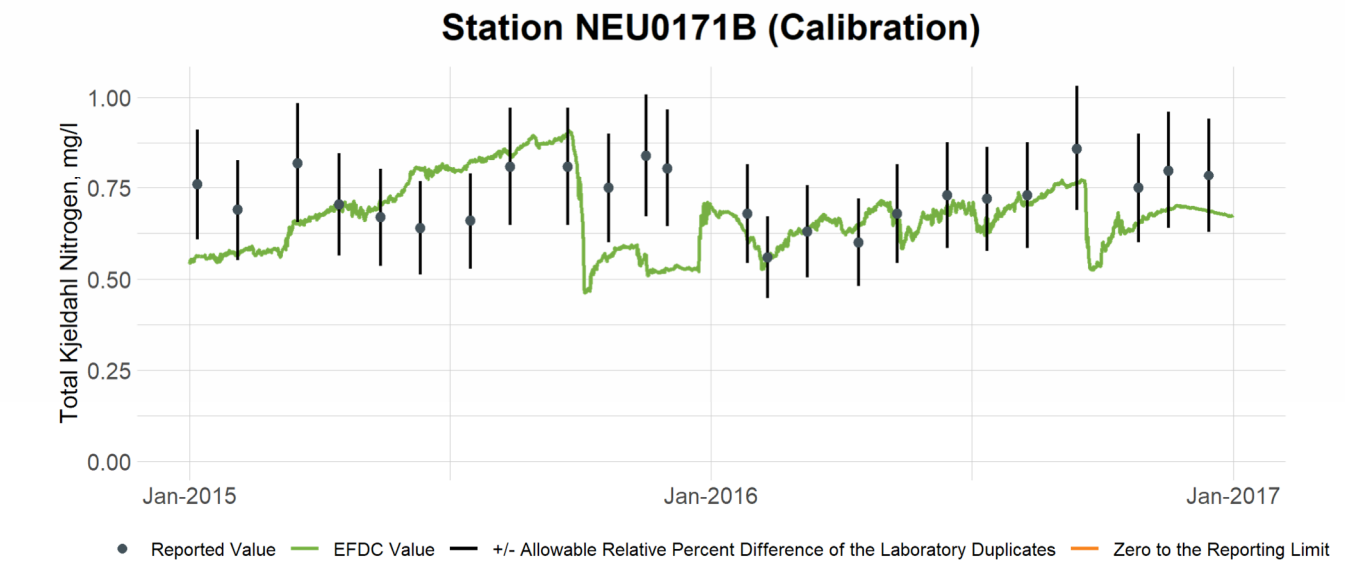

Figure 10-6 Calibration Plot of TKN at Station NEU0171B

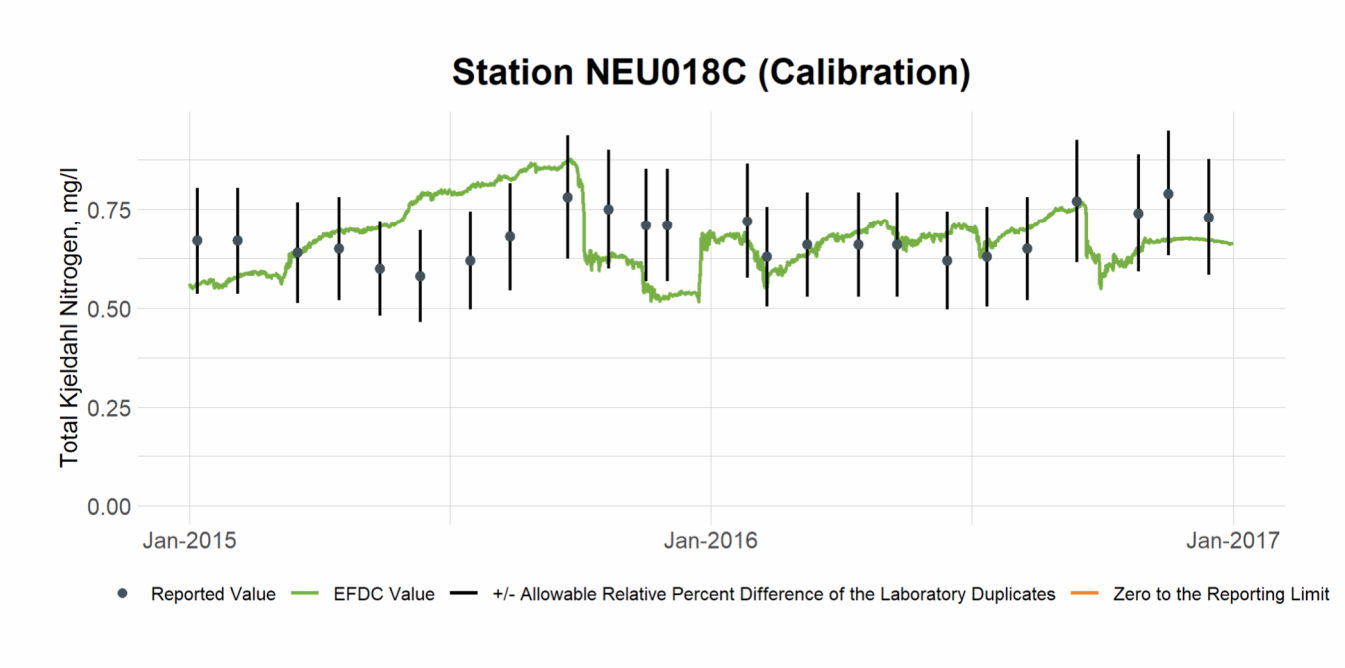

Figure 10-7 Calibration Plot of TKN at Station NEU018C

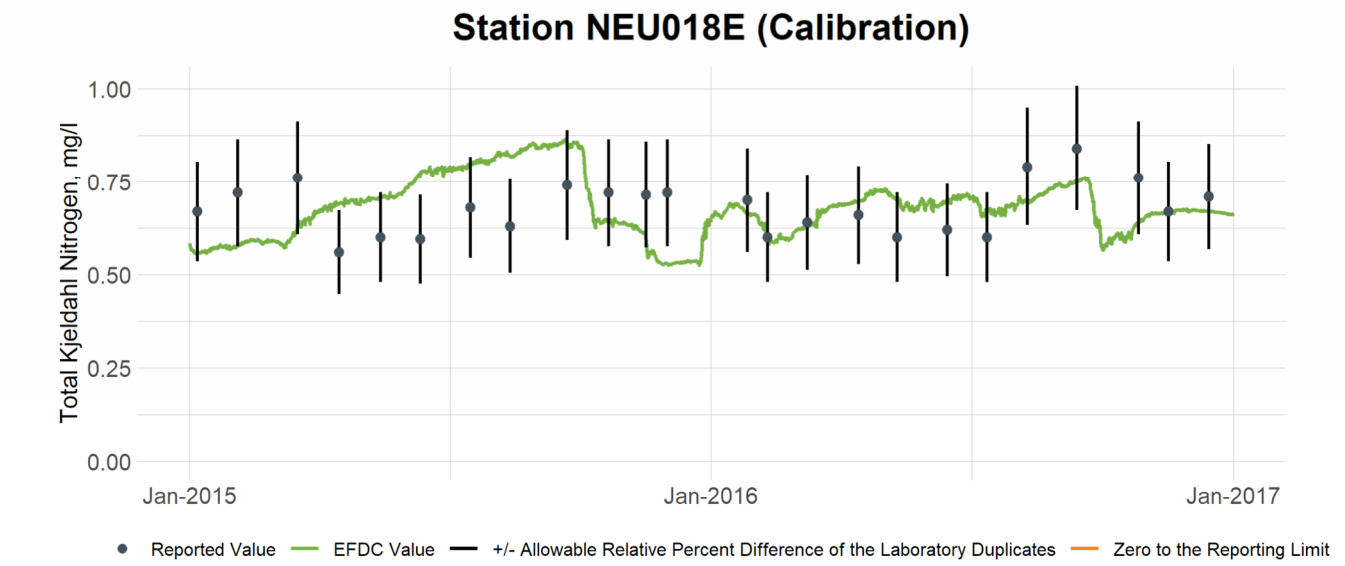

Figure 10-8 Calibration Plot of TKN at Station NEU018E

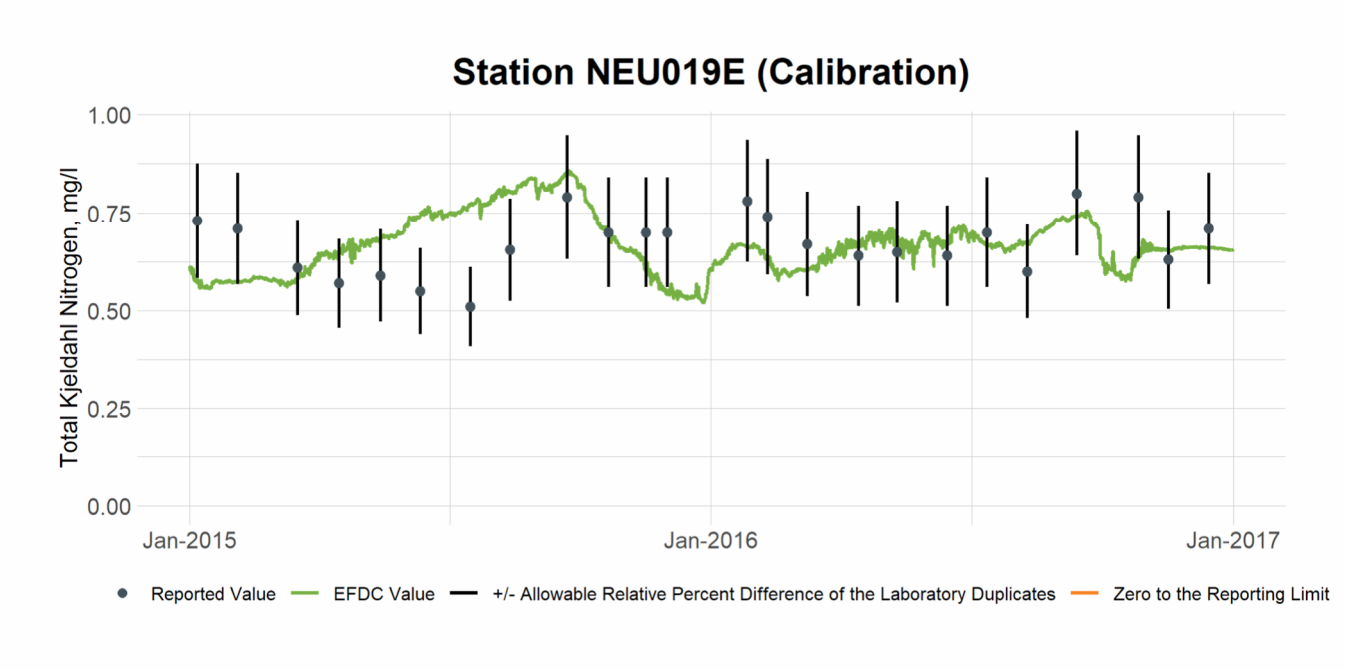

Figure 10-9 Calibration Plot of TKN at Station NEU019E

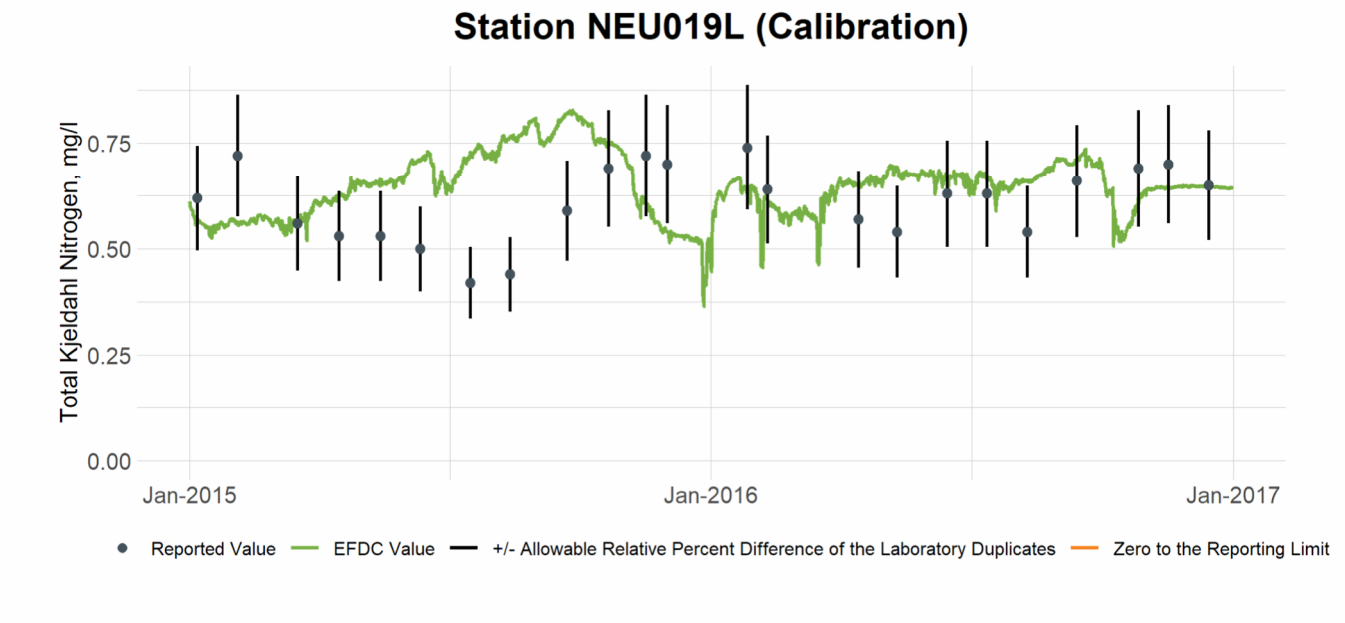

Figure 10-10 Calibration Plot of TKN at Station NEU019L

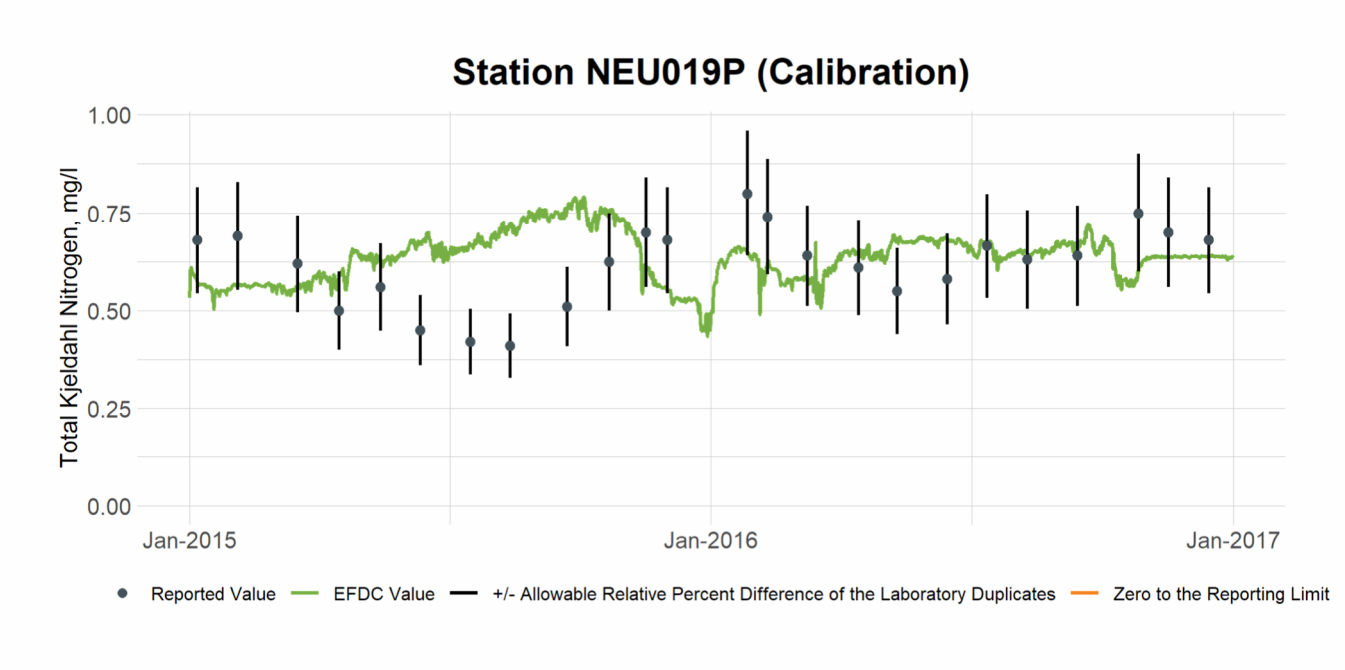

Figure 10-11 Calibration Plot of TKN at Station NEU019P

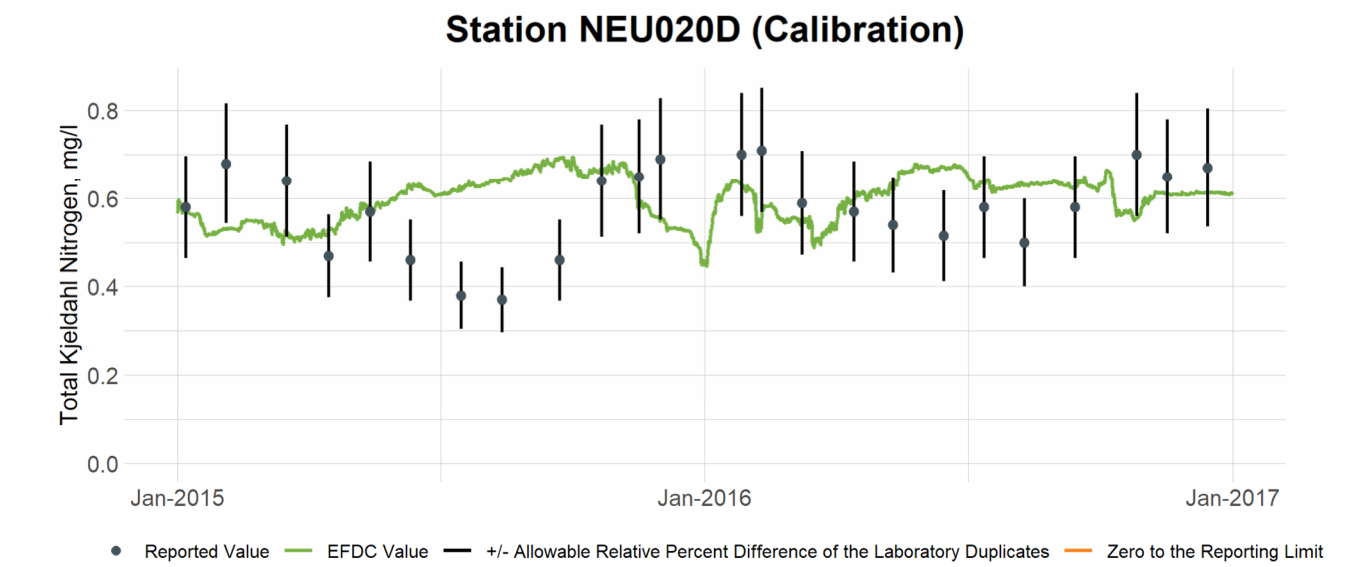

Figure 10-12 Calibration Plot of TKN at Station NEU020D

10.2 TKN Validation

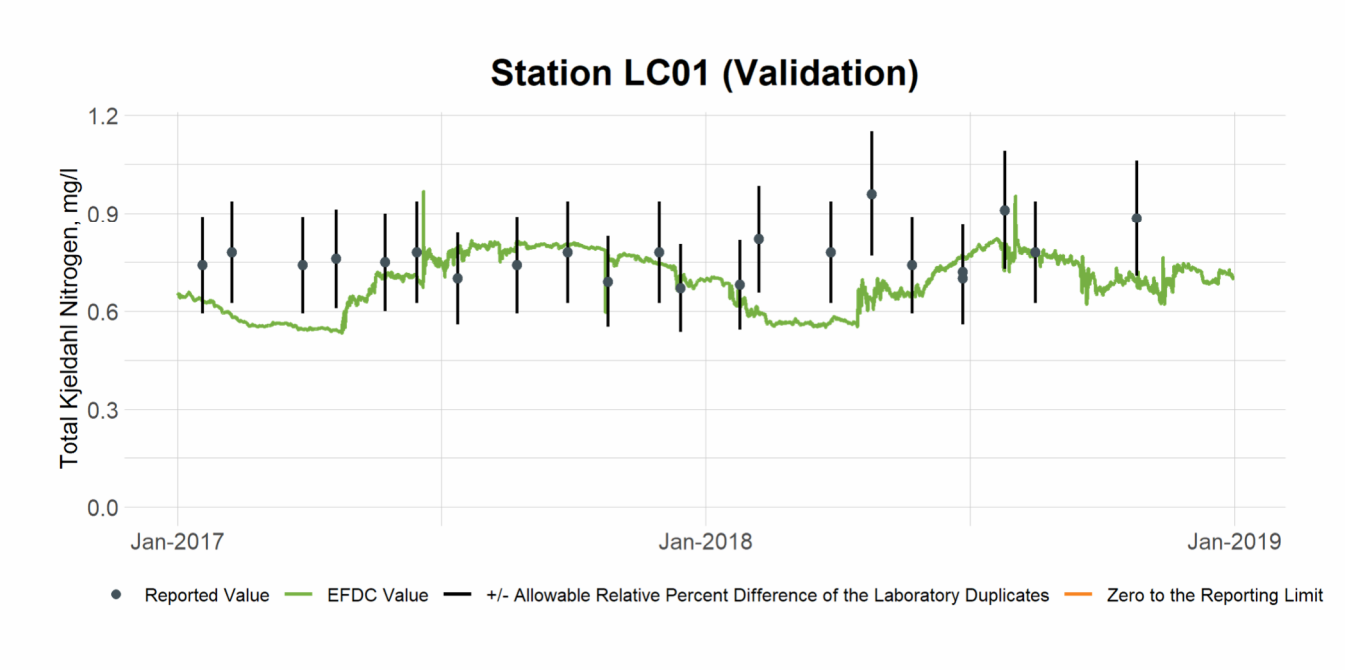

Figure 10-13 Validation Plot of TKN at Station LC01

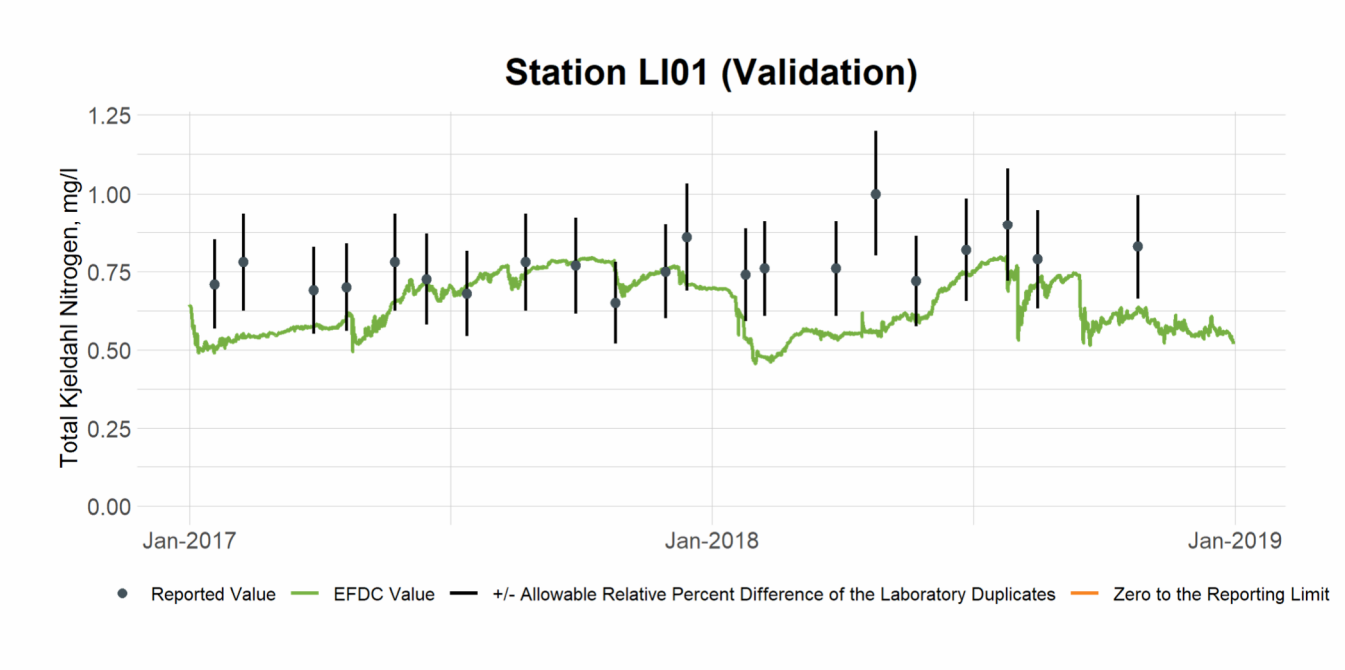

Figure 10-14 Validation Plot of TKN at Station LI01

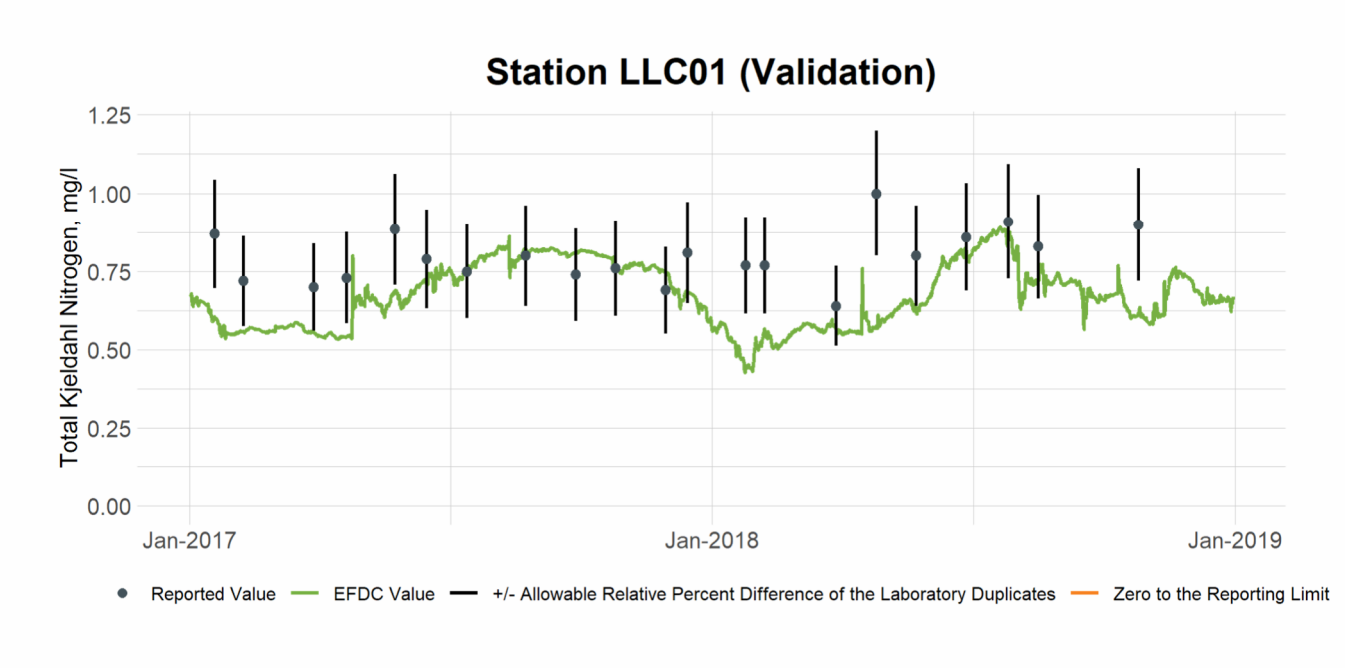

Figure 10-15 Validation Plot of TKN at Station LLC01

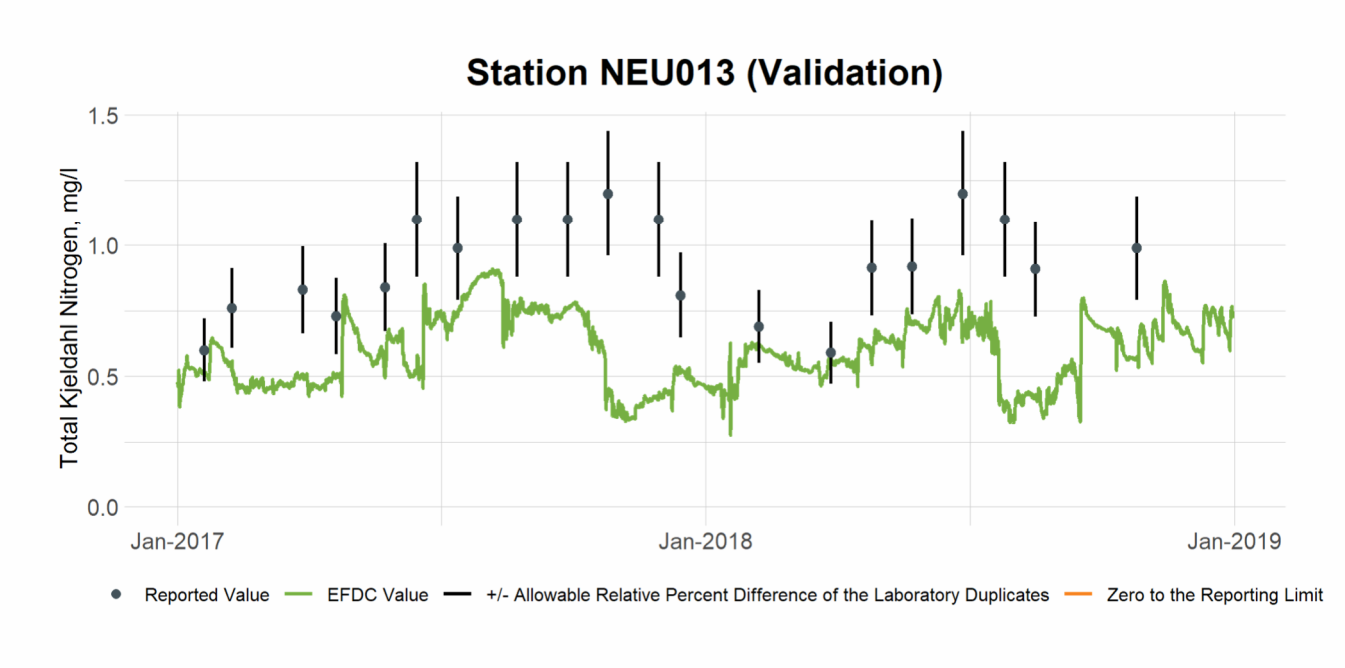

Figure 10-16 Validation Plot of TKN at Station NEU013

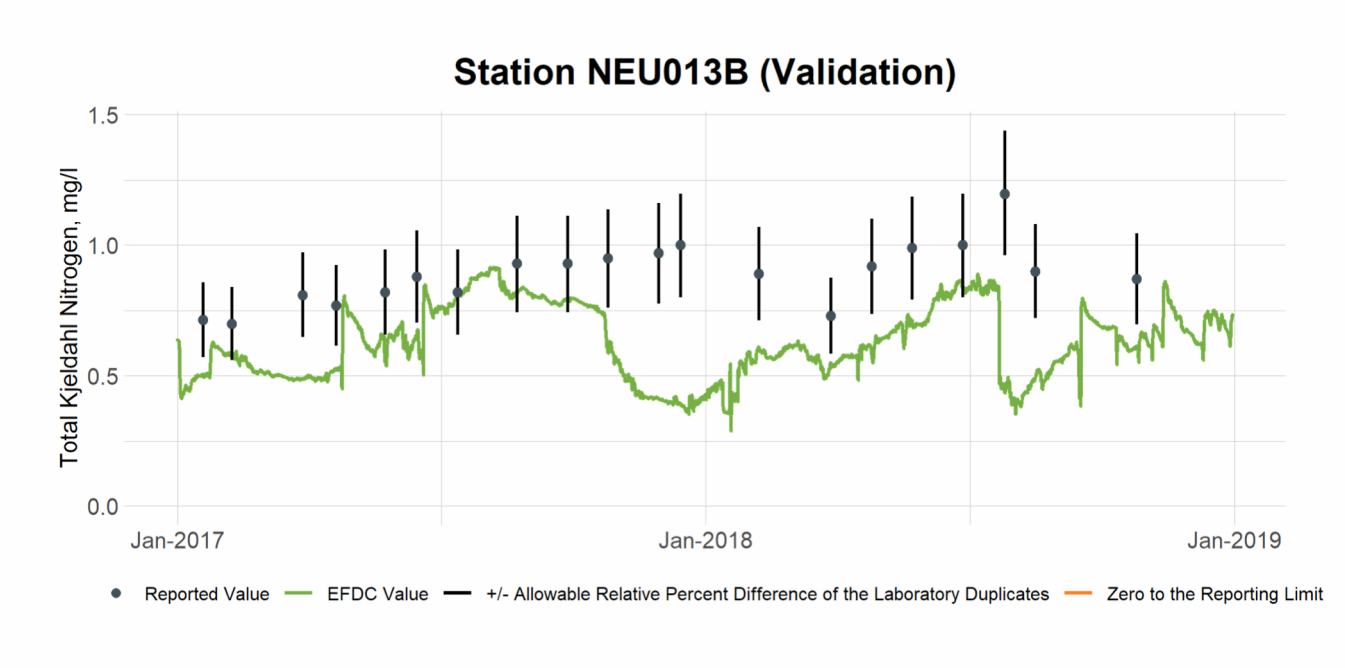

Figure 10-17 Validation Plot of TKN at Station NEU013B

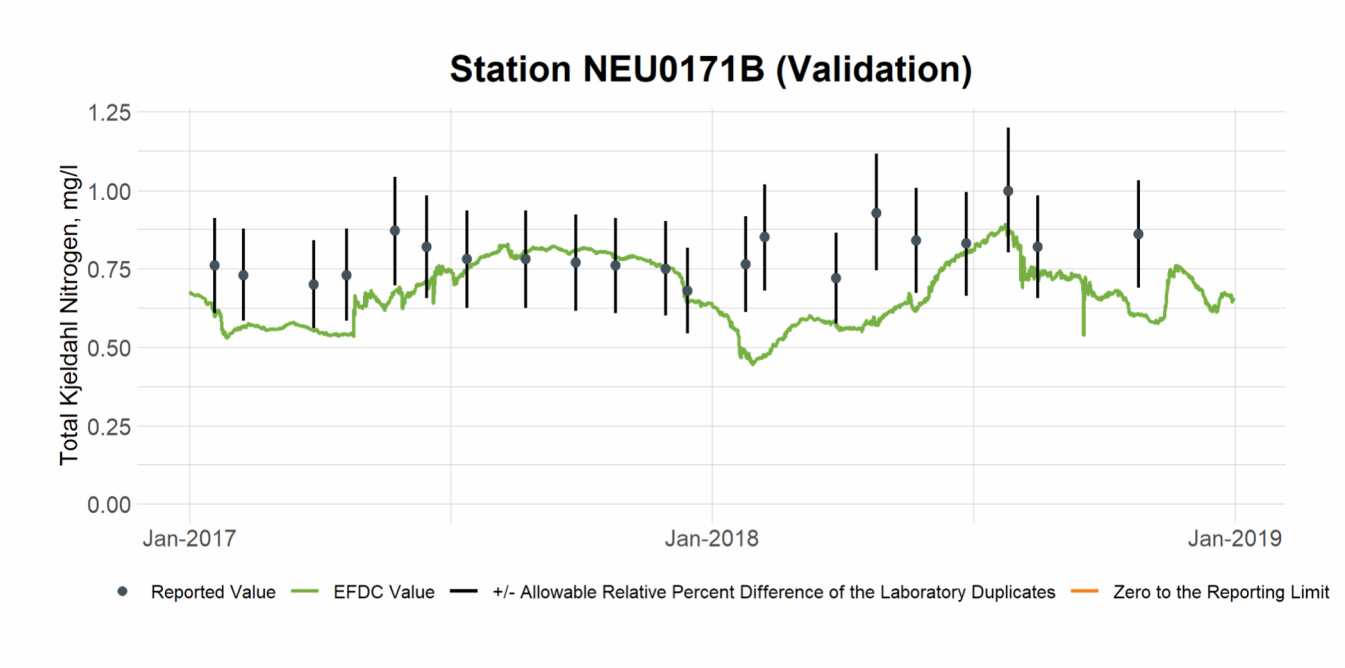

Figure 10-18 Validation Plot of TKN at Station NEU0171B

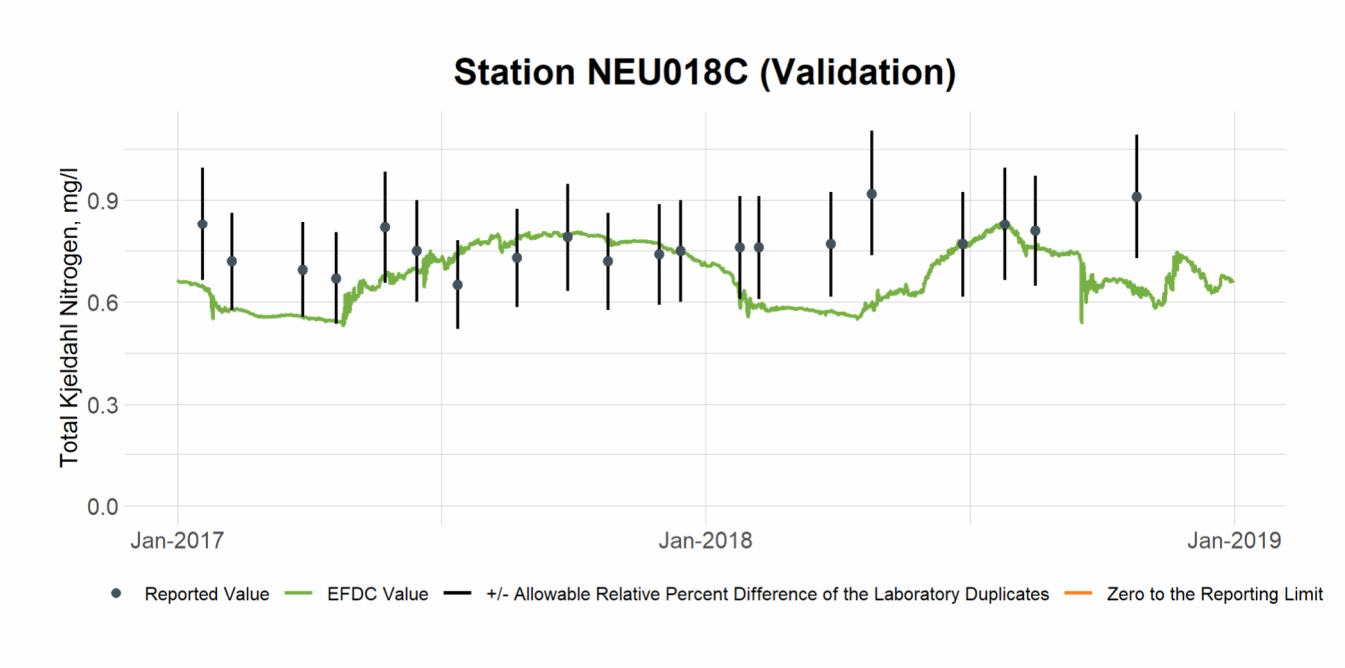

Figure 10-19 Validation Plot of TKN at Station NEU018C

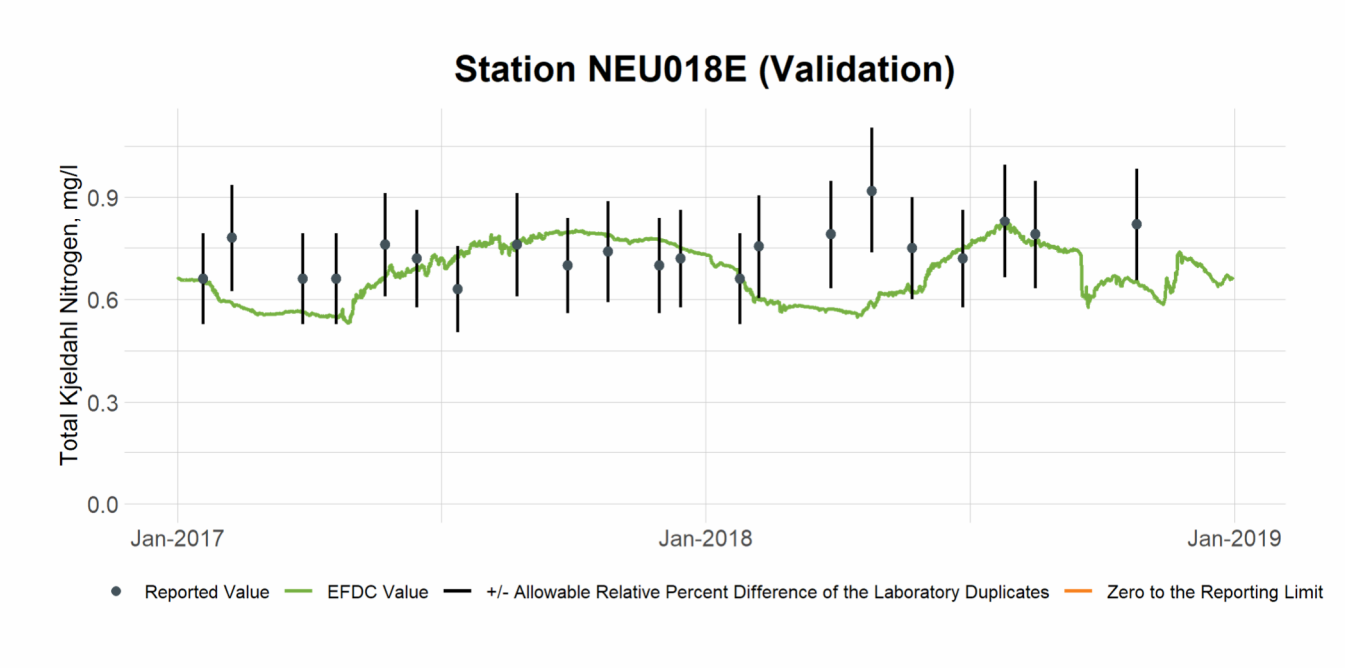

Figure 10-20 Validation Plot of TKN at Station NEU018E

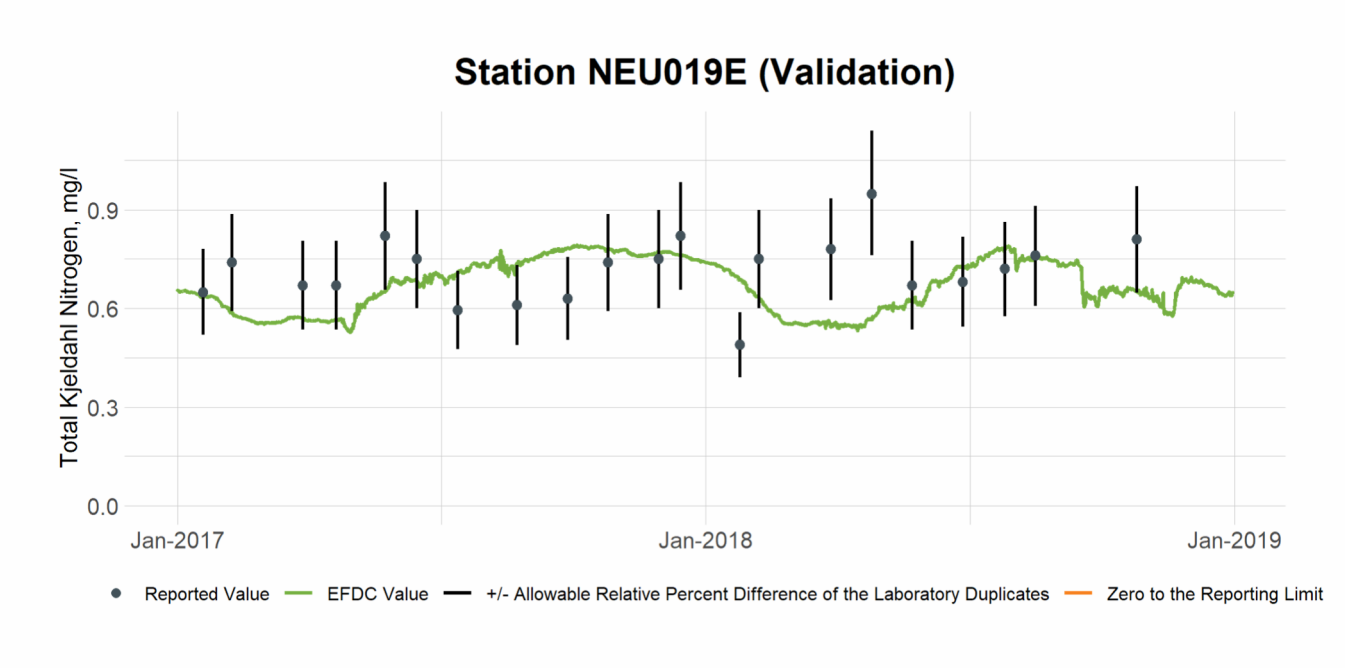

Figure 10-21 Validation Plot of TKN at Station NEU019E

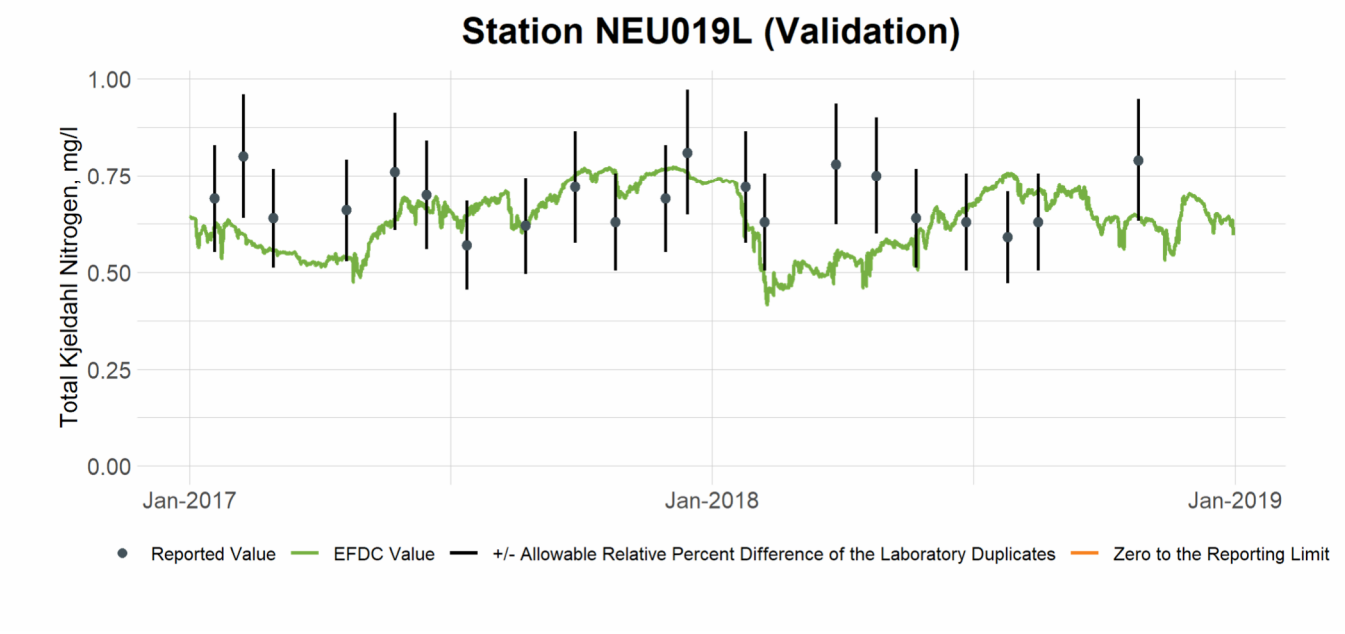

Figure 10-22 Validation Plot of TKN at Station NEU019L

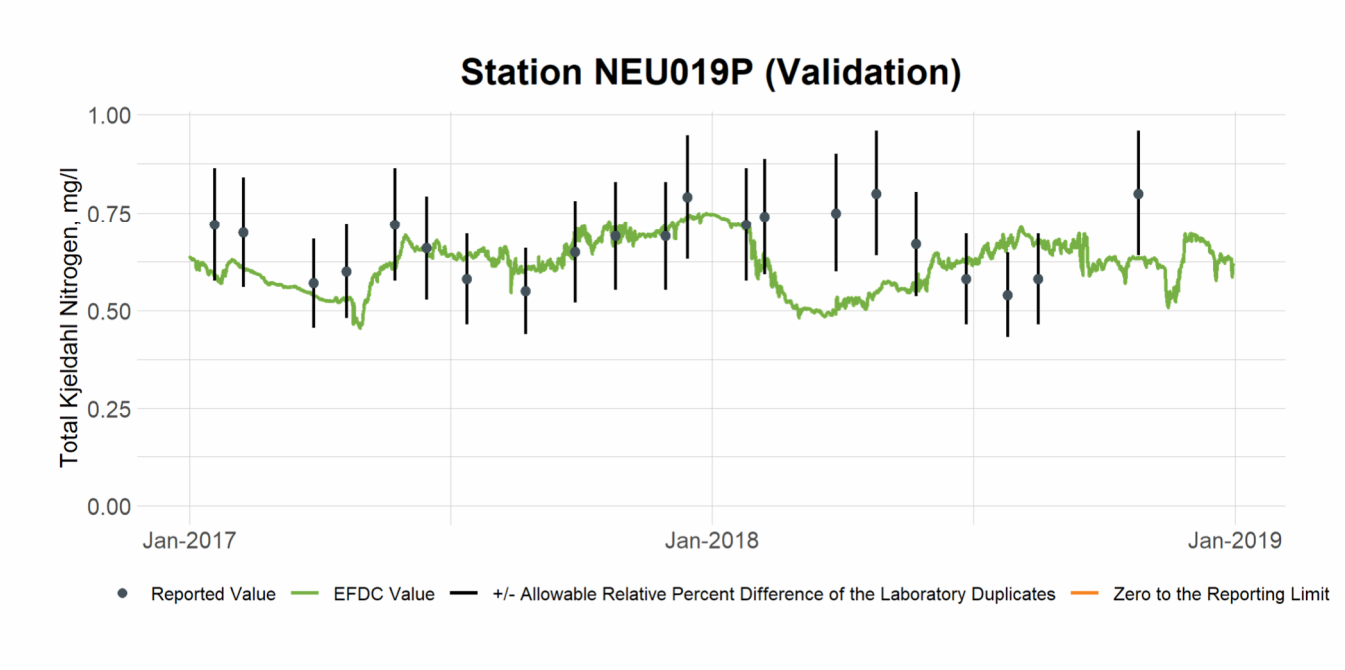

Figure 10-23 Validation Plot of TKN at Station NEU019P

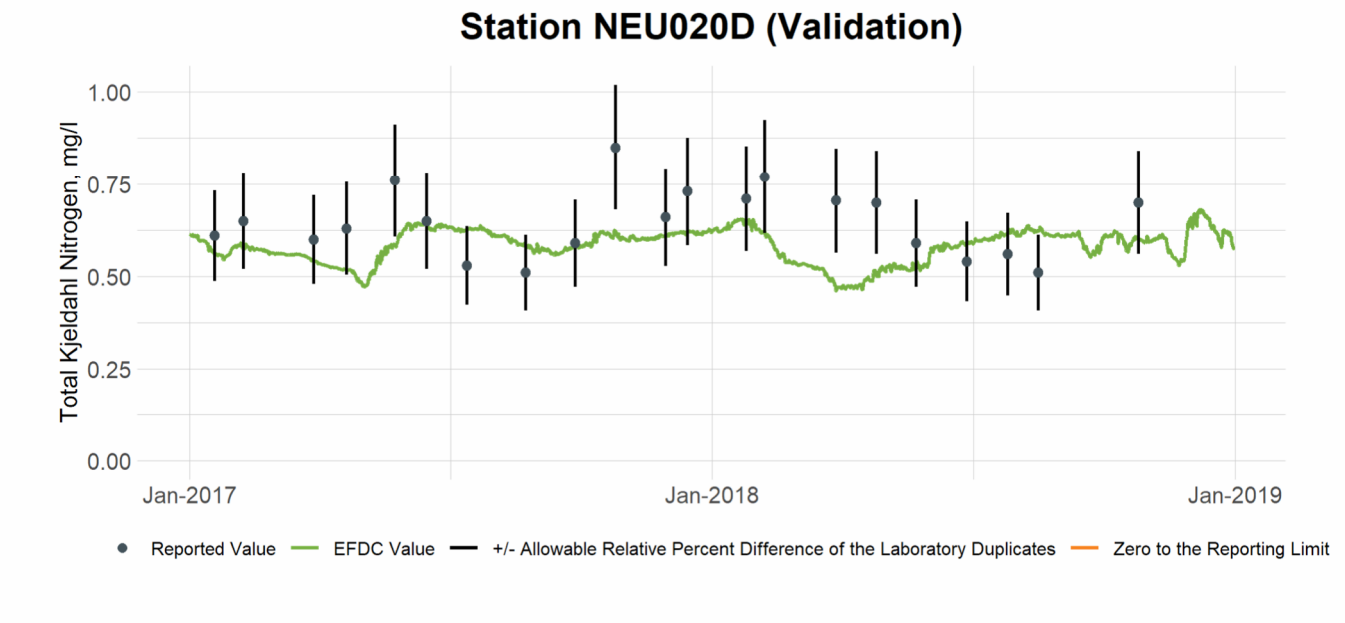

Figure 10-24 Validation Plot of TKN at Station NEU020D

11. TON

11.1 TON Calibration

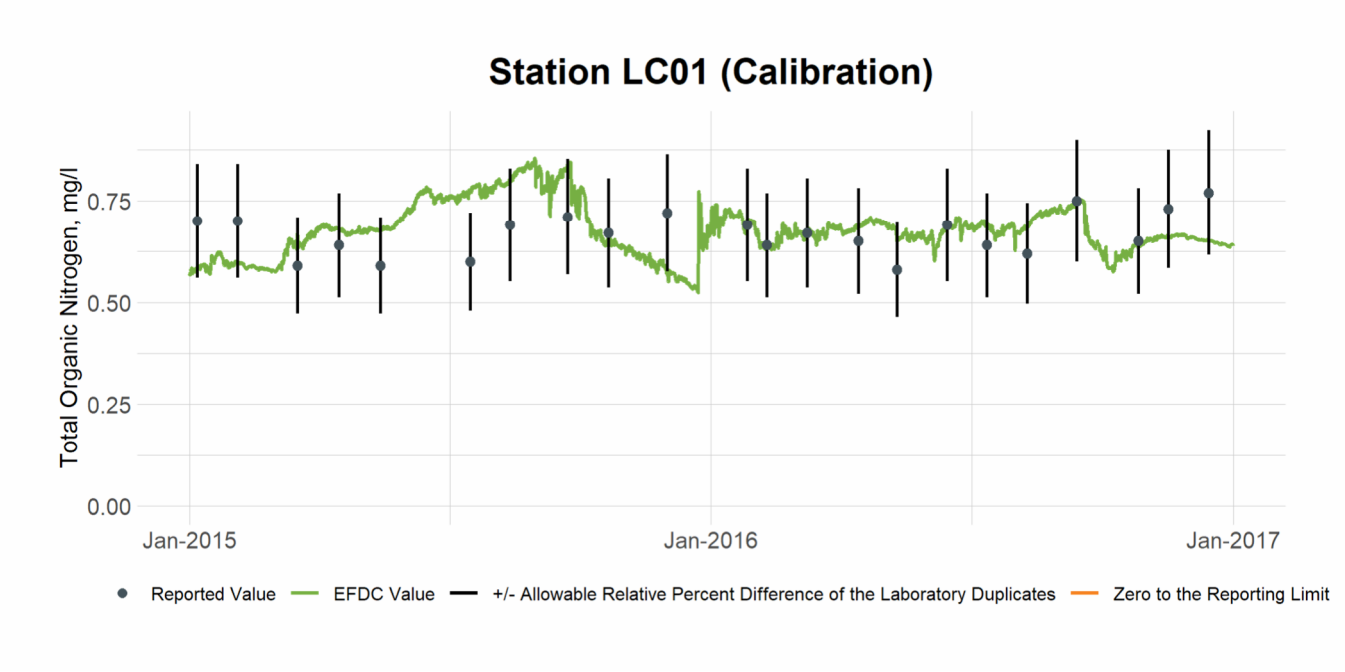

Figure 11-1 Calibration Plot of TON at Station LC01

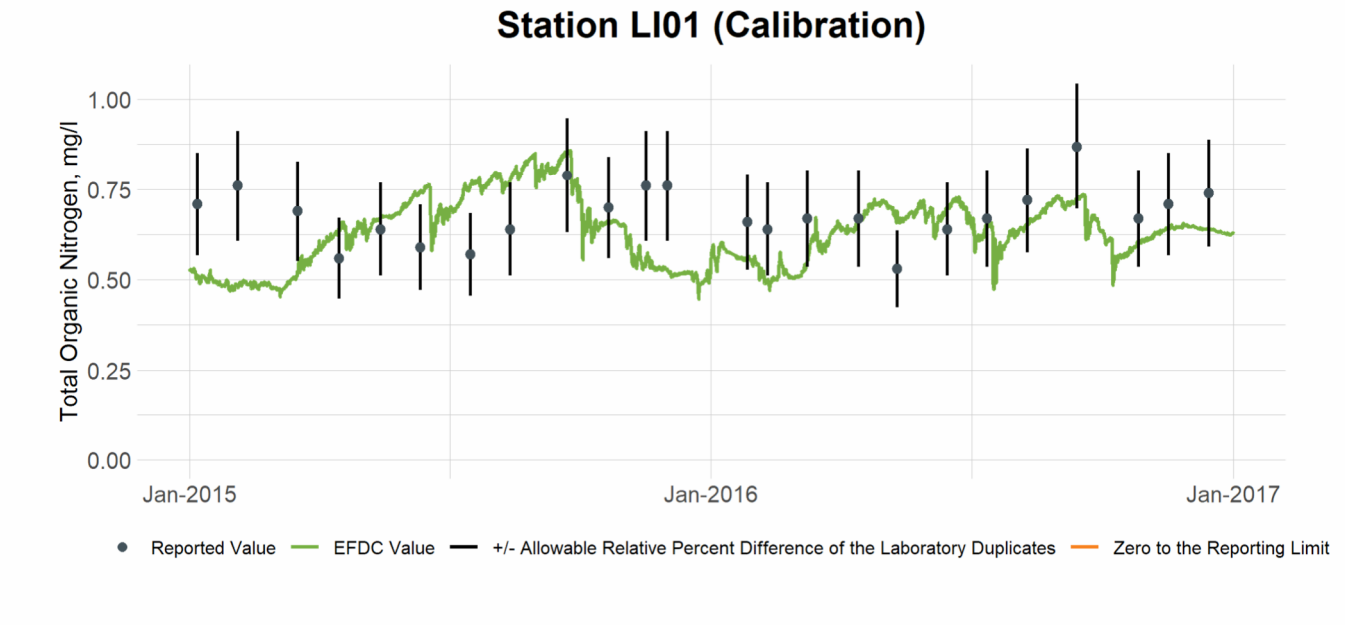

Figure 11-2 Calibration Plot of TON at Station LI01

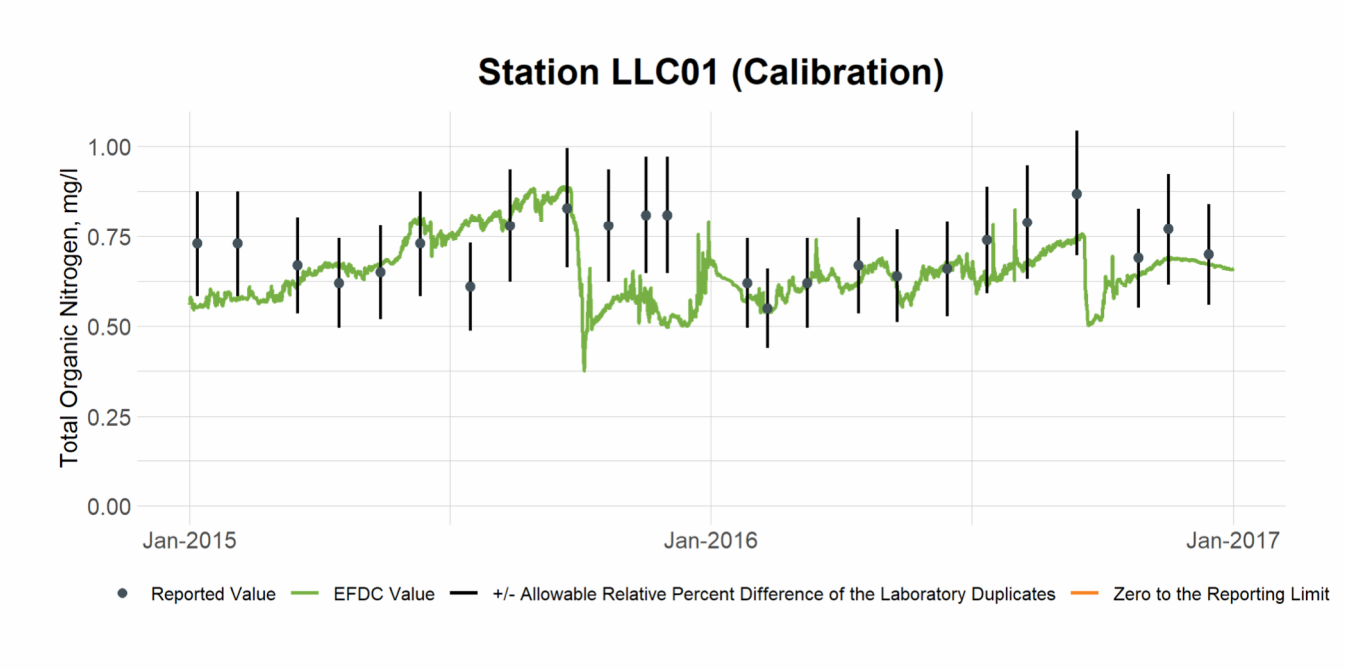

Figure 11-3 Calibration Plot of TON at Station LLC01

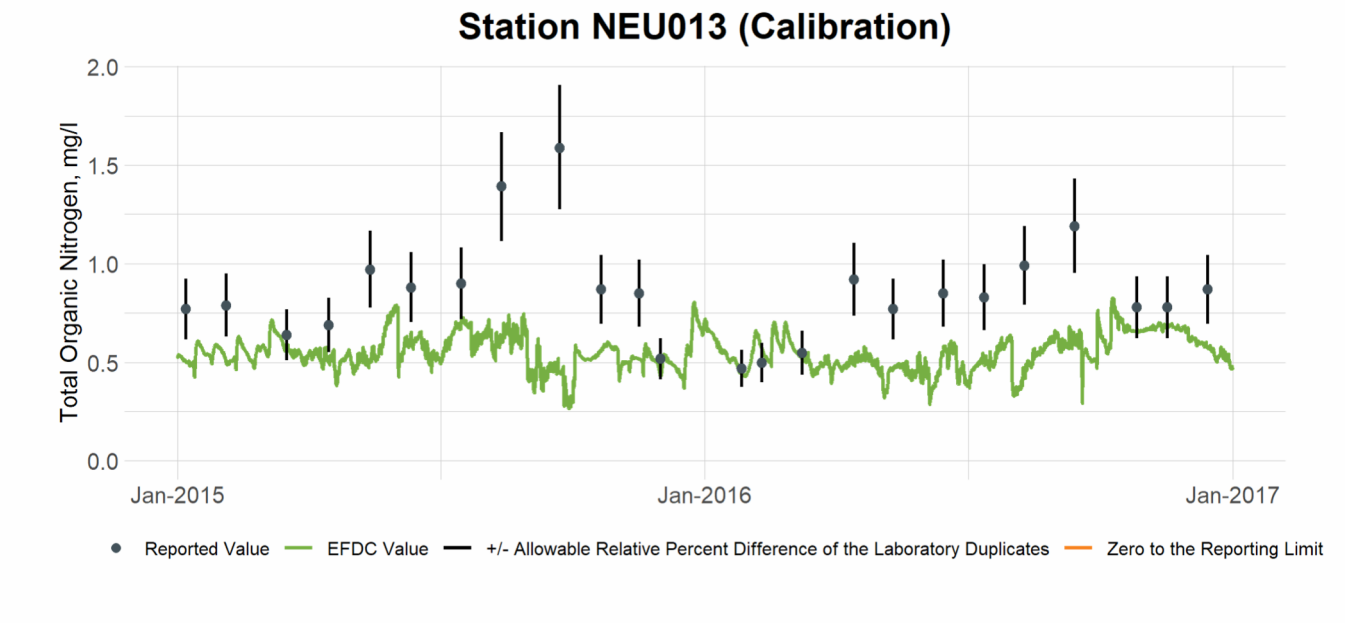

Figure 11-4 Calibration Plot of TON at Station NEU013

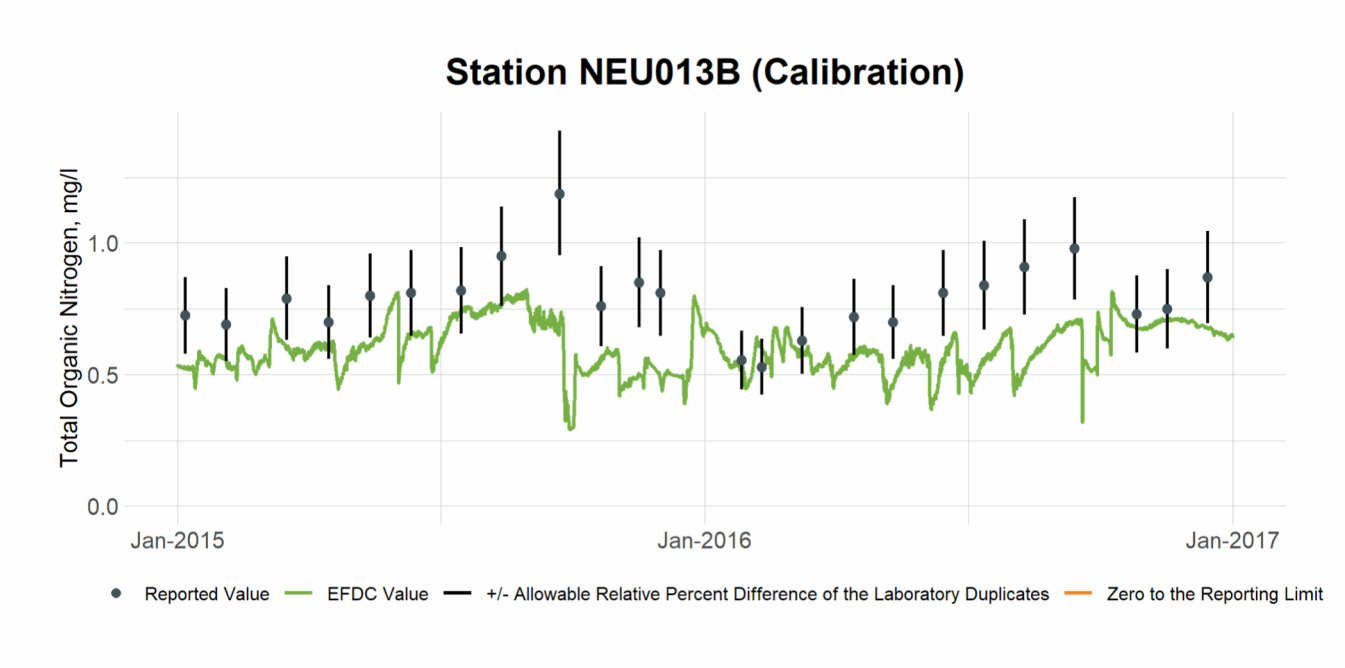

Figure 11-5 Calibration Plot of TON at Station NEU013B

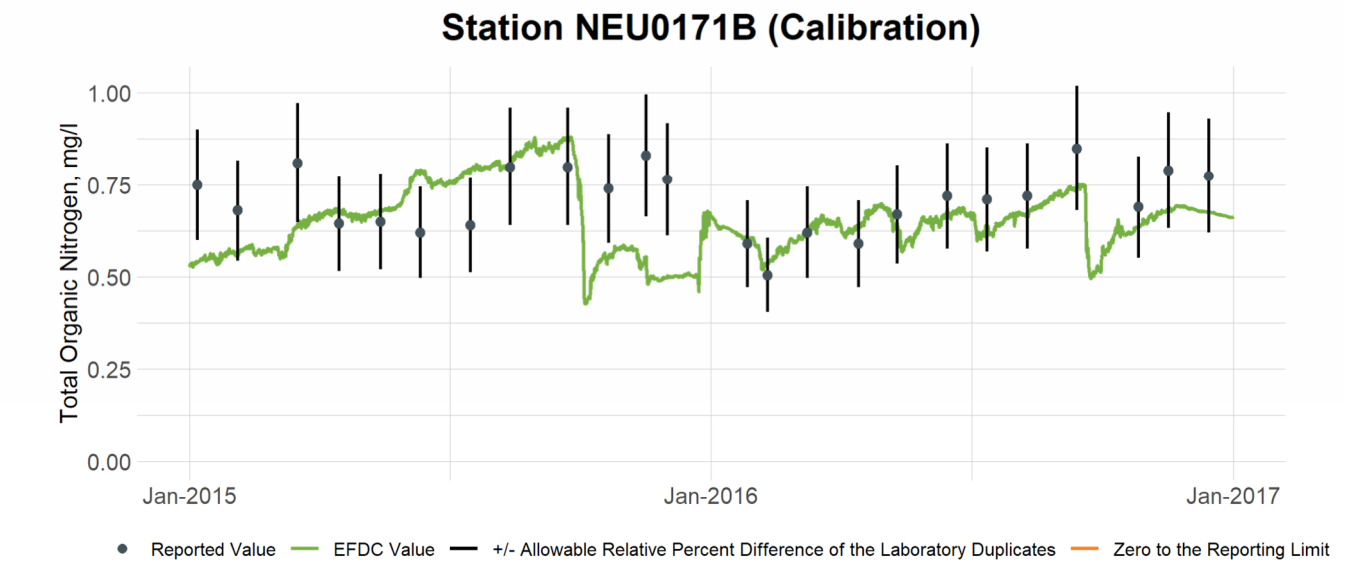

Figure 11-6 Calibration Plot of TON at Station NEU0171B

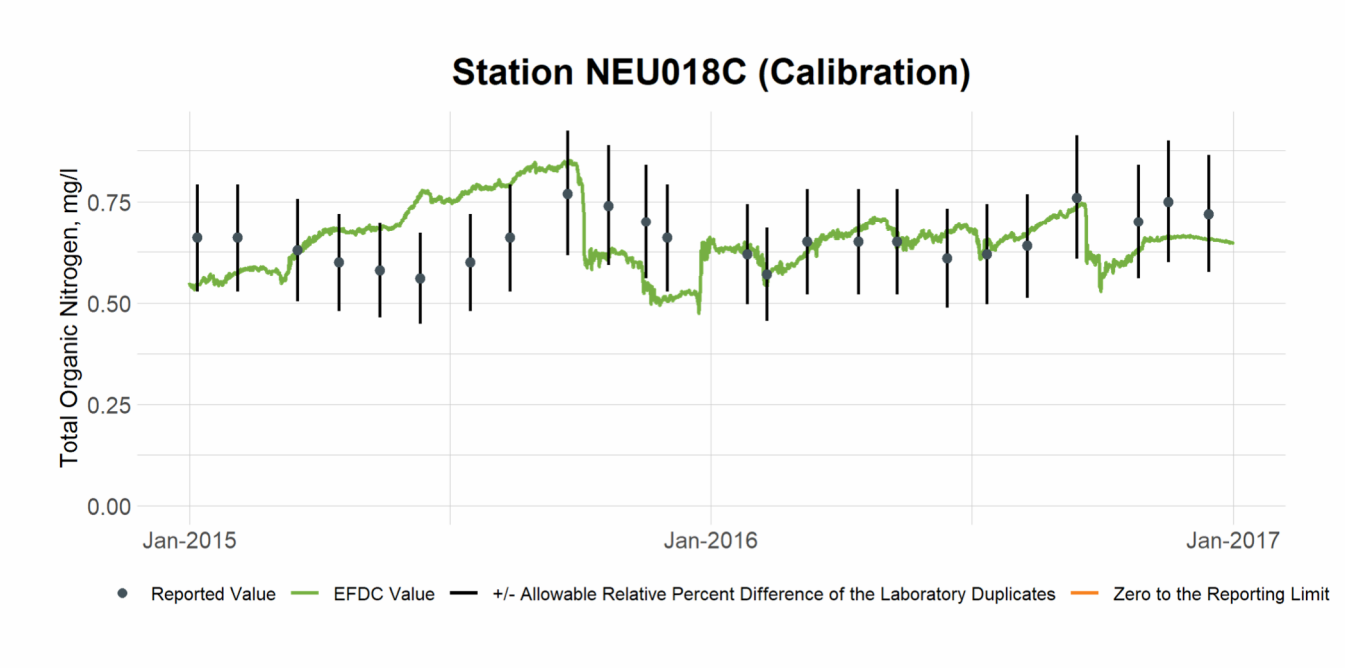

Figure 11-7 Calibration Plot of TON at Station NEU018C

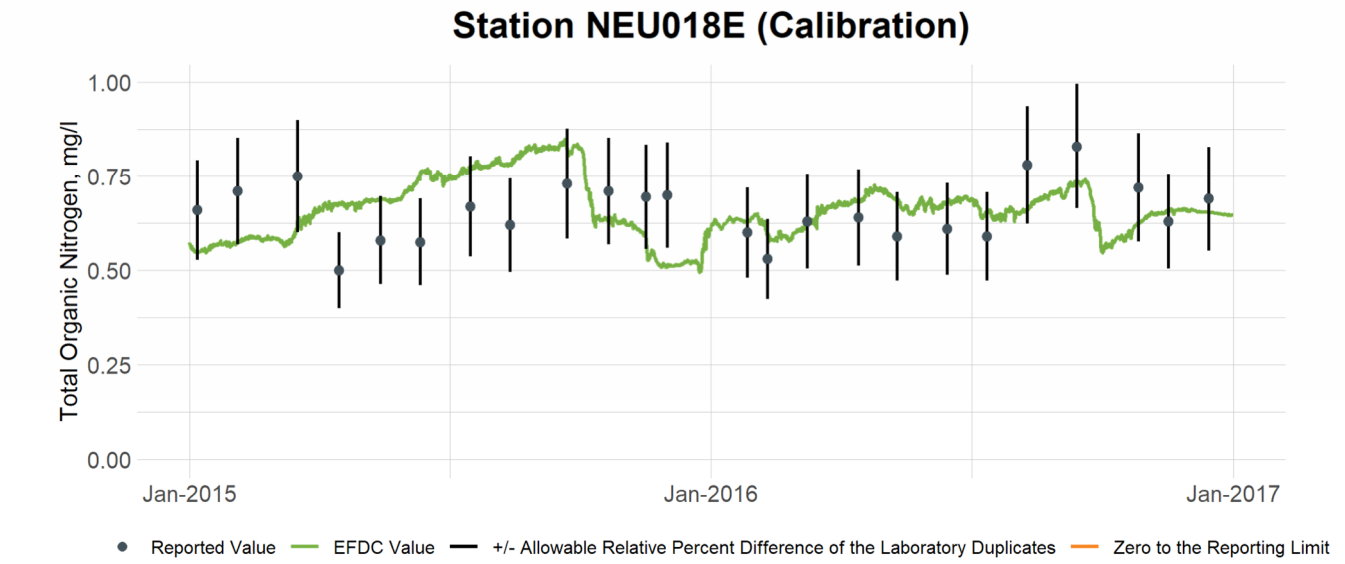

Figure 11-8 Calibration Plot of TON at Station NEU018E

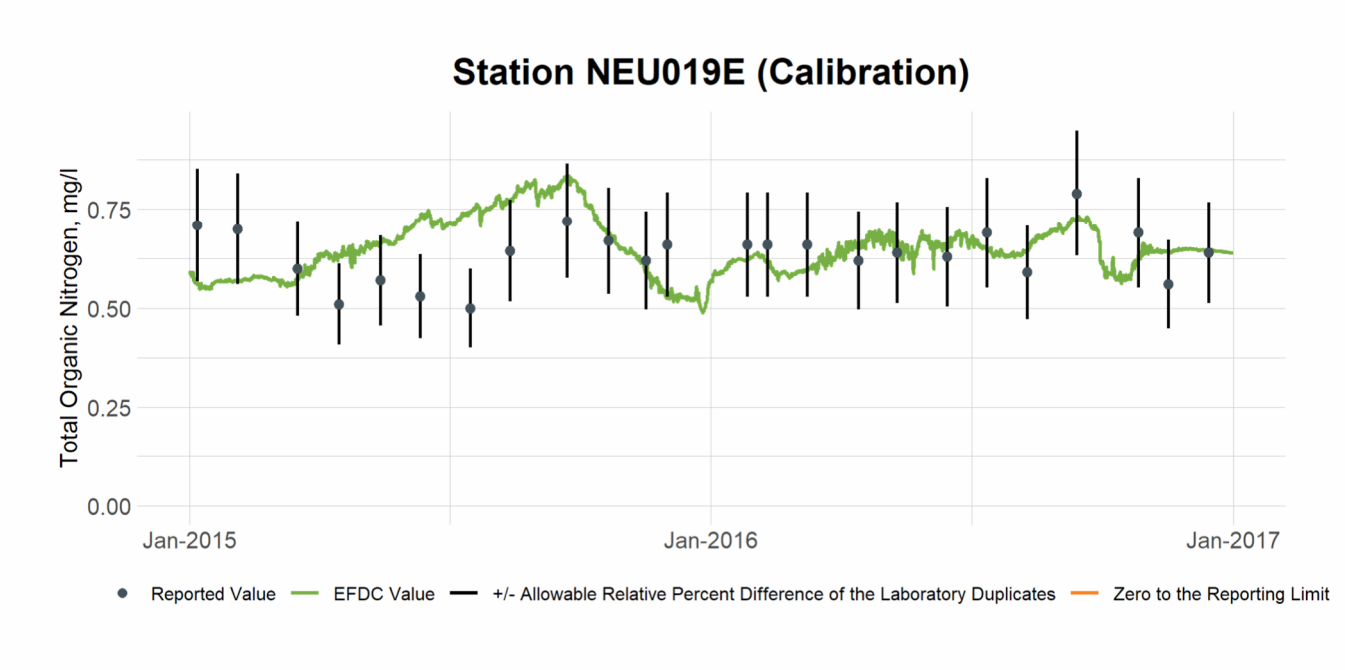

Figure 11-9 Calibration Plot of TON at Station NEU019E

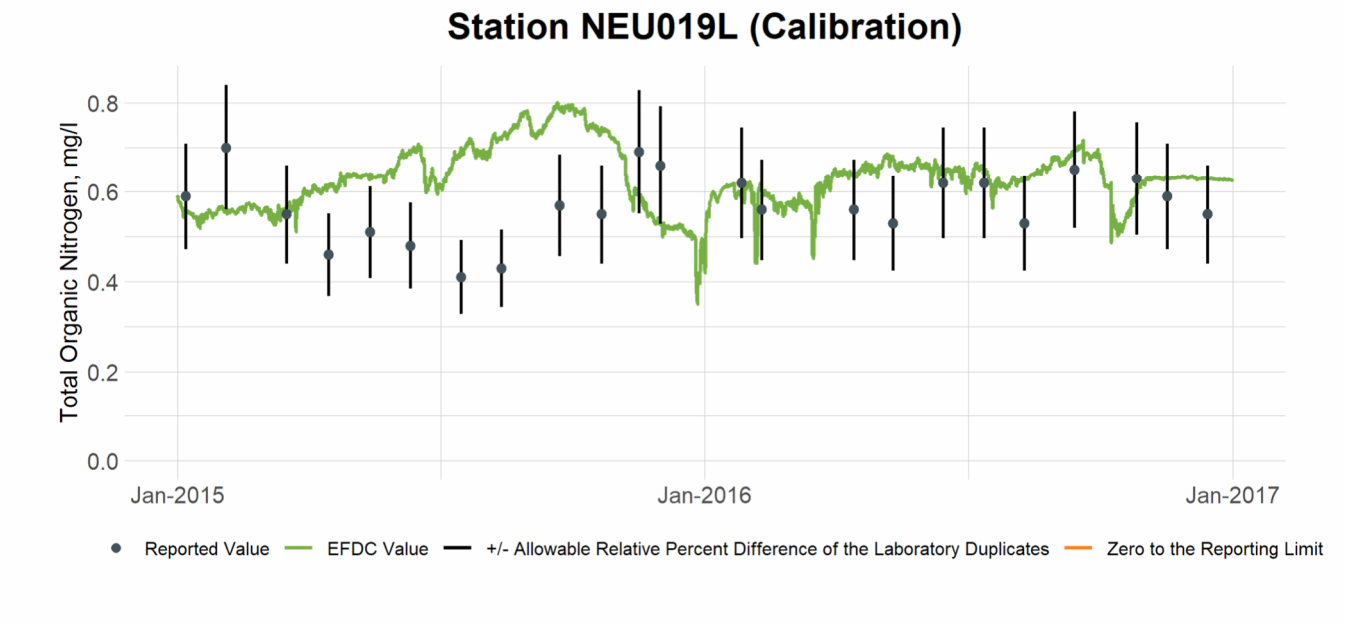

Figure 11-10 Calibration Plot of TON at Station NEU019L

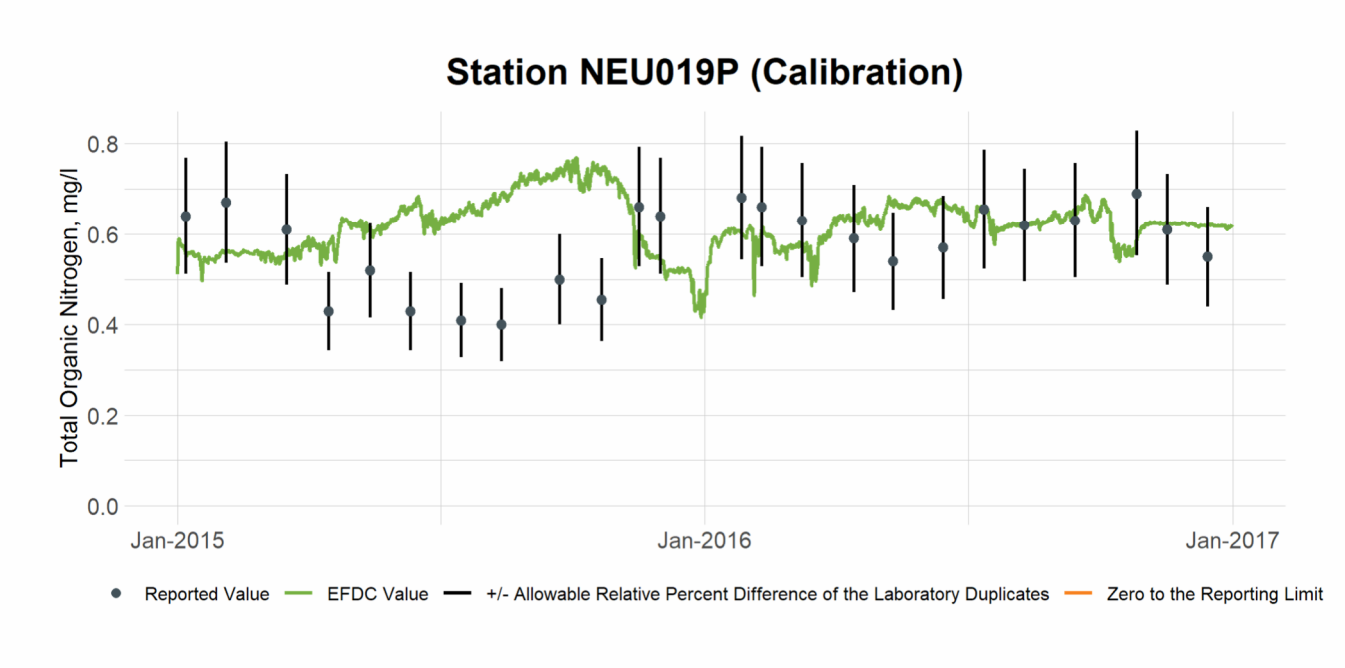

Figure 11-11 Calibration Plot of TON at Station NEU019P

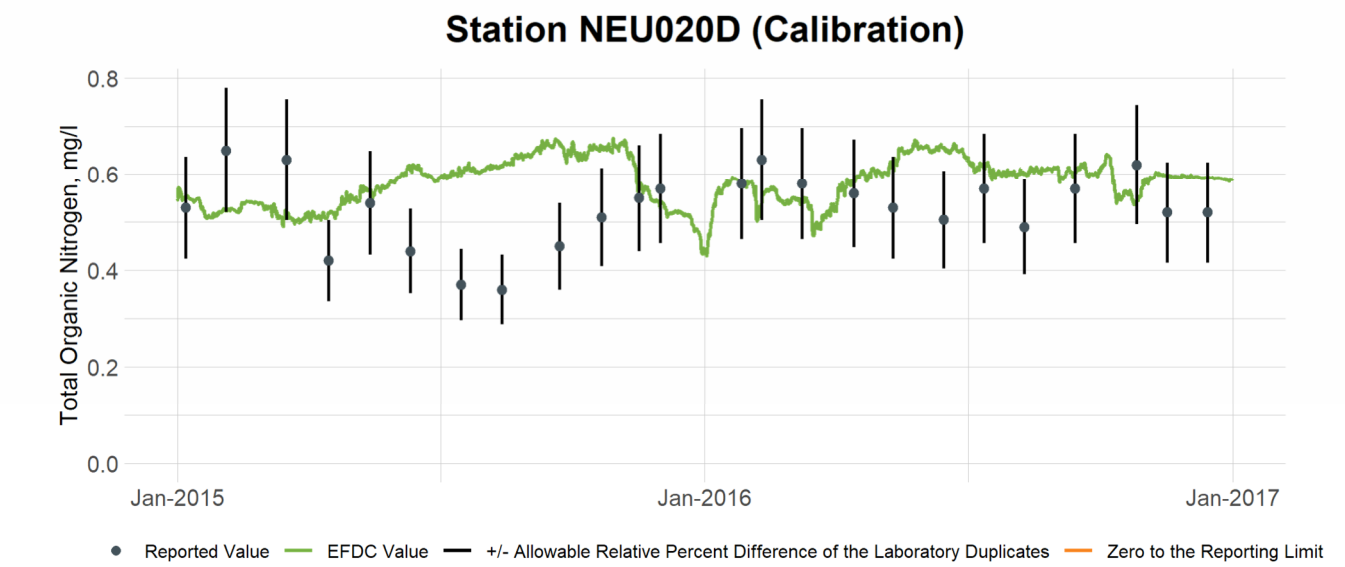

Figure 11-12 Calibration Plot of TON at Station NEU020D

11.2 TON Validation

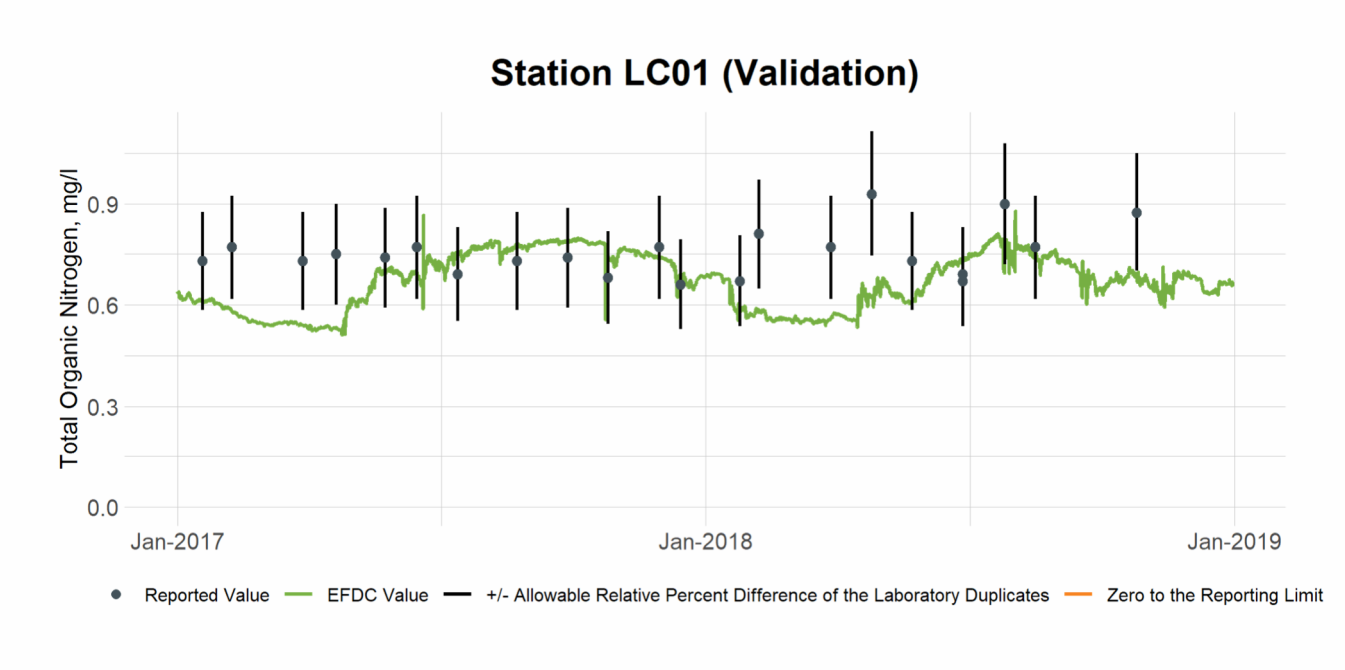

Figure 11-13 Validation Plot of TON at Station LC01

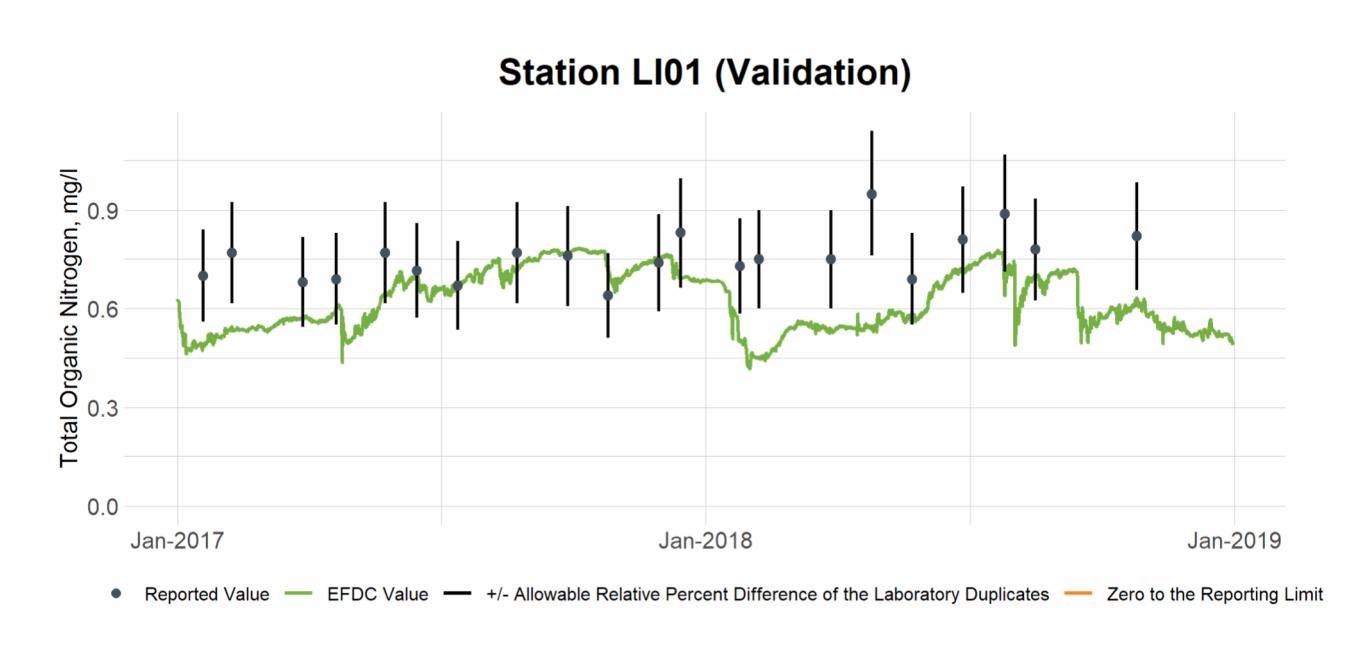

Figure 11-14 Validation Plot of TON at Station LI01

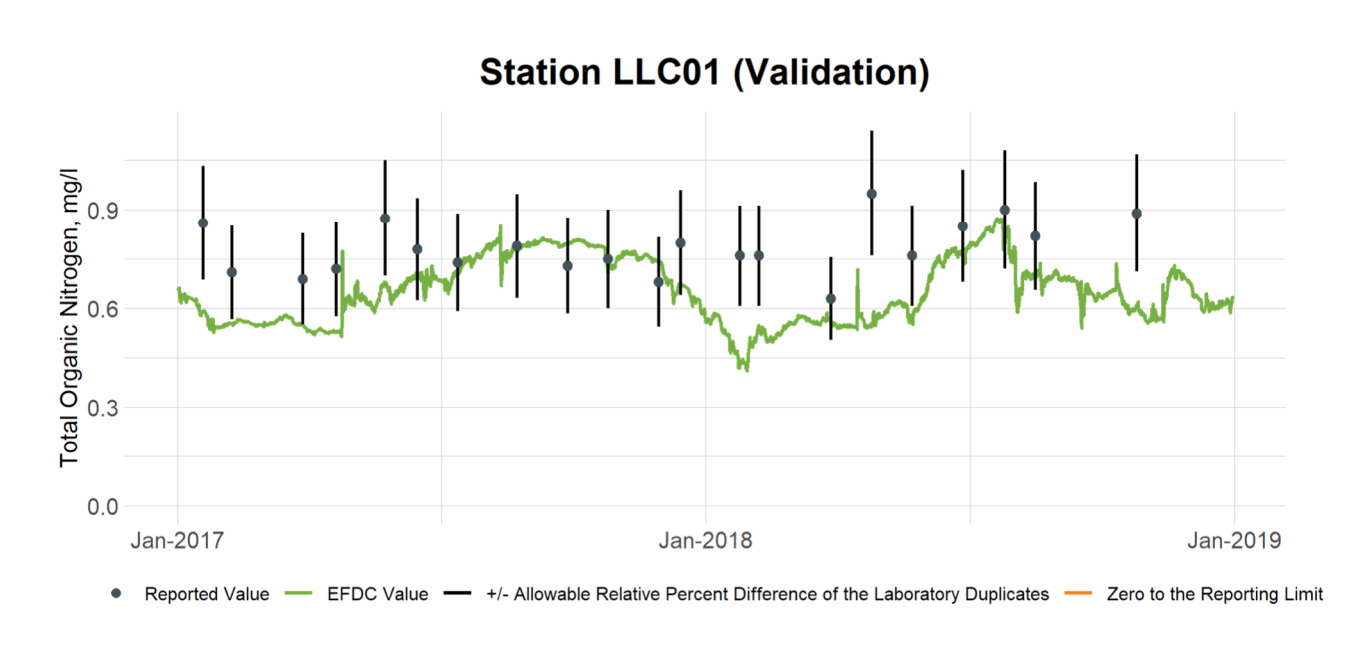

Figure 11-15 Validation Plot of TON at Station LLC01

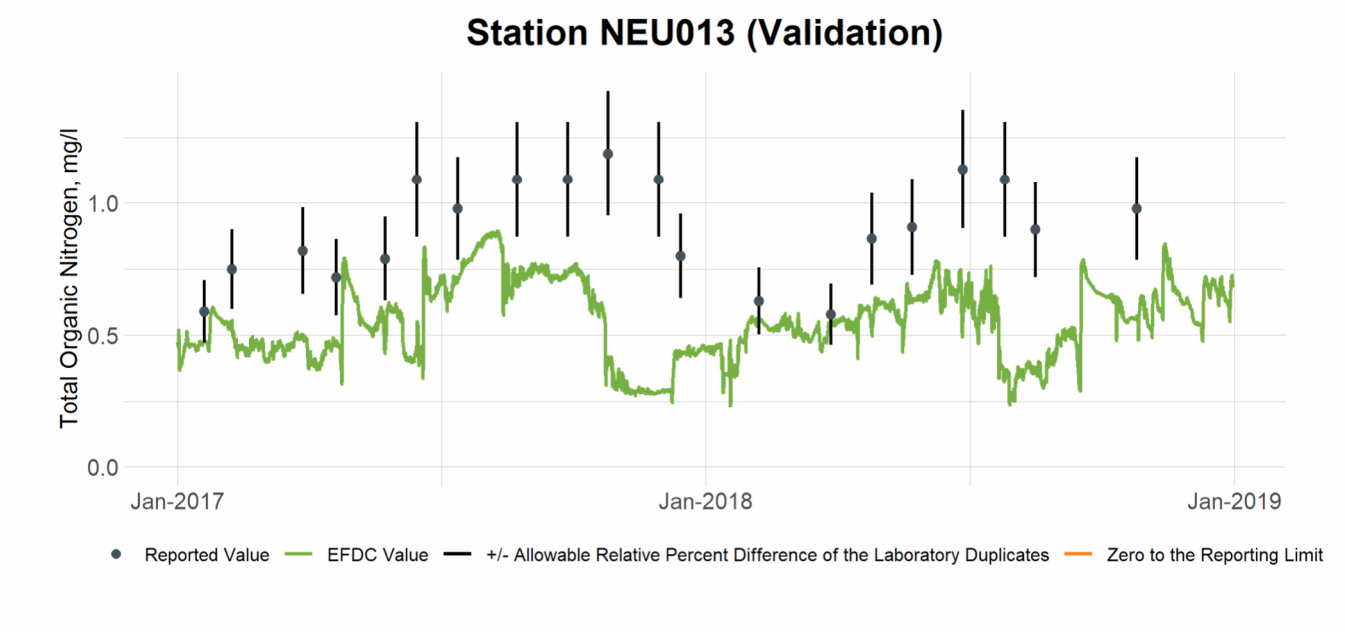

Figure 11-16 Validation Plot of TON at Station NEU013

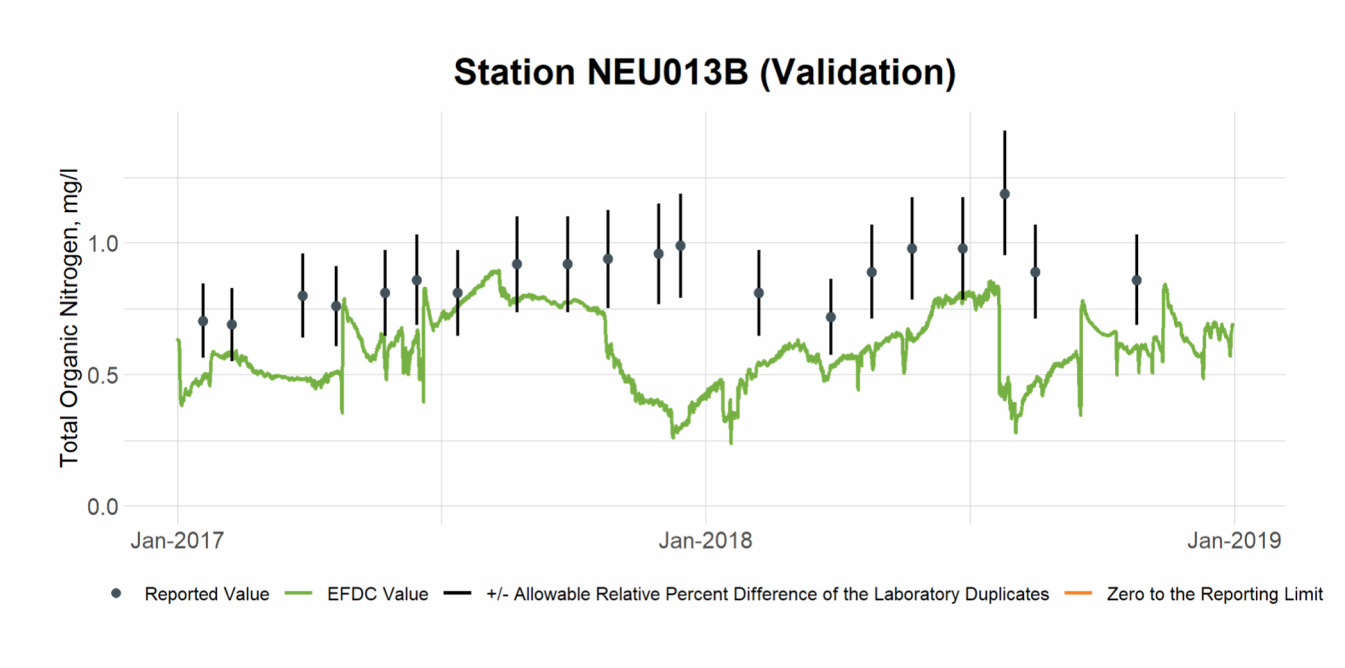

Figure 11-17 Validation Plot of TON at Station NEU013B

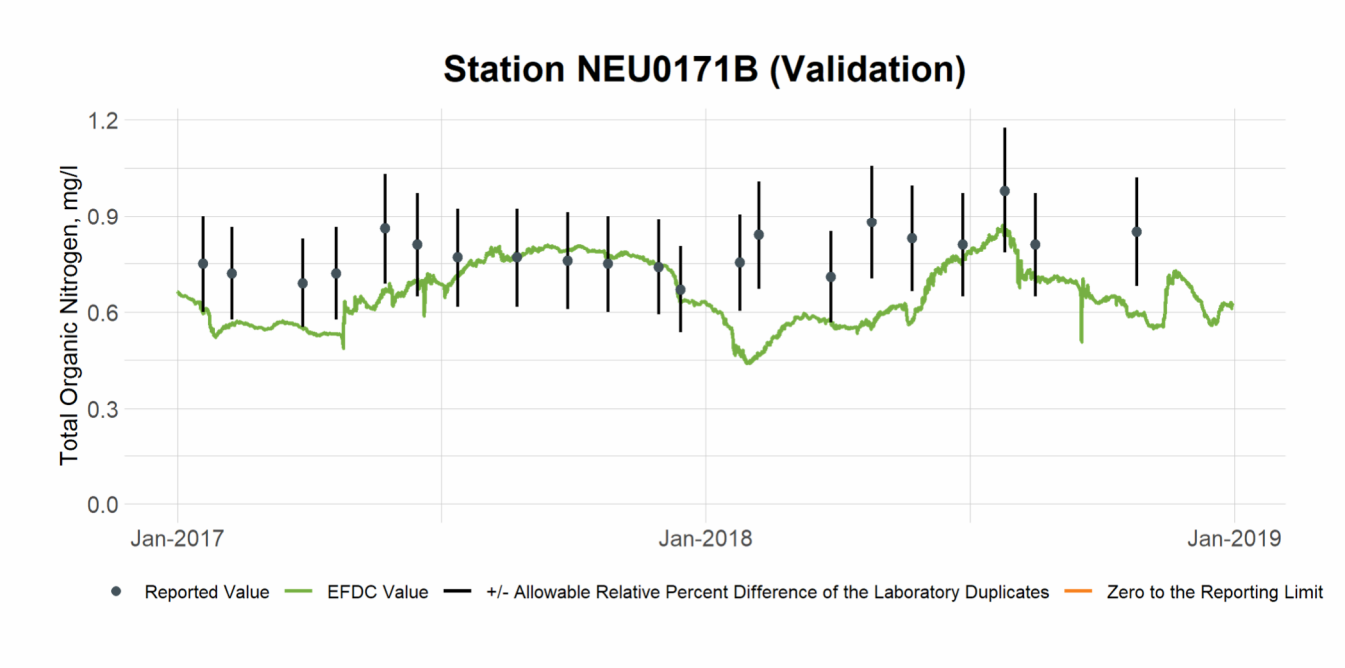

Figure 11-18 Validation Plot of TON at Station NEU0171B

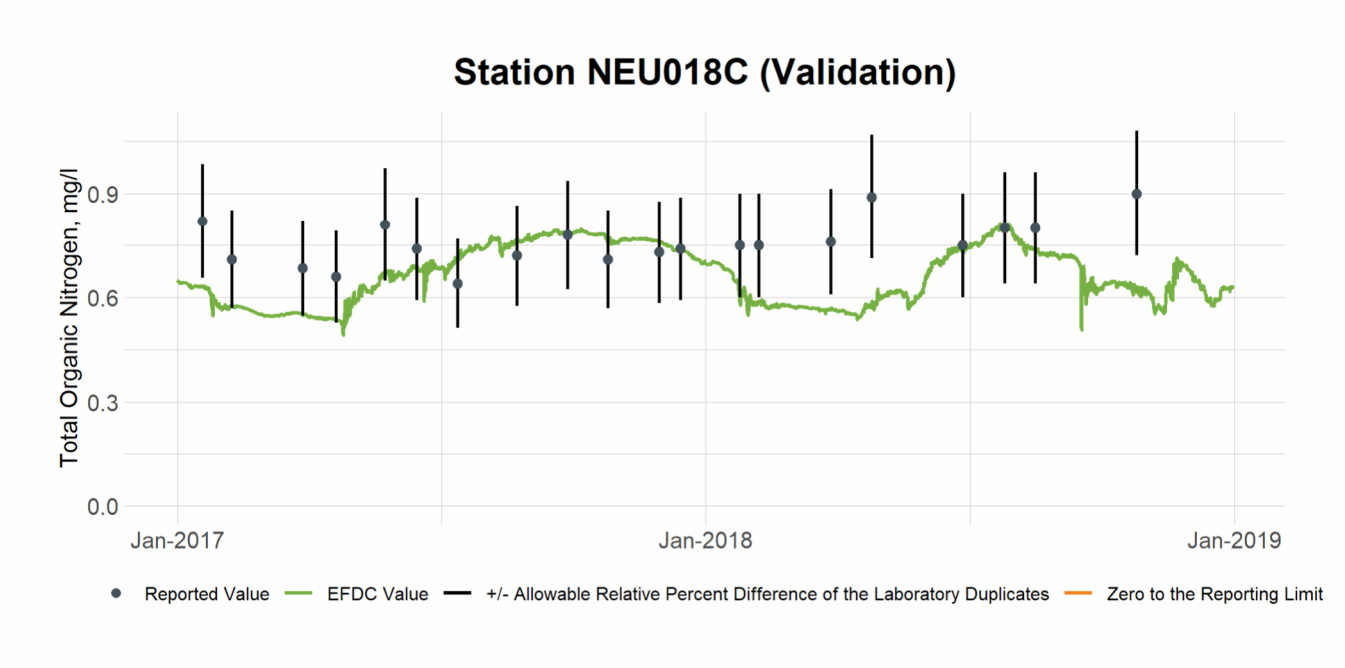

Figure 11-19 Validation Plot of TON at Station NEU018C

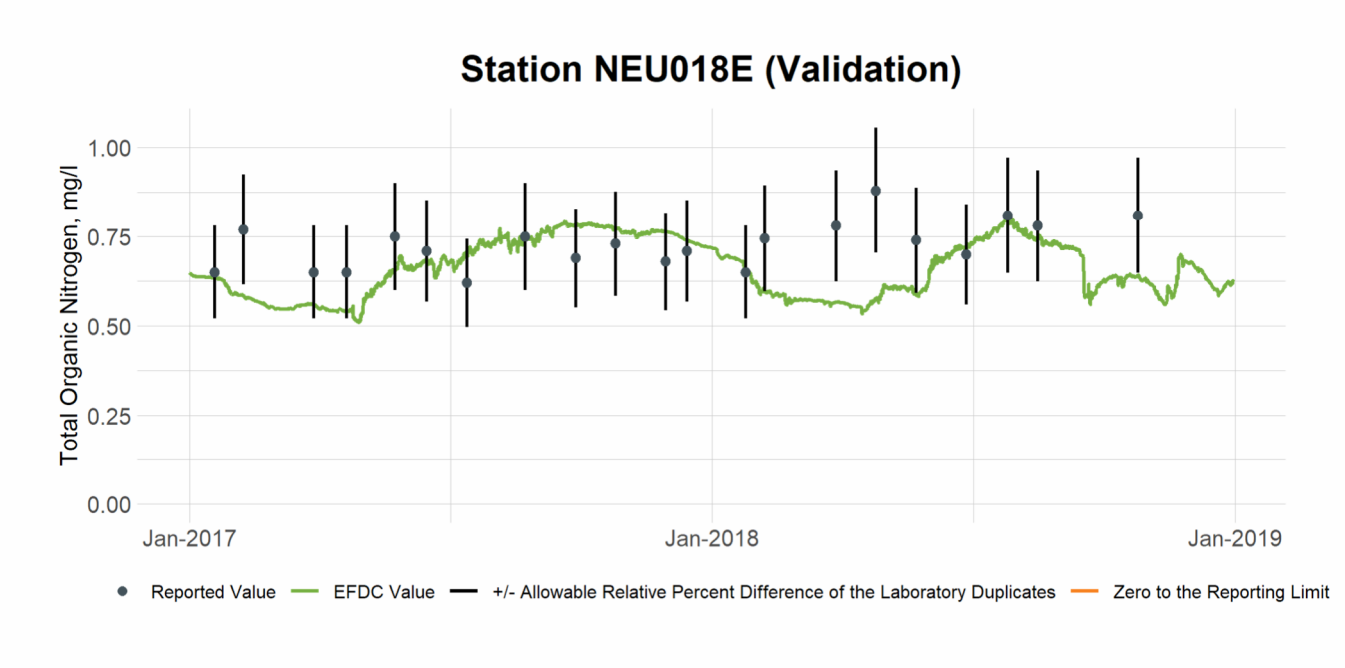

Figure 11-20 Validation Plot of TON at Station NEU018E

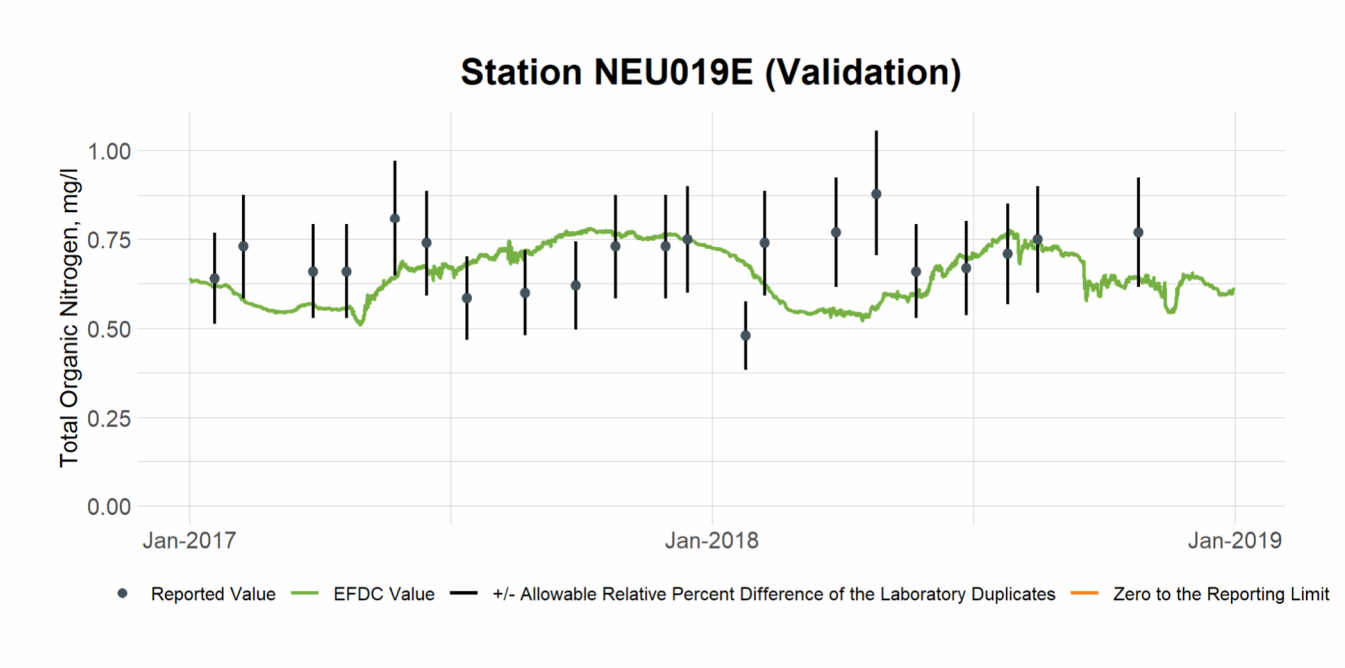

Figure 11-21 Validation Plot of TON at Station NEU019E

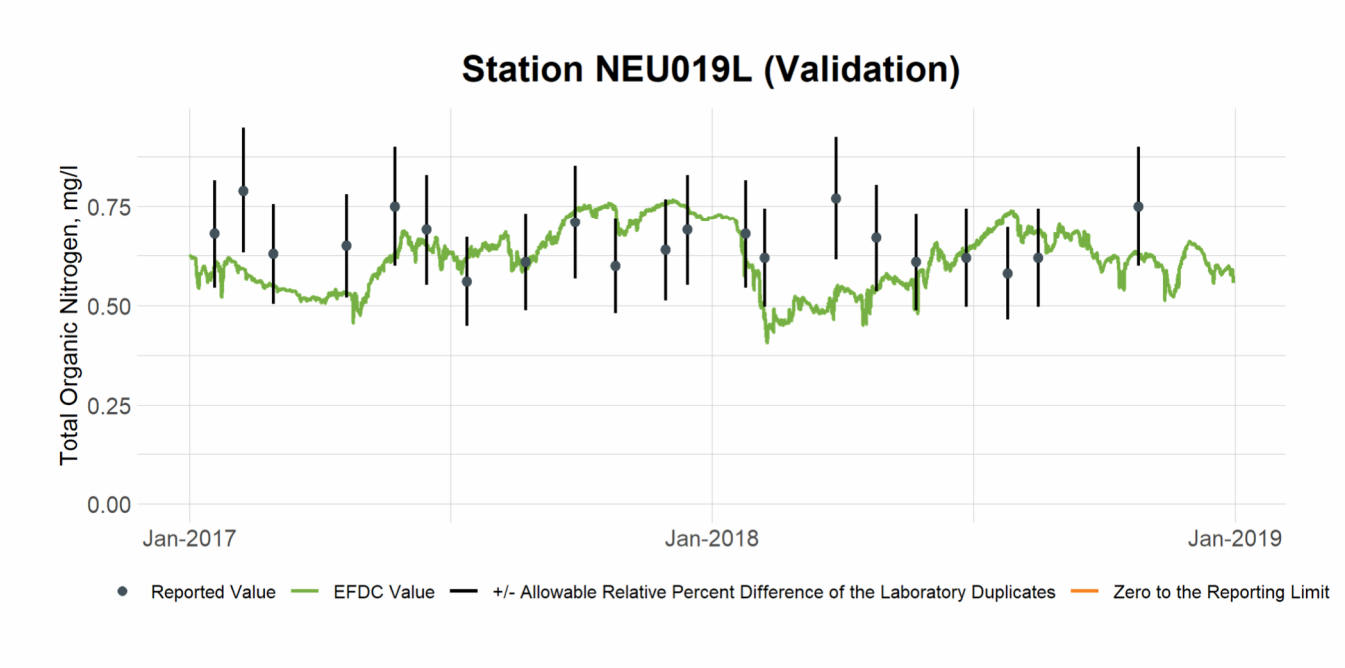

Figure 11-22 Validation Plot of TON at Station NEU019L

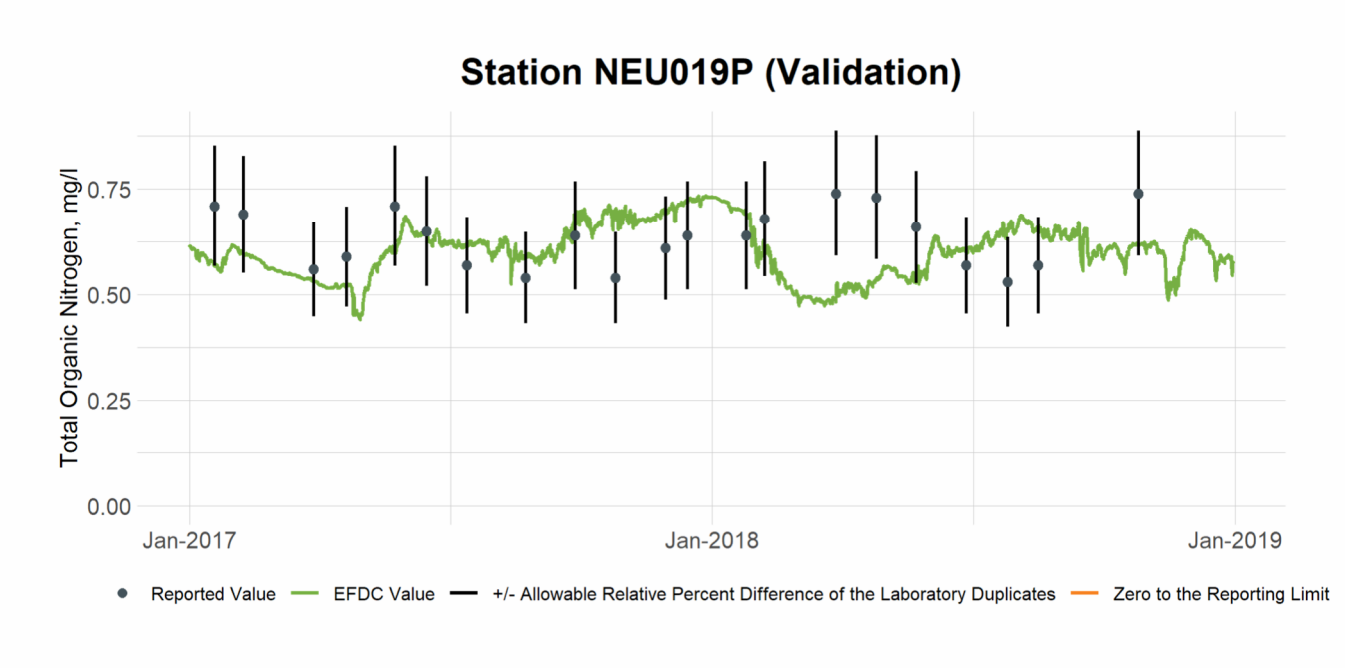

Figure 11-23 Validation Plot of TON at Station NEU019P

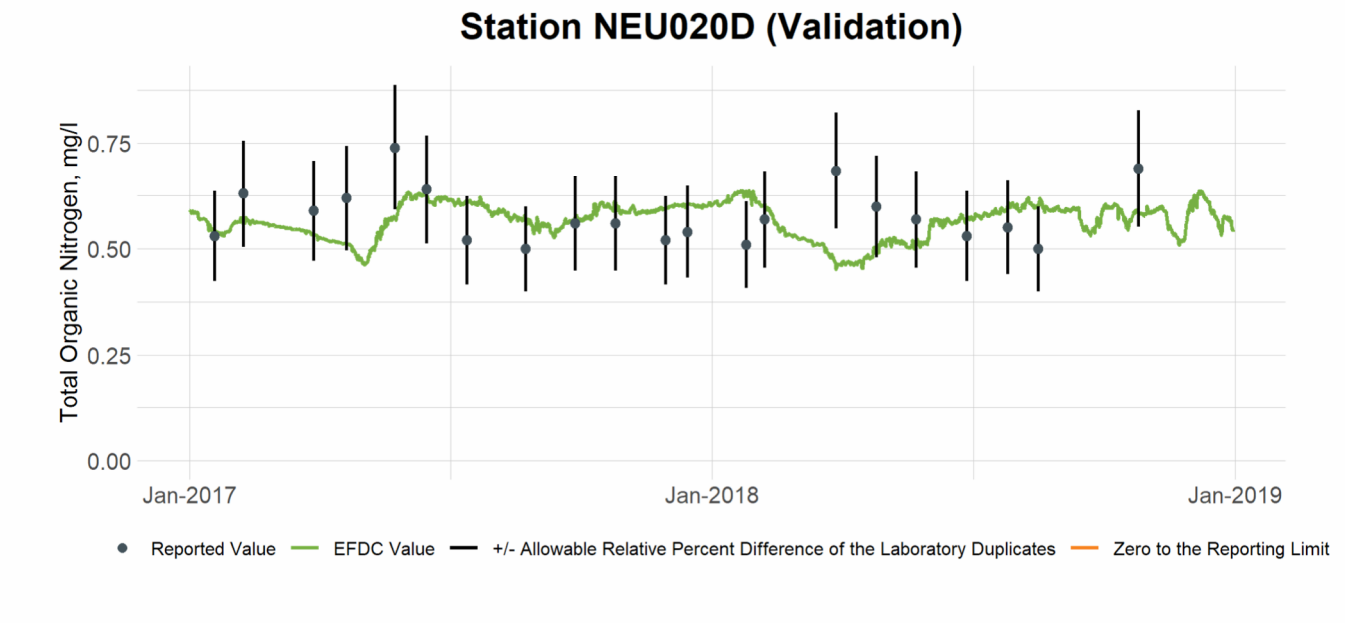

Figure 11-24 Validation Plot of TON at Station NEU020D

12. TSS

12.1 TSS Calibration

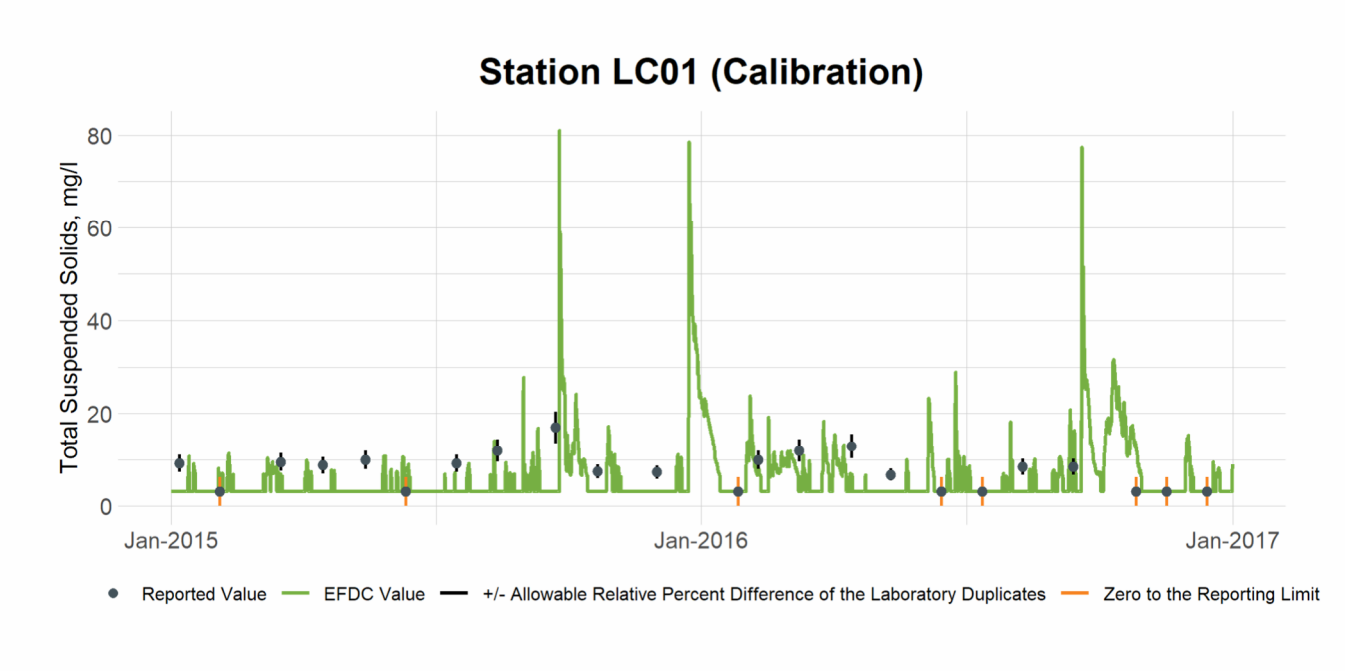

Figure 12-1 Calibration Plot of TSS at Station LC01

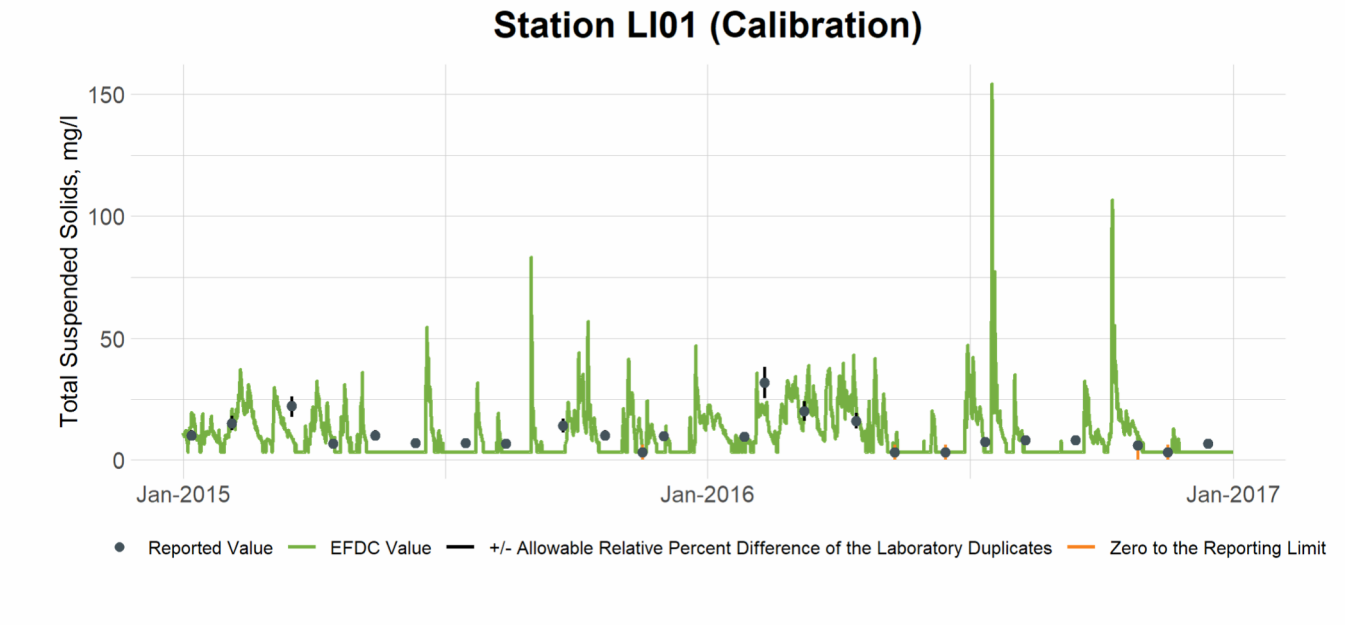

Figure 12-2 Calibration Plot of TSS at Station LI01

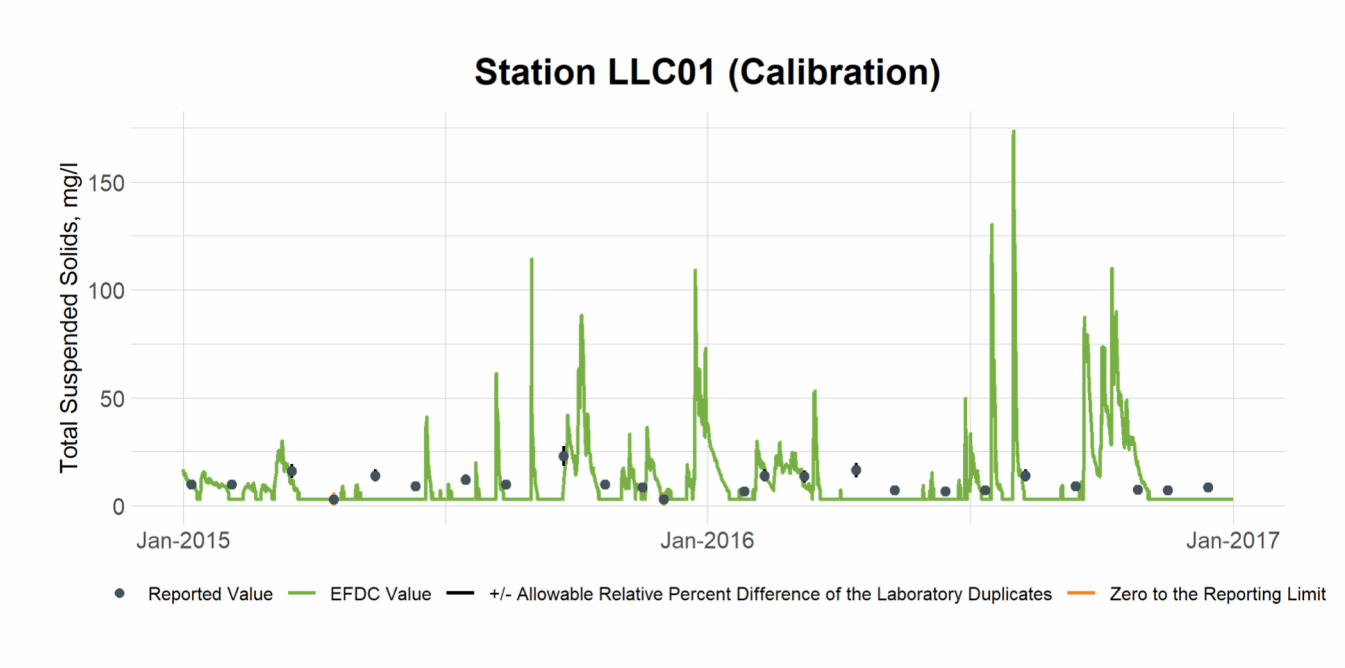

Figure 12-3 Calibration Plot of TSS at Station LLC01

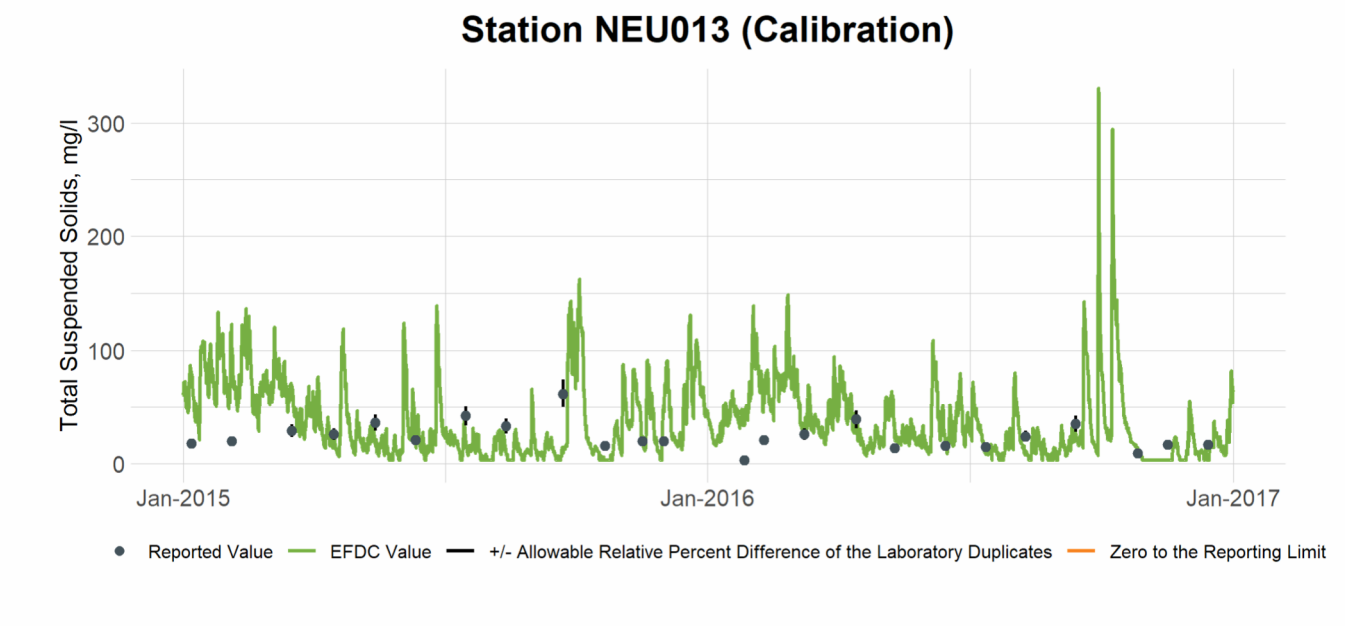

Figure 12-4 Calibration Plot of TSS at Station NEU013

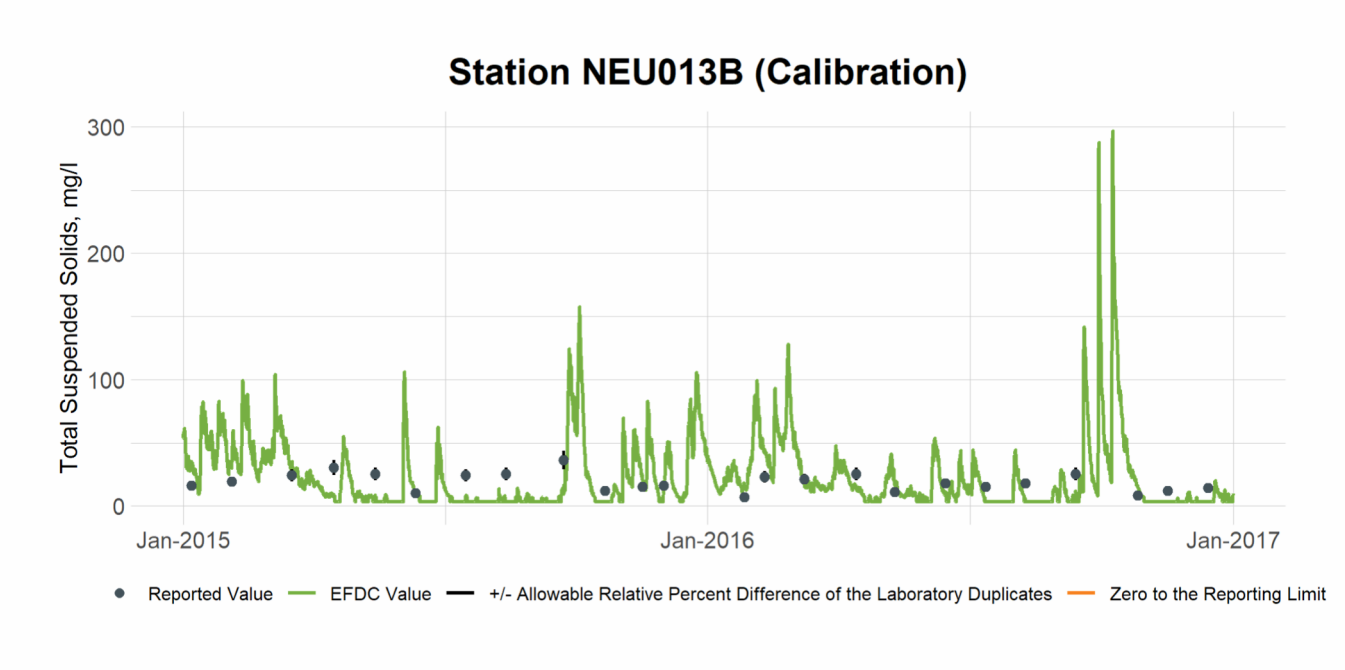

Figure 12-5 Calibration Plot of TSS at Station NEU013B

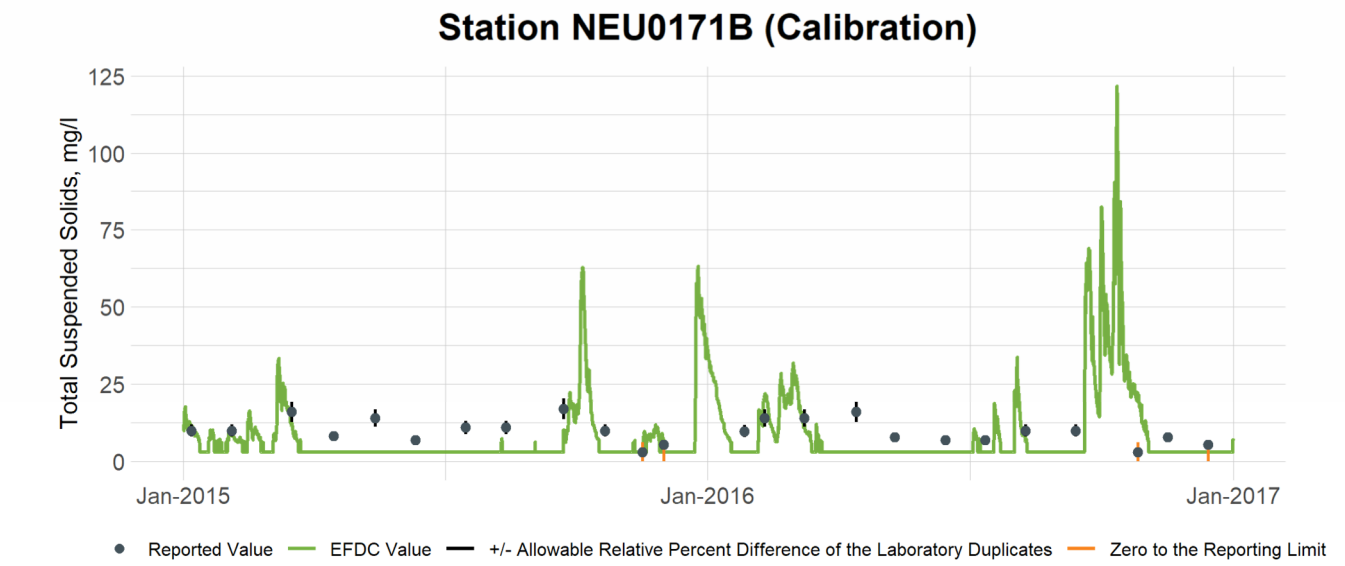

Figure 12-6 Calibration Plot of TSS at Station NEU0171B

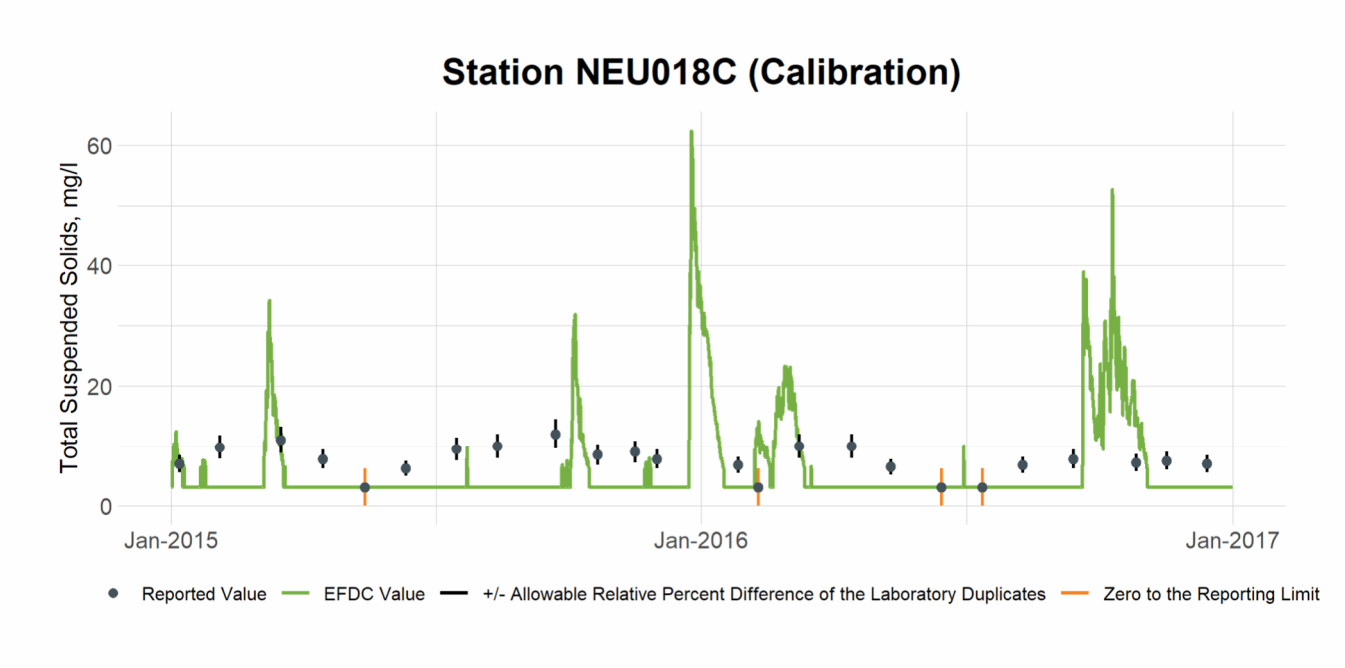

Figure 12-7 Calibration Plot of TSS at Station NEU018C

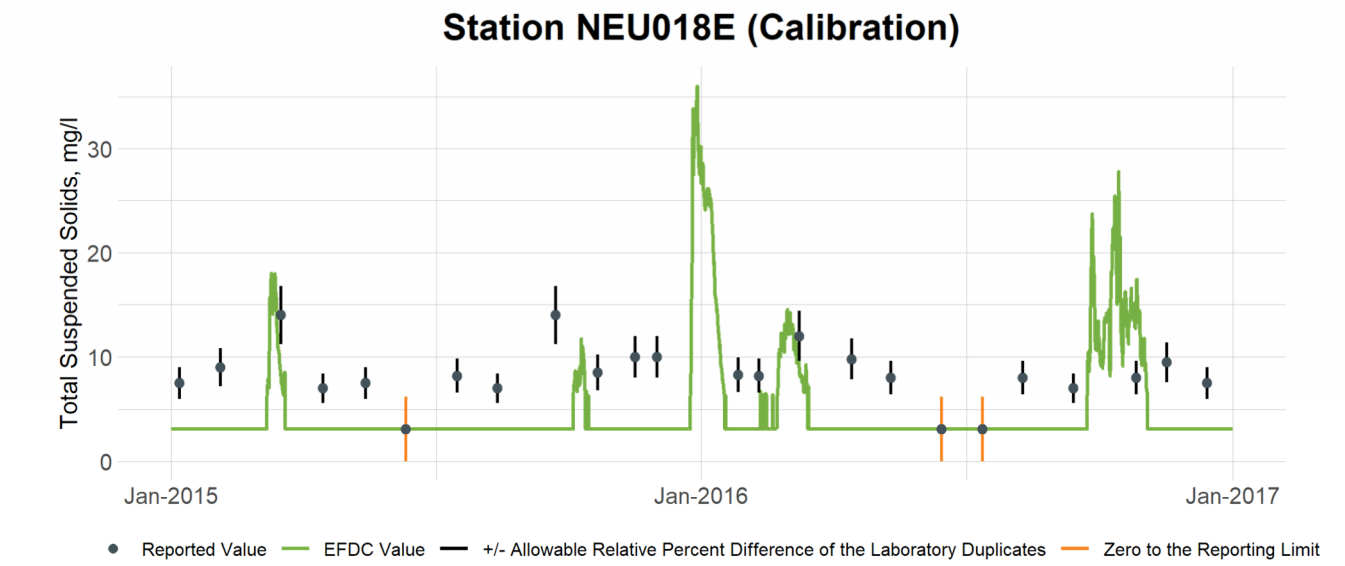

Figure 12-8 Calibration Plot of TSS at Station NEU018E

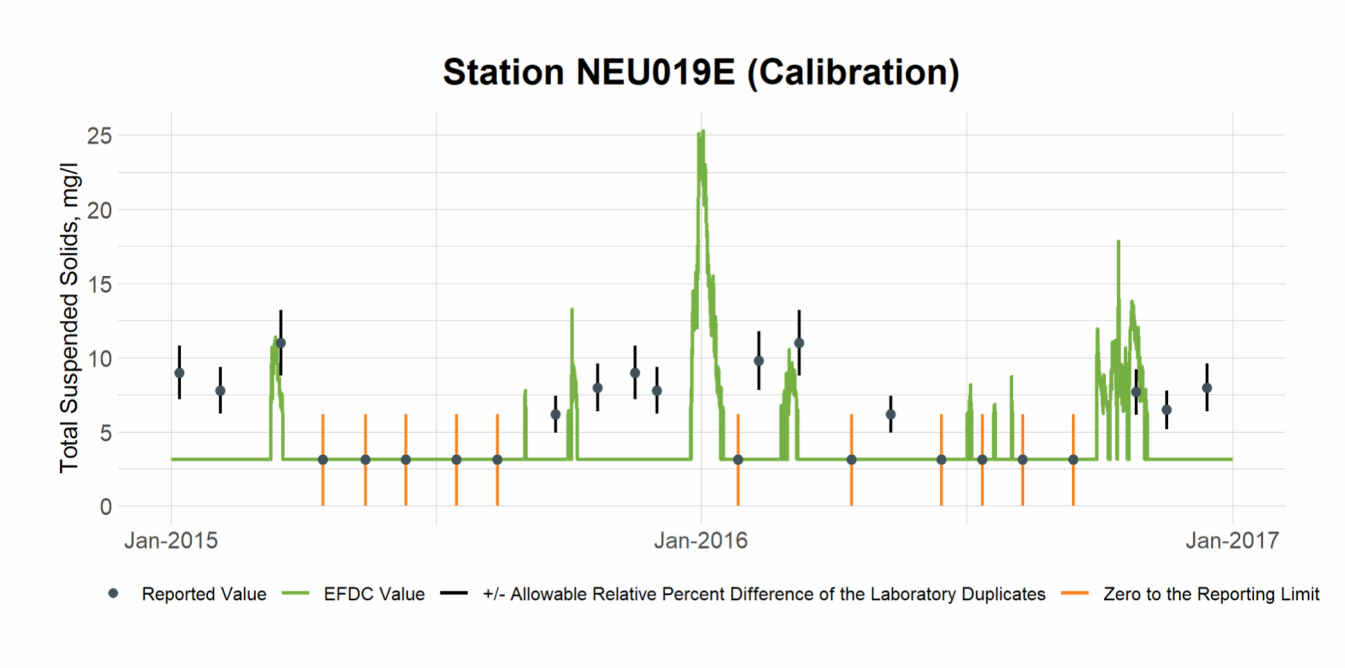

Figure 12-9 Calibration Plot of TSS at Station NEU019E

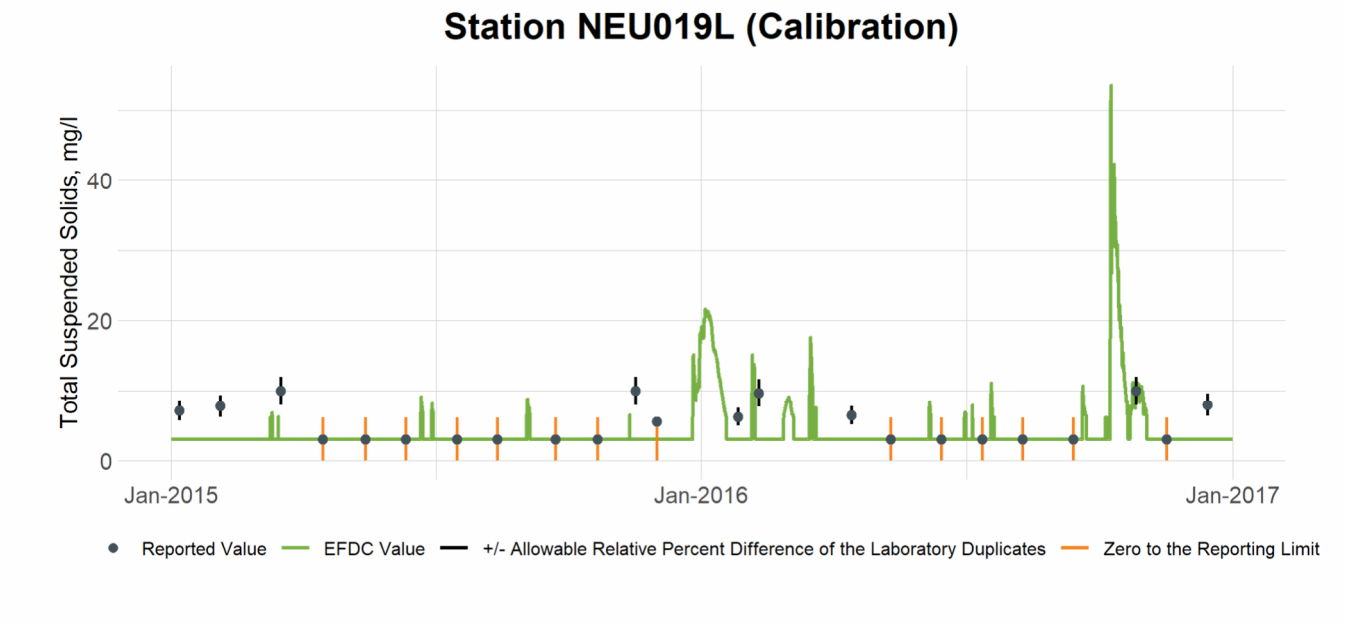

Figure 12-10 Calibration Plot of TSS at Station NEU019L

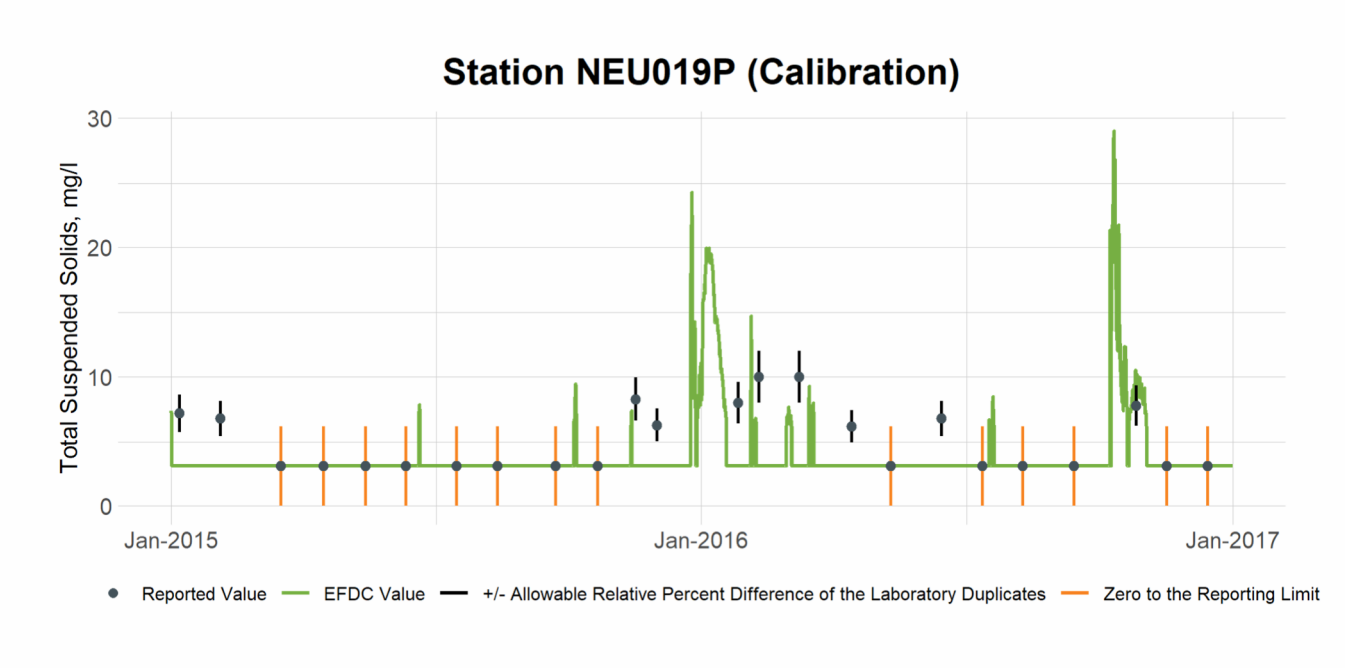

Figure 12-11 Calibration Plot of TSS at Station NEU019P

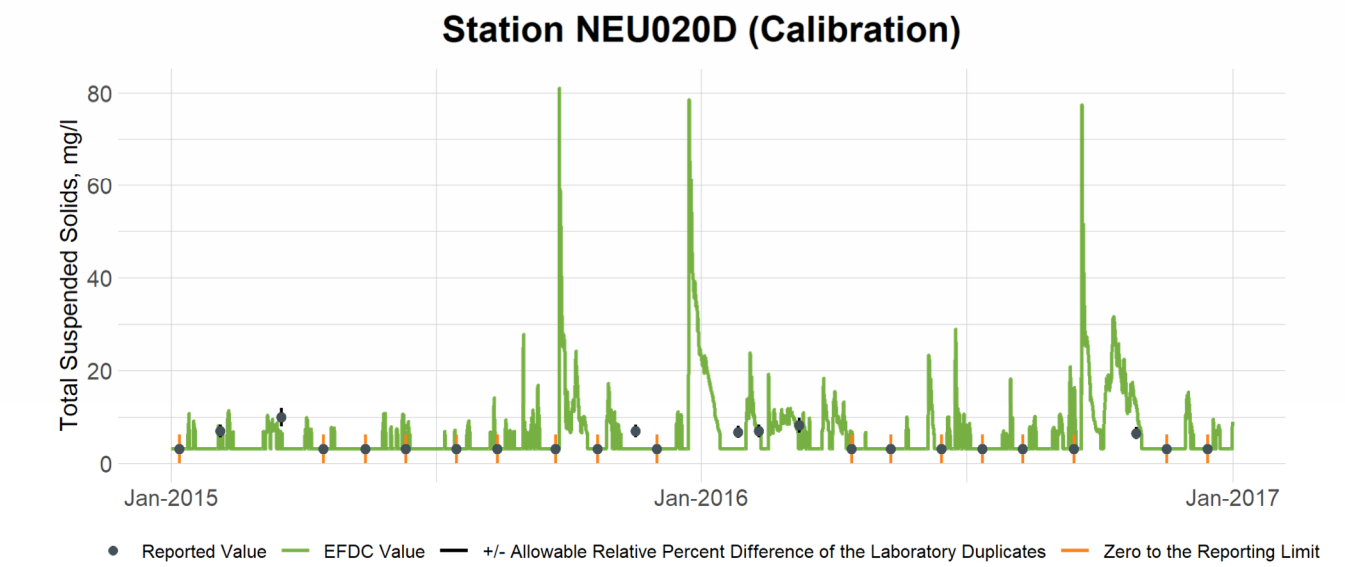

Figure 12-12 Calibration Plot of TSS at Station NEU020D

12.2 TSS Validation

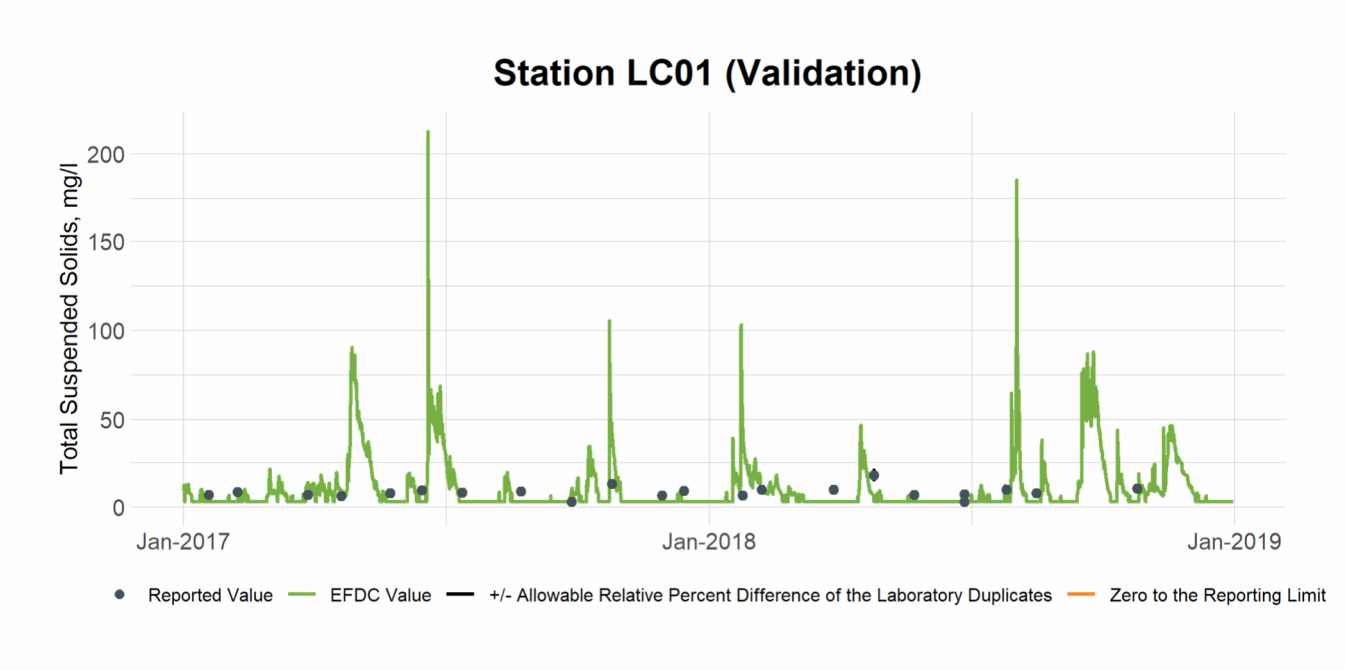

Figure 12-13 Validation Plot of TSS at Station LC01

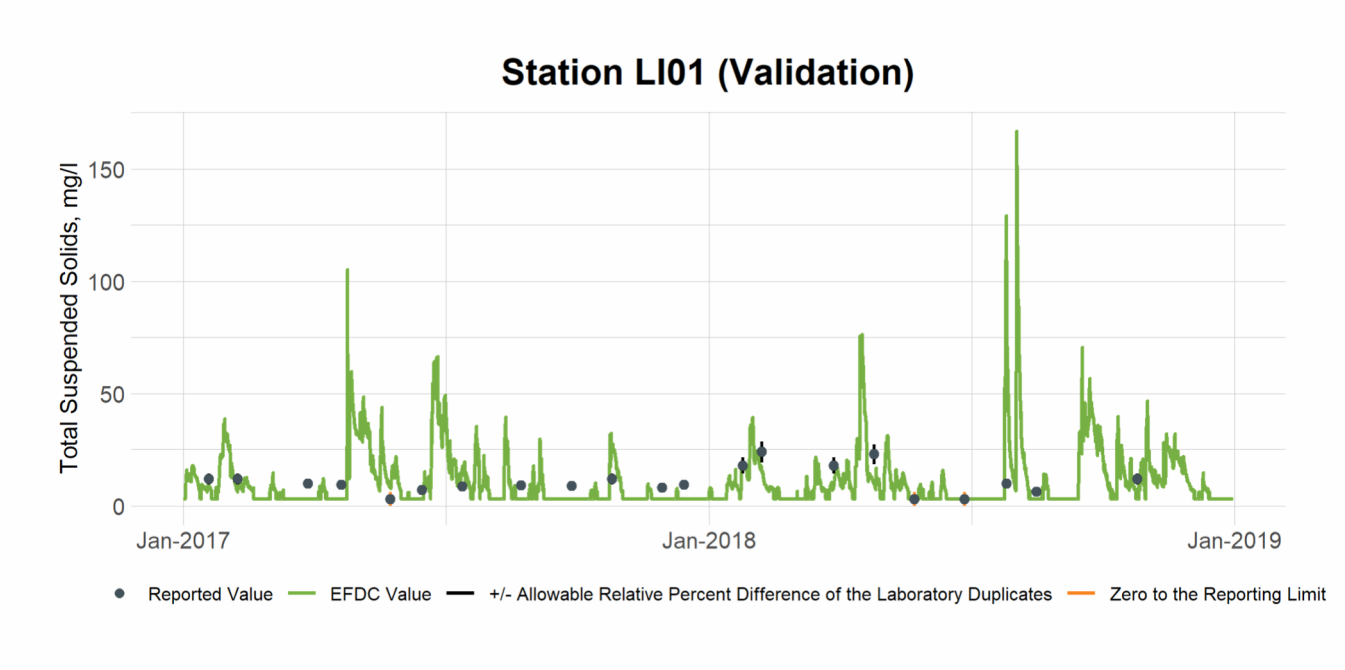

Figure 12-14 Validation Plot of TSS at Station LI01

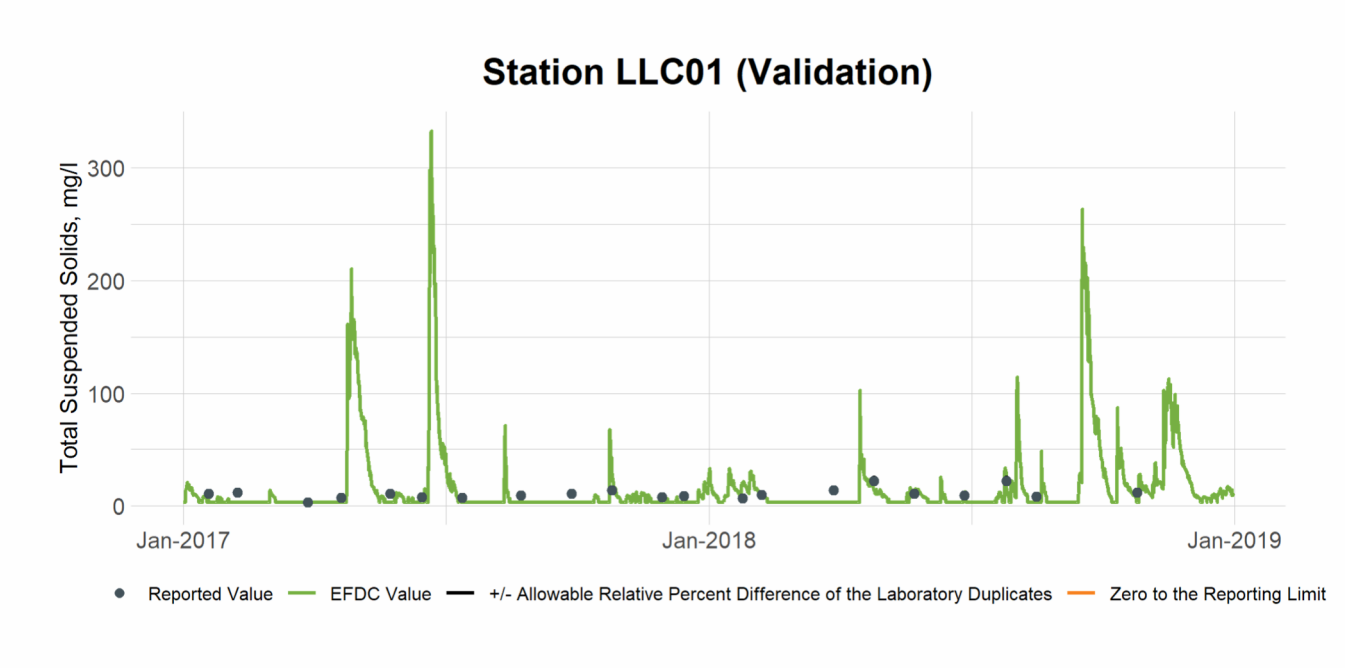

Figure 12-15 Validation Plot of TSS at Station LLC01

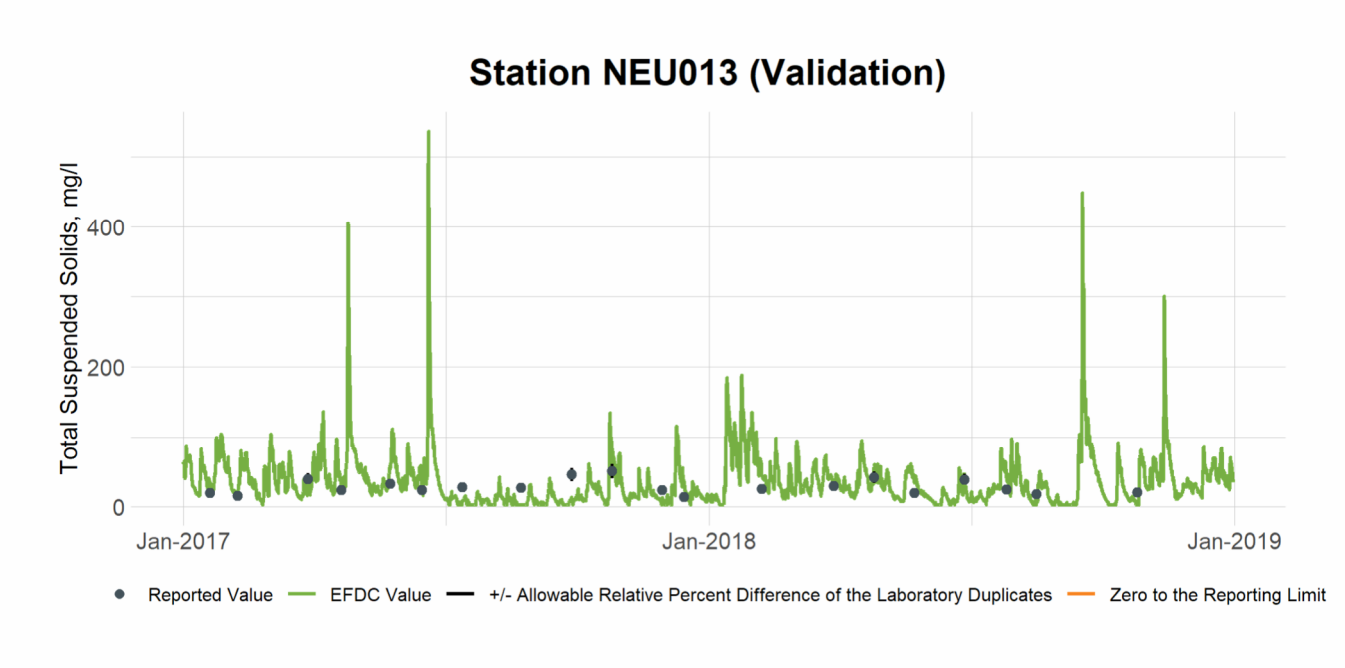

Figure 12-16 Validation Plot of TSS at Station NEU013

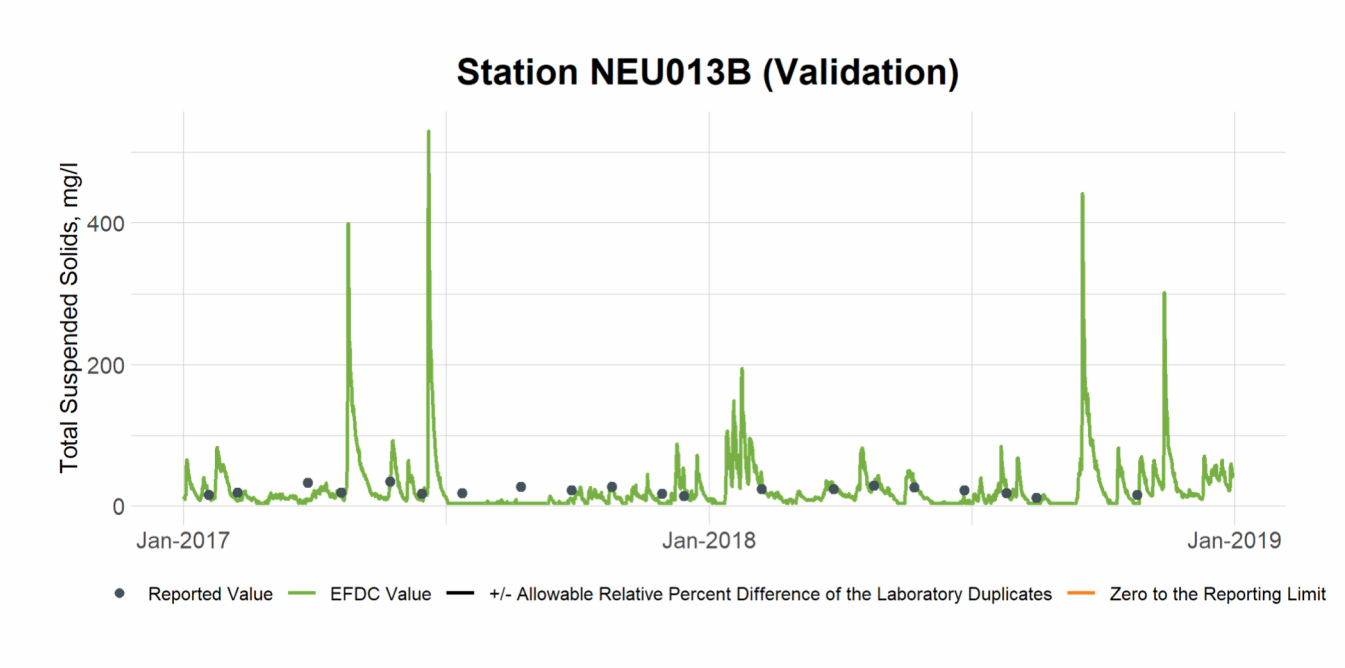

Figure 12-17 Validation Plot of TSS at Station NEU013B

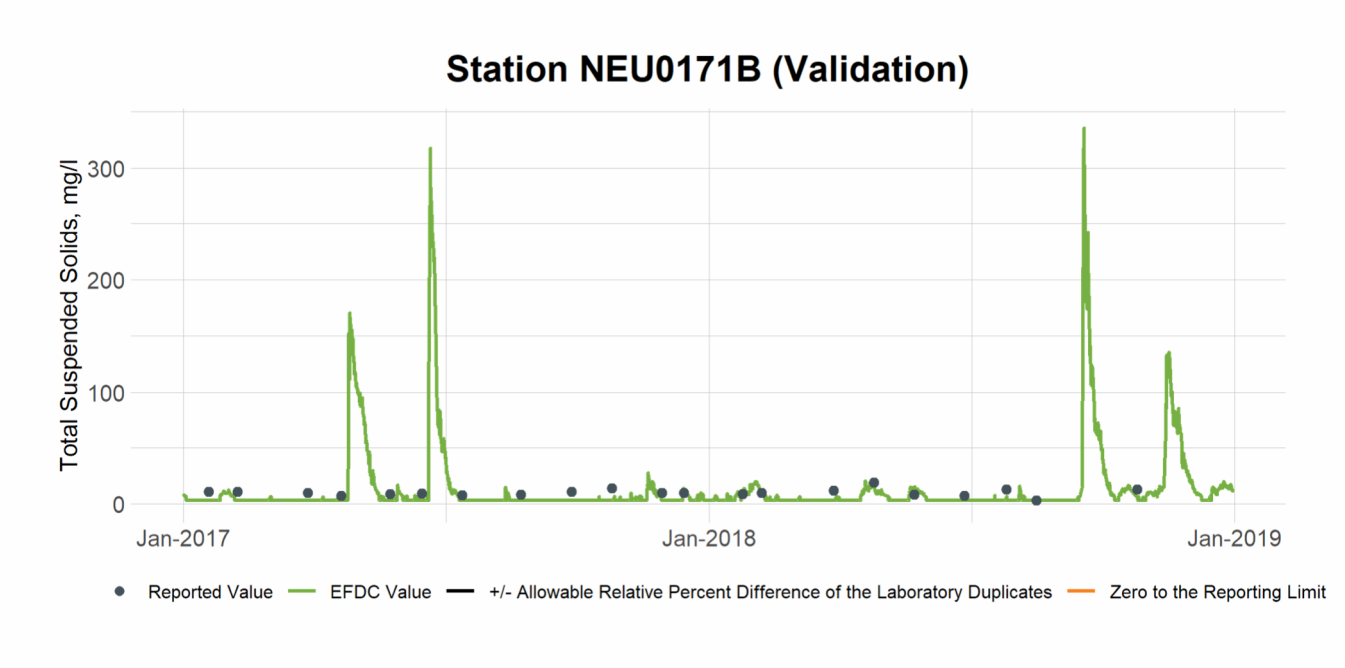

Figure 12-18 Validation Plot of TSS at Station NEU0171B

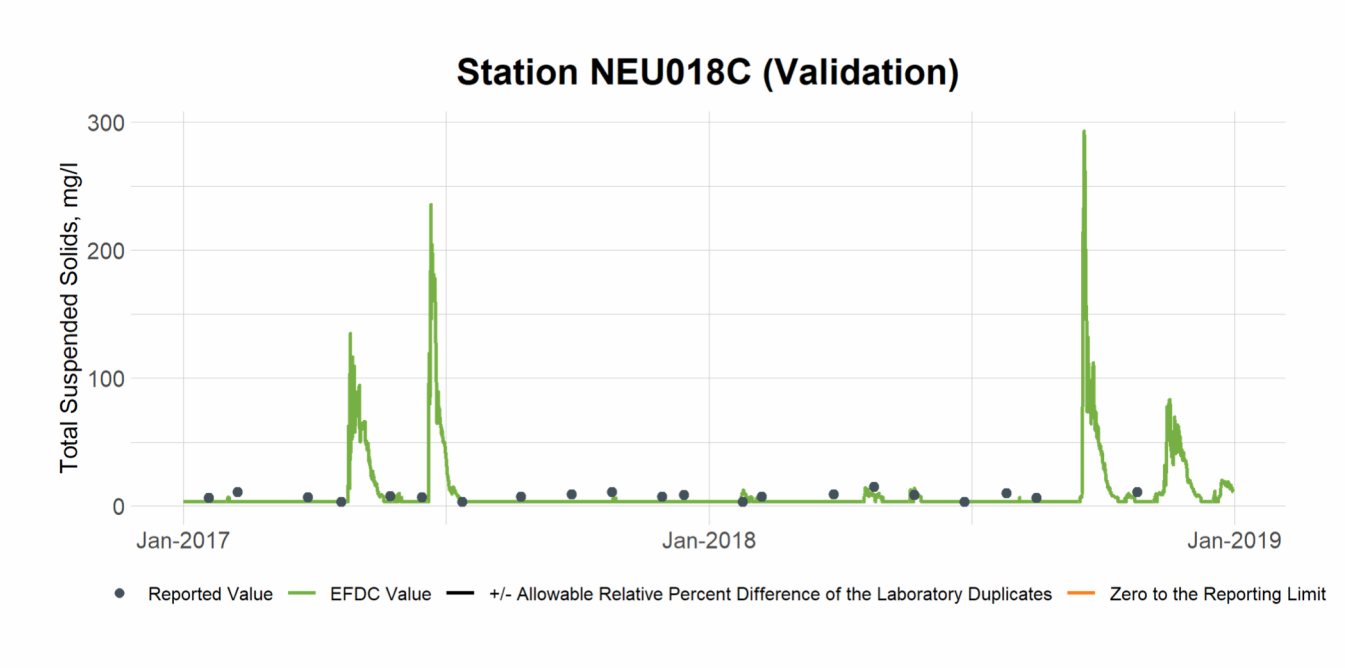

Figure 12-19 Validation Plot of TSS at Station NEU018C

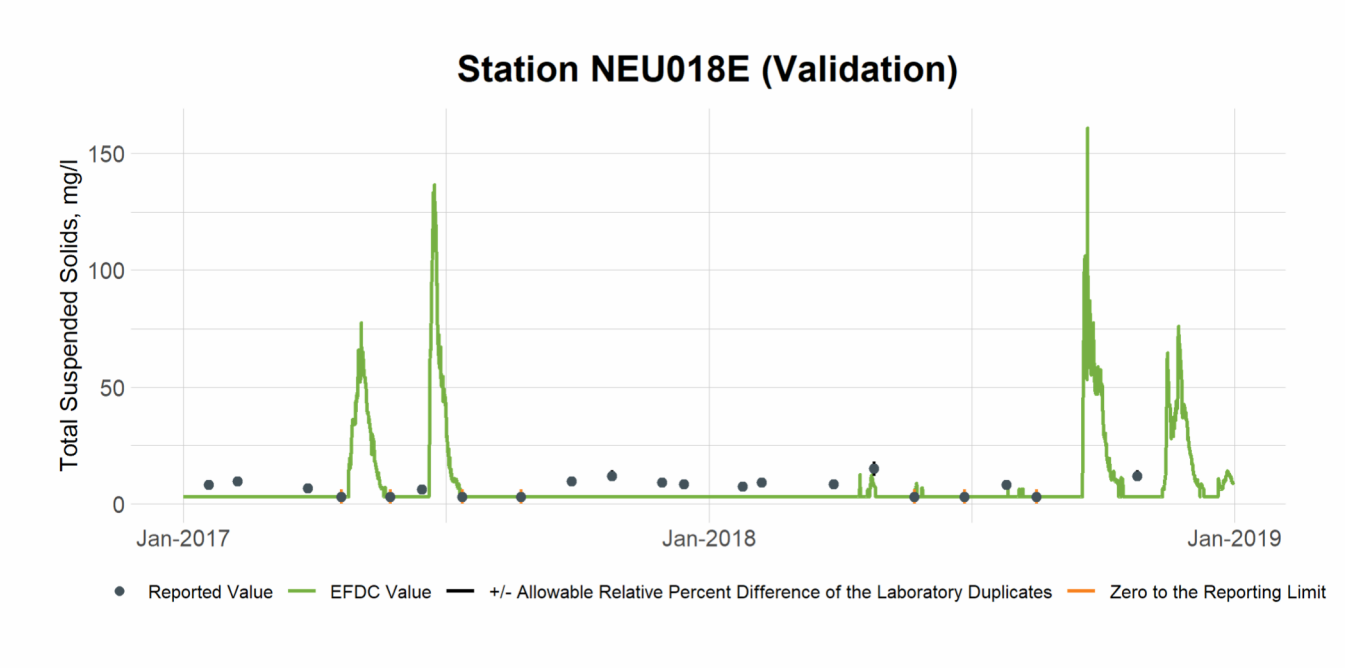

Figure 12-20 Validation Plot of TSS at Station NEU018E

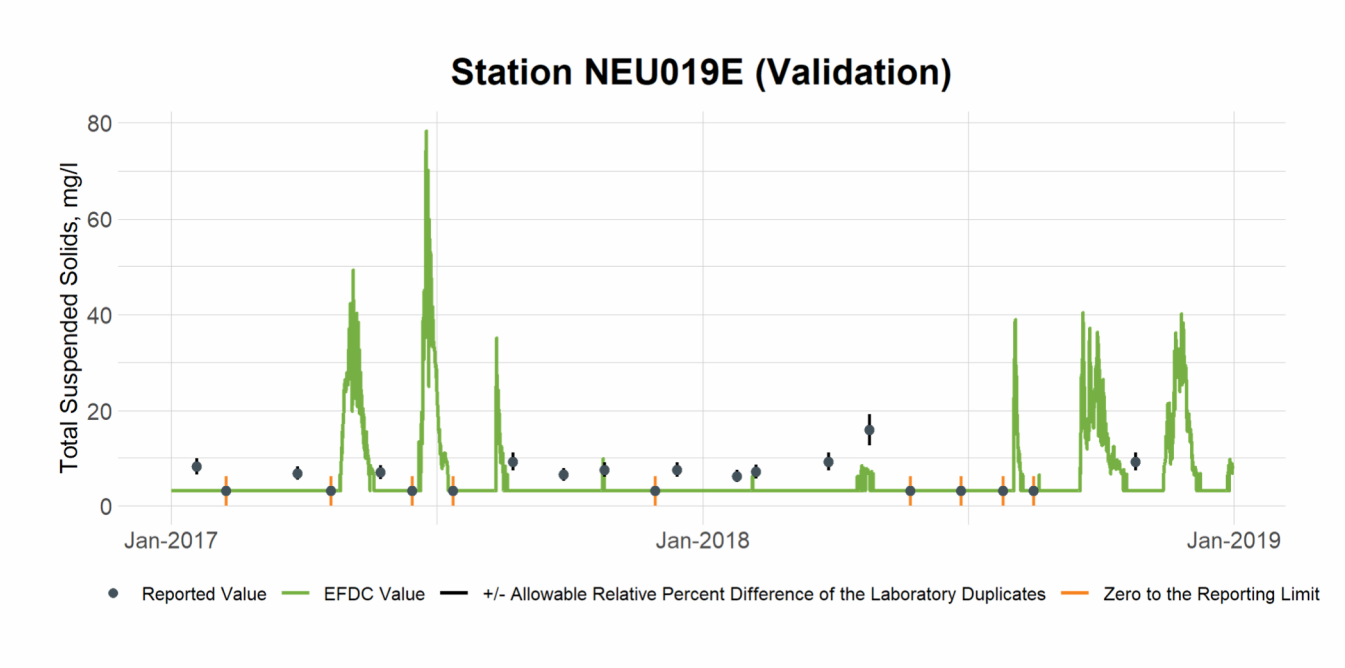

Figure 12-21 Validation Plot of TSS at Station NEU019E

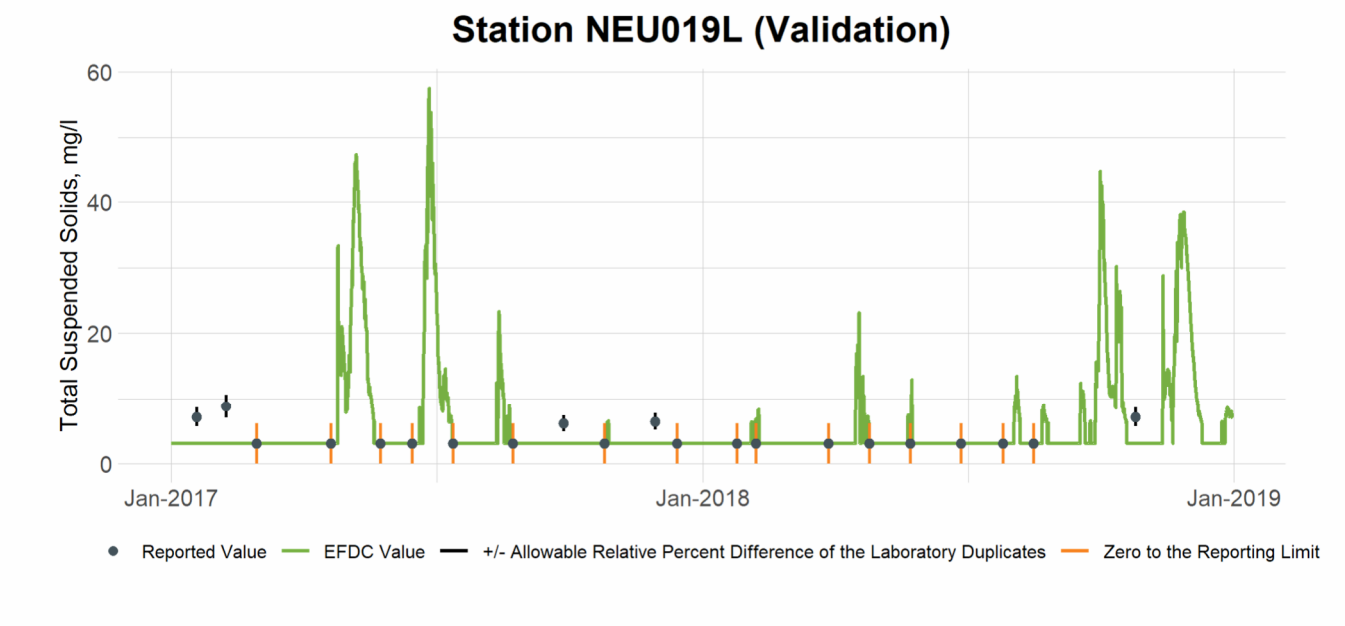

Figure 12-22 Validation Plot of TSS at Station NEU019L

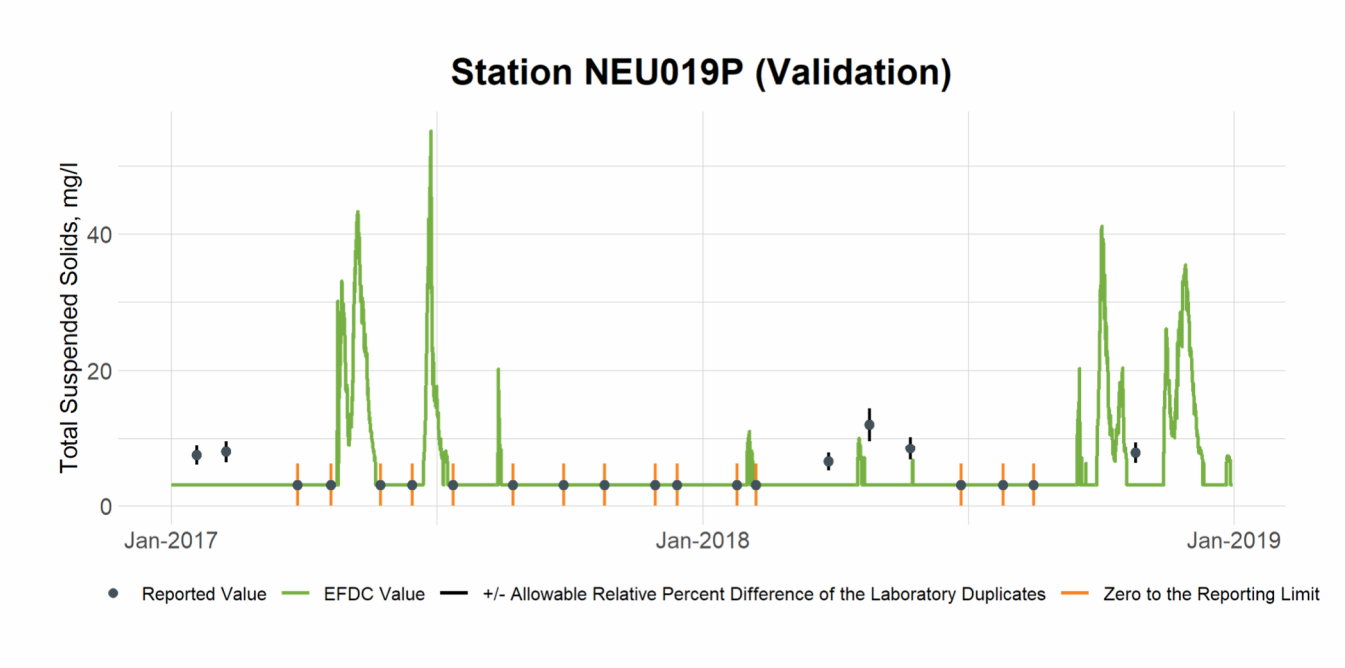

Figure 12-23 Validation Plot of TSS at Station NEU019P

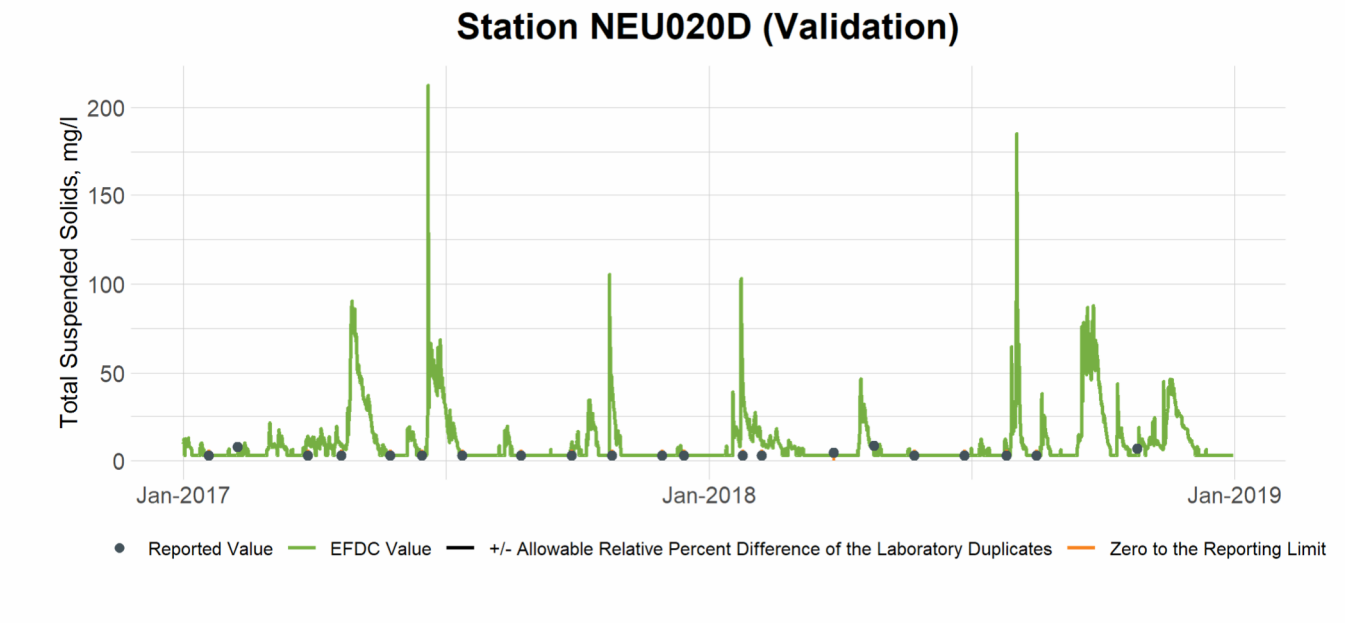

Figure 12-24 Validation Plot of TSS at Station NEU020D

13. Secchi Depth

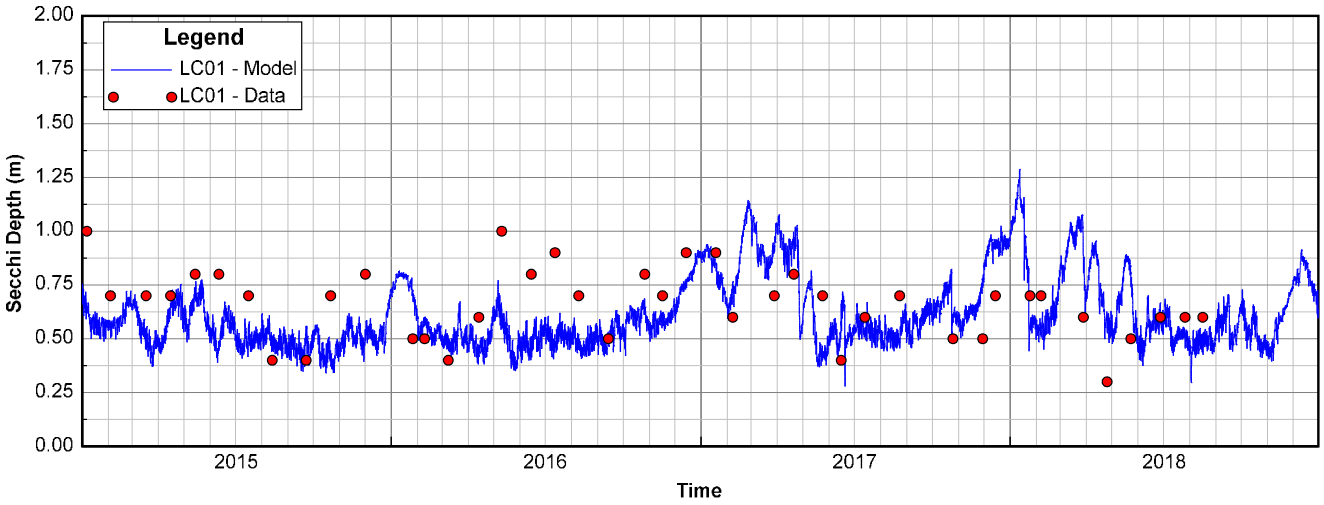

Figure 13-1 Plot of Secchi Depth at Station LC01

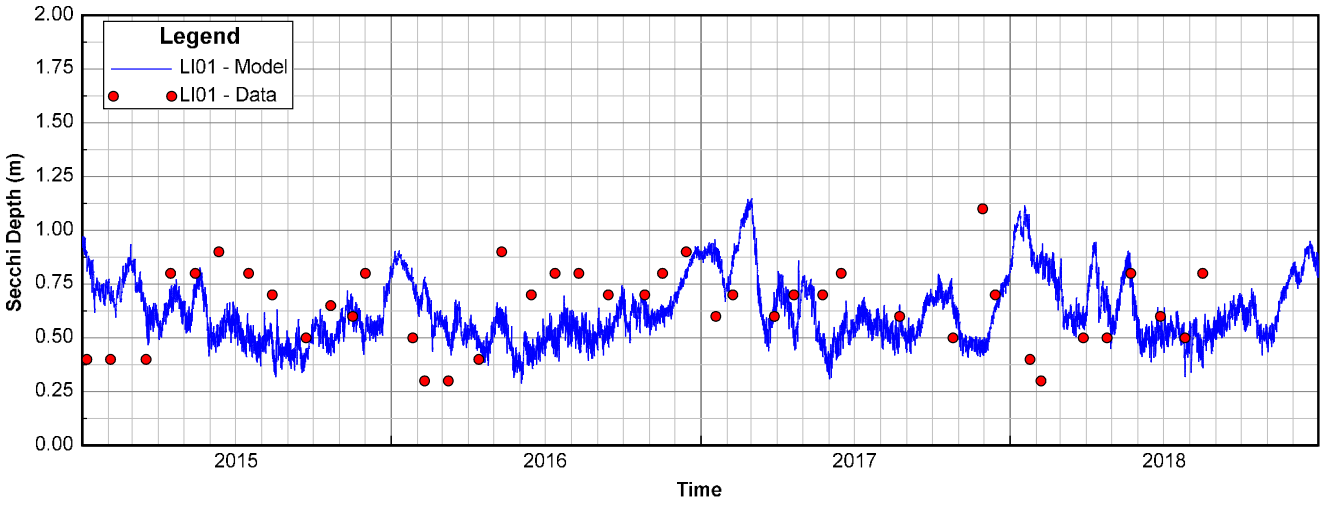

Figure 13-2 Plot of Secchi Depth at Station LI01

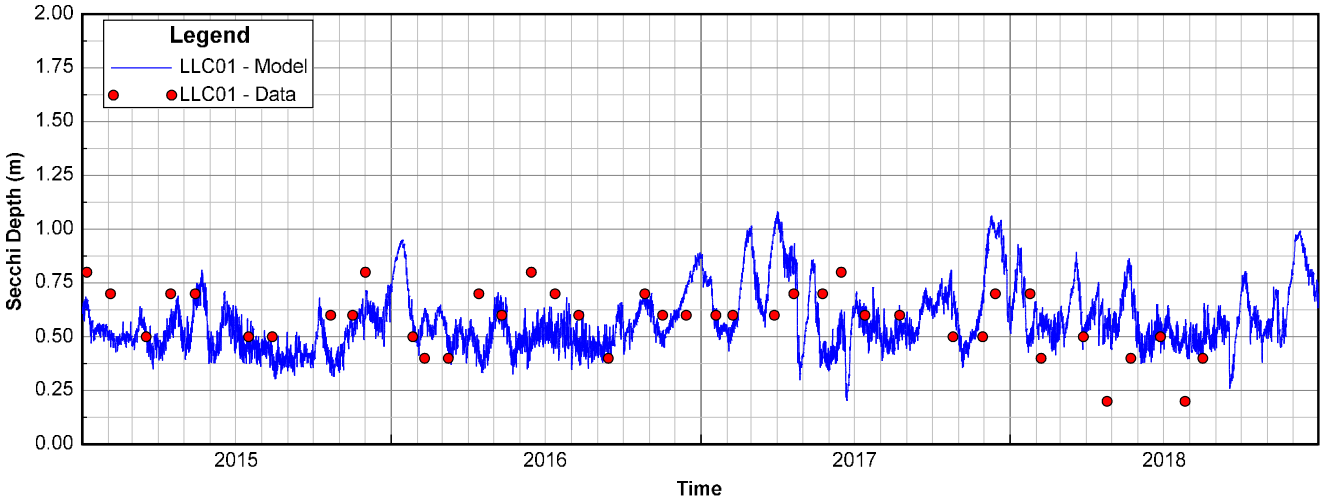

Figure 13-3 Plot of Secchi Depth at Station LLC01

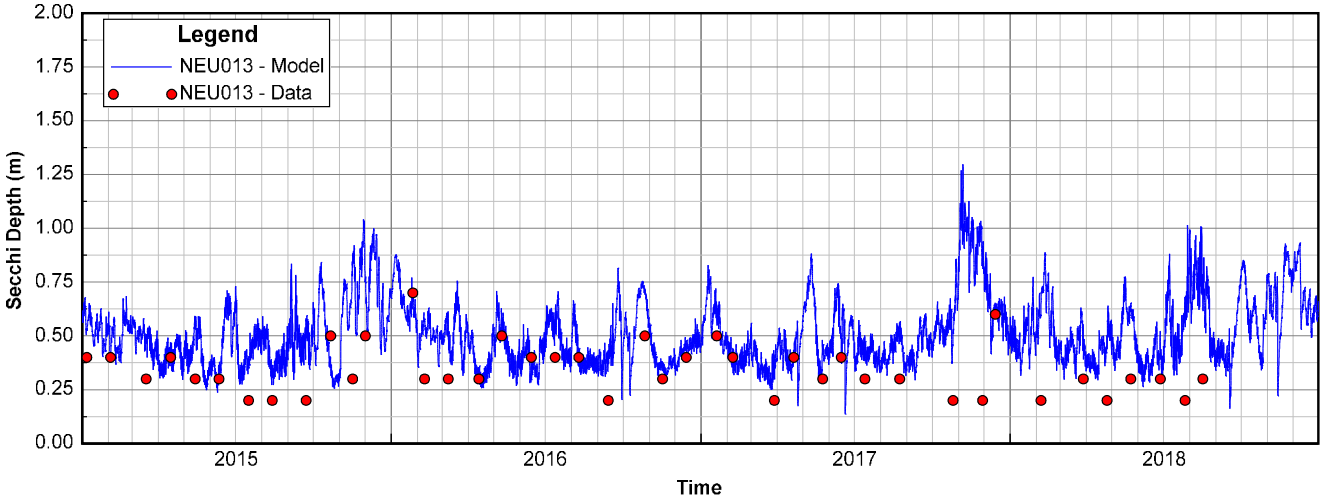

Figure 13-4 Plot of Secchi Depth at Station NEU013

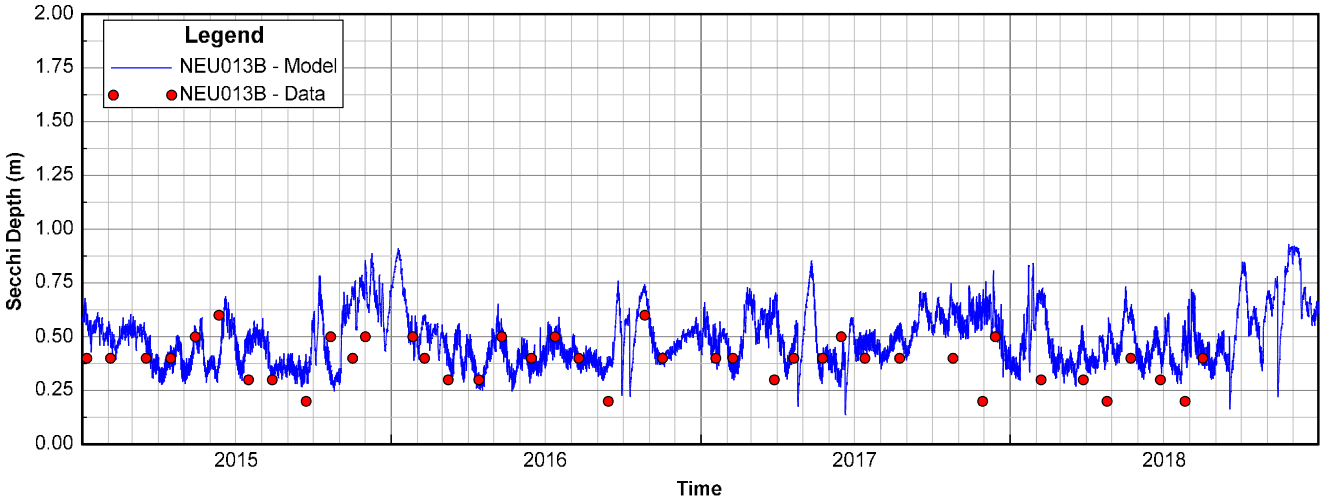

Figure 13-5 Plot of Secchi Depth at Station NEU013B

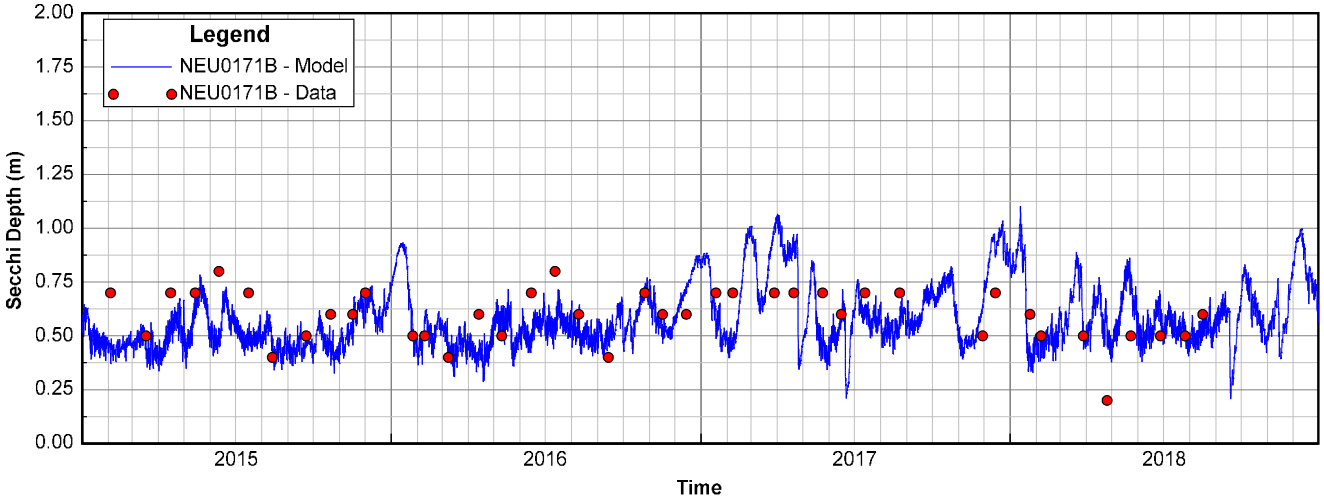

Figure 13-6 Plot of Secchi Depth at Station NEU01171B

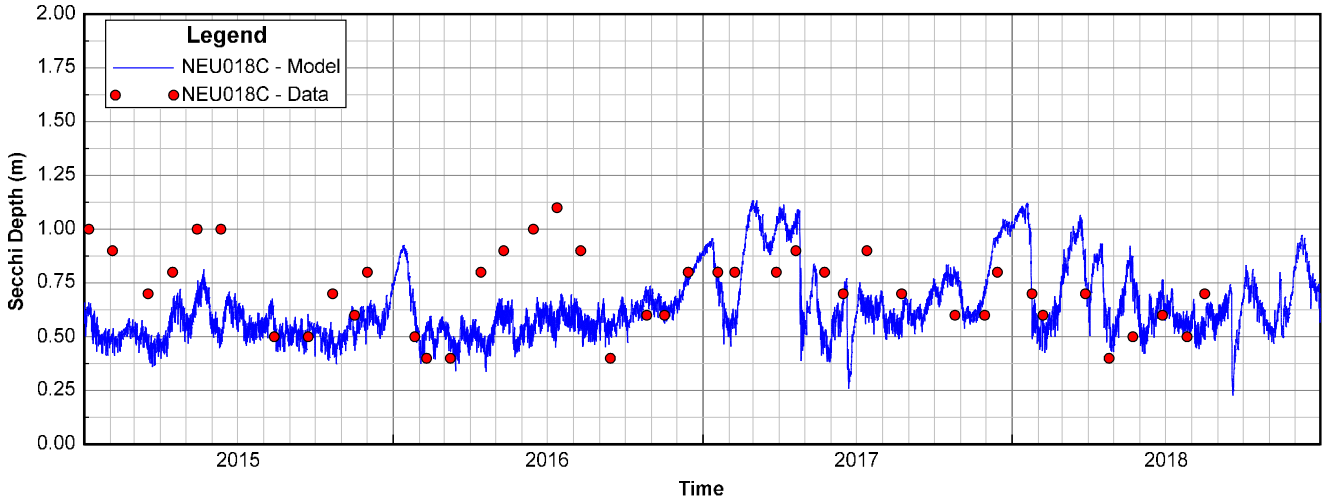

Figure 13-7 Plot of Secchi Depth at Station NEU018C

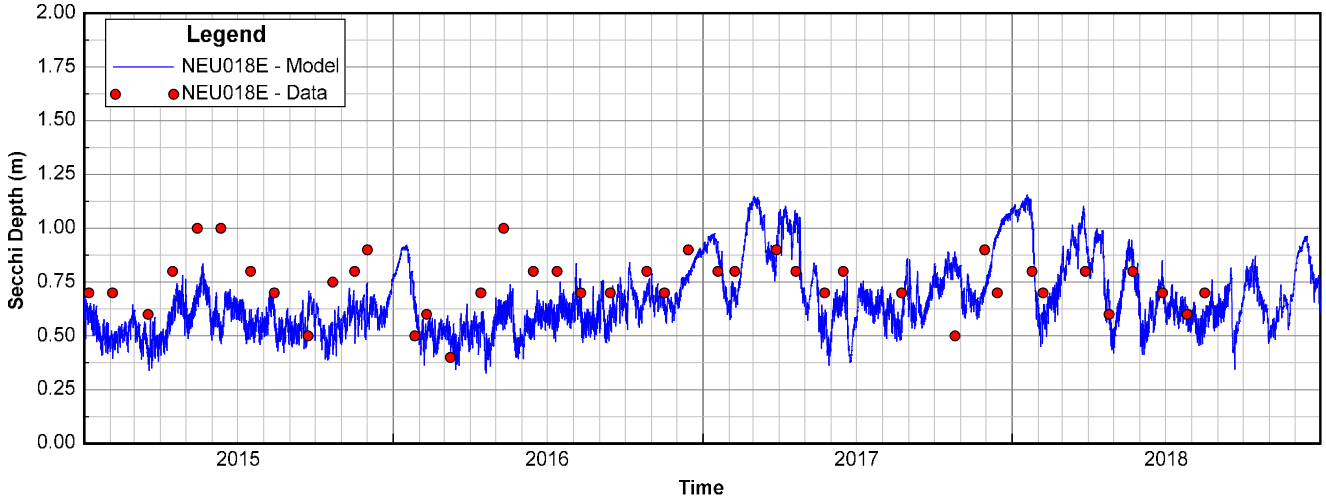

Figure 13-8 Plot of Secchi Depth at Station NEU018E

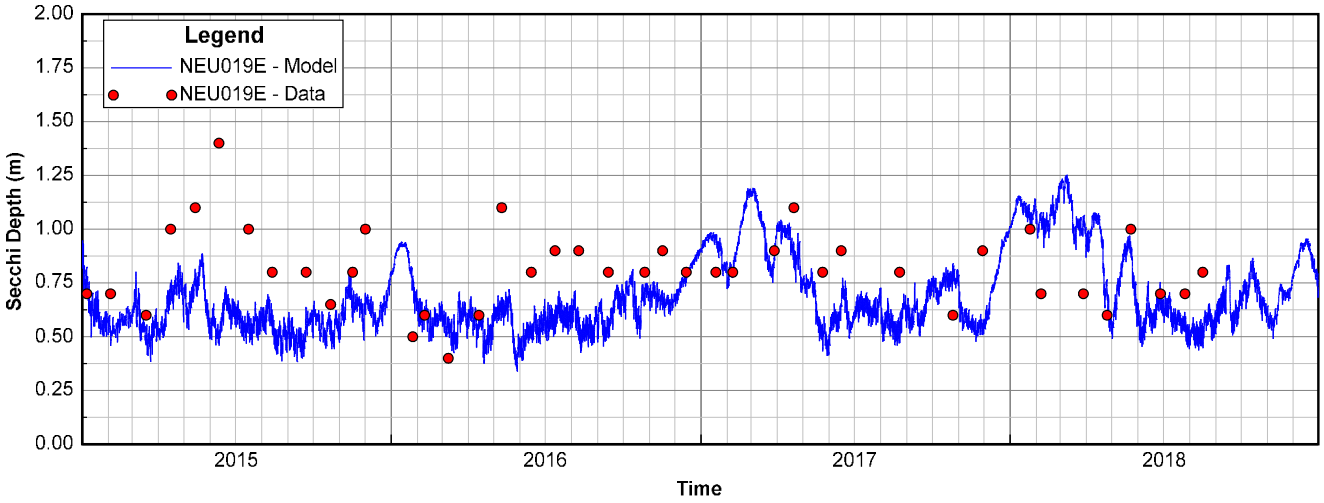

Figure 13-9 Plot of Secchi Depth at Station NEU019E

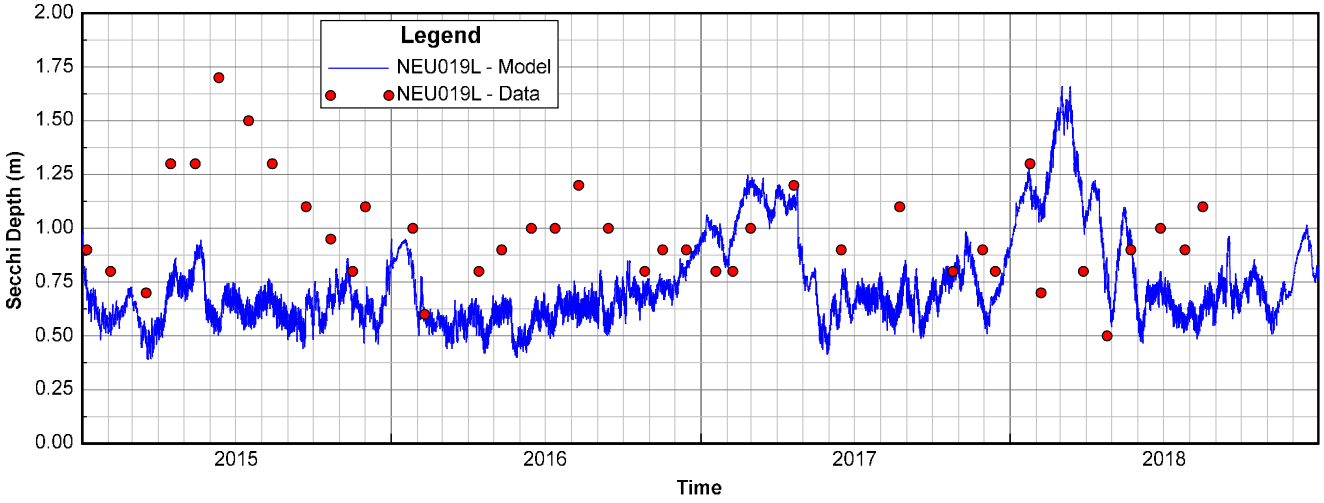

Figure 13-10 Plot of Secchi Depth at Station NEU019L

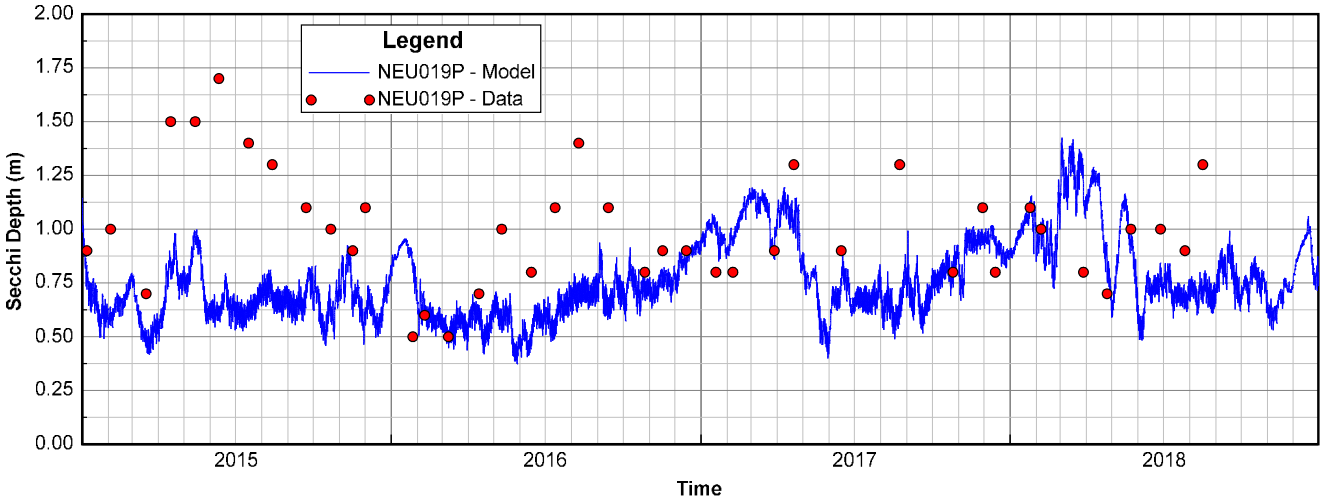

Figure 13-11 Plot of Secchi Depth at Station NEU019P

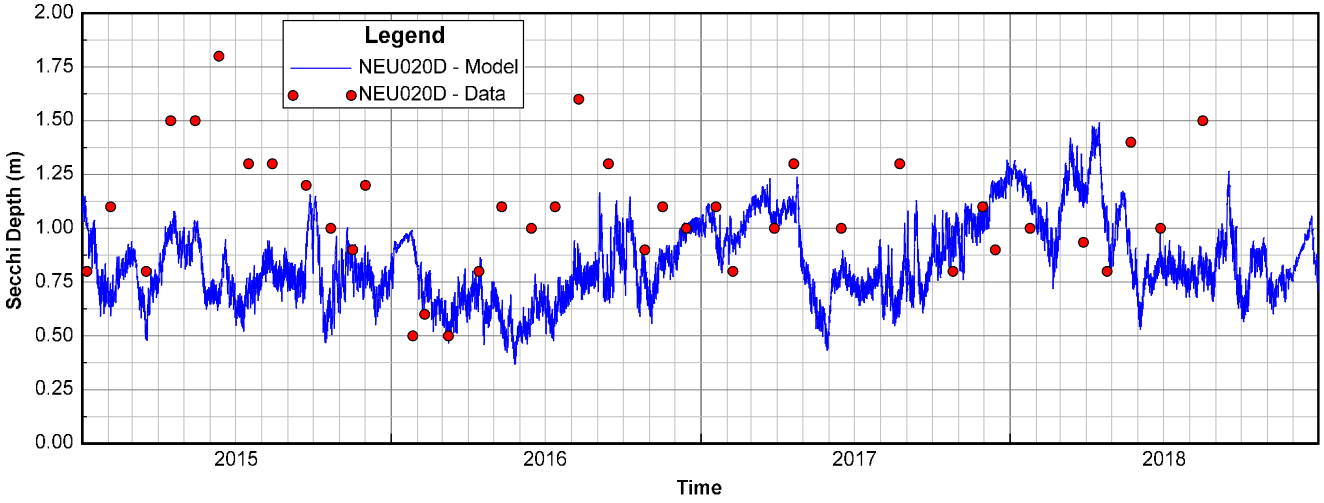

Figure 13-12 Plot of Secchi Depth at Station NEU020D

14. Scatter Plots

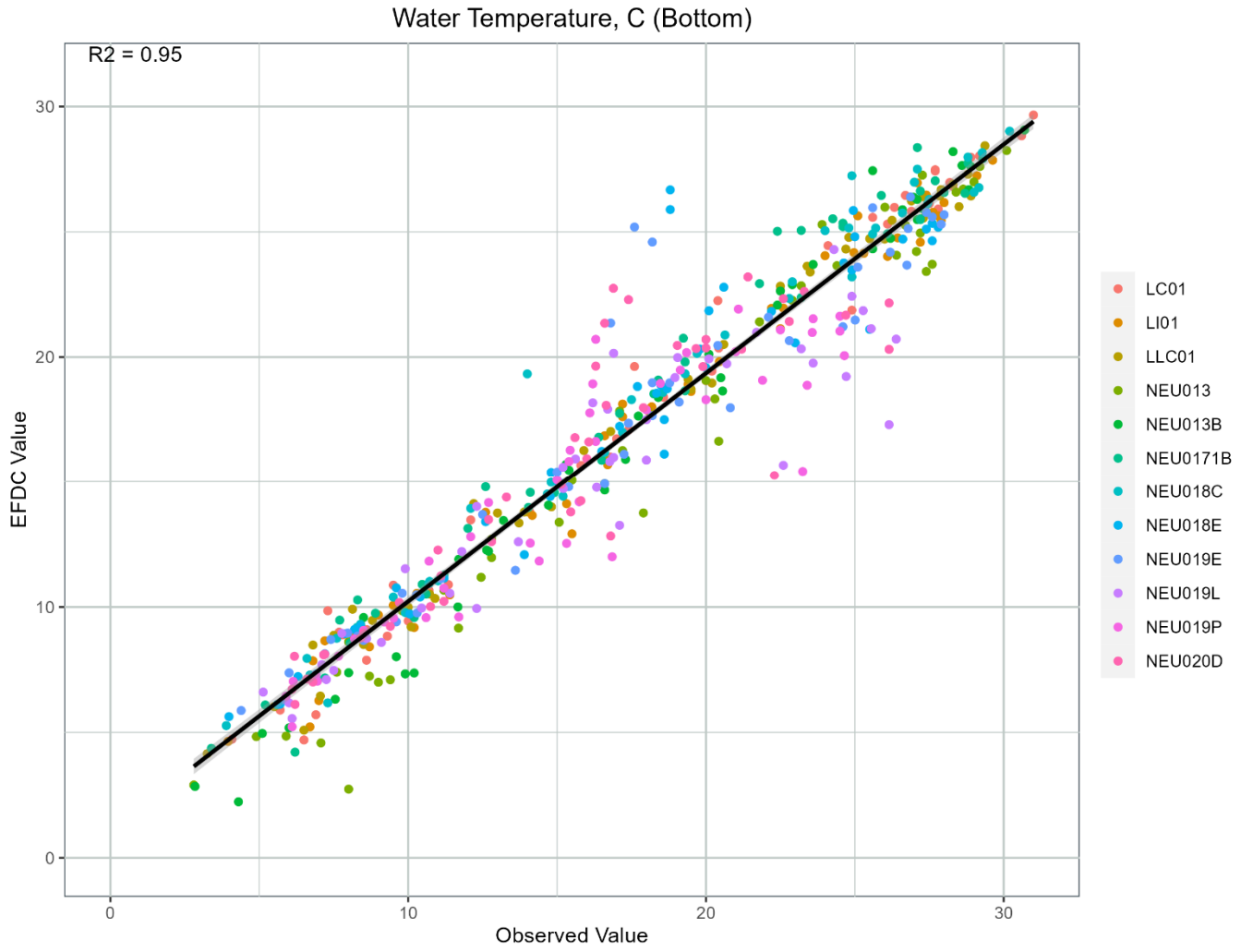

Figure 14-1. Scatter plot of observed versus modeled bottom water temperatures.

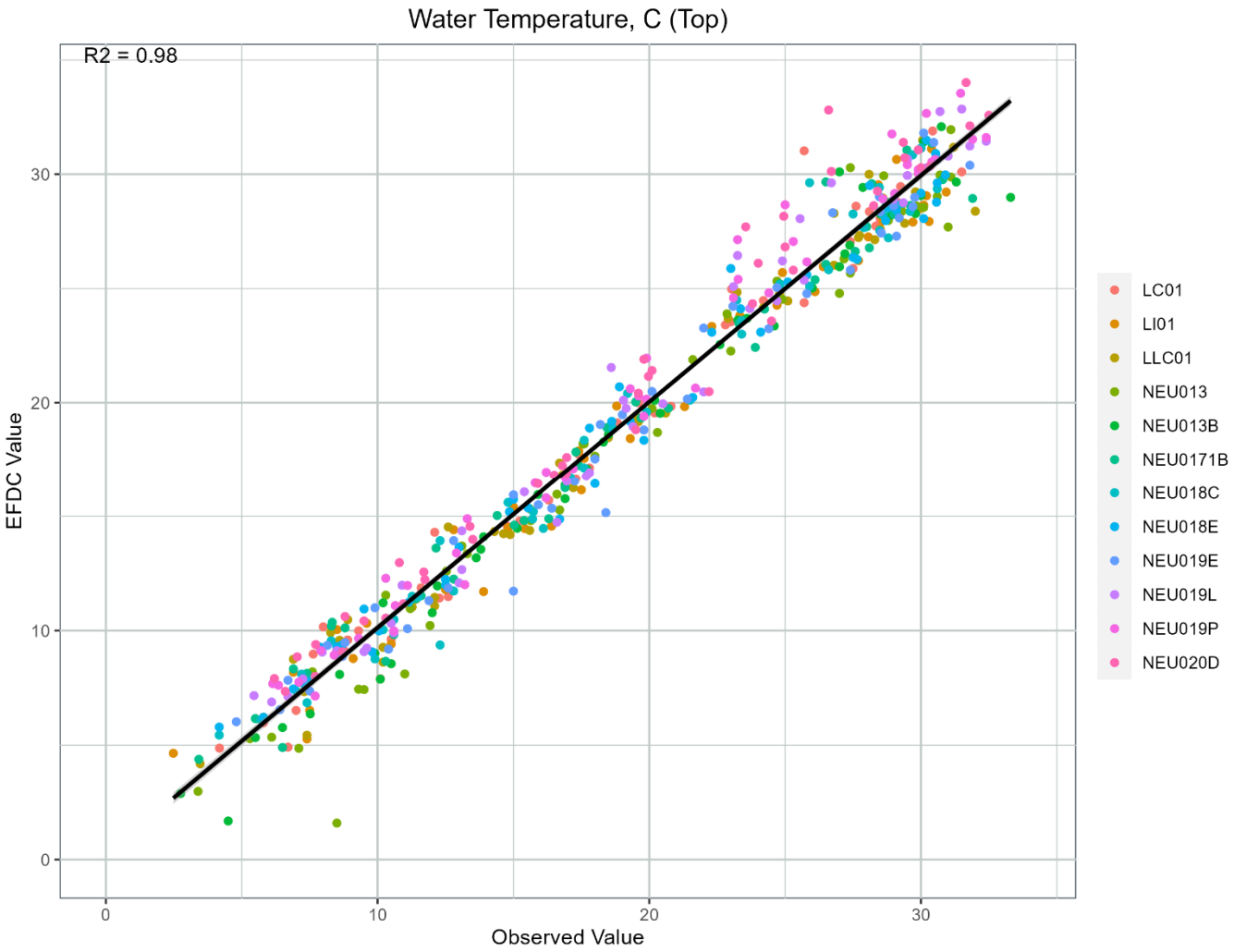

Figure 14-2. Scatter plot of observed versus modeled surface water temperatures.

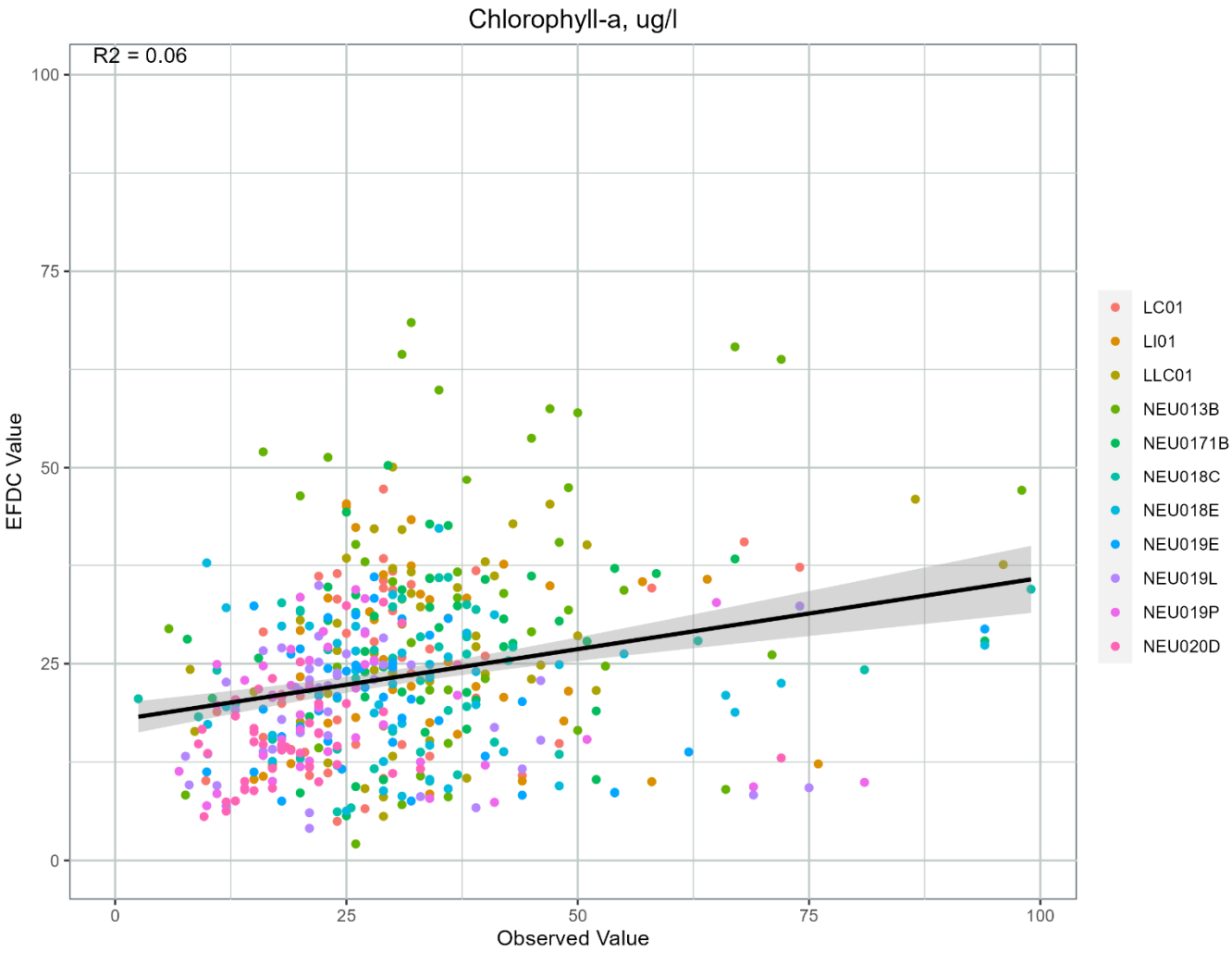

Figure 14-3. Scatter plot of observed versus modeled chlorophyll-a concentrations.

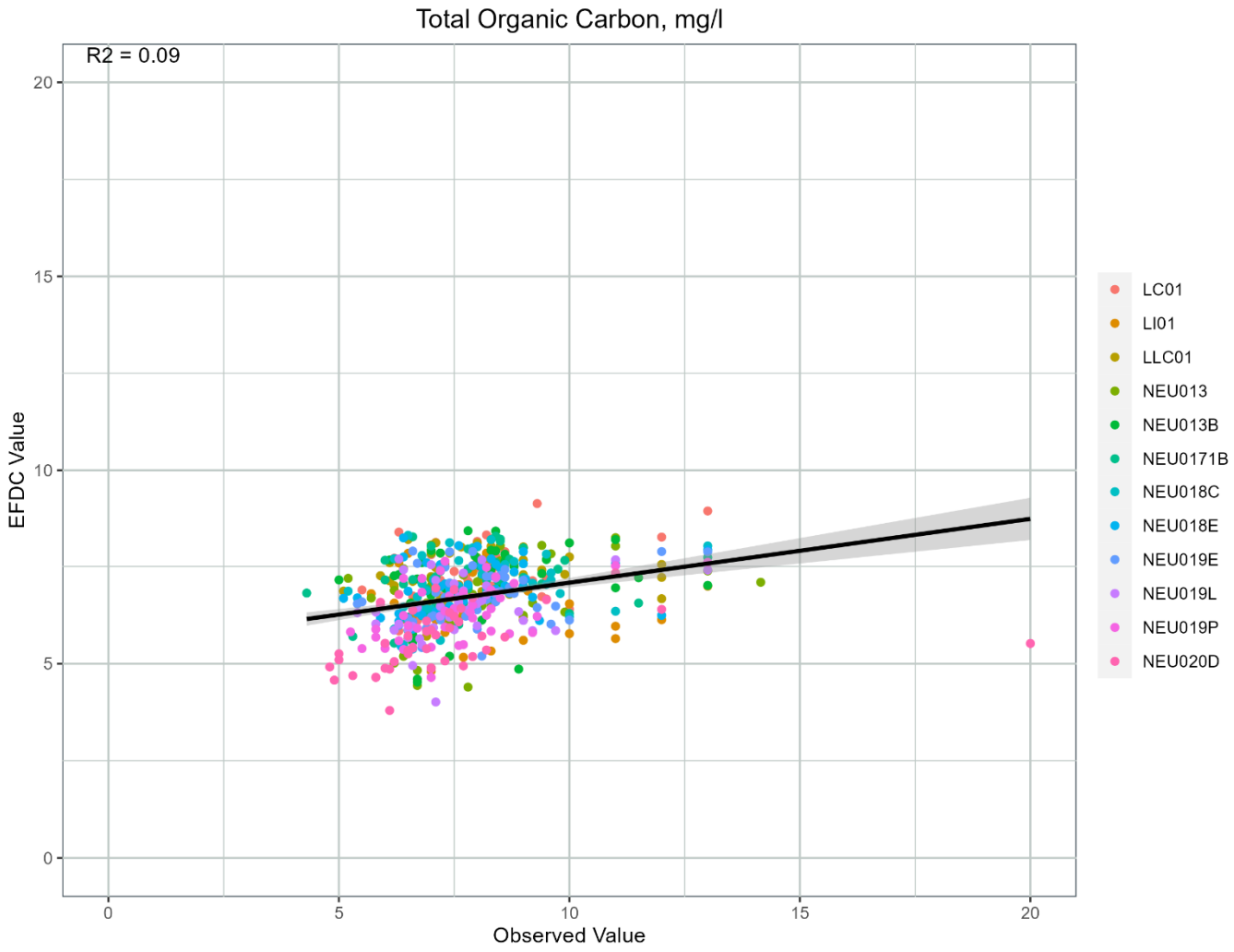

Figure 14-4. Scatter plot of observed versus modeled total organic carbon concentrations.

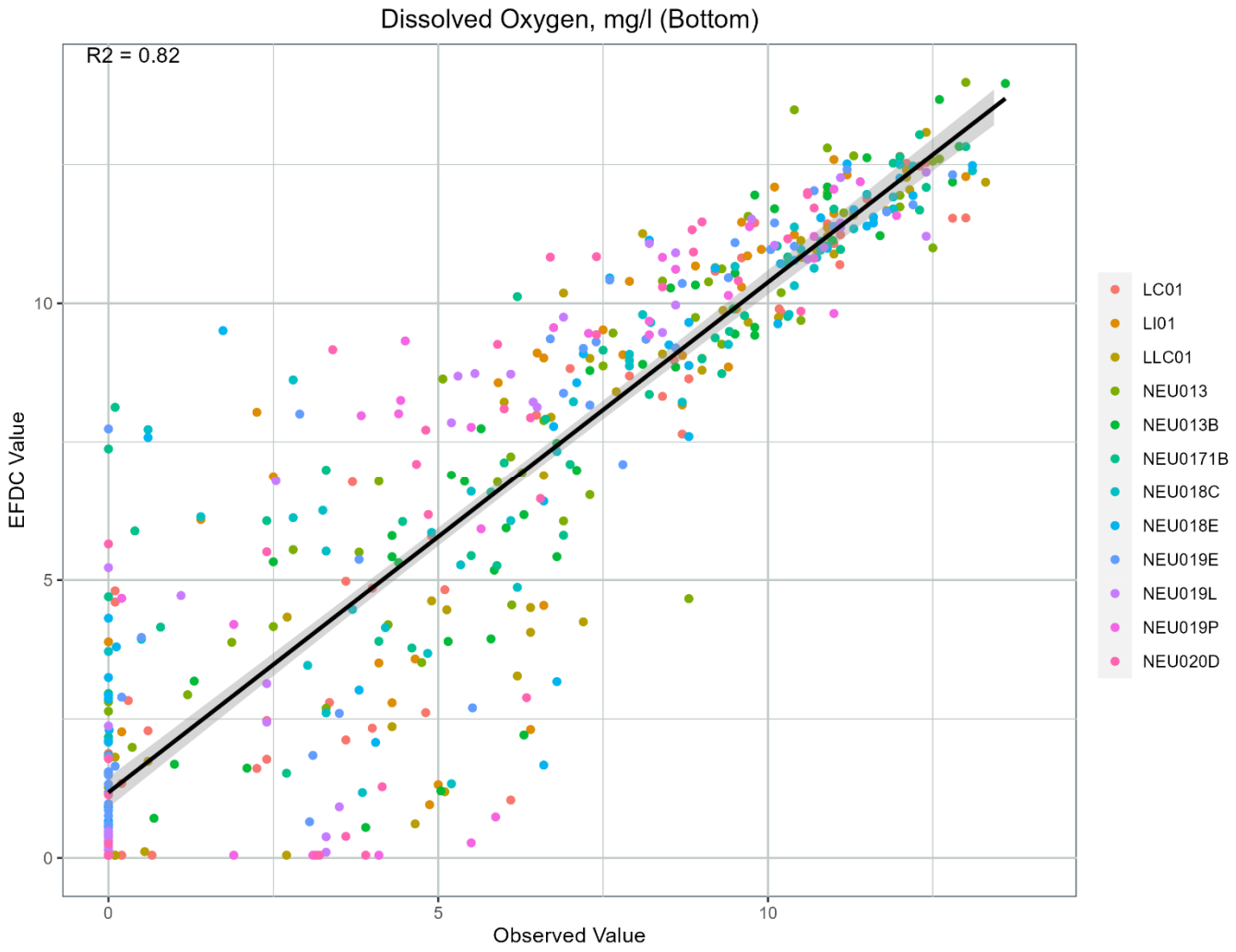

Figure 14-5. Scatter plot of observed versus modeled bottom water dissolved oxygen concentrations.

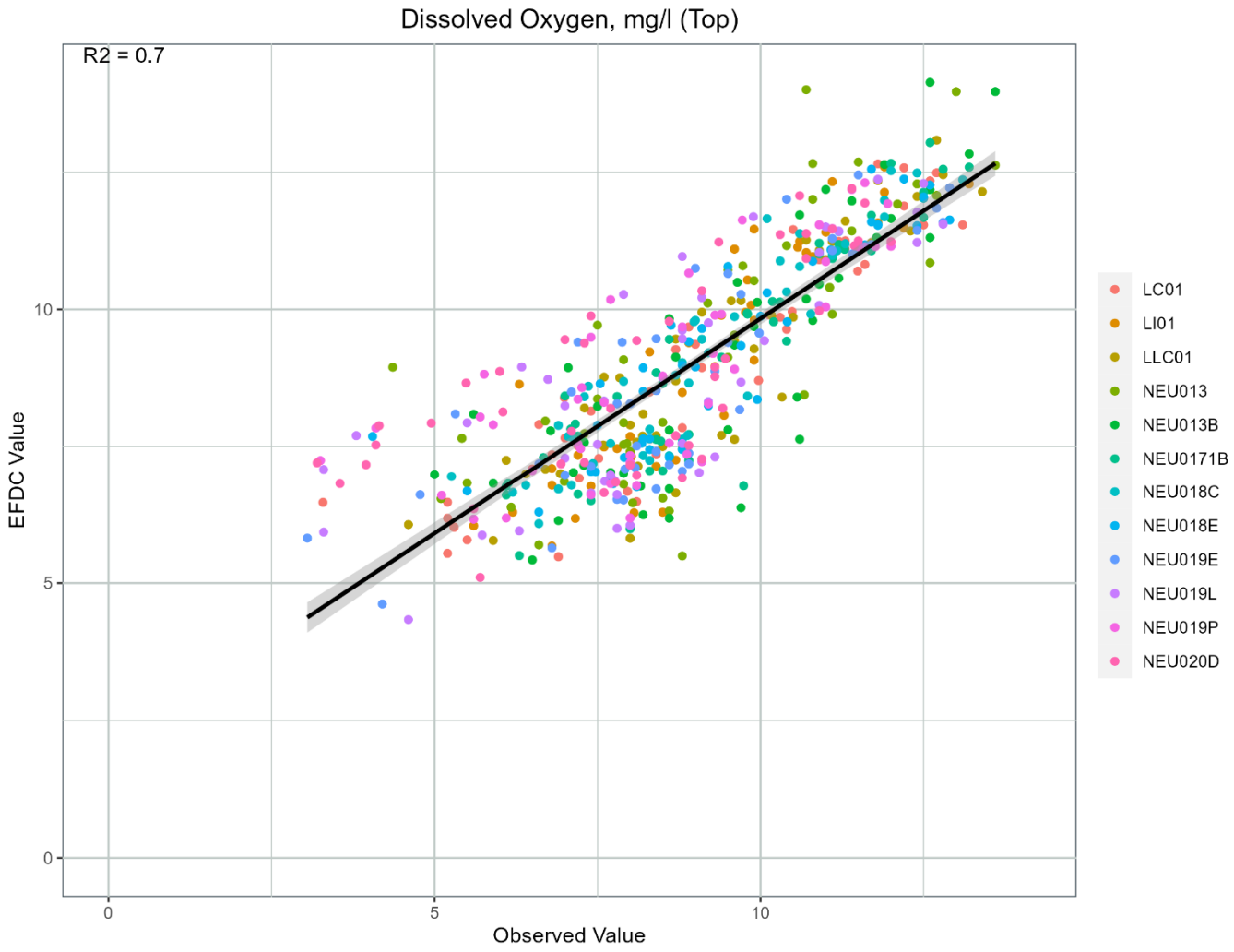

Figure 14-6. Scatter plot of observed versus modeled surface water dissolved oxygen concentrations.

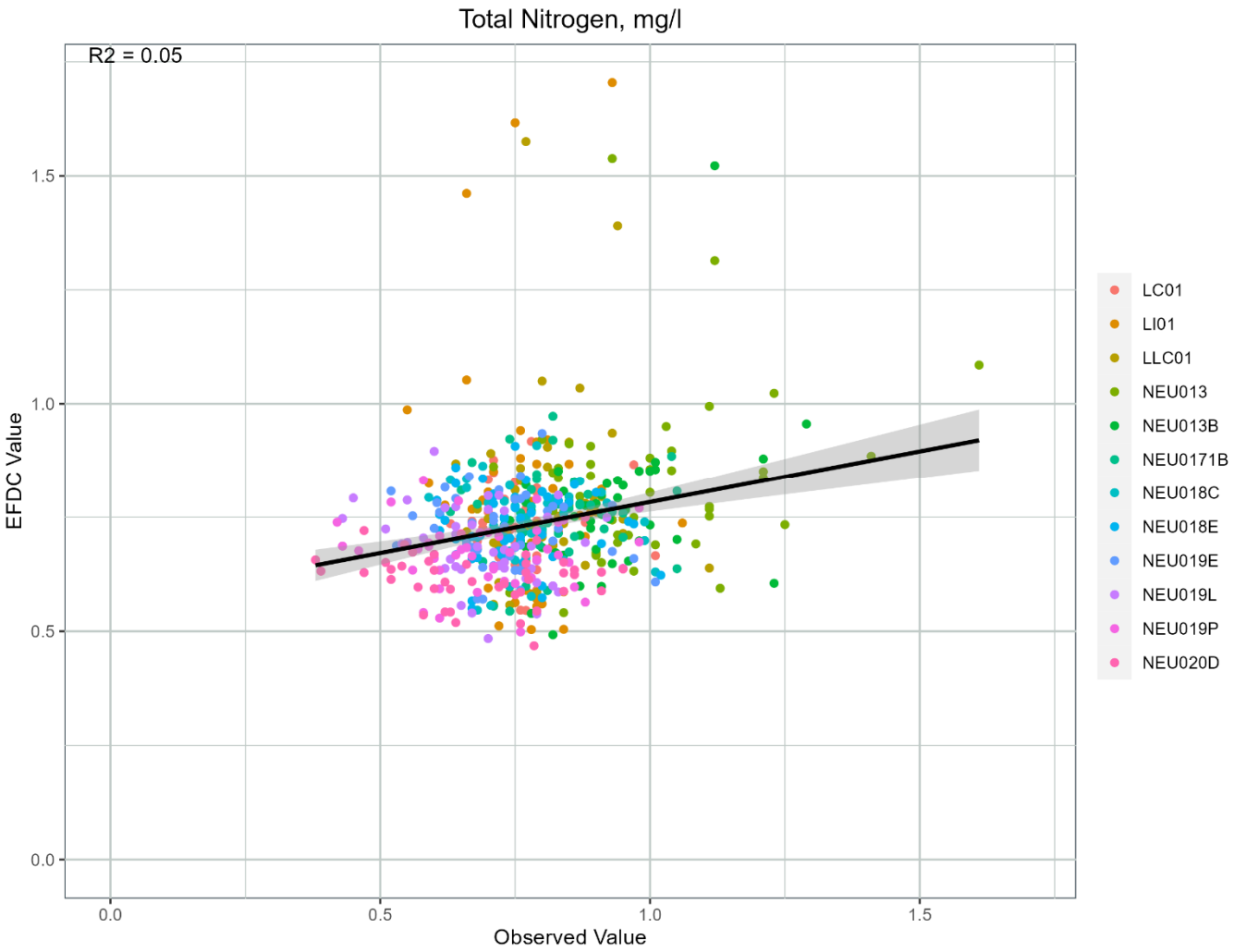

Figure 14-7. Scatter plot of observed versus modeled total nitrogen concentrations.

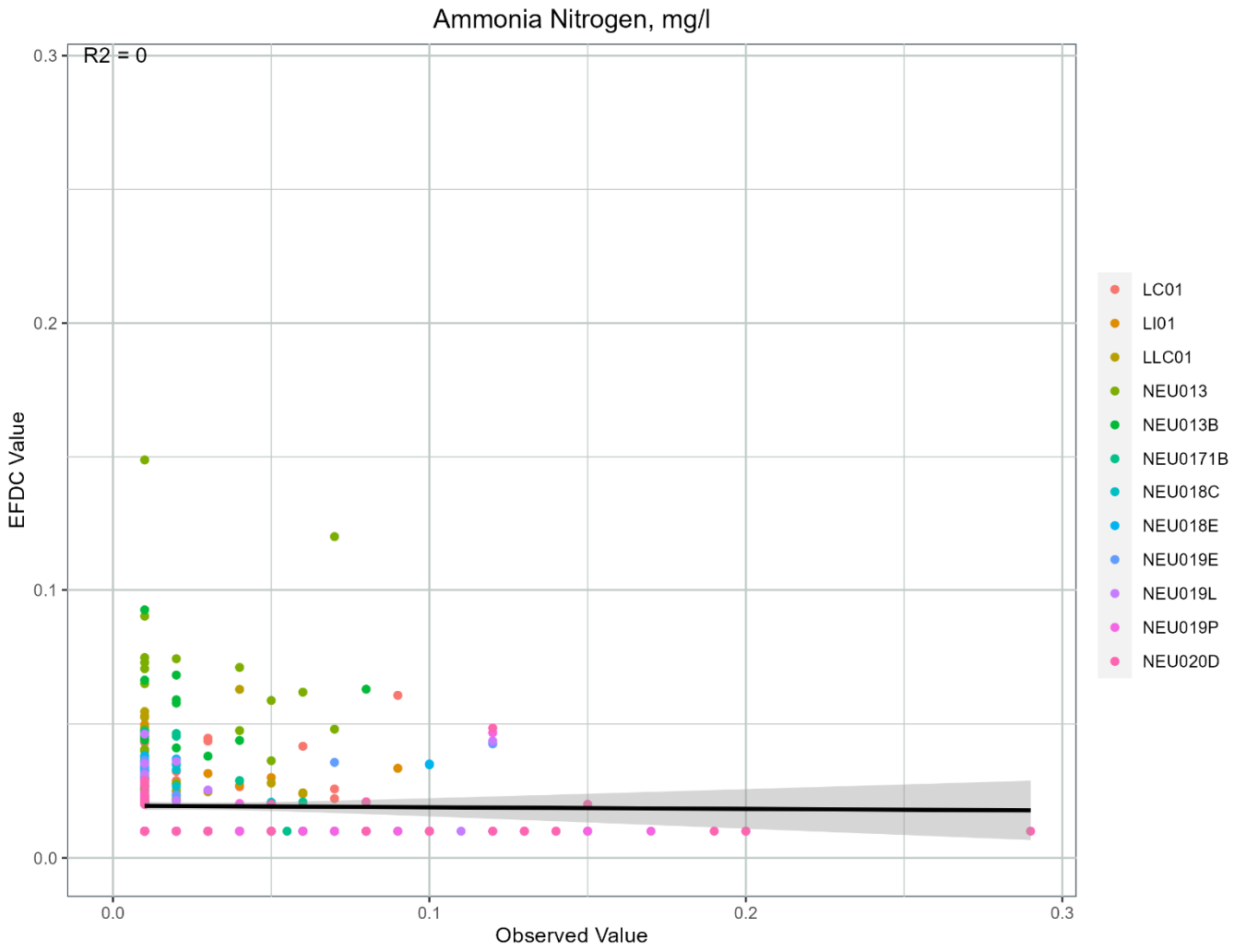

Figure 14-8. Scatter plot of observed versus modeled ammonia concentrations.

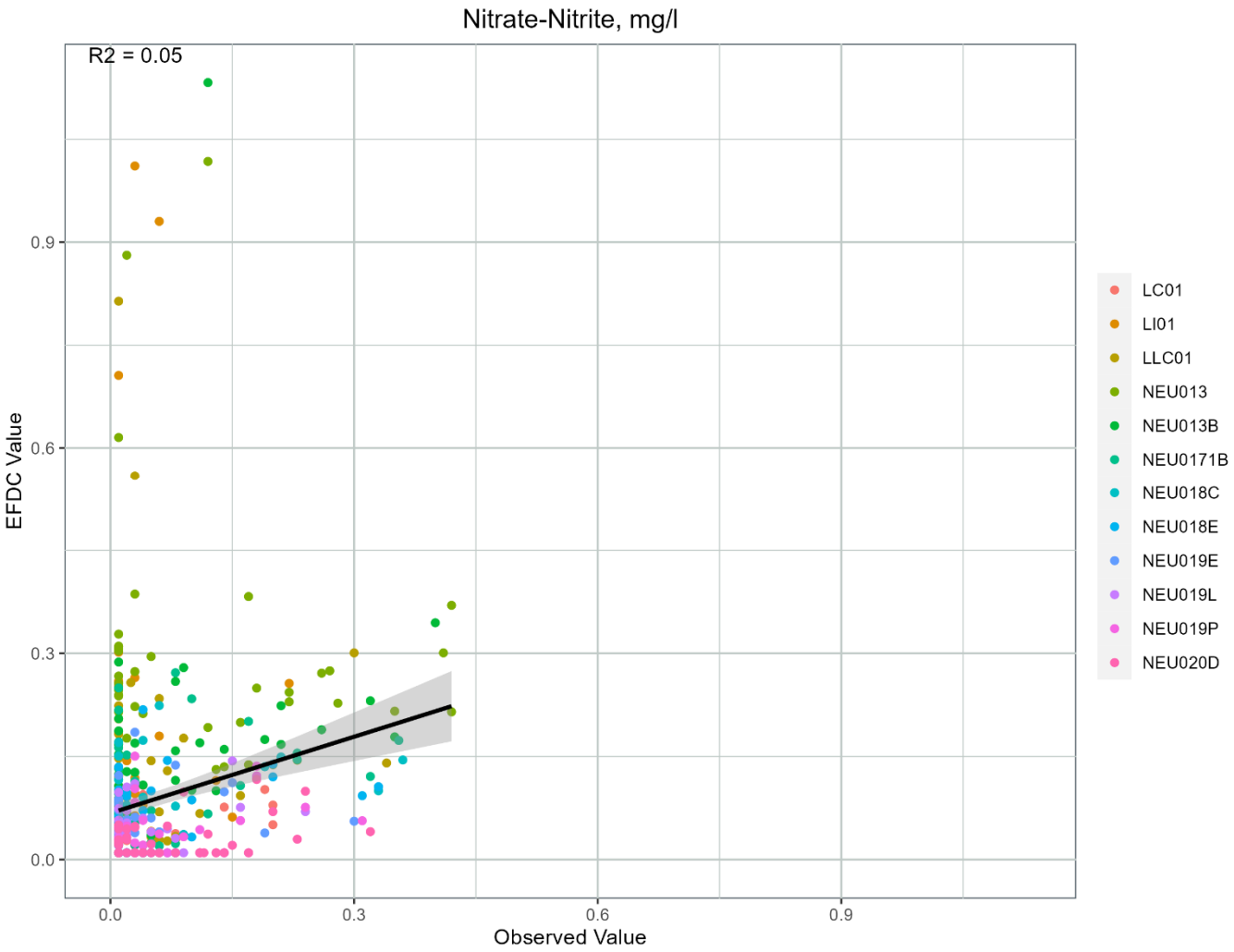

Figure 14-9. Scatter plot of observed versus modeled nitrate-nitrite concentrations.

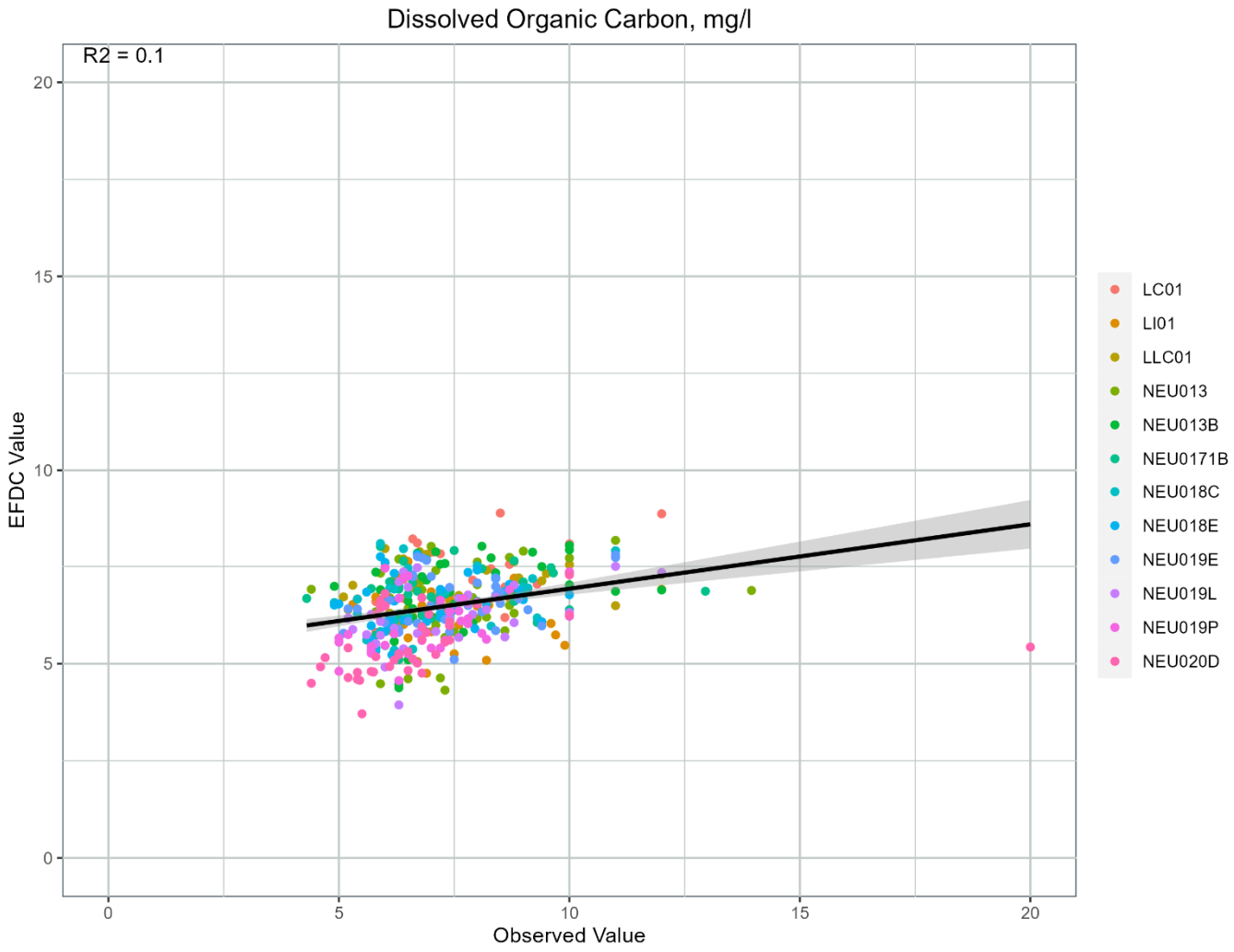

Figure 14-10. Scatter plot of observed versus modeled dissolved organic carbon concentrations.

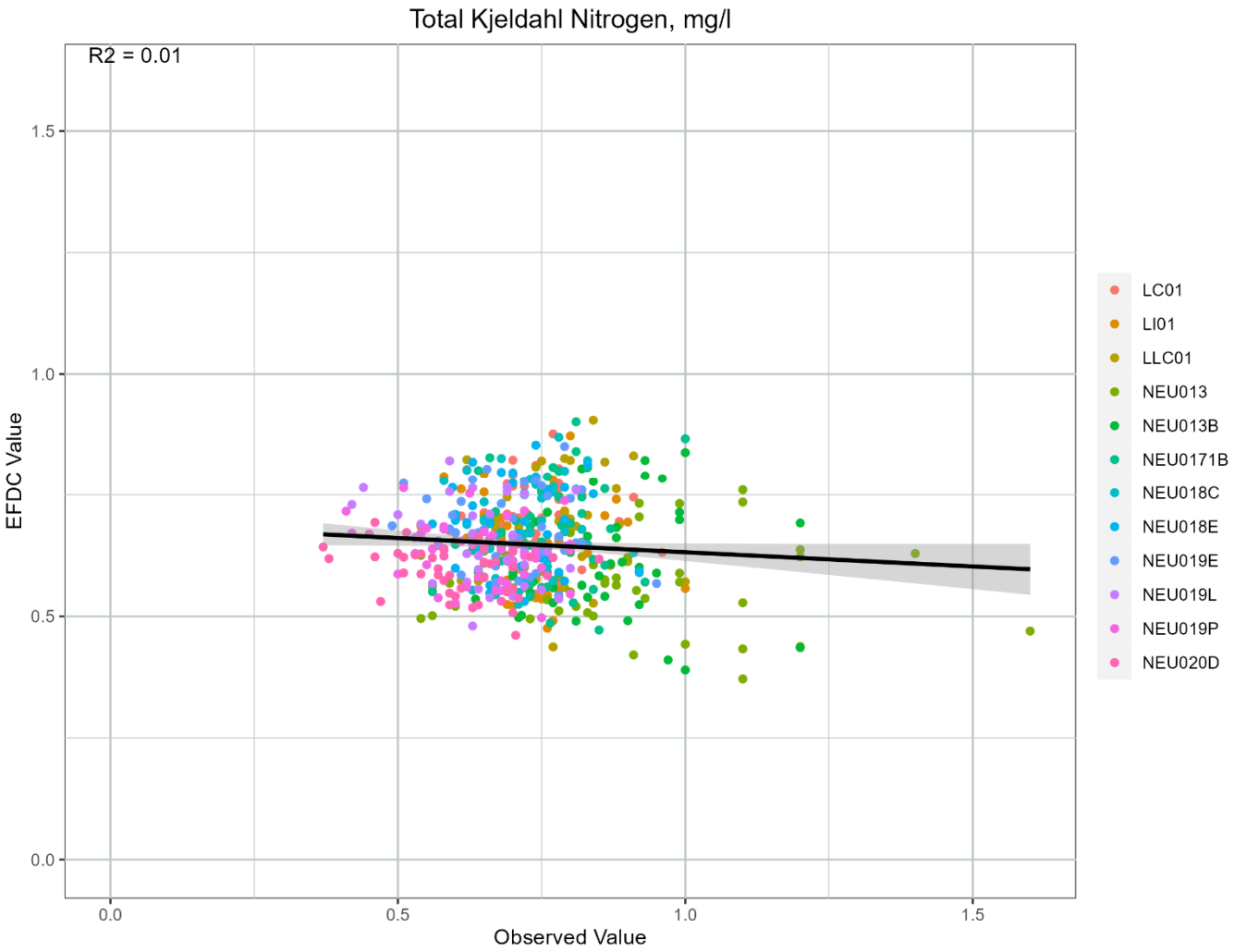

Figure 14-11. Scatter plot of observed versus modeled total Kjeldahl nitrogen concentrations.

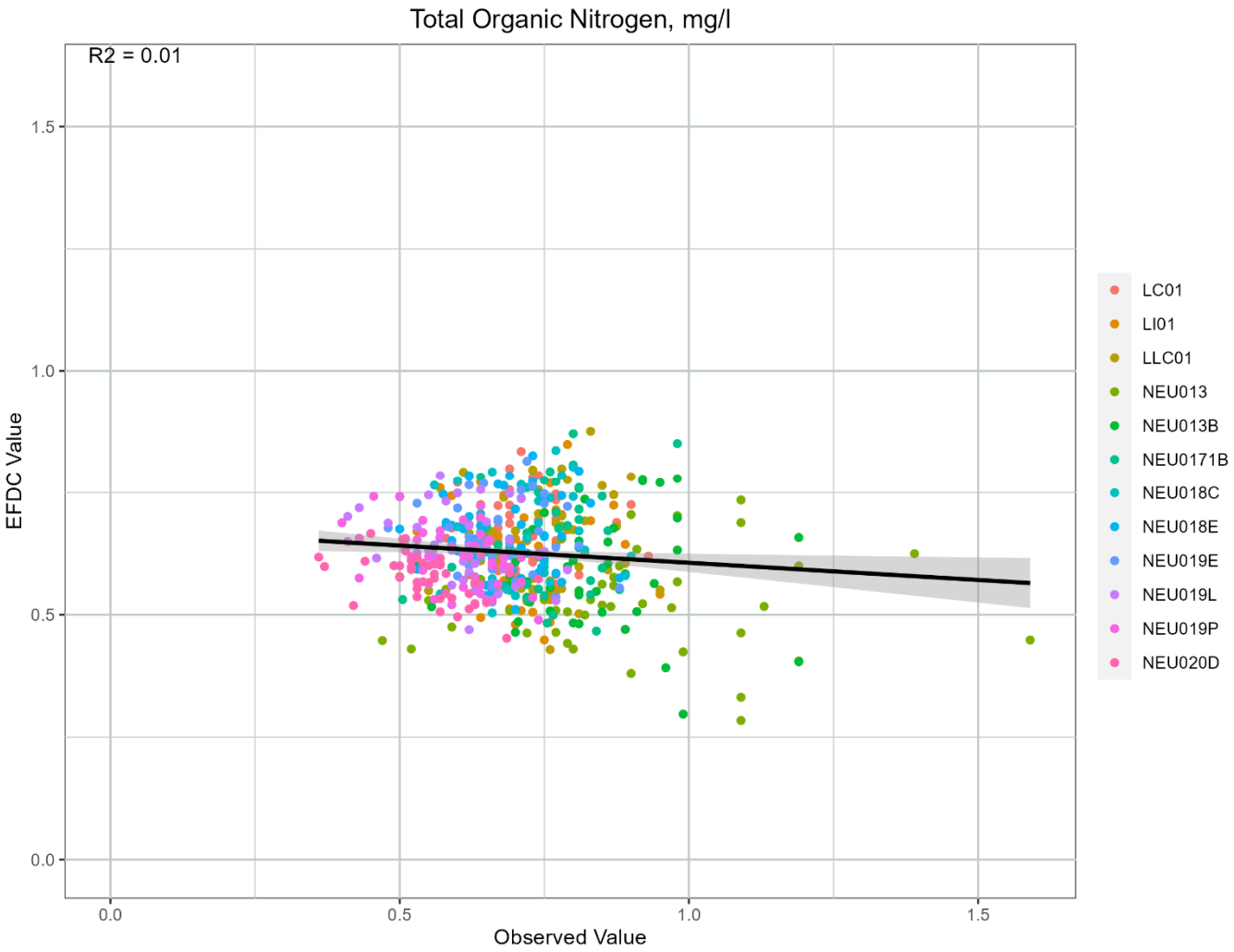

Figure 14-12. Scatter plot of observed versus modeled total organic nitrogen concentrations.

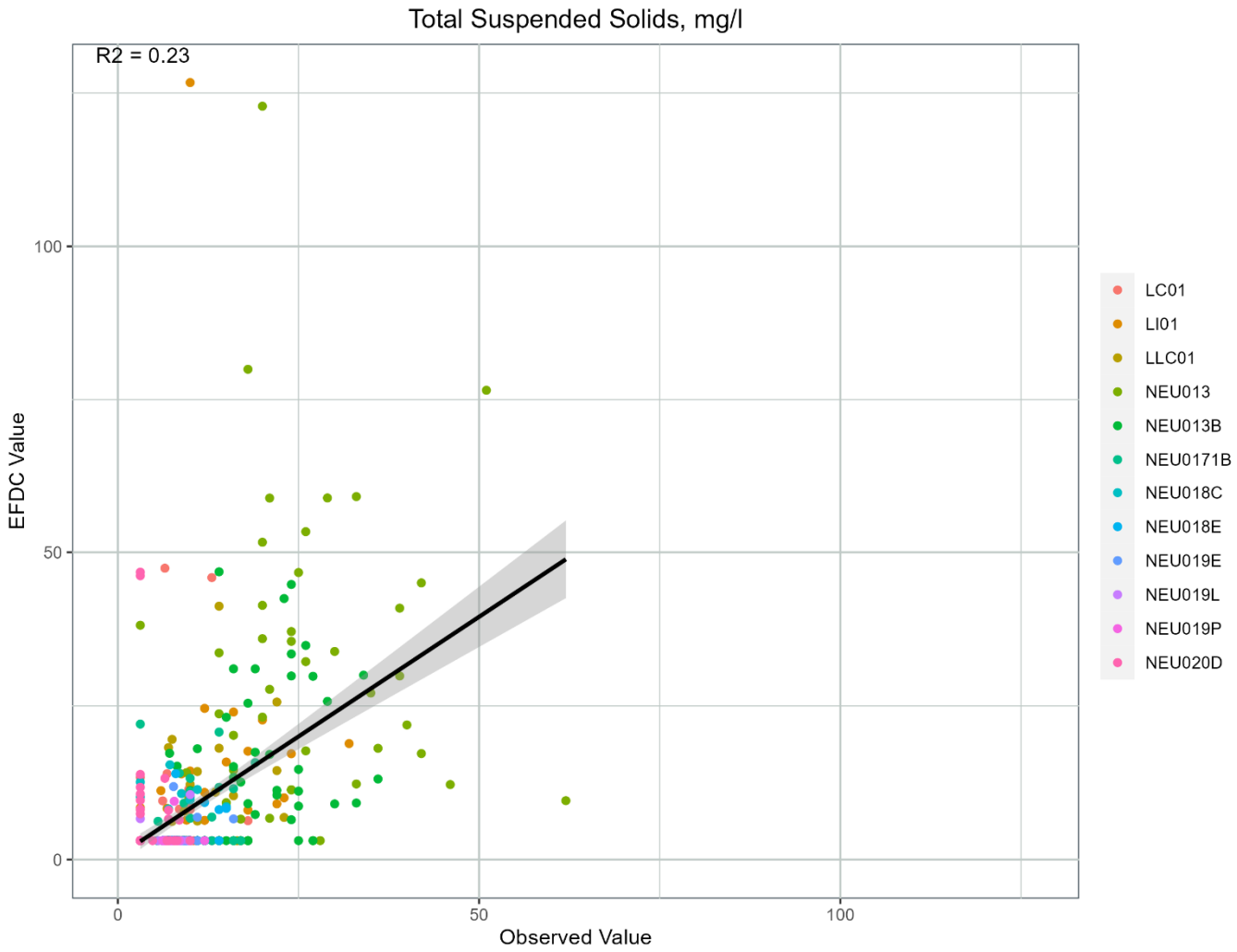

Figure 14-13. Scatter plot of observed versus modeled total suspended solids concentrations.

Appendix A.3

Falls Lake EFDC Model Vertical Profile Plots

Table of Contents

List of Figures

1. Water Temperature Vertical Profile Plots

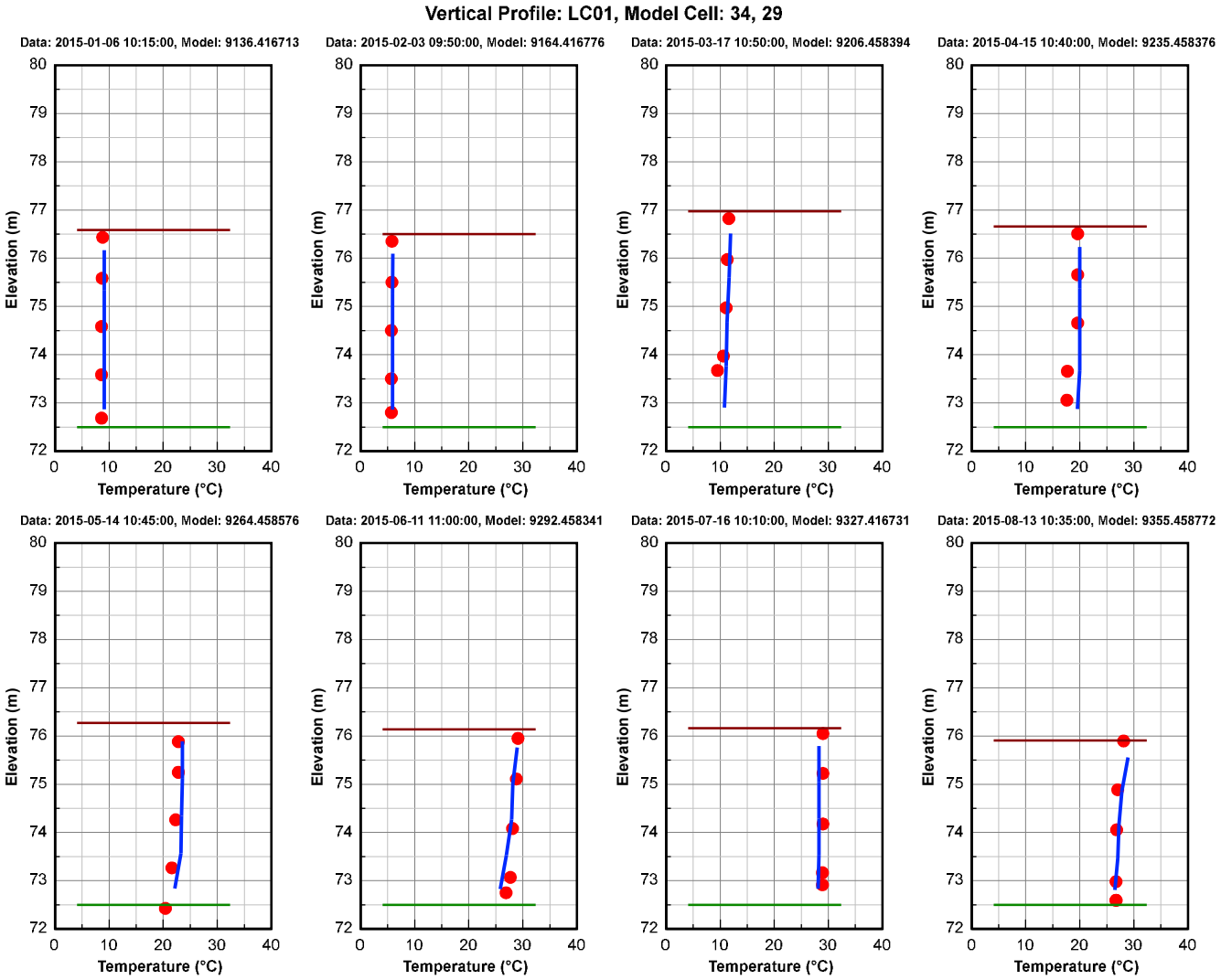

January 2015 – August 2015 (1 of 6)

Vertical Profile: LC01, Model Cell: 34, 29

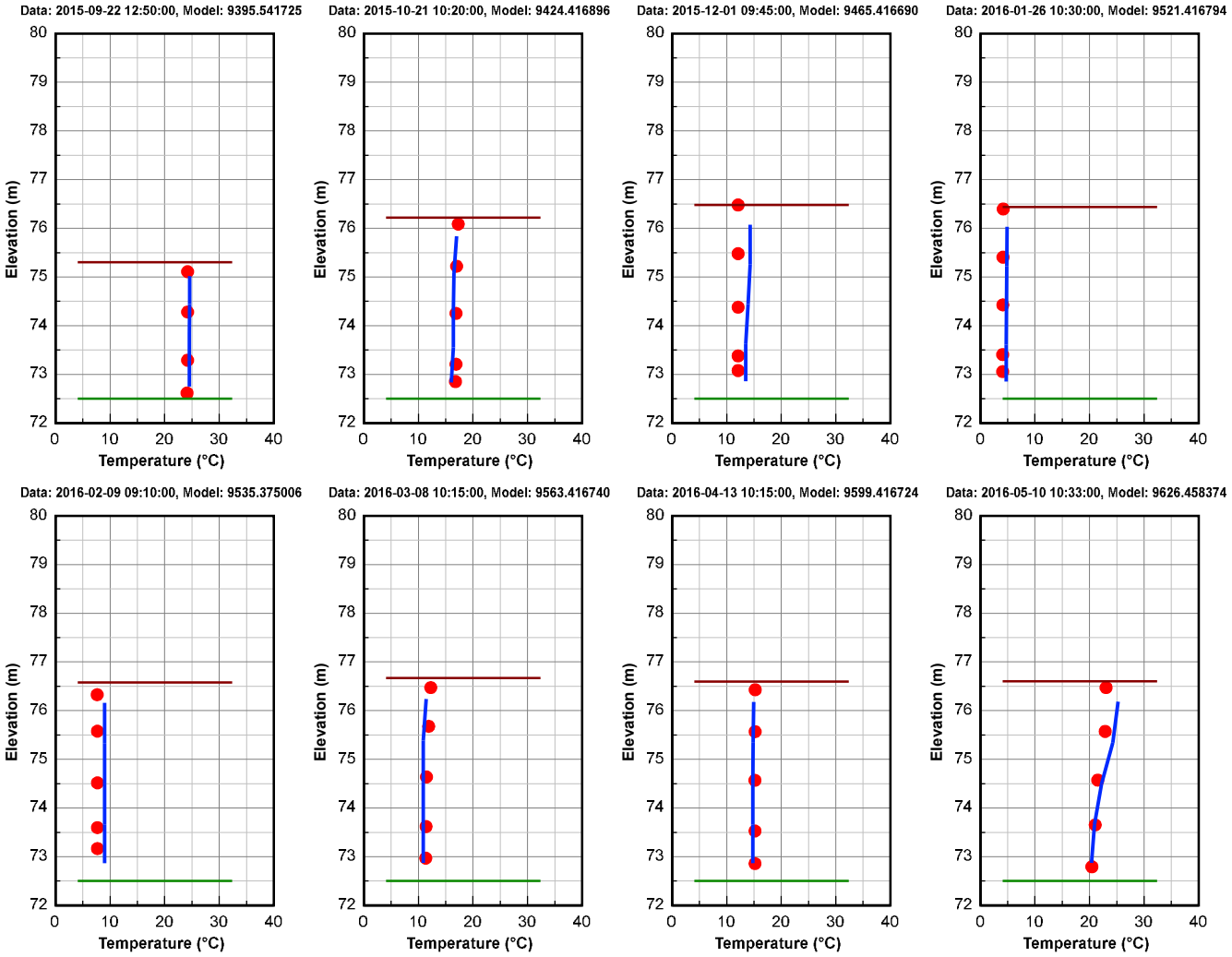

September 2015 – May 2016 (2 of 6)

Vertical Profile: LC01, Model Cell: 34, 29

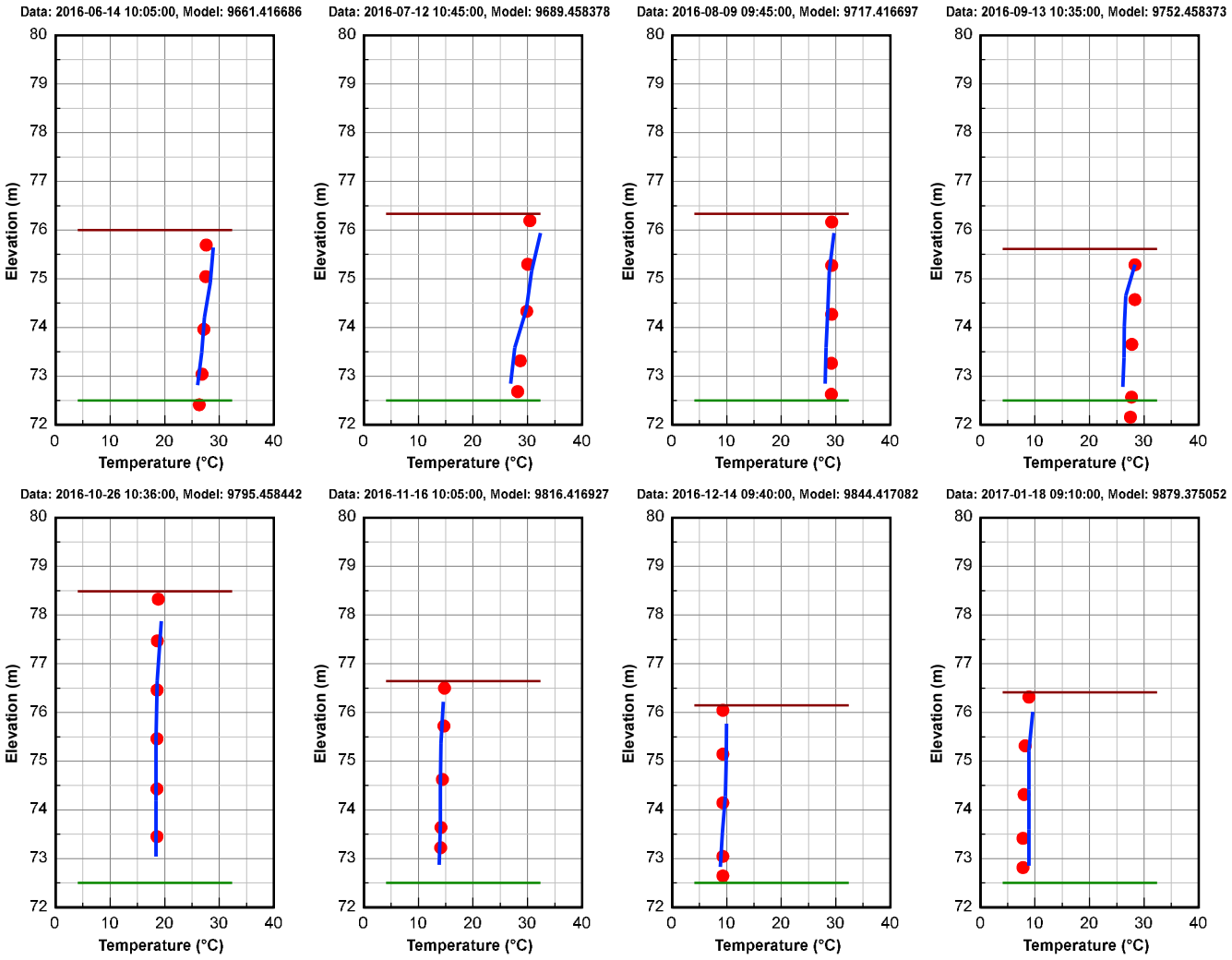

June 2016 – January 2017 (3 of 6)

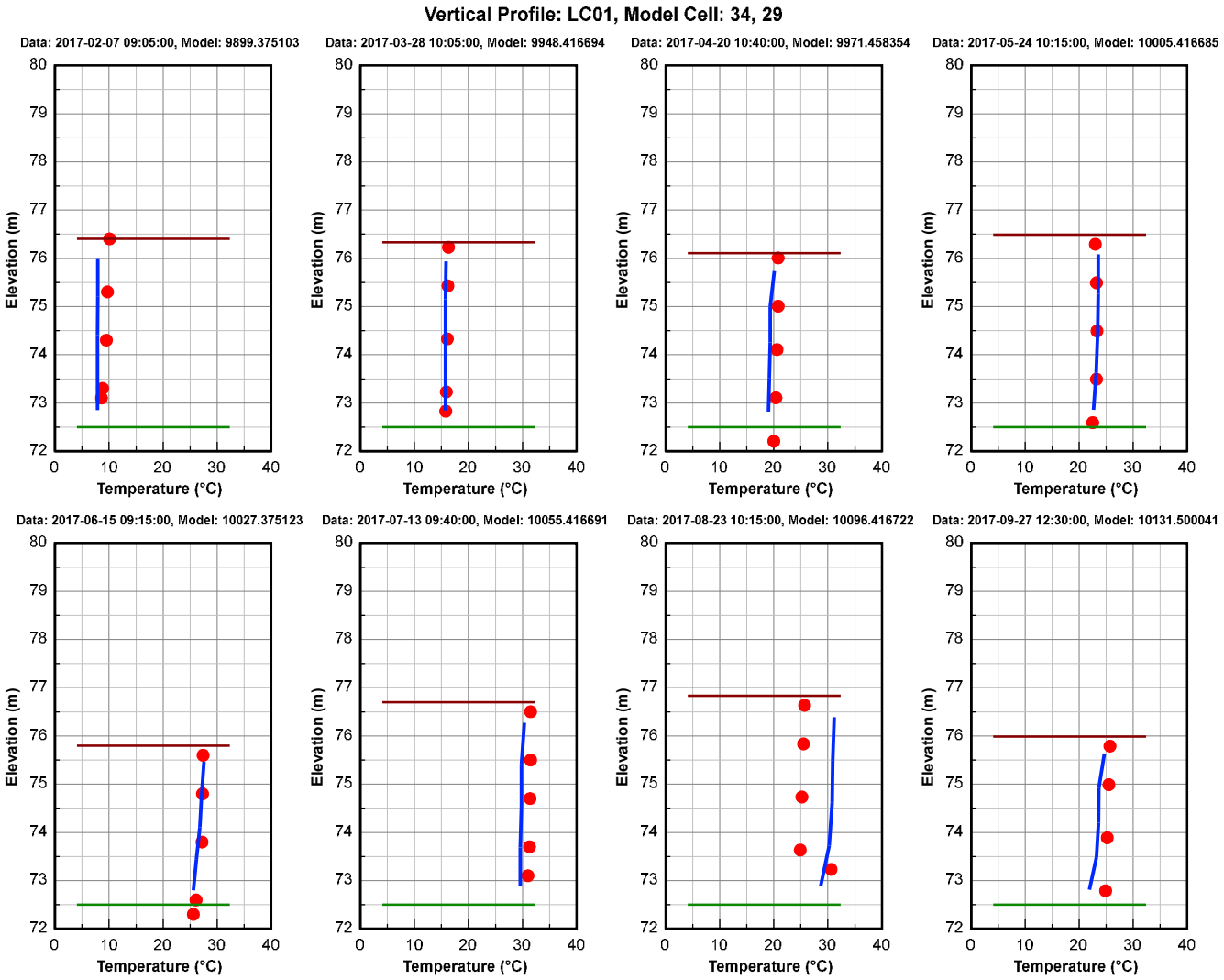

February 2017 – September 2017 (4 of 6)

Vertical Profile: LC01, Model Cell: 34, 29

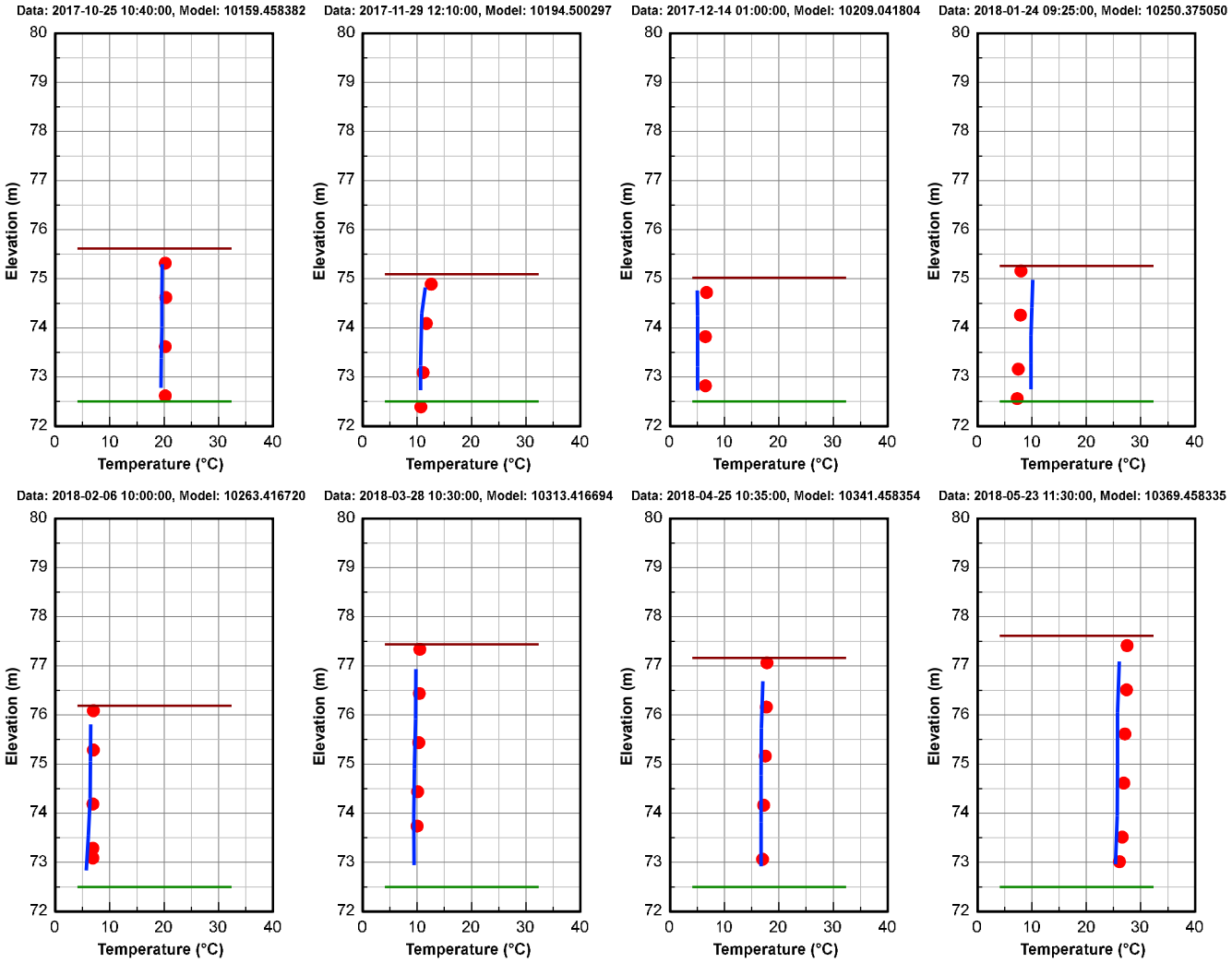

October 2017 – May 2018 (5 of 6)

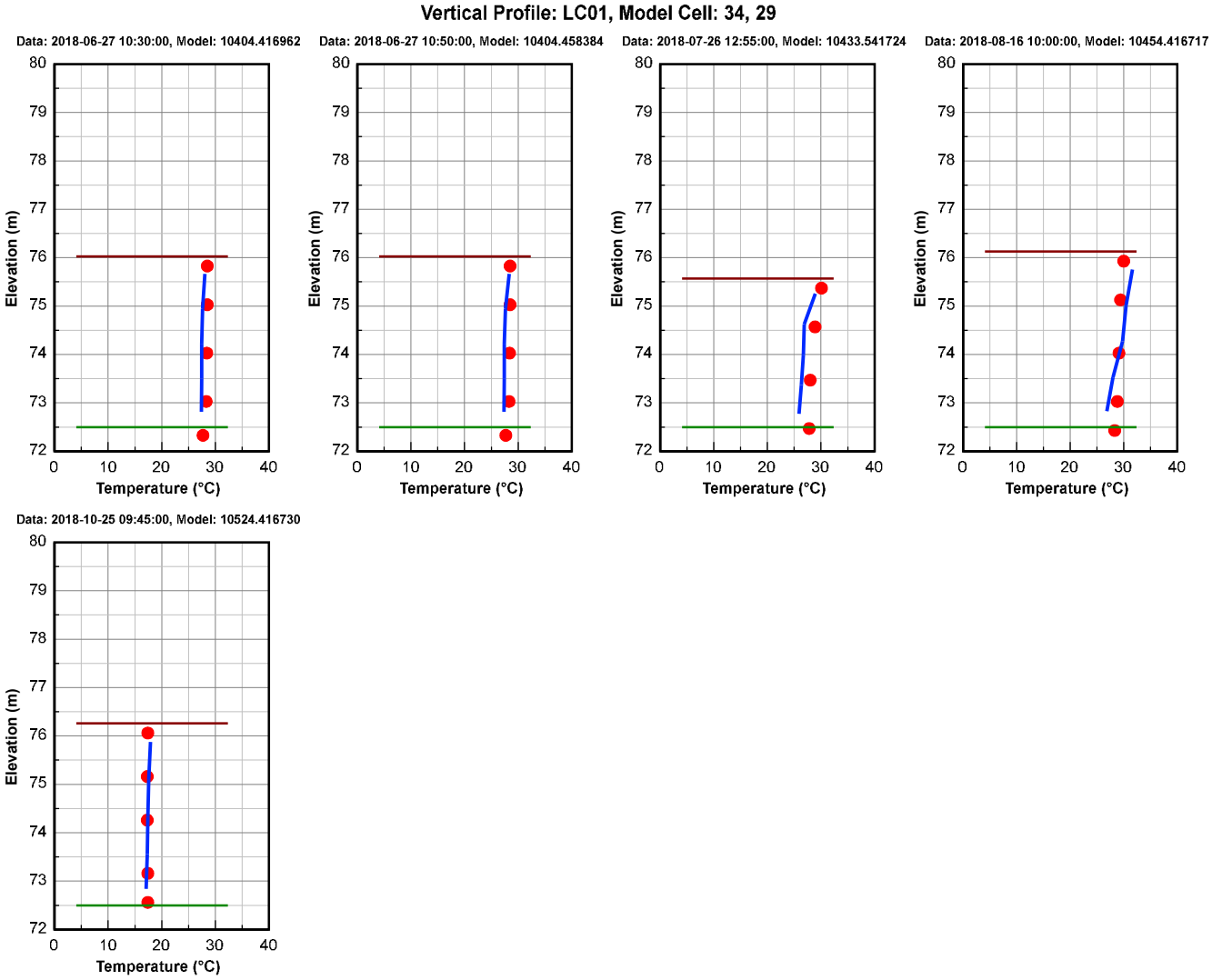

June 2018 – October 2018 (6 of 6)

Figure 1-1 Water Temperature Vertical Profile Comparison Plot at Station LC01 during the calibration and validation period. Red dots are data, and blue continuous lines are model results.

Vertical Profile: LI01, Model Cell: 39, 43

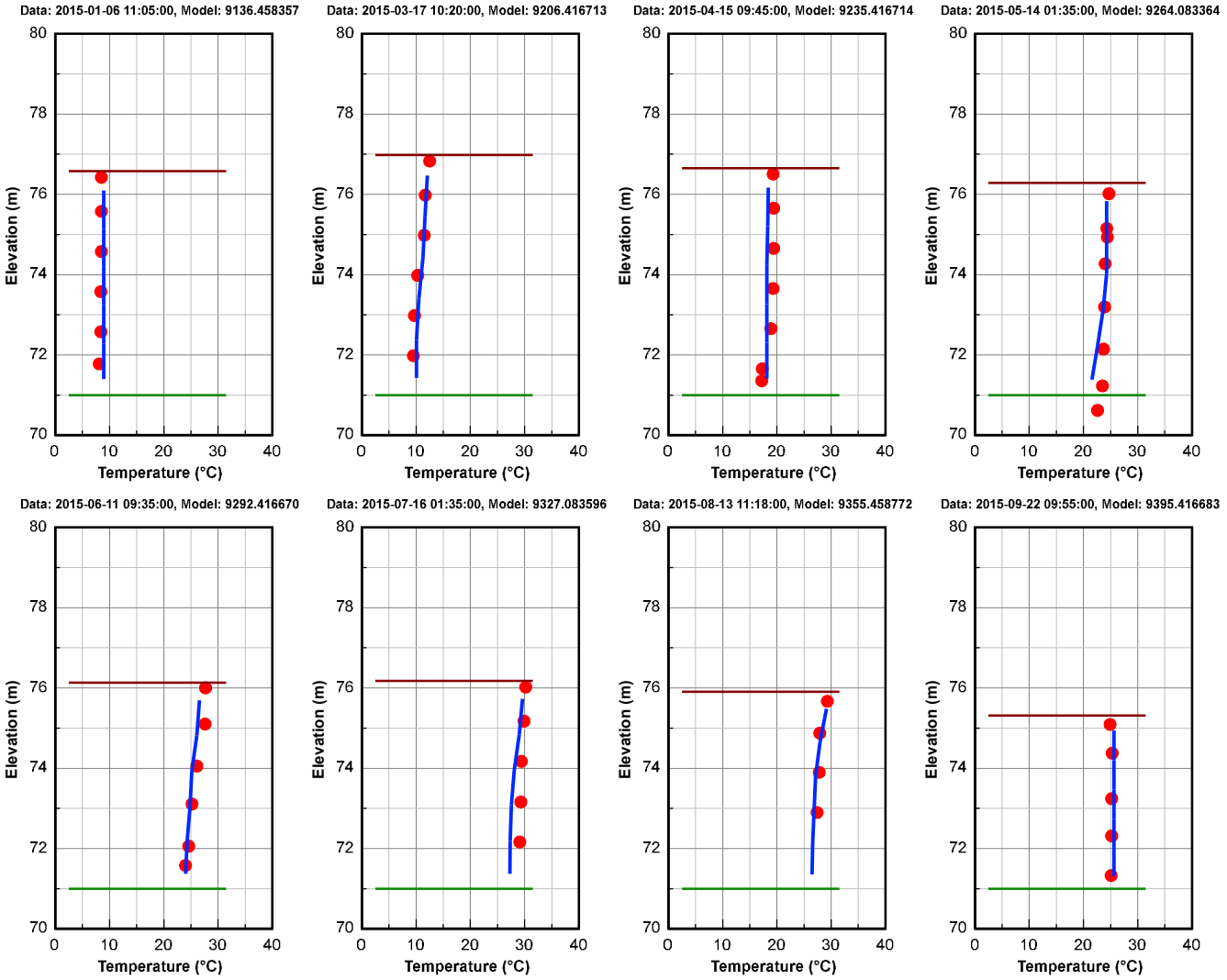

January 2015 – September 2015 (1 of 6)

Vertical Profile: LI01, Model Cell: 39, 43

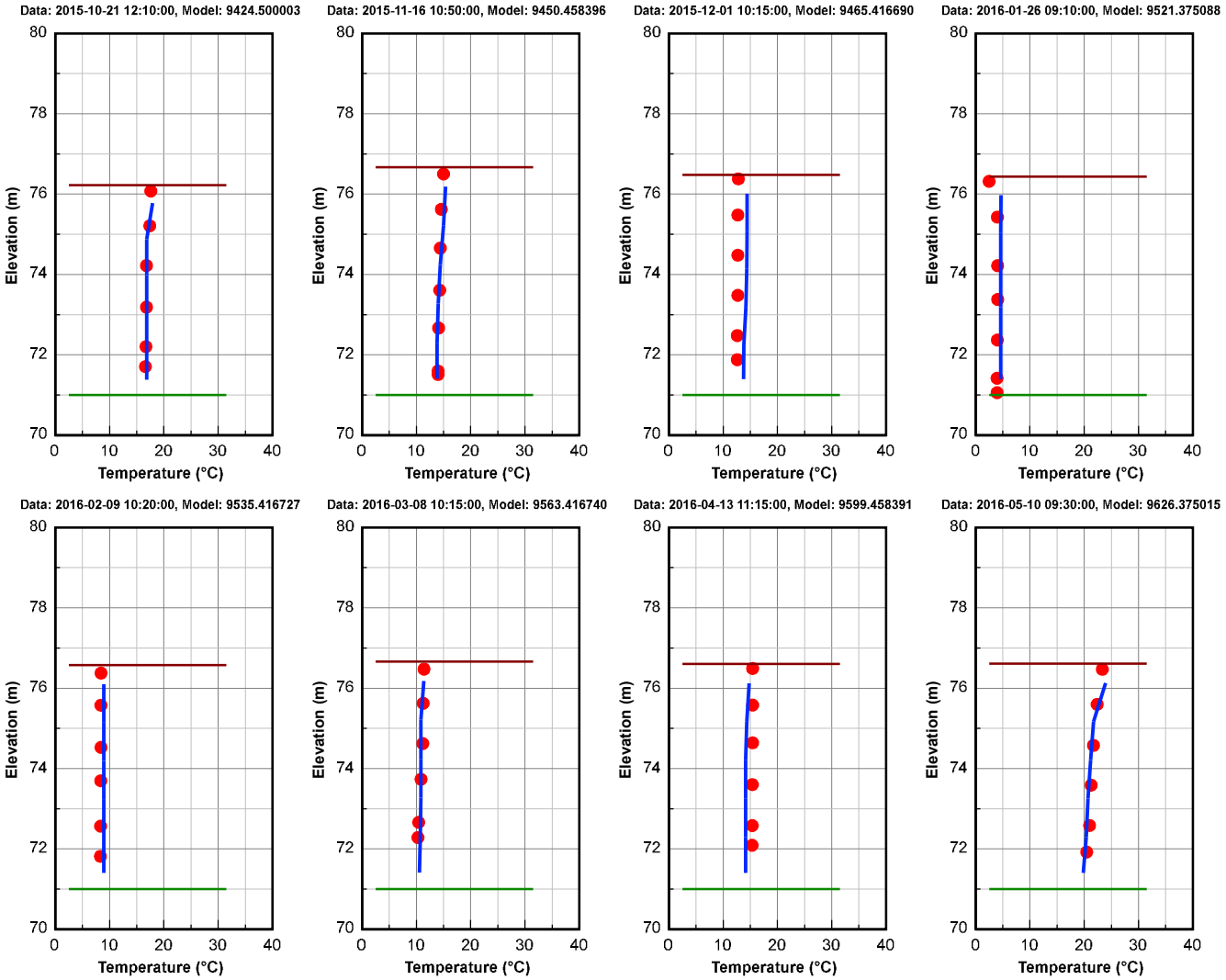

October 2015 – May 2016 (2 of 6)

Vertical Profile: LI01, Model Cell: 39, 43

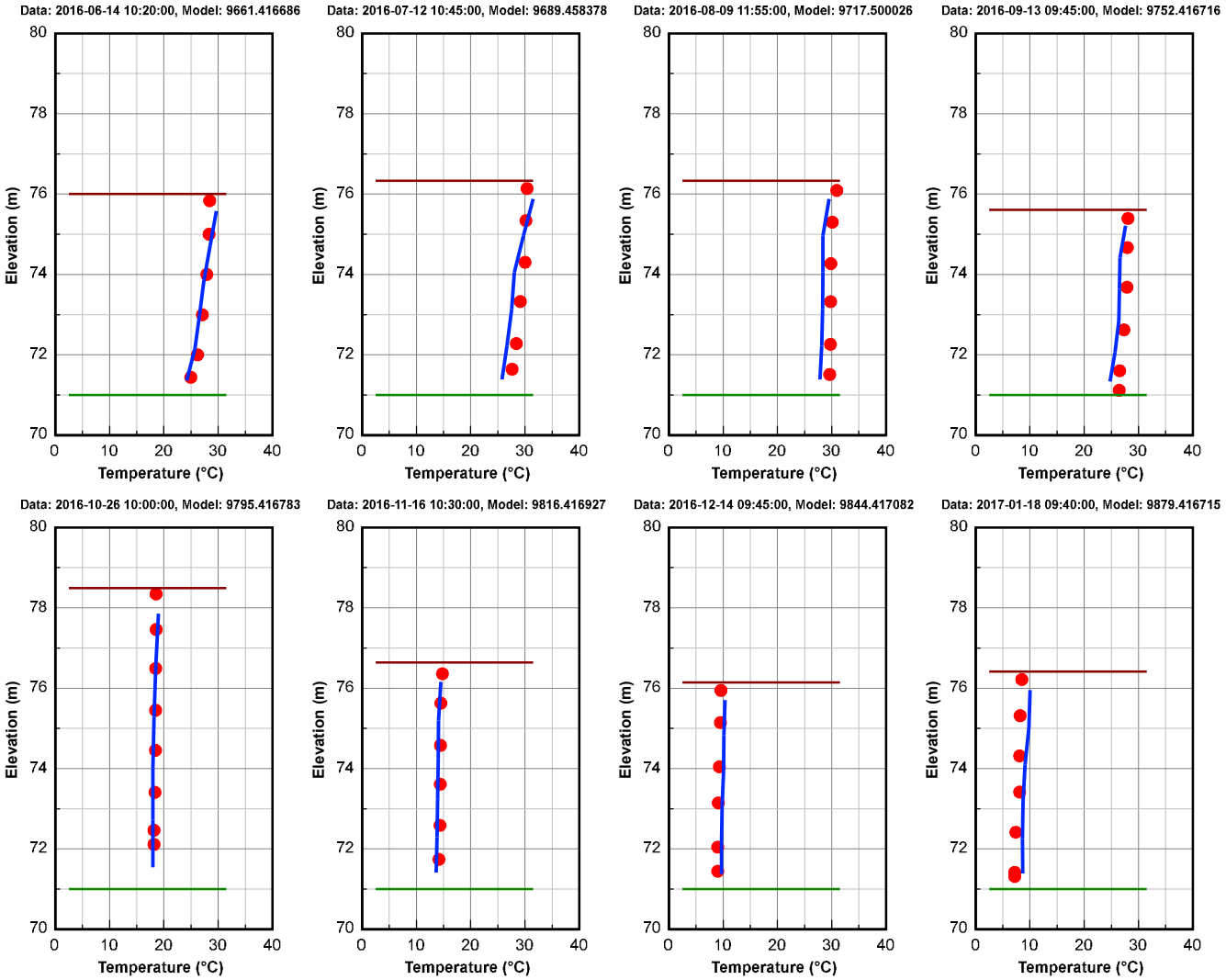

June 2016 – January 2017 (3 of 6)

Vertical Profile: LI01, Model Cell: 39, 43

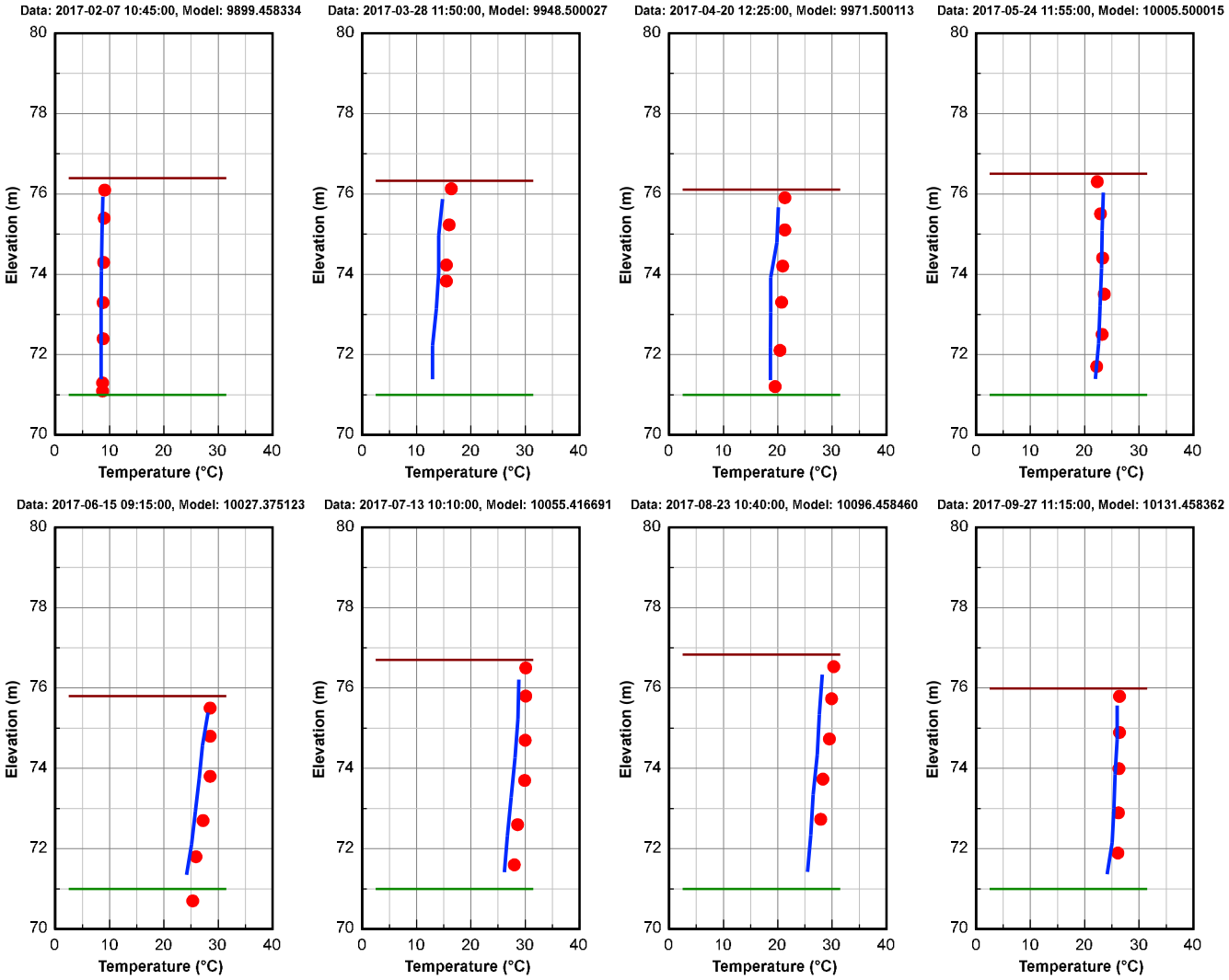

February 2017 – September 2017 (4 of 6)

Vertical Profile: LI01, Model Cell: 39, 43

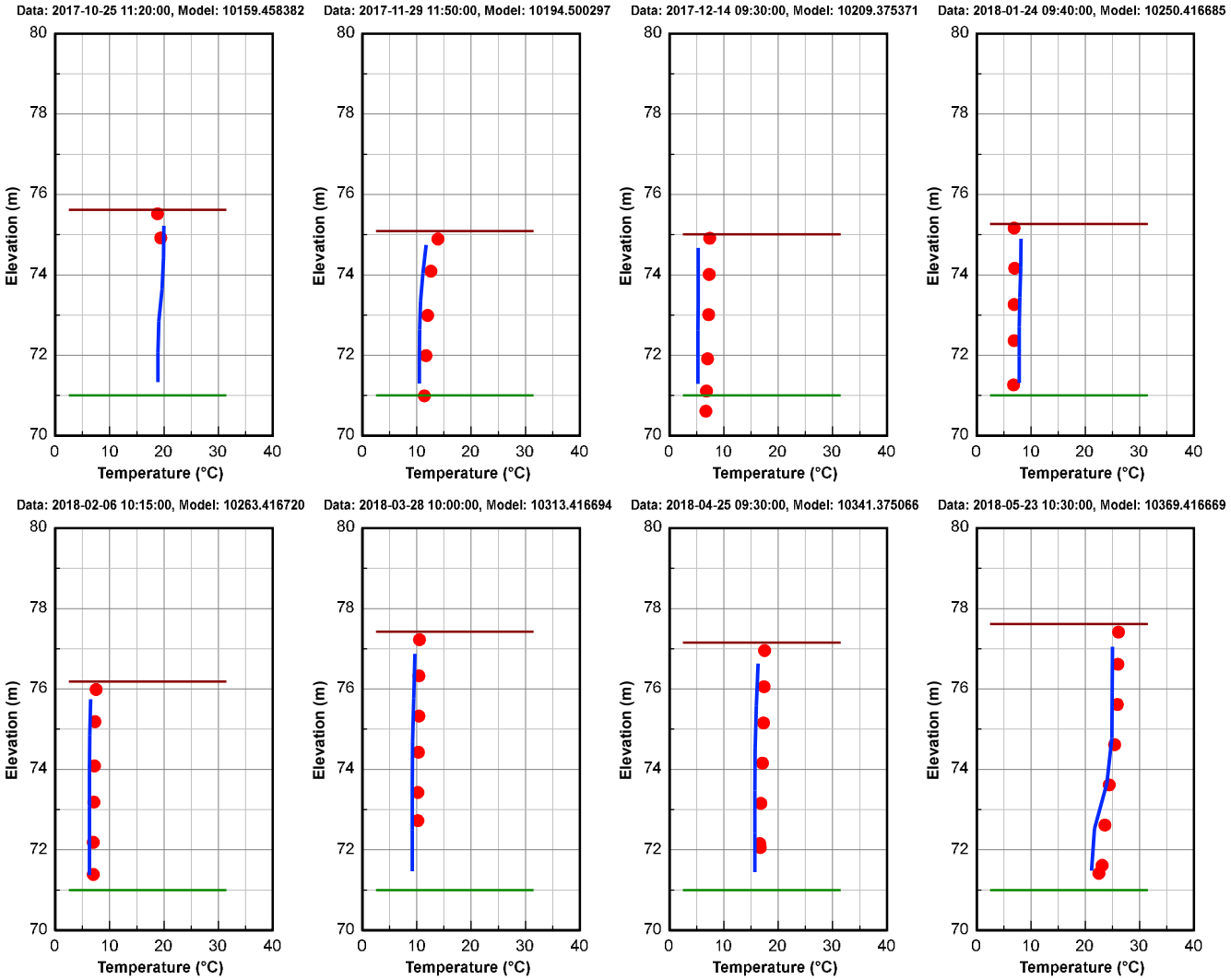

October 2017 – May 2018 (5 of 6)

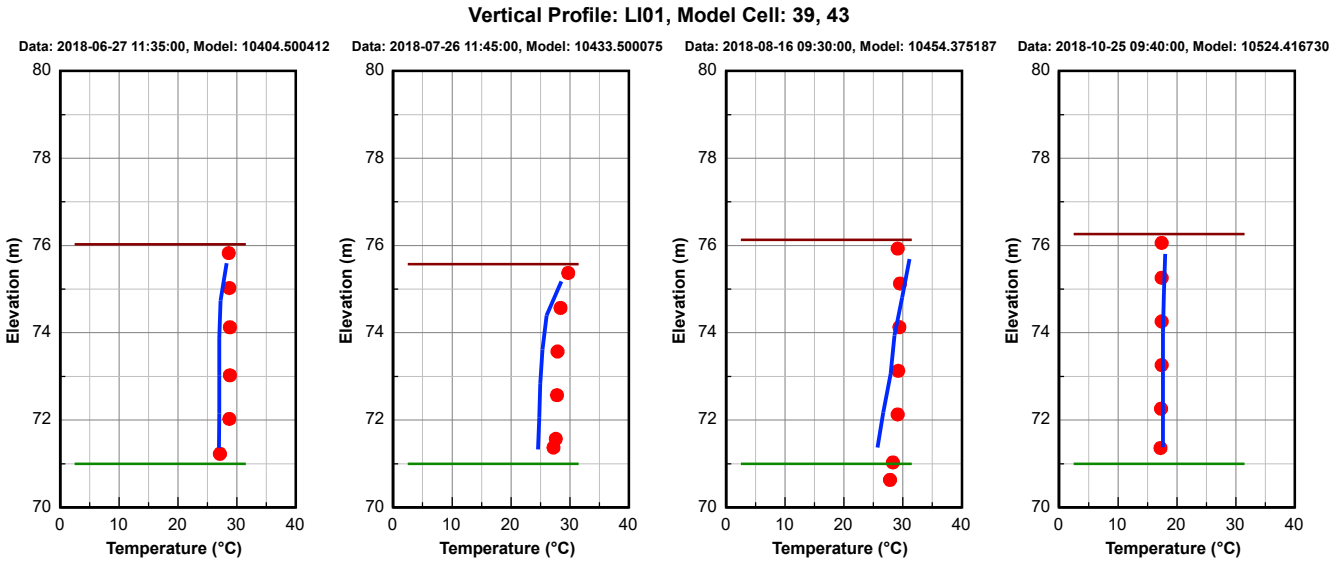

June 2018 – October 2018 (6 of 6)

Figure 1-2 Water Temperature Vertical Profile Comparison Plot at Station LI01 during the calibration and validation period. Red dots are data, and blue continuous lines are model results.

Vertical Profile: LLC01, Model Cell: 47, 33

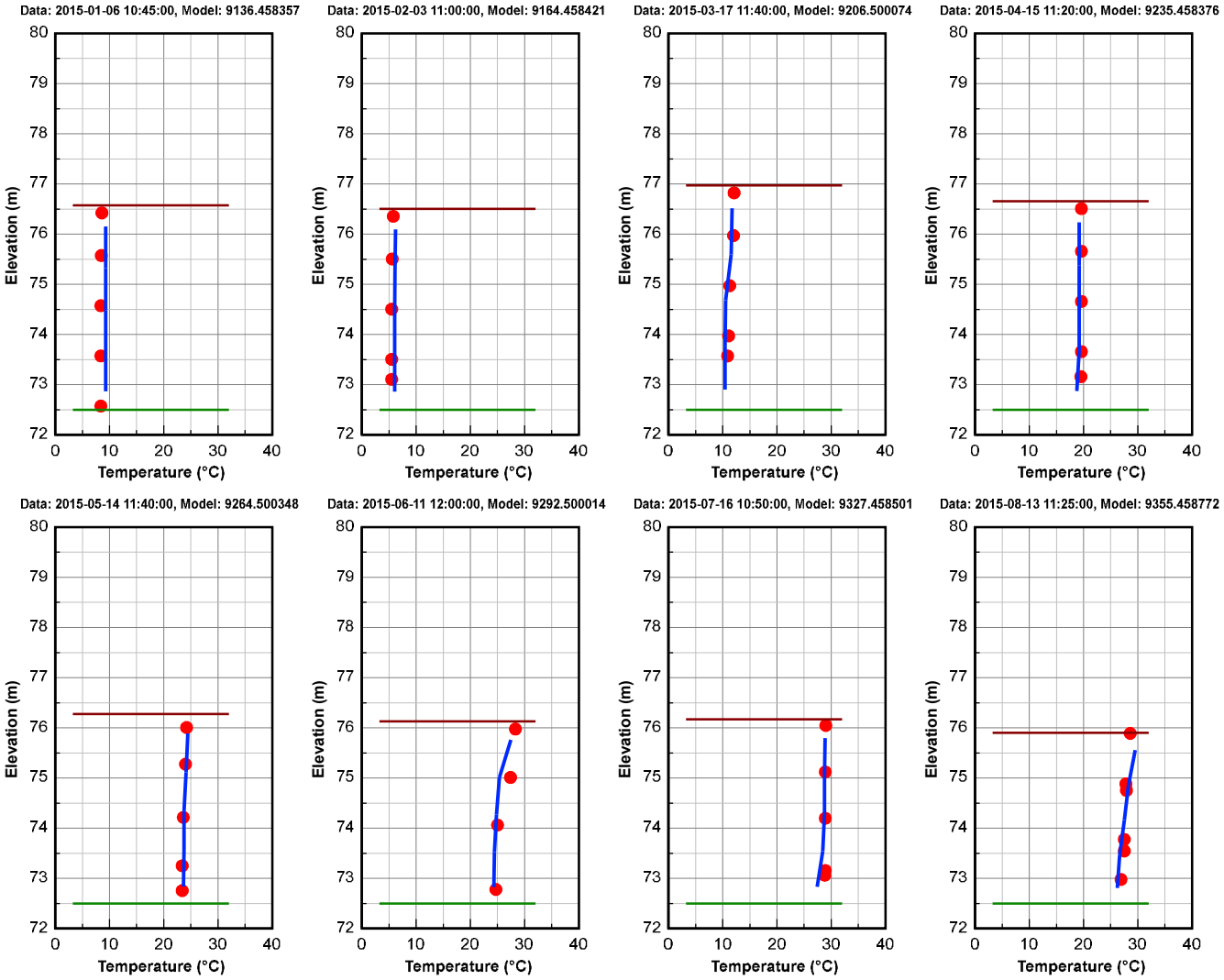

January 2015 – August 2015 (1 of 6)

Vertical Profile: LLC01, Model Cell: 47, 33

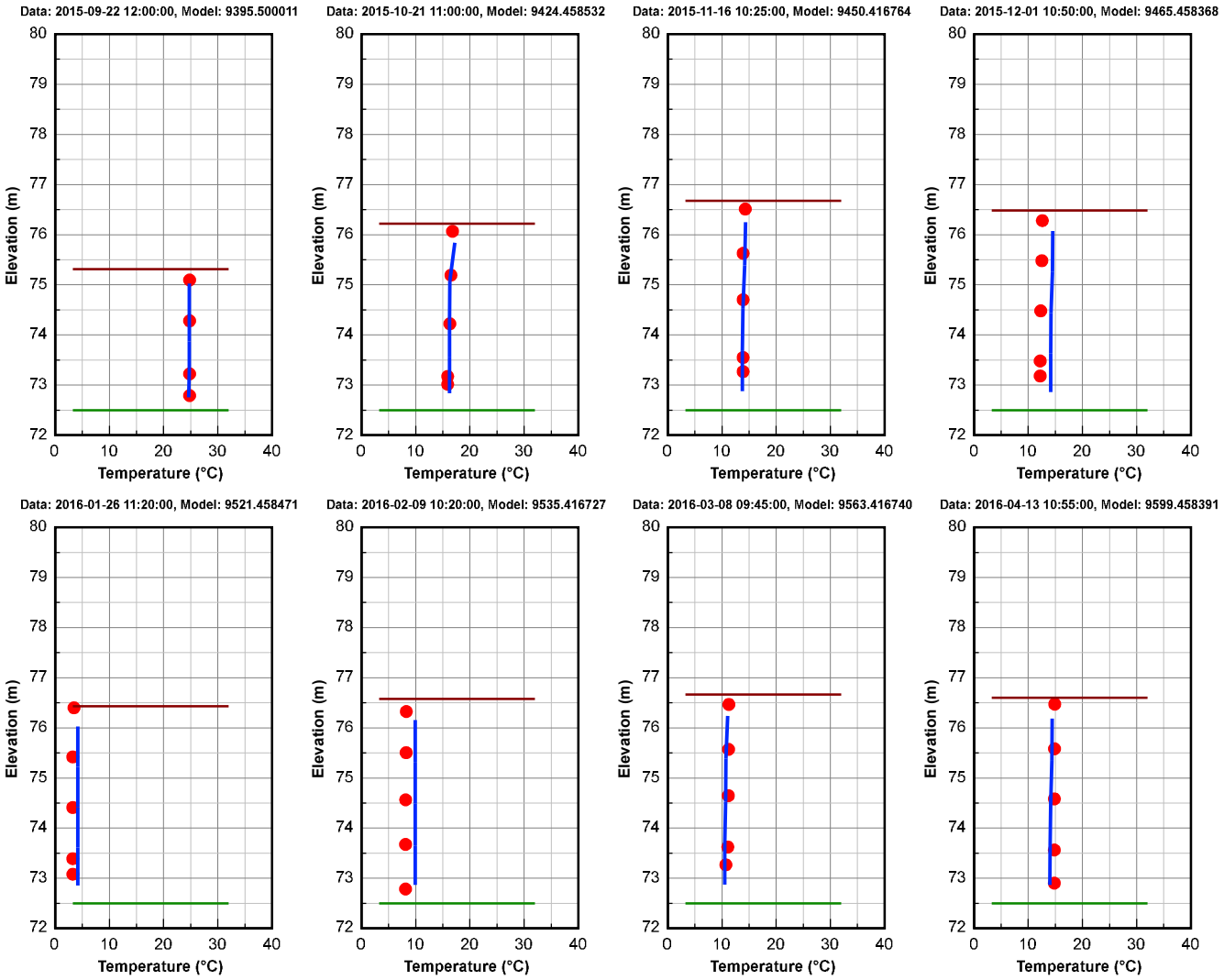

September 2015 – April 2016 (2 of 6)

Vertical Profile: LLC01, Model Cell: 47, 33

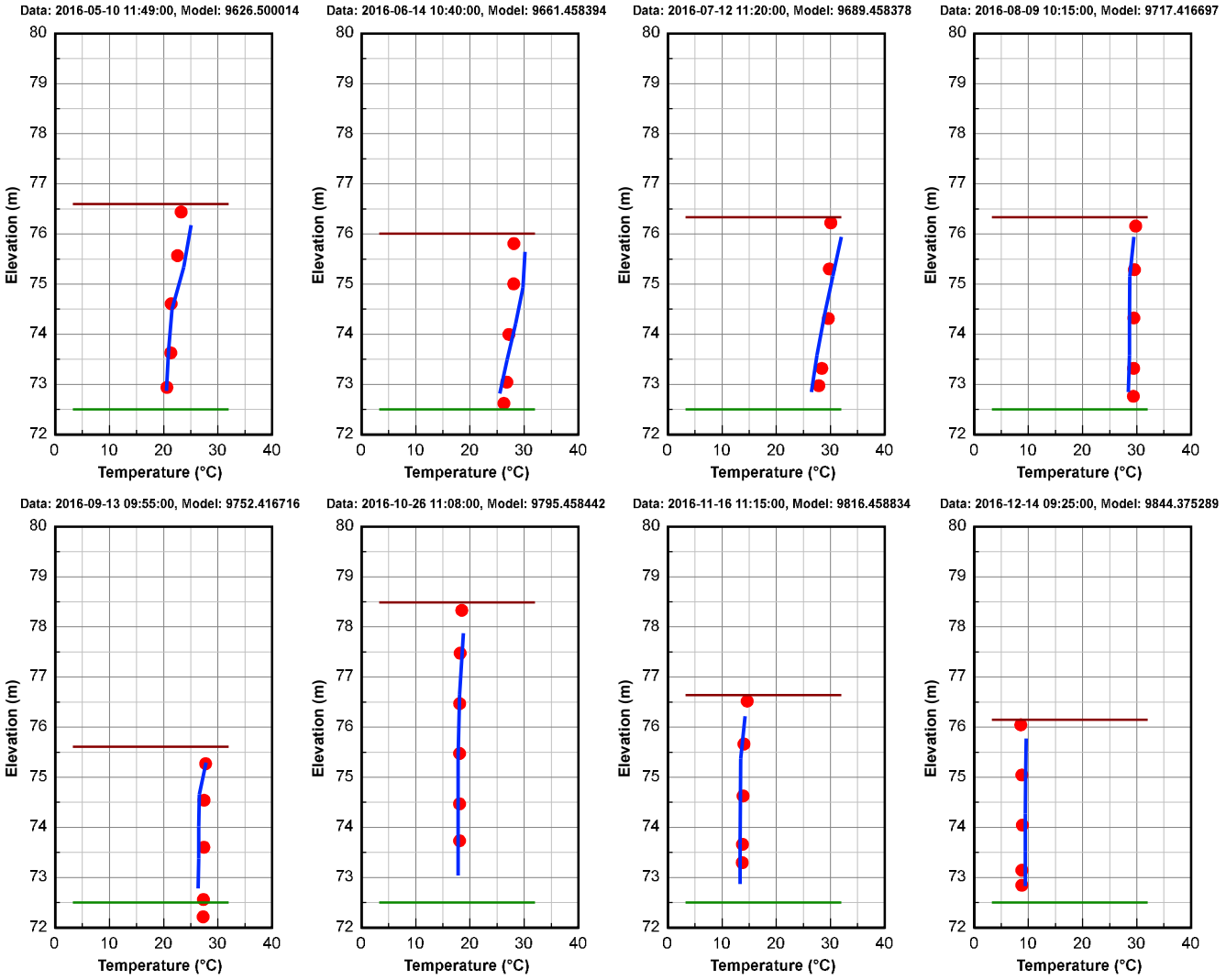

May 2016 – December 2016 (3 of 6)

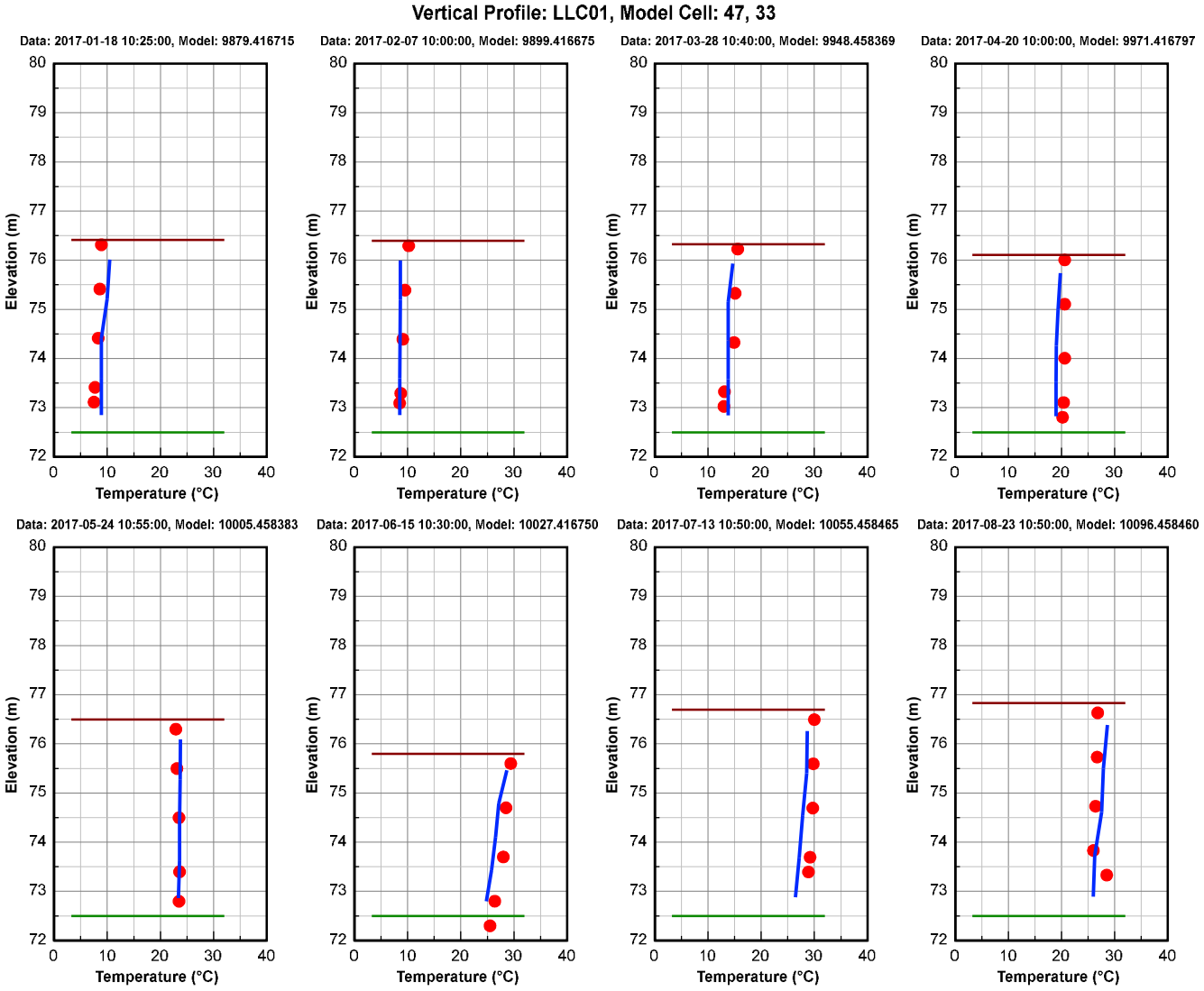

January 2017 – August 2017 (4 of 6)

Vertical Profile: LLC01, Model Cell: 47, 33

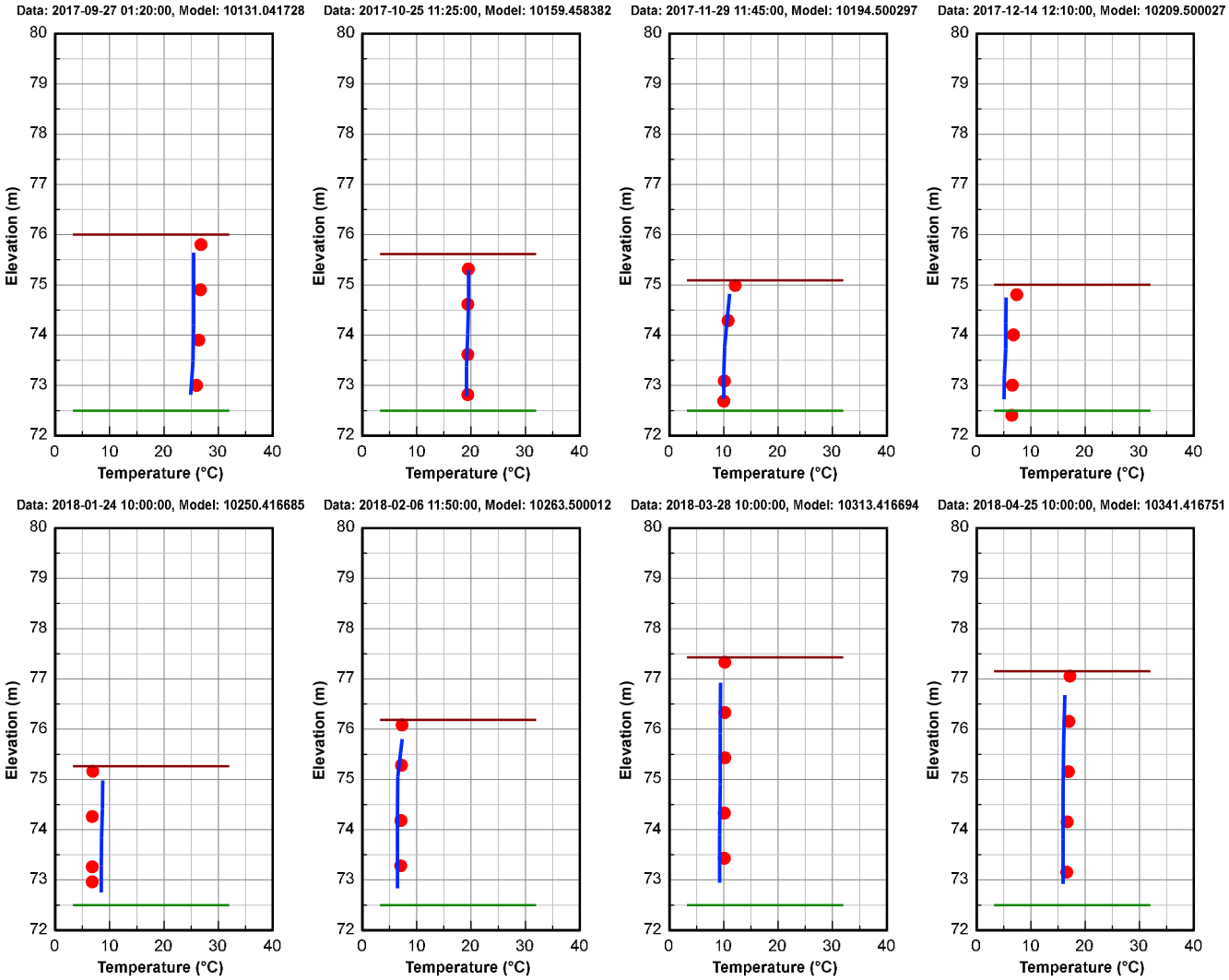

September 2017 – April 2018 (5 of 6)

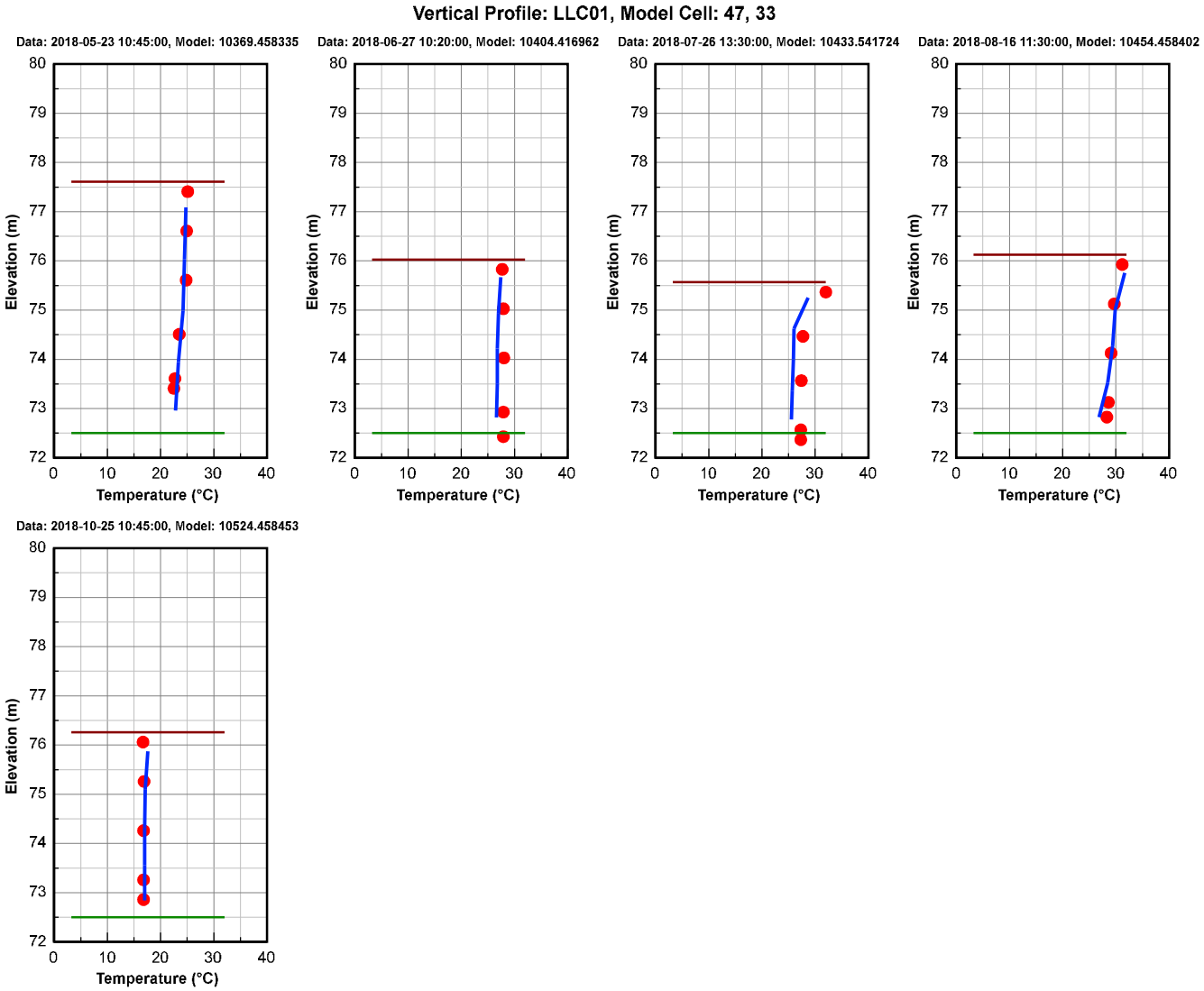

May 2018 – October 2018 (6 of 6)

Figure 1-3 Water Temperature Vertical Profile Comparison Plot at Station LLC01 during the calibration and validation period. Red dots are data, and blue continuous lines are model results.

Vertical Profile: NEU013, Model Cell: 42, 17

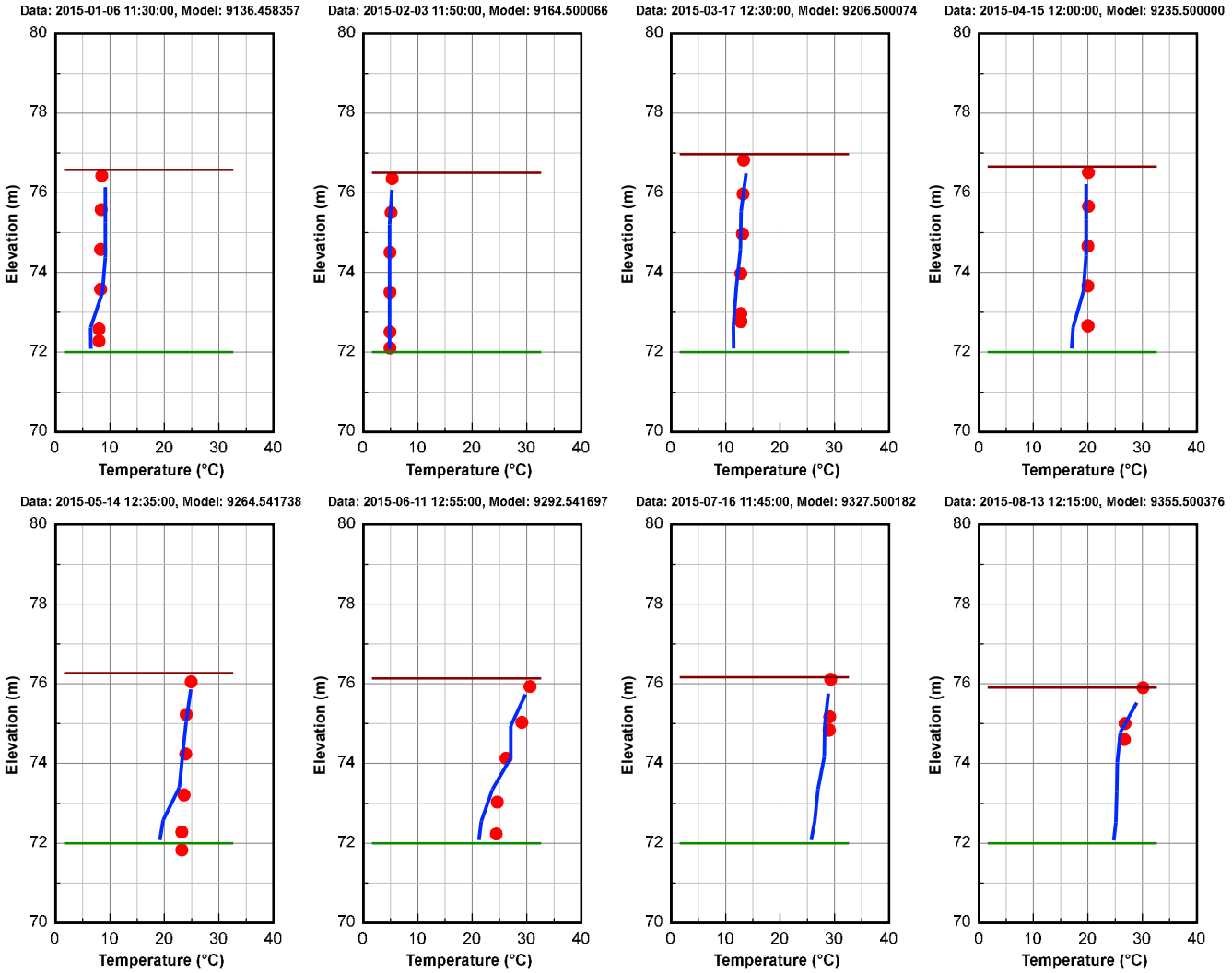

January 2015 – August 2015 (1 of 6)

Vertical Profile: NEU013, Model Cell: 42, 17

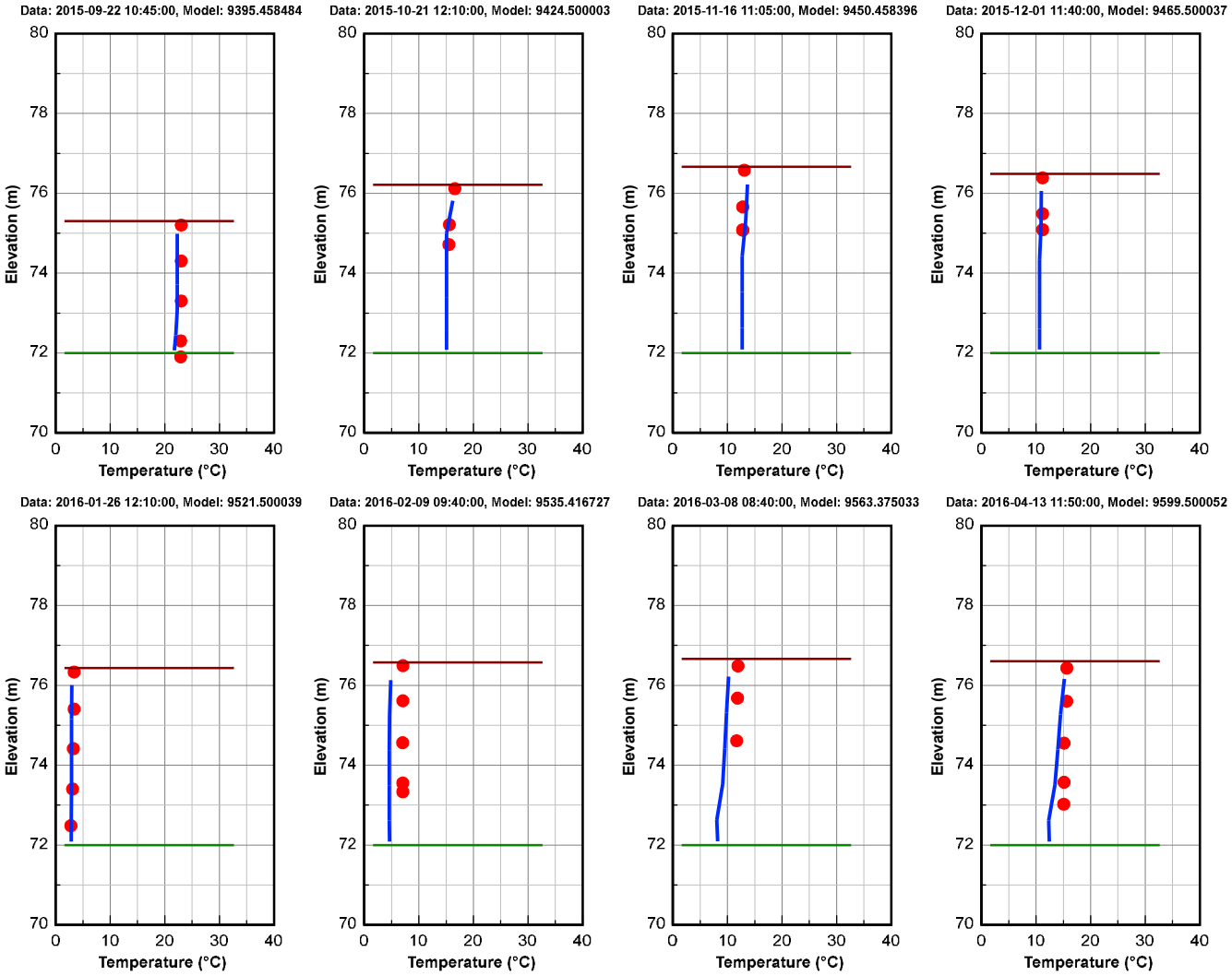

September 2015 – April 2016 (2 of 6)

Vertical Profile: NEU013, Model Cell: 42, 17

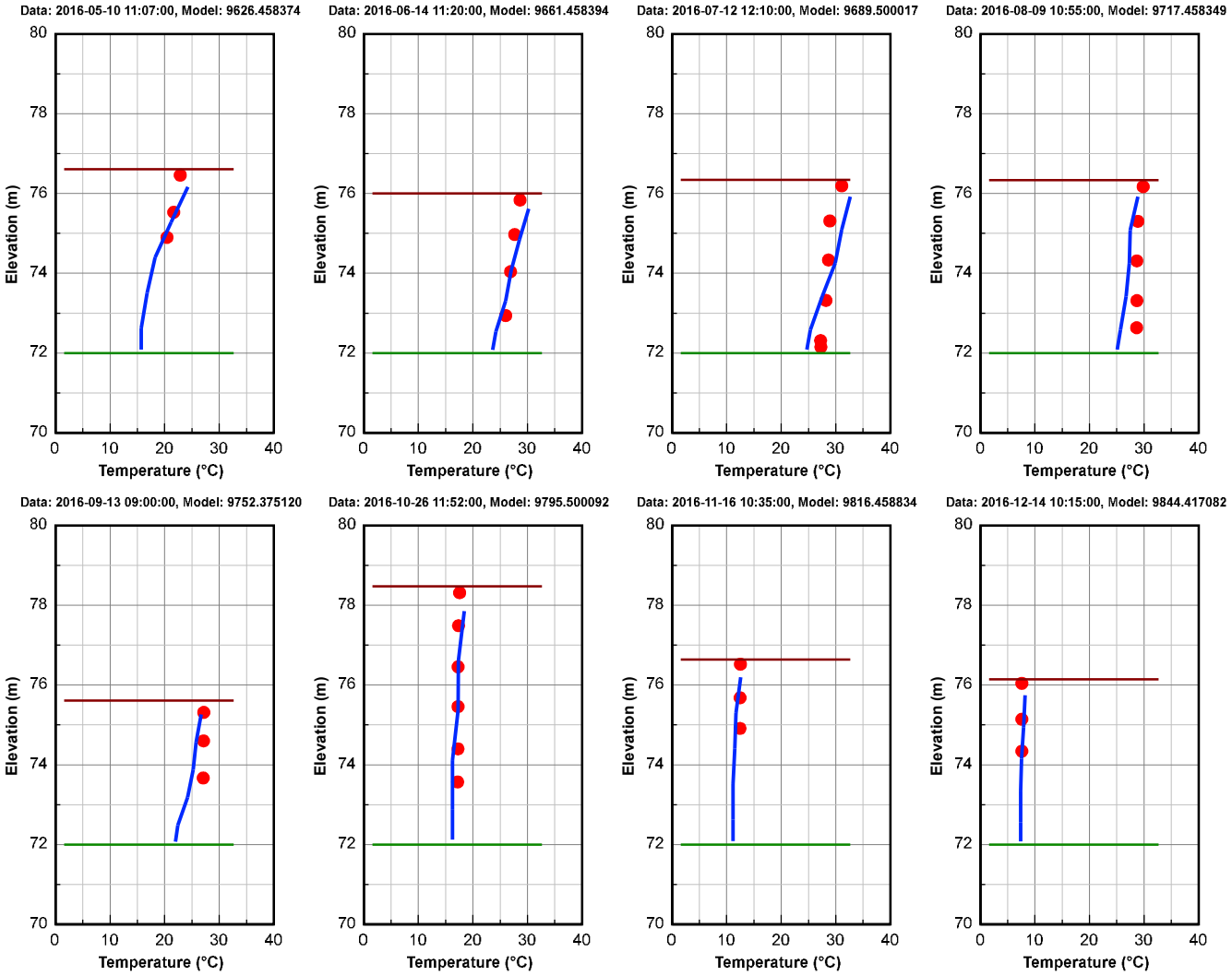

May 2016 – December 2016 (3 of 6)

Vertical Profile: NEU013, Model Cell: 42, 17

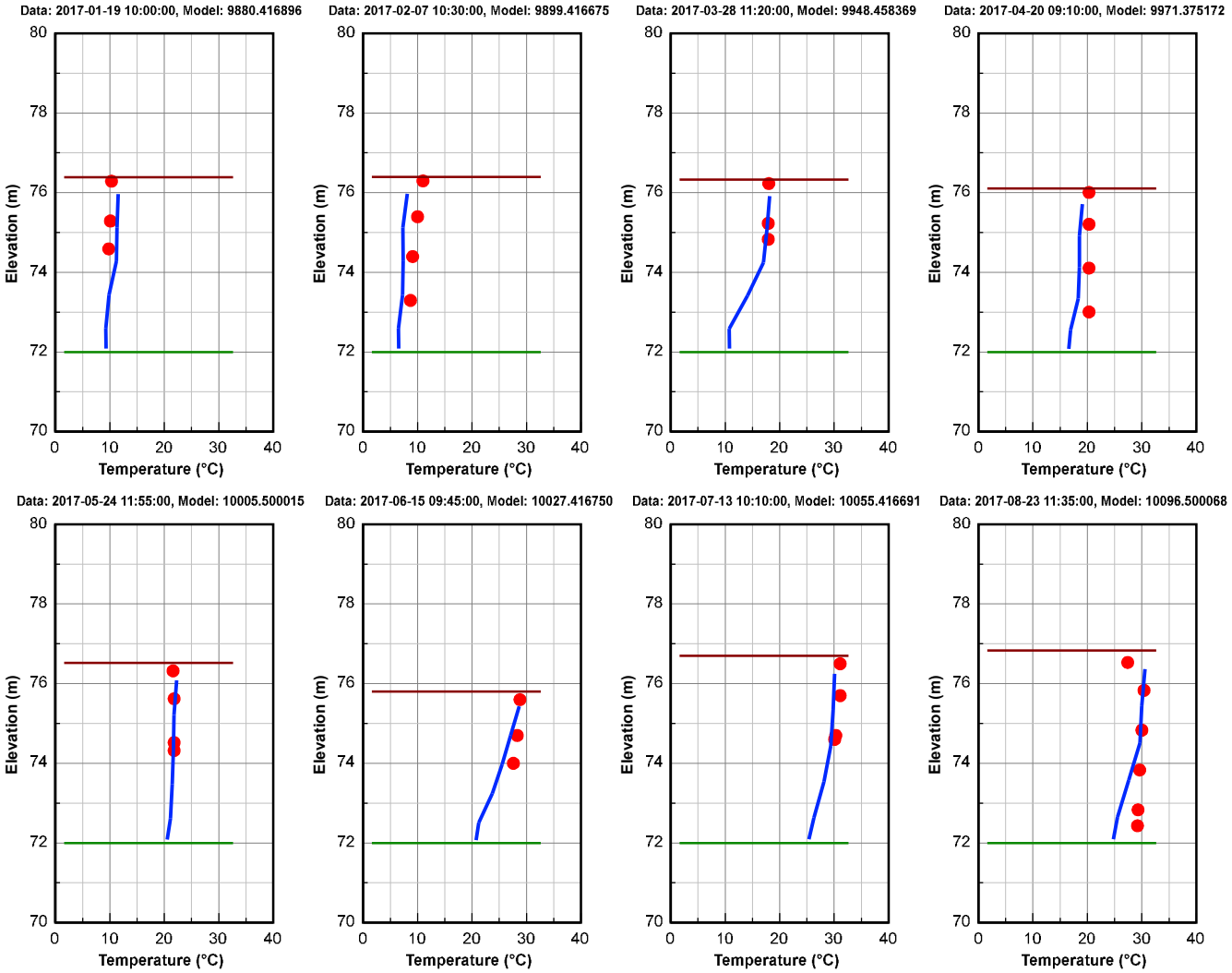

January 2017 – August 2017 (4 of 6)

Vertical Profile: NEU013, Model Cell: 42, 17

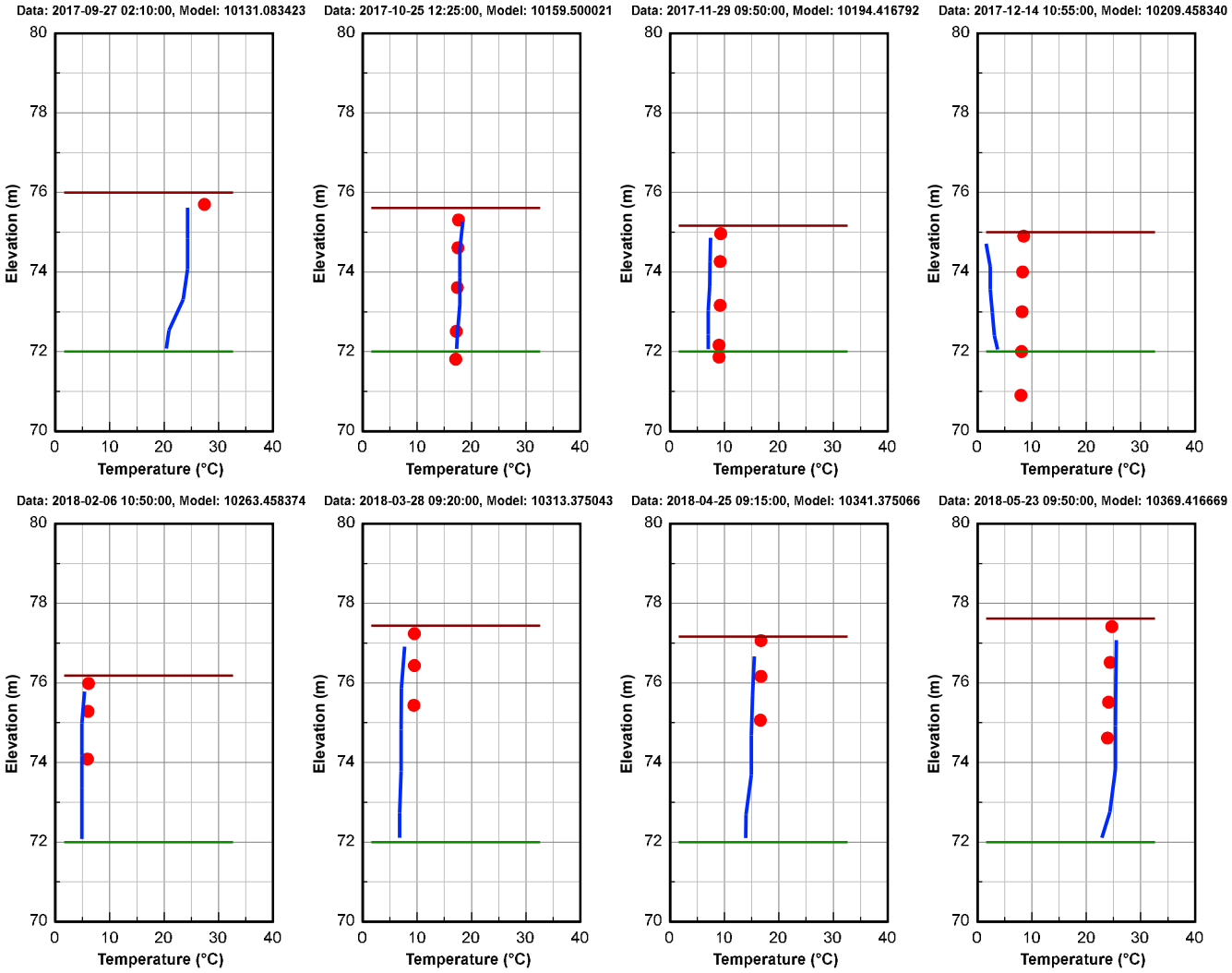

September 2017 – May 2018 (5 of 6)

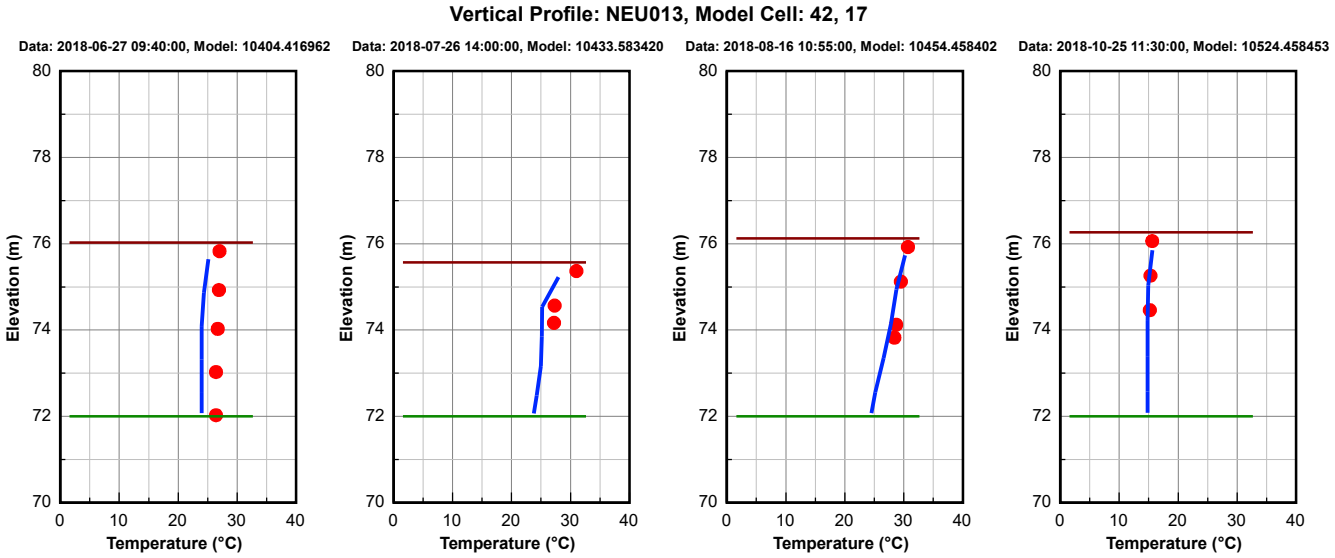

June 2018 – October 2018 (6 of 6)

Figure 1-4 Water Temperature Vertical Profile Comparison Plot at Station NEU013 during the calibration and validation period. Red dots are data, and blue continuous lines are model results.

Vertical Profile: NEU0171B, Model Cell: 42, 36

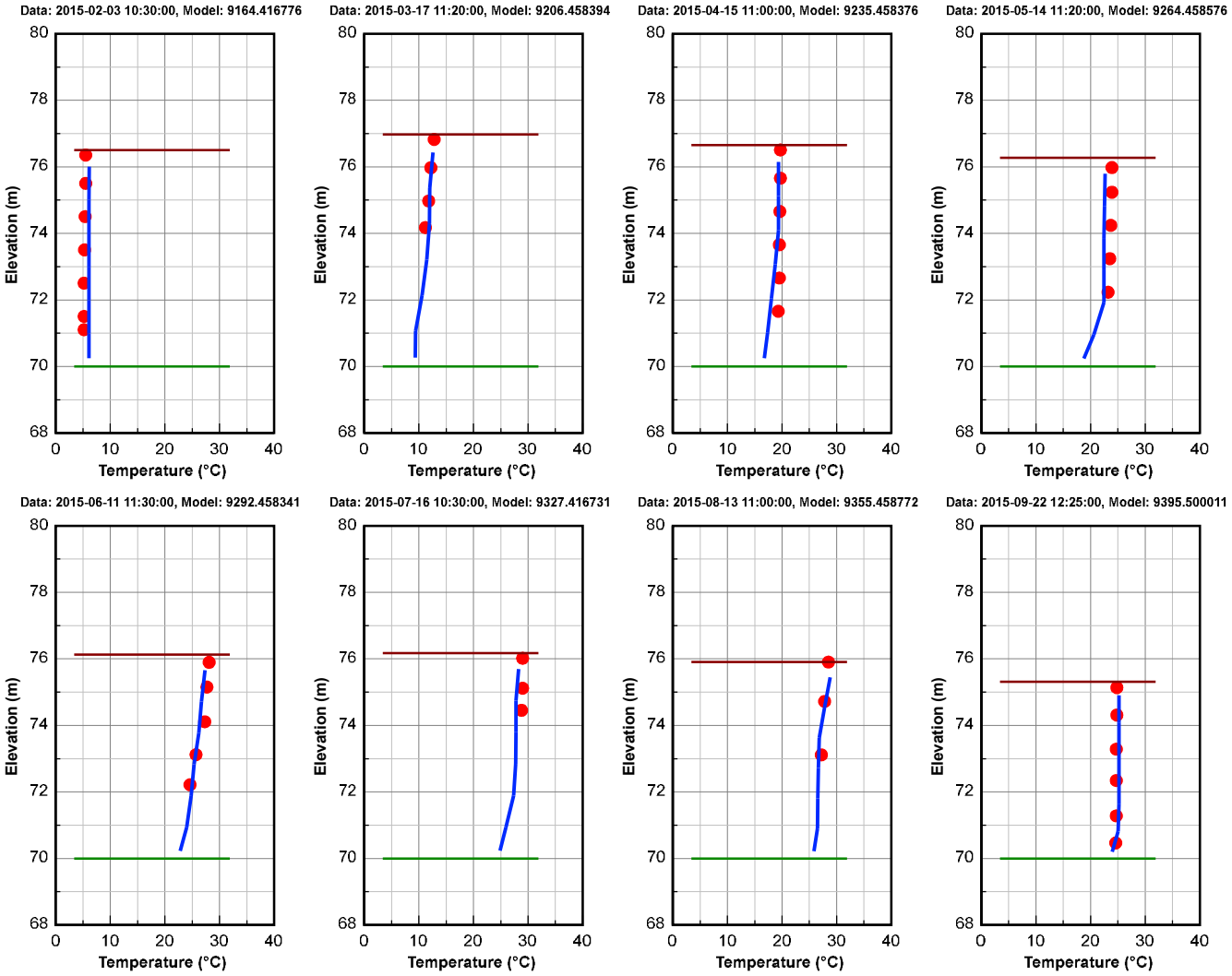

February 2015 – September 2015 (1 of 6)

Vertical Profile: NEU0171B, Model Cell: 42, 36

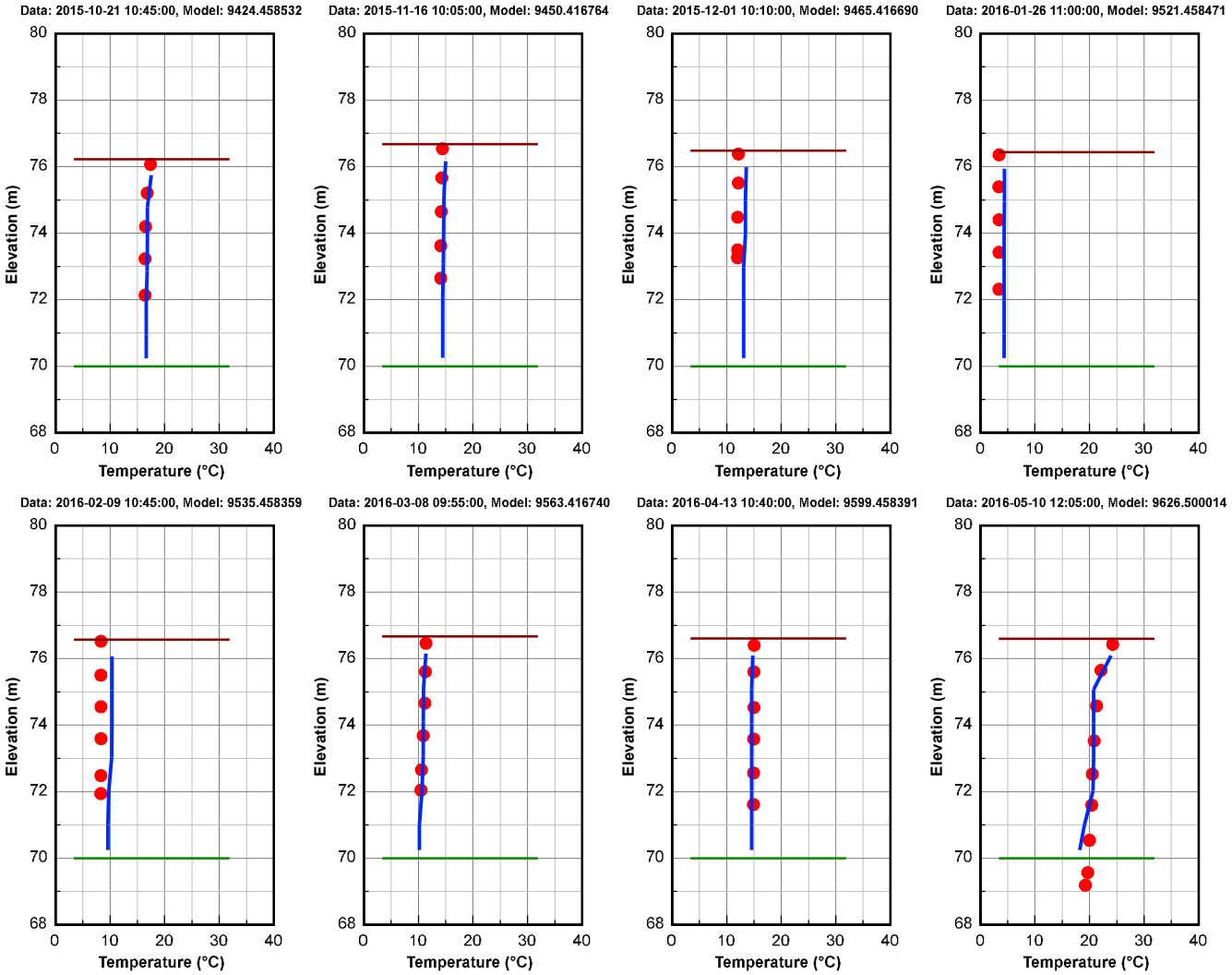

October 2015 – May 2016 (2 of 6)

Vertical Profile: NEU0171B, Model Cell: 42, 36

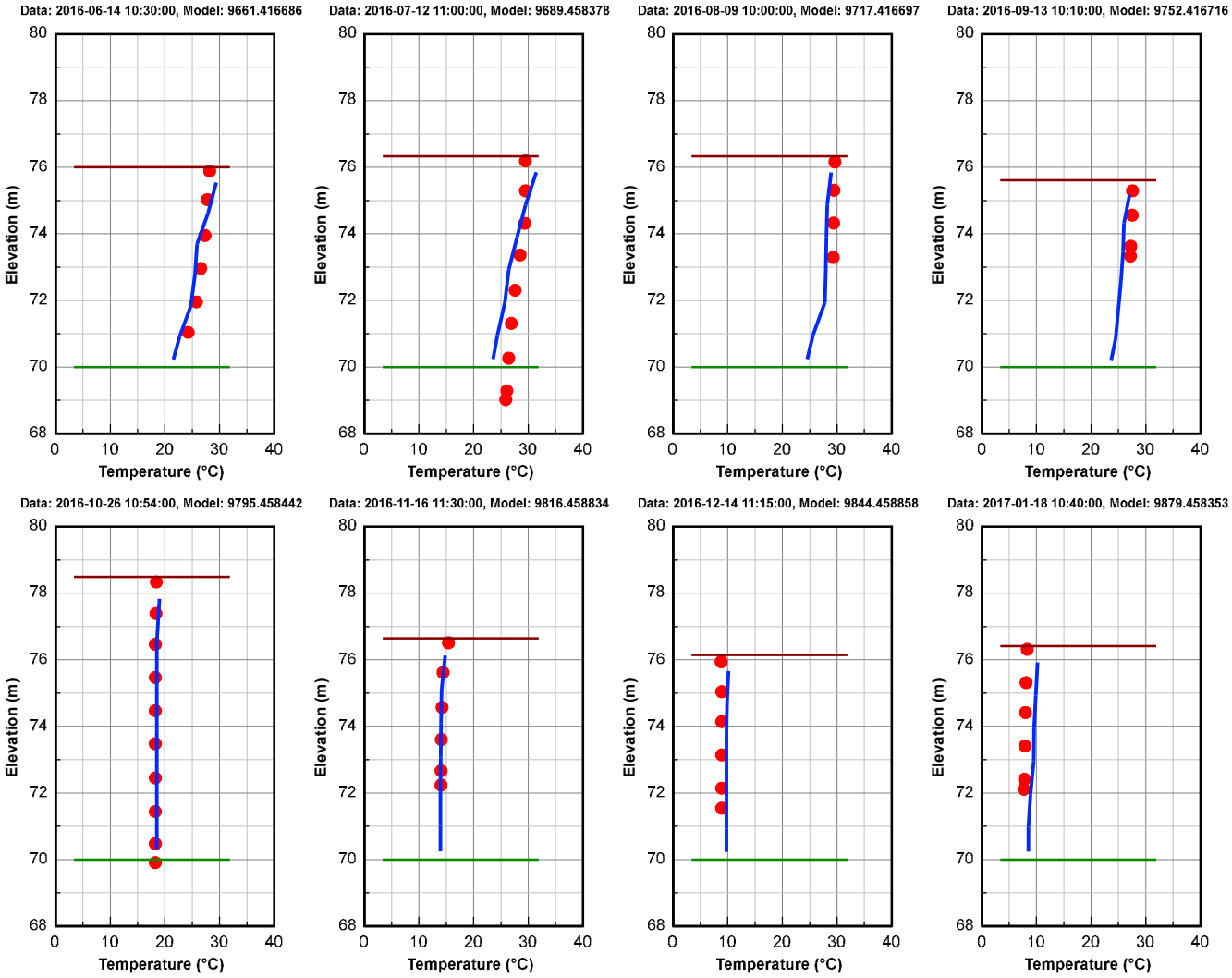

June 2016 – January 2017 (3 of 6)

Vertical Profile: NEU0171B, Model Cell: 42, 36

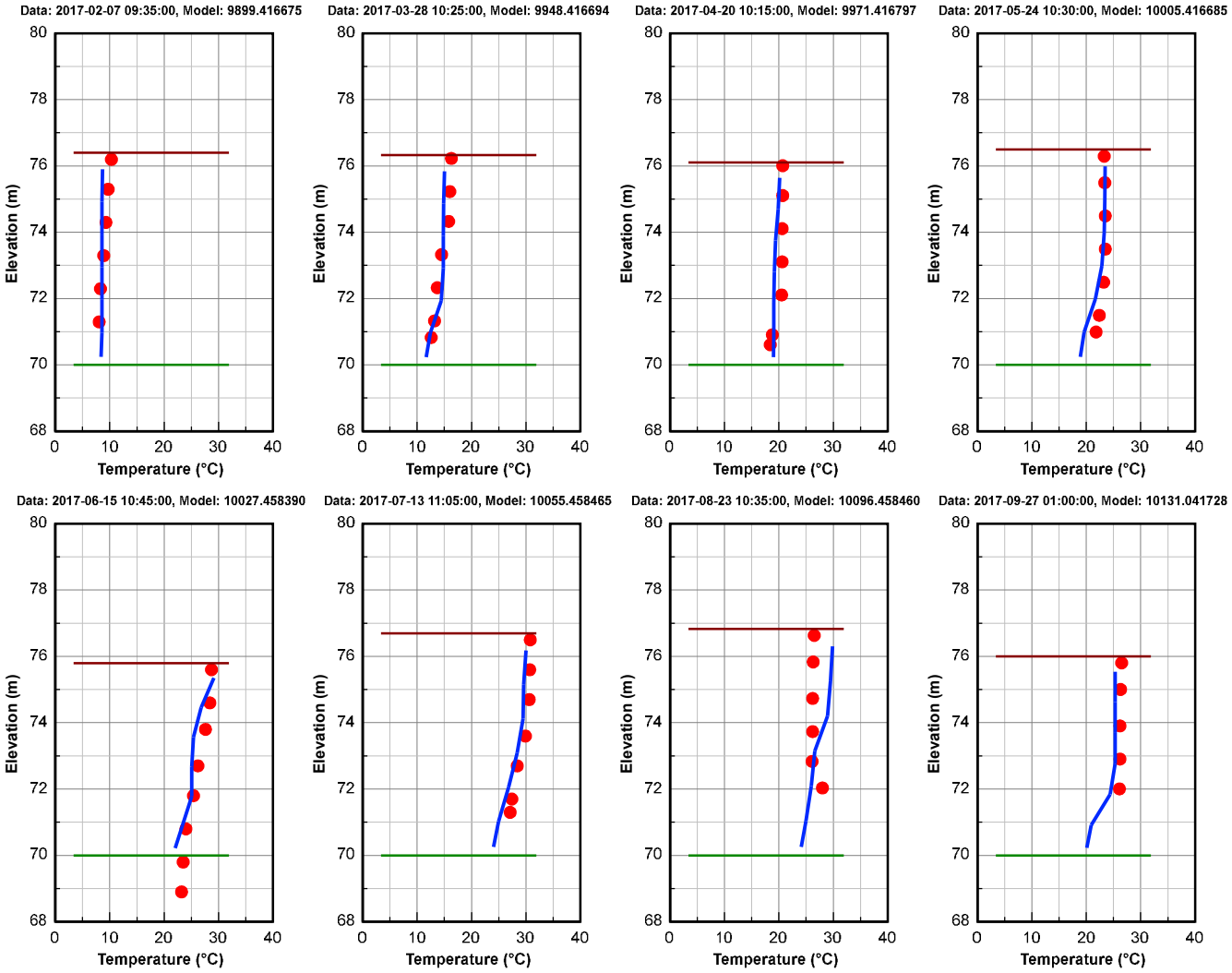

February 2017 – September 2017 (4 of 6)

Vertical Profile: NEU0171B, Model Cell: 42, 36

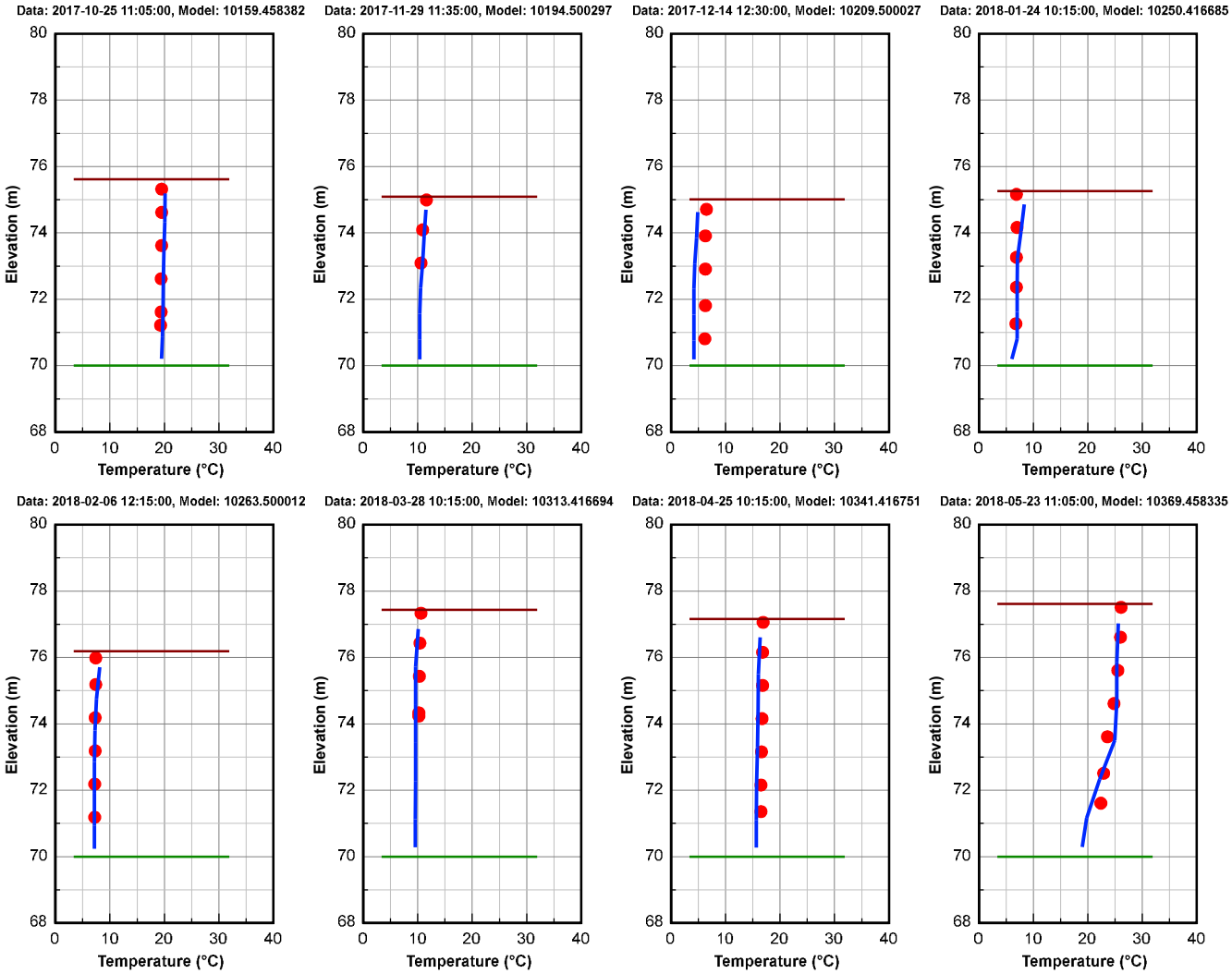

October 2017 – May 2018 (5 of 6)

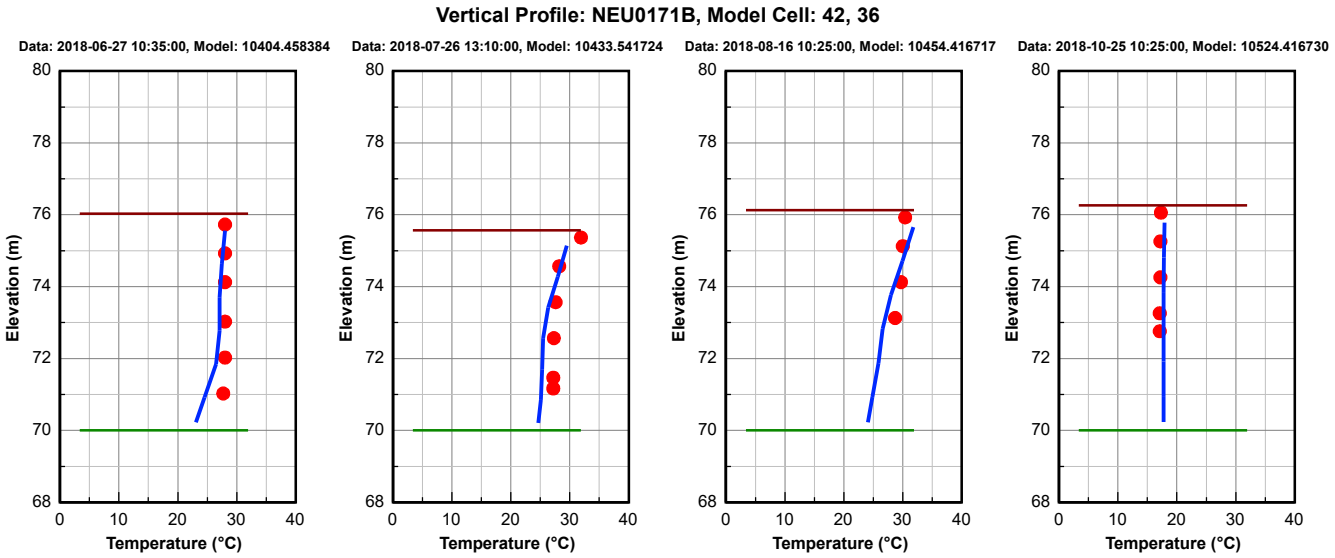

June 2018 – October 2018 (6 of 6)

Figure 1-5 Water Temperature Vertical Profile Comparison Plot at Station NEU0171B during the calibration and validation period. Red dots are data, and blue continuous lines are model results.

Vertical Profile: NEU018C, Model Cell: 35, 35

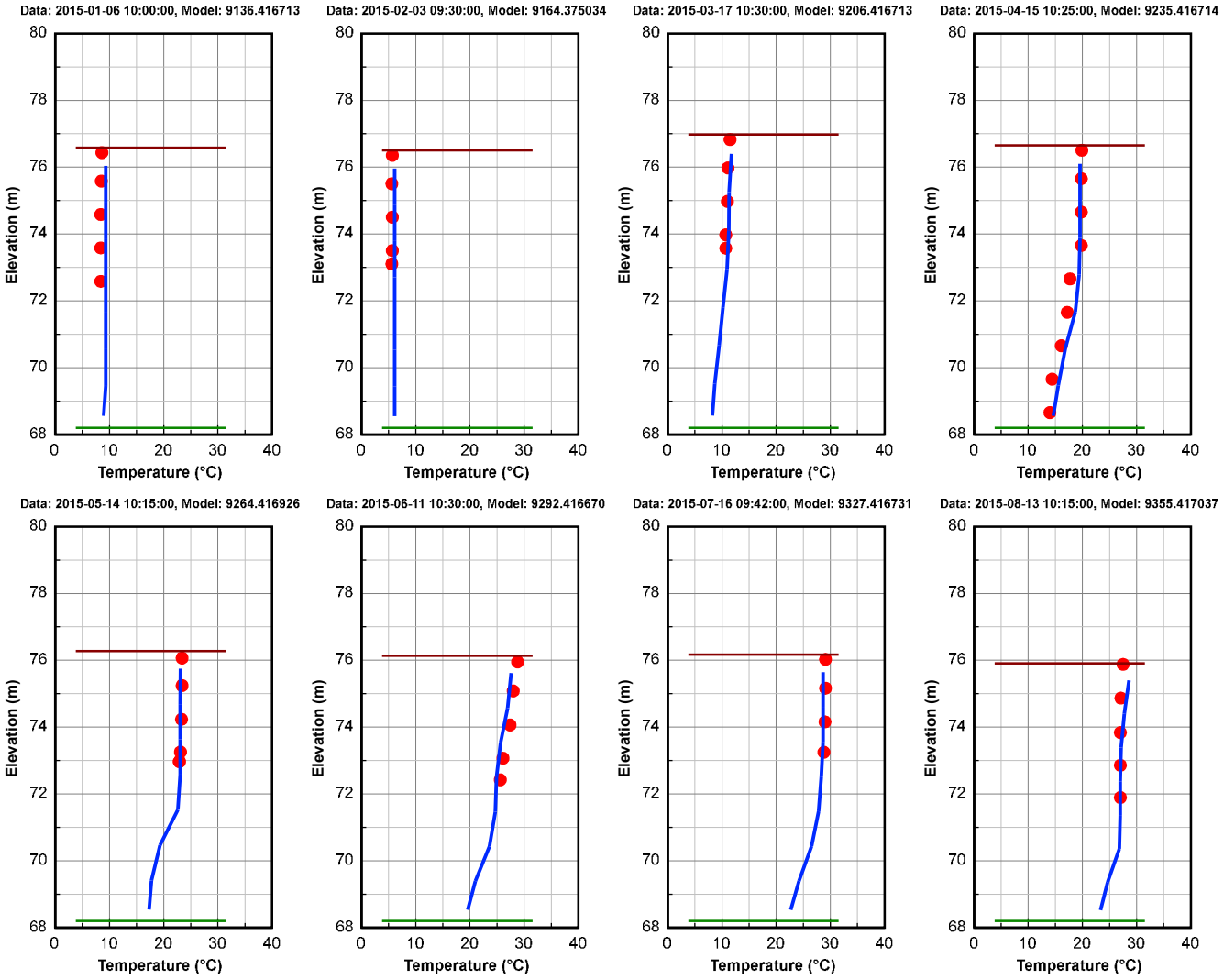

January 2015 – August 2015 (1 of 6)

Vertical Profile: NEU018C, Model Cell: 35, 35

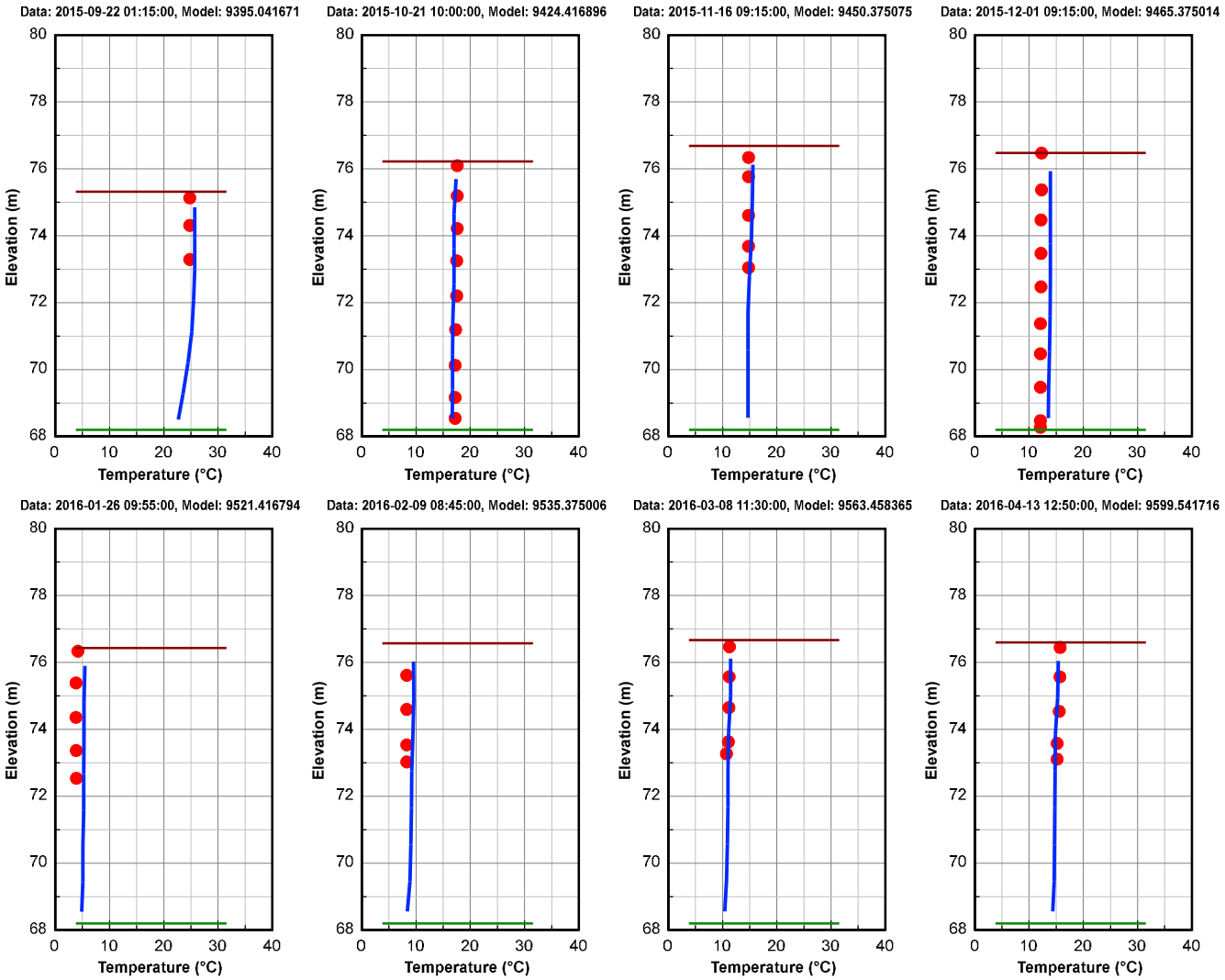

September 2015 – April 2016 (2 of 6)

Vertical Profile: NEU018C, Model Cell: 35, 35

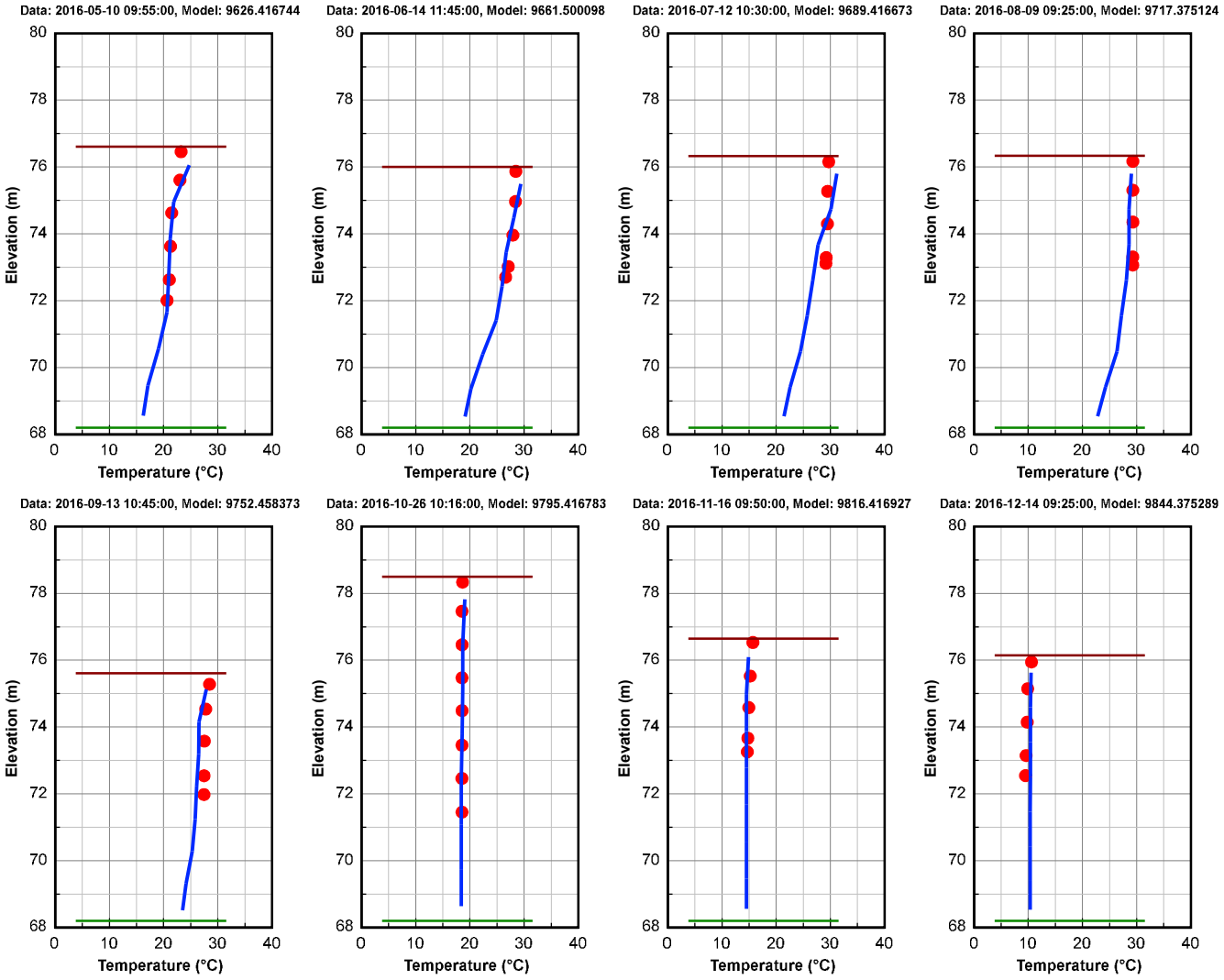

May 2016 – December 2016 (3 of 6)

Vertical Profile: NEU018C, Model Cell: 35, 35

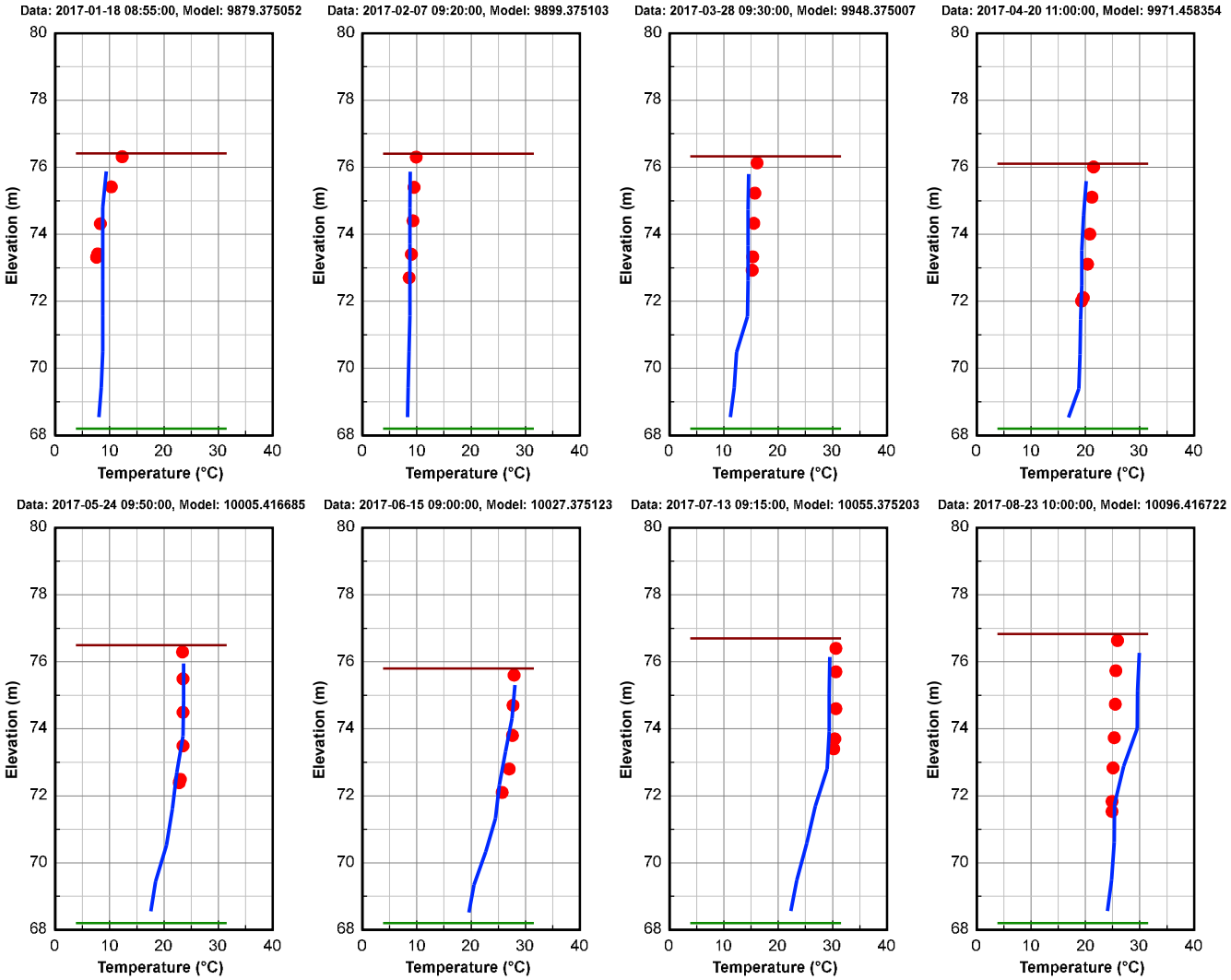

January 2017 – August 2017 (4 of 6)

Vertical Profile: NEU018C, Model Cell: 35, 35

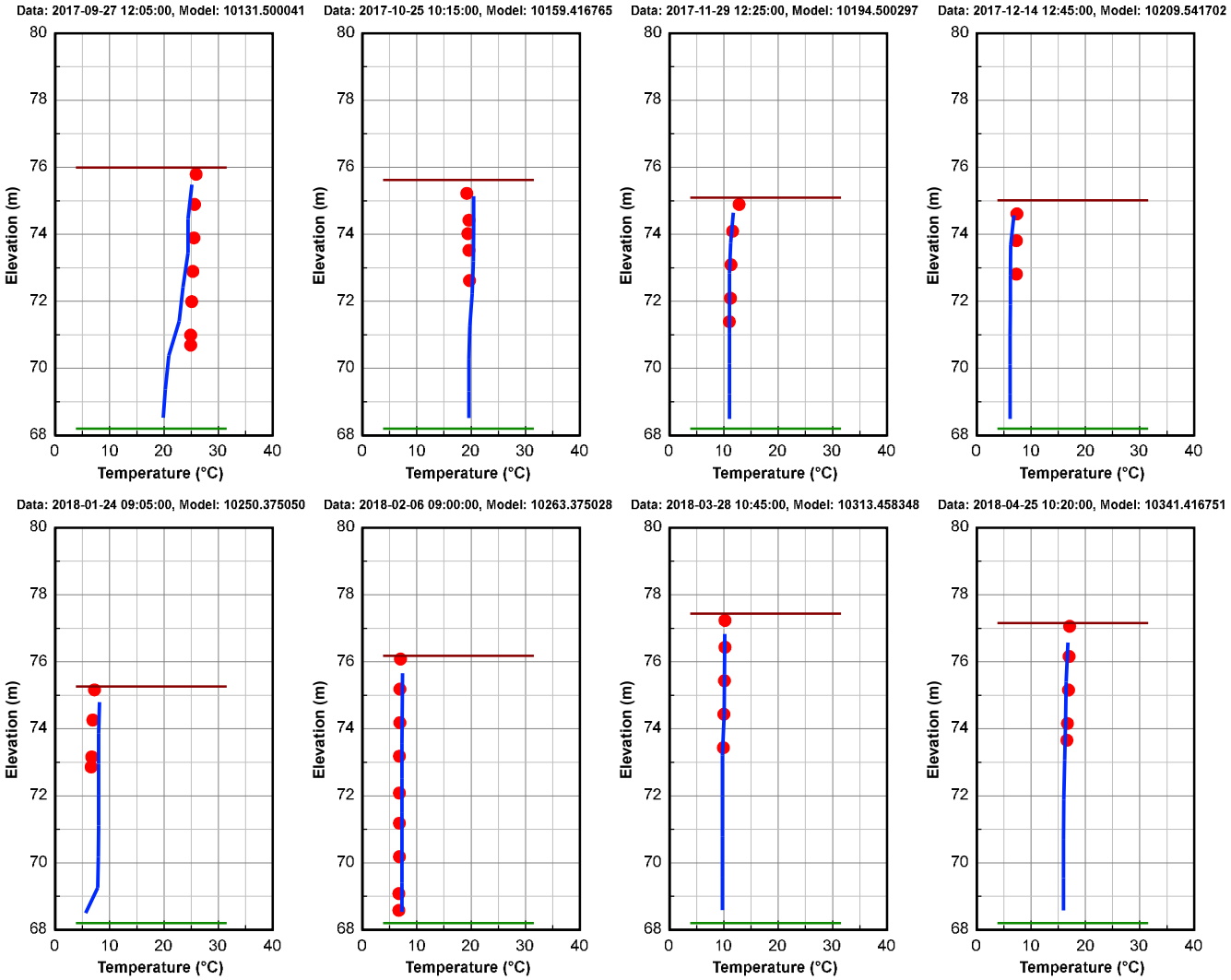

September 2017 – April 2018 (5 of 6)

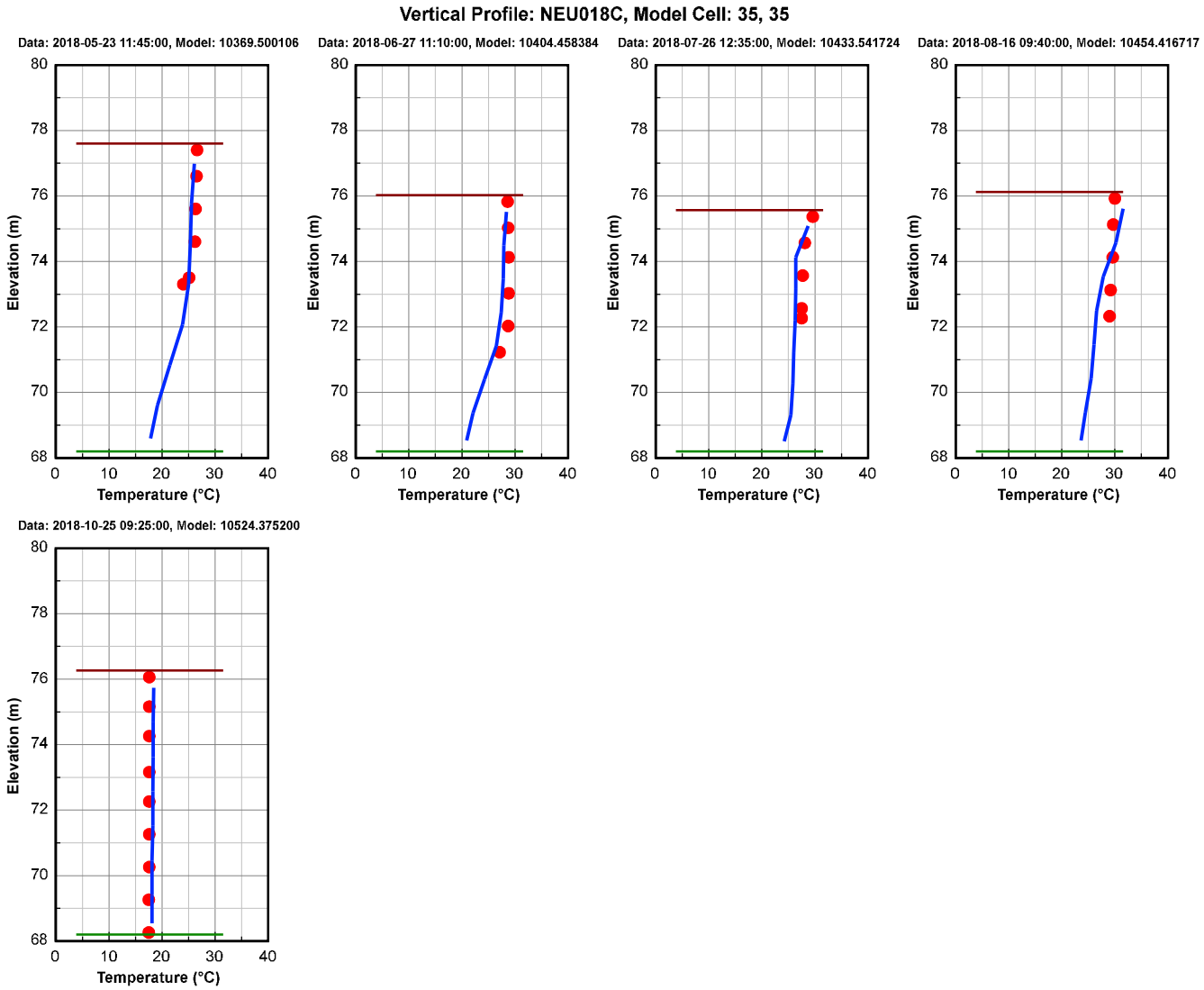

May 2018 – October 2018 (6 of 6)

Figure 1-6 Water Temperature Vertical Profile Comparison Plot at Station NEU018C during the calibration and validation period. Red dots are data, and blue continuous lines are model results.

Vertical Profile: NEU018E, Model Cell: 34, 40

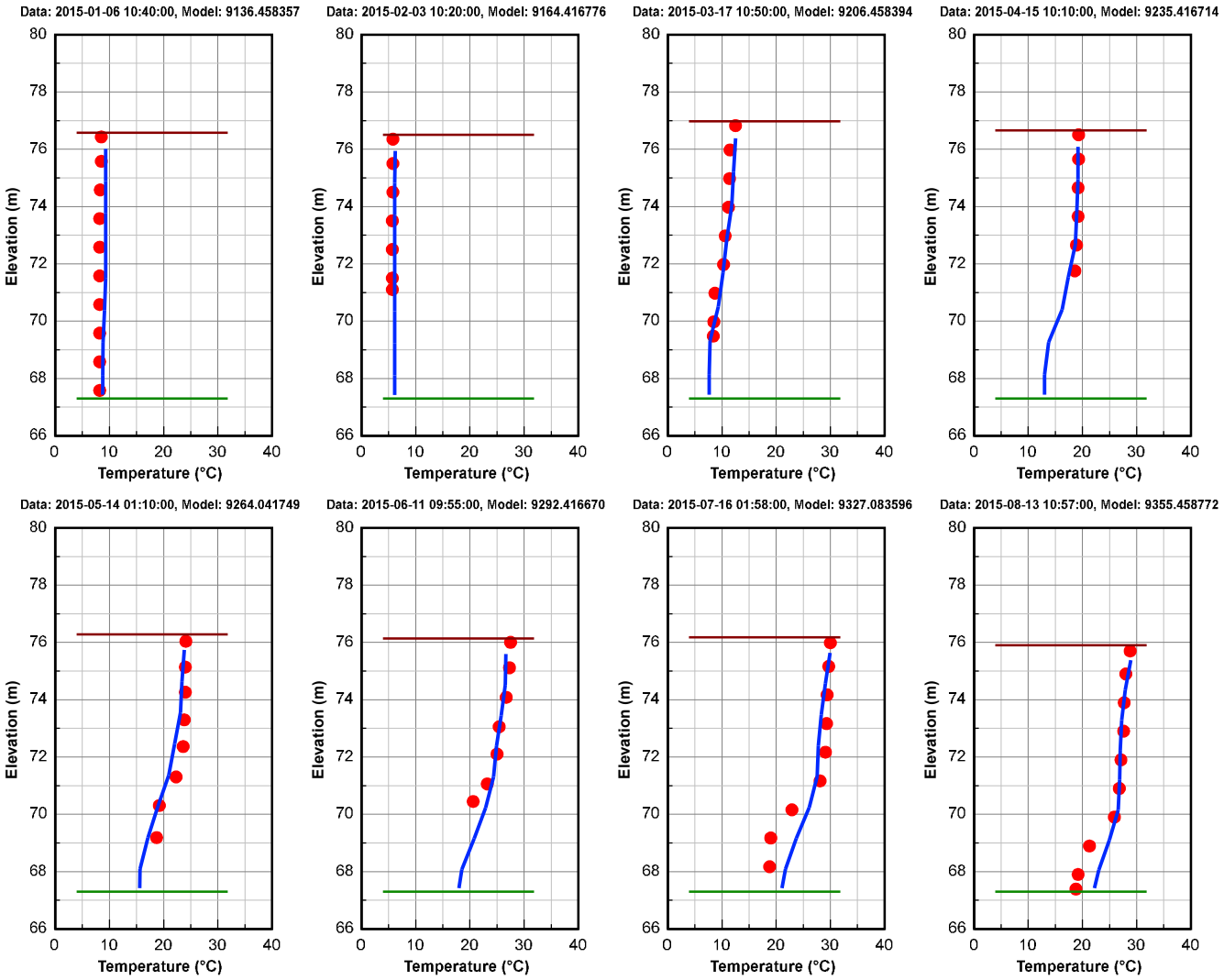

January 2015 – August 2015 (1 of 6)

Vertical Profile: NEU018E, Model Cell: 34, 40

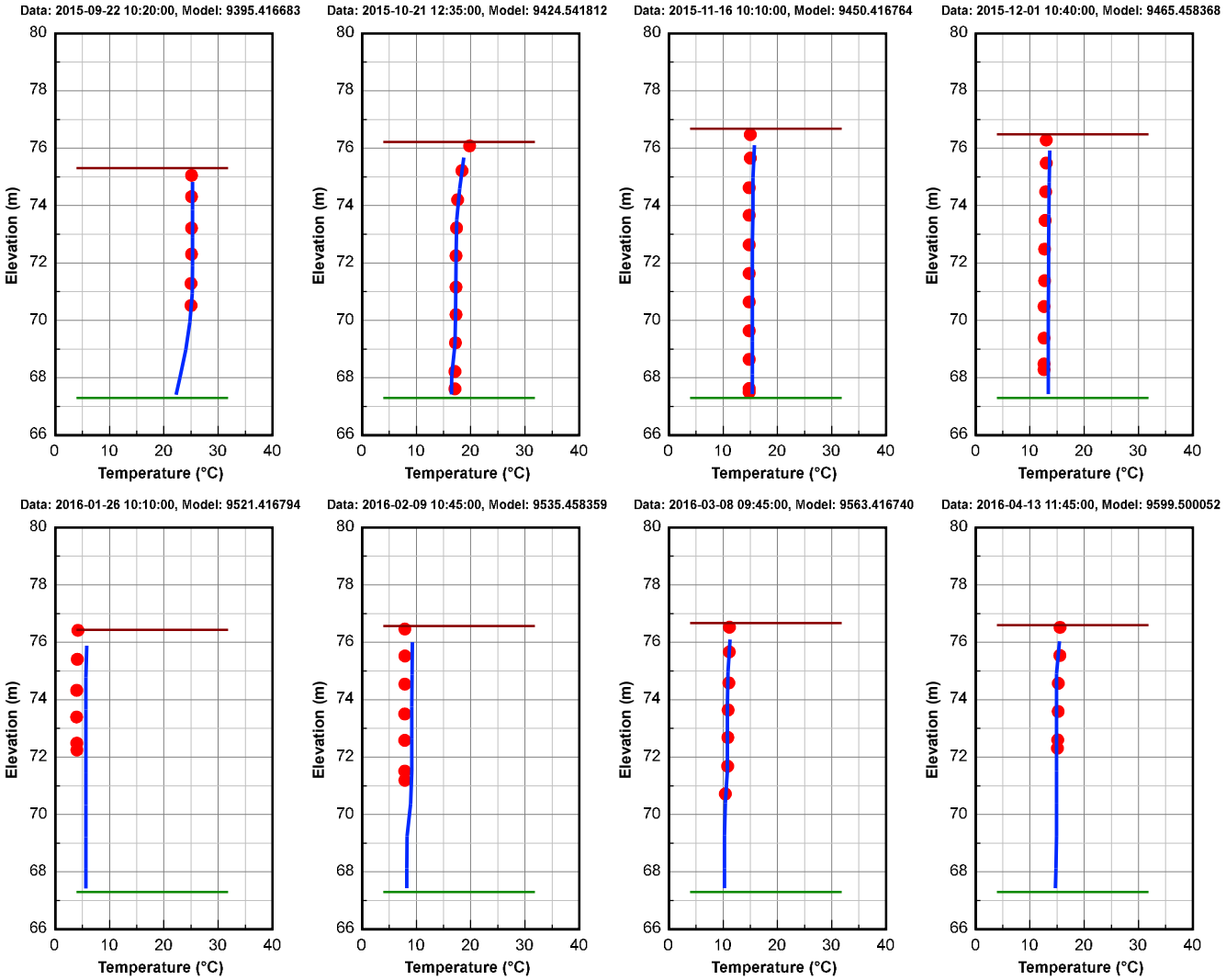

September 2015 – April 2016 (2 of 6)

Vertical Profile: NEU018E, Model Cell: 34, 40

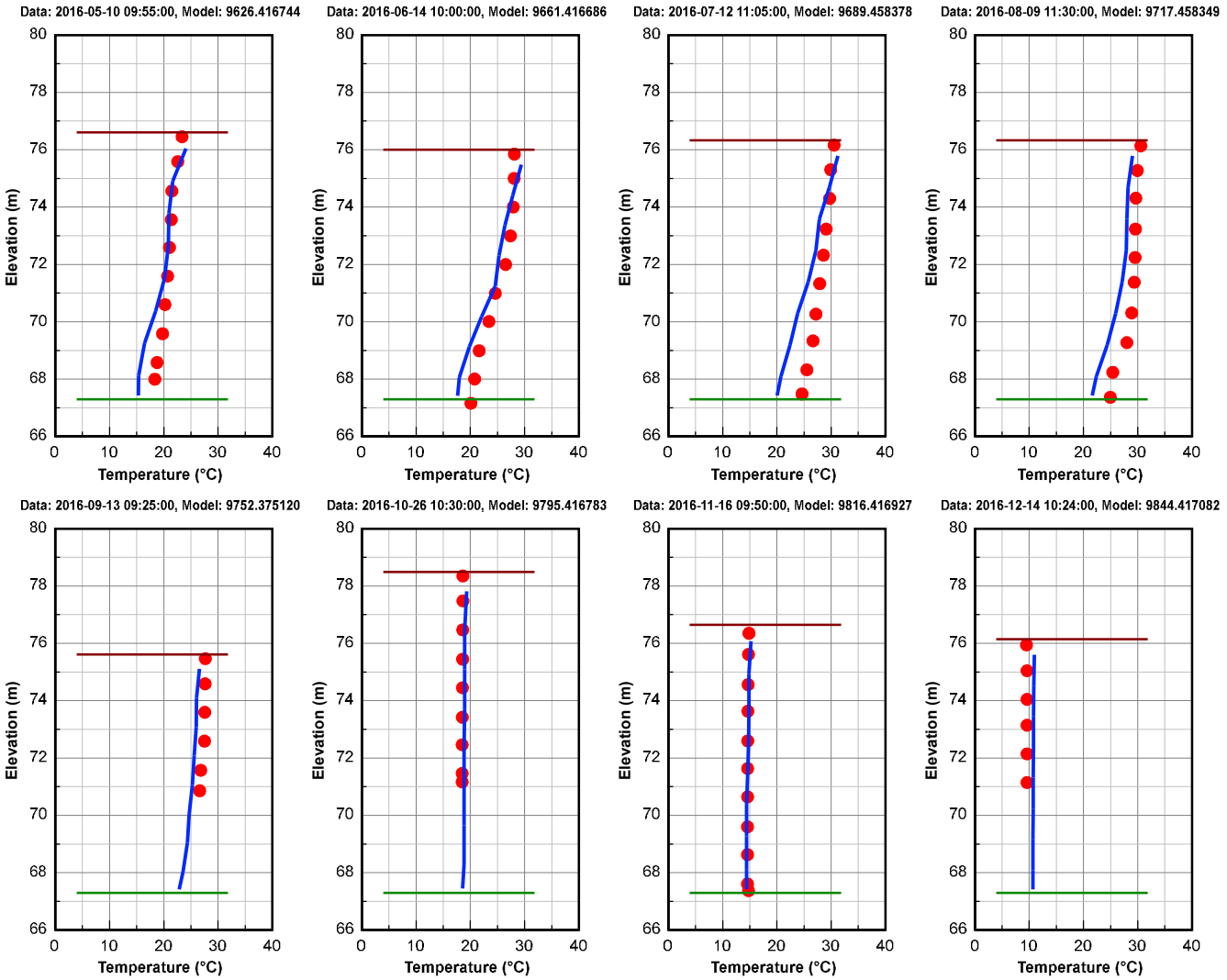

May 2016 – December 2016 (3 of 6)

Vertical Profile: NEU018E, Model Cell: 34, 40

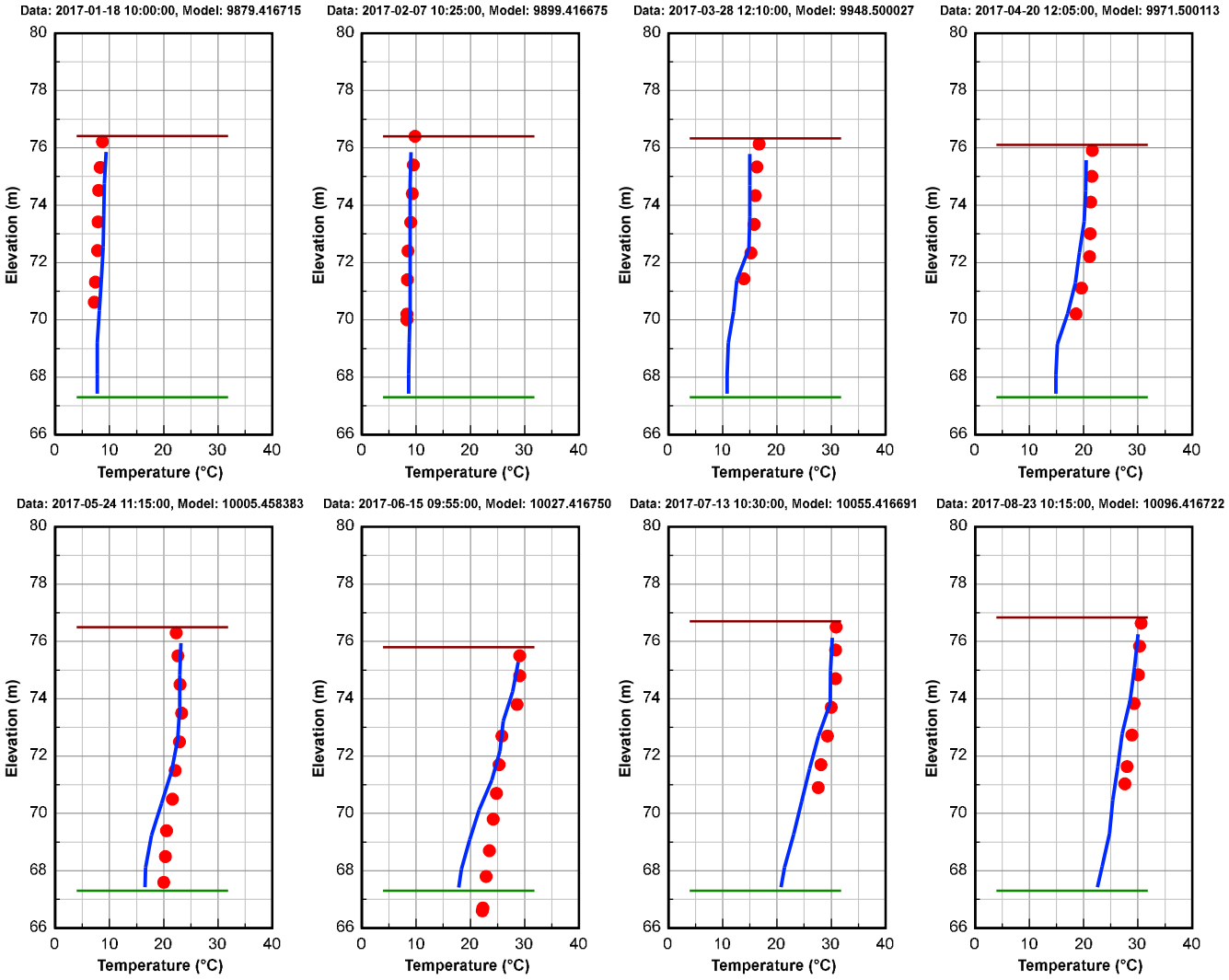

January 2017 – August 2017 (4 of 6)

Vertical Profile: NEU018E, Model Cell: 34, 40

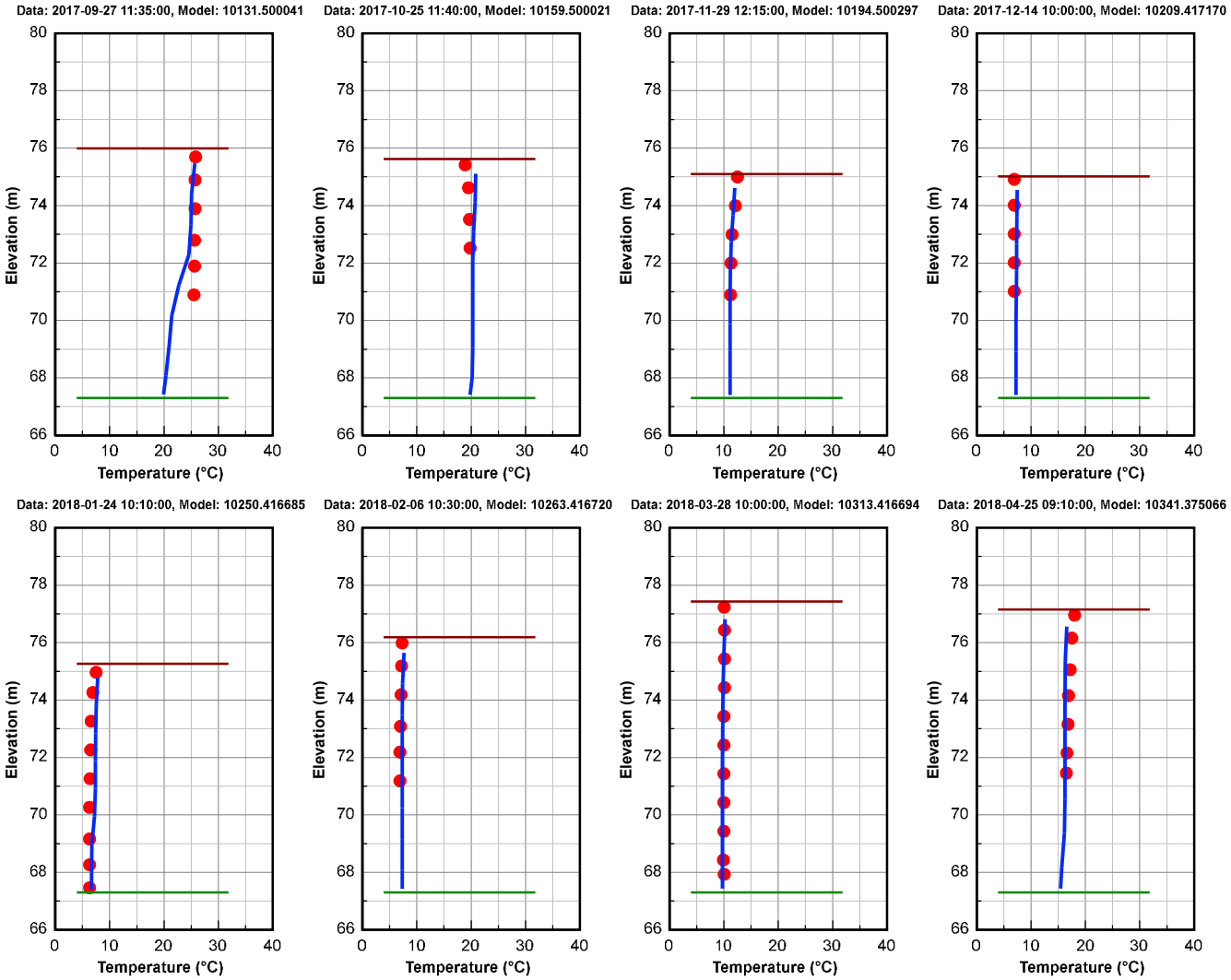

September 2017 – April 2018 (5 of 6)

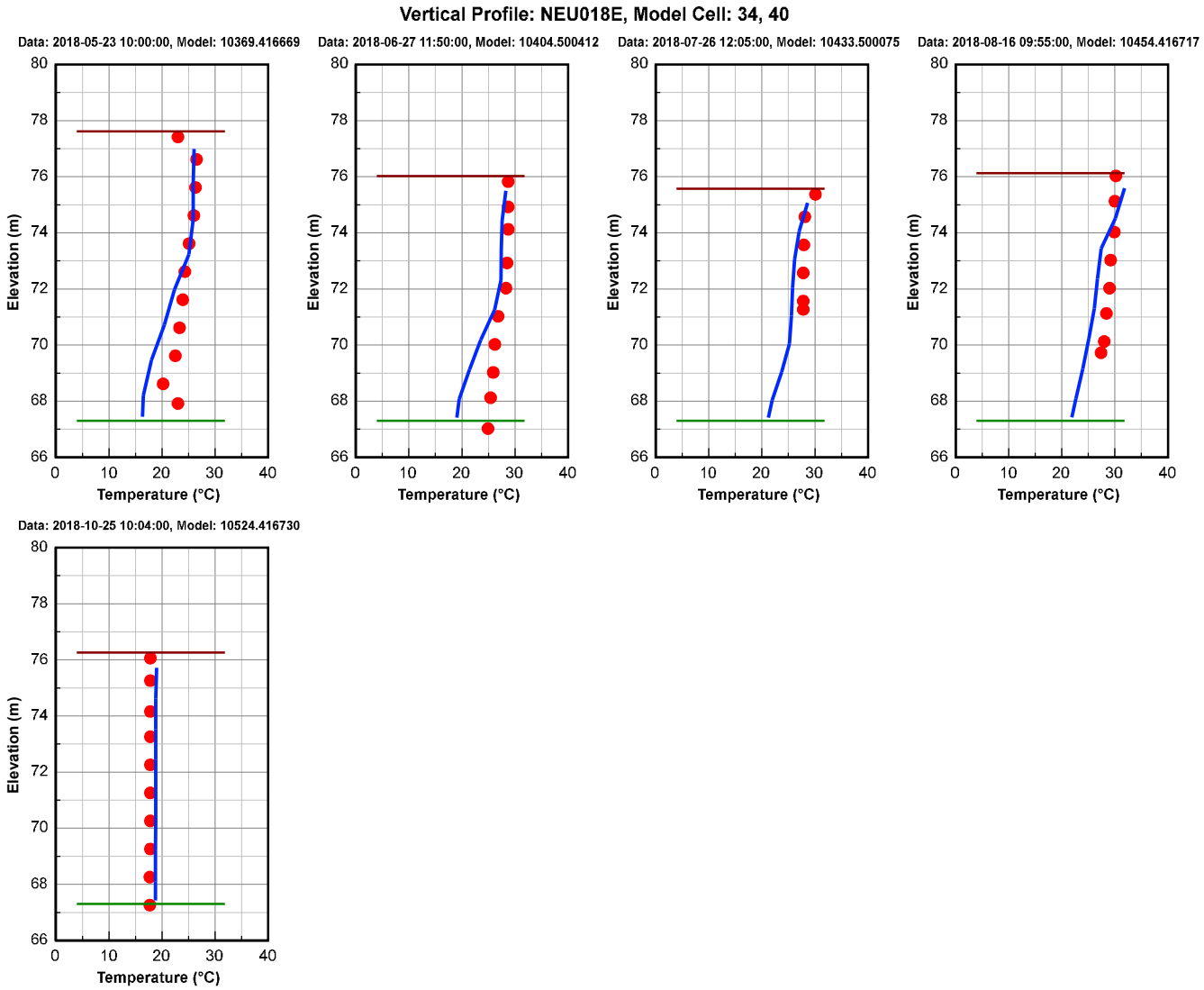

May 2018 – October 2018 (6 of 6)

Figure 1-7 Water Temperature Vertical Profile Comparison Plot at Station NEU018E during the calibration and validation period. Red dots are data, and blue continuous lines are model results.

Vertical Profile: NEU019E, Model Cell: 26, 43

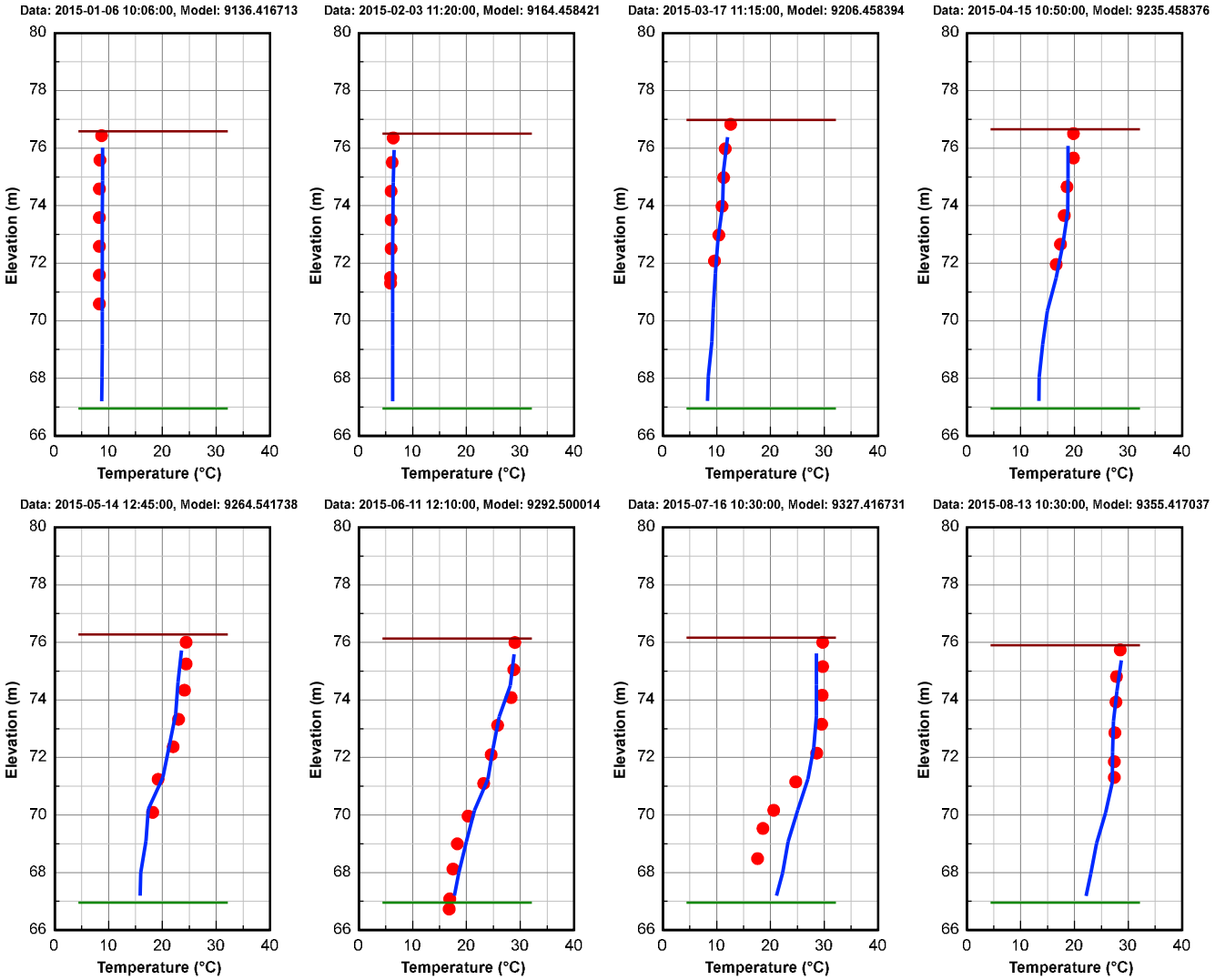

January 2015 – August 2015 (1 of 6)

Vertical Profile: NEU019E, Model Cell: 26, 43

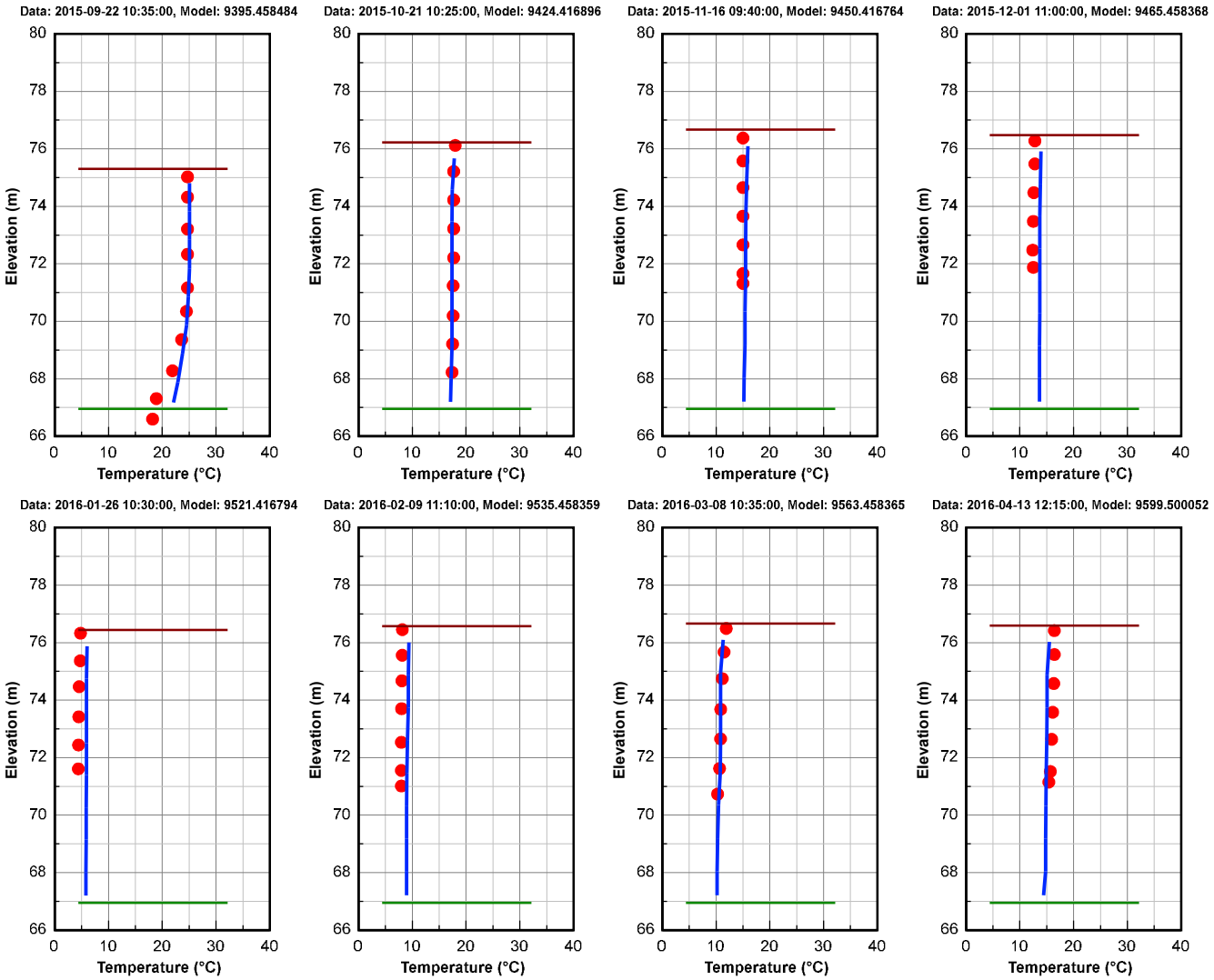

September 2015 – April 2016 (2 of 6)

Vertical Profile: NEU019E, Model Cell: 26, 43

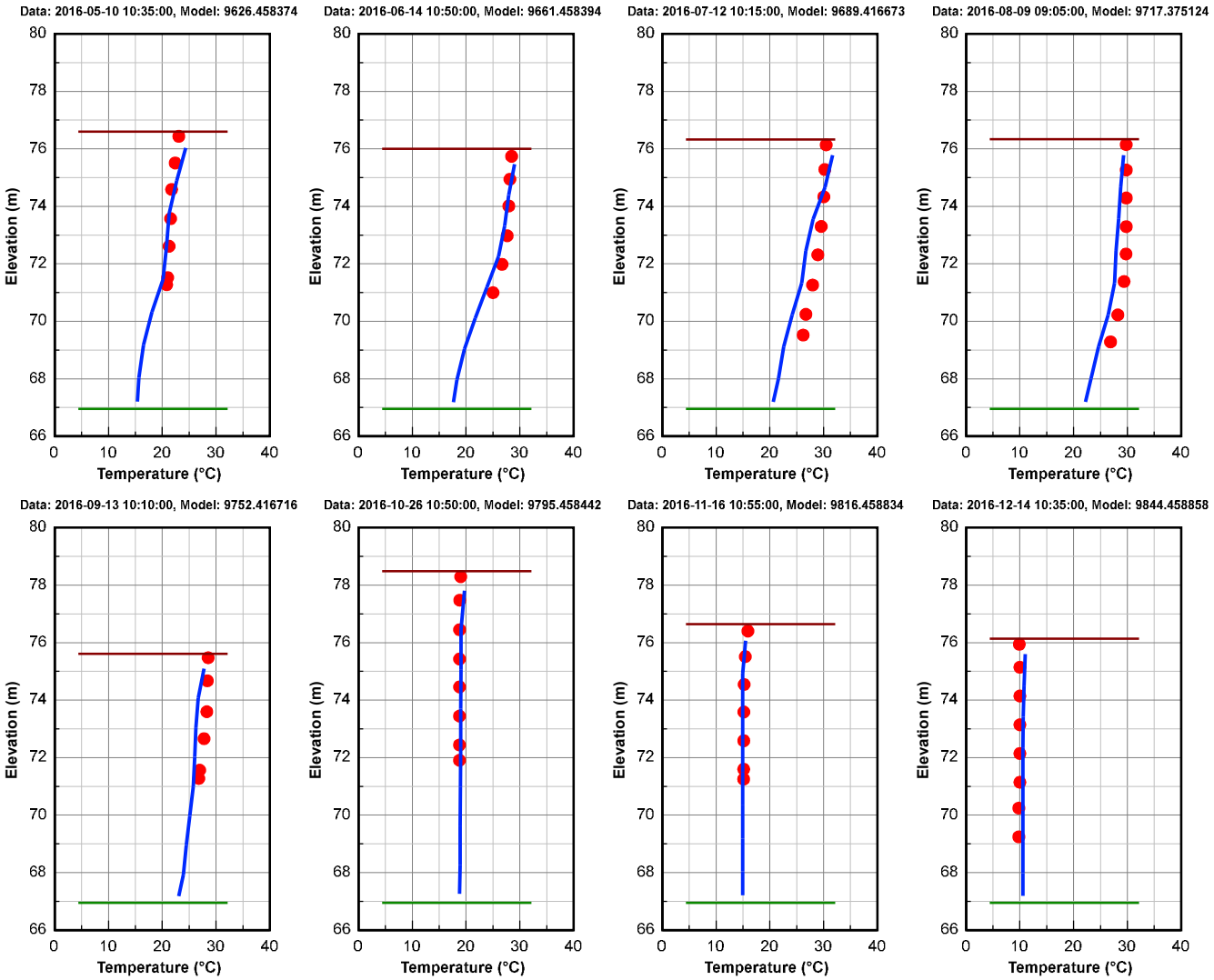

May 2016 – December 2016 (3 of 6)

Vertical Profile: NEU019E, Model Cell: 26, 43

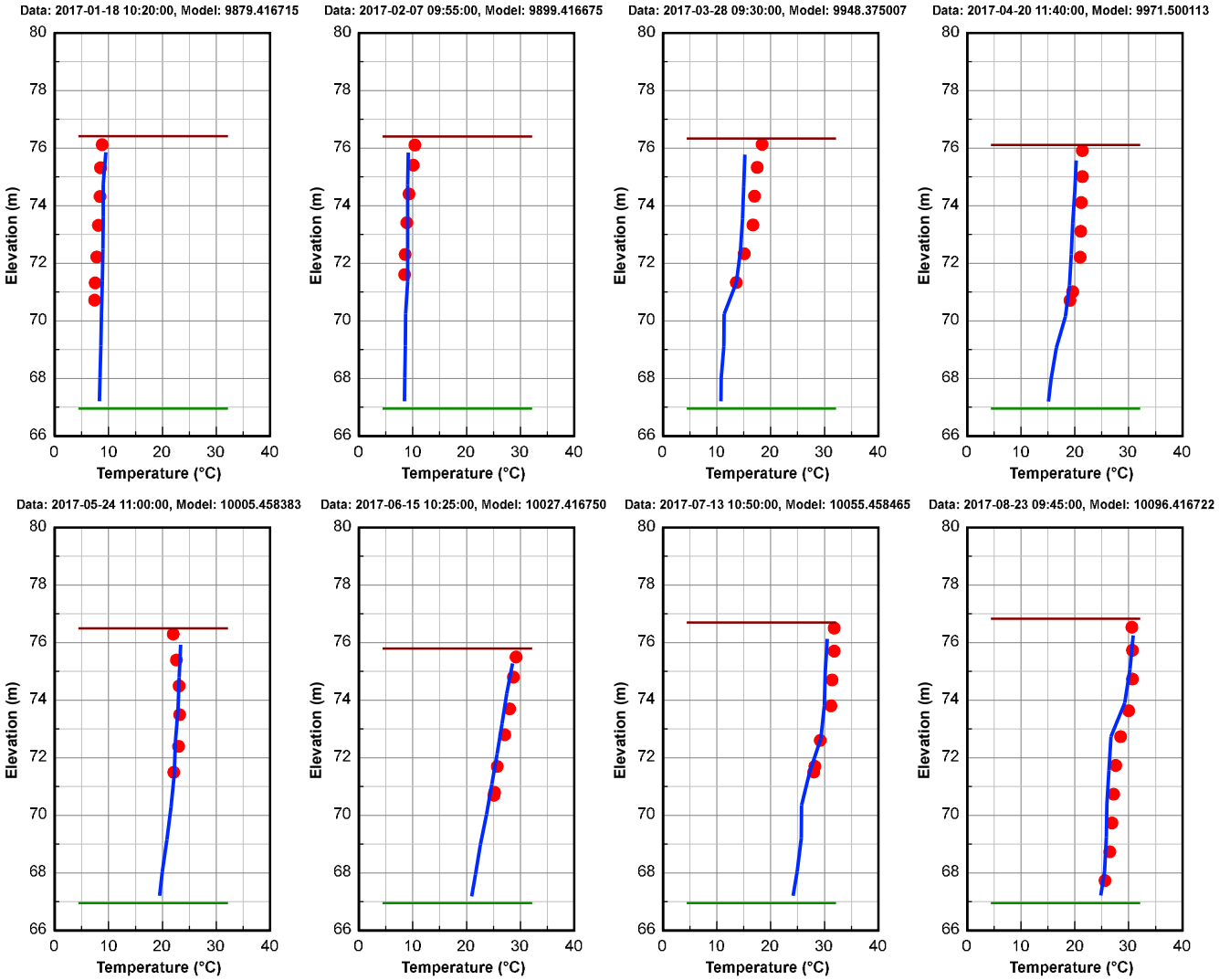

January 2017 – August 2017 (4 of 6)

Vertical Profile: NEU019E, Model Cell: 26, 43

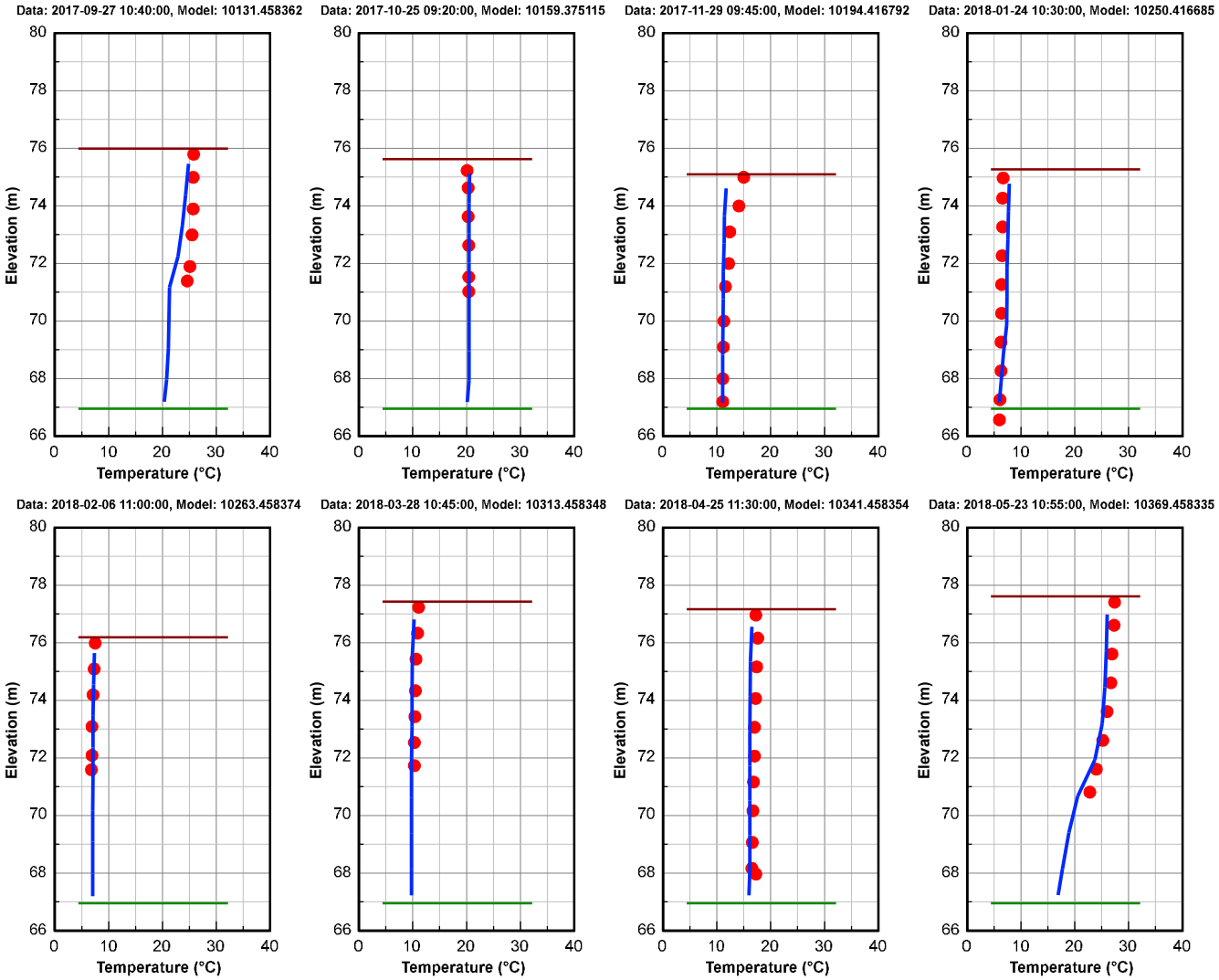

September 2017 – May 2018 (5 of 6)

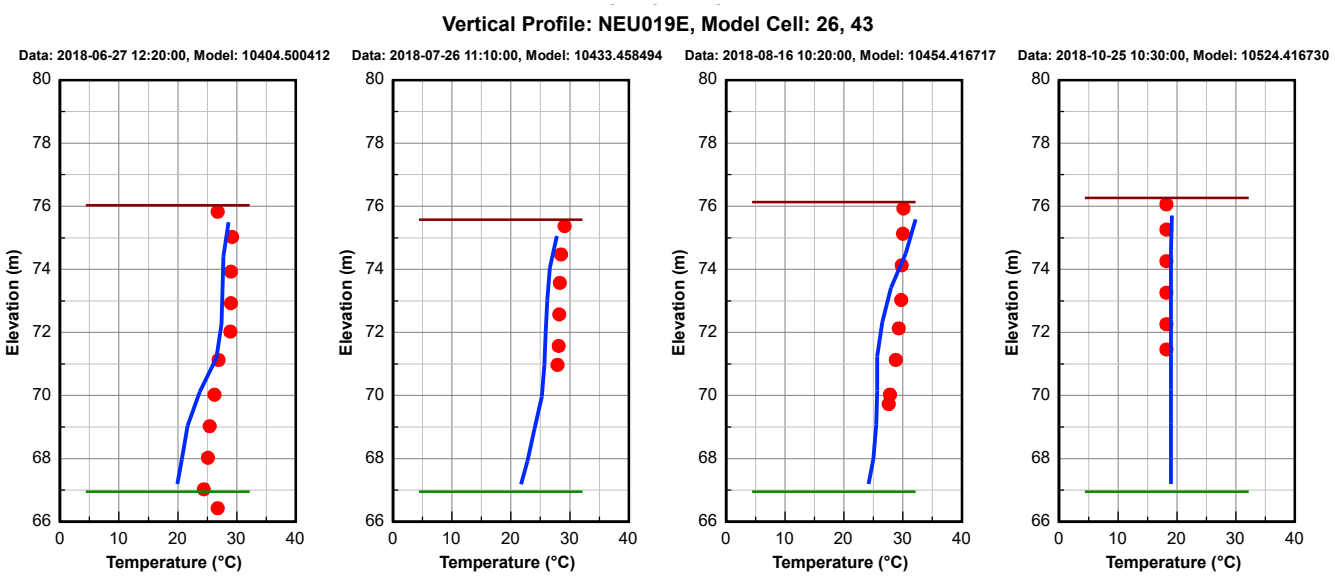

June 2018 – October 2018 (6 of 6)

Figure 1-8 Water Temperature Vertical Profile Comparison Plot at Station NEU019E during the calibration and validation period. Red dots are data, and blue continuous lines are model results.

Vertical Profile: NEU019L, Model Cell: 33, 75

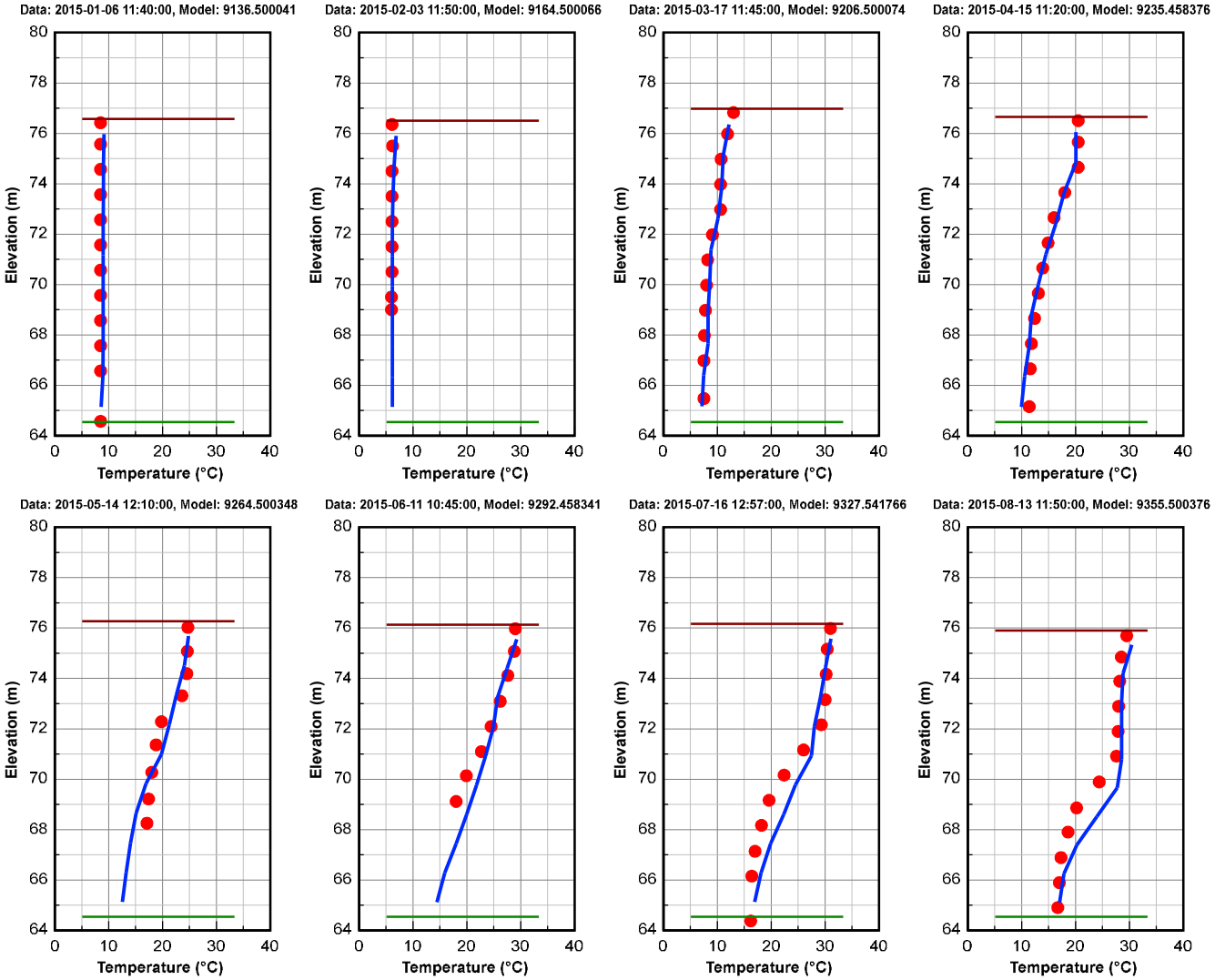

January 2015 – August 2015 (1 of 6)

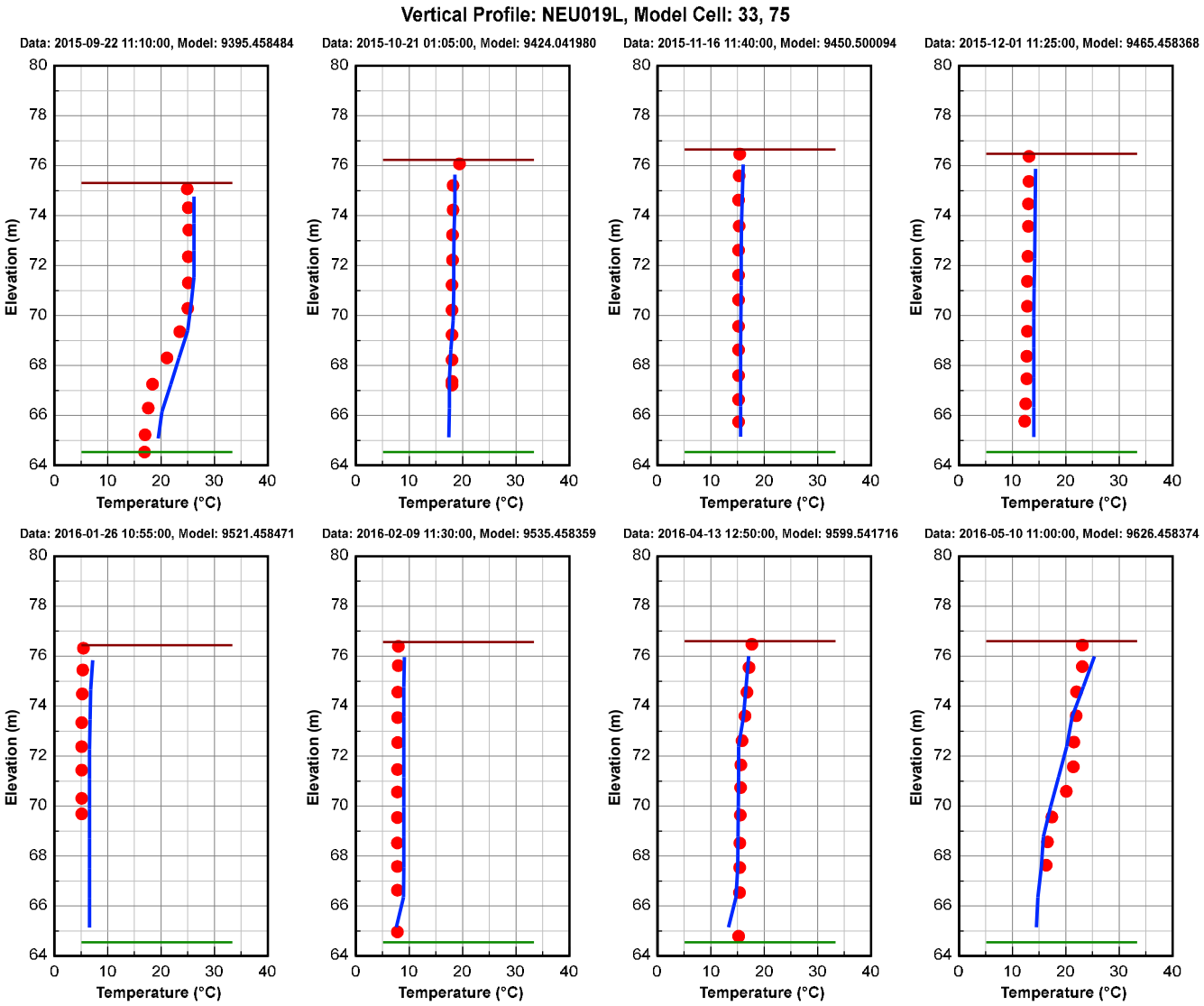

September 2015 – May 2016 (2 of 6)

Vertical Profile: NEU019L, Model Cell: 33, 75

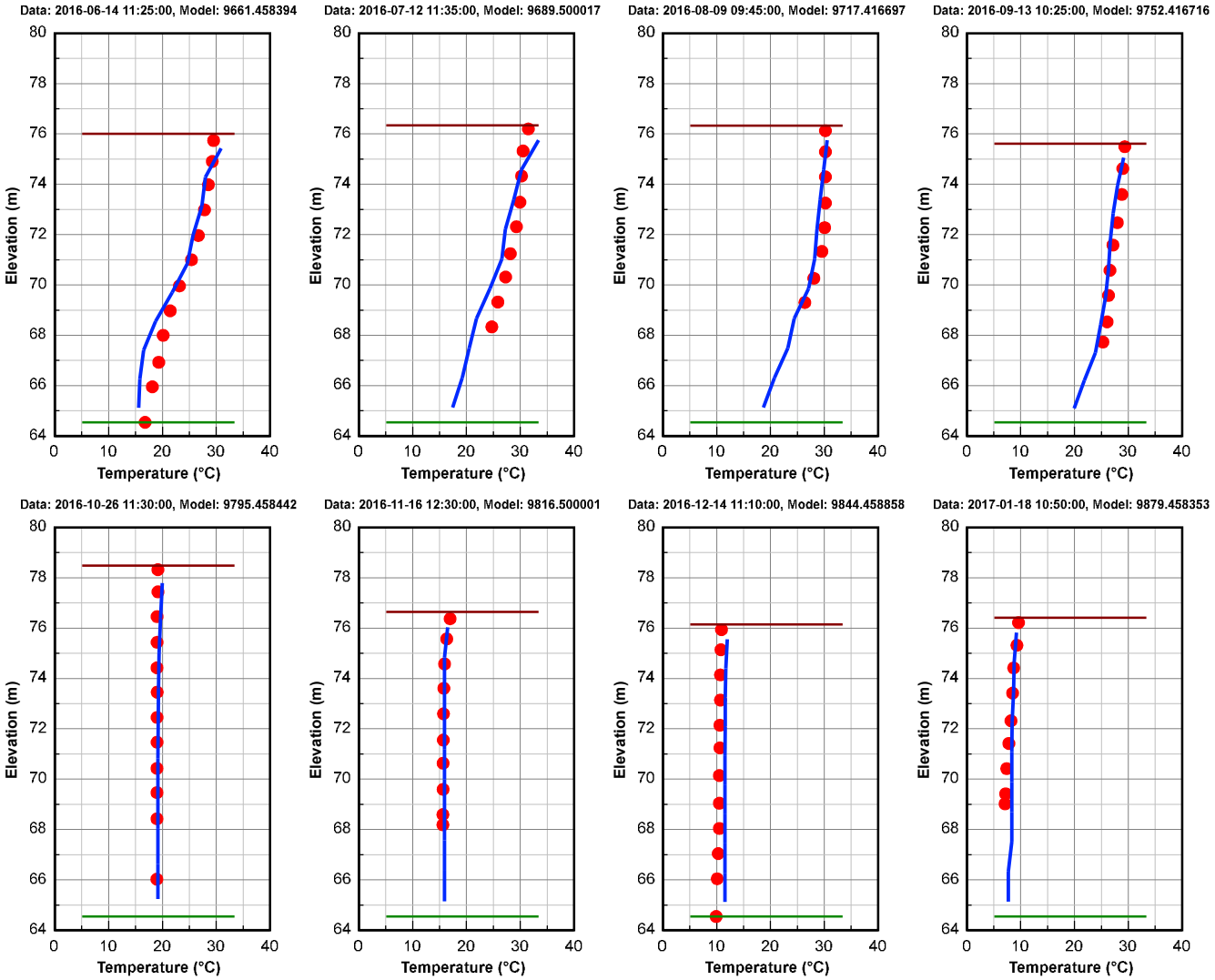

June 2016 – January 2017 (3 of 6)

Vertical Profile: NEU019L, Model Cell: 33, 75

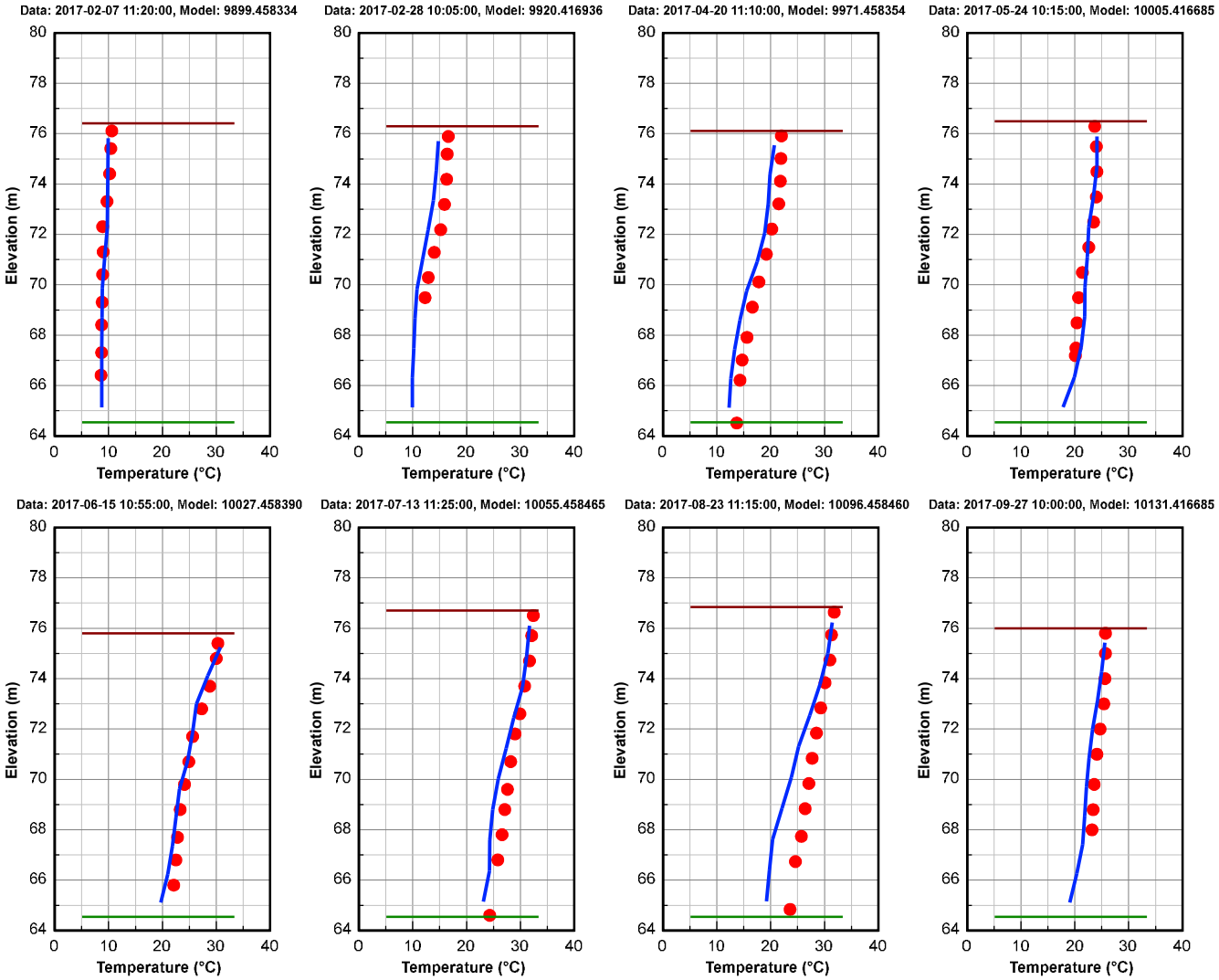

February 2017 – September 2017 (4 of 6)

Vertical Profile: NEU019L, Model Cell: 33, 75

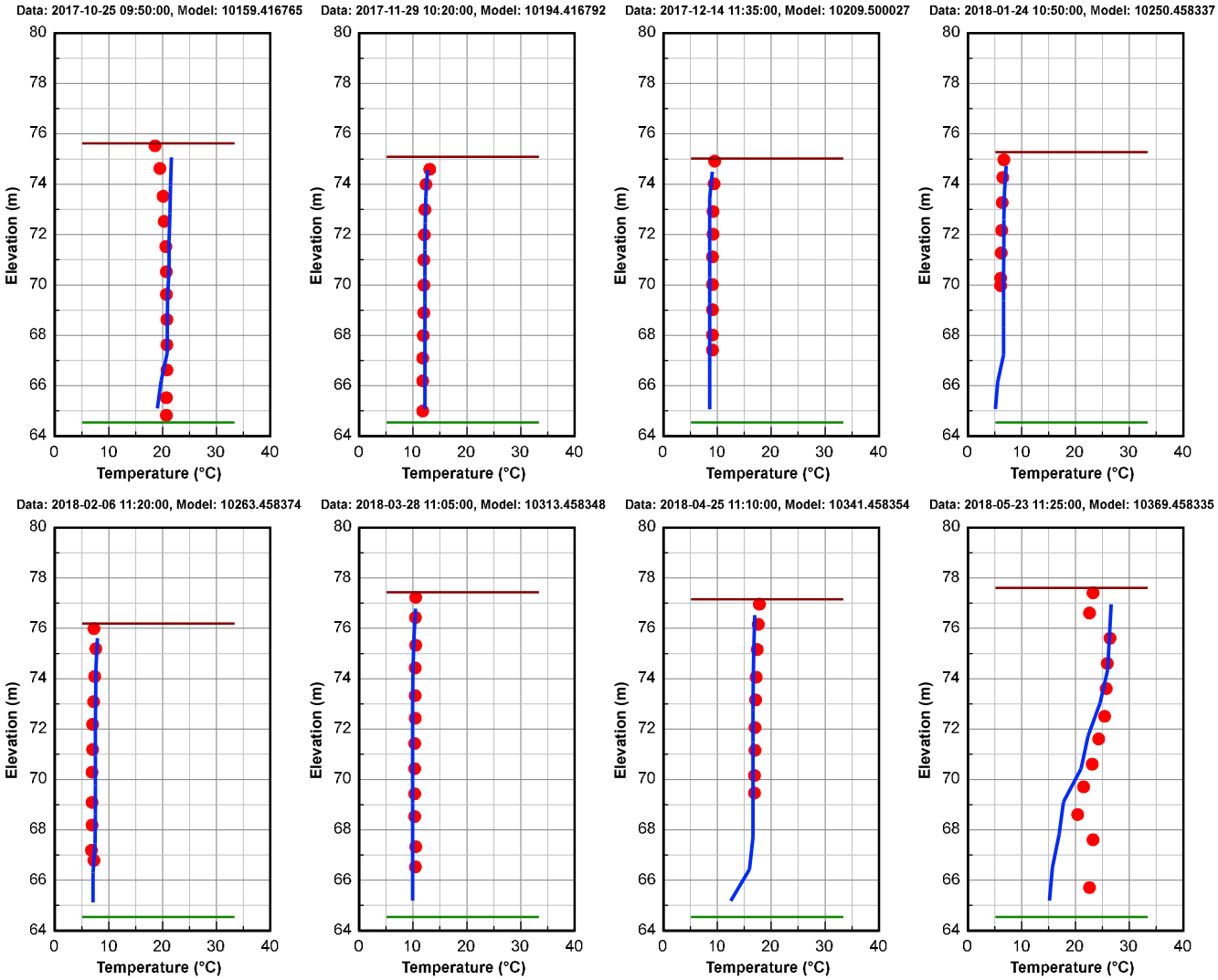

October 2017 – May 2018 (5 of 6)

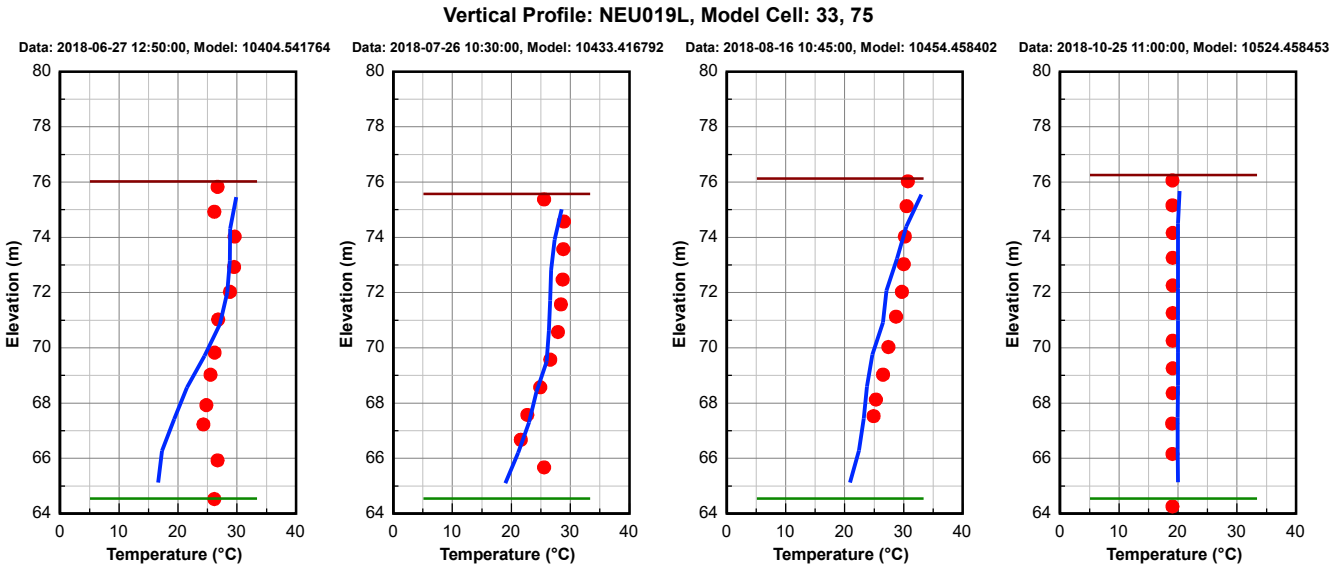

June 2018 – October 2018 (6 of 6)

Figure 1-9 Water Temperature Vertical Profile Comparison Plot at Station NEU019L during the calibration and validation period. Red dots are data, and blue continuous lines are model results.

Vertical Profile: NEU020D, Model Cell: 12, 98

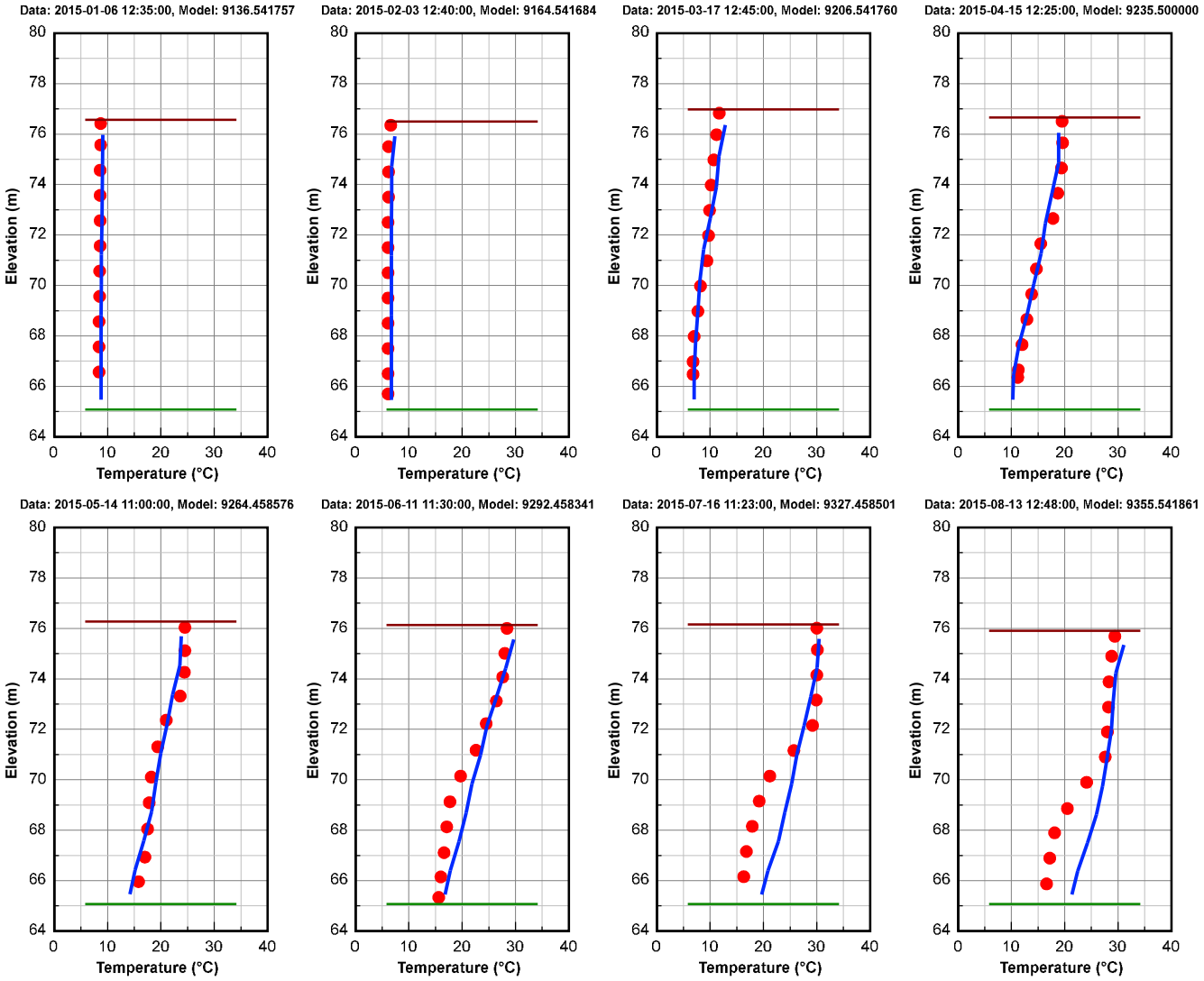

January 2015 – August 2015 (1 of 6)

Vertical Profile: NEU020D, Model Cell: 12, 98

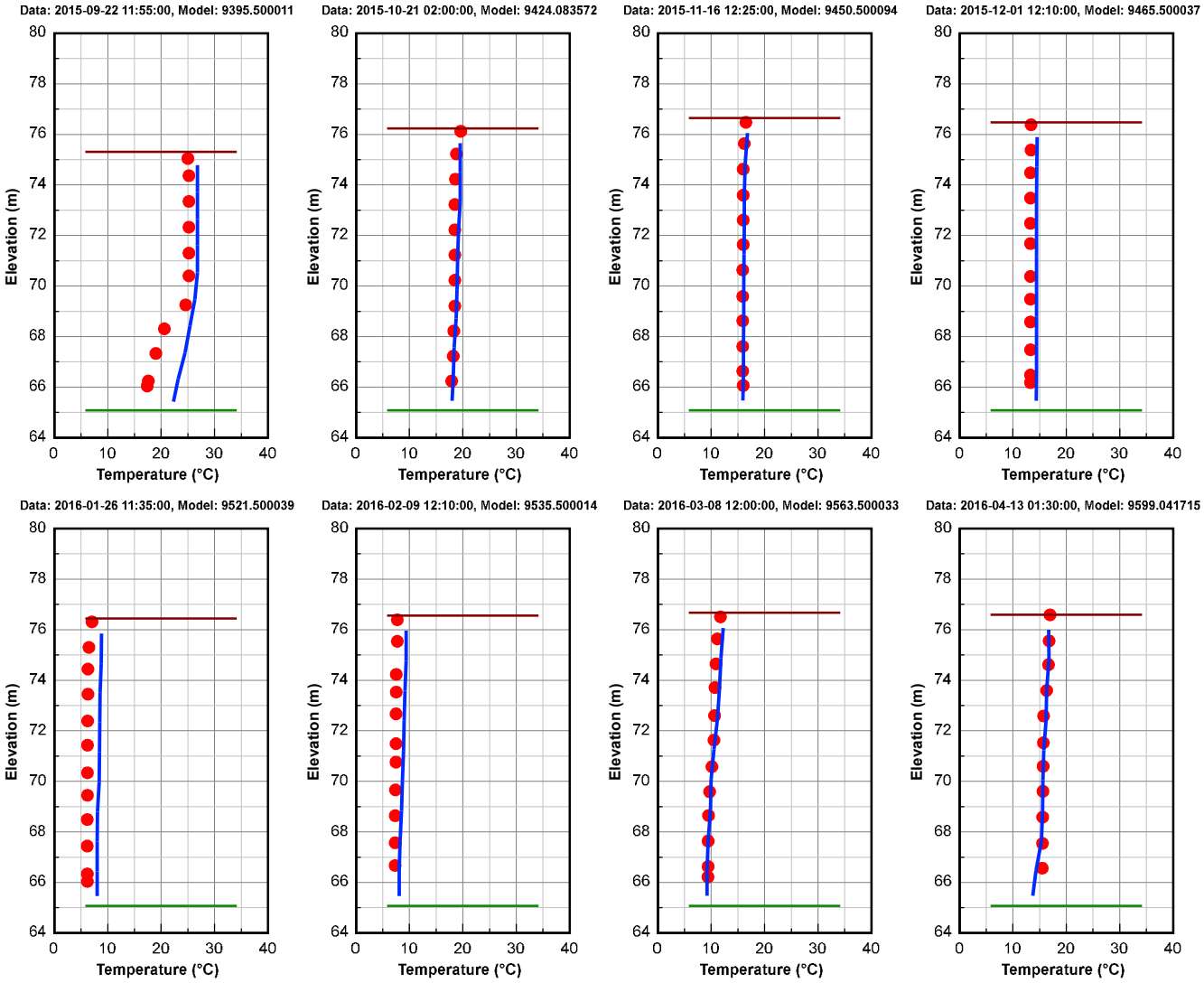

September 2015 – April 2016 (2 of 6)

Vertical Profile: NEU020D, Model Cell: 12, 98

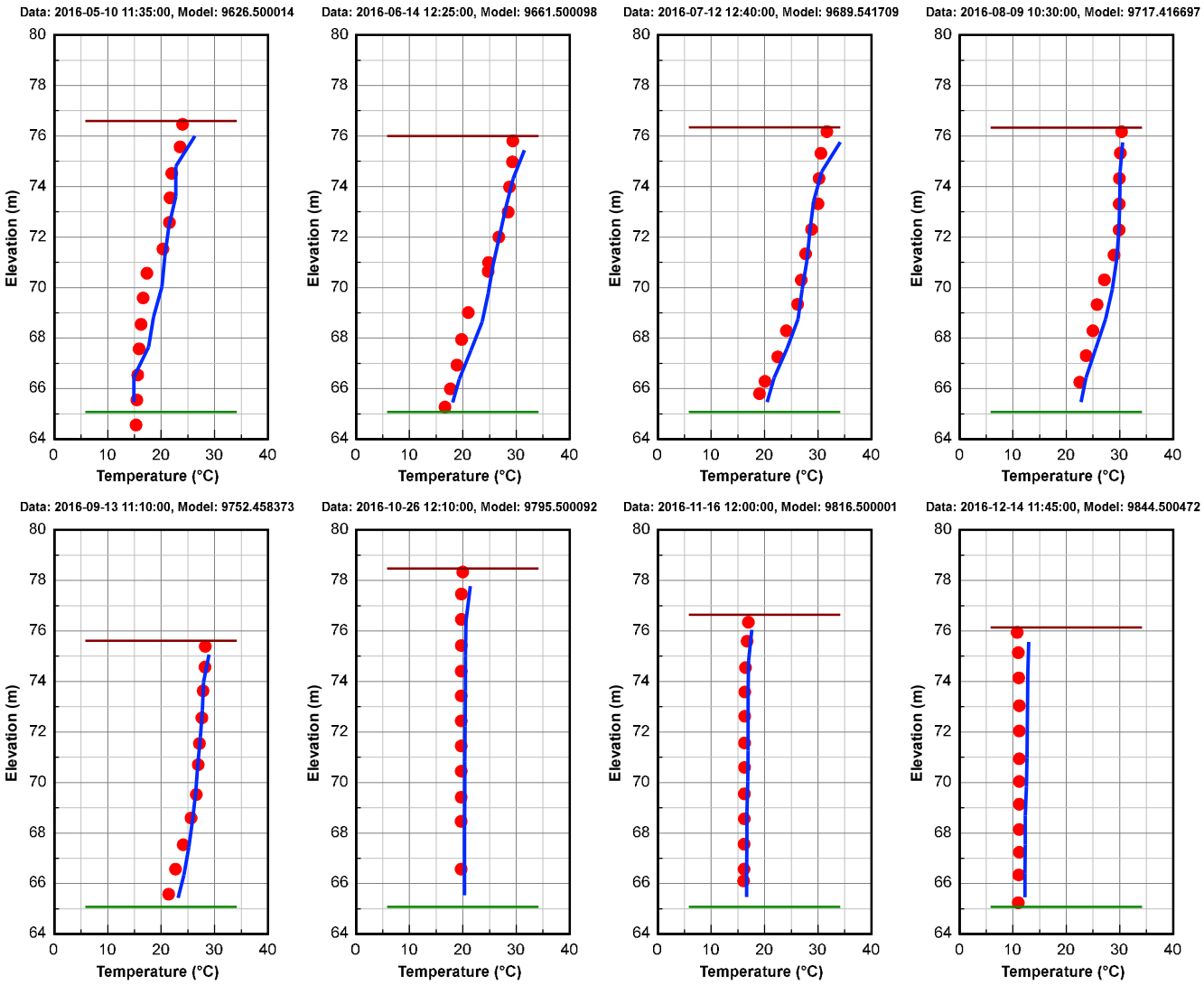

May 2016 – December 2016 (3 of 6)

Vertical Profile: NEU020D, Model Cell: 12, 98

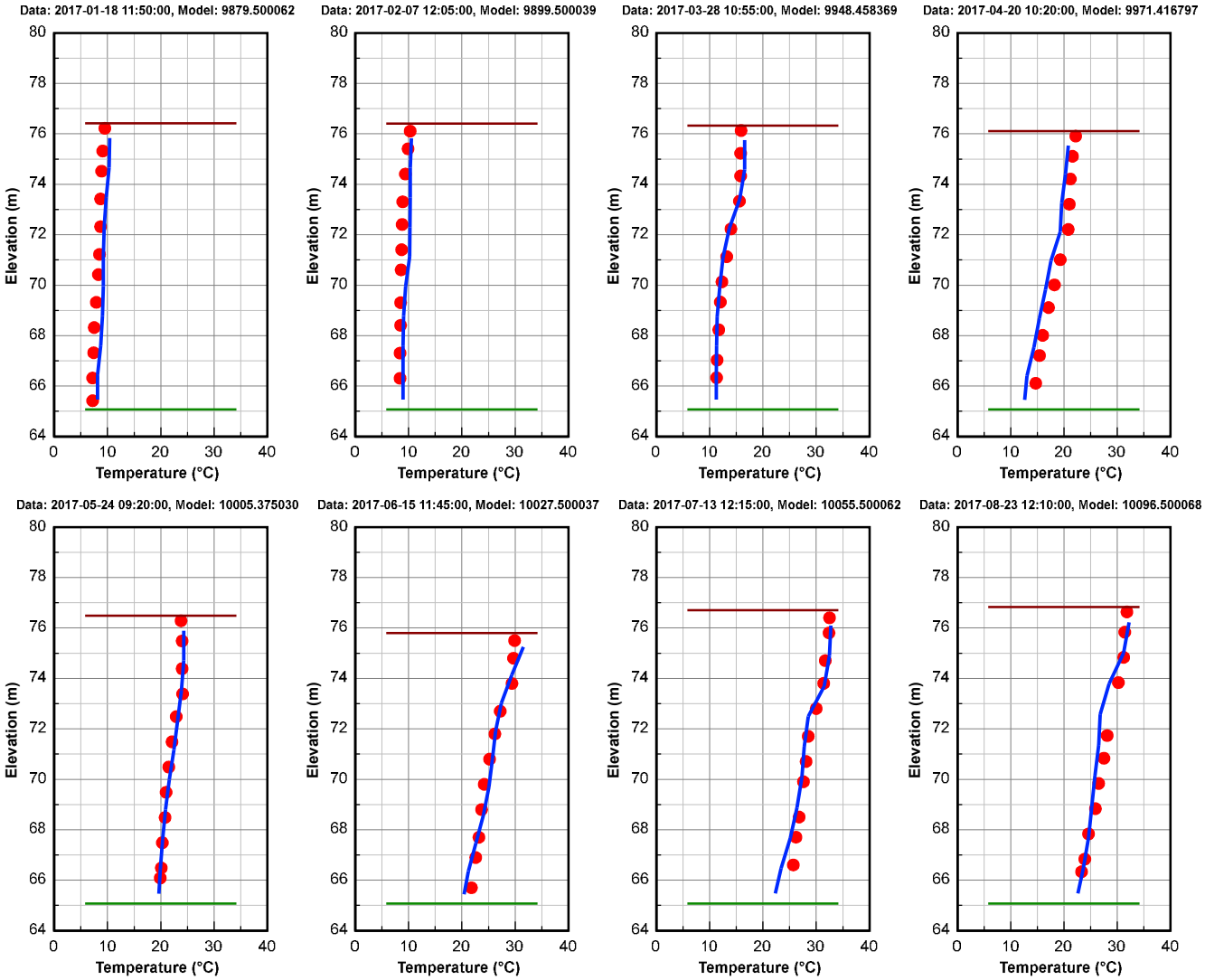

January 2017 – August 2017 (4 of 6)

Vertical Profile: NEU020D, Model Cell: 12, 98

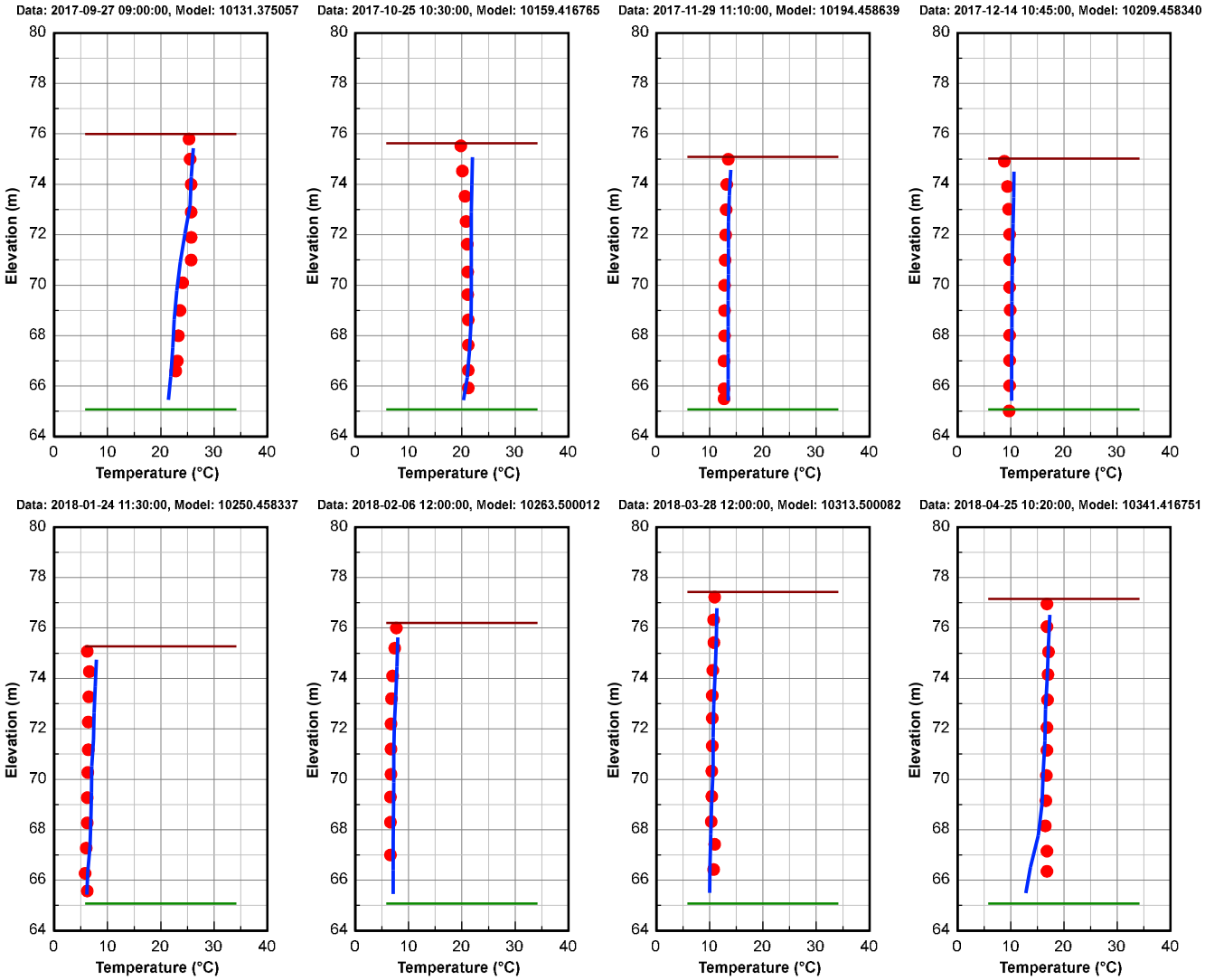

September 2017 – April 2018 (5 of 6)

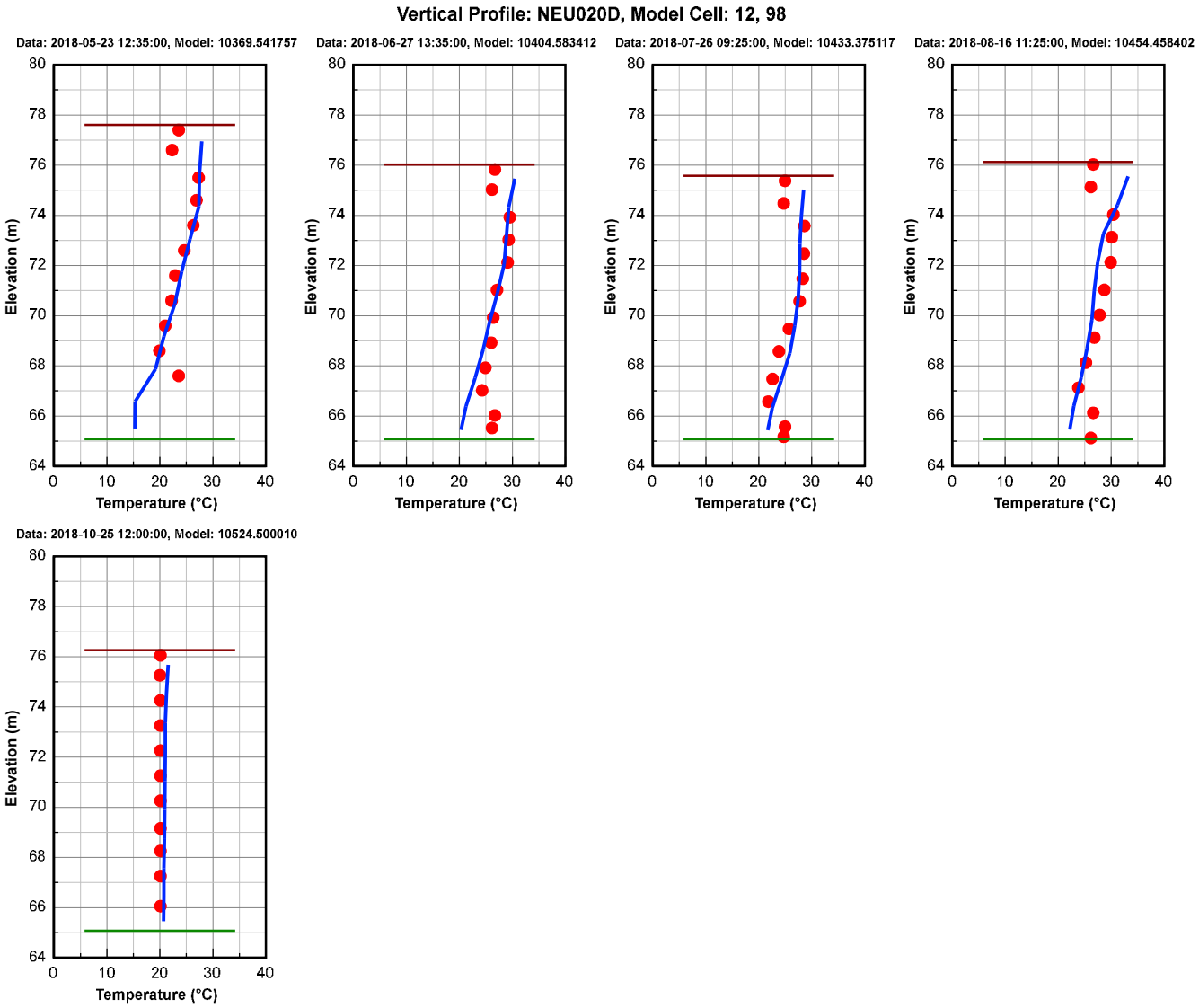

May 2018 – October 2018 (6 of 6)

Figure 1-10 Water Temperature Vertical Profile Comparison Plot at Station NEU020D during the calibration and validation period. Red dots are data, and blue continuous lines are model results.

2. DO Vertical Profile Plots

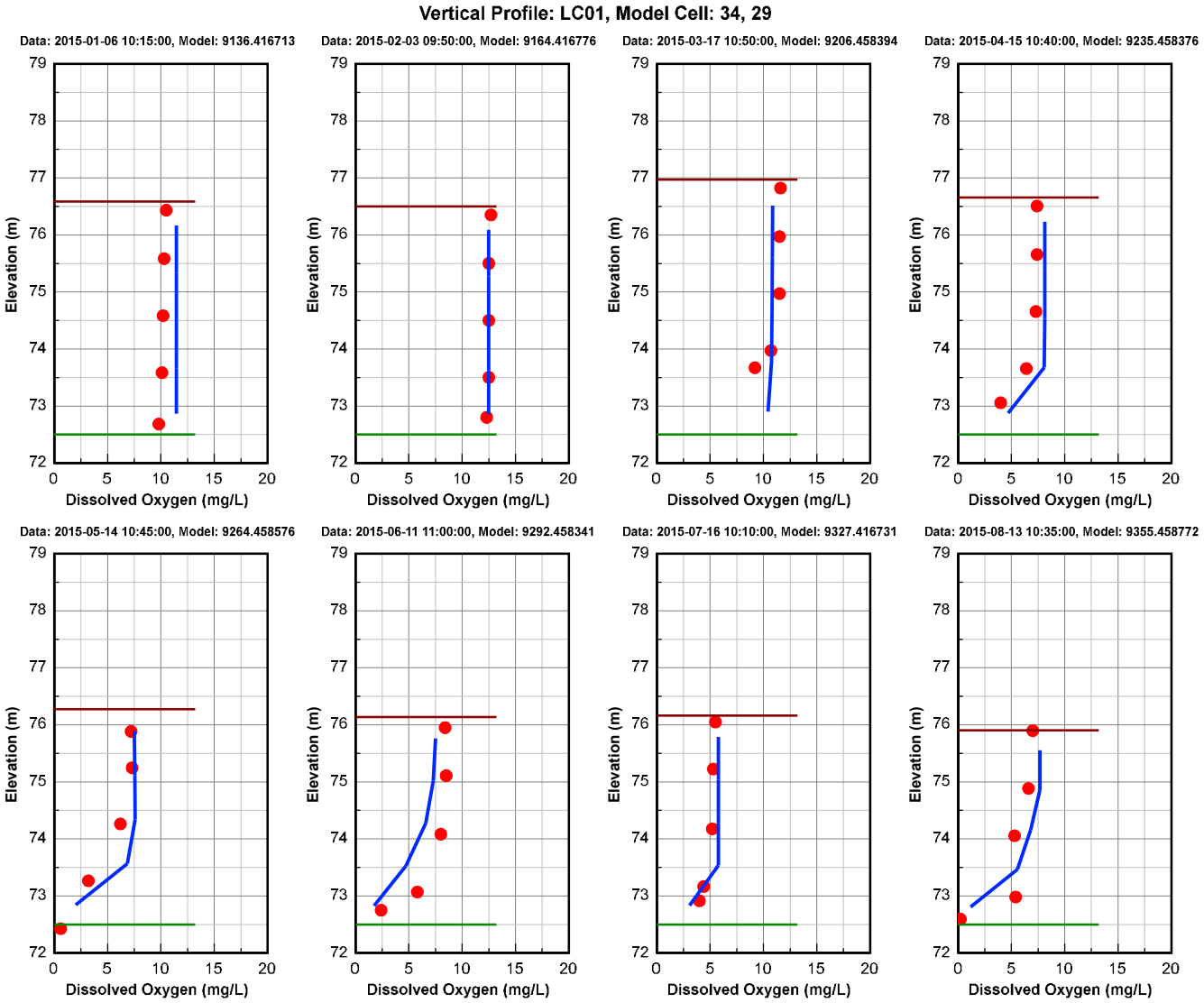

January 2015 – August 2015 (1 of 6)

Vertical Profile: LC01, Model Cell: 34, 29

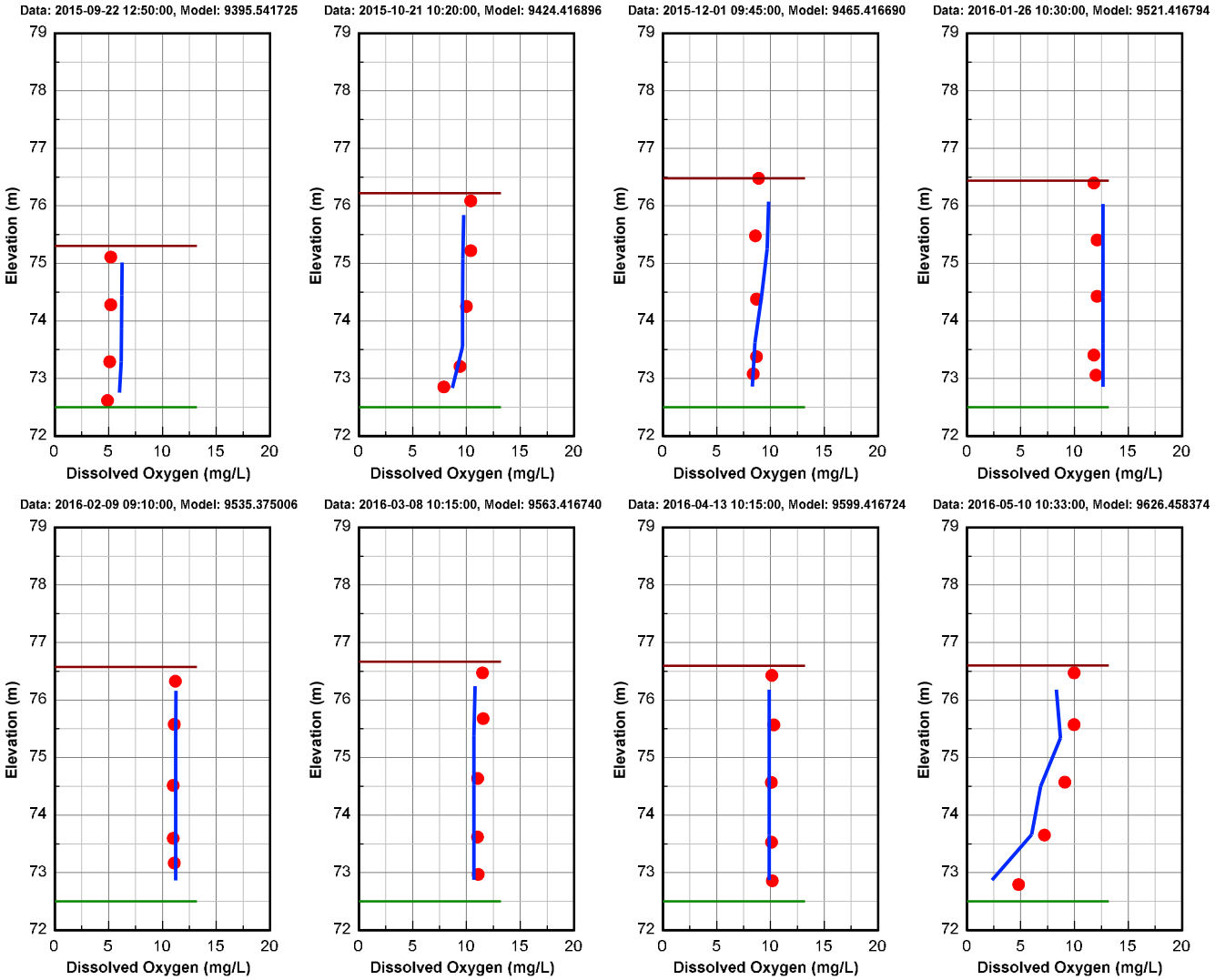

September 2015 – May 2016 (2 of 6)

Vertical Profile: LC01, Model Cell: 34, 29

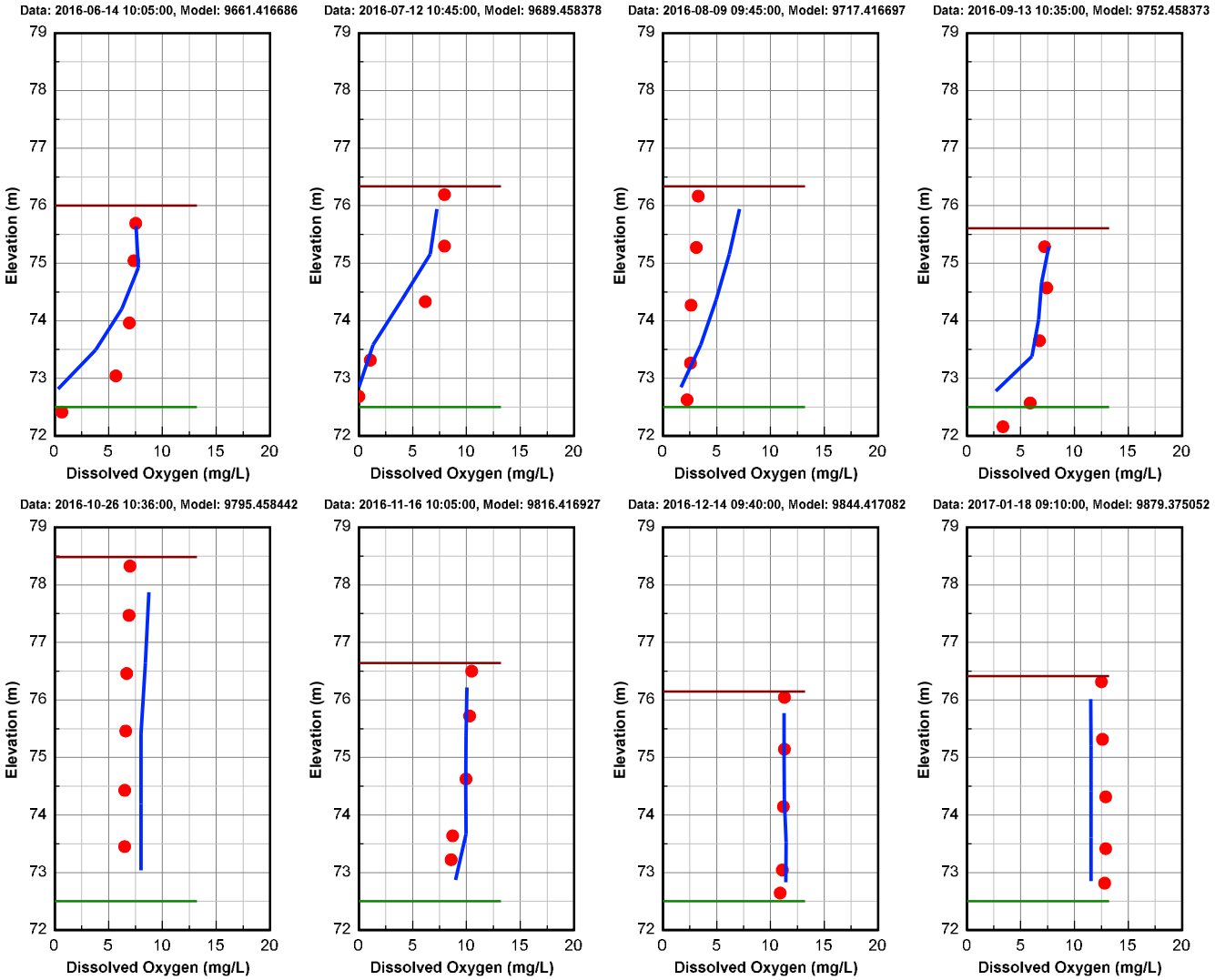

June 2016 – January 2017 (3 of 6)

Vertical Profile: LC01, Model Cell: 34, 29

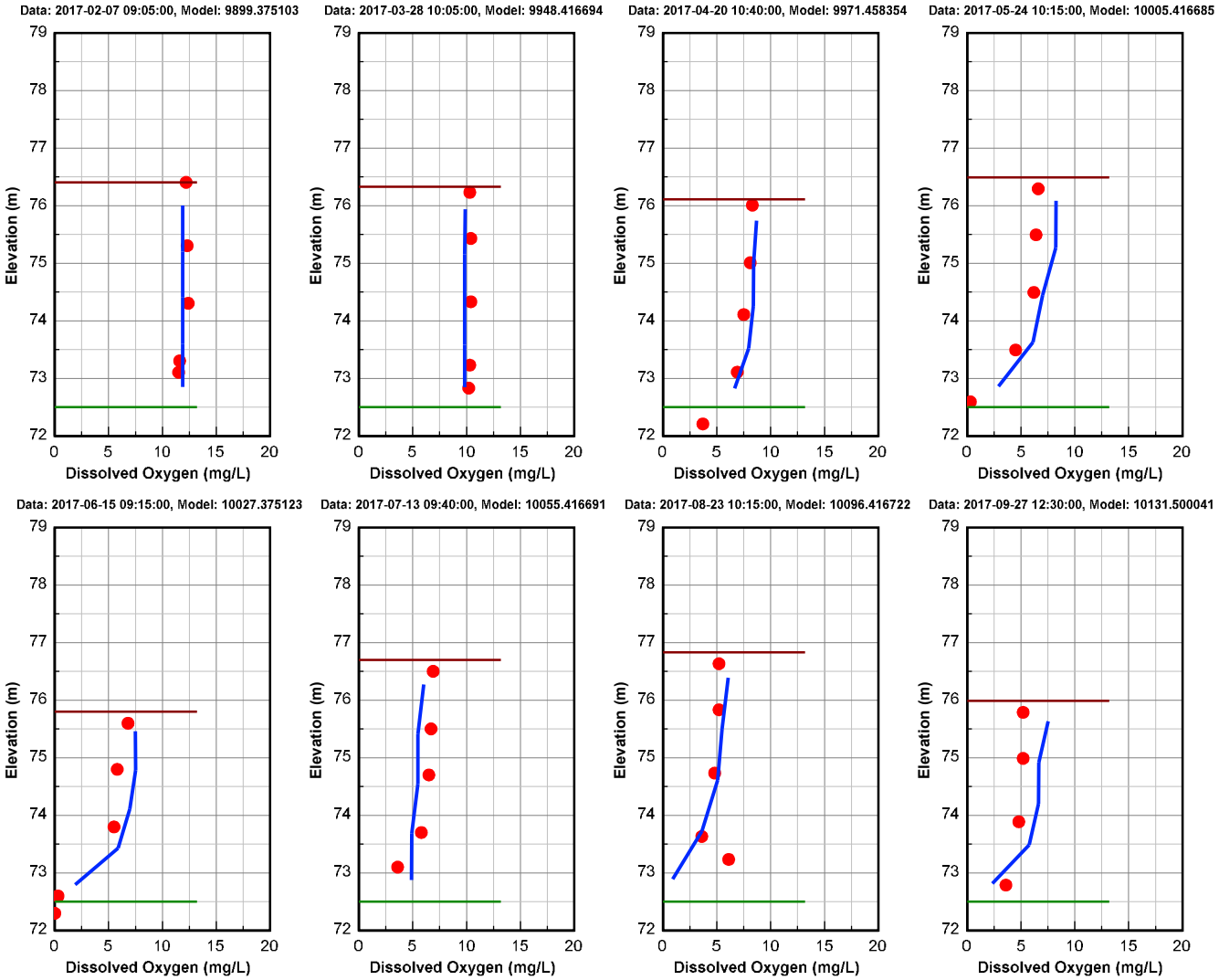

February 2017 – September 2017 (4 of 6)

Vertical Profile: LC01, Model Cell: 34, 29

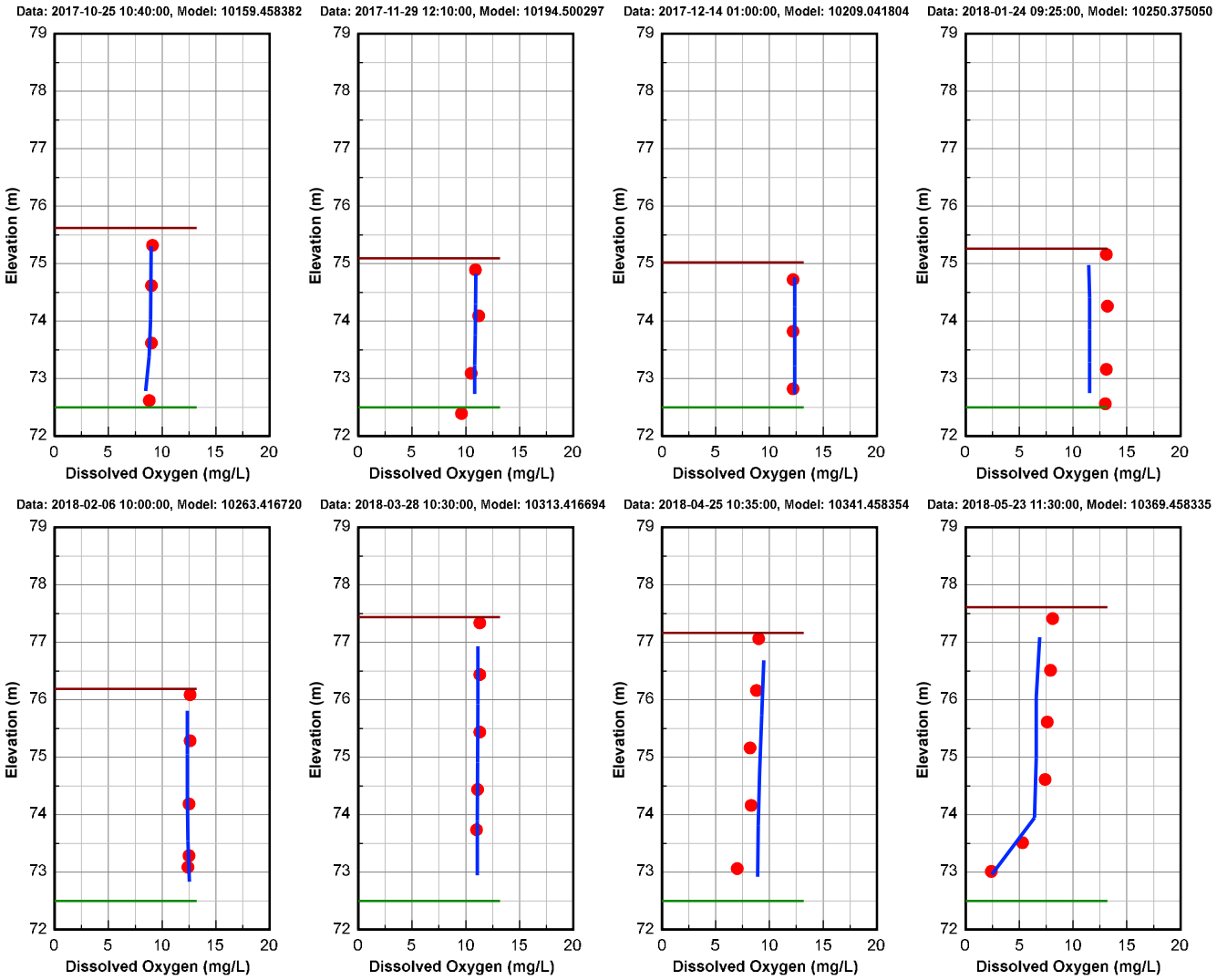

October 2017 – May 2018 (5 of 6)

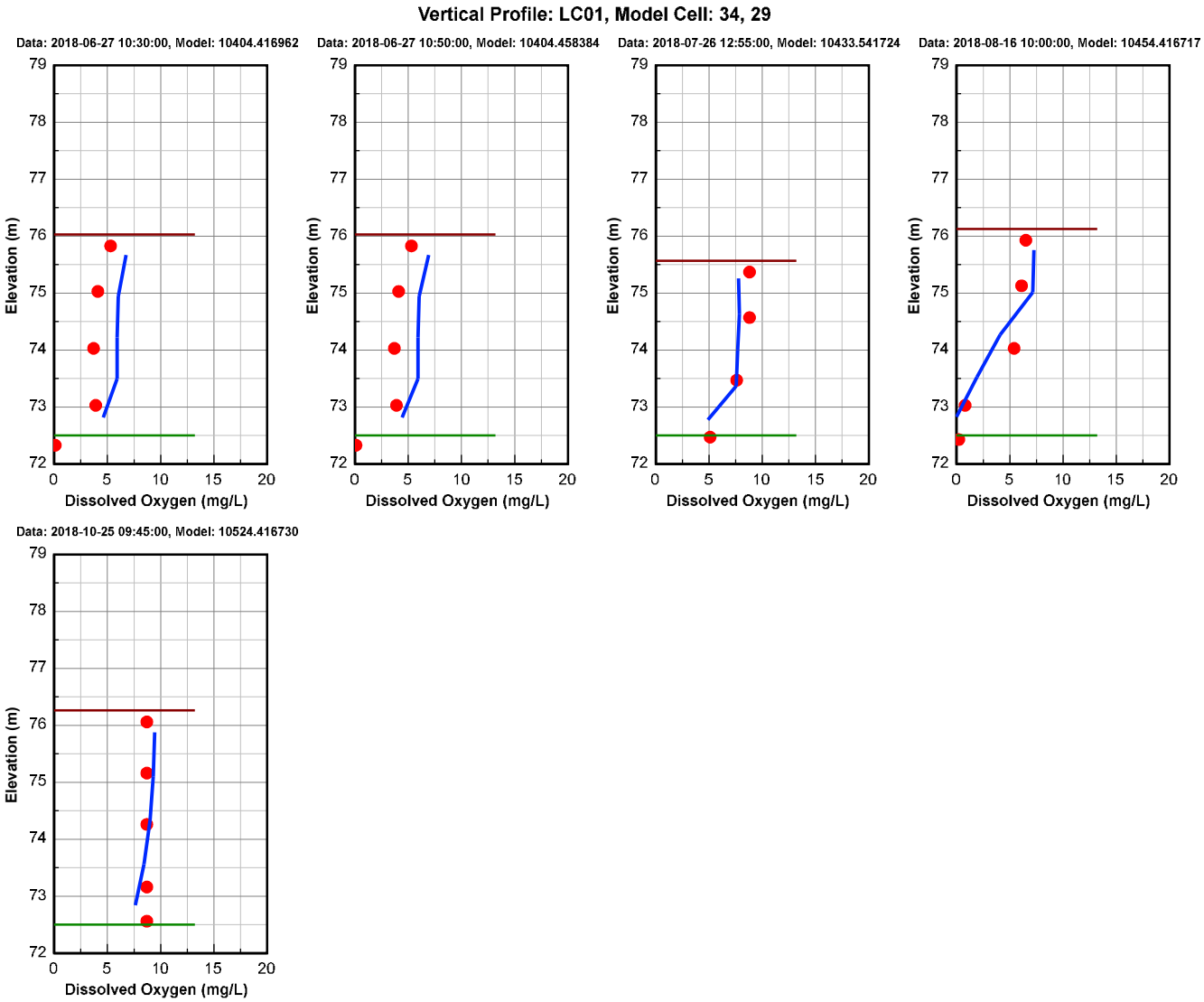

June 2018 – October 2018 (6 of 6)

Figure 2-1 DO Vertical Profile Comparison Plot at Station LC01 during the calibration and validation period. Red dots are data, and blue continuous lines are model results.

Vertical Profile: LI01, Model Cell: 39, 43

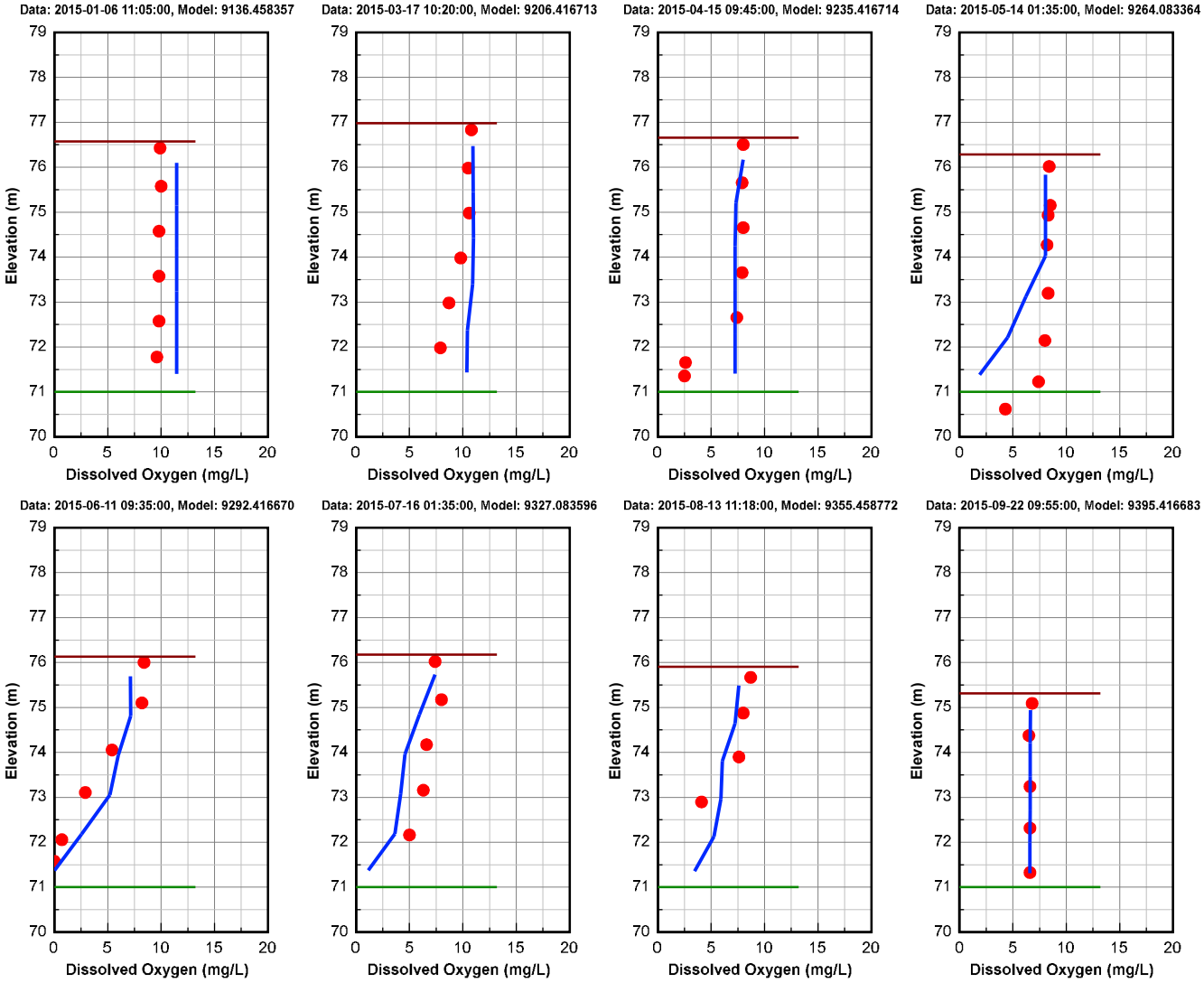

January 2015 – September 2015 (1 of 6)

Vertical Profile: LI01, Model Cell: 39, 43

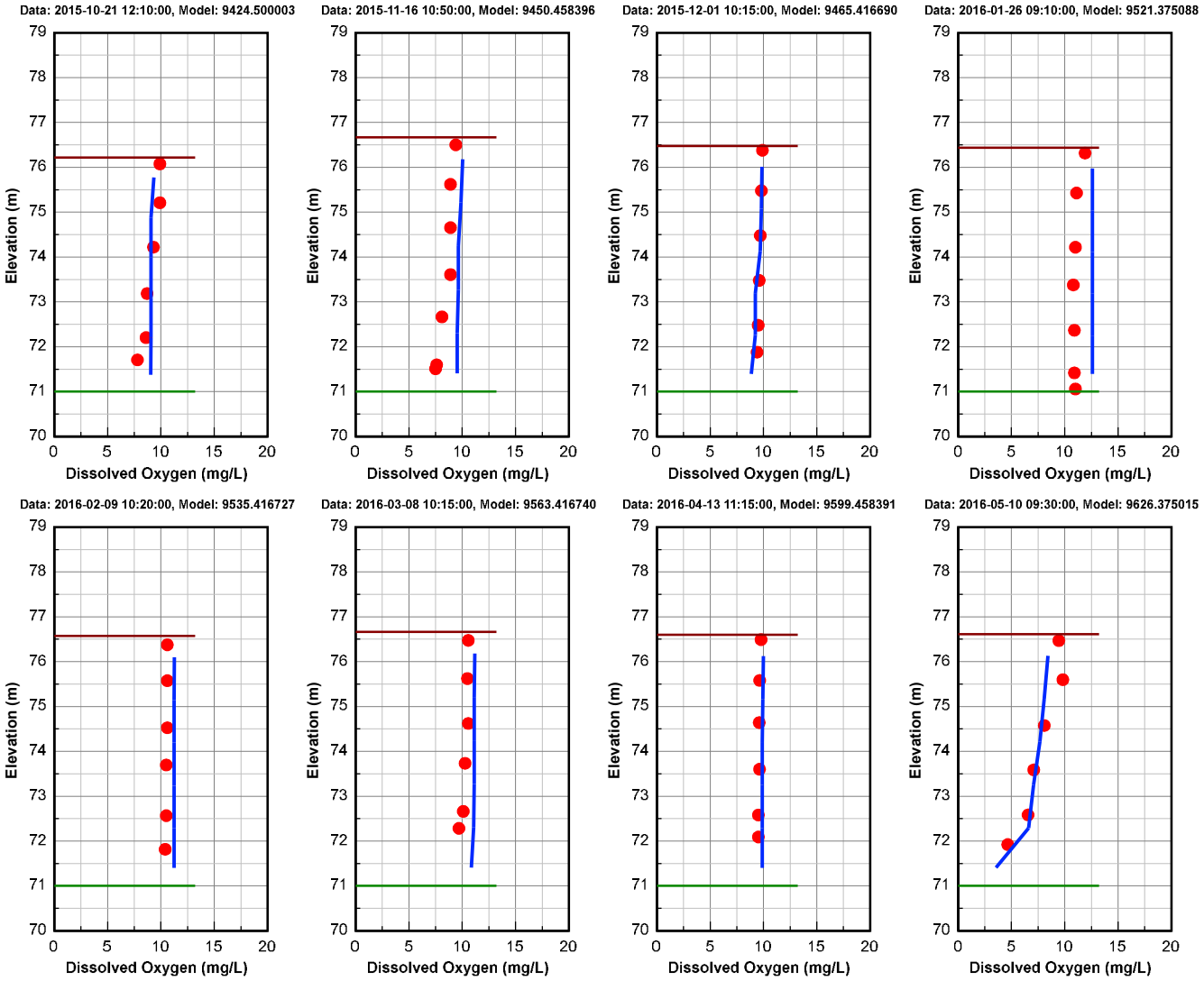

October 2015 – May 2016 (2 of 6)

Vertical Profile: LI01, Model Cell: 39, 43

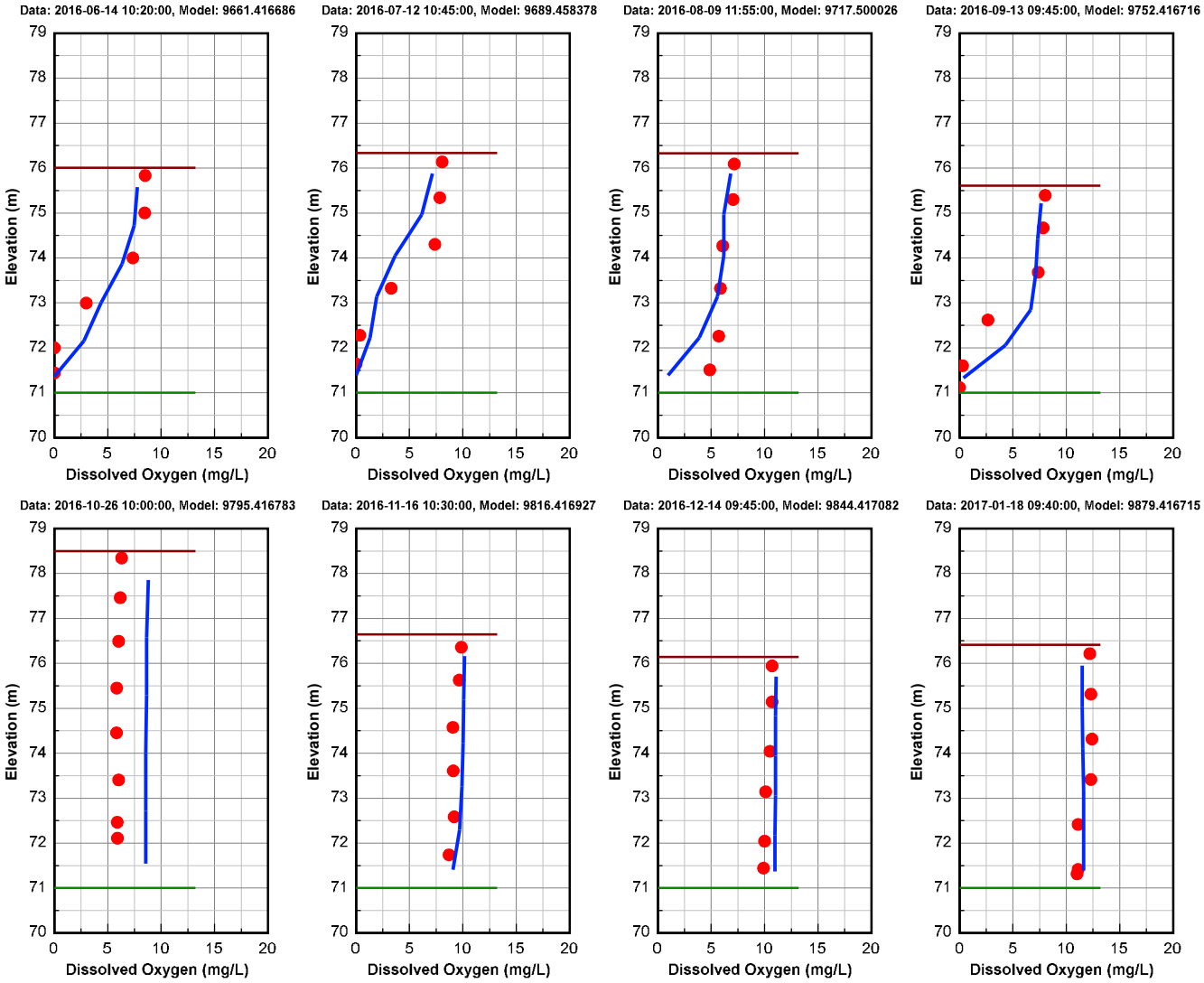

June 2016 – January 2017 (3 of 6)

Vertical Profile: LI01, Model Cell: 39, 43

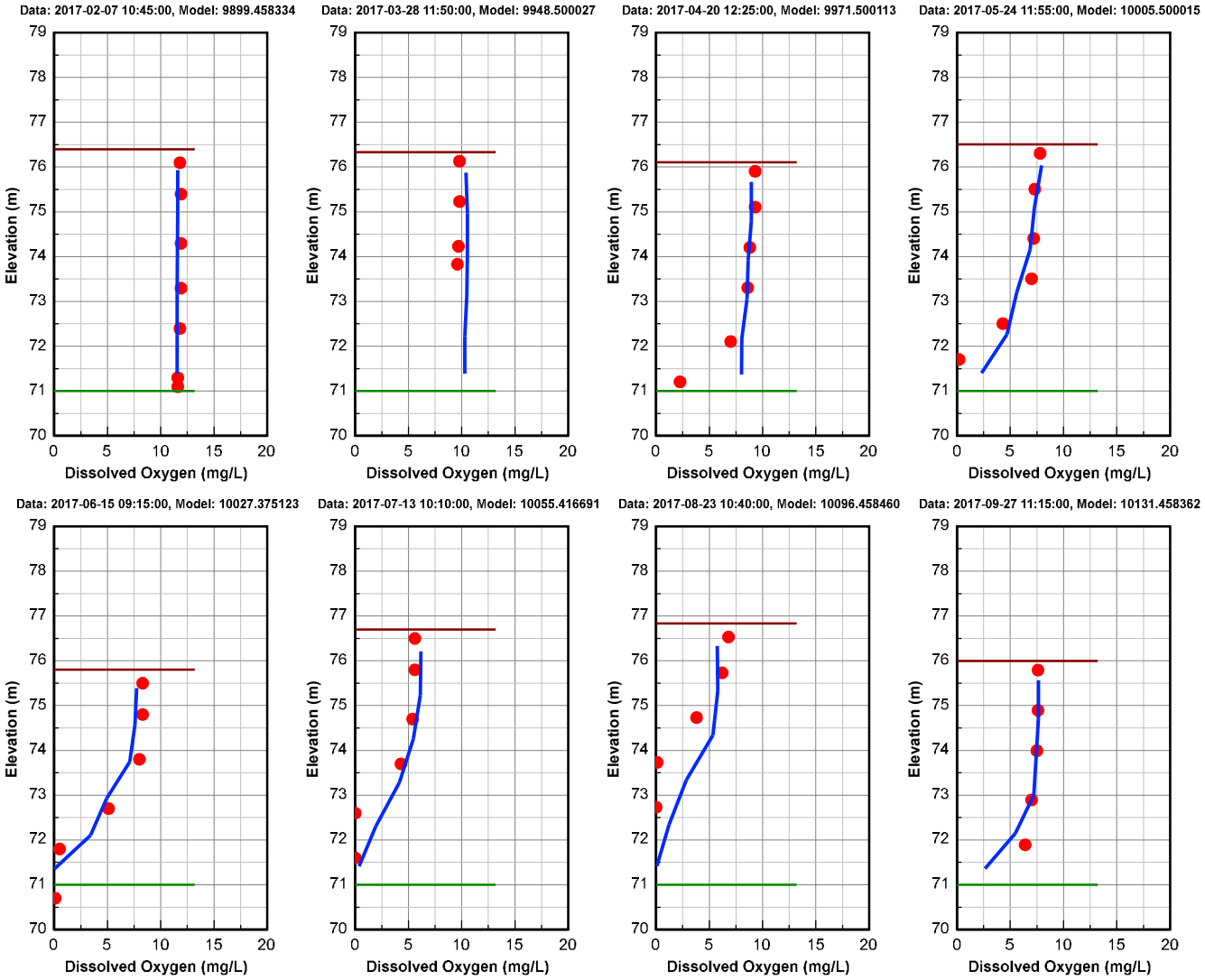

February 2017 – September 2017 (4 of 6)

Vertical Profile: LI01, Model Cell: 39, 43

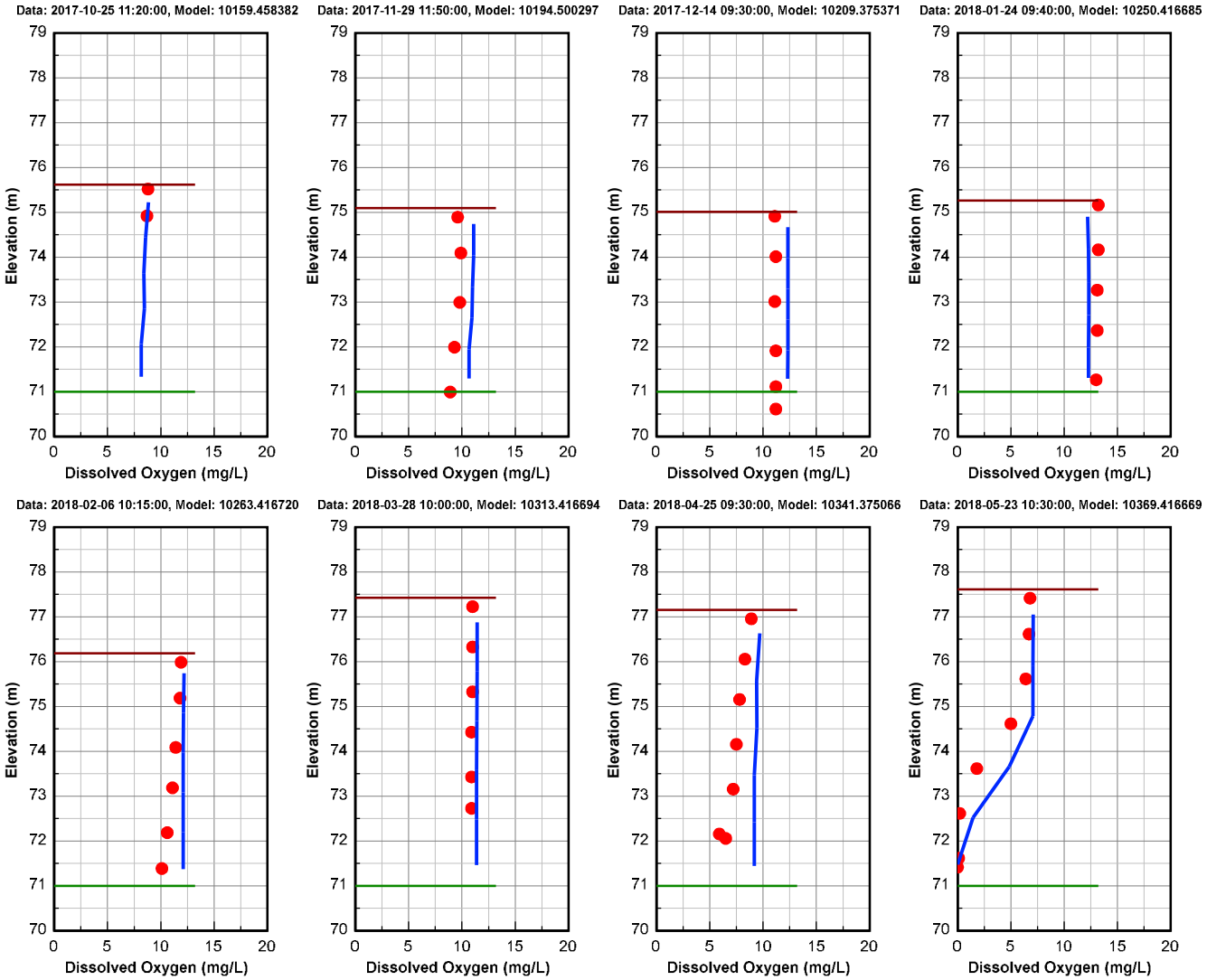

October 2017 – May 2018 (5 of 6)

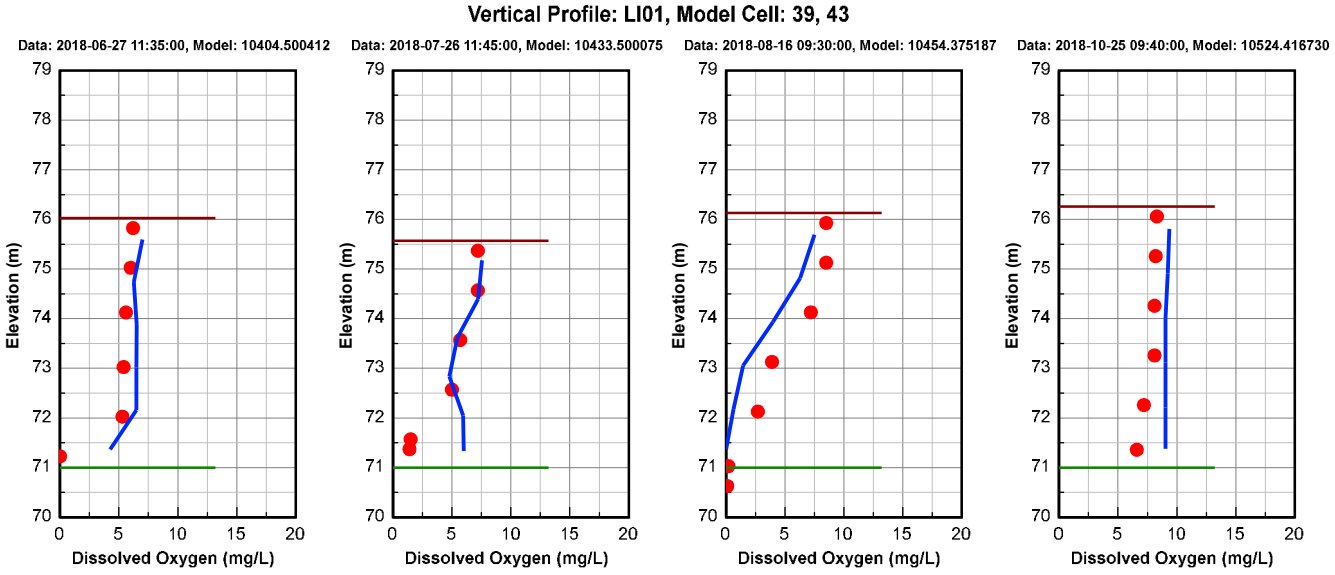

June 2018 – October 2018 (6 of 6)

Figure 2-2 DO Vertical Profile Comparison Plot at Station LI01 during the calibration and validation period. Red dots are data, and blue continuous lines are model results.

Vertical Profile: LLC01, Model Cell: 47, 33

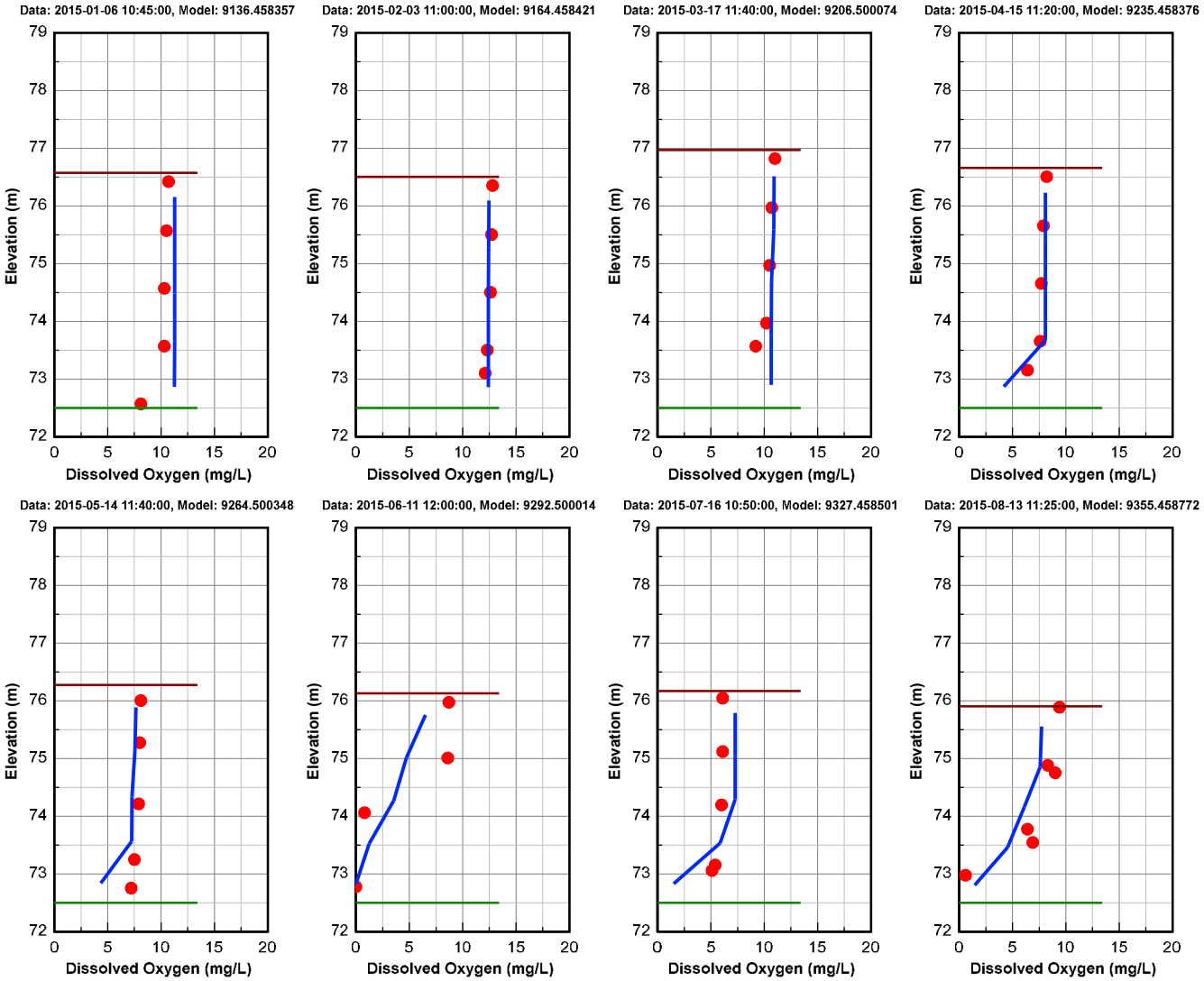

January 2015 – August 2015 (1 of 6)

Vertical Profile: LLC01, Model Cell: 47, 33

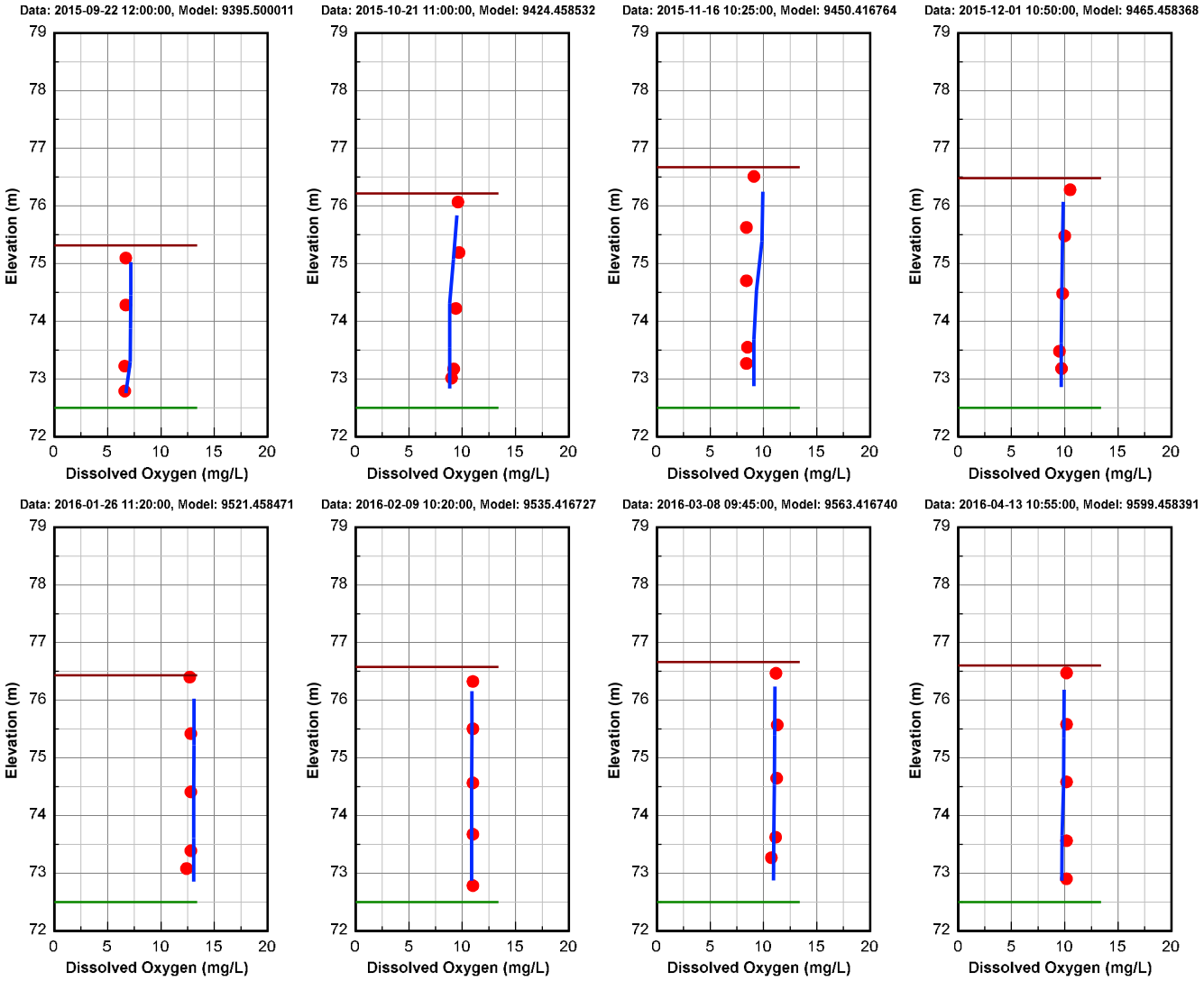

September 2015 – April 2016 (2 of 6)

Vertical Profile: LLC01, Model Cell: 47, 33

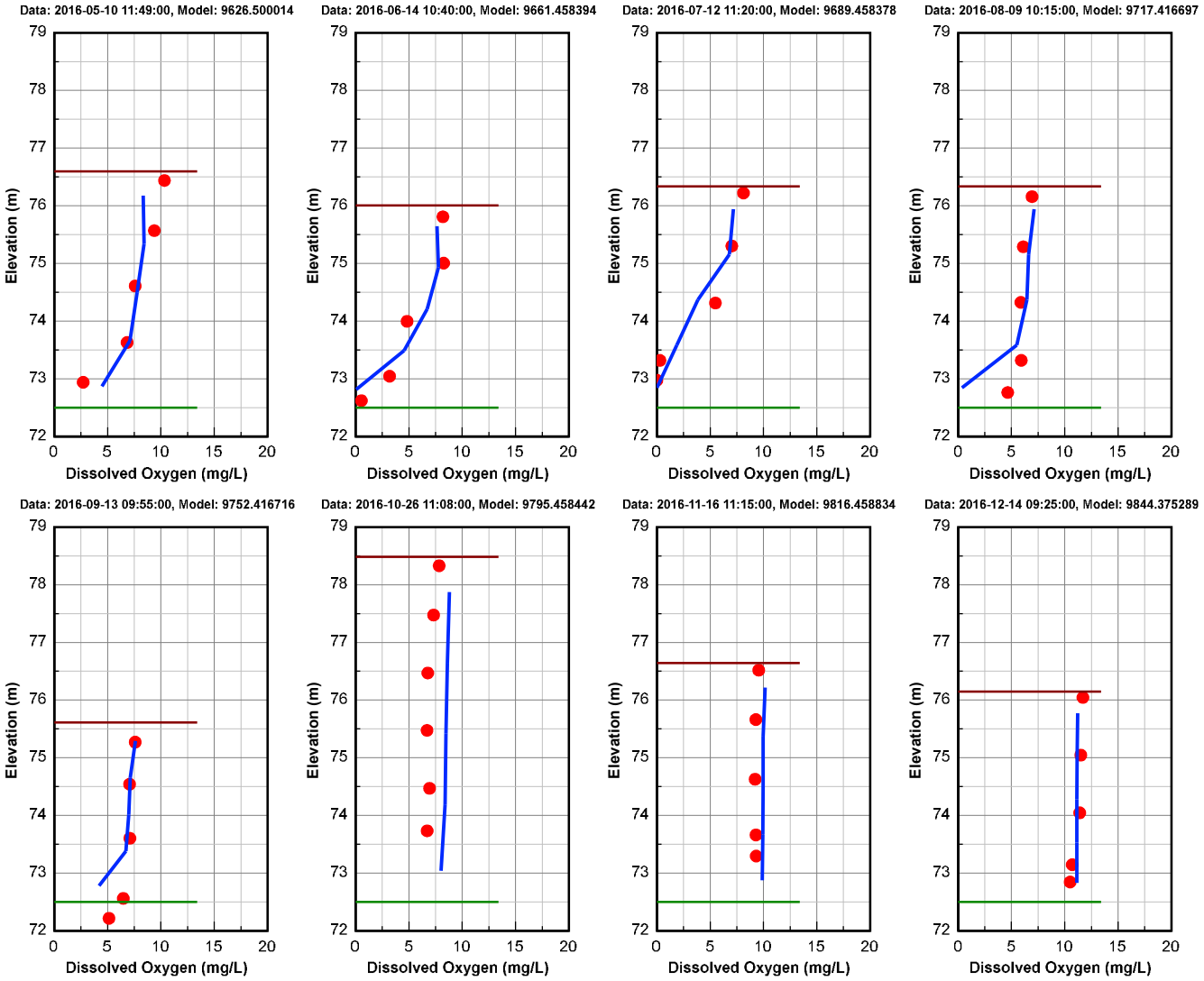

May 2016 – December 2016 (3 of 6)

Vertical Profile: LLC01, Model Cell: 47, 33

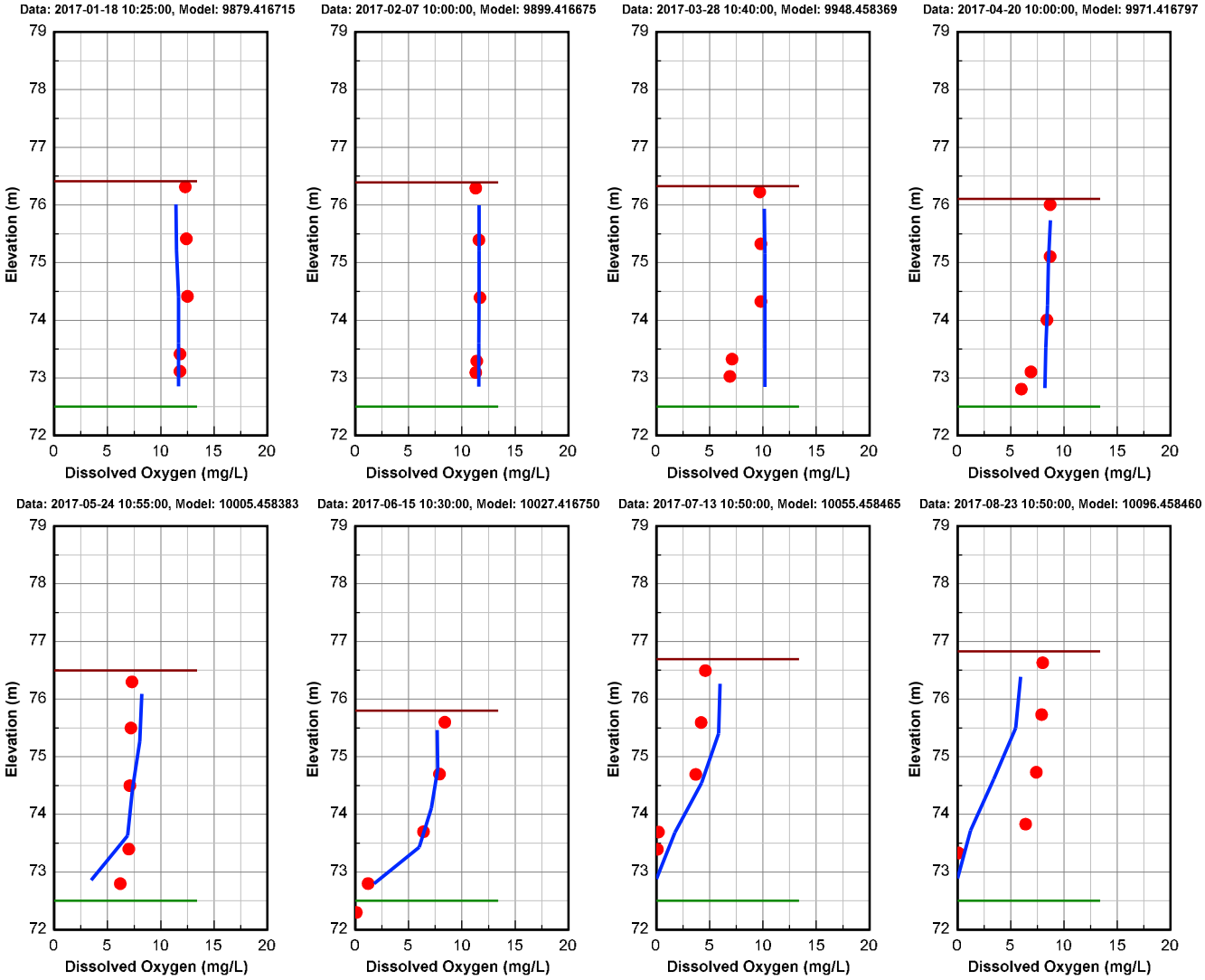

January 2017 – August 2017 (4 of 6)

Vertical Profile: LLC01, Model Cell: 47, 33

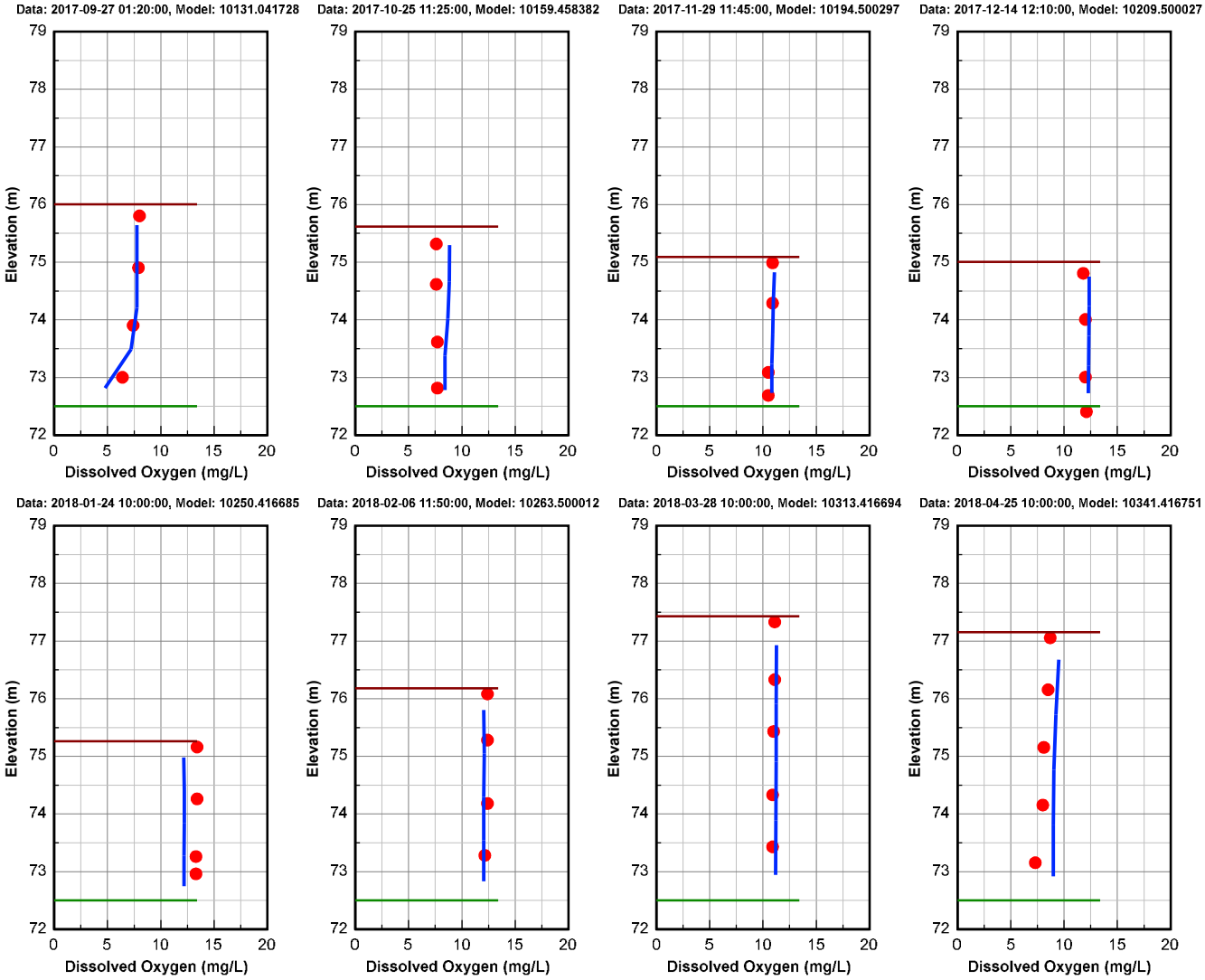

September 2017 – April 2018 (5 of 6)

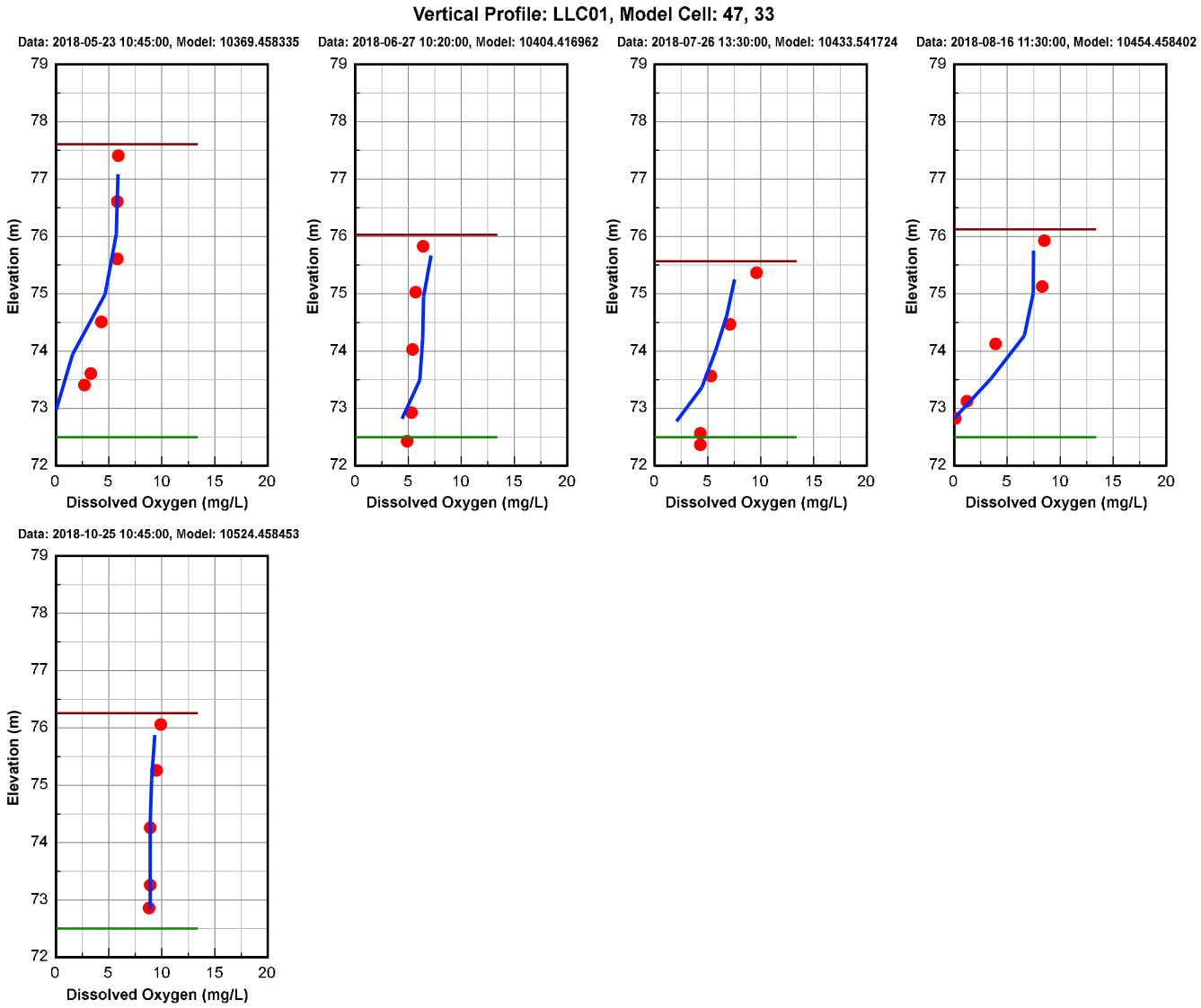

May 2018 – October 2018 (6 of 6)

Figure 2-3 DO Vertical Profile Comparison Plot at Station LLC01 during the calibration and validation period. Red dots are data, and blue continuous lines are model results.

Vertical Profile: NEU013, Model Cell: 42, 17

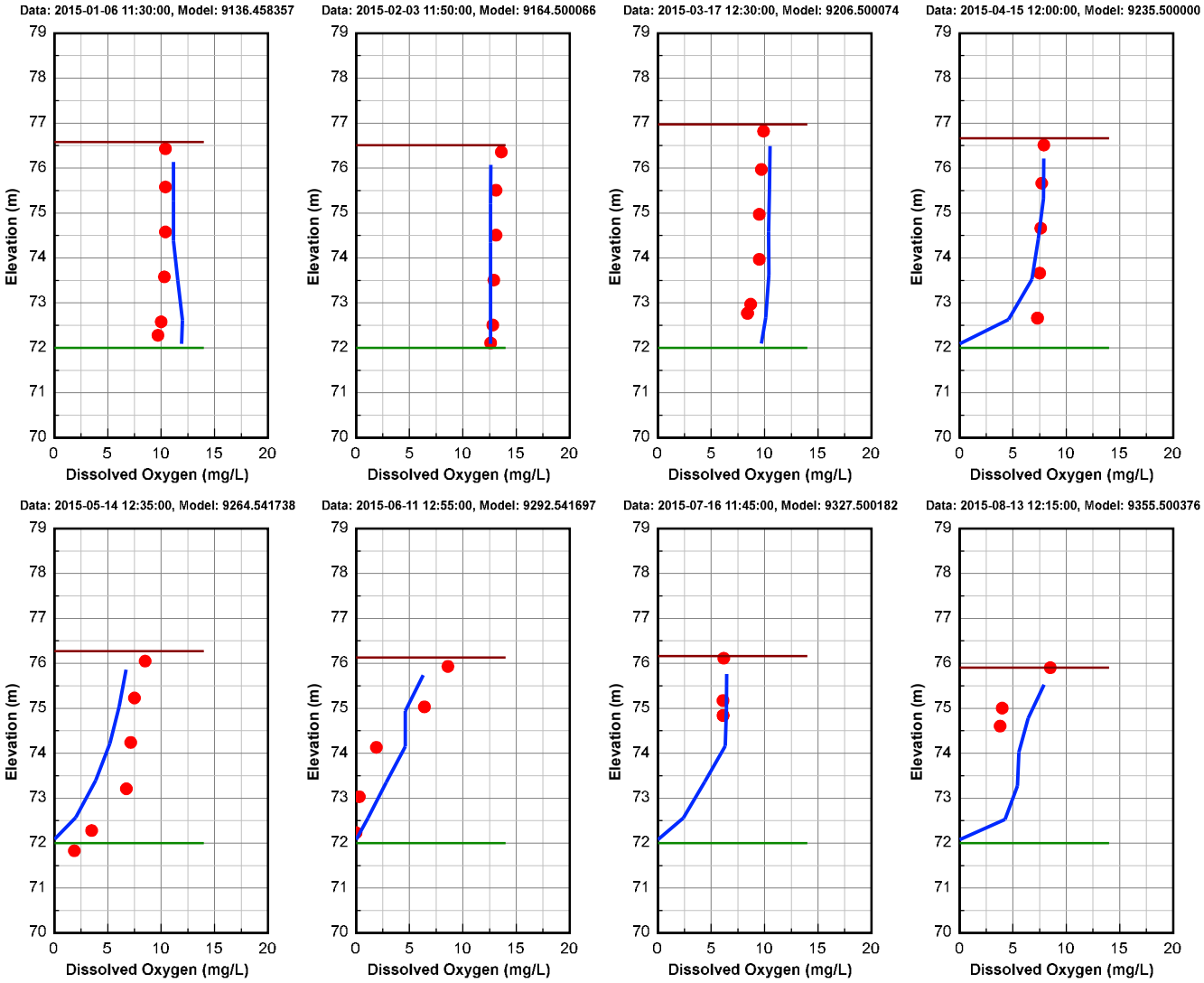

January 2015 – August 2015 (1 of 6)

Vertical Profile: NEU013, Model Cell: 42, 17

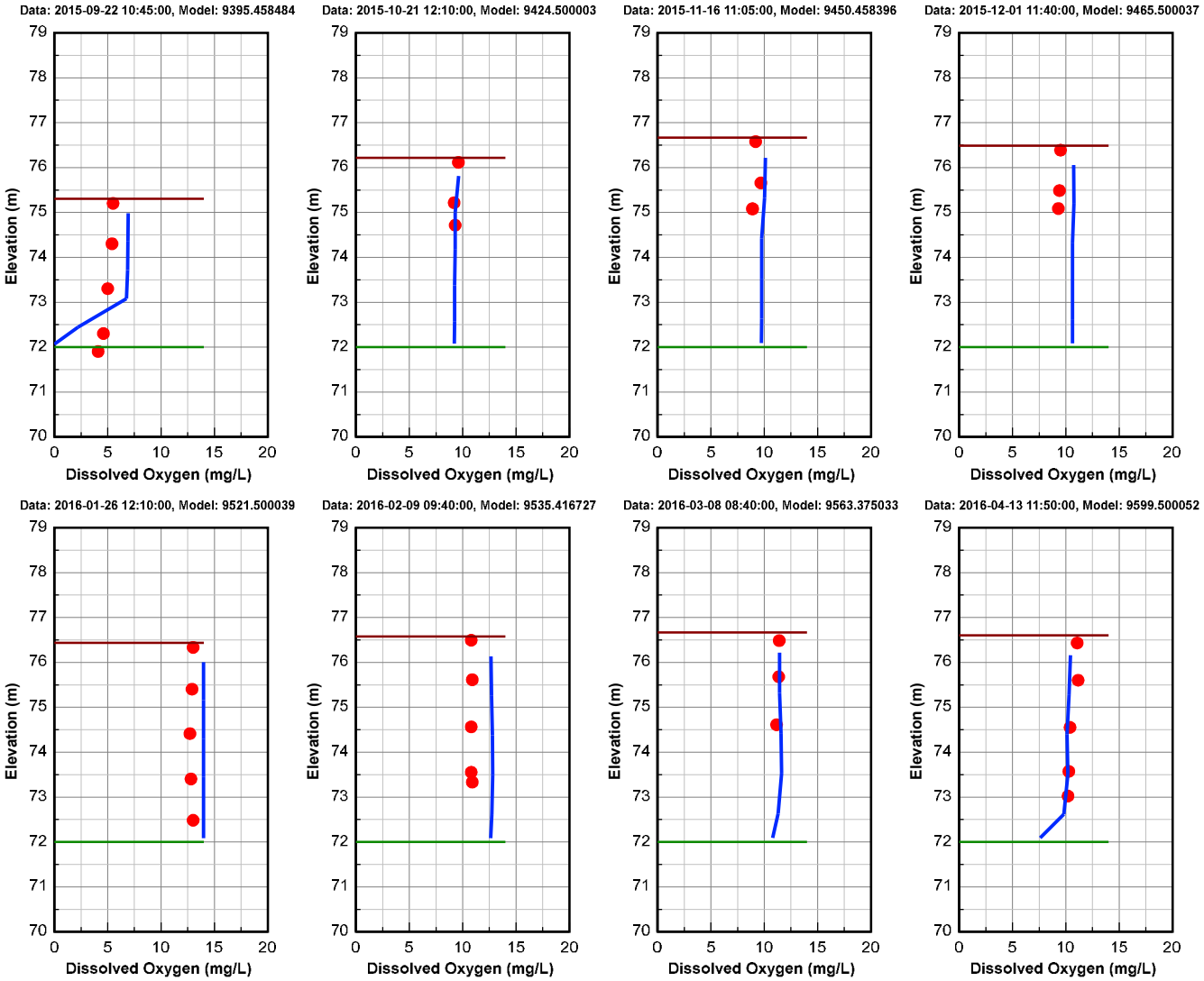

September 2015 – April 2016 (2 of 6)

Vertical Profile: NEU013, Model Cell: 42, 17

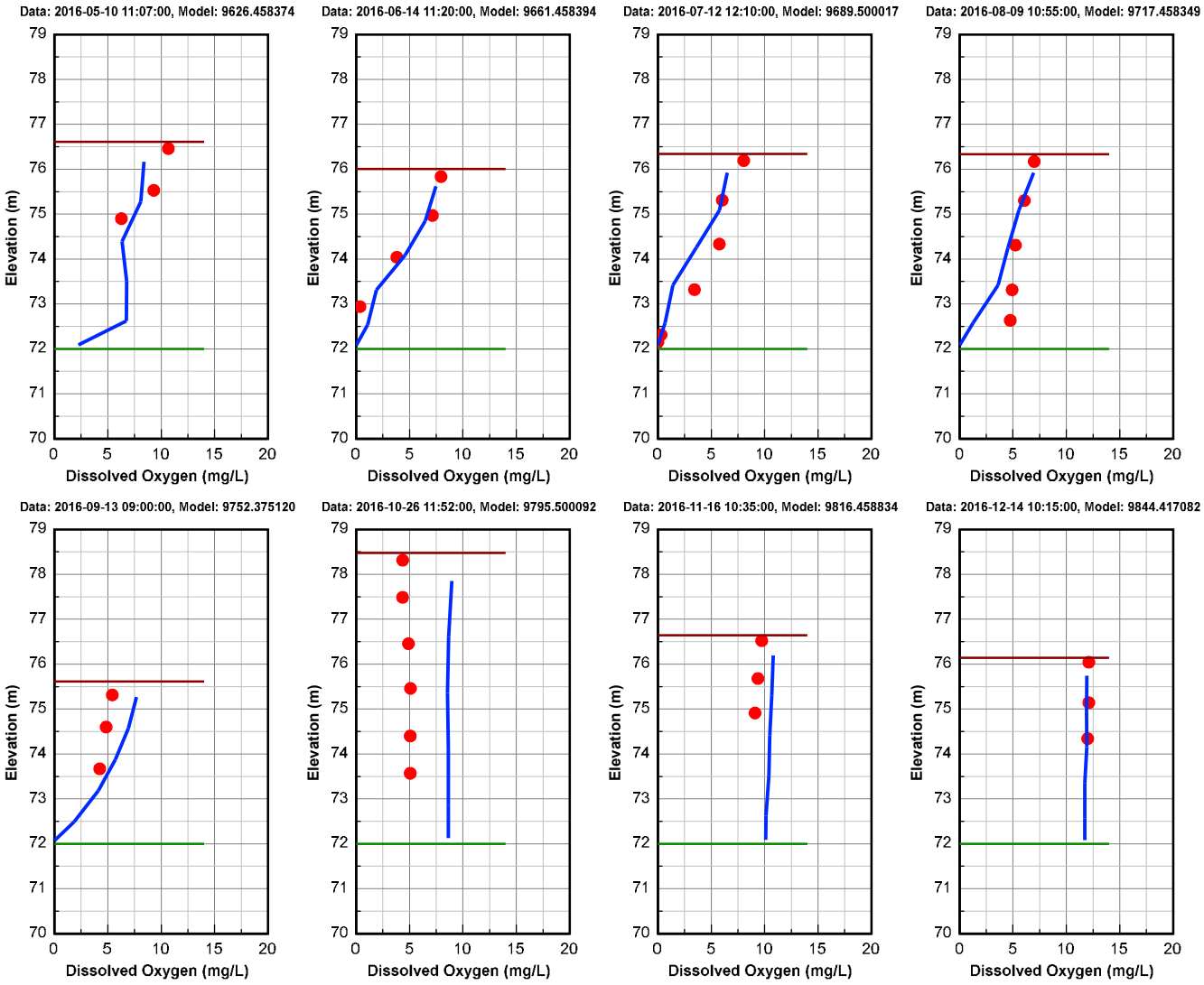

May 2016 – December 2016 (3 of 6)

Vertical Profile: NEU013, Model Cell: 42, 17

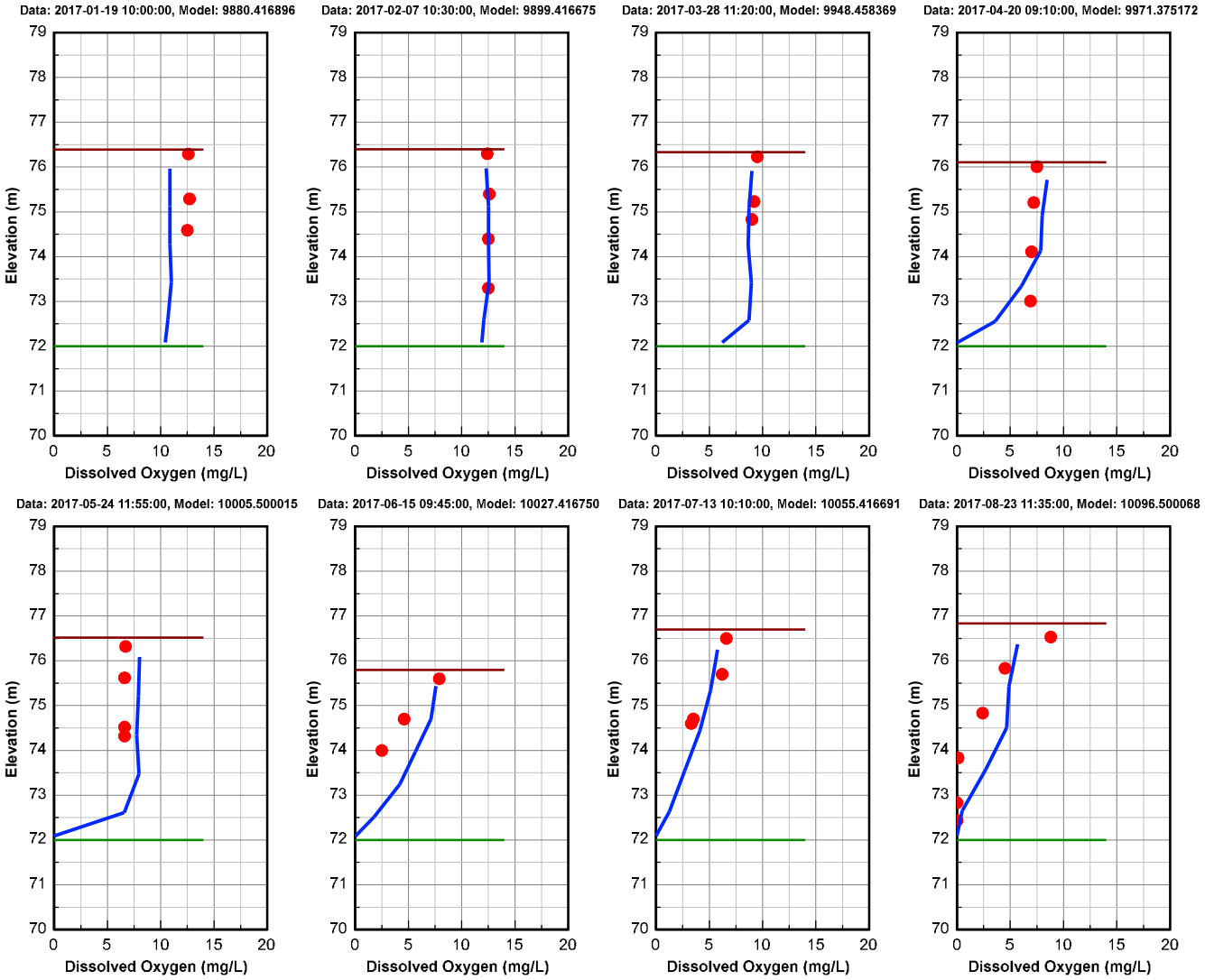

January 2017 – August 2017 (4 of 6)

Vertical Profile: NEU013, Model Cell: 42, 17

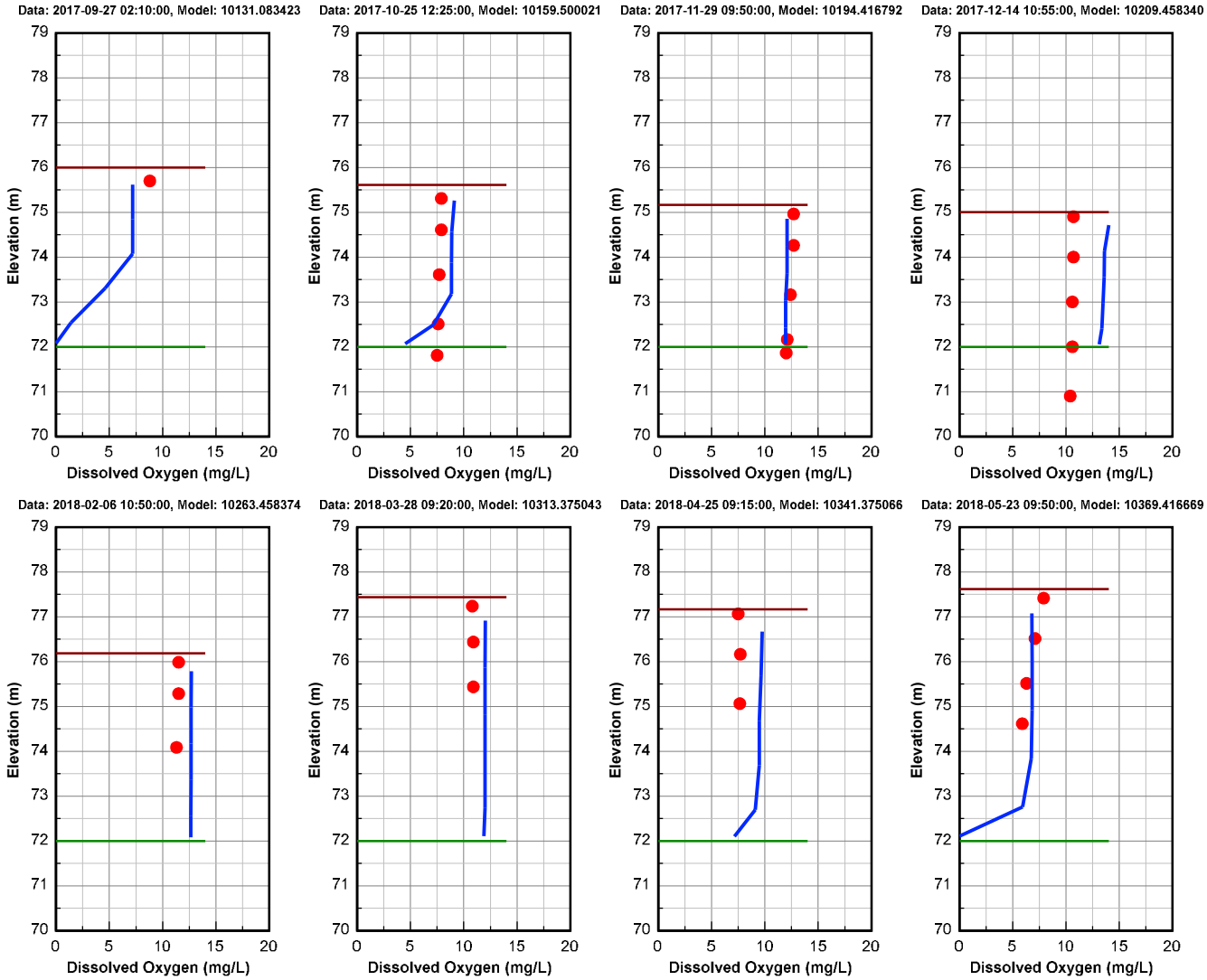

September 2017 – May 2018 (5 of 6)

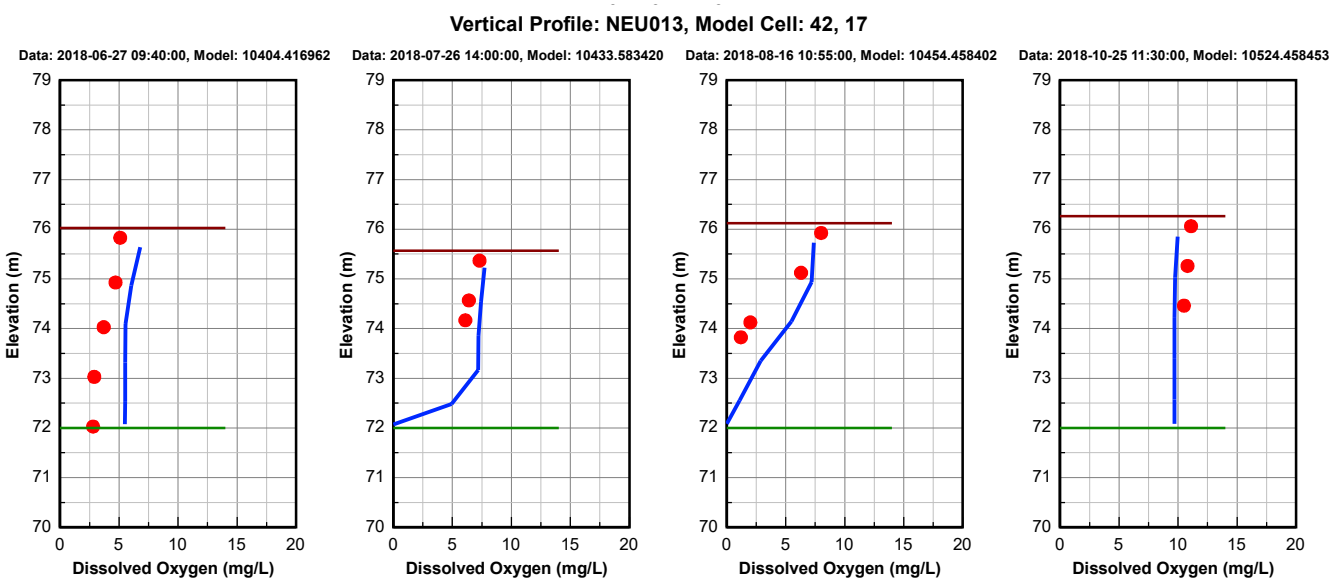

June 2018 – October 2018 (6 of 6)

Figure 2-4 DO Vertical Profile Comparison Plot at Station NEU013 during the calibration and validation period. Red dots are data, and blue continuous lines are model results.

Vertical Profile: NEU0171B, Model Cell: 42, 36

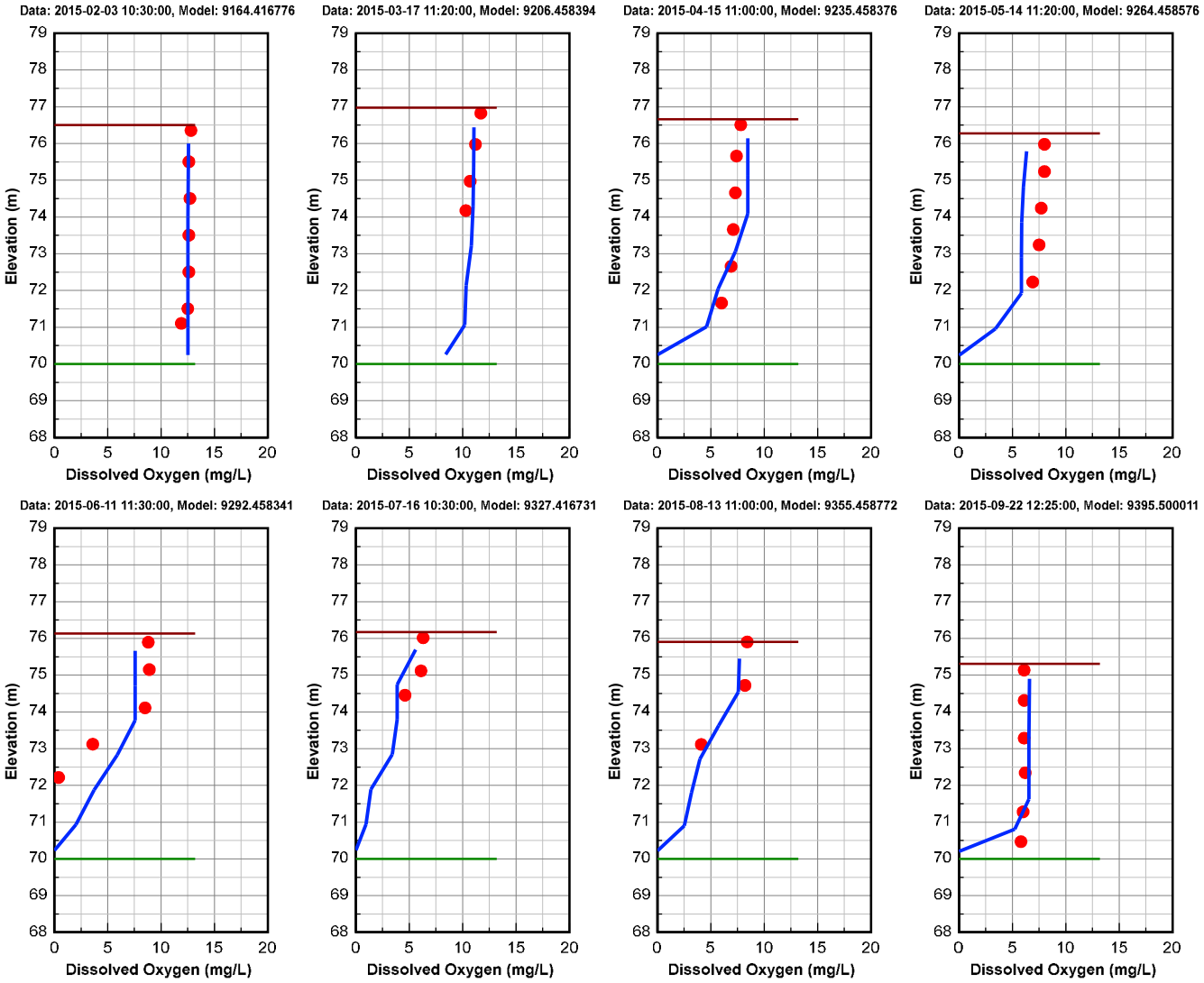

February 2015 – September 2015 (1 of 6)

Vertical Profile: NEU0171B, Model Cell: 42, 36

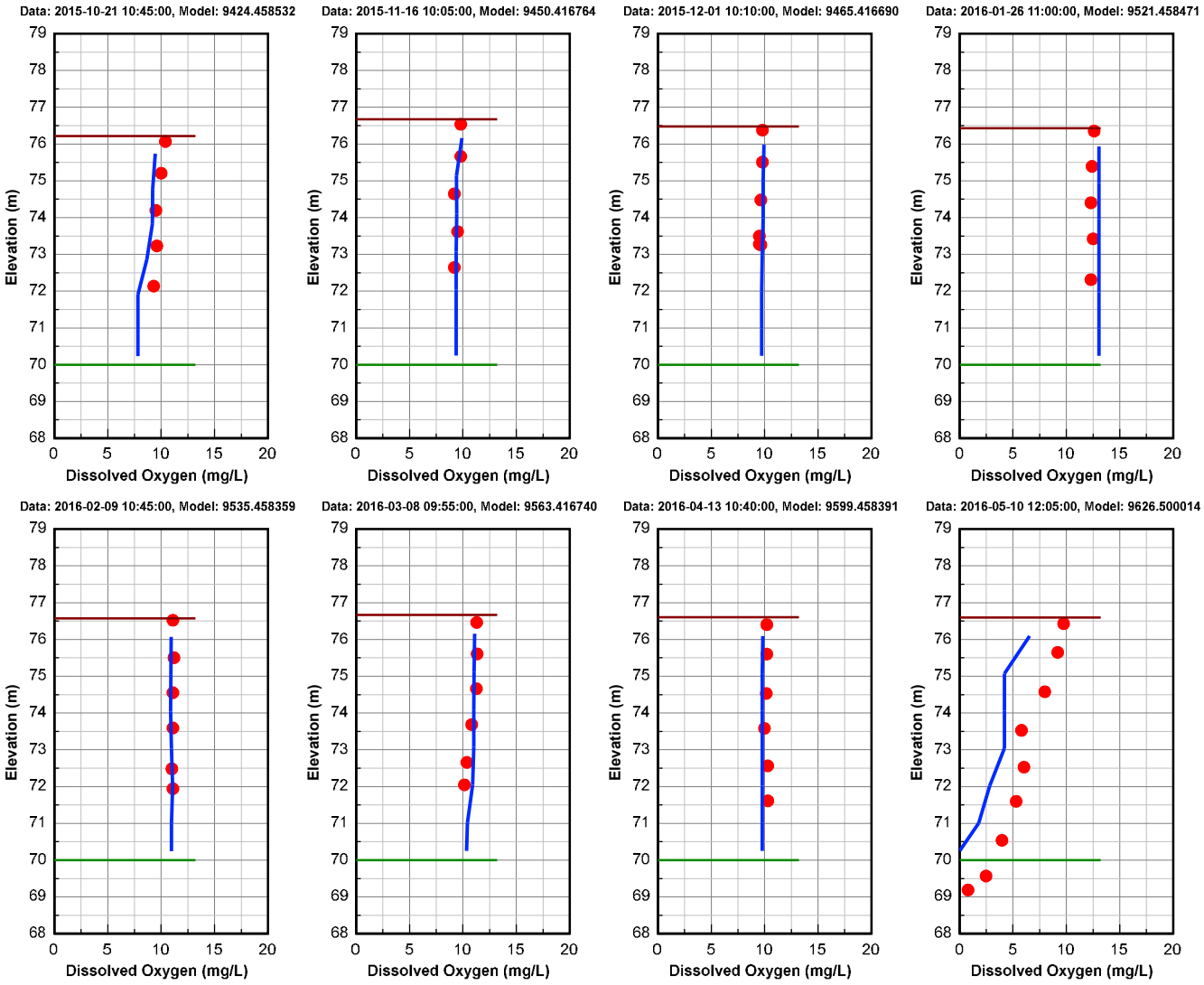

October 2015 – May 2016 (2 of 6)

Vertical Profile: NEU0171B, Model Cell: 42, 36

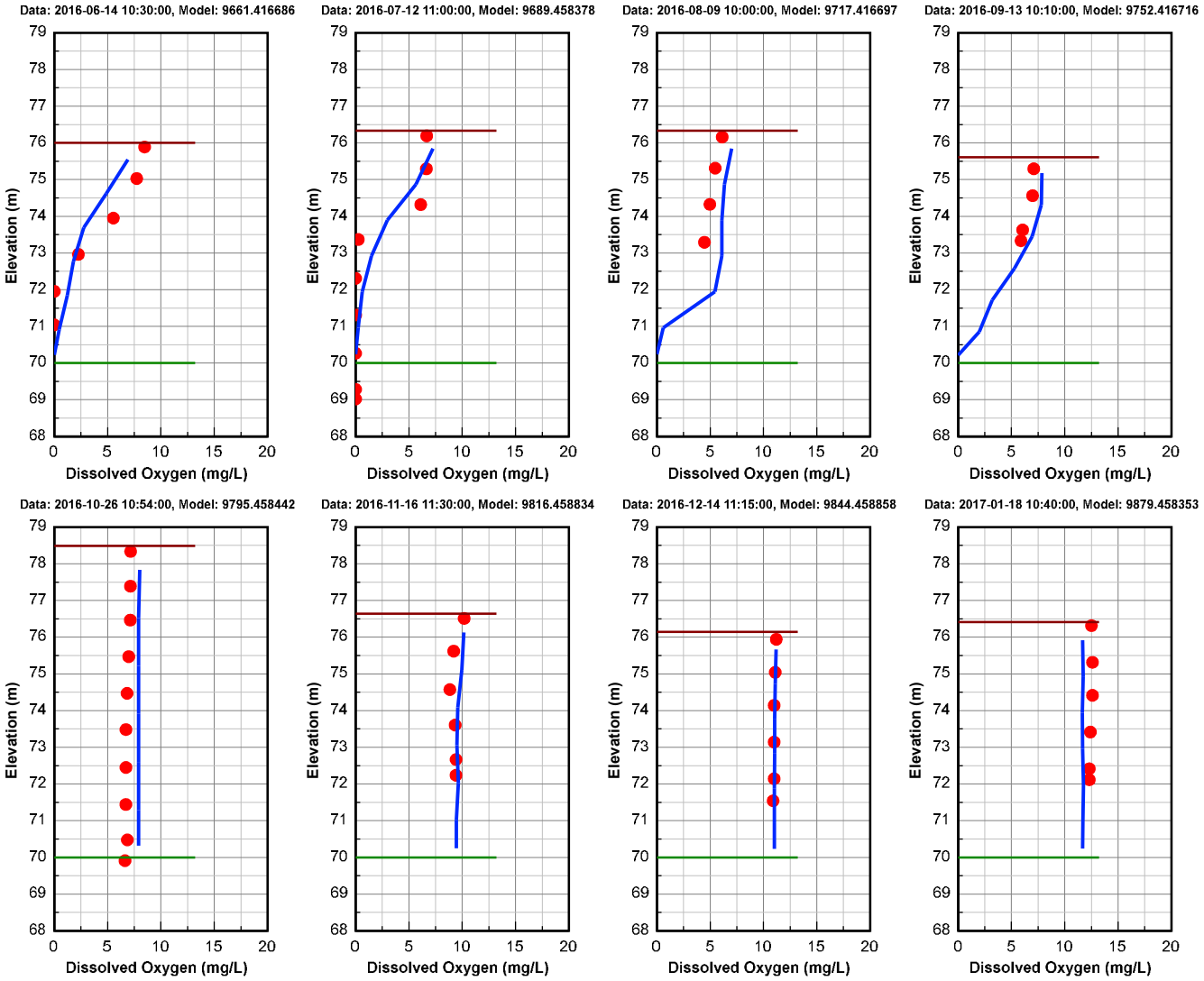

June 2016 – January 2017 (3 of 6)

Vertical Profile: NEU0171B, Model Cell: 42, 36

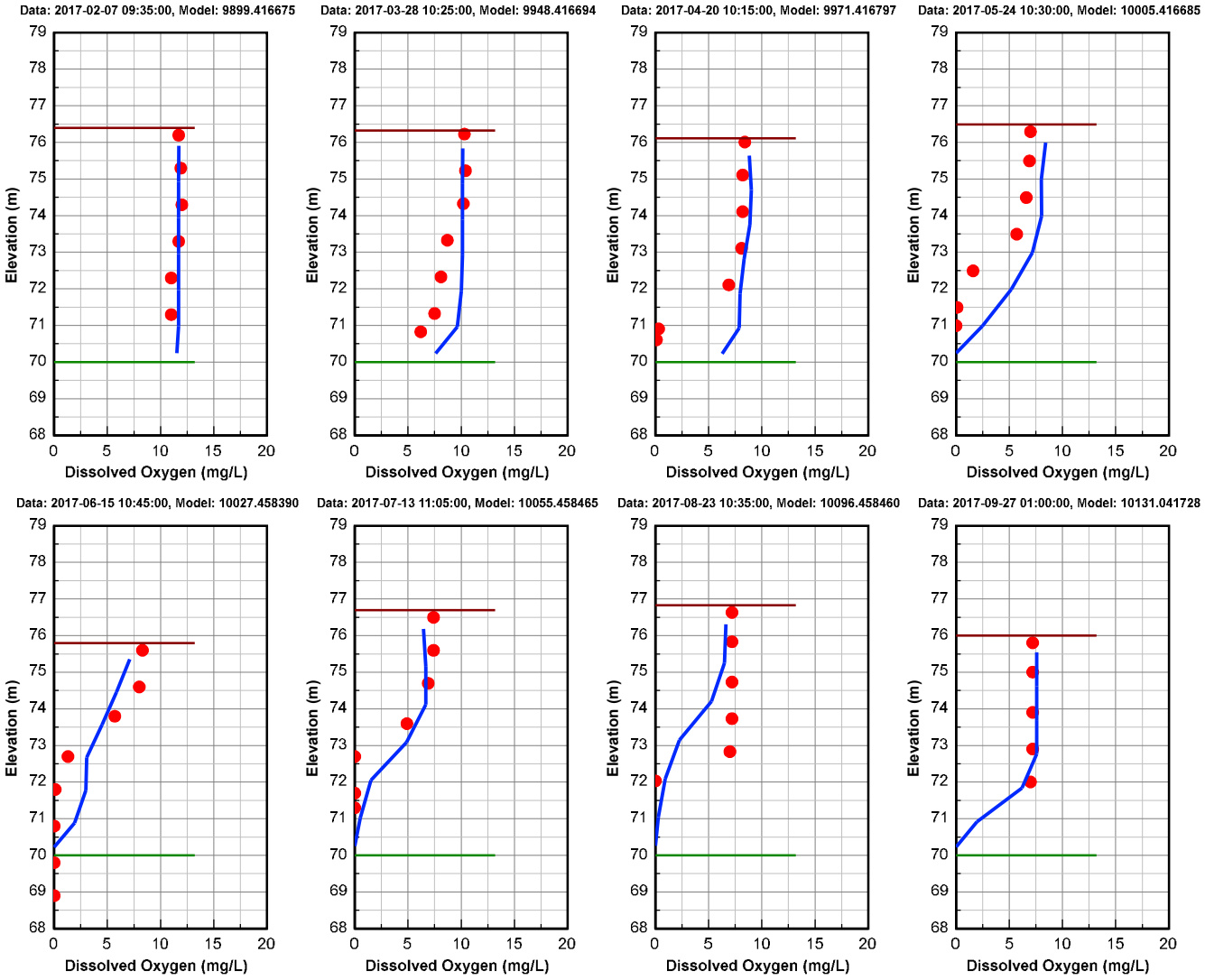

February 2017 – September 2017 (4 of 6)

Vertical Profile: NEU0171B, Model Cell: 42, 36

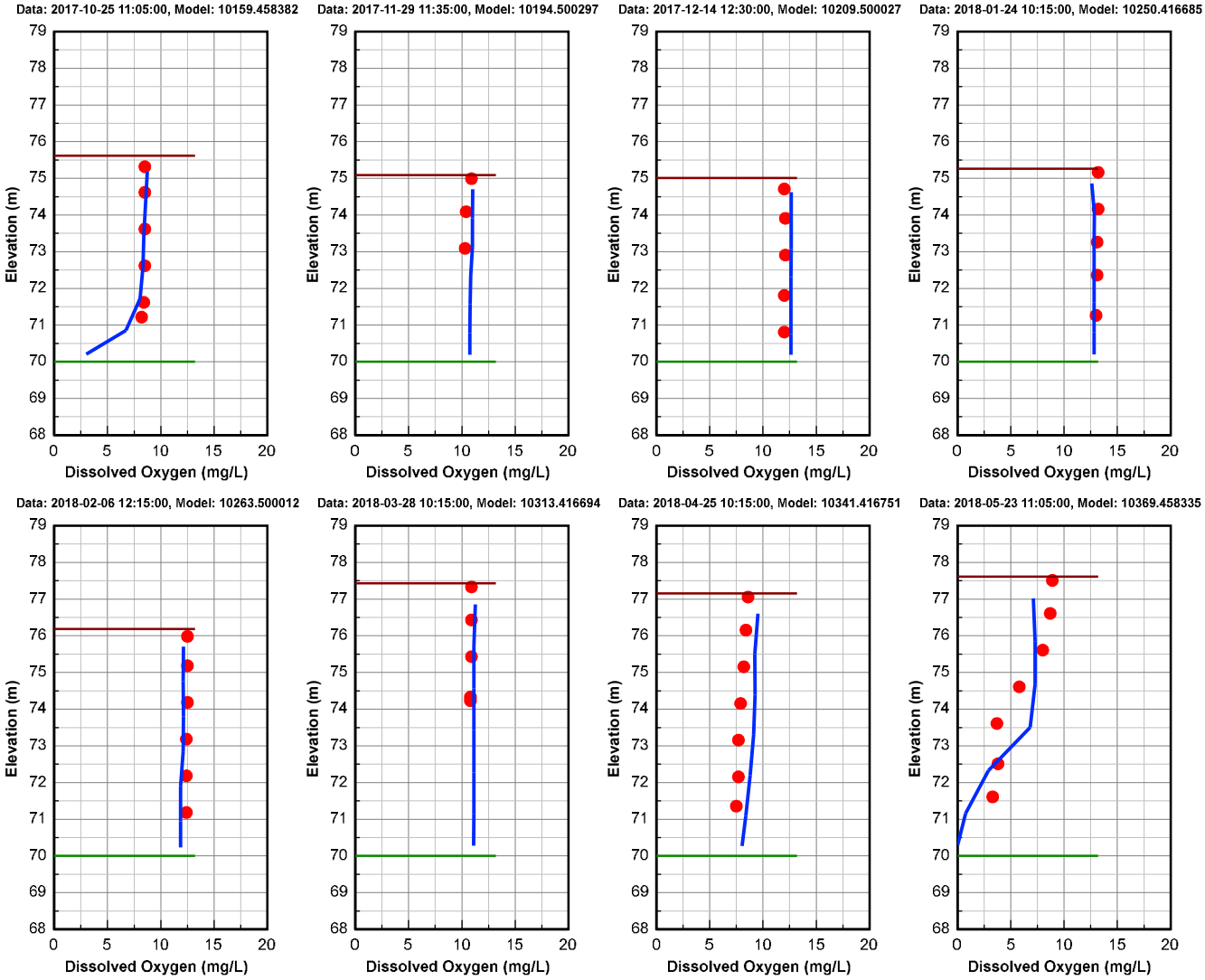

October 2017 – May 2018 (5 of 6)

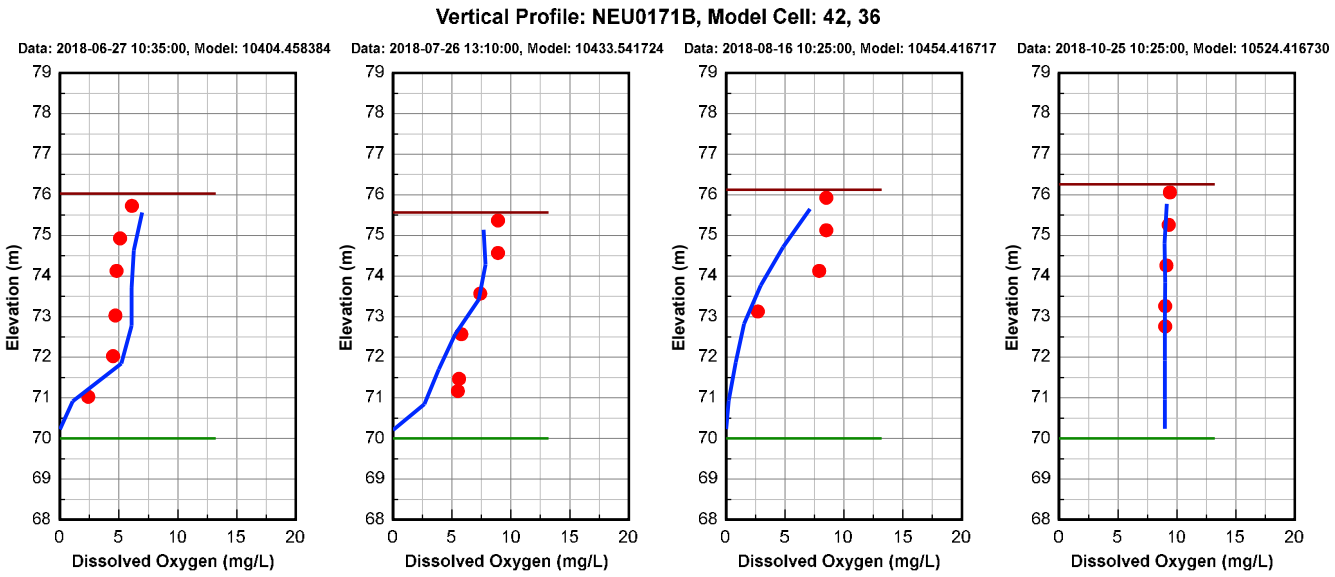

June 2018 – October 2018 (6 of 6)

Figure 2-5 DO Vertical Profile Comparison Plot at Station NEU0171B during the calibration and validation period. Red dots are data, and blue continuous lines are model results.

Vertical Profile: NEU018C, Model Cell: 35, 35

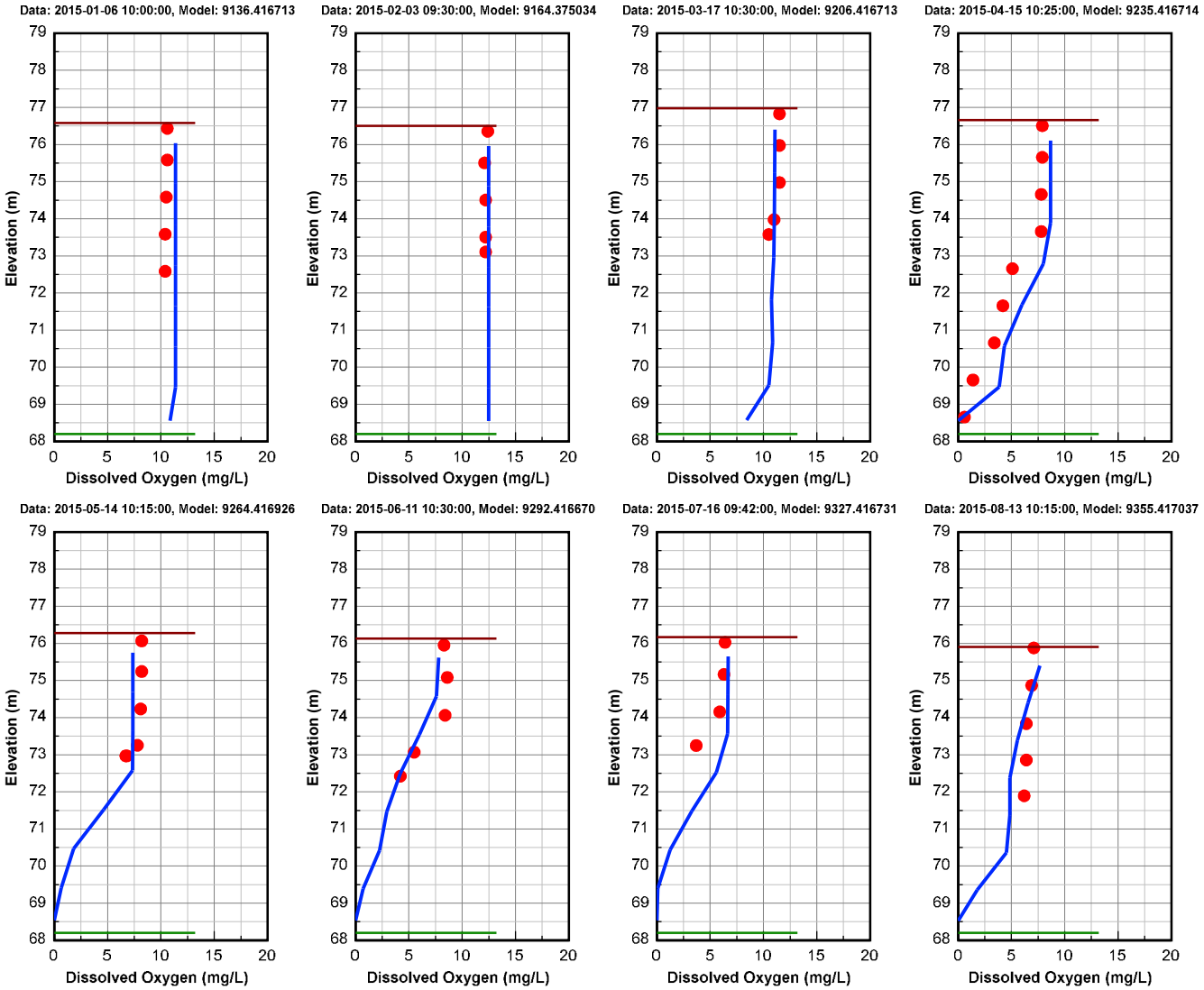

January 2015 – August 2015 (1 of 6)

Vertical Profile: NEU018C, Model Cell: 35, 35

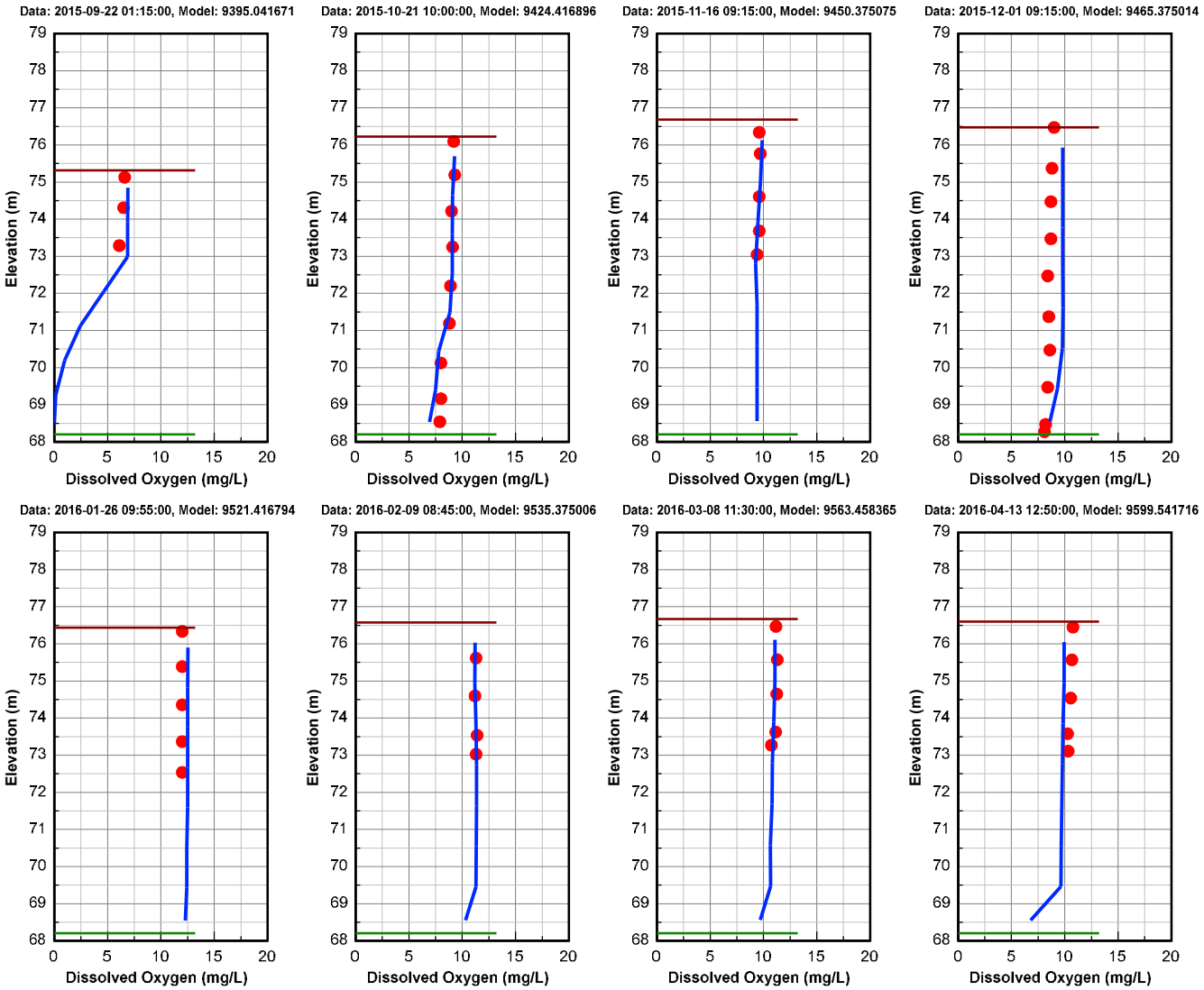

September 2015 – April 2016 (2 of 6)

Vertical Profile: NEU018C, Model Cell: 35, 35

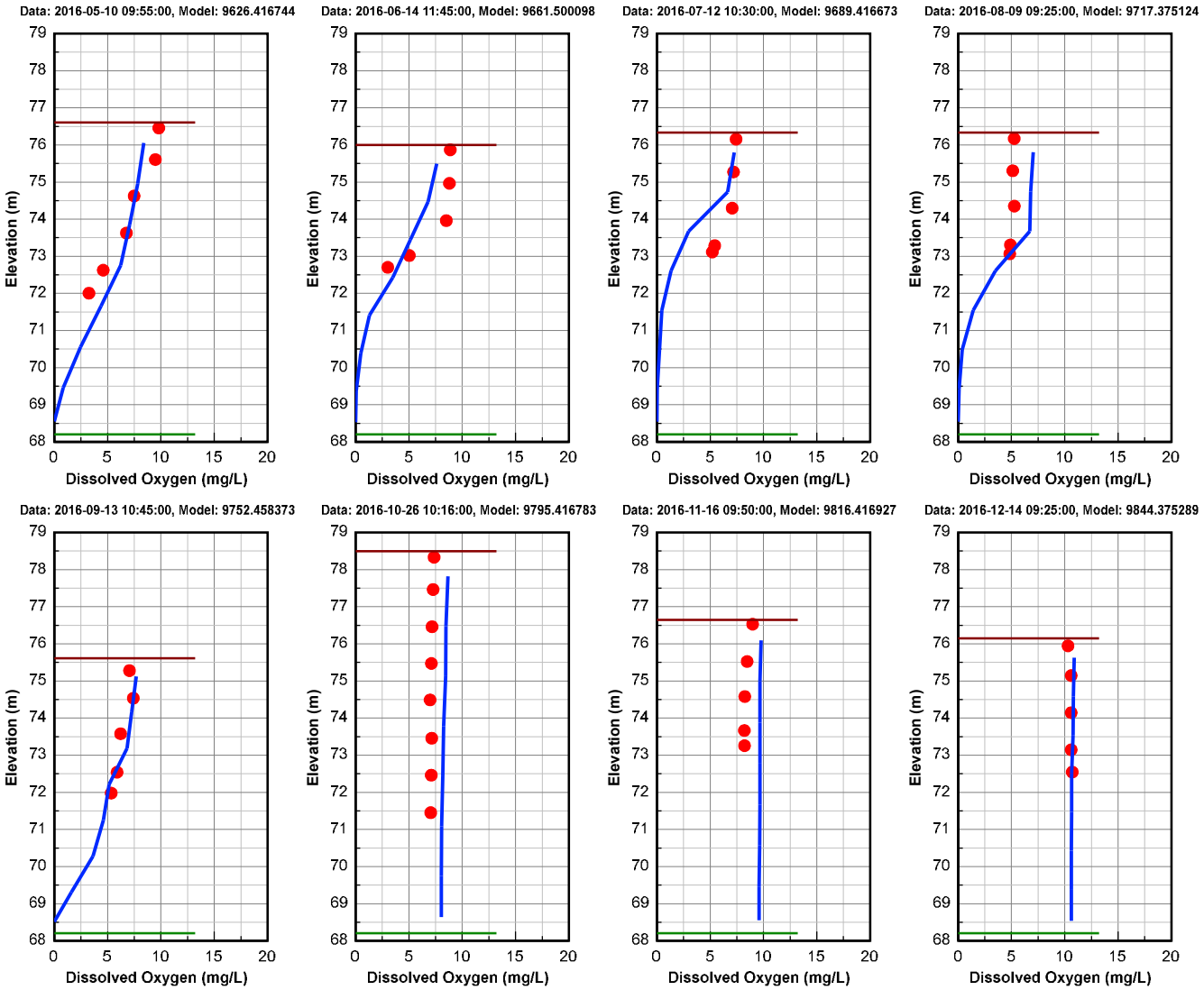

May 2016 – December 2016 (3 of 6)

Vertical Profile: NEU018C, Model Cell: 35, 35

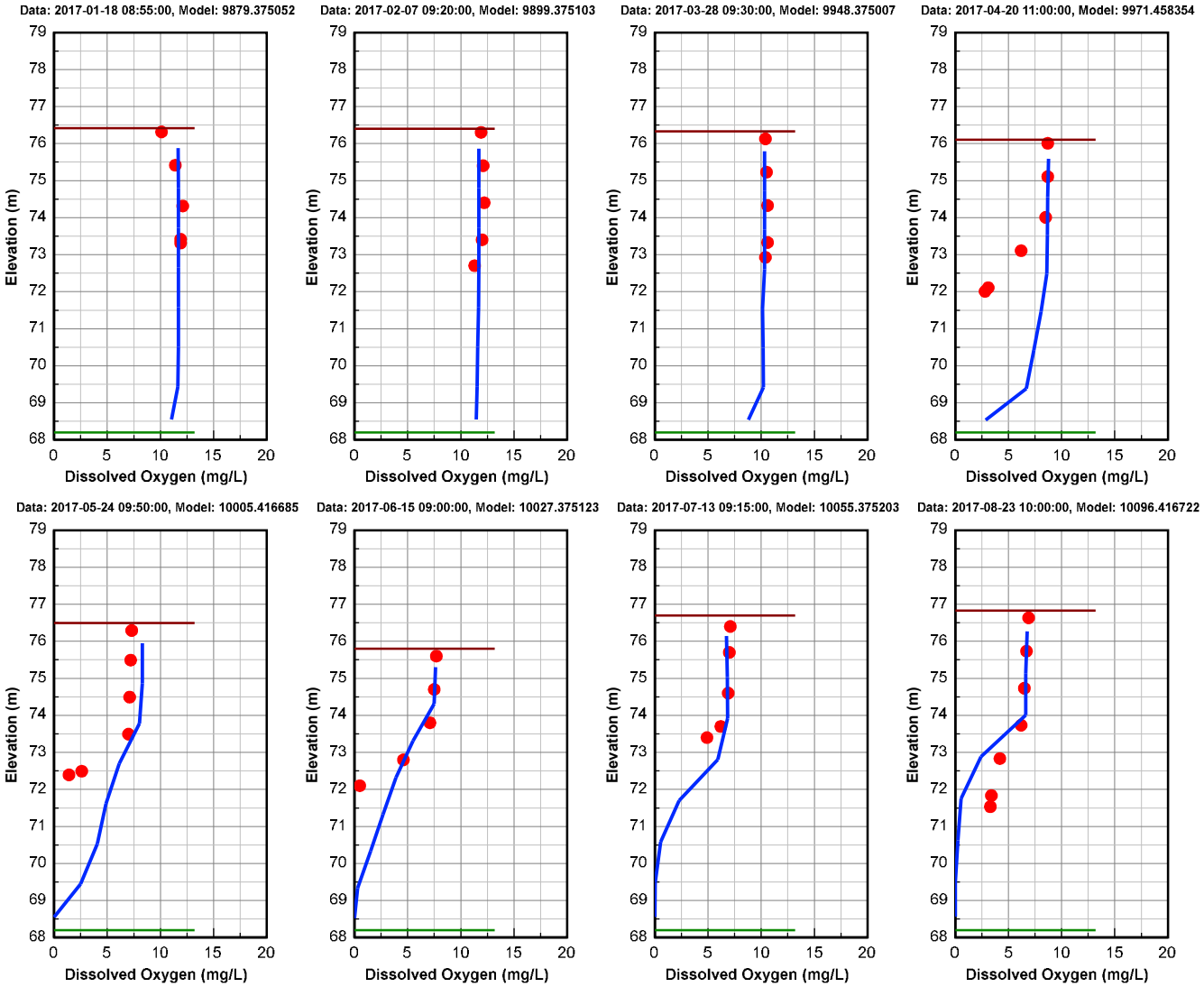

January 2017 – August 2017 (4 of 6)

Vertical Profile: NEU018C, Model Cell: 35, 35

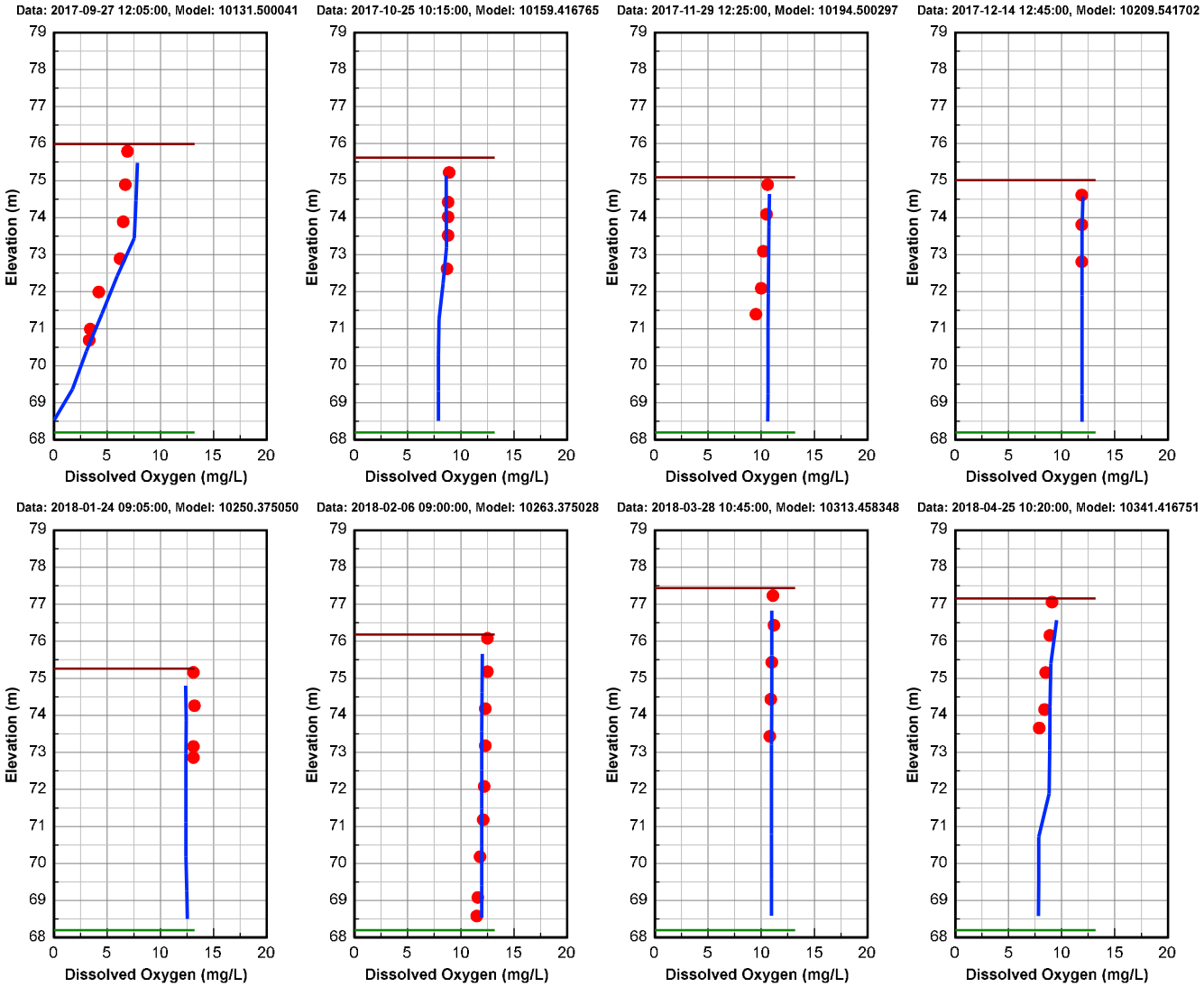

September 2017 – April 2018 (5 of 6)

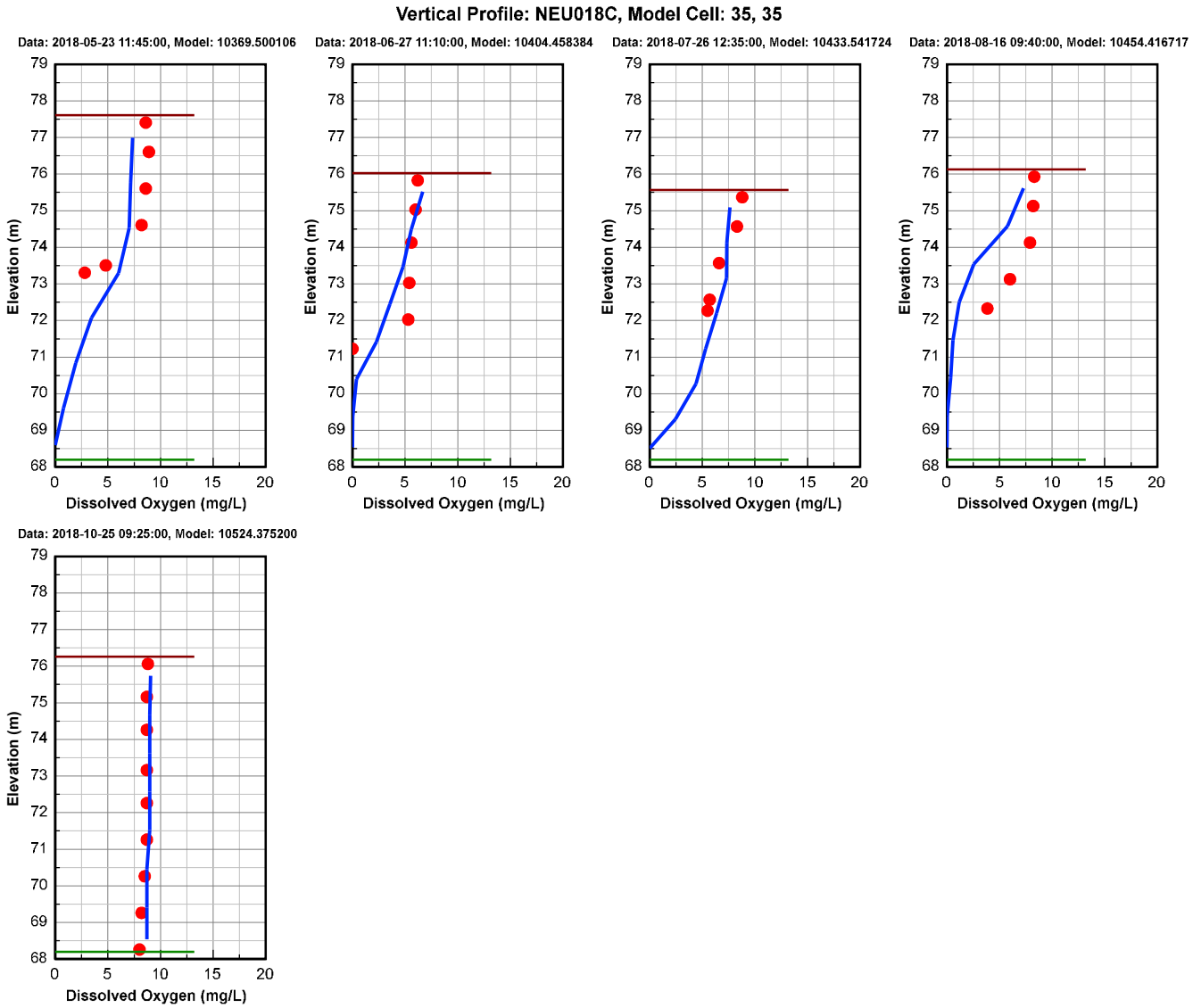

May 2018 – October 2018 (6 of 6)

Figure 2-6 DO Vertical Profile Comparison Plot at Station NEU018C during the calibration and validation period. Red dots are data, and blue continuous lines are model results.

Vertical Profile: NEU018E, Model Cell: 34, 40

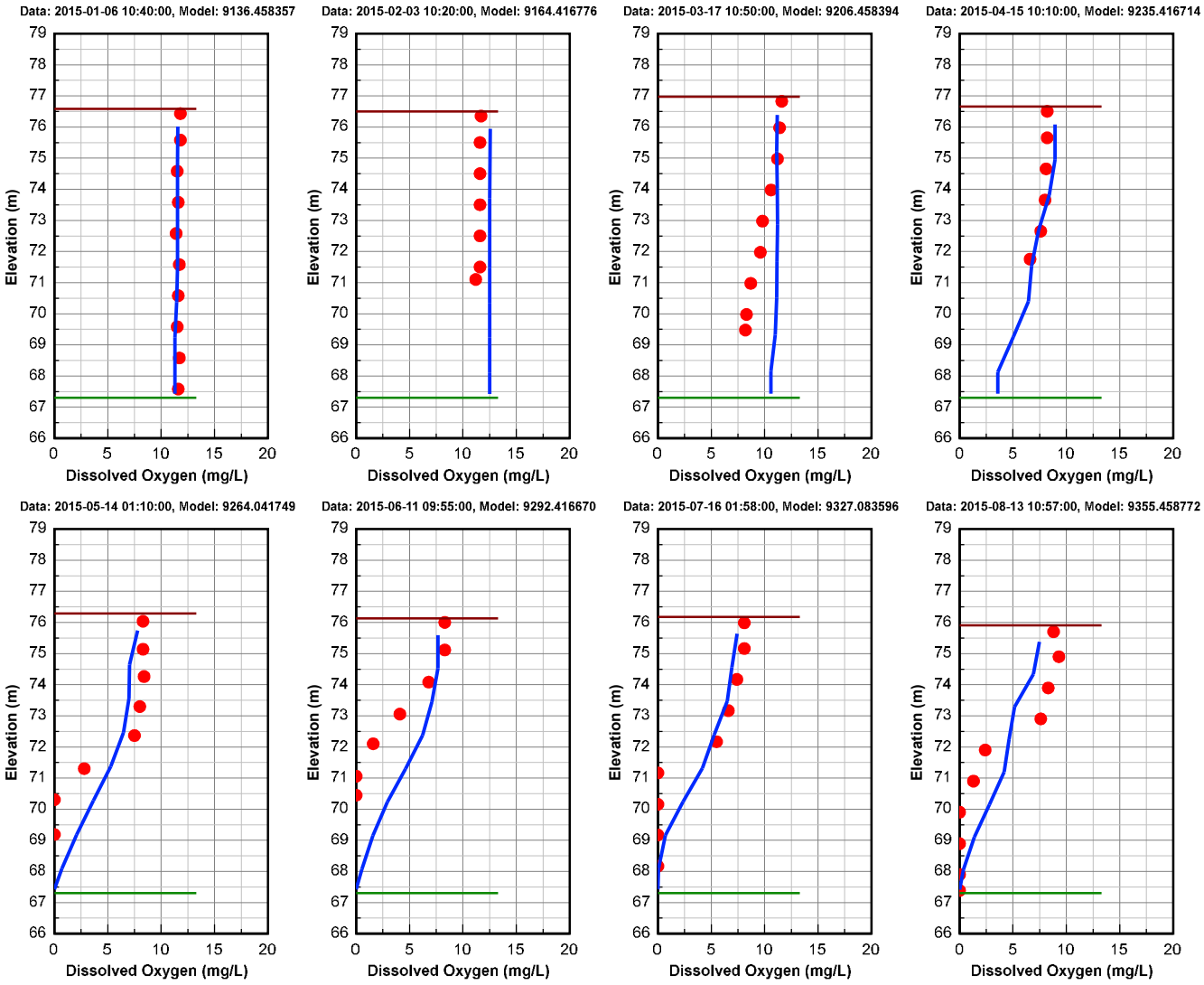

January 2015 – August 2015 (1 of 6)

Vertical Profile: NEU018E, Model Cell: 34, 40

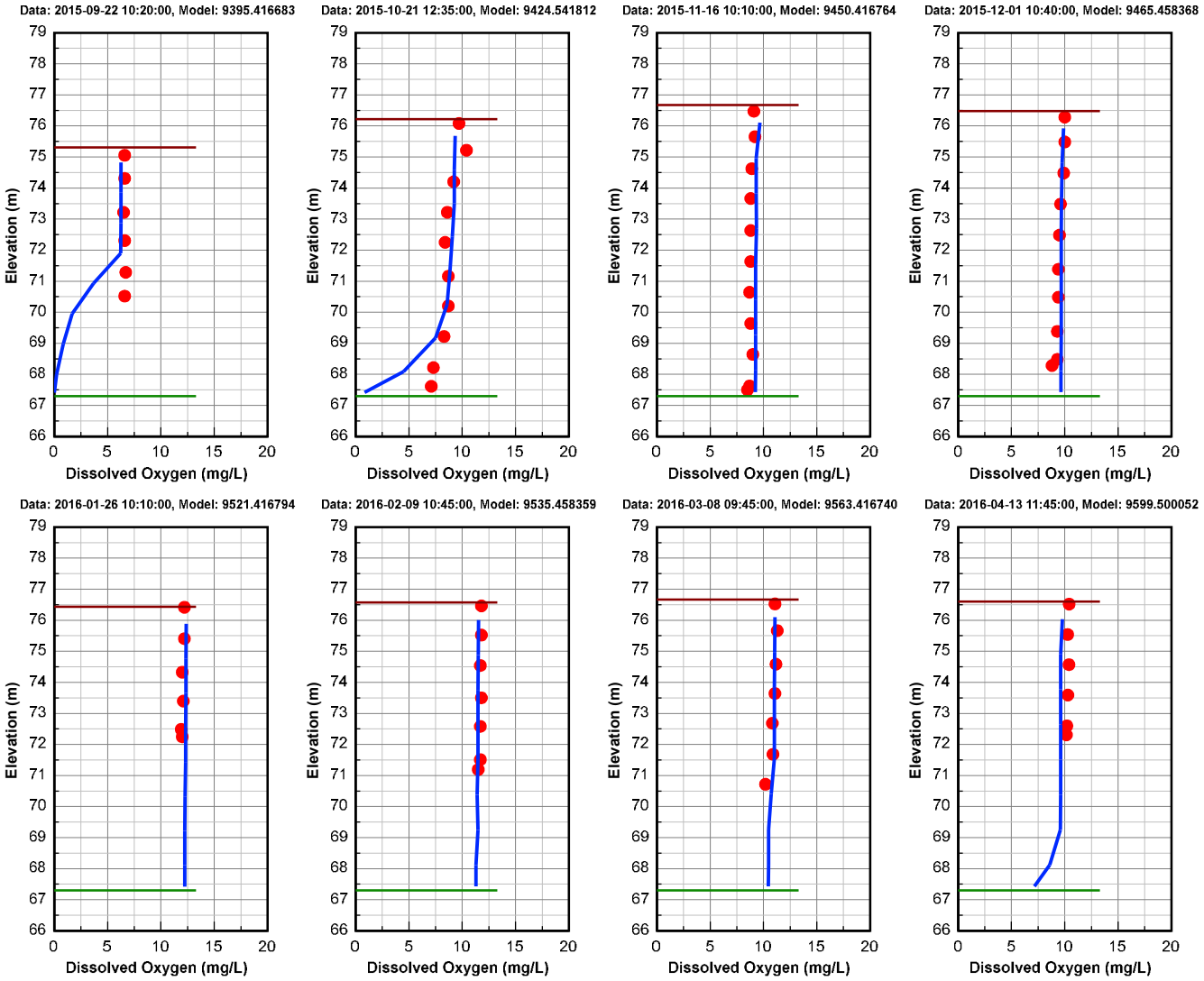

September 2015 – April 2016 (2 of 6)

Vertical Profile: NEU018E, Model Cell: 34, 40

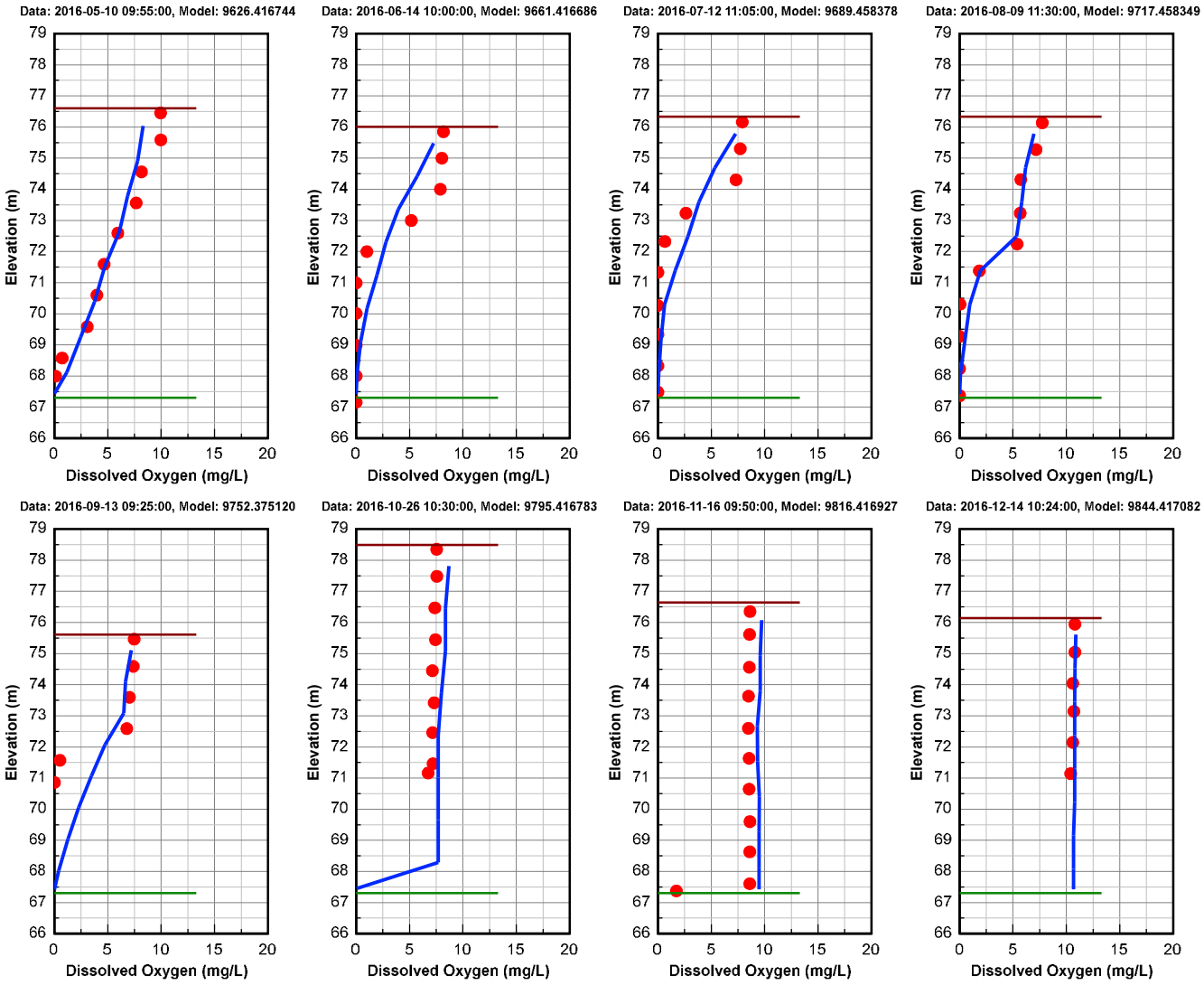

May 2016 – December 2016 (3 of 6)

Vertical Profile: NEU018E, Model Cell: 34, 40

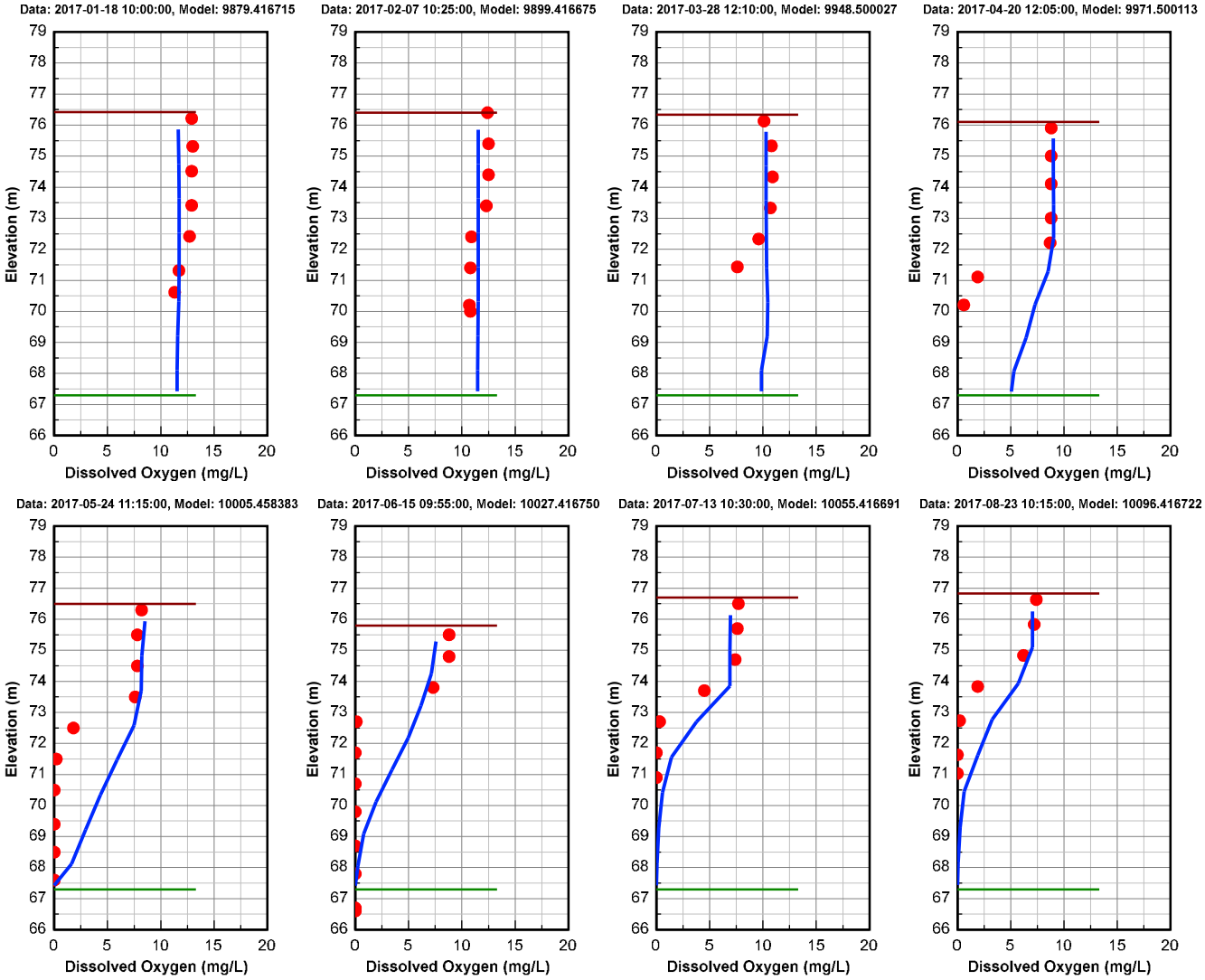

January 2017 – August 2017 (4 of 6)

Vertical Profile: NEU018E, Model Cell: 34, 40

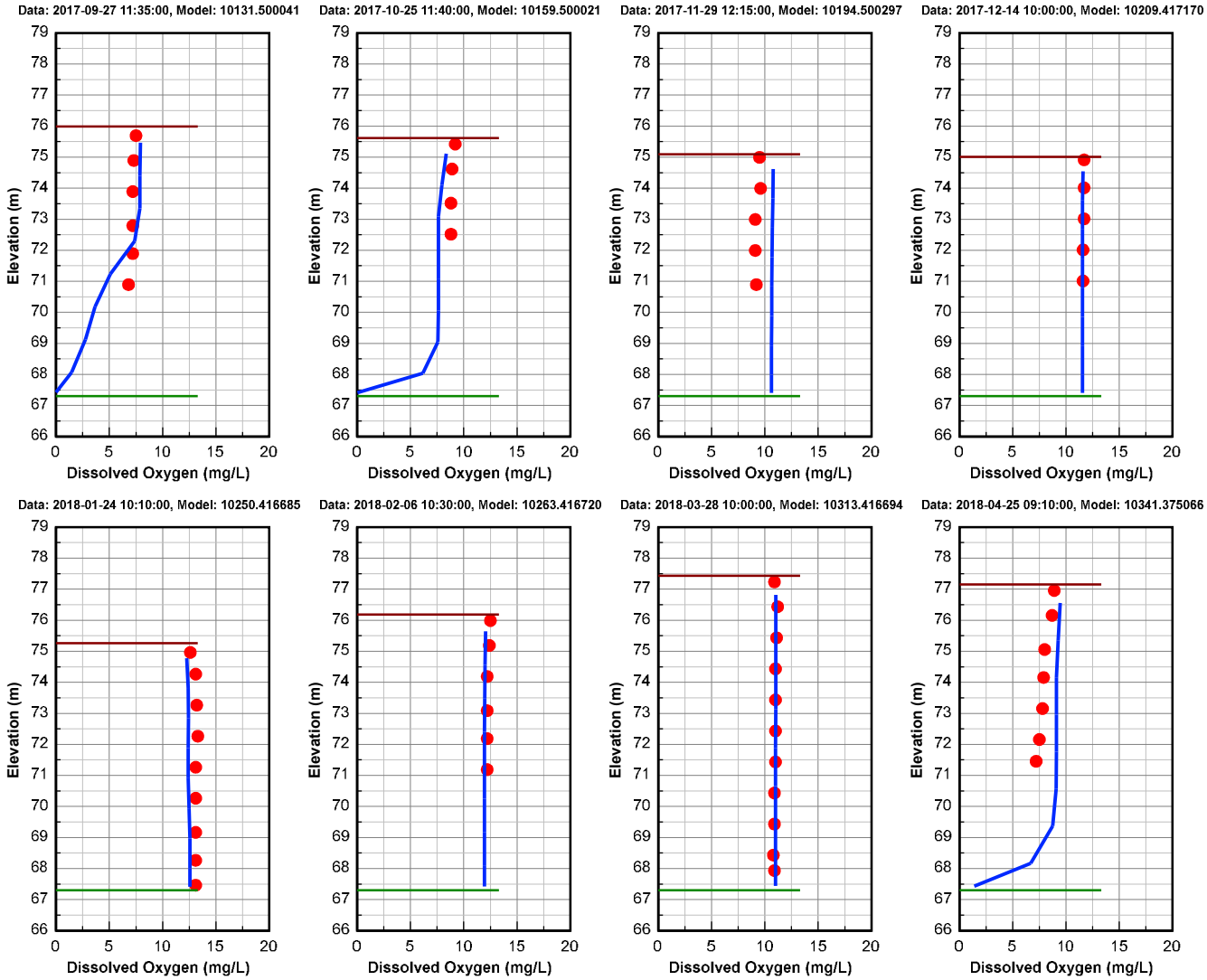

September 2017 – April 2018 (5 of 6)

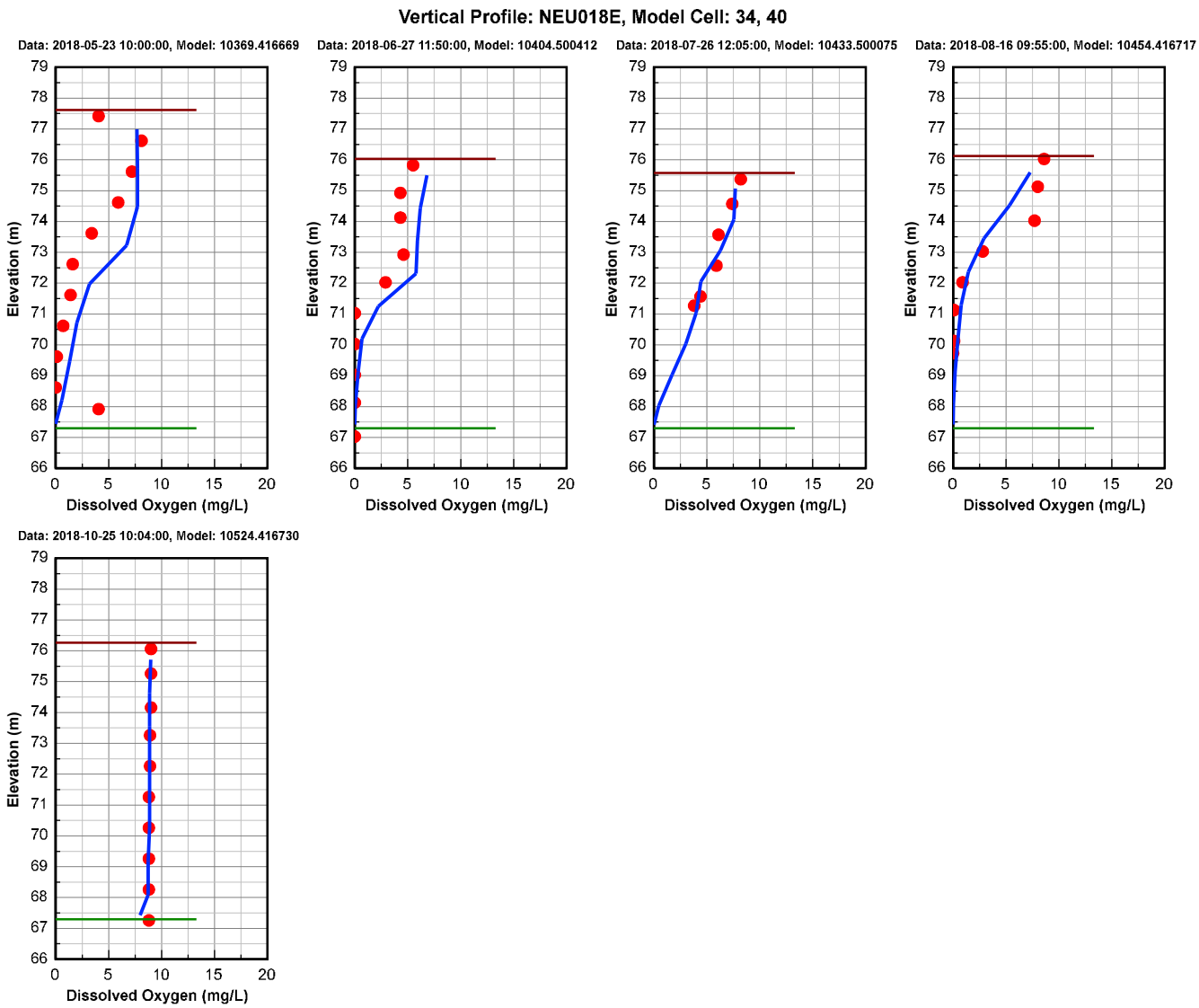

May 2018 – October 2018 (6 of 6)

Figure 2-7 DO Vertical Profile Comparison Plot at Station NEU018E during the calibration and validation period. Red dots are data, and blue continuous lines are model results.

Vertical Profile: NEU019E, Model Cell: 26, 43

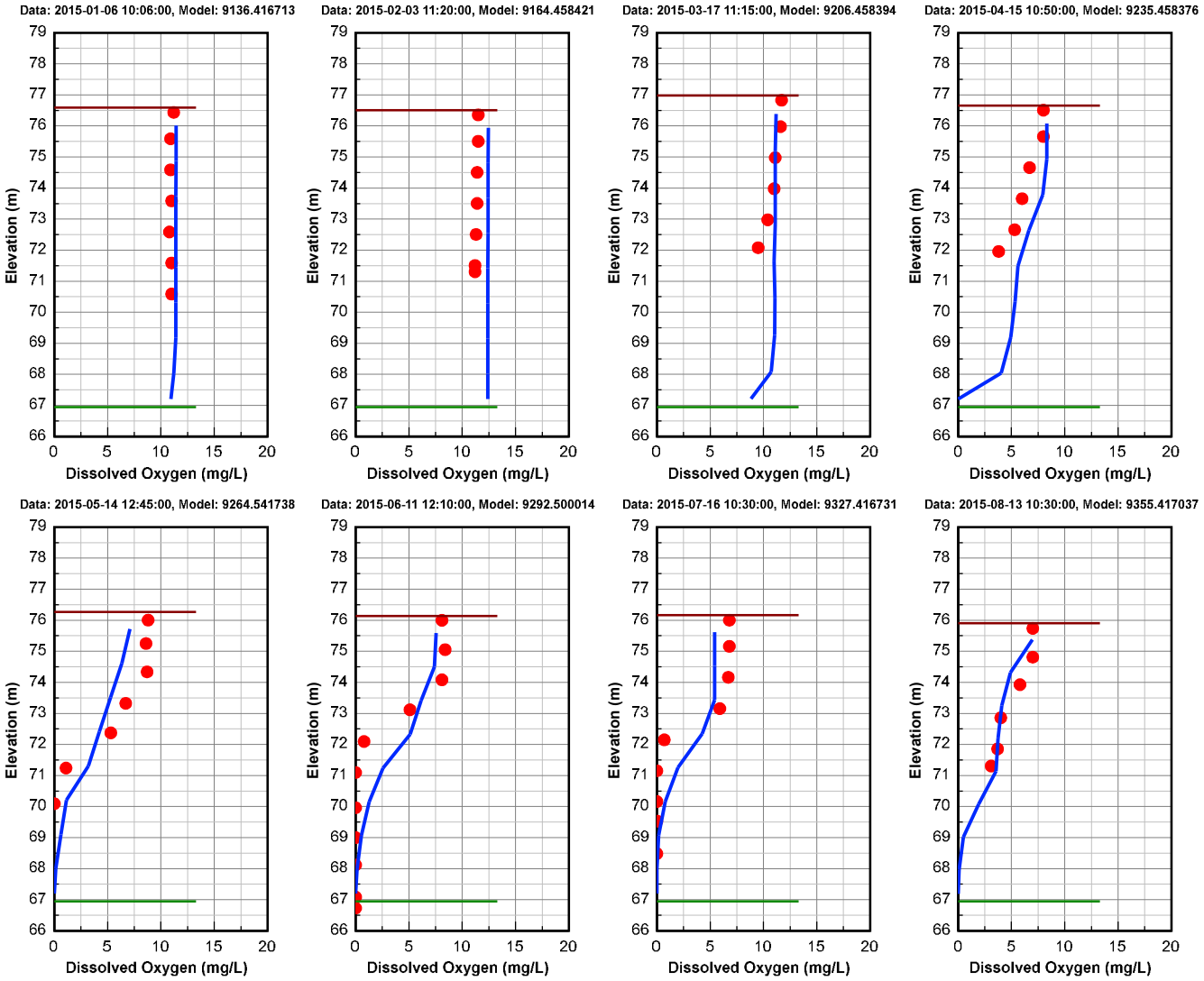

January 2015 – August 2015 (1 of 6)

Vertical Profile: NEU019E, Model Cell: 26, 43

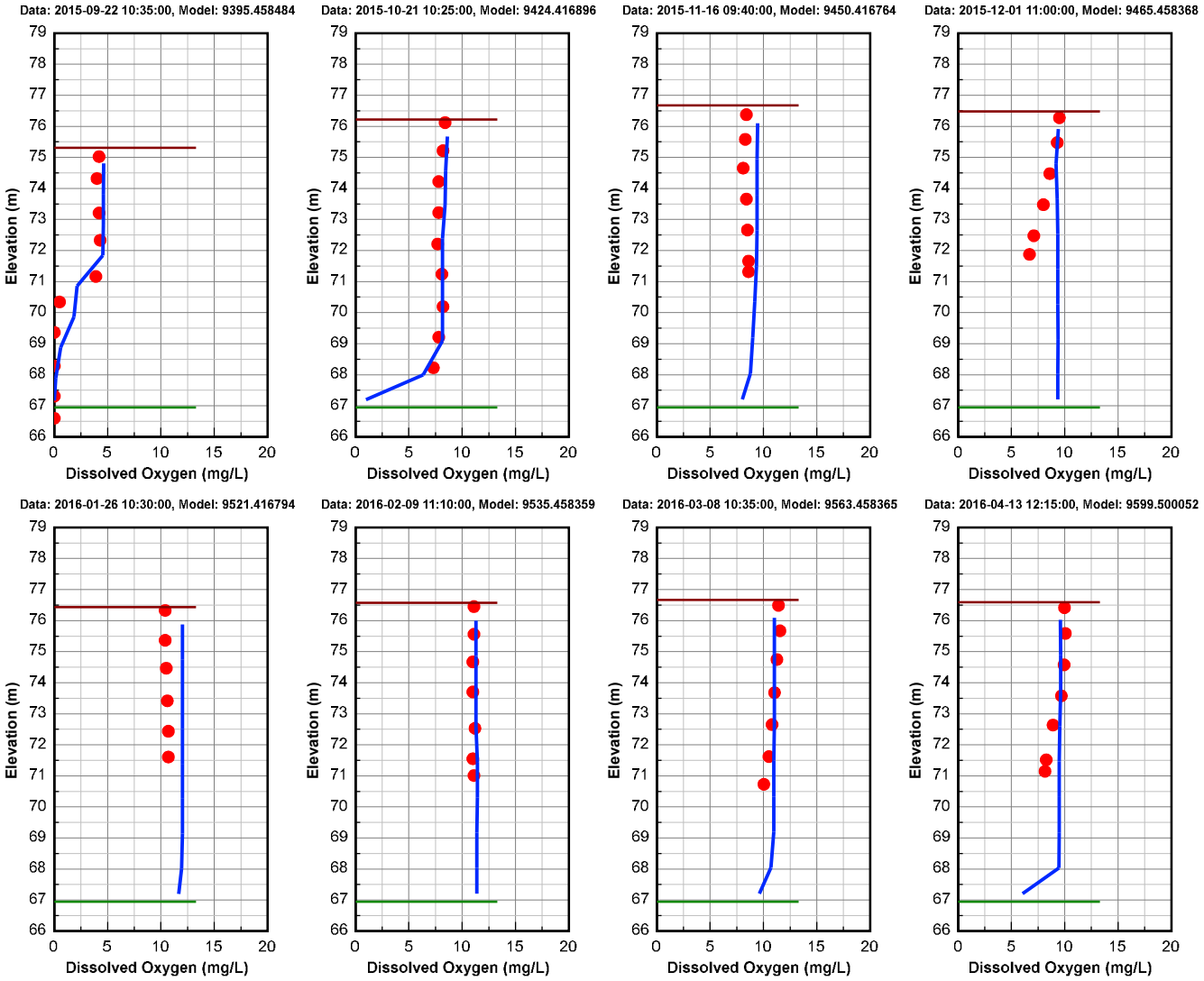

September 2015 – April 2016 (2 of 6)

Vertical Profile: NEU019E, Model Cell: 26, 43

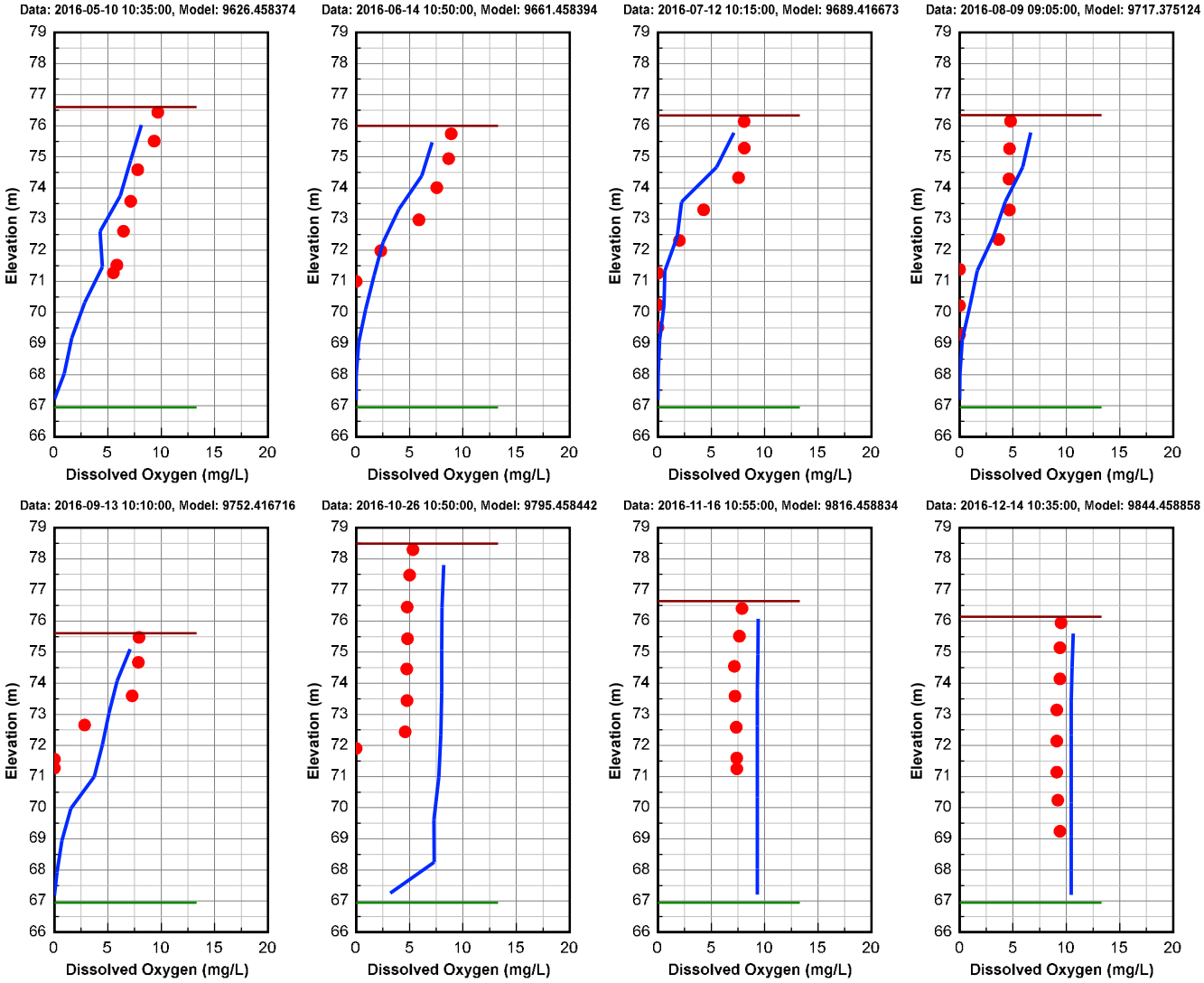

May 2016 – December 2016 (3 of 6)

Vertical Profile: NEU019E, Model Cell: 26, 43

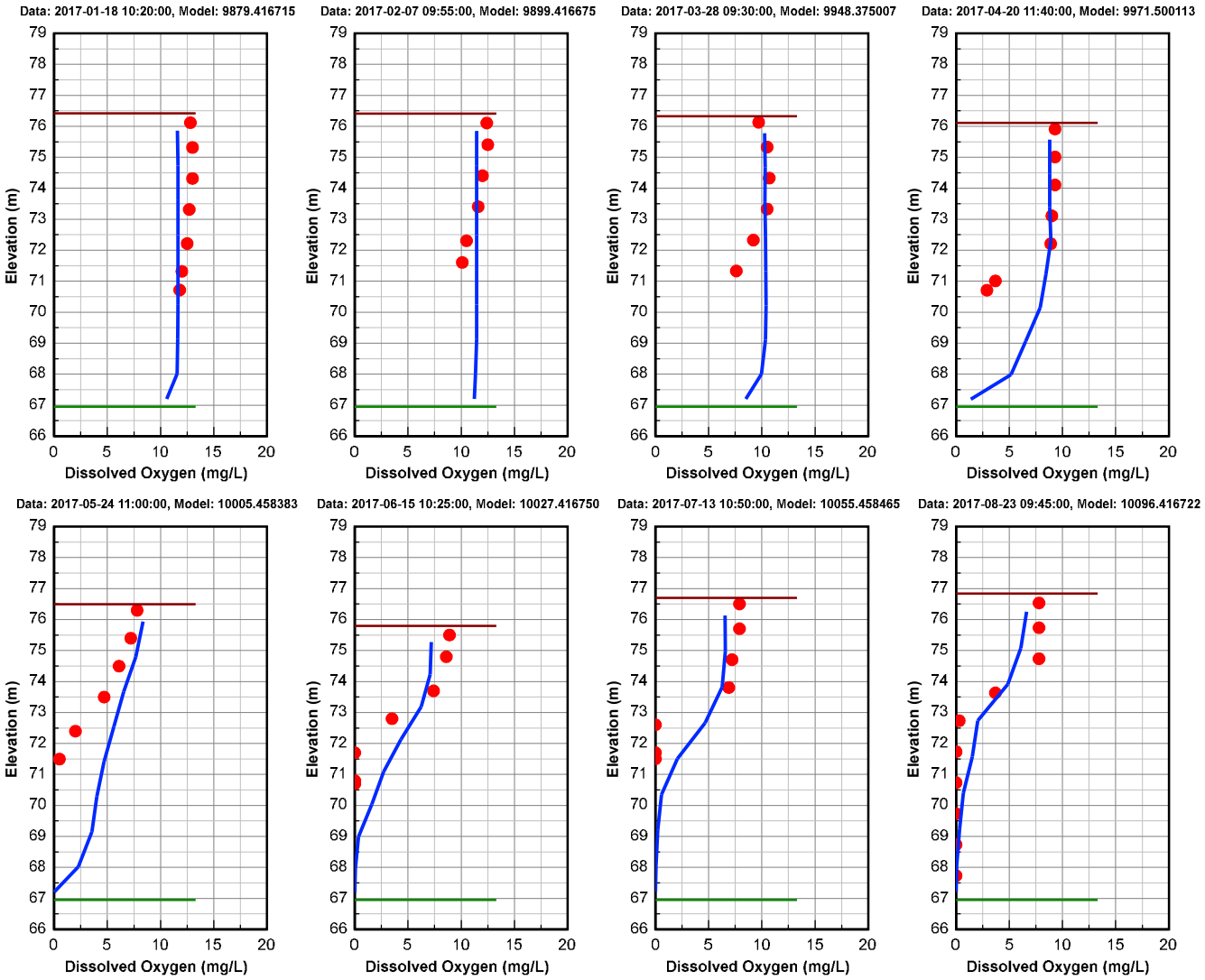

January 2017 – August 2017 (4 of 6)

Vertical Profile: NEU019E, Model Cell: 26, 43

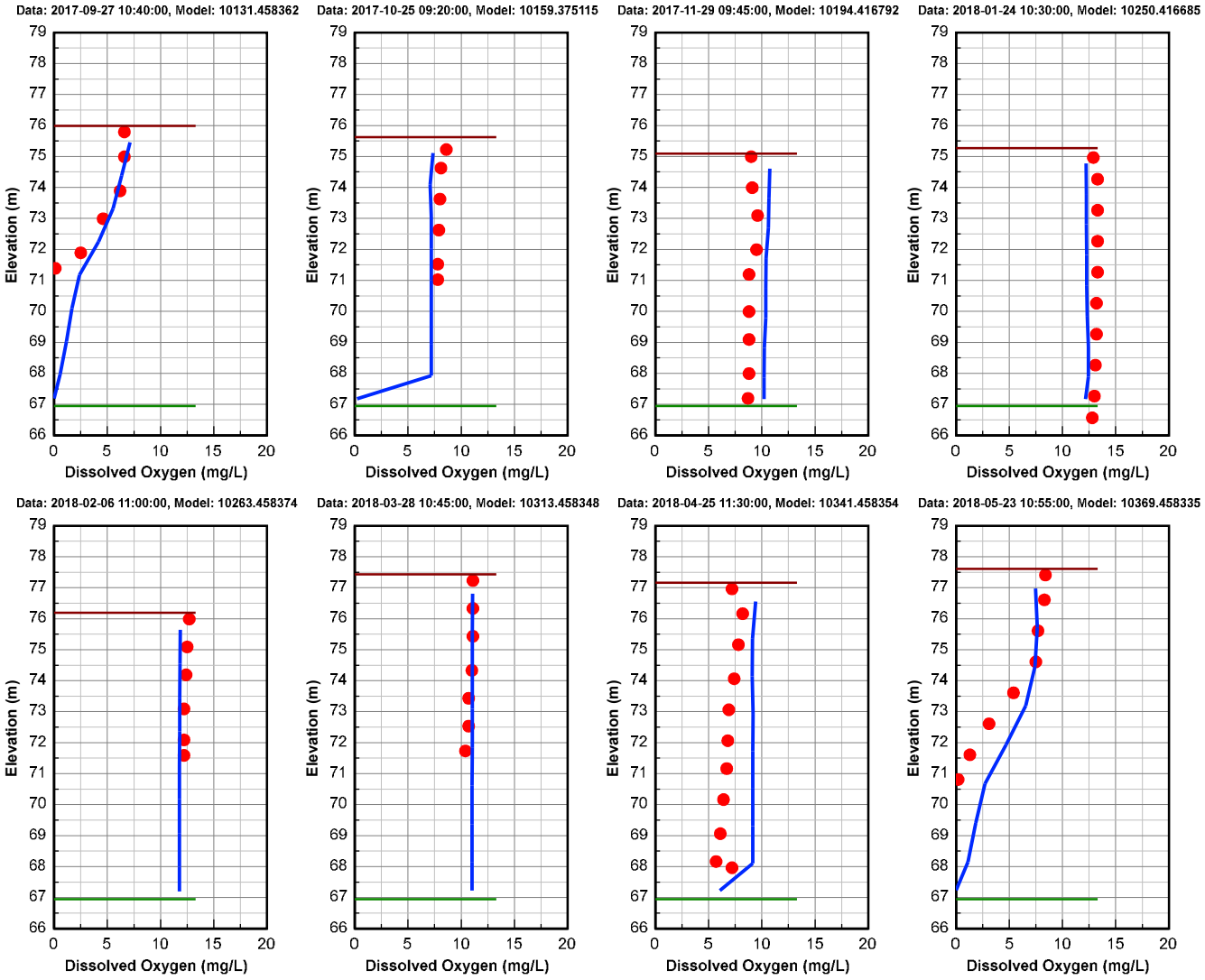

September 2017 – May 2018 (5 of 6)

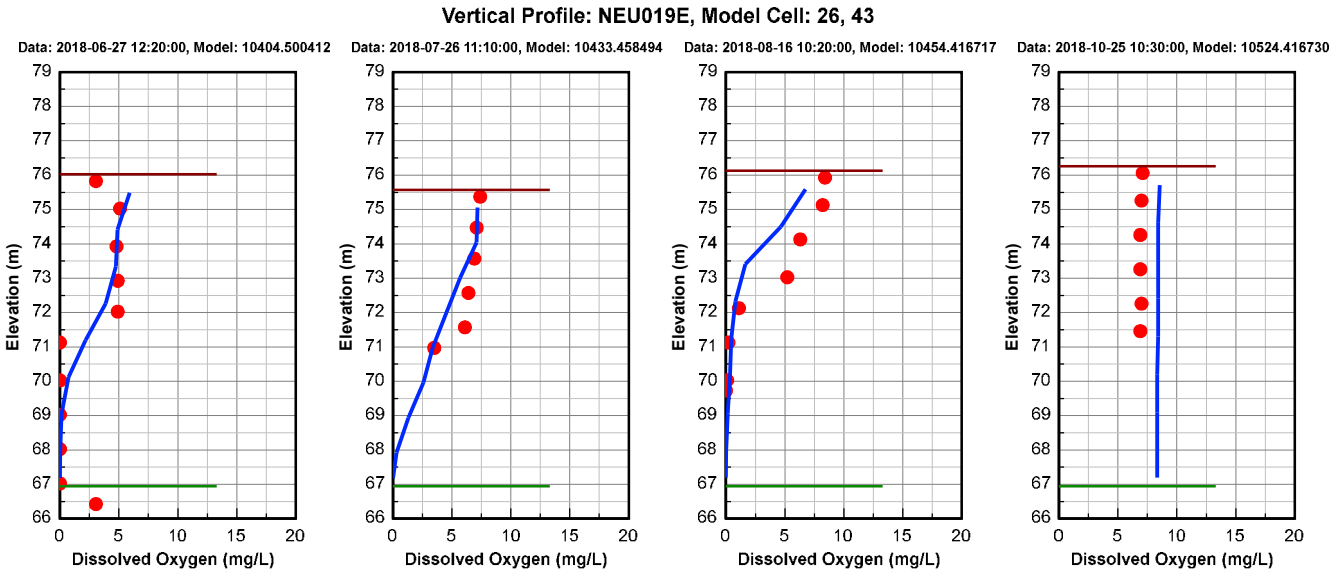

June 2018 – October 2018 (6 of 6)

Figure 2-8 DO Vertical Profile Comparison Plot at Station NEU019E during the calibration and validation period. Red dots are data, and blue continuous lines are model results.

Vertical Profile: NEU019L, Model Cell: 33, 75

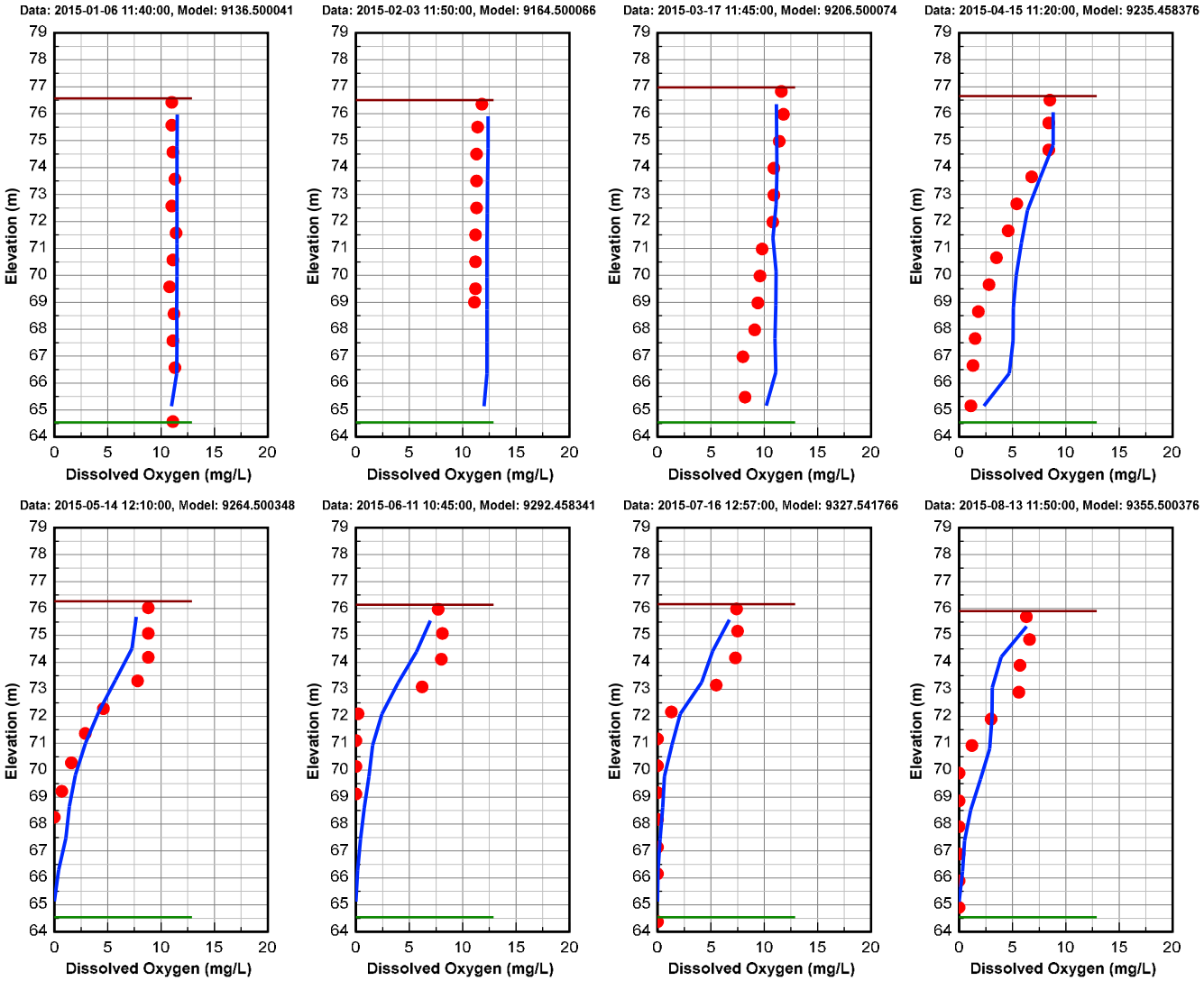

January 2015 – August 2015 (1 of 6)

Vertical Profile: NEU019L, Model Cell: 33, 75

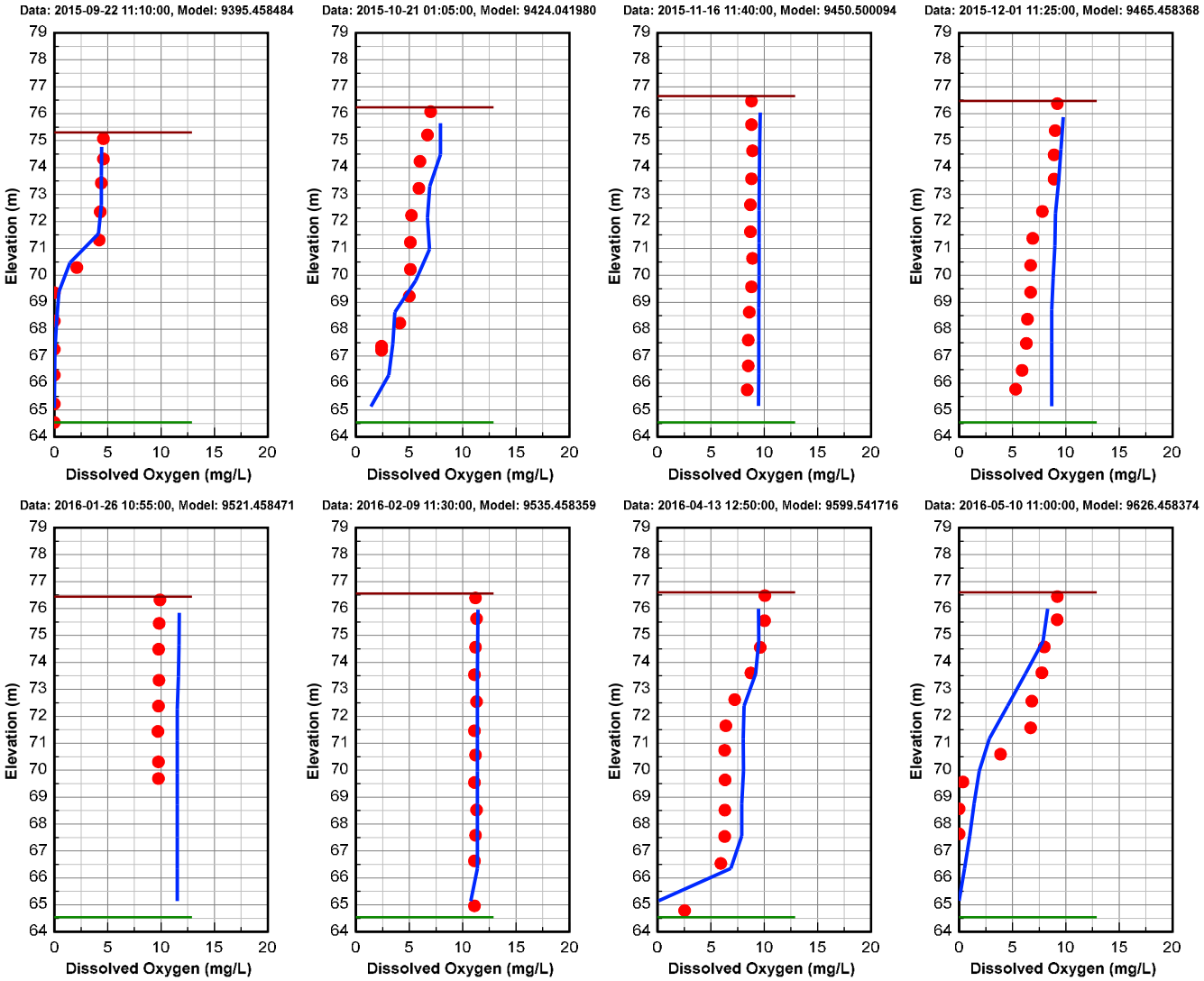

September 2015 – May 2016 (2 of 6)

Vertical Profile: NEU019L, Model Cell: 33, 75

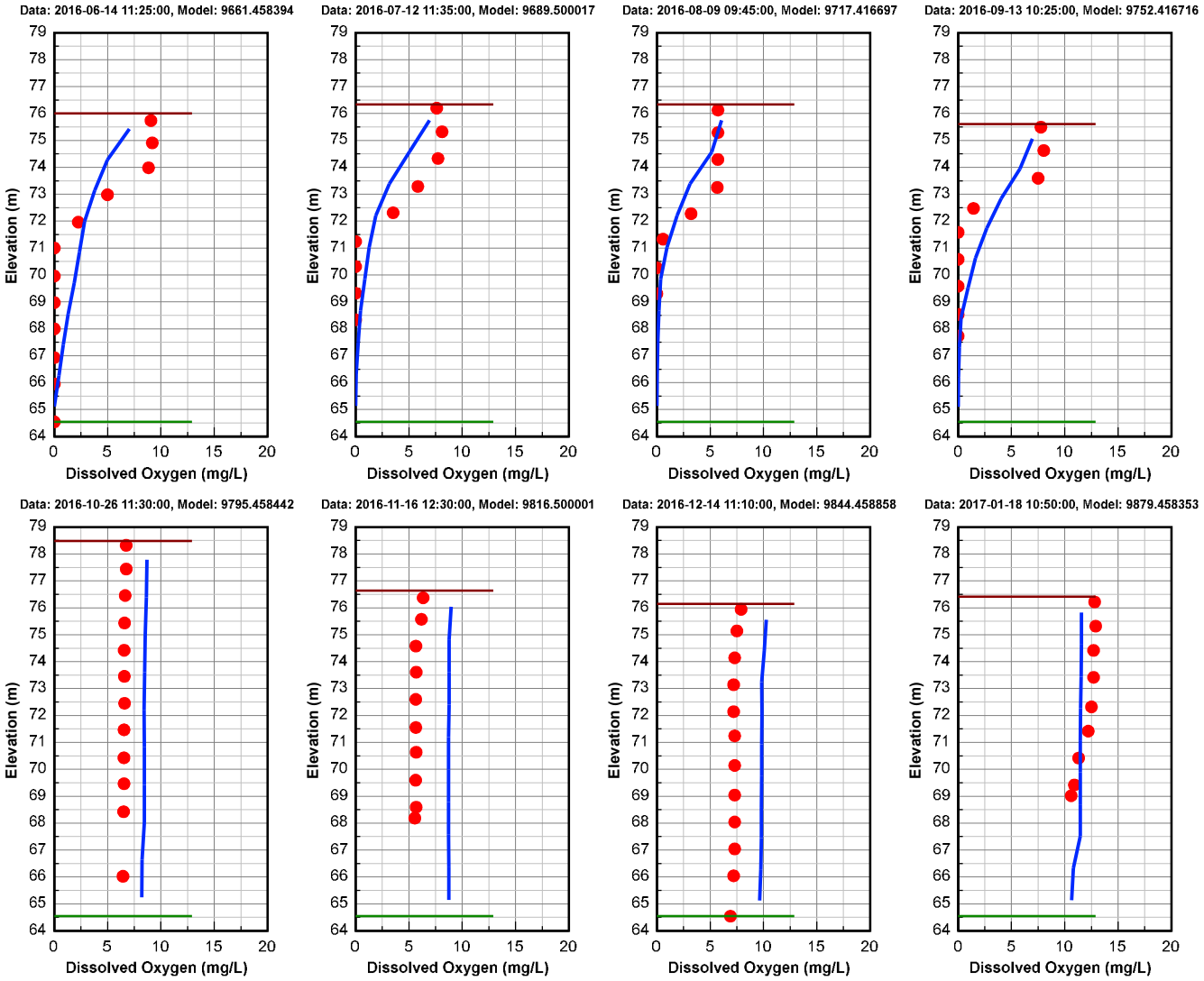

June 2016 – January 2017 (3 of 6)

Vertical Profile: NEU019L, Model Cell: 33, 75

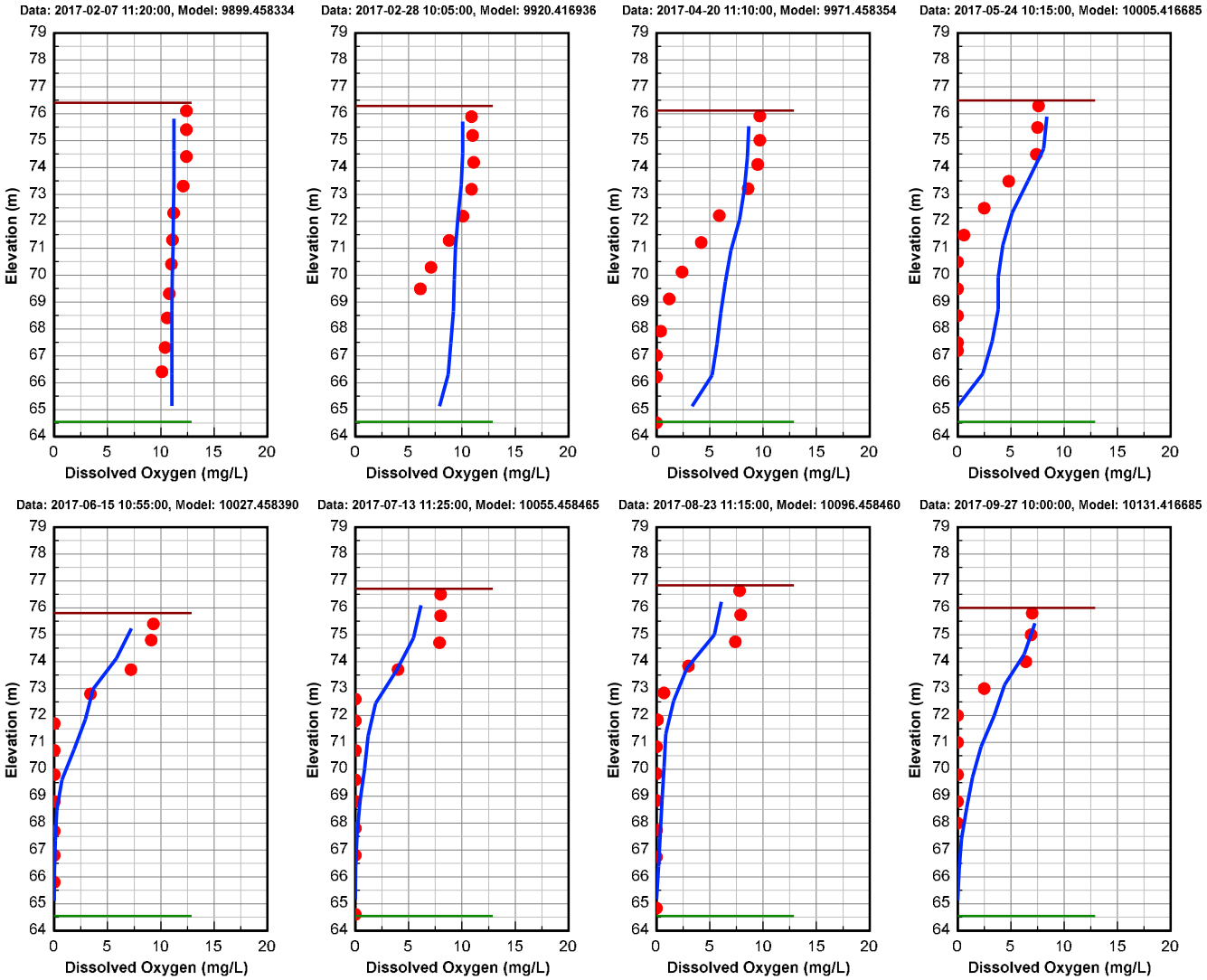

February 2017 – September 2017 (4 of 6)

Vertical Profile: NEU019L, Model Cell: 33, 75

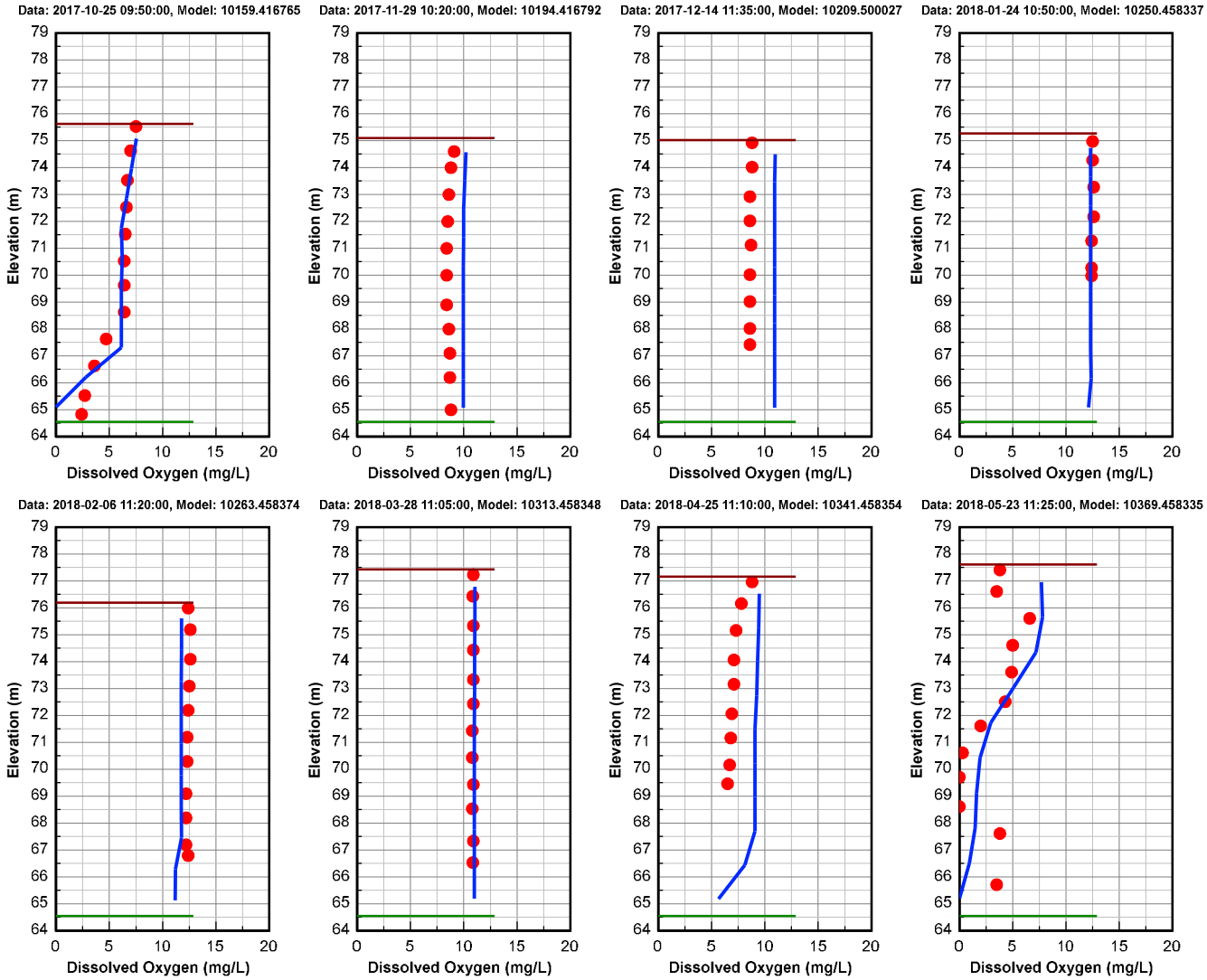

October 2017 – May 2018 (5 of 6)

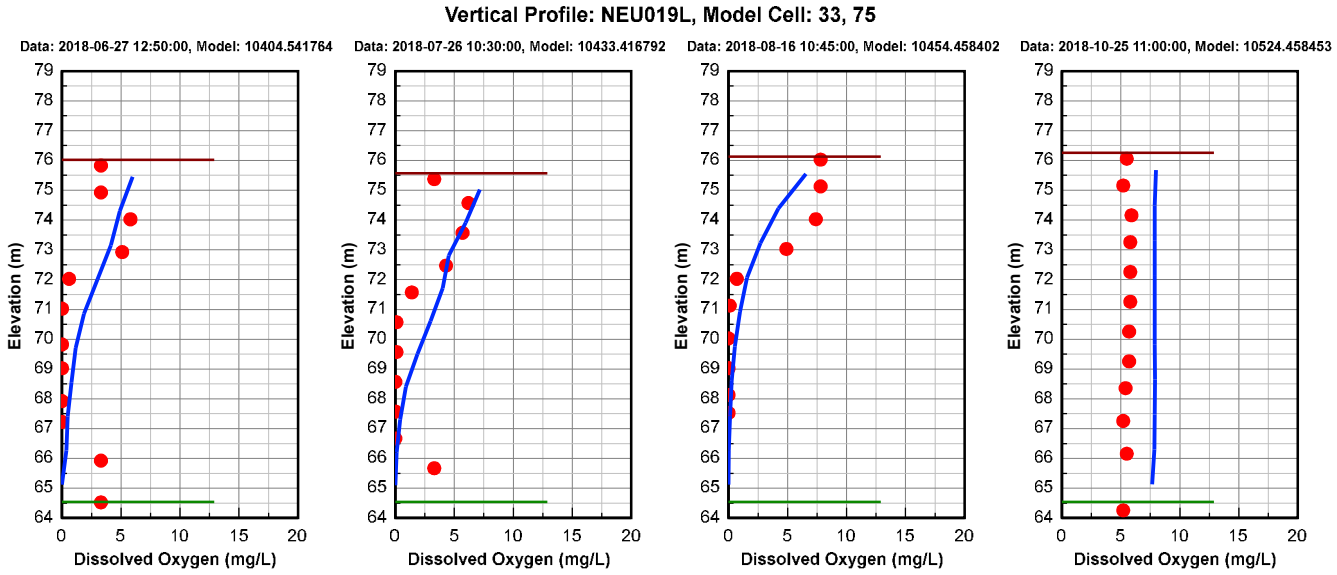

June 2018 – October 2018 (6 of 6)

Figure 2-9 DO Vertical Profile Comparison Plot at Station NEU019L during the calibration and validation period. Red dots are data, and blue continuous lines are model results.

Vertical Profile: NEU019P, Model Cell: 33, 95

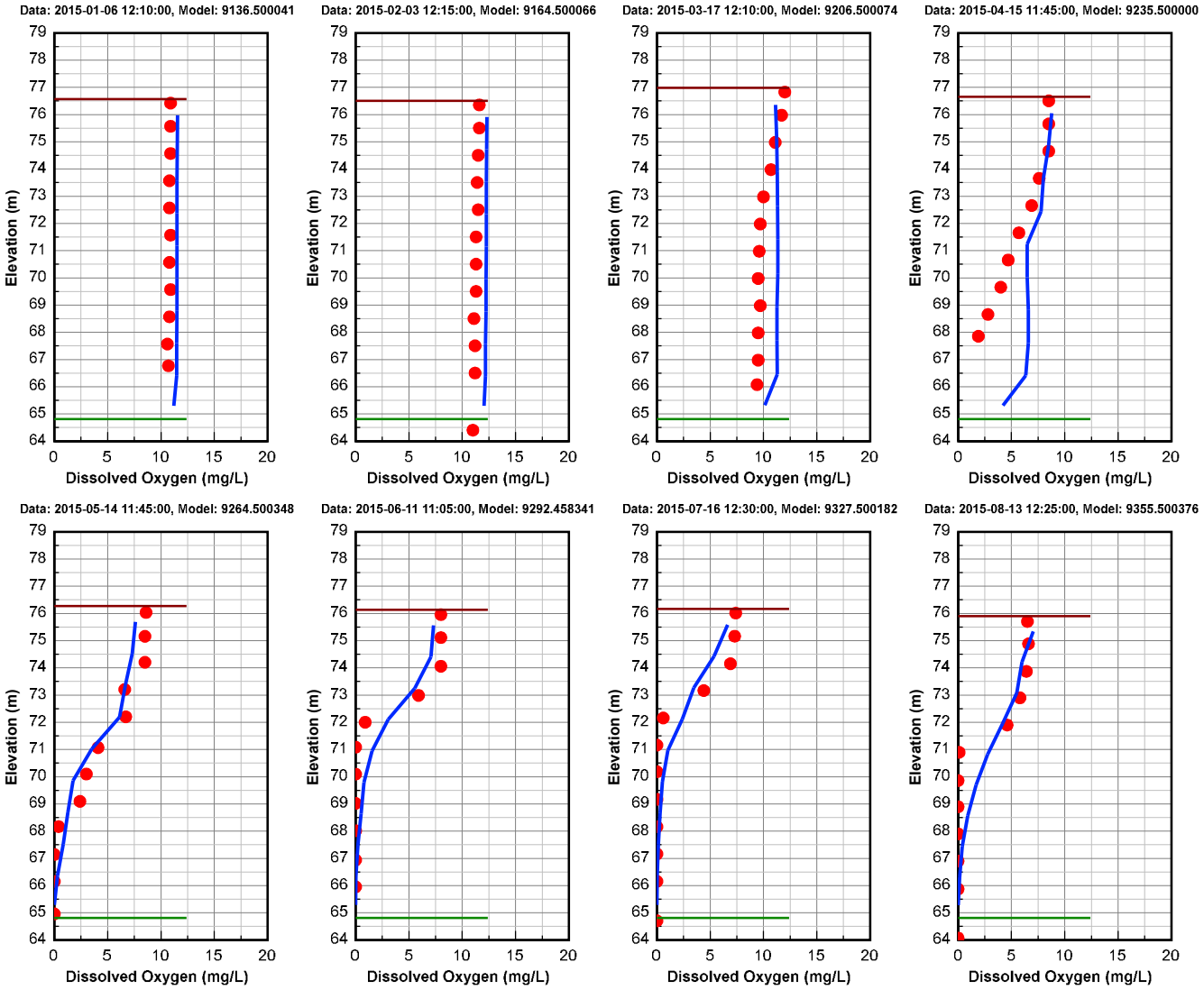

January 2015 – August 2015 (1 of 6)

Vertical Profile: NEU019P, Model Cell: 33, 95

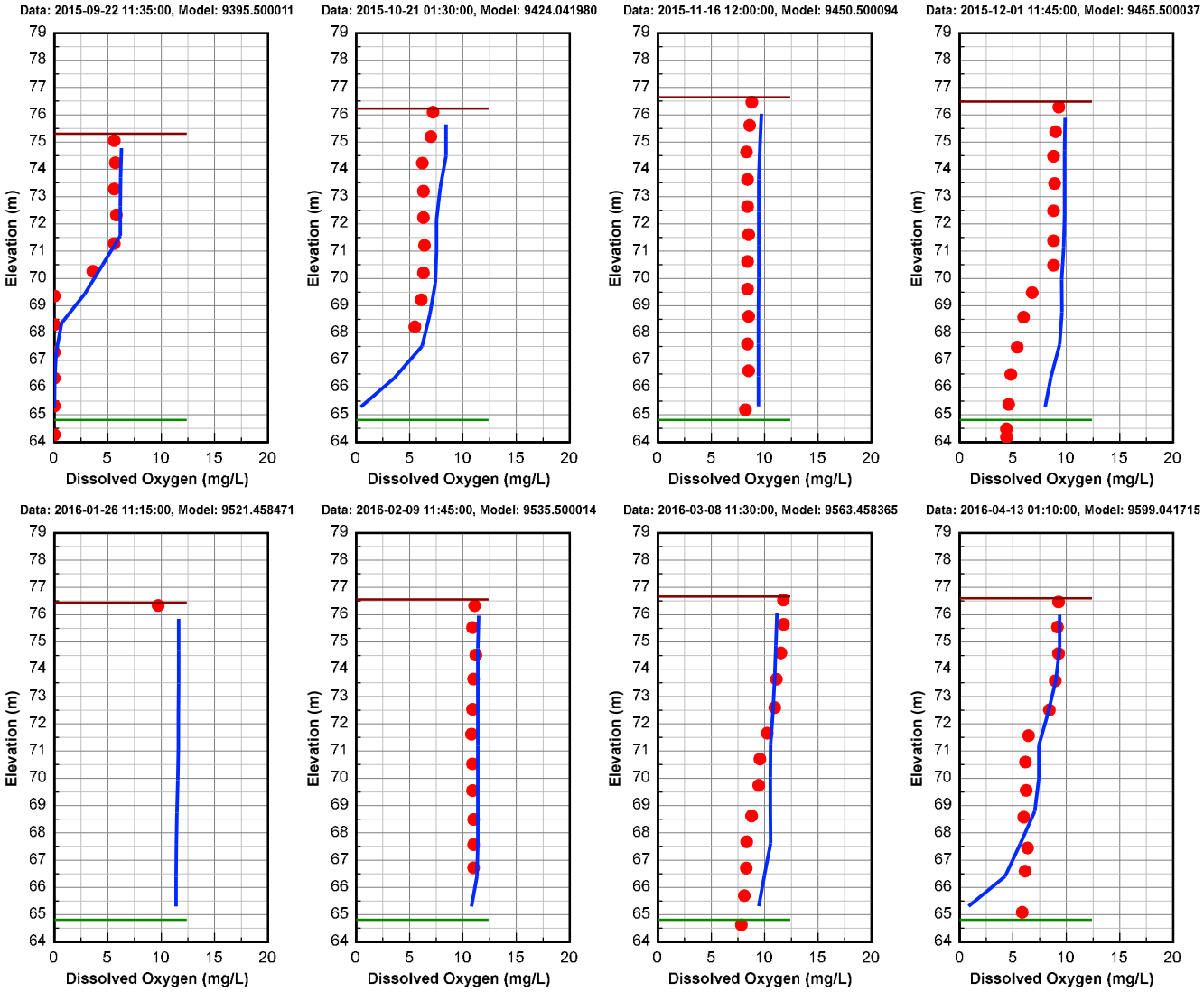

September 2015 – April 2016 (2 of 6)

Vertical Profile: NEU019P, Model Cell: 33, 95

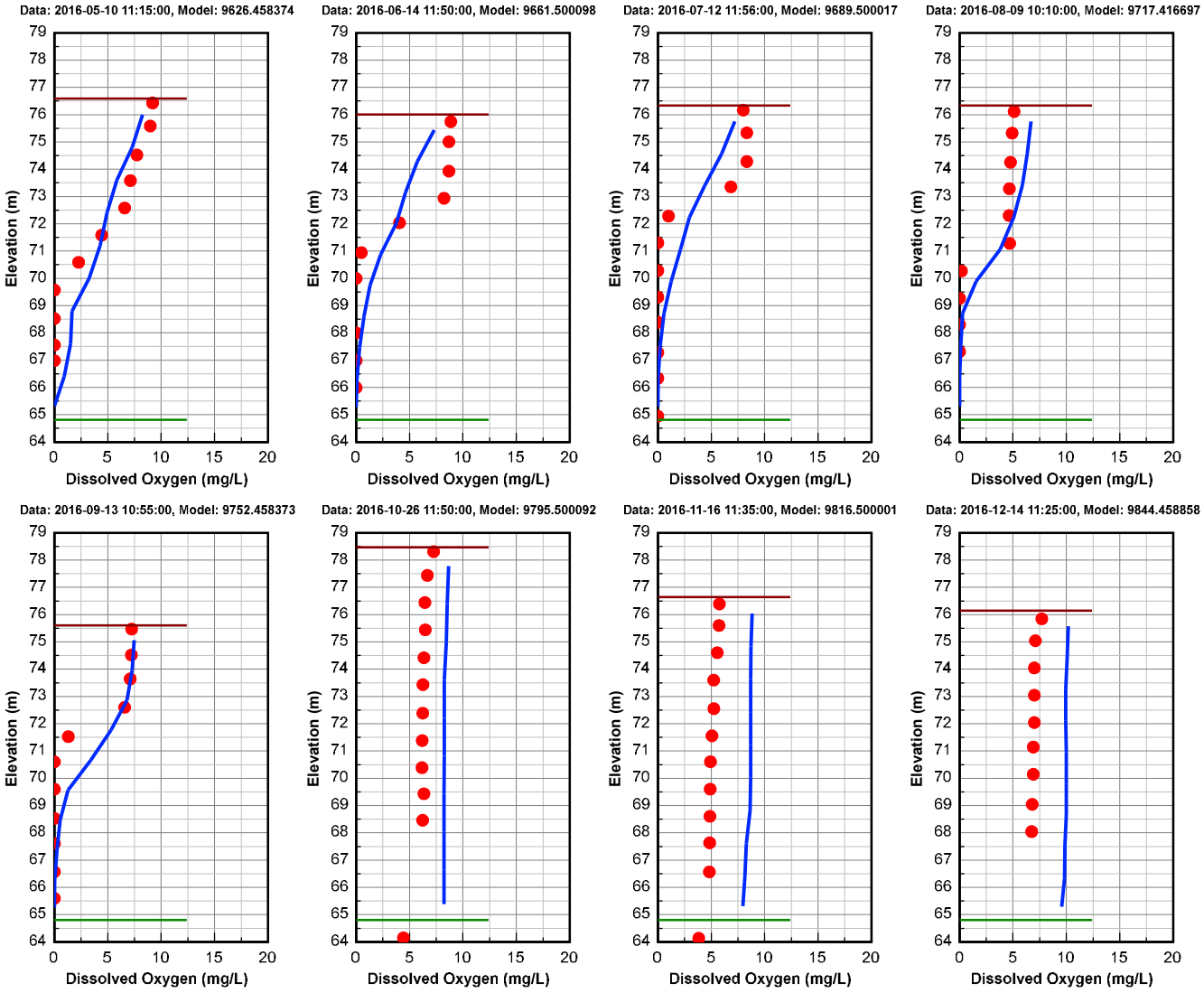

May 2016 – December 2016 (3 of 6)

Vertical Profile: NEU019P, Model Cell: 33, 95

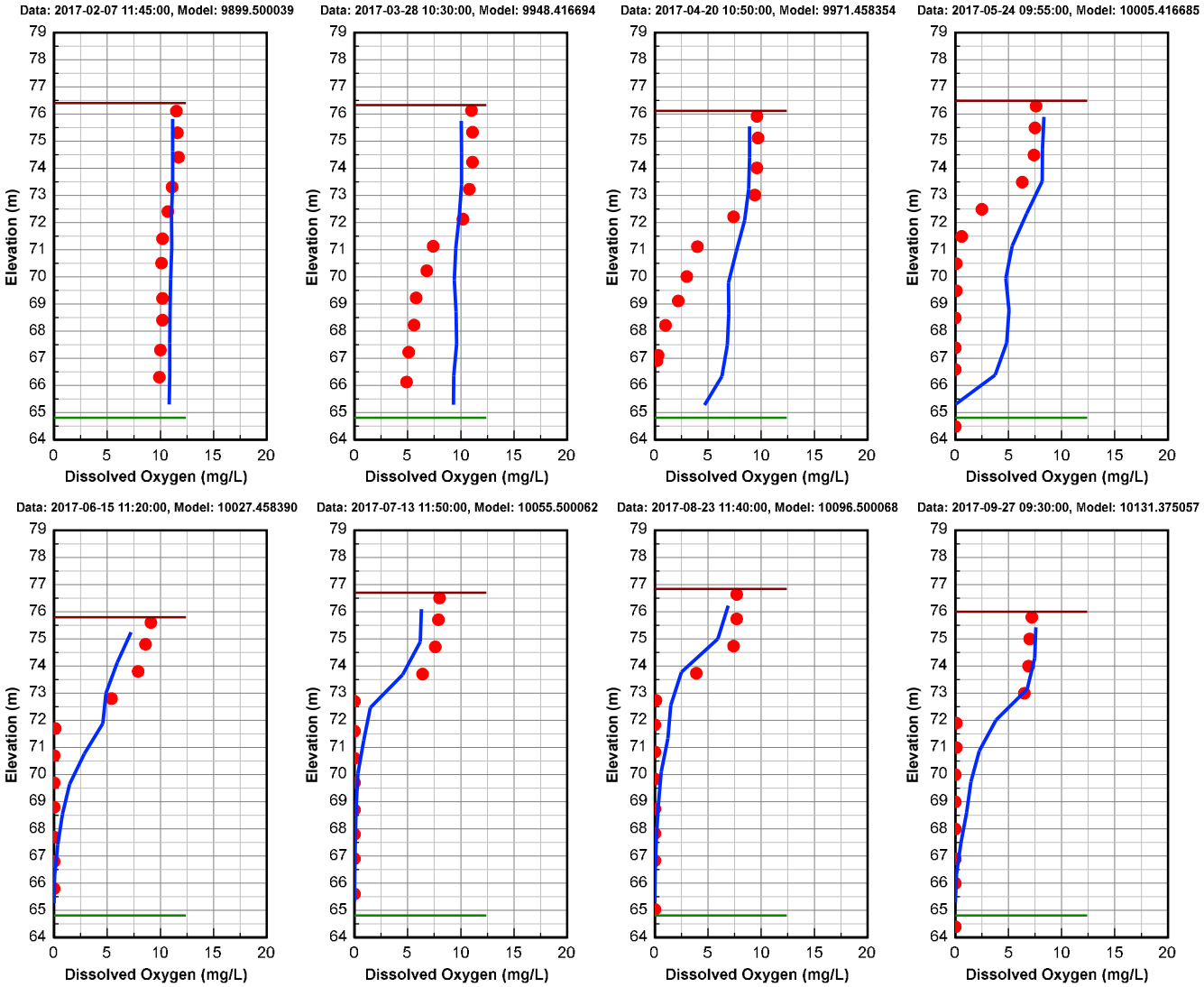

February 2017 – September 2017 (4 of 6)

Vertical Profile: NEU019P, Model Cell: 33, 95

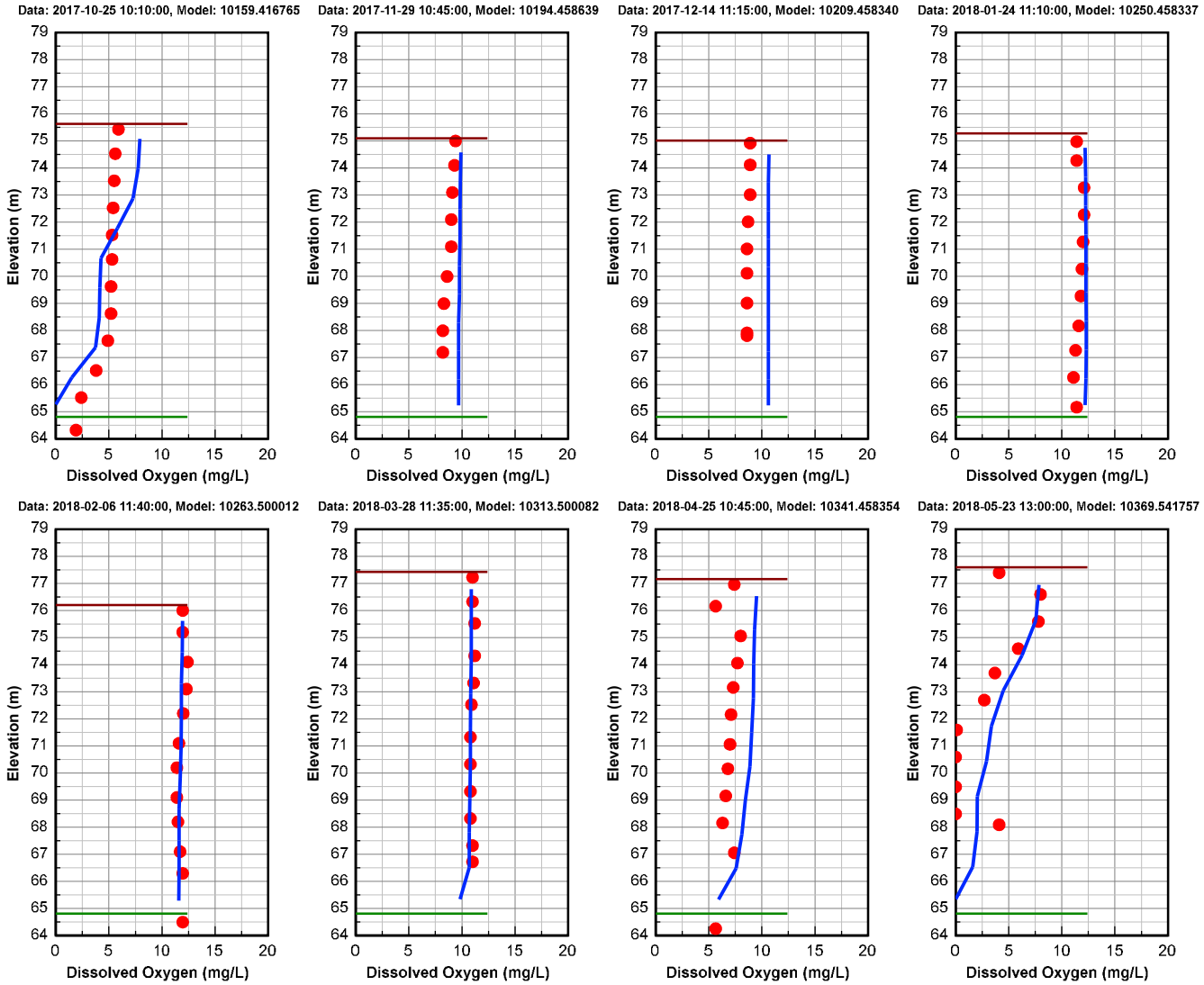

October 2017 – May 2018 (5 of 6)

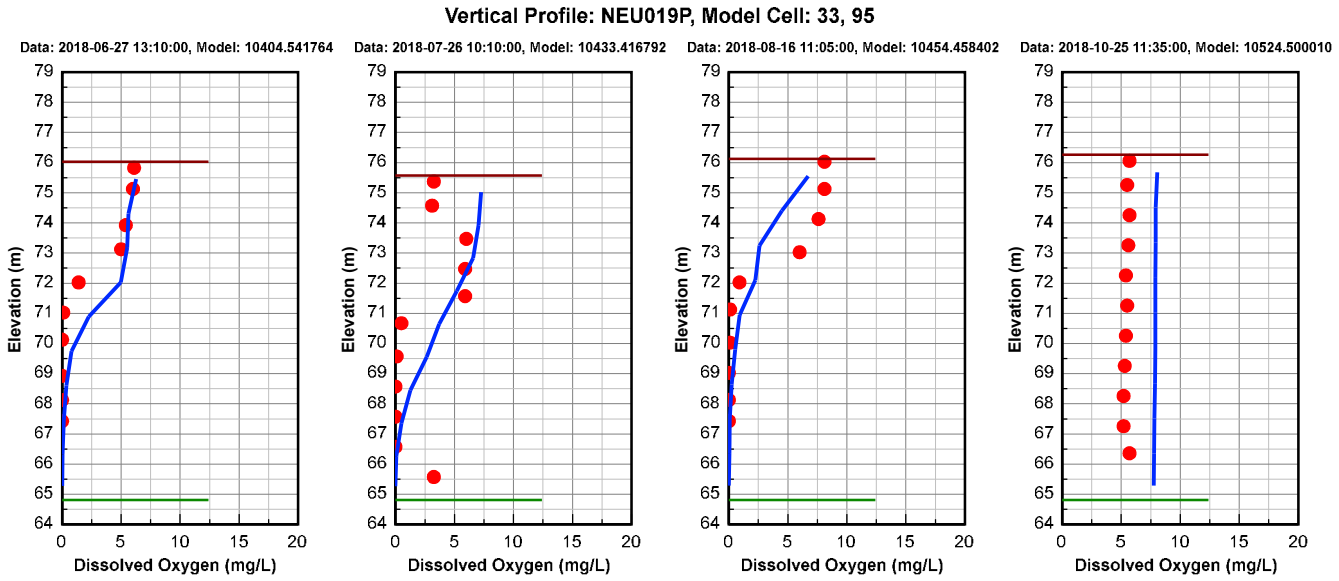

June 2018 – October 2018 (6 of 6)

Figure 2-10 DO Vertical Profile Comparison Plot at Station NEU019P during the calibration and validation period. Red dots are data, and blue continuous lines are model results.

Appendix A.4

Falls Lake EFDC Model Calibration and Validation Statistics Tables For Additional Parameters Not Provided in the Main Appendix A Document

Table of Contents

List of Tables

1. Ammonia Nitrogen (NH_4)

Table 1-1 Calibration Statistics for Ammonia Nitrogen

Station ID	Starting	Ending	# Pairs	Data Average (mg/L)	Model Average (mg/L)	R^2	RMSE (mg/L)	RSR (%)	RE (%)	AE (mg/L)	CE	pBias (%)
LC01	1/6/2015	12/14/2016	22	0.028	0.020	0.427	0.021	82	54.3	-0.007	0.31	-27.0
LI01	1/6/2015	12/14/2016	24	0.021	0.017	0.355	0.016	87	50.9	-0.004	0.28	-17.6
LLC01	1/6/2015	12/14/2016	24	0.020	0.020	0.027	0.021	101	70.1	0.000	-0.01	2.5
NEU013	1/6/2015	12/14/2016	24	0.017	0.034	0.092	0.029	209	129.3	0.017	-3.34	103.7
NEU013B	1/6/2015	12/14/2016	24	0.017	0.026	0.026	0.023	151	99.9	0.010	-1.23	57.9
NEU0171B	1/6/2015	12/14/2016	24	0.022	0.021	0.000	0.024	109	77.7	-0.001	-0.23	-4.4
NEU018C	1/6/2015	12/14/2016	24	0.023	0.017	0.098	0.022	99	62.1	-0.006	0.02	-25.3
NEU018E	1/6/2015	12/14/2016	24	0.023	0.018	0.006	0.025	107	69.9	-0.006	-0.17	-24.8
NEU019E	1/6/2015	12/14/2016	24	0.038	0.019	0.075	0.037	113	71.7	-0.019	-0.24	-49.7
NEU019L	1/6/2015	12/14/2016	23	0.041	0.019	0.006	0.048	120	81.6	-0.022	-0.42	-53.8
NEU019P	1/6/2015	12/14/2016	24	0.043	0.016	0.041	0.051	117	77.9	-0.028	-0.35	-63.7
NEU020D	1/6/2015	12/14/2016	24	0.050	0.017	0.010	0.059	122	82.3	-0.033	-0.46	-66.0

Table 1-2 Validation Statistics for Ammonia Nitrogen

Station ID	Starting	Ending	# Pairs	Data Average (mg/L)	Model Average (mg/L)	R^2	RMSE (mg/L)	RSR (%)	RE (%)	AE (mg/L)	CE	pBias (%)
LC01	1/18/2017	10/25/2018	22	0.014	0.021	0.049	0.016	182	91.1	0.007	-2.41	51.5
LI01	1/18/2017	10/25/2018	21	0.014	0.019	0.000	0.018	176	93.1	0.006	-2.10	40.3
LLC01	1/18/2017	10/25/2018	21	0.013	0.022	0.075	0.021	214	105.7	0.009	-3.25	68.2
NEU013	1/19/2017	10/25/2018	20	0.020	0.048	0.110	0.045	237	162.7	0.029	-4.42	147.4
NEU013B	1/18/2017	10/25/2018	20	0.016	0.029	0.086	0.028	174	125.3	0.014	-2.15	87.8
NEU0171B	1/18/2017	10/25/2018	21	0.013	0.016	0.019	0.015	170	80.5	0.003	-2.01	24.2
NEU018C	1/18/2017	10/25/2018	20	0.013	0.013	0.101	0.009	145	51.3	0.001	-0.94	5.2
NEU018E	1/18/2017	10/25/2018	21	0.013	0.014	0.022	0.011	153	59.7	0.001	-1.36	10.9
NEU019E	1/18/2017	10/25/2018	21	0.018	0.015	0.019	0.021	118	79.6	-0.003	-0.36	-15.5
NEU019L	1/18/2017	10/25/2018	21	0.025	0.015	0.024	0.031	112	73.8	-0.010	-0.27	-39.0
NEU019P	1/18/2017	10/25/2018	21	0.038	0.014	0.000	0.050	115	80.0	-0.023	-0.28	-62.2
NEU020D	1/18/2017	10/25/2018	21	0.067	0.014	0.021	0.098	118	85.3	-0.052	-0.38	-78.3

2. Nitrate+Nitrite Nitrogen (NO_3)

Table 2-1 Calibration Statistics for Nitrate+Nitrite Nitrogen

Station ID	Starting	Ending	# Pairs	Data Average (mg/L)	Model Average (mg/L)	R^2	RMSE (mg/L)	RSR (%)	RE (%)	AE (mg/L)	CE	pBias (%)
LC01	1/6/2015	12/14/2016	22	0.055	0.051	0.168	0.059	91	85.4	-0.004	0.16	-7.2
LI01	1/6/2015	12/14/2016	24	0.040	0.124	0.039	0.197	379	244.7	0.083	-13.11	205.9
LLC01	1/6/2015	12/14/2016	24	0.071	0.110	0.152	0.108	111	111.4	0.038	-0.24	53.8
NEU013	1/6/2015	12/14/2016	24	0.111	0.246	0.001	0.222	162	155.4	0.135	-1.61	121.8
NEU013B	1/6/2015	12/14/2016	24	0.085	0.134	0.288	0.104	98	97.6	0.049	0.03	57.3
NEU0171B	1/6/2015	12/14/2016	24	0.078	0.100	0.178	0.101	97	98.1	0.022	0.06	27.8
NEU018C	1/6/2015	12/14/2016	24	0.068	0.080	0.151	0.095	95	101.1	0.013	0.08	19.1
NEU018E	1/6/2015	12/14/2016	24	0.068	0.073	0.152	0.087	93	93.4	0.005	0.13	7.4
NEU019E	1/6/2015	12/14/2016	24	0.053	0.057	0.031	0.075	106	95.7	0.003	-0.13	6.2
NEU019L	1/6/2015	12/14/2016	23	0.058	0.051	0.151	0.063	94	79.1	-0.006	0.11	-11.2
NEU019P	1/6/2015	12/14/2016	24	0.076	0.048	0.136	0.084	100	72.8	-0.028	0.02	-37.1
NEU020D	1/6/2015	12/14/2016	24	0.078	0.036	0.232	0.088	102	72.2	-0.042	-0.04	-53.7

Table 2-2 Validation Statistics for Nitrate+Nitrite Nitrogen

Station ID	Starting	Ending	# Pairs	Data Average (mg/L)	Model Average (mg/L)	R^2	RMSE (mg/L)	RSR (%)	RE (%)	AE (mg/L)	CE	pBias (%)
LC01	1/18/2017	10/25/2018	22	0.015	0.035	0.025	0.044	397	190.7	0.019	-14.31	125.8
LI01	1/18/2017	10/25/2018	21	0.020	0.161	0.000	0.284	1493	727.4	0.140	-212.93	685.9
LLC01	1/18/2017	10/25/2018	21	0.027	0.131	0.008	0.227	784	452.2	0.104	-58.38	389.7
NEU013	1/19/2017	10/25/2018	20	0.092	0.264	0.014	0.314	288	202.5	0.173	-7.35	188.7
NEU013B	1/18/2017	10/25/2018	20	0.062	0.162	0.137	0.244	269	180.3	0.101	-6.21	163.7
NEU0171B	1/18/2017	10/25/2018	21	0.028	0.062	0.042	0.083	259	189.4	0.034	-5.67	124.4
NEU018C	1/18/2017	10/25/2018	20	0.018	0.031	0.002	0.046	242	168.1	0.013	-4.92	71.7
NEU018E	1/18/2017	10/25/2018	21	0.018	0.031	0.002	0.047	245	183.3	0.014	-4.72	78.3
NEU019E	1/18/2017	10/25/2018	21	0.019	0.031	0.076	0.043	305	166.4	0.012	-8.16	63.2
NEU019L	1/18/2017	10/25/2018	21	0.026	0.023	0.029	0.038	156	110.8	-0.003	-1.48	-12.3
NEU019P	1/18/2017	10/25/2018	21	0.033	0.019	0.001	0.044	130	95.4	-0.015	-0.71	-43.7
NEU020D	1/18/2017	10/25/2018	21	0.062	0.016	0.003	0.077	128	85.1	-0.045	-0.66	-73.5

3. DOC

Table 3-1 Calibration Statistics for DOC

Station ID	Starting	Ending	# Pairs	Data Average (mg/L)	Model Average (mg/L)	R^2	RMSE (mg/L)	RSR (%)	RE (%)	AE (mg/L)	CE	pBias (%)
LC01	1/6/2015	12/14/2016	22	7.6	7.1	0.132	1.632	100	17.2	-0.510	0.01	-6.7
LI01	1/6/2015	12/14/2016	22	7.6	6.5	0.059	2.189	140	23.1	-1.188	-0.95	-15.5
LLC01	1/6/2015	12/14/2016	22	7.6	7.0	0.000	1.827	111	20.0	-0.583	-0.23	-7.7
NEU013	1/6/2015	12/14/2016	22	7.8	6.6	0.164	1.890	120	20.4	-1.190	-0.43	-15.3
NEU013B	1/6/2015	12/14/2016	23	8.0	6.9	0.118	2.023	115	19.5	-1.155	-0.32	-14.4
NEU0171B	1/6/2015	12/14/2016	21	7.6	6.9	0.018	1.875	109	19.3	-0.695	-0.20	-9.2
NEU018C	1/6/2015	12/14/2016	22	7.2	6.9	0.013	1.626	108	19.3	-0.343	-0.16	-4.7
NEU018E	1/6/2015	12/14/2016	21	7.0	6.8	0.001	1.566	114	18.8	-0.204	-0.30	-2.9
NEU019E	1/6/2015	12/14/2016	22	7.6	6.8	0.078	1.704	110	18.6	-0.798	-0.21	-10.6
NEU019L	1/6/2015	12/14/2016	23	7.1	6.5	0.120	1.685	102	18.3	-0.639	-0.03	-9.0
NEU019P	1/6/2015	12/14/2016	22	7.0	6.4	0.147	1.451	104	17.4	-0.640	-0.09	-9.1
NEU020D	1/6/2015	12/14/2016	23	6.5	5.8	0.208	1.394	107	16.9	-0.761	-0.14	-11.7

Table 3-2 Validation Statistics for DOC

Station ID	Starting	Ending	# Pairs	Data Average (mg/L)	Model Average (mg/L)	R^2	RMSE (mg/L)	RSR (%)	RE (%)	AE (mg/L)	CE	pBias (%)
LC01	4/20/2017	5/23/2018	10	7.3	6.9	0.242	0.795	101	10.3	-0.377	-0.02	-5.2
LI01	4/20/2017	5/23/2018	10	7.2	6.2	0.032	1.468	148	16.4	-0.941	-1.20	-13.1
LLC01	4/20/2017	5/23/2018	10	7.2	6.7	0.294	1.098	98	13.0	-0.559	0.03	-7.7
NEU013	1/18/2017	5/23/2018	16	7.3	6.5	0.023	2.278	112	21.0	-0.816	-0.26	-11.1
NEU013B	1/18/2017	5/23/2018	16	7.0	6.6	0.194	1.146	115	13.9	-0.335	-0.31	-4.8
NEU0171B	1/18/2017	5/23/2018	16	7.4	6.5	0.193	1.864	100	16.5	-0.808	0.00	-11.0
NEU018C	1/18/2017	5/23/2018	17	7.0	6.5	0.360	0.957	97	10.9	-0.536	0.07	-7.6
NEU018E	1/18/2017	5/23/2018	17	7.1	6.4	0.363	1.253	98	12.7	-0.704	0.04	-9.9
NEU019E	1/18/2017	5/23/2018	17	7.3	6.3	0.212	1.288	139	15.2	-0.980	-0.92	-13.5
NEU019L	1/18/2017	5/23/2018	17	7.1	5.9	0.277	1.614	129	18.9	-1.210	-0.65	-17.1
NEU019P	1/18/2017	5/23/2018	17	6.9	5.7	0.528	1.573	118	18.8	-1.232	-0.40	-17.8
NEU020D	1/18/2017	5/23/2018	17	6.3	5.1	0.773	1.223	128	18.2	-1.128	-0.65	-18.0

4. TKN

Table 4-1 Calibration Statistics for TKN

Station ID	Starting	Ending	# Pairs	Data Average (mg/L)	Model Average (mg/L)	R^2	RMSE (mg/L)	RSR (%)	RE (%)	AE (mg/L)	CE	pBias (%)
LC01	1/6/2015	12/14/2016	22	0.695	0.698	0.002	0.089	156	9.9	0.003	-1.44	0.4
LI01	1/6/2015	12/14/2016	24	0.703	0.652	0.053	0.144	194	17.5	-0.051	-2.81	-7.3
LLC01	1/6/2015	12/14/2016	24	0.731	0.674	0.027	0.123	166	12.8	-0.057	-1.80	-7.8
NEU013	1/6/2015	12/14/2016	24	0.865	0.578	0.002	0.387	156	34.0	-0.287	-1.42	-33.1
NEU013B	1/6/2015	12/14/2016	24	0.805	0.625	0.142	0.218	170	23.2	-0.180	-1.88	-22.4
NEU0171B	1/6/2015	12/14/2016	24	0.729	0.674	0.016	0.129	165	13.8	-0.054	-1.75	-7.5
NEU018C	1/6/2015	12/14/2016	24	0.680	0.674	0.000	0.103	182	12.7	-0.006	-2.29	-0.9
NEU018E	1/6/2015	12/14/2016	24	0.679	0.677	0.005	0.108	155	13.9	-0.002	-1.41	-0.3
NEU019E	1/6/2015	12/14/2016	24	0.674	0.668	0.007	0.110	143	13.4	-0.005	-1.04	-0.8
NEU019L	1/6/2015	12/14/2016	23	0.609	0.657	0.206	0.142	160	18.5	0.048	-1.58	7.9
NEU019P	1/6/2015	12/14/2016	24	0.618	0.641	0.205	0.137	136	18.4	0.023	-0.85	3.7
NEU020D	1/6/2015	12/14/2016	24	0.579	0.600	0.198	0.128	131	18.1	0.021	-0.71	3.6

Table 4-2 Validation Statistics for TKN

Station ID	Starting	Ending	# Pairs	Data Average (mg/L)	Model Average (mg/L)	R^2	RMSE (mg/L)	RSR (%)	RE (%)	AE (mg/L)	CE	pBias (%)
LC01	1/18/2017	10/25/2018	22	0.768	0.689	0.020	0.142	197	14.9	-0.079	-2.94	-10.3
LI01	1/18/2017	10/25/2018	21	0.771	0.645	0.000	0.175	224	18.2	-0.126	-4.03	-16.3
LLC01	1/18/2017	10/25/2018	21	0.796	0.666	0.025	0.182	216	18.2	-0.130	-3.71	-16.3
NEU013	1/19/2017	10/25/2018	20	0.924	0.558	0.008	0.419	227	39.6	-0.366	-4.16	-39.6
NEU013B	1/18/2017	10/25/2018	20	0.890	0.599	0.000	0.341	294	32.7	-0.291	-7.66	-32.7
NEU0171B	1/18/2017	10/25/2018	21	0.797	0.664	0.070	0.179	235	17.9	-0.134	-4.58	-16.8
NEU018C	1/18/2017	10/25/2018	20	0.770	0.684	0.000	0.142	208	14.4	-0.086	-3.35	-11.2
NEU018E	1/18/2017	10/25/2018	21	0.739	0.683	0.001	0.124	182	12.5	-0.056	-2.33	-7.6
NEU019E	1/18/2017	10/25/2018	21	0.717	0.676	0.042	0.142	148	15.7	-0.041	-1.19	-5.7
NEU019L	1/18/2017	10/25/2018	21	0.688	0.642	0.003	0.121	170	15.0	-0.046	-1.94	-6.6
NEU019P	1/18/2017	10/25/2018	21	0.671	0.627	0.002	0.111	136	12.9	-0.044	-0.87	-6.6
NEU020D	1/18/2017	10/25/2018	21	0.645	0.584	0.000	0.118	131	15.4	-0.062	-0.73	-9.6

5. TON

Table 5-1 Calibration Statistics for TON

Station ID	Starting	Ending	# Pairs	Data Average (mg/L)	Model Average (mg/L)	R^2	RMSE (mg/L)	RSR (%)	RE (%)	AE (mg/L)	CE	pBias (%)
LC01	1/6/2015	12/14/2016	22	0.668	0.678	0.000	0.083	160	9.9	0.010	-1.58	1.5
LI01	1/6/2015	12/14/2016	24	0.682	0.634	0.016	0.137	181	17.4	-0.047	-2.26	-7.0
LLC01	1/6/2015	12/14/2016	24	0.711	0.654	0.056	0.121	149	12.7	-0.058	-1.24	-8.1
NEU013	1/6/2015	12/14/2016	24	0.848	0.544	0.010	0.399	156	36.6	-0.304	-1.45	-35.8
NEU013B	1/6/2015	12/14/2016	24	0.788	0.598	0.137	0.230	170	24.9	-0.190	-1.89	-24.1
NEU0171B	1/6/2015	12/14/2016	24	0.707	0.653	0.032	0.127	147	14.0	-0.053	-1.15	-7.6
NEU018C	1/6/2015	12/14/2016	24	0.657	0.656	0.007	0.097	167	11.9	0.000	-1.74	0.0
NEU018E	1/6/2015	12/14/2016	24	0.656	0.660	0.001	0.107	140	14.6	0.004	-0.92	0.6
NEU019E	1/6/2015	12/14/2016	24	0.636	0.649	0.003	0.099	145	12.4	0.013	-1.13	2.1
NEU019L	1/6/2015	12/14/2016	23	0.568	0.638	0.234	0.138	182	19.5	0.070	-2.34	12.4
NEU019P	1/6/2015	12/14/2016	24	0.575	0.625	0.319	0.137	151	18.7	0.050	-1.29	8.8
NEU020D	1/6/2015	12/14/2016	24	0.529	0.583	0.253	0.117	154	17.9	0.054	-1.40	10.2

Table 5-2 Validation Statistics for TON

Station ID	Starting	Ending	# Pairs	Data Average (mg/L)	Model Average (mg/L)	R^2	RMSE (mg/L)	RSR (%)	RE (%)	AE (mg/L)	CE	pBias (%)
LC01	1/18/2017	10/25/2018	22	0.753	0.667	0.009	0.141	198	15.2	-0.086	-2.95	-11.4
LI01	1/18/2017	10/25/2018	21	0.757	0.626	0.000	0.175	244	18.8	-0.131	-4.86	-17.3
LLC01	1/18/2017	10/25/2018	21	0.783	0.644	0.031	0.182	227	19.3	-0.139	-4.22	-17.8
NEU013	1/19/2017	10/25/2018	20	0.904	0.510	0.000	0.452	244	43.6	-0.394	-4.95	-43.6
NEU013B	1/18/2017	10/25/2018	20	0.874	0.569	0.011	0.356	307	34.9	-0.305	-8.40	-34.9
NEU0171B	1/18/2017	10/25/2018	21	0.785	0.648	0.070	0.177	250	18.3	-0.137	-5.19	-17.4
NEU018C	1/18/2017	10/25/2018	20	0.757	0.670	0.000	0.138	212	14.2	-0.087	-3.50	-11.5
NEU018E	1/18/2017	10/25/2018	21	0.726	0.669	0.001	0.120	188	12.5	-0.058	-2.51	-8.0
NEU019E	1/18/2017	10/25/2018	21	0.699	0.661	0.041	0.130	153	14.9	-0.038	-1.34	-5.5
NEU019L	1/18/2017	10/25/2018	21	0.663	0.627	0.018	0.114	184	14.6	-0.036	-2.37	-5.4
NEU019P	1/18/2017	10/25/2018	21	0.634	0.613	0.090	0.109	160	14.5	-0.021	-1.53	-3.3
NEU020D	1/18/2017	10/25/2018	21	0.579	0.569	0.137	0.093	141	13.4	-0.009	-1.03	-1.6

6. TSS

Table 6-1 Calibration Statistics for TSS

Station ID	Starting	Ending	# Pairs	Data Average (mg/L)	Model Average (mg/L)	R^2	RMSE (mg/L)	RSR (%)	RE (%)	AE (mg/L)	CE	pBias (%)
LC01	1/6/2015	12/14/2016	23	7.6	3.8	0.000	6.144	159	64.4	-3.730	-1.54	-49.3
LI01	1/6/2015	12/14/2016	24	10.2	7.2	0.455	6.176	92	49.5	-3.023	0.15	-29.6
LLC01	1/6/2015	12/14/2016	24	10.3	5.2	0.075	7.615	174	63.4	-5.079	-2.02	-49.4
NEU013	1/6/2015	12/14/2016	24	24.2	29.8	0.017	31.851	263	92.0	5.602	-5.90	23.2
NEU013B	1/6/2015	12/14/2016	24	18.7	14.3	0.007	13.115	186	62.7	-4.384	-2.44	-23.4
NEU0171B	1/6/2015	12/14/2016	24	9.8	5.8	0.018	7.596	200	64.3	-3.942	-3.01	-40.3
NEU018C	1/6/2015	12/14/2016	24	7.5	3.9	0.000	6.020	244	69.5	-3.631	-4.97	-48.3
NEU018E	1/6/2015	12/14/2016	24	8.3	2.9	0.105	6.376	235	70.7	-5.352	-4.51	-64.8
NEU019E	1/6/2015	12/14/2016	24	5.9	2.5	0.239	4.366	154	63.9	-3.457	-1.38	-58.4
NEU019L	1/6/2015	12/14/2016	23	5.3	1.7	0.389	4.193	155	68.3	-3.602	-1.40	-68.3
NEU019P	1/6/2015	12/14/2016	24	5.0	1.6	0.239	4.076	167	71.5	-3.398	-1.79	-67.5
NEU020D	1/6/2015	12/14/2016	24	4.4	1.7	0.392	3.204	153	63.8	-2.714	-1.35	-61.9

Table 6-2 Validation Statistics for TSS

Station ID	Starting	Ending	# Pairs	Data Average (mg/L)	Model Average (mg/L)	R^2	RMSE (mg/L)	RSR (%)	RE (%)	AE (mg/L)	CE	pBias (%)
LC01	1/18/2017	10/25/2018	22	8.4	8.8	0.014	12.364	406	93.7	0.428	-15.52	5.1
LI01	1/18/2017	10/25/2018	21	10.9	13.2	0.008	26.327	468	101.7	2.382	-20.93	21.9
LLC01	1/18/2017	10/25/2018	21	10.8	8.5	0.241	8.365	191	60.3	-2.295	-2.64	-21.3
NEU013	1/19/2017	10/25/2018	20	28.4	30.8	0.158	17.683	176	54.0	2.397	-2.10	8.4
NEU013B	1/18/2017	10/25/2018	20	21.7	18.1	0.065	13.800	230	51.7	-3.596	-4.27	-16.6
NEU0171B	1/18/2017	10/25/2018	21	10.2	5.5	0.186	6.215	204	55.0	-4.711	-3.14	-46.3
NEU018C	1/18/2017	10/25/2018	21	7.7	3.5	0.015	5.781	193	70.0	-4.221	-2.74	-54.6
NEU018E	1/18/2017	10/25/2018	21	7.3	2.2	0.037	6.240	180	75.6	-5.072	-2.23	-69.8
NEU019E	1/18/2017	10/25/2018	21	6.1	2.6	0.239	4.489	139	60.6	-3.494	-0.94	-57.2
NEU019L	1/18/2017	10/25/2018	21	4.1	2.1	0.058	3.642	203	74.6	-2.002	-3.13	-49.2
NEU019P	1/18/2017	10/25/2018	21	4.6	1.7	0.259	3.631	142	66.1	-2.880	-1.01	-62.5
NEU020D	1/18/2017	10/25/2018	21	3.8	1.4	0.342	2.842	173	65.3	-2.450	-2.01	-63.8

Appendix A.5

Sensitivity Analysis of Falls Lake EFDC Model Time Series and Box-Whisker Plots

Table of Contents

List of Figures

1. Time Series

1.1 Chl-a

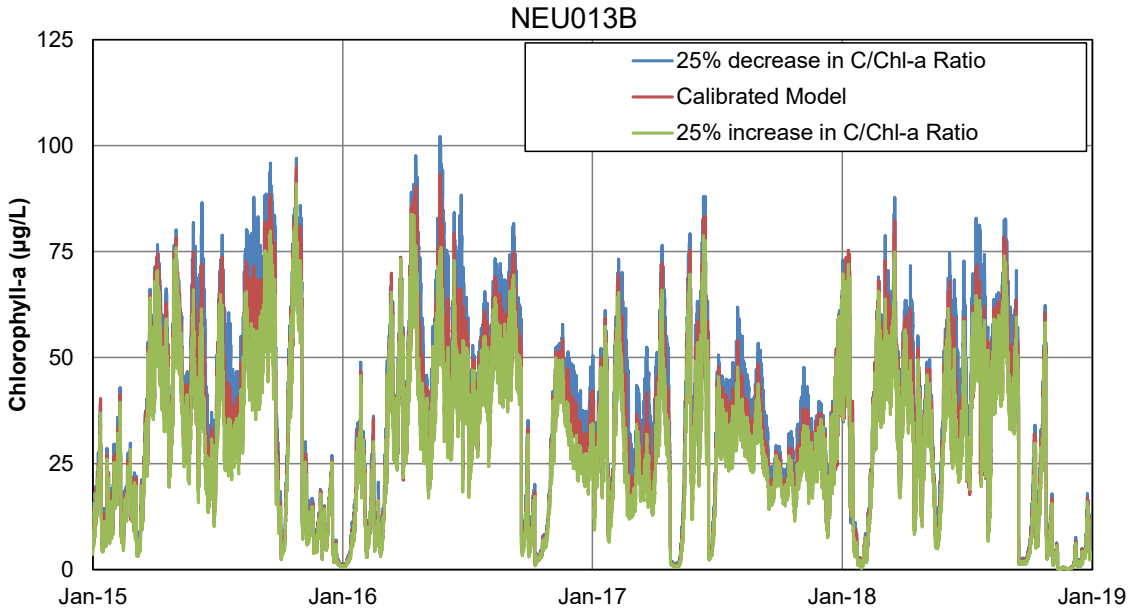

Figure 1 Modeled Chl-a at NEU013B under Perturbation Levels of C/Chl-a Ratio

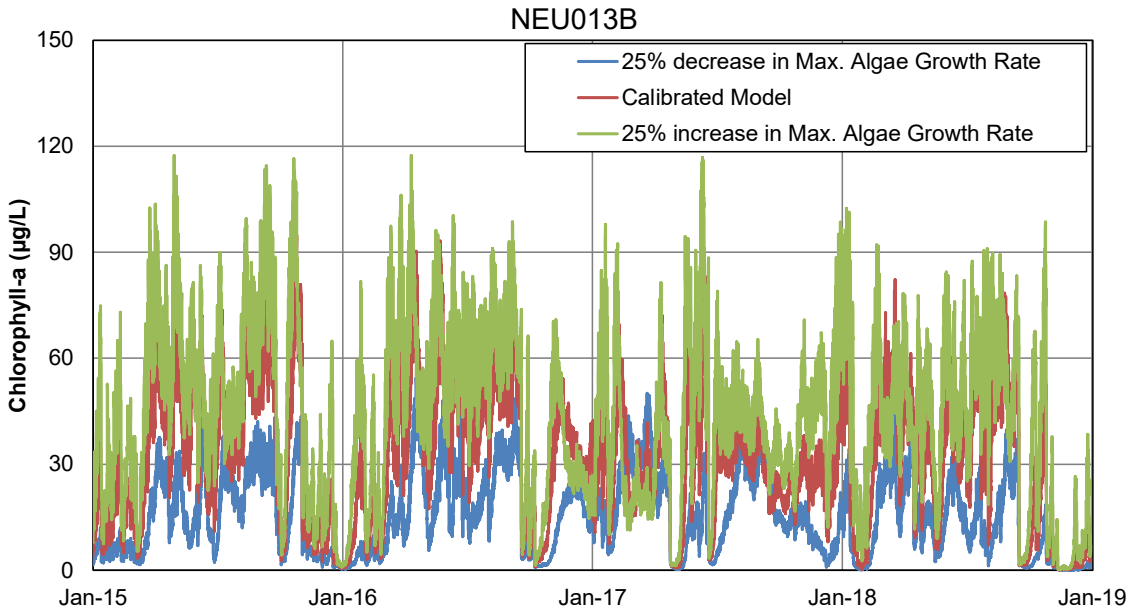

Figure 2 Modeled Chl-a at NEU013B under Perturbation Levels of Algal Growth Rate

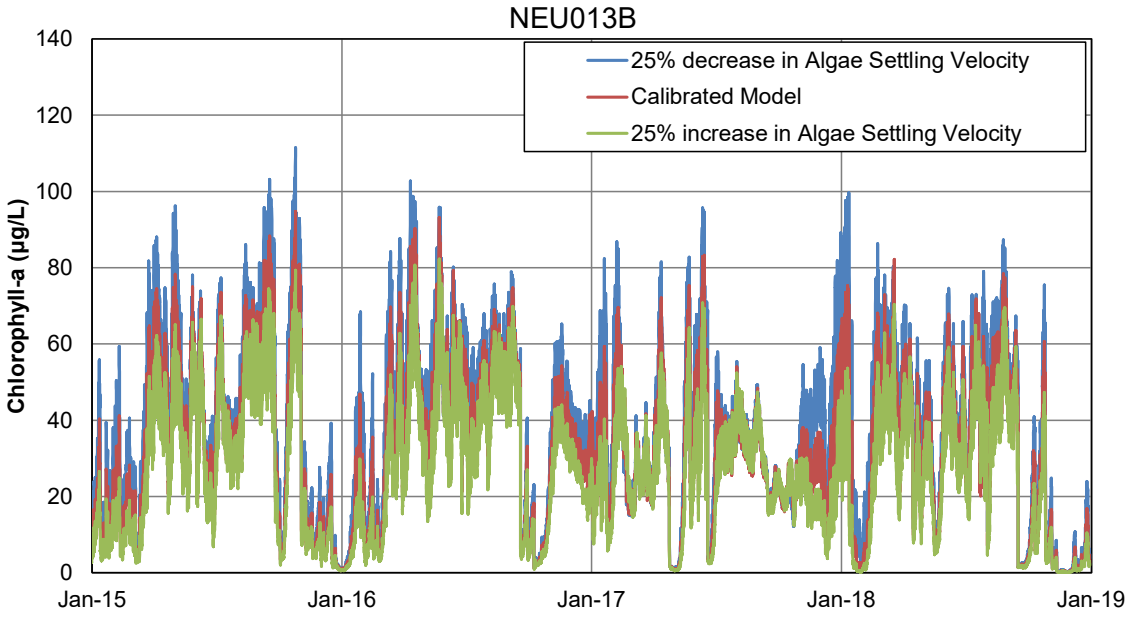

Figure 3 Modeled Chl-a at NEU013B under Perturbation of Algal Settling Velocity

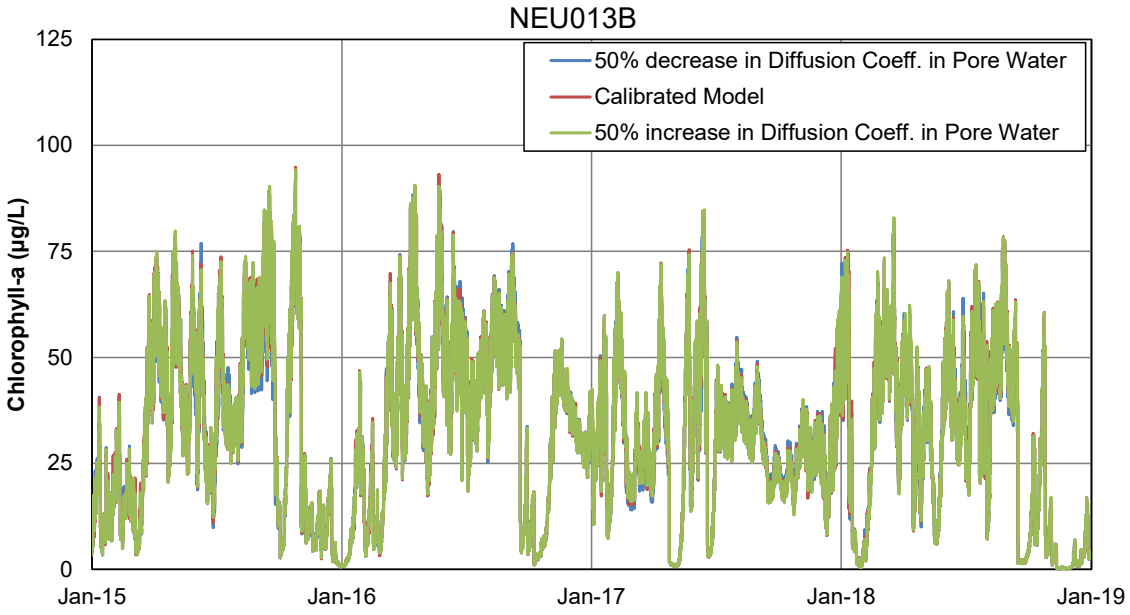

Figure 4 Modeled Chl-a at NEU013B under Perturbation of Diffusion Coefficient in Pore Water

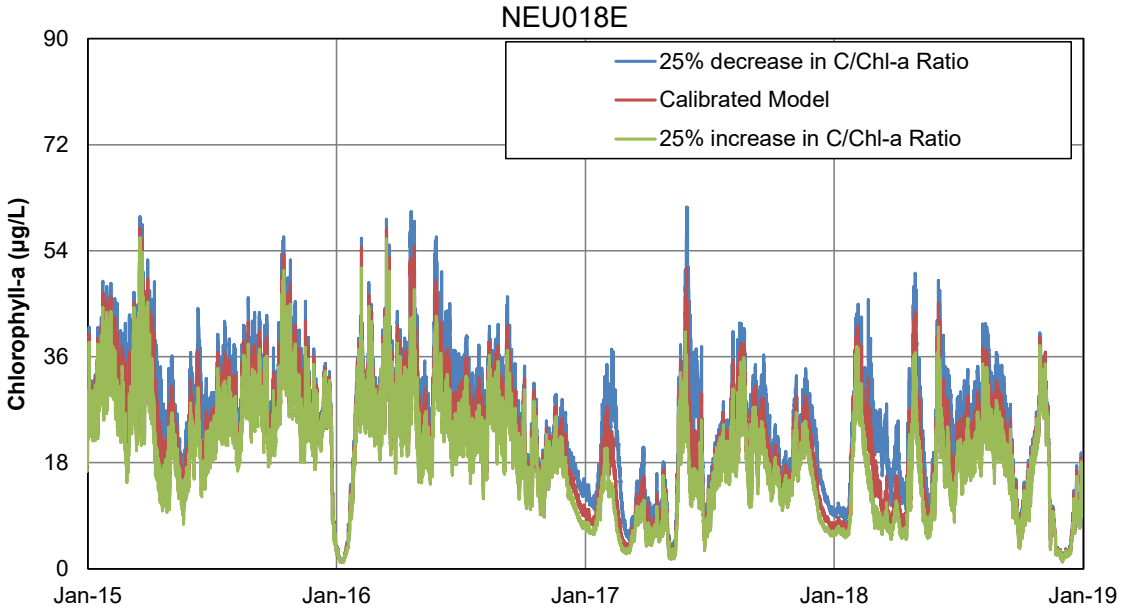

Figure 5 Modeled Chl-a at NEU018E under Perturbation Levels of C/Chl-a Ratio

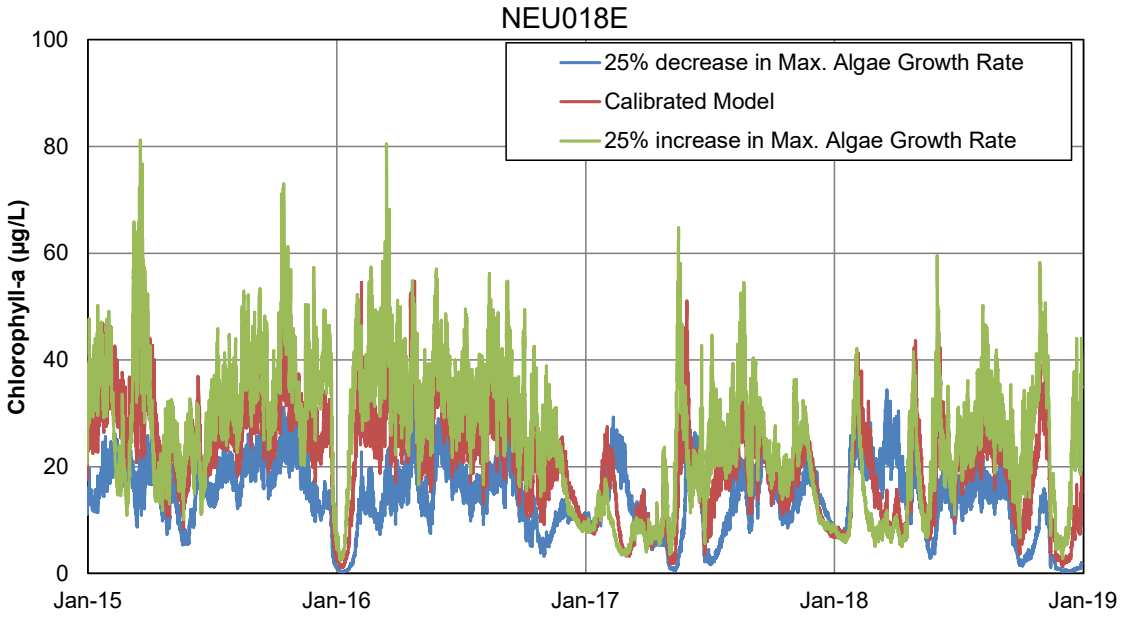

Figure 6 Modeled Chl-a at NEU018E under Perturbation Levels of Algal Growth Rate

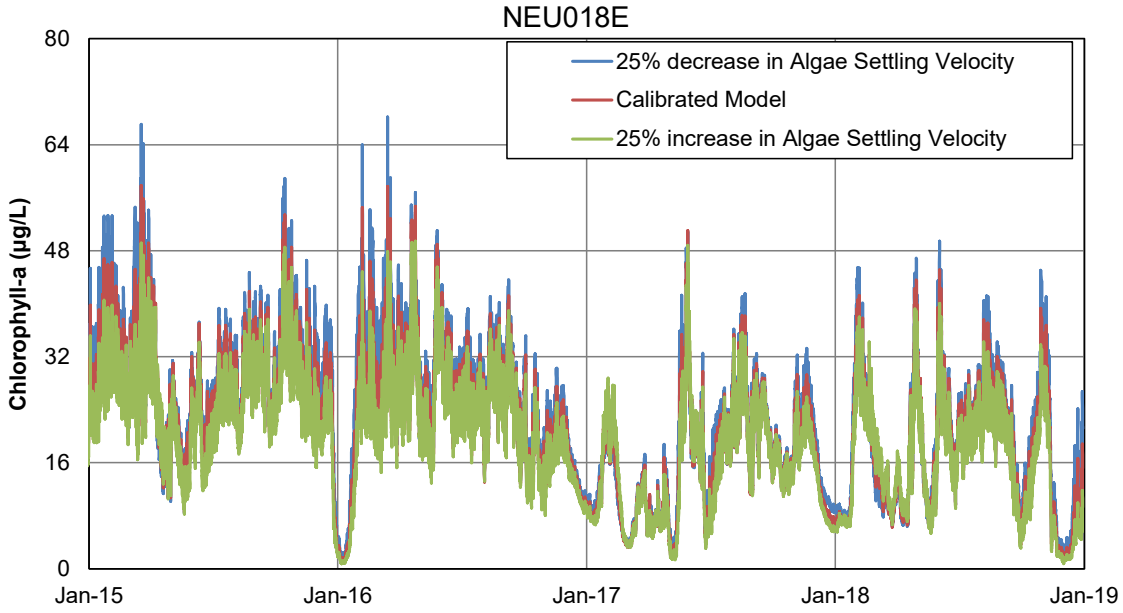

Figure 7 Modeled Chl-a at NEU018E under Perturbation of Algal Settling Velocity

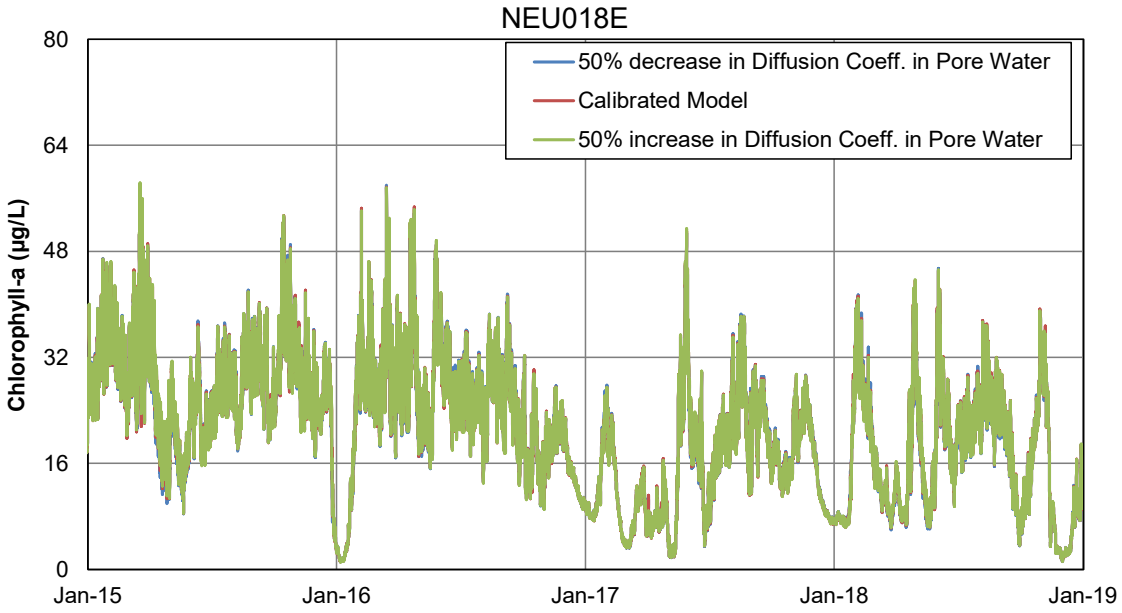

Figure 8 Modeled Chl-a at NEU018E under Perturbation of Diffusion Coefficient in Pore Water

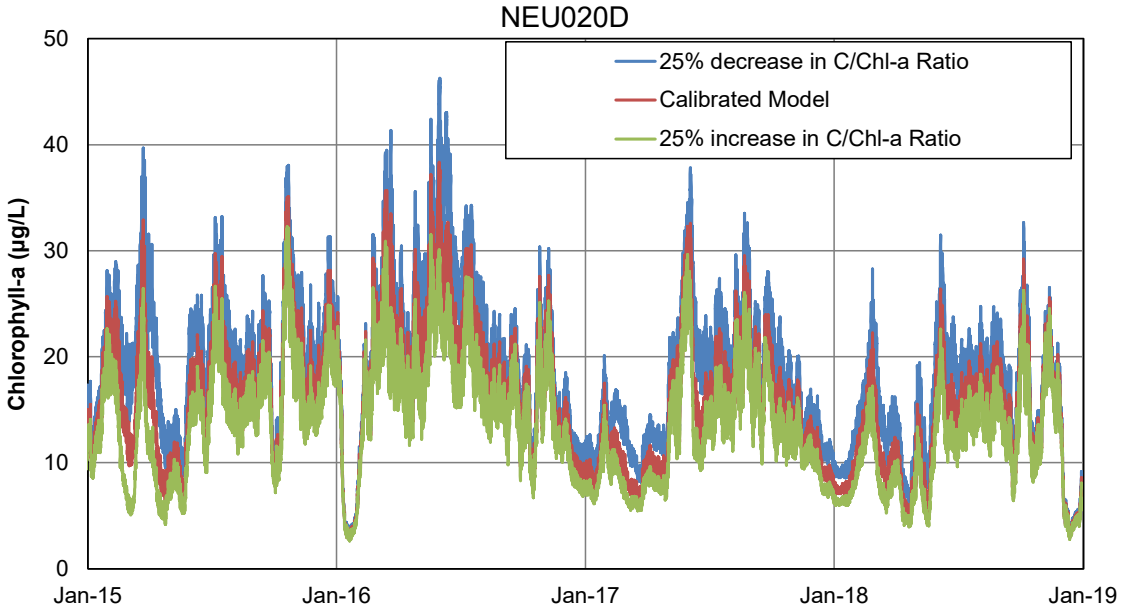

Figure 9 Modeled Chl-a at NEU020D under Perturbation Levels of C/Chl-a Ratio

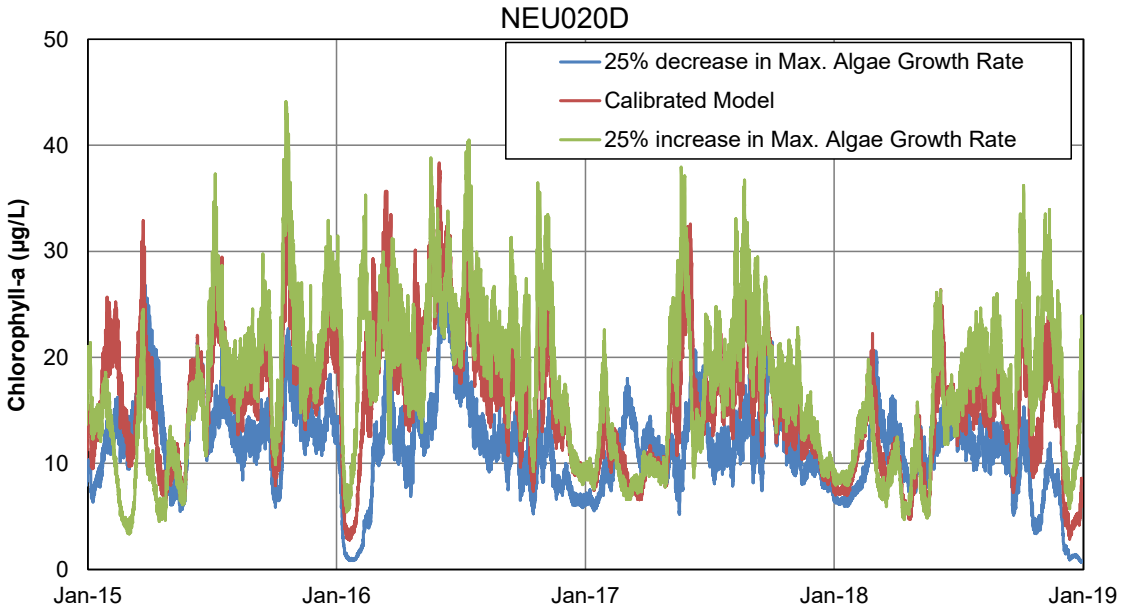

Figure 10 Modeled Chl-a at NEU020D under Perturbation Levels of Algal Growth Rate

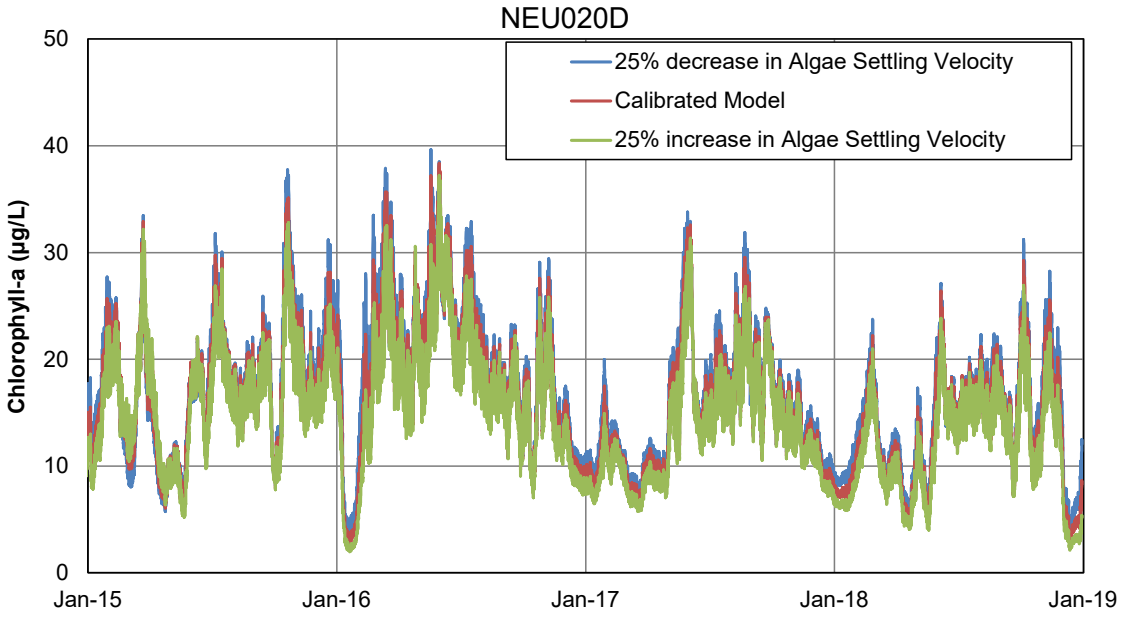

Figure 11 Modeled Chl-a at NEU020D under Perturbation of Algal Settling Velocity

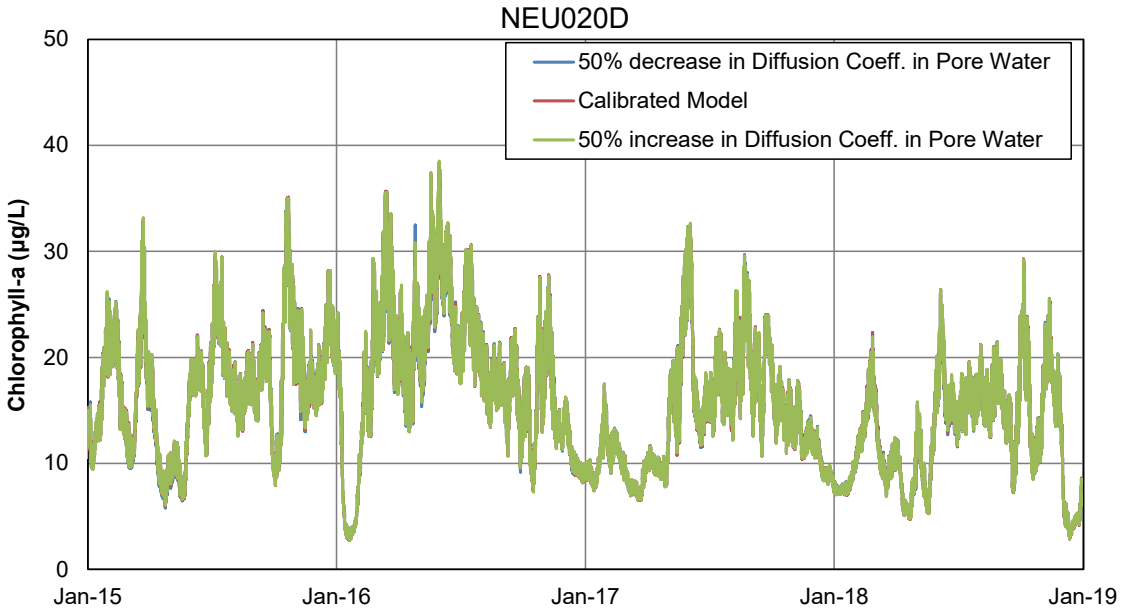

Figure 12 Modeled Chl-a at NEU020D under Perturbation of Diffusion Coefficient in Pore Water

1.2 TOC

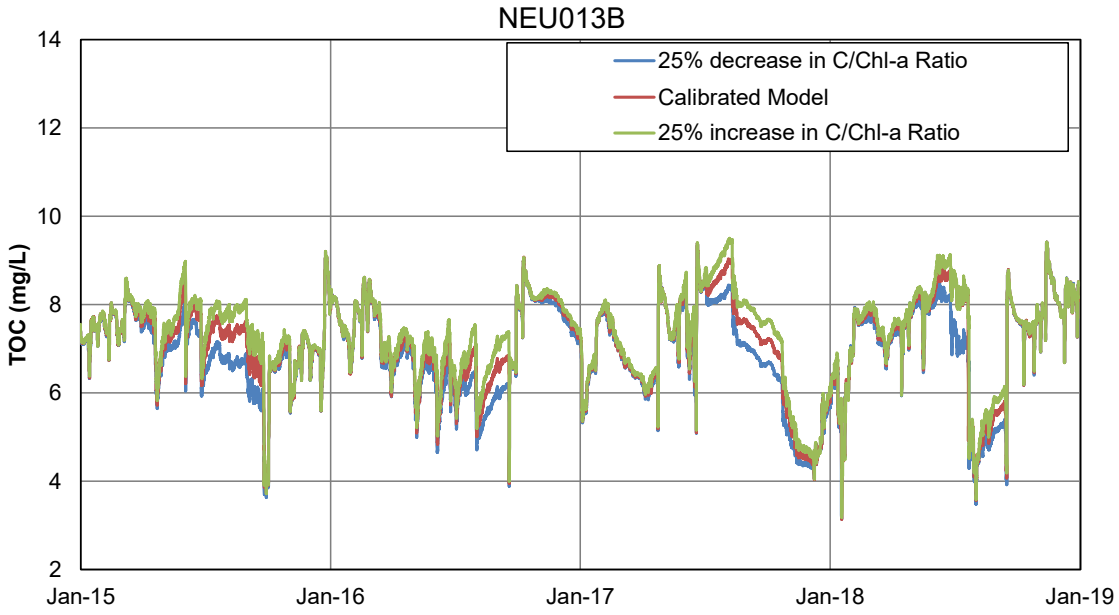

Figure 13 Modeled TOC at NEU013B under Perturbation Levels of C/Chl-a Ratio

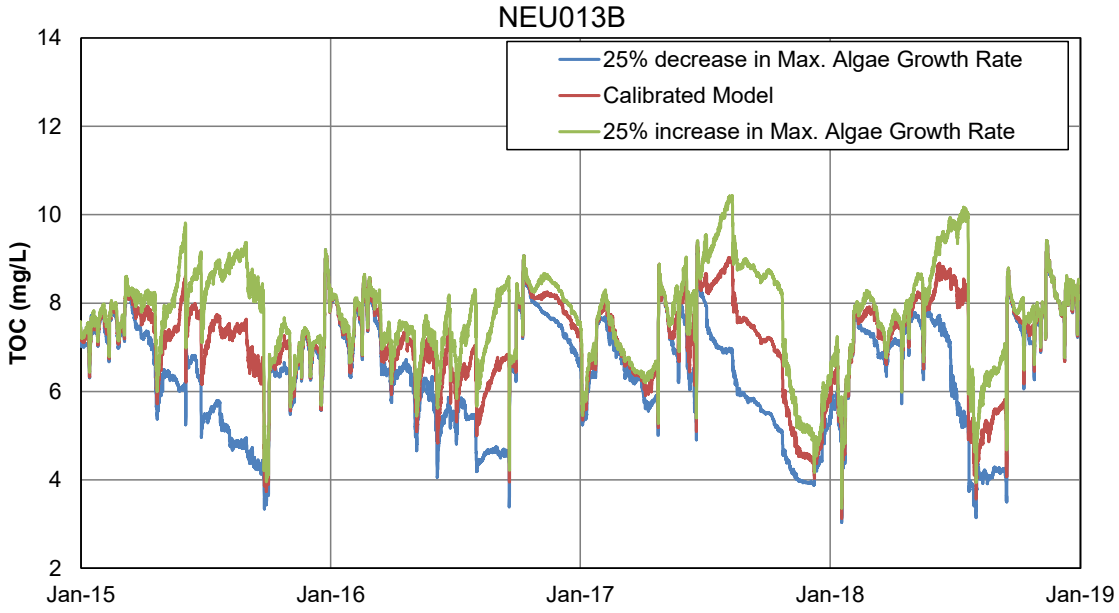

Figure 14 Modeled TOC at NEU013B under Perturbation Levels of Algal Growth Rate

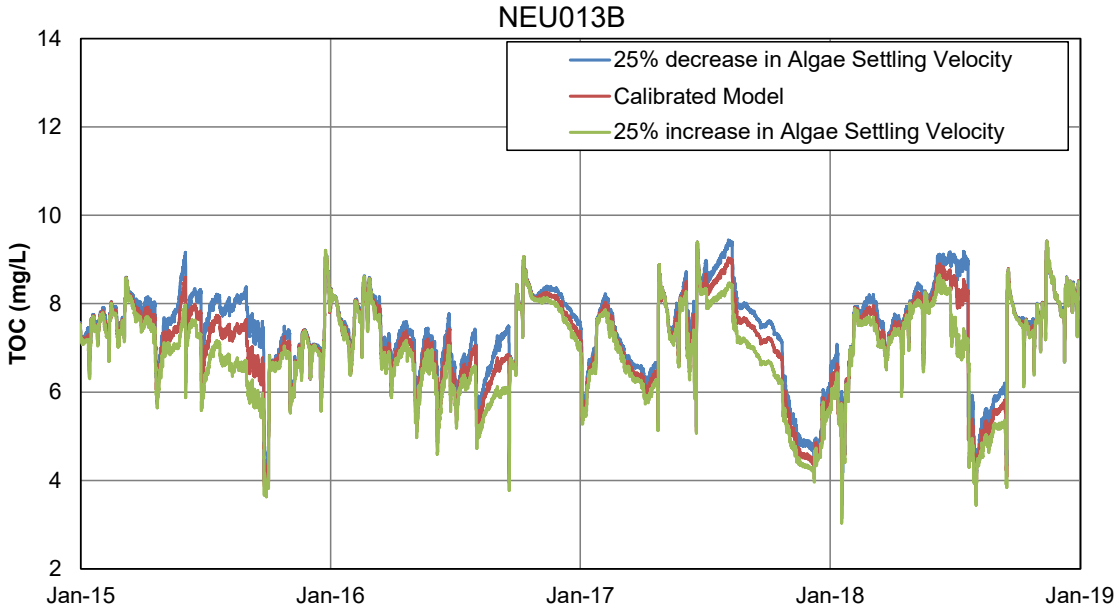

Figure 15 Modeled TOC at NEU013B under Perturbation of Algal Settling Velocity

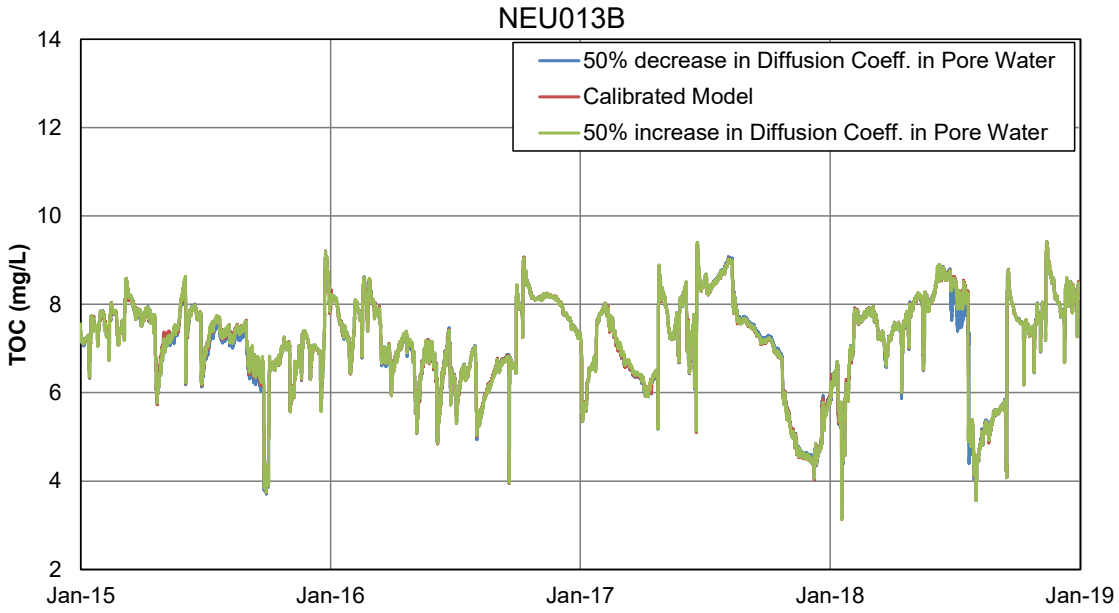

Figure 16 Modeled TOC at NEU013B under Perturbation of Diffusion Coefficient in Pore Water

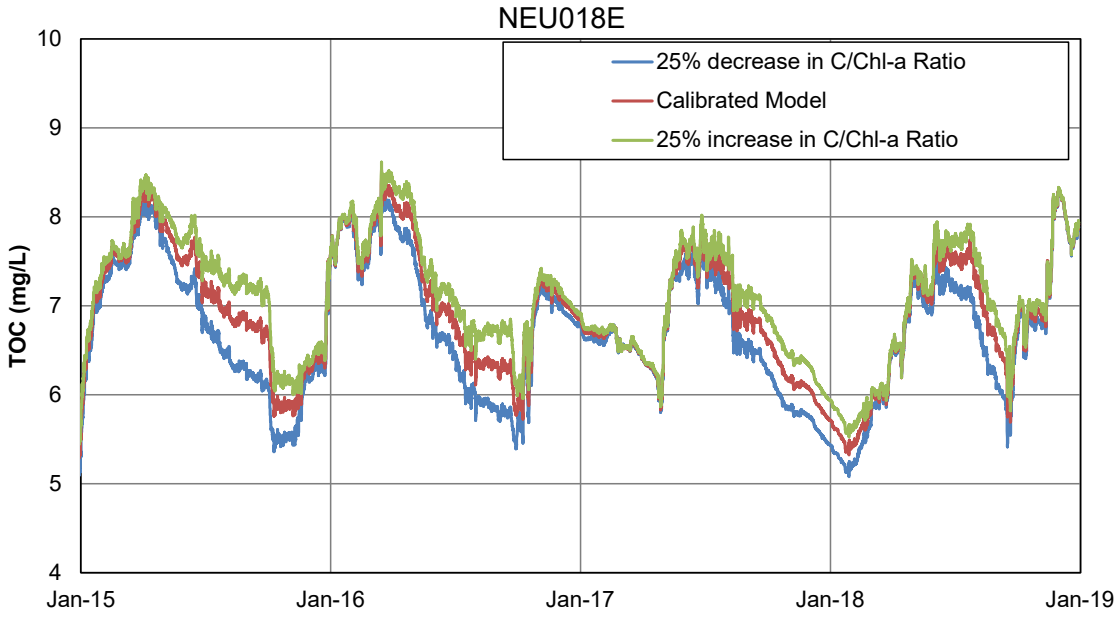

Figure 17 Modeled TOC at NEU018E under Perturbation Levels of C/Chl-a Ratio

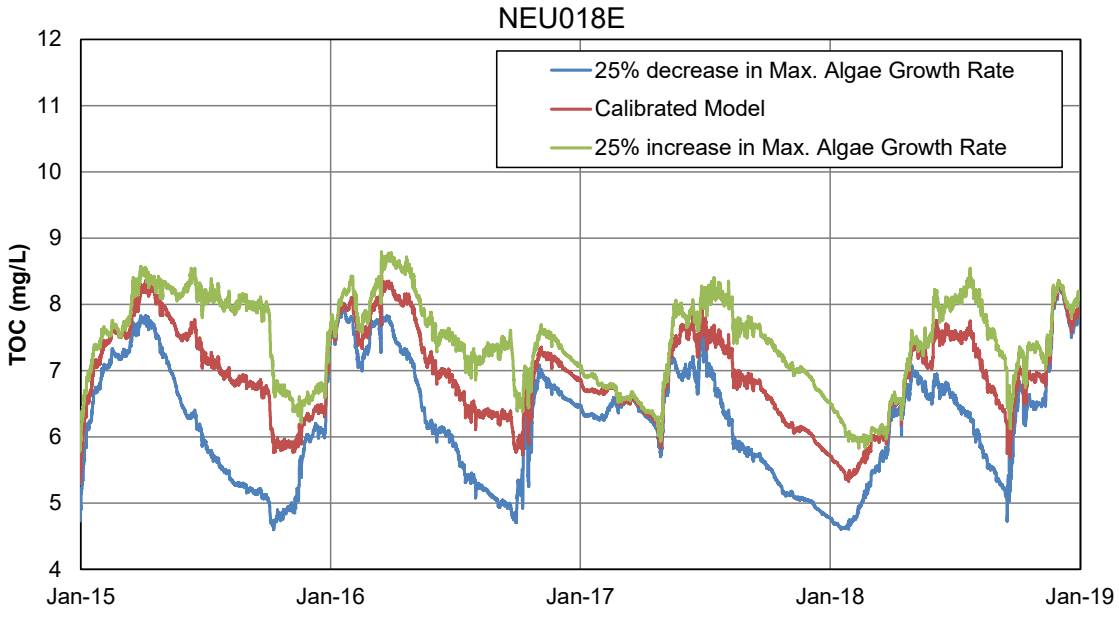

Figure 18 Modeled TOC at NEU018E under Perturbation Levels of Algal Growth Rate

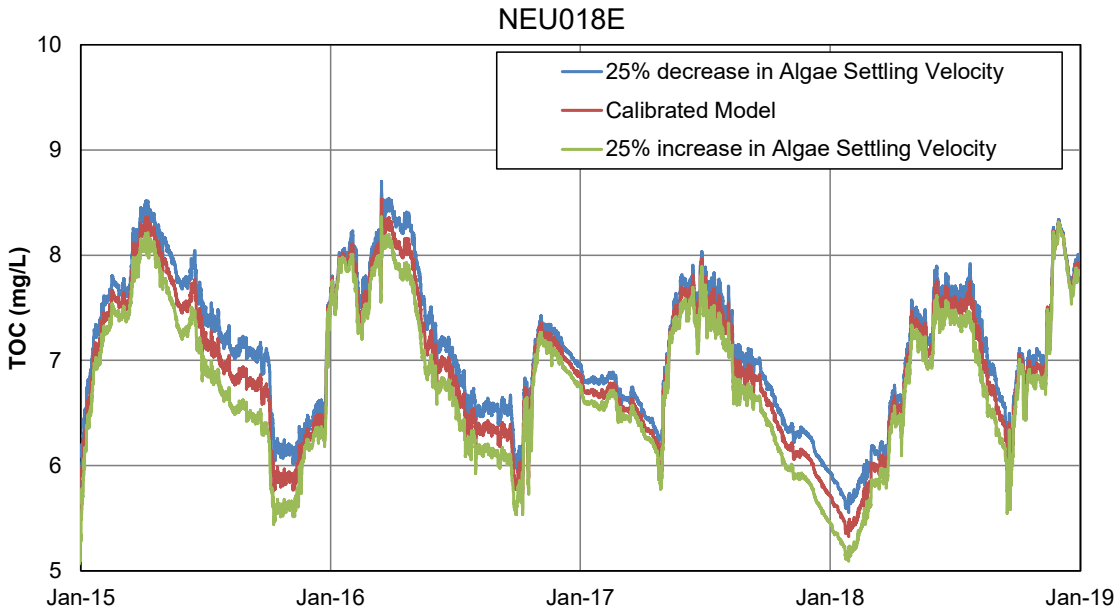

Figure 19 Modeled TOC at NEU018E under Perturbation of Algal Settling Velocity

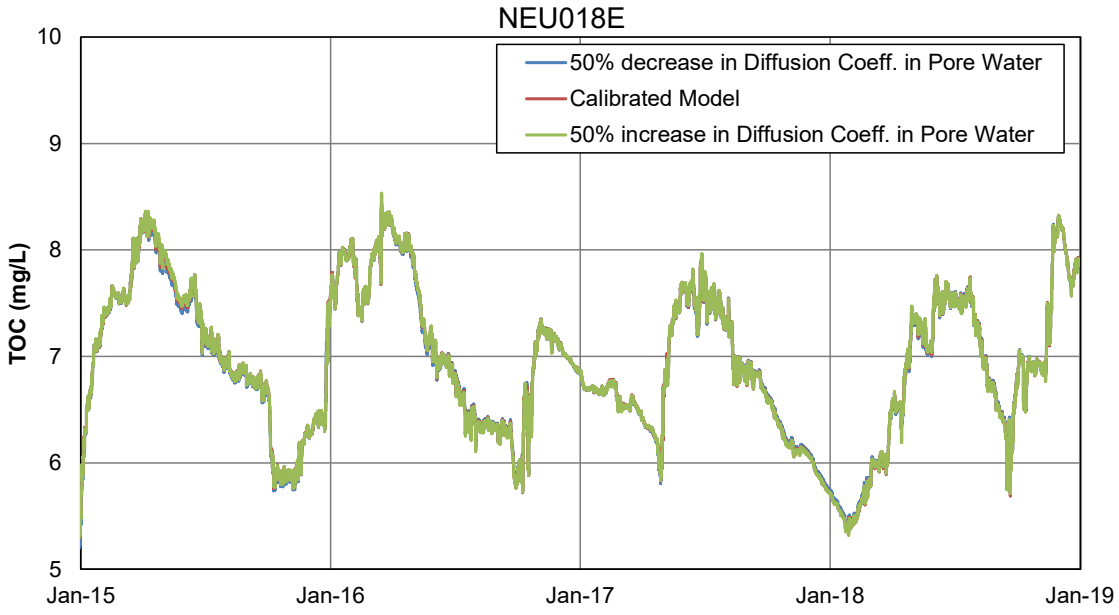

Figure 20 Modeled TOC at NEU018E under Perturbation of Diffusion Coefficient in Pore Water

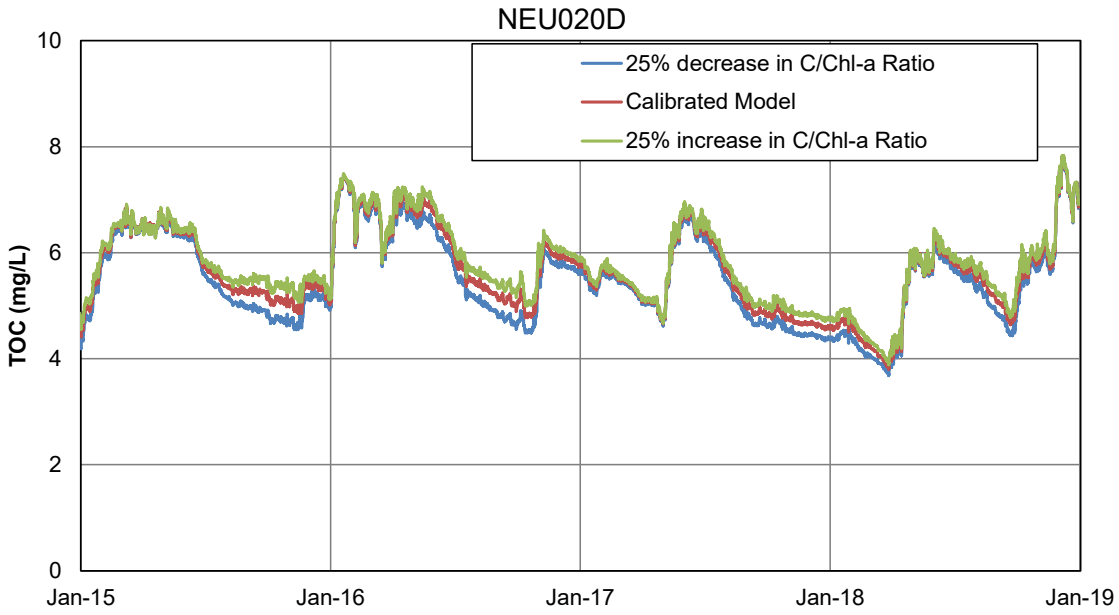

Figure 21 Modeled TOC at NEU020D under Perturbation Levels of C/Chl-a Ratio

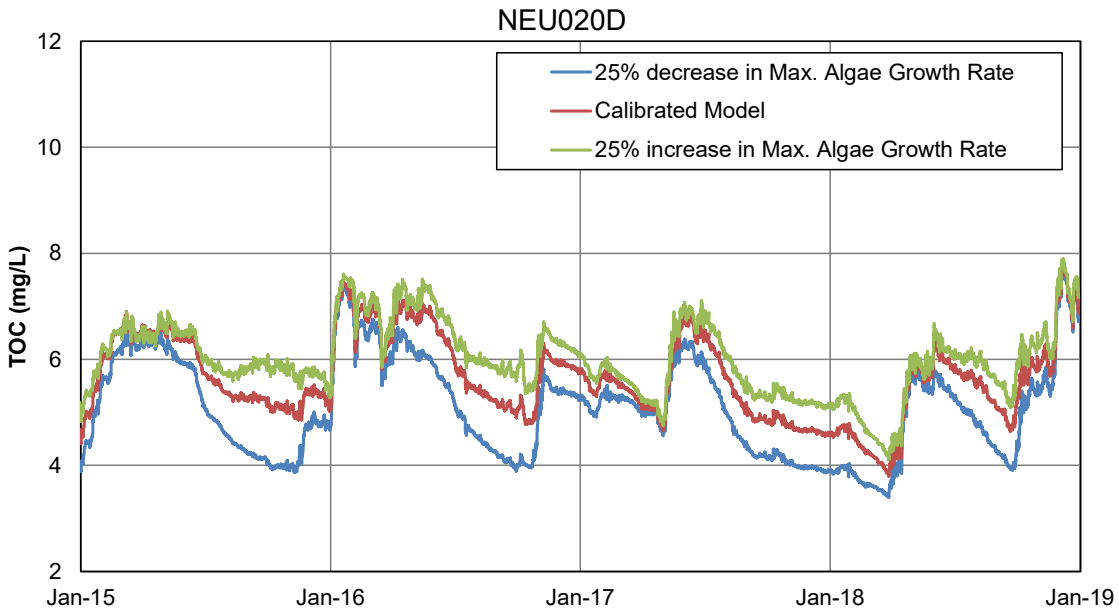

Figure 22 Modeled TOC at NEU020D under Perturbation Levels of Algal Growth Rate

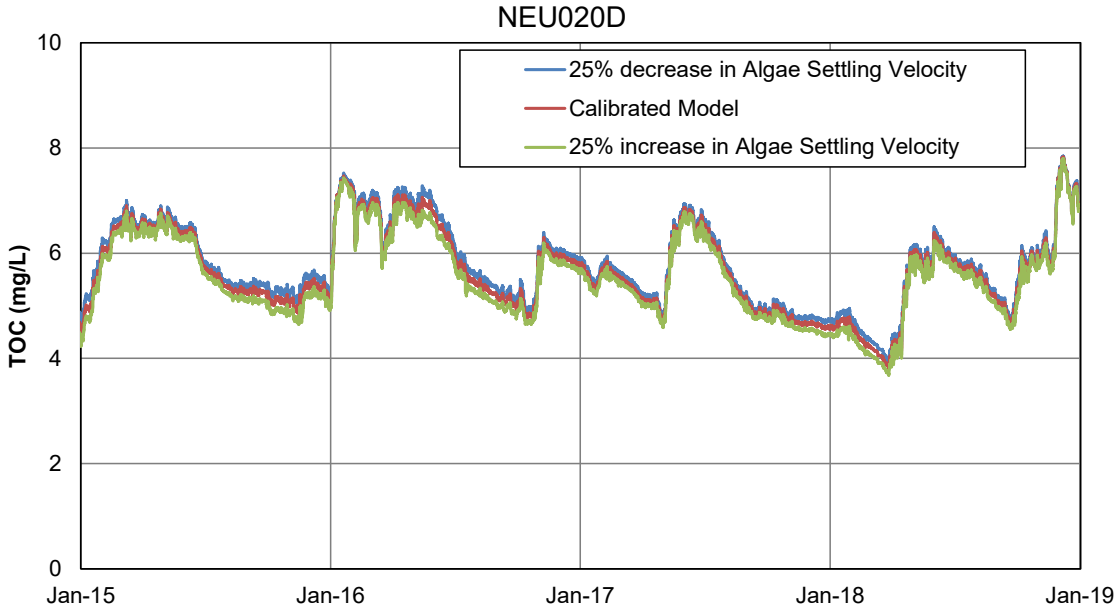

Figure 23 Modeled TOC at NEU020D under Perturbation of Algal Settling Velocity

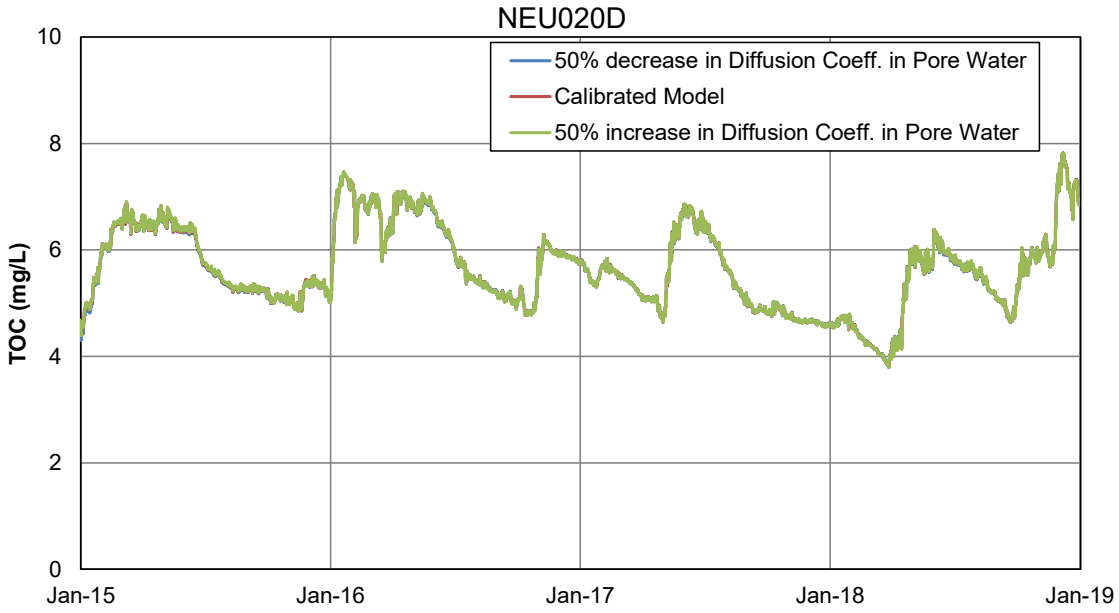

Figure 24 Modeled TOC at NEU020D under Perturbation of Diffusion Coefficient in Pore Water

1.3 TN

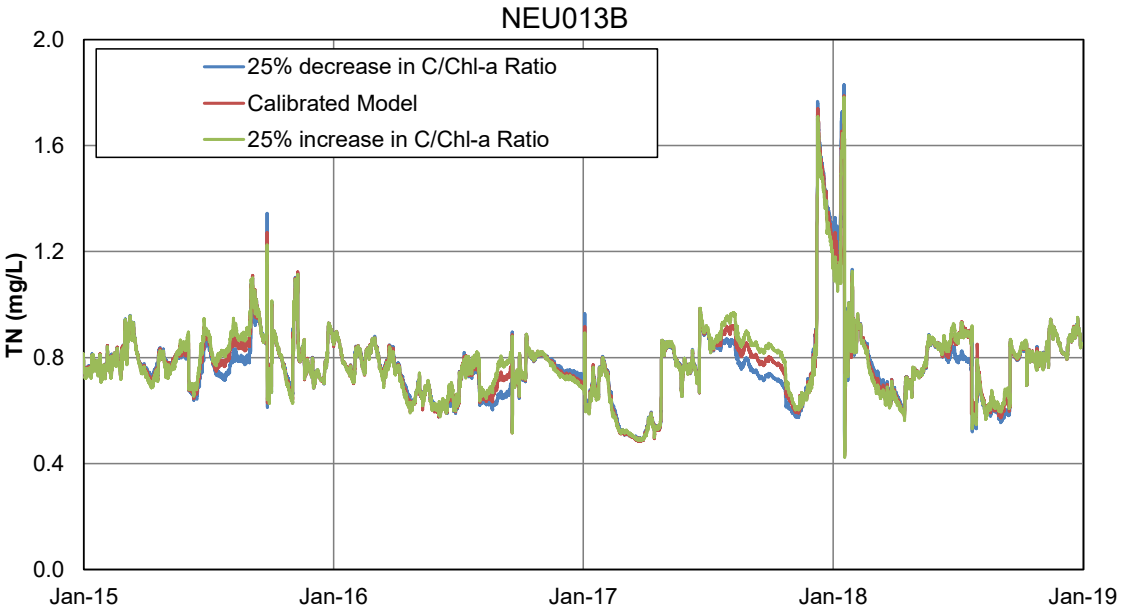

Figure 25 Modeled TN at NEU013B under Perturbation Levels of C/Chl-a Ratio

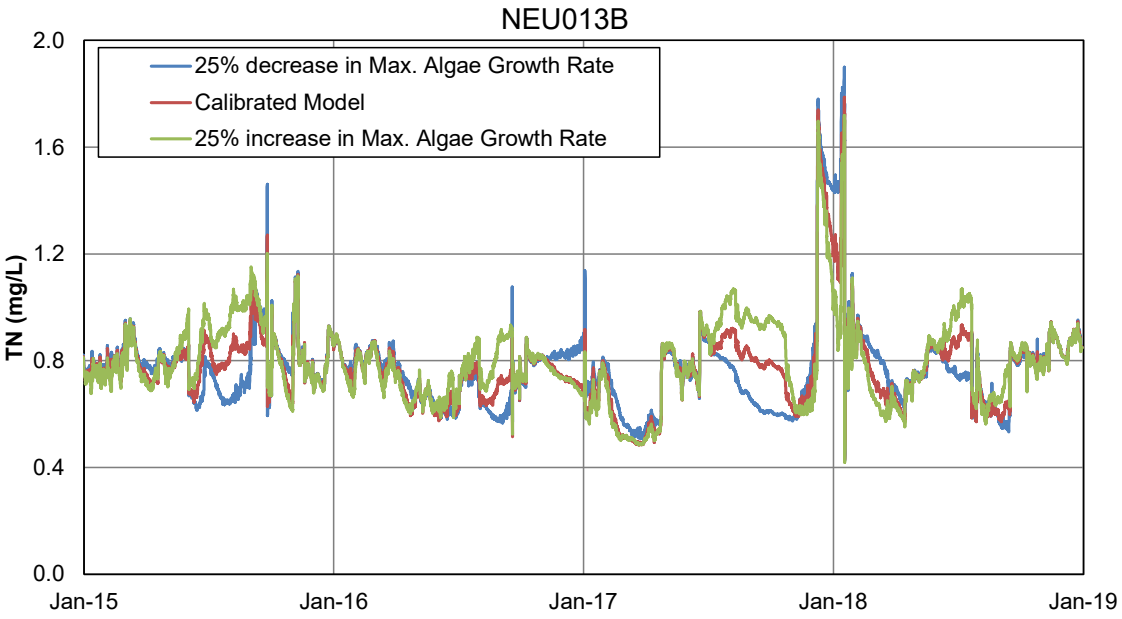

Figure 26 Modeled TN at NEU013B under Perturbation Levels of Algal Growth Rate

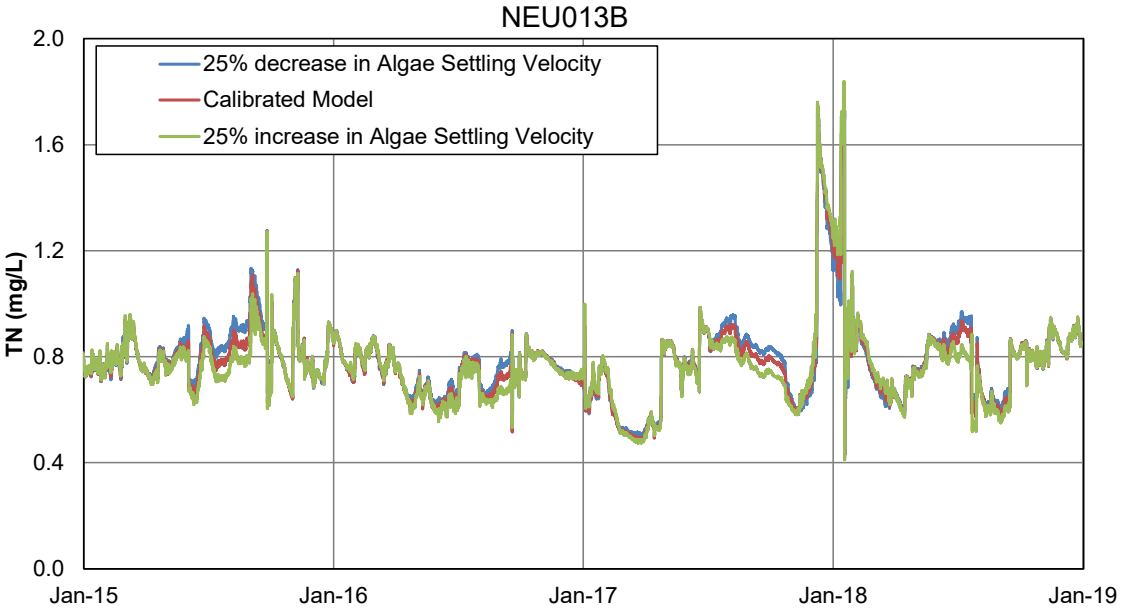

Figure 27 Modeled TN at NEU013B under Perturbation of Algal Settling Velocity

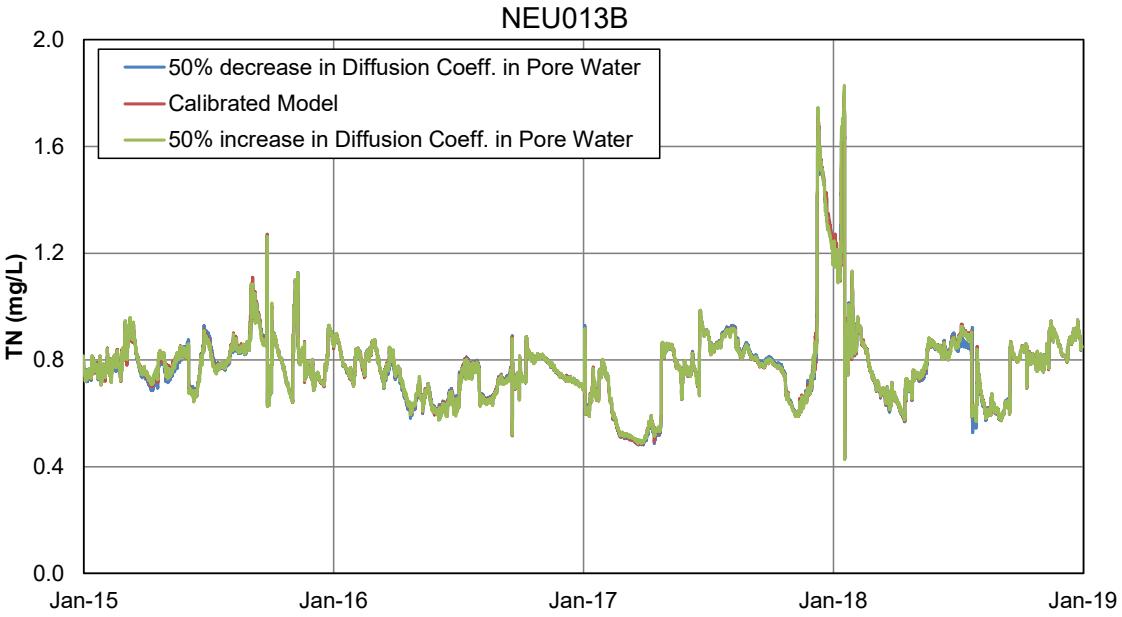

Figure 28 Modeled TN at NEU013B under Perturbation of Diffusion Coefficient in Pore Water

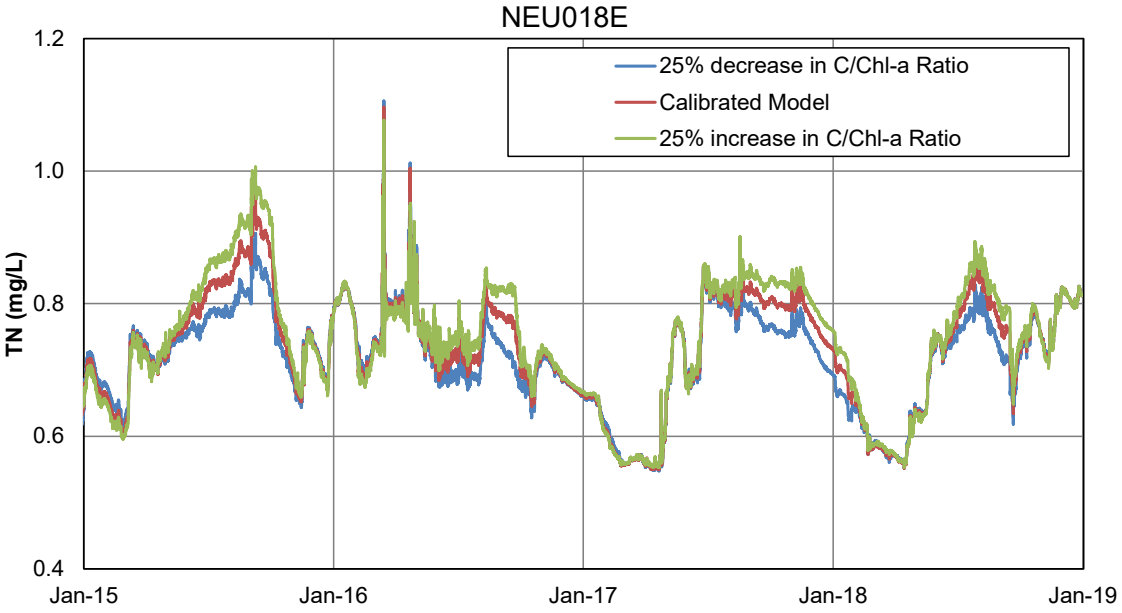

Figure 29 Modeled TN at NEU018E under Perturbation Levels of C/Chl-a Ratio

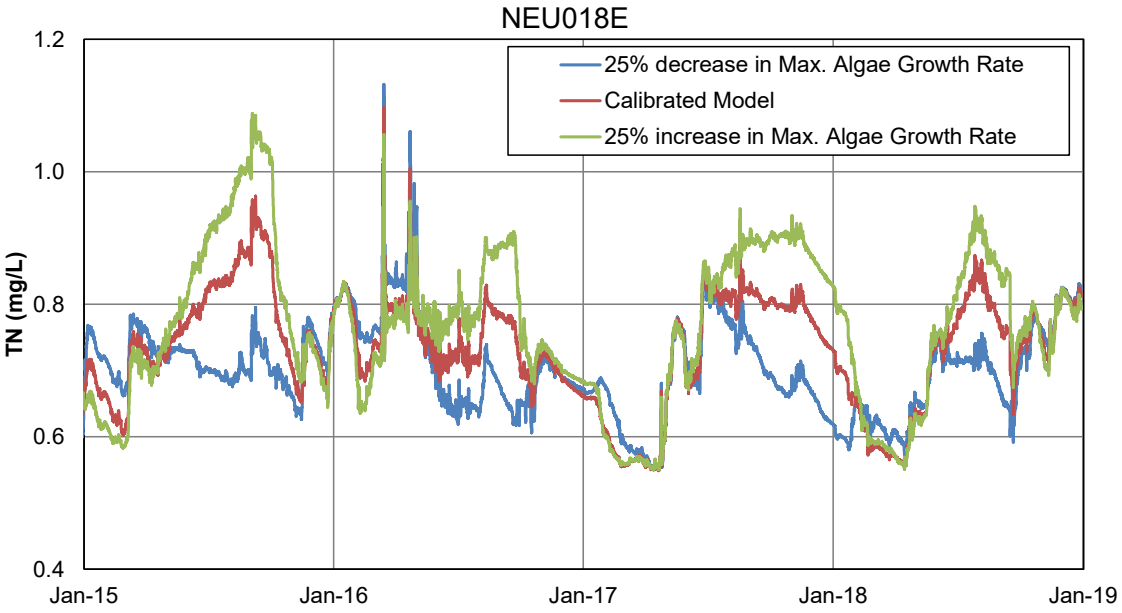

Figure 30 Modeled TN at NEU018E under Perturbation Levels of Algal Growth Rate

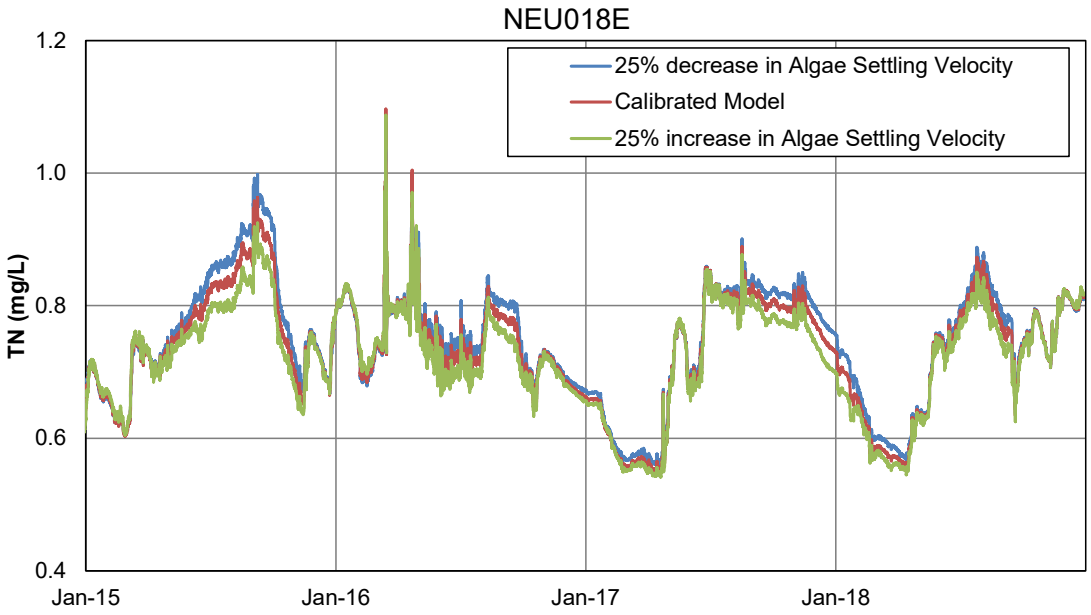

Figure 31 Modeled TN at NEU018E under Perturbation of Algal Settling Velocity

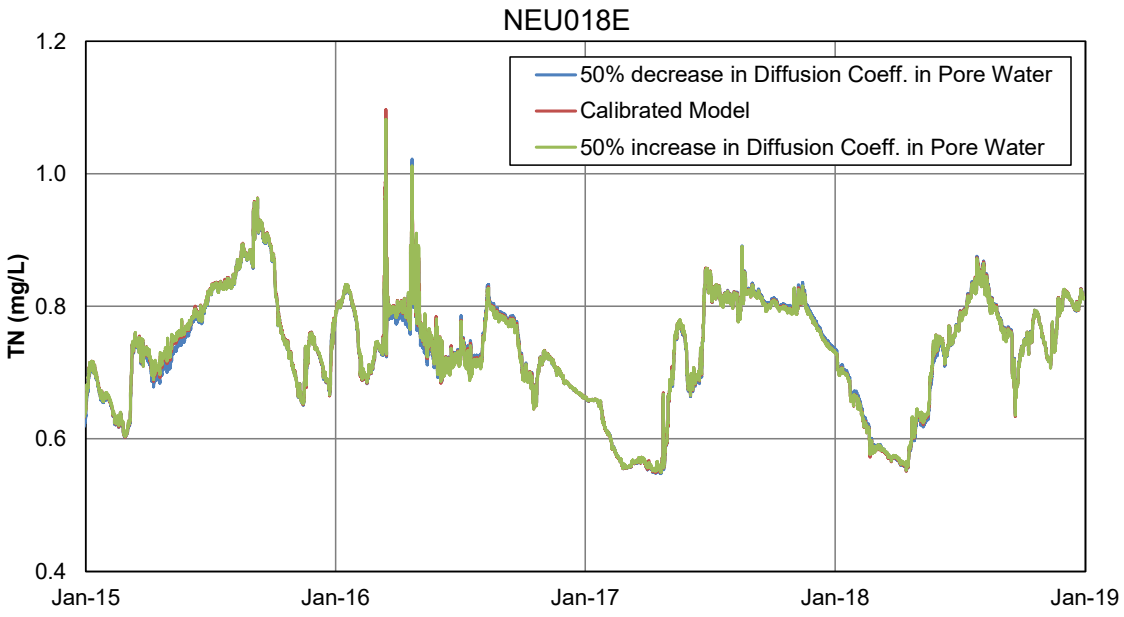

Figure 32 Modeled TN at NEU018E under Perturbation of Diffusion Coefficient in Pore Water

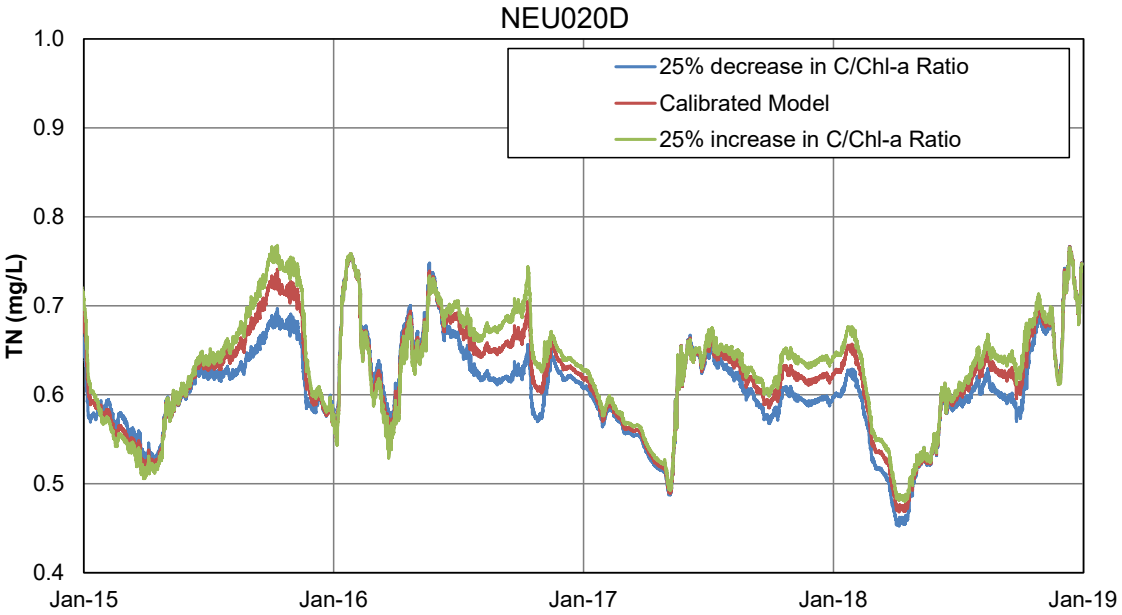

Figure 33 Modeled TN at NEU020D under Perturbation Levels of C/Chl-a Ratio

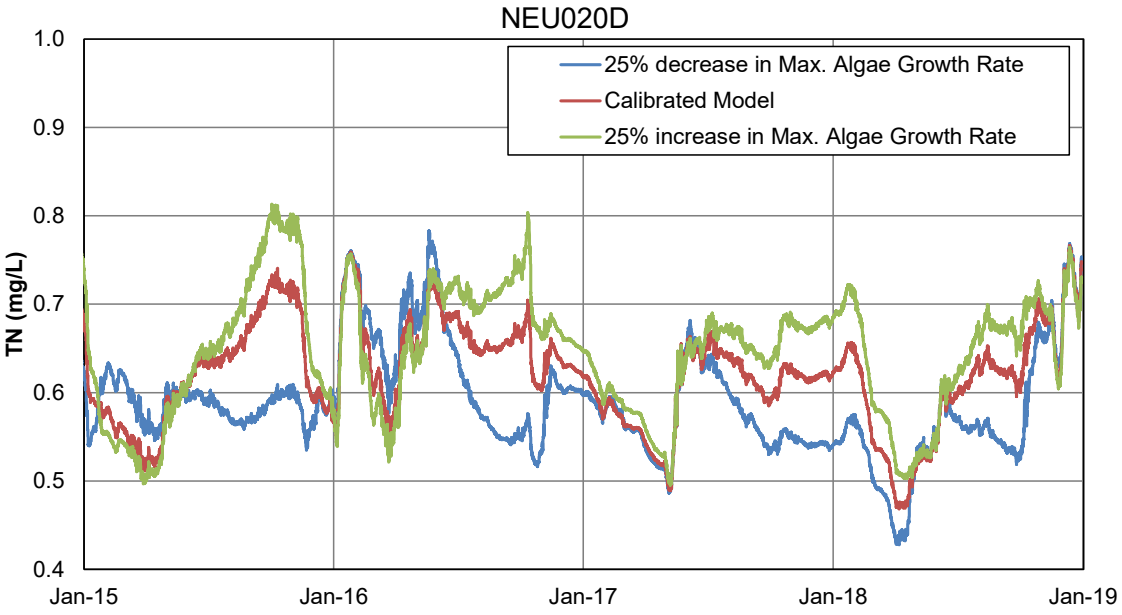

Figure 34 Modeled TN at NEU020D under Perturbation Levels of Algal Growth Rate

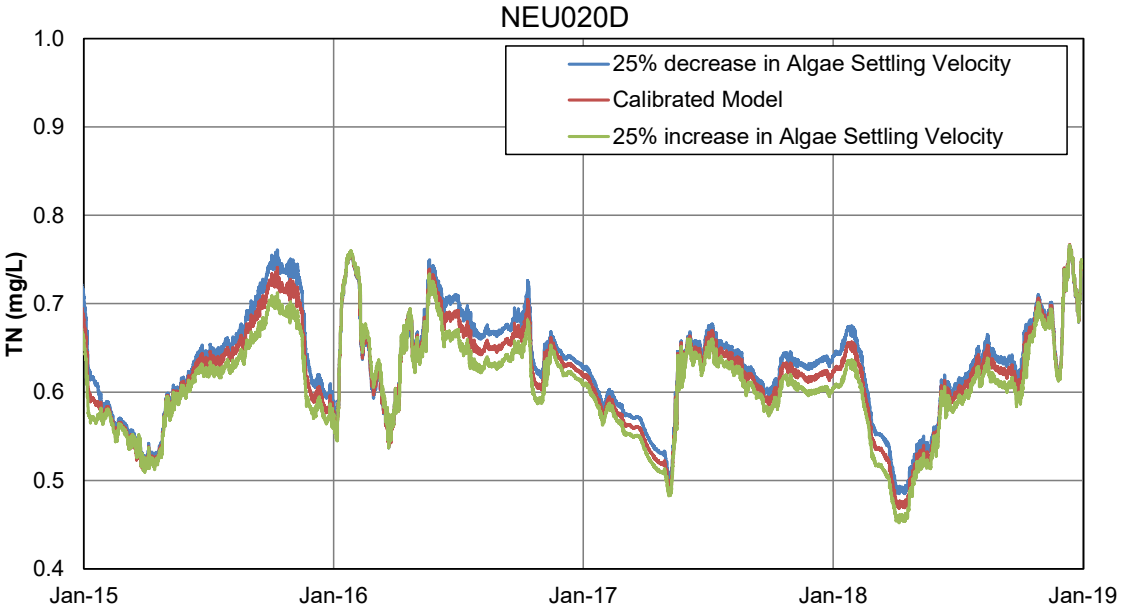

Figure 35 Modeled TN at NEU020D under Perturbation of Algal Settling Velocity

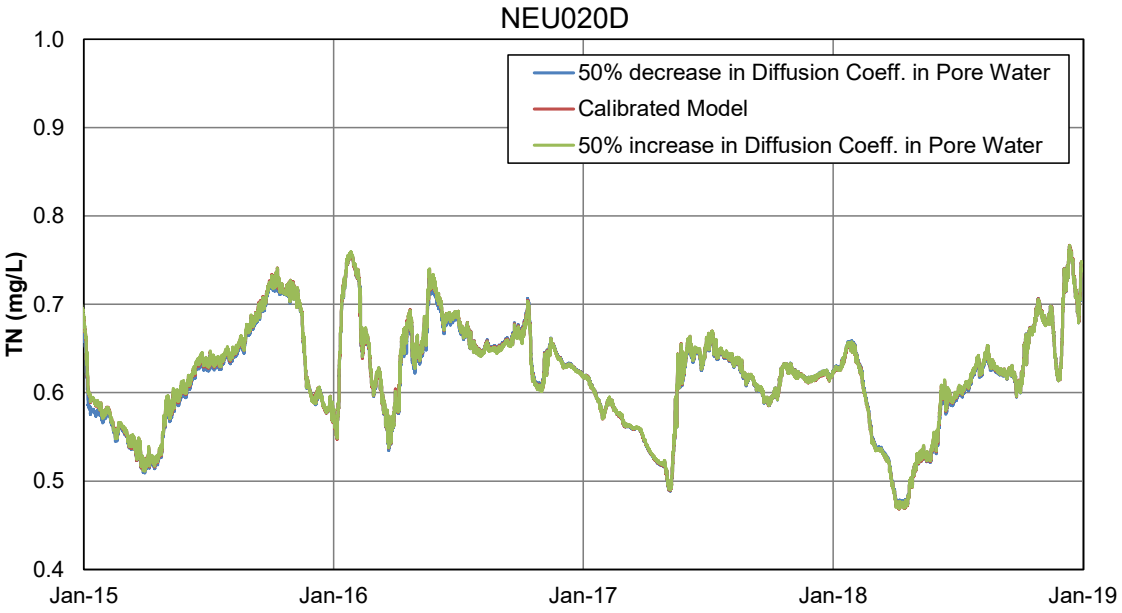

Figure 36 Modeled TN at NEU020D under Perturbation of Diffusion Coefficient in Pore Water

1.4 TP

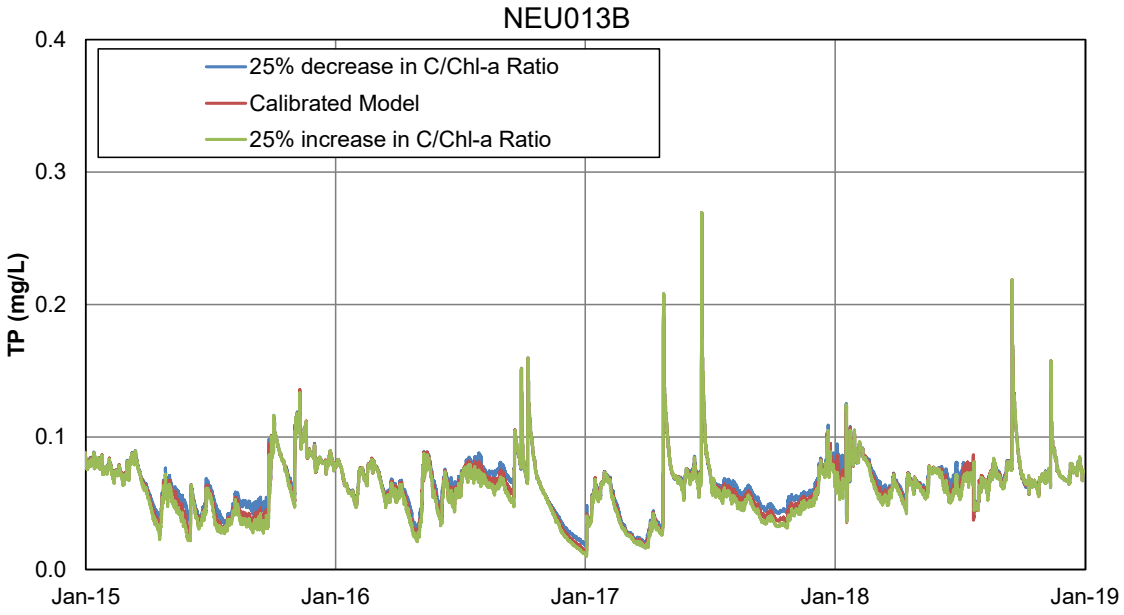

Figure 37 Modeled TP at NEU013B under Perturbation Levels of C/Chl-a Ratio

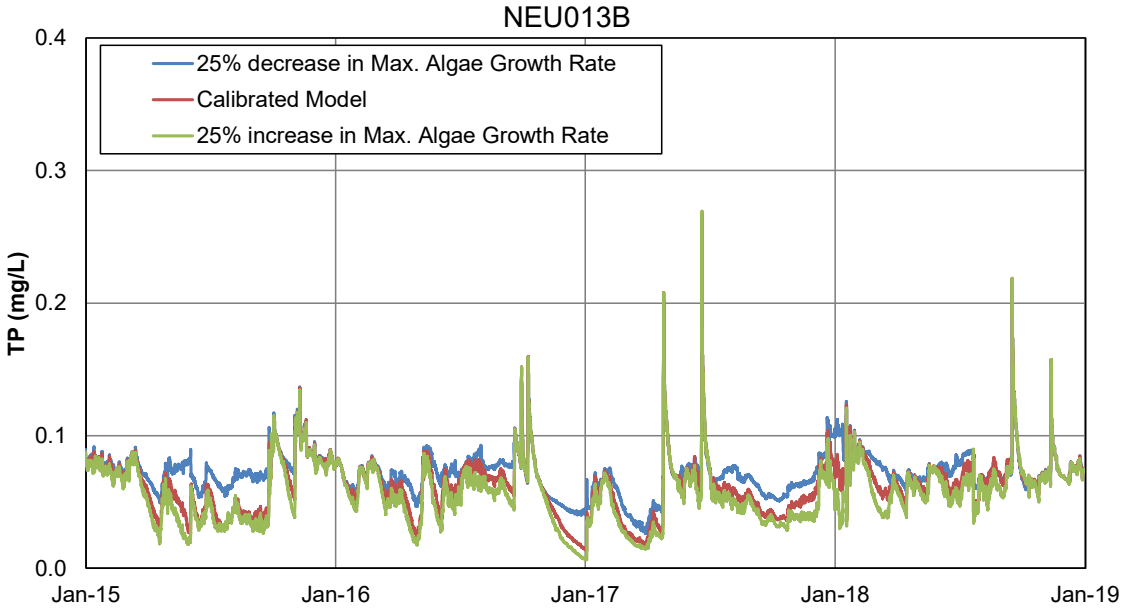

Figure 38 Modeled TP at NEU013B under Perturbation Levels of Algal Growth Rate

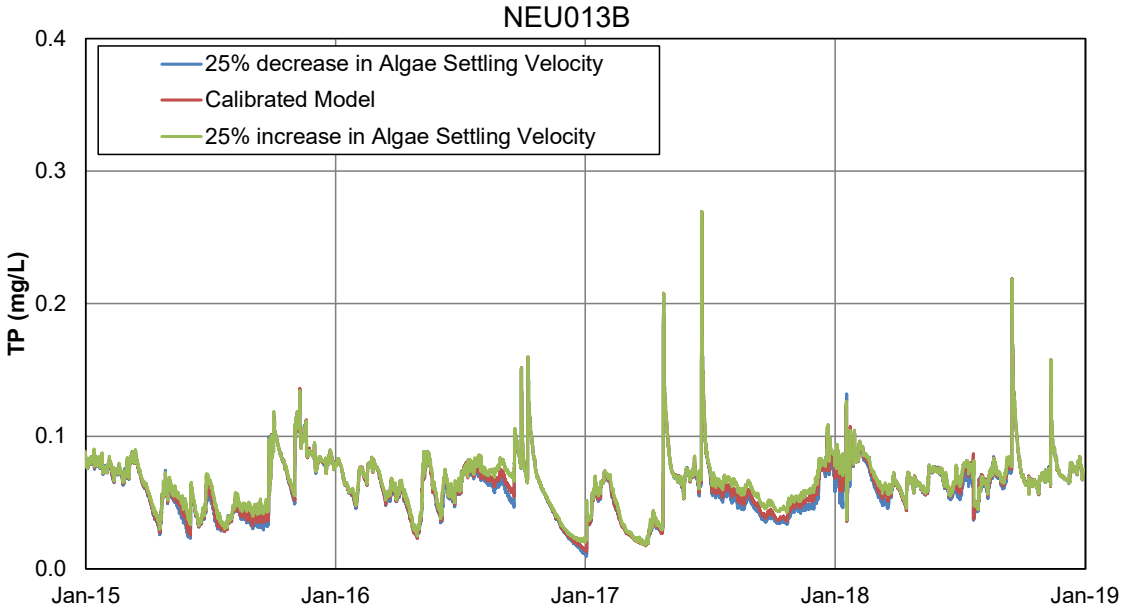

Figure 39 Modeled TP at NEU013B under Perturbation of Algal Settling Velocity

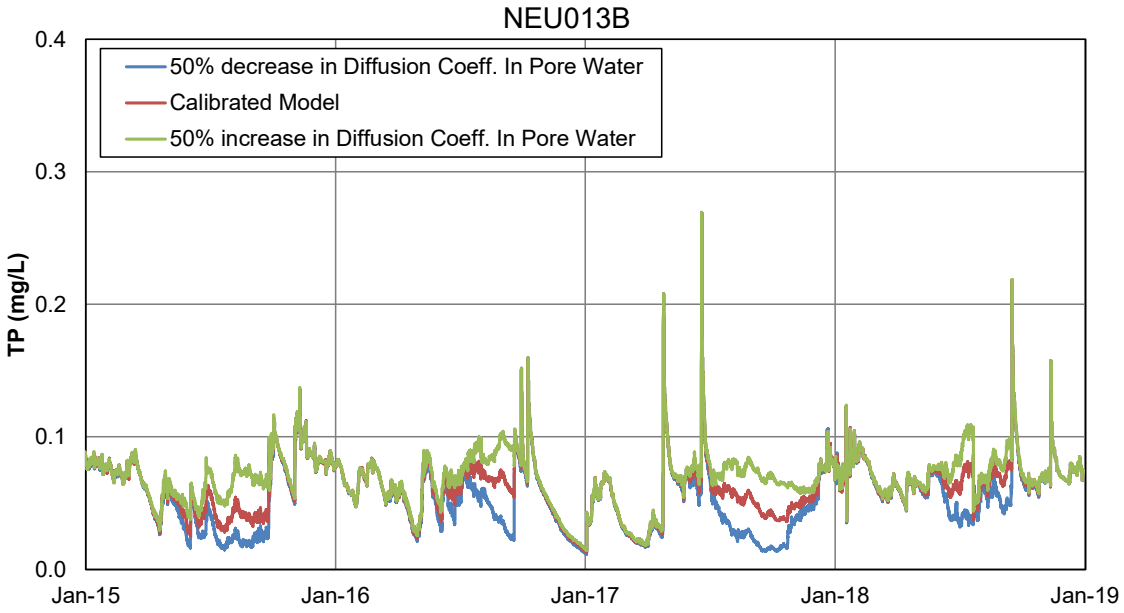

Figure 40 Modeled TP at NEU013B under Perturbation of Diffusion Coefficient in Pore Water

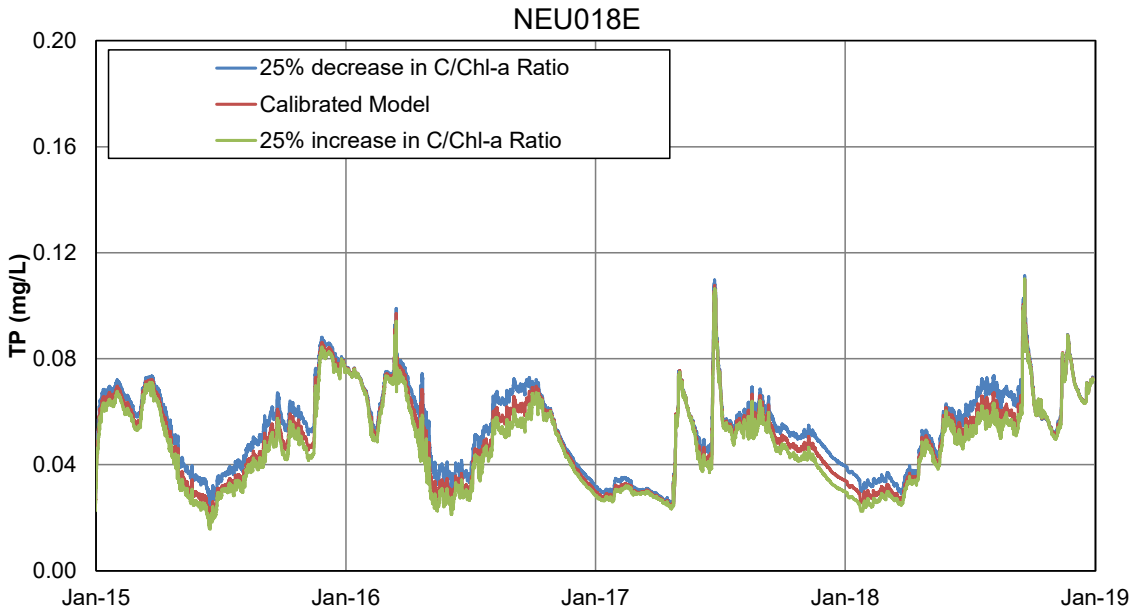

Figure 41 Modeled TP at NEU018E under Perturbation Levels of C/Chl-a Ratio

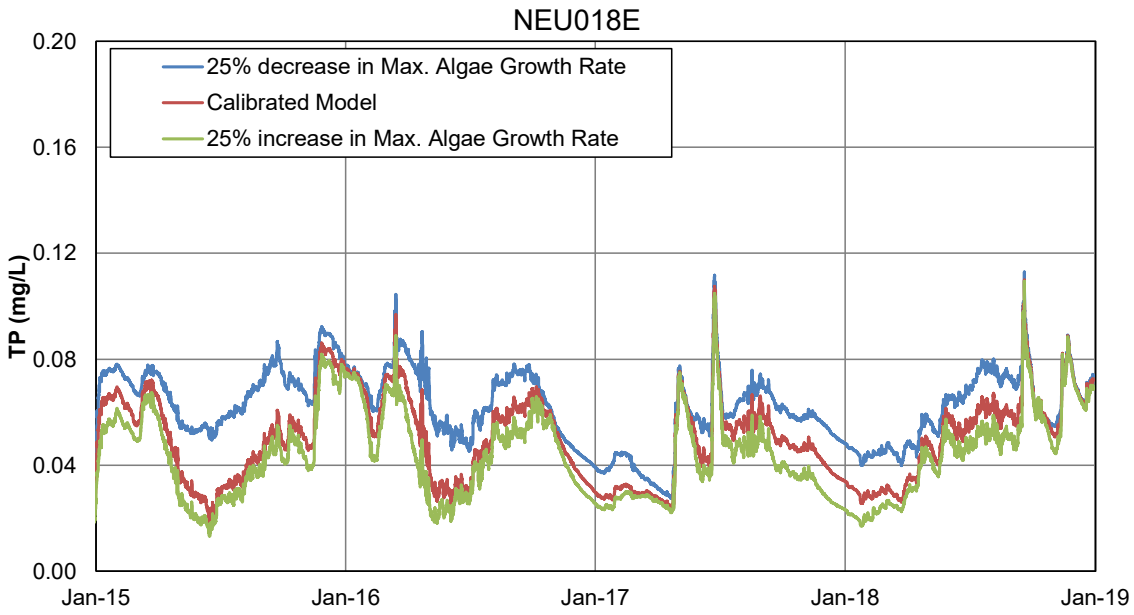

Figure 42 Modeled TP at NEU018E under Perturbation Levels of Algal Growth Rate

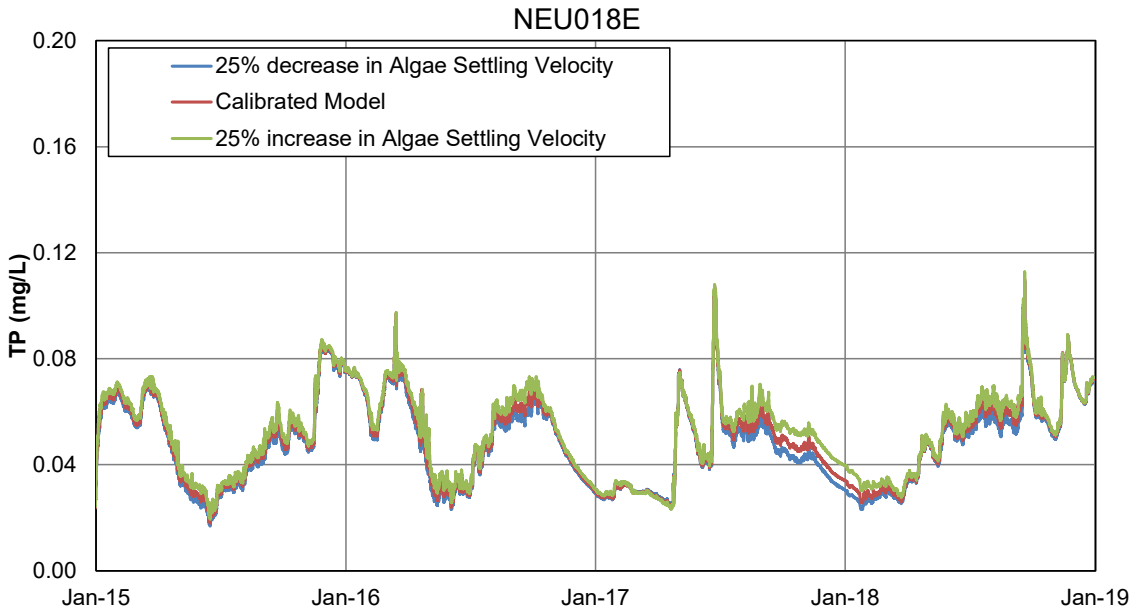

Figure 43 Modeled TP at NEU018E under Perturbation of Algal Settling Velocity

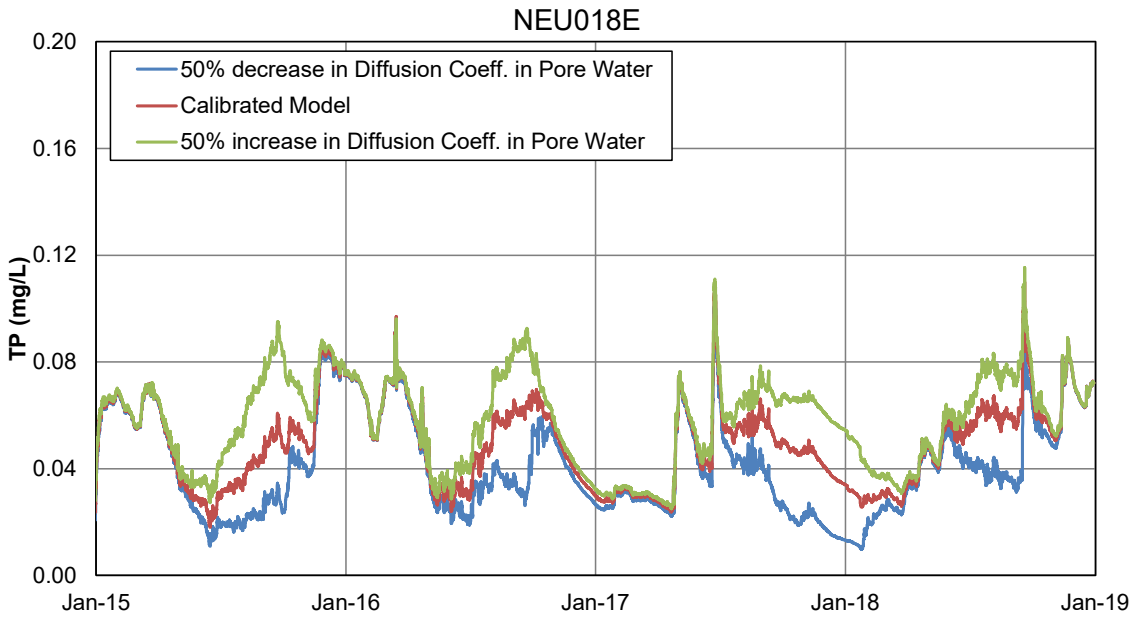

Figure 44 Modeled TP at NEU018E under Perturbation of Diffusion Coefficient in Pore Water

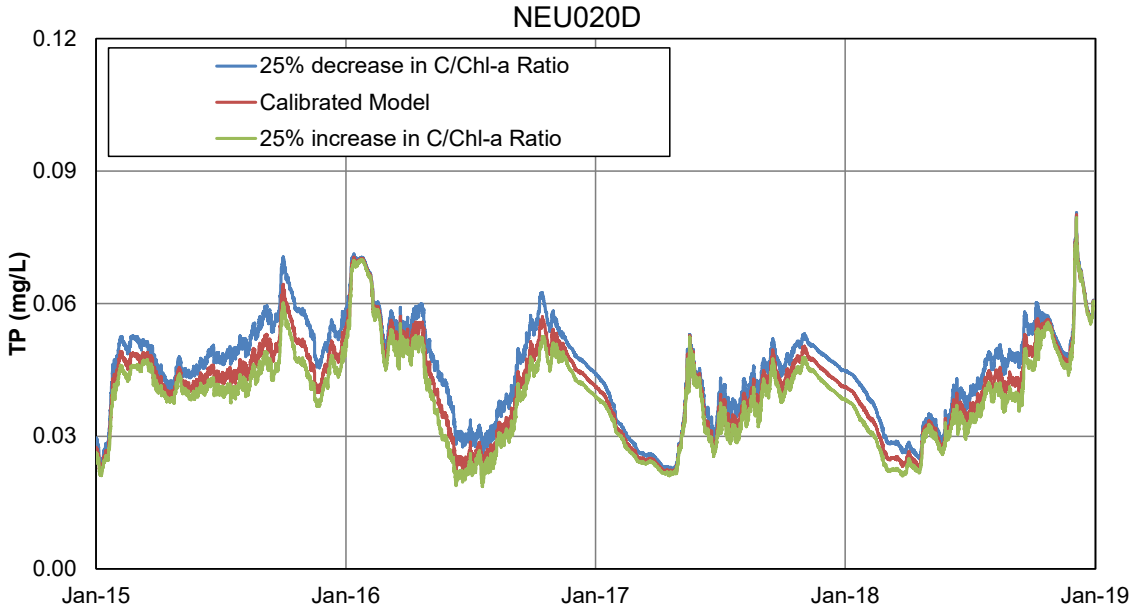

Figure 45 Modeled TP at NEU020D under Perturbation Levels of C/Chl-a Ratio

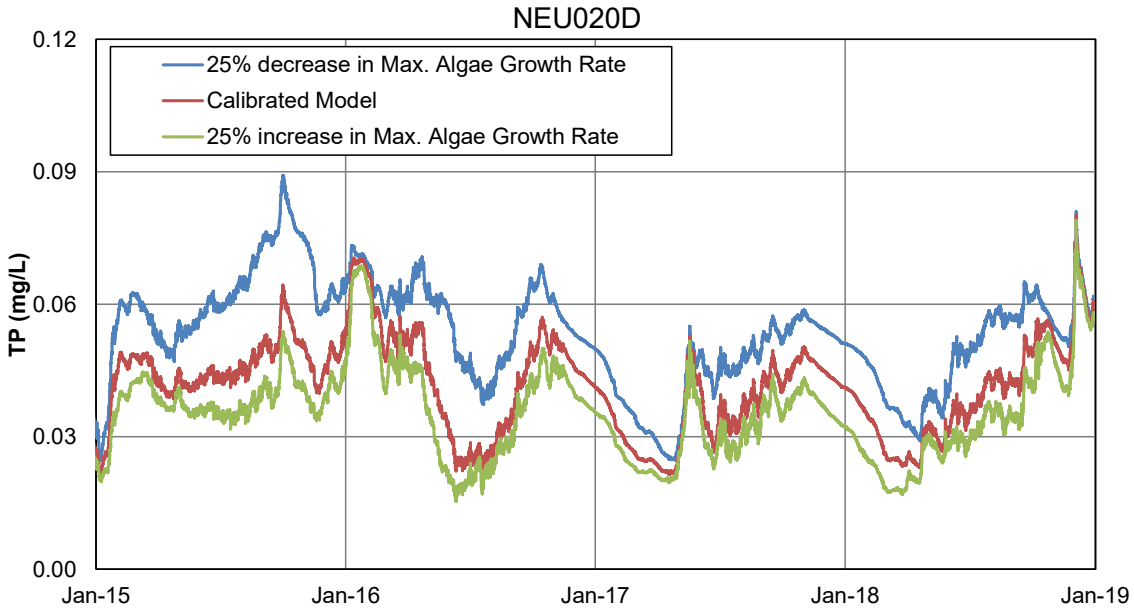

Figure 46 Modeled TP at NEU020D under Perturbation Levels of Algal Growth Rate

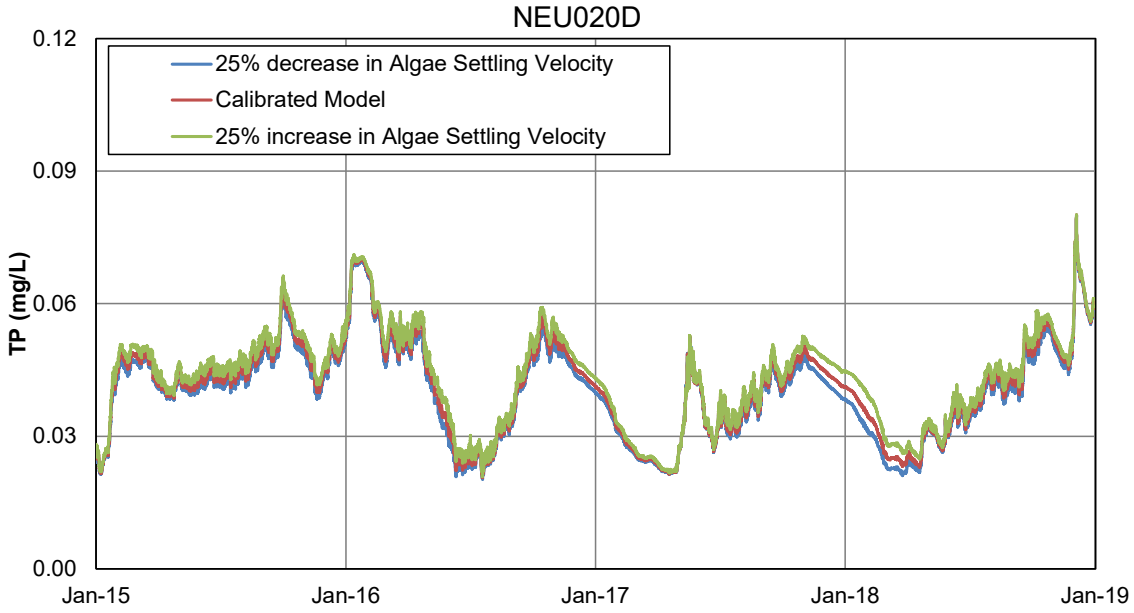

Figure 47 Modeled TP at NEU020D under Perturbation of Algal Settling Velocity

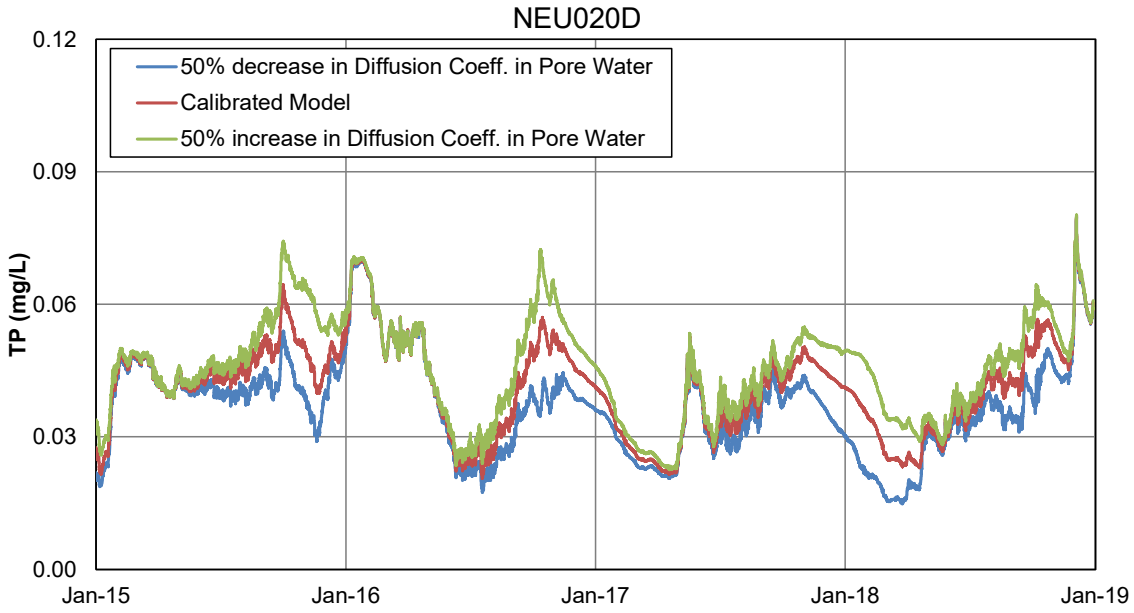

Figure 48 Modeled TP at NEU020D under Perturbation of Diffusion Coefficient in Pore Water

2. Box-Whisker Plot

2.1 Chl-a

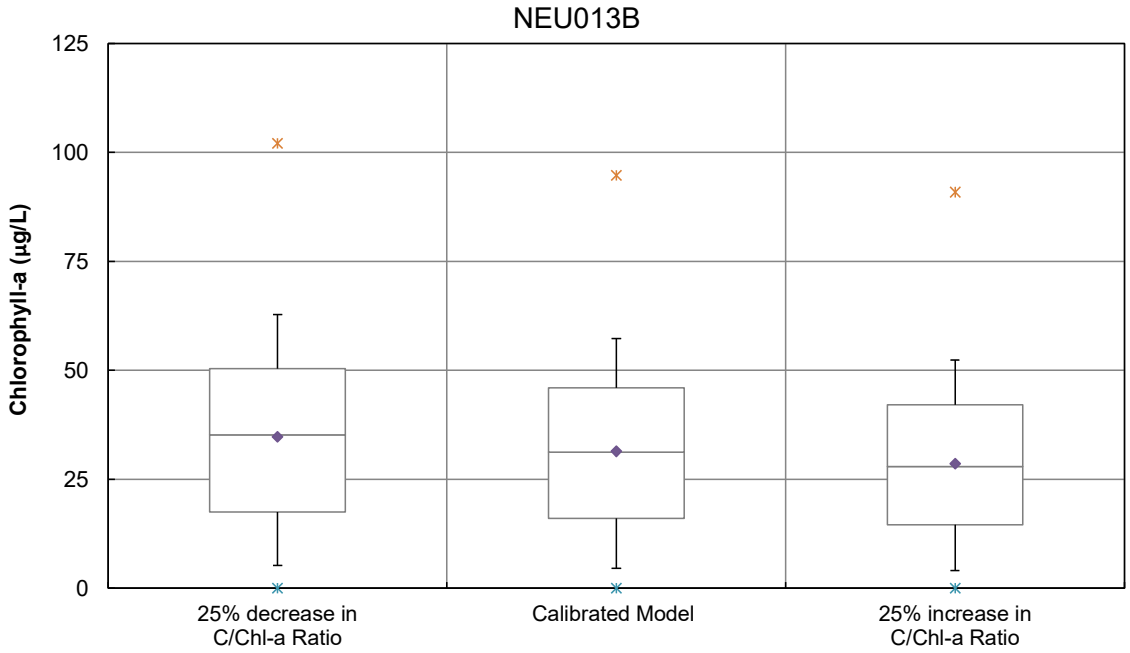

Figure 49 Box-Whisker Plot of Chl-a at NEU013B under C/Chl-a Ratio Perturbation

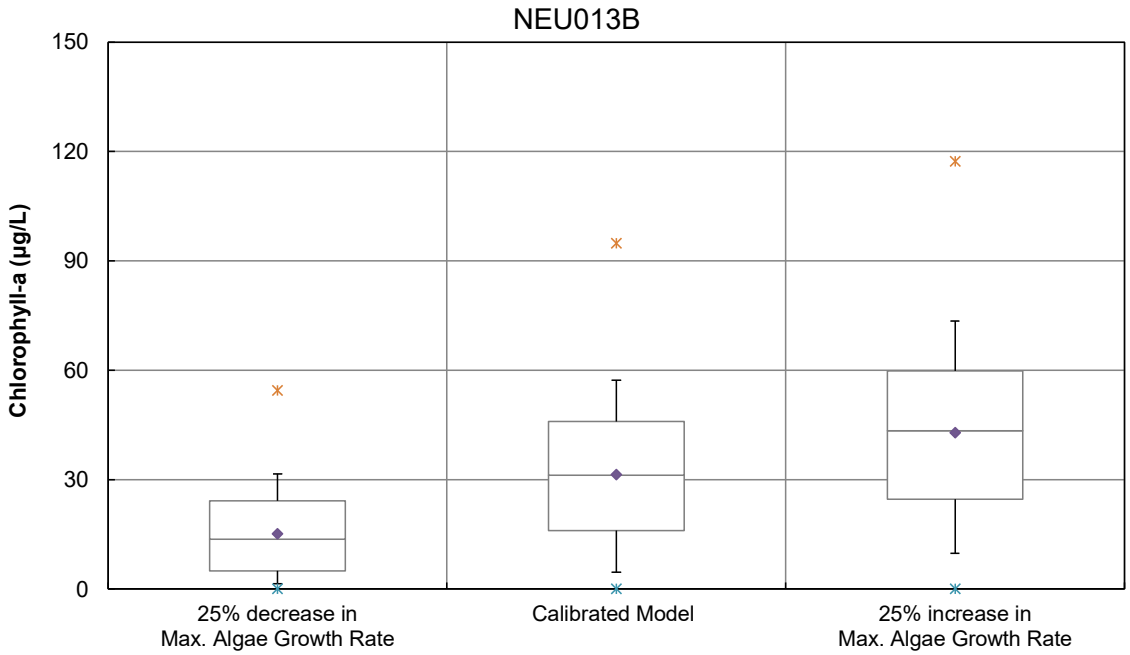

Figure 50 Box-Whisker Plot of Chl-a at NEU013B under Algal Growth Rate Perturbation

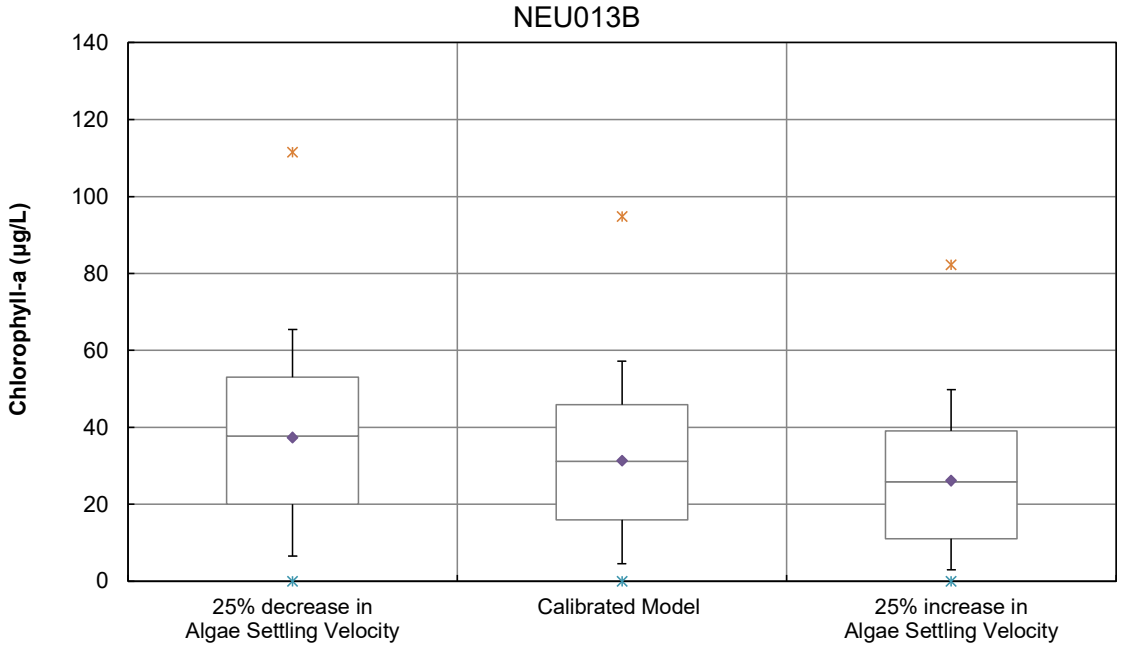

Figure 51 Box-Whisker Plot of Chl-a at NEU013B under Algal Settling Velocity Perturbation

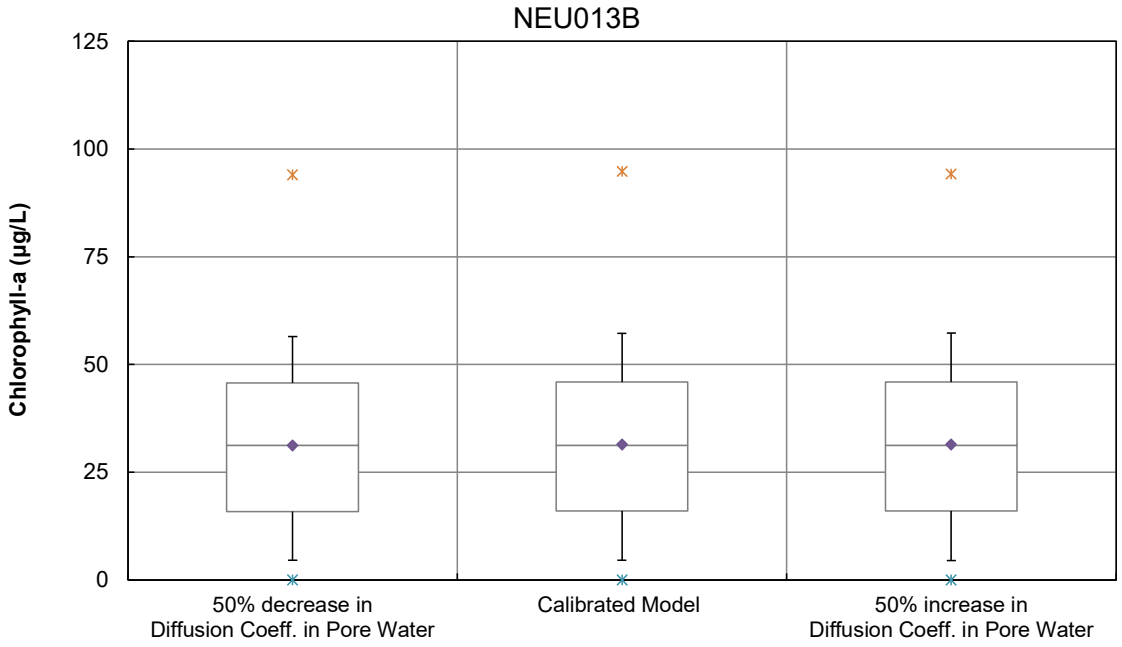

Figure 52 Box-Whisker Plot of Chl-a at NEU013B under Diffusion Coefficient in Pore Water Perturbation

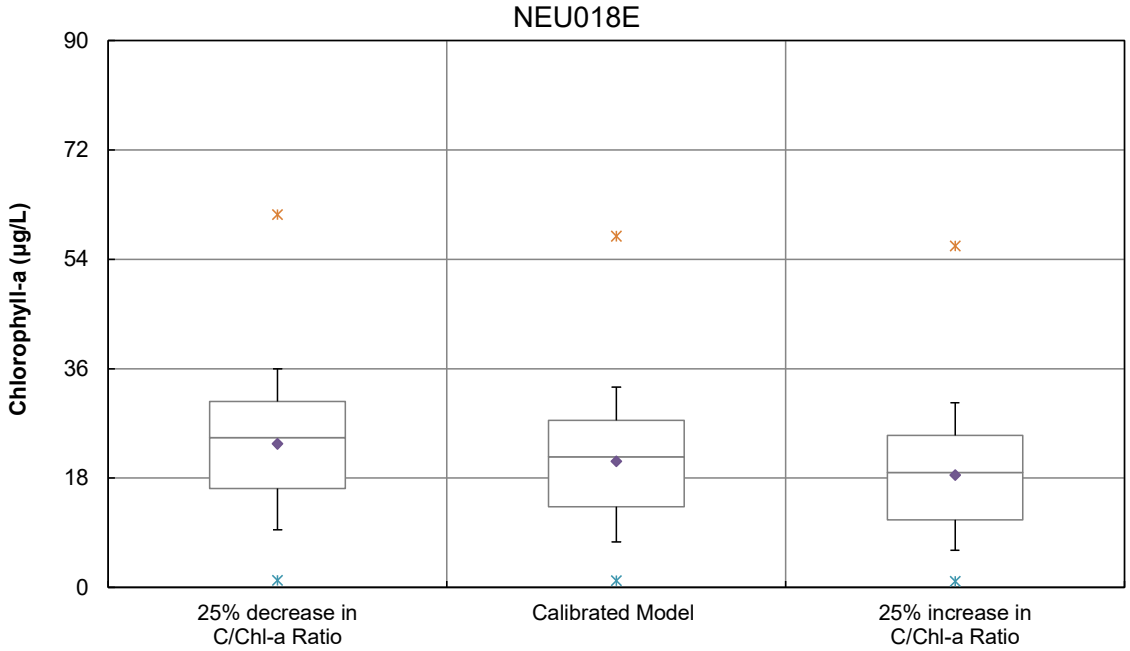

Figure 53 Box-Whisker Plot of Chl-a at NEU018E under C/Chl-a Ratio Perturbation

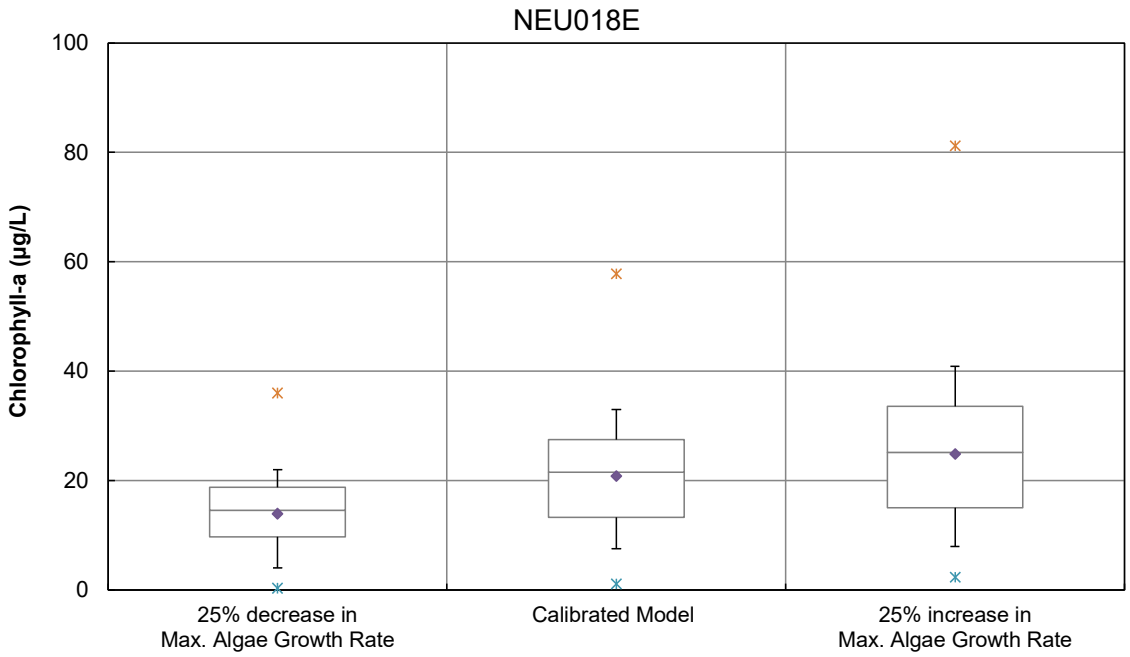

Figure 54 Box-Whisker Plot of Chl-a at NEU018E under Algal Growth Rate Perturbation

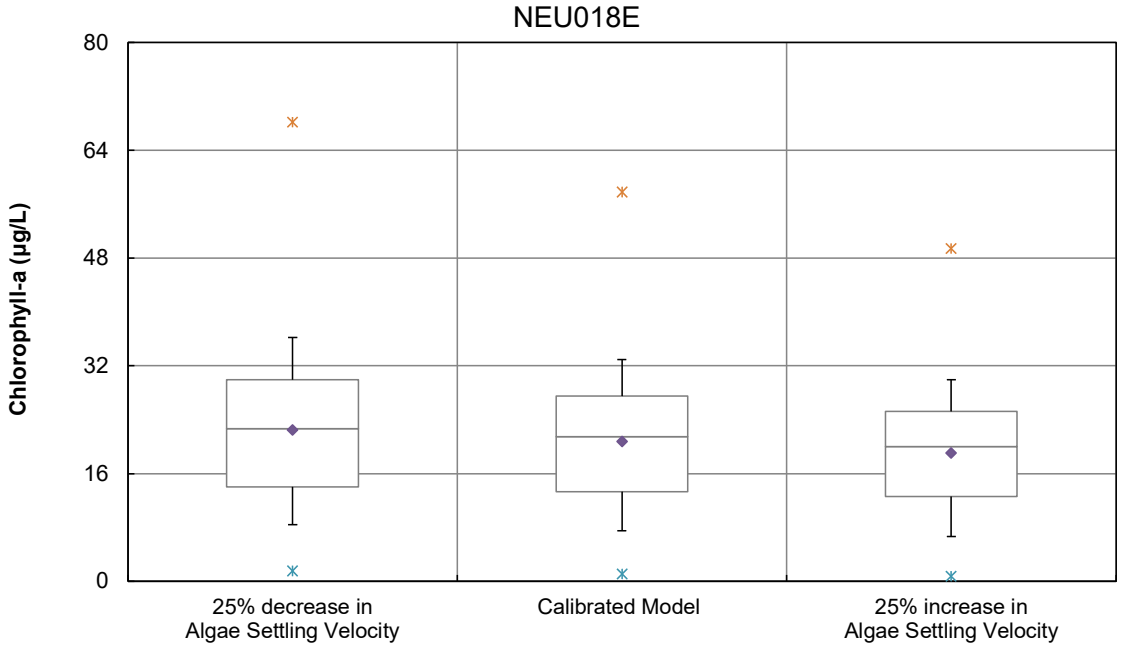

Figure 55 Box-Whisker Plot of Chl-a at NEU018E under Algal Settling Velocity Perturbation

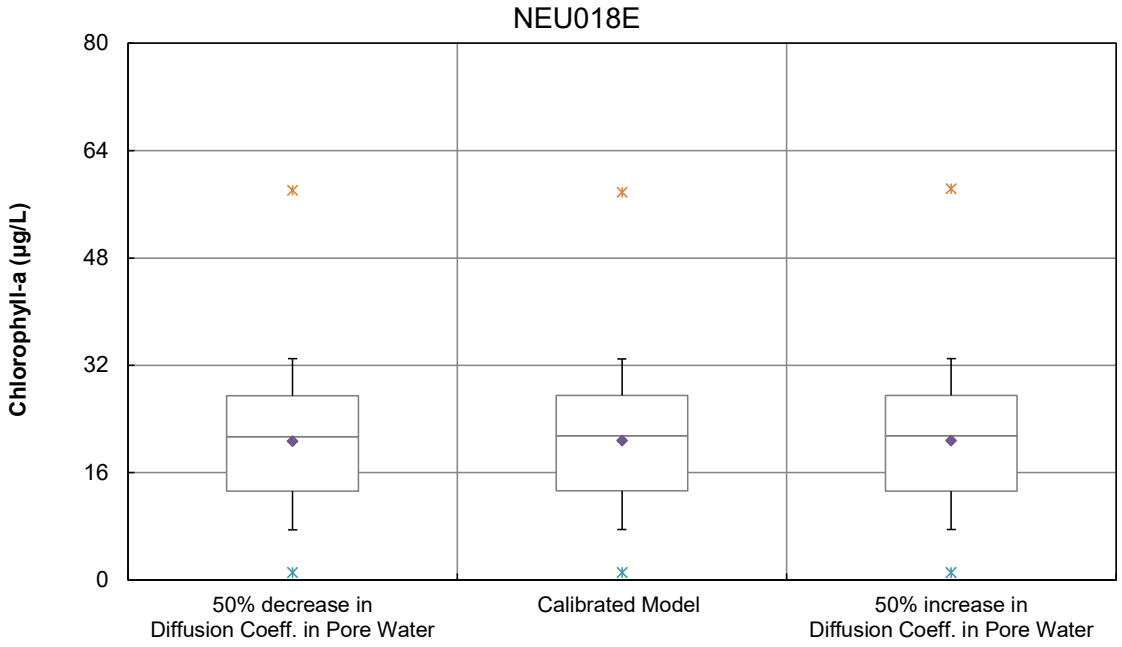

Figure 56 Box-Whisker Plot of Chl-a at NEU018E under Diffusion Coefficient in Pore Water Perturbation

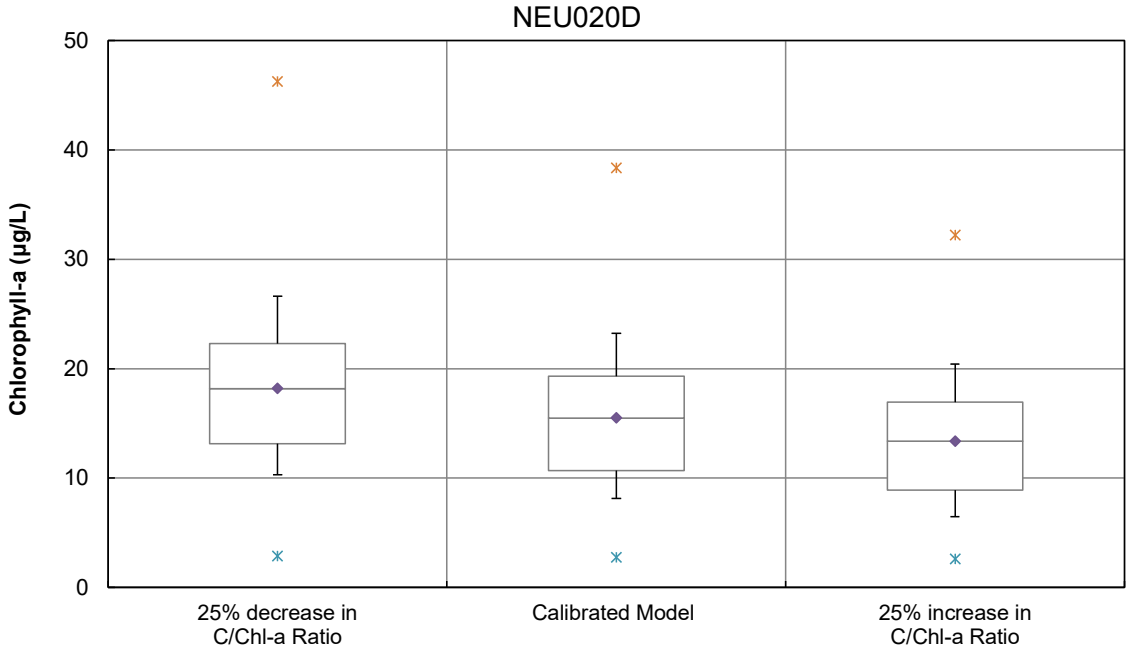

Figure 57 Box-Whisker Plot of Chl-a at NEU020D under C/Chl-a Ratio Perturbation

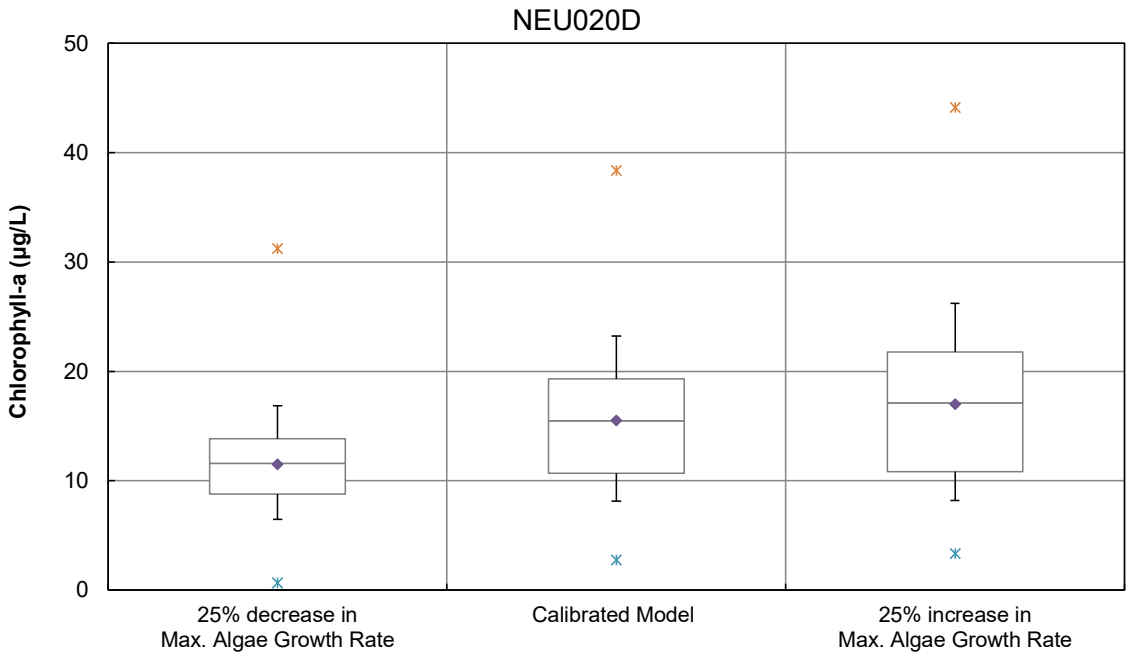

Figure 58 Box-Whisker Plot of Chl-a at NEU020D under Algal Growth Rate Perturbation

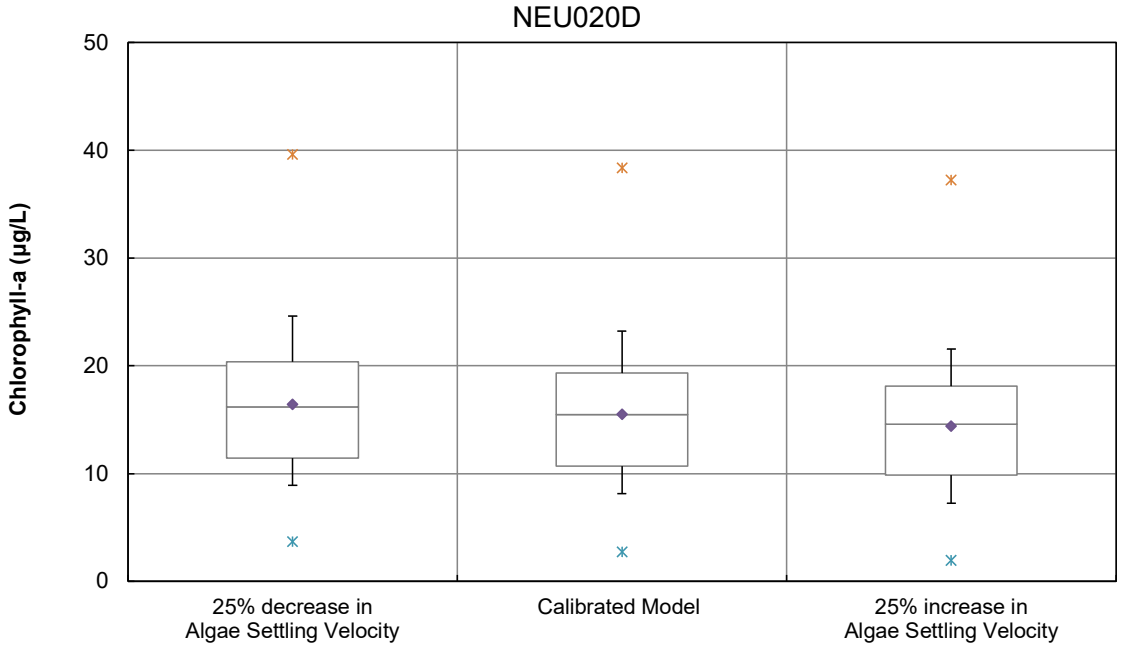

Figure 59 Box-Whisker Plot of Chl-a at NEU020D under Algal Settling Velocity Perturbation

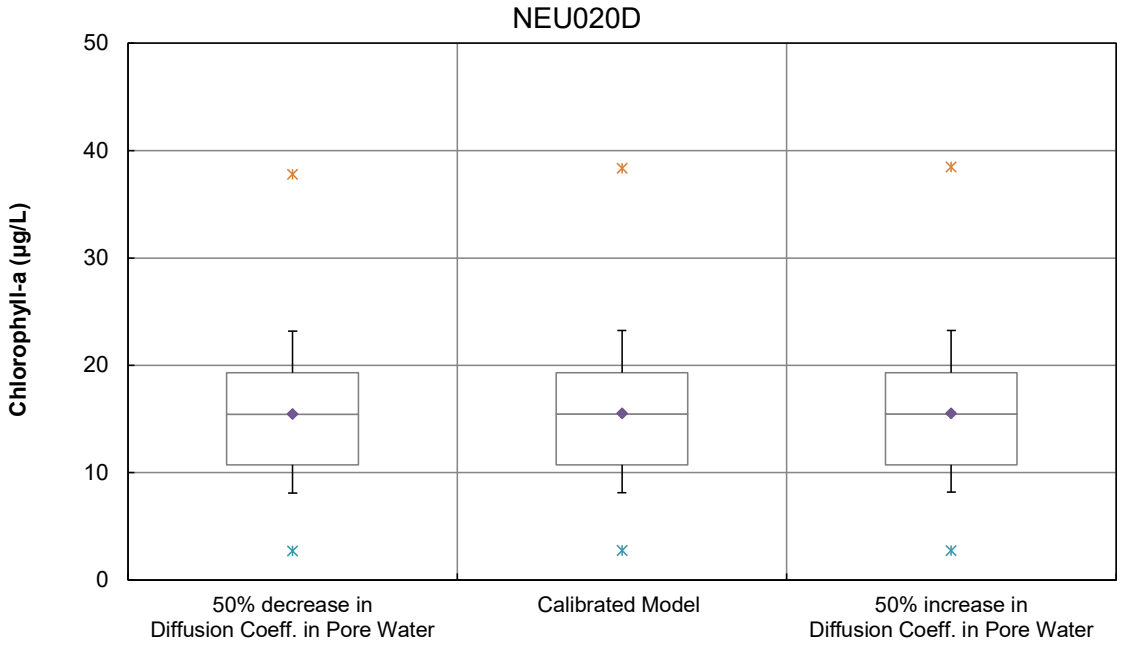

Figure 60 Box-Whisker Plot of Chl-a at NEU020D under Diffusion Coefficient in Pore Water Perturbation

2.2 TOC

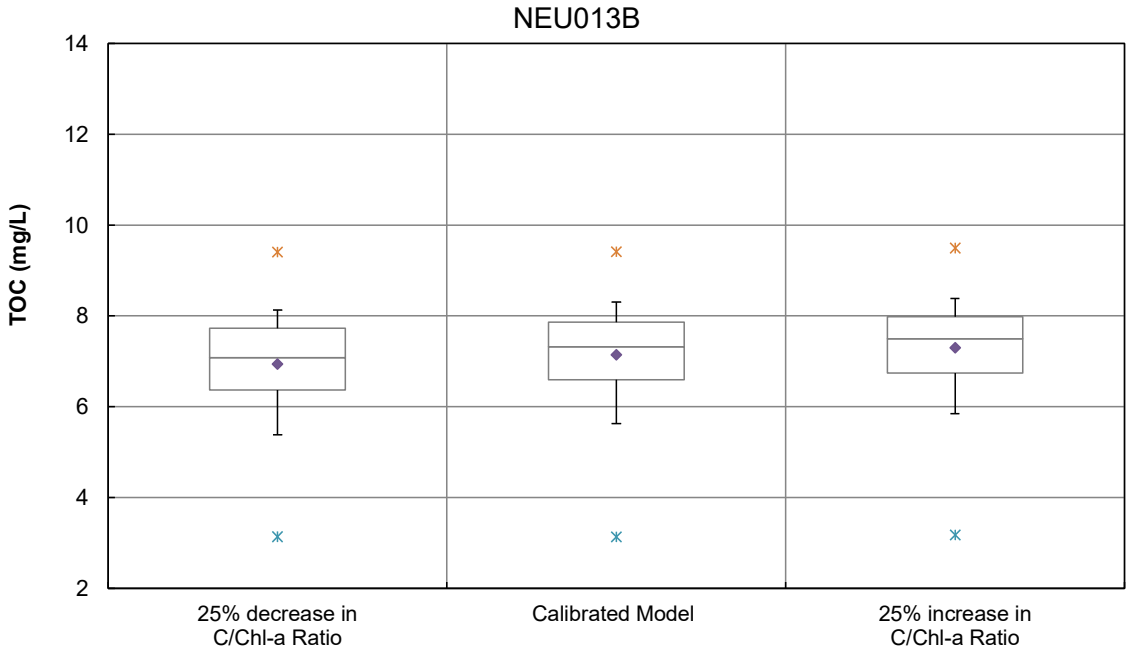

Figure 61 Box-Whisker Plot of TOC at NEU013B under C/Chl-a Ratio Perturbation

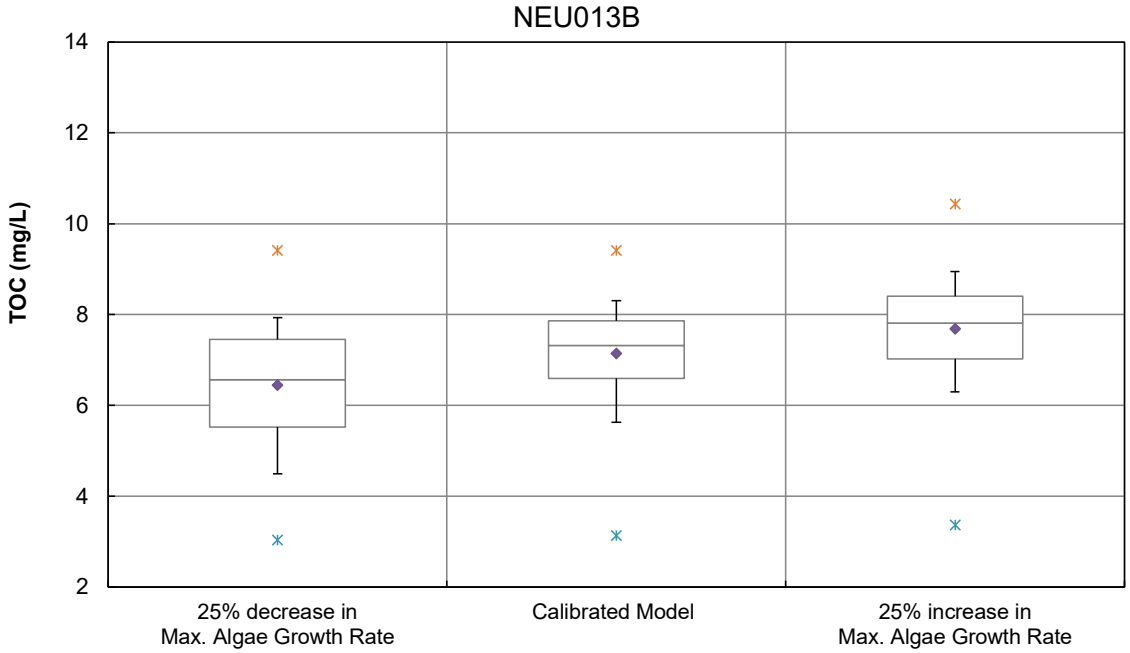

Figure 62 Box-Whisker Plot of TOC at NEU013B under Algal Growth Rate Perturbation

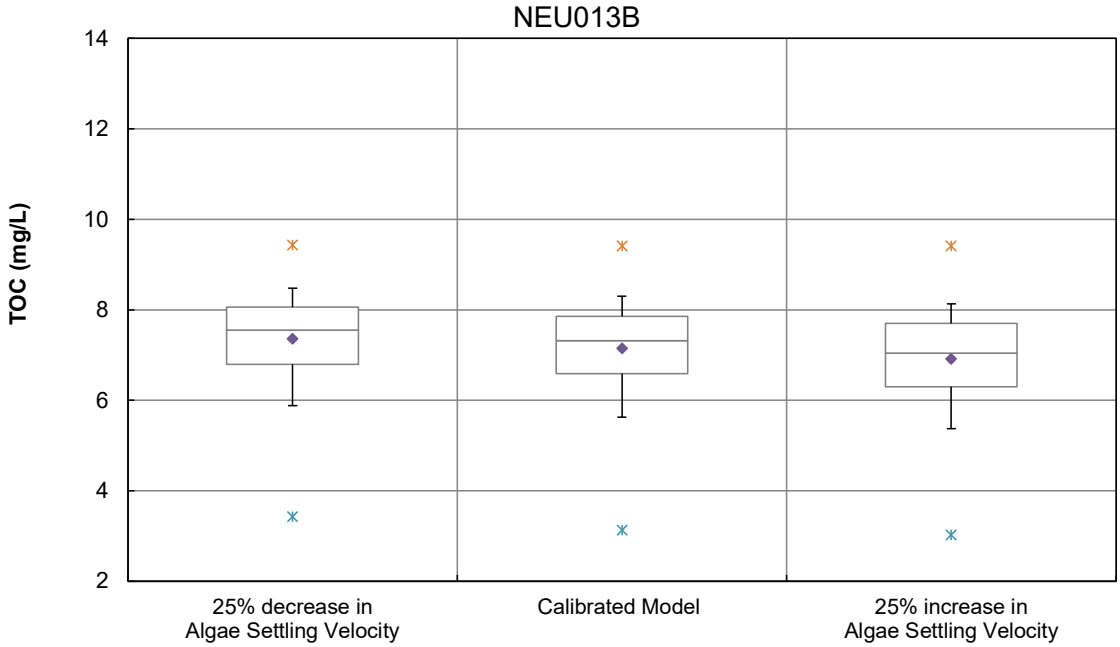

Figure 63 Box-Whisker Plot of TOC at NEU013B under Algal Settling Velocity Perturbation

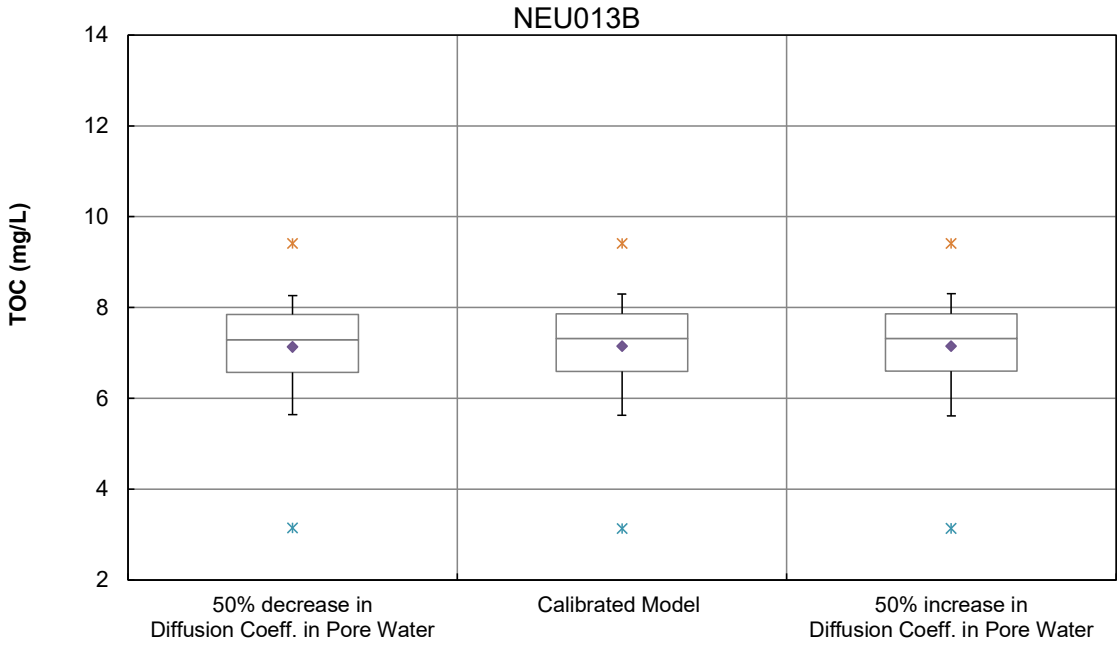

Figure 64 Box-Whisker Plot of TOC at NEU013B under Diffusion Coefficient in Pore Water Perturbation

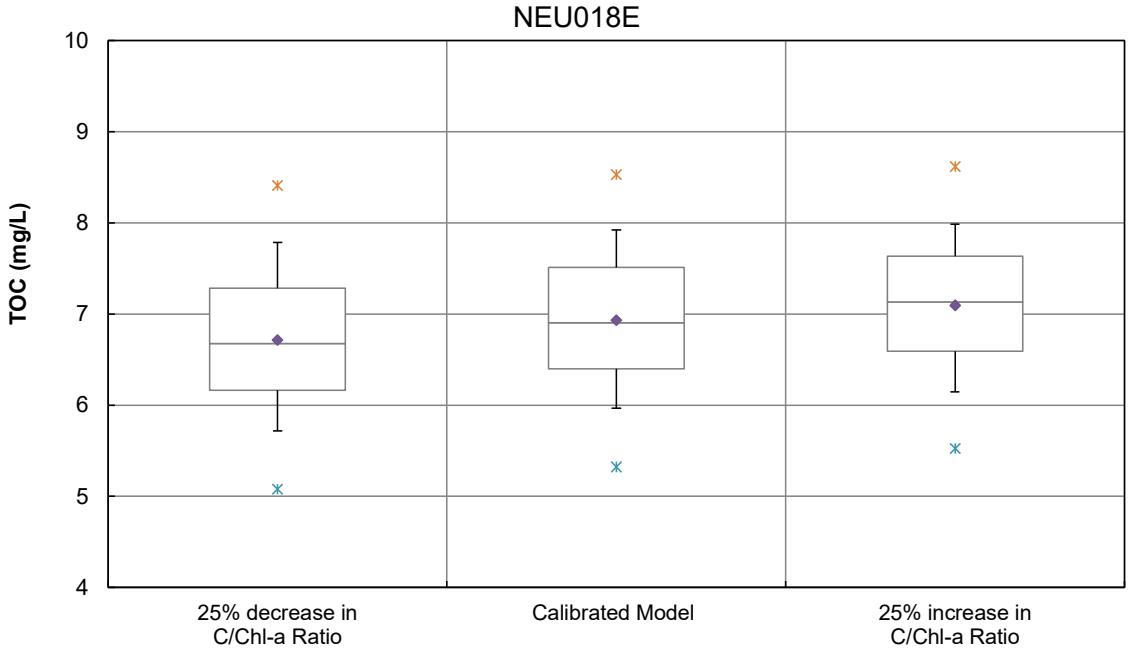

Figure 65 Box-Whisker Plot of TOC at NEU018E under C/Chl-a Ratio Perturbation

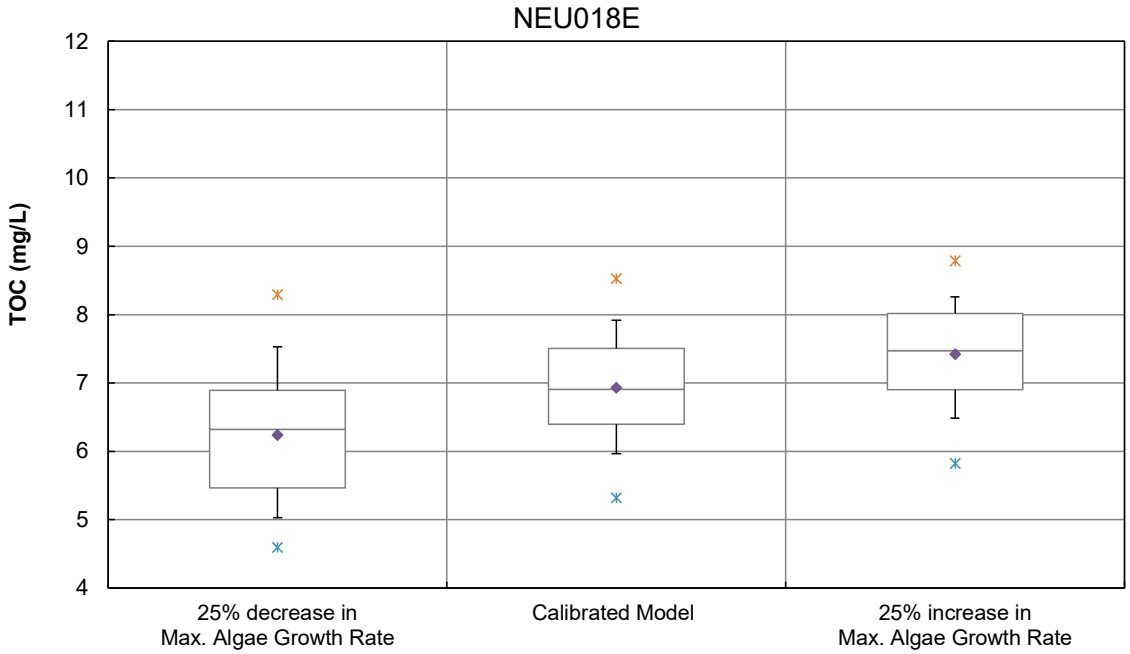

Figure 66 Box-Whisker Plot of TOC at NEU018E under Algal Growth Rate Perturbation

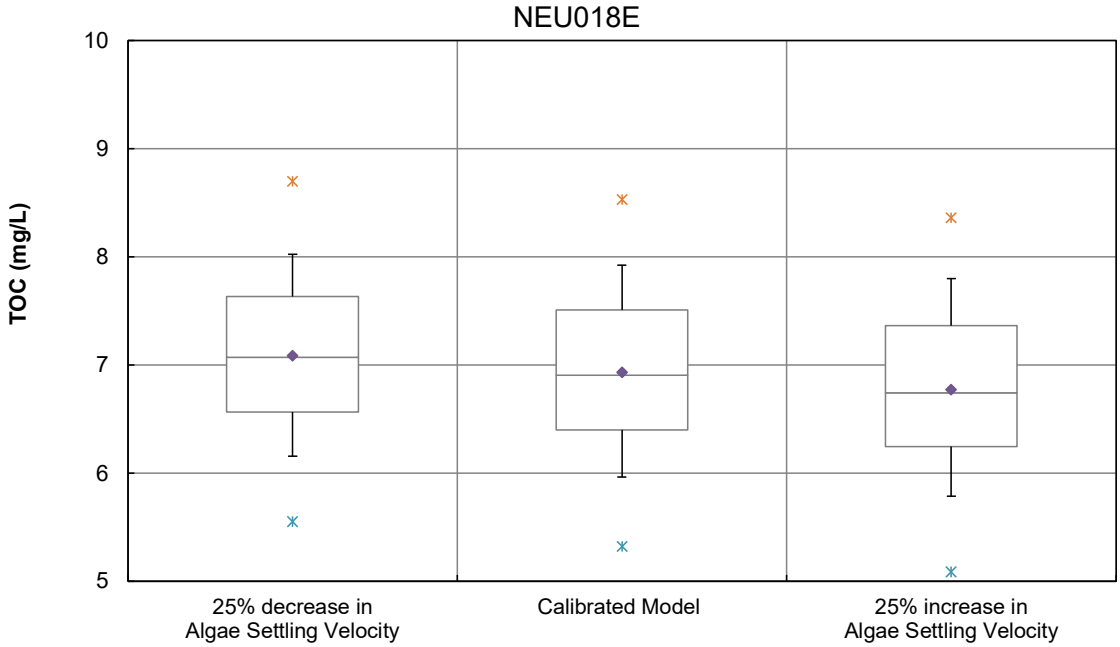

Figure 67 Box-Whisker Plot of TOC at NEU018E under Algal Settling Velocity Perturbation

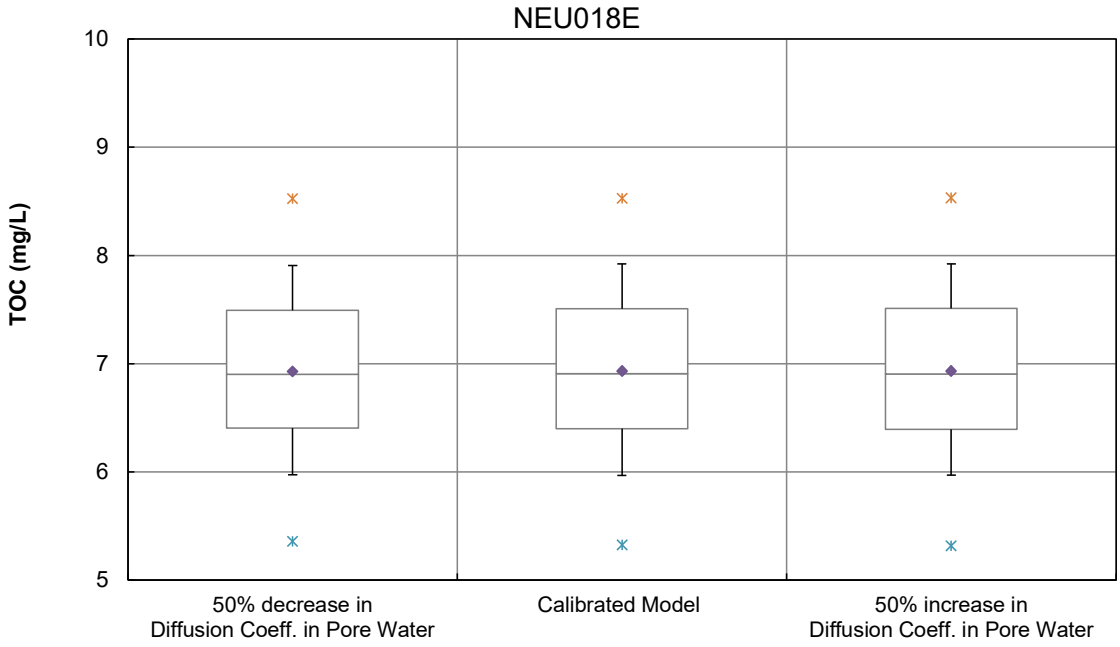

Figure 68 Box-Whisker Plot of TOC at NEU018E under Diffusion Coefficient in Pore Water Perturbation

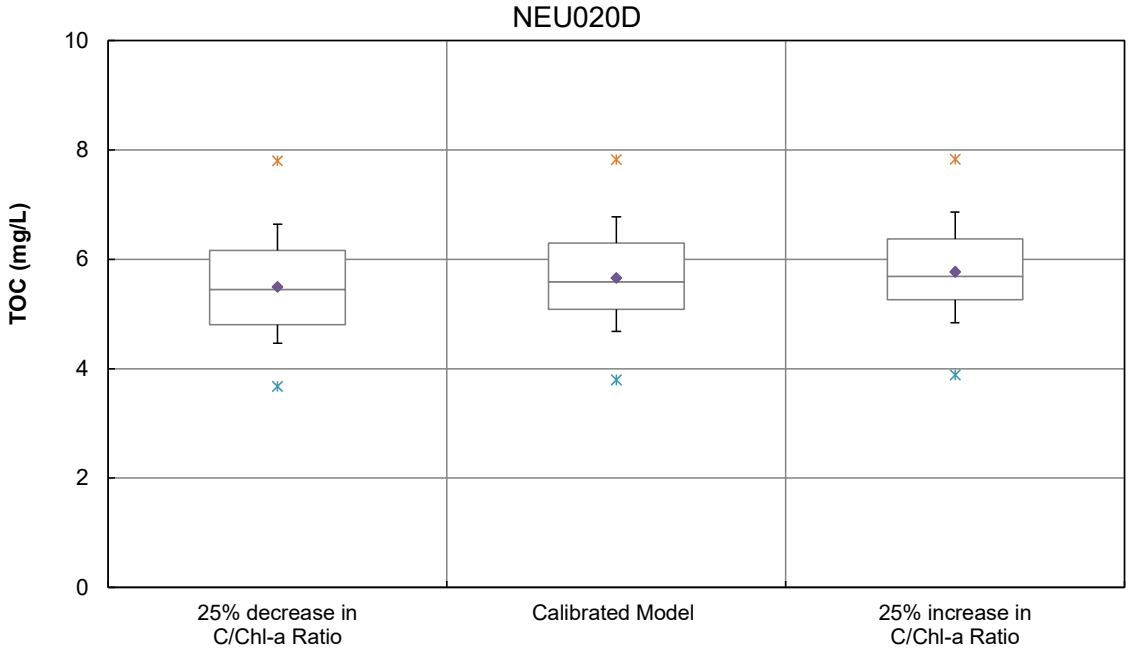

Figure 69 Box-Whisker Plot of TOC at NEU020D under C/Chl-a Ratio Perturbation

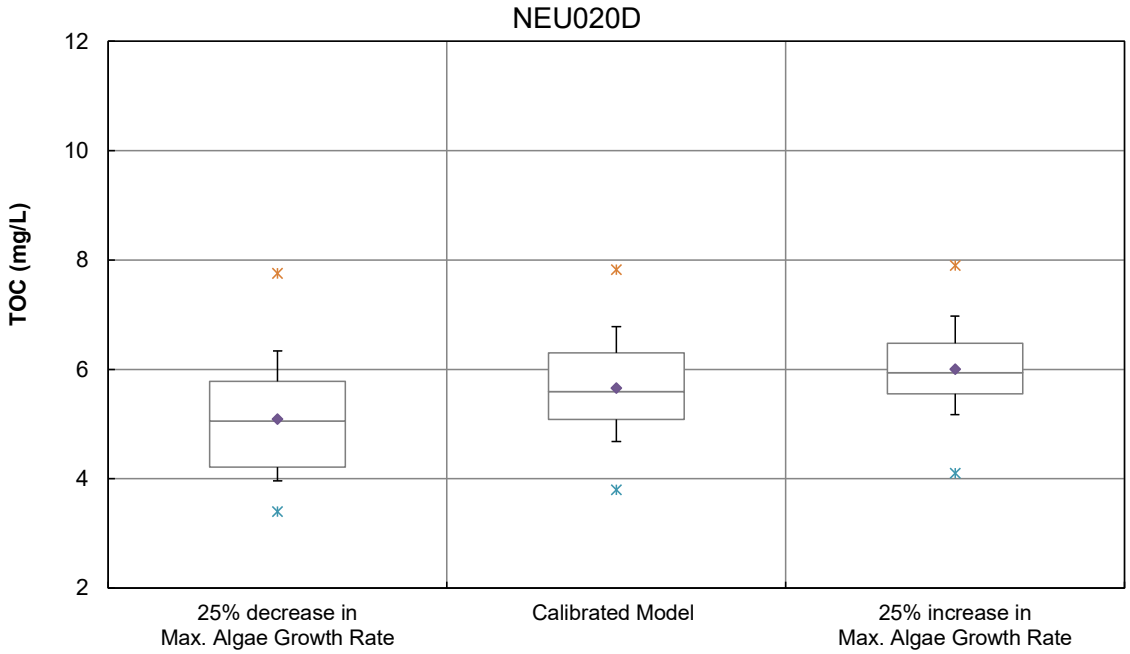

Figure 70 Box-Whisker Plot of TOC at NEU020D under Algal Growth Rate Perturbation

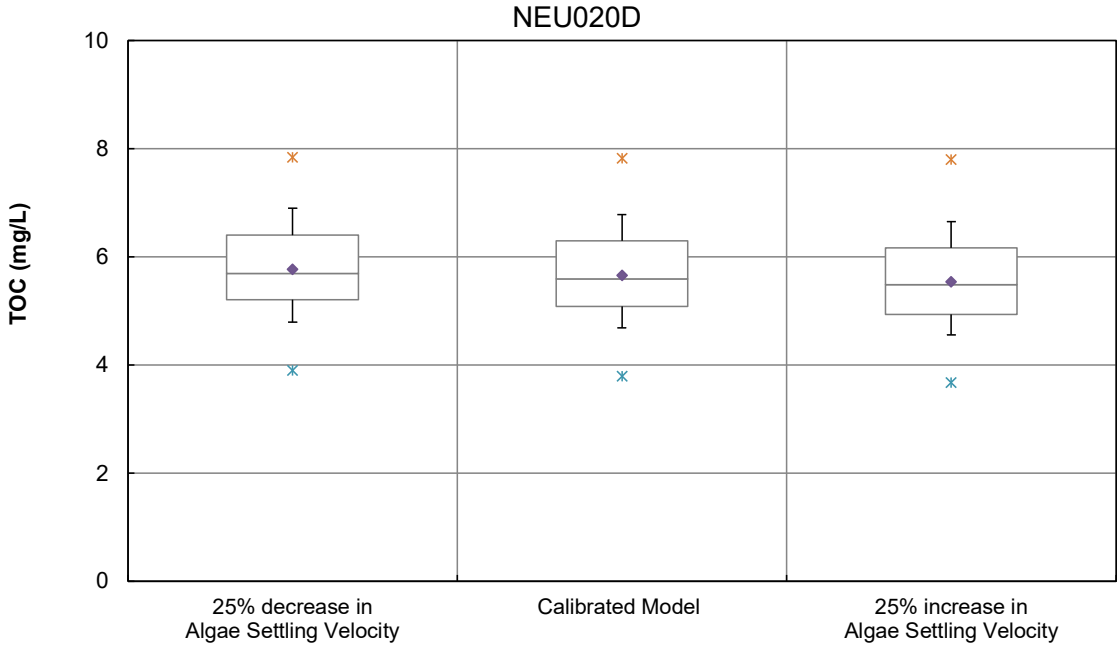

Figure 71 Box-Whisker Plot of TOC at NEU020D under Algal Settling Velocity Perturbation

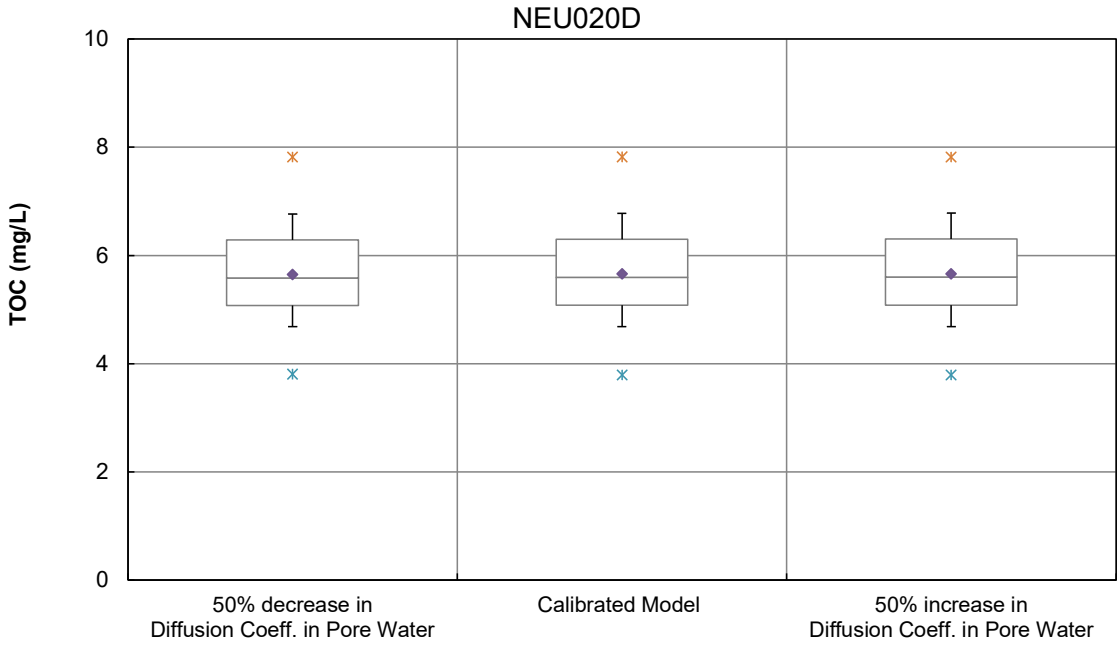

Figure 72 Box-Whisker Plot of TOC at NEU020D under Diffusion Coefficient in Pore Water Perturbation

2.3 TN

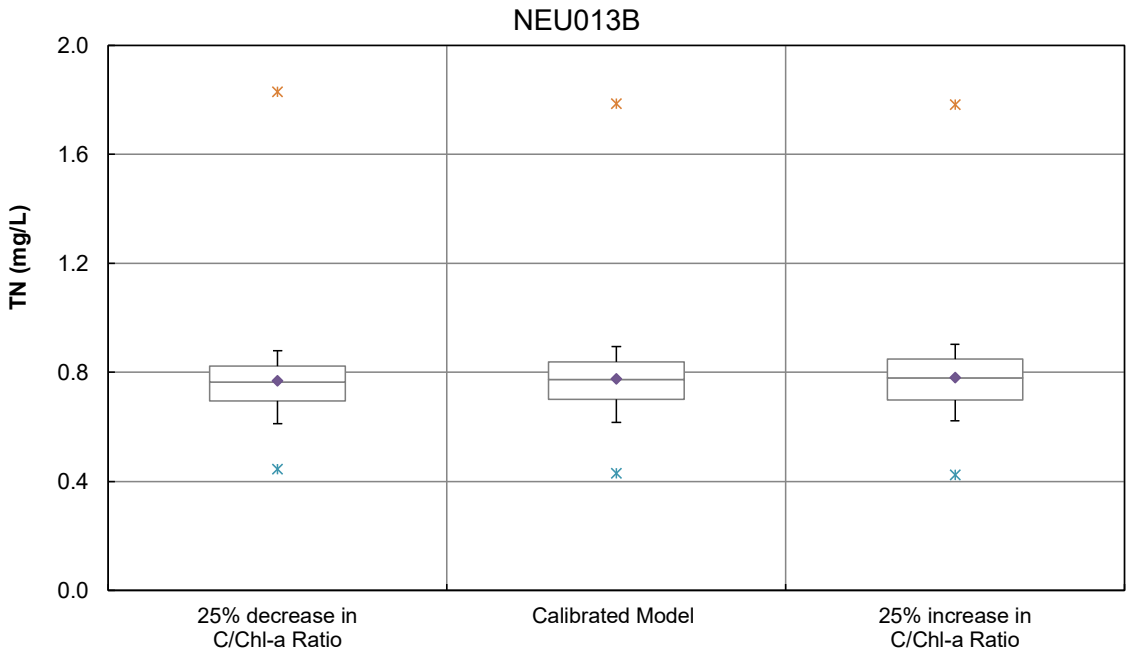

Figure 73 Box-Whisker Plot of TN at NEU013B under C/Chl-a Ratio Perturbation

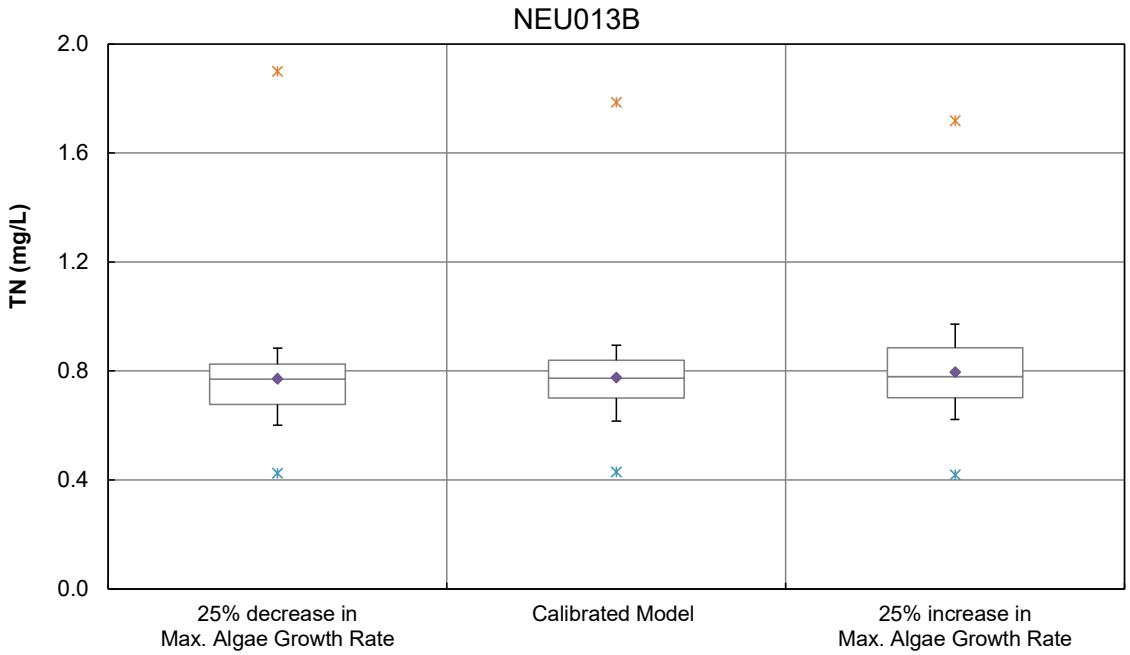

Figure 74 Box-Whisker Plot of TN at NEU013B under Algal Growth Rate Perturbation

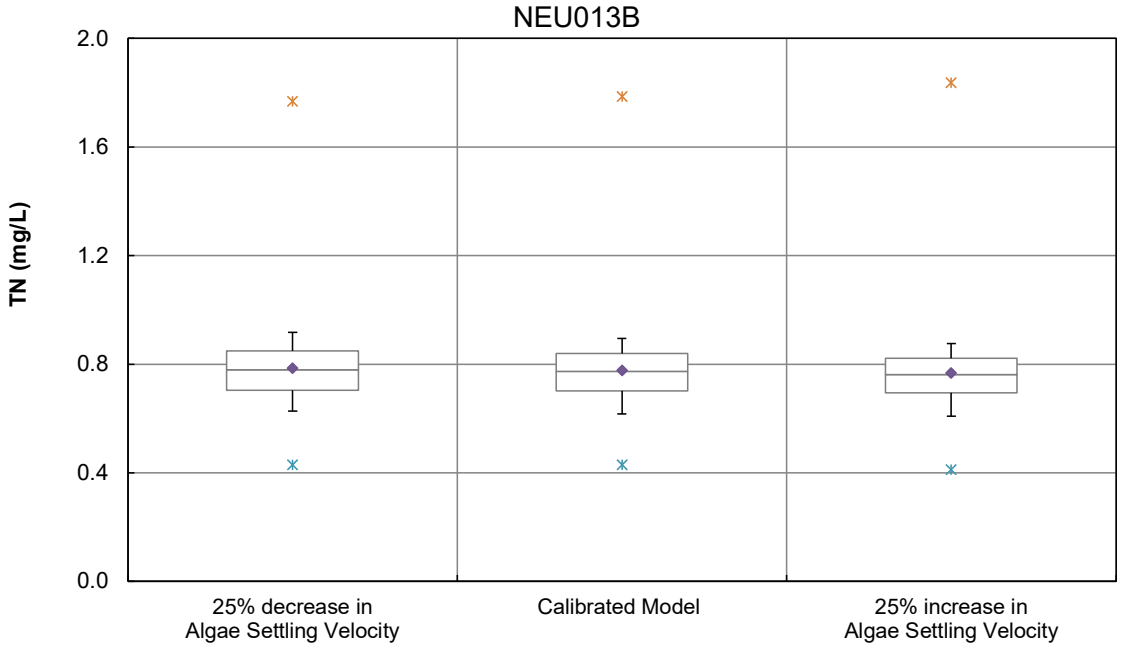

Figure 75 Box-Whisker Plot of TN at NEU013B under Algal Settling Velocity Perturbation

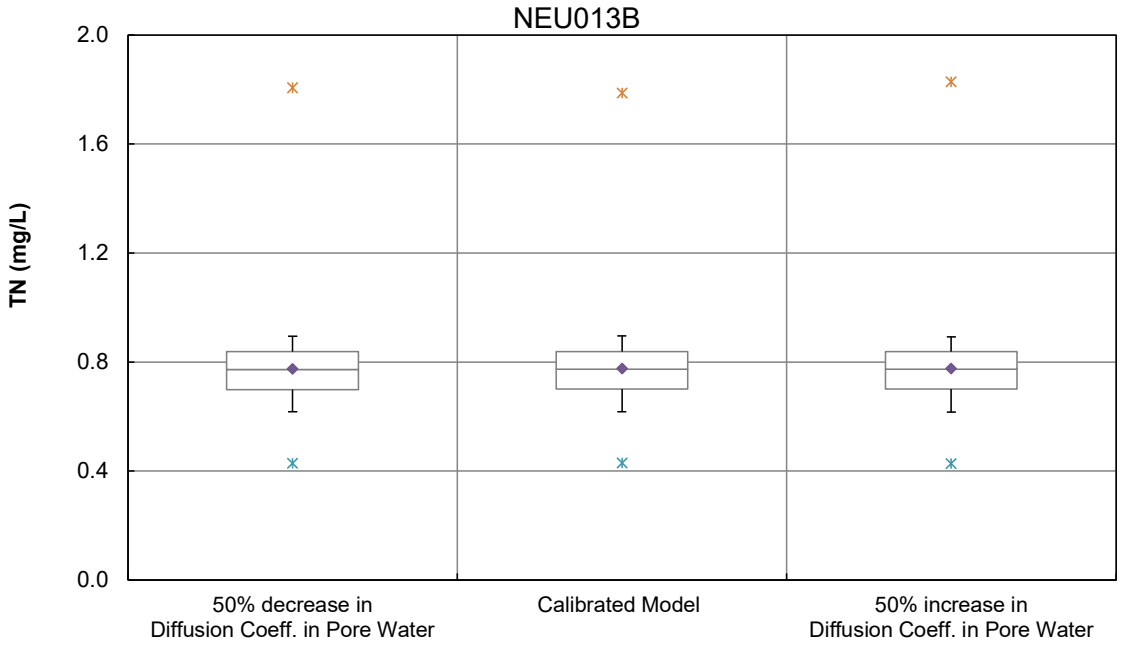

Figure 76 Box-Whisker Plot of TN at NEU013B under Diffusion Coefficient in Pore Water Perturbation

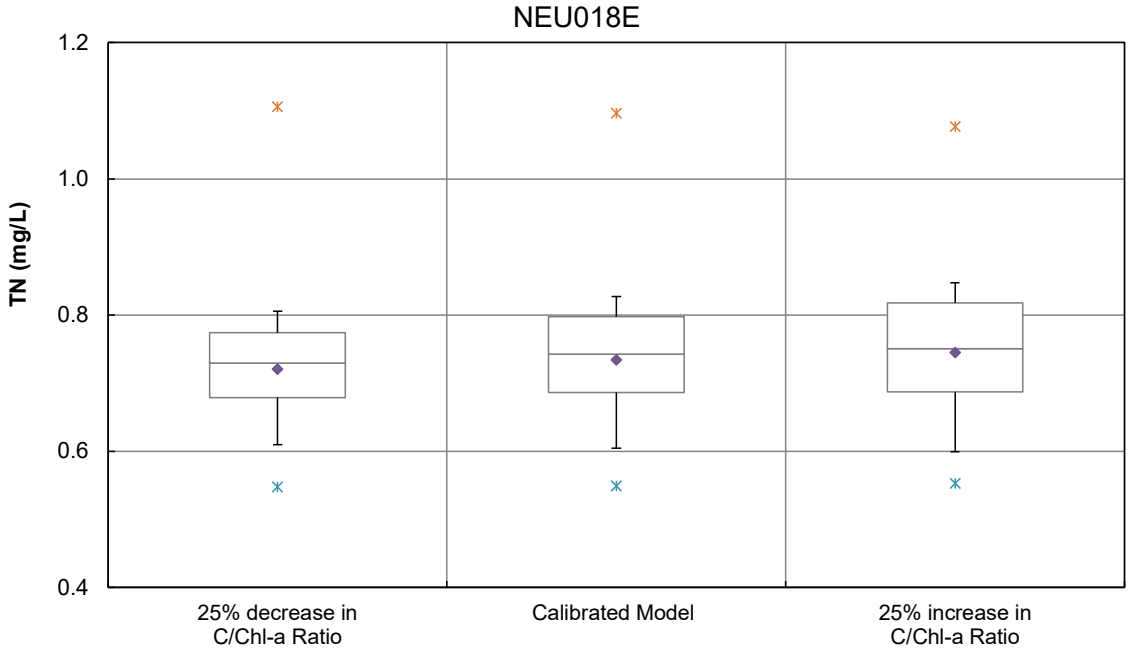

Figure 77 Box-Whisker Plot of TN at NEU018E under C/Chl-a Ratio Perturbation

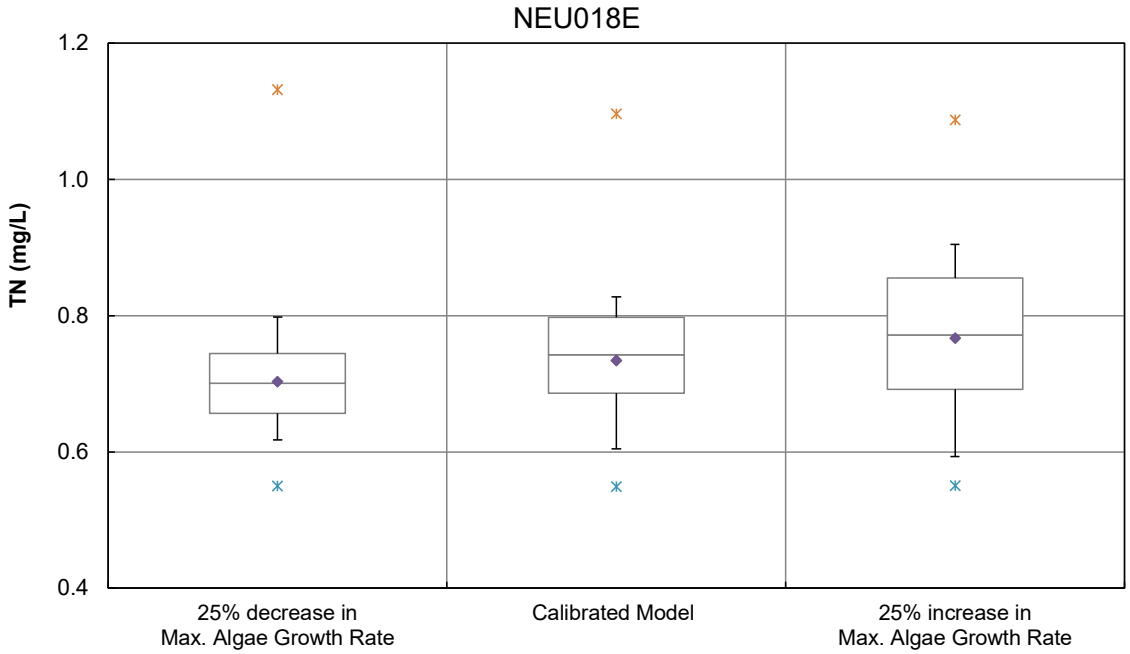

Figure 78 Box-Whisker Plot of TN at NEU018E under Algal Growth Rate Perturbation

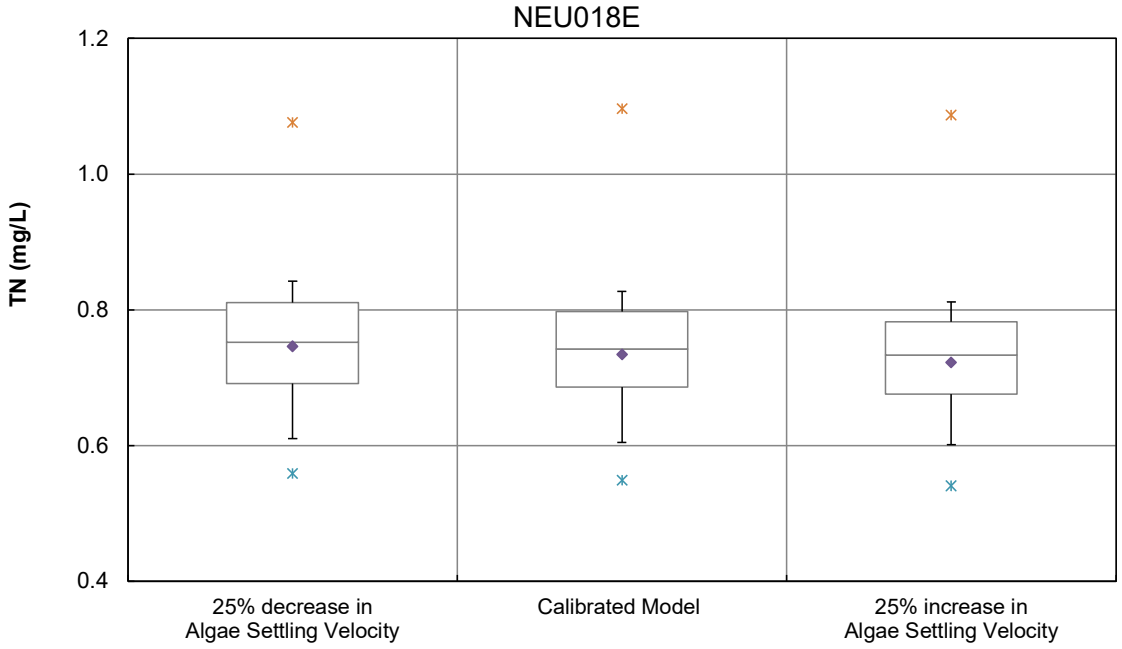

Figure 79 Box-Whisker Plot of TN at NEU018E under Algal Settling Velocity Perturbation

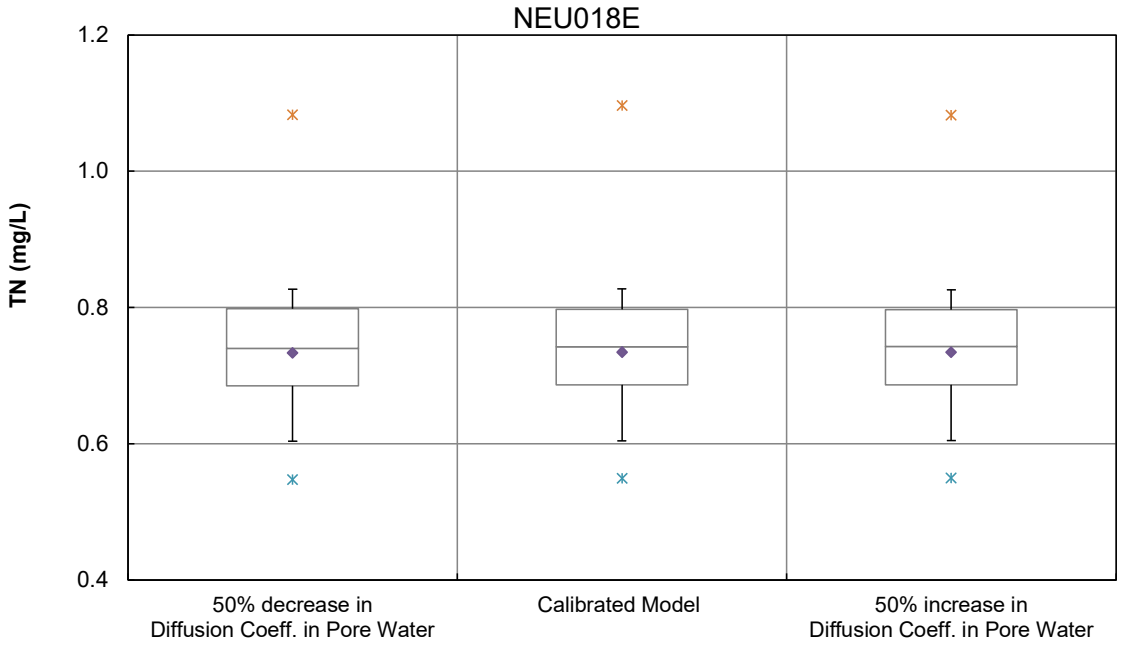

Figure 80 Box-Whisker Plot of TN at NEU018E under Diffusion Coefficient in Pore Water Perturbation

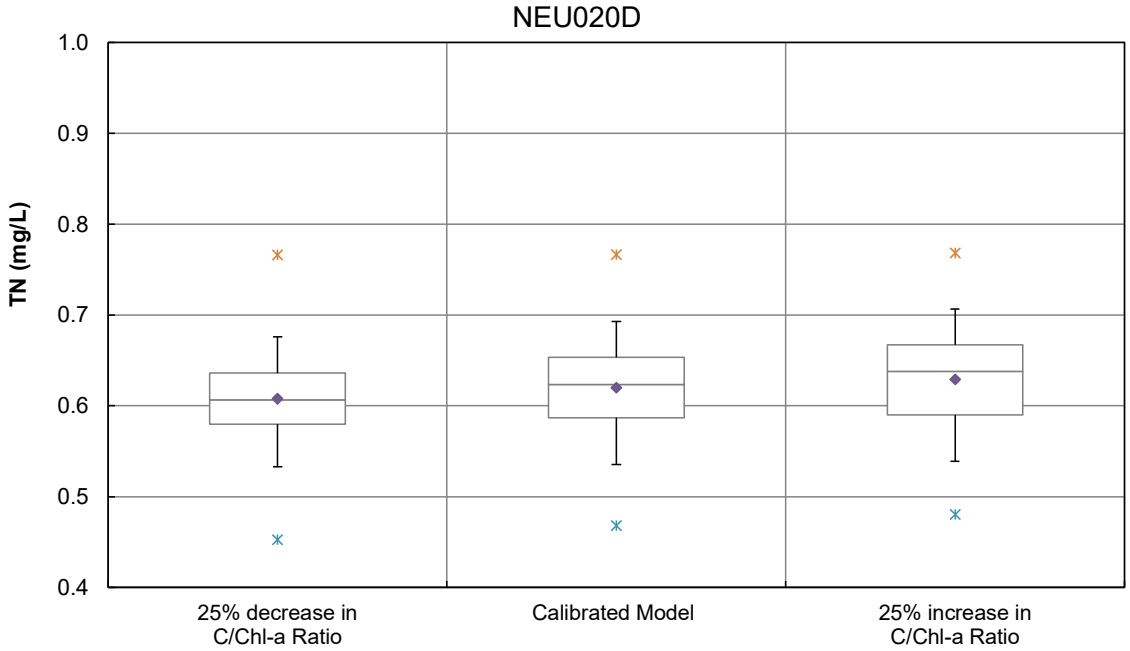

Figure 81 Box-Whisker Plot of TN at NEU020D under C/Chl-a Ratio Perturbation

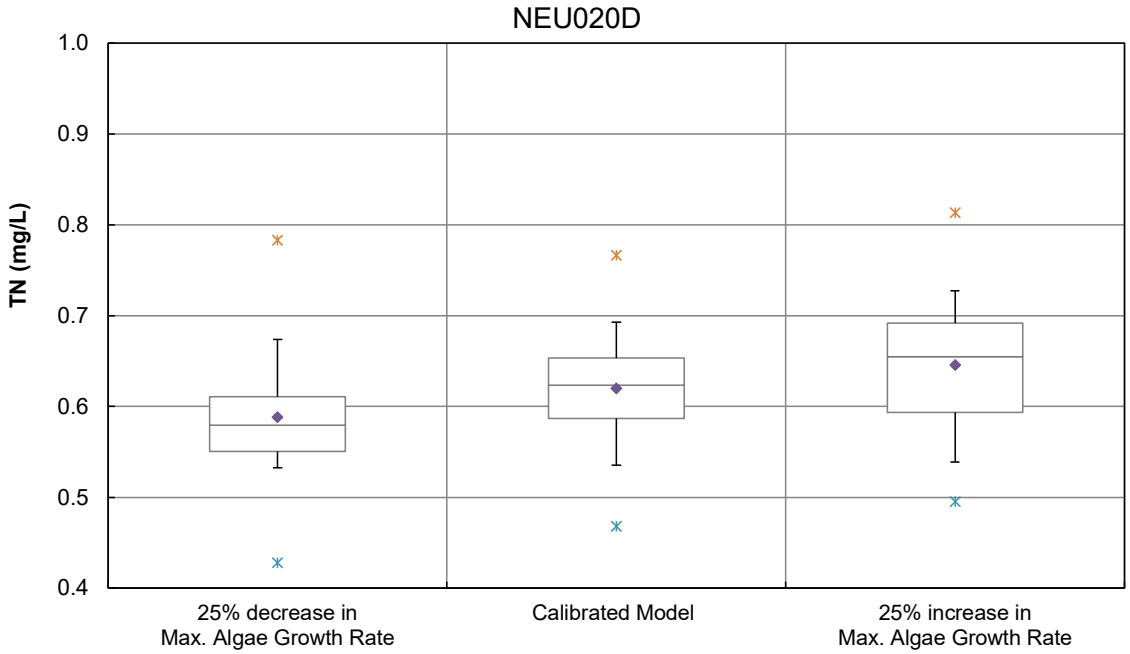

Figure 82 Box-Whisker Plot of TN at NEU020D under Algal Growth Rate Perturbation

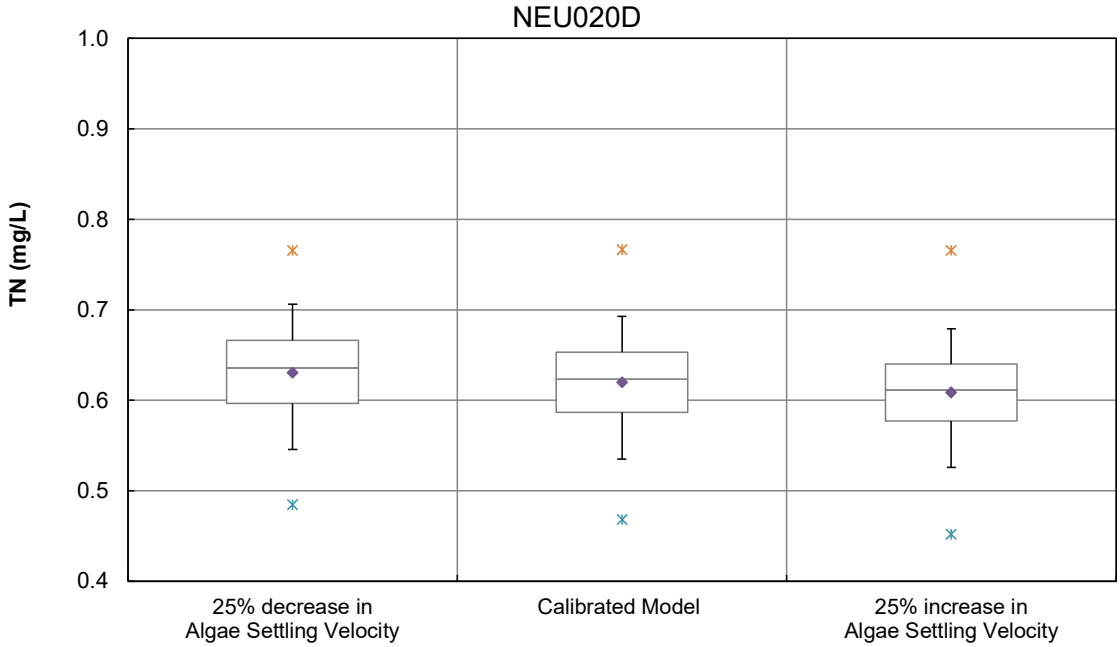

Figure 83 Box-Whisker Plot of TN at NEU020D under Algal Settling Velocity Perturbation

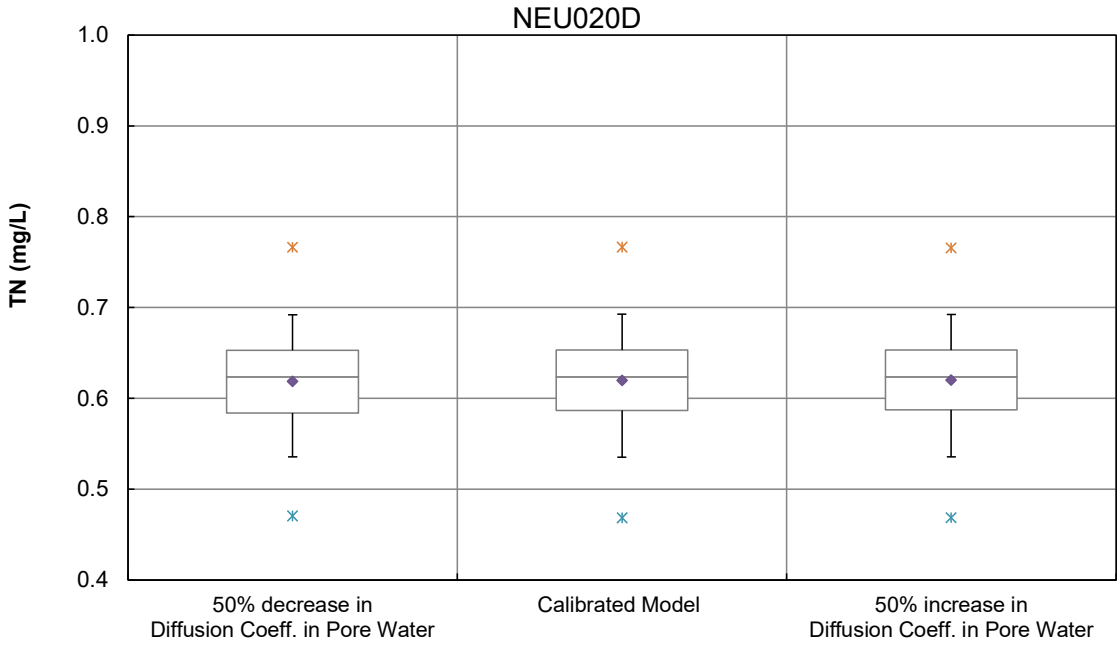

Figure 84 Box-Whisker Plot of TN at NEU020D under Diffusion Coefficient in Pore Water Perturbation

2.4 TP

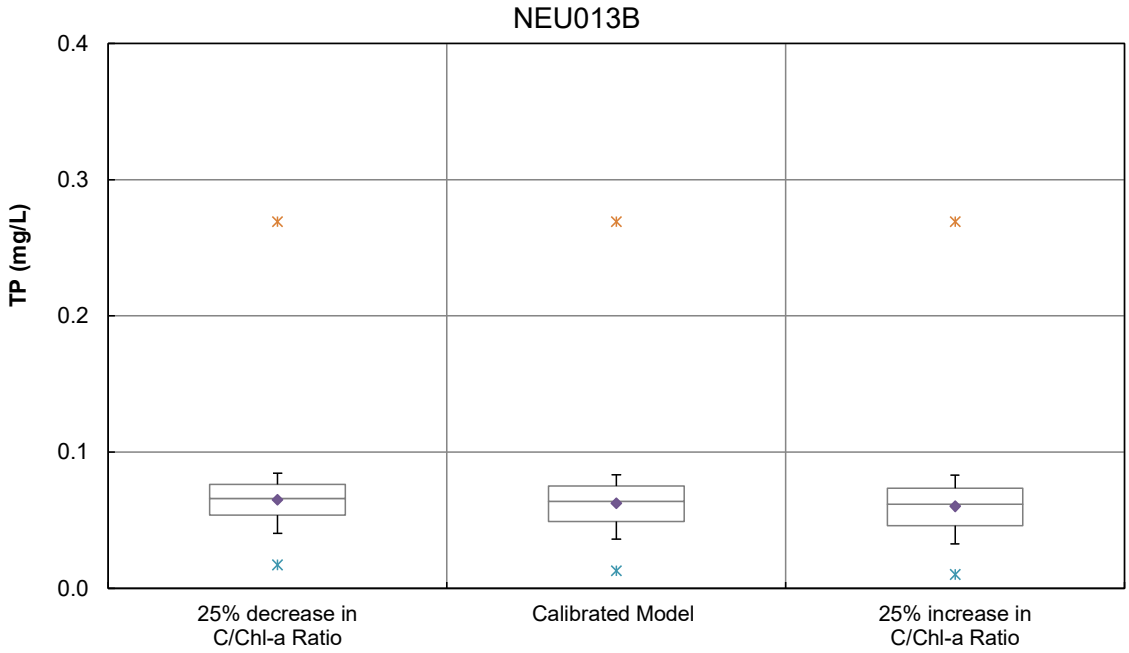

Figure 85 Box-Whisker Plot of TP at NEU013B under C/Chl-a Ratio Perturbation

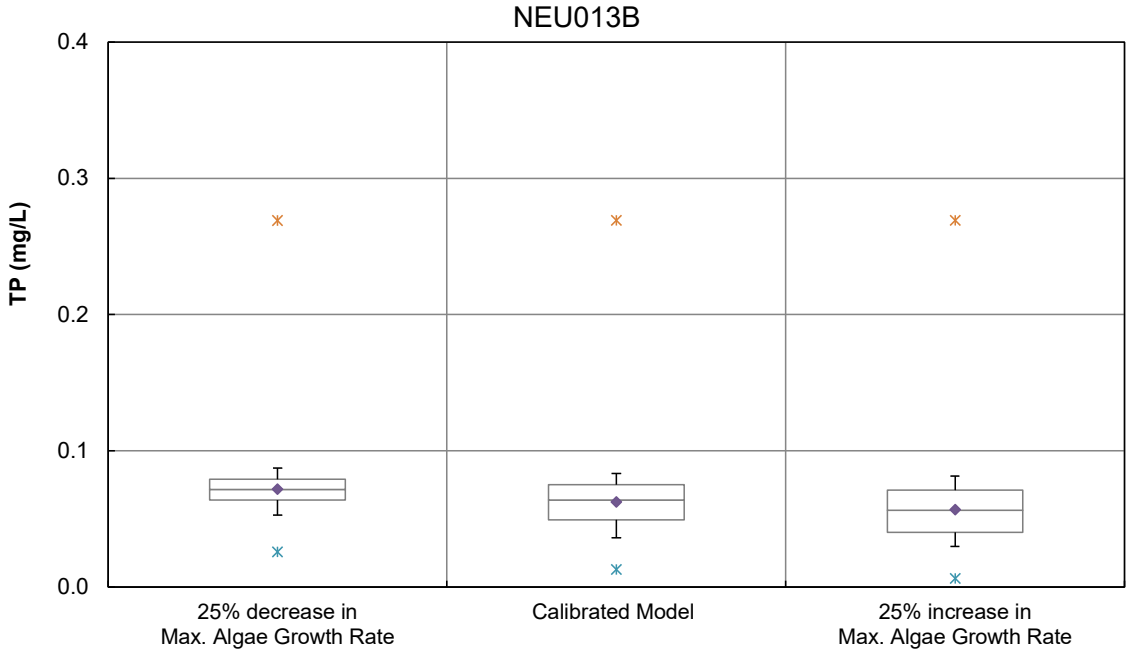

Figure 86 Box-Whisker Plot of TP at NEU013B under Algal Growth Rate Perturbation

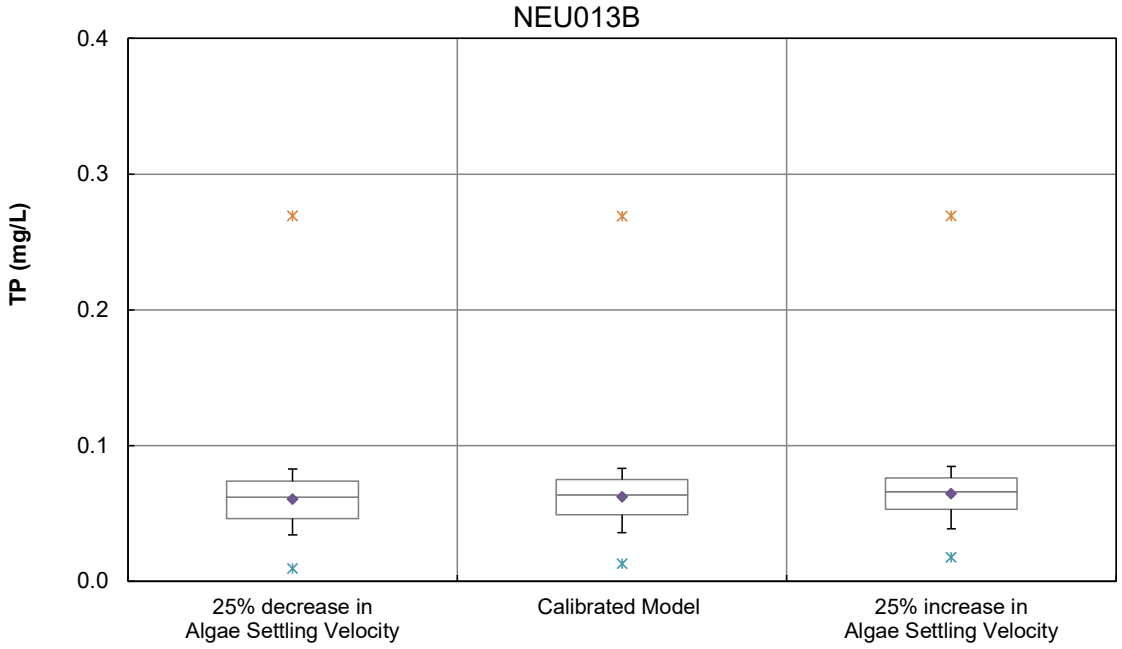

Figure 87 Box-Whisker Plot of TP at NEU013B under Algal Settling Velocity Perturbation

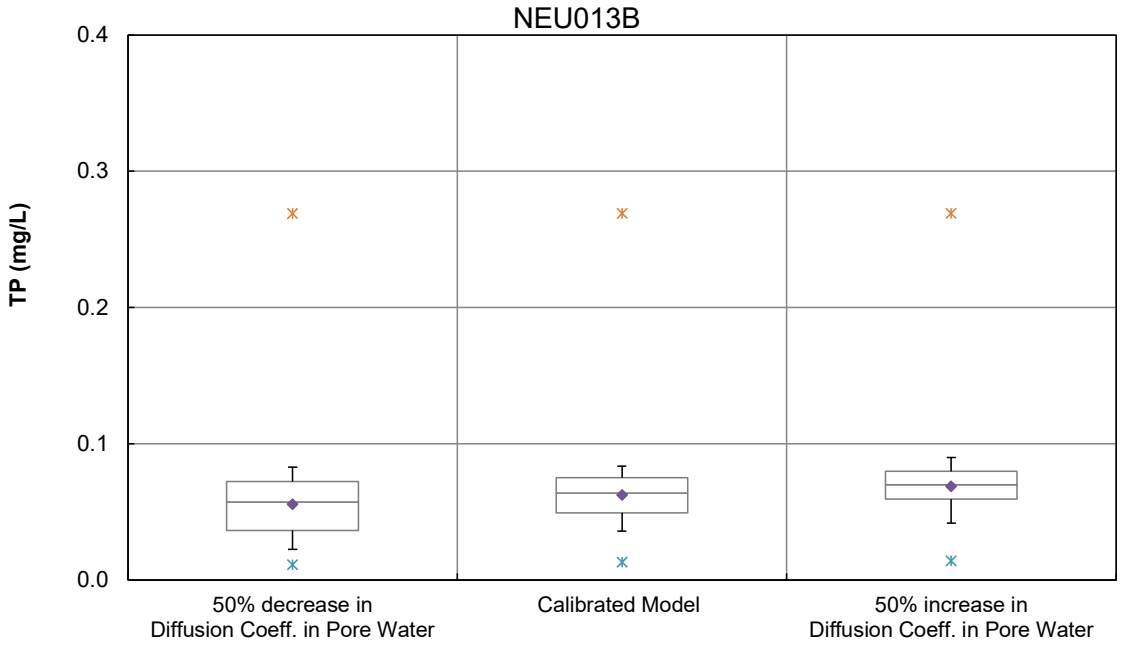

Figure 88 Box-Whisker Plot of TP at NEU013B under Diffusion Coefficient in Pore Water Perturbation

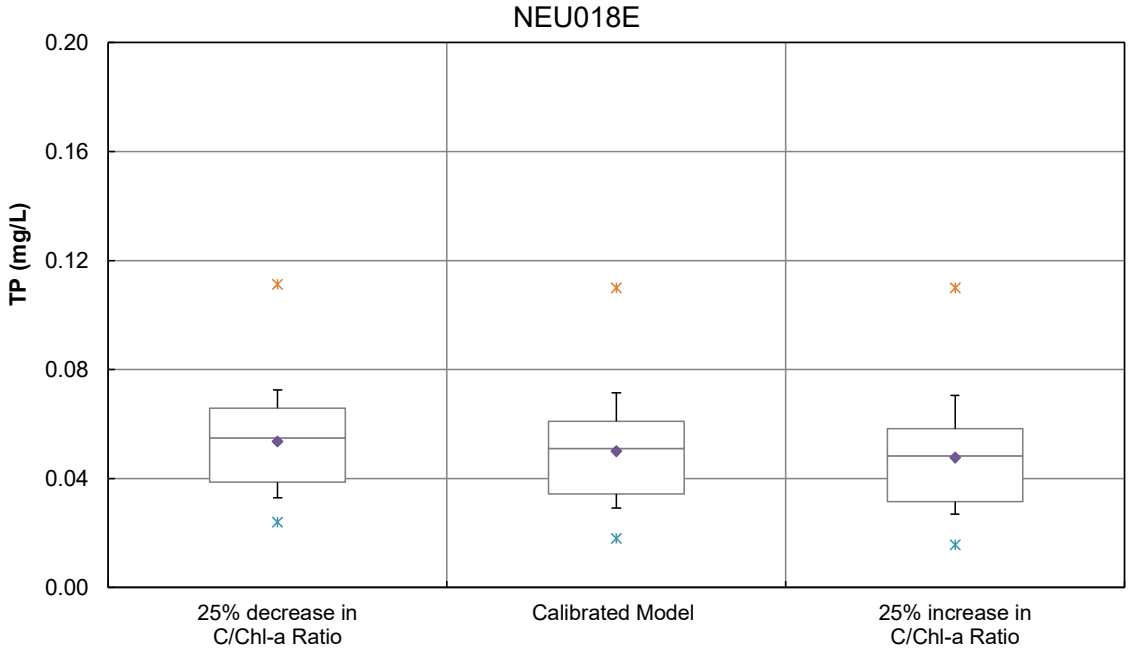

Figure 89 Box-Whisker Plot of TP at NEU018E under C/Chl-a Ratio Perturbation

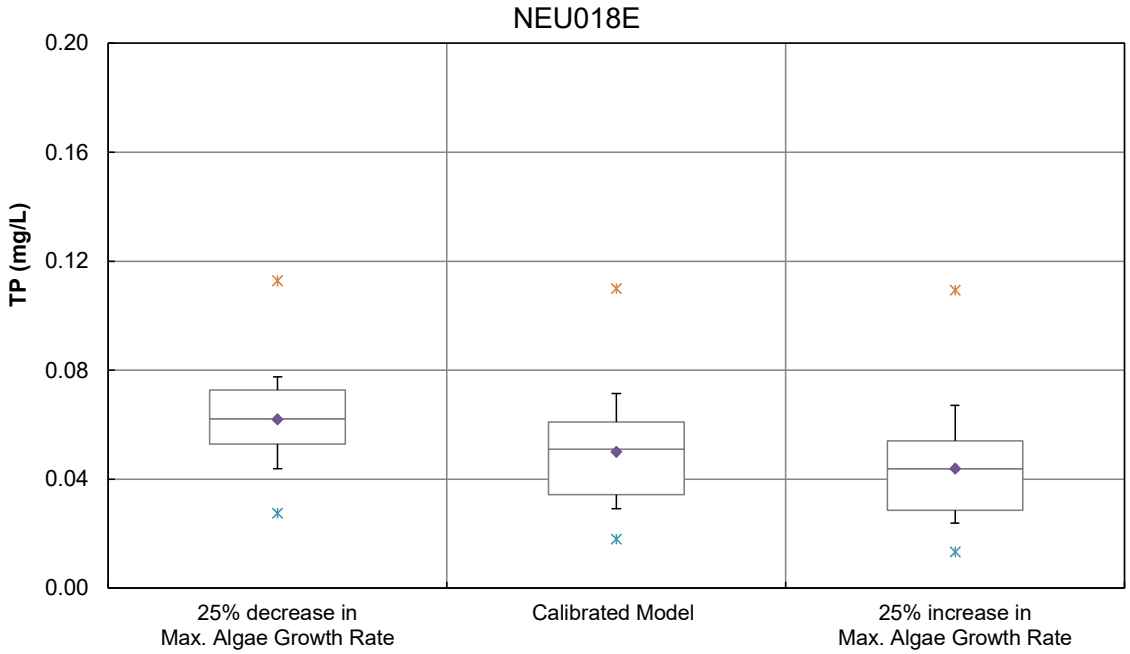

Figure 90 Box-Whisker Plot of TP at NEU018E under Algal Growth Rate Perturbation

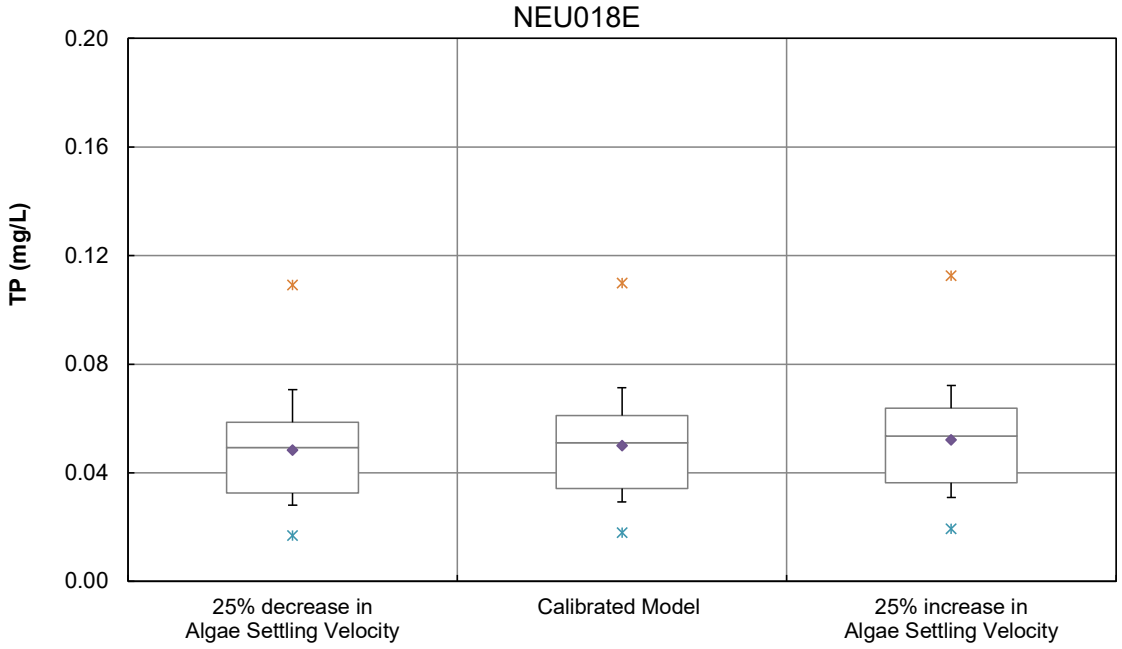

Figure 91 Box-Whisker Plot of TP at NEU018E under Algal Settling Velocity Perturbation

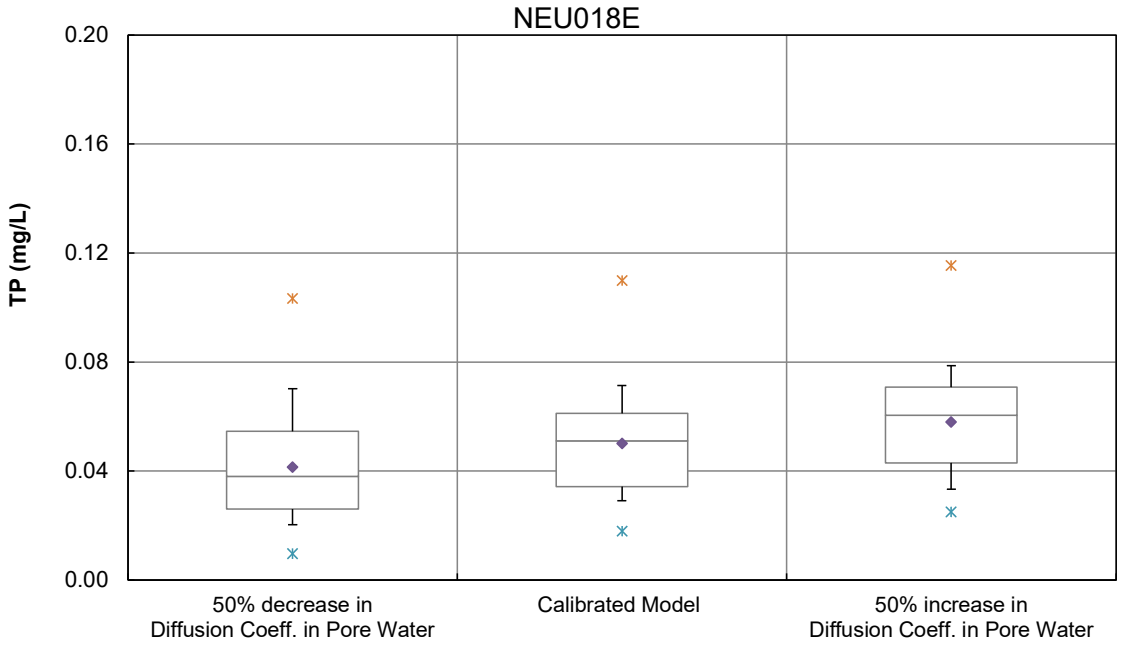

Figure 92 Box-Whisker Plot of TP at NEU018E under Diffusion Coefficient in Pore Water Perturbation

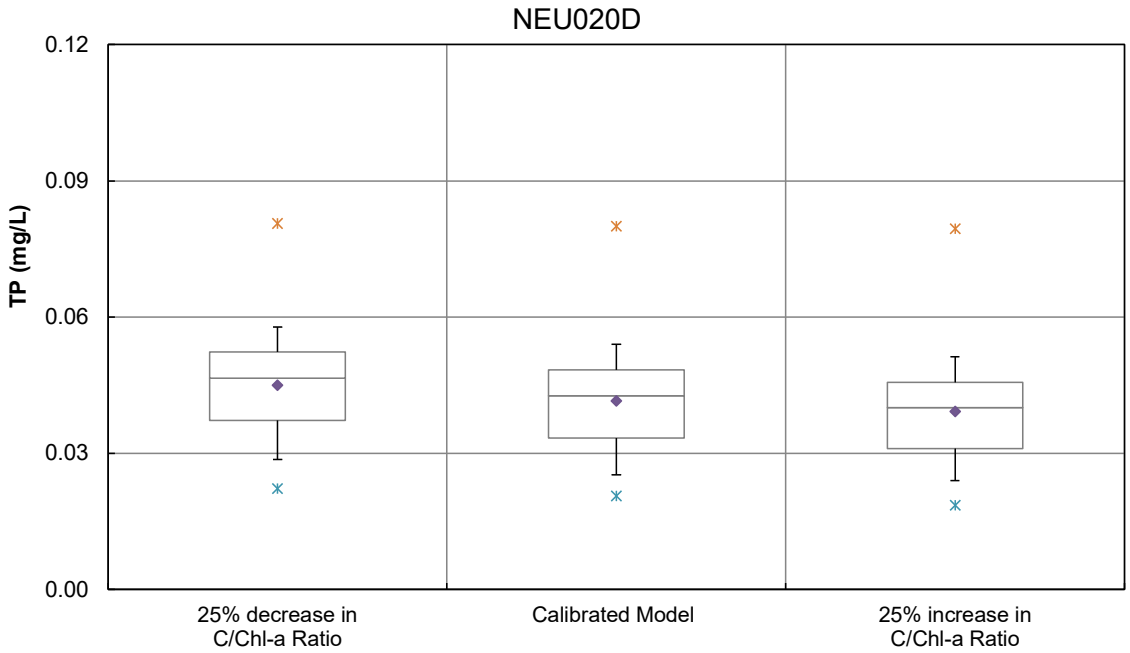

Figure 93 Box-Whisker Plot of TP at NEU020D under C/Chl-a Ratio Perturbation

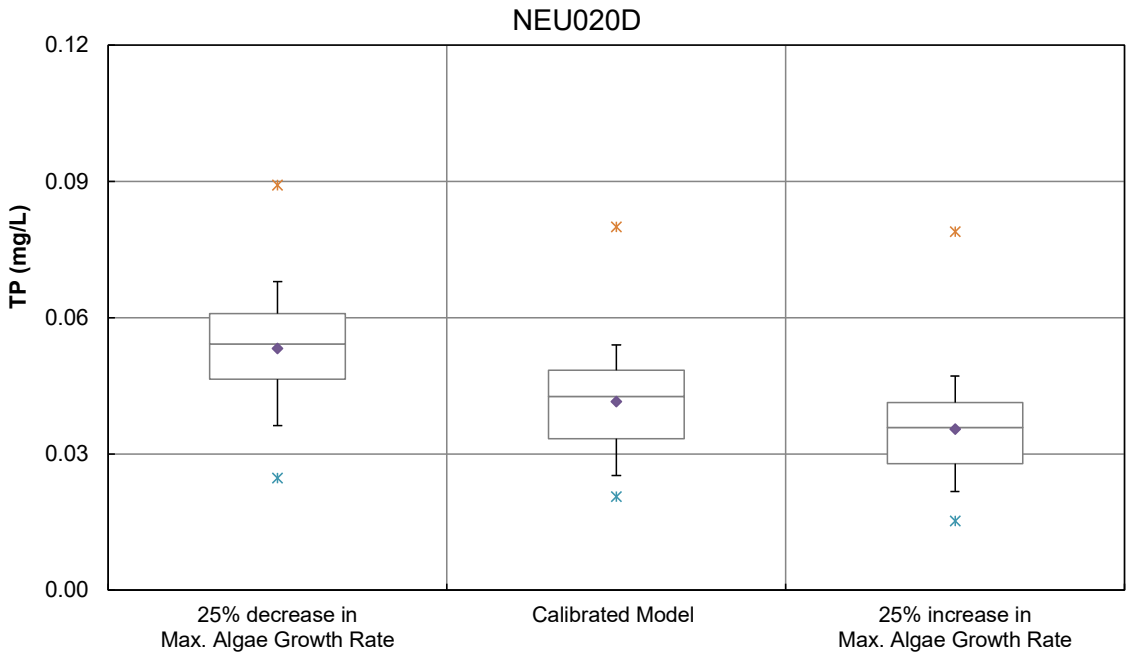

Figure 94 Box-Whisker Plot of TP at NEU020D under Algal Growth Rate Perturbation

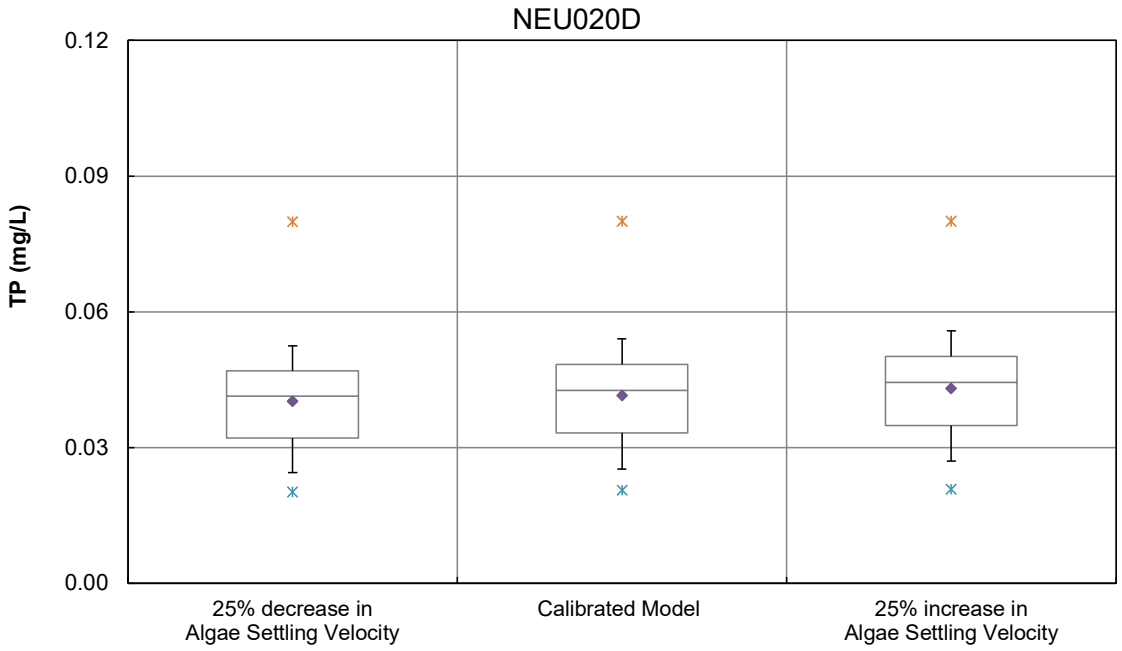

Figure 95 Box-Whisker Plot of TP at NEU020D under Algal Settling Velocity Perturbation

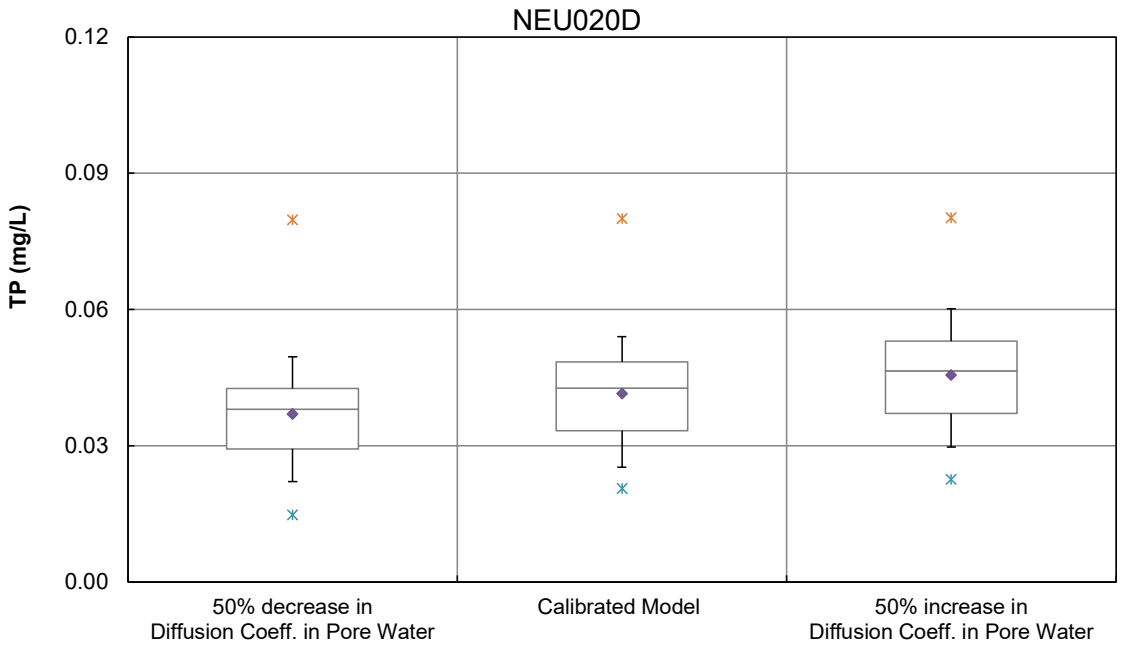

Figure 96 Box-Whisker Plot of TP at NEU020D under Diffusion Coefficient in Pore Water Perturbation